PROCEEDINGS
8th JOCG AIRCRAFT/STORES COMPATIBILITY SYMPOSIUM

23-25 OCTOBER 1990 FORT WALTON BEACH, FLORIDA

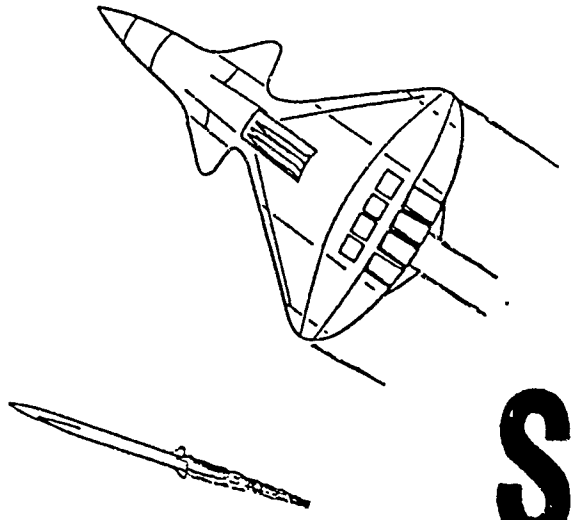

Sponsored by the
JOINT ORDNANCE COMMANDERS GROUP
AIRCRAFT/STORES COMPATIBILITY SUBGROUP

Hosted by the
Office for Aircraft Compatibility, 3246th TEST WING, Eglin Air Force Base, Florida
and the
Northwest Florida Section,
AMERICAN INSTITUTE OF AERONAUTICS AND ASTRONAUTICS

Symposium Objective

The purpose of this Symposium is to discuss the challenges of Aircraft/Stores Compatibility including lessons learned from the past, to review current problems and their solutions, and to investigate future technology trends. The program has been designed to provide presentations on analytical and experimental methods for current and future integration efforts.

→ to p. 1-1

Aircraft/Stores Compatibility Sub-Group Steering Committee

Sub-Group Chairman	Wiley J. Robinson	Air Force Systems Command
Study Group Chairmen		
Electrical Interface	Joe Ennis	Air Force Systems Command
Aerodynamics and Structures	Al Curry	LTV Aircraft Products Group
Aircraft Armament	Lanny Drummond	Pacific Missile Test Center (USN)
Compatibility Technology	William White	Air Force Systems Command

Symposium Paper Selection Committee

Wiley J. Robinson	Air Force Seek Eagle Office
Wayne Ingram	Air Force Development Test Center
Charles Epstein	Armcon, Incorporated
Joel Knight	Air Force Development Test Center

Hosting Organizations

3246th Test Wing
Office for Aircraft Compatibility
Eglin Air Force Base, Florida

Northwest Florida Section
American Institute of Aeronautics
and Astronautics

8th JOCG Aircraft/Stores Compatibility Symposium

Table of Contents

General Topics

Computational Fluid Dynamics Methods for Store Carriage and Separation

8th JOCG Aircraft/Stores Compatibility Symposium

Table of Contents (Continued)

8th JOCG Aircraft/Stores Compatibility Symposium

Table of Contents (Continued)

8th JOCG Aircraft/Stores Compatibility Symposium

Table of Contents (Concluded)

*Paper included in Proceedings but not presented at Symposium.

STORES INTEGRATION IN SMALL INTEGRATED MULTIROLE-MULTI USERS COMBAT AIRCRAFT NECESSITY OF A SYSTEM APPROACH

Claude CONNAN - DASSAULT AVIATION - FRANCE

1. INTRODUCTION

There are various aspects of stores integration on an aircraft. This paper is only related with the weapon system aspects and not with aerodynamics, mechanical, separation or any other aspect of the subject.

Integration of many different types of stores in a small multirole - multi users aircraft integrated weapon system has impacts much deeper than at the aircraft/store interface. Through three generations of systems this paper emphasizes lessons learnt on system design and development.

Starting from explaining the stores integration problem on such aircrafts (§2) it goes through the different solutions chosen for each generation of system (§3) to explain the progresses and problems encountered (§4) and concludes on working direction for the future (§5) to improve store integration in the systems and the consequences on interoperability improvements.

2. INTEGRATED WEAPON SYSTEM

The sizes of Dassault aircrafts are such that since the beginning of the seventies it was found necessary to have very integrated navigation and weapon systems sharing as much resources as possible instead of having several separate subsystems. Integrating as many different types of stores as possible leading to a great number of flying configurations has then to be made continuously all over the life of the aircraft by modifying the system as least as possible.

The main constraints of such stores integration are :

- integrate a new store in a short time
- keep the cost as low as possible
- be sure nothing already in the system is degraded when adding this store (non regression)
- the diversity of the technologies and techniques involved

3. SYSTEMS DESCRIPTION

This paragraph gives only a description of the most important areas implied in weapon integration :

- installation
- hardware architecture
- store station wiring and connecting
- functionnal architecture
- software architecture
- safety features
- supportability

Is does not describe the development methods and tooling which are used.

3.1. FIRST GENERATION SYSTEM (FIGURE 1)

This is a system designed in the beginning to middle seventies.

3.1.1. TECHNOLOGICAL STATUS

This system was designed at a time when :

- the stores were mainly
  - air to air missiles (analog)
  - ballistic simple weapons
  - recce/ECM pods requiring few informations

  The more sophisticated weapons and pods requiring more informations even if already existing were not required to be installed at the beginning but later during the life of the system.
- restricted computation and memory capabilities of the airborne computers
- beginning of multiplex data bus use

Main design constraints :

- use of one store at a time and one mission store (excluding self protection stores) per mission
- be able to integrate a large number of stores (table 1)
- implement the integration of a store in a limited time

- keep as often as possible the aircraft capable of using all stores when a new one is added.

3.1.2. INSTALLATION

- The pylons and launchers are specific for each type of store except for bombs and rockets.
- Three spaces are reserved for interchangeable interface boxes inside the equipment bay :
  - one connecting to most important store stations (central fuselage and internal wing stations)
  - one connecting to external wing stations
  - one connecting to wing tips (air to air infrared missiles)
- Two spaces are reserved for interchangeable control boxes in the cockpit
  - one for missile, recce pods, ECM (fuselage + internal wing stations)
  - one for ECM (external wing stations)

3.1.3. HARDWARE ARCHITECTURE

The main characteristics of the chosen architecture are :

- centralised architecture around one main computer with a limited avionics multiplexed data bus terminals including the main sensors and symbol generators
- Non multiplexed controls except for store selection and few "hands on stick and throttle" controls. Specific control boxes and interface boxes for pods and missiles
- Linkage between avionics system and store stations through a complete set of boxes :
  - one power distribution box and firing interface box : one circuit for each type of weapon (missiles, bombs, rockets) and a separate circuit for jettison and emergency jettison
  - two sets of interface boxes (cf § 3.1.2)
- Separate store stations connectors and wiring for each type of weapon : missiles, bombs, rockets
- One box for weapon code setting

3.1.4. STORE STATION WIRING AND CONNECTING

Each store station requires :

- one connector for : bombs, rockets
- one connector for missiles
- one or two connector (s) for pods

The connectors types are different at each store station

For the data bus several steps have existed during the life of the programm

1. No store station on data bus

2. Central fuselage store station can be a remote terminal of the avionics bus. A special plug has to be put on the connector when the pod requiring the bus is not installed.

3. Central fuselage is connected through a long strub with no need for special plug when not in use.

3.1.5. FUNCTIONNAL ARCHITECTURE

The main characteristics of the functionnal architecture are :

- safety critical circuitry separated in specific box
- no (or few) common point between specific function of different types of stores
- the only store functional resources between the different specific store functions are : safety controls, display terminal
- back up operationnal mode only for ballistic weapons :
  - first step : simple ballistics weapons (hard wired)
  - second step : all ballistics weapons (software implemented)

3.1.6. SOFTWARE ARCHITECTURE

The involved software are limited to :

- main computer software
- symbol generator software

And in a second step : weapon code setting box : used to set the stores codes

The addition of each new store leads to test the overall software of the system on the stimulated integration test bench.

3.1.7. SAFETY

Each type of weapon has its own ground safety equipment and procedure. The system is built so that only simple hardwired circuitry is involved in the safety.

3.1.8. SUPPORTABILITY

A centralised external system is used to test the overall system but each type of external store station equipment has its specific maintenance box(es).

3.2. SECOND GENERATION SYSTEM (FIGURE 2)

This is a system design of the end of the seventies-beginning of the eighties.

3.2.1. TECHNOLOGY SITUATION

This system was designed at a time when the stores still used mainly analog data transmission except for complex pods which were beginning to be digitized but completely digitized stores were only foreseen in the near or further future.

The computation and memory capabilities were increasing and permitting more flexible functional and software architectures. The multiplex data bus technique has been widely used in the system.

New design constraints for stores integration :

- have one installation including wiring for the overall life of the aircraft
- be able to add a new store without retesting the already existing software of the main computers (or as little as possible) : non regression.

3.2.2. INSTALLATION

- pylons and carriage stores are non specific to a weapon
- launchers are specific to each missile except one case where two missiles use the same launcher (one box has to be replaced in the launcher depending on which missile is used)
- One space is reserved for interchangeable interface box (main store stations) : four different boxes.

3.2.3. HARDWARE ARCHITECTURE

The main characteristics of the chosen architecture are :

- centralized architecture around two main computers with two avionics multiplexed data buses (one mainly oriented avionics, one mainly oriented ECM and stores management)
- Largely multiplexed controls except safety controls and power distribution controls. No replaceable control box in the cockpit.
- Linkage between avionics system and store stations through a limited number of boxes :
  - one store power distribution box : 10 Amps DC and 3 phase AC (+ additionnal power for central fuselage store station in a second step)
  - one firing interface box :
    - normal operationnal firing circuitry
    - selective jettison circuitry
    - emergency jettison circuitry
    - guns interface
  - one replaceable missile/pod interface box connected mainly to the central fuselage and internal wing station (cf § 3.2.2)
  - one interface box for Air to Air infrared missiles (connected to the external wing stations)
  - later in the definition ; one multiplex interface box for store stations not connected to the replaceable missile/pod interface box.

3.2.4. STORE STATION WIRING AND CONNECTING

Each store station requires :

- one connector for firing or release functions (one size of connector for main store stations, another for the other stations)
- one connector for power distribution and functionnal interface (analog and digital). Same connector for all store stations ; specific wiring for each station exept for main store stations.
- only for central fuselage store station : auxiliary connector (additionnal power and gun pod interface)

3.2.5. FUNCTIONNAL ARCHITECTURE

THe main characteristics of the functionnal architecture are :

- centralized architecture with the main functions in the two main computers :
  - fire control and main avionics functions in first computer : the stores are divided in two types : self protection (guns, missiles, ECM) and main mission store (one and only one per mission). The architecture is such that adding new main mission store can be done without modifying the remaining of the computer software.
  - stores management function in second computer.
- When a backup mode is developed for a store function it is implemented in both main computers. It is implemented only when it covers a large amount of the overall possible failures implied in the function). There is no specific hardware for back up modes. The firing back up mode uses the selective jettison circuitry.
- selective jettison is not hardwired but software implemented in both computers.

3.2.6. SOFTWARE ARCHITECTURE

Two main phases during the development :

1. Use of tables mainly for ballistic weapons management so that a new weapon is integrated by adding only a new list of parameters in the existing tables.
2. Use of tables extended to all weapons. Then a new weapon integration leads to add a new list of parameters and a very restricted number of interface functions between the appropriate fire control function and stores management (which interface is standard) or beetween the store itself and stores management.

3.2.7. SAFETY

Each type of weapon has its own ground safety equipment and features. The system is built so that almost only hardwired circuitry is involved in safety. The restricted amount of very simple safety involved software is isolated and developed with a specific method.

3.2.8. SUPPORTABILITY

The online maintenance is self contained in the aircraft, the only external equipment required to test the stores management and fire/release circuitry are wired plugs connected in place of the store. Some plugs are specific to some stores.

3.3. THIRD GENERATION SYSTEM (FIGURE 3)

This is a system designed in the middle to late eighties.

3.3.1. TECHNOLOGY STATUS

The digital technologies is prevailing which gives a lot of flexibility but the old existing analog stores still need to be intergrated in this system. To improve interoperability the system has to be compatible with MIL STD 1760 stores interfacing.

New design constraints :

- be able to use several types of weapons during the same mission and simultaneously (at the pilot's level).
- only allowed hardware development for a new store integration is in the launcher or pylon (no interface box inside the aircraft, all aircraft capable of all implemented stores without installation reconfiguration).

3.3.2. INSTALLATION

- pylons and carriage stores are non specific to a store
- launchers are designed for a family of weapons with no (or a minimum of) operations to change a weapon.
- no specific hardware inside the aircraft for any store.

3.3.3. HARDWARE ARCHITECTURE

The main characteristics of the chosen architecture are :

- several multiplexed data buses : MIL STD 1553B and NATO STANAG 3910
- distributed architecture but the data buses management is centralized
- completly multiplexed controls in the cockpit (exept safety fire controls)
- MIL STD 1760 connections between avionics system and store stations through :

- limited power distribution (no auxiliary except on central fuselage store station)
- three stores management physical MIL STD 1553 B data busses (to reduce vulnerability)
- high hanbwidth switching network (one network for video, one network for synch and blanking)
- safety involved through "Release consent " hardware implementation mainly
- interface boxes in pylons and/or launchers

3.3.4. STORE STATION WIRING AND CONNECTING

- the pylons are equiped with MIL STD1760 connectors
- The interface between the aircraft skin and the pylons (or the launchers) have a signal set which is capable of :
  - MIL STD 1760 signal set
  - emergency jettison
  - very few specific stores wirings

3.3.5. FUNCTIONNAL ARCHITECTURE

The main characteristics of the functional architecture are :

- distributed architecture so that it mainly consists of the management of an important amount of "resources" which are located in different boxes :
  - sensor informations
  - computation algorithms or logic computations such as ballistic computation, steering laws computations, firing envelopes computations, missions preparation data, etc.... non specific to a store. Each store can be characterized by a specific data set and algorithm set.
- clear separation of safety critical software from other software.
- back up modes are studied case by case and for each "resource" instead than each overall store function.

3.3.6. SOFTWARE ARCHITECTURE

The requirements are such that the functional and the software architectures are getting closer and closer (and almost identical) at the level where you need to have standard interfaces are needed between modules (which have to be considered as functionnal or software resources). This is possible because of an important in increase in computation, memory and data bus capabilities.

3.3.7. SAFETY

The ground safeties are standardized. The increasing amount of safety critical store management software is increased. Specific design and development criteria continue to be used for this software. But the main firing safety element is the "release consent" circuitry which is independant of software.

3.3.8. SUPPORTABILITY

The online maintenance is self contained in the aircraft except where pyrotechnic cartridges are used (replaced by special plugs) for safety critical cricuitry testing.

4. PROBLEMS AND INTERESTS OF EACH SYSTEM

They are described using the following main criteria :

- necessary preliminary design of the system
- main consequences of integrating a new store :
  - amount and complexity of work
  - new developments
  - modifications of existing system
- user's learning and training
- quality of the result and global cost
- interoperability

4.1. FIRST GENERATION SYSTEM

4.1.1. DESIGN OF THE SYSTEM (TABLE 2)

The preliminary design criteria which could be taken into account in a standardization approach at that time were :

- emergency jettison and selective jettison circuitry
- few controls
- room for boxes at specific places
- ballistic algorithm

The preliminary design is mainly restricted to installation, wiring, and some power distribution and jettison circuitry.

4.1.2. NEW STORE INTEGRATION

4.1.2.1 AMOUNT AND COMPLEXITY OF WORK

The type of work to be done is in fact a new part of an overall system design with all its aspects (installation, wiring, hardware and software development and modifications, new supportability equipment development)

4.1.2.2 NEW DEVELOPMENTS

Each new store integration generally implies the development of :

- a new interface box
- a new specific control box
- a new section in the main computer

One major redevelopment of an existing box occured during the program : change from a hardwired back up mode in the "weapon code setting box" to a software implemented back up mode in the same box.

The arrival of more and more digital stores at the end of the eighties implies connection of most of the store stations to the multiple data bus : a new digital interface box needed in addition (and simultaneously) to the other interface boxes with corresponding wires and connectors : It is a major wing installation modification.

4.1.2.3 MODIFICATION OF EXISTING SYSTEM

Scarcely : modify existing interface box and specific control box

For several stores : modify armement control box, wiring between boxes and at the store station level.

For all stores :

- modify a small part (but a part) of mission computer existing software and test the overall software
- modify the display computer software and test it all

4.1.3. USER'S LEARNING AND TRAINING

The lack of standardization at several levels is such that the training is almost specific for each usage for the ground crew and the pilot's (who have to be quite specialized for one type of mission)

4.1.4. QUALITY OF THE RESULT - COST

The overall quality of the product is good but necessitates an important amount of work and development for each new store integration with consequencies on the overall cost.

4.1.5. INTEROPERABILITY

It is quite difficult to speak of possible interoperability with this type of system.

4.1.6. LESSONS LEARNT

The lessons learnt quite rapidly on this program are :

- an important commonality exists in the types of necessary wirings for each store even if the transmitted information is completely lately different
- the firing circuitry for stores can be standardized
- stores management needs are very similar from store to store
- even back up modes for quite simple weapons are too complex to be hardwired. They need a software implementation.
- non regression adjunction to a system can be made easily only if there is no modification to the installation, wiring and hardware of common equipment.

  This implies :

  - to design the basic system carafully taking the potential adjunction into account.
  - to use a rigorous top down methodology with well identified steps.

4.2. SECOND GENERATION SYSTEM

4.2.1. DESIGN OF THE SYSTEM (TABLE 2)

The main design criteria for this second generation system were :

- taken from the lessons learnt on the first generation system :
  - common wiring between interface boxes and store stations
  - standardized fire and release circuitry for all weapons :
    - one operationnal firing circuit
    - one selective jettison circuit
    - one emergency jettison circuit
  - more standardization in stores management functional and software architecture in two steps :
    - first step (which did not imply long studies) use of restricted amount of parametric tables and interfaces

- second step : stores management built so that a new store is a set of data, specific algorithms or logics (with standard interfaces) to interface with fire control or store.

- new requirements :
  - non regression on software development : each fire control function is a completely separate function with interfaces with other functions which are as standard as possible.
  - less space in the cockpit for controls : implies a more extensive use of multiplexed controls
    - first step : 2 lines of multiplexed keys armement control box
    - second step : use of a CRT display with multiplexed keys.

    The power distribution and conditionning are hardwired per store station with a standard control box.

4.2.2. NEW STORE INTEGRATION

4.2.2.1 AMOUNT AND COMPLEXITY OF WORK

The necessary work to add a new store in this case is much more oriented toward functionnal and software design and developement. There is no more installation or wiring work required exept to check that what already exists is compatible with the new store needs.

4.2.2.2 NEW DEVELOPMENTS

Each new store integratior generally implies the development of :

- a new function and a new backup function in the main computers
- most times a new specific interface box

One major hardware development implying installation modification during the system development : multiplex data bus toward some of the store stations which were not all connected since the beginning.

One connector had to be added during development at the central fuselage store station for additional power supply.

4.2.2.3 MODIFICATION OF EXISTING SYSTEM

- not one modification of hardware of interface boxes or control box (the first step control box had no software)
- no one modification of the wings wiring and connectors and only one grounding modification to the central fuselage station
- only one main equipment bay modification (multiplex data bus stores interface box)

- at the beginning of the development it was difficult not to modify the existing main computers software but the modular evolutive architecture was rapidly improved and afterwards the only main computers modifications were : addition of a new fire control function and a set of interface modules and data for stores management and cockpit interface. The multiplexed data bus management had still to be modified and tested each time.

- display computers software

- some of the interface boxes between avionics system and stores have only to be partly modified to be able to interface a new store : stores built by the same manufacturer are using the same type of interface hardware (even not for same information)

4.2.3. USER'S LEARNING AND TRAINING

The improvements from the first generation system are mainly :

- for the ground crews : better standardization of the procedures (safety, stores loading, maintenance)
- for the pilot : similar controls use from one store to another but still quite specific use of the overall system and displays.

4.2.4. QUALITY OF THE RESULT - COST

The quality of the product is still as good as before with : more work at the specification level and less work at the test level : because regression and better specifications. This means a better cost result.

The operationnal wiring, circuits and store management software have been used for all the weapons separation test : so the number of hours of use of this part of the system is quite important. It increases the confidence in this safety critical part of the system.

4.2.5. INTEROPERABILITY

A step has been made toward interoperability but the result is still far from a really interoperable system :

- the operations needed to change the mission store loaded under the aircraft are reduced compared to the proceding generation :

  - change of launcher (when a specific launcher is needed)
  - change of one interface box (for a restricted number af cases)

- The system work to integrate a "MIL STD 1760 store" is generally reduced to : software fire control implementation (main computers and display computers), addition of stores management software and data interface modules.

4.2.6. LESSONS LEARNT

The main lessons learnt on this program are :

- the lessons learnt from the first generation system are confirmed and the standardization implemented in the system to answer those lessons is an important improvement toward an easier integration of a new store and in operation rapid loading of a different store.

- modularity of the fire control functions toward a better evolutivity of the system is possible. A very strict top down methodology of software development has to be used to arrive to a good result : from operational requirements to functionnal specification toward software specification and coding

- use of data tables and interface modules in the stores management function simplifies greatly the addition of a new store in the system. An important standardization effort needs to be made at the very beginning of the system design to define the content of those tables and the standard interfaces between the different modules

- a lot of similarities can be found inside the fire control functions, cockpit interface and store functional interfacing.

- even when giving acceptable results in the needed environment the originally designed wiring arrives at its usable limits (no more growth potential, signal to noise and other transmission characteristics need to be improved for future foreseen applications)

- confirmation that bad design has to be corrected as early as possible : it is important to validate the system before beginning the implementation itself to reduce the cost.

- the system is not flexible enough to allow all loading configurations which are wanted by the operational user.

4.3. THIRD GENERATION SYSTEM

4.3.1. DESIGN OF THE SYSTEM (TABLE 2)

The main design criteria for this third generation system are :

- keep a very strict top down development approach and improve it by more of early simulations to detect the problems as soon as possible and reduce the overall cost.

- the aircraft installation, wiring and hardware has to be able to support the integration of the foreseen stores without one modification. The transmission characteristics of the wiring has to be improved from the second generation system to accept new signals.

- simultaneous use of several stores, the need for the same operational user to cope with several types of stores, and the fact that similarities can be found in the system algorithms and logics implies that :

  - more common algorithms and logics need to be used
  - more commonality is needed in the user's interface
  - the data tables and interface modules concept has to be extended over the stores management function
  - the overall system has to be thought as a management system of an important amount of shared "resources"
  - the evolutions of the system have to be thought not only as the addition of a new store but also as :
    - the improvement of one of the resources
    - the easy integration of a new store (very similar to one already integrated) by the operationnal user.
  - when needed (for old existing stores) the adaptation interface (mainly hardware) has to be done in the launcher or other mechanical external interface.

4.3.2. NEW STORE INTEGRATION

4.3.2.1 AMOUNT AND COMPLEXITY OF WORK

The most important work has to be done at the first design phase of the systems with a prevalidation of the overall architecture with at least two different representative stores. The previous generation architecture can be taken as a basis and modified to design this one. What is important is to define the right standard functionnal module interfaces ans capabilities. Use of simulation is needed to optimize the standard interfacing.

The integration of a new store necessitates a smaller amount of work that for the previous generation.

4.3.2.2 NEW DEVELOPMENTS

Each new store integration implies the development of :

- a data set
- software interface modules and specific algorithms and logic
- if the store is not a MIL STD 1760 store possibly the development of an interface module (hardware and software) to be inserted in the pylon or launcher.

4.3.2.3 MODIFICATION OF EXISTING SYSTEM

The modifications foreseen are modification because the capabilities are not in the existing main frame of the system : computation capability, memory capacity, transmission capability, new types of signal, completely new interface with the pilot.

4.3.3. USER'S LEARNING AND TRAINING

The objective is also to have a basic having such that it is easier to transfer the knowledge from one store's to another.

4.3.4. QUALITY OF THE RESULT - COST

The objective is to decrease the cost of new store integration and the number of modifications to have better time schedules and cost.

4.3.5. INTEROPERABILITY

A new step has been made toward interoperability :

- the operations needed to change a mission store under the aircraft are reduced compared with the preceding generation : change of launcher (when a specific launcher is needed) : essentially for old non MIL STD 1760 stores or of an interface module inside the pylon launcher
- the system development work to integrate a new store tends to be only the introduction of a set of data and interface modules.

4.3.6. LESSONS LEARNT

It is too early at this stage of the program to speak of lessons learnt because it is under development.

5. CONCLUSION

Through the different generations of systems a cost effective method of store integration is beeing continuously improved. The main keys of this possible progression are :

- a rigourous top down methodology of system development with a priotity to a functional approach instead of a subsystems approach.
- a step by step progress in finding the different technical functions (installation, hardware, software) and operating function (fire control modules, stones management modules) and use of previous lessons learnt on the preceding systems. This results in a progressive standardization of the different elements of the overall weapon system involved in stores integration and use. In appearance this step by step approach takes a long time to arrive to a good standardization but in this areas it seems impossible to make instantaneously an important step but the real possibilities are learnt quite slowly.

Indirectly, it also results in getting closer and closer to the complete interoperability needs.

The efforts of standardization toward a more effective and easier store integration to aircrafts and better interoperability are of great interest. All the work made on MIL STD 1760 is very important for this progression but as shown in the preceding paragraphs, much more than MIL STD 1760 is implied for complete store integration to systems and for interoperability. The arising technologies are now giving much more capabilities : computation power, memory capacity, data bus transmission capabilities. Furthermore, there is more and more interoperability between the different elements : standard languages, operationnal systems, etc.... The past has shown that there is a lot of similarities which can be found between the different store needs and a lot of them can be expressed in terms of data sets plus some specific algorithms or logics.

Regardless of the implementation some modular functions can be defined to help this standardization effort :

- they have to be defined as "generic functions" which can be algorithms, logics, or more complex functions.
- the level of definition is at the interface of the "generic function" so that different implementations can be made by different manufacturers to be used in systems having different architectures.

Some of the main stores characteristics are already defacto non written standards, and more could be found so that all the system and functions designers can speak the same language and exchange coherent data.

TABLE 1 - STORES TO BE INTEGRATED			
TYPE OF STORE	1st GENERATION	2sd GENERATION	3rd GENARATION
Ballistic weap-ons	20	25	30
Missiles			
- Air to Air	5	7	7
- Air to Surface	3	10	15
Pods			
PHOTO/OPTRONIC	6	5	-
RADAR	1	1	1
ELECTRONIC RECCE	1	1	-
ECM	4	4	-
OTHER	5	5	-

TABLE 2 - SYSTEM DESIGN			
TYPE OF STORE	1st GENERATION	2sd GENERATION	3rd GENARATION
COCKPIT			
Controls	Partly : multiplexed Partly : specific	Partly : multiplexed soft driven Partly : multiplexed hardwired	All : multiplexed soft driven Exept safety release controls
Displays	Reprogrammable Test needed	Reprogrammable Test needed	Reprogrammable Non regressive
EQUIPMENT BAY			
- Power distribution	partly standard	totally standard	MIL STD 1760 limited
- Fire/release Circuit			
Emergency JET Selective JET	1 circuit	1 circuit	1 circuit
(Back up fire) Operational FIRE	1 circuit per weapon	1 circuit	1 circuit
- Interface boxes	specific 8 boxes developed	5 boxes developed with commodities	standard MIL STD 1760 Interfacing
- Computers involved	1 main computer + displays	2 mai computers + displays	2 mission computers + displays + controls
- Standard wiring	Release wires	Yes	MIL STD 1760 compatible
- Standard store station connectors	No	Yes	Yes
Functionnal architecture			
- Evolutive fire control software	No	Yes	Yes
- Software resources	No	No	Yes
- Digital interface at store stations	No	Yes	Yes

TABLE 3 - INTERESTS AND PROBLEMS OF EACH GENERATION OF SYSTEMS			
TYPE OF STORE	1st GENERATION	2sd GENERATION	3rd GENARATION
DESIGN METHOD-OLOGY			
Top Down	No	Yes	Yes
Main Technical Areas	Installation	Installation Hardware (partly common) Functional (Evolutive per stores)	Common installation Common hardware Functional multicible resources
DEVELOPMENT			
Per Store	INstallation - hard - soft	Hardware software	Interface software
Non regression	No	Hardware main computer software	Complete
Modifications on existing system			
Installation	Yes	No	No
Hardware	Yes	Yes	No (exept pylons and launchers)
Wiring	Scarcely	No	No
Software	Yes	No	No
OPERATIONAL USE			
Store Change	Pylon/launcher, interface boy, control box	Pylon, Launcher, interface box	Launcher
Training of Ground crew and Pilot	No commonalities	Few commonalities	As many commonalities as possible
REUSABILITY			
Installation	Partial	Yes	Yes
Equipment	"	Yes	Yes
Functional specs			
. Architecture	No	Yes	Yes
. Module specs	No	Partial	Yes
Software modules	No	No	Yes

DASSAULT AVIATION

1 ST GENERATION SYSTEM

DSA

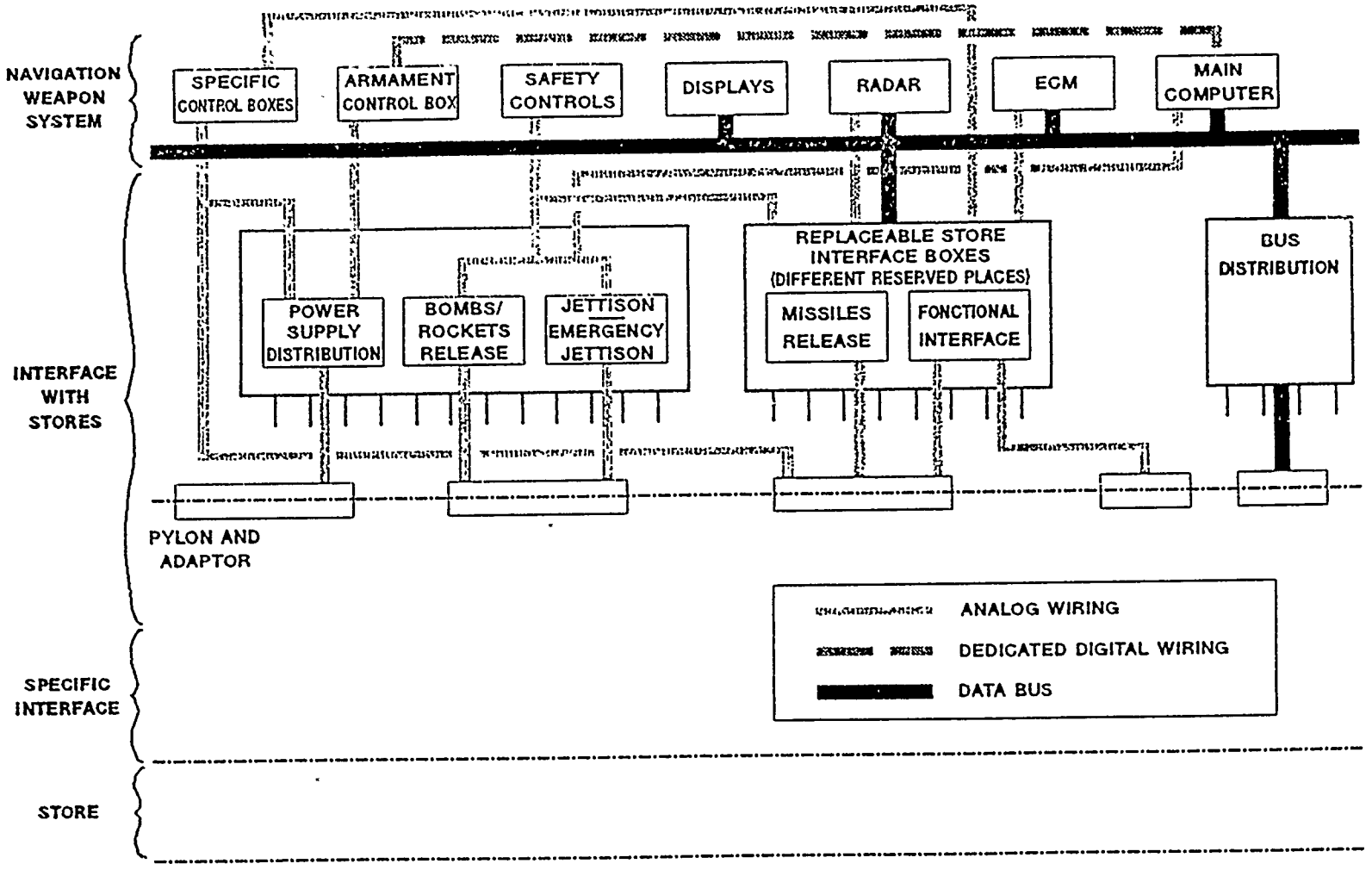

FIGURE 1

CLEARED FOR PUBLIC RELEASE

DASSAULT AVIATION

2 ND GENERATION SYSTEM

DSA

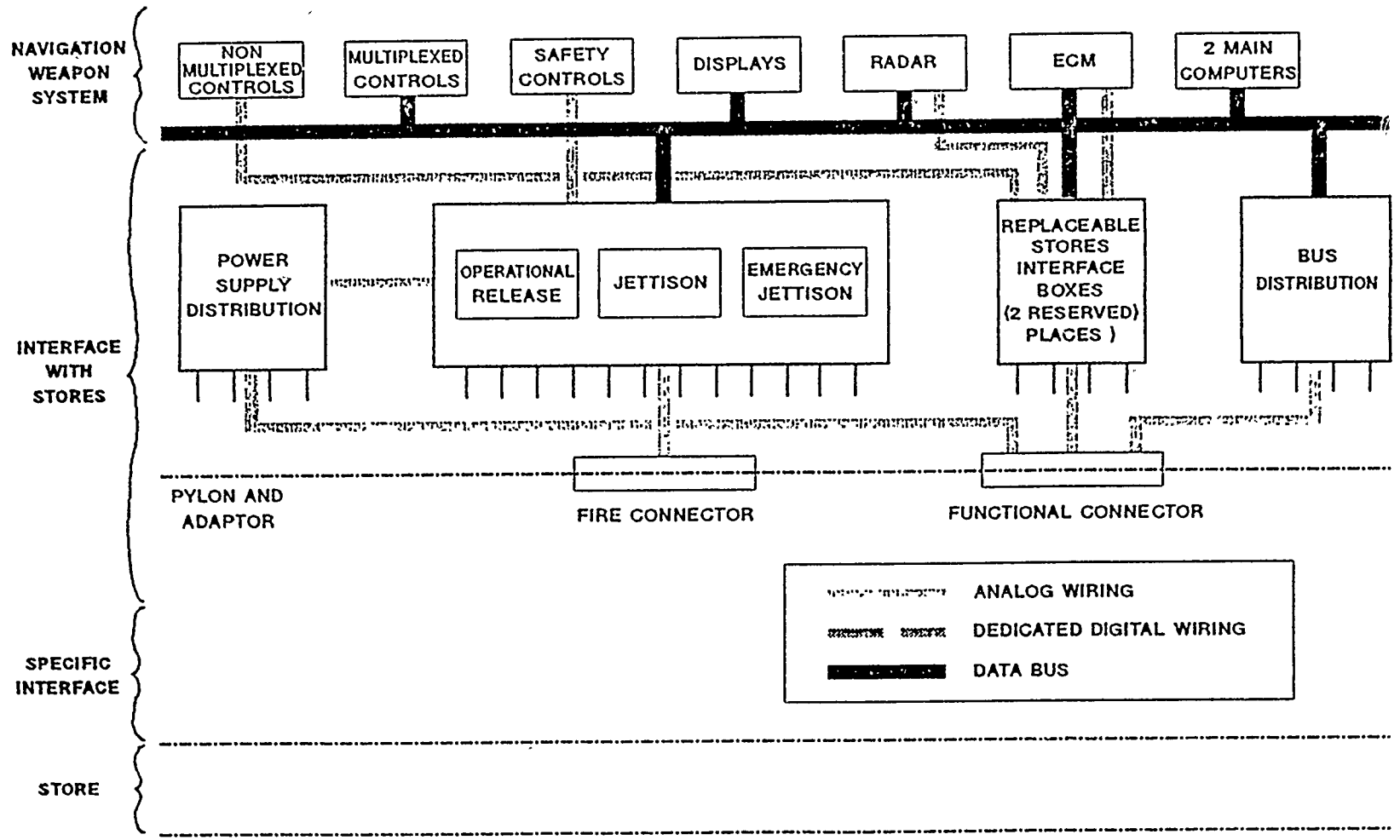

FIGURE 2

CLEARED FOR PUBLIC RELEASE

CLEARED FOR PUBLIC RELEASE

DASSAULT AVIATION

3 RD GENERATION SYSTEM

DSA

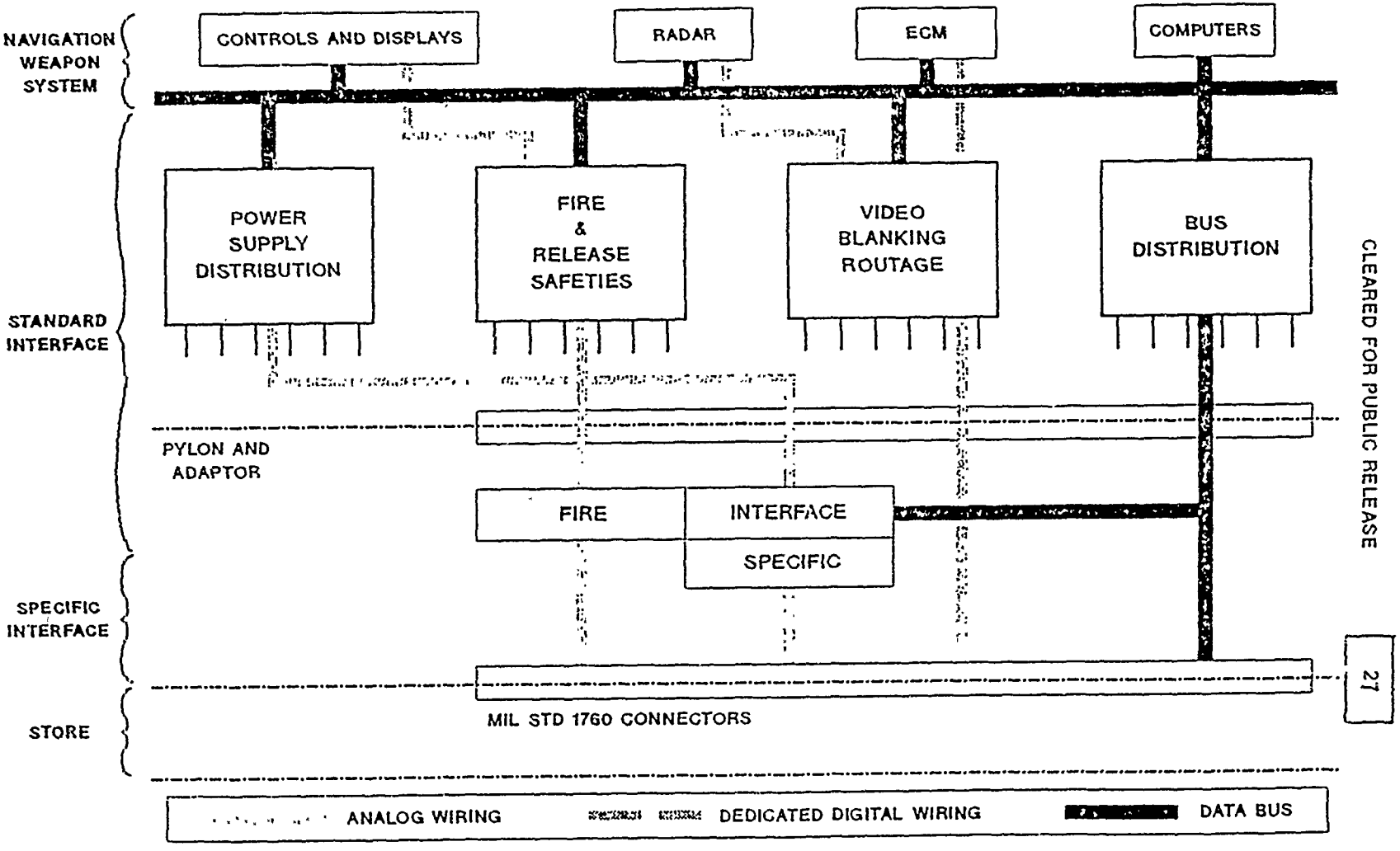

FIGURE 3

CLEARED FOR PUBLIC RELEASE

CLEARED FOR PUBLIC RELEASE

27

CLAUDE CONNAN

BACKGROUND

He graduated in 1971 in electronics engineering at Ecole Française de Radio électricité et d'Electronique (Paris - France) and specialized in systems engineering in 1972 at Ecole Nationale Supérieure d'Aéronautique et de l'Espace (Toulouse - France).

He joined Avions Marcel Dassault-Breguet Aviation in the Avionics Systems Division in 1972, where he worked on different areas such as civil aircraft cat III certification, navigation and air to ground functions for a Navy Fighter from 1972 to 1976. In 1976 he joined the Mirage 2000 Avionics System Program team to lead the stores management functions and main avionics controls. He led the stores management system team from 1983 to 1985, the stores integration group (stores management, fire control) from 1985 to 1988. Since 1988 he is in the technical board of the avionics division (for stores integration and system architecture)

Active member of the SAE - ASD - AS1 A MIL STD 1760 users task group since 1983

CLEARED FOR PUBLICATION RELEASE

FOLDING FIN ACTUATOR, FFA

E. K. TAKATA

SCOT INCORPORATED
GOVERNMENT PRODUCTS DIVISION
FSCM 93455

SEPTEMBER 1990

Prepared for

8th Aircraft/Store Compatibility Symposium
23-25 October, 1990
Ramada Beach Resort
Fort Walton Beach, Florida

SCOT INCORPORATED

FOLDING FIN ACTUATOR, FFA

1.0 INTRODUCTION

Maximum loading density of missiles in the aircraft storage area is provided by the Folding Fin Actuator, (FFA). This cylindrically shaped device is operated by a ballistic cartridge to unfold a missile fin from stowed to deployed position ready for flight. Design goal for deployment time is 0.050 sec. maximum, with resisting or aiding airloads acting on the fin and with a temperature range of -65°F to +200°F.

Scot Inc. has designed and tested a FFA consisting of dual oil damped rotary actuators located on the hinge axis of the fin to be deployed. These actuators transmit torque to the forward and aft sections of the fin using a single ballistic cartridge centrally located in the fin control shaft. A helical spline drive mechanism in each actuator act to convert gas piston linear displacement to rotational motion at the fin. Major design features incorporated in the FFA include gas operated initial locks, variable orifice fluid damping, final fin deployed locks and a threaded gas port for preflight manual actuation for ground checkout.

Development test results with a FFA prototype test model, with 1.000 inch outside diameter and 11.000 inch installed length, are presented herein. Full actuator stroke for 120° fin rotation with resisting torque up to 2500 in-lb. was accomplished with hydraulic pressure input. Preliminary ballistic cartridge operation resulted in a stroke time of 0.050 sec. with

1400 in.-lb. of constant resisting torque acting. Final test fin angular velocity was maintained less than 50 radians per second. The test fixture consisted of a nitrogen operated gas cylinder with cylindrical cam and torque arm mechanism. The cylindrical cam rotates the torque arm which bears against the test fin during deployment. A miniature hydraulic cylinder at the end of the torque arm is used to measure contact force between the test fin and torque arm.

For reduced torque load requirements conventional cylindrical harmonic cam with multiple cam followers is used. This improves rotary mechanism mechanical efficiency and significantly reduces the assisting/resisting load spread transferred from the cam mechanism to the FFA gas and fluid damping pistons. The overall mechanical and ballistic efficiency of the rotary actuator and oil damping system is thereby maximized. Scot has designed and fabricated a double acting FFA with a cylindrical cam and with a constant orifice area fluid damping system. Two cartridges are required to deploy and later restow fin if missile is not launched.

Scot has developed a computer ballistic program for the FFA. This provides an accurate means to predict performance by use of an internal ballistic analysis in combination with the mechanical design parameters of the FFA.

Effects of aiding and resisting torque loads in addition to extreme operating temperature range are quickly evaluated. The ballistic program is used to determine optimum values by analysis of test data, variable orifice fluid damping and ballistic para-

meters. This reduces development time and cost to a minimum.

2.0 DESIGN DESCRIPTION

The Folding Fin Actuator, FFA, consists of dual rotary actuators, each 5.50 inch long. Both actuators are identical in design except the (-1) unit contains a left hand spline drive and the (-2) unit contains a right hand spline drive. As shown in Fig. 1, both actuators are located in hubs on the fin hinge axis and act to rotate the fin 120° during deployment. The electrically initiated cartridge is threaded and sealed in the control shaft so that propellant gas is introduced through the stationary hub and acts simultaneously on both the (-1) and (-2) actuators in the forward and aft directions. Gas pistons in both units are displaced and the spline drives act to rotate the fin 120° to full deployment.

Oil damping with a variable orifice area is incorporated in the FFA, as shown in Fig. 2, to reduce the fin end of stroke angular velocity to less than 50 rad. per sec. The variable orifice design is necessary to accurately reduce the fin angular acceleration and deceleration to a minimum under aiding and resisting torque load conditions.

A gas operated initial lock is provided in each (-1) and (-2) actuator to lock the fin in the stowed position prior to cartridge actuation. Final locks are installed in the fin to rigidly support the fin during flight under an airload torque of ±6000 in.-lb. maximum.

As installed in the fin, the central portion of the 11.00 inch length of the FFA is fastened to the control shaft fin hub

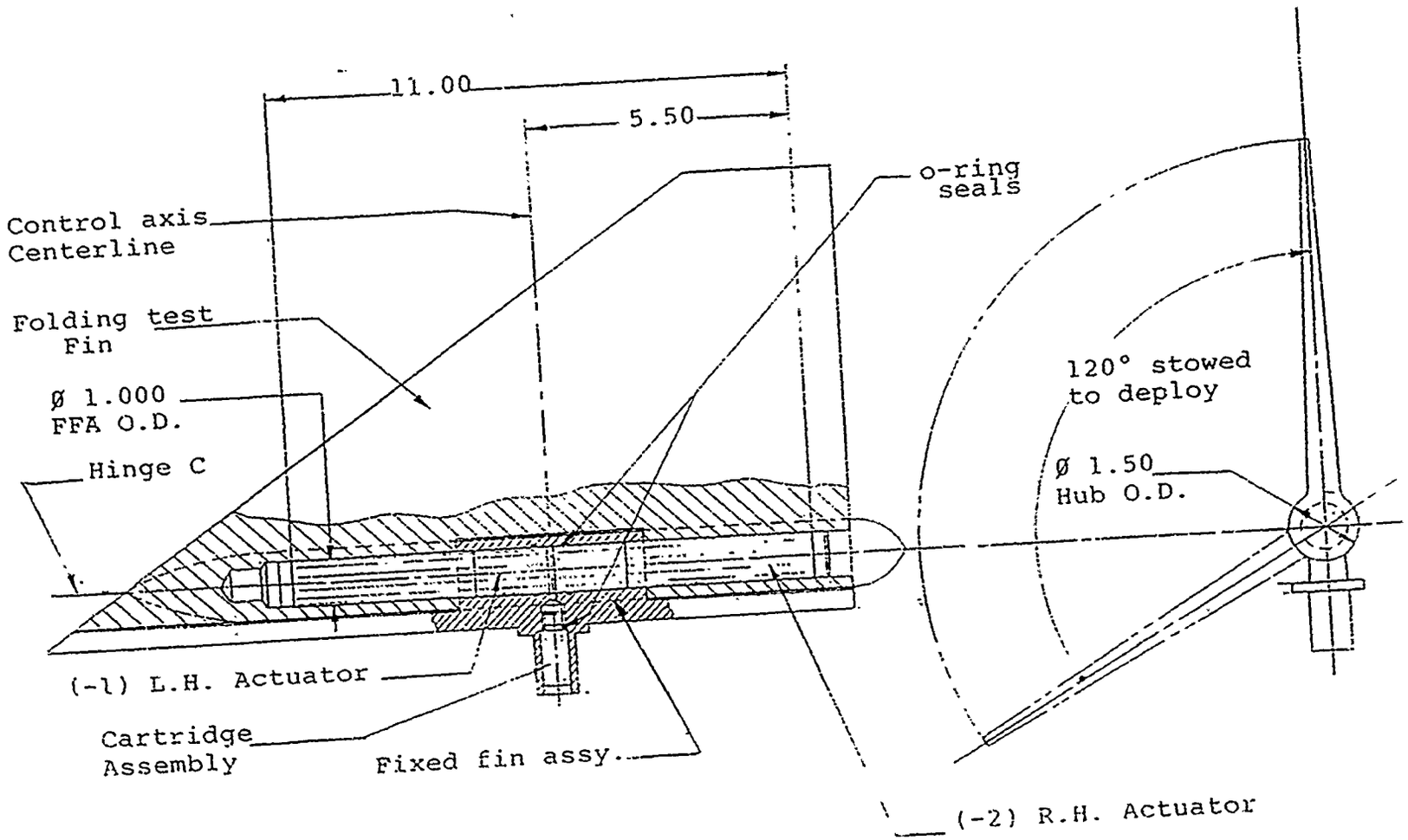

Figure 1 Folding Fin Actuator Installed

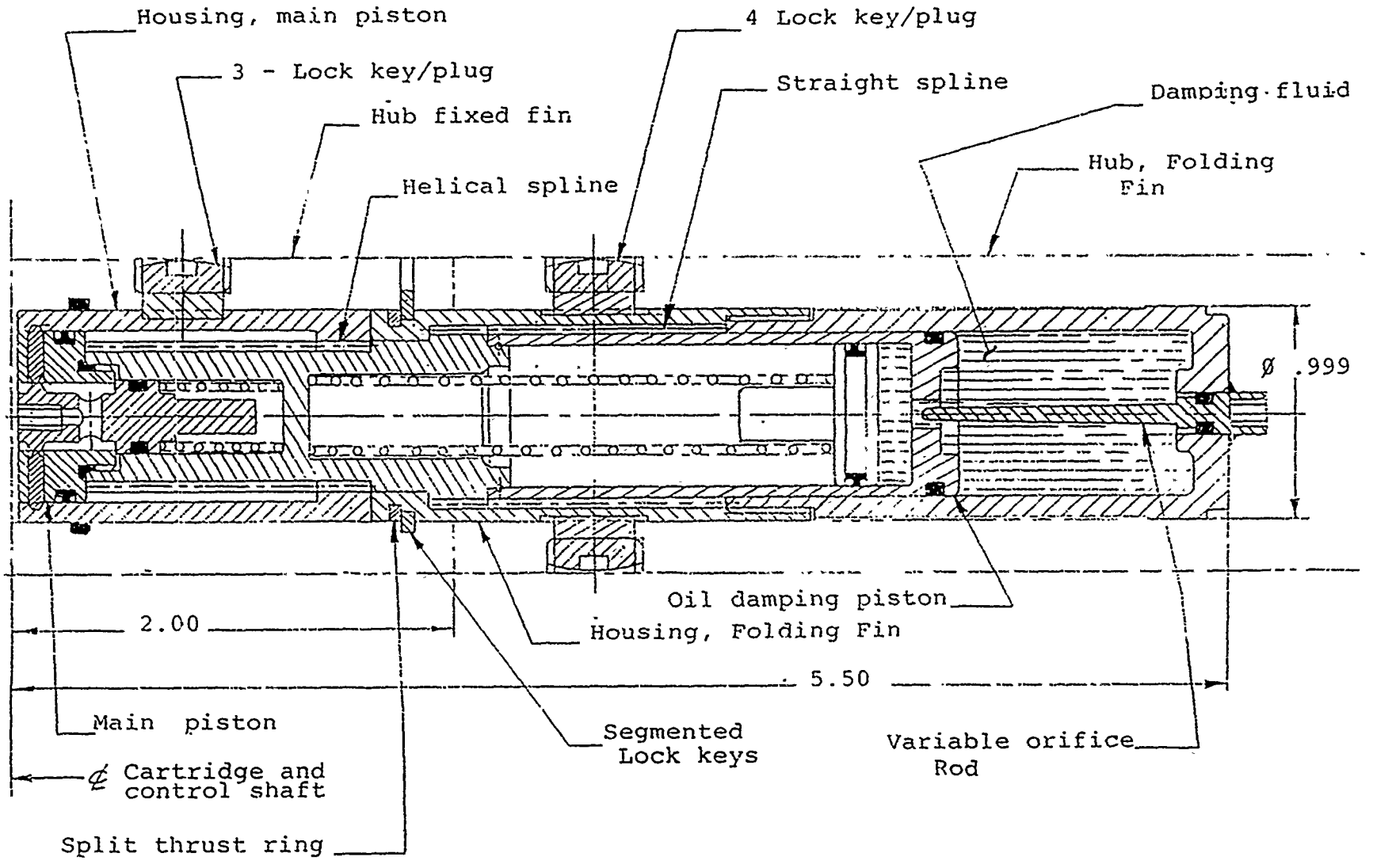

Figure 2 (-2) R.H. Actuator, FFA

with three lock keys per actuator. The (-1) and (-2) actuators of the FFA transmit torque to the folding fin hubs through four lock keys per actuator.

Major design features of the FFA include:

(1) Eight (8) tooth helical spline drive, with 35° helix angle and 0.250 inch long driver, is incorporated in each actuator to support the airload torque during actuation. The mating helical splines are accurately manufactured by broaching, grinding and final lapping to provide smooth mating surfaces with maximum bearing area. This results in minimum bearing stress and allows use of dry film lubricant coating of all mating spline surfaces. The sliding coefficient of friction is thereby minimized and the FFA mechanical efficiency is maximized.

(2) Dual actuator concept results in two (2) 5.50 inch long rotary actuators with all parts common except the L.H. and R.H. helical spline drive and driven components. This reduces the lengths of all major components to a minimum and reduces production fabrication costs. In addition to providing convenient propellant gas porting for the ballistic cartridge located in the fin control shaft, the output torque to the fin is equally distributed to the aft and forward fin hubs by the dual actuators.

(3) Variable orifice area oil damping design provides the best means to reduce the fin final angular velocity to less than 50 rad. per sec. Relative displacement of the cir-

cular orifice over a stationary tapered and stepped diameter rod gradually reduces the orifice area to the required small size at the end of stroke.

(4) Dual o-ring seals, spaced approximately 0.30 inch about the cartridge inlet port, provide a gas seal between the dual rotary actuators and the fixed fin hub bore. Continuous surfaces without spline grooves or slots at the sealing surfaces of FFA and fixed hub bore is necessary for this seal design. Gas porting from the cartridge volume in the control shaft passes through the fixed hub and into the bore between the (-1) and (-2) actuators. In this manner propellant gas acts on the gas piston end of each actuator simultaneously.

(5) During installation, each (-1) and (-2) actuator is inserted into the fin hubs from the aft end of the missile. The lock keys are then assembled through the slots and holes in the hubs and accurately mate with slots or grooves in the FFA housings. This serves to fasten the fixed fin hub to the gas end side of each actuator and the folding fin hubs to the opposite or output end of each actuator.

(6) Axial thrust from the gas piston and helical spline drive is carried by a split ring thrust bearing. A segmented lockring is assembled into an internal groove in the fixed hub to retain the axial thrust bearing. Dry film lubricant at mating thrust surfaces acts to maximize the mechanical efficiency of the rotary actuator.

(7) Reliable and simple initial and final actuator lock mechanisms for stowed and deployed fin positions, respectively.

(8) Manual actuation incorporated for ground checkout.

(9) Weight is minimized while satisfying structural integrity. (-1) and (-2) actuators, with envelope of 1.00 inch diameter and 11.00 inch total installed length, weigh approximately 1.4 lb. with cartridge assembly.

(10) Stress corrosion potential is minimized by proper material selection.

(11) Operating temperature is -65°F to +200°F.

(12) Reployment Angle is 120°.

(13) Maximum resisting deployment torque is 1400 in.-lb. based on ballistic testing and 2500 in.-lb. based on hydraulic actuation tests.

(14) Final angular velocity of fin is 50 rad./sec.

(15) Friction Time is less than 0.050 sec. by ballistic tests.

(16) Initial lock design torque load is $\pm$2500 in.-lb. for four (4) lock keys.

(17) Final lock design torque is $\pm$6000 in.-lb. for four (4) lock pins contained in fin hubs.

(18) Cartridge Major Design Features:

(a) two independent bridgewires with a third bridgewire shunt across both bridgewires for safely shunting of electrostatic potential.

(b) all fire current is 3.5 to 34 amps with 28 VDC within 0.005 sec. at -65°F to +200°F.

(c) no fire current is one amp of DC current for 5 minutes minimum.

(d) no fire power is one watt of DC power for 5 minutes minimum.

(e) bridgewire resistance is 1.1 $\pm$0.2 ohms

(f) insulation resistance is 50 megohm minimum at 500 VDC for 60 sec., all pins to case.

(19) Structural strength minimum margin of safety:

(a) ultimate strength under gas pressure loading. . . . . 1.67 proof
2.50 burst

(b) ultimate strength by all other loading 1.50

(c) limit load strength 1.25

2.1 FFA Installation

Each (-1) L.H. and (-2) R.H. FFA is a self contained unit of 1.000 inch maximum diameter x 5.50 inch maximum length as shown in Fig. 2. For installation, each L.H. and R.H. actuator is assembled into the fin hubs with access from the aft end after assembly of two (2) o-ring seals. The housings at the main piston end are keyed to the fixed fin hub with three (3) lock keys to carry axial and torque loads. Each key engages shallow slots in the outside diameter of the FFA housing and is retained with a threaded plug. The output housing of the FFA is joined to the folding fin hub with four (4) lock keys. Shallow slots in the outer diameter of the FFA housing mate with the keys and only transmit torque loads. A close fit of all keys is provided to

reduce lash to a minimum. A segmented lockring is then assembled to retain the axial thrust bearing which consists of a polished and dry film lubricated split washer. EC2216 adhesive/sealant is used to seal all threaded plugs and slots in the fin hubs.

The stowed position of the fin is retained by the initial lock mechanism which consists of:

- 4 - rectangular shaped lock keys which are contained in slots in the main gas piston and engage an internal groove in the main piston housing.
- 1 - initial lock piston retains 4 lock keys in engaged position.
- 1 - compression spring which retains lock piston in locked position.

2.2 FFA Operation

During ballistic operation, the cartridge in the control shaft is initiated and propellant gas flows into the center of the fixed hub bore and acts on the main piston and lock piston of each (-1) and (-2) FFA. The lock piston is displaced and the four (4) lock keys are cammed out of engagement with the housing releasing the main piston. A subassembly of the main piston, helical spline drive sleeve and oil damping piston then stroke 1.05 inch while rotating. An eight (8) tooth helical spline, integral with the sleeve, mates with 0.250 inch length of spline integral with the main piston housing which is attached to the fixed hub. In addition, an eight (8) tooth straight spline at the forward end of the sleeve mates with an internal spline contained in the output housing.

During the main piston stroke of 1.05 inch, the main

piston housing remains stationary and the output housing rotates 120°. The oil damping system for each rotary actuator consists of:

1 - oil damping rod which is profiled to vary the orifice flow area during 1.05 inch displacement of the main piston.

1 - oil damping orifice contained in the oil damping piston which is displaced with the main gas piston.

1 - oil reservoir to contain the oil damping fluid without voids over the operating temperature range.

1 - oil reservoir piston to displace when damping fluid expands and contracts.

1 - oil reservoir spring to retain piston in contact with the damping fluid.

AR - DC 200 damping fluid.

During FFA operation the oil damping force is transmitted to the main gas piston and helical drive spline from the oil reservoir housing. After full stroke the deployed position of the fin is retained by the final lock mechanism contained in the fixed hub and folding fin hub. Four (4) spring loaded pins are contained and sealed in the fixed hub prior to fin deployment. At the completion of fin deployment the spring loaded pins engage four holes in the folding fin hub to retain the locked position of the deployed fin. The lock pins are designed to support $\pm$6000 in.-lb. of aerodynamic hinge moment.

2.3 Development Testing

Development testing included:

(a) Hydraulic input tests to evaluate functional operation of rotary actuator to determine mechanical efficiency during full stroke deployment of 120°. This testing included application of resisting load torque by the test fixture and then applying hydraulic pressure at

the cartridge port to complete 120° fin angular displacement.

(b) Hot gas testing using a ballistic cartridge and application of resisting load torque with the test fixture.

A schematic of the FFA test fixture is shown in Fig. 3. An air cylinder provides the input energy to a cylindrical cam with dual cam follower slides located at 180°. The camshaft of the cylindrical cam is connected to a torque arm at 4.00 inch radius from the cylindrical cam axis of rotation. The 7.8 inch long torque arm swings through 120° angle at 4.0 in. radius as it applies load directly to the center of pressure of the test fin. A small hydraulic cylinder on the end of the torque arm bears against the test fin and is used to measure the tangential force applied to the test fin. Two different cylindrical cams, one for resisting load and one for assisting load, are used to reproduce the maximum aerodynamic loads at the fin. During resisting load tests the test fin acts to rotate the torque arm and cylindrical cam against a resisting load generated by the air cylinder and cylindrical cam. This acts to retract the cam follower slide and air cylinder piston into the air cylinder, compressing the air in the cylinder.

During assisting load tests the gas cylinder force is transmitted through the dual cam follower slides to the cylincrical cam. This serves to drive the cam and rotate the torque arm against the test fin. Air cylinder displacement during resisting load tests is approximately 2.50 inch and assisting load tests is approximately 5.20 inch. This is necessary to maintain

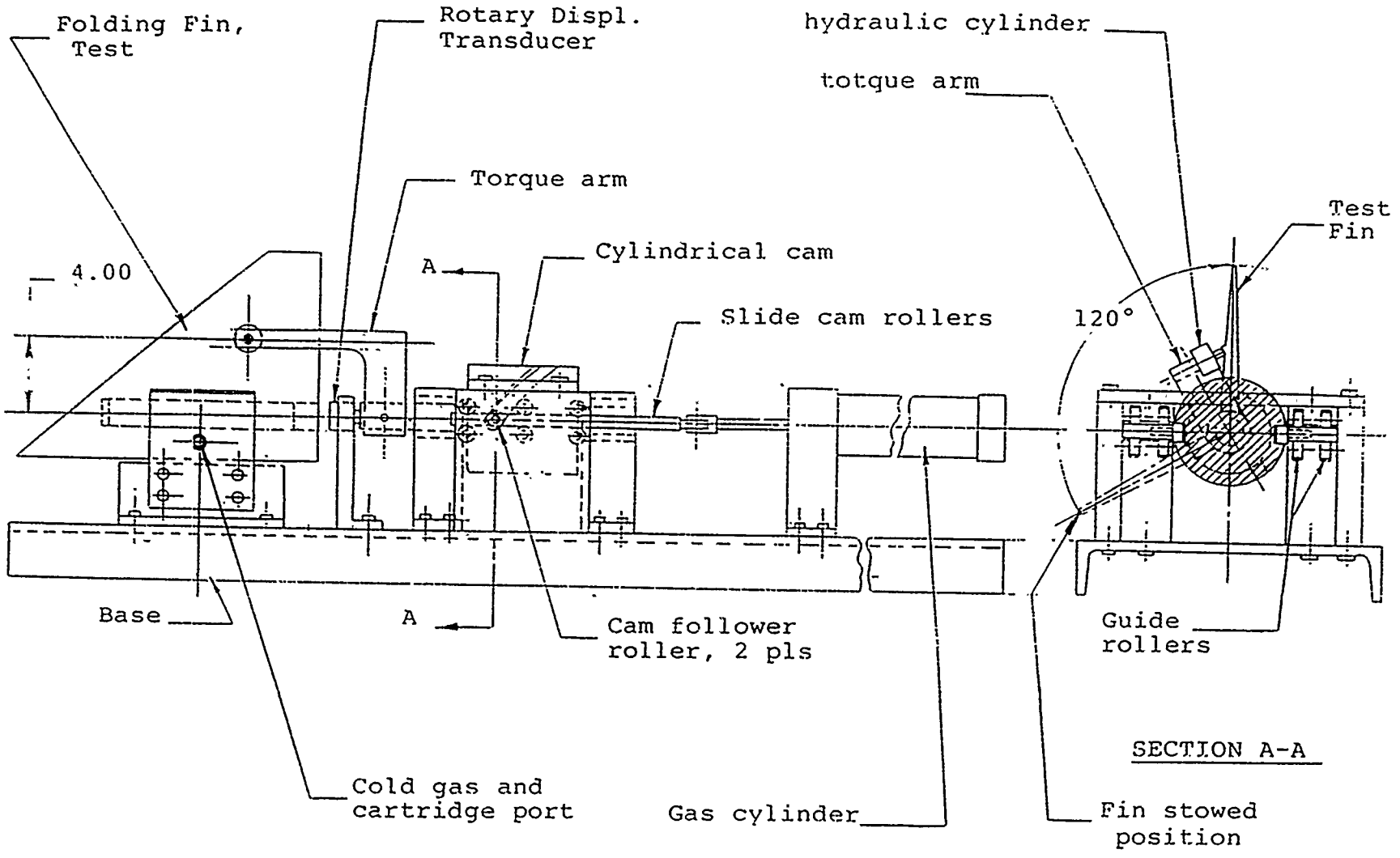

Figure 3 FFA Test Fixture Schematic

a maximum cam track to cam follower pressure angle less than 40°.

The mass moment of inertia of the test fixture fin, torque arm, cylindrical cam, slide and air cylinder piston are minimized and accurately calculated for ballistic/mechanical FFA computer analysis.

The digital simulation code results for performance at -65°F and +200°F for full resisting and assisting load of 2850 in.-lb., to satisfy stroke time of 0.050 sec. max. is shown below.

operating pressure	2950 to 15,000 psig
stopping velocity	32 to 50 rad./sec.
operating time	0.031 to 0.050 sec.
oil pressure	6500 to 15,700 psig
gas piston area	0.516 $in.^2$
oil piston area	0.428 $in.^2$
piston stroke	1.05 in.
propellant charge	2.15 gm., 7 perf. 0.16 in. web.

Based on test results to date and computer design analysis the approximate design data shown in Table 1 was prepared for FFA output torque as a function of design envelope.

Table 1 FFA Output Torque Versus Envelope

FFA Envelope		Maximum Constant	Fin Rotation
Diameter inch	Length inch	Resisting Torque in.-lb.	Deg.
1.000	11.0	1400	120
1.000	13.0	1500	120
1.200	14.0	2400	125
1.500	15.0	3500	90
1.750	16.0	4500	120

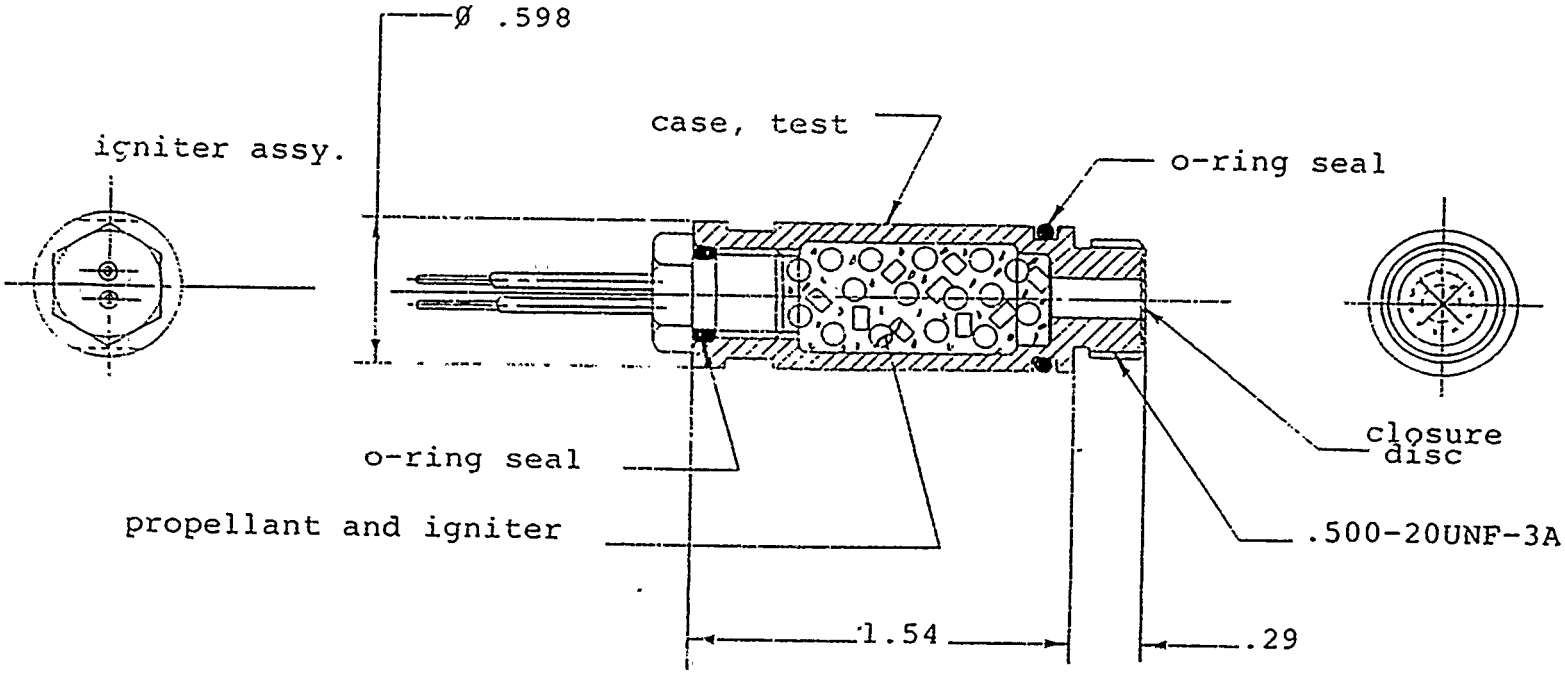

Figure 4 Cartridge Assembly, Test

Specified assisting torque load, stroke time and maximum end of stroke angular velocity will have an effect on these design values. The interior ballistic analysis with airload torque and FFA mechanical design parameters provide an accurate means to predict performance over temperature range of -65°F to +200°F.

The two extreme operating conditions for the FFA based on fin airload torque and temperature include:

(A) Maximum resisting load torque at -65°F temperature conditioning. FFA must complete full 120° fin deployment within maximum specified time. A large resisting airload torque near the end of FFA stroke dictates the extent of peak ballistic gas pressure required during operation. This is a result of adiabatic expansion of the gas from the peak pressure near the beginning of stroke in addition to gas pressure reduction from heat loss during stroke. A propellant grain with a progressive burning area provides an increased gas generation rate during FFA stroke. This acts to decrease the reduction in gas pressure and therefore minimize the peak gas pressure.

(B) Maximum assisting load torque at hot or +200°F temperature conditioning. FFA end of stroke angular velocity must not exceed the maximum specified value. The maximum energy dissipation by oil damping takes place during assisting load conditions.

The energy output of the ballistic cartridge must be a maximum under condition (A) above which includes opposing forces from airload, fluid damping forces, inertia forces from test fin and fixture and friction in FFA. This condition dictates the energy output design of the cartridge including the selection of propellant design.

The maximum energy input to the FFA occurs which condition (B) in which the ballistic cartridge energy and the assisting load energy combine to overcome forces from oil damping, inertia of fin and test fixture and friction in FFA, test

fin and test fixture. This results in the minimum stroke time and the maximum end of stroke fin angular velocity. This condition controls the oil damping orifice area design which is varied by profile modifications of the oil damping rod.

The FFA length has an important effect on FFA performance from the standpoint of helix angle of the spline drive. As the FFA length is increased the gas piston stroke is increased and the spline drive helix angle is reduced. This reduces the fin airload transfer through the spline drive to the gas and oil damping pistons. In addition, a reduced helix angle with respect to the main gas piston axis reduces both the operating gas pressure and oil damping pressure.

AUTOBIOGRAPHY

Earl K. Takata, B.S.M.E. and M.S.M.E.

With 30 years of experience, major successful projects in ordnance devices, high speed automatic machinery, special test equipment and machine design include:

AT AMF/MRD - Hydraulic Deceleration Tower, Precision Weighing System, Fin Deployment Mechanism and Indexing Drive Unit for Rocket Launcher.

AT OEA - Seat Retraction Thruster for B70 Bomber; Primary Initiator and seven shaped charge assemblies for F-111 Escape Module; and Primary Initiator, G-Altitude Initiator and Front Spoiler Thruster for B-1 Bomber.

AT SCOT - ASAT/F15 Missile Ejector; Modified MAU-12 Ejector for CSRL; Barostatic Mechanism, Parachute Release; Mode Selector for B-1 Bomber; Thruster Assembly for Trident D-2 Missile and FTSO for SRAM II Missile.

Earl K. Takata

Mr. Takata has more than 20 years varied experience in research and development of which more than 15 of the past years have been devoted to ordnance items. He has successfully designed the new missile ejector for the ASAT/F15 Aircraft interface and an unique modified MAU-12 Ejector for the CSRL Program. He was project engineer on the development of a rocket catapult system for personnel ejection from aircraft. In conjunction with this work, he has personally completed many of the design features of the system in addition to supervising the loading, preparation of propellant and test firing. Mr. Takata has extensive experience in the application of explosives to flexible linear shaped charge (FLSC) and mild detonating cord (MDC) systems including the development and qualification of five complete FLSC severance systems for the F-111 crew module and including the development of new tooling and manufacturing methods required for latest high temperature explosives. Mr. Takata earned a B.S. and M.S. from Illinois Institute of Technology.

Creating A Technical Information Base

For the Mass and Physical Properties of Stores

Michael J. Martell
3246 Test Wing
Eglin AFB, FL

Robert Dumoulin
Orlando Technology Inc.
Shalimar, Florida

CLEARED FOR PUBLIC RELEASE

1.0 ABSTRACT

Data engineering concepts with hardware and software technologies were applied to improve the utility of store mass and physical properties used in the aircraft/store compatibility field. User's data needs and short-falls of the pre-existing paper system have brought about requirements for a Store Technical And Mass Properties (STAMP) database. Discussed are how STAMP data elements were selected and then defined through the production of a data dictionary. Also shown are how hardware and software considerations indicated in the system requirements analysis were evaluated concurrently to produce a system design for the multi-purpose store database. A primary conclusion is that users must become more involved in defining the hardware, software and information standards to insure operability.

2.0 INTRODUCTION

The store compatibility process is designed to identify physical and functional store limitations which may inhibit pilot and aircraft safety prior to and during flight. Flight simulation tests which require access to consistently accurate Store Technical And Mass Properties (STAMP) data are performed. A brief list of these data fields are:

- Three axis center of gravity (c.g.) locations (both full and empty, if applicable)
- Three axis moment of inertia values (both full and empty, if applicable)
- Store length, width and height (restrictive definitions apply to the terms "length", "width" and "height")
- Weight (both full and empty, if applicable)
- Weapon nomenclature, model, and common name
- Suspension location
- Physical properties such as fuze type, submunition type, and fin type

A complete list of all STAMP data fields and definitions can be found in the Appendix A. STAMP data is used in almost all elements of compatibility engineering from loading stores on aircraft, through analysis of forces acting upon the store during flight, to safe escape of the aircraft after store employment. Safe carriage and employment limits vary directly with the mass properties of the store. Carriage speeds proven safe for one set of mass properties may result in catastrophic failure with an apparently minor change in mass properties. The following compatibility engineering analyses depend on accurate mass and physical property information:

Fit and Function analyses are performed before a store is ever loaded on an aircraft. These analyses use dimensional data and fin measurements to insure no spatial conflicts exist between the store and aircraft. Conflicts with landing gear doors or control surfaces and ground clearance available during emergency landing conditions such as landing with flat tires can usually be identified without actually mounting the store, although a physical loadout is accomplished before first flight.

Store and aircraft loads analyses use store inertia, center of gravity location, weight, suspension mounting location, and suspension spacing measurements in analyzing the forces experienced through aircraft maneuvers. These computations result in store carriage and employment load limits.

Flutter analyses determine undesirable flight conditions where the center of gravity and weight of the store combined with the elasticity and aerodynamics of the wing result in resonance. Flutter is a potentially destructive phenomenon which must be avoided by establishment of safe velocity and altitude placards.

Stability and control analyses utilize store weight, center of gravity, and inertia to evaluate the potential for an aircraft to depart from stable flight. Excessive roll rates can result in lack of adequate control effectiveness to assure recovery.

Ballistic analyses use store weight, center of gravity, and fins/fuze information in weapon delivery calculations to determine release altitude and dive angle envelopes.

Separations analyses use store weight, moments of inertia, center of gravity, and suspension location to establish safe separation characteristics. Improper ejection force input relative to the center of gravity can result in the store striking the aircraft because of adverse pitch conditions.

2.1 Purpose

Prior to 1968 information on the mass properties of stores were collected using paper forms. This was supplemented with information in a variety of formats from Government and commercial sources. After 1968 an AF Form 694 improved the recording of information by describing, in detail, the measured item. This reduced the chance that the data was incorrectly assigned to the wrong store. The AF Form 694's were collected in binders by category until 1988 when the data was entered into computer format which became STAMP. During the process of converting the bound paper products into a computer data base, the following limitations were uncovered:

1. Stores nomenclature was not standardized. A host of published technical orders, manuals, and manufacturer's data were either assigned different names for the same store or many stores had the same name. This is a common problem in database design and implementation ([1]).
2. Terminology was not standardized. The previous paper products were not supported with documentation to explain the individual blocks on the form. This led to an open format. As an example, the center of gravity measurement was not standardized and required extensive research to select a proper convention. There are currently three major reference points for c.g. measurement used by the store community (see Figure 1).

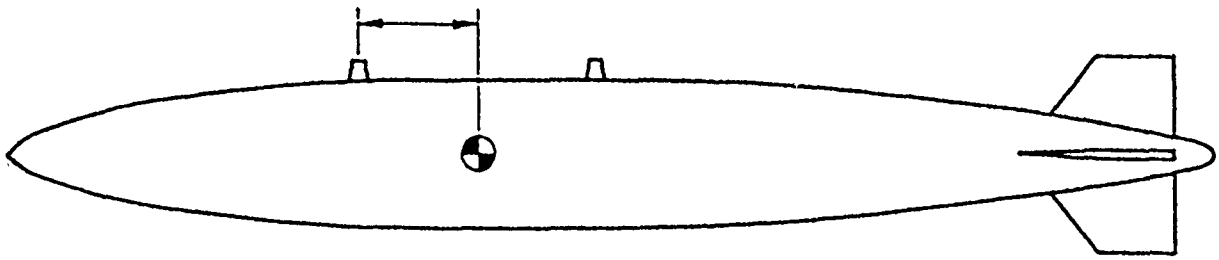

CONVENTIONAL WEAPON
AFT OF FWD ATTACHMENT POINT CENTERLINE

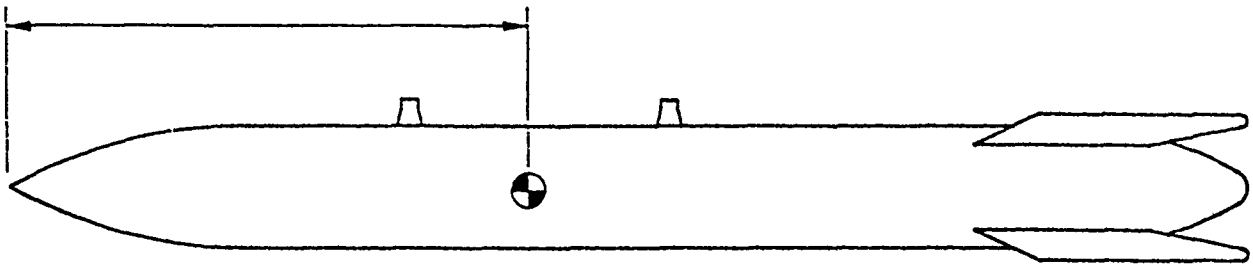

NUCLEAR WEAPON
AFT OF NOSE

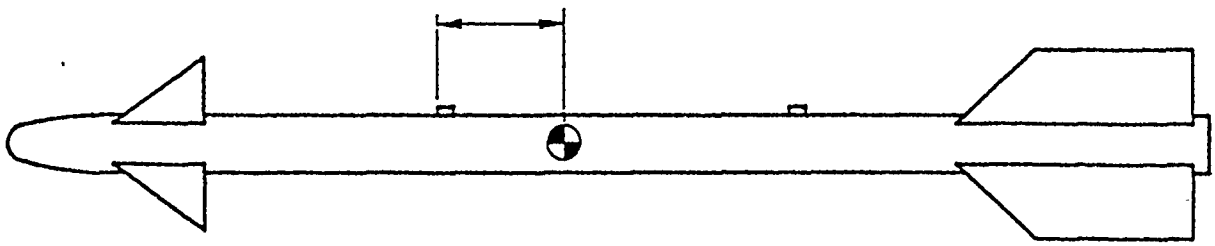

MISSILE
AFT OF FWD ATTACHMENT POINT
LEADING EDGE

Figure 1. Center of Gravity Reference Points

Conventional Munitions C.G. has been referenced from nose, tail, warhead fuse interface, and many other locations. C.G. measured from the center of the forward attachment point has been the most logical for three reasons:

1. The distance is usually smaller than other reference points offering less opportunity for error in measurement.
2. The forward attachment point is most often used for resolving moments during captive carriage on the aircraft. Generally, an MAU-12 hook will center the lug force with swaybraces accounting for the remaining forces.
3. Nose and tail reference points are subjected to fit and manufacture variations.

Nuclear Weapons C.G. is measured from the nose of the weapon.

Missiles C.G. is measured from the leading edge of the forward hanger. Some other examples of non-standardizations are:

1. Fin span (open or closed).
2. Convention of c.g. in the X direction is positive when measured from aft of the reference point. C.G. in the Y direction (viewed from aft) is positive when right of center- line. C.G. in Z direction is considered positive when measured up from the centerline of the store.

These conventions assume attachment hardware is on top of store. In all cases, documentation for standardization issues were non-existing or confusing.

3. Data Credibility Because terminology was not standardized, there was no basis to insure credibility. The sources of data used different reference points and measurement techniques. MIL-HDBK 244 [(3)] assigns a tolerance of ±.5 inches for c.g. and ±10% for inertias. The ±.5 inches is not based on practical measurement because a 2900-pound guided bomb and a 200-pound missile are required to have a ±.5 inch tolerance for c.g. location. Therefore, the credibility problem was a major concern. Why computerize "bad" data?

3.0 STAMP ORGANIZATION AND DESIGN

Users were asked to determine their needs. Those needs (data elements) were requested in a prioritized list. The lists were combined, and the final list was reduced by eliminating data elements which were out of scope, of low priority, or least requested. These remaining data elements (fields) were used in an information systems planning approach ([2]) to determine what functions the database needed to perform. Data elements were combined with cross-reference index fields to form over 30 data fields of STAMP information.

The sources for data were reviewed and found to be poor. Information was lacking or could not easily be verified. When information could be located, the source was often difficult to match with a unique store name. As previously mentioned, the store nomenclature system is not standardized. This led to development of information credibility categories. Data credibility started as levels 1, 2, and 3; however, the word labels of Historical, Calculated, and Measured, respectively, were adopted for ease of use. Definitions of the three credibility levels are:

. Historical - (least confidence) Information could not be verified.

. Calculated - (average confidence) Documented proof or source identified and reliable. However, information could not be linked to a reliable measurement system.

. Measured - (greatest confidence) Item was properly identified and measured by a DoD organization, and this measurement was confirmed by signature of a measurement technician.

All source information was reviewed by a committee of users (engineers and analysts) who compared the data acquired against established guidelines.

A data evaluation guide was created to provide the first documentation of standards and definitions for data. Each data field was explained in detail and reviewed by personnel who required the original information and would become the users. The data evaluation guide became the source for mass and physical properties terminology. In data engineering concepts, this became the data dictionary or meta data for STAMP. By nature, relational data design and computer logic dictated a standardized format. This helped the creation of STAMP by educating the users in understanding the data. The original source for STAMP was a collection of seven binders with approximately 800 different store types. To assist in finding a specific store, categories and subcategories were chosen. Categories are an aid for human selection of a store. A computerized database only required the exact name to retrieve a record of information. Since 800 exact names are difficult to memorize and a family of stores are often considered, a list of 34 categories/sub-categories was created. This also allowed in most cases, a full subcategory on a single terminal screen. There are many sources for store categories; MIL HDBK 244 describes 25 categories, and these 25 were expanded into 34 to accommodate the 800 +

stores. Consideration was given to an equal distribution of the stores between categories if possible. The definition of each category was explained in detail and added to the data evaluation guide.

The organization, content, and utility of the database is driven by the users. User input resulted in changes to many preconceived design criteria. In addition, the capabilities of the software and hardware were shared with the users to evaluate tradeoffs in requested functionality with system capabilities. An example is the concept of the user wanting more than one basic element in a data field (i.e., length + weight; 87-1500 for 87 inches and 1500 pounds). For utility purposes, separation of fields allows more flexibility by allowing searches by weight or length and will reduce edit error.

3.1 Hardware and Software Considerations

Once STAMP data elements were defined, a system requirements analysis was performed to determine what functions the STAMP database needed to perform. During this phase, users were asked to prioritize their use of the STAMP data fields in performing their particular jobs. This survey resulted in the identification of three unique data display subsets: one for program managers, one for engineers, and one for ballistic analysts. An additional format was also added which contained all STAMP data fields available. The requirements analysis also resulted in the following list of immediate and long-range capability requirements. The ideal STAMP database would have:

- Graphics form printing capability
- Multi-user access
- Transportability across a wide variety of computers
- Multi-level password protection
- Connectability to various distributed databases on multiple computers
- Capability of storing large amounts of data

. Maintainability
. A menu and/or mouse-driven user-interface
. Connectability with artificial intelligence packages
. Compatibility with existing programs
. Flexibility to allow for changing requirements and data elements.
. Ad-hoc query capability

Hardware and software specifications were determined from capabilities defined in the system requirements analysis. These specifications can be categorized into three groups: hardware and operating system; database management system; and compatibility with other software. These three system requirement groups are inter-dependent and cannot be evaluated separately. For this reason, the discussion of each group includes references to the other groups.

Hardware requirements focused on insuring that the operational platform was compatible with the selected DBMS software and possessed adequate speed to support the host database. System peripherals such as graphics terminals, disk space, and laser printers are system enhancements which may be added to most all systems and were not considered an immediate concern. Existing hardware in use at the computing facility of Eglin (SC) was considered a cost-effective alternative to purchasing a specialized system. Available systems included several DEC VAX models, a CDC CYBER 7600, and many personal computers which could also be used as smart or dumb terminals. The end-product needed to be multi-user, but initial database population could be performed on a personal computer if the chosen DBMS would allow data to be transported.

At the time, another database was already using a table containing store nomenclature, model, and symbol information on a Zenith Z-248 (80286) personal computer connected to a DEC LN03+ laser printer. The host DBMS for this database and store table was ORACLE, which is a mature

relational database management system (RDBMS) providing useful utilities and continued product support. The store table became the main table of the STAMP database. The single-user limitation of the PC was acceptable in the interim because ORACLE was scheduled to be installed on an SC VAX 11780 and ORACLE data is easily transported across supported host platforms. Data accessibility and security requirements were also met through ORACLE's relational architecture and multi-level password protection. The relational structure, along with ORACLE tools, allows multiple databases, distributed or local, to share common data through index key fields without data redundancy.

The utility of STAMP data can be measured not only by data credibility but also by data accessibility. The STAMP database was envisioned as being a store data source for several other engineering databases needing access to store information. Other uses included direct terminal access of data by engineers and access to customized computer programs needing store information.

Creating an acceptable and transportable user-interface compatible on the operating platforms supported by ORACLE was not a trivial task. Differences in display terminal control codes and mouse support software were major obstacles for compatibility across different systems. To satisfy the initial database population requirement, custom edit, view, and print programs were developed on a PC. The programs interfaced with the database via the ORACLE PRO utility which allows Structured Query Language (SQL) commands to be embedded in high level language programs. These programs were not mouse-driven, but were menu oriented, supported color, and were very keyboard friendly. PRO* utilities currently exist for FORTRAN, Pascal, COBOL, PL/I, Ada, and C language programs running either

on a computer hosting the database or a remote computer connected to the host DBMS system through DECNET, TCP/IP, or asynchronous communication protocols. Compatibility with high-level language compilers allows system-specific I/O and analysis programs to be developed, but does not insure a transportable application due to differences in system display terminals.

The VAX version of ORACLE became available shortly after the initial STAMP population was complete. Data was easily transported between systems using the export and import utilities. The chosen solution to supporting the growing number of computer platforms with the same source code was to use the ORACLE utility SQL*FORMS. This forms utility is a Computer-Aided Software Engineering (CASE) tool allowing a functional and transportable database interface created interactively and easily maintained. Even though the customized SQL*FORMS applications were functionally complete, they were not mouse-driven and lacked keyboard friendliness to the casual user. Consequently, the SQL*FORMS applications were not accepted by non-technical data entry support personnel expecting a MacIntosh look and feel. Another option allowing a windowing and pull-down menu system using a recently released portable windows toolkit is currently being researched.

The STAMP database was designed to have a modular structure allowing distributed databases access to STAMP data. Using a static approach to database design [4], global views of several data dictionaries are combined into one query statement making data access across multiple databases transparent to the user. The result of this modular design allows the STAMP database to fulfill its designated purpose as a multi-purpose store technical information authority.

4.0 CONCLUSIONS

This paper presented the experiences involved in the creation of a technical information database. We utilized data engineering concepts in the integration of hardware and software to meet the needs of users. From our efforts, we conclude the following:

a. Data standardization methods must be developed and accepted by the users.

b. Data credibility must be a concern in a technical information database.

c. A data dictionary should be maintained and users must insure that they are involved in its creation and use.

d. User involvement must be maintained throughout development to react to constantly changing user needs.

e. Users do not adapt to the structure of a database. This problem must be solved by involving the users in defining data field types and lengths. Also all internal database indexes MUST be removed from the user's sight.

f. Where possible, equipment should be standardized for ease of software integration.

References

1. Integrating Relational Databases With Support For Updates, "M. Sammy Gramal - Eldin, Gomer Thomas", Ramey Elmasri Data Engineering Symposium, 1988 IEEE

2. An Introduction To Information Engineering, "Clive Finkelstein Information Engineering Systems Corporation".

3. MIL-HDBK - 244

4. International Symposium On Databases In Parallel And Distributed Systems - A Logic Multidatabase System, "Thomas Ludwig, eva Kuhn", IEEE Computer Society Press

APPENDIX A

STAMP Data Fields and Definitions

GENERAL

This guide is divided into two sections: Section 1 describes the various blocks and information contained in the attached PMD STAMP Book, and Section I defines the store categories as currently established. These categories will be reviewed by 3246 TESTW/SK for deletion, revision or acceptance.

PURPOSE

The information in this guide is provided to help standardize the interpretation/classification of data and assist data managers in understanding terminology used in the attached PMD STAMP Book. The book contains information currently available on the PMD list of stores shown in attachment 1.

Stores for which no data exists have been omitted and will be included as data becomes available. Each block on the forms presented in the PMD STAMP Book is defined below:

1. Date of Last Revision - The date when the store was initially put into the database or the date when mass properties were last changed.

2. Nomenclature - The officially designated name for an item (Bomb, Guided, Modular GBU-15(V)6/B, or LAUNCHER, GUIDED MISSILE, AIRCRAFT LAU-117/A). For the purposes of the SEDB, stores will be identified by their abbreviated name in the nomenclature block until all stores have been assigned official nomenclature, i.e., GBU-15(V)6/B or GBU-24.

3. Model - The numbers and/or letters which uniquely identify a variant

of the official nomenclature. If no model is identified, the letters "N/A" will not be used in this field to avoid confusion.

4. Common Name - The commonly used name typically identifying a series of stores (Sparrow, Sidewinder, Gator, etc.) Common names are included to assist users in identification of families of stores.

5. Description - Used to describe the intended use of the store (e.g., "Antiradiation Vehicle" for an AGM-136A)

6. Stamp Store Number - A four-digit number assigned to each store/model as a unique identifier. These numbers can be obtained from the SEDB manager and should be considered an interim step until a universal standard store identification can be instituted.

7. Stamp Category/subcategory - One of the numbers or letters used to organize stores into families with similar characteristics, i.e., Cluster, Missile, etc. This list is pending final review and approval by SK.

8. Store Status - The tentative plan is to use this block to identify whether the store is in inventory, production, experimental, etc..., however, this block will be TBD until a final decision is made.

9. Reference Document/Drawing - Identifies government or contractor drawing numbers or documentation which can be used for engineering data. May include some detail drawings but typically a general arrangement view to define length, diameter, electrical connector locations, lug position, etc.

10. Data Credibility - An indication of the accuracy or uncertainty of the physical characteristics for each store. The following levels of credibility are subject to change following SEEK EAGLE review:

Level 1 - Exists as historical data and is termed historical.

Level 2 - Nominal mass properties as identified in manufacturers' specifications and is termed calculated.

Level 3 - Measured data averaged for N samples and is termed measured.

11. Length (inches) - Overall length from extreme fore and aft points to include fuzes and fins (see Figure A).

12. Location of FWD Suspension Point Centerline - Definition of the longitudinal forward mounting lug position so that a c.g. location referenced to the centerline of the forward lug will have physical meaning (see Figure A).

13. Diameter/Height/or Lug Axis (inches) - The maximum diameter for a store of circular cross section or the height of a non-circular cross section in relation to the lugs. This figure refers to the body of the store only and does not include the fin (see Figure B).

14. Width or Cross Lug Axis (if applicable - inches) - The width of the lateral cross section in concert with 13, above. This field will show N/A if the store has a circular cross section (see Figure B).

15. Office of Primary Responsibility - This block will not be included initially since insufficient data exists to identify sources; however, inclusion of this block is planned when sufficient data becomes available

to provide those offices/individuals identified in the Data Accession List responsible for updates or corrections to the PMD list.

16. Suspension Spacing - Distance between lugs (or notation that a unique suspension arrangement is being used as is common for missiles, etc.), typically 14 inches or 30 inches (see Figure A, for lug spacing).

17. Functions - Text block used to identify events in the store's employment profile such as fin opening, skin cutting charge initiation, altitude of submunition dispersal, etc.

18. Fin Number/Nomenclature - Official name or number to uniquely identify the fin group attached to the store.

19. Fin Span (inches) - Measure of the maximum fin width (i.e., Tip-to-Tip through the centerline, not between tips of two adjacent fins - see Figure A).

20. Fin Angle from Lugs - Used to define the orientation of the fin relative to the body of the store.

21. Fuze Number/Nomenclature - Official name or number which uniquely identifies the fuze to be used.

22. Submunitions - Nomenclature for the submunitions used in a dispenser or cluster-type munition.

23. Weight Full - Measured or projected weight for the store as an all up round (go-to-war configuration).

24. Weight Empty - Store weight without submunitions or fill (chaff and flare dispensers, fuel tanks, CBUs, etc.)

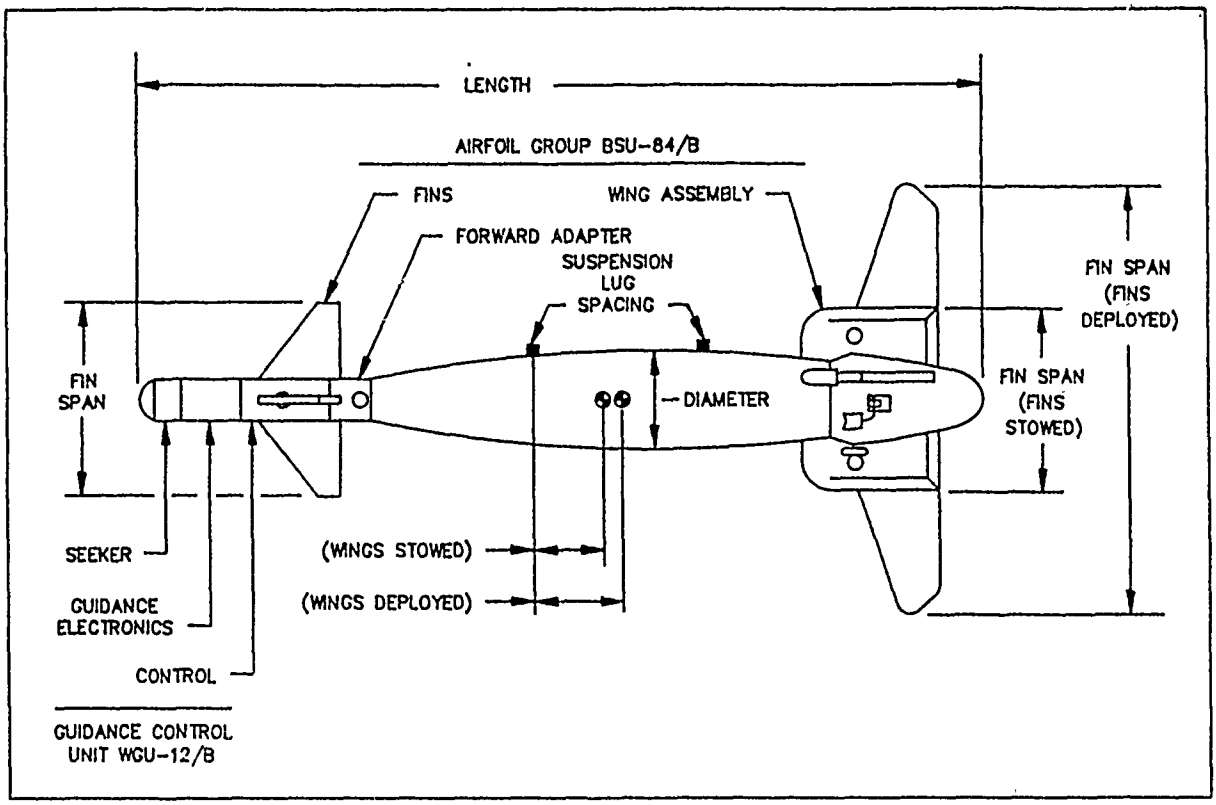

Figure A. Dimensions

25. X Axis Center of Gravity (inches) - X is defined as the longitudinal axis of the store. For the majority of stores, the c.g. location is referenced to the forward mounting lug. For stores with relocatable lugs or other unique attachment mechanisms, the c.g. will be referenced to the store nose in nuclear weapons and to the forward edge of the forward hanger for missiles (see Figure B).

26. Y Axis Center of Gravity (inches) - The lateral location of the center of gravity referenced to the geometric centerline of the store (see Figure B).

27. Z Axis Center of Gravity (inches) - The vertical location of the center of gravity referenced to the geometric centerline of the store (see Figure B).

28. Roll Inertia (Slug*Ft^2) - Mass moment of inertia about the roll ax referenced to the store center of gravity (see Figure B).

29. Pitch Inertia (Slug*Ft^2) - Mass moment of inertia about the pitch axis referenced to the store center of gravity (see Figure B).

30. Yaw Inertia (Slug*Ft^2) - Mass moment of inertia about the yaw axis referenced to the store center of gravity (see Figure B).

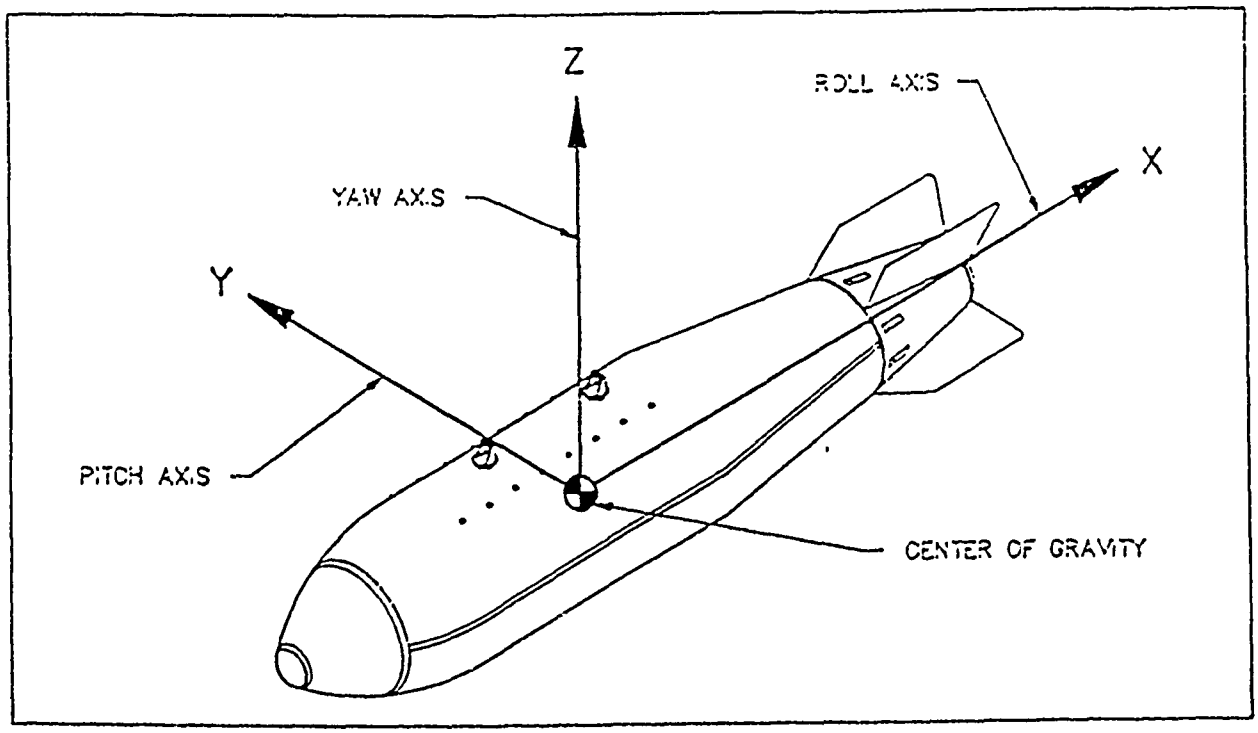

Figure B. Moments of Inertia

31. Tolerances - Set up as three text fields so that acceptable parameter variations can be identified (e.g., c.g. +/- 1/2 inch, WT +/- 5%, INERTIA +/-10%), as outlined in MIL-HDBK-244.

32. Remarks - General comments about the store which do not fit into any previously defined data field. Also used to provide additional information about parameters which require further definition or unique characteristics.

Biography

Michael J. Martell has an Associate of Applied Science in Electronic Engineering Technology and Aircraft Electronic Systems. He has worked on the Universal Store Loads Program for the AGM-130 and AIM-9P weapons systems. Prior to the aircraft/store compatibility work, he spent 9 years in the metrology fields of optics, temperature, force, vibration radiation, time and electrical measurement. His current work is in database design and data element definition for store mass property and technical information bases.

Robert L. Dumoulin has a Bachelor of Science degree in Computer Science and with a minor in Mathematics from Florida State University. He has 6 years experience in systems and applications programming on IBM, DG, CDC, SUN, DEC, mainframe, mini, and personal computers. Language experience includes Fortran, C, Pascal, ADA, Cobol, Basic, CICS, ORACLE SQL, JCL, CCL, XVT, along with DG, IBM, and CDC assembler. Robert has particular experience in database development to include micro and mainframe file transfer, graphical user interfaces and hard copy form production from relational data bases, development of user guides, and code documentation to reduce the man-print in database systems.

THIS PAGE INTENTIONALLY LEFT BLANK

FLIGHT TEST CERTIFICATION OF A 480 GALLON COMPOSITE FUEL TANK ON CF-18

by
Captain Mario B.J. Lagrange
Aerospace Engineering Test Establishment
Canadian Forces Base Cold Lake
Medley, Alberta, T0A 2M0, Canada

ABSTRACT

The Aerospace Engineering Test Establishment (AETE), as the Canadian Forces (CF) flight test authority, has recently completed flight tests and analysis of a major store certification program to establish an operational flight envelope for the carriage and jettison of a newly designed 480 gallon external fuel tank (EFT) for the CF-18 aircraft. The certification process involved a progressive series of analysis, wind tunnel tests, qualification tests, ground tests and flight tests activities. Most of the pre-flight activities were performed by the designer, McDonnell Aircraft Company (McAir), while all flight testing was the responsibility of AETE with engineering support from McAir. The progression of events from the qualification testing to the final flight testing recommendations are summarized herein. The primary focus of this paper is on the flying activities such as flutter, loads, stability and control, separation/jettison and performance. Special instrumentation, flight test techniques and test concept philosophy are also discussed. This paper highlights various technical problems encountered, such as the near flutter onset condition observed with tanks 50 percent full, the premature failure of the inboard wing spar pylon receptacle discovered after the last manoeuvring loads flight and the localized pitch-up phenomena observed during stab. , and control S&C testing. A glance at the increased range and payload capabilities is also included. Overall, the 480 gallon EFT was determined to be a viable option for the CF-18 aircraft.

INTRODUCTION

1. Background. To increase the war stock of external fuel tanks for the CF-18 aircraft, the Government of Canada established a follow-on fuel tank acquisition program. The options considered were either buying more of the currently used 330 US gallon EFTs or supporting the development of a new composite material 480 US gallon EFT designed by McAir. The decision was made to subsidize the testing of the composite 480 EFT on the CF-18 aircraft. This option was selected because of the technological benefits which could be accrued ' ' transferring filament wound composite technology to Canadian industry and for the potential of prov: increased range performance and payload capacity. Hence, AETE was tasked by the National Defence Hea Quarters (NDHQ) to support McAir and Canadian industry in the flight test certification of the 480 gallon EFT on the CF-18 aircraft.

2. Objectives. The 480 gallon EFT certification program was divided into two distinct phases. Phase I consisted of conducting a proof of concept demonstration so that a war time clearance could be issued for the carriage of the 480 gallon EFT on the CF-18 aircraft. This category I flight testing was conducted in concert with the designer, McAir, who was responsible for the qualification tests, pre-flight analyses, proposed test matrix, and post-flight data analyses. This phase included flight activities such as flutter, carriage and stores ejection loads, S&C, tank separation/jettison (Sep/Jett), performance and limited electromagnetic interference/compatibility (EMI/EMC) ground tests. In addition, a Royal Australian Air Force (RAAF) requirement to certify the 480 gallon EFT for carriage on the centreline station was originally incorporated into this test program. However, the

withdrawal of the RAAF from the joint venture resulted in the cancellation of any further centreline carriage effort. Phase II testing, currently under planning, will establish a full clearance envelope for the employment of various weapons in the presence of the 480 gallon EFT. This category II testing will involved engineering support from Canadair Incorporated.

3. Test Item Description. The 480 gallon EFT is a lightweight, survivable structure fabricated from two graphite filament wound shells with a foam filled honeycomb core between them. Glass cloth laminate core inserts are used to provide frames for attaching a graphite strongback box, three large access doors and all the required aircraft interface hardware. The tank does not contain baffles, and has been optimized for low manufacturing cost and ease of maintenance. Figure 1 depicts the physical characteristics of the 480 gallon EFT and compares them with the 330 gallon EFT. The extended length of the 480 gallon EFT does not permit to jettison the tank with the trailing edge flaps (TEF) fully deflected without collision between the tank and the TEF. Also, the centreline carriage requires a five inches extension/adapter (figure 2) between the 480 gallon EFTs and the aircraft to allow for landing gear extension without interference. The adapter is fastened to the tank through extended suspension lugs and remains with the tank during a jettison. The production 480 gallon EFT are fitted with a more reliable modular fuel valve assembly and, as a result of shortcomings identified during this test program, a low pass filter and a metal based wrap layer for better EMI protection.

PRE-FLIGHT TEST ACTIVITIES

4. Store Clearance Process. AETE was assigned the overall responsibility of recommending a clearance envelope for the 480 gallon EFT on the CF-18 aircraft to the NDHQ store clearance office. McAir was also contracted by NDHQ for engineering support to AETE. Thus, the store clearance plan used for this test program was very similar to that used for the F-15 and F/A-18 full scale development programs. The plan consisted of a logical progression of qualification tests, laboratory tests, engineering analysis, ground tests and flight tests. A block diagram of the 480 gallon EFT store clearance process is shown in figure 3. As the primary contractor, McAir carried out, under NDHQ contract, several engineering analyses and laboratory. Throughout the early phases of this process, the CF, including AETE personnel, continuously reviewed McAir progression to ensure that the CF vested interests in the program were met. AETE active participation in this store clearance process started with a EMI/EMC safety of flight test (SOFT). All flight test activities were carried out at Cold Lake using AETE's instrumented CF-18 and personnel. The flight test matrices were recommended by McAir and approved by AETE. The test team consisted of an AETE Project Officer (PO) who was essentially the team leader, AETE test pilots and several engineers from McAir and AETE. McAir was responsible for all data analysis which was subsequently reviewed by AETE's engineers. Again, the decision to proceed to the next test point was made by an AETE test controller (often the PO himself) based on concurrent recommendations from McAir and AETE engineers. The procedure used in this test program was safe, efficient and worked well either in the Flight Test Control Room (FTCR) or in the briefing room preparing for the following mission. AETE is most likely to use a similar procedure for the Category II flight trials.

5. Qualification Tests. A series of laboratory tests were carried out by the supplier, Brunswick Corporation of Lincoln, Nebraska, to ensure that the 480 gallon EFT met the procurement specifications established by McAir The qualification test program consisted of several tests including maintainability, lightning, slosh & vibration, ejection, fragment impact, flame engulfment, environmental and explosion containment. The qualification tests identified several shortcomings with the 480 gallon EFT. The most significant was the inability of the tank to withstand a lightning strike without internal arcing. The original tank design resulted in internal arcs on five different locations within the tank. Fixing this shortcoming would have required several months and, to remain

within the planned test program schedule, it was decided then to complete the flight testing using tanks that were not shielded for lightning and EMI protection. A flight test restriction not to fly through precipitation static conditions was imposed for all sorties. Also an EMI Safety of Flight Test (SOFT) was required prior to start flight testing. In this case, the flexibility given to the program office and the early involvement of the flight test agency, AETE, allowed to reach a compromise which helped expedite the completion of this certification program.

6. Similarly, delays in the design and production of the modular fuel valve assembly required the initial flight testing to be carried out with the existing 330 gallon EFT fuel valve system instead. The flight test certification of the modular fuel valve assembly was the subject of a separate test program which identified only one problem area involving the valve manual precheck assembly which will be rectified in the production 480 gallon EFT.

7. Wind Tunnel Tests. A series of wind tunnel tests were conducted by McAir, under NDHQ contract, to gather aerodynamic coefficients and derivatives required for the subsequent engineering analysis. The wind tunnel tests were grouped into five different sessions using various facilities. The Calspan eight foot wind tunnel was used to obtain S&C data as well as transonic performance data on a six percent scale model. The McAir Low Speed Wind Tunnel (LSWT) provided S&C characteristics for low speed and power approach with and without flap configuration using a 12 percent scale model. The same McAir LSWT was used to gather flutter data using a 17.5 percent scale flutter model. Trials conducted on a six percent scale model in the McAir Polysonic Wind Tunnel in 1984 provided the necessary information to derive the aerodynamic loads predictions. Last but not least, the Naval Ship Research and Development Center (NSRDC) wind tunnel was used to investigate the Separation and Jettison (Sep/Jett) characteristics of the 480 gallon EFT and of various other stores in the presence of the tank. The data obtained during these wind tunnel tests were used in various engineering analyses to determine the most critical configurations for flight testing and to establish the initial flight test envelopes. A list of flight test configurations is reproduced in figure 4.

8. Ground Fit and Function Test. Several ground tests were required prior to the start of the flight test program. The ground fit and function test, carried out on a production aircraft off the McAir assembly line in ST-Louis, showed that the 480 gallon EFT was compatible with the CF-18 and successful fuel transfer was demonstrated. This test also revealed that clearances from the centreline 480 gallon EFT to the nose wheel hold back bar and to the launch bar actuator were less than minimum distances specified in MIL-STD-1289A (Reference 1). Similarly, ground clearance for the centreline 480 gallon EFT was only 2.8 inches with soft tires and deserviced struts. This is less than the minimum requirements listed in reference 1. Because these deviations were only observed with either deserviced struts or the nose wheel rotated 30 degrees, and because no physical contact was observed, it was agreed to proceed with the test program as is. Again, AETE participation in this ground fit and function test helped in reaching a quick compromise with the contractor, McAir.

9. Ground Vibration Tests. Four different ground vibration tests (GVTs) were carried out in support of this certification program. The cantilevered pylon GVT, the full aircraft GVT and the structural mode interaction (SMI) GVT were performed at McAir, with CF participation, using a production aircraft. A rigging check GVT was carried out at AETE, with McAir involvement, for each configuration to be flutter tested, using the test aircraft. The cantilevered pylon GVT was performed to determine the liquid fuel correction factors as a function of the tank fuel level. The test set up consisted of a 480 gallon EFT loaded on a CF-18 wing pylon attached to a rigid test fixture. Five fuel levels were tested from empty to full. A dynamic model of the 480 gallon EFT and wing pylon was developed based on the correction factors. This model was then used to help identify three critical configurations to be tested in the full aircraft GVT. Subsequently, this dynamic model was modified to improve its correlation with the full aircraft GVT results. This refined model was then used for all flutter prediction analysis.

10. As previously mentioned, three configurations were tested during the full aircraft GVT (Figure 4). The aircraft, a production single-seat CF-18, was supported by soft jacks designed to dynamically uncouple the aircraft from the ground which allowed the measurement of aircraft rigid body modes at frequencies less than two Hz. The tests were performed with the landing gear retracted, canopy closed and all access panel secured. Selecting the "RIG" mode on the flight control system (FCS) ensured that all control surfaces were in the neutral position. The pylons and stores were rigged to minimize freeplay such that maximum mechanical energy was transmitted through all interfaces. The dynamic symmetry of the store rigging was verified by comparing the store resonant frequencies on both sides of the aircraft during dwell excitation. Where required, adjustments were made to obtain acceptable dynamic symmetry. Symmetric and antisymmetric frequency response surveys were conducted to obtain transfer function plots using a sine sweep excitation at constant force provided by two electrodynamic exciters. Modal frequencies were obtained from these plots while damping coefficients were derived using the log-decrement method on single mode decay time histories. The mode shapes were then mapped using the multi-mode sinusoidal excitation technique.

11. The vibration data obtained from this test were used to verify the McAir analytical aircraft/480 gallon EFT dynamic model used to perform flutter analysis. The GVT data also served as a baseline for comparison with vibration mode frequencies and damping coefficients measured during flutter flight testing. Overall, the frequency and mode shape results showed good correlation between the analysis, the full aircraft GVT and the rigging check GVT. Figure 5 tabulates the results for one of the configuration tested.

12. The Structural Mode Interaction (SMI) GVT check was required to verify that low frequency tank modes do not couple with the aircraft FCS to produce an unacceptable dynamic response. The two configurations tested are also depicted in figure 4. These tests were performed during the full aircraft GVT using exciters attached at the stick position and the FCS feedback accelerometer package. The tests consisted of a series of sinusoidal sweeps through the tank mode frequency ranges using maximum force lateral excitation on the tanks, followed by a dwell at the antisymmetric roll frequency. The SMI was investigated with the control stick in each of the four stick position quadrants and for all flap deflections. The results of this GVT showed no instabilities, sustained oscillations, or unacceptable dynamic response of the FCS.

13. Prior to commence flutter testing, a rigging check GVT was carried out on the two most critical flutter configurations to ensure proper installation of stores on the test aircraft. Freeplay was minimized to achieve dynamic similarity on both side of the test aircraft. Although the test procedure was similar to that used for the full aircraft GVT, this rigging check GVT was performed with the landing gear extended using the soft tire suspension technique. Transfer function plots were gathered at selected locations on the test aircraft. The modes of interest were partially mapped by manually recording response amplitude and phase relative to a reference location on the structure. The results correlate relatively well with the modal frequencies obtained during the full aircraft GVT (Figure 5). One discrepancy was found during one rigging check GVT which identified an antisymmetric mode at 7.46 Hz. This mode, which resembled to wing first antisymmetric bending mode but with reverse relative phasing between tank pitch and fuselage lateral motion, was not found by the analysis nor during the full aircraft GVT. This phenomena was believed to be the result of modal interferences of the aircraft structure elastic modes with the soft tire suspension system.

14. Electromagnetic Compatibility Ground Tests. The electromagnetic compatibility (EMC) of the 480 gallon EFT with the CF-18 avionic/electrical systems was partially evaluated through several contractor ground tests. Owing to the lack of EMC control plan, AETE was required to conduct an extensive analysis of potential electromagnetic interference (EMI) and EMC concerns based on contractor lightning and fuel probe radio frequency (RF) susceptibility test results. With composite walls, RF radiation is capable of passing through the

480 gallon EFT with more ease than a conventional metal tank. Such radiations could be coupled to the internal aircraft electrical/avionic system degrading their performance. Also, a potential exists for ignition of fuel vapour by RF radiation. Static charge build-up, because of friction, can occur from fuel flowing within the tank plumbing, from fuel sloshing within the tank, or from flying through moisture or dust (precipitation static). Static build-up may also affects the aircraft electric/avionic as well as ignite fuel vapour. This analysis categorized the EMI problems as either flight or mission critical. Those which were flight critical were addressed and ground tested, if proper resources were available at AETE, prior to flight testing. The EMI/EMC tests carried out at AETE prior to flight testing included a thorough inspection for design specification compliance; measurement of bonding, limited conducted emissions, and static potential build-ups; and CF-18 critical system victim functional checks with limited potential source interference for a Safety of Flight Test (SOFT). Several observations were made that indicated deficiencies with the tank design were made throughout the EMI/EMC ground testing. However, none of these were severe enough to halt flight testing with the 480 gallon EFT. As a precautionary measure, a restriction not to fly through visible moisture or any precipitation static potential environment was imposed on the pre-production 480 gallon EFT until a conductive coating/wrapping is applied to the tank. Similarly, flight in high electromagnetic environment areas was not recommended for the 480 gallon EFT without fuel probe line EMI protection (low pass filter).

FLIGHT TESTING

15. This section of the paper will provide the reader with an overview of the aircraft instrumentation and AETE installations used in support of this certification program. Then each flight test activities such as flutter, manoeuvring loads, store ejection dynamic loads, stability and control, separation/jettison and performance will be discussed.

16. Aircraft Instrumentation. Both AETE's instrumented CF-18 aircraft, used throughout this certification program, have identical data acquisition system capable of selecting data from the avionics multiplex (mux) buses and from various other sources. The current system provides a 64 channel analogue data acquisition capability. Data from the analogue signal conditioners along with selected data from direct analogue and digital inputs, mux buses, time code generator and the Flutter Exciter Control Unit (FECU) are encoded into a pulse code modulation (PCM) format and stored on the onboard MARS-2000 tape recorder. Pilot voice and selected direct analogue signal can also be recorded on dedicated FM channels. All PCM data are telemetered to the Flight Test Control Room (FTCR) for real time monitoring. Wing strain gauges were also installed during production assembly as part of the basic instrumentation package. These gauges, located at three different spanwise locations, are sensitive to either bending or torsion and allow identification of the wing overall motion during flutter testing. The additional instrumentation required for specific flight activities are discussed later in each of the flight test sub-sections.

17. For reasons of flight safety, the FTCR was used for most flight test missions. This facility permits real-time monitoring of selected parameters from the telemetered PCM data. Several monitoring devices are available, from simple strip chart recorders to large television screens, which can be use to display either raw telemetered data or near real-time processed data in engineering units. The FTCR is also equipped with a flutter analysis workstation comprising a fast Fourier analyser for near real-time spectral analysis, four lissajous scopes, and a display for monitoring the test aircraft FECU parameters. The FTCR set-up can be adapted to the user requirements The communication system in the FTCR provides each operator with capability to transmit/receive through UHF radio. During this test program, while everyone could receive pilot transmission, only the test controller (an AETE personnel) and in an abort situation, the lead engineer (normally a McAir personnel) were

allowed to transmit to the test aircraft. Later in the test program, a hot mike capability was installed in one of the test aircraft which allowed all intercom within the test vehicle to be telemetered to the FTCR. This feature enhanced the safety of flight and reduced pilot workload.

18. All test sorties were flown over Cold Lake Air Weapons Range (CLAWR) which also includes the AETE's Primerose Lake Evaluation Range (PLER). PLER is located on the southern boundary of CLAWR and approx 25 miles north of the airfield. This range is exclusively used by AETE for test and evaluation purpose. PLER facilities used in support to this test program included telemetry rebroadcast and tracking radars for all sorties while phototheodolites and meteorological data were required only for the Sep/Jett trials.

19. Structural Mode Interaction (SMI) Testing. SMI testing consisted of two high speeds taxi runs and several flight test points integrated within the flutter flight testing test matrix. Since configuration 1 (Figure 4) was identified as the most critical SMI configuration, it was decided to fly this configuration first during the flutter flight testing. The first taxi run was carried out on a smooth runway while the second run used a rougher runway in an attempt to induce structural mode coupling with the FCS. Both tests were performed with full 480 gallon EFTs and half flap selected. During these taxi runs the control stick was firmly held in the aft right and forward left quadrants for about 10 seconds to see if an oscillation build-up would result. The SMI flight testing consisted of exciting the aircraft structure with lateral and longitudinal stick raps while monitoring the aircraft FCS response. This exercise was performed at various flight regime including take-off and climb-out. The SMI taxi and flight testing confirmed the expectation, based on previous flight test experience with similar store configuration, that no FCS coupling with aircraft vibration modes will occur for the CF-18 while carrying the 480 gallon EFT.

20. Flutter Flight Testing. These tests were carried out to verify that the allowable carriage envelope of the CF-18 configured with 480 gallon EFT is flutter free up to 1.15 times limit speed. The testing consisted on monitoring modal damping trends and frequency coalescence of the different modes involved in the flutter mechanism, previously identified during the pre-flight flutter analysis and supported by the full aircraft GVT results. The left digital display indicator, on test aircraft CF-188907, was replaced by a flutter exciter control unit (FECU), shown in figure 6, which provides aileron displacement signals to the FCS. Three modes of aileron excitation are available through the FECU; sinusoidal sweep (from one frequency to another), dwell (at one frequency for a given time) and random (random noise within a selected frequency band). The FECU has built-in safety features which automatically shut down aileron excitation whenever roll rate or normal acceleration exceed a certain value or whenever the pilot depress the paddle switch. The FECU can hold up to 15 pre-programmed set ups which can be activated at the touch of one button. The FECU control display is also reproduced via telemetry on a monitor in the FTCR.

21. Flutter flight testing consisted of sinusoidal sweeps and single frequency dwells conducted over a range of altitude d airspeeds. The test points were divided into distinct dynamic pressure groups with each group representing a higher dynamic pressure zone. The FECU was the primary mode of inputing in-flight aileron excitation while stick raps had to be used when testing was carried out beyond the normal acceleration limits of the FECU. Functional check of the FECU, including the built-in safety features, was carried out by the pilot on each flight prior to commence flutter testing. Upon clearance from the flight test controller in the FTCR, the pilot proceeded with the mission. Symmetric or antisymmetric excitations were used at different fuel states and aircraft attitudes to excite the mode of interest which was a function of the configuration and the flutter mechanism involved. Sweeps were used to determine resonant frequencies while dwells provided the damping characteristics at and near these frequencies. Engineers in the FTCR constantly monitored key parameters using strip chart recorders and lissajous displays. Review of near real-time transmissibility plots (T-plots) was performed as sine sweeps were completed and review of decay trace was carried out during dwell excitations. The flutter speed was

determined through extrapolation of the flight test data using the Zimmerman flutter margin method and through correlation with the various flutter analyses. When it became too difficult to follow both damping modes with the Zimmerman method, testing continued by tracking only the lesser damped mode. Both McAir and AETE flutter engineers analysed and reviewed the processed data after each flight and test points from the subsequent higher dynamic pressure zone were selected for the next test sortie. The last test points consisted of a series of dives performed at maximum velocities from 30,000 feet to 5,000 mean sea level (MSL) with one second dwell excitations at selected altitudes. This was performed to demonstrated flutter free operations of the configuration tested.

22. The pre-flight flutter analysis predicted that full 480 gallon EFT was the critical tank fuel level for flutter testing regardless of the configuration flown. Flutter testing of configuration 1 confirmed this prediction. The flight test projected flutter antisymmetric flutter speed for configuration 1 correlated well with the analytical prediction, and allowed flight to the full CF-18 tank envelope. The stability of configuration 1 was also verified by low level flight to maximum velocity and demonstration dives out to the allowable flight limits, with acceptable modal damping being exhibited in all cases. However, flutter testing of configuration 2 (Figure 4) showed that half full 480 gallon EFT has the lowest projected flutter speed. A near flutter onset condition was observed during a dwell excitation at maximum velocity and low altitude. Real-time monitoring of wing gauge outputs (Figure 7) indicated a significant reduction in damping resulting in the test point being aborted. Previous testing with full 480 gallon EFT was successfully completed at similar test conditions. The flutter mechanism involved wing first bending and fuselage first lateral bending modes, as predicted by analysis. This lower flight test projected flutter speed will result in a carriage speed restriction for that particular configuration. The demonstration dives for this configuration 2, carried out at various fuel states, were successfully completed to expand the higher altitude envelope out to the specified Mach number. The remaining flutter flight testing proceeded quickly and without incident. The use of aerial refuelling helped expedite the flutter test program specially for the test points involving high drag configurations where a minimum of 5000 lb internal fuel was required.

23. Active Oscillation Control (AOC) testing. When configured with heavy stores on the outboard pylon and wing tip missiles on, the CF-18 encounters a 5.6 Hz limit cycle oscillation (LCO). Unlike flutter, LCO is not divergent in nature but creates unacceptable lateral oscillation levels in the cockpit which affect pilot performance. This phenomena, characterized by wing first bending and torsional motion which couples with the fuselage to produce lateral fuselage bending, is caused by a structural/aerodynamic interaction which excites the antisymmetric outboard store pitch mode. This oscillation is suppressed by the AOC system which is implemented in the CF-18 FCS. The AOC system is automatically activated when the aircraft is flying below 9,000 ft MSL or above 0.82 Mach and for heavy outboard stores configuration with wing tip missile on. The AOC system is essentially a feedback loop integrated into the FCS which senses the forward lateral accelerations, passes the signal through a passive bandpass filter, then through a phase shifter and output to the aileron to suppress the oscillation. The oscillation is aggravated slightly by an inboard fuel tank and since it is not predicted analytically, the certification of a 480 gallon EFT required flight testing to verify that the current AOC system adequately controls the oscillation with the larger fuel tank installed. The configuration used for AOC testing is depicted in figure 4. Flight testing was also conducted with the AOC system deactivated under similar flight regime so that a system effectiveness assessment could be made. A slight modification to the flight control computer wiring was required to disable the AOC system in-flight. The test approach consisted of flying symmetric manoeuvres under increasing normal acceleration and Mach number while simultaneously exciting the structure through lateral stick raps. The pilot seat lateral accelerations were monitored by engineers in the FTCR using strip charts recorders. A soft limit of 0.15 g lateral acceleration was defined as the abort criteria. Simulated weapon delivery manoeuvres using 20 to 35 degree dive angle and maximum velocity were performed to demonstrate the AOC system effectiveness. For most flights the AOC system was effective in reducing the 5.6 Hz LCO to within acceptable

levels (Figure 8). However, relatively high 5.6 Hz oscillation levels remained with half full 480 gallon EFT at high speed and low altitude. Flight restrictions will be required to maintain the oscillation levels within acceptable limits.

24. Manoeuvring Loads Testing. Extensive loads testing was required to demonstrate the safe manoeuvring envelope of the 480 gallon EFT since it is heavier and larger than any other stores flown on the CF-18. The manoeuvring loads testing was divided into two separate parts. The centreline carriage loads testing was carried out on aircraft CF-188701 while the wing carriage loads testing was done using aircraft CF-188907. Each aircraft had different specific instrumentation added to its basic system to support these tests. For flight safety reason centreline loads testing were combined with stability and control (S&C) testing to form a carriage test matrix. This was necessary as some of the loads test points required aircraft attitudes and flight regimes which were considered critical for aircraft departure and similarly some S&C test points were loads critical. Hence, it was common to have loads and S&C test point intermixed in one test card. However, the S&C issues will be reported in a separate section of this paper. The configurations selected for centreline and wing carriage loads testing are depicted in figure 4. The testing consisted of a build-up approach based on both progression in dynamic pressure and criticality of the manoeuvre performed including the amplitude of the control input. Once stabilized at a flight condition, the pilot performed certain manoeuvres known, from previous flight test program, to induce large loading at the pylon/aircraft interface. These included steady state pull-ups, wind-up turns (WUT), steady state push downs, 1 g 360 degree rolls, -1 g 180 degree rolls, rudder kicks, and rolling pull-outs (RPO). After a test point, the data was reviewed by McAir and AETE engineers in the FTCR and the test controller cleared the pilot to the next test point.

25. Centreline Carriage Loads. Aircraft CF-188701 was specially instrumented with an aircraft centre of gravity accelerometer and approximately 30 strain gauges for in-flight strain monitoring at designated critical locations in the centreline pylon, pylon adapter and at the aft attachment fuse. The gauges in the centreline pylon adapter were installed in an attempt to provide real-time measurements of load data through gauge calibrations. This method of measuring centreline loads had the advantage of being quick and allowing for immediate clearance to the next test point. However, the confidence in using this method was relatively low because of the limited instrumentation used in the calibration process. The second method used to obtain centreline loads values was the trajectory analysis. This method uses measured aircraft flight path with previously derived wind tunnel data to compute inertial and aerodynamic forces, and ultimately to calculate the pylon/aircraft interface loads. This technique requires a considerable amount of post-flight data because of the large number of time slice within one manoeuvre. All centreline loads testing was carried out using a three fuel tanks configuration with the centreline fuel quantity ranging from full to empty while the wing tanks remained empty.

26. A total of nine test sorties were required to complete the centreline loads test matrix. The first flight indicated that the centreline adapter strain outputs were only producing 10 percent of their expected values. Owing to time constraints it was then decided to proceed with the testing using the trajectory analysis method to derive the loads data. In the mean time, AETE found that the strain value range supplied by McAir were erroneous by a factor of 10. Corrections were made to the instrumentation gains but these gauges still only provided limited data because they were installed in an area too far away from the main load path. Hence, the trajectory analysis was the only reliable method to obtain centreline loads values.

27. The first two flight were carried out with the centreline tank filled up with 2600 lb of fuel (400 US gallons). Post-flight data analysis revealed that the centreline pylon aft attachment bolt had reached 108 percent its design load limit during a 360 degree, full aileron roll. On the same manoeuvre, the centreline pylon strain gauges, located at a critical fillet radii, was estimated to be over twice the maximum strain value predicted by

McAir pre-flight analysis. Some of the strains recorded were well beyond the yield point of the material. The pylon was removed and inspected using non-destructive techniques (NDT) and no defect was found. However, in view of the inconsistency between the predicted attachment strain values and those measured in flight testing, the centreline loads test matrix was completed with an empty centreline tank. A usable flight envelope was determined using the trajectory analysis method and analytically include fuel to predict attachment loads for a full 480 gallon EFT. It should be pointed out that even with an empty 480 gallon EFT, the centreline pylon strains at the critical fillet radii were near the maximum allowable level predicted by McAir. One of the reasons for poor correlation between predicted and flight test strain values is the lower two-dimensional stress concentration factor used by McAir in their analysis applied to a critical region featuring double curvature (three-dimensional). Also it is quite possible that the centreline loads model is erroneous by itself. Nevertheless, previous flight testing conducted at AETE has revealed that this problem was not unique to the 480 gallon EFT but also applied to the 330 gallon EFT currently used by the CF. A structural loads monitoring program has been established and the impact of these high strains manoeuvre on the fatigue life of the CF-18 is being investigated.

28. Wing Carriage Loads. In support of these trials, test aircraft CF-188907 was configured with two specially instrumented wing pylons. Each pylon were modified with several strain gauges at McAir. These calibrated gauges enabled real-time measurement in the FTCR of load data at the pylon hook, pylon post roll moment, pylon post pre-load, aft attachment vertical and side loads, and aft tie fuse load. Later in the test program, aircraft CF-188907 was also fitted with five strain gauges in the critical radius of the wing pylon receptacle to verify that pylon measured loads were within the maximum permissible strains of the wing pylon receptacle. As per the centreline loads testing, symmetric and asymmetric manoeuvres that were not considered to be departure critical were carried out first while the remaining test points were performed after the S&C flight testing was successfully competed for that configuration/manoeuvre. The wing carriage loads test matrix and manoeuvres performed were similar to that of the centreline testing. Because real time monitoring of the pylon/wing interface loads was available and the confidence level of the instrumentation used was much higher than that of the centreline pylon, a more practical build-up approach was used to expand the 480 gallon EFT wing carriage envelope during flight testing. Upon review of the data by both AETE and McAir engineers in the FTCR, the test controller cleared the pilot to proceed with a more critical test point. Generally, envelope expansion was carried out in build-up increments of 0.5 g for symmetric manoeuvres keeping the entry conditions constant. Asymmetric manoeuvres used similar build-up increments but also performed the manoeuvres using half control inputs first followed by full control inputs. This was continued until either a limit value was exceeded or if the next test point was likely to have overshot any limits.

29. The wing carriage loads testing was uneventful until a premature failure in the port inboard wing pylon receptacle was discover after the test aircraft had safely landed from its last manoeuvring loads mission. This failure was transparent to the engineers manning the FTCR as well as to the test pilot. The crack was discovered during the post-flight routine check as fuel was found leaking from the pylon receptacle area. Since the cracked receptacle (Figure 9) is an integral part of the number three wing spar, the entire inner wing had to be removed and shipped to McAir for repair. A new port inner wing was installed and testing was resumed after a three month delay. Part of this delay was because of the installation of strain gauges on the inboard starboard wing pylon receptacle to monitor and coorelate receptacle strain levels with pylon hook loads. Also the replacement inner wing was a production non-instrumented item which had no provision for installation of test instrumentation. However, the existing instrumentation in the starboard wing was similar to that in the original port wing and, after a re-calibration of the instrumented pylon on the starboard side, testing was resumed using the starboard wing vice the port wing to collect flight test data. A pylon receptacle strain survey was carried out using full 330 gallon EFT Symmetric WUTs and Asymmetric RPOs were performed at various load factor and the receptacle strains were plotted as a function of pylon loads (Figure 10). This survey provided data which permitted to correlate, by extrapolation, pylon loads flight test data from previously flown missions to receptacle strain levels. This exercise

showed that even the maximum pylon hook load values previously recorded was well within the allowable yield strain level of the receptacle and that it should have not failed from the 480 gallon EFT loads alone.

30. McAir conducted and extensive investigation as to the cause of this premature failure (Reference 2). Several failure causes were investigated including stress corrosion cracking, low cycle fatigue and static overstress, although the design loads for the wing spar receptacle had never been exceeded during any parts of this test program. During disassembly of the wing pylon receptacle, the beryllium-copper wear that attach to the lower flange (the sill which the pylon hook bears on) was installed incorrectly. The wear plate are installed correctly when its thin edge is located inboard as shown in figure 11 (the wear plate angle is exaggerated for better visualization). The localized wear surfaces and crack observed on the wear plates is reproduced in figure 12. Further investigation by the CF revealed that other CF-18 aircraft also had incorrectly installed wear plates. Upon further review of historical data by McAir it was discovered that a USN F/A-18 had suffered a port wing failure in virtually the same location as CF-188907. Fractographic inspection of the failure indicated that both failure were identical; however, it could not be ascertained if the wear plate on the USN aircraft was installed incorrectly. The findings of the McAir investigation were that no material discrepancies were found and that there was no evidence of stress corrosion cracking or fatigue. The investigation report conclusion states that the pylon receptacle failure on CF-188907 was owing to static overload and was precipitated by a reversed wear plate. The expected fatigue life of the CF-18 inboard pylon receptacles, with the wear plate installed correctly, was determined to be well beyond the life expectancy of the aircraft.

31. Store Ejection Dynamic Loads. Previous testing and analysis indicated the need for store ejection dynamic loads flight testing because of the load increment caused by the dynamic response of the structure during store ejection. Hence, these tests were carried out to obtain flight test data to establish release load factor limits of selected CF-18 outboard wing pylon stores while retaining 480 gallon EFT on the inboard wing pylon. Although the tests were performed using full 480 gallon EFT, allowable limits were analytically derived for full, partially full and empty 480 gallon EFT. These tests were carried out on CF-188907 after the wing pylon receptacle failure. Therefore, not only pylon hook loads were monitored but also the receptacle strain levels. In addition, accelerometers were installed on the starboard wing tip, wing fold, outboard pylon, and on the nose of the starboard 480 gallon EFT. The FTCR was used to monitor all store ejection dynamic loads sorties with the critical parameters being pylon hook load, pylon aft attachment vertical and side loads, and pylon receptacle strains.

32. The ejection of a store produces a transient response on the aircraft structure and retained stores/pylons which can be separated into steady-state and dynamic components. The steady state component consists of inertia and aerodynamic loads occurring just before the store release. The dynamic component results from the ejector piston force, the sudden weight released from the wing, and the application of the unbalanced airloads as lift exceeds the inertia load immediately after the stores are released. As a result it was necessary to use a build-up approach increasing normal acceleration at release. Two critical configurations (Figure 4) were identified for testing; the release of two MK-84 in salvo and the ripple salvo release of four MK-83 with 200 millisecond release interval. Pre-flight analysis indicated that the release interval was an important factor in the severity of the resulting dynamic loads. The analysis dictated that 200 millisecond was the most critical release interval for that particular MK-83 configuration, even more so than the MK-84 salvo release at the same load factor. All releases were carried out at the same flight conditions except for load factor which was progressively increased based on the results of the previous drop. The store ejection dynamic loads testing was complete quickly without major unserviceabilities. The flight test data showed, as expected, that the pylon hook loads and aft attach vertical loads were the most critical components. The maximum inboard pylon hook loads measured in flight were considerably less than predicted values and contrary to the pre-flight analysis the salvo release of two MK-84 bombs was indeed more severe than the ripple salvo release of four MK-83 bombs with the most critical release interval

setting as shown by figure 13. The inboard pylon vertical aft attach limit loads was exceeded by four percent during the last MK-84 release sortie. This limit was driven by the pylon structure and not the wing interface, both inboard pylons were checked and no irregularities were found. The final normal accelerations recommended for store release in the presence of the 480 gallon EFT are limited by the pylon aft attachment which is definitely not the pylon primary load path. This stresses the importance of harmonized aircraft design in that a secondary structure should not restrict the employment of the primary structure to its full potential.

33. Stability and Control Testing. The larger size and fuel weight of the 480 gallon EFT dictated that the effects of this new tank on CF-18 stability and control (S&C) characteristics be evaluated. As previously mentioned, S&C testing was integrated into the manoeuvring loads tests to form a safe carriage test matrix. The specific objectives of these flight trials were to determine and demonstrate a departure free envelope for the CF-18 loaded with 480 gallon EFT configurations as well as to evaluate CF-18 flying qualities with such configurations. Both CF-188701 and CF-188907 were used for these trials. Special instrumentation included a flight test nose boom with pitot head, total temperature probe, AOA and angle of sideslip vanes. Testing consisted of evaluating the flying qualities and departure resistance of the selected 480 gallon EFT configurations using a build-up approach in a series of standard test manoeuvres. These manoeuvres included level accelerations/decelerations, control doublets, steady heading sideslips, WUT, rudder rolls, lateral stick rolls, coordinated rolls, cross control and several operational mission tasks. All these were performed at various flight regimes and flap/gear configurations. The production aircraft yaw rate tone threshold was used as a soft flight test limit for yaw rate. After review of preliminary flight test results the sideslip angle test limit, initially defined, was slowly increased by 50 percent, using one degree increments, because the original limit was reached with less than full rudder pedal deflection early in the S&C testing.

34. The three empty 480 gallon EFTs S&C configuration (Figure 4) was determined to be the worst case for lateral-directional stability and henceforth was flight tested on both single-seat and dual-seat aircraft. Provision was made to replace the centreline 480 gallon EFT with a 330 gallon EFT if a loads or S&C limit was encountered, since the centreline 480 gallon EFT was a RAAF configuration only. When the RAAF withdraw from this program, all subsequent testing were carried out with a 330 gallon EFT on the centreline. Baseline flights with three 330 gallon EFTs were performed as a benchmark for the qualitative evaluation of aircraft flying qualities with 480 gallon EFT. Because of the reduced directional stability of the dual-seat aircraft, and unavailability of wind tunnel data for the three tank configuration, two flights were flown with only two 480 gallon EFTs on the wing stations as a build-up for departure resistance. All end points of the test matrix were flown with 3000 lb total fuel or less to verify the departure free envelope at the aft CG conditions. The interdiction S&C configuration, which includes three 480 gallon EFTs and four MK-83 bombs (Figure 4), represented the worst case for longitudinal stability at low fuel state (aft CG) and was only tested on the dual-seat CF-188907.

35. The S&C testing was completed without aircraft departures and a departure free envelope for the CF-18 configured with 480 gallon EFT was determined. Overall the flying qualities of the CF-18 configured with 480 gallon EFT was similar to that of comparable 330 gallon EFT configurations. Apparent lateral directional stability was positive on both the single and dual aircraft at all AOA and for all configurations tested. Regions of negative airframe lateral-directional stability were observed in mid to high AOA because of the large adverse yawing moment of the aircraft rolling surfaces. In all occurrences the FCS was successful in turning these instability regions transparent to the pilot. One coordinated input 360 degree roll performed in the high subsonic, mid AOA region resulted in a 30 degrees/second yaw rate build-up. Post-flight data analysis revealed that the very large proverse contribution of the rudder, commanded by the full rudder pedal input, was fundamentally responsible for the overall high level of yawing moment and yaw rate observed. Although the aircraft remained quite controllable throughout this manoeuvre, it was decided nevertheless to include a note in the AOI advising the pilot of these potentially high yaw rate flight regimes and manoeuvres.

36. Pitch response and damping were satisfactory on the single and dual aircraft for all 480 gallon EFT configurations at most flight conditions tested. Pitch response became quite sensitive above 0.8 Mach and high AOA with AOA soft limits often overshot. However, the aircraft never departed and the pilot always regained precise pitch control. Review of the flight test data revealed several regions of negative airframe stability mostly above 20 degrees AOA and high subsonic Mach number. One of the most interesting phenomena observed during this test program was a longitudinal stick reversal experienced by CF-188701 with three 480 gallon EFT during a WUT at 0.8 Mach/35,000 ft. Post-flight data analysis confirmed this negative apparent longitudinal stability (Figure 14). Further review of the data indicated that this pitch up phenomena was partially caused by the quickness of the manoeuvre relative to the large time constant of the filtered AOA to the trailing edge flap (TEF) controller. Review of the TEF position relative to the AOA showed deflections much greater that the scheduled position as the manoeuvre progresses (Figure 15) which significantly increased the nose up pitch moment. The control laws of the CF-18 are based on a commanded load factor system which in theory should provide the precise load factor at all times such that stick reversal should not happened. However, as the aircraft enters the region of airframe instability, the trim stabilator requirement changes from trailing edge up to trailing edge down. This momentary imbalance, aggravated by the previously mentioned TEF lag, results in a pitch-up, although the pilot holds a nearly constant longitudinal stick input. The natural reaction of the pilot is then to introduce forward stick to augment the control laws. McAir is confident that, given enough time and oscillations, the control laws should have eventually seek out the commanded load factor. Although the pilots have found these localized pitch-up phenomena bothersome, they were not considered hazardous. An AOI note advising the pilot about the pitch-up tendency of the CF-18 configured with 480 gallon EFT in certain flight regime will be recommended. Basically the departure free envelope for the CF-18 with 480 gallon EFT is practically identical to that of the CF-18 with 330 gallon EFT.

37. Lift-off speeds using military power and maximum power were recorded for several aircraft configurations throughout this test program. In general, carriage of full 480 gallon EFT resulted in normalized take-off speeds comparable to that of the 330 gallon EFT. A consistent trend depicted in the analysis of the take-off data indicates that the aircraft operating instructions (AOI) are in average 6 knots lower than the normalized flight test data. It is recognized that take off testing intrinsically produce large variances; however, three test pilots were involved in this testing and all were briefed to use 12 degree nose-up stabilator initial trim with full aft stick deflection during take off roll, yet hardly none of the test point recorded had a take-off speed less than that published in the AOI. Further testing to spot check the validity of AOI take-off data will be recommended.

38. Separation/Jettison Testing. The separation/jettison (Sep/Jett) testing were performed to demonstrate safe jettison of the 480 gallon EFT from the CF-18 aircraft and to compare the tank flight separation results with those predicted using the wind tunnel database and McAir six degrees of freedom (SDF) computer code. The pre-flight analysis conducted by McAir identified a total of seven jettison trials for flight testing; five from the wing stations and two from the centreline station. The later was deleted from the Sep/Jett test matrix as a results of the RAAF withdrawal from this program. All Sep/Jett testing was carried out on CF-188701 equipped with a flight test nose boom. In addition, three photosonic 1PL high speed cine cameras were installed on the starboard wing tip missile launcher while a fourth camera was located at the keel position. The tip cameras were calibrated so that their film could be used to provide SDF trajectories through photometric data reduction. Each of the 480 gallon EFT dropped during these trials were prepared with numbered decals to aid in the photometric data reduction. All jettison were done with empty and purged tanks since this was the predicted worst case fuel level. The FTCR was used to monitor the trials.

39. The overall test approach used a build-up procedure increasing Mach and airspeed independently by varying the release altitude and finishing with an end point demonstration. A total of four ejected and one auxiliary release (non-ejected) of 480 gallon EFT were successfully demonstrated during this test program. The auxiliary jettison of an empty 480 gallon EFT from the CF-18 wing station was carried out once good correlation was established between flight test data and McAir's SDF computer program predicted separation trajectories. The last jettison trial was conducted with two MK-83 low drag bombs on a vertical ejector rack (VER) mounted on the outboard wing station adjacent to the jettisoned 480 gallon EFT. To distribute the aerodynamic asymmetry between take-off and landing, an empty 330 gallon EFT was loaded on the port inboard wing station of the test aircraft and retained throughout the flight. All releases were carried out with flaps and landing gear up. At the highest dynamic pressure release, the tank aft end projected several inches above the plane of the wing pylon lower surface. Although this area is used by the TEF when fully deflected, at such high dynamic pressure the TEF are not deflected enough to be in the area of concern. However, the jettison of the 480 gallon EFT with the TEF fully deflected may be hazardous and an AOI warning to that effect is warranted. Overall, the 480 gallon EFT separation photometric data adequately matched the separation trajectories predicted by McAir's SDF computer program with some variations in pitch rate and yawing tendency of the 480 gallon EFT. The larger predicted angular motion may be attributed to the tank deforming under the ejector area thereby absorbing some of the ejection force. But most probably, the variance in angular motion may be from the different magnitude of the full scale aerodynamic characteristics from the predicted values since wind tunnel data was only available up to 35 degree pitch attitude. Nevertheless, the ejected and auxiliary jettison envelopes of the 480 gallon EFT on the CF-18 were successfully demonstrated to the desired limits.

40. Performance Testing. Limited performance testing was conducted to verify the wind tunnel predicted drag indices for various 480 gallon EFT configurations. At a typical cruise condition, the predicted drag increment for the 480 gallon EFT from wind tunnel testing was reported (Reference 3) to be three counts higher for centreline carriage and 13 counts more for two wing carriage than a similar configuration using 330 gallon EFT. All performance sorties were flown on CF-188701 configured with a flight test noseboom. Apart from this flight test noseboom, which had a drag index (DI) of 1.3, the test aircraft was representative of a fleet aircraft. Performance data was gathered during five flights using level accelerated flight and stabilized level flight using the constant weight to pressure ratio (W/δ) technique. Owing to the limited number of flights available and the several configurations to be tested only one weight, 34,000 lbs, and one altitude, 25,000 ft was verified in flight. Because of the lack in the trust measuring devices on AETE's instrumentated aircraft and the non-residency of a CF-18 trust deck at AETE, data reduction was rather archaic. It consisted of extrapolating drag indices from the AOI based on a measured Mach number and calculated fuel flow from fuel quantity variations over a two minute time period. A sensitivity analysis was performed and the flight test derived drag indices were estimated to be within seven counts of the true value at 0.8 Mach.

41. The clean aircraft, configured with only wing tip missiles, was first tested to verify the baseline drag index. The result showed that the baseline aircraft had an average DI of 25. This was approximately 15 drag indices higher than the expected value, accounting for aircraft modifications, fuselage launchers and flight test noseboom. The difference in the DI was attributed to normal inservice degradation of the aircraft performance. Similar results were obtained during a subsequent performance test program carried out to evaluate the CF-18 performance at low altitudes for various configurations including the 480 gallon EFT. Thus, a basic aircraft DI was recommended for insertion in the performance part of the AOI. Contrary to the AOI which considers the DI to be independent of Mach number, the test results showed that the variation of actual DI with Mach will affect some of the range and combat radius predictions from these AOI. However, test data indicates that this assumption may be considered valid for flight regime anywhere between 0.7 and 0.92 Mach. Essentially the flight test data showed that, allowing for the baseline offset and at a typical cruise condition, the actual DI for the 480 gallon EFT configurations closely

.../14

matches the McAir predicted values. The flight test performance results also confirmed the predictions that a CF-18 configured with two 480 gallon EFTs was essentially the same DI as a three 330 gallon EFT configuration. Since these two configurations carry similar amount of fuel, the utilization of two 480 gallon EFTs has the advantage or freeing up one additional weapon station for an increased payload capability. Overall, the limited performance data gathered during this test program have indicated that the carriage of 480 gallon EFT instead of 330 gallon EFT substantially increases the range and endurance of the CF-18 aircraft.

SUMMARY

42. This flight test program was successful in demonstrating safe carriage and jettison of a composite 480 gallon EFT for the CF-18 aircraft. A recommendation will be forwarded to NDHQ so that a certification clearance can be issued. A total of 98 test sorties were flown on CF-188701 and CF-188907 in support of these trials, 34 for flutter, AOC and SMI, 28 for S&C, 18 for manoeuvring loads, six for dynamic loads, five for Sep/Jett, five for performance, and two for wing receptacle strain survey. Except for performance testing, most of these flights required a safety/photo chase aircraft.

43. The minor deficiencies identified throughout this test program on the prototype 480 gallon EFT have been corrected on the production model. The EMI/EMC concerns with this composite material tank were addressed by incorporating an EMI low pass filter on the fuel quantity probe and including a metal based wrapping near the tank surface. Most EMI/EMC testing were repeated with this improved design with the final test currently being carried out at AETE.

44. Data gathered from all analysis, ground and flight tests have indicated that the 480 gallon EFT is a viable option for the CF-18 aircraft. As predicted analytically, no SMI will occur from the carriage of this tank. Minor speed limitations will be required for certain configurations based on the flutter and AOC test results. The higher than predicted strain values from the centreline loads testing may result in additional flight restriction if centreline carriage is reconsidered, but as previously mentioned centreline carriage was not a Canadian driven requirement. The wing inboard pylon receptacle failure will not restrict the wing carriage of the 480 gallon EFT since this failure was attributed to an incorrectly installed wear plate. Based on the dynamic loads flight test results, the wing pylon aft attachment load limits will somewhat restrict the permissible normal acceleration for outboard store releases in the presence of a 480 gallon EFT. Safe separation and jettison of the tank was demonstrated to the desired limits and performance testing has shown that the use of 480 gallon EFT increases the range and capability of the CF-18 aircraft. The follow-on test program, currently under planning, will establish a full clearance for employment of various stores adjacent to the 480 gallon EFT. Overall, this test program provided AETE personnel with valuable experience which will most likely be reflected in future store certification programs.

REFERENCES

[1] MIL-STD-1289A, Military Standard Ground Fit and Compatibility Tests of Airborne Stores, 11 November 1976

[2] McAir Letter M47-330-19537, Results of Canadian Aircraft CFB7 Inboard Pylon Receptacle Failure Investigation, 11 August 1989

[3] McAir Report MDC B0024, Stability and Control / Drag test on a Six-percent Scale F/A-18 Model With External 480 Gallon Fuel Tanks in the Calspan Eight-foot Transonic Wind Tunnel, 15 March 1987

PHYSICAL COMPARISONS EFT'S		
330	VS	480
ALL METAL/SURVIVABLE	WRAPPED	COMPOSITES
188·4/189 IN	LENGTH	215 IN
28·2/28·8 IN	DIAMETER	31·9 IN
220/290 LBS	DRY WEIGHT	310 LBS
330 GALS 2,244 LBS	USABLE FUEL	480 GALS 3,264 LBS

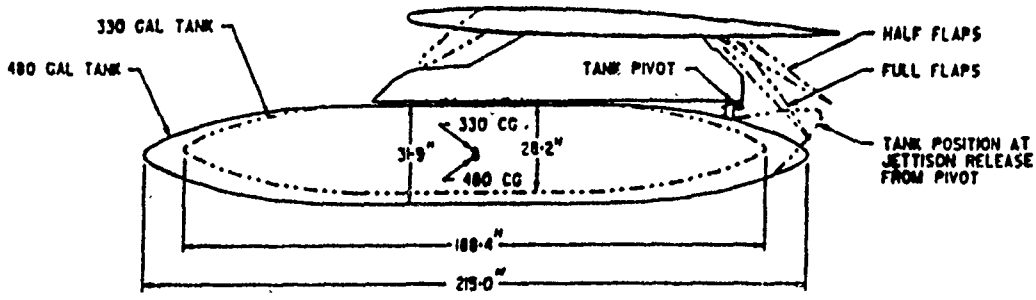

FIGURE 1 – COMPARISON OF EXTERNAL FUEL TANKS PHYSICAL CHARACTERISTICS

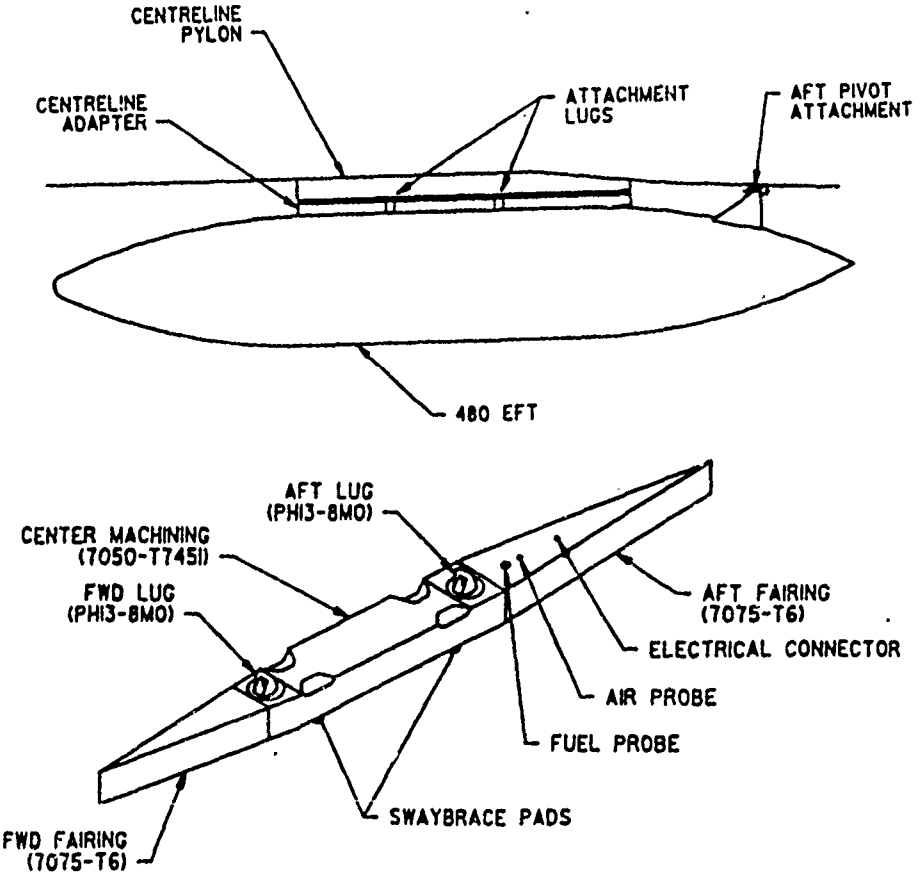

FIGURE 2 – CENTRELINE ADAPTOR FOR 480 GALLON EFT

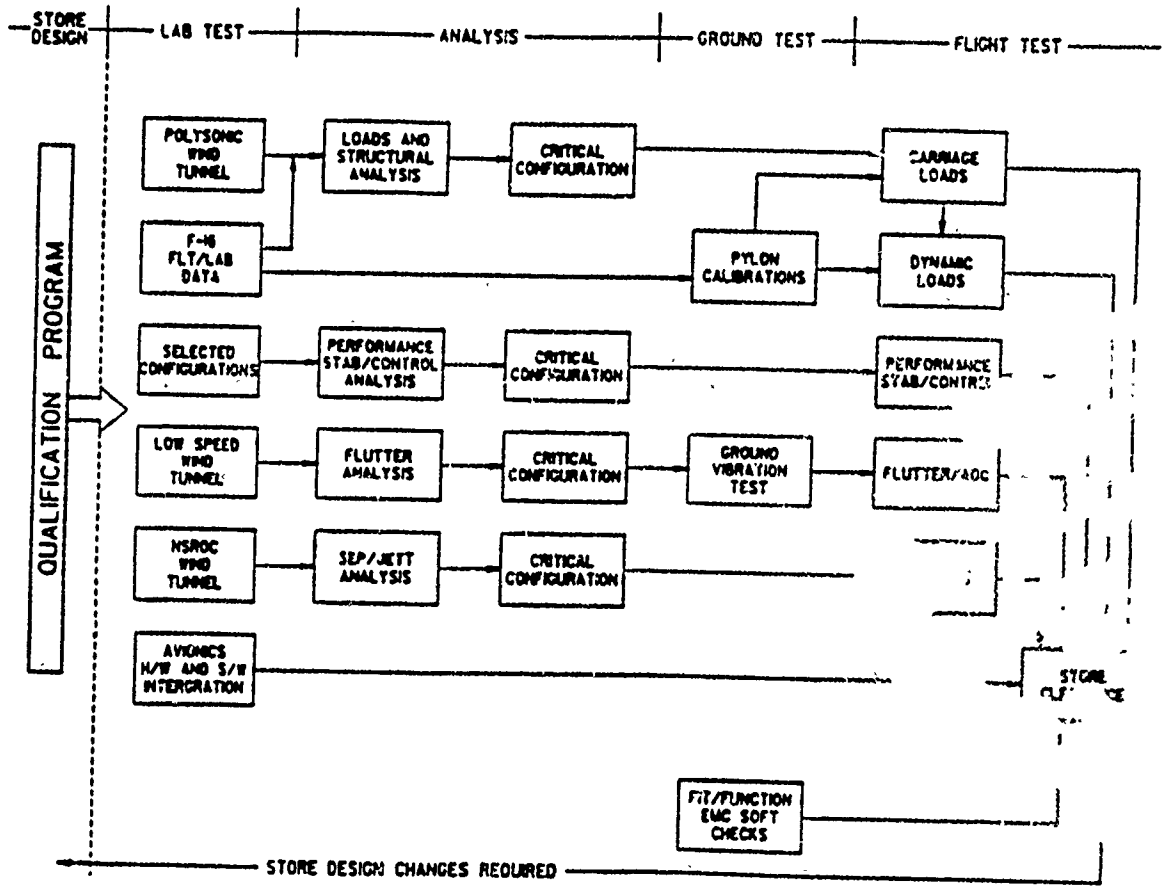

FIGURE 3 – 480 GALLON EFT STORES CLEARANCE PROCESS

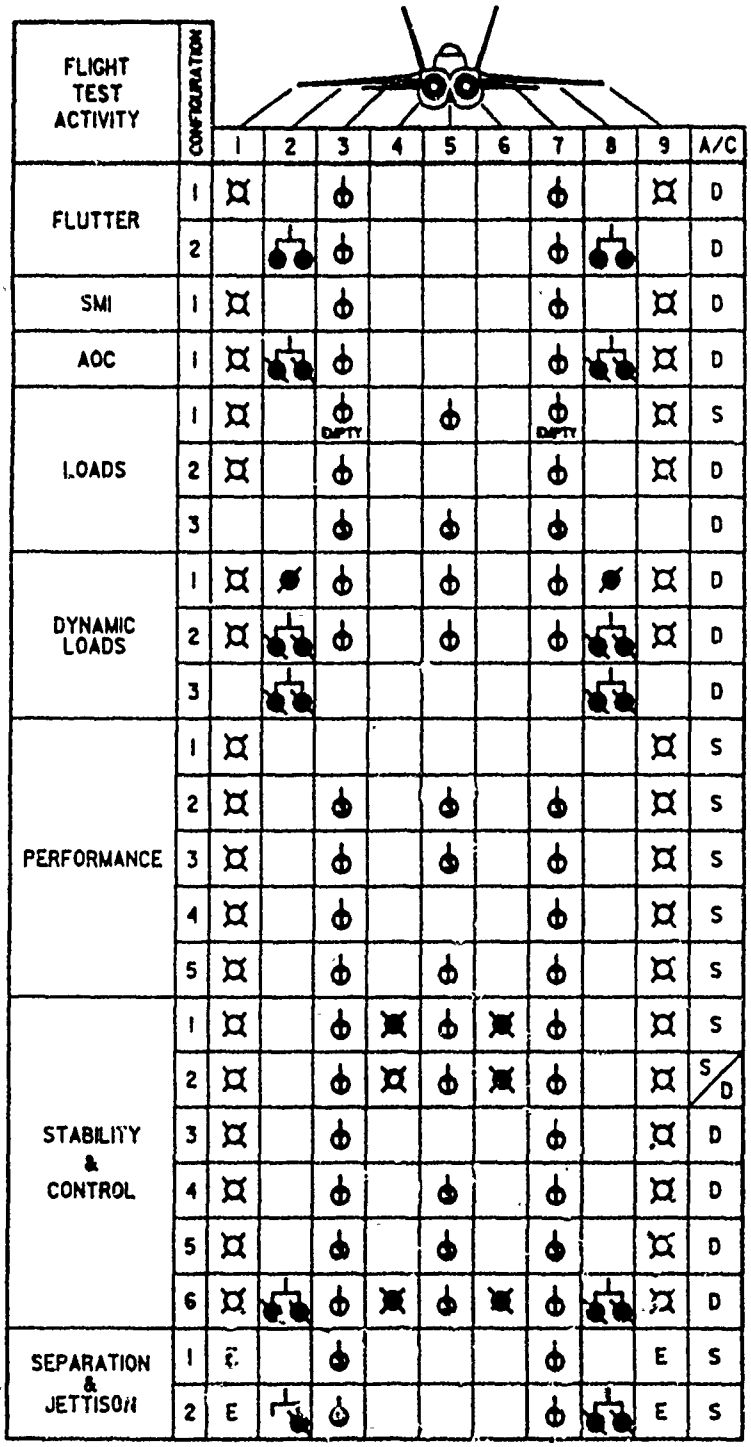

FIGURE 4 – CONFIGURATIONS FLIGHT TESTED

TIP MISSILES OFF, 2 MK-82 OUTBOARD, 100% 480 EFT INBOARD

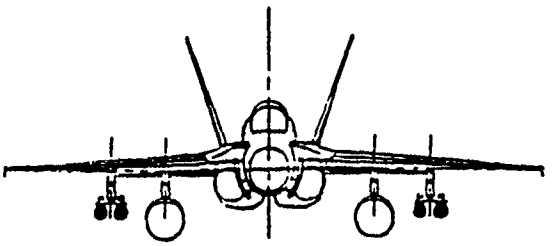

ANALYTIC MODE DESCRIPTION	SYMMETRIC			ANTI-SYMMETRIC		
	ANALYSIS HZ	GVT HZ	RIG HZ	ANALYSIS HZ	GVT HZ	RIG HZ
TANK ROLL	2.45	2.51	*NM	3.05	3.14	NM
TANK PITCH	6.00	6.17	6.19	5.75	5.72	5.89
TANK YAW	5.92	6.04	NM	5.93	6.42	NM
OUTBOARD STORE ROLL	4.05	4.41	4.45	4.63	4.73	4.45
OUTBOARD STORE PITCH	7.88	8.14	8.43	7.60	8.60	8.77
OUTBOARD STORE YAW	12.49	13.49	13.19	12.53	13.36	13.37
WING 1ST BENDING	5.53	5.91	5.77	8.31	8.08	8.12
WING 1ST TORSION	17.50	17.36	16.42	17.47	17.19	16.96
WING 2ND BENDING	11.90	12.60	NM	14.78	NM	NM
FUSELAGE 1ST BENDING	9.42	10.33	NM	8.80	9.74	9.31

*NM - NOT MEASURED

FIGURE 5 – SUMMARY OF TYPICAL 480 GALLON EFT GVT RESULTS

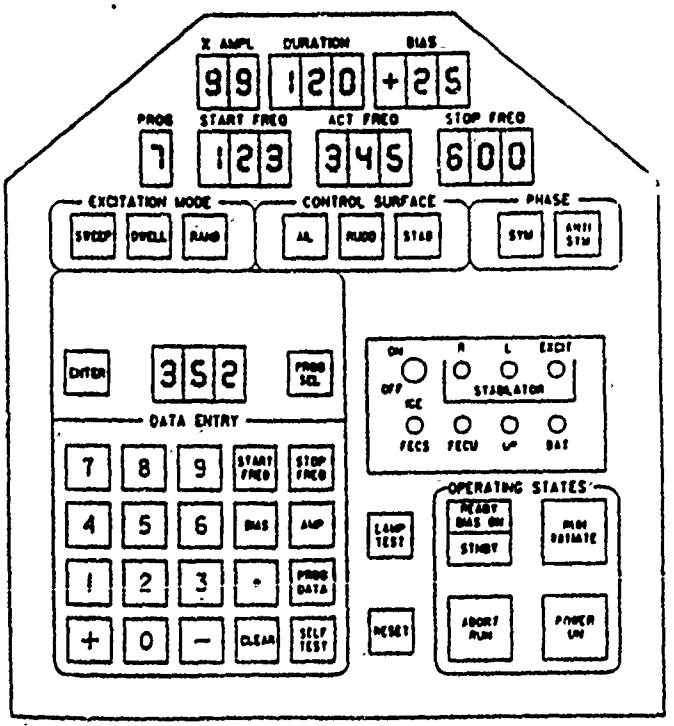

FIGURE 6 – FLUTTER EXCITER CONTROL UNIT

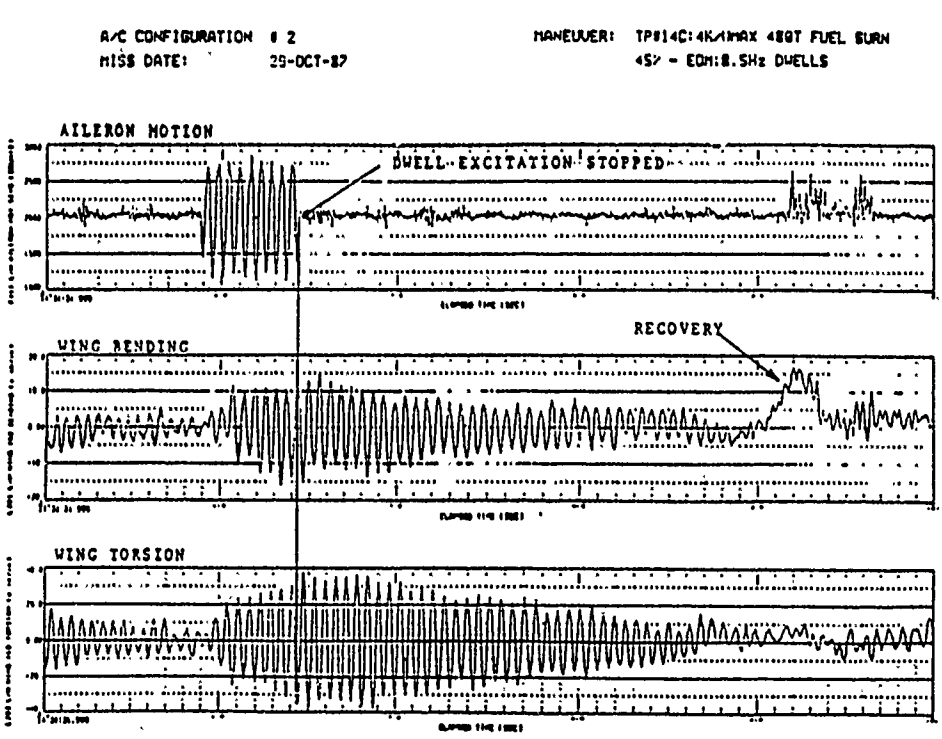

FIGURE 7 – RESPONSE OF WING STRAIN GAUGES AT LOW DAMPING

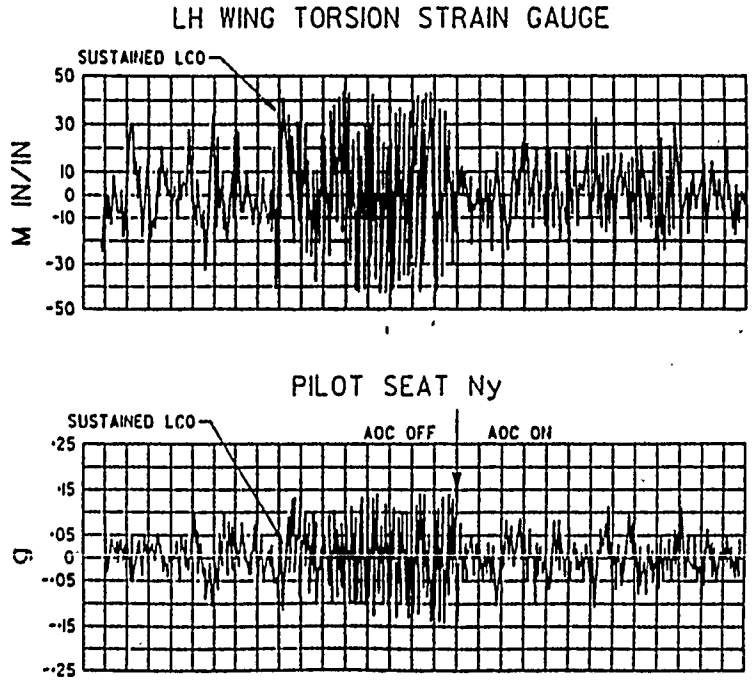

FIGURE 8 – AOC SYSTEM EFFECTIVENESS

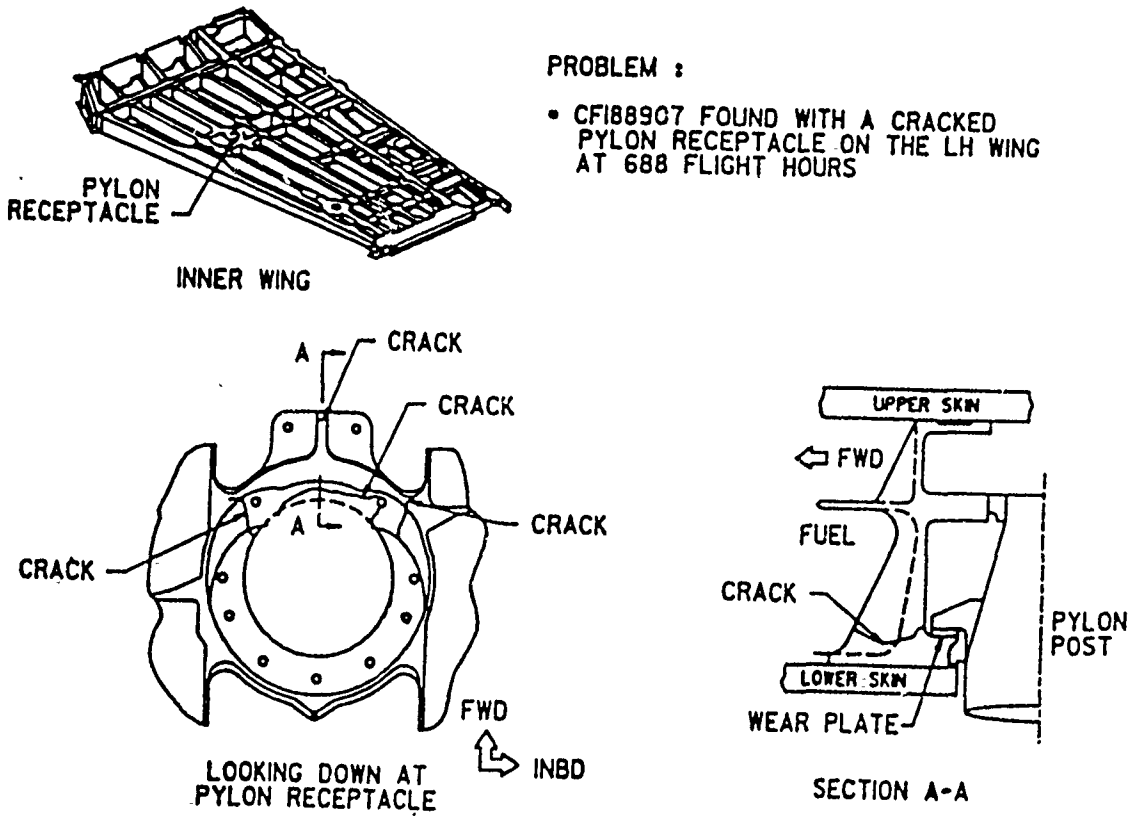

FIGURE 9 – INBOARD WING PYLON RECEPTACLE CRACK

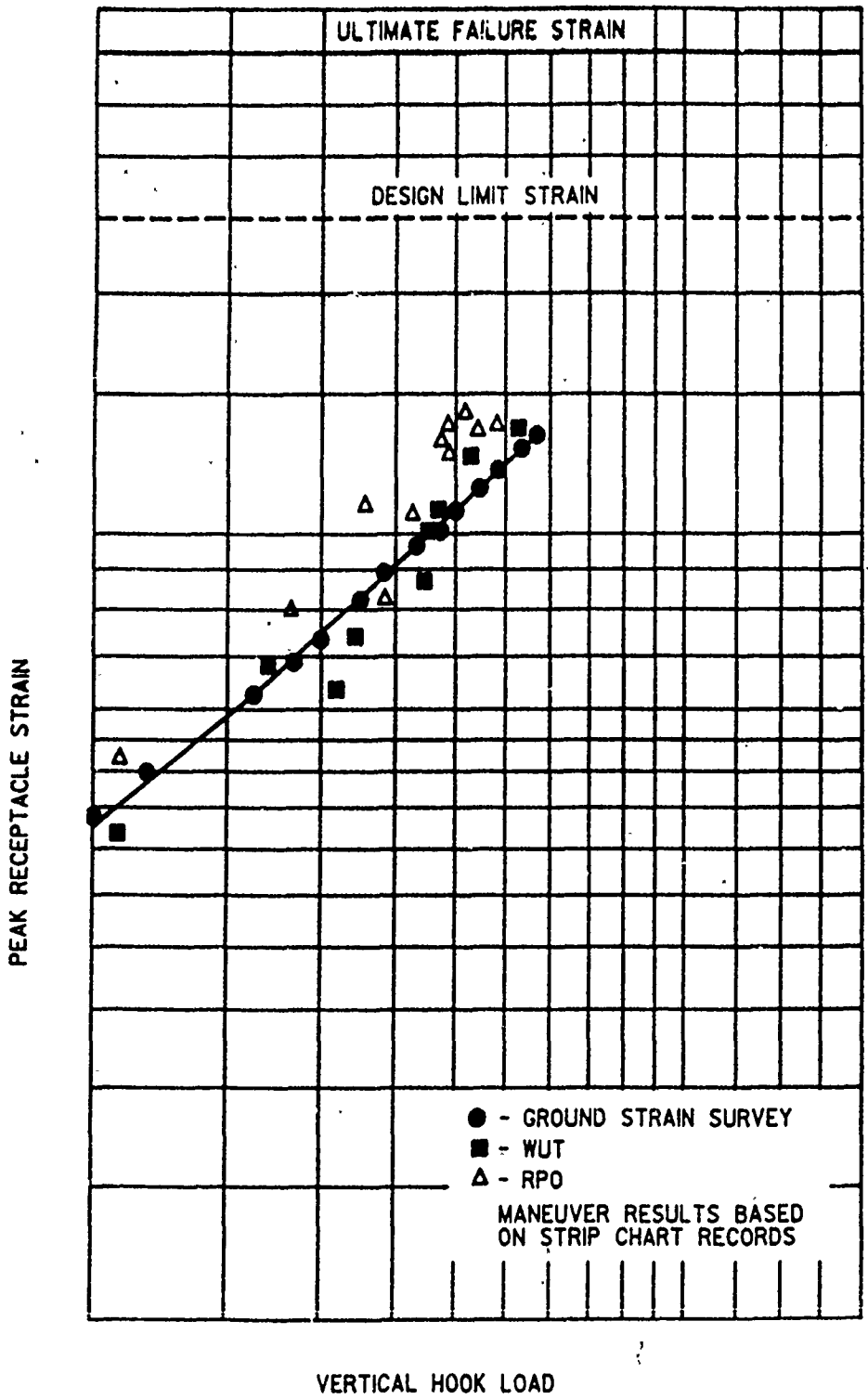

FIGURE 10 – INBOARD WING PYLON RECEPTACLE STRAIN/LOADS SURVEY

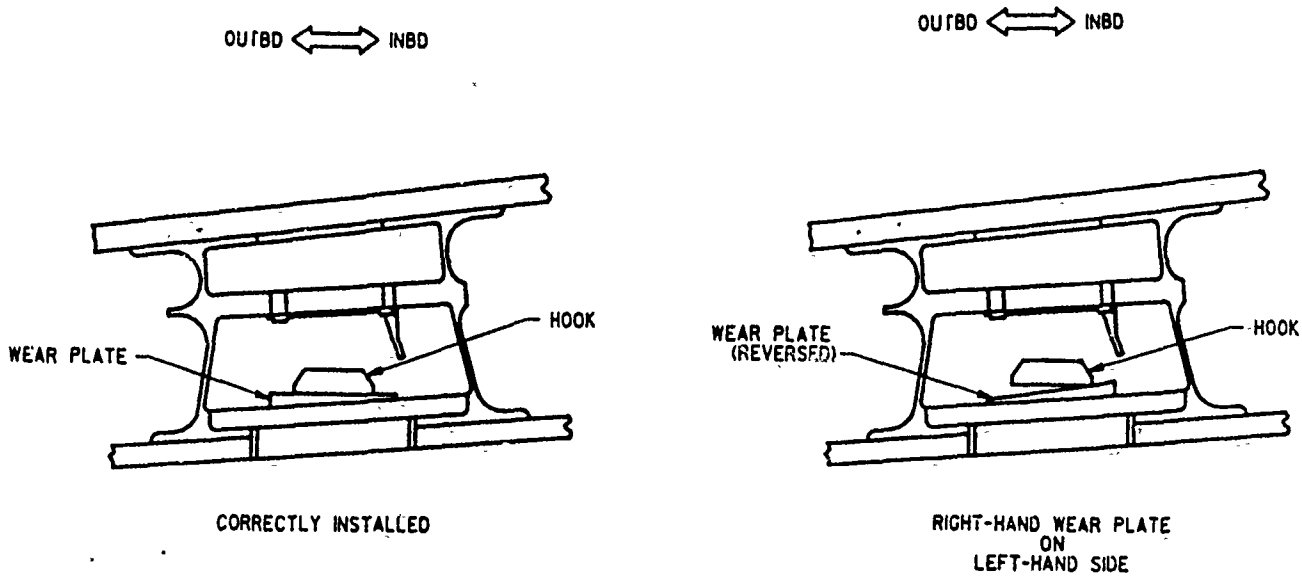

FIGURE 11 - CUT AWAY VIEWS OF WING PYLON RECEPTACLE & PYLON HOOK

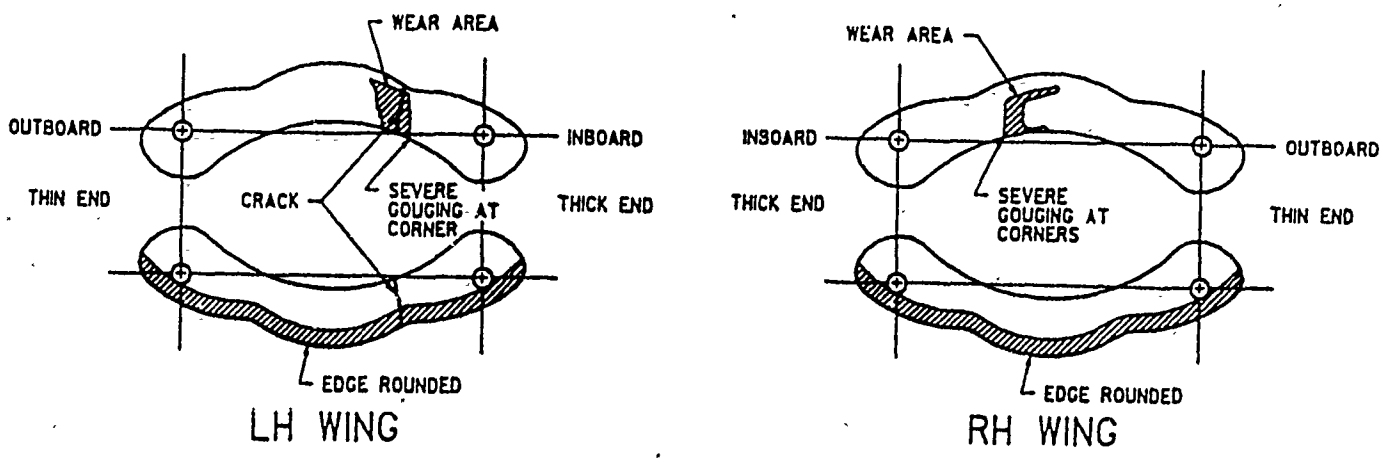

FIGURE 12 - WING PYLON RECEPTACLE WEAR PLATES FROM CF-188907

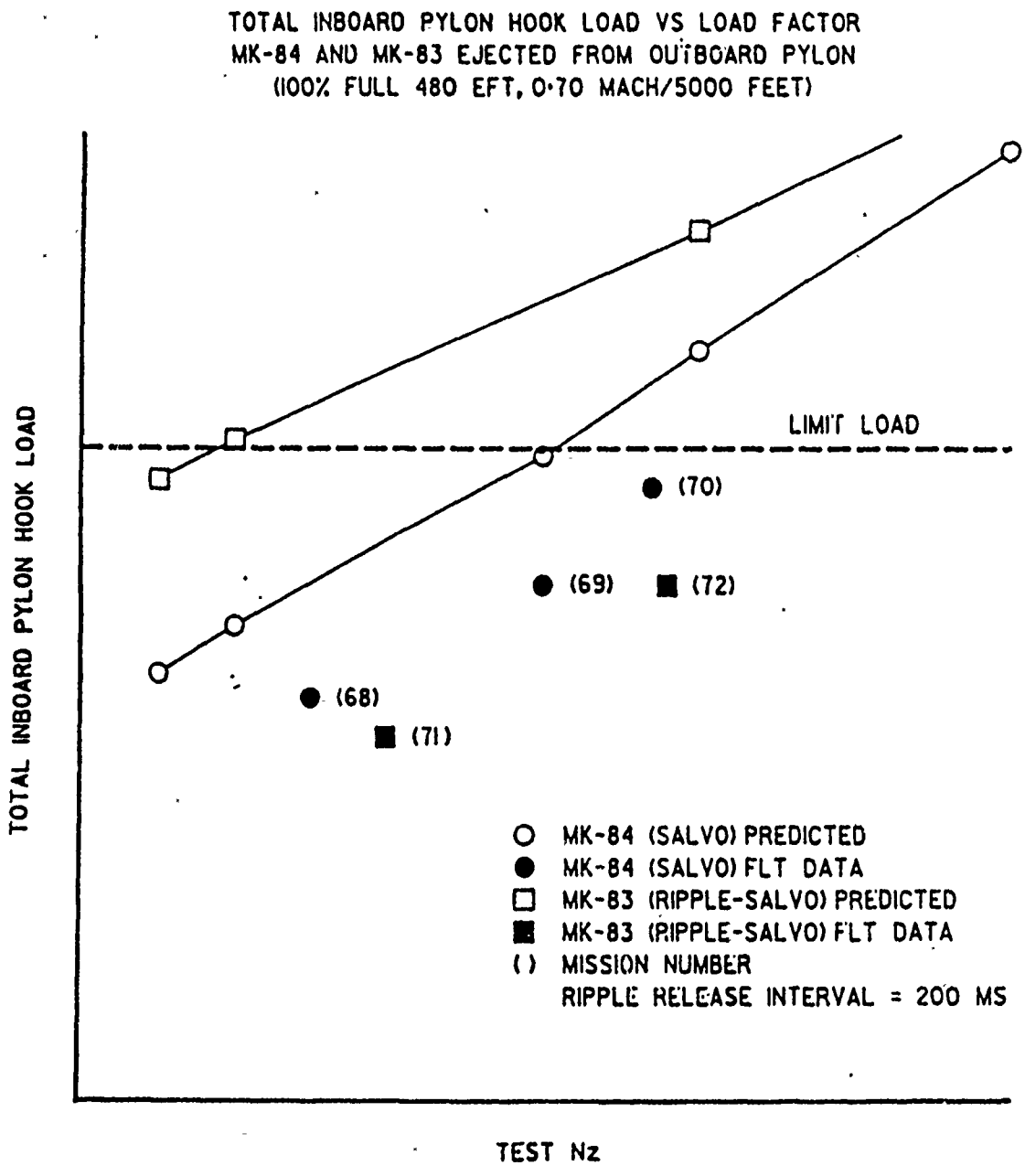

FIGURE 13 – PYLON HOOK LOADS FROM STORE EJECTION DYNAMIC LOADS TESTING

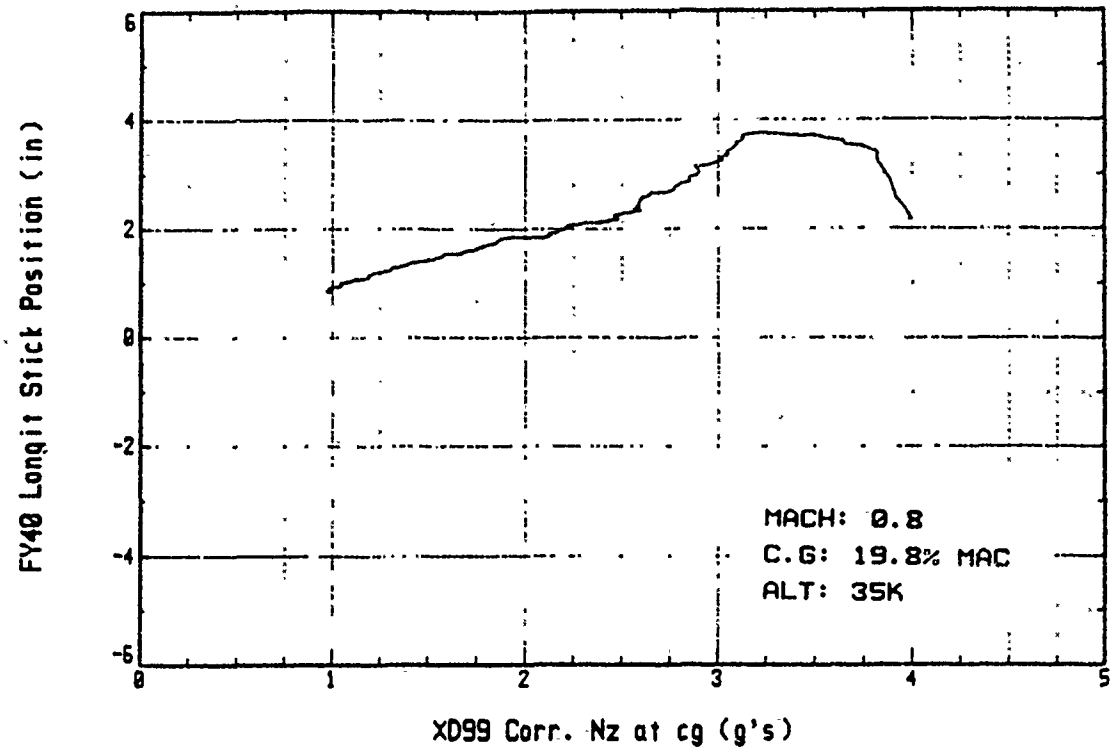

FIGURE 14 – LONGITUDINAL APPARENT STABILITY DURING WIND-UP TURN (3 x 480 EFT)

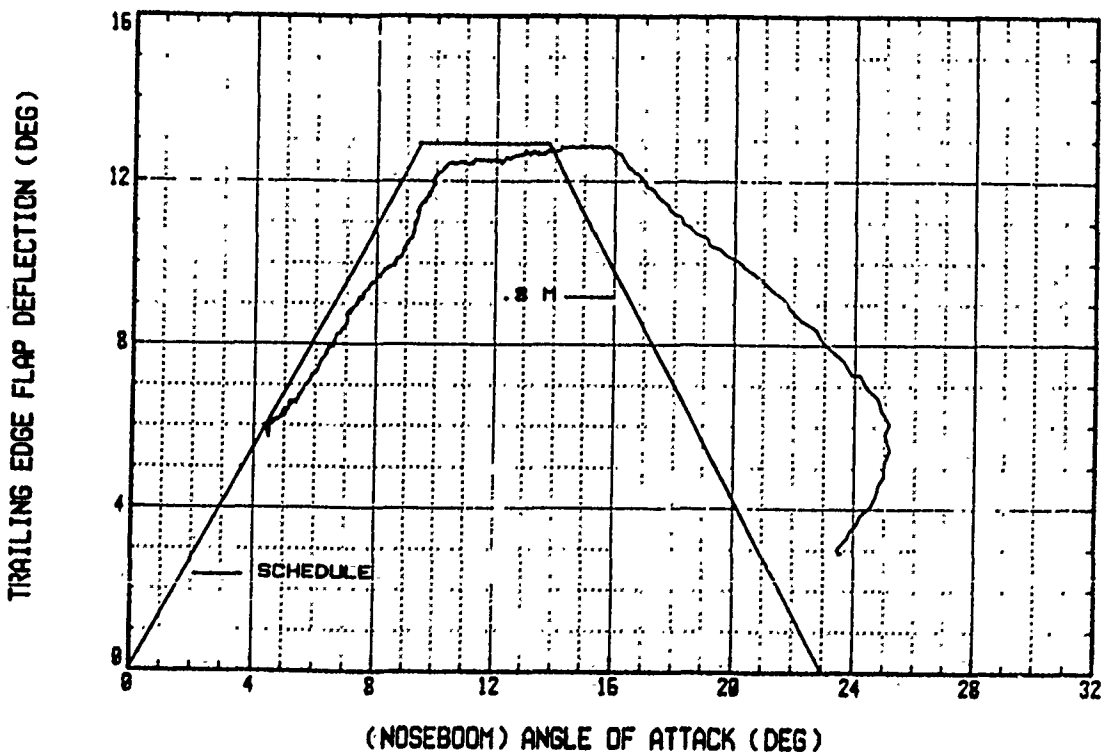

FIGURE 15 – TRAILING EDGE FLAP POSITION VERSUS SCHEDULE DURING WIND-UP TURN

BIOGRAPHY

CAPTAIN MARIO B.J. LAGRANGE

Captain Mario Lagrange was born in Quebec City in 1960. He is a graduate of the Royal Military College of Canada. In 1983 he received a master of applied science in aerodynamics from the University of Toronto Institute for Aerospace Studies. As a flight test engineer he is a proud member of Class 87B of the USAF Test Pilot School. Captain Lagrange is in his second tour of duty with the Aerospace Engineering Test Establishment and he is currently employed in the Armament System Engineering section. His primary responsibilities lie as a project manager and test director for various weapons clearance programs on the CF-18 aircraft. Among other test programs he was responsible for the clearance of the CRV-7 rocket weapon system, the MK-82/BSU-49 and the Category I testing of the 480 gallon external fuel tank on the CF-18. He is the Canadian representative to the AGARD Flight Mechanics Panel Working Group 19 on Aircraft Functional Agility. Captain Lagrange is a Professional Engineer and a member of the Society of Flight Test Engineers.

THIS PAGE INTENTIONALLY LEFT BLANK

CLEARED FOR PUBLIC RELEASE

THE ROYAL AUSTRALIAN AIR FORCE

AIRCRAFT STORES CLEARANCE PHILOSOPHY

BY

WING COMMANDER J.W. STEINBACH

DIRECTOR OF WEAPONS ENGINEERING

HEADQUARTERS LOGISTICS COMMAND

ROYAL AUSTRALIAN AIR FORCE

INTRODUCTION

The Royal Australian Air Force has a strength of around 20 000 permanent members and operates aircraft in the following force element groups:

Tactical Fighter	MCDONNELL DOUGLAS F/A-18 HORNET
Strike/Reconnaissance	GENERAL DYNAMICS F111C/RF111C
Maritime Patrol	LOCKHEED P3C/P3W ORION
Transport	DEHAVILLAND OF CANADA DHC4 CARIBOU LOCKHEED C130E/H HERCULES
Training	AERMACCHI MB326H PILATUS PC-9/A

As well, through a Memorandum of Understanding between the Chief of the General Staff and the Chief of the Air Staff, the RAAF exercises logistics responsibility for Army aircraft. These include:

SIKORSKI S70A Blackhawk

AEROSPATIALE AS350B Ecureuil

PILATUS PC-6 Porter

AEROSPACE TECHNOLOGIES OF AUSTRALIA Nomad

BELL UH-1H Iroquois

Although RAAF and Army aircraft are predominantly of US origin, some have been sourced in Europe while at least one is wholly Australian in design. In theory we would like to think that this eclecticism is to our advantage in that we acquire weapons systems that most closely satisfy our operational requirements at the best price. From an airworthiness perspective, this variety of sources means that we need to acquaint ourselves with the philosophies, standards and practices that apply in the countries of their origin. This is not necessarily bad because it enables

us to compare different approaches, selectively adopting what we think are the best features of each for ourselves. The other side of the picture is that from this derivation we may have created a system which is overly conservative with an in-built rigidity and inflexibility, one that cannot always react quickly enough in the event of some contingency.

While on eclecticism, I should add that while we naturally favour procuring stores and weapons that have been cleared on the type in its country of origin we often require stores or specify stores configurations to meet a peculiar Australian requirement. Our configurations or loading patterns can be therefore quite unique. For example we are presently working on a mixed stores clearance on the F111C that features Captive Carriage AIM-9L/M Sidewinder missiles, Harpoon Captive Carriage Weapons Systems (a Harpoon Simulator) and SUU-20A/A Practice Bomb Dispensers to allow our crews to undertake a variety of training missions in one sortie. It can also be a convenient way of transporting such stores on deployments.

We have cleared US-sourced aircraft stores on European aircraft (and occasionally vice-versa) and even a USN digital electronic weapon on a USAF analogue electronic aircraft, as we did with the AGM-84A Harpoon anti-shipping missile on the F111C, to provide this aircraft with a maritime strike capability. This brings me to another feature of our airforce: smallness, which can have a number of effects. It provides a rationale although not a very satisfactory one, to 'multi-role' our aircraft so we need to come up with some fairly original configurations (as with the Harpoon on the F111C) and bear the consequences of having to fully integrate systems into aircraft by ourselves. This naturally conflicts with another consequence of 'smallness', namely a limited capacity for conducting flight trials which is now compounded by reductions in flying hours available for flight test purposes. For example, flight testing of F/A-18 aircraft gets done at the expense of operational training as there are no dedicated test aircraft assigned to the trials unit. We do have two fully instrumented Hornets but these belong to operational units. Therefore greater emphasis must be placed on clearing stores and configurations by other means, notably by analogy. This technique has well known limitations and its appropriateness to any aircraft stores clearance must be understood.

Airworthiness Requirements

The Aircraft Stores Clearance (ASC) process is part of the broader airworthiness function, technical responsibility for which is vested in the engineering community of the RAAF. It is necessary to briefly review the RAAF concept of airworthiness as a basis for discussing the ASC process. Airworthiness is seen as a management system that exists to apply positive control over activities essential to safe and reliable air operations.
In the Royal Australian Air Force, the Chief of the Air Staff has statutory responsibility for airworthiness, for which he is answerable to the Minister of Defence. That responsibility is delegated, for a new aircraft project at the procurement stage to the Materiel Division manager, a two-star officer; while for in-service aircraft, it is assigned to the Air Officer Commanding Logistics Command (AOCLC), who for entirely practical reasons, delegates it to his senior engineering officer, the Director-General of Logistics Engineering, a one-star appointment. It should be noted that this is the minimum rank level at which an Aircraft Stores Clearance can be approved in the RAAF.

Airworthiness is seen as a concept which in its application defines the condition of an aircraft's suitability for flight. Furthermore, it forms the basis for judgement that an aircraft has been designed, constructed and maintained to approved standards by competent and approved individuals who are acting as members of an approved organization.

This then is the starting point for arriving, in the general sense, at the objectives of the Aircraft Stores Clearance process. Whenever new stores, configurations or employment limits are being introduced, certain technical activities must be performed to ensure that prevailing accepted standards of safety and reliable performance of the weapons system are not going to be compromised. However, the process goes beyond simply ensuring mechanical and electrical compatibility. It requires that all logistics support for the new store or configuration be provided, and especially that procedures for store preparation and loading be available. It is in fact a hard and fast rule in the RAAF that stores cannot be loaded to an aircraft unless an approved loading checklist exists. It can therefore be seen that the Aircraft Stores Clearance process is a wide ranging staff activity which looks at every facet having a bearing on airworthiness. This is accomplished by the use of proformae that require comment from key systems engineers within the Logistics Engineering Branch who must indicate whether or not some new stores fit or configuration impacts on the various sub-systems within their area of responsibility, and if so what they have done to accommodate the load change.

Objectives

We define an Aircraft Stores Clearance as being the approval to load, carry and employ (that is release, eject, launch, jettison, or 'captive carry') aircraft stores within stated limits on specified RAAF and Army aircraft. An aircraft store, for the purposes of the Stores Clearance is any device, excluding internally carried air cargo, intended for internal or external carriage and mounted to aircraft stores suspension equipment, whether or not the item is intended to be separated from the aircraft in flight. Aircraft stores can be classified into two categories:

Expendable Stores - which are normally separated from the aircraft in flight, and include bombs, rockets, missiles, mines, torpedoes, pyrotechnic devices, chaff, sonobuoys, and signals underwater sound.

Non-expendable Stores - those which are not normally separated from the aircraft during flight, but which may be jettisoned in an emergency; such as bomb racks, cargo pods, target canisters, data link pods, gun pods and munitions dispensers.

These definitions delimitate the scope of the ASC process. Stores that are externally attached to an aircraft but which are not capable of being released are not covered. Neither are items extracted from an aircraft by parachute. To reiterate, before an Aircraft Stores Clearance can be authorized and issued for a particular aircraft stores configuration, the airworthiness authority must ensure that certain criteria relating to

operational, safety, engineering and support issues have been addressed satisfactorily. The specific and formal objectives of the Aircraft Stores process are to certify the following.

* That the required aircraft stores configuration can be carried and employed safely and reliably to acceptable aircraft limits.

* That prerequisite aircraft modifications have been addressed and modification kits, where relevant, are available.

* That operator and maintenance publications including stores preparation and loading manuals have been issued or amended.

* That all other logistics support requirements, including provision of operator level maintenance special tools, test equipment, maintenance spares and training have been satisfied.

Initiation of Aircraft Stores Clearances

In any Aircraft Stores Clearance task we follow one cardinal rule, and that is that once RAAF has accepted design approval authority, in other words responsibility for airworthiness, then any proposed variation to the design including an approved stores configuration, is only ever accepted after a conscious, and deliberative exercise has been conducted by RAAF engineers. A corollary to that is that a foreign service Aircraft Stores Clearance is not in itself an authority for RAAF aircraft to carry or employ stores covered by that clearance. This means that in practice the Approved Load Charts appearing in Flight Manuals for aircraft bought overseas simply don't apply.

To accept a foreign service clearance we are required to obtain and consult copies of flight tests or any other reports that were used as a basis for establishing that clearance. This is quite a rigorous process, and only after we have convinced ourselves that the trials and analyses were conducted in accordance with standards comparable to our own do we accept the clearance as valid. There are other more practical reasons why we do not accept a foreign-source stores clearance. We may not use the same fuze, preferring a mechanical to an electrical one; or we may need to design a new arming control system. Recently we developed a new MK84 Low Drag Mechanical Arming Control System or MACS, to overcome a supply problem. We deliberately try to standardise wherever possible on all aircraft types. We cannot forget that our F111C is different to the F111 D, E, F or G variants so we often perform flight trials for weapons carriage and release to demonstrate that the physical differences between these models can be disregarded.

Details of clearances approved by the RAAF, whether based on in-house testing or on overseas clearances are promulgated in foreign-source Flight Manuals in supplementary pages.

The need for a new stores clearance generally arises from the identification of a new capability requirement. While it is possible for

any unit commander or Headquarters to identify a new requirement, it ultimately requires the concurrence of the Deputy Chief of the Air Staff before clearance action will commence. Once a requirement for the new capability or expansion of an existing one has been validated, weapons systems engineering staff will begin the task. As we all know it is extensive and time consuming. Even for a relatively straight-forward Clearance which may entail little more than checking the details of a foreign service Clearance (assuming that flight test reports from overseas are available) may take several months. A complex task (to cite the example of the Harpoon on the F111C) may take several years, particularly where carriage and stores release trials are involved.

Progression

Co-ordination of the Aircraft Stores Clearance task is the responsibility of the Director of Weapons Engineering in our Logistics Command. He is required to carry out the following functions:

* For overall planning purposes, assess the complexity of the effort, with an itemised estimated time and cost to complete.

* Conduct a thorough survey of local and overseas data, including data covering stores qualification trials, ground fit and compatibility trials, wind tunnel studies, aeroelastic studies, weight and balance studies, ballistic drops and any operational flight programmes. This is aimed to determine the extent if any, of additional in-house testing required to provide the Aircraft Stores Clearance.

* Co-ordinate feasibility studies and trials of aircraft store configurations, aircraft stores delivery systems and aircraft stores.

* From the results of all tests, trials and studies, demonstrate that the requisite stores configuration:

  (1) is functional for carriage and employment within the operating limits sought, and

  (2) does not compromise the airworthiness of the aircraft with carriage and employment conditions.

* Complete all technical administration and co-ordination, including liaison with all concerned agencies, before seeking formal airworthiness authority acceptance.

The Aircraft Stores Clearance Certificate

The medium used to progress a Stores Clearance process through the engineering bureaucracy is the Aircraft Stores Clearance Certificate. This is really a combination of a comprehensive 'questionnaire' type of document, and a detailed record of actions taken to complete the Clearance. Specifically it:

* details the approved stores configuration in a format appropriate for incorporation into the Flight Manual, and includes operating limits (airspeed, roll rate, acceleration and release attitudes) for carriage and employment of aircraft stores;

* refers to all test reports and engineering studies used to validate the Aircraft Stores Clearance.

* certifies that all actions prerequisite to the issue of the Clearance have been completed, and

* certifies that the completed Aircraft Stores Clearance is operationally acceptable.

This last certification was introduced to 'close-the-loop', so that operational commanders could endorse what is in effect a recommendation drawn from a process staffed principally by engineers. Each Clearance Certificate must also be signed off by each of the four principal Directors of Engineering who have responsibility for the various technologies, namely aircraft, avionics, weapons and explosives. Once operational aspects of the Aircraft Stores Clearance have been agreed to, the Stores Clearance Certificate is approved by the airworthiness authority, the Director General of Logistics Engineering. Amendments to the Flight Manual are then passed to aircrew publications managers for incorporation. It is at this stage that the Clearance takes effect.

Once a clearance has been approved, it cannot be amended. To change its content requires a re-issue which entails following the full procedure.

Some Problems and Prospects

We are painfully aware that the Aircraft Stores Clearance process is too time consuming, and we frequently receive criticism from operational staffs that we are not sufficiently responsive to their needs, so we are continually looking at shortening the time to issue a Clearance.

We have as yet no policies for managing Aircraft Stores Clearances to meet operational emergencies, but we are now considering abbreviating the process once we can identify and quantify the risks involved.

With the introduction of digital aircraft, and especially in the context of the F111C Avionics Update Programme, a lot more attention has to be given to operational flight programmes that interact with the weapons delivery systems. Some thought is being given to qualifying weapons delivery accuracy under the auspices of a Stores Clearance.

Conclusions

I would like to conclude this presentation not with a summary but by stating that in Logistics Command, we issue around twenty stores clearances per year, and that while we may be overly cautious, we are rarely put into a position where we are required to revise and re-issue a clearance because of any difficulties encountered during operations. This is not to say that we have always had trouble-free application, but on balance, I think we have a viable process which with the refinements I mentioned will continue to serve the Royal Australian Air Force well.

BIOGRAPHICAL DETAILS

WING COMMANDER J.W. STEINBACH

Wing Commander John Steinbach is presently the Director of Weapons Engineering at Headquarters Logistics Command Royal Australian Air Force (RAAF). He graduated from the RAAF Academy in 1970 and was commissioned as an Engineer (Armament). He is a graduate of the University of Melbourne, the Royal Melbourne Institute of Technology, the University of Canberra and the Royal Air Force College Cranwell (Aerosystems Engineering Course). He has attended the RAAF Advanced Staff College and the Australian Joint Services Staff College. For most of his service career he has been associated with the maintenance, engineering and introduction into service of airborne guided weapons systems. Prior to taking up his current appointment he served as a Technical Liaison Officer and as Defence Attache at the Australian Embassy, Paris France.

THIS PAGE INTENTIONALLY LEFT BLANK

INTEGRATION OF COMPUTATIONAL FLUID DYNAMICS INTO STORE SEPARATION METHODOLOGIES

*George A. Howell**
*Jack D. Watts***
General Dynamics Fort Worth Division

1. ABSTRACT

Advances in the technologies of computational fluid dynamics and computer science are examined to show that the capability to simulate the dynamic separation of weapons from parent vehicles is a near-term possibility. Progress in recent years is reviewed, and solutions are presented from potential-flow methods, Euler methods, and Navier-Stokes methods used to compute the mutual aerodynamic interference effects of aircraft and separating stores. The impact of structured, overset, and unstructured grids on problem solutions is also discussed, as are advanced computers that may enhance the ability to solve computationally intensive engineering tasks. The integration of computational fluid dynamics into store separation methodologies is justified through improvements in flight safety, turn-around time, and cost.

2. INTRODUCTION

Certain classes of military aircraft are designed for missions that require the inflight release of weapons and external fuel tanks. In striving for diversity, these aircraft are generally qualified to carry and drop as many different types of these stores as feasible. Configuring an aircraft to carry stores begins at an early stage in the design process. Wind tunnel tests are conducted to establish preliminary verification that the stores can be safely carried and released within a specified range of flight conditions. Final hardware certification procedures require that flight tests be conducted to verify that the stores can be safely carried and released and to assess the trajectory of weapons for delivery accuracy. Each store that is to be certified for an aircraft must be tested for each flight condition and for each store loading configuration (i.e. for each unique combination of pylon type, store position, and neighboring stores). These variables can lead to large matrices of flight tests that include the destructive use of expensive store hardware, in order to qualify a store for use with an aircraft.

In another arena, the explosion of supercomputer computational power in the past decade has provided a tool for scientists to begin applying computational fluid dynamics (CFD) to many real-world problems that were previously impractical to solve. In aircraft design, CFD has become an accepted tool for resolving problems in localized areas of complex flow. Still, much ingenuity is required to obtain successful simulations. The formulation of the equations of fluid motion to be used (Navier-Stokes, Parabolized Navier-Stokes, Thin-Layer Navier-Stokes, or Euler) must be carefully matched to the complexity of the flow field as well as the computational resources that can be applied to the solution of the problem. The status of CFD in today's aircraft design world can be characterized as a balance between the extent of the aircraft geometry to be analyzed, the complexity of the equations to be used in the solution, and the computational resources available.

A CFD method to simulate store separation will require the handling of complex geometries and moving bodies. Capabilities to handle complex geometries have been demonstrated with several steady-state solutions of the complete F-16 geometry with Euler and Navier-Stokes equations (References 1, 2 and 3). Time-accurate

* Engineering Specialist, Sr., Computational Fluid Dynamics
** Engineering Chief, Weapons Technology

solutions have also been made on simple shapes with moving bodies. Today's demonstrated capabilities of CFD, coupled with projections for revolutionary enhancements in computer technology, set the stage for development of a leading-edge capability to accurately simulate the dynamic separation of stores from aircraft.

3. AIRCRAFT/STORE INTERFERENCE EFFECTS

Store separation studies have historically concentrated on the effects of the parent vehicle on the store trajectory. First, tests must be conducted to certify that the store moves safely away from the vehicle. And second, the speed and orientation of the store as it escapes the influence of the parent vehicle must be estimated for use in computing the store trajectory. Many cases have been documented in which unexpected aerodynamic forces caused a released store to impact the parent vehicle or miss the target.

In the future, new problems in store separation will be introduced by high performance aircraft that deliver stores at supersonic and hypersonic speeds. Since aerodynamic forces on bodies increase approximately in portion to the square of the speed, stores that simply drop from an aircraft at low speeds may be unpredictable and fly along erratic trajectories when released at higher speeds. In addition, large aerodynamic loads on the parent vehicle can be caused by the shock waves from stores released at high-speed. The impact of this is illustrated below by two of General Dynamics' experiences in major aircraft programs.

On the B-58 program, seventy-four supersonic releases were made with configurations involving four types of weapons and an external fuel tank. A portion of these releases were made to establish the altitude/speed weapons delivery envelope shown in Figure 1. The original high speed limit was reduced for several reasons, but below Mach 1.35, the reduction was due to the aerodynamic loads generated on the wing when the lower component of the external fuel pod (TCP) was released.

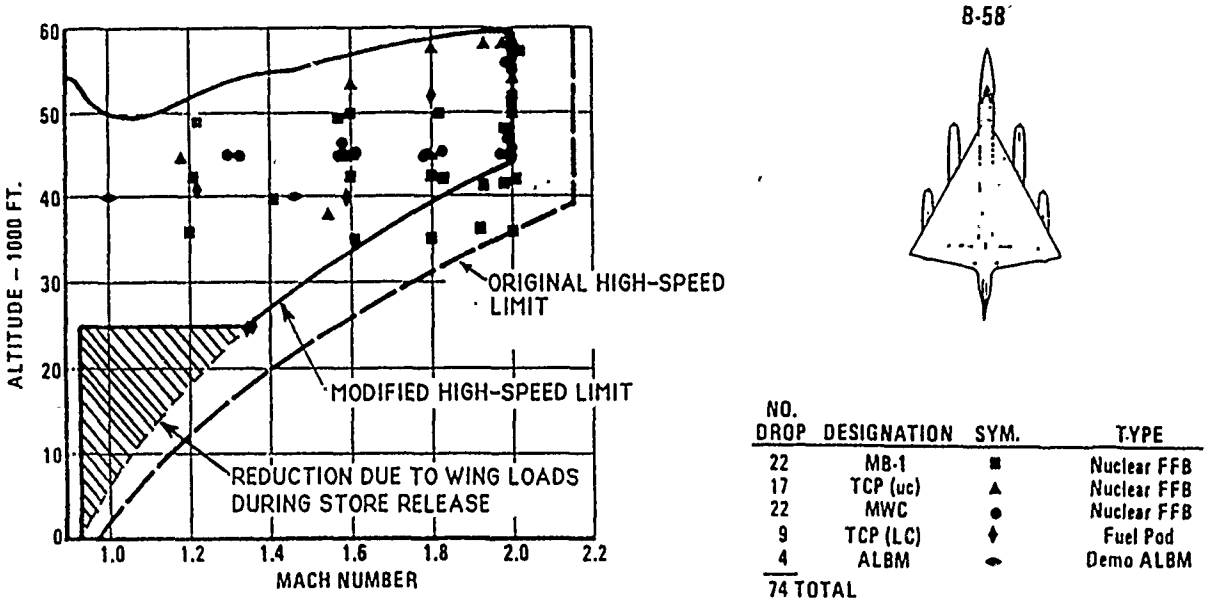

Figure 1. B-58 Wing Loads Restricted Weapon Release Envelope

On the F-16 program, fourteen 370-gallon tank drops were made between 1.1 and 1.6 Mach number as reported in Reference 4. As the tank is dropped, it is pivoted downward about the rear attachment point, as illustrated in Figure 2, generating a strong shock wave as it falls away from the wing. The shock wave impinges first on the wing and then on the horizontal tail, producing normal accelerations at the aircraft cg of up to 3.2 g's. The shock waves from the dropping tank also produced accelerations of approximately 12 g's on wing-mounted AIM-9s (stations 3 & 7) and up to 40 g's on the tail of wing-tip mounted AIM-9s (stations 1 & 9).

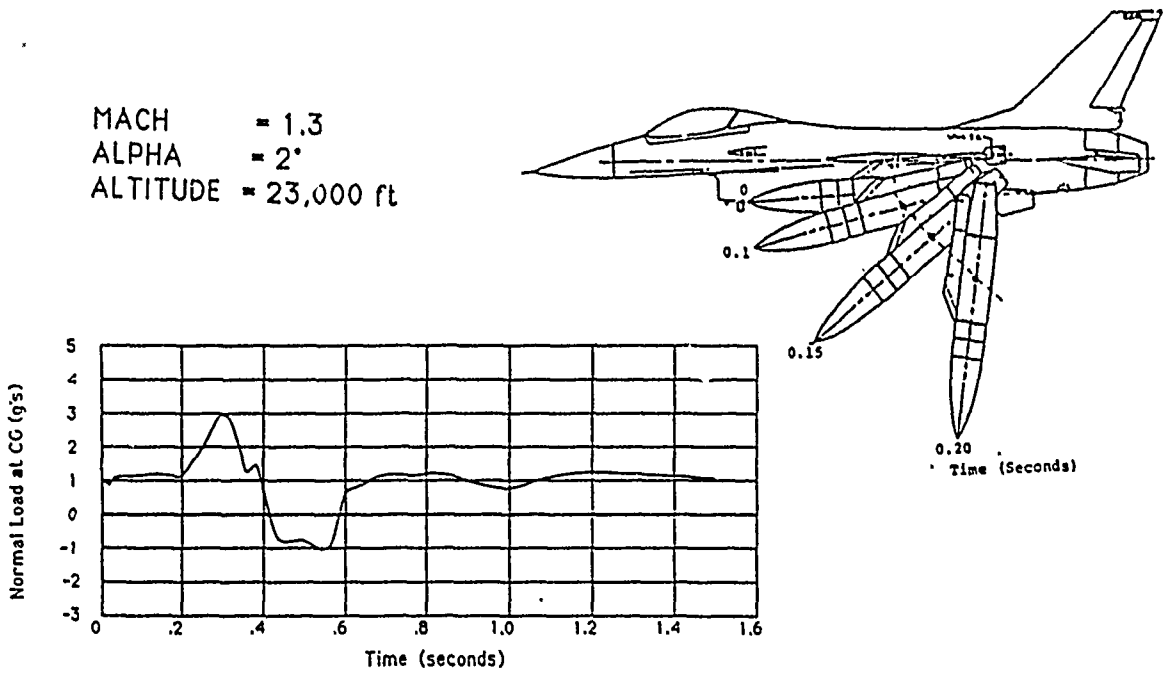

Figure 2. F-16 Pilot Is Subjected to Strong Accelerations When 370-Gal Fuel Tank Is Released

4. CFD TECHNOLOGIES FOR STORE SEPARATION

Recent advances in the application of CFD techniques for predicting complex aircraft flow fields and increases in computing power (with accompanying reductions in cost) have made simulation of aircraft/store separation appear to be practical in the near future. CFD methods used for this purpose can be characterized by the degree of simplification used in deriving the governing equations of fluid dynamics and by the type of grid that is used to discretize, or model, the physical space around the aircraft. These two factors are described in this section.

Governing Equations of Fluid Dynamics

The most general form of the governing equations of fluid dynamics is the Navier-Stokes equations. These equations describe viscous, compressible or incompressible fluid flow. They can simulate a broad class of real-world aerodynamic phenomena, including boundary layer buildup, flow separation, shock waves, and unsteady flows. Unfortunately, solutions of the Navier-Stokes equations on grids that can resolve these detailed flow aspects are very expensive to compute, which forces engineers to consider simplified forms of the equations to reduce cost. By understanding the predominant flow phenomena present in the problem being solved and choosing the right simplifications, an experienced CFD practioner can reduce the computer time needed to obtain a solution by several orders of magnitude, while still modeling the important flow features of the problem. Several widely-used forms of the governing equations are discussed below.

Navier-Stokes - The Navier-Stokes equations have the most capability to accurately simulate the real-world aerodynamic phenomena mentioned above. However, they require a dense grid, particularly in the boundary layer, in order to resolve viscous effects. Although the equations can model the physics associated with the turbulent phenomena (direct simulation of turbulence), an exorbitant number of grid points and time steps required render such a solution impractical for complete aircraft. Practical approaches to simulating turbulence are provided by algebraic and two-equation models. Turbulence modeling is still very much a pacing item for solving fighter aircraft flow fields.

Euler - The Euler equations are a subset of the Navier-Stokes equations that ignore the viscosity of the fluid. They simulate unsteady, incompressible or compressible flows including shock waves, expansion waves, and vortices introduced into the flow through curved shocks. These equations do not model boundary layers, flow

separation, or vortex dominated flows. Solutions using the Euler equations are cheaper than solutions using the Navier-Stokes equations because the equations are simpler and resolution of inviscid flow phenomena requires fewer grid points, the synergism of which results in large reductions in computer time. Solutions to these equations can be useful in preliminary design environments where a high degree of accuracy is not required and/or viscous effects are not predominant.

Potential Flow - The potential flow equations are an even further simplification of the Navier-Stokes equations. They do not model flow field vorticity and assume constant entropy, prohibiting accurate solutions for strong shock waves. For flows where they are applicable, potential flow solutions are cheaper than Euler solutions because only one equation has to be solved for each control point, rather than the five equations required for a three-dimensional Euler solution. An even simpler approximation, linearized potential flow, can be used for flows that are fully supersonic or fully subsonic (i.e. not transonic). The linearized potential equation can be solved by superimposing elementary solutions that are specified on a set of body panels. Only the body needs to be gridded (paneled), and off-body grid points are used only for panels that are for flow field surveys. Linearized potential solutions are very inexpensive.

Grid Models

Before an aerodynamic problem can be solved with a CFD method, the geometry and flow field must be represented mathematically, which can be either a set of grid points or a set of surface panels, depending on the type of fluid dynamic equations being solved. A distinguishing requirement of grid models for store separation problems is the need to simulate several bodies with large relative movements. Therefore, the grid must dynamically adapt to the positions of the stores as they move through the flow field. This factor alone makes the selection of a grid model a critically important decision.

Several other design problems share the need to handle body movement, including the separation of multi-stage orbital vehicles, escape capsule ejection, control surface deflections for dynamic maneuvering, and wing flutter. Four types of grid models that have been used for aircraft/store simulations are surface panels, structured grids, overset grids, and unstructured grids. Examples of the use of these grids are presented below.

Surface Panels - Geometry modeling with surface panels is a technique used in linear potential flow solutions. Each smooth section of a configuration is represented by a body-conforming network of panels. Depending on the geometric complexity, complete configurations are typically modeled with from one thousand to several thousand panels. An application of surface panels in a potential flow solution to the problem of aircraft/store separation is presented in Reference 5, where the PAN AIR Pilot Code was used to compute the flow field of a store in two stationary positions near a generic aircraft. The paneling arrangement representing the configuration with two tandem-mounted stores is shown in Figure 3. A flow field survey was computed for 1.2 Mach at approximately

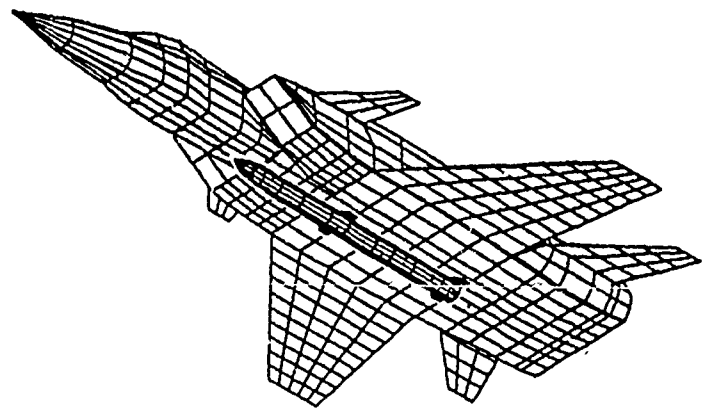

Figure 3. Surface Panels Represent A Generic Aircraft With Tandum-Mounted Stores

one store diameter beneath the configuration and compared with experimental data in Figure 4. The computed flow field pressures show the correct trends and match the data reasonably well. In another series of computations, the leading store was kept in the captive position while the trailing store was moved to several locations in the flow field beneath the fuselage. The aircraft was placed at 2.5 degrees angle of attack, and the store was placed at 6 degrees. The position of the moving store and the lift forces that were generated on the store are shown in Figure 5. These results indicate that when the moving store is near the captured store, nonlinear aerodynamic effects are present that are not simulated in potential flow solutions.

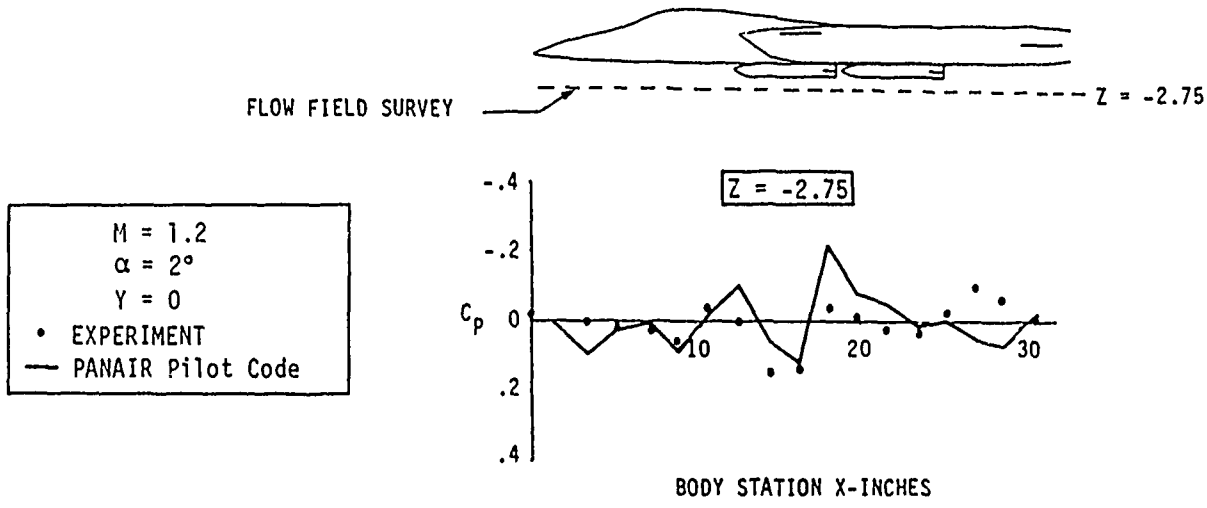

Figure 4. Computed Flow Field Pressures Are Near Experimental Values

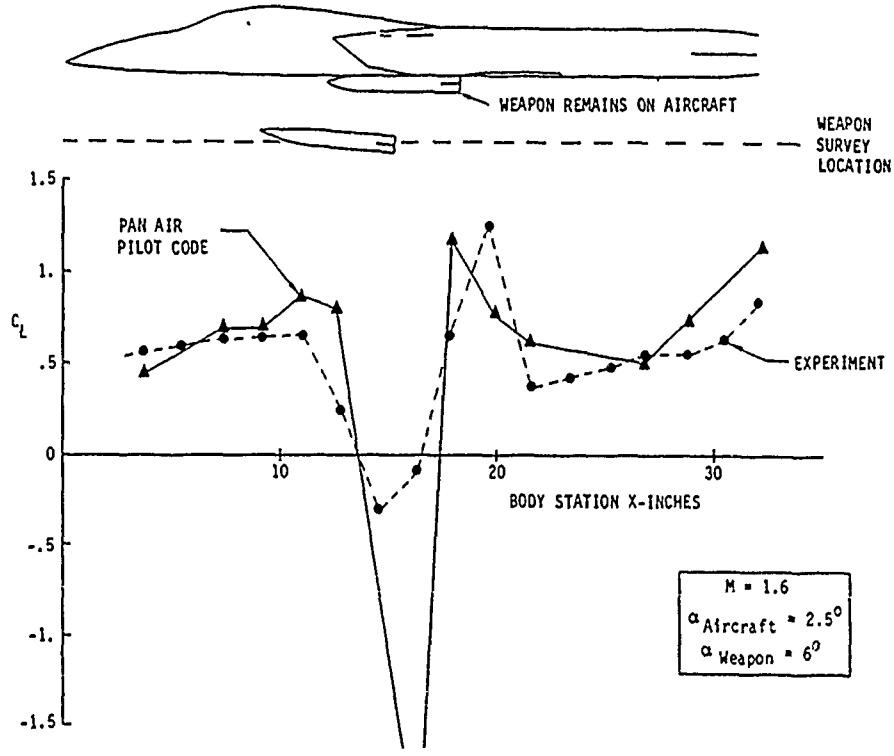

Figure 5. Non-Linear Aerodynamic Effects Are Absent From Potential Flow Calculations

The surface panel approach has several significant disadvantages, including the inability to simulate viscous effects, boundary layer effects, separated flow, and transonic flow. However, this approach requires little computer time, relative to other sophisticated techniques, and may be the only practical means for obtaining solutions in some design environments.

Structured Grids - For static geometries, multi-block structured grid schemes are the most popular means currently available for use in solving either the Euler or Navier-Stokes equations. A structured grid for the centerline plane of an F-16 and a store is illustrated in Figure 6. When the weapon is moved in this type of grid system, the grid must adapt to the weapon boundary or a new grid system must be generated. CFD codes can be written to automatically stretch the grid to account for small store movements, but when the grid cells become highly skewed, the complete grid must be re-generated. This is an overwhelming disadvantage of structured grids for dynamic configurations. The simulation of a store released from a captive position to a position outside the aircraft flow field would likely require numerous re-generations of the grid, a very labor-intensive task.

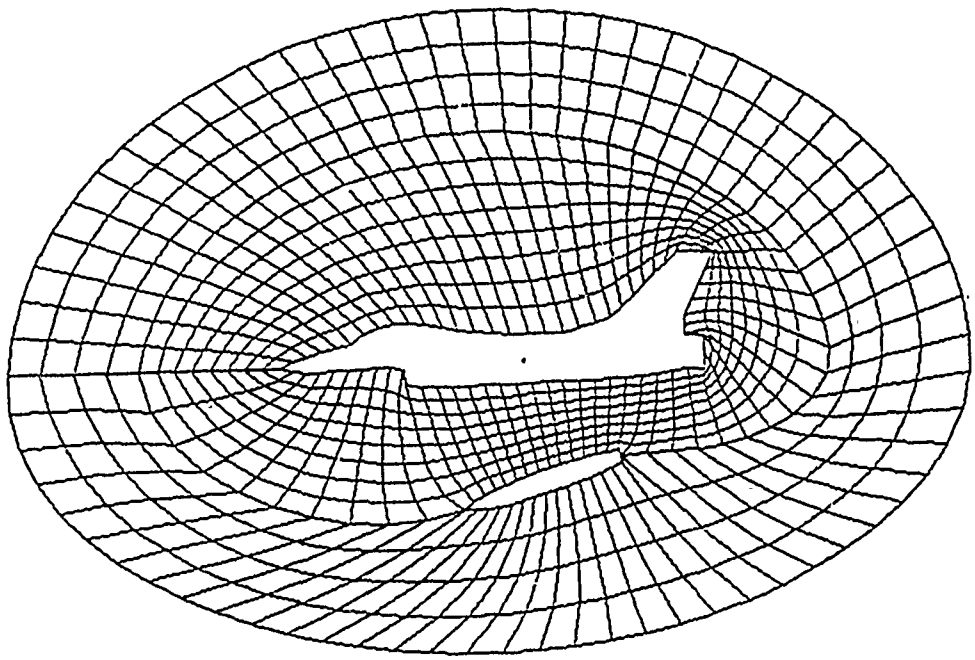

Figure 6. Weapon Movement in Structured Grid Systems Requires Stretching Cells or Regridding

An application of a structured grid to a three-dimensional wing/pylon/store configuration is presented by Whitfield and Thompson in Reference 6. The configuration was comprised of a symmetrical airfoil with a 45-degree leading-edge sweep, a pylon with a biconvex airfoil shape, and a store represented by an ogive-cylinder supported with a cylindrical sting joined to the store boattail. A three-dimensional structured grid comprised of approximately 220,000 points in 30 blocks was used to model the flow field about this configuration and is shown in Figure 7.

Two different solutions were obtained for this configuration. The first was a steady-state solution with the store mounted on the pylon. The second was an unsteady solution accounting for the dynamic movement of the store as it moved away from the captive position on the pylon. A comparison of computed and experimental surface pressures on the outboard side of the store are shown in Figure 8.

Overset Grids - The overset grid scheme, commonly referred to as the Chimera Scheme, is a promising approach that uses multiple overset structured grids to allow relative movement between bodies. The aircraft can be modeled with a global grid about the aircraft and minor grids about each store. The minor grids are overset on the global mesh without any requirements for point-to-point matching along the boundaries of the global and minor grid systems. The minor grids can then be moved freely within the global grid. Figure 9 illustrates this scheme. In a

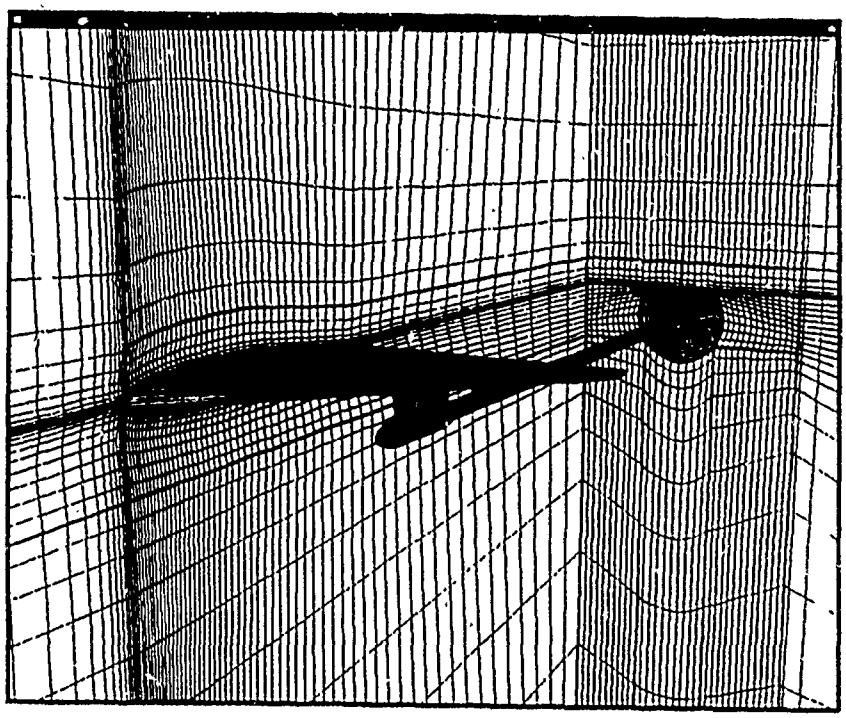

Figure 7. Surface Layer Of Structured Grid About Wing/Pylon/Store Configuration

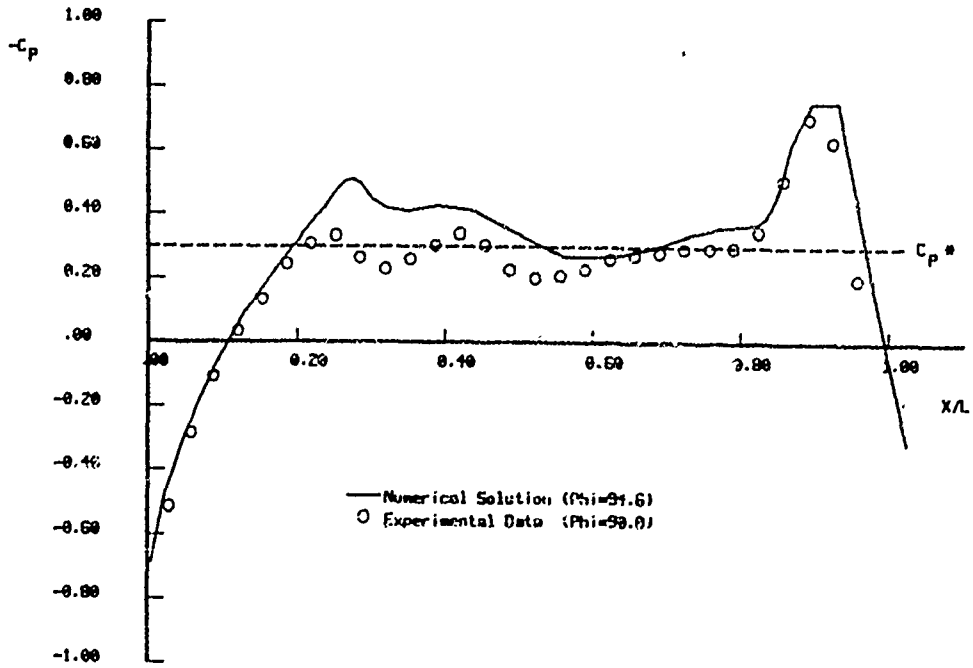

Figure 8. Surface Pressures Reflect Store Position

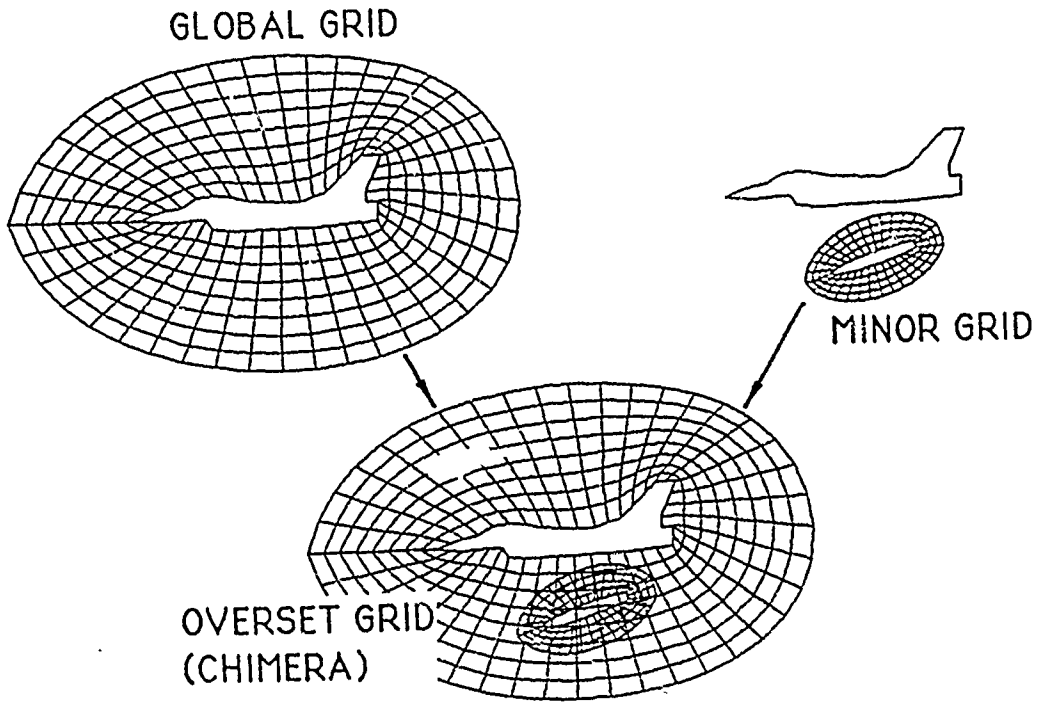

Figure 9. Chimera Grid Scheme Allows Minor Grids About Stores To Overset Global Grid

single iteration, the flow solver computes the aerodynamics on the global grid, interpolates for flow properties at the boundary of the minor grid, computes the aerodynamics on the minor grid, and finally, interpolates the flow properties at the boundary of the minor grid back to the global grid.

The overset grid scheme allows grids to be generated more rapidly, points to be clustered in critical regions, and relative movement between bodies. The primary disadvantage is that a complex bookkeeping system is required to handle the information exchange between the global and minor grids. This problem is compounded by the fact that small errors in the interpolation schemes can build into substantial errors during the many iterations required to obtain converged solutions.

The dynamic simulation of a three-dimensional body of revolution moving relative to a flat plate is presented in Reference 7. In this example, Figure 10, the store was placed initially at a position equivalent to 15% of the chord of the store below the flat plate and moved along a prescribed path at the rate of approximately a half chord length per second. Computed density contours after 660 iterations are shown in Figure 11.

Unstructured Grids - Unstructured grids are an even more promising and newer approach for simulating dynamic aircraft/store separation that does not impose any order requirements on the distribution or connection of grid points, such as that imposed by structured grid techniques. This approach offers geometric flexibility and ease of gridding compared with structured grid methods. Only the surface of the configuration and the outer boundary of the computational domain must be explicitly defined. Subsequently, unstructured grid generation techniques automatically discretize the region with a set of tetrahedral cells. This approach to grid generation can significantly reduce time to develop complex grid systems. Among the techniques for generating three-dimensional grids are Octree, Advancing Front, and Delaunay methods.

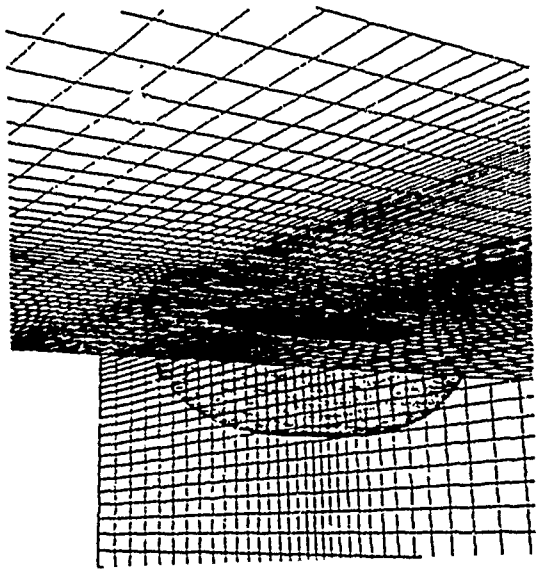

Figure 10. Overset Grid For A Store Near A Flat Plate

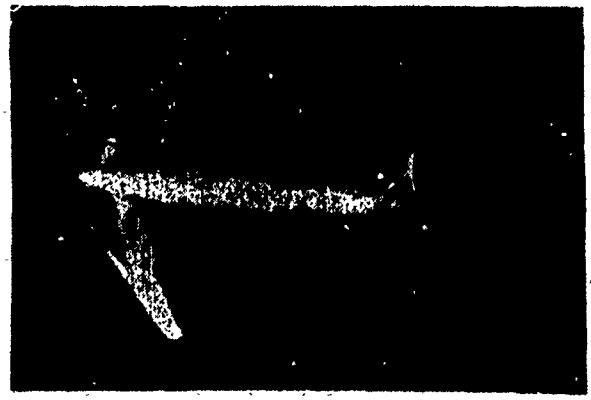

Figure 11. Chimera Grid Flow Field Solution Of Store Near Flat Plate

In a project at General Dynamics Fort Worth Division, a 2-D unstructured grid was generated with a Delaunay method to represent the symmetry plane of the F-16 and a generic store for a Mach 2.0 Euler solution. The initial grid was composed of 5,000 points, as shown in Figure 12. The redistributed solution adaptive grid and the steady-state flow solution for the geometry with the store in its captive position is shown in Figure 13a. High pressure gradients near the nose of the store and along shock waves are clearly delineated by the automatic clustering of the cells.

A major advantage of unstructured grids for aircraft/store separation is that cells can be added or deleted at runtime to adapt the grid to both flow field gradients and moving boundaries. As the store is moved along its path, the cells are stretched until they meet a skewness criteria. At this point, flow field gradients determine whether the skewed cells are split to increase grid resolution or combined with neighboring cells to reduce grid resolution. In this manner, the local flow field gradients drive the grid density as the solution evolves. The F-16 grid with the store a substantial distance along its trajectory is shown in Figure 13b. In this grid, the number of points was allowed to increase to approximately 10,000 points to improve the resolution of shock waves and to divide skewed cells as the weapon moved.

Objectives For A Near-Term CFD Code

Each of the examples shown above (and all others in open literature) include simplifications that preclude accurate predictions for actual hardware releases. However, the capability to accurately simulate aircraft/store flow fields during separation is judged by the authors to be within the near-term grasp of the CFD community. The approach that should be used is illustrated in Figure 14. First, a steady-state solution should be computed with the store in the captive trajectory. Then, unsteady calculations should start that include ejection forces on the store, the inertial characteristics of the store, and unsteady aerodynamic fluctuations. The iterative solution should generally entail the following four steps:

1. Sum external aerodynamic and ejection forces on the store.
2. Employ the six-degree-of-freedom equations of motion to compute a new store position after a small increment in time.
3. Automatically modify the grid to accommodate the new position of the store. This may entail minor modifications to the existing grid or periodic major modifications, depending on the type of grid system.
4. With the new grid and the previous CFD solution, compute a new iteration of the solution with the CFD solver.
5. Evaluate criteria to determine if the store is outside the influence of the parent vehicle.

CFD codes with the capability to perform this task must be able to simulate a wide range of aerodynamic phenomena and have certain other characteristics relevant to implementation procedures. Some of these issues are addressed for several combinations of the CFD equations and grid models in Figure 15. The issues involved are divided into two groups: those primarily dependent on the CFD equations and those primarily dependent on the type of grid model.

The combinations of equations and grid models in Figure 15 are arranged in order of increasing capability. But unfortunately, this is also the order of decreasing maturity and increasing computer time requirements. Potential-flow codes are presently available that can exploit this technology to its fullest extent at reasonable computer costs. Euler and Navier-Stokes codes are currently available that can produce static solutions on structured grids with large amounts of computer time. On the other hand, Euler and Navier-Stokes codes for overset and unstructured grids promise excellent solutions of the dynamics of store separation, but require extremely large amounts of computer time and are several years away from a mature capability.

5. COMPUTING POWER REQUIREMENTS

If a time-accurate, turbulent Navier-Stokes code with all the capabilities discussed above were available, it could simulate aircraft/store separation, even on today's supercomputers. However, the large amount of time required to accomplish this would render the solution highly impractical. The CFD equations and/or the geometry would have to be simplified in order to keep computer run time at a tolerable level. So, why invest in CFD codes if adequate computer hardware is not available?

Recent history has shown that exceptional increases in computer speed and memory capacity and reductions in computing cost are realized on a continuous basis. NASA's Numerical Aerodynamic Simulator (NAS) Facility program plan for 1989 (Reference 8) reported that their eight-processor CRAY Y/MP was delivering one GFLOP of sustained computing performance at that time. It also projected that new generations of computers would provide TeraFLOP performance (one trillion operations per second) by the year 2000. The pace of this 1000-fold increase is shown in Table 1. A computer with this speed could provide for the simulation of entire aerospace vehicle systems

TABLE 1. PERFORMANCE OBJECTIVES FOR NAS SYSTEM

YEAR	SUSTAINED GFLOPS	COMPUTER
1989	1	CRAY Y/MP
1991	3	UNDEFINED
1994	20	UNDEFINED
1997	100	UNDEFINED
2000	1000 (TERAFLOP)	UNDEFINED

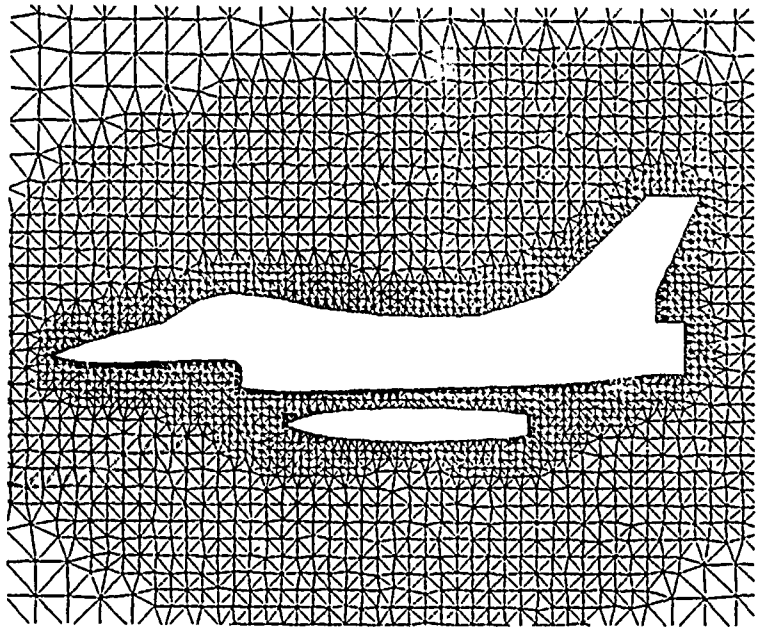

Figure 12. Initial 2-D Unstructured Grid For The F-16

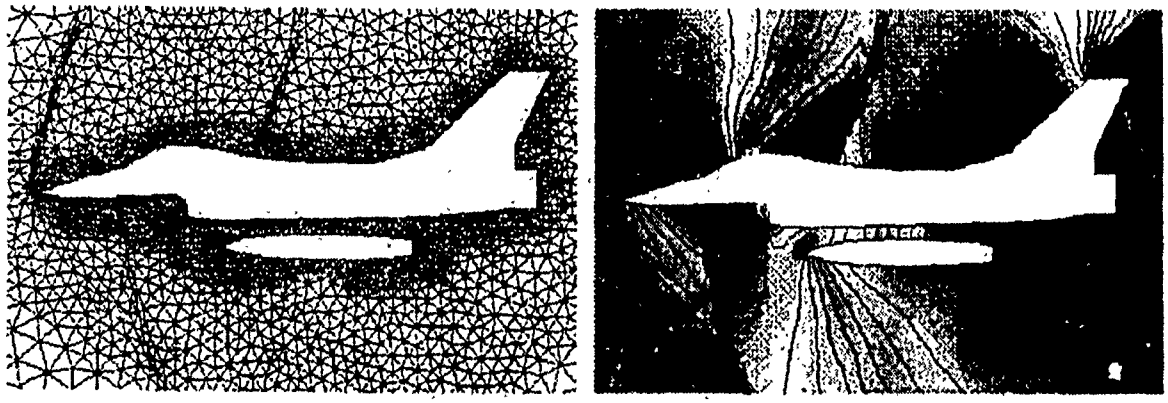

(a) Converged Solution on Adapted Grid

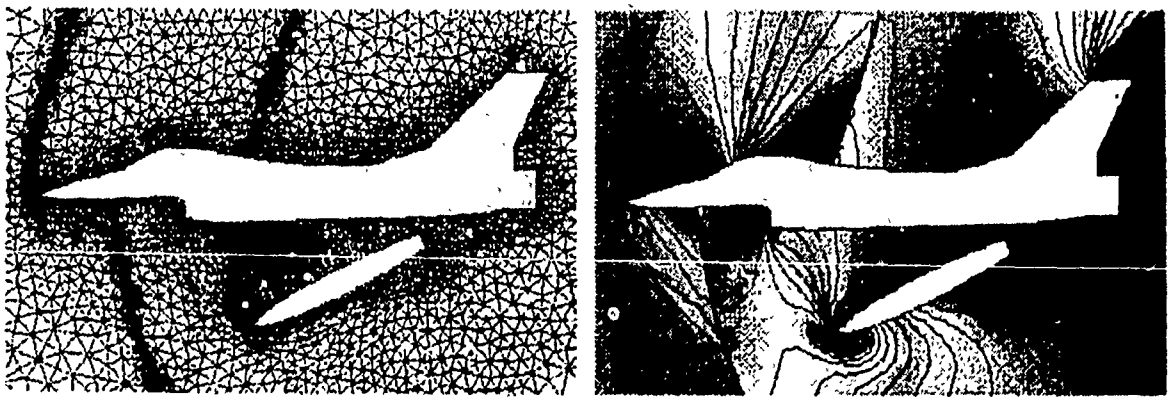

(b) Time Accurate Solution on Moving Grid

Figure 13. Unstructured Grid Capabilities Are Represented By A 2-D Solution On The Symmetry Plane Of An F-16

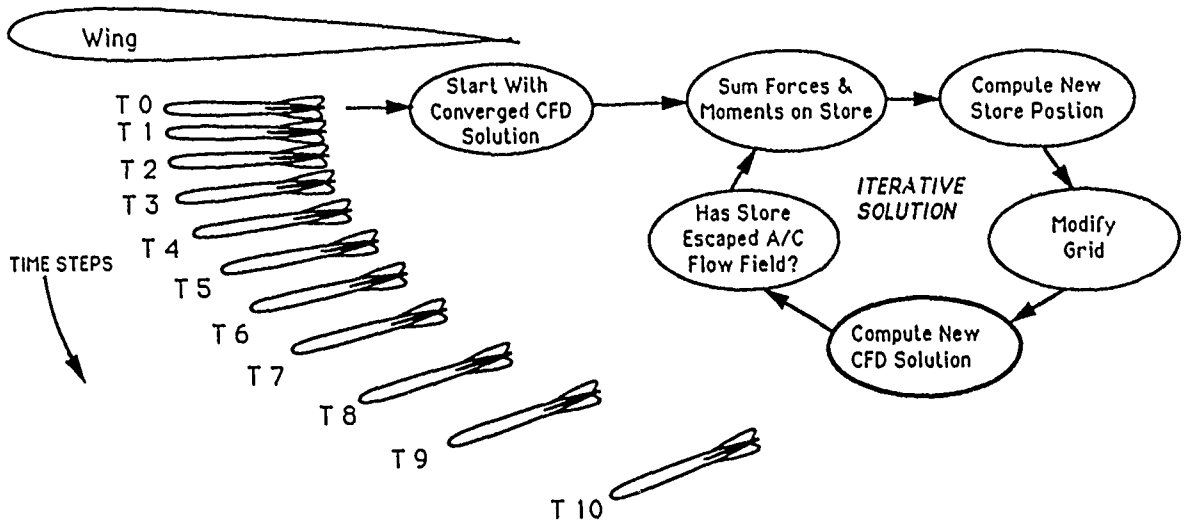

Figure 14. CFD Equations And Mechanical Equations Of Motion Can Be Coupled For Accurate Aircraft/Store Simulations

		EQUATION ISSUES						GRID ISSUES		
CFD EQUATIONS	GRID MODEL	Aircraft/Store Interference	Surface Pressures	Flow Field Properties	Vortices	Viscous B.L. Effects (Separation)	Unsteady Effects	Adaptive to Flow Field	Moving Bodies	Ease of Solution
Potential Flow	Surface Panels	√	√	limited						
Euler	Structured	√	√	√	limited		√	limited		
Navier-Stokes	Structured	√	√	√	√	√	√	limited		
Navier-Stokes	Overset	√	√	√	√	√	√	limited	√	
Navier-Stokes	Unstructured	√	√	√	√	√	√	√	√	√

Figure 15. Equation Forms And Grid Types Determine The Applicability Of CFD To Aircraft/Store Compatibility Studies

in a few hours. These capabilities are projected to come from advanced commercial systems, which are expected to be highly parallel. Computer companies are exceeding expectations and are developing systems that may provide TeraFLOP computing in the 1993 to 1995 time period. Four of these systems are discussed below.

Cray Research, Inc. is working on an advanced computing architecture for the mid-90s that will be a general-purpose machine with TeraFLOP-class performance for scientific problems. Their C-95 design, for instance, is expected to have 64 processors, a clock cycle time of 2 nano-seconds, longer vector lengths, an increased number of parallel pipes per processor, and a reduced number of instructions per floating point operation.

The Mega Machine is being developed by Thinking Machines, Inc. with a $12 Million grant from the Defense Advanced Research Projects Agency (DARPA). According to Reference 9, this is to be a TeraFLOP computer with as many as a million processors. It is based on the Connection Machine, which contains 64,000 simple processors and performs many tasks at speeds significantly above the Cray X/MP. Unstructured grid CFD codes are easily adaptable to this type of architecture. A recent publication (Reference 10), indicated that an unstructured grid solution could be computed about four times faster on a fully configured Connection Machine than on the Cray X/MP. Furthermore, new interprocessor communication software promises to increase this factor to about ten times the Cray X/MP speed.

The Touchstone computer is a promising next generation computer being developed by Intel Scientific Computers Inc. According to Reference 11, this computer is being partially funded by a $7.6 million DARPA contract. It will eventually have as many as 2,048 processors, each of which will have power near that of a Cray-1 supercomputer. Plans call for a Touchstone by the early 1990s with a performance level 50 to 100 times that of the Cray Y-MP.

Another recent entry into the next-generation supercomputer competition is the DARPA-sponsored DST computer, which is in the early stages of development by a team composed of Titan Corporation, Supercomputing Solutions, Inc., and Princeton University (Reference 12). The name DST is derived from the ultimate objective of the computer, which is to compute direct simulation of turbulence (DST), one of the grand challenges in computational fluid dynamics. The architecture of this machine is different in that it includes three levels of parallelism and is being specifically designed for selected scientific applications, primarily computational fluid dynamics.

It is obvious that computers with the power to handle unsteady, viscous, 3D flow field computations with a reasonable amount of time and money will be available in just a few years. Therefore, the answer to the question raised at the beginning of this section is, yes, it is worthwhile to invest in CFD methods, even though they are not practical on current computers.

6. THE ROLE OF CFD

The maturity of CFD must be advanced before it can significantly impact the current conventional approach to defining aircraft/store compatibility. Computer codes must be validated under a wide variety of conditions to establish confidence in their ability to model store releases. The general philosophy for integrating CFD into aircraft/store separation activities should be to consider it as a tool for supplementing hardware testing that can substantially reduce the number of test parameter variations in experimental programs.

As an example, consider a hypothetical test program to establish the compatibility of a multiple-carriage smart bomb and a modern high-speed aircraft in which CFD is substituted for selected store releases. The weapons are to be wing-mounted adjacent to fuel tanks, which adds the requirement for tank releases to verify that interference effects of the new configuration will not adversely affect the safe release of the tank. Test plans for a certification program with and without CFD are shown in Table 2. Conventional certification tests for this store require the release of 20 weapons and 8 tanks at the flight conditions indicated. It is reasonable to assume that CFD solutions could substitute for about 50% of the hardware releases, leading to the indicated reduction in hardware. Hardware releases could be made at selected operating conditions, and CFD solutions could be computed at all conditions to fill in the gaps and to assure that the trends are reasonable. A similar test plan for trajectory analysis is shown in Table 3. Conventional tests to determine separation effects on ballistics of the weapon require the release of an additional 24 weapons at a variety of airspeed and g-loading conditions. Credence for the use of CFD on the particular configuration being tested should be established during the certification tests, and subsequent trajectory analysis could perhaps be accomplished with only 10 hardware releases.

7. ACCEPTANCE BY MANAGEMENT

Gaining the acceptance of CFD by management, ordnance commanders, and pilots will require substantiation of the accuracy of the methods and convincing arguments for the benefits, which include safety, timeliness, costs, and the ability to compute solutions at conditions were aircraft cannot or should not fly.

TABLE 2. TYPICAL STORE RELEASE REQUIREMENTS FOR CERTIFICATION

FLIGHT CONDITIONS			WITHOUT CFD		WITH CFD	
MACH	'g' LOAD	ALTITUDE	WEAPONS	TANKS *	WEAPONS	TANKS
0.8	1	5K	2	2	1	1
0.9	1	5K	2	1	1	1
0.95	1	8K	2	2	1	1
1.1	1	13K	2	1	1	
1.2	1	18K	4	2	2	1
1.2	0.7	18K	4		2	
1.2	0.5	18K	4		2	
		TOTAL =	20	8	10	4

First tank drop is with tank empty, second is with partial fuel.

TABLE 3. TYPICAL STORE RELEASE REQUIREMENTS FOR TRAJECTORY ANALYSIS

FLIGHT CONDITIONS			WITHOUT CFD		WITH CFD	
MACH	'g' LOAD	ALTITUDE	WEAPONS	TANKS	WEAPONS	TANKS
0.7	1	SL	4		2	
0.7	4	SL	4		2	
0.9	1	SL	4		2	
0.9	4	SL	4		2	
1.1	1	18K	4		1	
1.2	1	18K	4		1	
		TOTAL =	24	0	10	0

Accuracy

CFD solutions for aircraft/store separation test cases must be computed and compared with known experimental data in order to establish the accuracy of CFD. Data needed for this task are much more detailed than that normally acquired in compatibility studies. Most current wind tunnel tests for aircraft/store compatibility are primarily to determine the trajectory of the store. Therefore, selected wind tunnel tests should be conducted for the specific objective of providing detailed data with which to validate CFD codes. Instrumentation should be included to measure surface pressures, forces on the aircraft and store, and detailed flow field properties. The fundamental aerodynamic flow properties must be computed and compared with this type of data to assure that the computations accurately portray the flow field.

Safety

Experienced personnel in the area of aircraft/store compatibility are keenly aware that safety is of utmost importance. The carriage and release of new stores, or old stores in new arrangements, can result in unexpected trajectories for the released store. Collisions between stores and between store and aircraft are not uncommon. Wind tunnel tests and conventional analysis methods are used to assess potentially dangerous situations prior to actual flight tests, but unfortunately, these methods have not always alerted engineers to potential hazards. A fully developed and verified CFD method will provide a safe and accurate means for evaluation of new store loadings and/or expanded carriage and release conditions prior to flight tests.

Timeliness

The availability of stores sometimes delays flight tests or extends the schedule outside the window in which other assets, such as aircraft or test facility, are available. Stores produced in foreign countries and carried on American aircraft are a special problem. Transferring the store to the United States to analyze carriage, release, and ballistic separation effects for a foreign base or a foreign country can be a lengthy process. A validated CFD tool could be used to predict these effects, preventing scheduling problems commonly associated with these tests.

Special Flight Conditions

There are flight conditions at which conventional analytical methods and/or wind tunnel testing are not reliable. Store separation at transonic speeds, for instance, has proven extremely difficult to predict with conventional analytical methods and wind tunnel scale effects sometime distort the true separation picture. Supersonic store separation effects are also difficult to predict with conventional analytical methods and wind tunnels. This is compounded by the limited amount of data and experience for this speed regime.

The hardware community has not yet been faced with the problem of releasing stores at hypersonic speeds. However, aircraft with this capability are being studied, and store compatibility engineers are likely to encounter this problem in the future. Stores will not simply drop from the aircraft at these speeds because of the aerodynamic forces but will have to be ejected forward, aft, or upward from the parent vehicle. Additionally, hypersonic vehicles may carry stores internally, greatly affecting the aerodynamic flow field upon release. Existing technologies will likely be unacceptable for these cases, and CFD may be the only method that can be used to predict separation characteristics.

Costs

The most immediate and visible benefit of using CFD to supplement flight testing will be the cost savings, which are difficult to predict because of three important items:

- The role of CFD
- The cost of store hardware and aircraft operating expense
- The efficiency of the CFD solvers and computer costs

The best that can be done at this time is to make assumptions about these issues and derive corresponding cost savings that could be realized by using CFD in aircraft/store compatibility studies. Based on the role of CFD presented above, the following paragraphs present an approach to assessing the cost benefits. In the hypothetical flight test program discussed above, assume that the smart weapons are valued at $30,000 each, the fuel tanks are valued at $20,000 each, and the operational expenses of the aircraft average approximately $10,000 per released store. A summary of the total costs of this conventional flight test program is summarized in Table 4(a).

TABLE 4. COST OF COMPATIBILITY TESTS

(b) WITH CFD

COST ITEM	UNIT COST	NUMBER FOR CERTIFICATION	NUMBER FOR TRAJECTORY	NUMBER TOTAL	COST TOTAL
WEAPON	$30,000	10	10	20	$600,000
TANK	$20,000	4	0	4	$80,000
AIRCRAFT	$10,000	14	10	24	$240,000
CFD RUNS	$20,000	15	6	21	$420,000
					$1,340,000

(a) WITHOUT CFD

COST ITEM	UNIT COST	NUMBER FOR CERTIFICATION	NUMBER FOR TRAJECTORY	TOTAL STORES	COST TOTAL
WEAPON	$30,000	20	24	44	$1,320,000
TANK	$20,000	8	0	8	$160,000
AIRCRAFT	$10,000	28	24	52	$520,000
					$2,000,000

Each computer simulation of a store release in the mid-1990s is estimated to cost about $20,000 based on the following: steady-state, 3-D Euler solutions on simple bodies can be computed on today's supercomputers in about 10 hours at a cost of about $20,000. CFD algorithms are continually being improved and computer speeds are projected to increase by 2 to 3 orders of magnitude. Therefore, it should be reasonable to assume that an equal amount of computer time and computer cost should be ample for a Navier-Stokes simulation of an aircraft store release.

The cost of the program with CFD in the role described above is summarized in Table 4(b). With these assumptions, the overall cost could be reduced by $660,000, which is 33% of the total program cost. It should be noted that the cost of store hardware is a very important factor in determining the cost-effectiveness of CFD. If the approach discussed above is applied to low-cost stores, then CFD may not be an economical tool. On the other hand, when high-cost stores are involved, CFD may provide the only economically-feasible approach to assess aircraft/store compatibility. Similar estimates for the savings of using CFD to supplement tests involving weapons with a wide range of costs are presented in Figure 16.

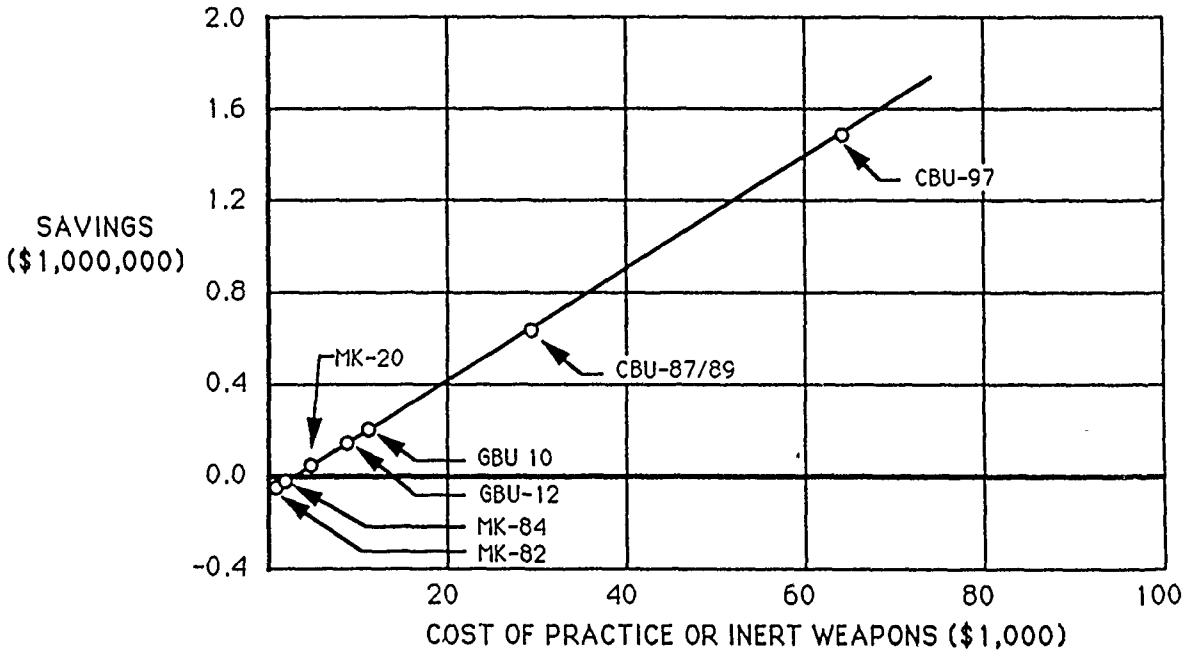

Figure 16. Cost Savings Are Strongly Dependent On The Value Of The Store

8. CLOSING REMARKS

When CFD methods reach maturity, aircraft designers, test engineers, and ordnance commanders will be able to use them to supplement wind tunnel and flight testing. Basic CFD technologies are available today for building codes to simulate the unsteady aerodynamics of multi-body problems, but developing a practical analysis tool will take a matter of years. In the meantime, computers with the memory and speed to calculate solutions will be developed. The CFD community, in the authors' opinion, should be working toward methods that will treat turbulence, vortices, and viscous separation, while adapting the grid to the flow field and allowing multiple bodies to move according to six-degree-of-freedom equations of motion. The potential benefits are extremely high and fully justify efforts to advance CFD technology for future integration into store separation methodologies.

REFERENCES

1. S.L. Karman, Jr., J.P. Steinbrenner and K.M. Kisielewski; "Analysis of the F-16 Flow Field by a Block Grid Euler Approach", AGARD 58th Symposium on Applications of Computational Fluid Dynamics in Aeronautics, Paper No. 18, 7-10 April 1986.
2. G.W. Huband, J.S. Shang, and M.J. Aftosmis; "Numerical Simulation of an F-16A at Angle of Attack", AIAA Paper 90-0100, January 1990.
3. J. Flores and J.M. Chaderjian; "A Zonal Navier-Stokes Methodology for Flow Simulation About A Complete Aircraft", AIAA Paper 88-2508, June 1988.
4. E. W. Harding; "F-16 Flight Load Survey and Dynamic Response Tests, Final Test Report", General Dynamic Report 16PR988, Addendum 1, September 17, 1984.
5. A. Cneko and E.N. Tinoco; "PAN AIR -Weapons, Carriage and Separation", AFFDL-TR-79-3142, December 1979.
6. David L. Whitfield and Joe F. Thompson; "Computation of Transonic Flow About Stores", AFATL-TR-89-20, June 1989.
7. F.C. Dougherty and J-H Kuan; "Transonic Store Separation Using a Three-Dimensional Chimera Grid Scheme", AIAA Paper 89-0637, January 1989.
8. "Numerical Aerodynamic Simulation Program Plan", Numerical Aerodynamic Simulation Systems Division, National Aeronautics and Space Administration, Ames Research Center, NP-1000-02-C00, October 21, 1988.
9. John Burgess; "$12 Million Grant for Fast Computer", The Washington Post, November 29, 1989.
10. J.S. Clary, G.A. Howell, and S.L. Karman, Jr.; "Benchmark Calculations With an Unstructured Grid Flow Solver On A SIMD Computer", Published in the Proceedings of the Supercomputing '89 Conference, Reno, Nevada, November 1989.
11. Gary H. Anthes; "Intel Lands DARPA Super Award", Federal Computer Week, Vol. 3, No. 15, April 10, 1989.
12. "Direct Solution of Turbulence (DST) Phase 0 Review", La Jolla, California, Sponsored by DARPA, 30-31 May 1990.

BIOGRAPHY: GEORGE A. HOWELL

Mr. Howell earned a Bachelor's degree in Aerospace Engineering from Auburn University in 1966 and a Master's degree in Aerospace Engineering from the University of Arizona in 1968. Since graduation, he has been continuously employed at the Fort Worth Division of General Dynamics, where he has gained a broad range of experience in aerodynamics.

For ten years, he provided aerodynamic support to advanced aircraft programs. Specific duties included the analysis of wind tunnel data, prediction of aerodynamic forces and moments, integrations of aircraft stores and weapons, and preparation of proposals. For the next five years, he was engaged in two projects: the development of a computer code to assess the aerodynamic degradation of an aircraft that sustains light to moderate damage from a nuclear encounter and a NASA-funded study to assess the aerodynamic characteristics of a STOL aircraft design.

In 1983, Mr. Howell joined a new group at General Dynamics to address the emerging science of computational fluid dynamics (CFD) and to integrate this science into the aircraft design environment. He is currently leading a research and development program to develop CFD software and validate its usefulness and accuracy for aircraft design. He is also managing a research project to investigate the advanced technologies of parallel computing and artificial intelligence for use in conjunction with computational fluid dynamics.

BIOGRAPHY: JACK D. WATTS

Mr. Watts received his BSEE from Texas Tech College in 1958. He joined General Dynamics (Fort Worth) in 1958. He is responsible for the F-16 weapon delivery performance. Mr. Watts developed, from scratch, the air-to-ground weapon delivery algorithms used on the F-16 aircraft. Mr. Watts was the program manager for the design and fabrication of a laboratory demonstration system for an airborne fuze control system (Fuze Function Control Technology) under a contract issued by ADTC/DLJF, Eglin AFB, Florida. Prior to the F-16 program, Mr. Watts participated in all phases of the A/C weapon delivery tasks for developing F-111 capabilities. He was the program manager for the Stores Identification Method Study conducted by General Dynamics for the Air Force Weapons Laboratory, Kirtland AFB. The objective of this study was to determine an optimum technique for a stores/stores characteristics identification system. Mr. Watts is currently the Engineering Chief in charge of the Weapons Technology Group. This group has the responsibilities for developing all of the weapon delivery algorithms (both air-to-air and air-to-ground) for all the GD/FW aircraft as well as developing the weapon/aircraft interface and integration.

THIS PAGE INTENTIONALLY LEFT BLANK

An Investigation of the Effect of Boundary Layer Gradients on Store Trajectory Predictions

F. Tessitore*, R. Romanowski and J. Laiosa
Grumman Aircraft Systems Div.
Bethpage, NY 11714

Abstract

Current methods for obtaining experimental aerodynamic data in support of aircraft/store carriage and separation simulation involves the use of scale model testing. As yet, no attempts to correct these data have been documented or are available in the open literature. While it is general practice to ignore local dynamic pressure gradients in the aircraft boundary layer in simulating the release of stores for conventional or traditional carriage, i. e., pylon mounted stores, the effect of reduced dynamic pressure on the trajectory of stores mounted within the boundary layer is unknown. Contemporary modes of carriage, namely tangent, semi-submerged and submerged (internal), have caused issues to arise such as wind tunnel to flight boundary layer correction and the effect of local dynamic pressure on store control effectiveness. The significance of these issues beg to be investigated.

With the advent of Navier Stokes solvers it is now possible to accurately calculate viscous flow effects such as those occurring in the aircraft boundary layer for both wind tunnel model scale as well as full scale flight conditions. The viscous dynamic pressure gradients within the boundary layer were thus predicted for the F-14 at a particular flight condition and comparisons of dynamic pressure gradients as well as their effect on store trajectory predictions were made for both wind tunnel scale and full scale flight. In this study, only the out of contour gradients were calculated since the control surfaces of the AIM-7 semi-submerged in the F-14 fuselage are actually slightly out of contour. Future work should consider the pressures in semi-submerged as well as fully submerged cavities with stores present.

FIGURES

INTRODUCTION

Recent investigations concerning the release of stores from cavities have revealed that significant reductions in dynamic pressure from free stream values occur in the cavity. These pressure gradients must be accounted for in both the acquisition of aerodynamic data as well as in the application of such data during the simulation of launch dynamics if reliable separation trajectory predictions are to be realized. These initial results raise the further question of the effect of dynamic pressure gradients that exist within the boundary layer of the external aircraft contour on the release characteristics of semi-submerged or tangent mounted stores. The semi-submerged fuselage carried AIM-7 serves as a typical example of such a configuration. A plan view of this configuration is shown in Fig. 1. For this investigation, the aft-most store location designated store station 4 shown shaded in the figure was chosen for analysis. The thickest boundary layer results at this aft location and it has proven to be the most difficult to obtain flight correlation with simulation using conventionally applied wind tunnel grid survey data techniques. Further it has the advantage of having a large wind tunnel data bank with which to correlate with flight test trajectories as a result of an aircraft/store recontact during early development flights, a problem that has since been corrected by improved ejector performance and subsequent improvements to the AIM-7F control system.

BOUNDARY LAYER PREDICTIONS

Methodology

Aircraft flow field simulations were obtained using the 3-D Navier-Stokes flow solver, PARC-3D[1]. This method, originally developed by NASA AMES[2], was extensively modified[1] to accommodate completely arbitrary internal/external geometries with a variety of fluid flow boundary conditions (i. e., solid boundaries, specified mass flow, and symmetry planes). Recent enhancements have been incorporated in the code by Grumman to include imbedded wakes, slip/lifting surfaces and periodic flows. Turbulent flows are simulated using the Baldwin-Lomax algebraic turbulence model.

Modelling/Grid Generation

Development of aircraft and flow field numerical representations began with the generation of a detailed surface contour model, Fig. 2. Actual aircraft surface definition was slightly modified to simplify the grid generation process and to overcome certain analysis code limitations. Primarily this modification consisted of the elimination of the inboard inlet diverter. In addition, the outer wing surfaces were not modelled in an attempt to reduce the grid size and computational running times. The outer flow field grid was generated using the 3-D grid generator 3DINGRID[3]. Grid density was increased near the surface, Fig. 3, to resolve the boundary layer flow gradients, and at the aircraft aft end location, Fig. 4, to accurately predict the effects of the horizontal and vertical tails.

Analysis

Analyses were performed for Mach = 0.98 and alpha = -2.0 degrees for both the wind tunnel test[4] Re = 2.00×10^6 and flight test Re = 5.45×10^6 per foot. Comparisons of these two cases were made by examining the aircraft lower surface local dynamic pressure fields at two particular fuselage station planes. These locations were selected to approximately correspond to the store station under investigation. The contour plots are presented in Figs. 5 & 6 for F.S. 547.3, and Figs. 7 & 8 for F.S. 626.2. As can be seen from these contours, the resulting flow fields are practically identical and therefore indicate that the subscale wind tunnel test accurately represent the full scale flight test conditions at this test condition.

APPLICATION OF DYNAMIC PRESSURE GRADIENTS

The flight condition for the store launch which was chosen for this investigation was M = 0.98, h_p = 5000 ft, hot atmosphere which corresponds to the Reynolds Number of 5.45×10^6 used in the analysis above. The dynamic pressure gradients calculated for the two fuselage stations shown above for this flight condition were plotted as a function of aircraft waterline at the fuselage centerline reference plane. Fig. 9 shows the dynamic pressure gradients at the two aircraft fuselage stations which correspond to the locations of the missile nose and the missile wing in the store station 4 carriage position shown in Fig. 1. It should be noted that the AIM-7 is a wing

controlled missile therefore fuselage station 626.2 provides the gradients at the appropriate location for the control system correction. Forming the ratio of local to free stream dynamic pressure results in a multiplier of flight free stream dynamic pressure and is shown in Fig. 10. The ratio thus formed was then incorporated into a six degree-of-freedom digital simulation of a zero "g" launch for this flight condition by correcting the aerodynamic forces and moments for reduced dynamic pressure according to the position of the store in its trajectory using several approaches.

TRAJECTORY PREDICTIONS

The first approach investigated was to apply the "q" correction to only the control effectiveness of the missile as postulated by Keen[5]. A comparison of this prediction with the uncorrected prediction as well as the flight trajectory is shown in Fig. 11. A more detailed comparison can be made for the same three trajectories by examining the path of the center of gravity of the missile, Fig. 12. As can be observed from the figure, although the correction moves the trajectory in the proper direction, i. e., toward the flight test trajectory, relatively little effect is observed due to applying the correction to the control parameters alone. The flight trajectory shown is that produced by simulation using the aerodynamic forces and moments derived by parameter identification from telemetered flight data of the early store recontact trajectory cited above.

In view of the relatively small correction realized from the application of the dynamic pressure ratio correction to the control effectiveness alone, a second approach was investigated. This consisted of applying the "q" ratio to the interference coefficient increments (delta coefficients) as well as the control parameters. A comparison of the results of the simulation using this approach with that of the former is shown by the last curve in Fig. 12. Using this approach a much larger effect is noted driving the trajectory much closer to the flight derived trajectory, however it should be noted that since the wind tunnel-to-flight boundary layer effects are virtually identical, the application of this ratio to the delta coefficients overcorrects the data and thus the prediction is not considered to be valid. It is, however, presented here in the interest of showing the potential sensitivity of the correction to the delta coefficients where vast differences might occur between local and free stream dynamic

pressure such as might be obtained from wind tunnel data where little or no boundary layer exists.

CONCLUSIONS

From the results of this study it was observed that, although small, the dynamic pressure gradients in the boundary layer are a factor to be considered in the application of wind tunnel acquired force and moment grid survey data to launch dynamics simulation. Though for the 10% scale data utilized in this study the gradients were virtually identical, the differences can be expected to be somewhat more pronounced with smaller scale testing at the same wind tunnel Reynolds numbers. Future studies of dynamic pressure within aircraft contours such as semi-submerged cavities or weapon bays should include the effects of the gradients on the total aerodynamic coefficient as well as the control power to provide a more complete assessment of the weapon bay effects on store launch dynamics.

References

1. Cooper, G. K.,"The PARC Code : Theory and Usage", AEDC-TR-87 24, October 1987.

2. Pulliam, T. H., "Euler and Thin Layer Navier-Stokes Codes : ARC2D, ARC3D", *Notes for Computational Fluid Dynamics User's Workshop*, The University of Tennessee Space Institute, Tullahoma, Tennessee, (UTSI Publication EO2-4005-023-84), March 12-16, 1984, pp. 15.1-15.85

3. Dorrel, Jr., E. W., and McClure, M. D., "3D INGRID : Interactive Three-Dimensional Grid Generation", AEDC-TR-87-40, April 1988.

4. de Kuyper, R.E., "Transonic Wind Tunnel Tests of a Sparrow Missile in the Presence of an F-14A Airplane (U)," Calspan Report No. AA-4001-W-18 (2 volumes), Dec. 1973.

5. Keen, K.S., "Evaluation of Missile Control Fin Effectiveness in a Bay Environment," Weapons Carriage and Separation Workshop, NADC, PA, 25-26 April 1989.

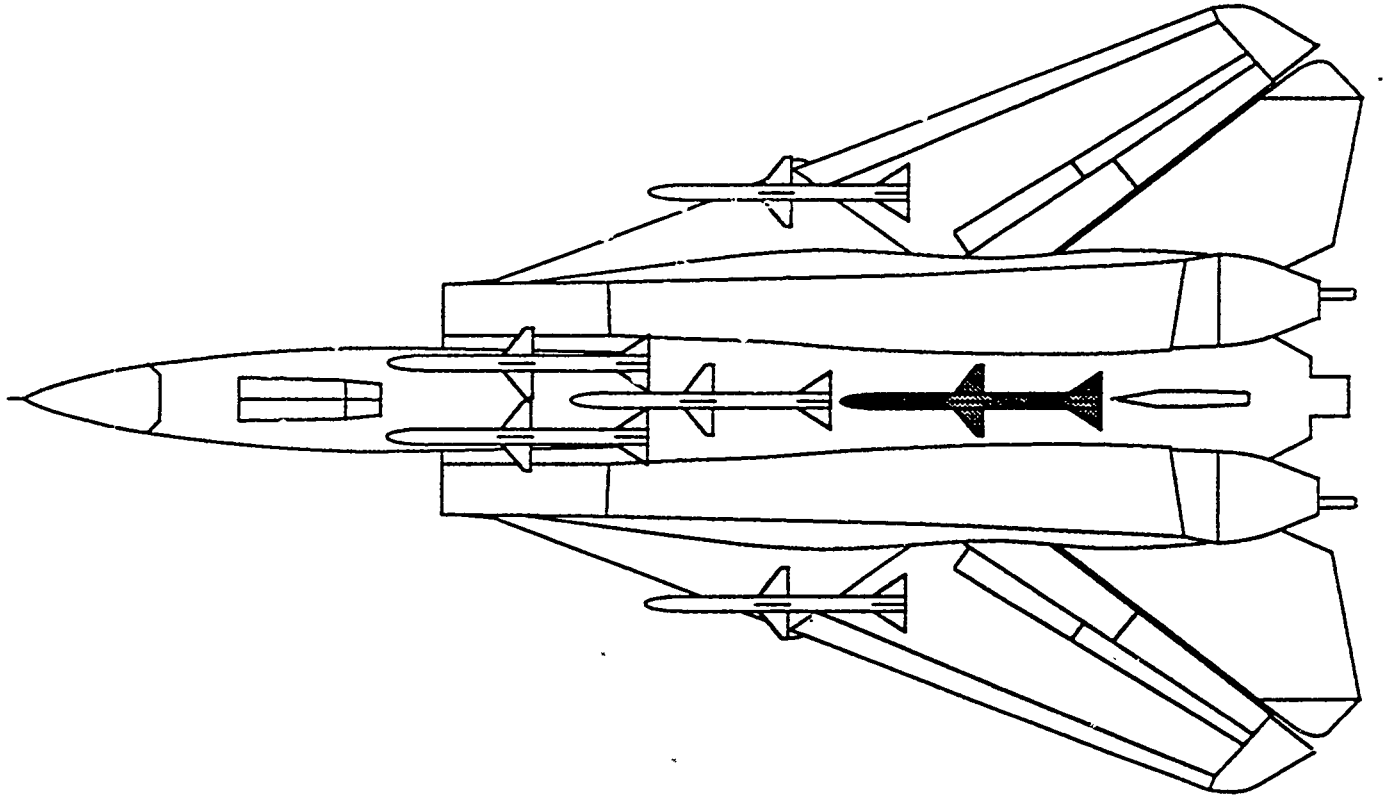

Fig. 1. F-14/AIM-7 Store Station Locations

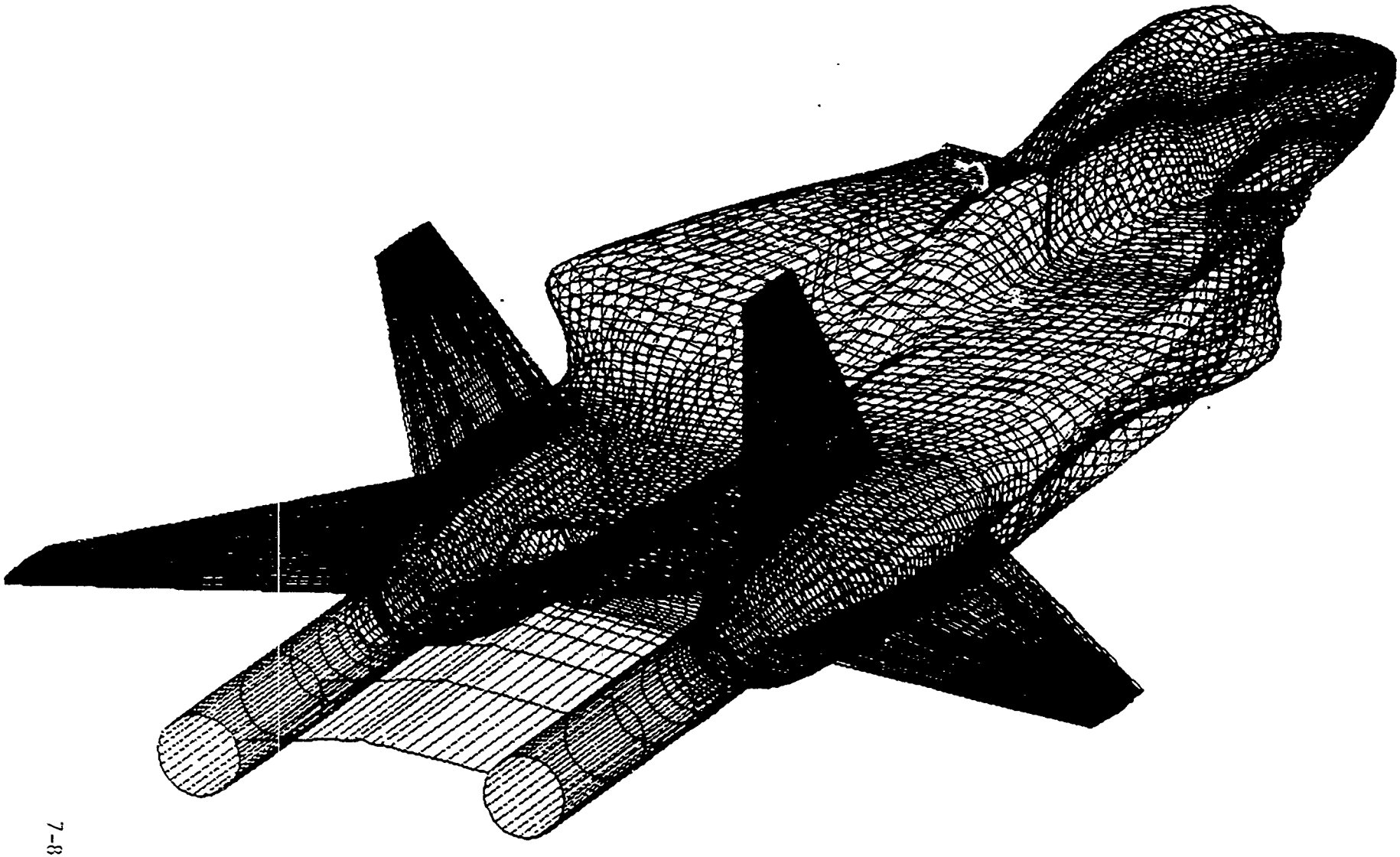

Fig. 2. F-14 Detailed Surface Contour Model

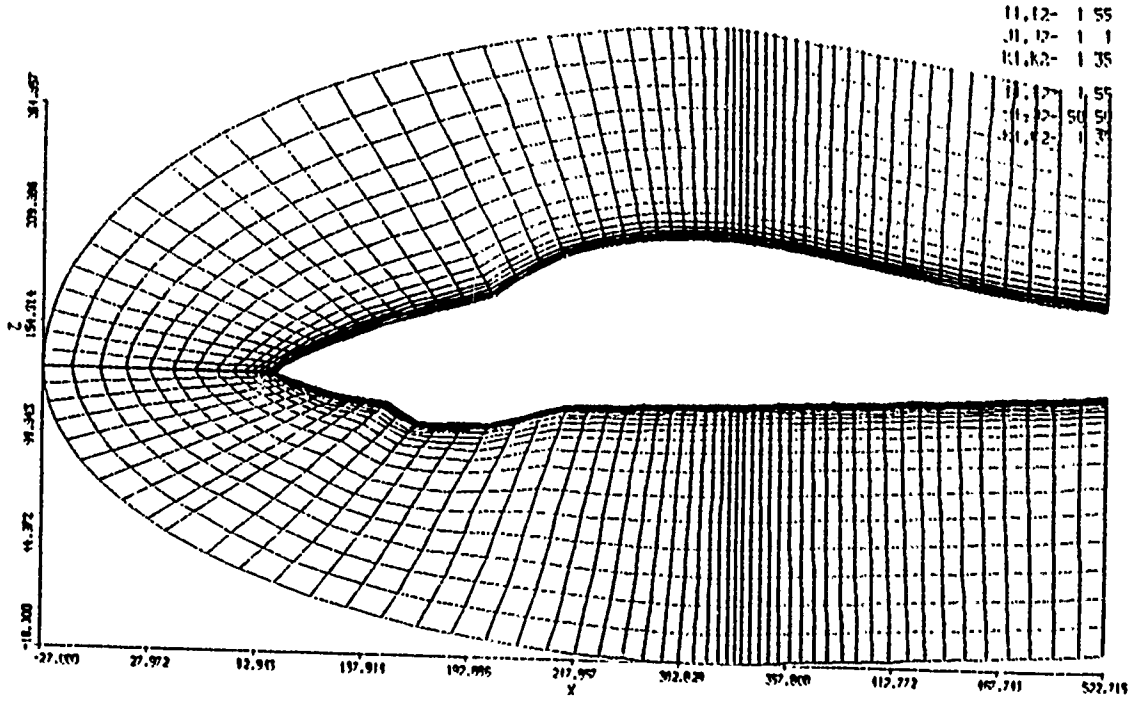

Fig. 3. F-14 Forward End Grid Density

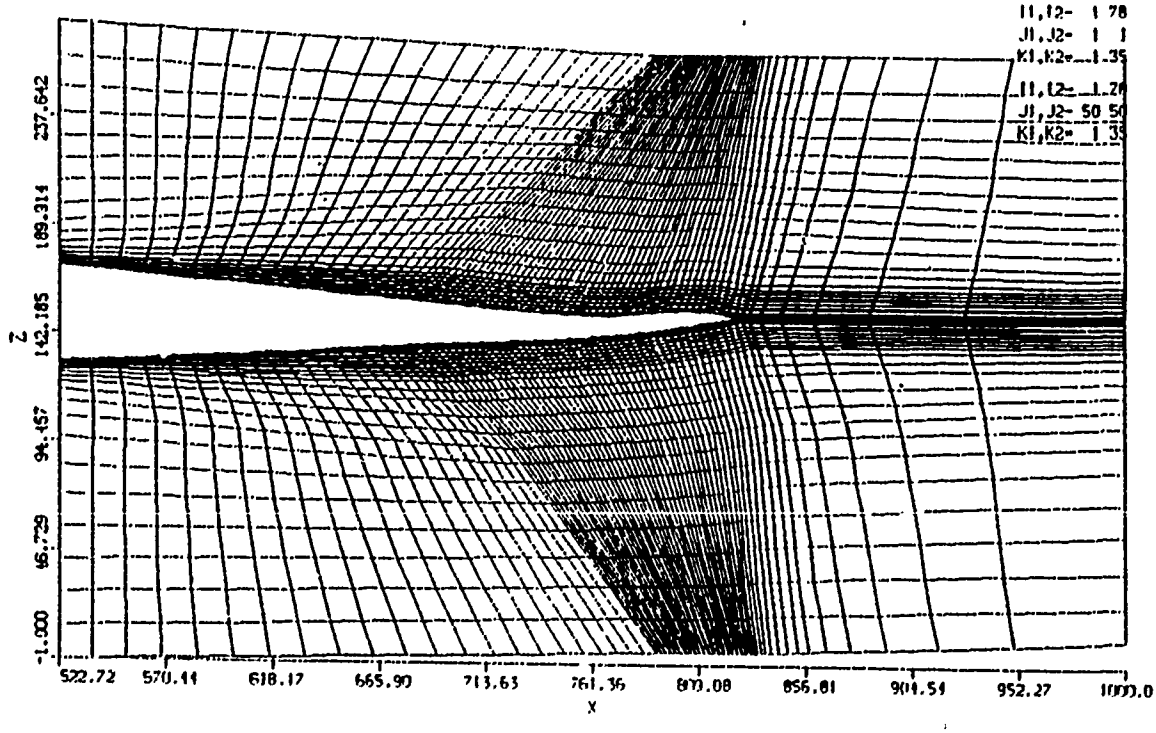

Fig. 4. F-14 Aft End Grid Density

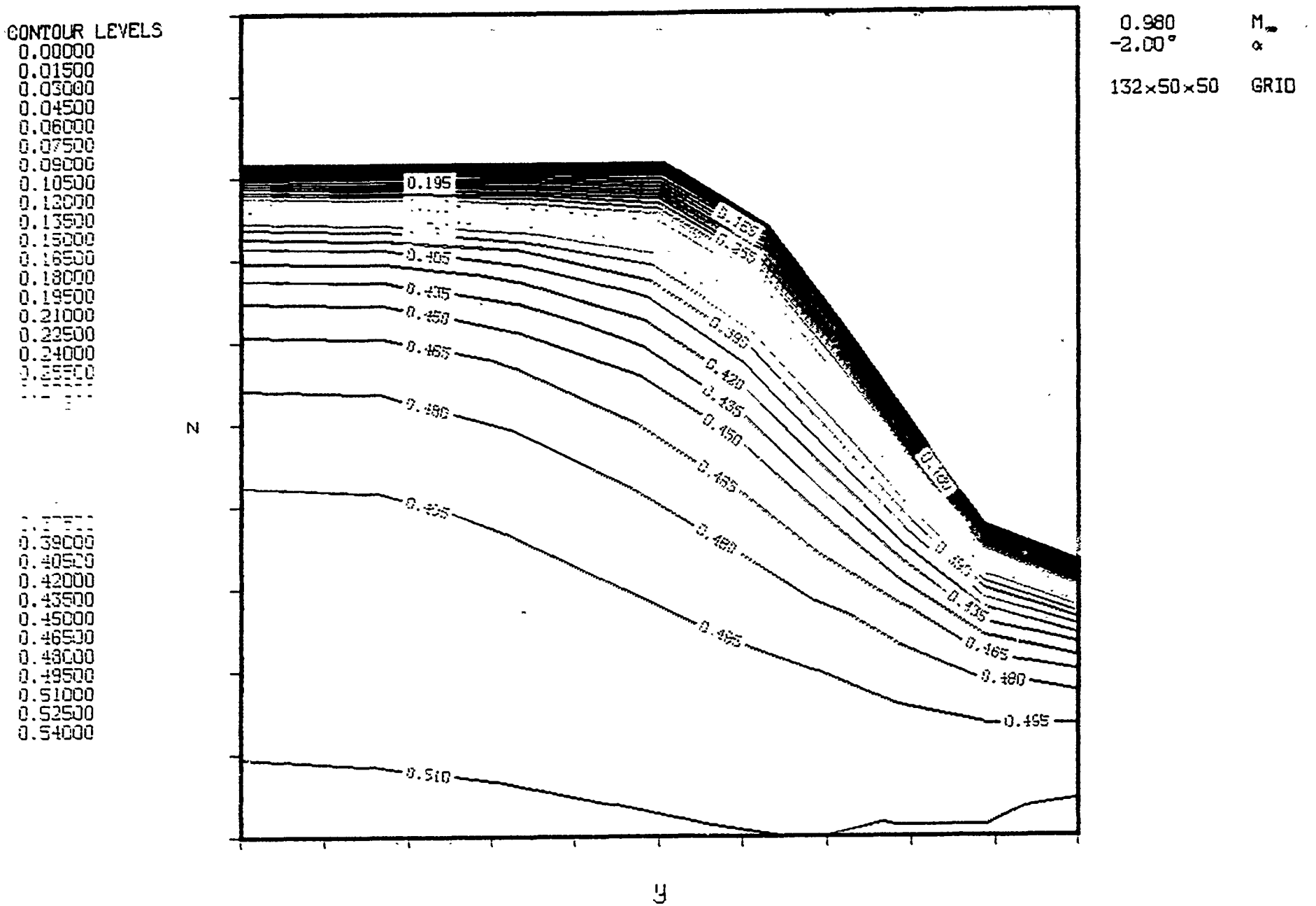

Fig. 5. Dynamic Pressure Contours for Wind Tunnel Test Conditions at FS 547.3

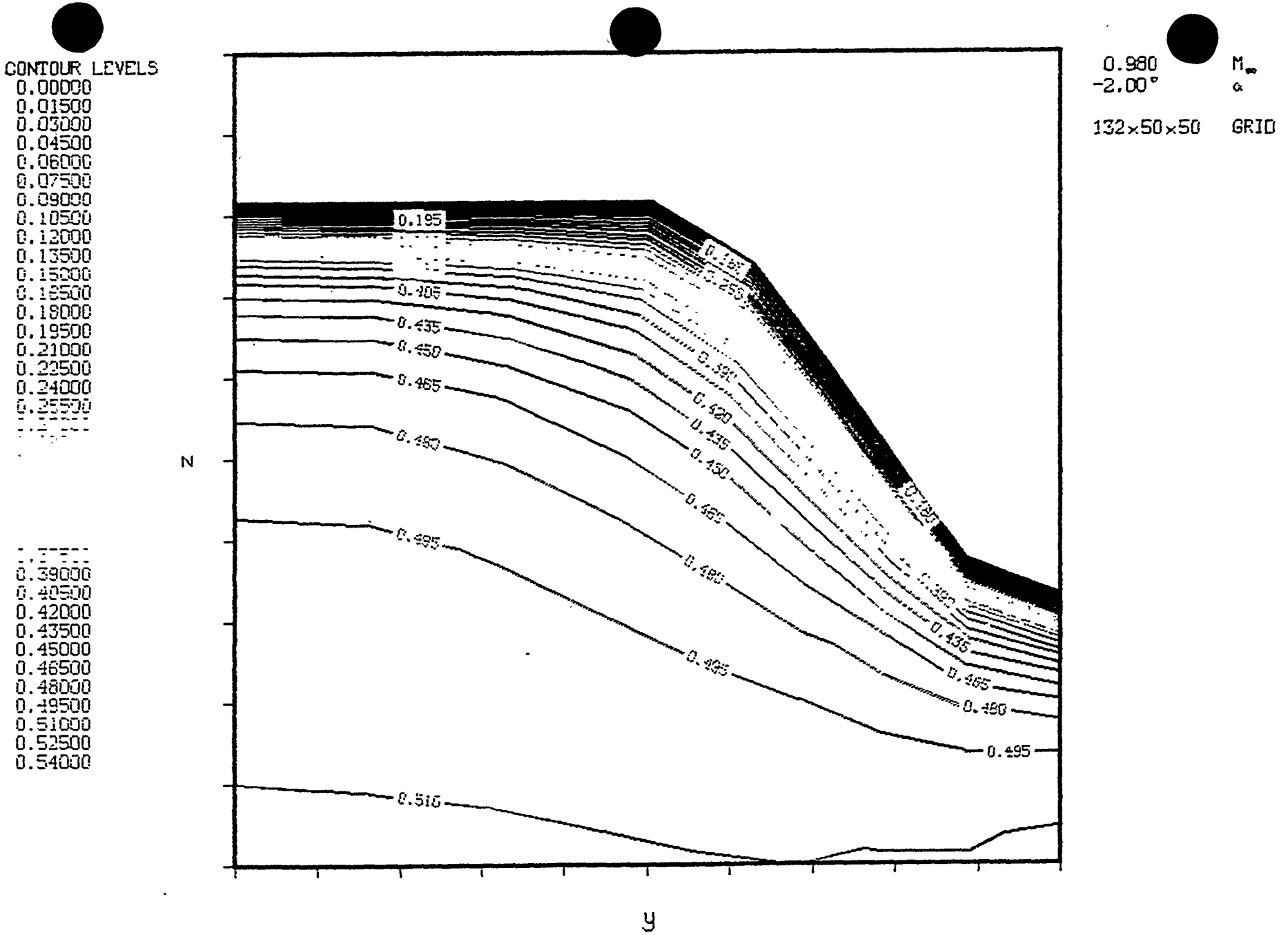

Fig. 6. Dynamic Pressure Contours for Flight Conditions at FS 547.3

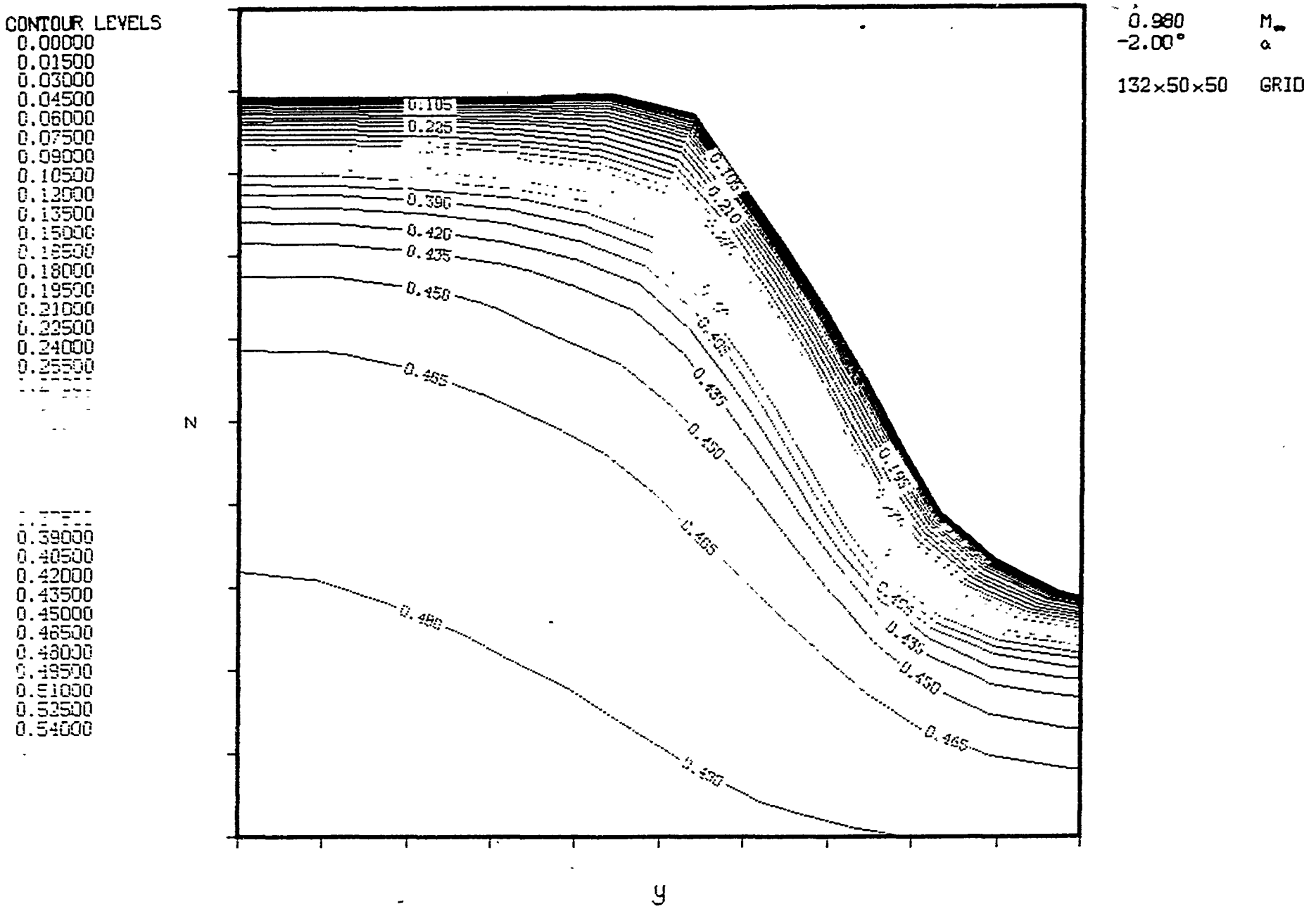

Fig. 7. Dynamic Pressure Contours for Wind Tunnel Test Conditions at FS 626.2

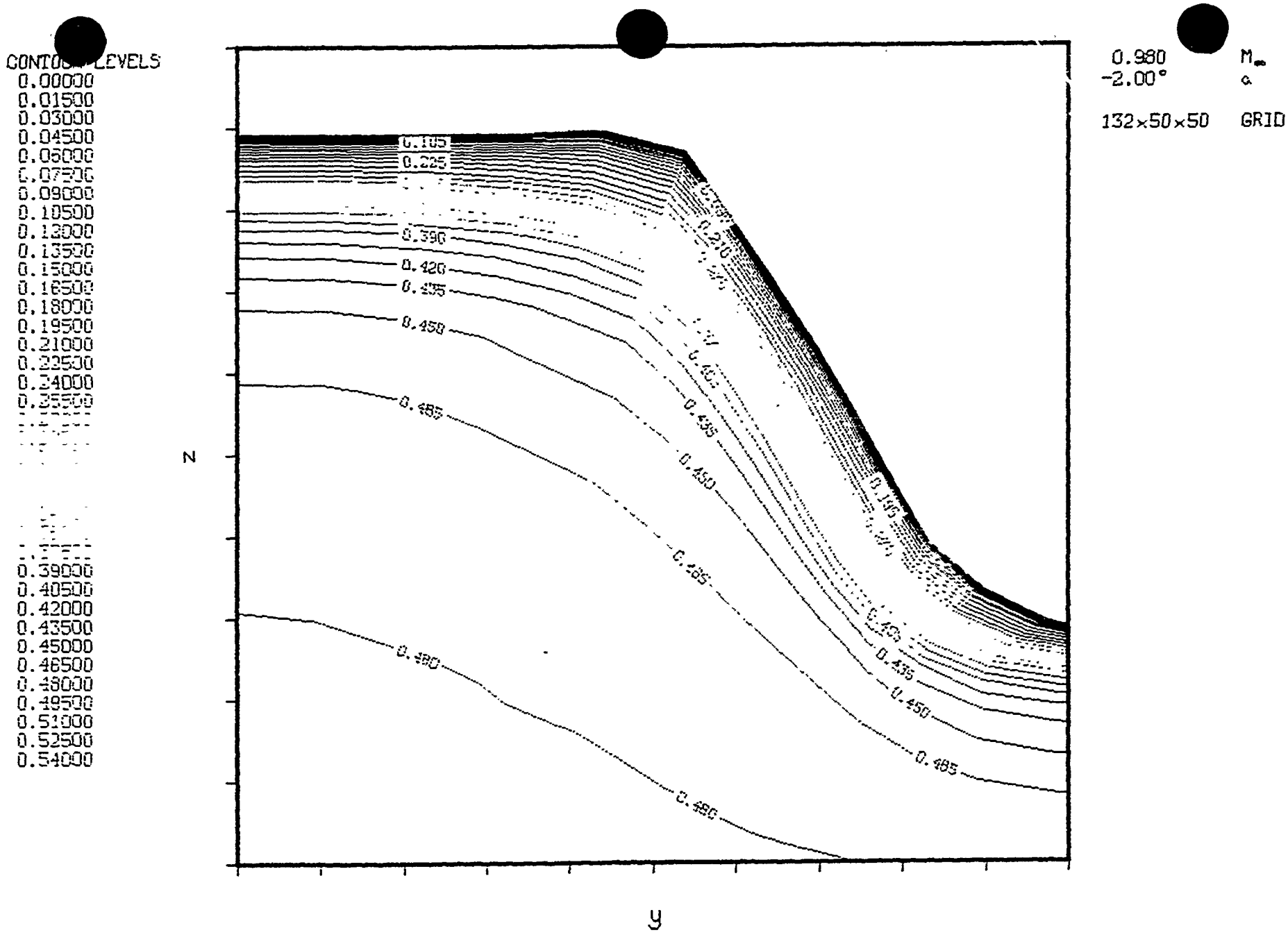

Fig. 8. Dynamic Pressure Contours for Flight Conditions at FS 626.2

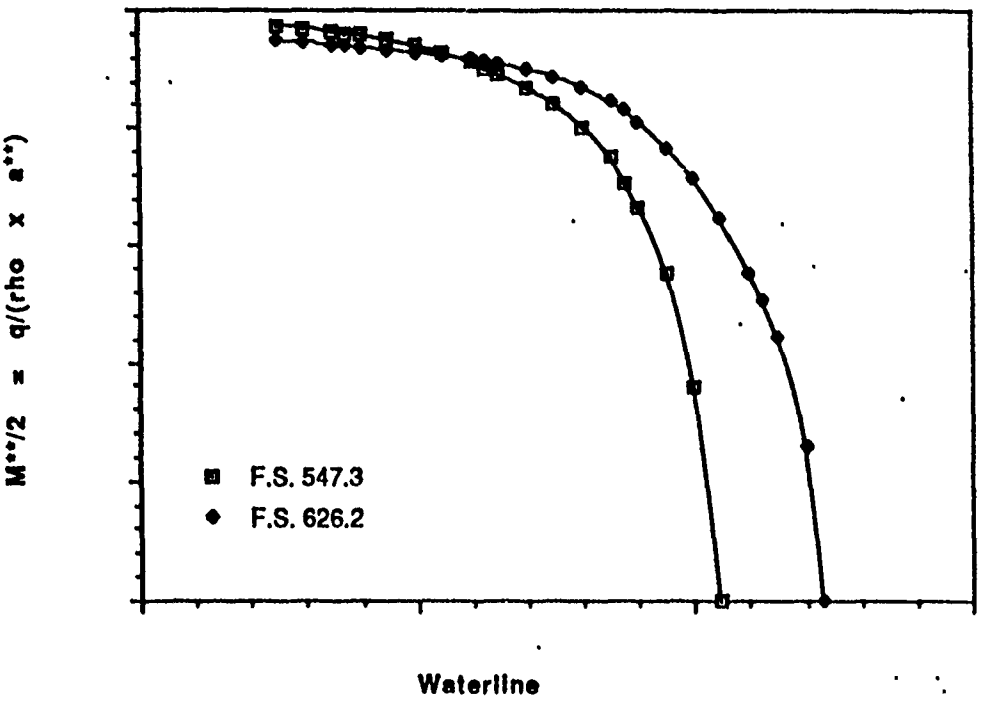

Fig. 9. F-14 Store Station 4 Centerline Dynamic Pressure Gradients

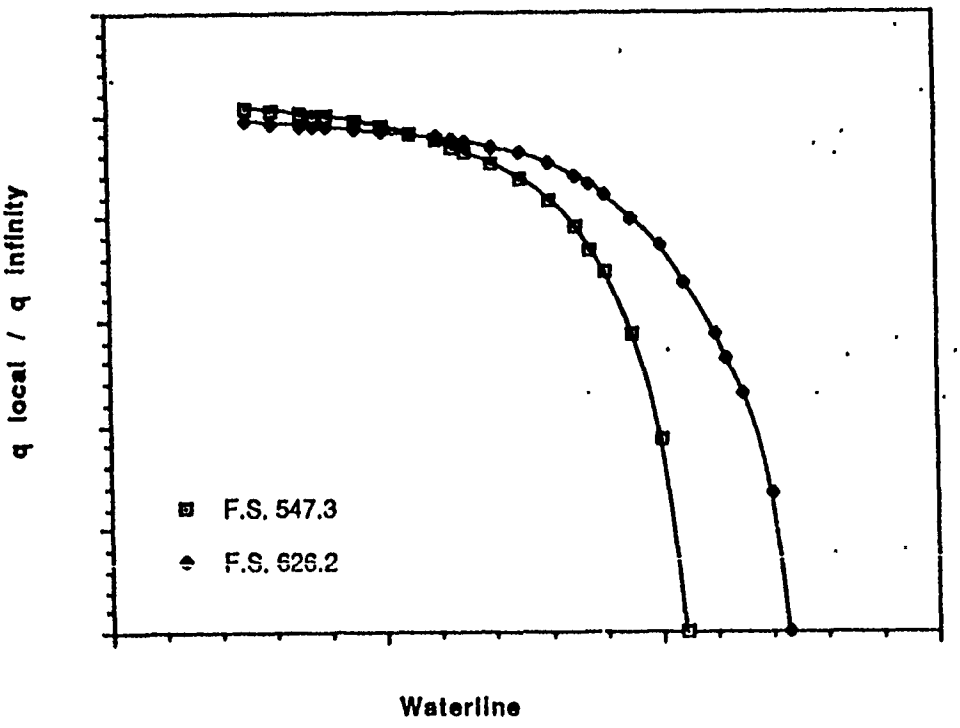

Fig. 10. F-14 Store Station 4 Centerline Dynamic Pressure Ratio

		DELTA sec	MACH NO	ALT ft	[illegible] s	N Z g s
F-14 AIM-7F SPARROW @ STA. 4, K9 AP, TELEMETRY FF, DROP 4 FL COND, ALPHA--1.5	□ -	0.100	0.98	5000	601	0.0
F-14 AIM-7F SPARROW @ STA. 4, K9 AP, CAL FF @ CG, DROP 4 FL COND, ALPHA--1.5	○ -	0.100	0.98	5000	601	0.0
F-14 AIM-7F SPARROW STA. 4, K9 AP, CAL FF, DROP 4, A - -1.5, O-CORR: CONTROL	△ -	0.100	0.98	5000	601	0.0

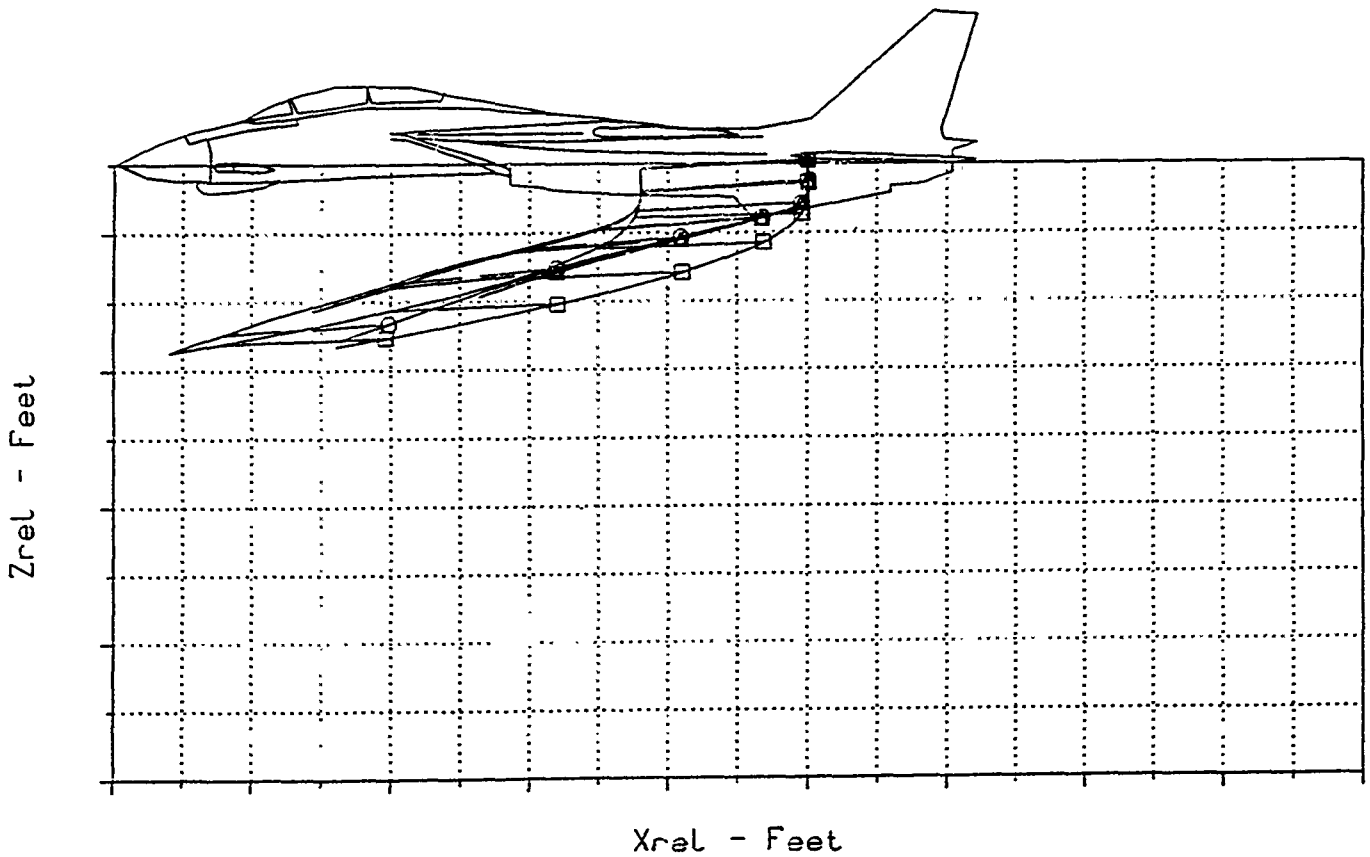

Fig. 11. F-14/AIM-7F Relative Separation Trajectory Predictions

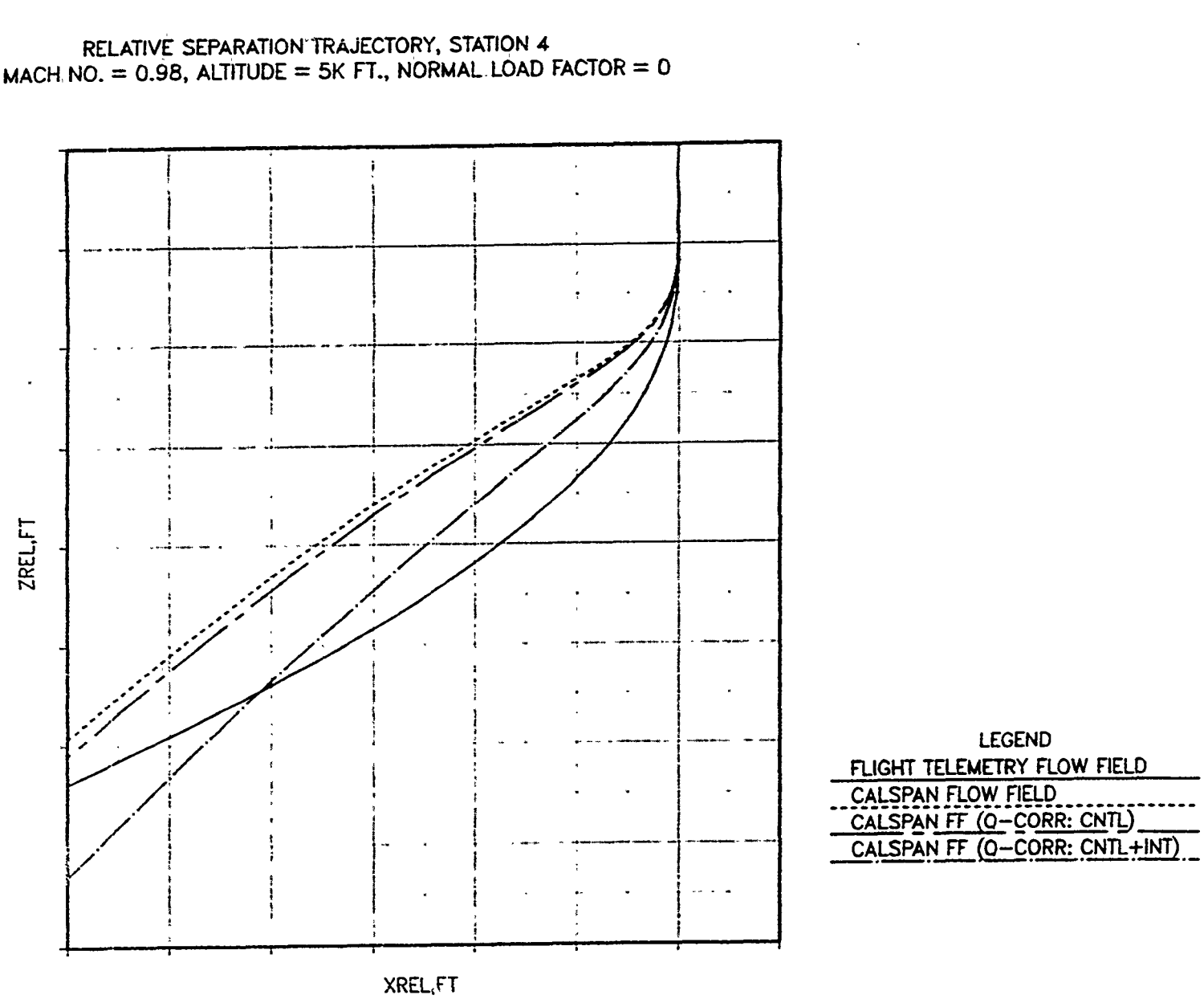

Fig. 12. F-14/AIM-7F Separation Trajectory C.G. Spatial Plot

BIOGRAPHY OF PRESENTER

Frank A. Tessitore

Mr. Tessitore has 32 years of experience in aerodynamic design analysis including the prediction of stability and control characteristics of designs ranging from VTOL through subsonic and supersonic aircraft as well as hypersonic reentry vehicles. During his 24 years with Grumman, he has been engaged in the development and mechanization of prediction methods for stability and control characteristics and has had responsibility for the design analysis of VSX, F-14, Space Shuttle, Threat and EF-111 aircraft. For the past 15 years he has been involved in the prediction of aerodynamic characteristics for weapon separation and was one of the principals in the development of the Influence Function Method (IFM) for the prediction of aerodynamic store loads under the influence of the aircraft interference flow field. He was Project Manager of the Inertial Guidance Technology Demonstration (smart bomb) program at Grumman and is currently Principal Engineer for all weapon separation studies. Mr. Tessitore is an Aeronautical Engineering Technology graduate from Northrop University - 1957 and holds a Bachelor of Science degree in Aeronautical Engineering from Tri State University - 1958. He has also pursued graduate studies at Long Island University, C W Post College.

BIOGRAPHIES OF CO-AUTHORS

Richard Romanowski

Mr. Romanowski holds a B.S.A.E. and an M.S.A.E. from the University of Notre Dame where he specialized in missile dynamics. He joined Grumman in 1968 and for 12 years gained extensive experience in aerodynamic, aerothermodynamic and propulsion wind tunnel testing on various programs including the F-14, A-6, E-2, Gulfstream, X-29, Space Shuttle, V/STOL and advanced aircraft. In 1980, he turned his efforts to the architectural design, programming, documentation and maintenance of interactive software systems which support the acquisition, processing, analysis, presentation and management of wind tunnel test data. Now an Engineering Specialist in Software Applications, he is currently involved in store separation simulation programming and analysis.

Joseph P. Laiosa

Mr. Laiosa has been an aerodynamicist with the Grumman Aerospace Corporation since 1979. Presently, he holds the position of Senior Engineer. Over the years, he has developed an expertise in the area of Computational Fluid Dynamics (CFD), by developing and applying state-of-the-art methods. Currently, he is developing an automated multi-element airfoil Navier-Stokes grid generator, which will be used to enhance the TOMCAT-21 aircraft high lift performance.

Mr. Laiosa has also served as Principal Investigator on many internal and NASA/DOD sponsored projects. In 1984 he provided a complete computational analysis of the Rockwell HiMAT RPRV configuration, under NASA Dryden contract NAS2-11424. Recently, he was assigned to the DARPA Advance Submarine Technology contract. In this capacity, he was responsible for the application of Navier-Stokes methodologies to the incompressible flow regime.

During the course of his career, Mr. Laiosa has gained valuable practical engineering experience by serving as Configuration Design and Analysis Engineer on such programs as the X-29 FSW Demonstrator, TOMCAT-21, ATF and other major classified aircraft programs. As Configuration Design and Analysis Engineer, he was primarily responsible for supervising low speed wind tunnel tests, performing pre- and post-test analyses, processing configuration contour geometry, and interfacing with various engineering disciplines.

In addition to the aircraft industry, Mr. Laiosa has extended his design/analysis expertise to the marine community. During the 1984-1987 time period, he supported the Sail America Foundation' s efforts to bring back the America' s Cup to the U.S.A.. His contributions, along with his fellow Grummanites, provided *Stars and Stripes*, the 1987 America's Cup winner, with a highly efficient winged-keel design. Mr. Laiosa holds a BS, Aeronautics & Astronautics - 1974 and a MS, Aerospace Engineering - 1976 from Polytechnic Institute of Brooklyn, and an Engineering Degree, Aerospace Engineering -1982, from Polytechnic Institute of New York.

ANALYSIS OF STORE TRAJECTORIES FROM TACTICAL FIGHTER AIRCRAFT*

T. L. Donegan and J. H. Fox
Calspan Corporation/AEDC Operations
Arnold Engineering Development Center
Arnold Air Force Base, Tennessee 37389

ABSTRACT

Use of the Euler equations to model complex transonic configurations and to predict store loads is well established. Results from further work in this area are presented. Of particular interest is the degree of complexity that can be readily accommodated by the methodology and still produce accurate store trajectories. Also of interest is the effect of geometric simplification on the trajectory of a store. Results indicate that what were heretofore thougnt of as minor simplifications to aircraft geometry may profoundly affect a store's trajectory.

Trajectories were computed based on Euler solutions for three aircraft configurations at a free-stream Mach number of 0.98 and aircraft angle of attack of 1.1 deg. All three configurations were comprised of the F-15E body, wing, ingesting inlet, pylons, and targeting pod as the basic geometric arrangement. The configurations differed with respect to the type and arrangement of the stores. For verification the trajectories were compared to both measured online trajectories and computed trajectories based on measured flow fields and measured store carriage loads. The results show that some aircraft geometric details may play a more important role than anticipated in computationally determining store trajectories. The results also demonstrate the capability of using computed store loads and computed flow-field information, independent of or in conjunction with wind tunnel data, to produce trajectories from extremely complex aircraft configurations.

INTRODUCTION

The determination of store trajectories has long been a source of uncertainty in the development of effective combat aircraft. To assure a safe and accurate store release, each aircraft-store combination must undergo a comprehensive wind tunnel and flight test store certification procedure. The store certification process can be extremely lengthy and costly, requiring several years to certify some configurations. However, with the advent of faster computers and advanced computational methodologies, emphasis is being placed on using computations to complement the current store certification process, in anticipation of shortening the process, cutting the cost, and improving the accuracy.

FIELD MODELING

Recent attempts to calculate the carriage loads on external stores have used algorithms that are based on either linearized potential flow solvers or transonic small disturbance formulations with modifications to capture oblique shock waves. A study of several different approaches was made by Cenko and Tessitore.[1] Conclusions of the study were mixed, citing limited advantages in practice because of restrictions in flow conditions and/or geometry. A similar transonic small disturbance algorithm of Rosen[2] produced good store carriage aerodynamics, but at present is limited to simple configurations such as wing-pylon mounted stores. The general problem of store separation requires solutions at transonic Mach numbers of a complex aircraft fuselage with various appendages such as wings, inlet housings, pylons in close proximity, fuel tanks, and other stores. The flow field about this complex configuration in the transonic regime will have shock waves in the neighborhood of the released store. Such a flow field cannot be modeled by descriptive equations simpler than the 3-D Euler

* The research reported herein was performed by the Arnold Engineering Development Center (AEDC), Air Force Systems Command. Work and analysis for this research were done by personnel of Calspan Corporation/AEDC Operations, operating contractor for the AEDC aerospace flight dynamics facilities. Further reproduction is authorized to satisfy needs of the U. S. Government.

equations. Also, since many components invariably exhibit mutual interference in such a flow field, solution of selected subsets will not suffice; the flow field must be solved in its entirety.

Recently, a program was initiated at AEDC to determine whether computational fluid dynamics (CFD) had matured sufficiently to provide quality flow-field and store load information in the near field of a complex aircraft/store configuration. The resulting study of Fox, et al.[3,4] showed comparisons between the CFD flow field produced by solution of the Euler equations and wind tunnel flow-field data in the vicinity of an F-15E fighter aircraft pylon system. The comparisons were made for three basic fighter configurations, and showed excellent overall agreement between the Euler solutions and wind tunnel data. In the study and in the present paper, the vertical and horizontal tails were omitted from both wind tunnel and Euler solution aircraft models.

The development of these computational tools now offers the opportunity to gain new insight into some of the complex characteristics of the aircraft flow-field environment into which a store is released. Presently, the extent to which the aircraft flow field influences a released store trajectory is not clear, especially in transonic flow. A specific concern is whether details in the aircraft geometry significantly affect the store trajectory.

TRAJECTORIES

An approach by Keen[5] proposes to use Euler computations to account for aircraft/store mutual interference near the aircraft in computing store separation and trajectories. Keen's technique may be applied by using computations alone, when experimental data do not exist, or in conjunction with data. The technique will be described in the Store Trajectory Computations section.

The present work uses this approach to investigate the store separation problem and the influence of the aircraft upon the store trajectory. Results are presented that further validate the computational method by comparison of computationally and experimentally determined trajectories for complex configurations.

GEOMETRY

The aircraft geometry used in the present work is the long-range, dual-role F-15E fighter aircraft (Fig. 1). The F-15E is equipped with large conformal fuel tanks (CFT) at the wing/inlet juncture and uses a pylon system for store carriage. Pylons are attached to hardened points on the CFT. Three store loading configurations were considered. The basic geometry for all three configurations was symmetric. Each side included the F-15E aircraft with CFT, inlet with scaled mass-flow rate, wing, four CFT pylons, wing pylon, targeting pod and pylon, and fuselage centerline pylon. The four CFT pylons include three stub outboard pylons and one long inboard pylon which can accommodate up to three stores.

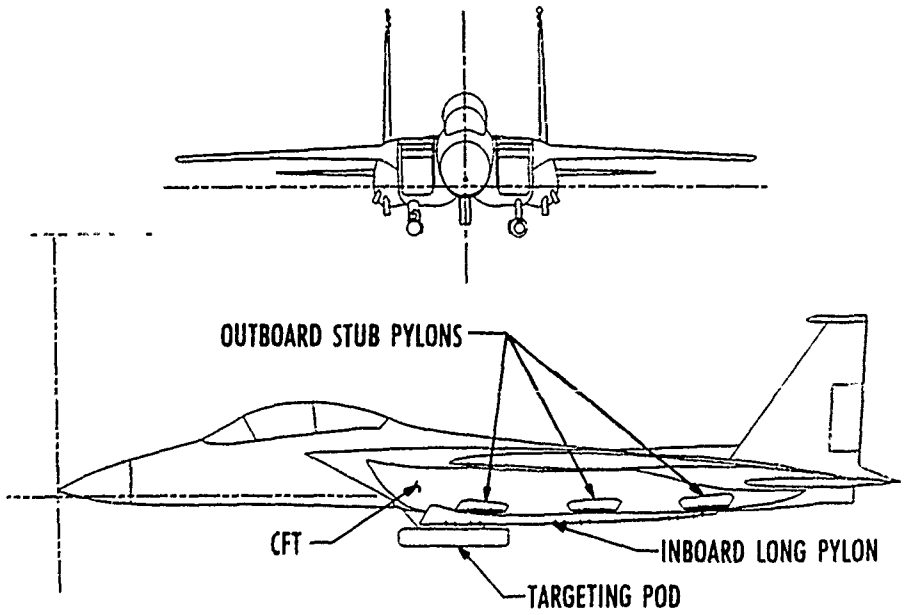

Fig. 1. Schematic of the F-15E aircraft.

Configuration 1 consisted of a laser-guided store (Fig. 2) attached to the forward-most outboard stub pylon of the basic geometry.

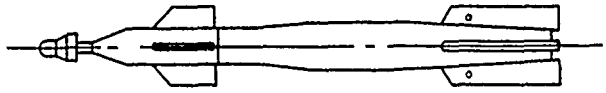

Fig. 2. Laser-guided store geometry.

Configuration 2 was comprised of Configuration 1 with an additional laser-guided store attached to the forward-most position of the long inboard pylon, as well as a large fuel tank added to the fuselage centerline pylon.

Configuration 3 included the basic geometry with a slender missile (Fig. 3) at the forward-most missile position of the long inboard pylon.

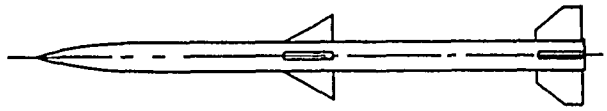

Fig. 3. Slender missile geometry.

Both the guided store and the slender missile are approximately the same length, although the missile body diameter is about half that of the guided store. Both stores have a set of four canards and a set of four fins. The missile canards are relatively much farther aft than those of the guided store, with the missile canards approximately at the center of gravity of the missile.

TEST ARRANGEMENT

The measured data used in this work were obtained in the AEDC's 4-ft Aerodynamic Wind Tunnel(4T). The test article was a 0.05-scale model of the F-15E aircraft, its targeting pod, pylon system, and selected stores. The flow-field data were acquired with a 20-deg half-angle cone probe. The data consisted of static pressure, total pressure, and flow angles. All data were acquired at a Mach number of 0.98 and an aircraft angle of attack of 1.1 deg. The aircraft model was mounted on the main pitch sector of the wind tunnel and the pressure probe was attached to the six-degree-of-freedom Captive Trajectory Support (CTS) system.

The CTS system may be used for several purposes. When obtaining flow-angle data, as above, the CTS rig is programmed to traverse a predetermined rectilinear grid volume beneath the aircraft to measure local flow angles in the vicinity of the pylon system, as shown in Fig. 4. The flow-angle data may be used for offline (i.e., post-test) trajectory calculations, as performed in the present work, or for validation of CFD methods. Validation of the methodology was made in Ref. 4. Also, by mounting a store model to the CTS, the rig may be used for measuring store force and moment data. Accordingly, store loads may be ascertained at the carriage position or any other position in the flow field. Until now, many of the trajectory determinations were made in this manner. Store loads were obtained for several angular orientations at each point in a grid volume beneath the aircraft, thereby creating a data base. The store load data base was interpolated to determine the loads at any arbitrary position and orientation relative to the aircraft. Trajectories were obtained by using store carriage loads, integrating in time to determine the next position and attitude, and deducing loads at each step in the flow field by interpolation of the measured data base. Finally, the CTS rig is also available to determine trajectories directly. The six-degree-of-freedom equations of motion are integrated online (i.e., during the test), and the trajectory is mapped by a step-wise process of moving the CTS rig to the next

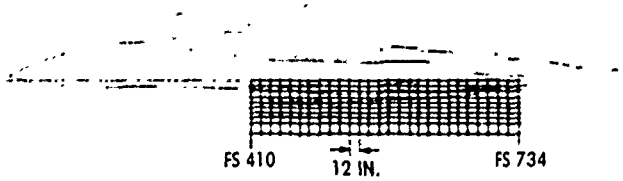

Fig.4. Schematic of cone-probe surveys.

trajectory location predicted using the measured forces and moments from the previous location. Since online trajectories are the most expensive and time-consuming, relatively few trajectories are determined in this manner. However, the available online trajectories provide a good source for comparison of computed offline trajectories.

CFD SOLUTIONS

Solution of the Euler equations was accomplished with the implicit, approximate factorization scheme of Beam and Warming.[6] The coded form of the scheme is a vectorized enhancement of the version developed by Pulliam and Steger.[7] The equations are solved on a boundary-conforming curvilinear coordinate grid system. The code is linked to the domain decomposition scheme of Benek, et al.,[8] which allows geometric components such as the fuselage, wing, pylons, and stores each to be modeled with an individual grid. In this manner each component may be more easily and more efficiently modeled. Each grid is overlapped with neighboring grids to allow for communication among the grids by trilinear interpolation on grid boundaries. The details of this scheme will not be explored in this paper, but are explained in Ref. 8 and by Dietz, et al.[9]

For a complex configuration such as the F-15E and the associated appendages considered here, this scheme is extremely effective. The complete structure may be built in parts and then assembled much like a physical model. Since each grid is independent of all others, another advantage of the scheme is the ability to remove and add stores (or any other component) without requiring alterations to any other grid in the system. Moreover, if necessary, different equation sets (such as Euler, Navier-Stokes, etc.) may be solved on different grids simultaneously. These capabilities provide the ability to produce solutions for flow fields about extremely complex configurations with relatively simple grids.

A basic simulation of the inlet spillage effect was included by using an inlet grid of rectangular cross section which protruded into the fuselage surface at the inlet location. Approximate mass-flow rate boundary conditions were applied on the downstream face of the inlet grid interior to the fuselage, while the exterior portion of the inlet grid communicated with the fuselage grid. Since the inlet spillage is only approximately modeled, some effect may be seen on a released store just underneath the inlet housing.

To simplify the complexity of the F-15E aircraft geometry, a liberty was taken initially, in describing the fuselage surface by omitting the boundary-layer gutter and diverter between the fuselage and inlet housing. The fuselage and inlet housing were combined by fairing over the gutter. The omission was made with the assumption that the gutter and diverter would have minimal effect on the underside of the aircraft from where the stores are released. This effect is investigated later in the present work by obtaining a solution with the diverter/gutter. All the remaining components making up the configurations were modeled as completely as possible. Standard grid generation procedures were used to create the grids with detailed descriptions presented in Ref. 3. The maximum number of grid points for the most complex configuration (i.e., Configuration 2) was 1.6 million points, requiring 42 grids. All configurations were symmetric and only the right side modeled for efficiency.

STORE TRAJECTORY COMPUTATIONS

Store trajectories in the present work were computed by the Flow Angle Trajectory Generation Program (FLOW TGP) of Keen.[5] The FLOW TGP package requires store carriage forces and moments along with the flow angularity description of the aircraft flow field in a rectilinear array of positions beneath the aircraft in order to compute the trajectory of the store through the described flow field.The required flow field does not contain the released store. Carriage loads and flow angles may be supplied by either CFD solutions or by experimental measurements. Moreover, the sources of information may be mixed (i.e., loads may be given by CFD and the flow angularity by measurements, or vice versa). A CFD solution determines the store carriage loads by an integration of the store surface pressures. Flow angularity is obtained naturally from the solution as velocity ratios at the grid locations of interest. Measurements establish store loads and flow angles with the CTS rig as described earlier. The store's

trajectory is obtained by specifying initial conditions such as zero linear and angular velocity and integrating the six-degree-of-freedom equations of motion. During the integration, store loads are required not only at the store carriage location, but throughout the flow field. The store loads away from the store carriage position are determined from the flow angles by use of a refined version of the Influence Function Method(IFM).[10]

In the IFM method, it is assumed that store loads can be expressed as linear combinations of local flow angles, where the coefficients are referred to as influence coefficients. The coefficients are determined either experimentally or computationally by passing the store through a known flow field with store forces and moments known, and deducing the influence coefficients by a regression analysis. Thus, if the influence coefficients for each store and the local flow angles are known, loads may be predicted for any location in a flow field.

The original IFM process is based on influence coefficients obtained by zero-angle traverses through a known flow field. Therefore, errors are inherent in the method when it is applied to stores with angular orientation. Since most store trajectories do not remain at very small angles with respect to the oncoming flow after release, the original process is not adequate for determining store loads for general flow fields very near the aircraft fuselage.

For this reason, FLOW TGP was created to allow for large angular orientations and to combine the IFM and trajectory calculations under one program. This was accomplished as follows. Store load coefficients are computed at the desired attitude in both the provided aircraft flow field and a constant free-stream flow field. As described above, these are determined from linear combinations of local flow angles. The results are differenced to provide "delta" coefficients. The "delta" formulation avoids the inherent errors associated with the IFM when it is applied to absolute flow angles. Delta force and moment coefficients are, in effect, aircraft interference increments to free-stream store loads. The most accurate store loads in the aircraft flow field are obtained by summing the delta loads to free-stream measured loads for a particular store at the designated attitude (where the latter data are generally available from separate free-stream tests). The carriage store loads may also be determined in this manner, but since the IFM method does not include the effects of mutual interference of the aircraft and store, the store loads will not be accurate in this region for transonic flows. Mutual interference is usually significant within the distance of one store diameter from the aircraft fuselage.

INCREMENTAL TRAJECTORY APPROACH

The above approach taken by the FLOW TGP program can be used to calculate trajectories through flow fields beneath extremely complex aircraft configurations. The trajectories obtained in this manner agree well with experiment, as will be shown in the results, but inherent errors associated with any aspect of the trajectory computation or the affiliated inputs may be apparent for some cases. To minimize the error for any part of the trajectory calculation and to make the store certification process more efficient, an incremental procedure has been proposed to take advantage of the strengths of CFD methods, yet anchor them to actual test measurements. In this manner, no part of the procedure will be relied upon in an absolute sense, but can be used to supply increments to measured information.

This incremental approach may be applied by using CFD results to correct for the aircraft/store mutual interference. The procedure is outlined in Fig. 5. For example, store carriage loads can be obtained by correcting measured free-stream loads with an increment determined from CFD (i.e., CFD carriage loads minus CFD free-stream loads). At a distance greater than one store diameter from the carriage position (recall that the aircraft/store mutual interference is significant within one store diameter), store loads are determined by the IFM delta method explained in the previous section. Within the first store diameter distance, the store loads are interpolated between the CFD corrected carriage loads and the IFM determined store loads. Simultaneously, CFD flow-field solutions may be used in the incremental approach to provide flow-angle increments to measured flow angles beneath the basic aircraft configuration (i.e., the aircraft without stores). The basic aircraft flow angles are measured once

to provide a baseline. If a configuration contains stores other than the store of interest, the effects of the additional stores on the baseline aircraft flow field may be represented with CFD flow-field increments (i.e., CFD flow angles with stores minus CFD baseline flow angles). The increments can be added to the measured baseline flow angles to account for the additional stores. Therefore, using the incremental approach, the store carriage loads and the flow angles are available to establish a trajectory that is based on measurements, yet enhanced by computations. This proposed methodology is detailed in Ref. 5 and shows promise for significantly reducing wind tunnel testing in the store certification process. The reduction is possible since one set of baseline flow-angle measurements may be used to create trajectories for many configurations of a particular aircraft. However, although the incremental approach has been proposed, it has not been verified until now. A trajectory determined by this procedure is presented in the results.

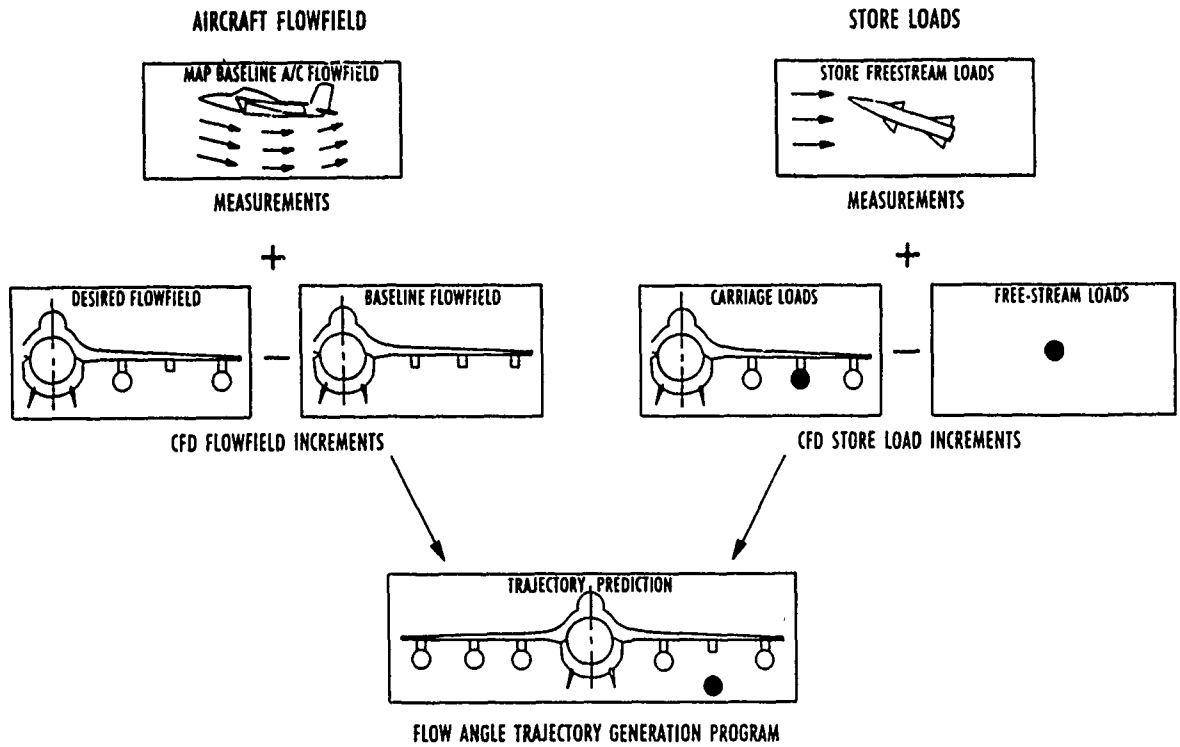

Fig. 5. Experimental/computational store clearance process.

RESULTS

Euler solutions were computed and FLOW TGP trajectories obtained for the three F-15E configurations described above. Trajectories based on CFD calculations are compared to experimentally-based trajectories and, if available, to CTS online trajectory data. All results are at a free-stream Mach number of 0.98 and aircraft angle of attack of 1.1 deg.

In Configuration 1, one laser-guided store is released from the forward outboard stub pylon position. Trajectories are determined with FLOW TGP for two input cases. The first trajectory is established with information obtained from a flow-field data base developed in the wind tunnel. Both the store carriage loads and flow angles are interpolated from measured data. The second trajectory is computed based on information supplied by CFD results only. In addition, CTS online data are available for comparison. The trajectories are compared by tracking the location of the center of gravity (cg) and store attitude. Figure 6 shows the two FLOW TGP trajectories and the CTS data. The dashed line represents the experimentally-based trajectory, the solid line depicts the CFD-based trajectory, and the open circles denote the CTS data. Cartesian components (X,Y,Z) give the location of the cg. Positive X is upstream, positive Y is outboard, and positive Z is down. The loci of the cg location for all three trajectories are virtually t he same. Many methods will yield trajectories with good cg locations, but have problems

predicting attitude variations which are essential for determining safe store releases. Yaw angles (ψ) and pitch angles (θ) are also presented in Fig. 6. The roll angle is not presented for this case since the store was not allowed to roll during the wind tunnel test. Positive yaw angles are nose out-board and positive pitch angles are nose up. The yaw angles compare very well for the two FLOW TGP determined trajectories, but are a few degrees off the CTS data at extreme yaw angles. Pitch angles compare well for the CTS data and experimentally-based FLOW TGP trajectory. The CFD-based FLOW TGP trajectory is underpredicted, possibly indicating some error in modeling the inlet spillage just upstream, thereby affecting the local upwash near the store.

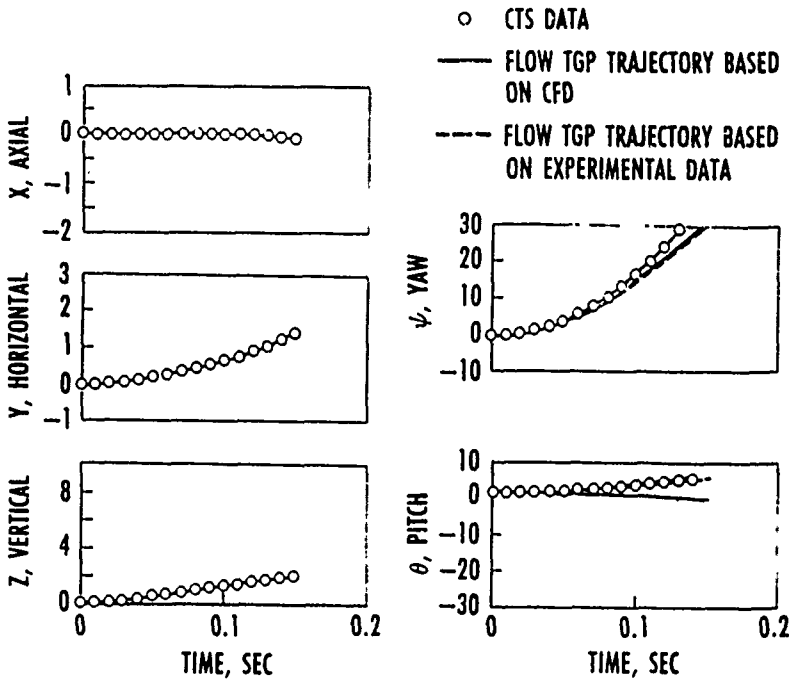

Fig. 6. Comparison of wind tunnel and computational trajectory simulations, Configuration 1.

To understand more clearly the characteristics of the flow field and its effects on the trajectory, a comparison of the measured and computed flow fields was made by analyzing the local flow angles in the region of the released store. In Fig. 7 the local sidewash and upwash angles are compared along an axial traverse. The relative store location is shown along the abscissa. The measured data were taken as described in the Test Arrangement section, with the cone probe secured to the CTS rig. Computed flow angles were interpolated from the Euler solution at the same positions for which data were available and overlaid for comparison. Here, positive sidewash angles represent flow turning outboard, while positive upwash angles denote flow turning upward. Although the flow field does not

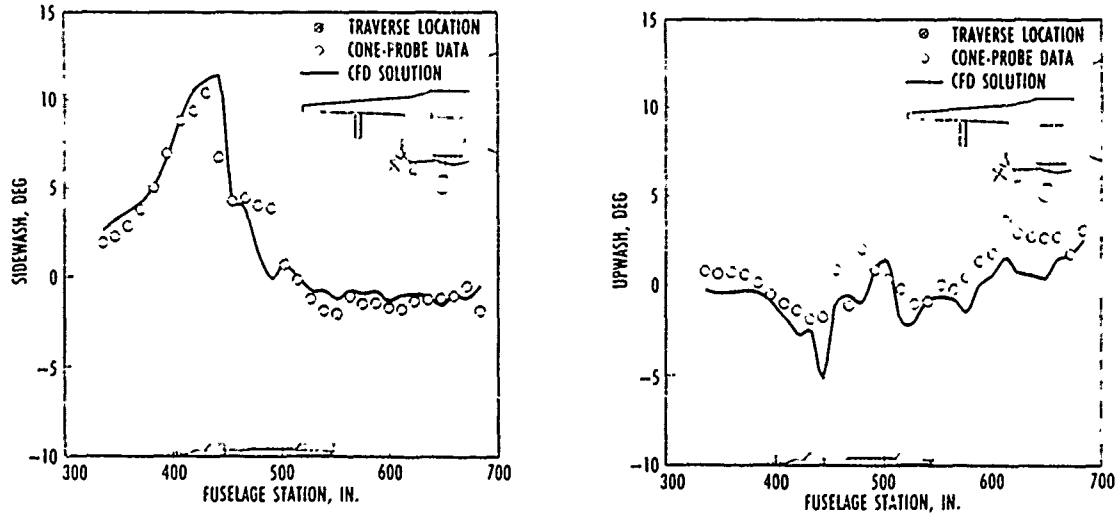

a. Sidewash comparisons

b. Upwash comparisons

Fig. 7. Computed and experimental flow-angle comparisons at store carriage location of Configuration 1.

contain the store itself, the flow angle comparisons are made at the carriage location of the store (i.e., near the forward outboard stub pylon as shown in the small aircraft figure in the plots). Therefore, the flow angles represent the nature of the flow that is imposed upon the store at the carriage location.

The sidewash comparison reveals a large outflux (outboard flow angle) at the location of the store nose and forward canards, and a slight influx in the area of the rear fins. This sidewash gradient results in the large yaw angle observed in the trajectory. The Euler solution follows the data very well and both methods predict similar yaw patterns. The observed pattern of substantial outflux followed by an influx is generally the one seen throughout the flow field underneath the basic aircraft. This would seem to be the dominant characteristic of the flow field about the basic aircraft. The upwash comparison indicates that even though the Euler solution exhibits the same trends as the data, there is enough discrepancy at critical points on the store to cause the pitch angle difference in the trajectory calculation. The Euler solution shows a larger downwash at the forward canards than the data, with little difference at the rear fins, thereby resulting in a lower pitch angle during the trajectory.

In addition to the guided store of the previous configuration, Configuration 2 consists of a second laser-guided store at the forward inboard position plus a large fuel tank on the centerline pylon. The inboard guided store is released from this configuration. Besides the influence of the major flow characteristics of the aircraft on the store trajectory, the local effects of two added components are now included. The trajectory for the inboard guided store is shown in Fig. 8. The symbols denote the CTS data and solid line the CFD-based trajectory. The incremental approach trajectory will be discussed later. There were no flow-field measurements made without the released store; consequently, there is no FLOW TGP trajectory based on measured quantities. To guarantee safe release, the CTS was programmed to constrain yaw for a short distance (roughly through the fourth data point). This constraint leads to very little yawing throughout the trajectory determined by the CTS rig. Placing the same constraint on the CFD-based trajectory, the two trajectories show good agreement. The CFD-based trajectory extends beyond the limits of the CTS and indicates eventual large yawing angles for

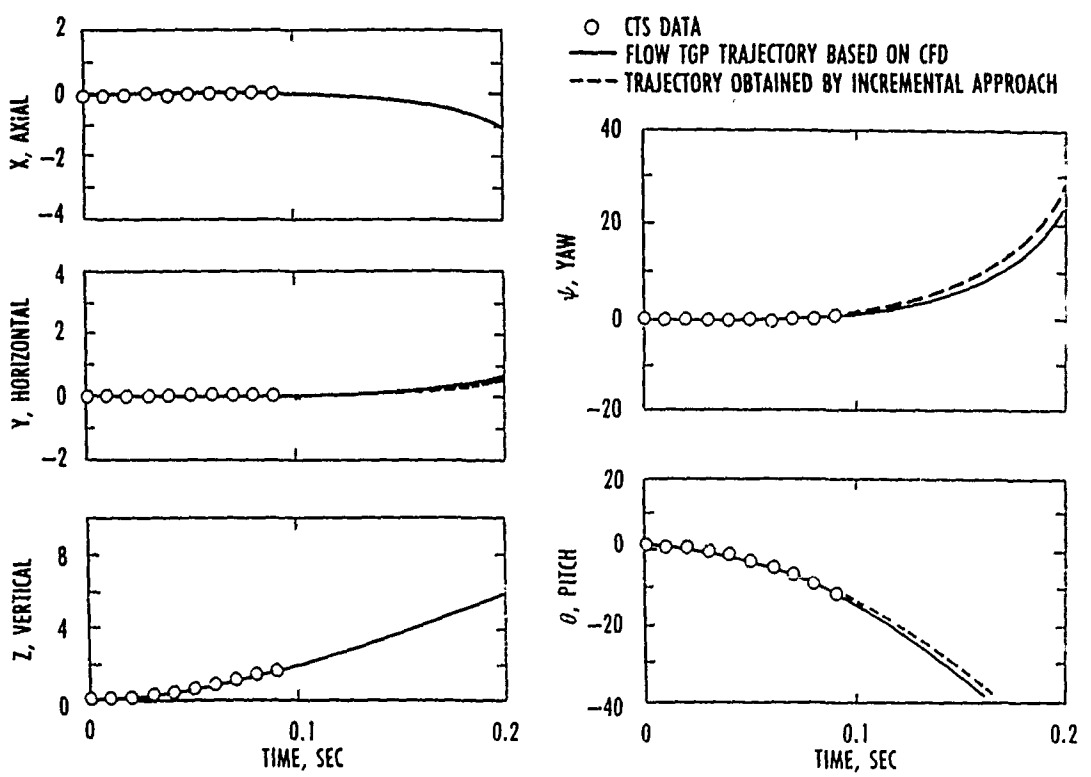

Fig. 8. Comparison of wind tunnel and computational trajectory simulations, Configuration 2.

the store. The yaw constraint dampens some of the initial motion of the store; however, the pitch was not constrained and the two trajectories also agree in this respect. No roll comparison is made since the store was not allowed to roll. The cg locations once again compare very well.

By inspecting the flow field near the released store carriage position, some observations may be made. Although no flow measurements were made without the released store, a flow-field measurement was made with the store in the carriage position. The sidewash comparison of Fig. 9 shows good agreement between measurements and the Euler solution near the front of the store, but begins to deviate near the rear. This difference is not realized in the trajectory calculations, probably because of the initial constraint of yaw. However, the upwash comparison indicates better agreement, and delivers good trajectory comparisons without pitch constraints.

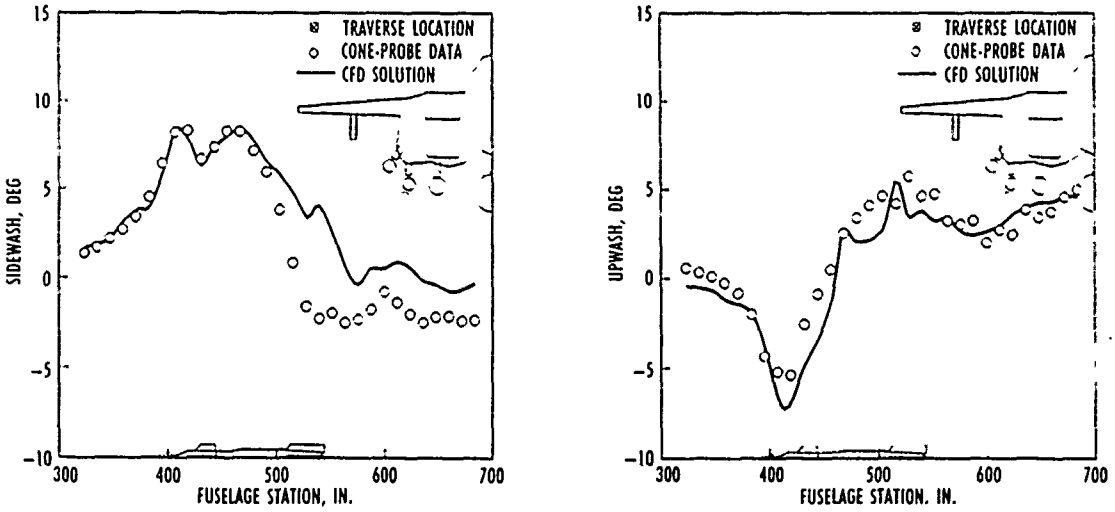

a. Sidewash comparisons b. Upwash comparisons

Fig. 9. Computed and experimental flow angle comparisons near store carriage location of Configuration 2.

Since Configuration 2 contains stores other than the one being released, this case presents the opportunity to evaluate the incremental trajectory approach discussed above. With CFD solutions, the effects of the two other stores (guided store and fuel tank) may be added, in an incremental fashion, to the measured baseline flow field evaluated in Fig. 7. CFD flow fields with and without the added stores are differenced and added to the measured flow field without the added stores. Free-stream store loads determined by CFD are subtracted from computed carriage loads and added to measured free-stream loads. Therefore, the measured free-stream loads and baseline flow field have been "corrected" for the two added stores. A new trajectory is now computed with these corrected quantities with FLOW TGP and is presented as the dashed line in Fig. 8. The incremental approach trajectory has the same cg location as the CFD-based trajectory. The yaw attitudes are 5 deg, at most, different at the extreme of the trajectory. Pitch attitude differences are even less. Overall, the incremental approach trajectory is in good agreement with the other trajectories. Adoption of this method could provide for more efficient testing by accommodating many configuration build-ups, with only baseline configuration flow-field measurements and free-stream store load measurements required.

Configuration 3 consists of the basic F-15E geometry and a slender missile at the forward inboard missile station. There are no CTS online data for this configuration, but trajectories are determined from FLOW TGP based on both measured data and CFD results, and are presented in Fig. 10. Open circles represent the experimentally-based trajectory and the solid line denotes the CFD-based trajectory. In this case, the greatest discrepancy exists between the two trajectories in yaw, although the cg locations

throughout the trajectory agree well. The basic trends in attitude are consistent since both trajectories exhibit an oscillatory pattern with basically the same period. The difference is mainly in the amplitude. The two trajectories also agree in roll angle (ϕ, positive clockwise looking upstream), which is significant since this is the first validation of the roll prediction. The roll angle comparison indicates the accuracy of the crossflow gradients since the roll angles are primarily a function of the crossflow gradients and not the axial-flow gradients.

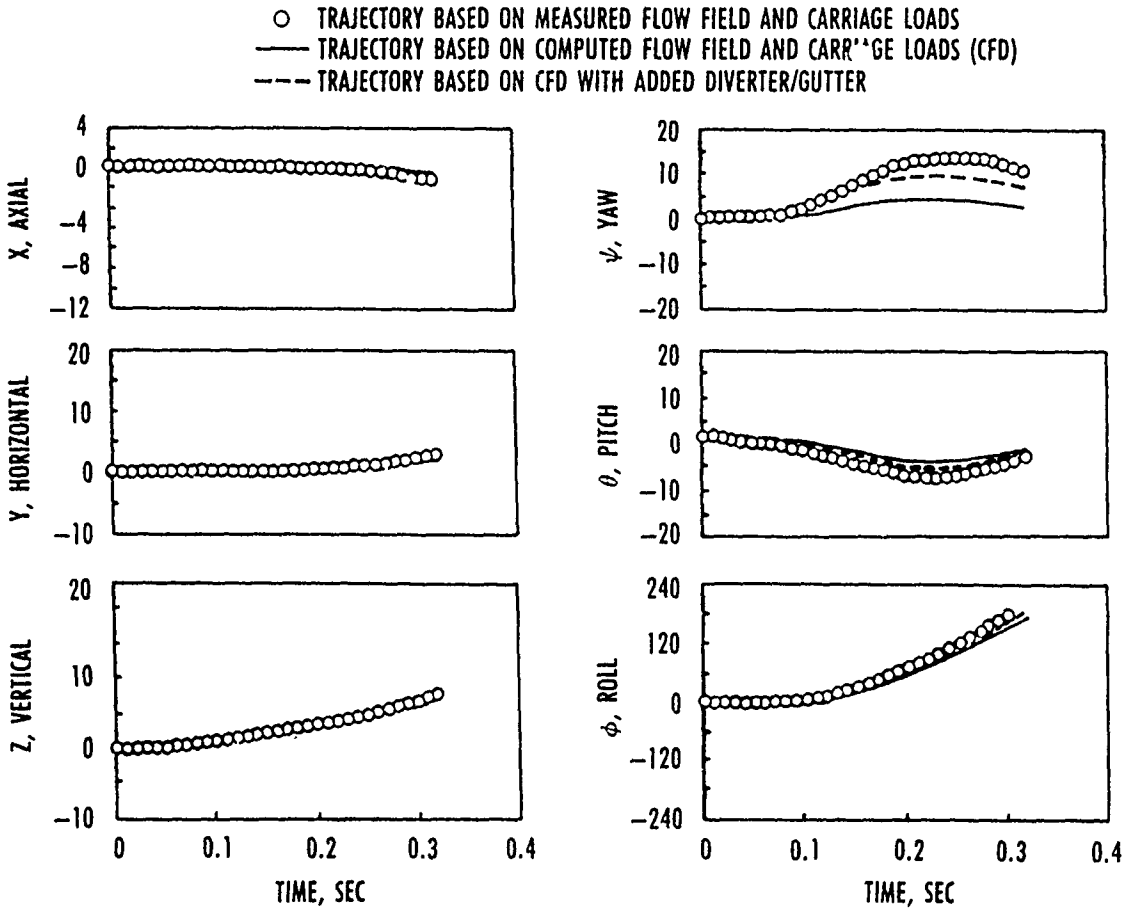

Fig. 10. Missile trajectory comparison, Configuration 3.

The flow field at the carriage position was examined to determine the cause of the noted discrepancies. Figure 11 shows the computed sidewash and upwash near the carriage position as dashed lines. The initial outflux at the store nose is computed well, but the rear influx prediction falls short of the data. Also, the location of the discrepancy on the missile is critical as it is near the rear fins. Since the front canards are approximately at the cg location, the outflux does not affect the missile moments as much as it did the guided store moments. The rear missile fins and associated influx now present the major portion of the initial yawing moment to the missile.

To correct the computed influx on the basic geometry, the fuselage modeling and associated assumptions were reconsidered. It was decided that the boundary-layer gutter and diverter initially omitted, if added, would allow more flow to be redirected to the lower portion of the fuselage, thereby acting as a sink and drawing the outer flow inboard. This would help the overall yawing moment on the missile in the trajectory. With the domain decomposition method being used to develop the computational grids, the gutter/diverter was easily added as another grid, leaving the original grids undisturbed. This underscores the effectiveness of the domain decomposition technique.

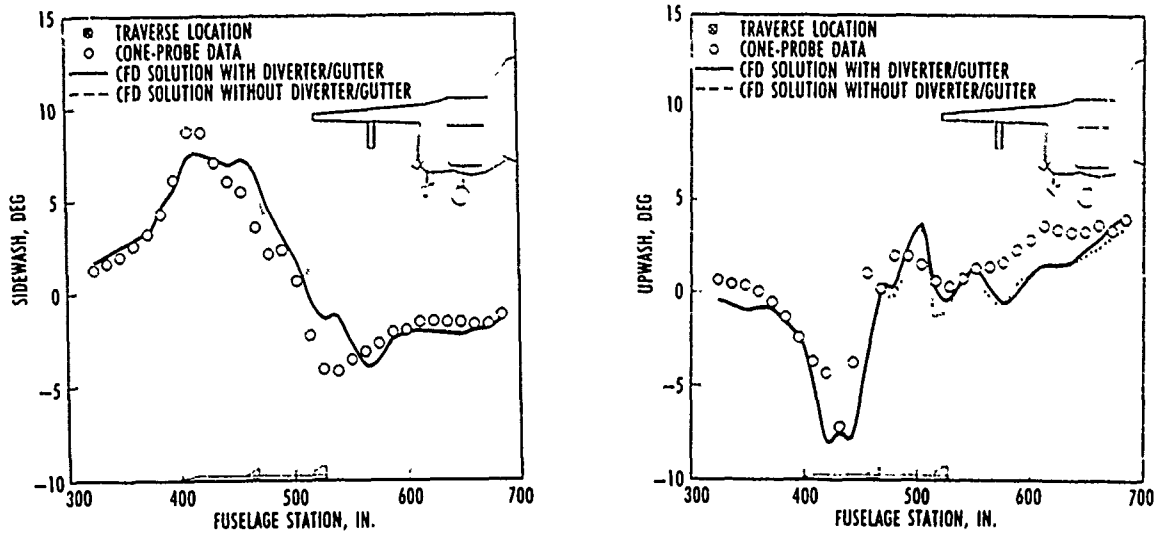

a. Sidewash comparisons b. Upwash comparisons

Fig. 11. Computed and experimental flow-angle comparisons at store carriage location of Configuration 3.

Updated CFD solutions were computed, and a new trajectory was determined accordingly. The results are shown in Fig. 10 as the dashed line. The yaw and pitch are significantly improved, although the entire discrepancy is not eliminated. The roll angle is also slightly improved. The solid lines of Fig. 11 depict the updated flow angles. While not affecting the upstream outflux, the influx at the rear of the missile is greatly improved. The upwash did not change appreciably, although the original upwash was not badly predicted, especially near the rear fins. In Fig. 12, the sidewash and upwash are plotted at a more inboard station and show a more marked improvement for both parameters. Sidewash is more affected by the gutter/diverter addition at both traverse locations; however, the upwash is significantly affected inboard. The gradients in upwash are much sharper at this location, but the improved solutions compare well with the data. The results indicate that the initial CFD solutions (i.e., without diverter/gutter) were improved upstream and outboard, and worsened inboard and downstream.

The Configuration 3 results demonstrate the importance of accurate geometric detail when modeling complex geometries. The initial omission of the gutter/diverter was made to simplify grid generation with

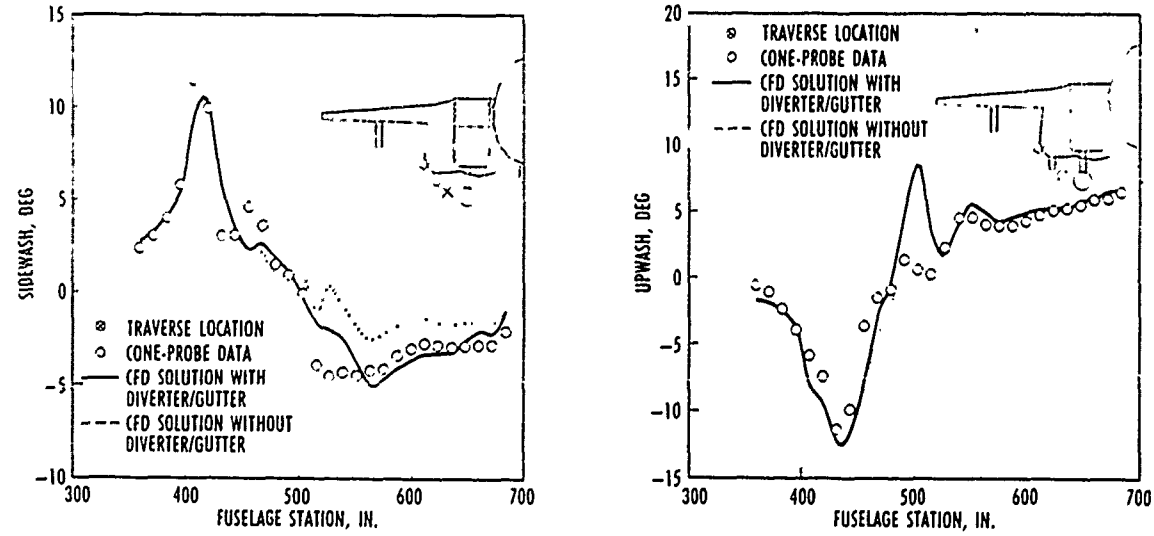

a. Sidewash comparisons b. Upwash comparisons

Fig. 12. Computed and experimental flow-angle comparisons inboard of store carriage location of Configuration 3.

the assumption that such a change would have little effect on trajectories since the stores were not proximate to the gutter. That this assumption was incorrect underscores the fact that approximations to simplify the store separation problem produce inaccurate results. It is difficult to know beforehand just what effect a simplification will have.

CONCLUSIONS

Trajectories were obtained based on Euler solutions and experimental data for two different stores from three configurations of the F-15E fighter aircraft. Trajectories based on CFD results were compared to trajectories based on experimental information, and to online trajectory data. Conclusions from the study are that moderate details in aircraft geometry may have a larger effect upon a store trajectory than originally anticipated, which necessitates accurate determination of the local flow field. Also, the study shows that trajectories may be obtained with the FLOW TGP trajectory method using CFD solutions and/or measured results. In this manner, safe trajectories may be determined more accurately and efficiently. This technology can be extremely useful in the store certification process by eliminating unnecessary testing of benign configurations, which can be more easily determined with CFD techniques, and confine needed testing to more critical configurations.

ACKNOWLEDGEMENT

The sponsor of this research is the F-15 System Program Office, Directorate of Test, ASD/VFT, at Wright-Patterson Air Force Base, Ohio.

REFERENCES

1. Cenko, A., and Tessitore, F. "Evaluation of Methods for Predicting Complex Aircraft Flowfields," *Journal of Aircraft*, Vol. 25, No. 5, May 1988, pp. 453-458.

2. Rosen, B. S. "External Store Carriage Loads Prediction at Transonic Speeds," AIAA-88-0003, January 1988.

3. Fox, J. H., Donegan, T. L., Jacocks, J. L., and Nichols, R. H. "Computation of the Euler Flow Field Produced by a Transonic Aircraft with Stores," AIAA-89-2219, July-August 1989.

4. Fox, J. H., and Allee, E. G. "Experimental/Computational Study of a Transonic Aircraft with Stores," AIAA-89-1832, June 1989.

5. Keen, K. S. "New Approaches to Computational Aircraft/Store Weapons Integration," AIAA-90-0274, January 1990.

6. Beam, R., and Warming, R. F. "An Implicit Finite-Difference Algorithm for Hyperbolic Systems in Conservation-Law Form," *Journal of Computational Physics*, Vol. 22, September 1976, pp. 87-110.

7. Pulliam, T. H., and Steger, J. L. "Implicit Finite-Difference Simulations of Three-Dimensional Compressible Flow," *AIAA Journal*, Vol. 18, No. 2, February 1980, pp. 156-169.

8. Benek, J. A., Buning, P. G., and Steger, J. L. "A 3-D Chimera Grid Embedding Technique," AIAA-85-1523, July 1985.

9. Dietz, W. E., Jacocks, J. L., and Fox, J. H. "Application of Domain Decomposition to the Analysis of Complex Aerodynamic Configurations," SIAM Conference on Domain Decomposition Methods, Houston, TX, March 1989.

10. Meyer, R., Cenko, A., and Yaros, S. "An Influence Function Method for Predicting Store Aerodynamics During Weapon Separation." Paper presented at the 12th Navy Symposium on Aeroballistics, David Taylor Ship Research and Development Center, Bethesda, Maryland, May 1981.

TRACY L. DONEGAN

Mr. Donegan received his formal education at the University of Tennessee, earning his B.S. degree in Mechanical Engineering in 1978. He received his M.S. in Aerospace Engineering in 1983 also from the University of Tennessee while employed with Calspan Corporation at the Arnold Engineering Development Center (AEDC) in Tennessee. He is currently pursuing the PhD degree part-time at the University of Tennessee Space Institute near AEDC.

In his twelve years of engineering experience at AEDC, he has worked in the computational fluid dynamics (CFD) section by modifying and applying CFD codes to advanced fluid mechanics problems. Specifically, the last three years he has been involved in the area of using CFD in the store certification process to determine aircraft/store flowfields.

THIS PAGE INTENTIONALLY LEFT BLANK

UNSTRUCTURED GRID METHODS FOR STORE SEPARATION

Rainald Löhner
CMEE, SEAS, The George Washington University
Washington, D.C. 20052, USA

and

Joseph D. Baum
SAIC, McLean, VA 22102

ABSTRACT

Recent advances in grid generation, flow solvers for unstructured grids, local or global adaptive remeshing, rigid body motion integrators, interactive flow visualization tools and computer hardware have made it possible to simulate store separation problems in three dimensions. The purpose of this paper is to document the steps that were necessary to achieve such a fully coupled fluid-structure simulation capability, dwelling in detail on the grid generation, flow solver, rigid body motion integration and adaptive remeshing algorithms employed. Several results, showing single and multiple 3-D store separation, are given to demonstrate the capabilities developed.

1. INTRODUCTION

Store separation from aircraft or submarines has been an outstanding computational challenge for many years. In order to be more specific, consider the store separation from aircrafts flying at supersonic or hypersonic speeds. Figure 1 illustrates some of the relevant physical processes involved in these situations:

- Shock/Shock Interactions: at supersonic speeds, the presence of shocks in the flowfields becomes unavoidable. With several bodies interfering with each other, the shocks emanating from them interact with each other in sometimes extremely complicated ways [1,2].
- Shock-Boundary-Layer Interaction: when shocks impact on a surface, the boundary layer is greatly influenced by parameters such as shock-reflection angle, shock-strength, the pressure gradients upstream and downstream of the impact zone and body curvature. The resulting flowfield may vary abruptly with only minor changes of flight conditions.
- Turbulent Separated Flows: given the highly complex and not aerodynamically streamlined geometries of bombbays, many of the flowfields contemplated will have vast regions of separated, turbulent flow. This implies that any hope of simulating them accurately with a conventional, algebraic turbulence model has to be forfeited. The lowest order turbulence model that can yield acceptable results for flows of this type is the k, ϵ model.
- Body Motion: a further degree of complexity is added for the class of problems considered here due to the relative motion of the bodies present. The bodies move through an already complex, highly nonlinear flowfield, modifying it constantly.

All of these aspects, taken together, make the intuitive prediction of these flows, as well as any extrapolation from past experience, a very unreliable design approach. The non-linear character of these flows also implies that safe deployment from a mid-cavity position does not guarantee safe deployment from a side-cavity position. The only other two alternative design prec dures besides CFD, wind-tunnel measurements ana ight testing, are either extremely expensive or impossible.

Wind-tunnel experiments for store separation in the supersonic regime are difficult because:

- Three non-dimensional numbers need to be reproduced on the scaled model at the same time: Reynolds-number, Mach-number and Froude-number. For supersonic flows in particular, the reproduction of all three non-dimensional numbers in the windtunnel is practically impossible.
- The release of ordnance stores requires several seconds, a time-frame that would be too power-consuming -and thus expensive- for most large windtunnels.
- The release of ordnance stores into a supersonic free stream tends to accelerate these objects drastically, propelling them to high velocities very soon. Thus, one can expect extensive damage from any experimental program of this sort.

Thus, in-flight experiments appear as the only viable choice. However, this is a very primitive, and extremely expensive design process:

- A prototype has to be built to attain certainty in the safety of the design. Production of a com-

plete prototype on such uncertain terms -there is no guarantee that it will deploy safely- appears almost unjustifiable.

- Unsafe deployment may damage or destroy the carrier vehicle. This high risk implies additional expenses in any test program.
- The prototype has to be tested for each new release position: safe deployment from a given position at a certain speed and height does not imply safe deployment from any other position and/or any other speed and/or any other height. As one can see, this can lead to an extremely lengthy, and costly, certification procedure for each new ordnace store entering service.

The situation outlined above for store separation is not much different from that encountered in many other engineering applications, such as interstage separation in rockets, shroud removal for interceptors, separation of MIRVs, torpedo launch, reciprocating engines, turbines, propellers, ventilators and valves. The main difficulty in predicting all of these flowfields stems from the fact that body motion will, in most cases, lead to complex, time-dependent flows. Advances in computer speed and memory over the next decade will allow the simulation of these flows on a routine basis. Thus, one can expect CFD to gradually take the lead role in the design process for these applications. The present effort represents a first step in this direction.

1.1 General Features of any CFD Methodology for Moving Bodies

The accurate simulation of 3-D time-dependent, compressible flows with moving bodies requires:

a) Interactive Grid Generation Methods: The fast, userfriendly, interactive generation of grids in 3-D is essential to the success and widespread acceptance of any CFD tool in the user community. Without such a capability, the set-up times for new problems run in the order of months, significantly reducing the benefits which may be realized from any CFD methodology. Thus, interactive grid generation methods for unstructured grids that reduce set-up times to days if not hours are a prime requirement.

b) Solvers for Moving Frames of Reference: Since at the very least the portions of the mesh close to the moving bodies will move in time, the ability to describe the equations of motion for the fluids in moving frames of reference becomes mandatory.

c) High-order Monotonicity-preserving Schemes: These schemes are needed to simulate time-dependent flows with strong shocks and other discontinuities that will arise in the flows of interest in this effort (supersonic and hypersonic speeds).

d) Modelling of Turbulent, Separated Flows: The flowfields considered will have vast regions of separated, turbulent flow. The lowest order turbulence model that can yield acceptable results for the flows considered here is the k, ϵ model.

e) Fast Regridding Capabilities: These are needed because the motion of bodies may be severe, leading to distorted elements which in turn lead to poor numerical results.

f) Adaptive Refinement Schemes: Experience over the last years [3-7] has demonstrated that self-adaptive refinement schemes are essential in reducing the total number of degrees of freedom without deteriorating the accuracy of the solution. In 3-D, the ability to refine locally regions of interest will determine the accuracy of the result and whether it can be obtained in a reasonable time. Given the currently available hardware, it is impossible to solve 3-D problems using uniformly fine grids everywhere in the computational domain.

g) Consistent Rigid Body Motion Integrators: In order to fully couple the motion of rigid bodies with the aerodynamic forces exerted on them, consistent rigid body motion integrators must be developed. This task is relatively simple in 2-D. However, in 3-D the temporal variation of the moments of inertia tensor can lead to difficulties.

h) Interactive Post-Processing Capabilities: Understanding of the complex, time-dependent, 3-D flowfields requires instantaneous visualization of several key parameters such as pressure, Mach number, density, etc. An engineer that cannot visualize immediately a computed flowfield, in order to make judicious changes in the design, will never accept CFD as a design tool. Thus, a fast, interactive, workstation-based post-processing capability is required.

This list indicates that techniques from several different areas of CFD and Computer Science must be combined to meet the desired goal. It is therefore not surprising that very few attempts have been made to tackle the complete class of problems. Currently, the chimera grid scheme [8] seems to be the most promising approach for structured grids. In this approach, local grids for each body are overset on a major grid that covers the complete computational domain. For unstructured grids, Formaggia et al. [9] have used local remeshing for regions of distorted elements in combination with Eulerian and Arbitrary Eulerian-Lagrangian solvers in 2-D to simulate store separation problems. In both cases, the body motion was prescribed, and no adaptive refinement techniques were

employed. In 1988 the author presented a fully coupled 2-D fluid-rigid body interaction algorithm [5,6]. This algorithm also employed adaptive remeshing to accurately simulate the flowfield at hand. This development represented the first attempt to combine and incorporate in a single, coherent software package all of the requirements listed above.

The present paper extends this methodology to 3-D. While conceptually the same as the 2-D algorithm, the 3-D extension required several important improvements: better 3-D grid generators, consistent 3-D rigid body motion integrators, interactive plotting tools, and access to a large memory supercomputer for debugging. Given the currently available computer hardware, and our lack of knowledge in turbulence modelling, it seems unreasonable to include turbulence modelling at the present stage of development. Therefore, the present discussion will center on Euler-solvers, rather than Navier-Stokes solvers for compressible flows.

The rest of the paper is divided as follows: Section 2 treats the equations of motion for the flowfield in arbitrary frames of reference, as well as their solution (items b and c above). Section 3 deals with the equations of motion for the moving bodies (item g). In the present case, we restrict the description to rigid bodies. Section 4 outlines the gridding technique used (items a and e). The gridding technique is also used to adaptively regrid the computational domain (item f). Finally, section 5 contains numerical examples that demonstrate the capabilities developed.

2. THE EQUATIONS OF MOTION FOR THE FLUID

In order to handle the moving frames of reference associated with the moving finite elements, the partial differential equations need to be modified. This is most easily accomplished by the Arbitrary Lagrangian-Eulerian (ALE) formulation. The derivation of the equations may be found in [10]. Here, we just state the final form of the equations of motion. Given the velocity field $\mathbf{w}$ for the elements

$$\mathbf{w} = (w^x, w^y, w^z) \quad , \tag{1}$$

the Euler equations that describe an inviscid, compressible fluid may be written as

$$\left\{ \begin{matrix} \rho \\ \rho u^x \\ \rho u^y \\ \rho u^z \\ \rho e \end{matrix} \right\}_{,t} + \left\{ \begin{matrix} (u^i - w^i)\rho \\ (u^i - w^i)\rho u^x + p \\ (u^i - w^i)\rho u^y \\ (u^i - w^i)\rho u^z \\ (u^i - w^i)\rho e + u^i p \end{matrix} \right\}_{,i} = -\nabla \cdot \mathbf{w} \left\{ \begin{matrix} \rho \\ \rho u^x \\ \rho u^y \\ \rho u^z \\ \rho e \end{matrix} \right\} \tag{2}$$

Observe that in the case of no element movement ($\mathbf{w} = 0$), we recover the usual Eulerian conservation-law form of the Euler equations. If, however, the elements move with the particle velocity ($\mathbf{w} = \mathbf{v}$), we recover the Lagrangian form of the equations of motion. From the numerical point of view, Eqn.(2) implies that all that is required when going from an Eulerian frame to an ALE-frame is a modified evaluation of the fluxes on the left-hand side, and the additional evaluation of source-terms on the right-hand side.

As the elements move, their geometric parameters (shape-function derivatives, jacobians, etc.) need to be recomputed every timestep. If the whole mesh is assumed to be in motion, then these geometric parameters need to be recomputed globally. In order to save CPU-time, only a small number of elements surrounding the bodies are actually moved. The remainder of the field is then treated in the usual Eulerian frame of reference, avoiding the need to recompute geometric parameters. This is accomplished by identifying several layers of elements surrounding the bodies, which are then moved. As the number of layers increases, the time-interval between regridding increases, but so also does the cost per timestep. Therefore, one has to strike a balance between the CPU requirements per timestep and the CPU requirements per regridding. In the present case, we found that two to five layers of elements represented a good compromise.

2.1 Boundary Conditions

When imposing the boundary conditions for the velocities at solid walls, we need to take the velocity of the surface $\mathbf{w}$ into consideration. Denoting the predicted momentum at the surface as $\Delta\rho\mathbf{v}^*$, we can decompose it as follows:

$$\Delta\rho\mathbf{v}^* = \Delta\left[\rho\left(\mathbf{w} + \alpha\mathbf{t} + \beta\mathbf{n}\right)\right] \quad , \tag{3}$$

where $\mathbf{t}, \mathbf{n}$ are the tangential and normal vectors. The desired momentum at the new timestep should, however, have no normal velocity component ($\beta = 0$) and has the form

$$\Delta\rho\mathbf{v}^{n+1} = \Delta\left[\rho\left(\mathbf{w} + \alpha\mathbf{t}\right)\right] \quad . \tag{4}$$

Combining Eqns.(3) and (4), we obtain for the two following cases:

a) Given $\mathbf{t}$:

$$\Delta\rho\mathbf{v}^{n+1} = \Delta\rho\mathbf{w} + \left[\left(\Delta\rho\mathbf{v}^* - \Delta\rho\mathbf{w}\right)\cdot\mathbf{t}\right]\cdot\mathbf{t} \quad , \tag{5}$$

b) Given **n** :

$$\Delta\rho\mathbf{v}^{n+1} = \Delta\rho\mathbf{v}^* - [(\Delta\rho\mathbf{v}^* - \Delta\rho\mathbf{w})\cdot\mathbf{n}]\cdot\mathbf{n} \quad . \qquad (6)$$

2.2 The Flow Solver (FEM-FCT)

For the compressible flows described by Eqn.(2), discontinuities in the variables may arise (e.g., shocks or contact discontinuities). Any numerical scheme of order higher than one will produce overshoots or ripples at such discontinuities (the so-called 'Godunov theorem'). In the present case the appearance of these overshoots, which may lead to numerical instability, is avoided by combining, in a conservative manner, a high-order scheme with a low-order scheme [11]. The temporal discretization of Eqn.(2) yields

$$U^{n+1} = U^n + \Delta U \quad , \qquad (7)$$

where ΔU is the increment of the unknowns obtained for a given scheme at time $t = t^n$. Our aim is to obtain a ΔU of as high an order as possible without introducing overshoots. To this end, we rewrite Eqn.(7) as:

$$U^{n+1} = U^n + \Delta U^l + (\Delta U^h - \Delta U^l), \qquad (8)$$

or

$$U^{n+1} = U^l + (\Delta U^h - \Delta U^l) \quad . \qquad (9)$$

Here ΔU^h and ΔU^l denote the increments obtained by some high- and low-order scheme respectively, whereas U^l is the monotone, ripple-free solution at time $t = t^{n+1}$ of the low-order scheme. The idea behind FCT is to limit the second term on the right-hand side of Eqn.(9):

$$U^{n+1} = U^l + lim(\Delta U^h - \Delta U^l), \qquad (10)$$

in such a way that no new overshoots or undershoots are created. It is at this point that a further constraint, given by the conservation law (2) itself, must be taken into account: strict conservation on the discrete level should be maintained. The simplest way to guarantee this for the node-centered schemes considered here is by constructing schemes for which the sum of the contributions of each individual element (cell) to its surrounding nodes vanishes. This means that the limiting process (Eqn.(10)) will have to be carried out in the elements (cells). Further details on the limiting procedure, its algorithmic implementation, and the high- and low-order schemes employed may be found in [11].

3. RIGID BODY MOTION

The movement of rigid bodies can be found in standard textbooks on classical mechanics. See, for example [12]. Due to its nonlinear character, rigid body motion in 3-D is not as straightforward as it may seem. Therefore, a more detailed description of the numerical implementation used is given here. The situation under consideration is shown in Figure 2. Given the position vector of any point of the body

$$\mathbf{r} = \mathbf{r}_c + \mathbf{r}_0 \quad , \qquad (11)$$

the velocity and acceleration of this point will be

$$\dot{\mathbf{r}} = \dot{\mathbf{r}_c} + \dot{\mathbf{r}_0} = \mathbf{v}_c + \omega \times \mathbf{r}_0 \quad , \qquad (12)$$

$$\ddot{\mathbf{r}} = \dot{\mathbf{v}_c} + \dot{\omega} \times \mathbf{r}_0 + \omega \times (\omega \times \mathbf{r}_0) \quad . \qquad (13)$$

Using the vector-relationships

$$\mathbf{r} \times (\omega \times (\omega \times \mathbf{r})) = (\mathbf{r} \cdot (\omega \times \mathbf{r}))\,\omega - (\mathbf{r}\cdot\omega)(\omega \times \mathbf{r})$$

$$= -\omega \times (\mathbf{r} \otimes \mathbf{r}) \cdot \omega \quad , \qquad (14)$$

and the following abbreviations

$$m = \int_\Omega dm = \int_\Omega \rho d\Omega \quad , \qquad (15)$$

$$I_{ij} = \int_\Omega r_0^i r_0^j \rho d\Omega \quad , \qquad (16)$$

$$\Theta = tr(\mathbf{I}) \cdot 1 - \mathbf{I} =$$

$$\begin{Bmatrix} I_{yy} + I_{zz} , & -I_{xy} , & -I_{xz} \\ -I_{xy} , & I_{xx} + I_{zz} , & -I_{yz} \\ -I_{xz} , & -I_{yz} , & I_{xx} + I_{yy} \end{Bmatrix} \quad , \qquad (17)$$

we then have the following equations describing balance of forces and moments:

$$m\dot{\mathbf{v}_c} = \sum \mathbf{F} = m\mathbf{g} - \int_\Gamma p\mathbf{n} d\Gamma \quad , \qquad (18)$$

$$\Theta\dot{\omega} - \omega \times (\mathbf{I}\cdot\omega) = \sum \mathbf{r}_0 \times \mathbf{F} = -\int_\Gamma p\mathbf{r}_0 \times \mathbf{n} d\Gamma \quad . \qquad (19)$$

Observe that in 2-D, the second term on the left-hand side disappears, considerably simplifying the equations. However, in 3-D it usually does not. Another complication that arises only in 3-D is the temporal variation of the inertial matrix Θ. As one can see from Eqn.(16), the values of Θ will vary as the body rotates. This implies that during the simulation one has to follow the local frame of reference of the body.

In order to update the velocities and positions of the bodies in time, we employ an explicit time-marching scheme. This seems reasonable, as in practical calculations the time-scales of the body-movement are much larger than those associated with the fluid flow. Thus, we update $\mathbf{v}_c, \omega$ as follows:

$$\mathbf{v}_c^{n+1} = \mathbf{v}_c^n + \Delta t\, \dot{\mathbf{v}}_c^n \quad , \tag{20}$$

$$\omega^{n+1} = \omega^n + \Delta t\, \dot{\omega}^n \quad . \tag{21}$$

A minor difficulty now becomes apparent: the magnitude of the timestep Δt is unknown before the start of the flowfield update. In the present case, the timestep of the previous timestep was taken instead. This implies that the body movement is 'lagging' behind the flowfield by at most one timestep. However, practical simulations show that the actual error is much smaller, as the magnitude of Δt does not change abruptly. For the time-interval $[t^n, t^{n+1}]$, we then have the average velocities

$$\mathbf{v}_c^{av} = 0.5 * (\mathbf{v}_c^{n+1} + \mathbf{v}_c^n) \quad , \tag{22}$$

$$\omega^{av} = 0.5 * (\omega^{n+1} + \omega^n) \quad . \tag{23}$$

Combining Eqns.(22,23) with Eqn.(12), we are now in a position to compute the velocities at the surface of the bodies, $\mathbf{w}_\Gamma$.

Some of the simulations shown below required several thousand timesteps. If one simply uses the velocities obtained at the boundary from Eqns.(22,23), the body shape becomes more and more distorted. This is a purely numerical artifact. It can be explained by looking at the situation depicted in Figure 3. The portions of the body with higher velocity tend to 'elongate' the body. This implies that one ought to impose the exact rigid body motion when updating points on the surface. With reference to Figure 4, we decompose a point lying on the body at time $t = t^n$ into three components:

$$\mathbf{r}^n = \mathbf{r}_c + \mathbf{r}_\varphi + \mathbf{r}_r \quad . \tag{24}$$

We can then define unit vectors in the directions of $\mathbf{r}_\varphi$ and $\mathbf{r}_r$:

$$\mathbf{e}_\varphi = \frac{\mathbf{r}_\varphi}{|\mathbf{r}_\varphi|} \quad , \quad \mathbf{e}_r = \frac{\mathbf{r}_r}{|\mathbf{r}_r|} \quad . \tag{25}$$

Furthermore, we define the vector $\mathbf{e}_n$ as:

$$\mathbf{e}_n = \mathbf{e}_\varphi \times \mathbf{e}_r \quad . \tag{26}$$

Then, given the incremental rotation angle $\Delta\varphi = |\omega^{av}|\Delta t$, the new position for $\mathbf{r}$ is obtained from

$$\mathbf{r}^{n+1} = \mathbf{r}_c + \Delta t \mathbf{v}_c^{av} + \mathbf{r}_\varphi + |\mathbf{r}_r|\,(cos(\Delta\varphi)\mathbf{e}_r + sin(\Delta\varphi)\mathbf{e}_n) \quad . \tag{27}$$

The complete rigid body algorithm then consists of the following steps:

B.1) Compute body forces and moments from Eqns.(18,19).

B.2) Transform moments to the local frame of reference of the body

$$M^{i'} = \left(\mathbf{e}^{i'} \cdot \mathbf{e}^{i}\right) M^{i} \quad . \tag{28}$$

B.3) Given the estimated timestep Δt, obtain the accelerations $\dot{\mathbf{v}}_c$, $\dot{\omega}$ from Eqns.(18,19).

B.4) Given the accelerations, compute average velocities $\mathbf{v}_c^{av}, \omega^{av}$ for time-interval $[t^n, t^{n+1}]$ from Eqns.(22,23).

B.5) Transform back the angular velocity ω^{av} from the local frame of reference of the body to cartesian coordinates

$$\omega^{i} = \left(\mathbf{e}^{i} \cdot \mathbf{e}^{i'}\right) \omega^{i'} \quad . \tag{29}$$

B.6) Given the actual timestep Δt, update the positions of the points lying on the surface of the body, as well as the points defining the body geometry using Eqns.(24-27).

B.7) Given the actual timestep Δt, update the positions of the centers of mass and the rotational frame of reference using Eqns.(24-27).

4. ADAPTIVE REMESHING

For typical compressible flow problems, we have small regions of rapid change in the solution embedded in large regions where the solution is smooth. In order to simulate correctly the interaction of these discontinuities or fronts, an appropriately fine mesh is required. It would however be extremely wasteful to have an overall fine mesh, as the regions where a fine mesh is required are small. Therefore, the use of adaptive refinement techniques becomes imperative. As the bodies in the flowfield may undergo arbitrary movement (see examples below), a fixed mesh structure will lead to badly distorted elements. This means that at least a partial regeneration of the computational domain is required. On the other hand, as the bodies move through the flowfield, the positions of relevant flow features will change. Therefore, in most of the computational domain a new mesh distribution will be required. The idea is to regenerate the whole computational domain adaptively, taking into consideration the current flowfield solution. In order to generate or regenerate a mesh we use the advancing front technique [4-7,13-15]:

F.1 Use the current grid and solution, together with appropriate error indicators, to define the spatial variation of the size, the stretching, and the stretching direction of the elements to be generated. At the nodes of the current grid we define the desired element size, element stretching, and stretching direction. In what follows we will denote this grid as background grid.

F.2 Define the boundaries of the domain to be gridded. This is typically accomplished by splines in 2-D and surface patches in 3-D.

F.3 Using the information stored on the background grid, set up faces on all these boundaries. This yields the initial front of faces. At the same time, find the generation parameters (element size, element stretching and stretching direction) for these faces from the background grid.

F.4 Select the next face to be deleted from the front; in order to avoid large elements crossing over regions of small elements, the face forming the smallest new element is selected as the next face to be deleted from the list of faces.

F.5 For the face to be deleted:

F.5.1 Select a 'best point' position for the introduction of a new point `IPNEW`.

F.5.2 Determine whether a point exists in the already generated grid that should be used in lieu of the new point. If there is such a point, set this point to `IPNEW` and continue searching (go to F.5.2).

F.5.3 Determine whether the element formed with the selected point `IPNEW` does not cross any given faces. If it does, select a new point as `IPNEW` and try again (go to F.5.3).

F.6 Add the new element, point, and faces to their respective lists.

F.7 Find the generation parameters for the new faces from the background grid.

F.8 Delete the known faces from the list of faces.

F.9 If there are any faces left in the front, go to F.4.

4.1 Recent Developments

A typical simulation where bodies undergo severe motion typically requires several tens, if not hundreds, of remeshings. Therefore, the grid generator must be reliable and fast.

4.1.1 Reliability:

We have recently increased the reliability of the grid generator to a point where it can be applied on a routine basis in a production environment. This significant increase in reliability was achieved by:
a) not allowing any bad elements during the generation process: and
b) enlarging and remeshing those regions where new elements could not be introduced.
Thus, we first attempt to complete the mesh, skipping those faces that do not give rise to good elements. If pockets of unmeshed regions remain, we enlarge them somewhat, and regrid them. This technique has proven extremely robust and reliable. It has also made smoothing of meshes possible: if elements with negative or small jacobians appear during smoothing, these elements are removed. The unmeshed regions of space are then regridded. By being able to smooth, the mesh quality was improved substantially.

4.1.2 Speed:

The following means are used to achieve speed:

a) Use of optimal data structures: The operations that could potentially reduce the efficiency of the algorithm to $O(N^{1.5})$ or even $O(N^2)$ are (see Section 2):

- Finding the next face to be deleted (step F.4).
- Finding the closest given points to a new point (Step F.5.2).
- Finding the faces adjacent to a given point (Step F.5.3).
- Finding for any given location the values of generation parameters from the background grid (Steps F.3 and F.7). This is an interpolation problem on unstructured grids.

The verb 'find' appears in all of these operations. The main task is to design the best data structures for performing these search operations as efficiently as possible. The data structures used are:

- Heap-lists to find the next face to be deleted from the front;
- Quad-trees (2-D) and Octrees (3-D) to locate points that are close to any given location;
- Linked lists to determine which faces are adjacent to a point.

The detailed implementation of these data-structures may be found in [13].

b) Filtering: Typically, the number of close points and faces is far too conservative, i.e. large. As an example, consider the search for close points: there may be up to eight points inside an octant, but of these only one may be close to the face to be taken out. The idea is to filter out these 'distant' faces and points in order to avoid extra work afterwards. While the search operations are difficult to vectorize, these filtering operations lend themselves to vectorization in a straightforward way, leading to a considerable overall reduction in CPU requirements.

c) Automatic Reduction of Unused Points: As the front advances into the domain and more and more tetrahedra are generated, the number of tree-levels increases. This automatically implies an increasing

CPU-time, as more steps are required to reach the lower levels of the trees. In order to reduce this CPU-increase as much as possible, all trees are automatically restructured. All points which are completely surrounded by tetrahedra are eliminated from the trees. We have found this procedure to be extremely effective. It reduced the asymptotic complexity of the grid generator to less than $O(N \log N)$. In fact, in most practical cases one observes a linear $O(N)$ asymptotic complexity, as CPU is traded between subroutine call overheads and less close faces on average for large problems.

d) Global h-refinement: While the basic advancing front algorithm is a scalar algorithm, h-refinement can be completely vectorized. Therefore, the adaptive remeshing process can be made considerably faster by first generating a coarser, but stretched mesh, and then refining globally this first mesh with classic h-refinement [6]. Typical speed-ups achieved by using this approach are 1:6 to 1:7.

Currently, the advancing front algorithm constructs grids at a rate of 25,000 tetrahedra per minute on the CRAY-XMP or CRAY-2. With one level of h-refinement, the rate is 190,000 to 200,000 tetrahedra per minute. This rate is essentially independent of grid-size, but may decrease for very small grids.

4.2 Local Remeshing

Practical simulations revealed that the appearance of badly distorted elements occurred at a frequency that was much higher than expected from the element size prescribed. Given the relatively high cost of global remeshing, we explored the idea of local remeshing in the vicinity of the elements that became too distorted. Thus, we proceed as follows:

L.1 Identify the badly distorted elements in the layers that move, writing them into a list `LEREM(1:NEREM)`.

L.2 Add to this list the elements surrounding these badly distorted elements.

L.3 Form 'holes' in the present mesh by:

- L.3.1 Forming a new background mesh with the elements stored in the list `LEREM` .
- L.3.2 Deleting the elements stored in `LEREM` from the current mesh.
- L.3.3 Removing all unused points from the grid thus obtained.

L.4 Recompute the error indicators and new element distribution for the background grid.

L.5 Regrid the 'holes' using the advancing front method.

Typically, only a very small number of elements (< 10) becomes so distorted that a remeshing is required. Thus, local remeshing is a very economical tool that has allowed us to reduce CPU-requirements by more than 60% for typical runs.

4.3 Determination of Element Sizes

In order to estimate the element size, stretchings, and stretching directions, we employ the modified interpolation theory error indicator proposed in [3]. In 1-D, on a uniform grid of element size h, this error indicator reduces to the following form:

$$E_i = \frac{|U_{i+1} - 2 \cdot U_i + U_{i-1}|}{|U_{i+1} - U_i| + |U_i - U_{i-1}| + c_n \left[|U_{i+1}| + 2 \cdot |U_i| + |U_{i-1}|\right]} \tag{30}$$

Defining the following 'derivative quantities':

$$D_i^0 = c_n \left(|U_{i+1}| + 2 \cdot |U_i| + |U_{i-1}|\right) \ , \tag{31}$$

$$D_i^1 = |U_{i+1} - U_i| + |U_i - U_{i-1}| \ , \tag{32}$$

$$D_i^2 = |U_{i+1} - 2 \cdot U_i + U_{i-1}| \ , \tag{33}$$

the error on the present ('old') grid is given by:

$$E_i^{old} = \frac{D_i^2}{D_i^1 + D_i^0} \ . \tag{34}$$

This implies that a reduction of the current element size h^{old} by a fraction ξ to

$$h^{new} = \xi \cdot h^{old} \tag{35}$$

will lead to the following estimated errors

$$E_i^{new} = \frac{D_i^2 \xi^2}{D_i^1 \xi + D_i^0} \ . \tag{36}$$

Thus, given the desired error value E^{new}, the reduction factor ξ becomes

$$\xi = \frac{E^{new}}{E^{old}} \frac{1}{2} \left[\frac{D_i^1 + \sqrt{(D_i^1)^2 + 4 D_i^0 \frac{E^{old}}{E^{new}} \left[D_i^1 + D_i^0\right]}}{\left[D_i^1 + D_i^0\right]} \right] \tag{37}$$

Notice that if the solution is smooth, implying $D^1 \ll D^0$, then the reduction factor reverts to

$$\xi = \sqrt{\frac{E^{new}}{E^{old}}} \ , \tag{38}$$

consistent with the second-order accuracy assumption of linear elements. However, close to a discontinuity, where $D^1 \gg D^0$, the reduction factor ξ is given by

$$\xi = \frac{E^{new}}{E^{old}} \ . \tag{39}$$

In 2-D and 3-D we define the corresponding matrices

$$(D^0)^I_{kl} = h^2 c_n \int_\Omega |N^I_{,k}||N^J_{,l}||U_J| d\Omega \ , \qquad (40)$$

$$(D^1)^I_{kl} = h^2 \int_\Omega |N^I_{,k}||N^J_{,l} U_J| d\Omega \ , \qquad (41)$$

$$(D^2)^I_{kl} = h^2 | \int_\Omega N^I_{,k} N^J_{,l} d\Omega \ U_J \ | \ , \qquad (42)$$

where N^I denotes shape-function of node I, and h is a typical element length. Given these matrices, we obtain the error-indicator matrix $\mathbf{E}$ and its modal decomposition

$$\mathbf{E} = \begin{Bmatrix} E_{xx} & E_{yx} & E_{zx} \\ E_{xy} & E_{yy} & E_{zy} \\ E_{xz} & E_{yz} & E_{zz} \end{Bmatrix} = \mathbf{X} \cdot \begin{Bmatrix} E_{11} & 0 & 0 \\ 0 & E_{22} & 0 \\ 0 & 0 & E_{33} \end{Bmatrix} \cdot \mathbf{X}^{-1} \qquad (43)$$

Each principal direction is then treated as a 1-D problem. Using Eqn.(37), we obtain three different element sizes δ_1, δ_2, δ_3 along the principal directions. This information is then used to regenerate a better grid for the problem at hand. We remark the following characteristics of the present error indicator:
a) The error indicator is non-dimensional. Therefore, several variables may be monitored at the same time in order to accurately track all physical phenomena present. Thus, we can monitor both density (shocks, contact discontinuities) and vorticity (boundary layers) for viscous flow problems.
b) The error indicator is bounded. This implies that the user does not have to change specified error tolerances from run to run. We have found that for large classes of problems the specified error tolerances could be left untouched without impediment to the adaptation process. We find this of particular value for the non-expert user environment.

Before proceeding to the overall algorithm, we summarize the steps required for one adaptive remeshing:

- R.1 Obtain the error indicator matrix for the gridpoints of the present grid.
- R.2 Given the error indicator matrix, get the element size, element stretching and stretching direction for the new grid.
- R.3 Using the old grid as the 'background grid', remesh the computational domain using the advancing front technique.
- R.4 If further levels of global h-refinement are desired: refine the new grid globally.
- R.5 Interpolate the solution from the old grid to the new one.

5. THE OVERALL ALGORITHM

The overall algorithm for the advancement of the solution in time looks as follows:

- O.1 Advance the solution one timestep.
  - A.1 Compute the body forces and moments from the pressure field and any exterior forces.
  - A.2 Taking into consideration the kinematic constraints for the body movements, update the velocities of the bodies at $t = t^{n+1}$: $\mathbf{v}_c^{n+1}, \omega^{n+1}$. At the same time, obtain the average velocities $\mathbf{v}_c^{av}, \omega^{av}$ for the time-interval $[t^n, t^{n+1}]$.
  - A.3 With the average velocities $\mathbf{v}_c^{av}, \omega^{av}$, obtain the velocities $\mathbf{w}_\Gamma$ on the surface of each body for the time-interval $[t^n, t^{n+1}]$.
  - A.4 Given the surface velocities $\mathbf{w}_\Gamma$ on the boundaries of the global domain, obtain the global velocity field $\mathbf{w}_\Omega$ for the element movement.
  - A.5 Advance the solution by one timestep using the ALE-FEM-FCT solver. This yields the actual timestep Δt^n.
  - A.6 Given the actual timestep Δt^n and the velocity field for the element movement $\mathbf{w}_\Omega$, update the coordinates of the points.
  - A.7 Update the shape-function derivatives and other geometric parameters for the elements that have been moved.
  - A.8 Update the centers of mass $\mathbf{r}_c$ for the bodies, as well as the coordinates of the points defining the body geometry.
- O.2 If the grid has become too distorted close to the moving bodies: adaptively remesh these regions.
- O.3 If the desired number of timesteps between global remeshings has elapsed: adaptively remesh the complete computational domain.
- O.4 If the desired time-interval has elapsed: Stop. Otherwise, advance the solution further (go to O.1)

6. NUMERICAL EXAMPLES

We consider two numerical examples that demonstrate the effectiveness of the algorithms developed. In both cases an idealized store release from a bay at supersonic speed ($Ma_\infty = 2.0$) is simulated. Because of symmetry, only half the flowfield domain needs to be simulated. Release into a supersonic flowfield will neccessitate the forceful ejection of stores. Therefore, the motion of the stores was prescribed, and the resulting forces computed. Adaptive remeshing was performed every 100 timesteps initially, while at later times the grid was modified every 40 timesteps. The maximum stretching ratio specified was $S = 6^5_8$

Density and the absolute value of the velocity were chosen as indicator variables. The latter provided suitable mesh adaptation to the shear layers in the cavity. Even though the grid shows considerable variation in element size, the average grid size was of the order of 280,000 tetrahedra for the first example, and 350,000 tetrahedra for the second one. On a uniform mesh, the required number of elements would have increased by more than an order of magnitude. The required CPU time for runs of this kind is of the order of several CRAY-XMP processor hours.

6.1 Single Store Ejection:

The computational domain is shown in Figs. 5.1 and 5.2. Observe that the doors of the bay simulated are somewhat thicker than in real life. The store is a slender object, resembling a missile. Figs. 5.1 and 5.2 show the mesh on the surface of the computational domain at time $T = 0.0$. The corresponding pressure contours (30) are show in Fig. 5.3. Figs. 5.4-5.6 show the surface mesh and the pressure contours (60) at time $T = 8.5$. One can clearly discern the extent of mesh adaptation, as well as the considerable change in shock-strengths and shock-positions that occurred due to body motion.

6.2 Multiple Store Ejection:

The computational domain is the same as before. The two stores resemble bombs. The store at the back of the cavity is ejected first, followed by the store in the front of the cavity. Figs. 6.1 and 6.2 show the mesh on the surface of the computational domain at time $T = 0.0$. The corresponding pressure contours (60) are show in Fig. 6.3. Figs. 6.4-6.6 show the surface mesh and the pressure contours (60) at time $T = 2.62$. While the store at the back of the cavity has already moved a considerable distance, the sore in the front has just begun to move. As before, one can clearly discern the extent of mesh adaptation, as well as the considerable change in shock-strengths and shock-positions that occurred due to body motion.

7. CONCLUSIONS

We have demonstrated how the combination of adaptive remeshing techniques, flow solvers for transient problems with moving grids, and integrators for rigid body motion allows the simulation of fully coupled fluid-rigid body interaction problems of arbitrary geometric complexity in three dimensions. The overall reduction in CPU-times as compared to uniformly fine grids depends strongly on the stretching ratios allowed by the physics of the problem, but typically lies between 10 and 50. Areas that deserve further study are:

- the diffusive effect of interpolation while remeshing,
- extension to Navier-Stokes problems,
- treatment of multifluid interactions, and
- extension to flexible bodies and structures.

8. ACKNOWLEDGEMENTS

This work was partially funded by AFOSR under contract AFOSR-89-0540. Dr. Leonidas Sakell was the technical monitor.
The generous support of CRAY Research, Inc. in the form of ample CPU-time on a CRAY-2S is also gratefully acknowledged.

9. REFERENCES

[1] B. Edney - Anomalous Heat Transfer and Pressure Distribution on Blunt Bodies at Hypersonic Speeds in the Presence of an Impinging Shock; *FAA Rep.* 115, Aero. Res. Inst. Sweden (1986).

[2] R. Thareja, J.R. Steward, O. Hassan, K. Morgan and J. Peraire - A Point-Implicit Unstructured Grid Solver for the Euler and Navier-Stokes Equations; *Int. J. Num. Meth. Fluids* 9, 405-425 (1989).

[3] R. Löhner - An Adaptive Finite Element Scheme for Transient Problems in CFD; *Comp. Meth. Appl. Mech. Eng.* 61, 323-338 (1987).

[4] J.D. Baum and R. Löhner - Numerical Simulation of Shock-Elevated Box Interaction Using an Adaptive Finite Element Shock Capturing Scheme; AIAA-89-0653 (1989).

[5] R. Löhner - An Adaptive Finite Element Solver for Transient Problems with Moving Bodies; *Comp. Struct.* 30, 303-317 (1988).

[6] R. Löhner - Adaptive Remeshing for Transient Problems; *Comp. Meth. Appl. Mech. Eng.* 75, 195-214 (1989).

[7] J. Peraire, M. Vahdati, K. Morgan and O.C. Zienkiewicz - Adaptive Remeshing for Compressible Flow Computations; *J. Comp. Phys.* 72, 449-466 (1987).

[8] F.C. Dougherty and J. Kuan - Transonic Store Separation Using a Three-Dimensional Chimera Grid Scheme; AIAA 89-0637 (1989).

[9] L. Formaggia, J. Peraire and K. Morgan - Simulation of a Store Separation Using the Finite Element Method; *Appl. Math. Mod.* 12, 175-181 (1988).

[10] J. Donea - An Arbitrary Lagrangian-Eulerian Finite Element Method for Transient Dynamic Fluid-Structure Interactions, *Comp. Meth. Appl. Mech. Eng.* 33, 689-723 (1982).

[11] R. Löhner, K. Morgan, J. Peraire and M. Vahdati - Finite Element Flux-Corrected Transport (FEM-FCT) for the Euler and Navier-Stokes

Equations; *Int. J. Num. Meth. Fluids* 7, 1093-1109 (1987).

[12] A. Sommerfeld - *Vorlesungen über Theoretische Mechanik*; Verlag Harri Deutsch, Frankfurt (1976).

[13] R. Löhner - Some Useful Data Structures for the Generation of Unstructured Grids; *Comm. Appl. Num. Meth.* 4, 123-135 (1988).

[14] R. Löhner and P. Parikh - Three-Dimensional Grid Generation by the Advancing Front Method; *Int. J. Num. Meth. Fluids* 8, 1135-1149 (1988).

[15] J. Peraire, K. Morgan and J. Peiro - Unstructured Finite Element Mesh Generation and Adaptive Procedures for CFD; AGARD-CP-464, 18 (1990).

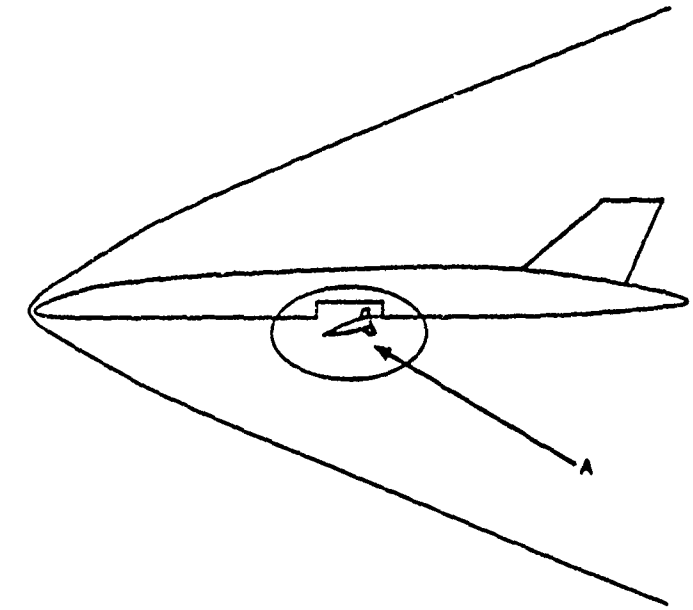

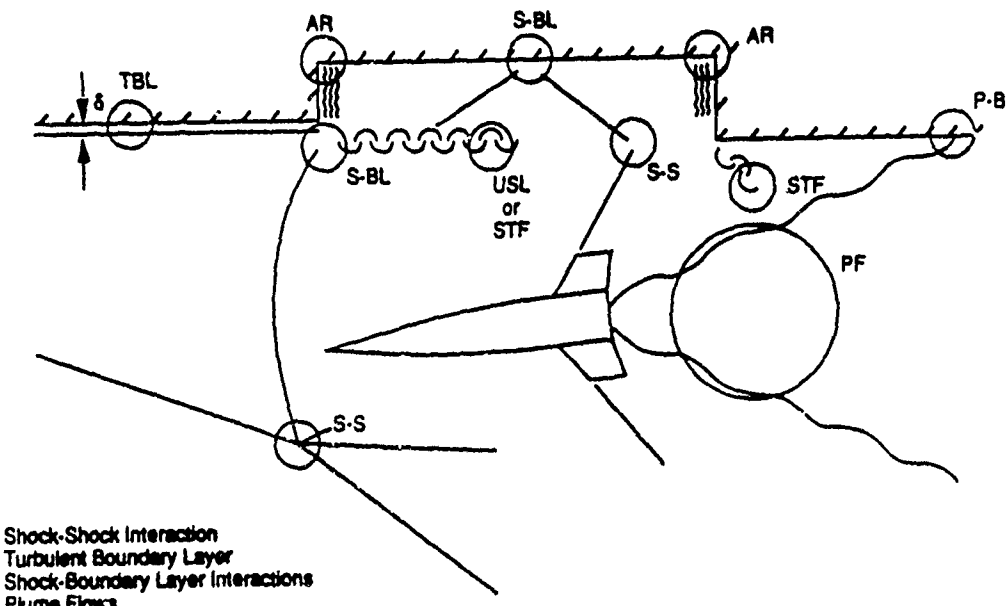

S-S: Shock-Shock Interaction
TBL: Turbulent Boundary Layer
S-BL: Shock-Boundary Layer Interactions
PF: Plume Flows
STF: Separated, Turbulent Flow Regions
AR: Acoustic Resonance
USL: Unstable Shear Layer
P-B: Plume-Body Interaction

Enlargement of Area A

Figure 1: Store Separation: Relevant Physical Processes

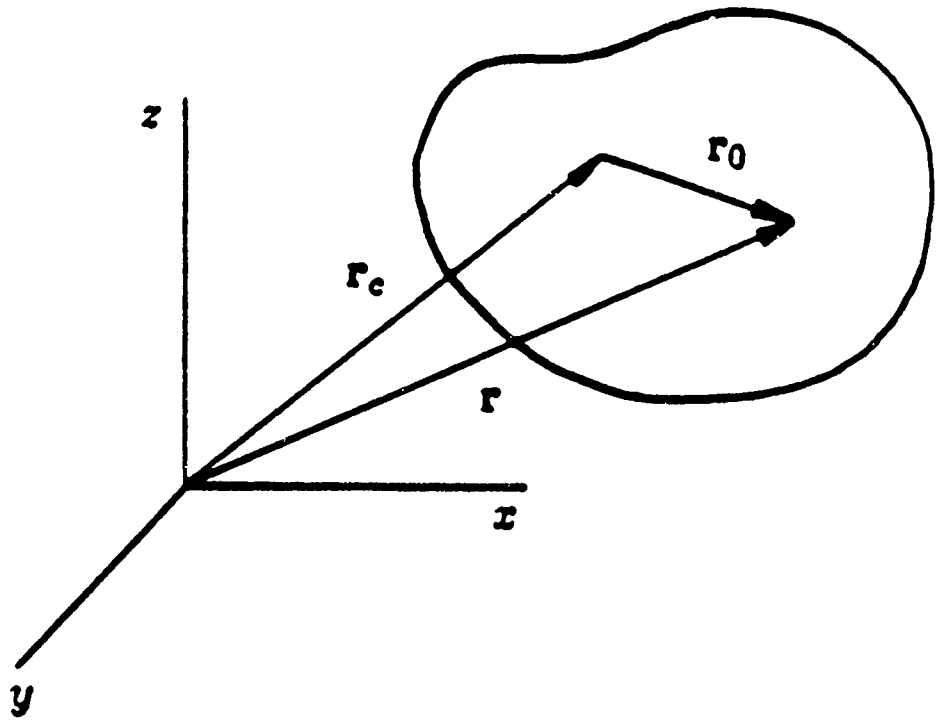

Figure 2: Rigid Body Motion

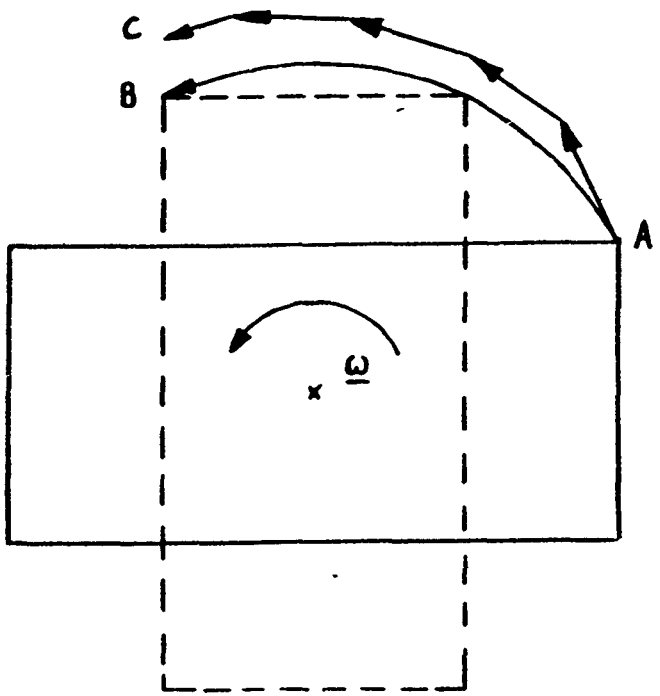

Figure 3: Elongation of Body. Correct Path: AB. Computed: AC.

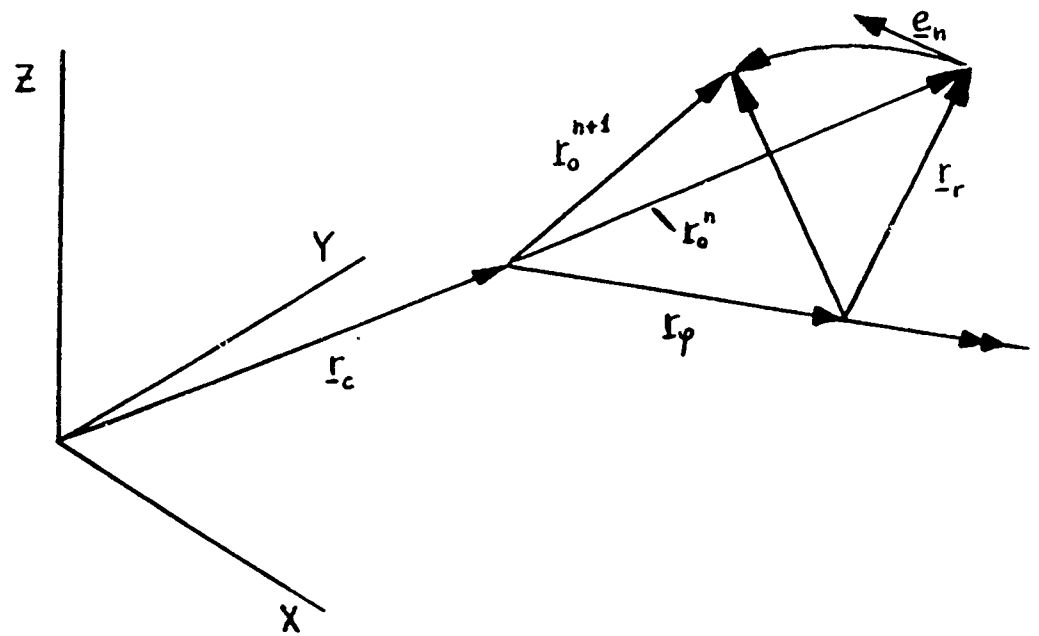

Figure 4: Decomposition of Surface Vector for Rigid Body Motion

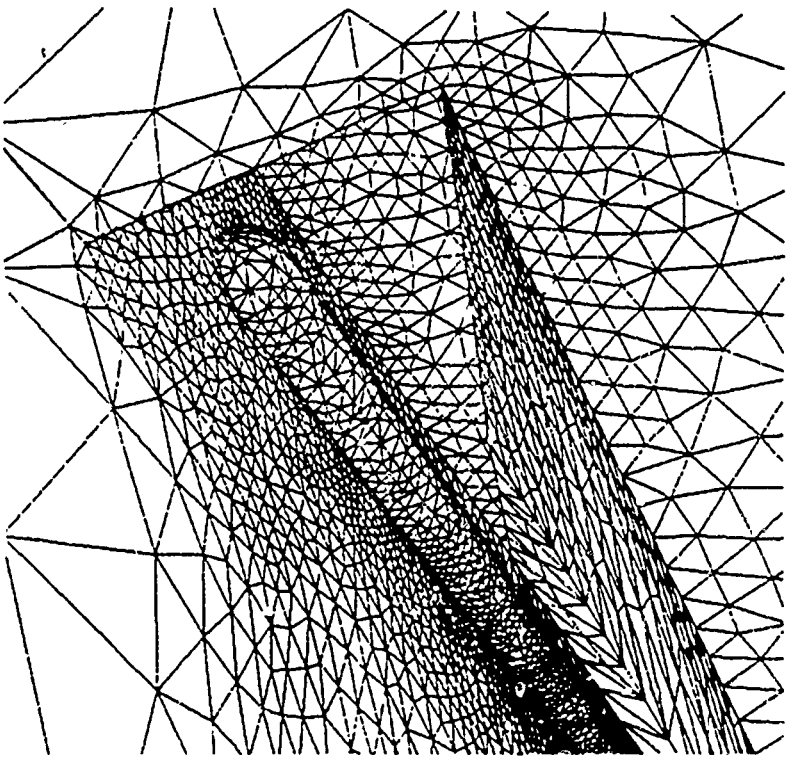

5 1

FEFLO52

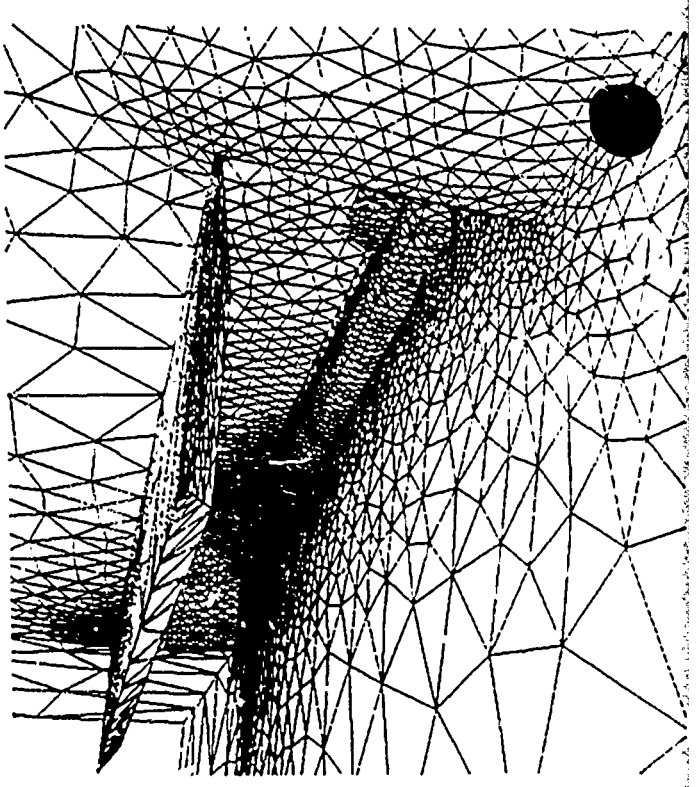

5 2

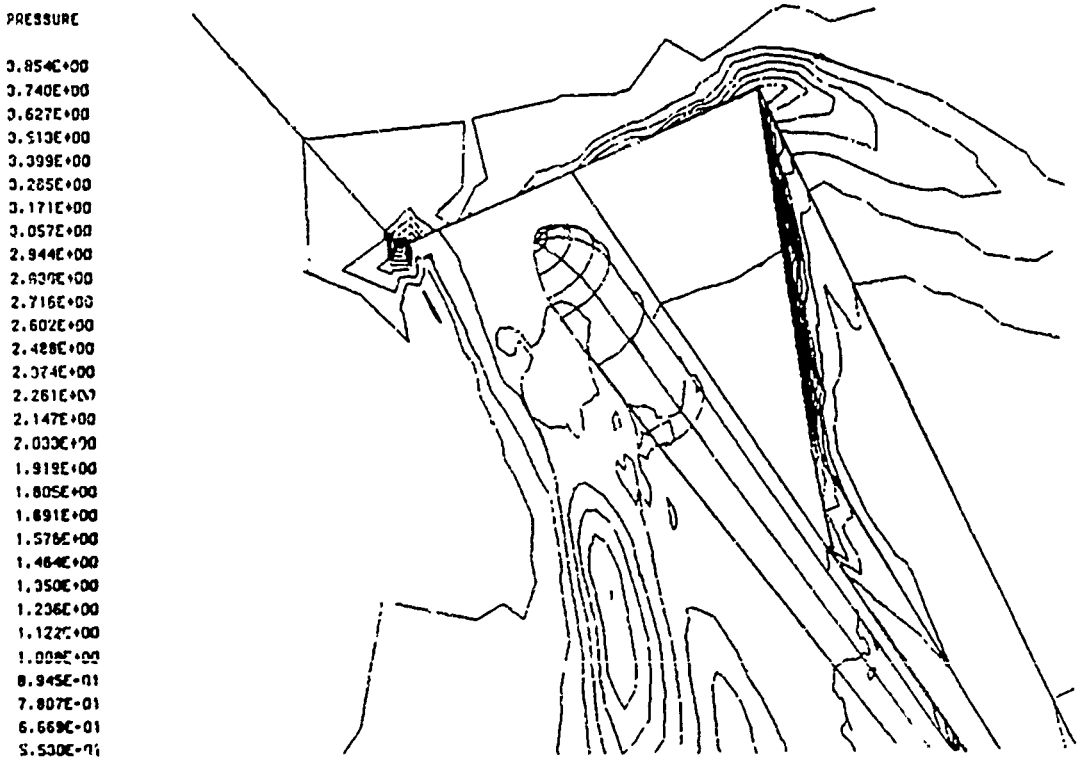

FEFLO52

5 3

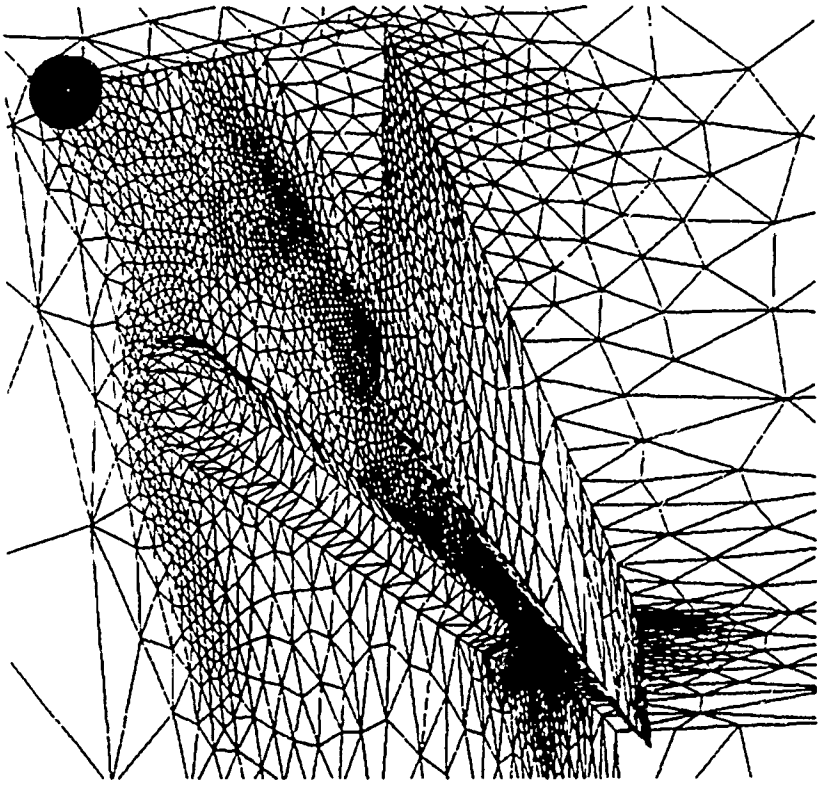

54

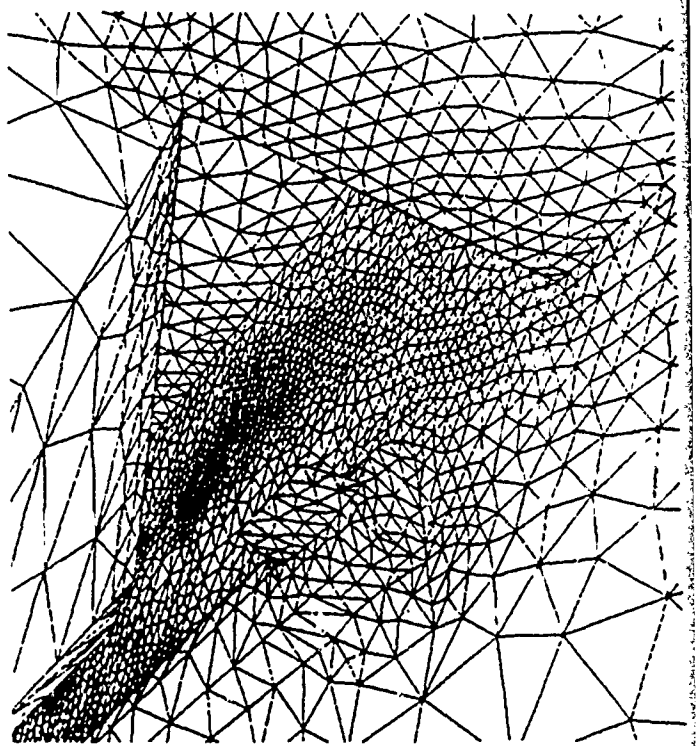

55

FEFLO52

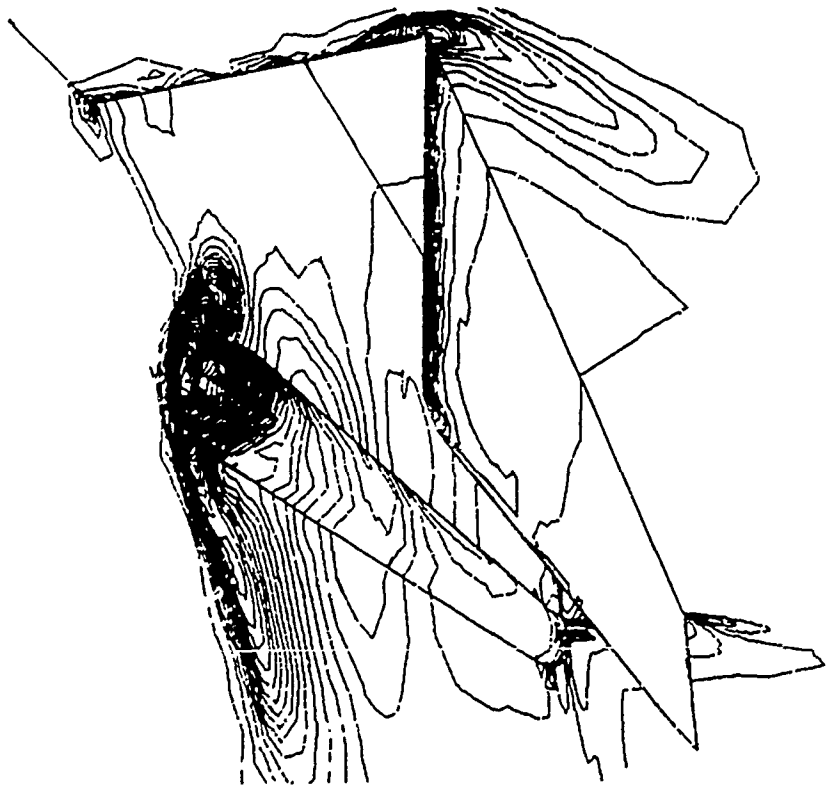

56

FEFLO52

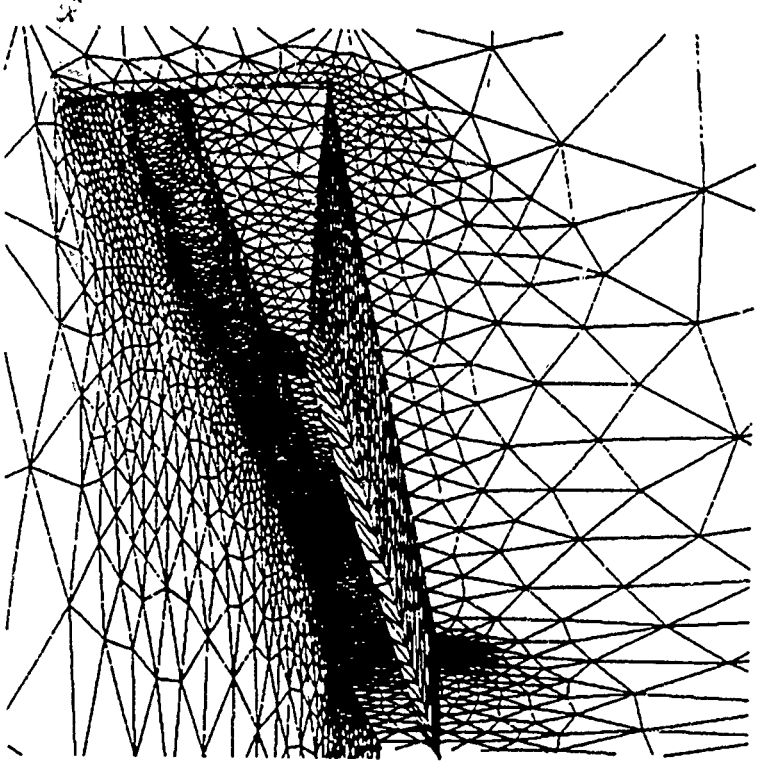

6.1

FEFLO52

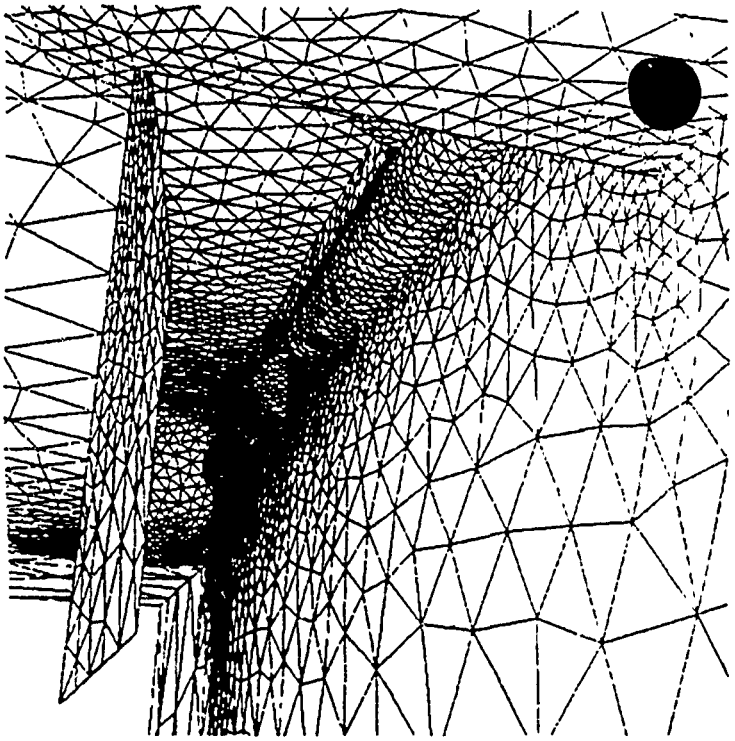

6.2

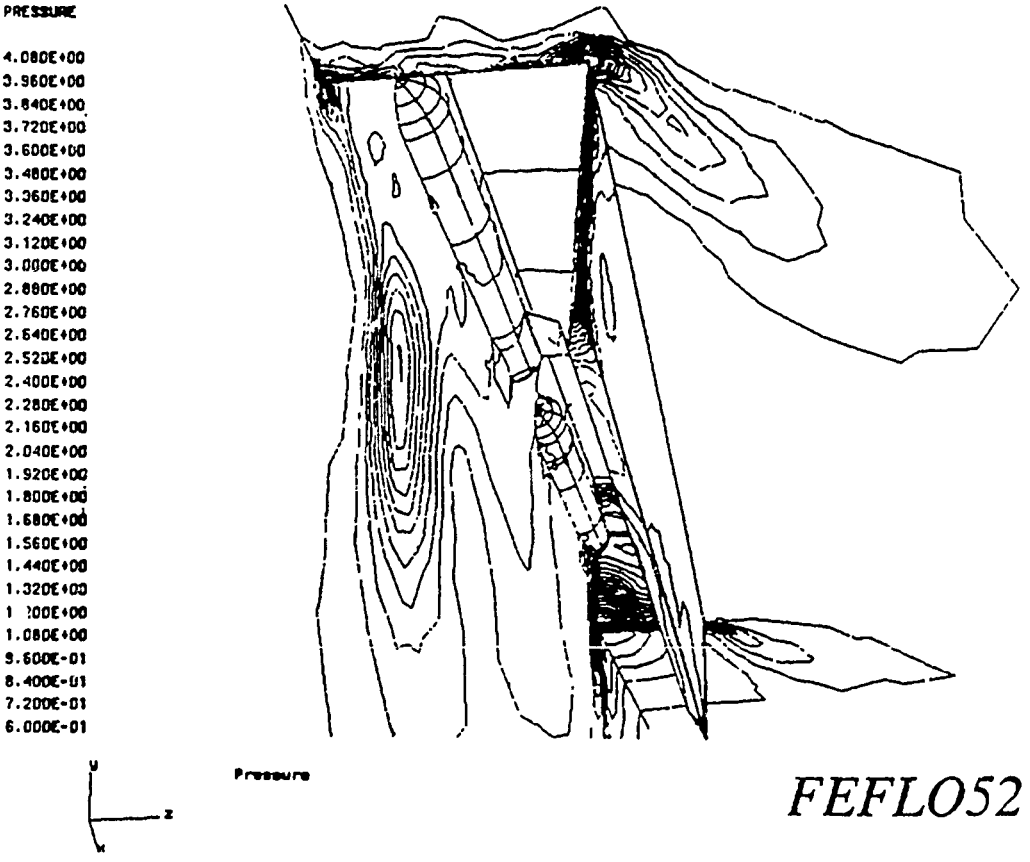

FEFLO52

6.3

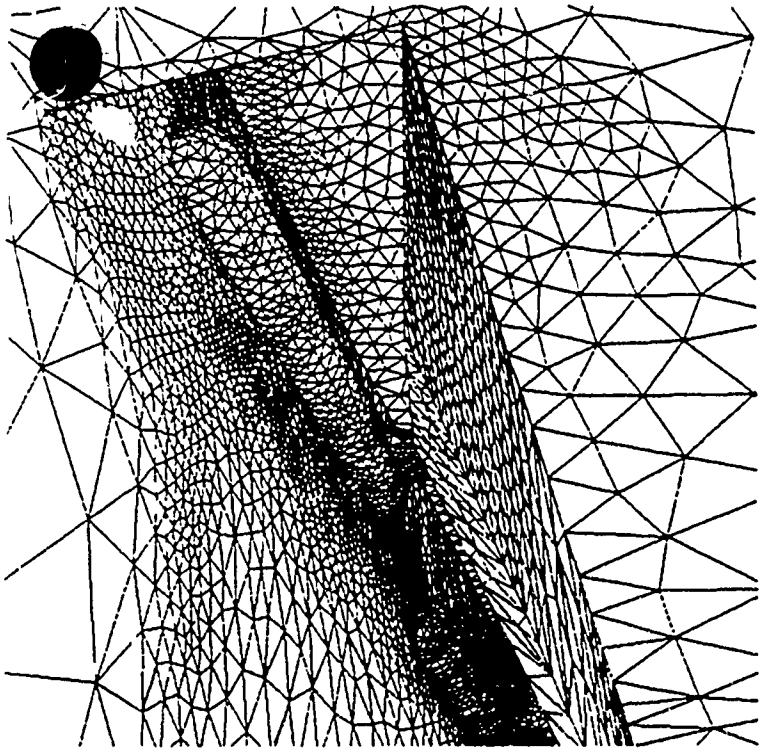

64

FEFLO52

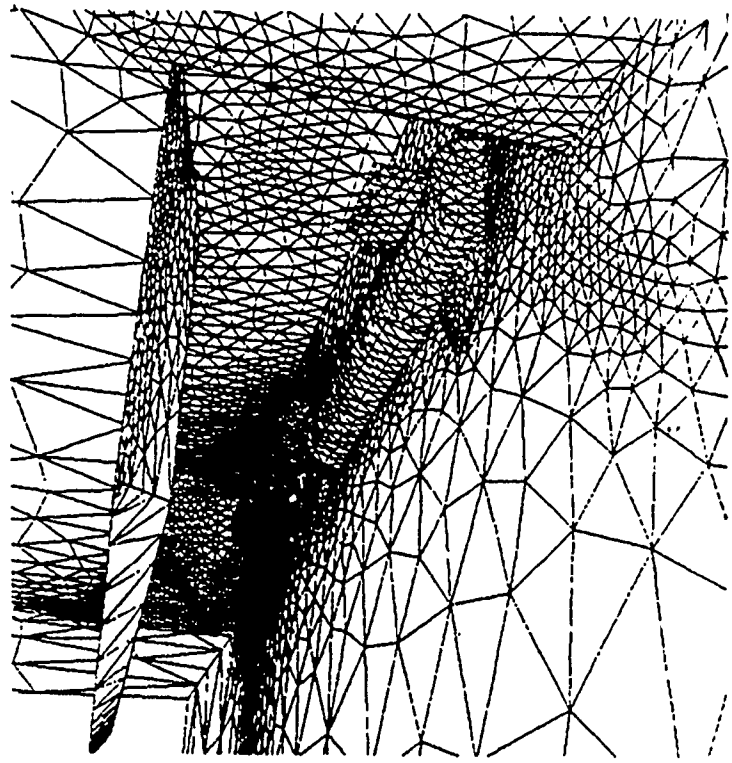

65

66

FEFLO52

Short Biographical Sketch of Rainald Löhner

Education

University: 1977-1982, Technische Universität Braunschweig, W. Germany; 8/3/1982: Diplom Ingenieur, Maschinenbau (MSc in Mechanical Engineering)

Postgraduate Study: 1982-1984, University College of Swansea, Wales, United Kingdom; 10/1984: PhD in Civil Engineering

Working Experience

Lectureship: 1984-1985, University College of Swansea, Wales, United Kingdom; lectured on Computational Mechanics, conducted research on Finite Element Methods for High Speed Compressible Flows

Research Scientist: 1985-1988, Laboratory for Computational Physics, Naval Research Laboratory, Washington. D.C.; developed New High Resolution Schemes, Adaptive Refinement Strategies for 2-D Unstructured Grids, 2-D and 3-D Grid Generators for Unstructured Grids

Associate Research Professor: 1988-present, Dept. of Civil, Mechanical and Environmental Engineering, The George Washington University, Washington, D.C.; currently developing Adaptive Refinement Strategies for 3-D Unstructured Grids, 3-D Graphics Packages for Unstructured Grids, Unstructured Grid Flow Solvers for Incompressible Flows, Maxwell Solvers and Particle-in Cell Codes

Membership in Editorial Panels of Journals: Member of the editorial panel of the international Journal 'Communications in Applied Numerical Methods', published by J. Wiley & Sons

Publications: Around 80 papers in Journals, Meetings, Workshops, etc

Computer Codes: Author of the FEFLO-family of flow simulation codes, as well as FEGEN2D/3D and FEPLOT2D/3D pre- and post-processors.

STORE INTERFERENCE AERODYNAMICS

Lawrence E. Lijewski
U.S. Air Force Armament Laboratory
Eglin AFB, Florida

INTRODUCTION

Accurate prediction of aerodynamic characteristics of missile shapes is of paramount importance to the airframe designer. The accomplishment of the mission is highly dependent on his ability to design an effective missile shape with desirable aerodynamic qualities, both in free-flight and in an interference flowfield. It is in the interference flowfield under the aircraft that aerodynamic forces are generated by two or more of these missile shapes that have a great influence on the speed, range and endurance of modern fighters. Furthermore, the release of these bodies from the parent aircraft is highly dependent on their aerodynamic interrelationship when in close proximity. This interrelationship, or mutual interference, is most pronounced in the transonic regime where modern tactical fighters often operate. All these factors must be taken into account by the engineer in the missile design process. The process is often a time-consuming iterative effort coupling an aerodynamic predictive method and expensive wind tunnel testing. The purpose of this chapter is to present methodology designed to improve this iterative process for missile configurations in aircraft interference flowfields.

Until recently, it has been difficult for the designer to numerically predict the aerodynamic flowfield about complex, mutually interfering body configurations in the transonic Mach range. The geometric complexity of the grid generation and the existence of embedded regions of subsonic and supersonic flow that preclude the use of space-marching codes have been major road blocks to the solution of the problem. With the advent of generalized, arbitrary geometry, multi-block grid codes [1,2] and sophisticated flow solvers [3,4] to work in concert with these grids, good inviscid flow solutions can be obtained for very complex configurations such as fighter aircraft with external weapons. Inviscid flow calculations have been successfully obtained on missiles with multiple lifting surfaces [5,6] multiple finned [7] and unfinned bodies [8,9] and a wing-pylon-unfinned store configuration [10] at low angles of attack. In addition, three-dimensional computations have been successfully obtained on overlapping or Chimera grids [11,12,13]. This method has been designed to simplify the grid generation and allow more timely and routine calculations of complex aircraft/weapon configurations. Steps in this direction have been taken by Benek [11] with multiple unfinned body calculations, and by Meakin [12] with calculations on a wing-unfinned body configuration.

The computational results presented here cover the range of interest from multiple finned stores to a wing-pylon-store configuration. Both the blocked grid and overlapping grid methods were used for the wing-pylon-store computation. All configuration grids were built using the elliptic method of Thompson [1] resident in the Eglin Arbitrary Geometry Implicit Euler (EAGLE) code. The inviscid solver is based on an implicit Euler algorithm described by Belk [14] and Whitfield [15]. The algorithm is a flux difference split (FDS) scheme based on Roe's [16] approximate Riemann solver. One version of the flow solver handles blocked-grids while a second version handles single block overlapped grids through

three-dimensional interpolation between grids outer boundaries.

GRID GENERATION

The EAGLE grid code is a general three-dimensional algebraic/elliptic grid generation system based on the block structure. This code allows any number of blocks to be used to fill an arbitrary three-dimensional region. Any block can be linked to any other block (or to itself) with complete (or lesser) continuity across the block interfaces as specified by input. The code uses an elliptic generation system with automatic evaluation of control functions, either directly from an initial algebraic grid (generated by the code using transfinite interpolation) and then smoothed, or by interpolation from the boundary point distribution.

The grid generation system [2] actually consists of two codes, one of which generates the boundary surface configuration, and the other of which generates a grid within the field. These codes are designed so that, once a configuration has been developed, changes can be made in a local manner without the necessity of corresponding changes scattered throughout the input. The grid in the field is then generated by the grid code. Three complex grid configurations generated with the EAGLE code are presented here. These particular configurations were chosen for their complex, though generic, geometry, and to cover a range of mutually interfering body applications.

Mutually Interfering Finned Bodies

The first case chosen emphasizes the aerodynamic interference between closely spaced finned bodies. One, two, and three finned body combinations were gridded to isolate the interference effects. Each finned body was identical to the others, comprised of a generic ogive-cylinder-ogive body and four swept fins with a tapered NACA 0008 airfoil cross-section and exposed aspect ratio of 0.257, Figure 1. The finned body was arranged in the one, two and three-body combinations illustrated in Figure 2. The most complex configuration was the three finned body combination, Figure 3. Since the separation distance between the bodies was less than one body diameter, the three bodies were arranged with physical clearance in mind. Hence, the top two bodies were in the x-fin arrangement, while the bottom body was in a +-fin arrangement. To expedite the solution process and save computational costs, advantage was taken of the vertical symmetry plane, cutting the configuration in half. The overall grid was nearly 300,000 points in 30 blocks. C-O grids were constructed around the bodies, with the remainder of the grid an H-O mesh. Blocks 1-8 and 19-22 comprise the C-O grids. Blocks 1-4 and 19 and 20 extend from the body nose to the fin leading edges. Upstream of these blocks are H-O grid blocks 9-12 and 23 and 24, which complete the tube-like structure forward to the front boundary. In this manner, three sections of 10 blocks each comprise the grid, the section being stacked axially, front to back.

A cut through the wireframe grid at the fin section, Figure 4, gives a closer view of how the blocking scheme was formulated. Blocks 1-8 around the upper body were each 10,309 points. Each block was 61 points axially, 13 points radially, and 13 points circumferentially (61 x 13 x 13). Blocks 19-22 around the lower half body were each 7,930 points (61 x 10 x 13). The twelve larger outer blocks completed the overall grid.

Figure 5 gives a three-dimensional perspective of the bodies in relation to the reflection plane, and a cross-sectional grid plane at the back boundary. The tube-like grid construction can be seen around the half body on the reflection plane, as well as the grid around the bodies in the rear plane.

In general, grid line distribution functions were used extensively within individual blocks to achieve smooth transition between blocks. A hyperbolic tangent distribution function was typically used. Nearly uniform spacing was generated on the body forward of the fins, while grid line clustering was used on the fin sections, concentrated at the leading edge. Typical longitudinal cell sizes were 1.2 percent on the body based on body length and 1.0 percent on the leading edge of the fins based on the local chord. The average cell on the fins was 2.6 percent local chord. The size of the first cell in the normal direction to the body and fin surfaces were typically 3.9 percent of the body diameter.

As noted earlier, an attempt was made to build all the grids in a similar fashion. Figure 6 shows a cross-section of the block-edge schematic for the two finned body case, comparable to Figure 4. The body is again built in a tube-like mesh composed of C-O and H-O grids. The overall grid is now 21 blocks (240,292 points), with three sections of seven blocks each stacked axially. The dimensions of blocks 1-12 are identical to those in the three body case, with the same grid spacings maintained whenever possible. A cross-section of the block-edge schematic for the single body configuration is shown in Figure 7. This grid is composed of 24 blocks (289,432 points), and is generated by adding three outer boundary blocks where the reflection plane was located in Figure 6. Here the size of the first 21 blocks are the same as before with the same spacing enforced where possible.

Wing-Pylon-Store Configurations

The next application of the EAGLE grid generation system to a multi-body problem is that of the wing-pylon-store configuration. The wing is a clipped delta (NACA 64A010 airfoil section) with 45 degrees of leading edge sweep. The pylon is an ogive-flatplate-ogive shape, while the store is an ogive-cylinder-ogive with an aft cylindrical sting. The basic configuration dimensions are shown in Figure 8.

The surface grid defining the geometry was built entirely with operations in the boundary code. Coordinates for the wing root and tip were read in, and the wing was built by interpolation between root and tip coordinates. The chordwise point distribution was set to allow control over spacing at both the leading and trailing edges.

The pylon, store, and sting were constructed according to dimensions and specifications by building up curve segments and then rotating these curves, or by interpolating between them. The pylon was generated separately and then affixed smoothly to the wing lower surface through an intersection operation. Since the ultimate purpose of the grid was to accurately model wind tunnel experiments, a gap was left between the lower surface of the pylon and the top of the store, consistent with the wind tunnel model. Figure 9 illustrates the surface grids and the 0.07 inch gap between the pylon and store.

The grid developed for this problem is a 30-block system containing approximately 650,000 points. The system consists of a C-O grid enclosing the pylon, store, and sting, with an H-type grid surrounding the wing and the embedded C-O structure. An H-O structure extends from the nose of the C-O to the upstream grid boundary. The boundary for the C-O grid was generated by rotating curves about the axis of the store and sting. This approach, while quite simple for an isolated body, was complicated considerably by the need to have the C-O boundary interface smoothly with the highly curved lower surface of the wing. Additional complexity was caused by the 45-degree sweep angle of the wing leading edge. The curves to be rotated each included a C-like segment emanating from a point ahead of the store nose and terminating at the leading edge of the wing at a point to the right or left of the pylon. A second segment of the rotated curves consisted of spar lines extracted from the lower wing grid. The third part extended from the wing trailing edge to the downstream boundary.

Figure 10 is a view of the blocking system at a plane about mid-chord. Block 6 is embedded in the gap as indicated. Points were clustered in the gap between the pylon and store to better resolve the flowfield. Figure 11 illustrates the elliptic grid at the same axial location. A side view of the block system on the outboard side of the pylon is shown in Figure 12. The large outer blocks are truncated here for easier viewing, accounting for their irregular boundaries. Figure 13 is a side view of the elliptic grid showing the interference of the pylon-store C-grid with the surrounding wing H-grid. The difficulties inherent in interfacing the C-grid with the wing are graphically evident at the leading edge.

The remainder of the grid system, consisting of 24 blocks, surrounds the C-O system. Except for the H-O cylindrical structure ahead of the C-O system, these remaining blocks are nearly rectangular. The far-field boundaries were placed 20 store diameters upstream and downstream of the nose of the store, and 15 diameters outboard of the store. Looking downstream from the front boundary, Figure 14 illustrates the blocking system in the grid upstream of the wing-pylon-store blocks.

The final application of the EAGLE grid generation system is the same wing-pylon-store configuration, but using Chimera overlapping grids. Here, grids are built separately around the wing, pylon, and store, then overlaid to obtain the final configuration. In addition, a fourth grid is built to assist in the interpolation between its coarser wing grid and the finer store and pylon grids.

The basic surface geometry is shown in Figure 15. The wing and pylon are the same as before, but the store has the sting removed to facilitate easier gridding. The resulting store grid is of O-type, Figure 16, with perpendicular planes shown. The body length consists of 95 points with 35 points radially and 73 points circumferentially. Figure 17 presents the wing grid with the wing surface, reflection plane and back plane. The grid is of C-C type with dimensions being 135 points from the leading edge to the back boundary, 31 points normal to the wing surface and 95 points spanwise from the top reflection plane to the bottom reflection plane wrapping around the wing tip.

A perspective of the pylon grid is shown in Figure 18. The grid was built by generating a surface coincident with a portion of the wing lower

surface and then wrapping this surface around the pylon from the outboard to the inboard side. The grid contains 61 points lengthwise on the pylon, 21 points normal to the pylon surface and 57 points wrapped around the pylon. Figure 19 illustrates the combination of these grids along with the interface grid. The front portions of each grid are eliminated for viewing purposes. The interface grid encompasses the store and pylon grids and is nearly rectangular except for the upper surface which conforms to the wing surface. This grid contains 111 points chordwise by 45 points normal to the lower wing surface by 47 points spanwise.

COMPUTATIONAL RESULTS

To investigate interference effects for the three configurations, a series of computational cases were solved.

Mutually Interfering Finned Bodies

For the first example case, Figure 2, Euler solutions were obtained at Mach numbers from 0.80 to 1.20 at zero degrees angle of attack. All cases were run to convergence at a Courant number of 5 for 1,000 iterations with a speed of approximately 4.9×10^{-5} sec/pt/iteration on a CRAY-2 supercomputer. For the three body case, 51.6×10^{6} words of central memory were used with a total run time of 3.76 hours for 1000 iterations.

Multi-Body Pressure Comparisons

To illustrate the aerodynamic interference in the multi-body cases, Figure 20 plots the pressure coefficients on the inboard side of the upper body for the three finned configurations at Mach 0.95 and zero degrees angle of attack. It is clear that by adding a second body and then a third, the flow accelerates between the bodies as indicated by the increasing expansion peaks, both on the forebody and between the fins. Also, the expansion regions increase in size, resulting in the shocks moving downstream. It is interesting to note that the expansion rise on the ogive nose generally reaches the same magnitude at the ogive-cylinder junction, X/L = 0.28, for all three configurations even though the rate of expansion for each case is different. The Euler code gives very good agreement with data in the one and two body cases, even though the interference effects are strong in the two body case. The Euler code, however, shows a crisp shock on the body at X/L = 0.45 in the two body case, whereas the data begins to indicate the effects of viscosity and a more smeared shock. This becomes even more evident when the third body is added, although the data does not show a large difference in the expansion change. Here again the flow solver predicts a sharp shock at X/L = 0.50, that is in contrast with the smeared shock indicated by the data. Also, the Euler prediction over-compresses after the shock, unlike in the one and two body cases, where the predictions and data more nearly agree after the shock. It is becoming evident from the Euler/data comparisons that the three-body case is much more viscous dominated than the two-body case. Finally, in the fin region, the expansion and subsequent shock is overpredicted and downstream as would be expected from an Euler code. However, the fin region is highly viscous, near Mach 1.0, as will be discussed later.

In contrast to the inboard side of the upper body, the outboard side, Figure 21, is much better predicted, even in the fin region. The main

interference effect here is the elongation of the expansion region near mid-body with the subsequent rearward movement of the shock, as the second and third bodies are added. In all three cases the flow solver does quite well. Interference effects are not felt on the outboard side of the ogive nose, compared to what was seen on the inboard side. In fact, the pressure distribution on the outboard side of the body in the multi-body cases closely resembles the distribution for the single body case, except for the shock location. Therefore, the interference flowfield shock formed on the body is not a local phenomenon on the inboard side of the body, but rather a shock disk extending around to the outboard side. The strength of the shock may vary from the inboard to the outboard side, but the outboard shock location is similar to the inboard shock location.

Multi-Body Aerodynamics

When investigating the aerodynamic interference phenomena of multiple bodies in close proximity, the question arises as to the mutual aerodynamics of such configurations. How the bodies react to each other and the underlying causes of the reaction are important to understand. The pressure distributions are integrated for the three-body configuration to obtain the force and moment coefficients from Mach 0.80 to 1.20. Figure 22 plots the normal and side forces of the upper body and normal force of the lower body. Figure 23 plots the pitching and yawing moments of the upper body and the pitching moment of the lower body. The moment reference center is located at X/L = 0.561. The axis system and sign convention from Figure 2 is in effect here for both the upper and lower bodies. Up and down refer to the vertical axis, while in and out refer to the horizontal axis.

What is evident immediately from Figure 22 is that the forces on the bodies tend to move the bodies together in subsonic flow, but move the bodies away from each other at supersonic Mach numbers. The inward force at Mach 0.80 also appears to be significantly stronger than the outward force at Mach 1.20. Here inward and outward refer to the direction from the center of the configuration. Figure 24 illustrates this strength by comparing the pressure distributions on the inboard and outboard sides of the upper body at Mach 0.80. The outboard side prediction is at 85 degrees clockwise from top center, while the inboard side prediction is at 265 degrees. The two expansion regions on the inboard side at the nose and tail provide a strong inboard force when compared to the same two outboard locations. This identical pattern was also observed on the upper/lower sides of both the upper and lower bodies, where the expansion peaks on the maximum interference sides determined the force direction. The result was an inward/outward force on the upper body and upward force on the lower body. Supersonically, the forces reverse themselves. The pressure distribution on inboard and outboard sides of the upper body, Figure 25, gives evidence for this reversal. In marked contrast to Mach 0.80, the flow expansion in the fin region is similar from one side of the body to the other. In addition, the pressure on the outboard side of the nose expands more rapidly than the inboard side, resulting in a net outboard force. However, the significant contributions to the outward force occurs as a result of the shock on the body near the fin leading edge region. Unlike at Mach number 0.80, where little difference was observed across the body in the compression region after the body shock, a significant difference occurs here across the body, resulting in an outward force. Only the large expansion region prior to the shock on the

inboard side, X/L = 0.30 to 0.60, serves to minimize the outward force. Again the identical behavior was seen on the upper/lower sides of the upper and lower bodies. Investigation of the moment coefficients yielded an equally interesting explanation. Figure 23 shows that the bodies react to the subsonic flow opposite to that in supersonic flow. Subsonically, the nose of each body moves away from the other, while the fin sections move toward each other. In supersonic flow the direct opposite occurs, where the body nose sections come together while the fin sections move apart. At Mach number 0.80, Figure 24, the flow expansion on the inboard side of the upper body dominates the pitching and yawing moments. The difference across the fin section from outboard to inboard is so great that the fin sections move toward each other. Since this also occurs in the vertical plane of both the upper and lower bodies, the result is that the nose of the upper body pitches upward and yaws outboard, while the nose of the lower body pitches downward. This phenomena has been observed in flight on numerous occasions during subsonic carriage and release of multiple bodies from aircraft. Reversal of this trend supersonically can be explained from Figure 25. The dominant feature here is the strong shock on the body at X/L = 0.67, with the accompanying expansion area before and sharp compression region after. This expansion/compression forms a couple that rotates the nose inward and the fin section outward. The magnitude of the moment is restricted by the proximity of the forces to the moment reference center and the counteracting nose compression on the inboard side. Since the vertical plane of both the upper and lower bodies is similarly loaded, the result is that the nose of the upper body pitches downward and yaws inward, while the nose of the lower body pitches upward.

The key element in establishing the observed multi-body force moment dependence on Mach numbers is the rearward movement of the body and fin region shocks, and elongation of the body flow expansion region. Figure 26 clearly illustrates this phenomena. The body shock near X/L = 0.30 for Mach 0.80 travels aft to X/L = 0.50 for Mach 0.95, and then to X/L = 0.67 for Mach 1.20. Meanwhile, the strong shock in the inboard fin region at Mach 0.80 moves off the body at Mach 1.20, leaving only an expansion region on the fins that was shown in Figure 25 to have little influence. The rearward elongation of the body flow expansion region is evident in Figure 26 and is clearly depicted in surface oil flows, Figures 27-29. The bright while region near the nose cylinder junction, Figure 27, coincides with the expansion region at X/L = 0.25, Figure 26. As the Mach number increases to 0.95, the flow expansion region now elongates from X/L = 0.25 to X/L = 0.50, in Figure 26. Figure 28 confirms the growing expansion region with the rearward movement of the bright oil. This side view of the three-body configuration shows the inward movement of the oil toward the interference side of the bodies and the areas of lowest pressure. In Figure 29 the shock has moved aft to the leading edge of the fins. The elongated expansion region upstream of the fins is clearly seen. By comparing the three oil flows, the shock in the fin region can be seen moving aft. At Mach 0.95, the shock is strong enough to induce a region of vorticity clearly visible in the last quarter chord of the fins, Figure 28. Understandably, the Euler code was not able to capture this region. The phenomena was very sensitive to the Mach number and interference flowfield in that it was only observed at Mach 0.95 and 1.05, and to various degrees of strength depending upon the fin orientation in the configuration.

The rearward movement of the fin region shock is further illustrated in Figures 30 and 31. Both figures show fin pressure distribution at 30 percent span on the 315 degree fin of the upper body. At Mach number 0.80 the shock is on the fin, although overpredicted and downstream of the data. Still, a clear, significant difference exists between the upper and lower surfaces, resulting in the inward/downward force as seen previously. Figure 31 shows the shock has moved off the fins and the differential between upper and lower surface pressures has lessened. This is consistent with the findings discussed earlier. These two figures are typical of the agreement between prediction and data on all the fins.

Wing-Pylon-Store Configurations

The second case is the wing-pylon and unfinned store, Figure 9, using blocked grids. Euler solutions were obtained at Mach numbers from 0.60 to 1.20 at zero degrees angle-of-attack. All cases were run to convergence at a Courant number of 5 for 500 iterations with a speed of approximately 8.4×10^{-5} sec/pt/iteration on a CRAY-2 computer using a slower, but greatly reduced memory requirement version of the Euler code.

Store Aerodynamics

The mutual aerodynamic interference phenomena of the wing-pylon-store configuration is of prime interest to both missile and aircraft system designers alike. Since these phenomena are important to both weapon carriage and release from aircraft, a better understanding of how these bodies react to each other in high speed flight would be invaluable. This section takes a cursory look at the forces and moments acting on the store and their underlying causes based on pressure distributions.

For the range of Mach numbers considered, Figure 32 plots the forces and moments acting on the store body. Normal force, yaw force, and pitching moment are all well-behaved through the Mach range. The yawing moment, however, changes sign with increasing Mach. First of all, the normal force coefficient indicates an upward force on the store toward the wing-pylon while the pitching moment shows a nose-down moment for all Mach numbers. This can be readily explained upon examination of the pressure distributions on the top and bottom of the store, Figure 33. This plot shows the pressures on a longitudinal body curve at zero degrees circumferentially (directly under the pylon) and at 180 degrees (directly under the store). The extensive low pressure region aft of 0.30 X/L on the top side compared to the bottom side accounts for the upward normal force on the body. This, coupled with the higher pressure region forward of the 0.30 X/L point compared to the bottom side, creates the nose-down pitching moment seen in Figure 32. Note that the agreement with wind tunnel data is quite good, even in the gap region between the pylon and store beginning at 0.30 X/L. This agreement was typical for the range of Mach numbers studied. Figure 34 confirms the normal force and pitching moment trends for the Mach number range. The plots indicate the pressure differential from the top to the bottom of the store (delta Cp) at three cases that span the Mach range. For all cases the pattern remains the same; a net downward pressure at the nose and net upward pressure under the pylon, resulting in a net upward force on the body and a nose-down pitching moment.

The side force remains inboard throughout the Mach number range. However, the yawing moment changes direction as Mach number increases from 0.60. These trends can be observed by examination of Figures 35-37. All three plots are pressure distributions spanning the Mach number range along both the inboard and outboard sides of the body. In all three cases, the inboard pressures at 275 degrees around the body are generally lower than the outboard pressure at 85 degrees, resulting in a net inboard force. The change in the distribution of this pressure differential from forward to aft of the center of gravity (c.g.) causes the reversal of the yawing moment as Mach number increases. At Mach 0.60, Figure 35, the largest pressure differential occurs near the nose, forward of the c.g., resulting in a nose inboard yawing moment. At Machs 0.95 and 1.20, Figures 36 and 37, the differential has moved aft of the c.g., causing the body aft section to move inboard and the nose to yaw outboard. Figure 38 summarizes these findings plotting the pressure differential (delta Cp) along the body sides for the three Mach numbers studied. Clearly the majority of the differential curves are negative, resulting in inboard forces for all Mach numbers. Movement of the maximum differential rearward on the body as Mach number increases, moves the net force from forward of the c.g. at Mach 0.60 to aft of the c.g. at higher Mach numbers, and reverses the yawing moment. This reversal can be critical to a safe store release, and therefore crucial to flight clearance engineers.

Overlapped Grids Solution

The last case is the wing-pylon and unfinned store, Figure 15, using overlapped grids. An Euler solution was obtained at Mach 0.95 and zero degrees angle of attack. The case was run to convergence at a Courant number of 2 for 1000 iterations with a speed of approximately 1.3×10^{-4} sec/pt/iteration on a CRAY-2 computer. The speed of the Euler code was significantly reduced due to the interpolation process between the overlapped grids, even though the basic solver algorithm remained the same. The solution took approximately 32.7 hours of run time using 61.5×10^{6} words of central memory.

This case was run to compare the flow solutions obtained usin the blocked grid and overlapping grid methods. Figures 39-42 present these comparisons on the unfinned store for four circumferential positions. Clearly both methods give similar results even though the grids are significantly different.

CONCLUSIONS

A complete grid generation and flow solver system has been demonstrated for complex aerodynamic interference configurations in the subsonic/transonic flight regime. The method combined an arbitrary geometry, blocked elliptic grid generator with compatible, yet generalized, implicit flow solvers. These solvers were Euler methods based on a flux difference split algorithms and capable of obtaining solutions on blocked or overlapping grids. The flow parameters obtained for configurations of various complexity compared favorably with experimental data. The pressure distributions on mutually interfering bodies were found to be as accurate as those on isolated airframes. Consequently, the forces and moments obtained from integrated surface pressure distributions resulted in physically realistic rigid body behavior in interference flowfields. This demonstrated accuracy in

interference flowfields make the system an attractive overall design tool for air launched missiles.

REFERENCES

1. Thompson, J. F., "A Composite Grid Generation Code for General Three-Dimensional Regions - The EAGLE Code," AIAA Journal, Volume 26, No. 3, p. 271, March 1988.

2. Thompson, J. F., and Gatlin, B., "Program EAGLE User's Manual, Volumes II and III, Surface and Grid Generation Codes," AFATL-TR-88-117, September 1988.

3. Belk, D. M., and Whitfield, D. L., "Three-Dimensional Euler Solutions on Blocked Grids Using an Implicit, Two-Pass Algorithm," AIAA-87-0450, January 1987.

4. Mounts, J. S., Belk, D. M., and Whitfield, D. L., "Program EAGLE User's Manual, Volume IV, Multi-Block, Implicit, Steady-State Euler Code," AFATL-TR-88-117, September 1988.

5. Lijewski, L. E., "Transonic Flow Solutions on a Blunt, Finned Body of Revolution Using the Euler Equations," AIAA-86-1082, May 1986.

6. Lijewski, L. E., "Transonic Flow Solutions on a Blunt, Body-Wing-Canard Configuration Using the Euler Equations," AIAA-87-2273, August 1987.

7. Lijewski, L. E., "Transonic Euler Solutions on Mutually Interfering Finned Bodies," AIAA-89-0264, AIAA 27th Aerospace Sciences Meeting, Jan. 1989.

8. Cottrell, C. J., Martinez, A., and Chapman, G. T., "A Study of Multi-Body Aerodynamic Interference at Transonic Mach Numbers," AIAA-87-0519, January 1987.

9. Cottrell, C. J. and Lijewski, L. E., "Finned, Multi-Body Aerodynamic Interference at Transonic Mach Numbers," Journal of Aircraft Volume 25, No. 9, pp. 827-834, September 1988.

10. Arabshahi, A., and Whitfield, D. L., "A Multi-Block Approach to Solving the Three-Dimensional Unsteady Euler Equations About a Wing-Pylon-Store Configuration," AIAA-89-3401, August 1989.

11. Benek, J. A., Donegan, T. L., and Suhs, N. E., "Extended Chimera Grid Embedding Scheme with Application to Viscous Flows," AIAA-87-1126, June 1987.

12. Meakin, R., "Unsteady Aerodynamic Simulation of Multiple Bodies in Relative Motion," AIAA-89-1996, June 1989.

13. Dietz, W. E., and Suhs, N. E., "Pegsus 3.0 User's Manual," AEDC-TR-89-7, August 1989.

14. Belk, D. M., Unsteady Three-Dimensional Euler Equations Solutions on Dynamic Blocked Grids, Ph.D. Dissertation, Mississippi State University, August 1986.

15. Whitfield, D. L., Janus, J. M., and Simpson, L. B., "Implicit Finite Volume High Resolution Wave-Split Scheme for Solving the Unsteady Three-Dimensional Euler and Navier-Stokes Equations on Stationary or Dynamic Grids," Mississippi State University Report MSSU-EIRS-ASE-88-2, 1988.

16 Roe, P. L., "Approximate Riemann Solvers, Parameter Vector, and Difference Schemes," Journal of Computational Physics, Vol. 43 1981, pp. 357-372.

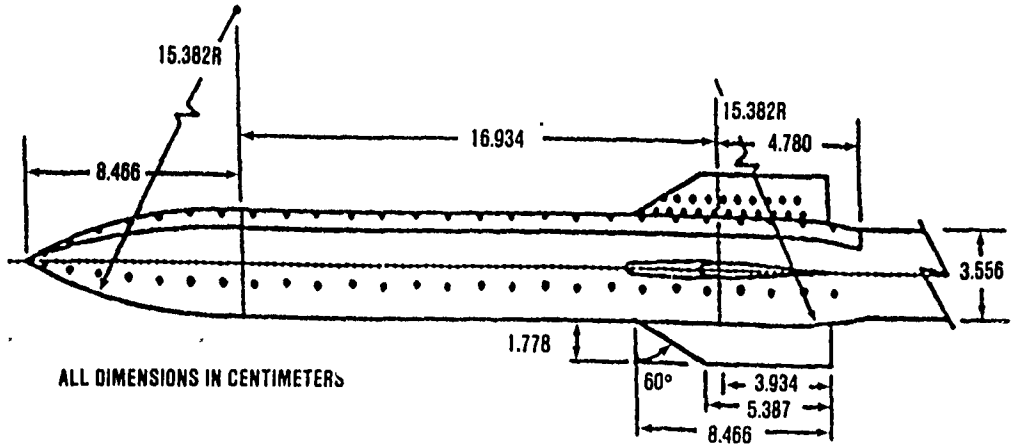

FIGURE 1. Finned Body Geometry

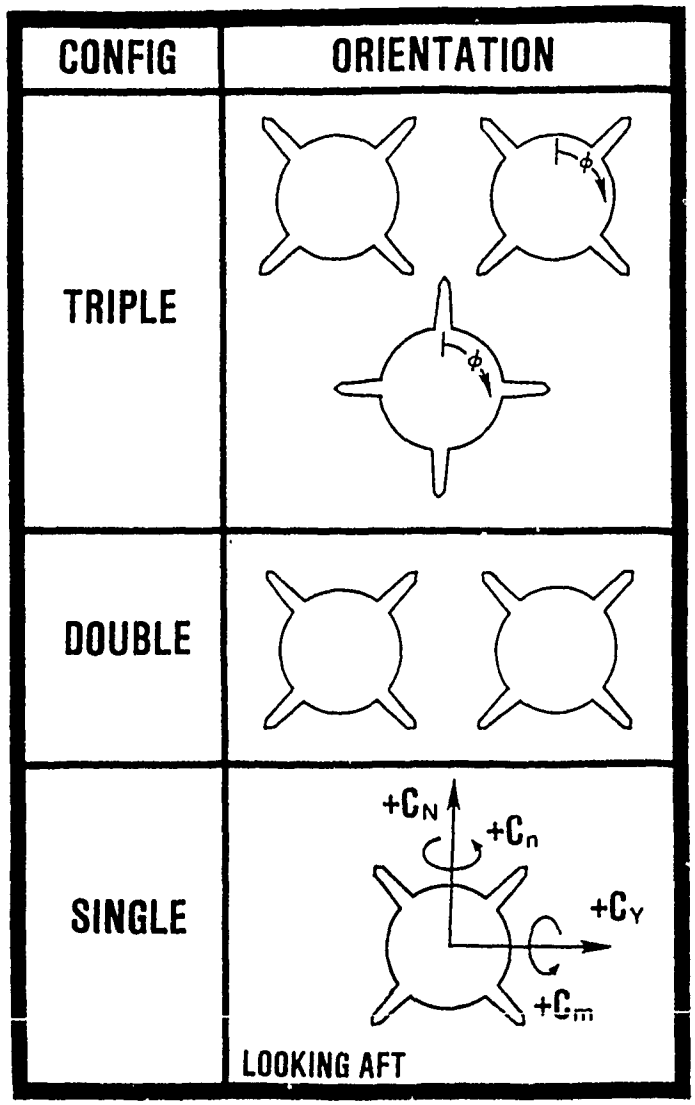

FIGURE 2. Finned Body Configurations

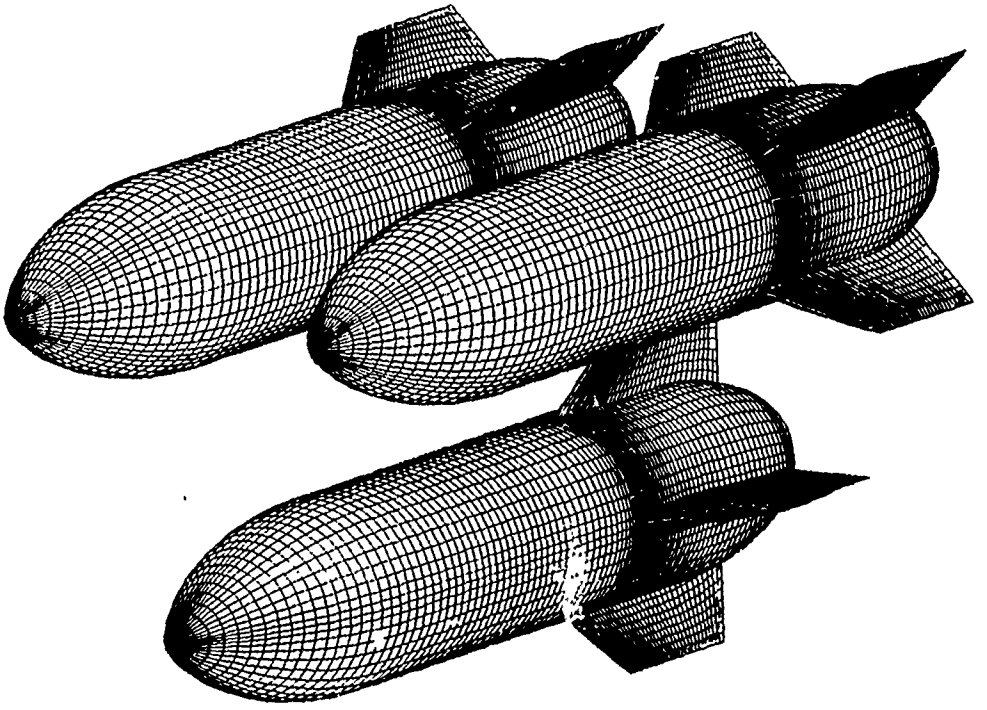

FIGURE 3. 3-Body Surface Gri.

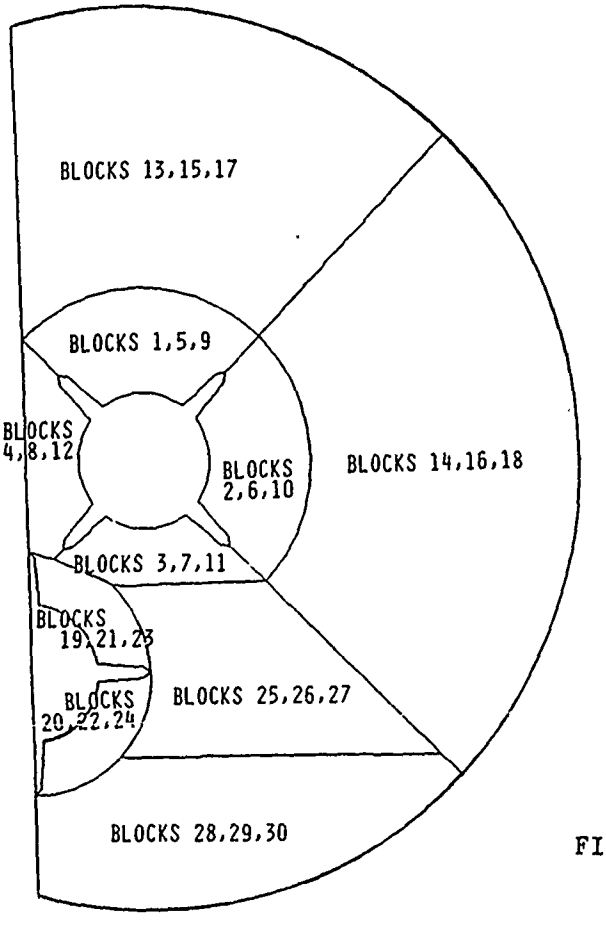

FIGURE 4. Blocking Scheme, 3-Body Case

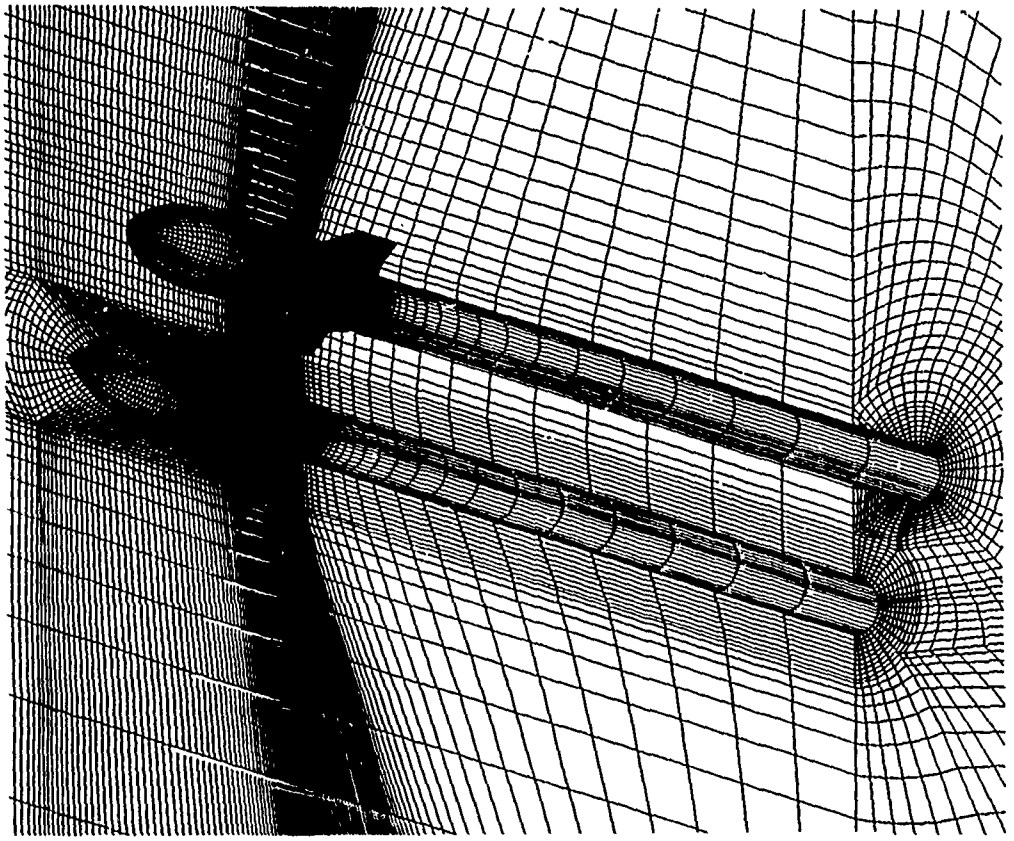

FIGURE 5. Reflection and Back Planes, 3-Body Case

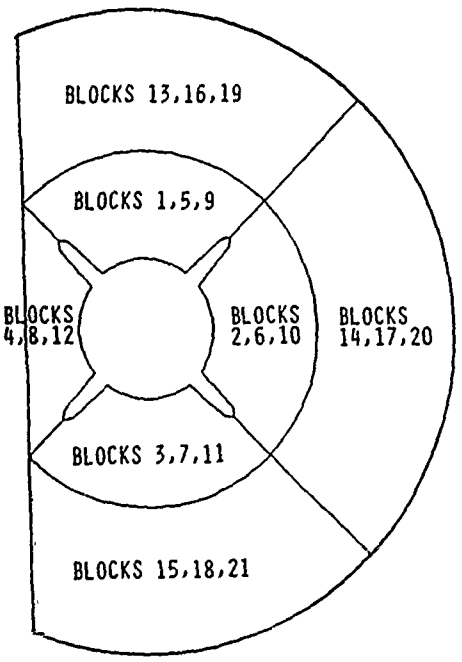

FIGURE 6. Blocking Scheme, 2-Body Case

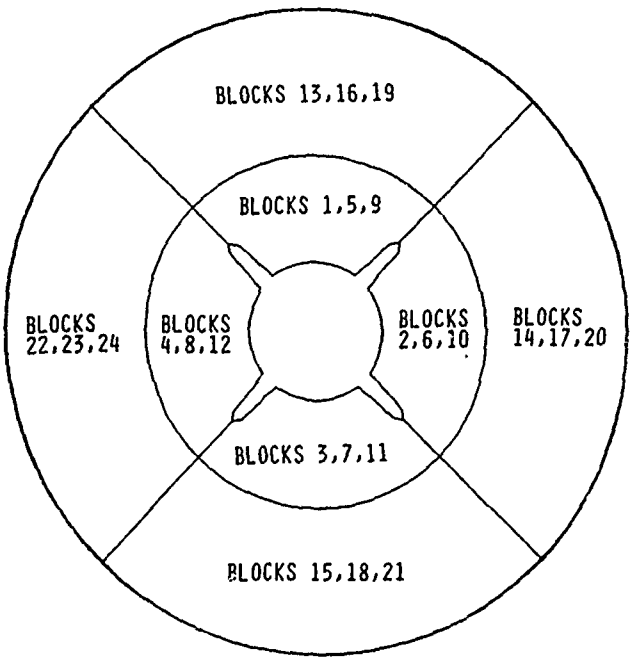

FIGURE 7. Blocking Scheme, 1-Body Case

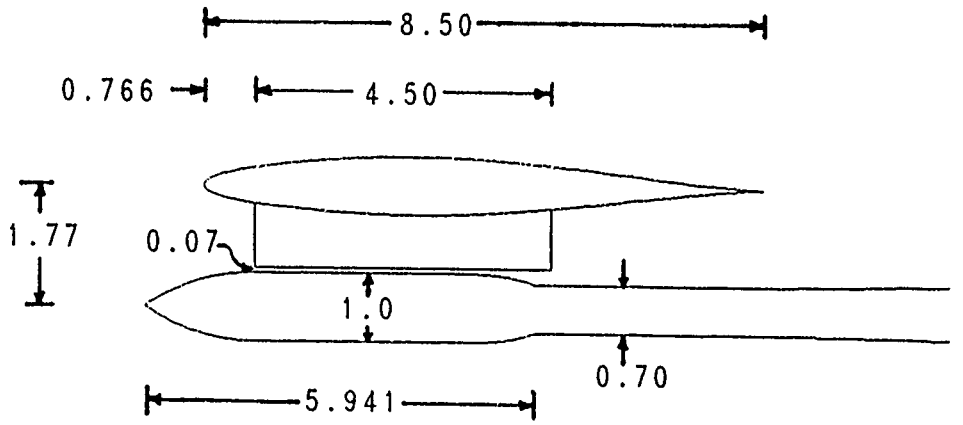

FIGURE 8. Wing-Pylon-Store Geometry

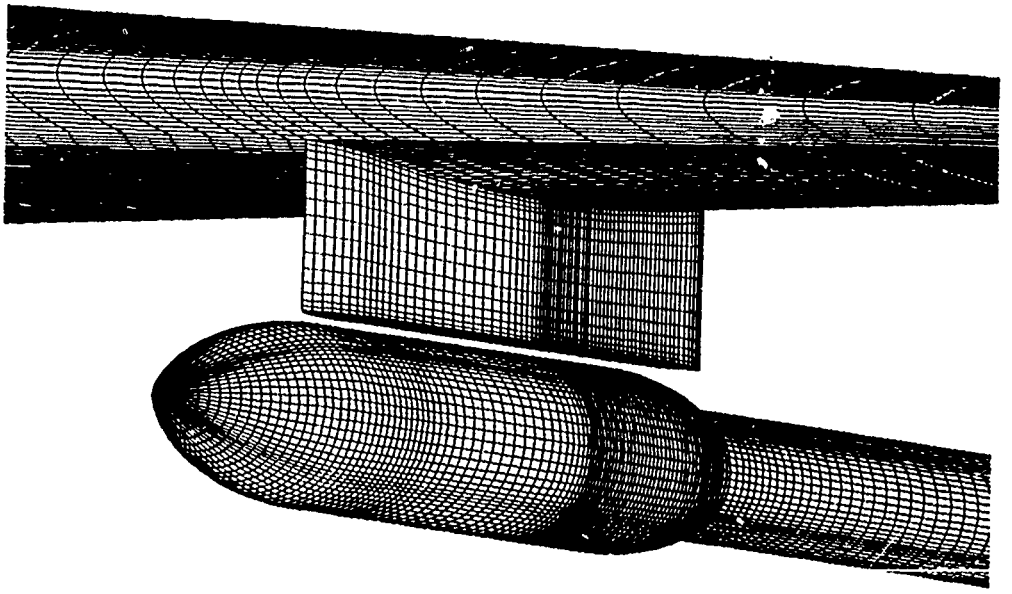

FIGURE 9. Wing-Pylon-Store Surface Grid (Blocked Grid)

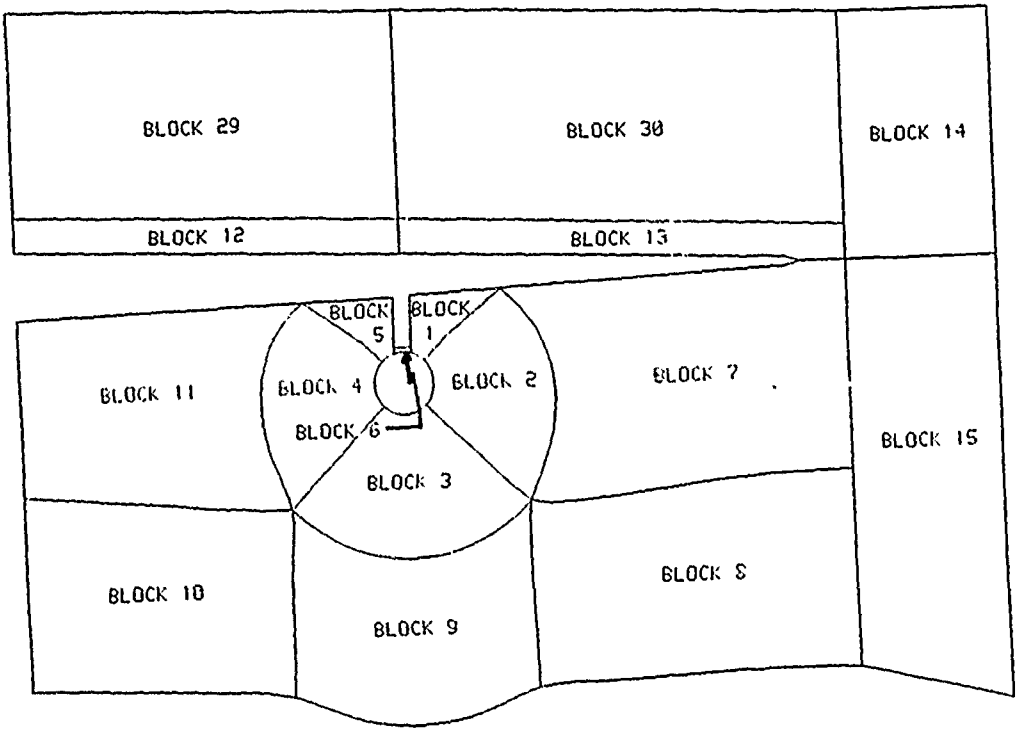

FIGURE 10. Wing-Pylon-Store Rear Blocking System, Rear Blocks, Front View

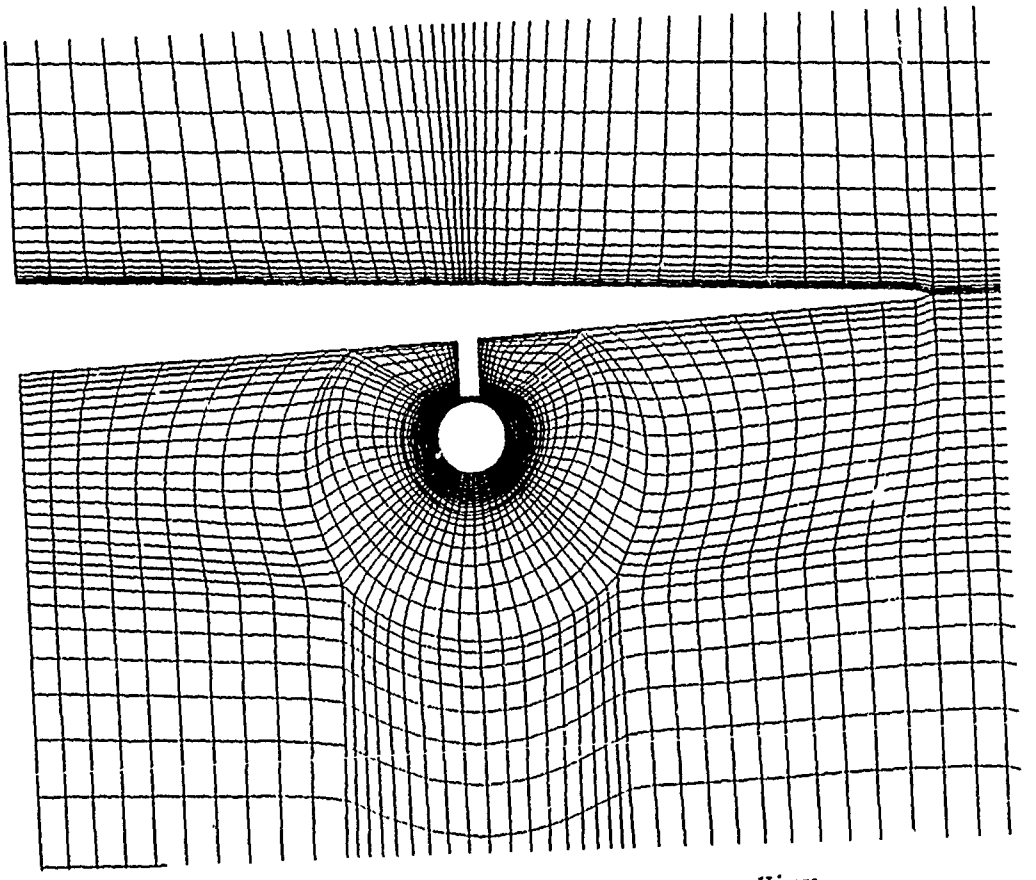

FIGURE 11. Elliptic Grid at Wing, Front View

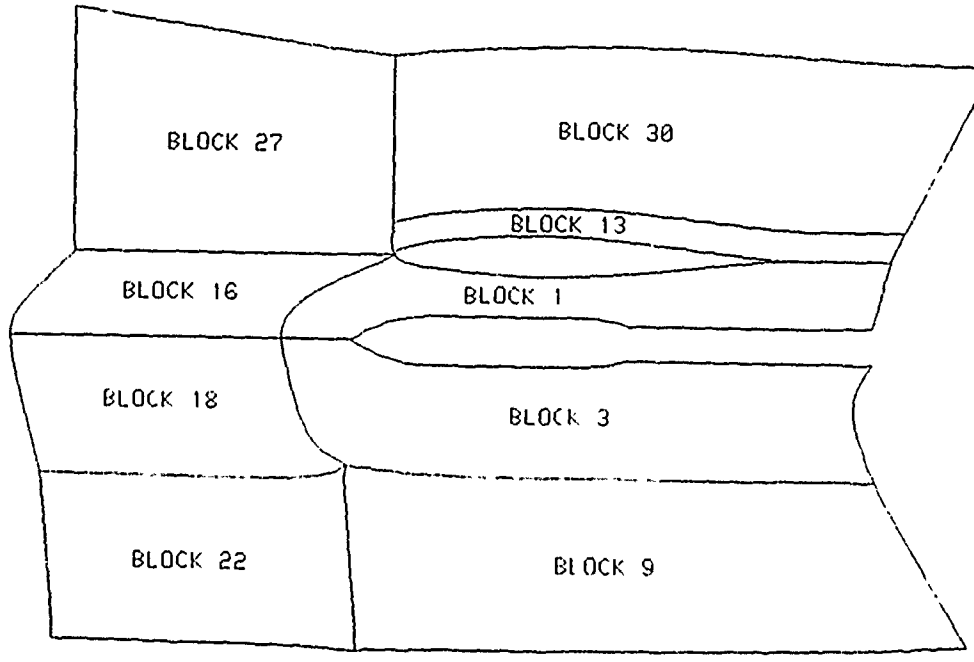

FIGURE 12. Wing-Pylon-Store Blocking System, Side View

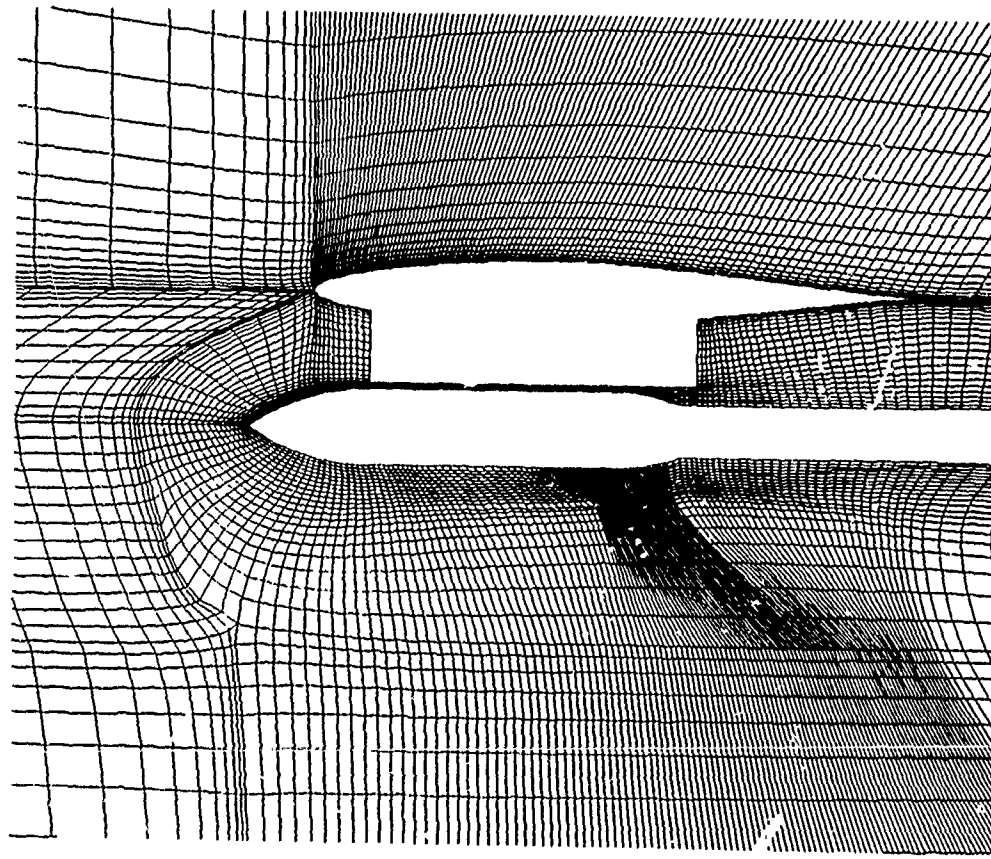

FIGURE 13. Elliptic Grid at Store Centerline, Side View

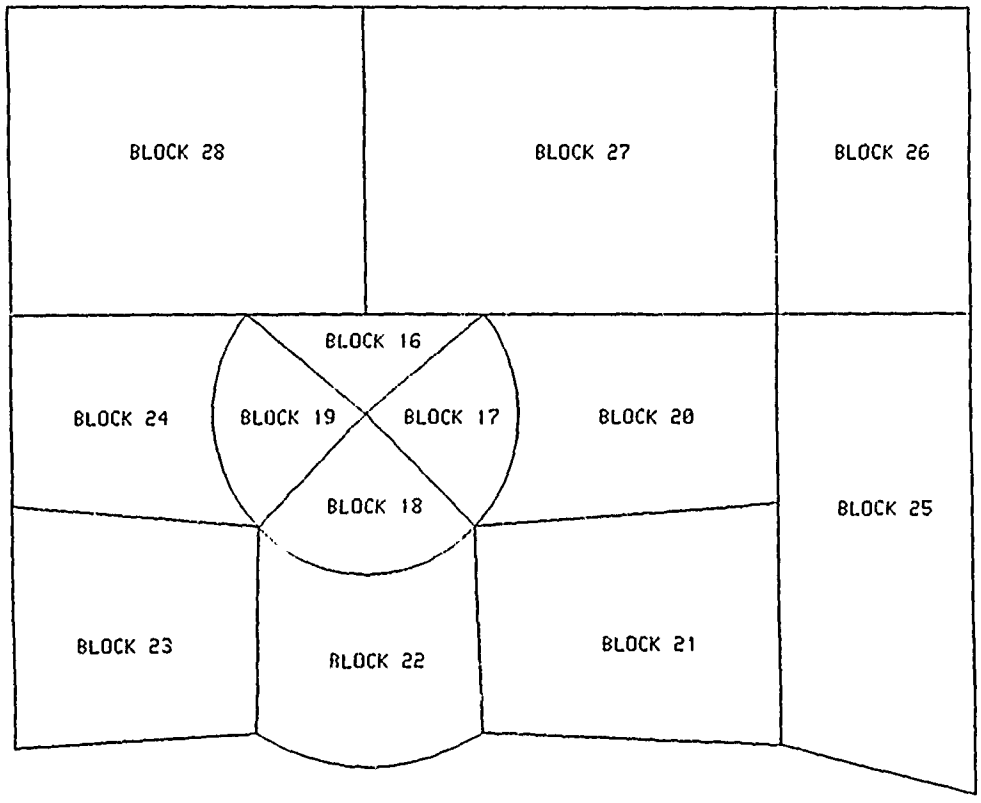

FIGURE 14. Wing-Pylon-Store Blocking System, Front Blocks, Front View

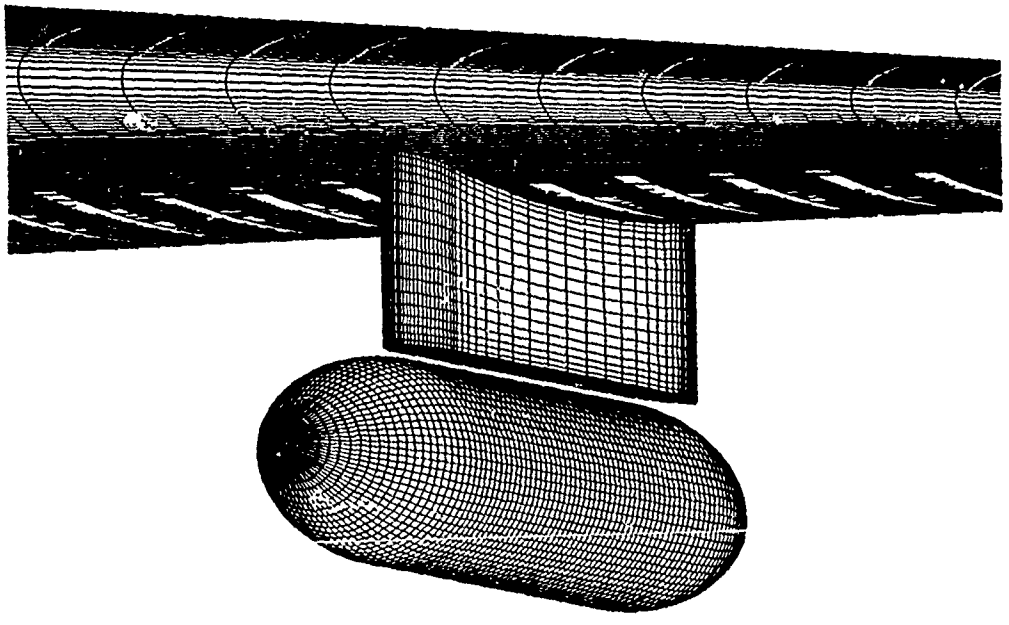

FIGURE 15. Wing-Pylon-Store Surface Grid (Overlap Grids)

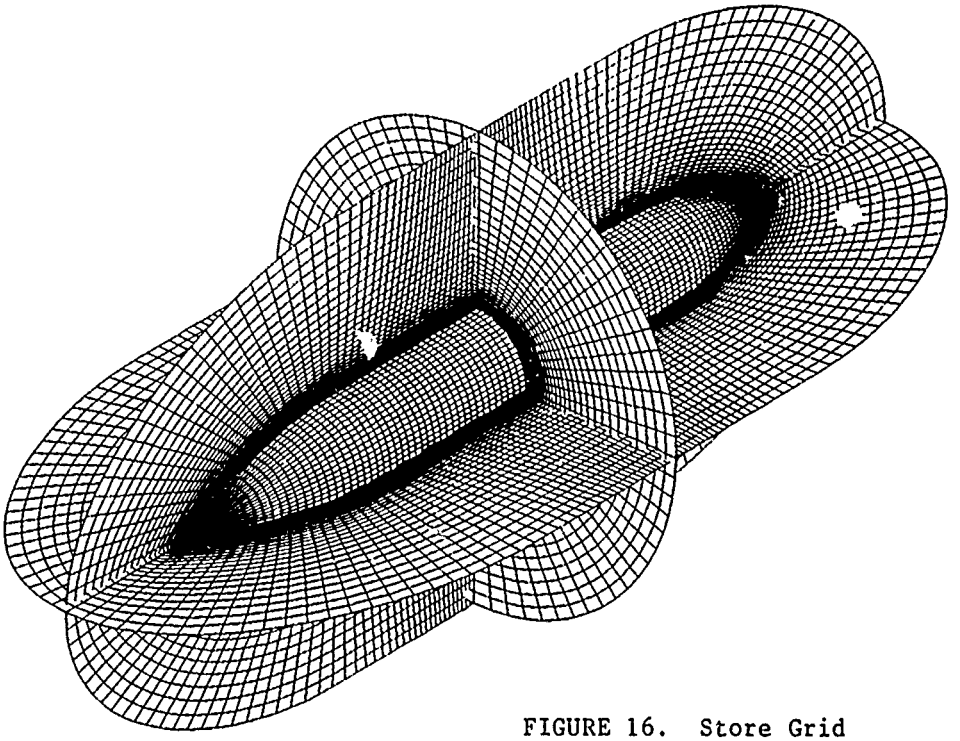

FIGURE 16. Store Grid

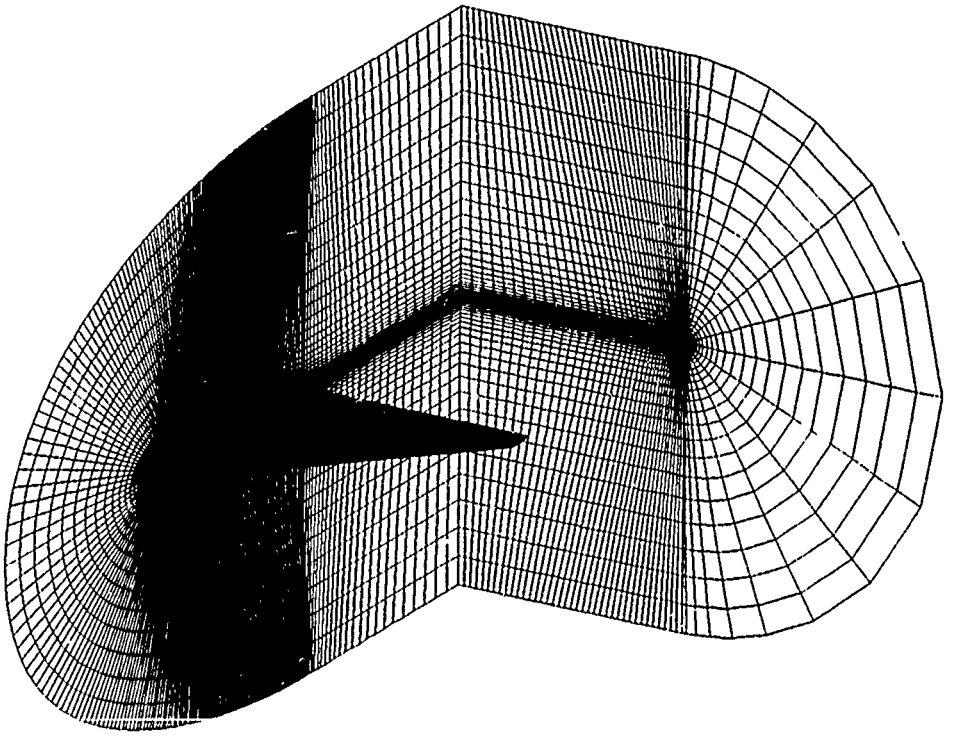

FIGURE 17. Wing Grid

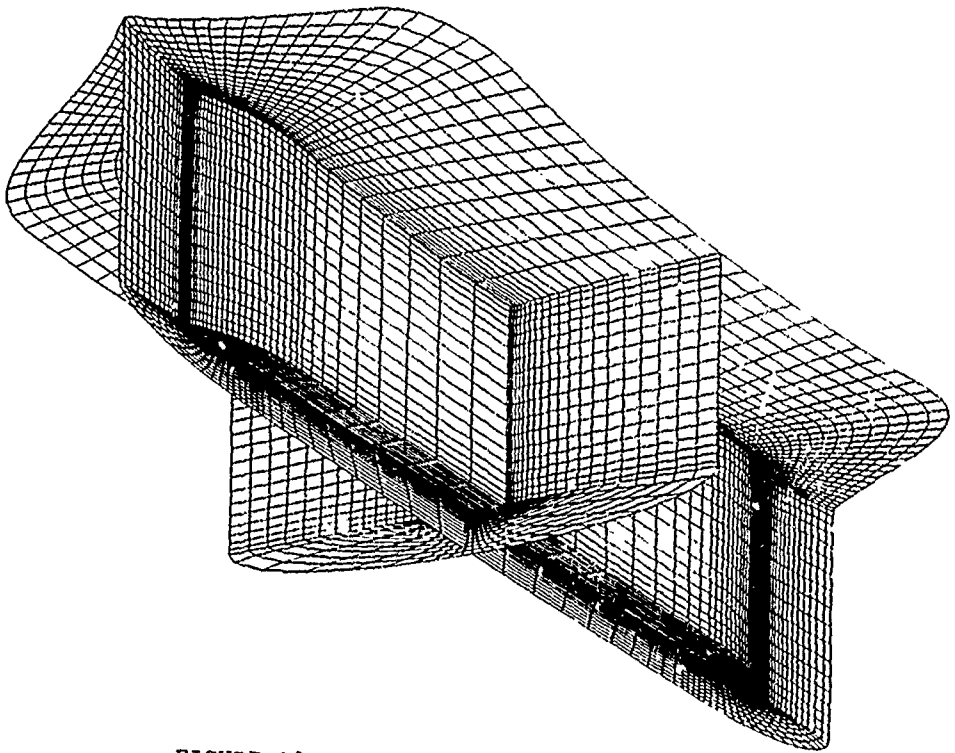

FIGURE 18. Pylon Grid

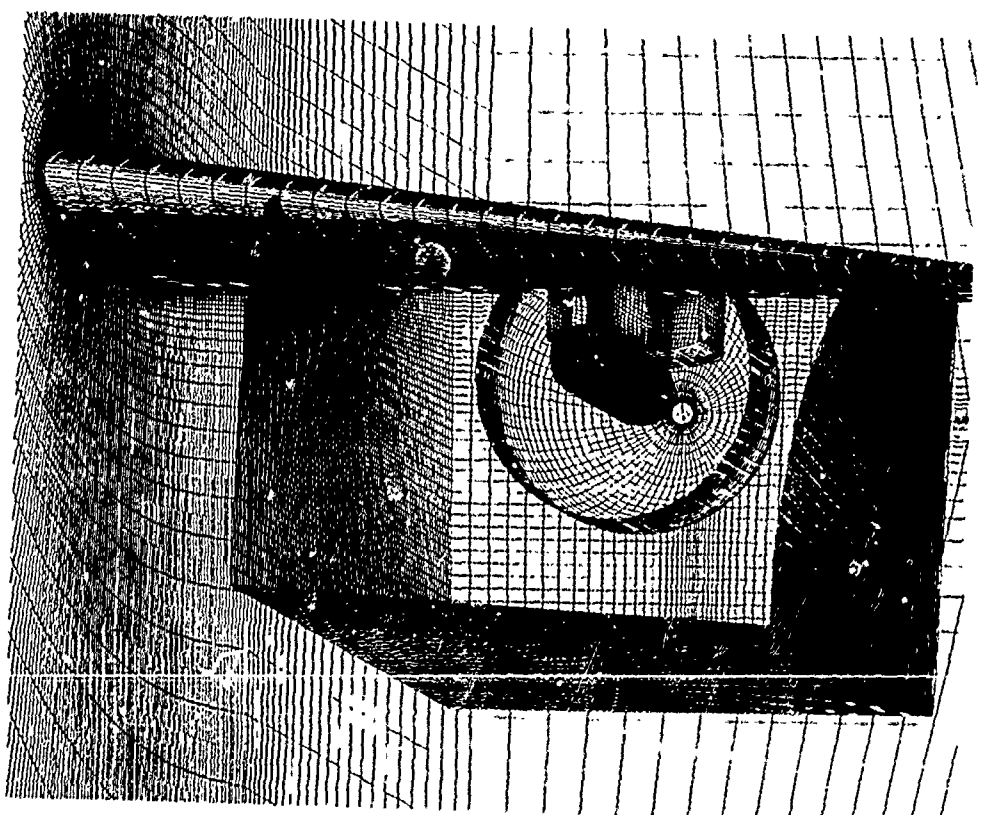

FIGURE 19. Wing-Pylon-Store Overlapped Grids

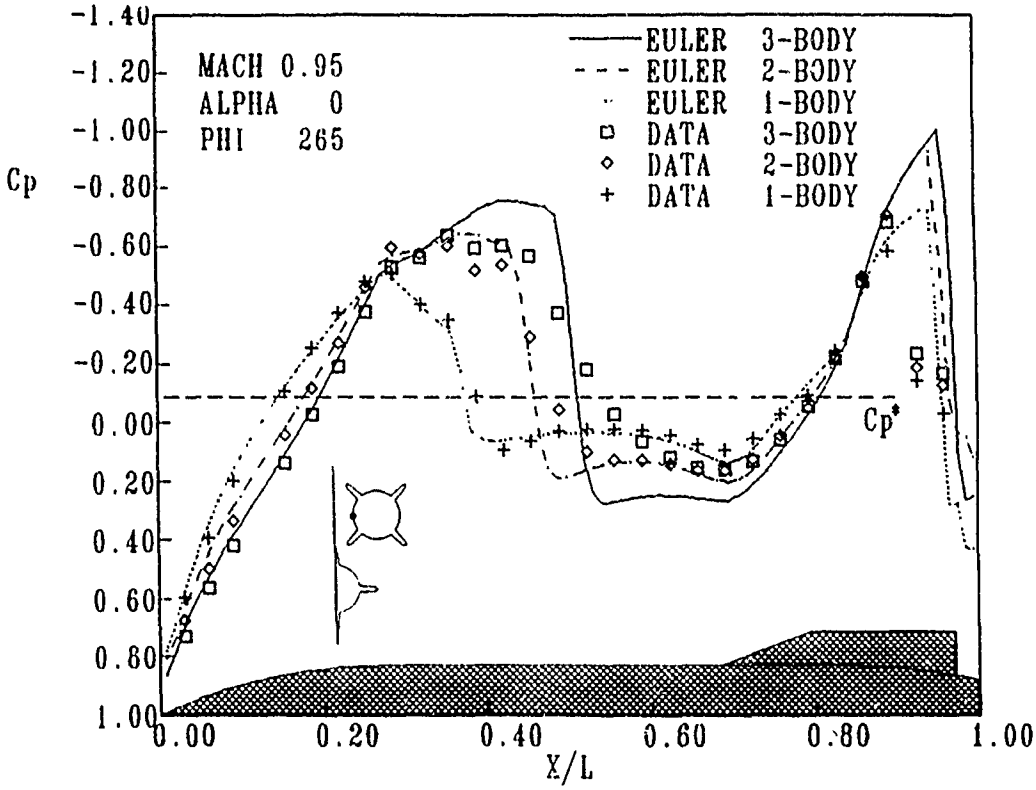

FIGURE 20. Finned Body Configuration Effects, Upper Body, Inboard Side

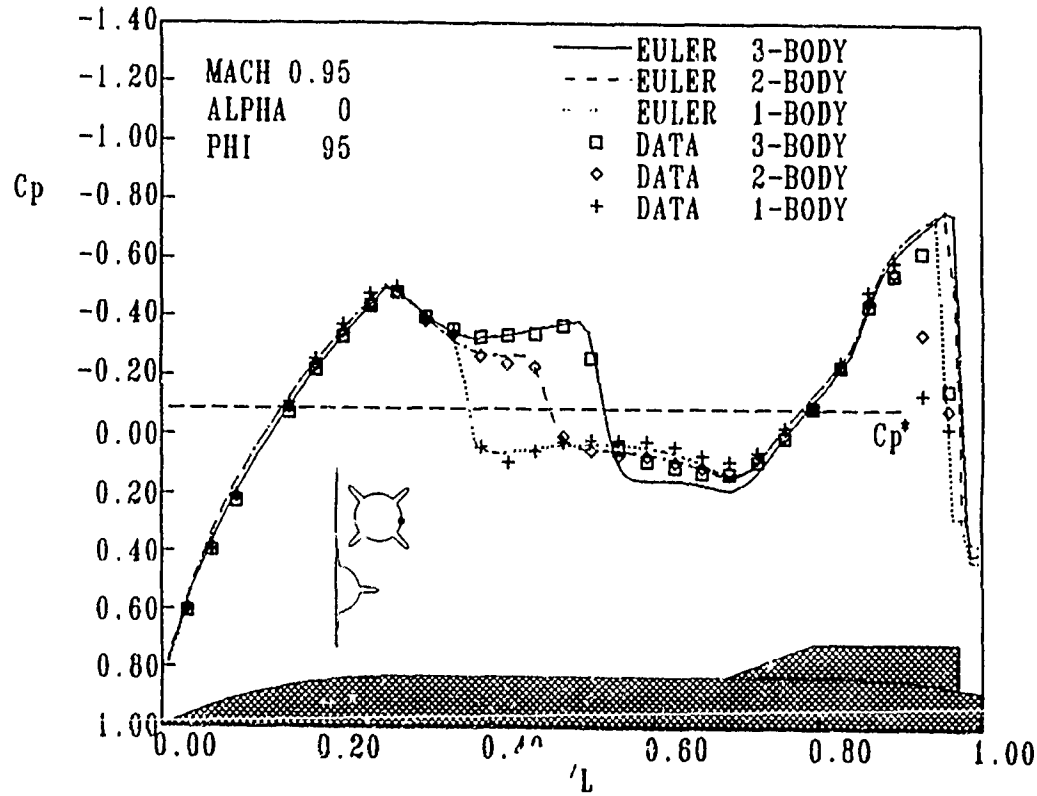

FIGURE 21. Finned Body Configuration Effects, Upper Body, Outboard Side

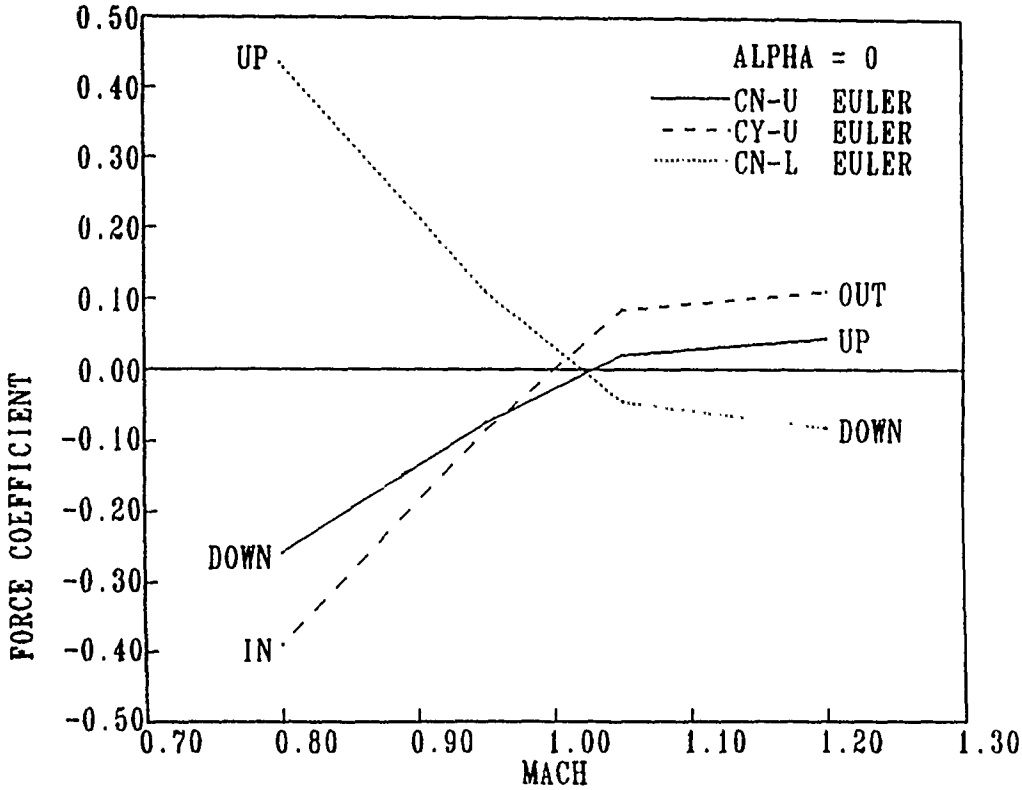

FIGURE 22. Finned Body Force Coefficients, 3-Body Case

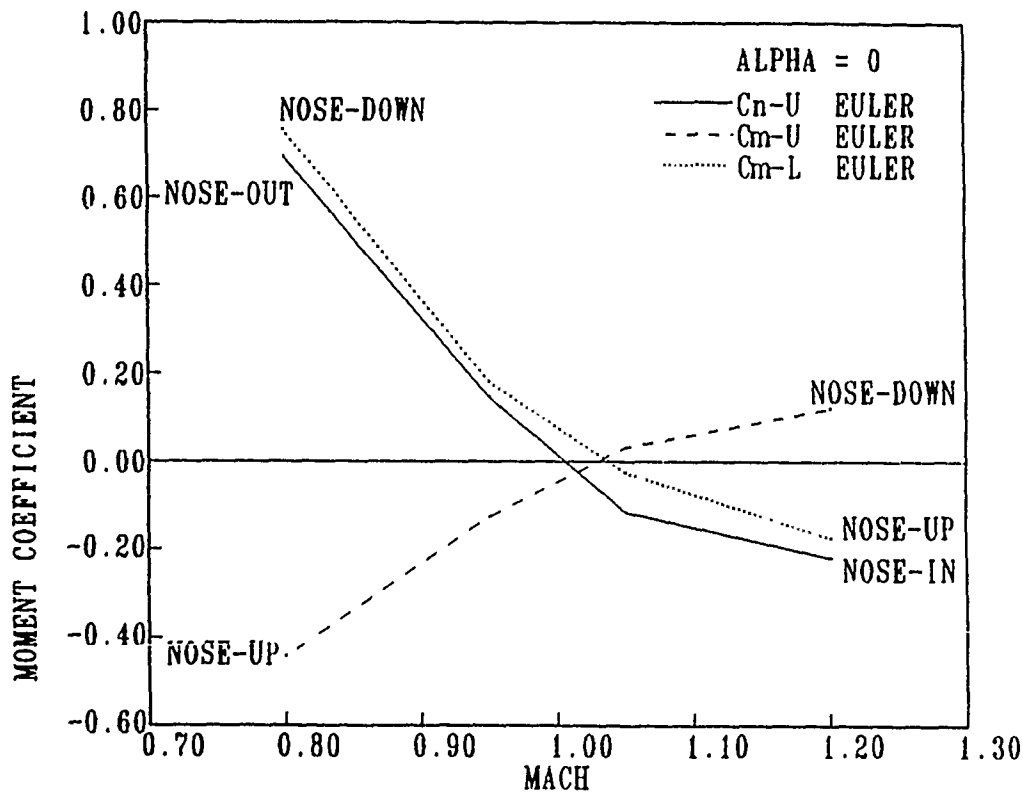

FIGURE 23. Finned Body Moment Coefficients, 3-Body Case

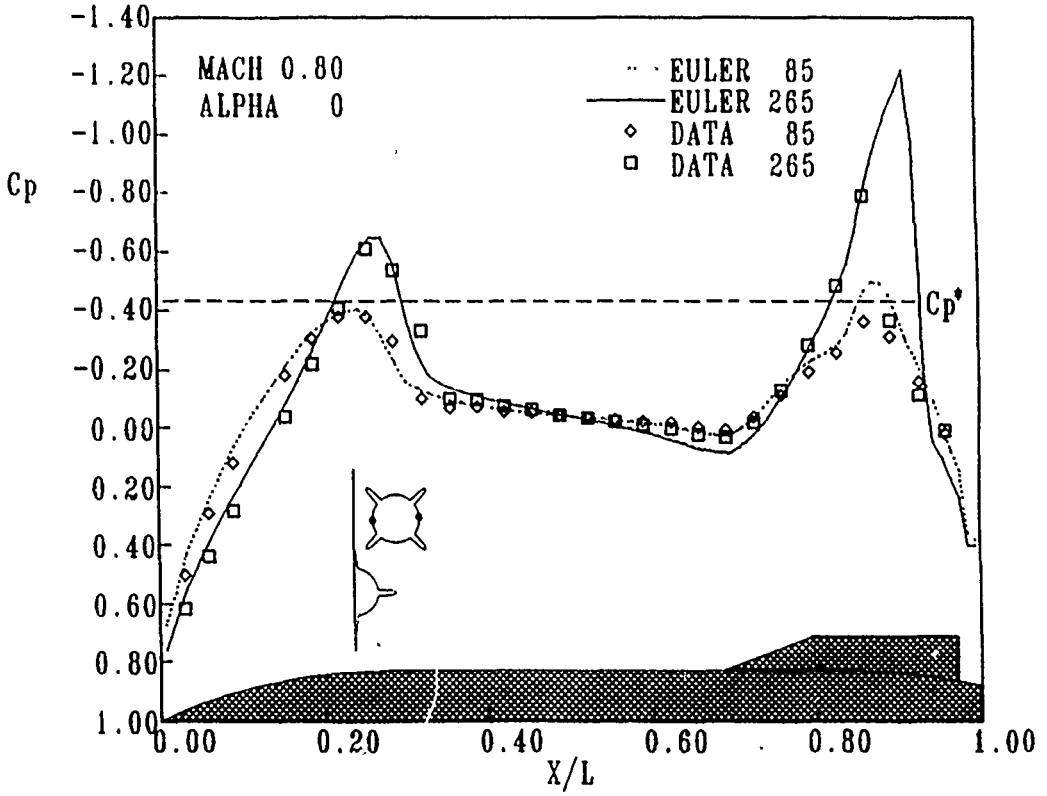

FIGURE 24. 3-Finned Body Subsonic Interference Effects, Upper Body

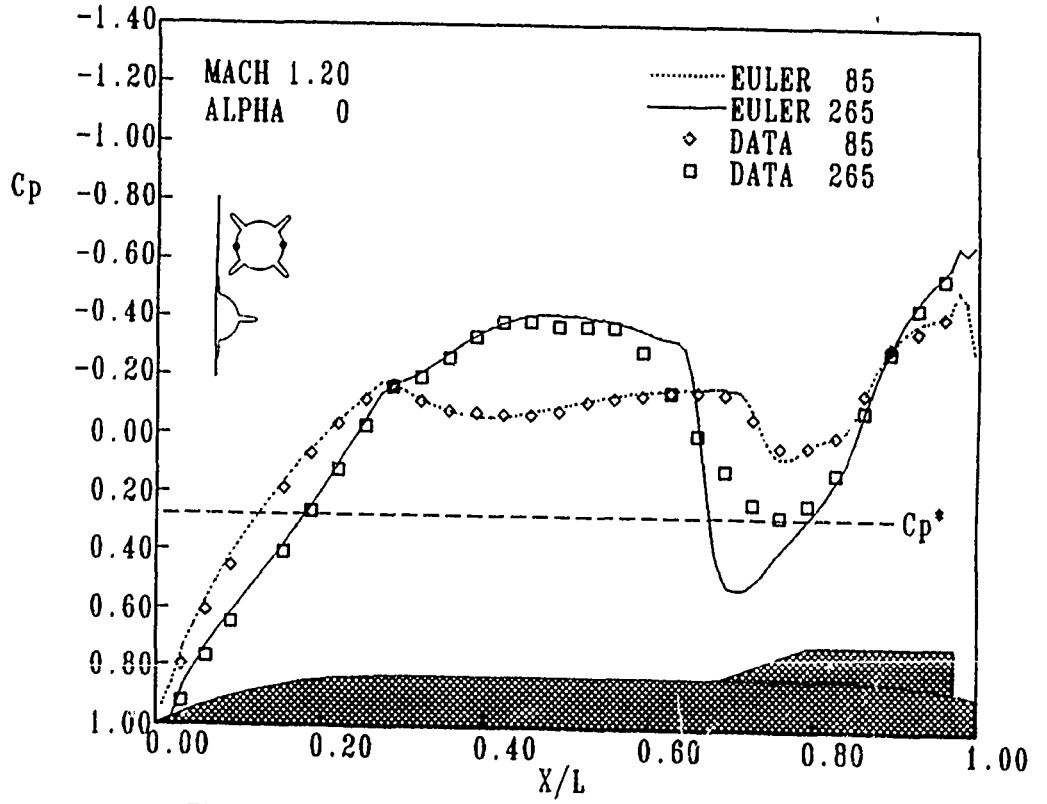

FIGURE 25. 3-Finned Body Supersonic Interference Effects, Upper Body

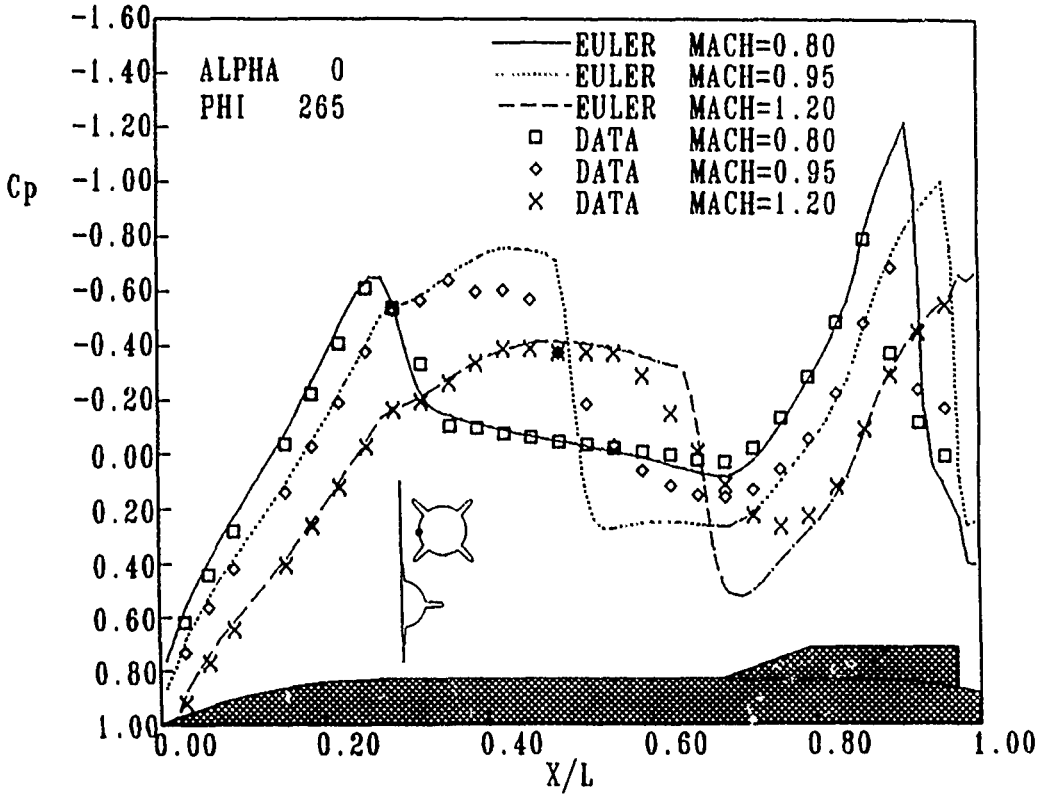

FIGURE 26. 3-Finned Body Mach Number Effects, Upper Body, Inboard Side

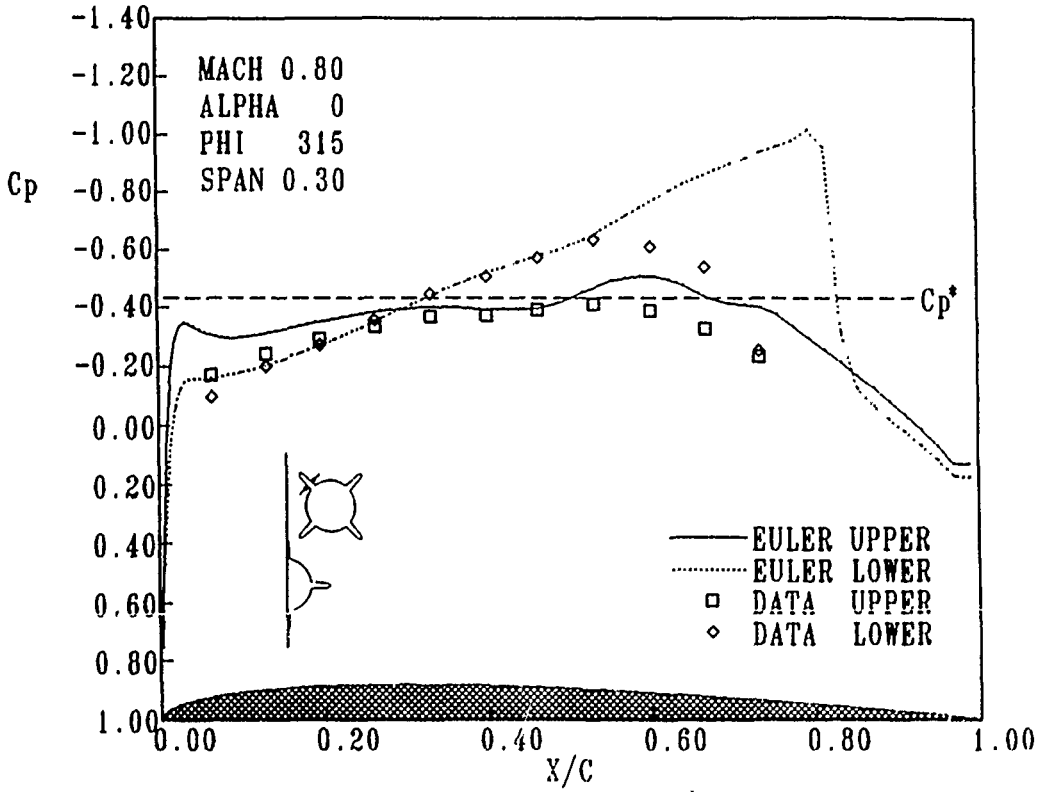

FIGURE 30. Fin Subsonic Interference Effects, 3-Body Case

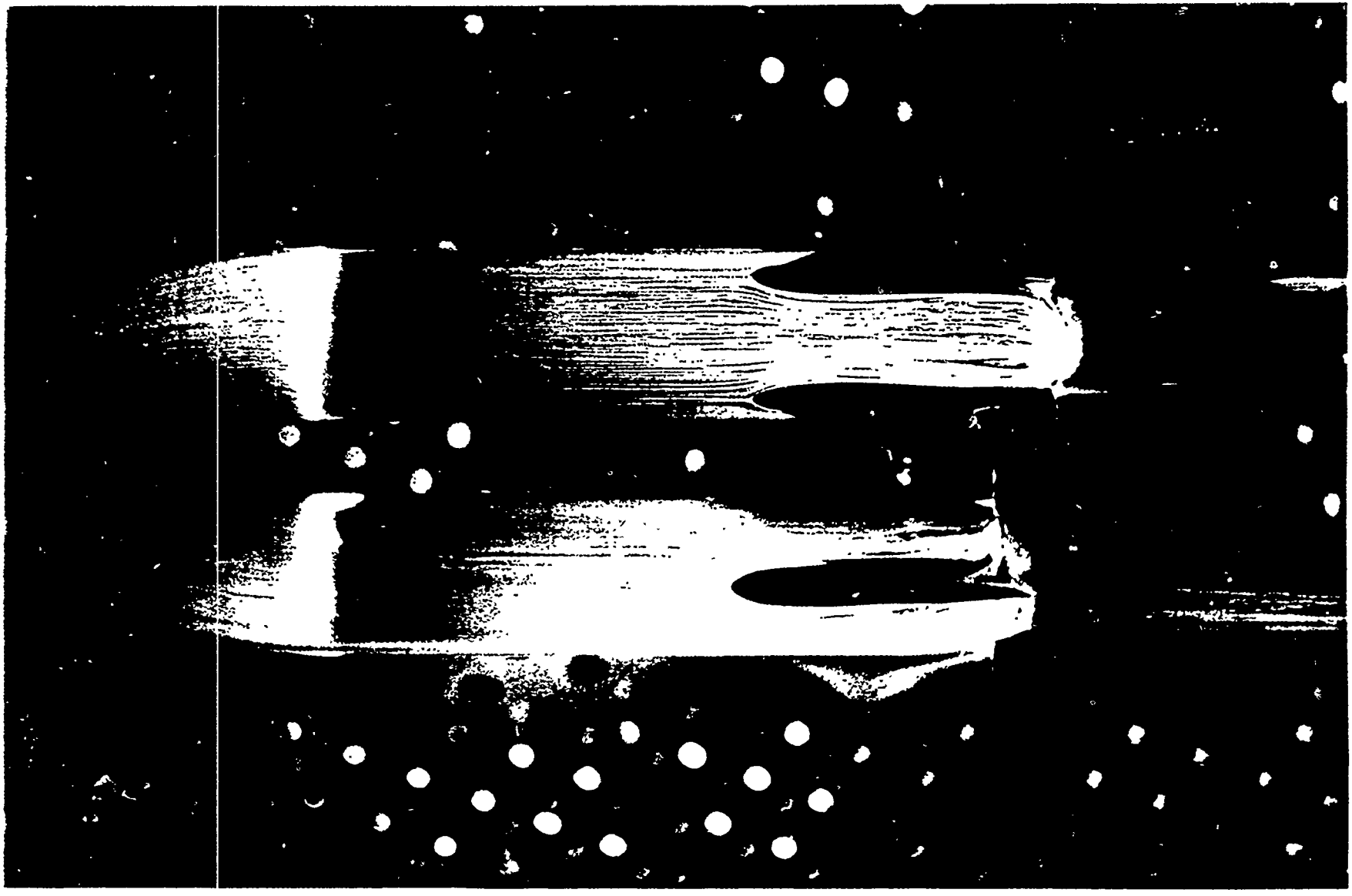

FIGURE 27. Surface Oil Flow, Mach 0.80,
3-Body Case, Side View

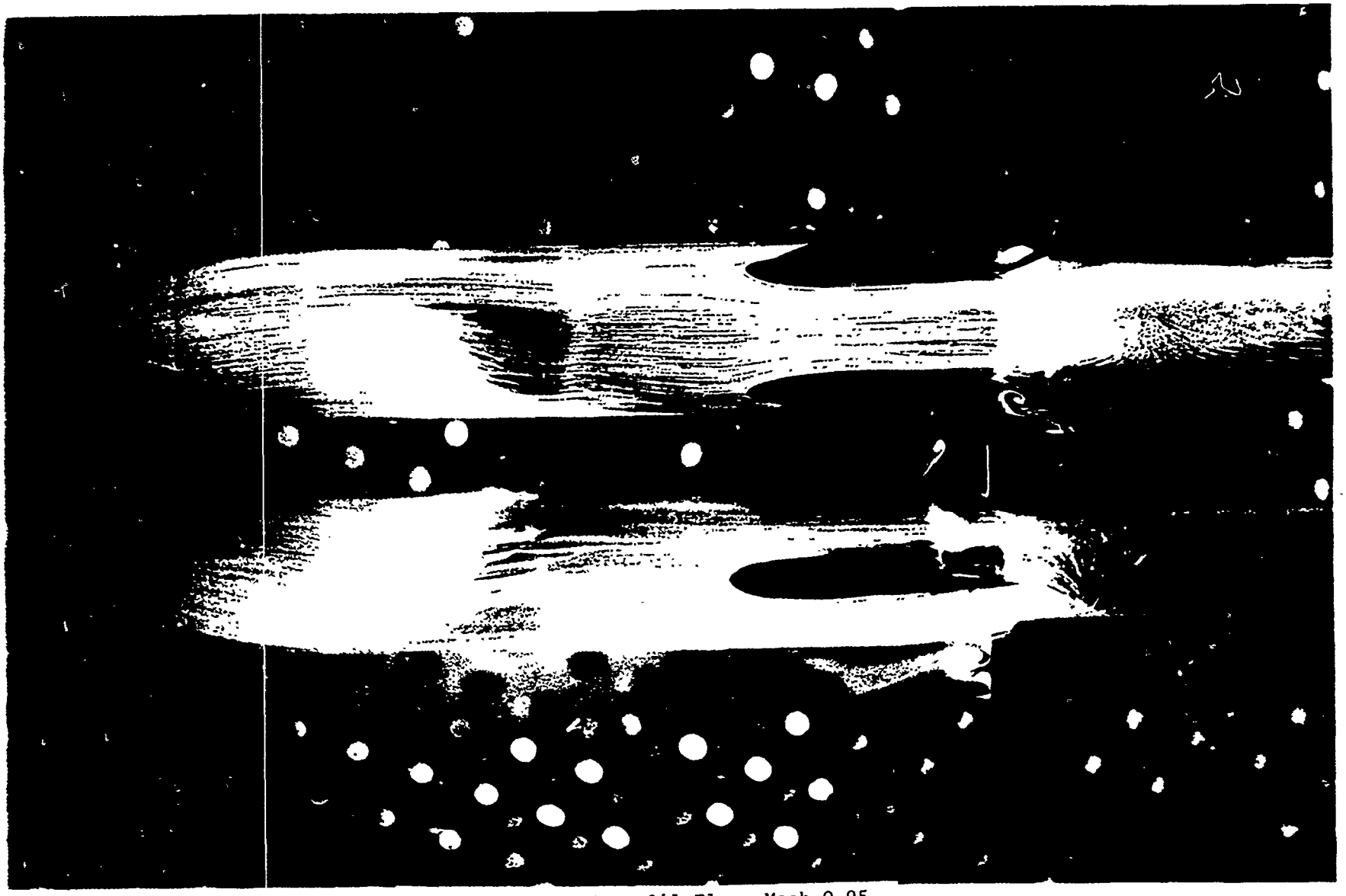

FIGURE 28. Surface Oil Flow, Mach 0.95, 3-Body Case, Side View

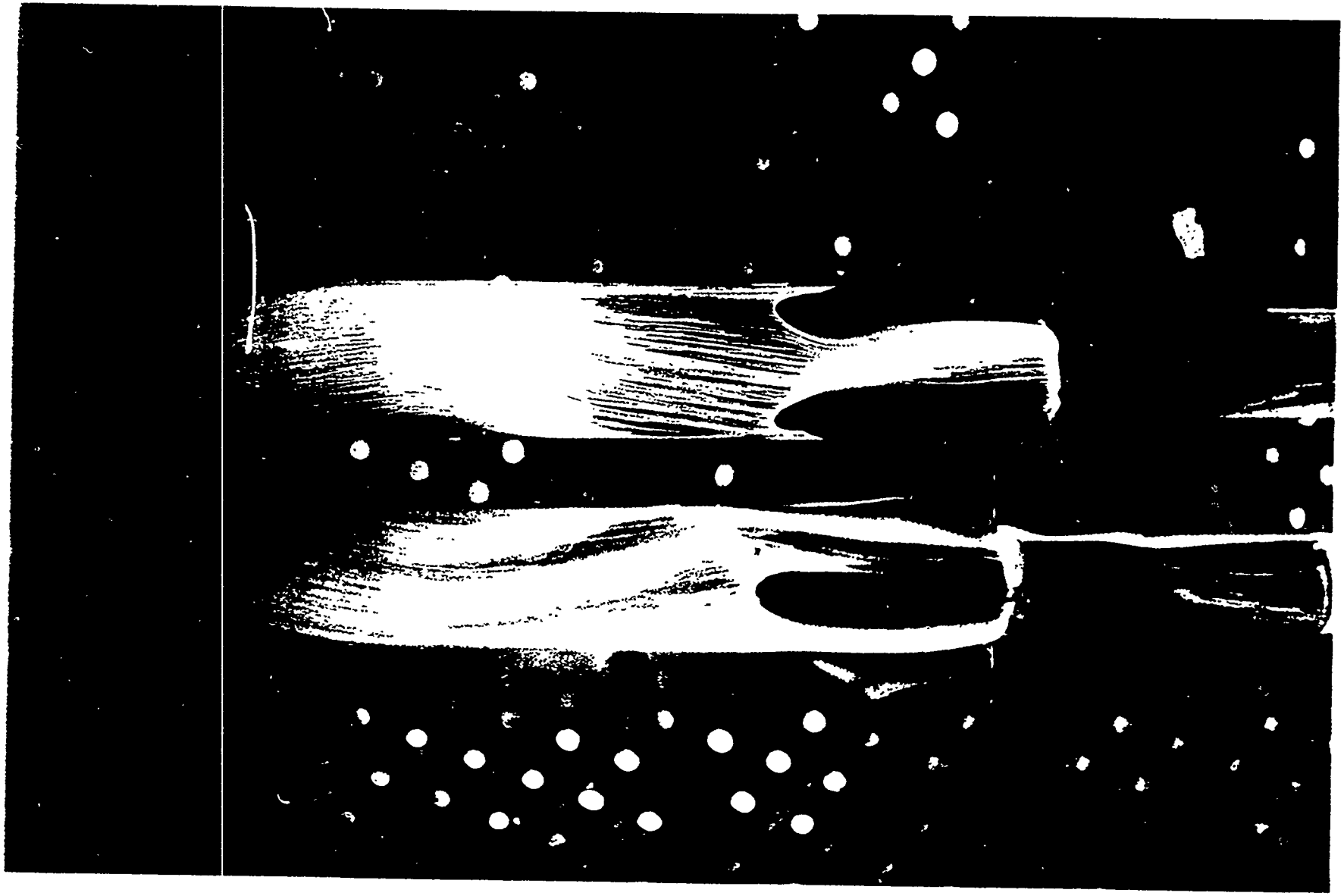

FIGURE 29. Surface Oil FLow, Mach 1.20, 3-Body Case, Side View

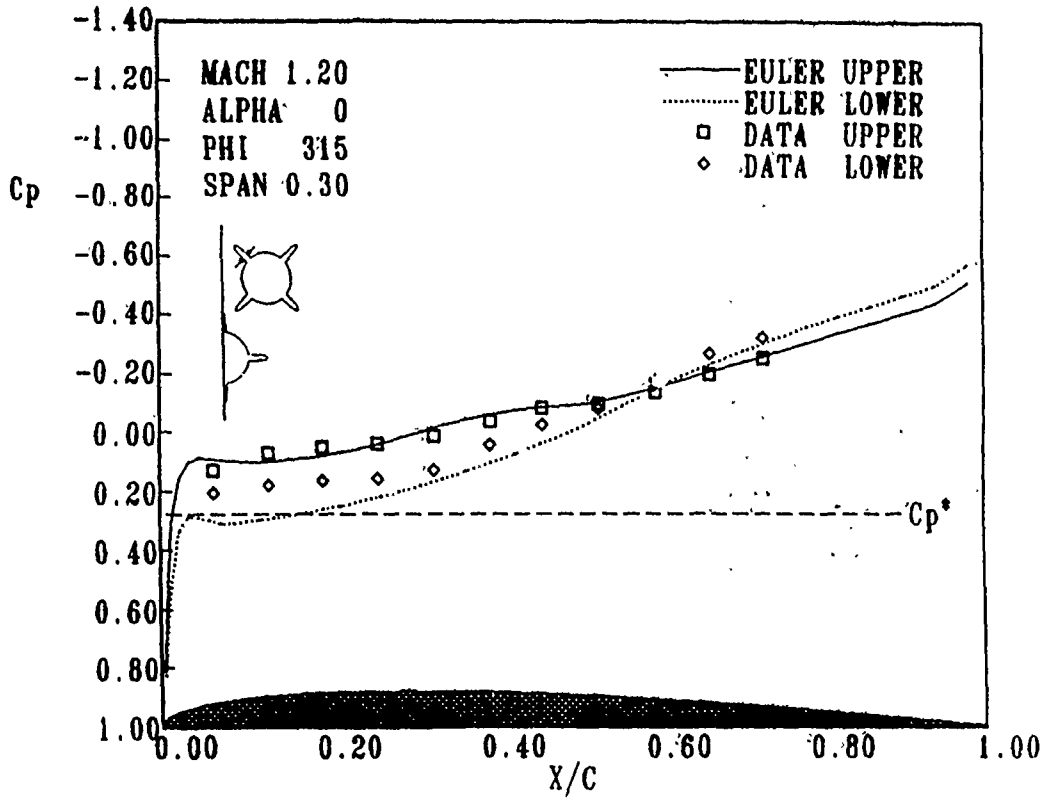

FIGURE 31. Fin Supersonic Interference Effects, 3-Body Case

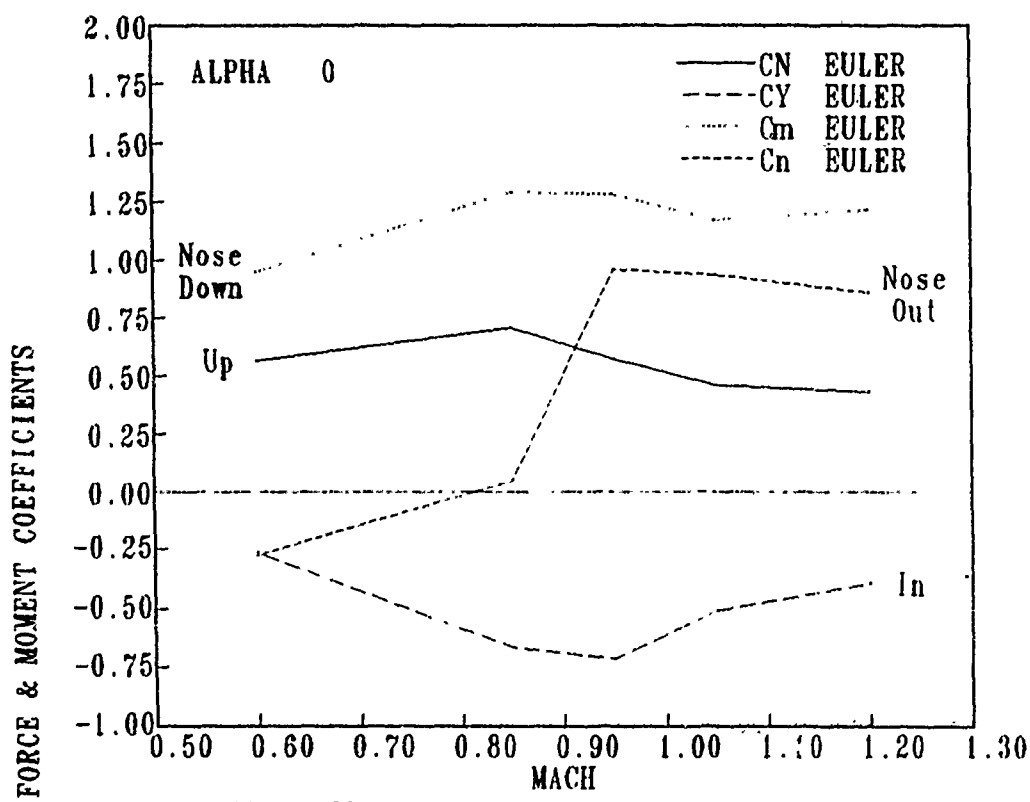

FIGURE 32. Store Force and Moment Coefficients, Wing-Pylon-Store Configuration

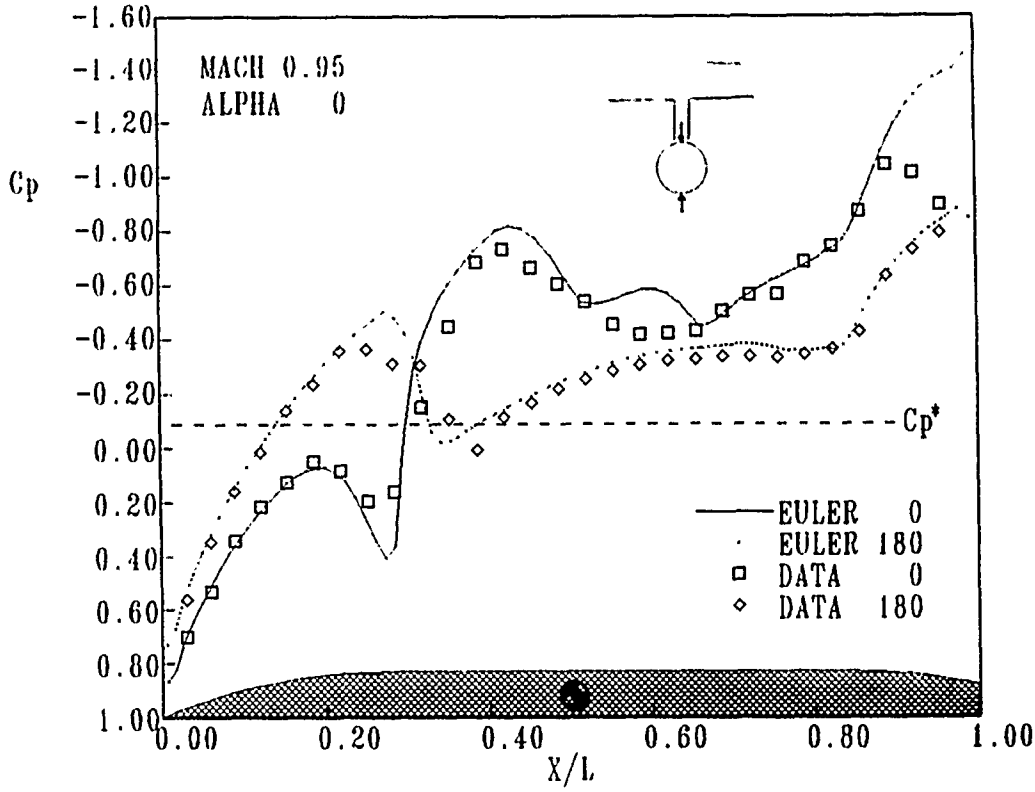

FIGURE 33. Store Surface Pressures, Top/Bottom

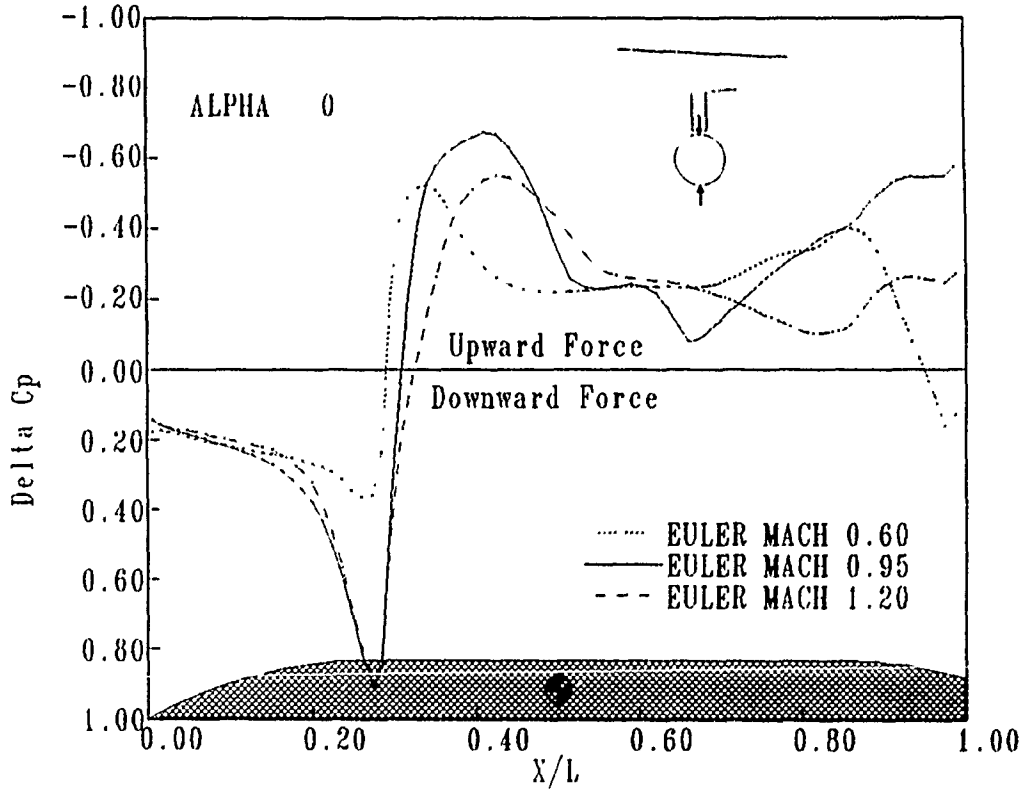

FIGURE 34. Store Pressure Differential, Top/Bottom

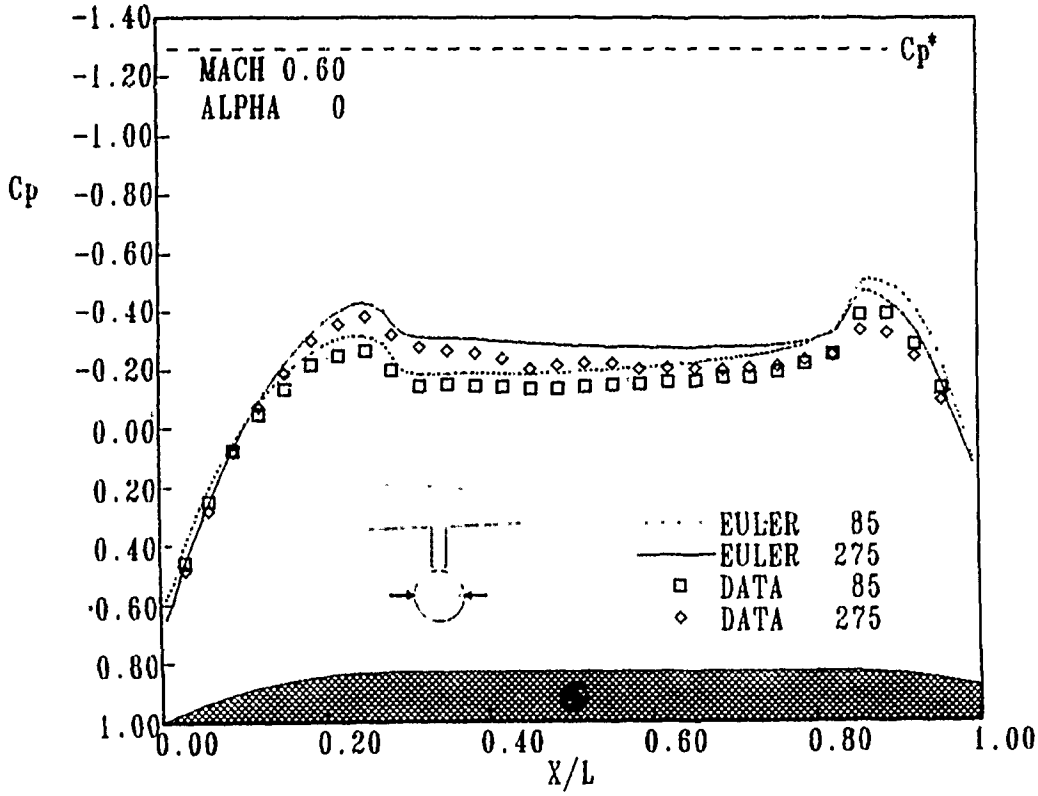

FIGURE 35. Store Surface Pressures, Mach 0.60, Inboard/Outboard

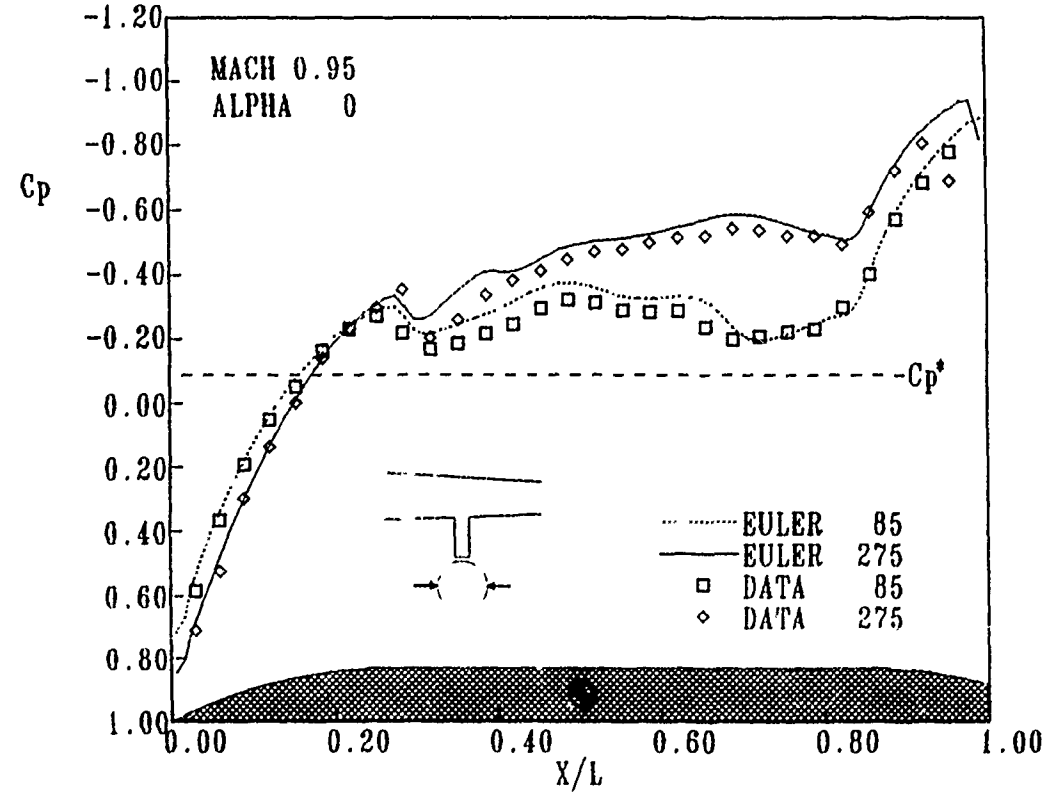

FIGURE 36. Store Surface Pressures, Mach 0.95, Inboard/Outboard

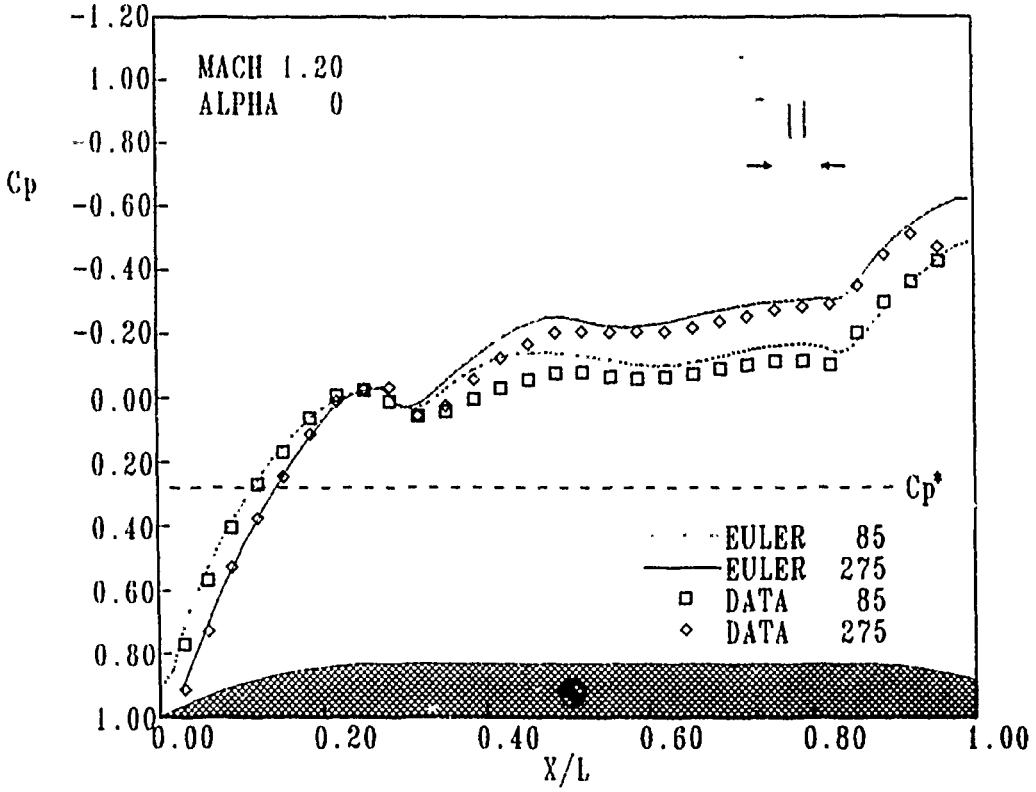

FIGURE 37. Store Surface Pressures, Mach 1.20, Inboard/Outboard

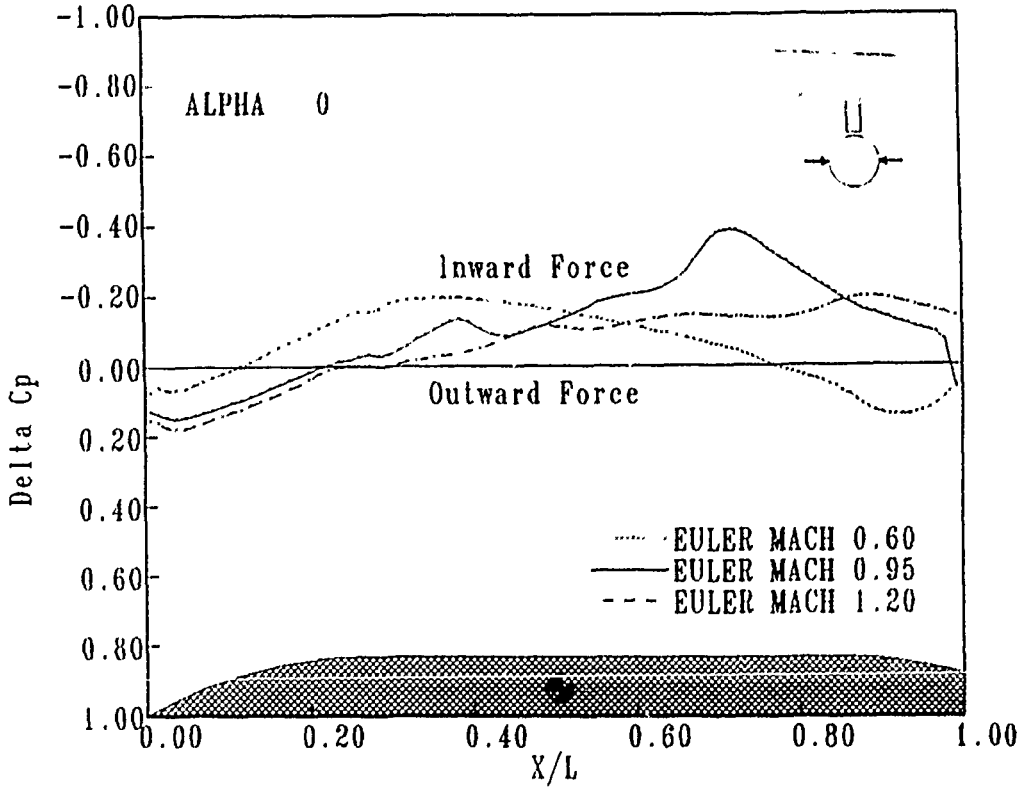

FIGURE 38. Store Pressure Differential, Inboard/Outboard

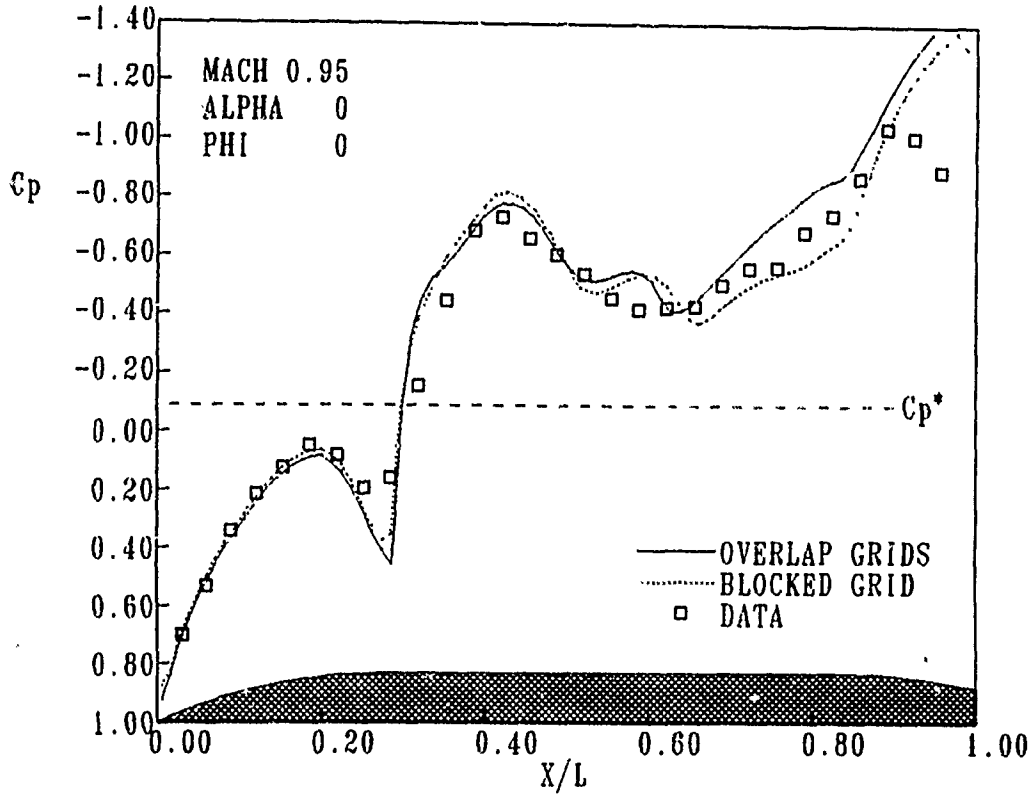

FIGURE 39. Store Surface Pressures, Top Side, Overlap/Blocked Grids

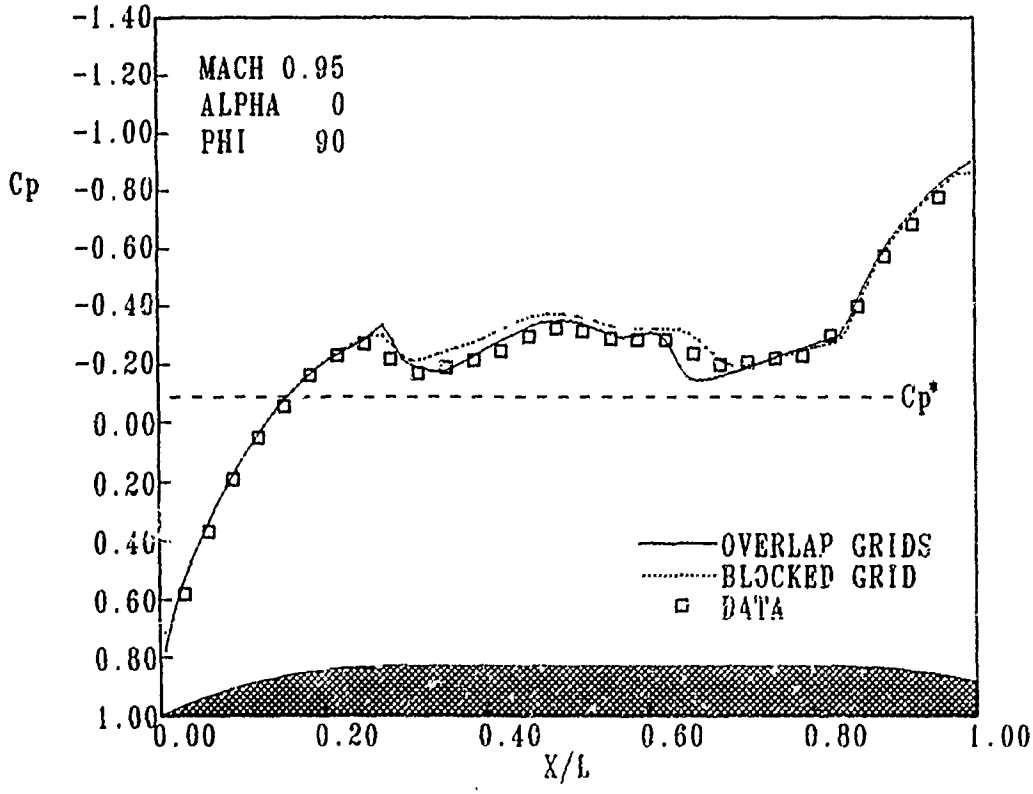

FIGURE 40. Store Surface Pressures, Outboard Side, Overlap/Blocked Grids

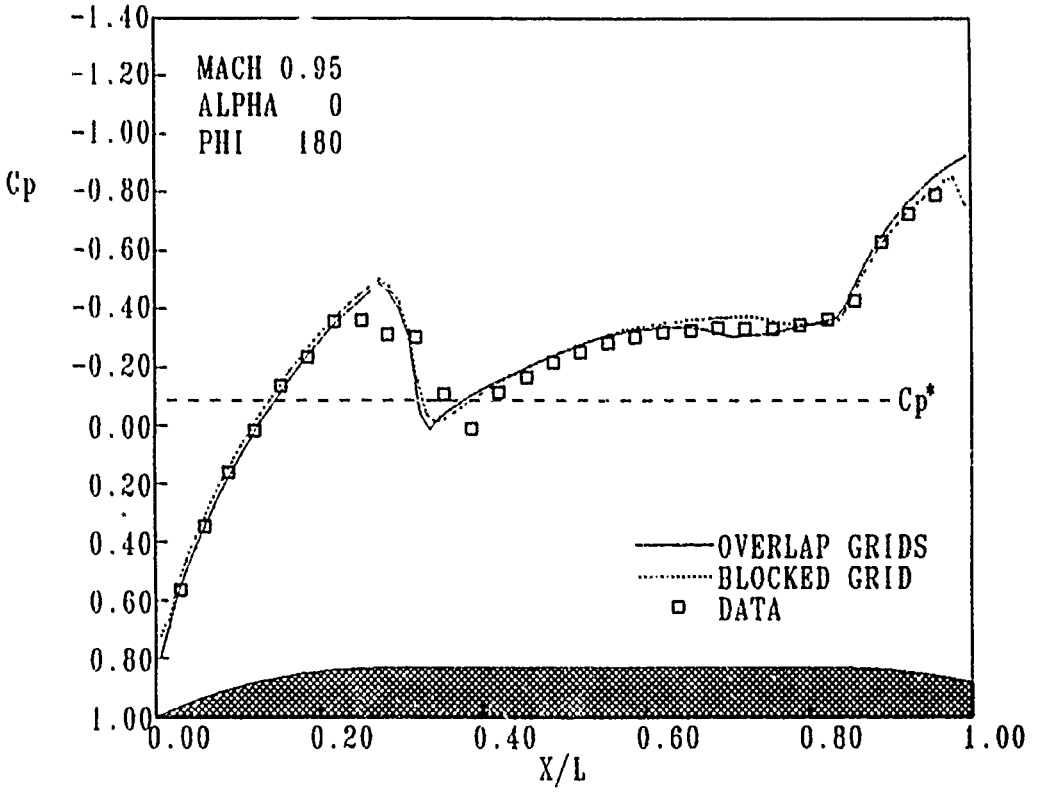

FIGURE 41. Store Surface Pressures, Bottom Side, Overlap/Blocked Grids

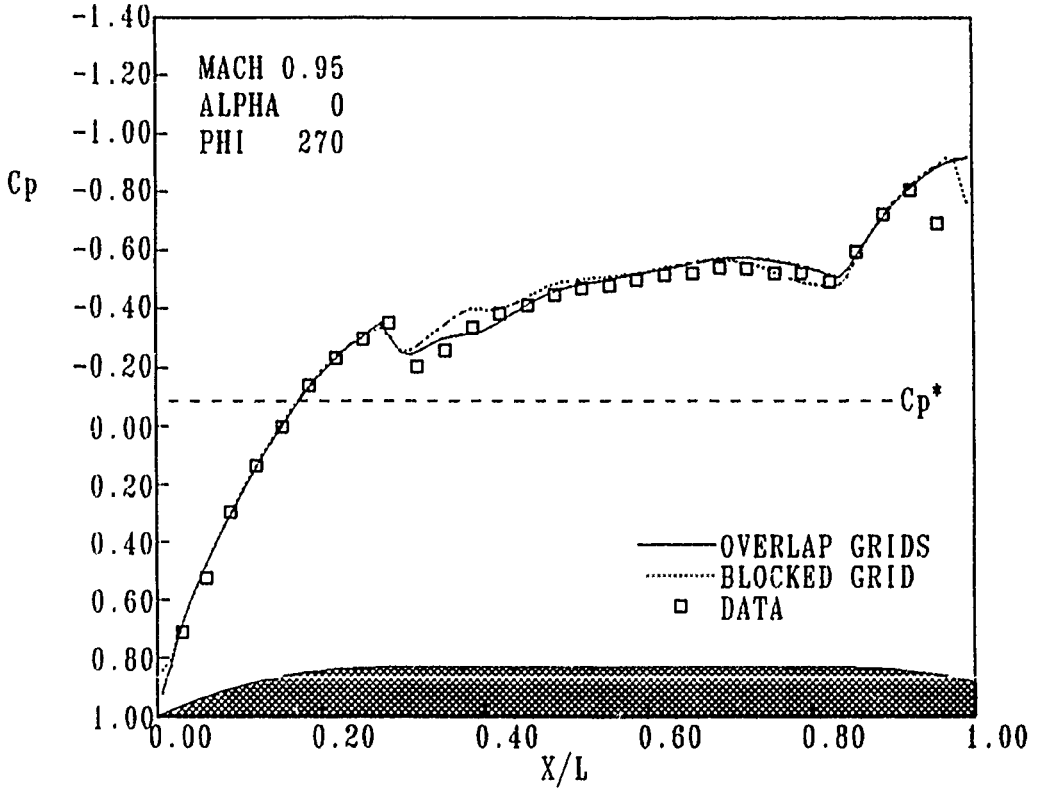

FIGURE 42. Store Surface Pressures, Inboard Side Overlap/Blocked Grids

Biography

Lawrence E. Lijewski was born in Milwaukee, Wisconsin, on March 12, 1948. He received the Bachelor of Science Degree in Aerospace Engineering from the University of Notre Dame in 1970. He later received the Master of Science in Aerospace Engineering and Doctor of Philosophy Degrees, also from the University of Notre Dame, in 1972 and 1974 respectively.

Upon graduation, he was employed as a mechanical engineer with the United States Army Aviation Systems Command in St Louis, diagnosing helicopter vibration problems.

From March 1977 to the present time, Dr Lijewski has been employed as an Aerospace Engineer at the Air Force Armament Laboratory, Eglin Air Force Base, Florida. His assignments have included Aircraft/Stores Compatibility Branch team chief positions in airloads and in research and technology; aerodynamics technology project and task manager; aerodynamics research task manager; and Computational Fluid Dynamics section chief. He is currently assigned as research scientist in charge of developing CFD techniques to predict freestream and carriage and release characteristics of weapon airframes in the transonic regime. His principal fields of aerodynamic interest include computational fluid dynamics, missile flight dynamics, and aircraft/store interference dynamics. He has authored or co-authored 25 technical reports and publications in these areas, and has lectured at scientific short courses and conferences.

Dr Lijewski is a senior member of the American Institute of Aeronautics and Astronautics (AIAA) and was named the Air Force Armament Laboratory Scientist of the Year in 1982.

CLEARED FOR PUBLIC RELEASE

NAVIER-STOKES SIMULATIONS OF INTERNAL AND EXTERNAL STORE CARRIAGE AND SEPARATION*

Oktay Baysal†
Kamran Fouladi
Victor R. Lessard

Old Dominion University
Norfolk, Virginia
and

David S. Miller
NASA Langley Research Center
Hampton, Virginia

JOCG 8th Aircraft/Stores Compatibility Symposium
Fort Walton Beach, Florida

October 23–25, 1990

---

* This paper is CLEARED FOR PUBLIC RELEASE.
† Author presenting the paper.

ABSTRACT

The objective is to demonstrate the numerical simulations of the interference flows about generic configurations of internally and externally carried stores at supersonic speeds. The efficiency and performance of fighter or bomber type aircrafts can be effected by stores in their proximity. The safe and effective separation of stores also become important as speed increases. External store carriage is the logical choice for existing aircrafts. The internal carriage of stores by the military aircraft, however, is an option for the possible reductions of both aerodynamic drag and radar observability. Trade studies of these options require studying the parent body and the stores together. With this motivation, a computer code was recently developed to solve the three-dimensional, Reynolds-averaged, unsteady, compressible, full Navier-Stokes equations on overlapped and block-structured grids. Each store location was assumed to be frozen at some close proximity of its parent body during its separation. Unsteady computations were performed for two types of internal-carriage configurations with two separate relative positions of each. Also, a steady flow simulation was performed for a store model near a flat plate wing. Time-averaged surface pressures were successfully compared with the experimental data.

INTRODUCTION

Aerodynamic effects of stores on a fighter or a bomber type of aircraft and their safe operations become more important as the speed of the aircraft increases. In addition to wind tunnel and flight tests, computations are now a viable option for the store-carriage-configuration design and trade studies. Computational fluid dynamics (CFD) is free from the problems of disturbing the flow with measurement probes or the wind tunnel walls, and it can reduce risks associated with flight tests. However, it is bounded by the truncation and the round-off errors, and the underlying physical assumptions. The aim of this study is to explain the application of a recently developed CFD code, and to contribute to the much needed database in understanding the interference between a parent body and a store during its separation. It is meant to augment wind tunnel tests, such as those reported in Refs. 1–5.

This investigation was divided into five building-block studies: (1) simulations of cavity flows (Refs. 6–9), (2) simulations of flows past cylindrical bodies at incidence (Refs. 10–12), (3) grid generation by a hybrid domain decomposition technique, DDT (Ref. 13), (4) simulations of interference flows past a cylinder near a flat plate wing (Refs. 13,14), (5) simulations of interference flows past two separate internal-carriage-configurations (Refs. 15,16).

The results included in this paper were compiled from References 13 through 16. Therefore, the description of the governing equations and their solution method are only summarized below. Also, the survey of pertinent literature on external and store carriages is omitted and the reader is referred to the proceedings of several conferences on this topic held in recent years (e.g., Refs. 3, 17, 18).

COMPUTATIONAL METHOD

A rectangular cavity consists of walls with outward normal vectors in three directions. Consequently, the diffusion effects of the viscous fluxes are not negligible, and their gradients are approximately of the same order of magnitude in all three directions. This requires the solution of the complete Navier-Stokes equations. Their reduced forms, such as, the thin layer approximation or the Euler equations produce nonphysical solutions to cavity flows.

The effects of Reynolds stresses were incorporated through the Baldwin-Lomax (Ref. 19) algebraic turbulence model. Several modifications have been done to the model for all the points in the cavity in order to determine the proper length and velocity scales in the highly vortical regions of massive separation, near three-dimensional corners and near the shear layer. Details of these modifications are given in Refs. 7–9.

Finite volume differencing was formulated by integrating the conservation equations over a stationary control volume. This equation was solved using the second-order accurate method described in Refs. 13, 15, 16, and 20. Either flux vector splitting (FVS) or flux-difference splitting (FDS) was used to construct the upwind differences for the convective and pressure terms. The diffusion terms were centrally differenced. Spatial approximate factorization and Euler backward integration after linearization in time resulted in the solution through 5x5 block-tridiagonal matrix inversions in each of the three directions.

A domain decomposition technique (DDT) subdivides the flow domain into simpler subdomains which accept easily constructed grids. these methods vary in constructing the grid interfaces and establishing the communication among the subdomain grids. Popular DDT's are the overlapped grids, the zonal grids, and the multiblock grids.

The standard block tridiagonal inversions of approximately factored, delta form of the Navier-Stokes equations can be easily extended for zonal and block structured grids. However, due to the existence of the overlap region and the holes in the overlapped grids, modification to the solution algorithm is necessary (Ref. 21). As subdomains are moved to their overlapped positions, some cells of one grid may be found to coincide with a solid boundary contained within another grid. Also, a significant number of cells may be interpolated, if every cell common to more than one subdomain grid is to be updated. This becomes computationally expensive and it could have an adverse effect on the global accuracy when cell sizes are not compatible in different subdomain grids. This problem can be avoided by updating only the boundary of the common region between subdomains, and excluding the other cells inside this region from the calculation. This process introduces an artificial boundary or a hole inside the overset subdomain. Hence, a search method was used to create and locate these holes. The details of the DDT's used in this study and the consequent modifications to the solution algorithm are given in Refs. 13 and 15.

CONFIGURATIONS AND GRIDS

Five computational examples were considered in this study. For the first two cases, a sharp ogive-nose-cylinder (ONC) was positioned near a cavity with a length-to-depth ratio of 6.73 (Fig. 1). The cavity was 29.363 in. long, 4.363 in. deep and 5.768 in. wide. The base diameter and the length of the cylinder were 1.2 in. and 24.028 in., respectively. The cylinder was mounted to a L-shaped offset sting, which had a 3.2 in. axial section (Ref. 2). The cylinder was placed 6.0 in. above the cavity opening for Case 1, and it was positioned 2.0 in. below the cavity opening for Case 2.

The computational domain was divided into four subdomains. The stretched Cartesian grid for the cavity had a lower block (81x23x43) inside the cavity and an upper block (103x28x57) above the cavity subdomain. The conservation across the grid interface is extremely important since the cavity flow is driven by the shear layer. To ensure the conservation, the grid lines were contiguous normal to the interface of these two blocks where the solutions were matched. A boundary fitted H-O grid was wrapped around the cylinder (121x29x33) and the sting was contained in an O-H grid (21x25x57). Both grids were embedded in the Cartesian grids. The end surface of the O-H grid containing the sting root was coincident with the cylinder solid surface. These component grids were used to form the composite grids for both cases. In fact, this is one of the advantages of the current algorithm in which the component grids are reusable. The total number of points in the composite grid was 390,219. The composite grids of Case 1 is shown in Fig. 2. Portions of the overlapped regions are marked by the solid circular dots.

For Cases 3 and 4, the parent body was represented by an 18 in. long, 4 in. wide and 2 in. deep cavity centered aft of the leading edge of a 47 in. by 16 in. flat plate (Fig. 3a). A boundary layer trip strip was installed 1 in. aft of the plate leading edge to promote transition to turbulent flow at the cavity lip. The store was represented by a 11.714 in. long cylinder with 0.5 in. diameter, which included a blunt-nose and a boat-tail (Fig. 3b). Four standard fins in cruciform arrangement and a curved offset sting were attached to the cylinder. Two flow cases were picked from the large test matrix reported in Ref. 4. The cylinder axis was aligned with the longitudinal center plane of the cavity at zero angle of attack, and was located 1.8 in. above the cavity opening for Case 3 and 0.9 in. below the cavity opening for Case 4. The flows of cases 1–4 were assumed symmetrical, which allowed the simulation of only half of the configuration. The cavity grid consisted of one block above the flat plate (122x40x50) and another block inside the cavity (91x31x45). The H-O grid of cylinder-fin-sting (CFS) assembly consisted of three blocks separated by the fin surfaces. The dimensions of these blocks were (121x17x41), (121x33x41), (121x17x41).

These individually generated subdomain grids were put together to form the composite grid. The three blocks of CFS were embedded in the two blocks of cavity with overlapped intergrid volumes, thus creating holes in the cavity grids (Fig. 4). The total number of points in the composite grid was 703,332. The locations of these holes were naturally different for Case 3 and Case 4. Composite grids can be generated for different positions of CFS, as it moves relative to the cavity, without having to change the subdomain grids.

The configuration of Case 5 was comprised of another ogive-nose-cylinder (ONC2) attached to a sting and in a proximity of a flat plate which was 70 in. long and 55 in. wide. The

base diameter and the length of ONC2 were 1.2 in. and 21.6 in., respectively. The nose of the cylinder was placed 34.42 in. aft of flat plate and its axis was 4.2 in. away from the flat plate (Fig. 5). A stretched Cartesian grid (97x57x73) was generated for the flat plate. The grid for ONC2 was a C-O grid (73x65x17) and it was completely embedded in the Cartesian grid (Fig. 6). The total number of points in the composite grid was 484,282.

BOUNDARY AND INITIAL CONDITIONS

Since the flow was two-dimensional on the flat plate ahead of the cavity, a two-dimensional, turbulent boundary layer profile was generated to match the experimentally determined thickness upstream of the cavity lip (0.40 in. for Cases 1 and 2, 0.26 in. for Cases 3 and 4, 0.85 in. for Case 5). Using this profile as an upstream boundary condition allowed the computational domain to start downstream of the flat plate leading edge (22 in. for Cases 1 and 2, 13 in. for Cases 3 and 4, 14 in. for Case 5), thus significant computational time and memory saving were realized. The conventional viscous flow boundary conditions, that is, no-slip, impermeability, and adiabatic-wall conditions were imposed on all solid surfaces. First order extrapolation of the primitive variables were used at the downstream boundary. One-dimensional characteristic boundary conditions were imposed at the outer boundary and the lateral outboard boundary. The symmetry of the flow at the plane, where symmetry was assumed (Cases 1–4), was ensured by setting the contravariant velocity normal to this plane equal to zero and extrapolating the other primitive variables.

Besides the physical boundaries of the computational domain, there were intergrid boundaries between the five subdomain grids. The conservative transfer of fluxes across a block interface, i.e., where the lines normal to the interface are contiguous, was maintained by using two sets of ghost cells on each side. Across an intergrid boundary with overlapped subdomain grids, the conserved variables were interpolated nonconservatively to one set of ghost cells on each side. The coefficients of this trilinear interpolation to one grid cell were determined based on the distances to the vertices of a hexahedron formed by the cell centers of the neighboring overlapped subdomain grid (Refs. 13, 15).

Since the governing equations were elliptic partial differential equations and were solved using time marching, the dependent variables, i.e. the conserved flow variables, needed to be initialized. This could be done by either an all-quiescent domain or by an all-freestream domain. However, a more efficient method was initializing the cavity subdomains with the solution for a clean cavity flow, i.e. in the absence of the cylinder. Similarly, the CFS, ONC, and ONC2 domains were initialized with the solution for a flow past CFS or ONC without the presence of the parent body in its proximity. This procedure required first solving time accurately for the unsteady clean cavity flow (Refs. 6–9), then solving for the steady flow past CFS or ONC (refs. 10, 12).

The block chart of the code developed for this class of flows is given in Fig. 7. The viscous internal store carriage code (VISCC) was run on the CRAY-2 computers of NASA Langley Research Center and Numerical Aerodynamic Simulation facility of NASA. The run time memory required by the solver of the flow equations (VUMXZ3) for the cases being considered here was about 136 megabytes for Cases 1 and 2, and 208 megabytes for Case 3

and 4, and 142 megabytes for Case 5 (approximately 295 bytes per grid point). The memory requirement can be reduced, if necessary, by simply dividing the domain into more subdomain grids. As discussed earlier, this is one of the advantages of employing DDT.

Two characteristic times were defined for two different reasons. The first characteristic time was defined as the maximum of all the times obtained as the ratio of a cavity dimension, l (length width) to the corresponding component of the freestream velocity, $t_{c1} = \max(l/u)$. It was used as a time scale for this unsteady flow. Numerical transients due to the nonphysical initialization of the clean cavity computational domain were assumed to be removed after running the solution algorithm for (4 t_{c1}). The second characteristic time was defined as the ratio of the minimum length of the discretization stencil used by the solution algorithm to the freestream value of the speed of sound, $t_{c2} = \min(5.\Delta x_m)/a_\infty$. Note that this second-order algorithm used five-point stencils in each direction. Time characteristic, t_{c2}, was used to determine the physical limitation set on the time step size of the solution algorithm which was advanced time accurately. To collect computational data at a rate faster than the wave propagation speed, computational time step should be an order of magnitude less than t_{c2}. This practice ensured capturing numerically the pressure fluctuations of the cavity flow. The values of t_{c1} and t_{c2} for the Case 3 cavity were 0.73 and 0.07 milliseconds, respectively. Their values for the cavity of Case 1 were 1.56 and 0.073 milliseconds, respectively. Since Case 5 involved a steady flow, t_{c1} and t_{c2} were not defined for this case.

DISCUSSION OF COMPUTATIONAL RESULTS

For Cases 1 and 2, the flow was turbulent at M = 1.65, R_e/ft = 2×10^6, $\alpha = 0°$, P_t = 1092 lb/ft^2, and T_t = 584°R, where P_t and T_t denote the freestream total pressure and temperature, respectively (Ref. 2). The nominal wind tunnel test conditions (Ref. 4) of the turbulent flow being simulated for Cases 3 and 4 were: Mach number, M = 2.75; unit Reynolds number, Re = 2.97 million per foot; total pressure, P_t = 18.3 psia; total temperature, T_t = 580°R. The major differences between the configurations of Refs. 2, 4 are: (1) CFS has four fins, (2) CFS has a blunt nose and a boat-tail, (3) the sting shapes are totally different. The configuration for Case 2 does not contain the sting in an attempt to obtain a better understanding of flow between the cylinder base and the cavity rear face. Besides, such a sting certainly does not exist in a realistic application such as an internally carried store separating from its parent body.

Case 5 represents an external store flow. The approaching turbulent flow was at M = 2.86, Re = 2 million per foot, T_t = 610°R. The ogive-nose-cylinder (ONC2) and the flat plate were at zero angle of attack.

Cases 1 and 2:

The clean cavity solution was obtained after 15 t_{c1}, which required about 17.5 hours of computer time. The steady-state solution for cylinder-sting in freestream was obtained by using one hour of computer time. The computer time to advance the interference flow for one t_{c1} was about 20 hours. The interference flow between the components of the configuration was observed in less than one t_{c1}, after the initialization of the flowfield. However, the solution was advanced for nearly 2 t_{c1}. The reasons for this extended calculation was to mimic the

experimental procedure for code validation purposes. In the experiment (Ref. 2), a steady flow measurement technique was used to measure these unsteady flows.

The computed values of the averaged pressure coefficient (C_p) distributions on the cavity surface and the cylinder for Case 1 are presented in Fig. 8 in comparison with the experimental data. In Figs. 8a-b, C_p distributions are plotted along the horizontal centerline of the floor (F) and the vertical centerline of the rear face (RF). The pressures are near the freestream value on most of the F, but they increase near and along the RF. The same trend is observed in Fig. 8c for the side wall (SW). The longitudinal C_p distribution on the inboard surface of the cylinder ($\eta = 180^o$) shows the sharp increase owing to the nose shock followed by the expansion around the forebody (Fig. 8d). In comparison with the results of clean cavity (Ref. 9), these results show that the cylinder has very small effect on pressure distributions on the centerline of the cavity. In any event, the computed C_p values compare very well with the experimental data at all locations. These values vary with time for this unsteady flow and the only basis for comparison is through time averaging. However, the initial time and the elapsed time of the averaging process are different for the computations and the measurements. Also, a true characteristic time for averaging is not evident since the flow fluctuations are non-periodic at supersonic speeds (Ref. 7–9). The measured surface pressure data were averaged values of over 100 measurements obtained within a time span of 2 to 3 seconds. The surface pressure distributions in this study were averaged over a period of approximately 3 milliseconds. The averaging was done over 11,000 computed values.

The instantaneous streamwise Mach number contours at the plane of symmetry (y = 0.0) for Case 1 are displayed in Fig. 9. Evident in this figure is the undulation of the free shear layer which is formed between the high speed external flow and the slower internal flow. When the pressure inside the cavity is below the freestream pressure, the shear layer is deflected down and air is pumped into the cavity. This air mass is then slowed down by various dissipative processes within the cavity and this in turn increases the cavity pressure above the freestream value. The shear layer is then deflected out of the cavity by the excess pressure and the mass is pumped out of the cavity. However, this cycle is changed when a cylinder is placed near the cavity. The pressure of the flow between the shear layer and the inboard side of the cylinder is increased due to the nose shock of the cylinder and its reflection off of the shear layer. As shown in Fig. 9, this rise in the pressure value then causes the shear layer to deflect downward deep inside the cavity. The formation of the wake flow at the base of the cylinder and the blunt trailing edge of the sting and its interference with the shear layer are also shown in Fig. 9.

The vortical nature of the shear layer is depicted in Fig. 10. This figure also shows the expansion at the sharp corner of the front face and the compression at the rear face of the cavity. Also shown is the nose shock on the cylinder and impingement of this shock on the shear layer. The unsteady nature of the cylinder near cavity flow was captured computationally and is presented in Fig. 11. The oscillation of the normal force coefficient, C_N, due to this unsteadiness is observed over a period of 1.59 milliseconds (ms). The computed mean value of the axial force coefficient C_A and C_N of the cylinder over this period were (0.3532) and (0.0056), respectively. The experimentally measured values of C_A and C_N were (0.3756) and (-0.0258), respectively.

The unsteady nature of the flowfield and the interaction of the shear layer with the cylinder are illustrated in Fig. 12, where Mach number contours of symmetry plane at five consecutive

instants over a period of 1 ms are shown. The shape of the shear layer and in turn its points of contact with the cylinder constantly change with time. This motion of the shear layer and its interaction with the rear lip of the cavity has been shown to generate shedding of vortices (Ref. 9).

Time averaged pressure coefficients on various surfaces of the cavity and the cylinder are presented in Fig. 13. The trend of computed C_p distributed on most surfaces agree very well with the data of Ref. 2. The discrepancy in the distribution of RF is attributed to the sting, which exists in the experimental model but not in the computational model. The computed C_p at the vertical centerline of RF is slightly higher than the experimental data. This effect is also evident on the surfaces of the cylinder. The predicted mean values of C_A and C_N for the cylinder over a period of 1.59 ms were (0.0580) and (-0.0551), respectively. The experimental values (Ref. 2) for C_A was (0.0283) and for C_N was (-0.0611). The variation of C_N over this period is illustrated in Fig. 11. The difference between a high and a low instantaneous values of C_N, which may be interpreted as the amplitude, is much larger for Case 2 than it is for Case 1. This is expected since the unsteadiness is much more pronounced inside the cavity.

Cases 3 and 4:

The clean cavity solution was obtained after 10 t_{c1}, which required about 25 hours of computer time. The steady state solution for CFS in freestream was obtained by using 1 hour of computer time. The interference flow solution was obtained for 2 t_{c1} after the initialization of the flowfield. The computer time needed for 1 t_{c1} of the interference flow was about 35 hours.

The instantaneous Mach contours of the symmetry plane (Fig. 14) show the flow structure of Case 3. As the boundary layer on the front plate separates at the front cavity lip, it forms the shear layer bridging this deep cavity. This open-type (Refs. 6-8) cavity flow is predominantly transonic inside the cavity. However, the impingement of the detached shock emanating from the nose of CFS causes the shear layer to deflect inwards, creating a supersonic pocket in this region. Above this region, between the incident shock and its reflection, the Mach number is greater than freestream.

At the inboard and outboard sides of the CFS, boundary layer growth is drastically different because of cavity flow interference. Another shock structure is evident just upstream of the fins. The interaction of this shock surface and the shear layer creates a highly vortical wake just downstream of the fins. At this instant, the shear layer is deflected upward upstream of the rear cavity lip. A strong detached shock surface extends from the base to the top of the vertical sting. The wake behind this sting is highly vortical. The flow on the rear flat plate is partially transonic and separated.

A spanwise cut of the shear layer and the flow in the fin region are depicted via the instantaneous and normalized pressure contours (Fig. 15). The boundary layer on the cavity side plate reaches the shear layer through a large crossflow vortex. Near the shear layer the elevated cavity pressure is reduced to freestream. As the lower surface of the inboard fin is approached, the pressure increases to its maximum value. A nonsymmetrical flow develops in the fin-to-fin region with cylinder-inboard fin and cylinder-outboard fin flows being significantly different. The resulting pressure distribution in the fin regions will create a normal force which

pushes CFS away from the cavity, and a moment which pitches the nose of CFS towards the cavity. This undesirable separation attitude is typical in the case of shallow cavities (Refs. 1–3).

Time averaged surface pressure coefficients are plotted and compared with the wind tunnel data (Ref. 4) for various locations of the cavity (Fig. 16). The trends of the computed pressure coefficients agree with the data. It should be noted that these values vary with time for this unsteady flow. Therefore, the initial time and the elapsed time of the averaging process become variables both for the computations and the measurements. The computed values appear slightly higher than the data in Fig. 16. However, the agreement improved with longer elapsed times of averaging. Since the flow fluctuations were nonperiodic at supersonic speeds (Refs. 6–9), a true characteristic time for averaging was not evident.

The flow structure of Case 4 is shown through the instantaneous Mach number contours of the symmetry plane (Fig. 17). The internal flow is accelerated from the nose of CFS to the point where the shear layer impinges on the cylinder. Sonic speeds are achieved near the fin region with shear-layer and detached shock surface interaction just ahead of the vertical sting. The flowfield at the fin region is depicted by the instantaneous density contours of the crossflow plane (Fig. 18). The shear layer is deflected inward after a large vortex near the side plate. The density values are larger around the upper fin as compared to the lower fin.

Shown in Fig. 19 are the normalized pressure contours of the symmetry plane at two different instants of time. A comparative observation of these figures reveals the unsteady nature of the flowfield. Two shocks, with an expansion in between, are visible due to the upward deflection of the shear layer at two locations. The normalized pressure after the first shock is about 1.3 and that of the second shock is 2.1. At some instant later, the angle of the first shock is smaller and the second shock moves significantly in the streamwise direction. Although not shown here for brevity, observation of the flowfield plots at 20 different instants indicated nonperiodic cycles of shock motion above the shear layer. Finally, the time averaged pressure coefficients on various surfaces are shown in comparison with the experimental data (Fig. 20). Generally, the trends agree very well, yet discrepancies exist in the numerical values.

Case 5:

Since only a frozen instant of the store separation was considered, the flow was assumed steady. Therefore, computations were performed through the local-time stepping and the multigrid convergence acceleration (Refs. 12, 13). The solution was obtained by utilizing 3.5 hours of computer time.

Presented in Figs. 21–24 are the results for the flow past the ogive-nose-cylinder (ONC2) at 3.5 diameter (D) distance from the flat plate. The Mach number contours of the longitudinal plane of symmetry are shown in Fig. 21. The interaction of the cylinder forebody shock and the boundary layer on the flat plate is followed by the reflected recompression waves impinging on the cylinder aftbody. The influence of the reduced pressures in the region between the cylinder and the flat plate is observed as reduction of the C_p values on the flat plate (Fig. 22). They are slightly negative almost everywhere except in the region where the shock impinges. The interference of the flows is further demonstrated by the Mach number (Fig. 23) contours at a crossflow plane. The shock imparts a significant momentum on the fluid particles in normal and

spanwise directions. This can be observed through the skin friction patterns (limiting streamlines) on the flat plate (Fig. 24). The outline of the cylinder is superimposed in order to indicate the relative location of the streamlines. The flow along the longitudinal centerline experiences an adverse pressure gradient (Fig. 22) until the point of shock impingement. This pressure gradient causes sharp spanwise turns of the streamlines with the crossflow velocities increasing, followed by inboard-direction turns to recover the freestream direction. The convergence of the limiting streamlines indicates trends of localized crossflow separations.

CONCLUSIONS

A computational fluid dynamics code was developed to simulate the interference flows experienced during the carriage and separation of internally and externally carried stores. The code was applied to two different internal-carriage configurations and one external-carriage configuration. Due to the existence of the cavity in the case of internal-carriage, the flowfields were unsteady, and they were simulated through time-accurate computations. The flow about the external-carriage case, however, was considered steady. Favorable comparisons obtained between the computed results and the experimental data contributed to the validation of the computational code. The results of this study, particularly, the computational unsteady data and the computational flow visualization, should contribute to the database needed for the design and trade studies on the store carriage and separation.

REFERENCES

1. Stallings, R. L., Jr., "Store Separation from Cavities at Supersonic Speeds," J. Spacecraft and Rockets, Vol. 20, No. 2, pp. 129–132, March-April 1983.

2. Stallings, R. L., Jr., Wilcox, F. J., Jr., Forrest, D. K., "Measurements of Pressures, Forces and Moments on a Generic Store Separating From a Box Cavity at Supersonic Speeds," Proposed NASA-TP, January 1990.

3. Dix, R. E., Butler, C., "Cavity Aeroacoustics," Proceedings of Store Carriage, Integration and Release Conference, Bath, U.K., The Royal Aeronautical Society, April 1990.

4. Crosby, W. A., Carman, J. B., Hawkins, W. R., Simons, S. A., "Store Separation Tests at Supersonic Speeds from Internal Carriage Position of a Generic Weapons Bay," AEDC-TSR-88-V9, Arnold Engineering Development Center, TN, May 1988.

5. Stallings, R. L., Jr., "Aerodynamic Characteristics of a Sparrow III Missile Model in the Flow Field of a Generalized Parent Body at Mach 2.86," NASA-TM-85713, February 1984.

6. Baysal, O., Stallings, R. L., Jr., "Computational and Experimental Investigation of Cavity Flowfields," AIAA J., Vol.. 26, No. 1, pp. 6–8, January 1988.

7. Baysal, O., Srinivasan, S., Stalling, R. L., Jr., "Unsteady and Viscous Calculations of Supersonic Flows Past Deep and Shallow 3-D Cavities," AIAA Paper No. 88–0101, January 1988.

8. Srinivasan, S., Baysal, O., Plentovich, E. B., "Navier-Stokes Calculation of Transonic Flows Past open and Transitional Cavities," Advances and Applications in CFD (Ed.: O. Baysal), ASME Special Publications, Vol. FED-66, pp. 169–180, December 1988.

9. Baysal, O., Yen, G.-W., "Implicit and Explicit Computations of Flows Past Cavities With and Without Yaw," AIAA Paper No. 90–0049, January 1990.

10. Baysal, O., Fouladi, K., "Viscous Calculations of Supersonic Flows Past Cylinders at Angles of Attack," AIAA Paper No. 87–2414 CP, Proceedings of 5th AIAA Applied Aerodynamics Conference, pp. 338–347, August 1987.

11. Baysal, O., Srinivasan, S., "Calculation of Wall and Free Turbulent Shear Flows at Supersonic Speeds," Turbulent Flow Forum (Ed.: W. Bower), ASME Special Publications, Vol. FED-51, pp. 55–60, June 1987.

12. Baysal, O., Fouladi, K., Miller, D. S., "Computation of Supersonic Flows Over a Body at High Angles of Attack," AIAA J., Vol. 27, No. 4, pp. 427–437, April 1989.

13. Baysal, O., Fouladi, K., Lessard, V. R., "A Multigrid Method to Solve 3–D Viscous Equations on Overlapped and Embedded Grids," AIAA J., Vol. 29, No. 4, 10 pages, April 1991 (expected). Also, AIAA Paper No. 89–0464, January 1989,

14. Baysal, O., Stallings, R. L., Jr., Plentovich, E. B., "Navier-Stokes Solutions for Store Separation and Related Problems," Proceedings of NASA Computational Fluid Dynamics Conference, NASA-CP-10038, Vol. 1, pp. 385–410, March 1989.

15. Fouladi, K., Baysal, O., " Viscous Simulation Method for Unsteady Flows Past a Configuration with Nonsimilar Multicomponents," Recent Advances and Applications in CFD (Ed.: O. Baysal), ASME Winter Annual Meeting, November 1990.

16. Baysal, O., Fouladi, K., Leung, R. W., and Sheftic, J. S., "Computing Interference Flows Past a Cylinder-Fin-Sting Assembly In and Near a Cavity," AIAA Paper No. 90–3095 CP, Proceedings of 8th Applied Aerodynamics Conference, August 1990.

17. Proceedings of Workshops on Weapons Carriage and Separation, Second, Wright-Patterson AFB, OH, April 1988; Third, Naval Air Development Center, Warminster, PA, April 1989.

18. Proceedings of Eighth JOCG Aircraft/Stores Compatibility Symposium, Ft. Walton Beach, FL, October 1990.

19. Baldwin, B. S. and Lomax, H., "Thin-Layer Approximation and Algebraic Model for Separated Turbulent Flows," AIAA Paper 78–257, 1978.

20. Thomas, J. L., Taylor, S. L., Anderson, W. K., "Navier-Stokes Computations of Vortical Flows Over Low Aspect Ratio Wings," AIAA Paper No. 87–0207, January 1987.

21. Benek, J. A., Steger, J. L., and Dougherty, F. C., "A Flexible Grid Embedding Technique with Application," AIAA Paper No. 83–1944, 1983.

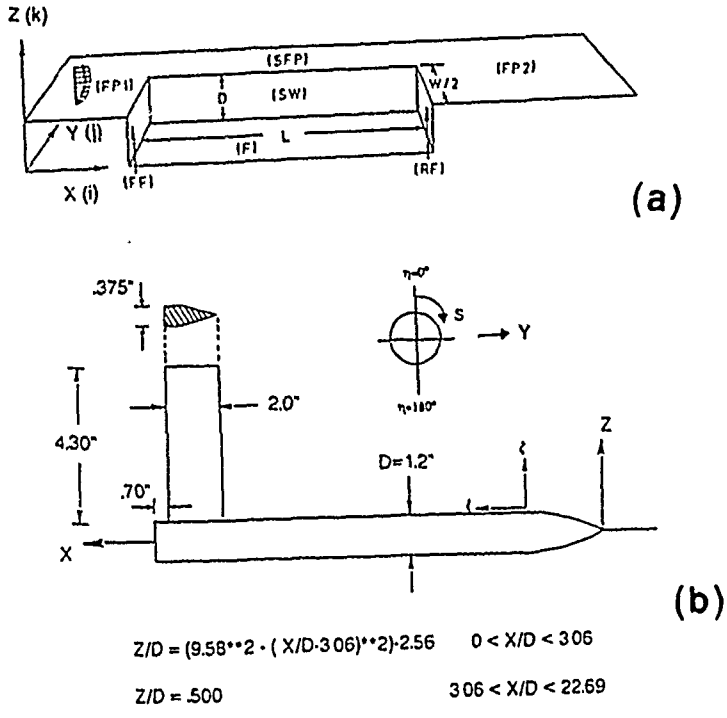

Fig. 1 Schematics of (a) rectangular cavity with L/D = 6.73, (b) ogive-nose-cylinder for Cases 1 and 2.

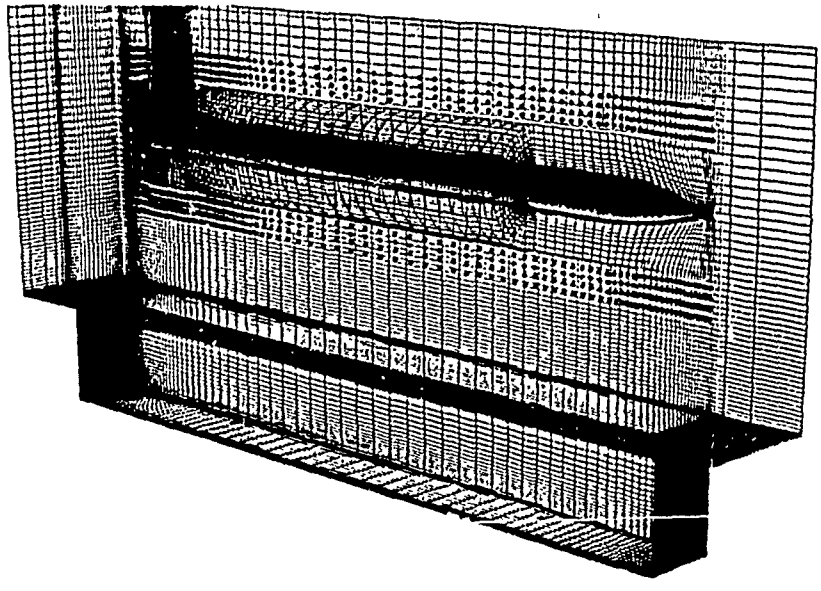

Fig. 2 Composite grid of ogive-nose-cylinder with sting near the cavity (Case 1).

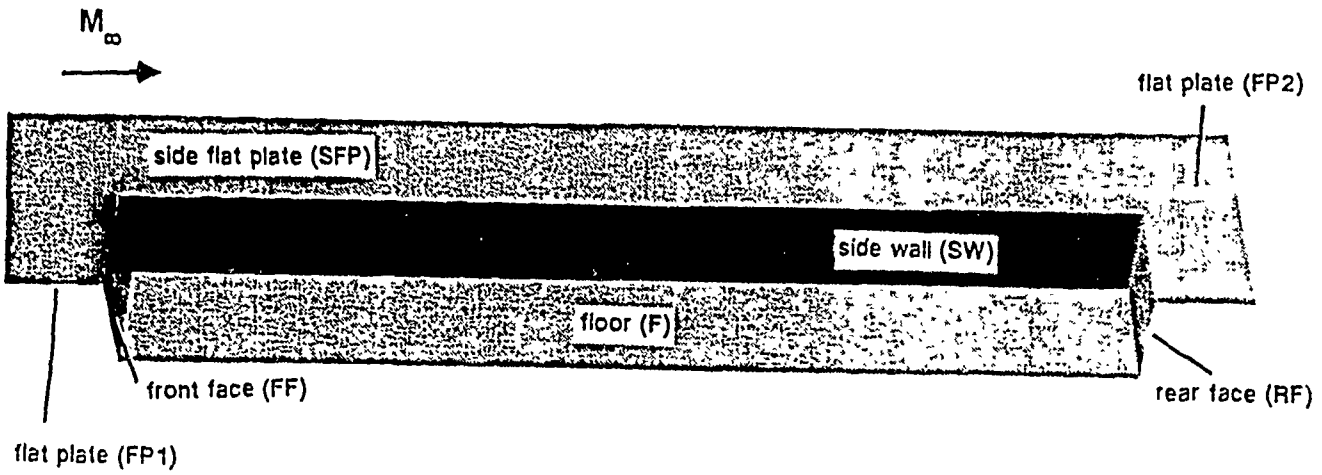

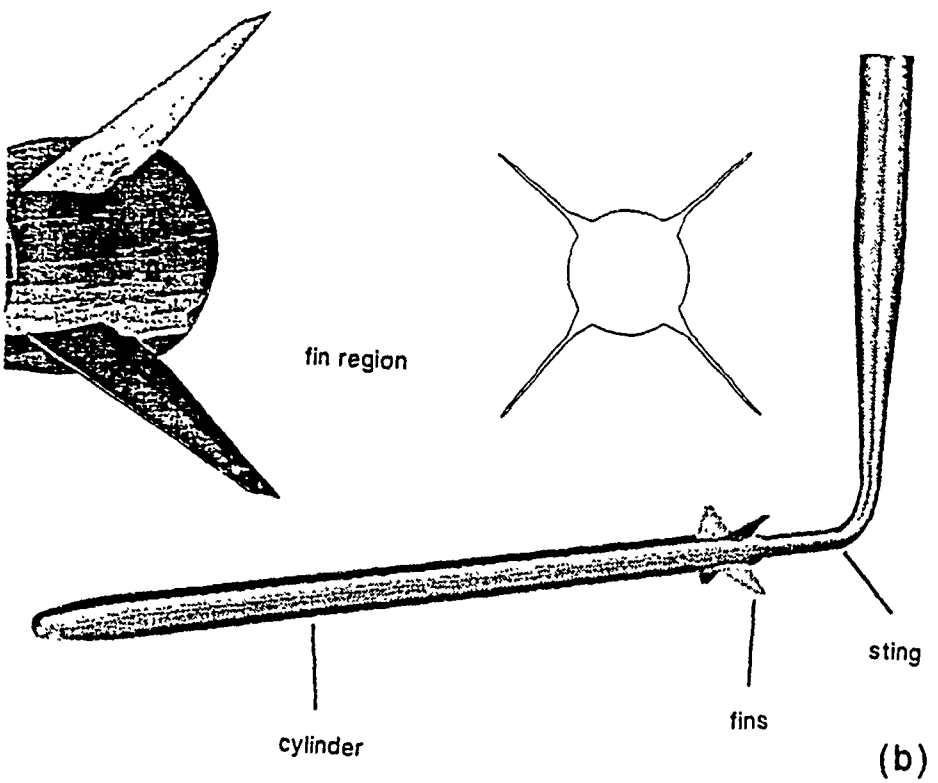

Fig. 3 Schematics of (a) the rectangular-box cavity with length-to-depth ratio of 9.0, (b) the cylinder-fin-sting (CFS) assembly with fin details, for Cases 3 and 4.

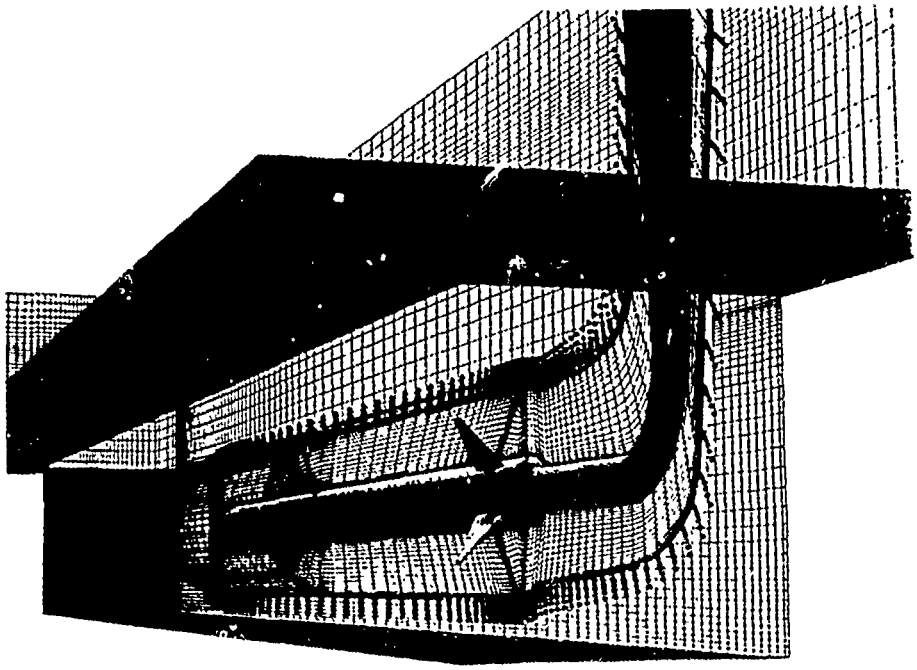

Fig. 4 Composite grid of CFS inside the cavity (Case 4).

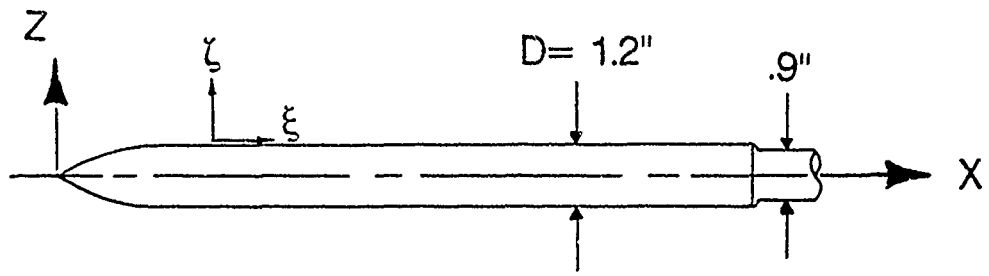

$$Z/D = \left(5.26^2-(X/D-2.25)^2\right)^{1/2}-4.76 \qquad 0.00 < X/D < 2.25$$

$$Z/D = .500 \qquad 2.25 < X/D < 18.00$$

Fig. 5 Schematic of the ogive-nose-cylinder for Case 5 (ONC2).

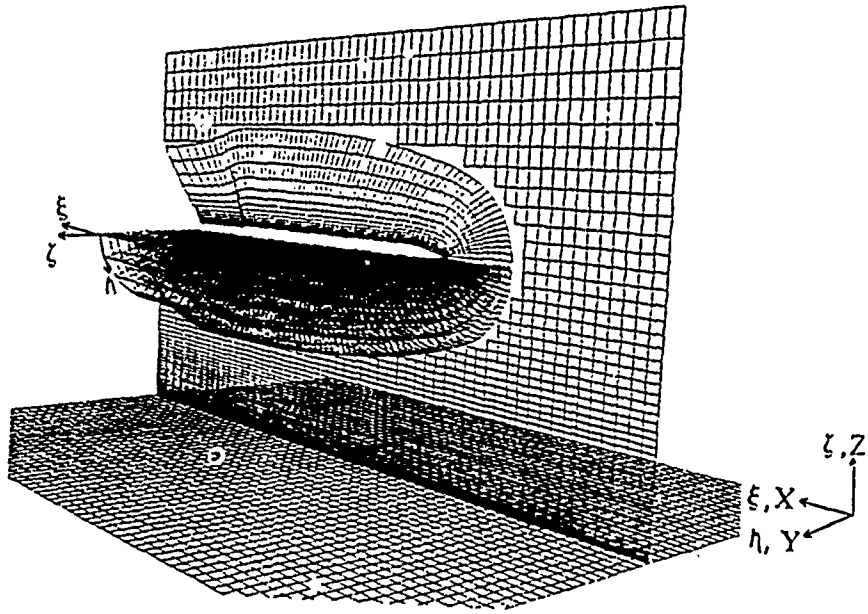

Fig. 6 Composite grid for the ogive-nose-cylinder (ONC2) in the proximity of a flat plate.

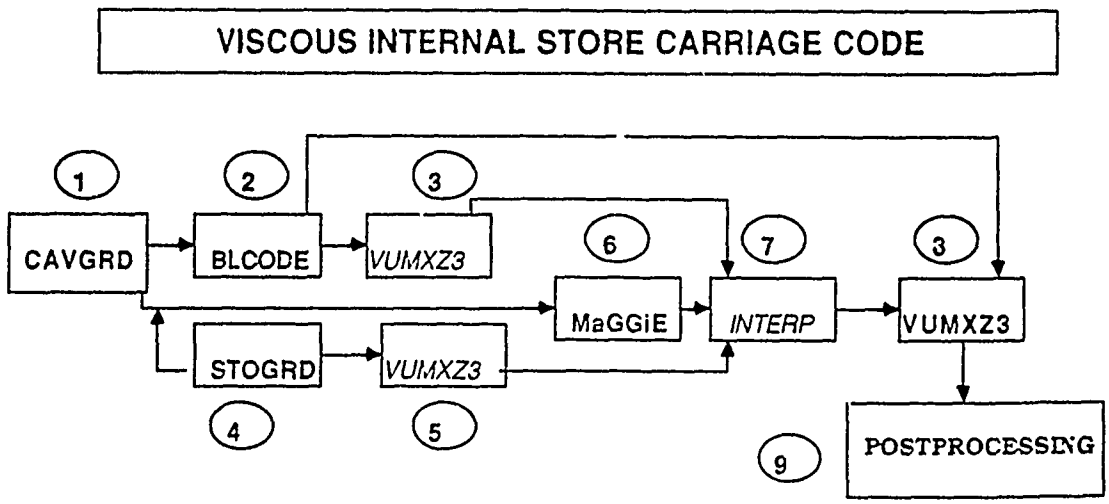

1 : GENERATE CAVITY GRID
2 :GENERATE BOUNDARY LAYER PROFILE
3 : SOLUTION FOR CLEAN CAVITY FLOW- optional
4 : GENERATE STORE GRID
5 : SOLUTION FOR FLOW PAST STORE IN FREESTREAM - optional
6 : GENERATE OVERLAPPED/ZONAL COMPOSITE GRID FROM 1 AND 4, CONNECTION DATA
7 :INTERPOLATE SOLUTIONS 3 AND 5 FOR ADVANCED INITIALIZATION TO COMPOSITE GRID 6 -optional
8 : SOLUTION FOR INTERFERENCE FLOW PAST STORE IN/NEAR CAVITY
9 : PLOTTING, PRINTING PACKAGES

Fig. 7 Block chart of viscous internal store carriage code (VISCC).

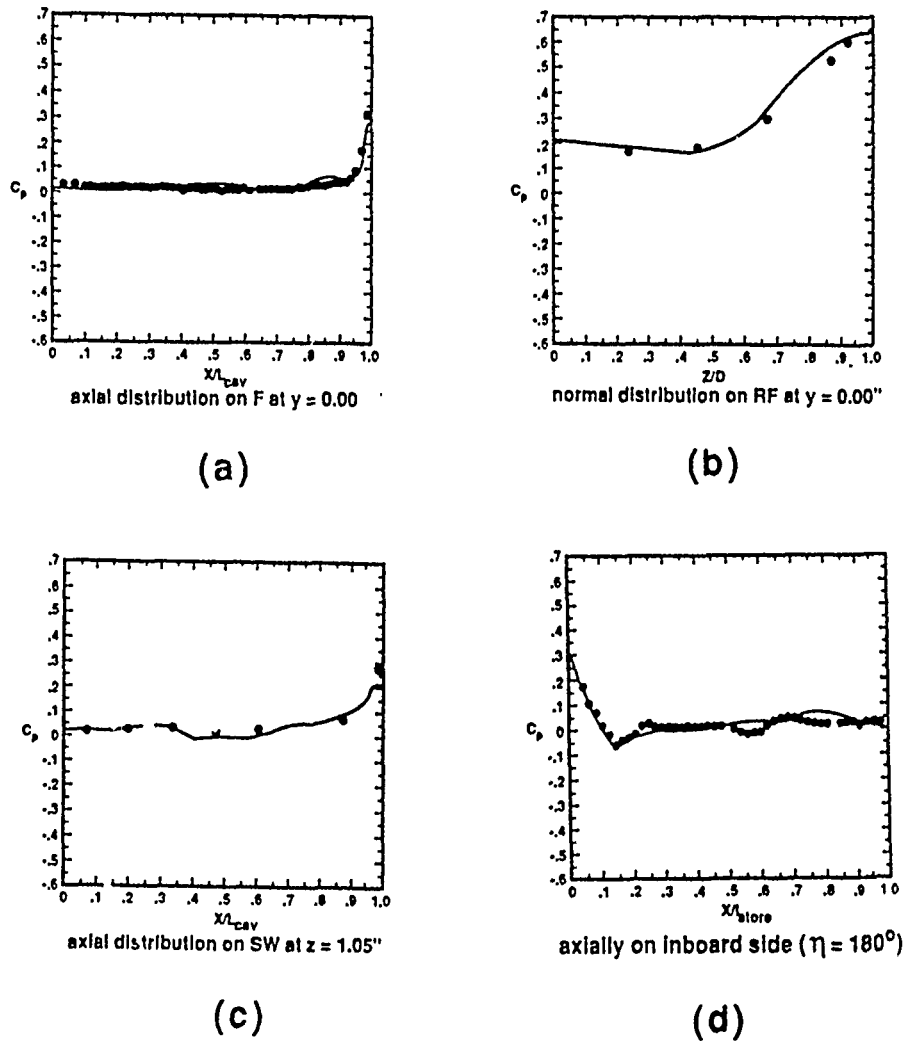

Fig. 8 Time averaged surface pressure coefficient distributions for Case 1.

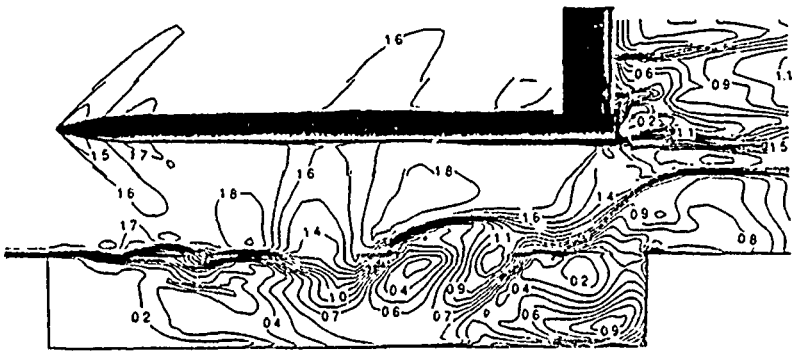

Fig. 9 Instantaneous Mach contours on the symmetry plane of Case 1.

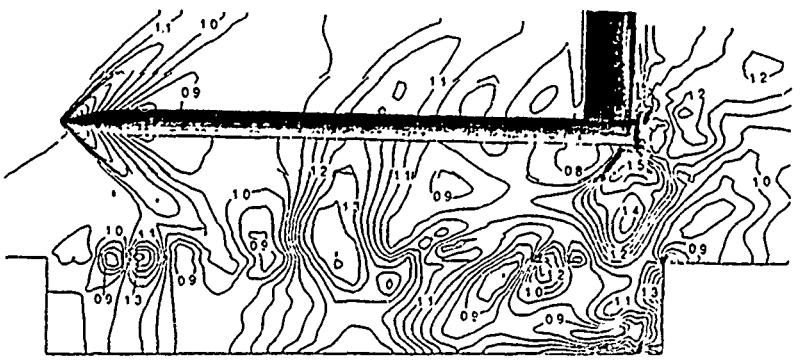

Fig. 10 Instantaneous normalized pressure contours on the symmetry plane of Case 1.

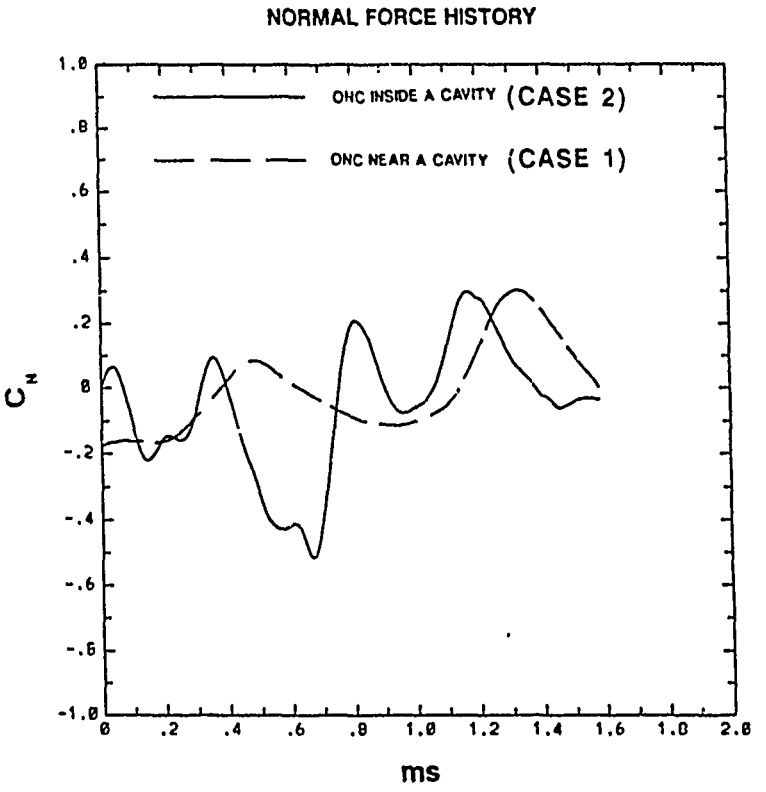

Fig. 11 Variation of C_N with time over a period of 1.59 ms for Case 1 and Case 2.

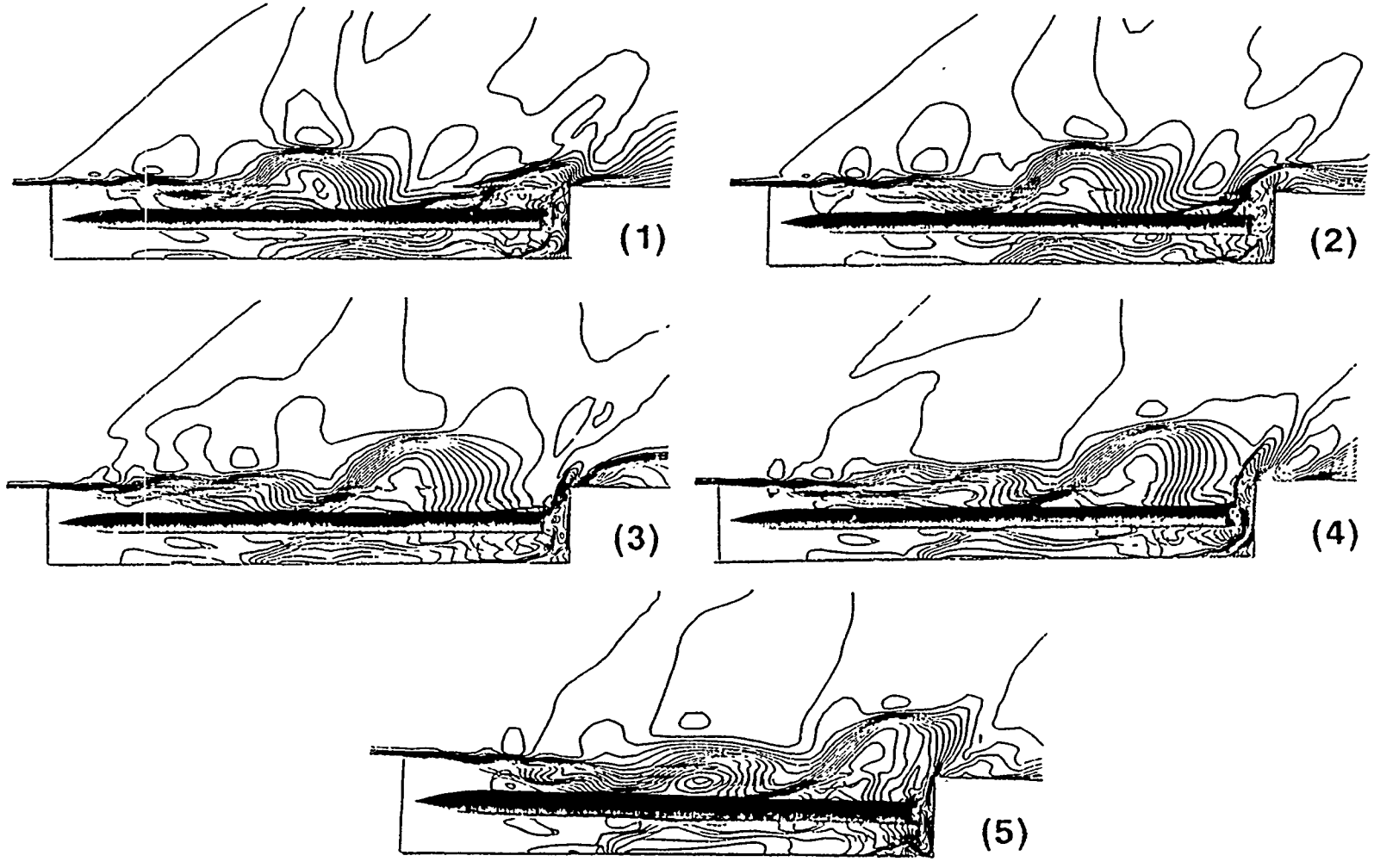

Fig. 12 Instantaneous Mach contours on symmetry plane of Case 2. Frame interval = 1/4 ms.

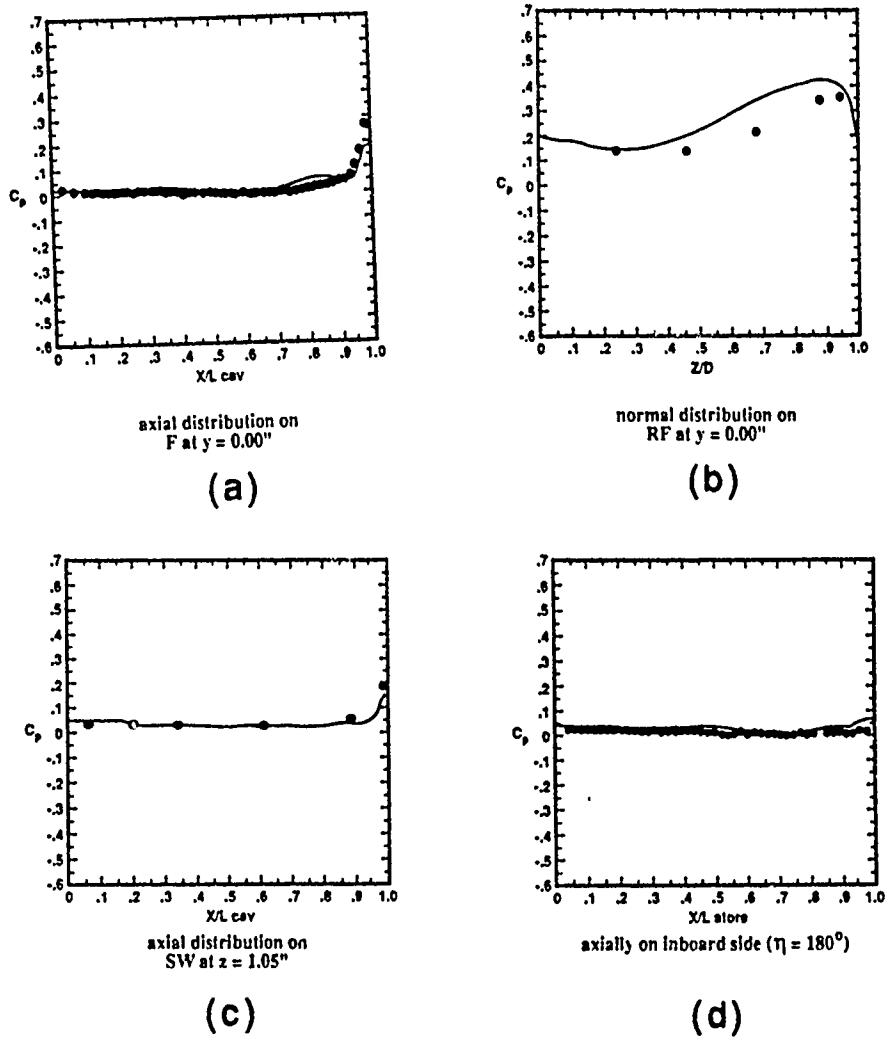

Fig. 13 Time averaged surface pressure coefficient distributions for Case 2.

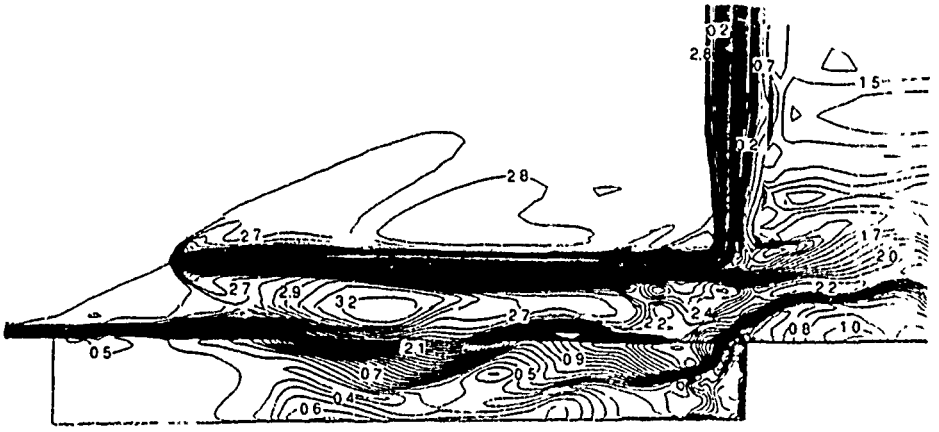

Fig. 14 Instantaneous Mach contours on the symmetry plane of Case 3.

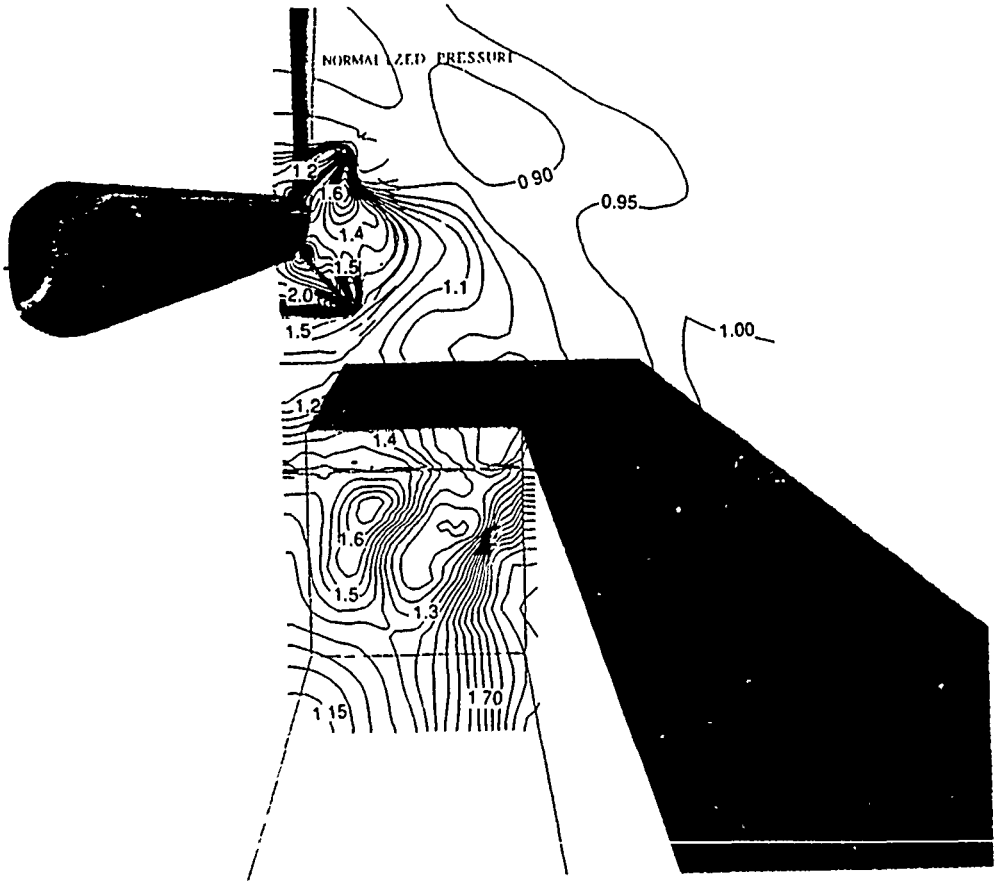

Fig. 15 Instantaneous and normalized pressure contours
at a spanwise cut in the fin region of CFS for Case 3.

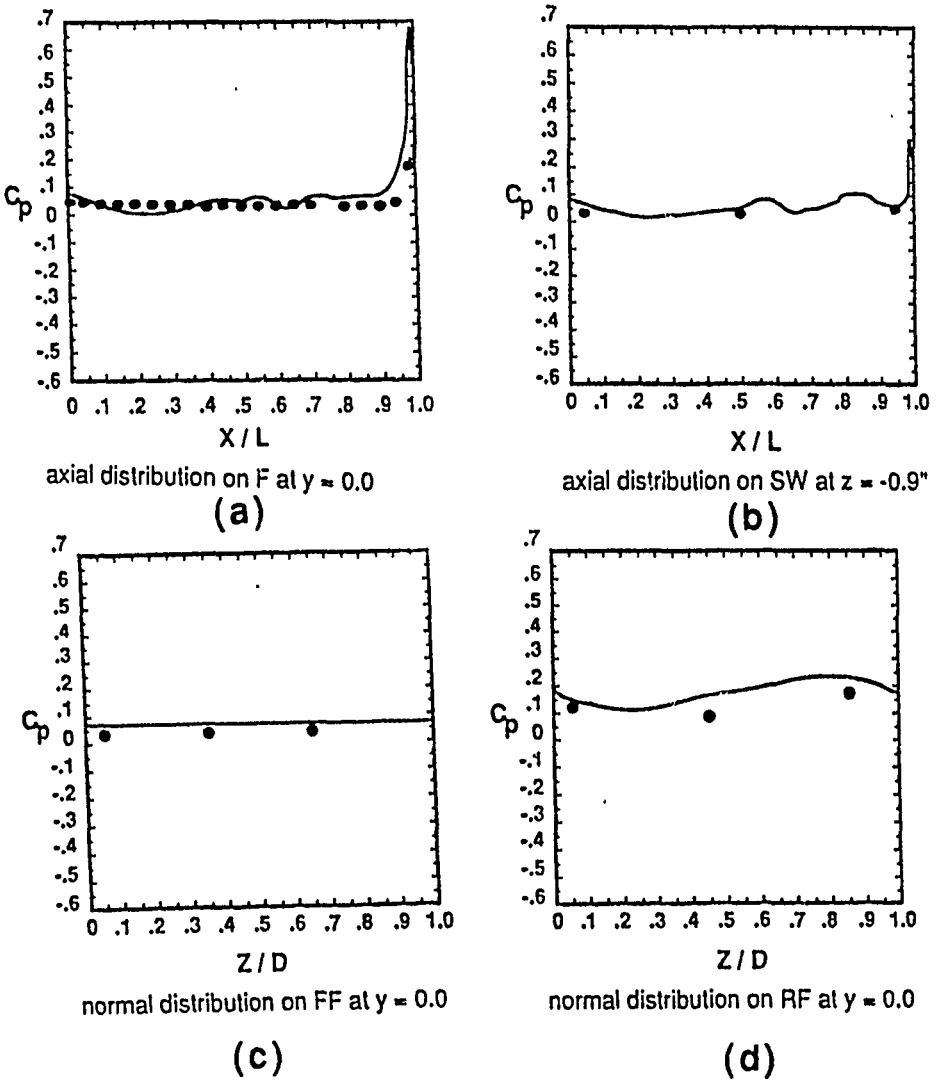

Fig. 16 Time averaged surface pressure coefficient distributions for Case 3.

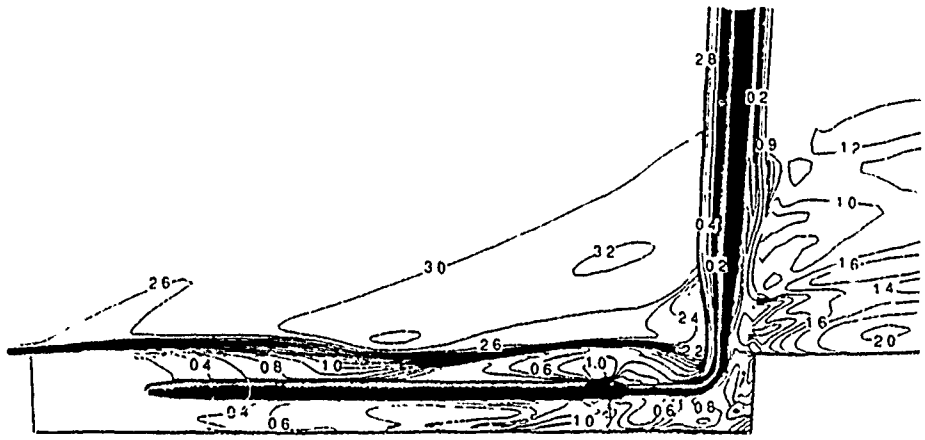

Fig. 17 Instantaneous Mach contours on the symmetry plane for Case 4.

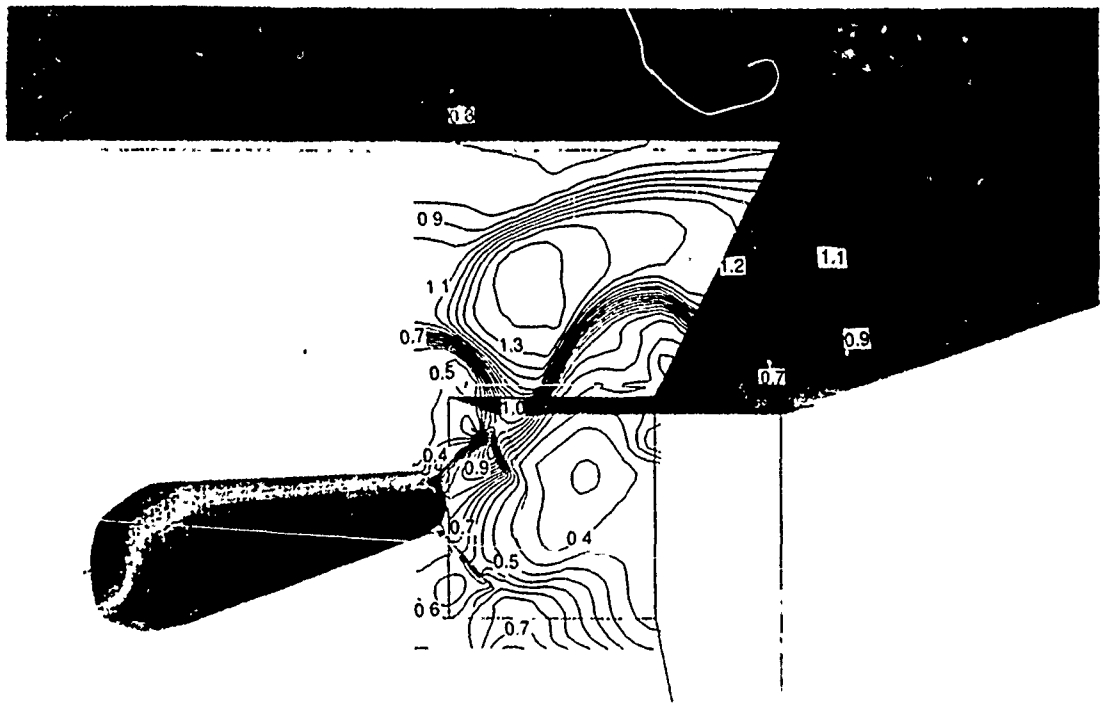

Fig. 18 Instantaneous and normalized density contours
at a spanwise cut in the fin region of CFS for Case 4.

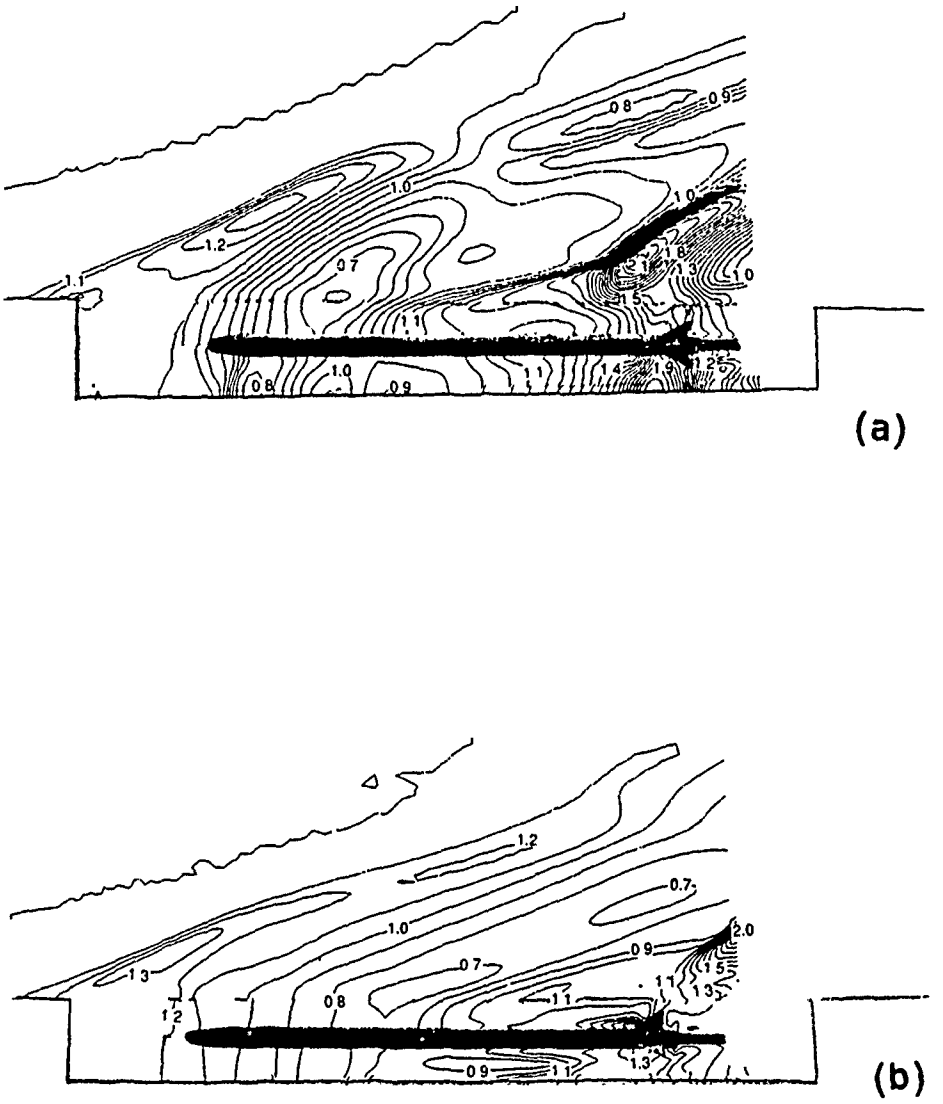

Fig. 19 Normalized pressure contours on the symmetry plane of Case 4 at two different instants.

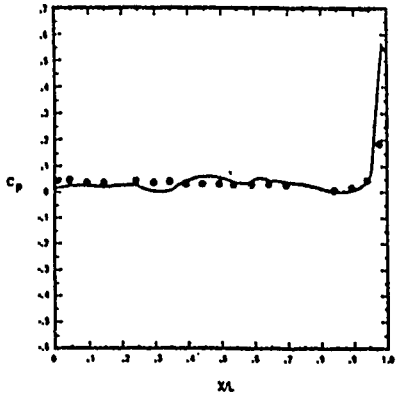

axial distribution on F at y = 0.0

(a)

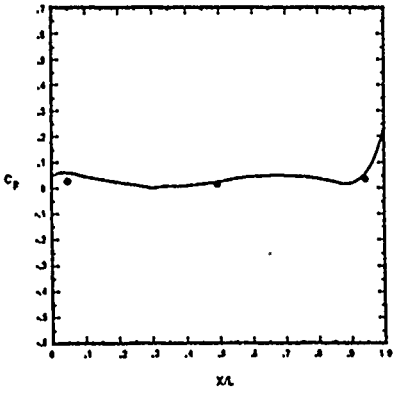

axial distribution on SW at z = -0.9"

(b)

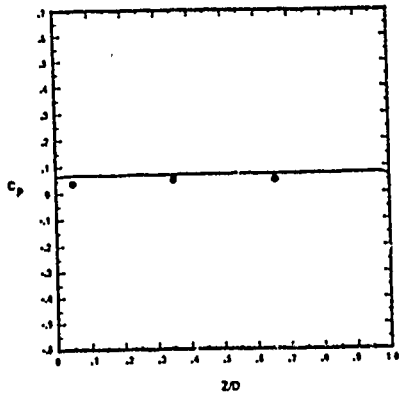

normal distribution on FF at y = 0.0

(c)

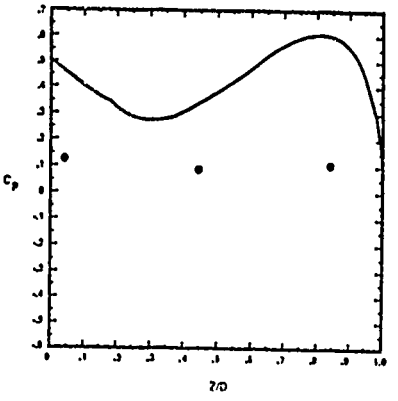

normal distribution on RF at y = 0.0

(d)

Fig. 20 Time averaged surface pressure coefficient distributions for Case 4.

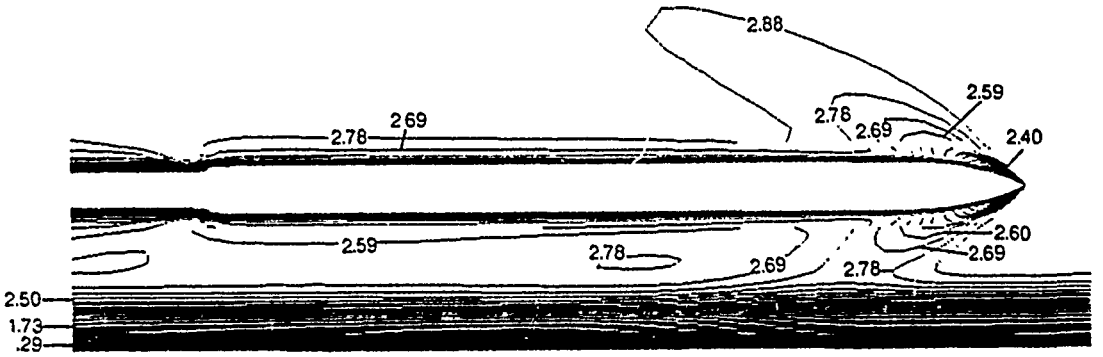

Fig. 21 Mach number contours on the symmetry plane of ONC2, which is at (3.5D) distance from the flat plate.

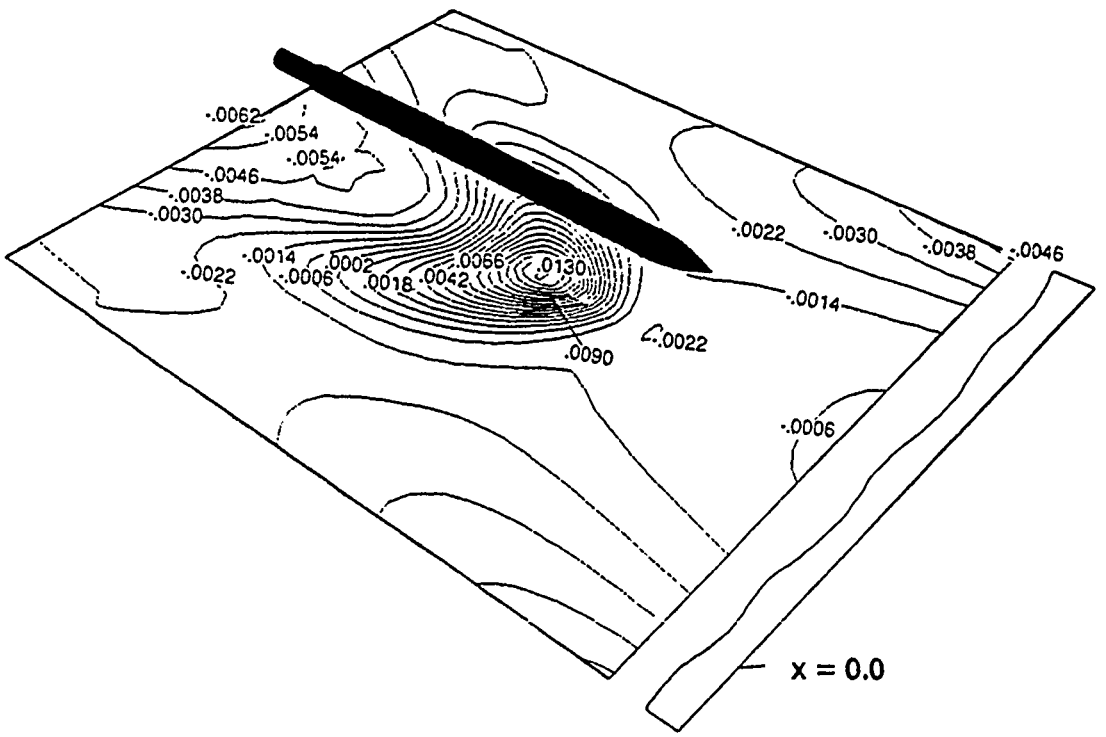

Fig. 22 Pressure coefficient contours on the surface of the flat plate with ONC2 at (3.5D) distance.

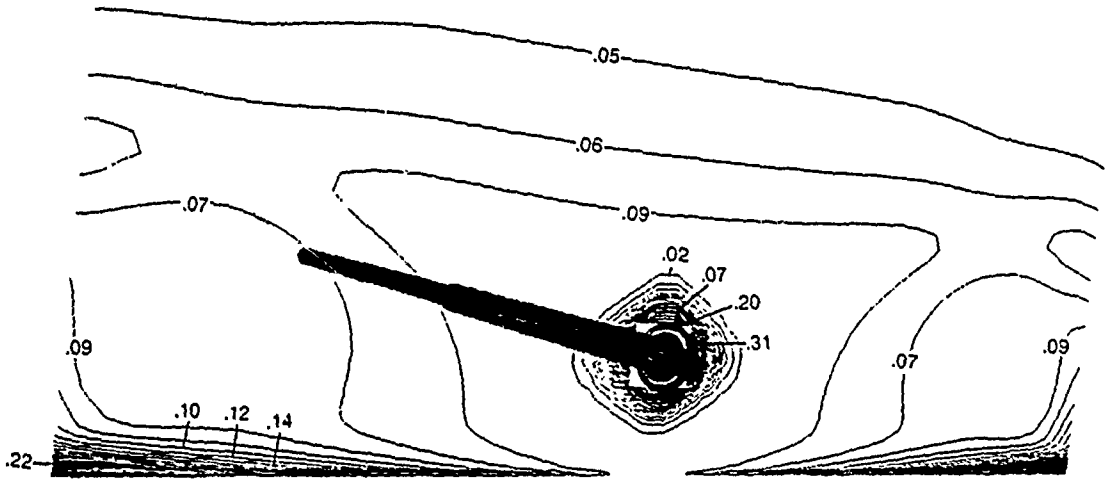

Fig. 23 Crossflow Mach number contours at forebody-cylinder junction of ONC2, which is at (3.5D) distance from the flat plate.

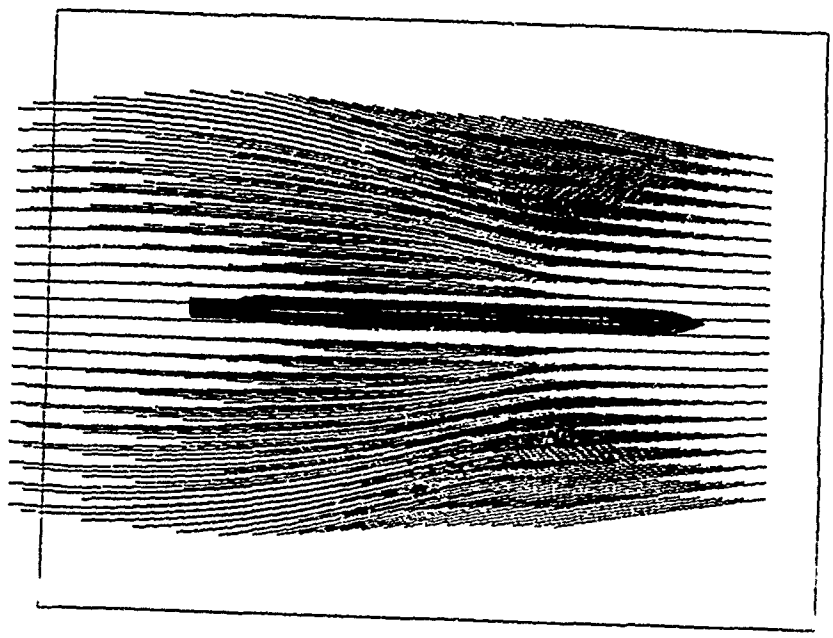

Fig. 24 Skin friction patterns on the flat plate surface with ONC2 at (3.5D) distance from the flat plate.

OVERSET GRID METHODS FOR AERODYNAMIC SIMULATION OF BODIES IN RELATIVE MOTION

Robert L. Meakin *
University of California
Department of Mechanical, Aeronautical,
and Materials Engineering
Davis, California 95616
U. S. A.

INTRODUCTION

Analysis of modern aircraft and launch vehicles often require accurate computation of aerodynamic flow fields about geometrically complicated regions. The present work adopts the point of view that geometric complexity can best be addressed computationally via overset grid (i.e., Chimera) techniques which decompose complex domains into a number of much simpler overlapping subdomains. This approach simplifies grid generation problems, since each component can be generated independently and grid boundaries are not required to match neighboring grids in any special way. Further, the approach facilitates the use of existing structured grid flow solvers which are highly vectorizable. Overset grid methods have been demonstrated for a wide variety of aerodynamic applications including, among many others, simulations about the integrated space shuttle vehicle for various ascent conditions [1], transonic computations about the entire F-15 aircraft with pylons and stores [2], simulation of the viscous flow about the F/A-18 at high angles of attack [3], and numerical studies of a delta wing planform with multiple jets in ground effects [4]. In addition, overset grid techniques represent a powerful tool for analyzing problems involving relative motion between vehicle components. Such applications have been carried out time-accurately in three-dimensions for the separation sequence of the Space Shuttle's solid rocket boosters [5] and aircraft store separation sequences [5,6]. The approach has also been successfuly applied to many non-aerodynamic problems ranging from applications in biomedical fluid mechanics [7] to environmental flow simulations [8].

Overset grid techniques allow each component of a given configuration to be gridded independently and overset onto a main grid to complete the discretization. Usually there is a major grid which is stretched over the entire field, and is often generated about a dominant boundary or surface. Minor grids are generated about remaining portions of the body. For example, a nine-grid discretization of the integrated space shuttle vehicle is represented in Figure 1, where the external tank is the major grid, and minor grids have been generated about the orbiter, solid rocket boosters (SRB), attach hardware, and the SRB and orbiter wakes. As can be seen from this example, minor grids may be used to resolve features of the geometry, such as details of the vehicle components, or features of the flow that are not adequately resolved by the major grid. In the case of moving body applications, all grids may move with six degrees of freedom relative to an inertial frame of reference. Accordingly, grid generation is not required during moving body problems.

An overset grid approach for moving body applications consists of three main func-

* Visiting Research Scientist and Lecturer

tional components; aerodynamics (ADF), body dynamics (BDF), and domain connectivity (DCF). The present paper presents the corresponding overset grid techniques which have been developed in support of a need to simulate a proposed space shuttle abort maneuver known as "fast sep", which called for an emergency separation of the orbiter from the rest of the launch vehicle during ascent. Most of the simulation results presented in the paper have been presented previously. However, the computational methods employed have been improved in terms of efficiency, general applicability, and accuracy. Accordingly, the most recent components of the overset grid techniques developed in support of the space shuttle are presented here.

THE COMPUTATIONAL METHOD

Aerodynamic Function (ADF)

The unsteady flow of a viscous, compressible, continuous fluid is governed by the Navier-Stokes equations. In the absence of any external body forces, and conditions which justify the "thin-layer" approximation, these equations can be nondimensionalized and written in a generalized coordinate system [9] as:

$$\partial_\tau \hat{Q} + \partial_\xi \hat{F} + \partial_\eta \hat{G} + \partial_\zeta \hat{H} = Re^{-1} \partial_\zeta \hat{S} \tag{1}$$

where the viscous terms in ζ have been collected into the vector $\hat{S}$, and

$$\hat{Q} = \begin{bmatrix} \rho \\ \rho u \\ \rho v \\ \rho w \\ e \end{bmatrix}, \quad \hat{E} = J^{-1} \begin{bmatrix} \rho U \\ \rho u U + \xi_x p \\ \rho v U + \xi_y p \\ \rho w U + \xi_z p \\ (e+p)U - \xi_t p \end{bmatrix}, \hat{F} = J^{-1} \begin{bmatrix} \rho V \\ \rho u V + \eta_x p \\ \rho v V + \eta_y p \\ \rho w V + \eta_z p \\ (e+p)V - \eta_t p \end{bmatrix},$$

and $\hat{G} = J^{-1} \begin{bmatrix} \rho W \\ \rho u W + \zeta_x p \\ \rho v W + \zeta_y p \\ \rho w W + \zeta_z p \\ (e+p)W - \zeta_t p \end{bmatrix}.$

The dependent variables represented by the Q array are defined with respect to an inertial reference frame (viz., a space-fixed Cartesian coordinate system). However, the independent variables have been transformed into a general curvilinear coordinate system that is body conforming in both space and time. Since the dependent variables are left in terms of an inertial frame of reference, apparent body forces due to rigid-body motion do not exist. This is not true for formulations which transform both the independent and dependent variables to the body conforming reference frame.

The variables u, v, and w are the Cartesian components of velocity. U, V, and W are the contravariant components of velocity, and are defined as

$$U = \xi_t + \xi_x u + \xi_y v + \xi_z w, \quad V = \eta_t + \eta_x u + \eta_y v + \eta_z w, \quad W = \zeta_t + \zeta_x u + \zeta_y v + \zeta_z w.$$

An implicit approximately factored algorithm for solving the thin-layer Navier-Stokes equations is used here. The algorithm requires the ζ direction to be oriented normal to body surfaces in order to resolve the boundary layer. It uses central differencing in the η and ζ directions and upwinding in ξ. The algorithm is formally presented in reference [10], however, for completeness, a brief description is presented here. The numerical analog of equation (1) can be written as

$$\left[I + i_b h \delta_\xi^b (\hat{A}^+)^n + i_b h \delta_\zeta \hat{C}^n - i_b h Re^{-1} \bar{\delta}_\zeta J^{-1} \hat{M}^n J - i_b D_i|_\zeta\right]$$
$$\times \left[I + i_b h \delta_\xi^f (\hat{A}^-)^n + i_b h \delta_\eta \hat{B}^n - i_b D_i|_\eta\right] \Delta\hat{Q}^n \qquad (2)$$
$$= -i_b \Delta t \{\delta_\xi^b (\hat{F}^+)^n + \delta_\xi^f (\hat{F}^-)^n + \delta_\eta \hat{G}^n + \delta_\zeta \hat{H}^n - Re^{-1} \bar{\delta}_\zeta \hat{S}^n\} - i_b (D_e|_\eta + D_e|_\zeta) \hat{Q}^n$$

where $h = \Delta t$ or $(\Delta t)/2$ for first or second order time accuracy. Here, δ is a three-point second order accurate central difference operator, and $\bar{\delta}$ is a midpoint operator used with the viscous terms. The flux F is eigensplit to facilitate use of the backward and forward spatial difference operators δ_ξ^b and δ_ξ^f. The flux differences themselves are midpoint differenced and backward or forward weights of the split fluxes are used in the manner of Thomas, et al. [11]. The matrices $\hat{A}, \hat{B}, \hat{C}$, and $\hat{M}$ result from local linearization of the fluxes about the previous time level. D_e and D_i are dissipation operators, and are used in the central space differencing directions. Presently, turbulence modeling is accomplished via the algebraic turbulence model of Baldwin and Lomax [12].

"Intergrid boundary points", or IGBPs, is a termonology that is used frequently throughout the balance of this paper. It refers specifically to the set of points which define "hole boundaries" and minor grid outer boundaries. "Holes" can exist in overset grid systems (examples are illustrated in Figures 1b, 2a, and 2b) and boundary conditions for the grid points which make up the corresponding boundaries must be interpolated from the solution field of a neighboring grid, just as for minor grid outer boundary points. Values for the i_b array and the interpolation coefficients needed to update the IGBPs are provided by the Domain Connectivity Function (DCF, to be discussed shortly). In the present work, problems involving multiple bodies in relative motion are of primary interest. The location of hole and intergrid boundaries are time dependent for such problems. Accordingly, the i_b array and required interpolation coefficients are also a function of time. Herein lies the close interdependence of the method's three functional parts for moving body problems. The AeroDynamics Function (ADF) depends on the DCF to supply hole and interpolation information. The DCF in turn, depends on the Body Dynamics Function (BDF) to supply the location and orientation of all moving bodies relative to the primary body, or set of bodies. Completing the cycle, the BDF depends on the ADF to provide aerodynamic loads and moments on the moving bodies, in order to perform its function.

Body Dynamics Function (BDF)

The thin-layer Navier-Stokes algorithm described above provides time dependent aerodynamic fields about multiple body configurations. Of course, the resulting aerodynamic loadings on the vehicles are derivable from this information and can be represented as instantaneous integral forces and moments applied at the center of mass for each body. Specifically, the loads for each body are determined as

$$\begin{aligned} F_x &= \int_s (\tau_{xx} - p + \tau_{xy} + \tau_{xz}) \cdot dA_x, & M_x &= \int_s [(y - y_o) dF_z - (z - z_o) dF_y], \\ F_y &= \int_s (\tau_{yx} + \tau_{yy} - p + \tau_{yz}) \cdot dA_y, & M_y &= \int_s [(z - z_o) dF_x - (x - x_o) dF_z], \\ F_z &= \int_s (\tau_{zx} + \tau_{zy} + \tau_{zz} - p) \cdot dA_z, & M_z &= \int_s [(x - x_o) dF_y - (y - y_o) dF_x]. \end{aligned} \qquad (3)$$

where the surface of integration is that of the body; x_o, y_o, z_o are coordinates of the body center of mass; τ_{ij} the ij components of the viscous stress tensor; and p the pressure; all defined relative to the inertial frame of reference adopted in the flow solver. It should be noted that the thin-layer and full Navier-Stokes viscous stress tensors are identical at a surface where the no-slip condition applies.

The present approach allows the trajectory of body components to either be prescribed, or allowed to respond to aerodynamic and applied loads (i.e., any load which can be

represented as a force and moment combination acting at the body center of mass). Applied loads may be, for example, vehicle weight, effects of separation motors, wind gusts, etc. In the present work, all applied loads are defined relative to the inertial frame of reference used by the flow solver, and are combined with the computed aerodynamic loads to form resultant F_x, F_y, F_z, M_x, M_y, and M_z values which act on the body.

The general motion of a rigid body is a combination of translation and rotation. The Newtonian linear momentum principle leads directly to relations which describe the translatory motion of the body mass center as it is acted upon by F_x, F_y, and F_z. Likewise, the angular momentum principle leads to relations which describe the angular motion of the body. The most convenient set of equations which describe the rotational motion of a rigid body about a fixed point can be defined if the frame of reference is fixed to the body and aligned with its principle axes.

$$\begin{aligned} M_1 &= I_1\dot{\omega_1} - (I_2 - I_3)\omega_2\omega_3, \\ M_2 &= I_2\dot{\omega_2} - (I_3 - I_1)\omega_3\omega_1, \\ M_3 &= I_3\dot{\omega_3} - (I_1 - I_2)\omega_1\omega_2. \end{aligned} \tag{4}$$

The above equations are known as Euler's equations for rigid body motion. The dependent variables of the equation set are ω_1, ω_2, and ω_3, which are the angular velocities about the body principle axes. M_1, M_2, and M_3 are the moments acting on the body relative to its principle axes, and are related to M_x, M_y, and M_z via the transformation relations:

$$\begin{aligned} M_1 &= c_{11}M_x + c_{12}M_y + c_{13}M_z, \\ M_2 &= c_{21}M_x + c_{22}M_y + c_{23}M_z, \\ M_3 &= c_{31}M_x + c_{32}M_y + c_{33}M_z. \end{aligned} \tag{5}$$

Finally, I_1, I_2, and I_3 are the principle moments of inertia. In the present work, the instantaneous moments acting on a body are assumed constant over Δt, and equation set (4) is integrated from time-level n to $n+1$ using the trapezoidal rule. With the body angular velocities now defined for the $n+1$ time level, the new body orientation can be determined. However, the angular velocities must be transformed back to the inertial reference frame via

$$\begin{aligned} \omega_x &= c_{11}\omega_1 + c_{21}\omega_2 + c_{31}\omega_3, \\ \omega_y &= c_{12}\omega_1 + c_{22}\omega_2 + c_{32}\omega_3, \\ \omega_z &= c_{13}\omega_1 + c_{23}\omega_2 + c_{33}\omega_3. \end{aligned} \tag{6}$$

The directional cosine tensor components, c_{ij} and c_{ji} facilitate transformation from the inertial to body frames, and from the body to inertial frames, respectively. The directional cosine tensor components can be defined in terms of the Euler vector $\vec{\epsilon}$ as

$$\begin{aligned} c_{11} &= 2(\epsilon_1\epsilon_1 + \epsilon_4\epsilon_4) - 1, & c_{21} &= 2(\epsilon_2\epsilon_1 + \epsilon_3\epsilon_4), & c_{31} &= 2(\epsilon_3\epsilon_1 - \epsilon_2\epsilon_4), \\ c_{12} &= 2(\epsilon_1\epsilon_2 - \epsilon_3\epsilon_4), & c_{22} &= 2(\epsilon_2\epsilon_2 + \epsilon_4\epsilon_4) - 1, & c_{32} &= 2(\epsilon_3\epsilon_2 + \epsilon_1\epsilon_4), \\ c_{13} &= 2(\epsilon_1\epsilon_3 + \epsilon_2\epsilon_4), & c_{23} &= 2(\epsilon_2\epsilon_3 - \epsilon_1\epsilon_4), & c_{33} &= 2(\epsilon_3\epsilon_3 + \epsilon_4\epsilon_4) - 1 \end{aligned} \tag{7}$$

where ϵ_1, ϵ_2, ϵ_3, ar . ϵ_4, are the components of $\vec{\epsilon}$ and are known as the Euler parameters. Any change in the relative orientation between a moving body and the inertial reference frame can be defined as a simple rotation of angle θ about an axis whose direction is defined by the unit vector $\vec{\lambda}$. The Euler parameters can be defined in terms of $\vec{\lambda}$ and θ as

$$\epsilon_1 = \lambda_1 sin(\tfrac{\theta}{2}), \quad \epsilon_2 = \lambda_2 sin(\tfrac{\theta}{2}), \quad \epsilon_3 = \lambda_3 sin(\tfrac{\theta}{2}), \quad \epsilon_4 = cos(\tfrac{\theta}{2}) \tag{8}$$

with the constraint relation

$$\epsilon_1^2 + \epsilon_2^2 + \epsilon_3^2 + \epsilon_4^2 = 1. \tag{9}$$

As a body moves, $\vec{\epsilon}$ must be consistently updated to facilitate transformation of vector quantities between the inertial and body fixed frames of reference. Accordingly, relations between $\vec{\epsilon}$ and angular motion of the body are required. The needed relationship is expressed as follows:

$$\begin{bmatrix} \dot{\epsilon}_1 \\ \dot{\epsilon}_2 \\ \dot{\epsilon}_3 \\ \dot{\epsilon}_4 \end{bmatrix} = \frac{1}{2} \begin{bmatrix} +\epsilon_4 & -\epsilon_3 & +\epsilon_2 & +\epsilon_1 \\ +\epsilon_3 & +\epsilon_4 & -\epsilon_1 & +\epsilon_2 \\ -\epsilon_2 & +\epsilon_1 & +\epsilon_4 & +\epsilon_3 \\ -\epsilon_1 & -\epsilon_2 & -\epsilon_3 & +\epsilon_4 \end{bmatrix} \begin{bmatrix} \omega_x \\ \omega_y \\ \omega_z \\ 0 \end{bmatrix}. \tag{10}$$

Since the angular velocities (ω_x, ω_y, and ω_z) are known at time level $n+1$ from the solution of equation set (4), equation (10) can be integrated over time Δt for the Euler parameters at $n+1$. In the present work, the constraint relation given by equation (9) is enforced in a least squares sense using a generalized inverse. However, given the time step sizes required to suitably resolve the transient processes in moving body problems, the constraint relation is usually satisfied. Accordingly, the least squares enforcement of equation (9) is not applied unless $\vec{\epsilon}^{n+1}$ lies outside a prescribed tolerance of the constraint.

A body dynamics code based on the above relations provides the $n+1$ Euler parameters and inertial frame center of mass coordinates for moving bodies. This information is sufficient to position and orient corresponding grid systems at their $n+1$ locations.

Domain Connectivity Function (DCF)

The price that must be paid for the geometric and computational freedoms provided by an overset grid approach lies in the need to provide free transfer of information between the various grid components. Again, intergrid boundaries are the outer boundaries of minor grids, and the boundaries around holes created by overset portions of bodies defined in a neighboring grid. Of course, the IGBPs (intergrid boundary points) are dependent upon solutions in the overlap region of neighboring grid systems. For example, the dependent flow variables for the hole boundaries in the external tank grid shown in Figure 1b must be interpolated from the overlap region of neighboring grid systems, possibly from the orbiter and SRB solution domains. Hence, a generalized procedure for identifying IGBPs and suitable donors for the required interpolations is needed. Various algorithms can be devised for performing this task automatically (e.g., PEGASUS [13] and CMPGRD [14]). For static grid cases, existing algorithms for performing this intergrid communication function may be sufficient. However, for moving body problems, such as for aircraft store separation and trajectory applications, staging sequences of launch vehicles, and others, it is essential that this function be very efficient since it is required with each grid movement. As interactive grid generation becomes increasingly common, the incentive to carry out interactive domain connectivity will also increase. Hence, the efficiency of current methods for performing this function must continue to improve.

The PEGASUS code has been modified and employed for aircraft store separation and the space shuttle SRB separation problems [5,15], and was also used in the tilting disk heart valve calculations of Kiris and Chang [7]. However, this algorithm represents a computational expense that is of the same order as the flow solver for aerodynamic applications [5]. In the present section, an entirely new approach to the domain connectivity problem is outlined (a complete description of the method is in preparation). It is hoped that this new approach will provide at least an order of magnitude reduction in expense for this function without loss of generality.

In general, each component grid in an overset grid approach represents a curvilinear coordinate system of points. However, the position of all points, regardless of component, are defined relative to an inertial frame of reference. Though the respective mappings

between physical and computational space are relatively simple, they still pose a problem when it comes to facilitating domain connectivity. The problem is that the computational space of each component grid is completely arbitrary. The ξ, η, ζ coordinates of a point in one grid, for example, are not related to the ξ, η, ζ coordinate system in any other component grid. This makes it difficult to identify suitable donor elements for the interpolation requirements of the IGBPs. Search methods can be employed for this purpose, but are computationally expensive and often are not easily vectorizable.

The present method employs non-search techniques to satisfy all interpolation requirements, and a highly efficient method of IGBP identification. The method contains 4 basic steps which include problem set-up, inverse mapping of key subsets of the several computational spaces, IGBP identification, and determination of IGBP donors and interpolation information.

Problem Set-Up

The "set-up" aspects of the new method require certain basic pieces of information to establish the problem. First, the ξ, η, ζ space of each grid component must be defined with respect to an inertial frame of reference. Usually, each grid component is associated with a vehicle component, such as the orbiter or external tank in the case of the space shuttle. It is convenient to define a body center of mass and Euler parameters for each grid component. However, these values are only significant for grid components associated with a moving body. In moving body problems, the corresponding body mass centers and Euler parameters (defined by equation (8)) are used to achieve proper spatial and rotational orientation of the several body components and associated grids. Hence, the center of mass that should be specified for each grid component is that of the body to which it is associated. For grids which never move from their initial mated positions, including fixed grids used to resolve flow features, the center of mass specified is not relevant. Accordingly, any grid component associated with a fixed body, or flow region, should have the Euler parameters specified as $\vec{\epsilon} = [0, 0, 0, 1]^T$.

Inverse Maps

In order to realize the computational gains hoped for in providing domain connectivity, it is necessary to be able to freely convert from inertial frame coordinates (x, y, z) to the computational space coordinates (ξ,η,ζ) of any component grid. Such a conversion facility, eliminates the need for costly search algorithms. The present method proposes the use of inverse mappings between the independent computational spaces of the component grids and a corresponding number of uniform Cartesian grids. Therefore, if suitable inverse maps can be created at a computational expense less than that required for the more traditional search methods, the present idea is valuable for fixed grid applications. In any case, however, the idea holds a great deal of promise for moving body problems, since the inverse maps need only be created once for any given grid component. Hence, moving body problems can be carried out with practically no searches, and with no cost for the inverse maps.

There are probably several ways the idea of inverse mappings could be implemented into a domain connectivity algorithm. In the present implementation, there are three slightly different contexts in which the inverse maps are used. First, an inverse map of the major grid computational space must be established. However, it is not necessary to map the entire major grid. The major grid inverse map only needs to extend over that portion of the domain where IGBP information is going to be exchanged. In fact, a number of inverse maps of the major grid can be created, each mapping different portions of the major grid domain in which connectivity may be needed. For example, a simplified space shuttle grid

system is illustrated in Figure 2. The example considers a three component discretization of the external tank (major grid), and the upper and lower (as depicted in the figure) solid rocket boosters. Figure 3a identifies the extent of the major grid inverse maps, which anticipate the limits of interest of an SRB trajectory during separation. The second type of inverse maps are those associated with minor grid components. The entire domain of each minor grid must be mapped (see Figure 3b).

Provided the grid components are rigid, the inverse maps are always valid, even for moving body problems. For example, consider an SRB separation sequence as suggested in Figure 4. Given inertial frame coordinates (x,y,z) which at any instant lie within the domain of an SRB grid, for example, the corresponding computational space coordinate (ξ, η, ζ) can be found immediately by "searching" the corresponding SRB inverse map. "Searching" an inverse map is a trivial operation.

With the approach taken in the present method, the preceding two types of inverse maps are sufficient to provide all domain connectivity requirements. However, it is easy to imagine that a uniform Cartesian distribution of grid points may not accurately resolve the variations in ξ, η, ζ for a number of situations. For example, if the ζ coordinate corresponds to grid lines normal to a body component, it is unlikely that a practically sized uniform Cartesian grid could resolve the variation in ζ for the boundary layer portion of a viscous grid. However, even a coarse uniform Cartesian system of points can be used to create an inverse mapping which will define the limits of ξ, η, ζ variation for a given component grid. Such is the premise of this new method. The inverse maps are used to identify, within a very narrow range, the ξ, η, ζ coordinates of donor elements for inter-grid boundary points. At best, the inverse maps identify the correct donors directly, which is usually the case. At worst, they identify a "neighborhood of points" for each IGBP wherein the correct donor element resides. A search of the neighborhood, then, will reveal the correct donor. The motive of the third and final context in which inverse maps are used in this method is to minimize neighborhood sizes in regions where the major and minor grid inverse maps do not sufficiently resolve ξ, η, ζ.

The present method allows for the creation of auxiliary inverse maps. Auxiliary inverse maps are not always required. However, for viscous grids, or grids which have rapid variation in ξ, η, ζ, perhaps to resolve details of a flow, such as a shock, auxiliary inverse maps may significantly reduce the computer time required to satisfy domain connectivity requirements. Any number of auxiliary inverse maps can be created for any of the component grids.

An example of where an auxiliary inverse map may prove useful is shown in Figure 5. The figure is a close-up of the gap between the external tank and the lower solid-rocket booster. The external tank grid is shown in the right-hand portion of Figure 5a, and the uniform Cartesian grid of the lower SRB inverse map is shown in the left-hand portion. The spacing of the external tank's inverse map grid is roughly the same as that shown for the lower SRB. Neither inverse map, however, resolves its respective ξ, η, ζ space. In this case it is possible that the present method would identify the entire grid as the neighborhood of the correct donor for a point within the gap. Fortunately, a very modestly sized auxiliary inverse map covering the gap (as in Figure 5b) would provide sufficient resolution of this region to identify the correct donor element within a neighborhood of a few points. In the case of moving body problems, such as SRB separation, the need for auxiliary grids may disappear as the distance between bodies increase. The present method automatically discards such auxiliary maps, saving the computational overhead required by their use. It is also possible that flow conditions, or even body motion, could create a situation that could benefit from an auxiliary inverse map. At present, the method does not recognize

this need automatically.

IGBP Identification

Consider, for a moment, procedures which could be employed to identify intergrid boundary points within overset grid systems. The IGBPs which correspond to minor grid outer boundaries are easy to identify. This can be done as simply as specifying ranges of coordinate indices. A more difficult task is that of identifying IGBPs resulting from holes created by a body, or bodies, in overset grids. Consider again the external tank and SRB grids shown in Figure 2. The SRBs, of course, cause holes in the external tank grid, and the external tank causes a hole in each of the SRBs. The respective body shapes of the external tank and SRBs could, for example, be used to create the holes and, hence, identify the resulting intergrid boundaries. The result, however, would not be acceptable. Intergrid boundary points created in this way could lie within the viscous portion of the donor grid, or even on the body surface. Due to the relative coarseness of the receiving grids in such regions, no useful information could be exchanged. Hence, it is desirable to define hole boundaries some distance from the actual body surface. Several factors may dictate the best offset for the hole cutting surfaces. In any case, it is necessary to provide a mechanism for cutting holes. The PEGASUS code, for example, uses a collection of surfaces defined by the component grids to create holes.

The approach adopted in this work is to cut holes using a collection of analytic shapes. Computationally, the task of hole creation in this way is very inexpensive. For example, the holes created in the external tank grid shown in Figure 2 were created using a cone, a cylinder, and a sphere positioned around each SRB. Similarly, the holes cut in the SRB grids were created by a cylinder and an sphere positioned around the external tank. Since each of the shapes are analytic, efficient routines can be written to determine if points lie in or outside of the shape. In the present work, an integer variable, I_b, is defined as 1 for all component grid points that are in the solution field, 0 for points which lie within a "hole," and -1 for an intergrid boundary. Again, intergrid boundary points are either minor grid outer boundaries, or are the fringe of points that surround a hole. Hence, I_b is set to -1 for all minor grid outer boundaries, and, once the holes have been cut via analytic shapes, the rest of the intergrid boundary points can readily be identified as well, setting $I_b = -1$. Once identified, it is convenient to compile a list of all IGBPs. In this method, points in the IGBP list are ordered by grid, viz. IGBPs from grid one occupy the first block in the list, IGBPs from grid two occupy the second block, etc.

The present method requires component grids and analytic shape parameter definitions to be made with respect to the initial mated position of the vehicle, or system of grids, being considered. This is true even for moving body problems. The component grids are never translated and rotated to their actual dynamic orientations. Rather, when cutting holes, the analytic shapes are oriented such that the holes are cut as if the grids were in their dynamic positions. Similarly, when the inverse maps are used to identify interpolation donors, only the list of IGBPs are translated and rotated to their effective dynamic positions. The component grids and inverse maps never move. In terms of computational expense, nine multiplies and six adds are required for every point rotated from one frame to another. Hole cutting requires transformation of only two points per analytic shape selected to position the set of hole cutters.

Determination of IGBP Donors

Given inverse mappings of all portions of the component grids which must participate in the domain connectivity process, and a complete list of intergrid boundary points, the only task that remains is to identify a suitable donor element for each point in the list. Of

course, this task also requires provision of the donor's J,K,L indices and ξ,η,ζ increments needed for interpolation. A certain amount of strategy is needed in order to accomplish this task efficiently. Two principles dictate the strategy employed here. The first principle is based on the fact that the inverse maps represent a large amount of data relative to that contained in the IGBP list. It is assumed that an auxiliary storage device will be employed, and the inverse maps will be rolled into main memory as needed. Accordingly, the first principle is to minimize requests for retrieval of the inverse maps from auxiliary storage, and is accomplished by exhausting the utility of a given map before retrieving the next map. Accordingly, each inverse map is used only once. The second principle is based on the fact that a certain amount of foreknowledge about the interconnectivity of the component grids is always available and should be exploited. Since points in the IGBP list are ordered by grid, obvious interconnections between grids can be made explicit via simple input. For example, grids which do not share a region of overlap will never have occasion to use one another's inverse map. Accordingly, entire blocks of points within the IGBP list can be skipped when the specified inverse map is in use. There are also interconnection issues which may not be readily discerned *a-priori*, but can easily be identified automatically via simple screening tests of the points in the IGBP list. In the present method, the simple screening tests are carried out for a single block of points from the IGBP list at a time. Accordingly, points within a block are skipped, and only a "short list" of points from the block need to be considered with respect to the inverse map in use. Such a situation exists, for example, when several grids share a common overlap region. There may be reason, perhaps based on grid characteristics, or physical features anticipated in the flow, which would suggest a hierarchy of preferred donor grids for the respective grid components. Accordingly, if several of the points within a block have already received suitable donors from their preferred donor grid, there is no need to use the current inverse map for these points.

The procedure for identifying suitable donor elements for a given block of points consists of five steps. First, a simple screening test is carried out on the block of IGBPs to see which, if any, have already received suitable donors from their preferred grid component. Such points are not entered into the "short list" of points to be considered further. Second, the inertial frame coordinates (x,y,z) of the IGBPs in the short list are transformed so that their relative orientation to the inverse map corresponds to the correct dynamic position between the respective grid systems. Of course, this step is omitted if a static grid problem is being considered. The third step is another simple screening test that determines which of the points in the short list are actually inside the domain of the current inverse map. Points which pass this screening make up the final list of IGBPs for which the current inverse map will be used to find interpolation donor elements. The fourth step is to actually find the donor elements.

After donor elements have been identified for as many of the points in the final list as possible, a final screening test, based in the donor's I_b array, is required. For example, a donor element which contains a hole point ($I_b = 0$) is not a suitable donor. The donor indices and ξ,η,ζ increments are saved for each point in the final list which passes the test. Points in the final list which fail the test must wait for a subsequent inverse map to identify a donor from a different component grid. Remember, in the present method, a new inverse map will not be rolled into main memory until the utility of the present inverse map has been exhausted, which is when all blocks within the main IGBP list have had access to the map. Once all of the inverse maps have been exhausted, any points within the main IGBP list for which a suitable donor element has not been found will have an I_b value of 0 and cannot be updated as an intergrid boundary point within the flow solver (ADF).

Donor elements and interpolation increments can thus be provided for the IGBPs within

a system of overset grids. A code has been built upon these principles and is named "DCF3D" (*D*omain *C*onnectivity *F*unction in *3 D*imensions). DCF3D has been tested on four different overset grid topologies, which include the simplified space shuttle grids illustrated in Figure 2, a wing and missile combination (Figure 6a), a generic helicopter and rotor combination (Figure 6b), and a pair of concentric cylinders. The latter case was used to test the code on grid systems where IGBP information must be exchanged in the vicinity of degenerate (i.e., non-hexahedral) elements. The efficiency of DCF3D in facilitating domain connectivity is proportional to the number of IGBPs which exist in an overset grid system. Figure 7 presents the efficiency of DCF3D in a "CRAY-2 seconds versus number of IGBPs" plot derived from several test cases including those illustrated in Figures 2 and 6. On average, DCF3D provided domain connectivity among static overset grid systems at a rate of 472 IGBPs per CRAY-2 second. For dynamic overset grid systems (i.e., moving body problems), the test computations indicate DCF3D could provide domain connectivity at rates on the order of 3,500 IGBPs per CRAY-2 second. Based on test computations using the PEGASUS code for the simplified space shuttle grids and the wing/missile combination, the corresponding static and dynamic rates for PEGASUS are about 45.3 and 123 IGBPs per CRAY-2 second, respectively.

The DCF3D test cases used to construct Figure 7 are relatively small grid systems, the largest being the 246,740 grid point generic helicopter and rotor grid system which has 6,294 IGBPs. Problems of more practical importance, such as the 9 component space shuttle grid illustrated in Figure 1, contain many more grid points and IGBP totals of over 50,000. DCF3D must be tested further on more complicated grid configurations. If the above DCF3D performance rates prove to be true even for large grid systems (which they should), the present DCF methods can effectively limit DCF expenses in moving body problems to a fraction of those of the ADF (flow solver). Also, static grid applications could be done interactively even for large grid systems.

RESULTS

As noted in the introduction, much of the motivation for the development of the present computational methods originated from the need to simulate the proposed "fast sep" shuttle abort maneuver. The SRB separation sequence was chosen as a stepping-stone to actual "fast sep" computations because of the existence of flight data (i.e., video and pressure data) and quasi-steady type wind-tunnel data. SRB separation occurs approximately two minutes into the shuttle's ascent at Mach 4, and at an altitude of about 50,000 meters. Longitudinal separation results naturally due to the greater axial acceleration of the combined orbiter and external tank (ET) vehicle relative to the spent SRBs. However, separation of the SRBs in the lateral and normal directions are caused by aerodynamic and applied forces. At separation, eight booster separation motors (BSMs) ignite and provide about 22,000 pounds of thrust each. The BSMs burn for only $\sim 2/3$ of a second and are oriented to ensure safe separation and minimize exhaust plume impingement on the orbiter thermal protection tiles. Given the BSM exhaust directions, (see Figure 8 and reference [16]), the BSM plumes are clearly a major contributor to the flow field transients during separation. However, simulation of the BSM plumes was not attempted as part of these calculations. Rather, the focus of the calculations was on the transients induced into the aerodynamic field due to SRB motion.

2-D SRB Separation Simulations

A two-dimensional overset grid system was generated to model the symmetry plane between the shuttle ET and both SRBs. The ET grid was again treated as the major grid and was resolved with 3x174x60 points in the respective coordinate directions. The SRBs were each resolved with 3x105x21 points and treated as minor grids. This representation of the

shuttle vehicle was constructed to further explore transients that may occur at separation, and to provide a preliminary evaluation of the overall computational method where body motion is driven by aerodynamic and applied loads, rather than a prescribed trajectory.

Unsteady results are presented and correspond to zero angle of attack ($\beta = 0$) and Mach 2.5 free-stream conditions. Though the BSM plumes were ignored throughout this work, their effect was accounted for in the present set of simulations as part of the body dynamics computation. The components of the BSM thrust vectors acting in the ET/SRB symmetry plane (see Figure 8) were treated as applied forces acting through the SRB centers of mass. The BSMs were assumed to provide a constant thrust during the burn-time and not to produce a net moment on the respective SRBs. The gravitational force vector was assumed to act in the positive Cartesian x direction, which is coaxial with the ET major axis. The effect of the ET's greater acceleration was accounted for by applying a corresponding force to each of the SRBs in the direction of the gravity vector.

The separation dynamics were resolved with 2,500 time-steps covering the $\sim 2/3$ second BSM burn time (dimensionless $\Delta t = 0.0024$). Figure 9 shows the instantaneous Mach field at three instants during separation ($t = 25\Delta t$, $650\Delta t$, and $1300\Delta t$). The ET base region is a highly unsteady regime. This has also been observed in other studies of the space shuttle's flowfield [15]. As the SRBs are blown away from the ET, the aerodynamic field responds. The bow shock "flexes" in response to the SRB motions, resulting in an increasing downstream region of transonic and subsonic flow (i.e., the lighter colored areas downstream of the bow shock and between the ET and SRBs in Figure 9).

3-D SRB Separation Simulation

A three-dimensional discretization of the integrated shuttle vehicle similar to that illustrated in Figure 1, but with lower resolution, was used to simulate the SRB separation sequence [5]. The composite grid contains approximately 350,000 points. The ET grid is treated as the major grid, the orbiter and SRB grids are minor ones. In all, there are 8 inter-grid boundaries within the composite grid system and represent 10,408 points. The corresponding computations assumed the following flight conditions at separation:

$M_\infty = 4.5$, $\alpha = +2^\circ$, and $R_e = 6.95 \times 10^6$

where the Reynolds number is based on the full-scale orbiter length. The simulation was carried out for the 2/3 second BSM burn-time, using 500 time-steps to resolve the motion temporally (dimensionless $\Delta t = 0.0136$). In this case, the SRB trajectory was prescribed.

A sequence of plots from the time-accurate solution are shown in Figure 10 at three instants during the separation ($t = 0$, $250\Delta t$, and $500\Delta t$). Figure 10 shows gray-scale images of the C_p distributions over the surface of the shuttle vehicle. In the top views, the orbiter is transparent, revealing the C_p distributions over the ET and SRBs (mirrored in the figure about the symmetry plane). Similarly, the SRB is transparent in the side views, revealing the C_p distributions over the orbiter and ET. The sequence of results presented in the figure illustrate the influence of the separation transients on the surface pressure distributions. As the SRBs move away from the ET and orbiter, the SRB bow shocks interact with the orbiter bow shock and impinge on the ET and orbiter surfaces causing localized zones of high pressure. As the SRBs continue to fall back and away, the high pressure zones correspondingly traverse back the length of the ET and orbiter.

The unsteady separation sequence required approximately 104 CRAY-2 seconds per time step. Of this, approximately 30.9 seconds were required by the ADF (flow solver), 72.6 seconds for the DCF (then the PEGASUS code run in dynamic mode), and a negligible amount of time for the BDF (a prescribed trajectory in this case, though the actual BDF

would still have been a very small fraction of the overall cost). Given the "IGBPs per CRAY-2 second" rates estimated for PEGASUS (dynamic mode) in the preceding section, domain connectivity for the 10,408 IGBPs of this problem should be satisfied in about 85 seconds, which is fairly close to the actual 72.6 seconds that were required. Similarly, given the "IGBPs per CRAY-2 second" rates estimated for DCF3D (dynamic mode), domain connectivity for this problem should be satisfied in approximately 3 seconds. In other words, if the same computation were carried out today using DCF3D, the total cost of the 500 time-steps would drop from the 14.4 CRAY-2 hours (using PEGASUS in dynamic mode as the DCF) to 4.7 hours.

CONCLUDING REMARKS

An overset grid method of the "chimera" type has been presented for time-accurate simulation of three-dimensional multiple body viscous flows, given arbitrary grid combinations, body shapes, and relative motion between grid systems. The components of the method have been tested individually on selected ideal and practical problems. The method components have also been tested collectively on several moving body problems; some of the space shuttle SRB separation results being presented in this paper. Recent improvements to the overall method include the addition of a body dynamics algorithm and a newly developed methodology for providing domain connectivity among systems of overset grids. Addition of the body dynamics algorithm allows the trajectory of body components to respond to aerodynamic and applied loads. The new domain connectivity methods embodied in the DCF3D code promise substantial reduction in the computational expense of providing domain connectivity among systems of overset grids.

It should be understood that overset grid techniques in general still represent a maturing methodology. Although the approach is well suited for geometrically complex problems, and represents by far the most computationally affordable alternative available for moving body problems, there still are a number issues which demand further algorithmic maturation. Of course, issues of efficiency and accuracy will continue to be pacing items as they are for all computational methods. Implementation and testing of a new delta form method for conservative interpolation of IGBP information [17] will be pursued. The need for adaptive grid (e.g., see reference [18]) capability for unsteady and moving body problems, represents an additional area in which significant contributions can be made.

ACKNOWLEDGEMENTS: The author is indebted to the members of the Space Shuttle Flow Simulation group at NASA Ames Research Center and Johnson Space Center who at various times during this research provided useful information and suggestions. Special thanks are due to Dr. Joseph Steger for encouraging this work and many helpful suggestions along the way. The body dynamics section of the paper does not represent original work. Rather, it is a compilation of well known ideas drawn from a variety of sources. The generic helicopter and rotor grid combination, and the pair of concentric cylinder grids, which were used as tests for the DCF3D code were furnished by Dr. Sharon Stanaway. All of the computational results presented in this paper were carried out on the NAS Cray Y-MP and Cray-2 computers at NASA Ames Research Center.

REFERENCES

1. NASA Ames Space Shuttle Flow Simulation Group, Buning, P., Chiu, I., Martin, F., Meakin, R., Obayashi, S., Rizk, Y., Steger, J., and Yarrow, M., "Numerical Simuation of the Integrated Space Shuttle Vehicle in Ascent," 4th Internat. Conf. on Super Computing, Santa Clara, Calif., April, 1989.

2. Fox, J., Donegan, T., Jacocks, J., and Nichols, R., "Computation of the Euler Flow Field Produced about a Transonic Aircraft with Stores," AIAA Paper

89-2219, July-August 1989.

3. Rizk, Y. and Schiff, L., "Numerical Simulation of the Viscous Flow Around a Simplified F/A-18 at High Angles of Attack," AIAA Paper 90-2999, August 1990.

4. Chawla, K., VanDalsem, W., and Rao, K., "Simulation and Analysis of a Delta Planform with Multiple Jets in Ground Effect," AIAA Paper 90-0299, January 1990

5. Meakin, R. and Suhs, N., "Unsteady Aerodynamic Simulation of Multiple Bodies in Relative Motion," AIAA Paper 89-1996, June 1989.

6. Dougherty, C. and Kuan, J., "Transonic Store Separation Using a Three-Dimensional Chimera Grid Scheme," AIAA Paper 89-0637, January 1989.

7. Kiris, C. and Chang, I., "Numerical Simulation of the Incompressible Internal Flow Through a Tilting Disk Valve," AIAA Paper 90-0682, January 1990

8. Meakin, R. and Street, R., "Simulation of Environmental Flow Problems in Geometrically Complex Domains. Part 2: A Domain-Splitting Method," Comp. Meths. Appl. Mech. Engrg., 68, 311-331, 1988.

9. Pulliam, T. and Steger, J., "On Implicit Finite-Difference Simulations of Three-Dimensional Flow", AIAA Paper 78-10, January 1978.

10. Steger, J., Ying, S., and Schiff, L., "Partially Flux-Split Algorithm for Numerical Simulation of Compressible Inviscid and Viscous Flow," Workshop on Computational Fluid Dynamics, Institute of Non-Linear Sciences, U. of Calif., Davis, Calif., 1986.

11. Thomas, J., Taylor, S., and Anderson, W., "Navier-Stokes Computations of Vortical Flows Over Low Aspect Ratio Wings," AIAA Paper 87-0207, January 1987.

12. Baldwin, B. and Lomax, H., "Thin Layer Approximation and Algebraic Model for Separated Turbulent Flows", AIAA Paper 78-257, January 1978.

13. Dietz, W., Jacocks, J., Fox, J., "Application of Domain Decomposition to the Analysis of Complex Aerodynamic Configurations." SIAM Conf. Domain Decomposition Meths., Houston, TX, March 1989.

14. Brown, D., Cheshire, G., Henshaw W., and Kreiss, O., "On Composite Overlapping Grids", 7th Internat. Conf. on Finite Element Methods in Flow Problems, Huntsville, AL, April 1989.

15. Meakin, R., "Transient Flow Field Responses about the Space Shuttle Vehicle During Ascent and SRB Separation," R. Aero. Soc. Store Carriage, Integration, and Release Conf., pp. 29.1-29.16, April 1990.

16. Craig, M. and Dresser, H., "Shuttle Booster Separation Aerodynamics", In Shuttle Performance: Lessons Learned, pp. 139-157, NASA Conference Publication 2283, NASA Langley Research Center. March 1983.

17. Steger, J. "Delta Form Boundary Interface Update for Chimera," unpublished notes, August 1990.

18. Berger, M. "Adaptive Finite Difference Methods in Fluid Dynamics," Courant Mathematics and Computer Laboratory Rept. DOE/ER/03077-277, 1987.

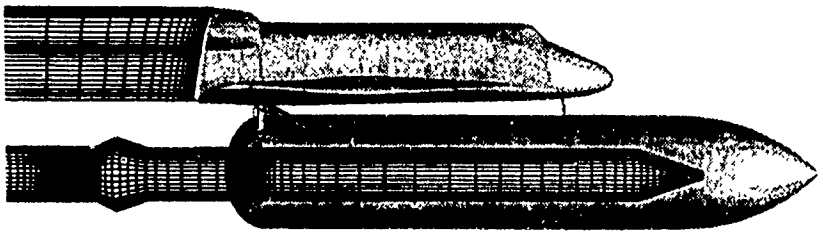

(a) Orbiter and SRB wake grids.

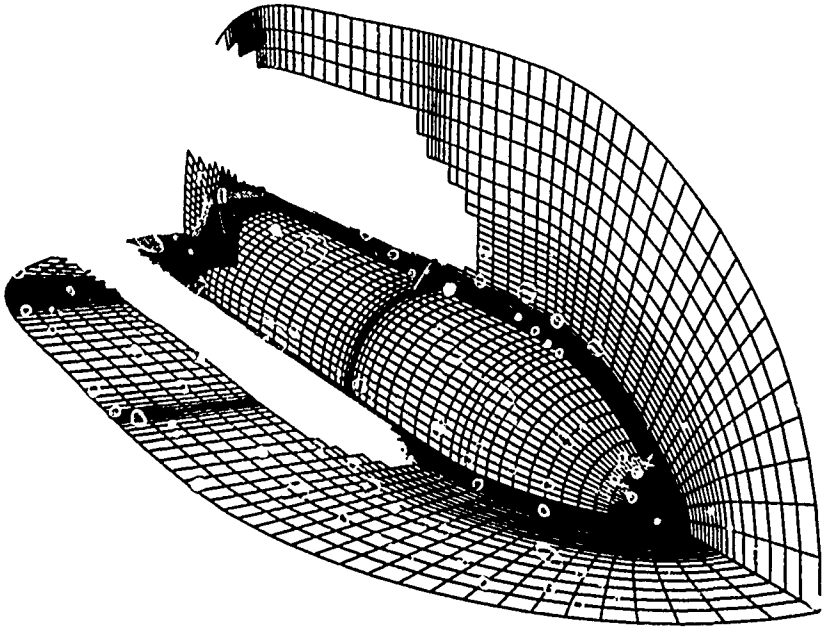

(b) Orbiter and SRB holes in ET grid.

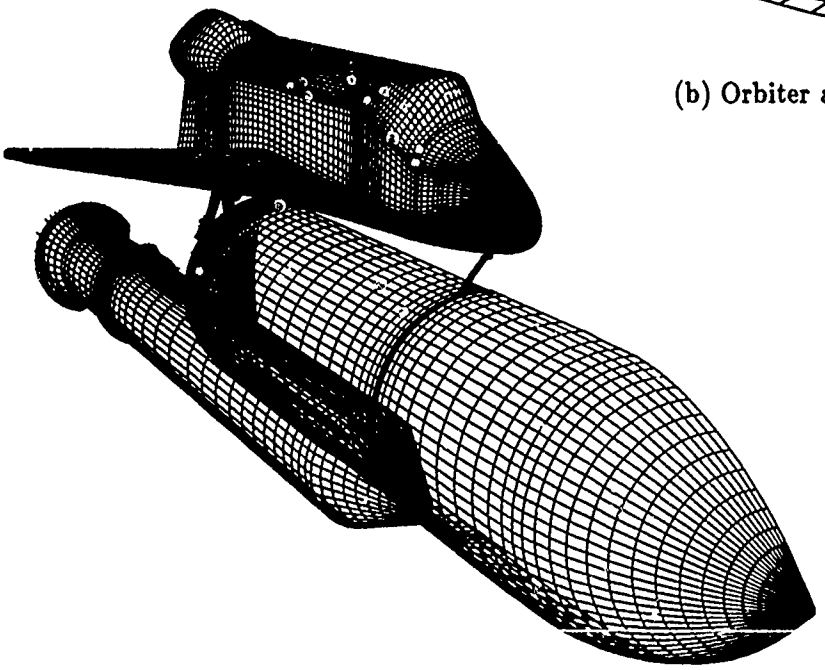

(c) Surface grids for Orbiter, ET, SRB and attach hardware.

Figure 1. Overset grid discretization of the integrated space shuttle vehicle.

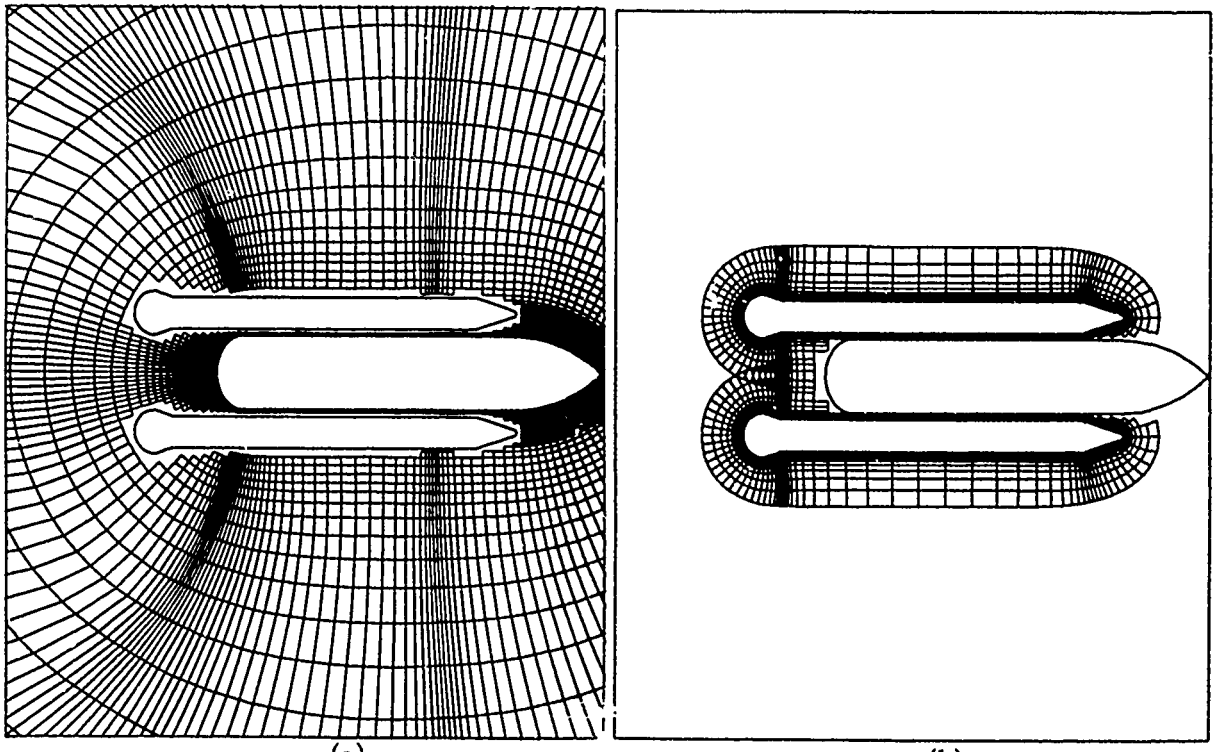

Figure 2. Simplified space shuttle grid system showing hole boundaries. (a)" Major" grid about the external tank. (b) "Minor" grids about the upper and lower solid rocket boosters.

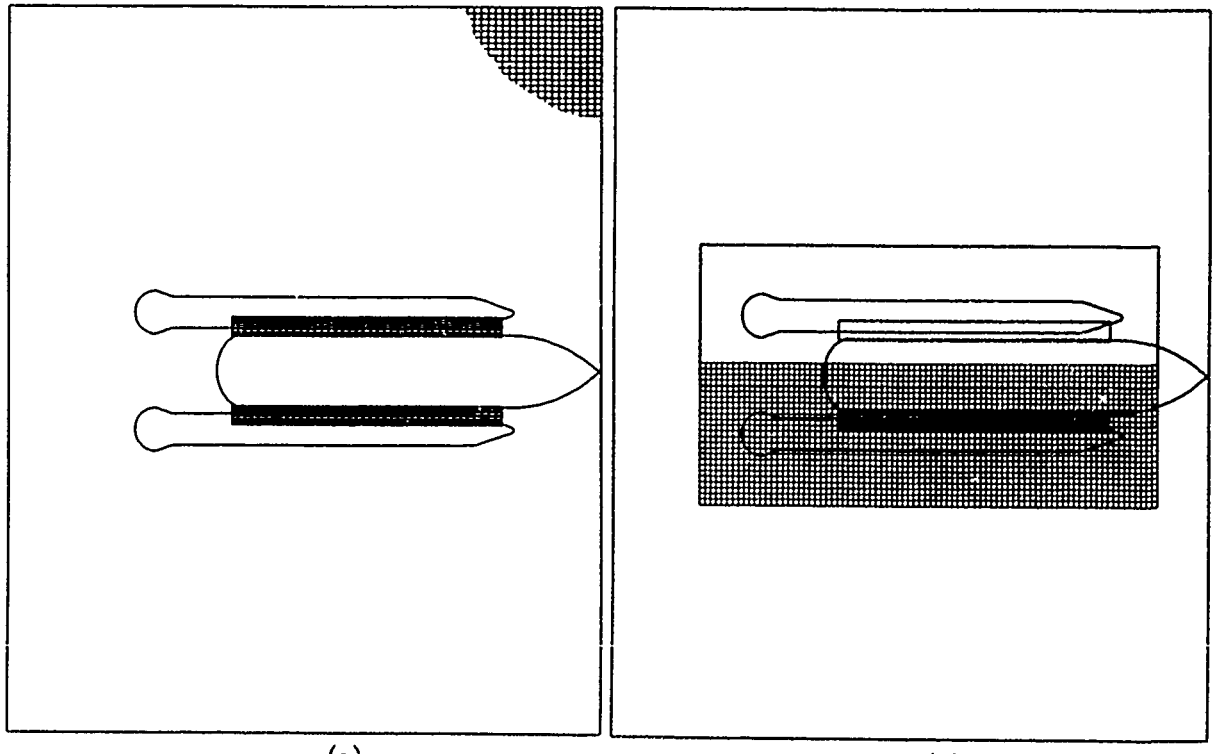

Figure 3. Inverse Maps. (a) Extent of the major grid inverse maps. (b) Extent of the minor grid inverse maps.

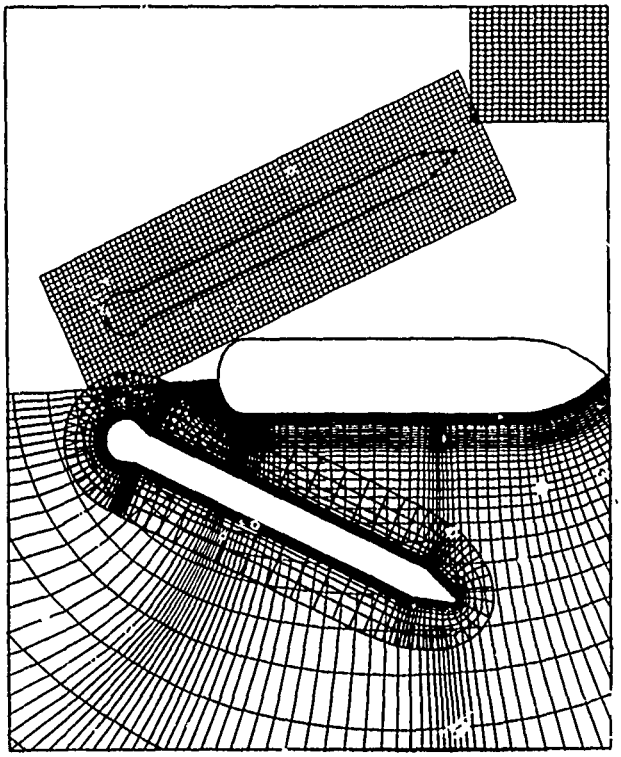

Figure 4. Representation of component grid and inverse map orientation during SRB separation. **note:** As stated in the text, the inverse maps *never* move. The upper SRB's inverse map is illustrated in this position only to indicate its association with the SRB.

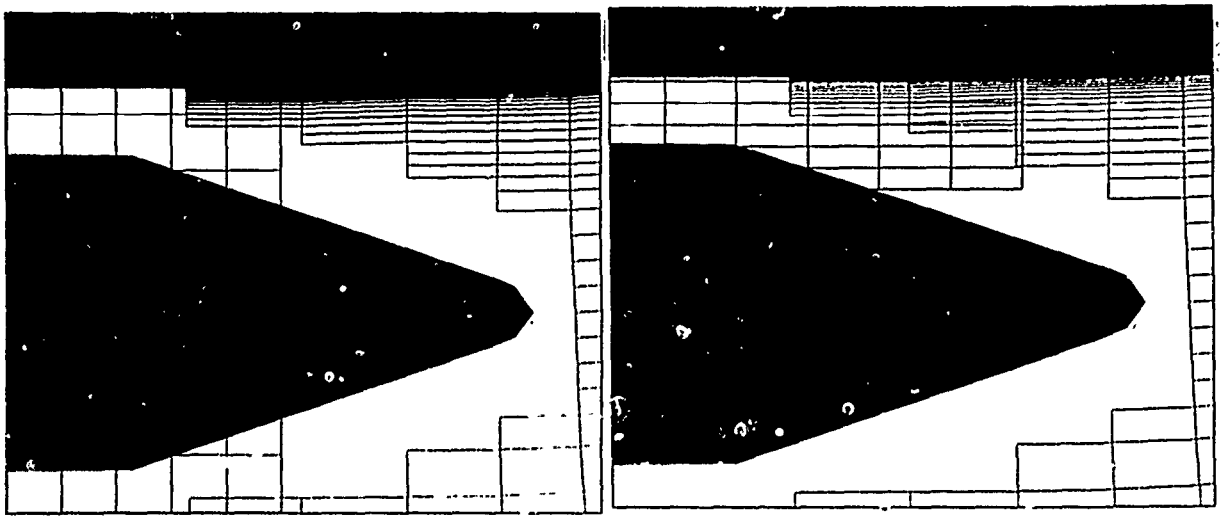

(a) (b)

Figure 5. Auxiliary inverse maps. (a) Major grid and lower SRB inverse map resolution between the external tank and lower SRB. (b) An auxiliary inverse map used to resolve ξ,η,ζ space within the gap.

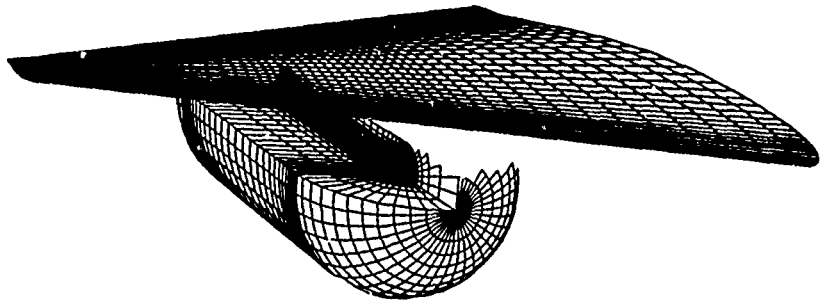

(a) Wing and missile grid (2,564 IGBPs).

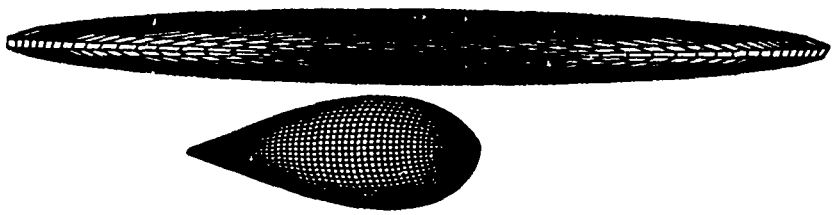

(b) Generic rotor/body combination (6,294 IGBPs).

Figure 6. Sample of DCF3D test cases.

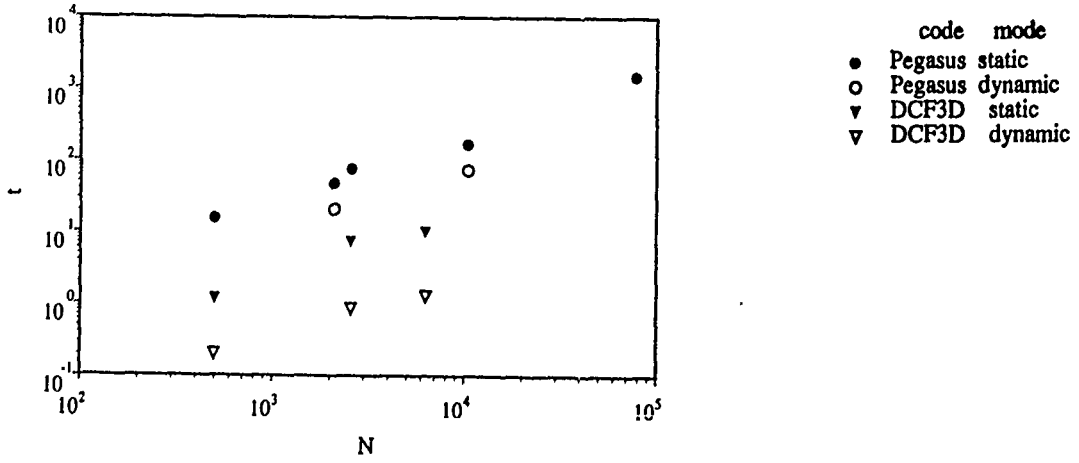

Figure 7. DCF3D efficiency plot (t versus N). Results from several test computations are plotted as Cray-2 seconds required to establish domain connectivity versus the total number of intergrid boundary points (IGBPs). Data from tests of PEGASUS code are provided for comparison.

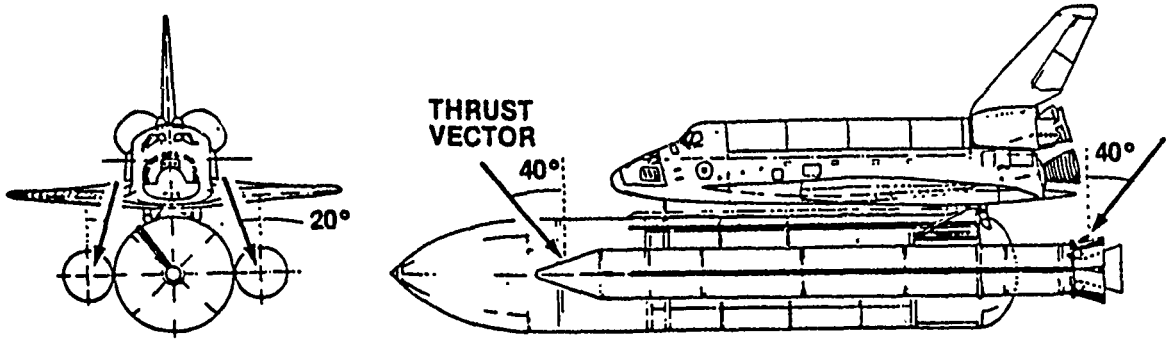

Figure 8. Booster separation motor (BSM) thrust vectors [16].

(a) $t = 25\Delta t$ (b) $t = 650\Delta t$ (c) $t = 1300\Delta t$

Figure 9. 2-D SRB separation simulation. Mach contours about the external tank and both SRBs during separation [15]. $M_\infty = 2.5$, $\beta = 0°$, and $R_e = 4.9x10^7$.

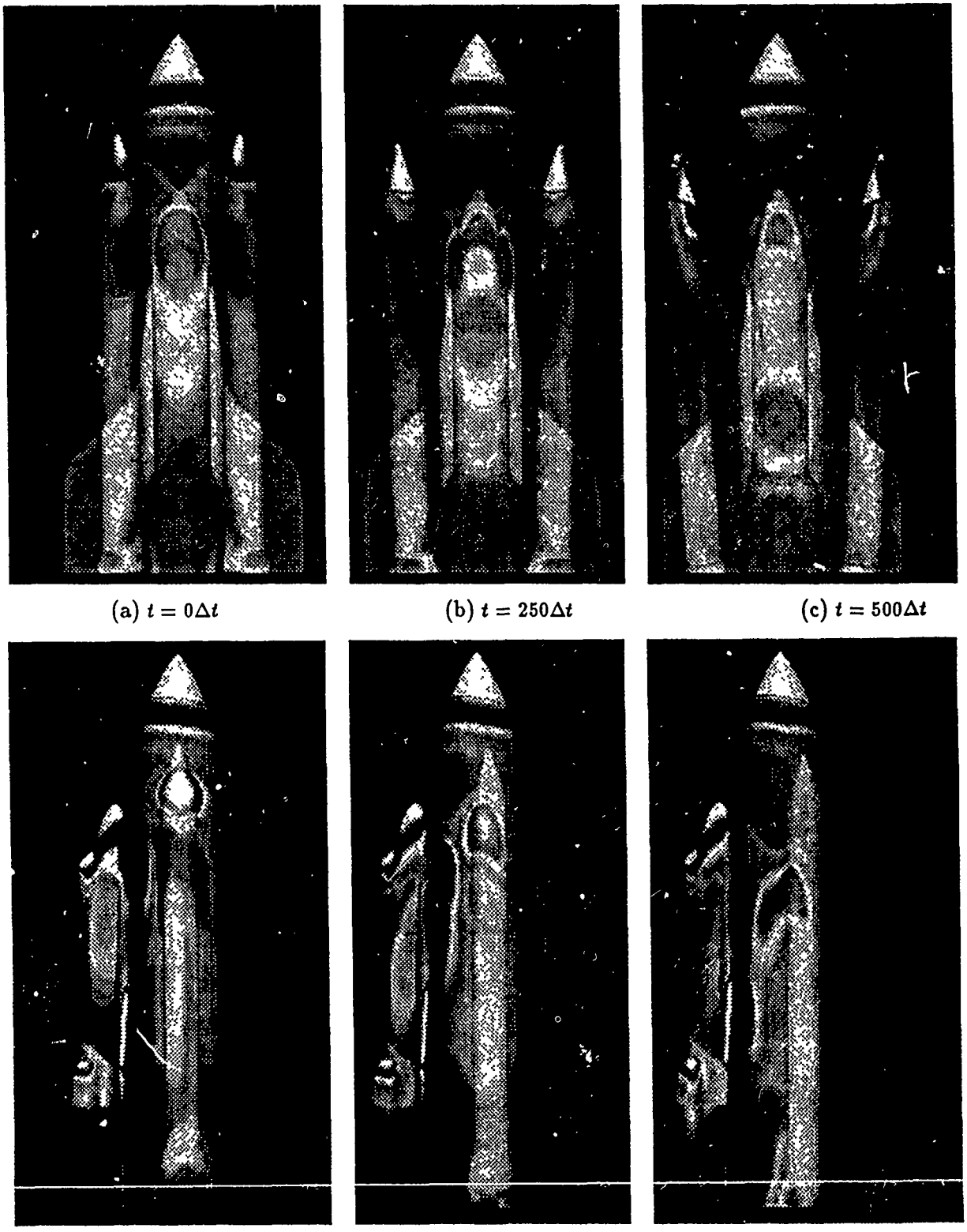

(a) $t = 0\Delta t$ (b) $t = 250\Delta t$ (c) $t = 500\Delta t$

Figure 10. 3-D SRB separation simulation. C_p contours about the integrated space shuttle vehicle during SRB separation [5]. $M_\infty = 4.5$, $\alpha = +2^o$, and $R_e = 6.95 \text{x} 10^6$.

Robert L. Meakin

Dr. Meakin is currently a "Visiting Research Scientist and Lecturer" in the Mechanical Engineering Department at the University of California, Davis. The emphasis of his research is on computational methods for unsteady fluid dynamic problems in geometrically complex domains. Much of his work over the past few years has been motivated by NASA's need to simulate the aerodynamics about the space shuttle vehicle for emergency abort maneuvers during ascent. Dr. Meakin received his education at Stanford University, and was awarded a Ph.D. degree in January of 1987.

BALLISTIC ACCURACY VERIFICATION PROCESS STANDARD

Air Force SEEK EAGLE Office

Capt David Smith

DSN 872-9711

(904) 882-9711

CLEARED FOR PUBLIC RELEASE

CONTENTS

FIGURES

TABLES

1. INTRODUCTION

The objective of this document is to define and standardize the ballistic accuracy verification process. The term ballistic accuracy as used in this document refers to how well an aircraft Operational Flight Program (OFP) models the freestream ballistics and separation effects characteristics of a weapon from the time of release until impact, dispenser opening, bomblet impact, or other special event (drag chute, rocket phase, etc). The ballistic accuracy verification process consists of three phases: the OFP ballistic evaluation phase (PHASE I), the separation effects derivation phase (PHASE II), and the OFP ballistic verification phase (PHASE III). Each of the phases will be defined in terms of its objective, when it occurs in the process, the recommended flight test matrix, the recommended number of weapons, and the acceptance criteria in terms of circular error probable (CEP) and range bias, where applicable. Weapon freestream ballistics must be determined and incorporated in the aircraft OFP as a prerequisite to conducting PHASE I of the ballistic accuracy verification process.

In determining the bombing accuracy of a weapon system, one of the most important decisions that must be made is determining the number of weapons to drop during the ballistic accuracy verification process. While too few weapons may result in erroneous conclusions, too many constitute a waste of scarce resources. Lack of effective analytical tools to make such a decision has resulted in test numbers ranging from just a few weapons to several hundred weapons. Since ballistic accuracy verification is one of the essential parts of OFP software development, the capability to determine the number of weapons required is extremely valuable. Table 1 shows the number of weapons needed to statistically estimate CEP for a particular confidence level and acceptable error in the actual CEP. Table 1 is based on a bivariate normal distribution--a two-dimensional, normal distribution where the distributions in either direction [range (along track) and deflection (across track)] are independent of each other. Reference Technical Memorandum 78-4 (TM 78-4 SA), Statistical Analysis of Weapon Impact Data, from the Naval Air Test Center for details on calculating CEP and defining Table 1. Requests for this document should be referred to Commander, Naval Air Test Center, Patuxent River, Maryland 20670.

2. DEFINITIONS

Aircraft Dispersion: Refers to the aircraft errors contributing to the weapon delivery error budget because of sensor errors, on-board avionics, timing delays, variation in rack ejection forces, etc.

Circular Error Probable (CEP): A measure of accuracy whose value is equal to the radius of a circle centered on the aimpoint or mean point of impact with an associated probability of containing 50 percent of the impact points. CEP is measured in the normal plane for level and dive deliveries and in the ground plane for loft deliveries.

Deflection Error Probable (DEP): A measure of accuracy whose value is equal to one-half of the distance between two lines that are equidistant from the aimpoint and parallel to the aircraft track at time of release with an associated probability of containing 50 percent of the impact points. DEP is measured in the ground plane.

Ground Plane: The plane level with the Earth's surface passing through the aimpoint.

Mean Point of Impact : A point which has as its range/deflection coordinates the arithmetic means of the range and deflection coordinates of the impact points.

Normal Plane: The plane perpendicular to the pilot's line of sight passing through the aimpoint.

Range Bias: The criteria that defines whether the weapon system is biased in range; that is, long/short weapon impacts about the target.

Range Error Probable (REP): A measure of accuracy whose value is equal to one-half of the distance between two lines that are equidistant from the aimpoint and perpendicular to the aircraft track at time of release with an associated probability of containing 50 percent of the impact points. REP is measured in the ground plane.

Standard Deviation: A measure of dispersion of a distribution.

System Dispersion: The total dispersion due to the combination of the weapon and aircraft dispersion.

Weapon Dispersion: Random weapon - to - weapon variations in the freestream ballistic characteristics which are attributed to, notably, manufacturing tolerances (e.g. weight) and accidental misalignments occurring during assembly and handling of the weapon (e.g., bent fins).

3. BALLISTIC ACCURACY VERIFICATION PROCESS

Figure 1 illustrates the ballistic accuracy verification process. The process begins after the incorporation of the freestream ballistics (and any available separation effects information) into the OFP, which were derived/gathered from either flight test or an existing data base. The ballistics (freestream plus separation effects) are incorporated into the OFP which is loaded into the aircraft weapon delivery computer. PHASE I, conducted by flight testing, provides an initial assessment of the aircraft/weapon ballistic accuracy. The process requires a properly functioning aircraft weapon delivery system, thereby eliminating the possibility of compensating errors in the system (separation effects causing weapons to go long, avionic timing problems causing it to go short, net result: weapons on target and system passes Phase I). From the CEP and range bias evaluations, the test agency can determine whether or not the ballistics

are acceptable at this point. If both the CEP and range bias evaluations meet the user's acceptance criteria, then the ballistic accuracy of the OFP for the particular aircraft/weapon combination in question will have been verified, and PHASE II and PHASE III will not be necessary. If either of the above fails, it must be determined whether the problem is in the OFP algorithm (e.g., the weapon release algorithm), the avionics, or the ballistics. If the problem is within the OFP algorithm or avionics, it must be determined whether it can be fixed; and if so, what level of verification testing will be required; nothing, spot check, or PHASE III. If the weapon separation effects are suspected to be the significant error source, then PHASE II flight testing is conducted as necessary (after acquiring as much separation effects data as practical from PHASE I testing) to derive the separation effects coefficients. These coefficients are then loaded into the OFP to model the weapon's trajectory through the aircraft flow field. PHASE III is then conducted by flight testing to validate the weapon ballistic accuracy. The CEP and range bias criteria in PHASE I are used to evaluate the PHASE III results. The process of refining the OFP can continue until the acceptance criteria is achieved or until the user accepts the results or cancels the requirement.

4. FREESTREAM BALLISTICS

The ballistic accuracy verification process requires that the freestream ballistics already be defined and incorporated in the aircraft OFP prior to beginning PHASE I testing. The freestream ballistics are independent of the aircraft and the delivery mode and provide the baseline ballistics for the OFP. Freestream ballistics model the weapon's trajectory from the time the weapon reaches steady state flight, approximately three seconds after release, until impact, dispenser opening, bomblet impact, or other special event (drag chute, rocket phase, etc).

5. PHASES OF THE BALLISTIC ACCURACY VERIFICATION PROCESS

5.1 OFP Ballistic Evaluation Phase (PHASE I)

The objective of this phase is to evaluate the initial aircraft/weapon ballistic accuracy of the OFP. As a minimum, the ballistics of the OFP during this phase consist of the freestream ballistics of the weapon. If available, separation effects gathered by analogy with a similar weapon, from wind tunnel tests, from aircraft contractor estimates, or from a data base will be incorporated to the maximum extent possible in the ballistics. The evaluation of the ballistics includes a CEP comparison test and a range bias test.

The number of weapons to be dropped for each delivery mode (e.g., level, dive/dive toss, loft) and flight condition that the user specifies is

dependent on the desired confidence level and acceptable error in the measured CEP. The statistical requirement must take into account funding, scheduling and weapon availability constraints and should be a management decision by the user and aircraft/store SPO or SPM. Also the philosophy of diminishing marginal return should be considered as described in the following example. Assume the user desires an 85 percent confidence level and wants the measured CEP to be within approximately 20 percent of the actual CEP. Using Table 1, 15 weapons would be required. However, using the philosophy of diminishing marginal return (each additional weapon dropped should result in at least a one percent incremental improvement in the acceptable error of the measured CEP) results in 13 weapons, with a measured CEP within 22 percent of the actual CEP. This number is determined by plotting the number of weapons versus the acceptable error in percent CEP, on a one - to - one scale in order to determine the knee in the curve, as shown in Figure 2. By drawing a 45 degree line to the 85 percent confidence level curve the tangential point is determined, and it defines the point of diminishing marginal return which correlates to the number of weapons. The user, after considering cost, may be willing to accept this result, realizing that the two additional weapons have little impact on the results. PHASE I test points should be selected to complete as much of the potential PHASE II test matrix as practical. Time-Space-Position-Information (TSPI) data should be gathered on each drop so that if PHASE II testing is required, the PHASE I test points will not need to be repeated.

After flight testing is completed, a CEP about the mean point of impact may be calculated. This represents the system CEP. The equation, CEP = 0.873 x (range error probable + deflection error probable) is used for calculating the system CEP. This equation will apply as a good approximation of CEP regardless of the ratios of the standard deviations of the range and deflection components as explained and proved in TM 78-4 SA. The system CEP is then corrected for weapon dispersion, which can be found in the Joint Munitions Effectiveness, Air to Surface Delivery Accuracy Manual. The resultant CEP represents the aircraft contribution to the ballistic dispersion. This value of CEP is compared to the user's requirements. The user determines whether or not it is acceptable.

A bias evaluation is also accomplished assuming a binomial distribution. Simply stated, if the median is expected to be a certain point (the aimpoint in our case), then for any given sample by definition of the median, you would expect half of the weapons to impact long of the median and half to impact short for no bias. With a 50-50 chance of being long or short, the binomial table, Table 2, can be used to evaluate bias. Those weapon combinations that fall to the right of the solid line in Table 2 pass the bias test. The line is based on assuming that the weapon delivery system is perfect. For a perfect system, those long/short combinations to the right of the line will occur 90 percent of the time and those to the left will occur only 10 percent of the time. Thus, if the weapon results fall to the left of the line there is most likely something wrong with the aircraft or weapon delivery system.

5.2 Separation Effects Derivation Phase (PHASE II)

The objective of this phase is to derive the separation effects coefficients for the aircraft/weapon loading configuration. Separation effects models account for the motion of the weapon from the moment it is released until it clears the air flow around the aircraft (reaches steady state flight). The weapon can be affected for up to approximately three seconds after release. Separation effects are currently modeled as a function of release variables such as Mach number, normal acceleration, and dynamic pressure.

In order to derive the separation effects coefficients for an aircraft/weapon loading configuration, weapons are dropped and tracked for TSPI in accordance with MIL-STD-1763, Test 290. The result of these tests and subsequent analysis of the data is a family of curves that create a multi-dimensional surface (e.g., velocity adjustment versus Mach number and normal acceleration), as in Figure 3. The number of weapons per selected flight condition is determined based on the same rationale as used in PHASE I. The flight conditions will be selected with the goal of acquiring enough data to derive the separation effects coefficients. These coefficients will be used to compensate for separation effects and may be incorporated into the separation effects algorithm in the OFP and/or the -34 T.O. ballistic tables (as implemented by aircraft with no computer - aided weapon delivery solutions, i.e., OFP). The coefficients used in an algorithm may result in adjustments to the aircraft velocities used in the air to surface trajectory calculations or may incorporate changes in the mode of trajectory calculation. Only those flight conditions and weapons which have significant separations effects will be tested in this phase. Table 3 represents the baseline test matrix and only those necessary flight conditions that were not flown in PHASE I will have to be flown in PHASE II.

The Table 3 three by three matrix (low, medium, and high g releases versus low, medium, and high airspeeds) represents the baseline test matrix for defining the separation effects coefficients because of the non-linearity of the separation effects. The test conditions chosen will depend on the aircraft/weapon loading configuration, the operational delivery conditions, and the expected shape of the multi-dimensional surface. There will be circumstances which do not warrant the use of the entire matrix. There are some weapons, for instance, which would never be released under high g conditions. There are also weapons designed to be released under only one set of flight conditions. Obviously under these circumstances a three by three matrix is unnecessary. A thorough understanding of the aircraft and weapon system being tested as well as the intended use of the weapon is paramount in designing a successful test matrix.

5.3 OFP Ballistic Verification Phase (PHASE III)

The objective of this phase is to verify the ballistic accuracy of the OFP. The ballistics at this point in the process consist of both the freestream ballistics and the derived separation effects adjustments.

PHASE III is identical to PHASE I. CEP and bias evaluations are performed and compared to the acceptance criteria. If the criteria is not met, then the decision for further analysis, rederivation of the separation effects, or modification to the delivery platform (aircraft) must be made versus accepting a less accurate weapon system or rejecting the aircraft/weapon loading configuration.

TABLE 1

NUMBER OF WEAPONS NEEDED TO ESTIMATE CEP
FOR A GIVEN CONFIDENCE LEVEL

CONFIDENCE LEVEL [1]

ACCEPTABLE ERROR (%) CEP	0.70	0.75	0.80	0.85	0.90	0.95	0.99
2.0	685	840	1038	1305	1698	2403	4149
4.0	175	214	263	329	427	602	1204
6.0	80	97	119	148	191	268	466
8.0	46	56	68	84	108	152	263
10.0	31	37	44	55	70	98	169
12.0	22	26	32	39	49	68	118
14.0	17	20	24	29	37	50	88
16.0	13	16	19	23	28	39	67
18.0	11	13	15	18	23	31	54
20.0	9	11	13	15	19	24	41
22.0	8	9	11	13	16	21	37
24.0	7	8	9	11	14	18	31
26.0	6	7	8	10	12	16	27
28.0	6	6	7	9	10	14	23
30.0	5	6	7	8	9	12	20
40.0	4	4	4	5	6	7	12
50.0	3	3	3	4	4	5	8
60.0	2	3	3	3	3	4	6
70.0	2	2	2	3	3	3	5
80.0	2	2	2	2	2	3	4
100.0	2	2	2	2	2	2	3

1. This is the number of weapons that need to be dropped so that when the sample standard deviation is used as the population standard deviation, the error induced will be less than the specified acceptable error with a probability as specified by the confidence level.

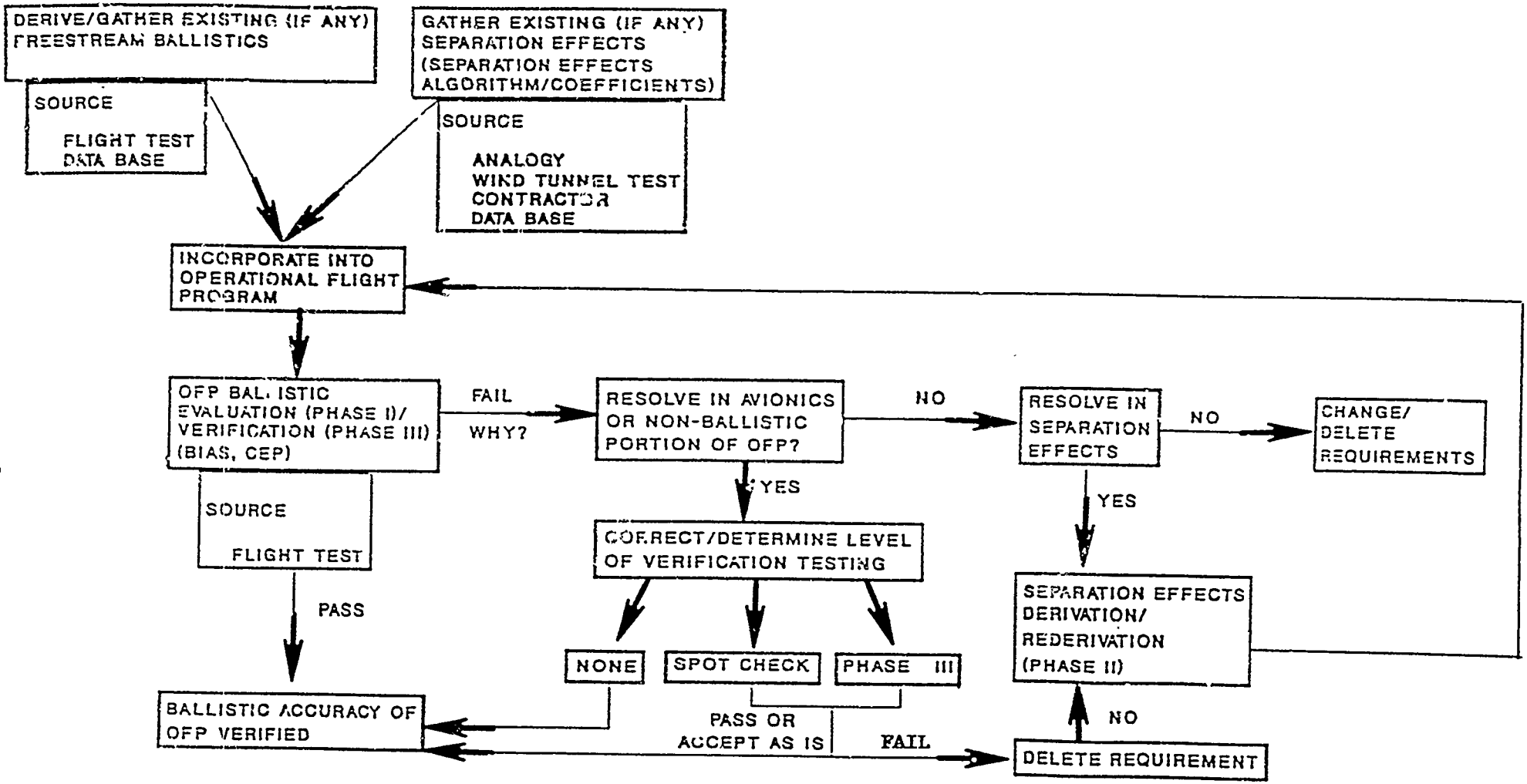

FIGURE 1. BALLISTIC ACCURACY VERIFICATION PROCESS

RECOMMENDED MAXIMUM NUMBER OF WEAPONS

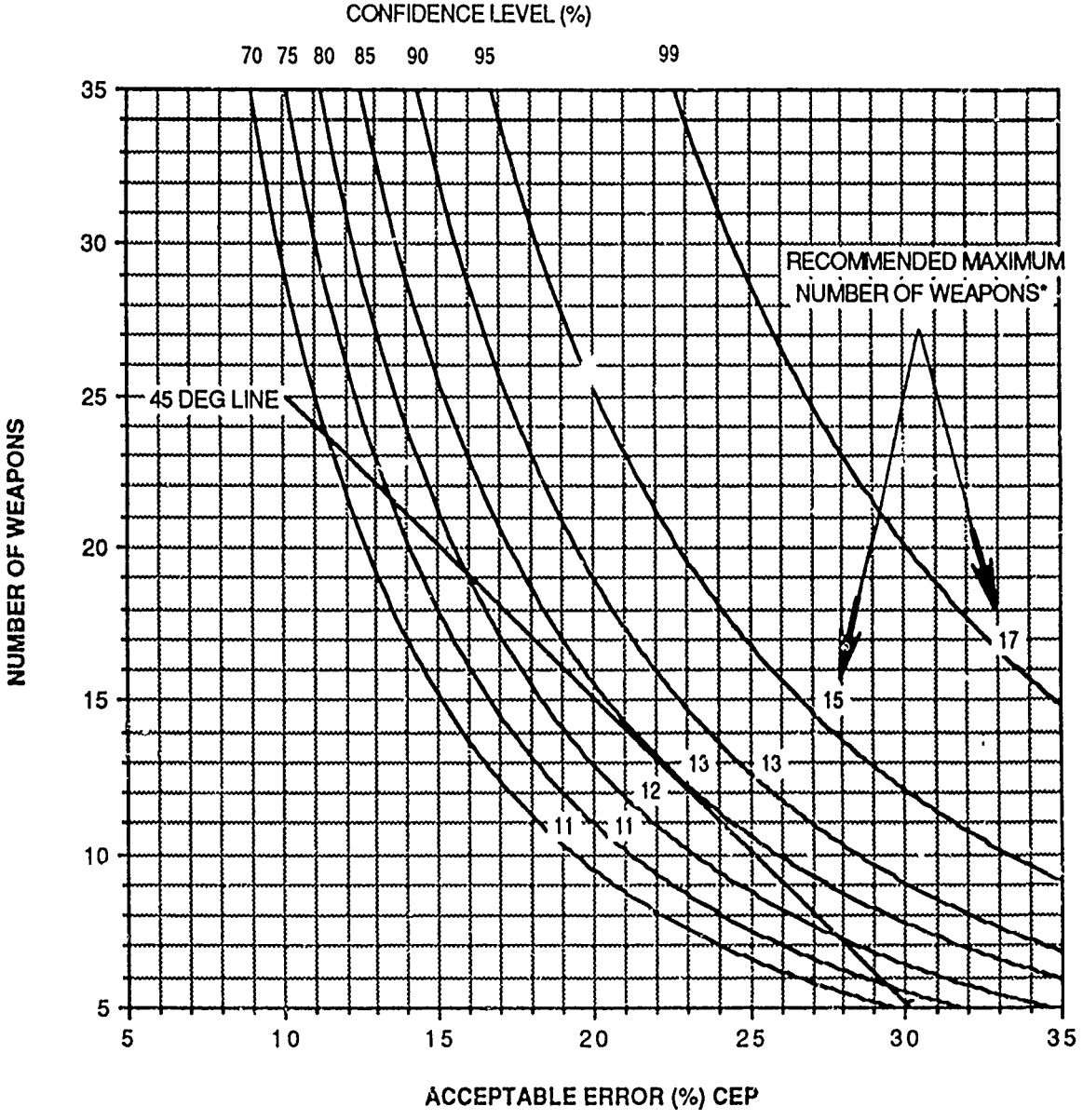

*NOTE: MAXIMUM NUMBER OF WEAPONS: EACH WEAPON DROPPED UP TO THE RECOMMENDED MAXIMUM NUMBER OF WEAPONS RESULTS IN AT LEAST A ONE PERCENT IMPROVEMENT IN ACCEPTABLE ERROR IN CEP. THE RECOMMENDED MAXIMUM NUMBER OF WEAPONS IS DEFINED AT THE TANGENTIAL POINT OF THE 45 DEG LINE AND THE APPROPRIATE CONFIDENCE LEVEL CURVE.

FIGURE 2 RECOMMENDED MAXIMUM NUMBER OF WEAPONS

TABLE 2

BIAS CRITERIA

	# WEAPONS SHORT OR LONG (WHICH EVER IS LEAST)												
N	0	1	2	3	4	5	6	7	8	9	10	11	12
5	031	188	500										
6	016	109	344	656									
7	008	062	227	500									
8	004	035	145	363	637								
9	002	020	090	254	500								
10	001	011	055	172	377	623							
11		006	033	113	274	500							
12		003	019	073	194	387	613						
13		002	011	046	133	291	500						
14		001	006	029	090	212	395	605					
15			004	018	059	151	304	500					
16			002	011	038	105	227	402	598				
17			001	006	025	072	166	315	500				
18			001	004	015	048	119	240	407	593			
19				002	010	032	084	180	324	500			
20				001	006	021	058	132	252	412	588		
21				001	004	013	039	095	192	332	500		
22					002	008	026	067	143	262	416	584	
23					001	005	017	047	105	202	339	500	
24					001	003	011	032	076	154	271	419	581
25						002	007	022	054	115	212	345	500

DIVIDE BY 1000 FOR PROBABILITY

DIVIDE BY 10 FOR PERCENT PROBABILITY

Notes:

1. This chart is based on a binomial distribution

$n/i=o\sum (N!/(N-n)!n!)p^{n}(1-p)^{N-n}$ where p = 0.5 because the weapon is either short or long, N = number of weapons in the sample, and n = number of weapons short or long, which ever is least.

2. Those weapon combinations that fall to the right of the solid line pass the bias test. Assuming that the weapon delivery system is perfect, there is a 50/50 percent chance of a weapon being long/short. Those combinations to the right of the line will occur 90 percent of the time with a perfect weapon delivery system and those combinations to the left will occur only 10 percent of the time. Thus, if the weapon results fall to the left of the line there is most likely something wrong with the aircraft or weapon delivery system.

SEPARATIONS EFFECTS CURVE
F-16/CBU-58

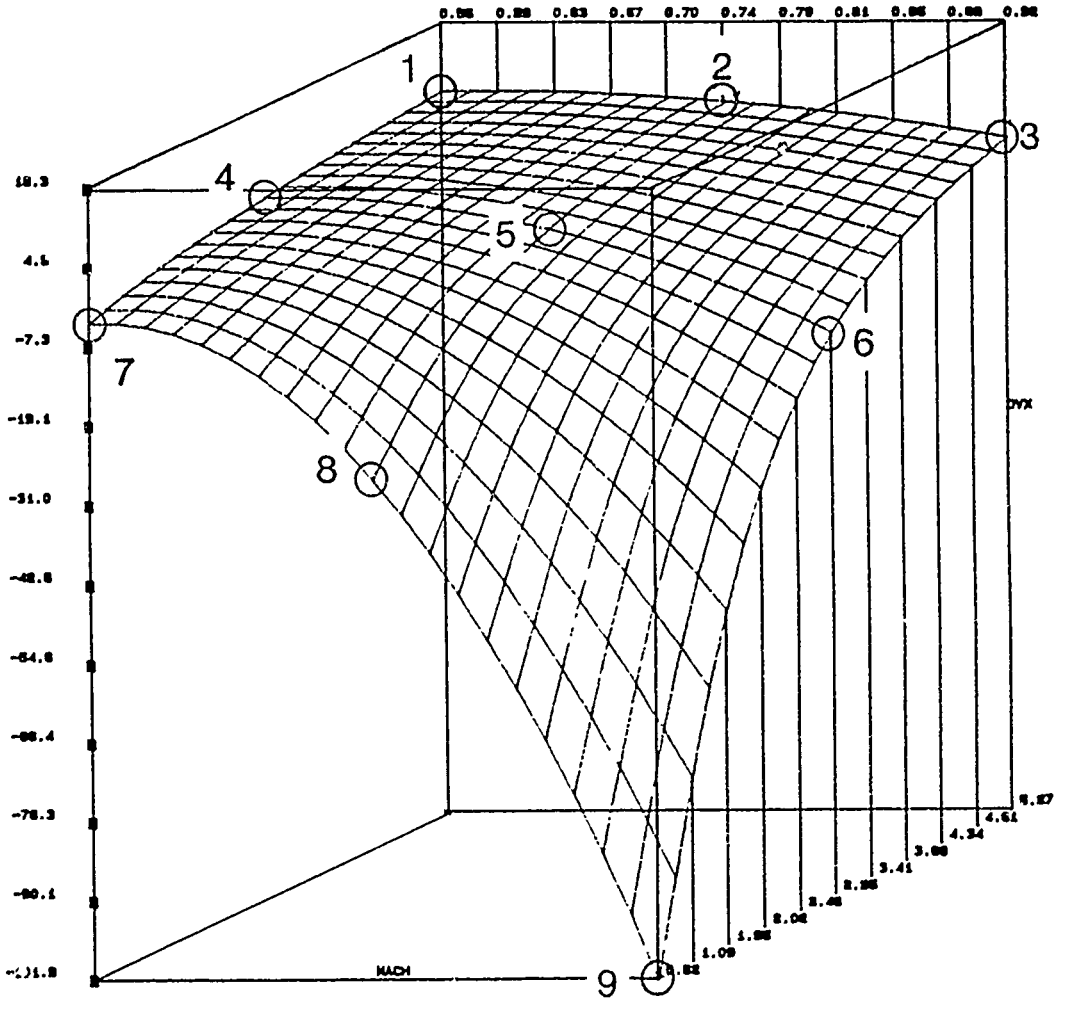

Figure 3 Separation Effects Curve Example

TABLE 3 SEPARATION EFFECTS MATRIX

1 LOW AIRSPEED HIGH G	2 MEDIUM AIRSPEED HIGH G	3 HIGH AIRSPEED HIGH G
4 LOW AIRSPEED MEDIUM G	5 MEDIUM AIRSPEED MEDIUM G	6 HIGH AIRSPEED MEDIUM G
7 LOW AIRSPEED LOW G	8 MEDIUM AIRSPEED LOW G	9 HIGH AIRSPEED LOW G

Note: The numbers in the upper right hand corner of each square corresponds to the numbers on Figure 3.

CAPTAIN DAVID SMITH

Captain Smith is assigned to the Air Force SEEK EAGLE Office (AFSEO), Air Force Systems Command, at Eglin Air Force Base. He is responsible for integrating, directing, and funding the analytical technology improvements currently being pursued by the SEEK EAGLE Office for the store certification process. He is also responsible for the development and standardization of the ballistic accuracy verification process.

Captain Smith received a bachelor of science degree in aeronautical engineering from the University of Illinois in 1984. His initial assignment was to the 6520 Test Group, flight dynamics branch, at Edwards AFB. He was assigned to the Advanced Cruise Missile Combined Test Force from June 84 to April 86 as a project engineer and then to the F-16 Combined Test Force until January 89 as a project manager/engineer. He then moved to the AFSEO at Eglin AFB, where he remains today.

THIS PAGE INTENTIONALLY LEFT BLANK

BALLISTIC DISPERSIONS

by Jürgen A. Lang
Messerschmidt-Bölkow-Blohm GmbH

Summary

This paper covers the tolerances of bomb ballistics. It is concentrated mainly on system aspects and statistical deviations caused by aircraft instrumentation data recording. A comparison of the individual tolerances show, that the main attention should be focused on air density corrections, target fixing accuracy and system time delay when shooting for improved ballistic performance of combat aircraft.

BALLISTIC DISPERSIONS

MBB Deutsche Aerospace

Table of Contents

BALLISTIC DISPERSIONS

MBB Deutsche Aerospace

1 Introduction

The success of bomb attacks by an aircraft depends mainly on the distance between the obtained impact point and the target point. To get a better accuracy, one can use guided bombs or one can try to generate a better model to calculate the flightpaths of bombs. The subject of this paper will be an investigation of the accuracy of ballistic calculations for freefall bombs and cluster bombs using an automatic mode of the aircraft attack computer.

The deviations of a flightpath predicted in a model compared to the real flightpath of a bomb are affected by

1) the calculation-algorithm,

2) the deviations of the values of measured flight data from their exact values (different initial conditions at release),

3) the initial conditions, which are not taken into account for release computations (e.g. Rolling, pitching, yawing, air density)

4) the system delay times,

5) the differences of altitude above ground and altitude above target, depending on aircraft sensors to be used

6) the bomb interference at ripple release or salvo, e.g. bomb to bomb interaction

7) the wind effects

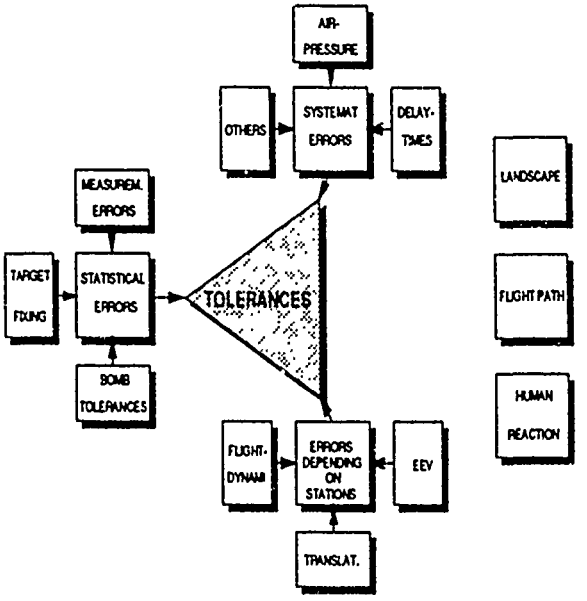

Figure 1: texture of the analysis

The paper is concentrated mainly on system aspects and statistical deviations caused by aircraft instrumentation data recording. Detailed aerodynamic flow and interference effects as well as deviations caused by wind effects are not dealt with.

2 Calculation Methods

In order to calculate ballistics a mass-point model can be used. In such a model it is assumed, that the bomb is a mass-point with the relevant drag of the bomb. Rotations of bomb and other aerodynamic effects like bomb lift and bomb pitching moments are not included.

The ballistic equations for mass-points cannot be solved analytically.

$$v \cdot \frac{dv}{ds} = -D - g \cdot \sin\theta$$

$$v^2 \cdot \frac{d\theta}{ds} = -g \cdot \cos\theta$$

v ... velocity
s ... length of trajectory
D ... drag
g ... acceleration of gravity
θ ... dive angle of bomb

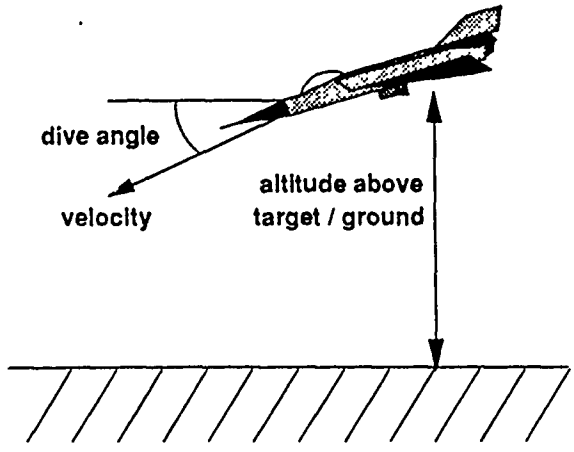

Figure 2: to define the variables

It is necessary to use a numerical method to integrat. these equations. The well-known fourth-order Runge-Kutta-procedure is such a method, which evaluates the derivative of a function four times in each step (initial point, two middle-points, end-point) to calculate the function value at the end of the step. The inaccuracy of the function value caused by the Runge-Kutta-algorithm at a Δy(a) depends on the step-width Δt (t: time) of integration and can be calculated as follows:

$$\Delta y(a,\Delta t) \approx \frac{Y_{Runge-Kutta}(a,\Delta t) - Y_{Runge-Kutta}(a,2\cdot\Delta t)}{2^5 - 1}$$

$Y_{Runge\text{-}Kutta}$ is the value calculated by the Runge-Kutta-procedure.

This numerical error can be limited by using a small step-width. An error of less then 0.1% can be obtained with a step-width of about one millisecond.

Unfortunately the Runge-Kutta-procedure takes a lot of calculation time. In addition this calculation time changes for different release conditions because it depends on them. Computers in todays aircraft cannot solve this time problem (e.g. no parallel processing capability).

This is the reason for using a different model to calculate the bomb's range and time of flight: one uses an analytical equation with some polynomial fitting of the parameters, which are generated from the results of Runge-Kutta-calculations. The parameters are optimized by using the least-square-method in a region around predefined values of velocity, altitude and dive angle.

The disadvantage of this method is a certain inaccuracy of the calculations at initial conditions far away from the optimum release requirement. But it is possible to get relatively exact results under usual bombing conditions.

In addition it needs much less time to calculate the bomb's range and its time of flight than the Runge-Kutta-procedure.

The accuracy of this approximation could increase with the number of the fit parameters. But the calculation time is also increasing with the number of the parameters. It is always necessary to find a compromise between ballistic accuracy and realtime requirement.

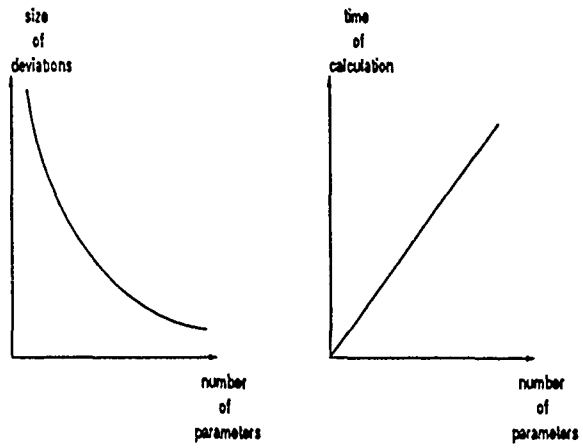

Figure 3: possible behaviour of a calculation procedure under optimal conditions

In the previous figure a possible behaviour of a calculation procedure is shown. This behaviour is a favourable case. Worse cases are possible too: rapidly increasing time of calculation or unsteady size of deviation.

3 Statistical Deviations

3.1 A/C Flight Data

The measurement of the flight data of the release conditions is not exact. There will always be statistical deviations from the exact values, as for every measurement and this cause deviations of the bomb's flight calculated by the Runge-Kutta-proc

The initial aircraft (and bomb) data ... for the ballistic calculation are as follo...
true airspeed: v_{TR}
altitude above target/grou...
dive angle: $\theta_{aircraft}$
angle of attack: α

In modern aircraft the scatt... measured data is small. Under ... conditions less then 2% for true airspeed ... altitude (using a Radar altimeter) and less then 10% for the angles.

A fifth factor influencing the mass-point ballistics is a value called "Equivalent Ejection Velocity" (EEV), which describes both the ejection process (ERU characteristics, aircraft structure effects) of the bomb and the release disturbance between the aircraft and the bomb after the release (aerodynamic interference). This value can be derived from flight testing or mathematical models applied for store separation. It depends mainly on the ERU type, the aircraft type, the bomb type, the release station and the true airspeed. In addition under real flight

conditions the EEV is changing as a function of the flight manoeuvre, the temperature dependence of cartridges and the changes of aerodynamic interference as a function of the density of air. It may scatter too, as a result of bomb installation tolerances and changing cartridge characteristics for the different lots.

The scattering of the EEV is in the order of 25%.

3.2 Bomb Tolerances

The bomb's mass and its drag may differ for different bombs of the same type. The tolerances used in these analysis are given by producer. These tolerances have a negligible influence on range and time of flight. An estimation shows an error of less then 0.1% in range. In reality higher tolerances of bomb's mass and drag were observed.

In addition fusing type, fusing location and lanyards arrangement are items, which must be taken into account for an analysis of a individual bomb configuration.

Another problem are the observed instabilities of some bomb (e.g. MK80 series), which may also influence the overall ballistic accuracy (changing drag, aerodynamics, Coriolis-effect).

3.3 Aircraft Behaviour

Unforeseen and statistical rolling, yawing and pitching of the aircraft changes the release conditions. It changes both the release position of bomb because of deviating roll-, pitch- and yaw-angles and the release-velocity because of the angular frequencies.

The influence of the statistical deviations from the required angles on range and time of flight are negligible (less then 0.1% in range).

On the other side the additional velocities in every direction caused by unforeseen angular frequencies are not negligible for the calculation of range. The influence of this effect depends on the distance between release station and roll-, yaw- or pitch-axis.

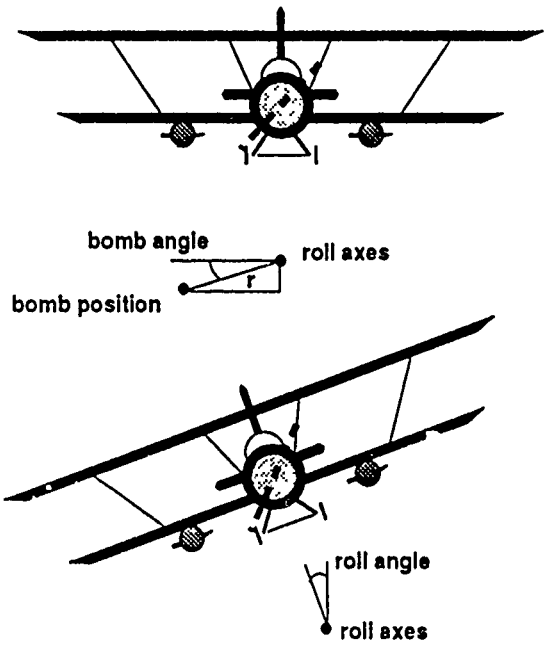

Figure 4: rolling aircraft

The additional release velocities caused by rolling can be calculated as follows:
lateral (y-direction):

$$v_y = \omega \cdot r \cdot \sin(\phi + \delta)$$

downwards (z-direction):

$$v_z = \omega \cdot r \cdot \cos(\phi + \delta)$$

with
v ... velocity
ω ... angular velocity of aircraft
r ... distance bomb - roll-axis
ϕ ... roll angle
δ ... bomb angle

In the same way the equations for yawing and pitching can be built up.

These additional release velocities must be added to the velocity (true airspeed) of the aircraft at the moment of bomb release. They cause both deviations in range and lateral displacement.

3.4 Target Fixing

To hit a target its position relative to the aircraft must be known. Consequentially it's necessary to measure the coordinates of target relative to aircraft.

The accuracy of this measurement depends on the quality of the sensors and the mathematical model used for processing of data obtained. Depending on the sensors and the attack mode, there always remains a statistical scattering, which is the reason for deviations in target fixing. The reasons for this scattering are the measurement errors of the sensors. An improvement of the sensors could reduce these deviations.

3.5 Methods to Determine The Overall Statistical Failure

In this investigation it is assumed that the statistical deviations can be described by the Gaussian distribution. The interesting question is, how strong does any of them influence the bomb range and the time of

flight. For analytical calculations this problem is simply solved by the error propagation formula:

$$\Delta f(x,y,z)=\sqrt{\left(\frac{\partial f}{\partial x}\right)^2\cdot\Delta x^2+\left(\frac{\partial f}{\partial y}\right)^2\cdot\Delta y^2+\left(\frac{\partial f}{\partial z}\right)^2\cdot\Delta z^2}$$

For equations, which only can be solved numerically, like the ballistic equations, this method cannot be used. An analytical function f(x,y,z) isn't known. To get the overall error and the dependence of the error from changing initial conditions in this case, it's necessary to calculate the deviations of the range for different initial conditions.

To get the assumed distribution one can use the Monte-Carlo method. This method generates the statistical errors of the initial conditions as input for the calculations of range. The distribution of the impact points on ground is a result of all these calculations. The accuracy of the distribution increases with an increasing number of calculations. The disadvantage of this method is the long computing time, which is necessary to get a accurate distribution of the impact points on ground.

The method used here, which needs less computing time is to calculate the range for the standard deviation of each initial parameter. The result is an ellipsoid, which includes the impact-points of bomb with a probability of 0.68 for each parameter. Now it can be assumed, that the distribution of impact-points is nearly Gaussian (the areas are nearly symmetric to the impact-point calculated for exact initial conditions, like it is expected for a Gaussian distribution). Consequential the variance of each area can be added to get whole variance (the variance is the square of the standard deviation).

3.6 Comparison of The Statistical Deviations

In the following figure the influence of the different statistical errors on the overall statistical deviation is shown for different heights and velocities. The deviations relative to the bomb range are shown:

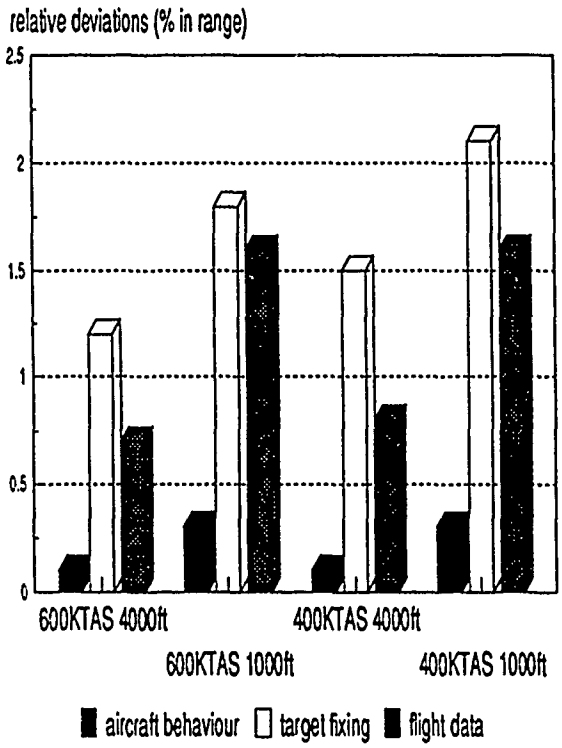

Figure 5: comparison of the statistical deviations

The main errors are caused by the target fixing. For lower altitudes flight data measurement errors become more dominant. The errors caused by bomb tolerances are negligible and not shown in the figure. They are about 0.1% in range. Changes of angle of attack caused by different aircraft mass and pilot's failure are not include .

The total statistical standard deviation in range is about 5%. The total standard deviation σ_{tot} is the square-root of the sum of the single standard deviations' σ square:

$$\sigma_{tot} = \sqrt{\sum_i \sigma_i^2}$$

The deviations in range caused by the errors of true airspeed, altitude above ground, dive angle, angle of attack an EEV are summed up under "flight data", like it is described above (square root of the sum of the variances). The following table shows some examples to give an impression of the order of the deviations in range.

statistical errors (percent deviation in range)	velocity 600KT AS altitude 4000ft	velocity 600KT AS altitude 1000ft	velocity 400KT AS altitude 4000ft	velocity 400KT AS altitude 1000ft
true airspeed	0.5	0.6	0.5	0.6
altitude above ground	0.1	0.4	0.1	0.5
dive angle	0.4	1.2	0.4	1.0
angle of attack	<0.1	<0.1	0.1	<0.1
EEV	0.2	0.7	0.4	0.9

4 Systematical Errors

4.1 Air Density

The ballistic flight-path is influenced by the air density ρ. Usually it is assumed that this density only depends on altitude above sea level h. It can be approximated as follows:

$$\rho = \rho_{sea} \cdot \left(1 - \frac{h}{41900}\right)^4$$

with h in meter and the air density ρ_{sea} at sea level.

Other approximation formulas for altitude dependence of density of air show small deviations up to 1200m (less then 0.1%, increasing with increasing altitude).

But air density also depends on temperature T and air pressure p, which are changing with weather. Looking at air as a ideal gas and assuming an isentropic process one can write for the air density at sea level:

$$\rho_{sea} = \rho_0 \cdot \left(\frac{p}{p_0}\right)^{\frac{1}{\gamma}}$$

and

$$\rho_{sea} = \rho_0 \cdot \left(\frac{T}{T_0}\right)^{\frac{1}{\gamma - 1}}$$

with T_0= 288.16K, p_0= 1013.25hPa, ρ_0= 1.225kg/m^3 at sea level and the isentropic exponent γ.

Consequential ρ at sea level varies usually between 1.0kg/m^3 and 1.5kg/m^3.

Higher density of air shortens the bomb range, lower one causes a longer range. The size of this effect depends on time of flight. For a time of flight of about 20s one can get a deviation in range of about 15% (both at 1.5kg/m^3 and 1.0kg/m^3).

The differences in air density could be included by calculation. A proposal to do this, is to measure the air pressure and the temperature at aircraft altitude. Then the density of air at sea level can be calculated. In the board computer some sets of parameters for the analytical equations should be stored. Every set should be valid for a little range of density of air. The relevant set could be chosen some seconds before the bomb release calculations are started. So that the realtime requirement can still be fulfilled.

4.2 Different Release Stations

In most cases bomb ballistics is calculated using an average value for the EEV, which covers all the different aircraft release-stations. The deviations in range caused by different EEV's are less then 0.5% compared with the range calculated for an average-value of EEV. The differences of EEV on the different stations are mainly caused by the different stiffness of aircraft structure and by the different aerodynamic flow around the different release stations.

The parallaxe corrections, which are a function of the different release positions of bomb, have average values too. The release positions at an aircraft differ only in the order of some feet. For differences parallel to the ground there will be a translation with the same value. Differences in upwards or downwards direction have little influence on bomb range (less then 0.5%). This influence is increasing when altitude is decreasing.

4.3 Coriolis Force

The rotation of the earth also causes deviations. They depend on the velocity in north-south- or south-north-direction. It could be shown, that these deviations are negligible for usual release conditions: they effect deviations of less then 0.1% in range.

5 System Delay

5.1 Causes

"System delay" means the difference between the time the bomb should be released and the time it is released. In general the delay times are generated by computing, data transfer and ejection delay.

The following figure shows a simplified hardware configuration which could be used for bomb release.

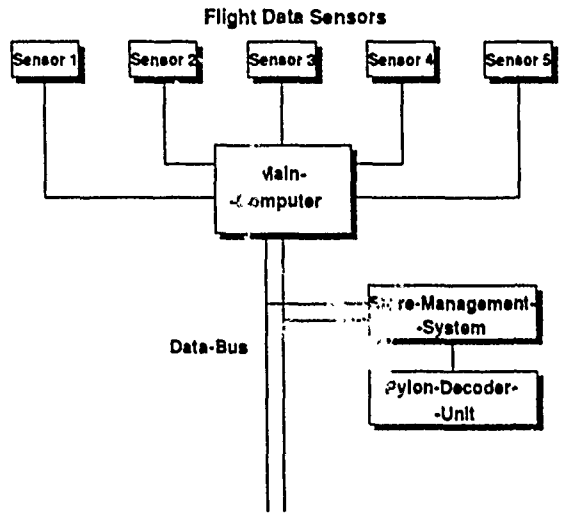

Figure 6: simplified hardware configuration for bomb release

The sensors provide flight data (angles, velocity, altitude,...) and target informations to the attack computer (AC) which calculates the impact point of the selected bomb. At the moment when the calculated impact point meets the target point, the board-computer gives a signal to the store management system (SMS) via the relevant bus systems. The SMS sends a signal to the pylon-decoder-unit (PDU), which sends a fusing signal to the cartridge. Now the pistons' ejection begins. The bomb will get its expected ejection velocity by piston stroke.

Each of these actions needs time. The sum of these times is the system equipment delay. The following figure gives an impression of this

delay time. The exact values are scattering and some of them (fusing, ERU piston behaviour) depend on external conditions.

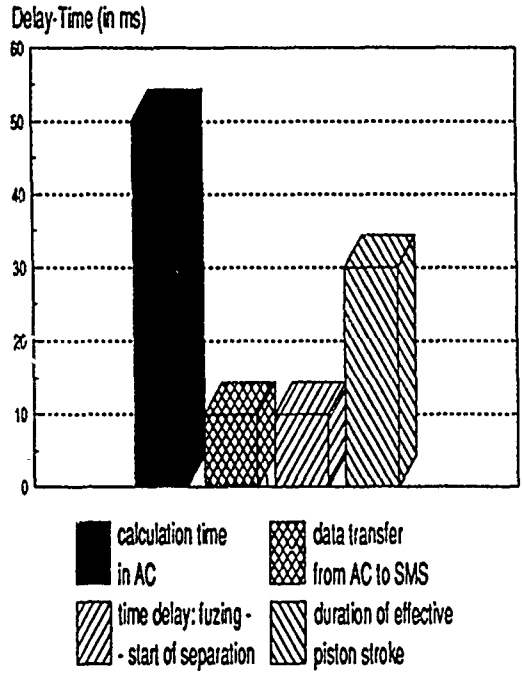

Figure 7: comparison of delay times

The time necessary for the ballistic calculation depends on the algorithm used for the solution of the ballistic equations (see also chapter 2), on the type of A/C attack computer and on the sharing concept of attack computer capability. It can be approximated by the following equation:

$$t_{calculation} = C_{algorithm} \cdot R \cdot \frac{100}{A_{ballistic}}$$

with the time necessary for calculation $t_{calculation}$, the complexity of algorithm $C_{algorithm}$ (number of operations necessary for calculations) and the number of operations which the computer perform do per second R. $A_{ballistic}$ is the percentage of CPU-time, the ballistic calculation gets. The time is in the order of 50ms.

The time necessary for data transfer via data bus system $t_{transfer}$ depends on the state of the bus system at the moment when the release signal should be sent from MC to SMS. In worst case the data transfer needs a whole cycle time (about 20ms) of bus system. The average delay is about 10ms (half cycle time).

The SMS has to execute the ejection algorithm. The execution time can be estimated in the same way as the calculation time of attack computer. Then it sends the fire signal to the pylon-decoder-unit. The total time necessary for these actions is $t_{ejection}$ (about 10ms).

The pistons need some time to accelerate the bomb up to the release velocity, which is a part of the ballistic calculations as a part of the EEV. This time t_{stroke} depends on stroke length, bomb mass, kind of propellants, release manoeuvre and environmental conditions (mainly temperature). The environmental conditions influence the effectiveness of cartridges. The acceleration time is in the order of 30ms.

The total delay time t_D can be calculated as follows:

$$t_D = t_{calculation} + t_{transfer} + t_{ejection} + t_{stroke}$$

It is in the order of some 100ms. The exact value depends on the parameters mentioned above.

5.2 Delay Effects

During the delay time the aircraft will change its position because of its velocity (true airspeed). Consequentially the impact point will change. In addition the aircraft could change its flight path.

When wether dive angle, altitude nor velocity are changed during delay time the deviation of range in flight-direction can be calculated as follows:

$$\Delta x = v_x \cdot t_{delay}$$

with

Δx .... deviation

v_x ..... velocity in x-direction

t_{delay} ... delay time

If the true airspeed is changing, the equation would be as follows:

$$\Delta x = \int_{t_{release} - t_{delay}}^{t_{release}} v_x(t)dt$$

with

$t_{release}$ ... time of real bomb release

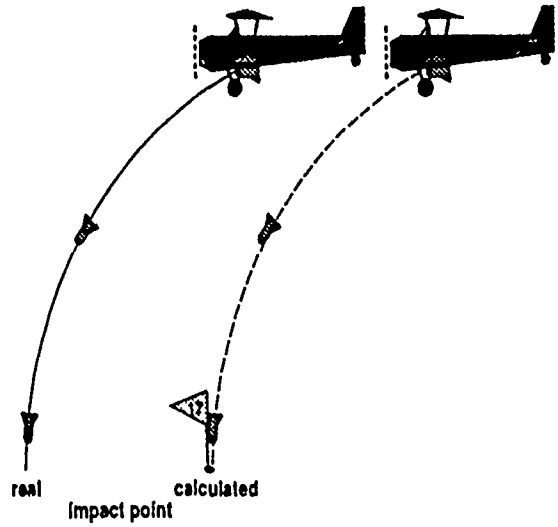

Figure 8: deviation of impact point caused by delay

Changes in aircraft flight-path can cause a total different bomb flight-path. The ballistic calculations for different altitudes, dive angles and velocities can give an impression of the deviations caused by changes of flight-path. These deviations are only limited by aircraft performance and duration of delay.

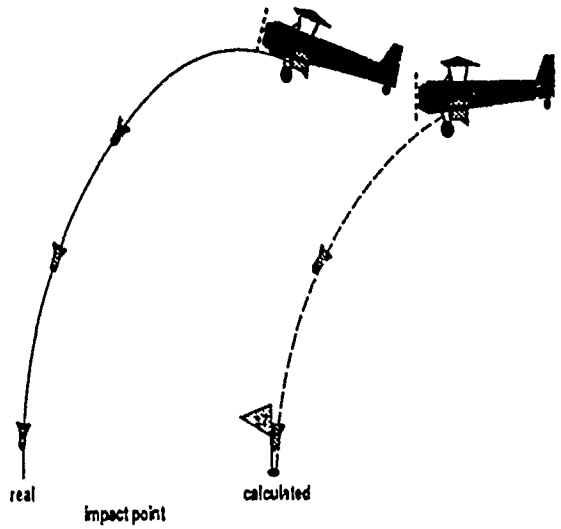

Figure 9: deviation of impact point caused by delay and change of flight path during delay time

The resulting errors caused by delay time can be minimized by including a "delay range" into the attack computer calculations. But there always will remain an error, because the delay-time is scattering and changes of velocity or flight-path during this time are not predictable.

5.3 Pilots Reaction Time

If a manual attack-mode is used, the delay would be much higher, as a result of pilot's reaction time and transfer time from pilot's release button to MC. This additional delay may be in the order of 1s. Consequentially the deviations in range would be higher and the probability of success would decrease.

In this case a "pilot delay-range" can be implementated into ballistic calculations too. But there would remain a big scattering because the reaction time depends on the person and his condition.

6 Influence of Landscape

If the landscape is not flat, some additional deviations would become possible:

a) Hills in flight-path of the bomb could stop the bomb before it reaches the target.

b) If an attack mode is used, which only measures the altitude above ground, then the altitude above target could differ from this value. A difference of about 3% of altitude causes deviations of 1% or more.

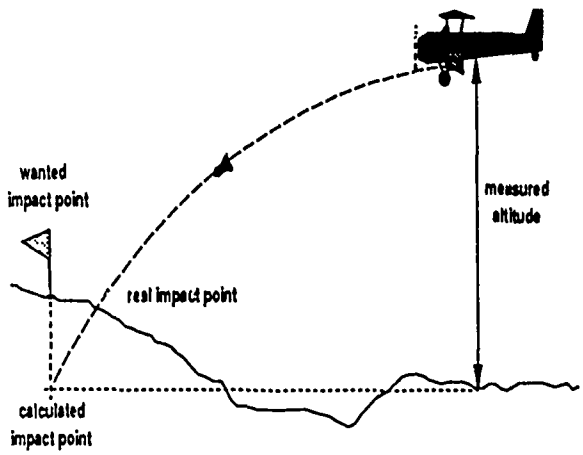

Figure 10: influence of landscape

An similar error to that in b) can be obtained by using a radar altimeter, which sends its signal not rectangular to ground (e.g. because of a bankangle)

7 Ripple Release and Salvo

At ripple release some additional deviations appear:

a) The selected release time interval between two releases scatters statistically. The scattering is in the order of 10ms. In a straight and level attack such a deviation in time would cause a deviation in range of about 10ft at a velocity of 600KTAS.

b) The statistical measurement error of velocity Δv also causes deviations in range Δr, which depends on the release time interval t_{ripple} as follows: $\Delta r = \Delta v \cdot t_{ripple}$

Figure 11 shows the expected ground pattern at a ripple release of seven cluster bombs (dark grey) and its deviation area (light grey) for a straight and level bomb release at 400KTAS, 1000ft altitude and a ripple interval of 540ms.

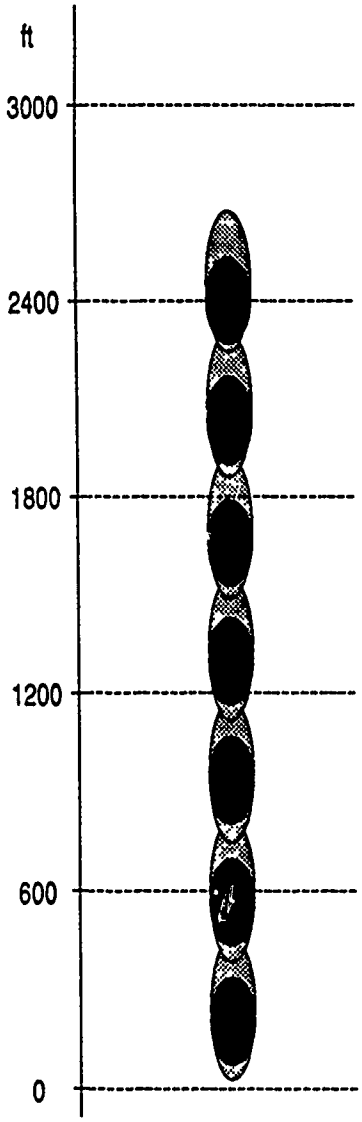

Figure 11: expected ground pattern length (dark grey) of a ripple release of seven cluster bombs and its tolerances (light grey)

The tolerances of the ground pattern dimensions of the cluster bomb are not shown in this figure.

At salvo the same kind of errors could be obtained, because a minimum release interval of about 10ms (depending on bomb type) makes the salvo comparable to a ripple release. The minimum release interval is necessary because without it the salvo may demolish the aircraft structure.

8 Conclusion

The most important deviations in ballistics as dealt in this paper are caused by air density (differences caused by weather conditions), target fixing and system time delay. For low altitudes the statistical errors of the dive angle become important too.

The following tolerances are negligible: the aircraft behaviour, the bomb tolerances, the different release stations, the Coriolis force and the statistical scattering of angle of attack.

BALLISTIC DISPERSIONS

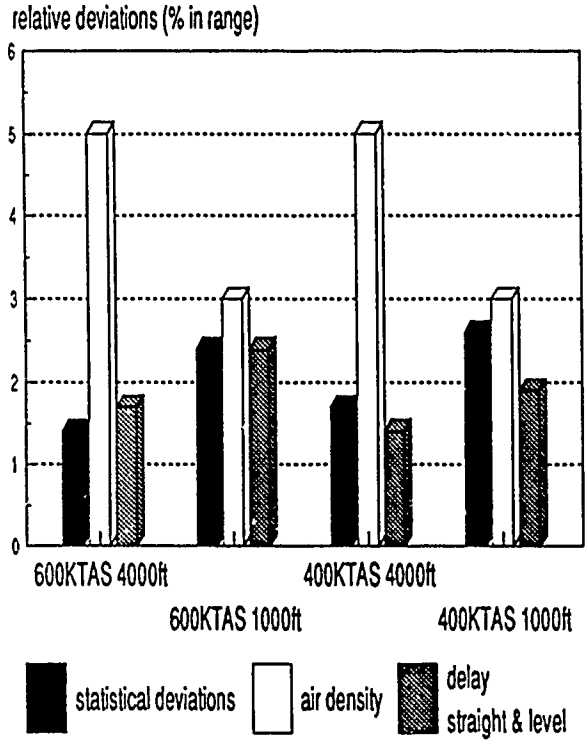

Figure 12: comparison of typical deviations

The ballistics improvement should be concentrated on target fixing, air density, delay times, bomb to bomb interaction and bomb to aircraft interaction.

Autobiography

-	Name	Jürgen A. Lang
-	Born	1963 in Rheinfelden (Baden / Germany)
-	1982-1983	joining the German Army
-	1983-1989	study of physics at the Universität Stuttgart main interests: - semiconductor physics - superconductor physics - theory of relativity - quantum theory
-	since 1989	system engineer at the Military Aircraft Division of the Messerschmitt-Bölkow-Blohm GmbH in Ottobrunn near Munich engaged in - system simulation - software testing

CLEARED FOR PUBLIC RELEASE

PROCESSING STORE SEPARATION CLEARANCES WITH THE MBB-STORE SEPARATION PROGRAM *

by
Ronald M. Deslandes
MBB GmbH, Deutsche Aerospace
Postfach 801160, FE121
D-8000 Munich 80, Germany

INTRODUCTION

The MBB Store Separation Program is a code,which in a most general form has been designed in order to determine store separation characteristics from a fighter aircraft and to establish the clearance declaration within the required zone of operation.

Since 1978 more than 30 different separation projects have been successfully processed with this tool in order to demonstrate feasibility of separation, to specify necessary ejection forces,rail-lengths or piston strokes or even control characteristics for separation autopilots.

Presently the SSP is an approved tool in use for the qualification of the store clearances required for the GE military aircraft.

The topic of this paper is to review the basic concepts of the SSP, emphasizing its versatility with respect to the adaption to several complex numerical tools such as Euler codes. After a description of the main ideas realized in this flow angularity technique some numerical results and trajectories computed with aerodynamic inputs preprocessed at different levels of complexity will be shown in order to underline the necessity of the higher order theories presently used.

In this part. it will be also demonstrated that a safety analysis also requests special facilities in order to accurately analyse the computed motions. Therefore, a typical case will be shown in which the geometrical clearance between the separating store and adjacent components of the aircraft can be no more obviously recognized.

In the second part the clearance philosophy is outlined. Here, the dependency between predictions, validation by flight test and level of accuracy achievable by upgrades is accentuated and demonstrated by current project results.

* Cleared for Public Release

Finally the completeness of the chosen approach will be underlined by the example of a missile with active autopilot, comparing analytical results with flight test data from telemetry.

PROGRAM CONCEPTS

In general, store separation predictions require a combination of two main engineering tasks:

- Flight mechanics to describe the store and aircraft motion
- Aerodynamics representing the interferences on the store during separation

Within a computation both tasks have to be consecutively called up within a loop, in which each sweep represents a time-step of the trajectory and which is repeated until the specified total separation time is achieved. This general set-up, sketched in Fig. 1, is representative for all known computer codes even operating captive trajectory systems or running the very much complex "chimera codes".

In all of these programmes the flight mechanical equations are operated in similar formulations for six degrees of freedom with the standard quarternion equations for matching arbitrary non-linear rotations.

As far as the aerodynamic task is concerned, the flow angularity technique as used in the MBB code is splitted in a basic subsonic approach and a supersonic extension. The subsonic part consists in concatenating three main families of aerodynamic loads arising from the

- aircraft flowfield interferences
- dynamic effects (store motion and damping)
- reciprocal interferences.

Within supersonic cases these increments are completed by the non-linearities arising from:

- steady sonic shocks
- time-dependently moving shocks reflected on the separating store

The basic concept of this approach is sketched in Fig. 2. In the most general case the aircraft flowfield and the freeflight aerodynamics of the store are separately preprocessed by means of higher order time-marching Euler solvers.

In a second step the aerodynamic characteristics of the store are decomposed into sectional load gradients for different combinations of angles of attack and sideslip.

Ten years ago, during the 5th Aircraft Store Compatibility Symposium the same concept was presented using lower order linear panel methods.

During a trajectory calculation the velocity components resulting from the non-uniform flowfield around the aircraft, from the store translation and rotation are superposed to effective sectional flow angles. These angles of attack and sideslip are imposed to the load gradients of each store section and summed up to total store loads.

Within this representation aerodynamic damping effects are automatically captured by converting the store rotation into discrete sectional velocities.

However, the higher order effects have to be separately implemented by upgrading these trajectory loads with measured installed loads or with postprocessed time accurate Euler computations for discrete store positions.

For this purpose, the Euler equations are formulated for moving control volumes, which allow an accurate description of the dynamic effects of the store surface in motion. A detailed description of this theory is given in Ref. 1. Worked out into the divergence formulation, this set of equations can be written as shown in Fig. 3, where ρ, l, m, n and e correspond to the conservative variables of the specific flow properties such as density, momentum and total energy. The store velocity is represented by $\dot{x}$, $\dot{y}$ and $\dot{z}$.

Using this formulation in a suitable CFD code, it is possible to analyse the major part of nonlinear inviscid flow problems occuring during a launch situation. Even in cases of an extraction of a pilot escape module, boosted out of a cavity, this formulation has been applied successfully. The complexity of the flow computations for this cases are illustrated in Fig. 4 and 5, which show the extracted cabin of the European Shuttle HERMES in a post-launch position.

The robustness of the flux vector splitting algorithm is well demonstrated for this supersonic case at Ma=2., where also the booster plume has been represented blowing into the cavity with a local peak Mach-number of Ma=4.5. The complexity of this analysis was additionally increased by an aperture at the bottom of the cavity, which enables the plume to expend outside of the space plane, and therefore reduces the acceleration levels during the first moment of separation. The 3D-grids used within this feasibility study are shown in Fig. 6 and 7.

As far as interference was concerned,no wind tunnel results were available to validate the theoretical results. However, for the freeflight aerodynamics of the cabin several entries were performed up to Ma=6.

Fig. 8, 9 and 10 are showing a comparison between theory and experiment based on the entry at Ma=2. There, drag, lift and pitching moment are shown for angles of attack from -40° up to 30°. Throughout this range there is a good agreement between experiment and computation.

The trajectory shown in Fig. 11 was iteratively computed, following the above mentioned concept by using aerodynamic inputs such as:

- 35 x 6 preprocessed sectional coefficient to represent the freeflight aerodynamics and the damping terms
- the preprocessed space plane flowfield
- 3 sets of postprocessed post-launch positions.

The main target of this analysis was to demonstrate the safe separation of the cabin without exceeding the physiological limits of the pilots during the boosted phase. From this analysis, specifications for the nozzle deflection range, for the actuators and for the separation control system could be deduced within the required technical feasibility limits.

Considering a normal store integration project on a known aircraft with well defined launchers and ejectors, the essential clearance analysis to be performed is in general less exotic but still complex enough. Depending on the release characteristics, the local geometrical clearances are often reduced to a minimum. In such cases the clearance analysis affords not only completeness of the mathematical modelling, but also proper tools in order to accurately investigate the separation behaviour. Fig. 12 represents, for instance, the launch behaviour of a typical air to surface missile during a wind-up turn at 60° bank.

Without the complex mathematical representation of the missile motion on the rail, incorporating not only the physical constraints of the rail, but also the major characteristics of the hangers as well as their frictional properties, the separation behaviour would appear to be safe.

Taking all these effects into account and additionally representing all relevant geometrical lines of the aircraft inclusively launcher/adapter and rail the risk of a collision was detected between the upper left rudder of the missile and the launcher nose as shown in Fig. 13. Without such advanced 3D-graphical postprocessing facilities it would be nearly impossible to synthesize the store and aircraft motions simultaneously for this

type of non-trivial manoeuvring condition. An interpretation of the local geometrical clearances would then become marginal.

The collision occuring in this flight condition was initiated by a very strong release disturbance with respect to the roll rate. Using aerodynamic inputs generated by linear theory this collision would not be well represented due to an underprediction of the initial roll motion during the first 0.4 s, as shown in Fig. 14.

There the roll motion computed by panel methods is compared with the results generated by means of an Euler preprocessed data set. The oscillation of the roll rate is not realistic due to a mismatch of the cross coupling terms between lateral and longitudinal motion. In panel methods, these terms are evaluated by linear superposition of the sideslip and the angle of attack flow under the assumption of small disturbance theory, whereas such effects are non-linearily captured by the Euler equations. The very good quality of this approach is documented in Fig. 15 by the comparison between a flight tested roll rate and the SSP result based on Euler preprocessed aerodynamics. For the missile shown in this example nearly 80000 finite volume cells were used to evaluate the freeflight aerodynamics. A typical section of this grid is shown in Fig. 16. Normally, reasonable results would already be achievable with a total of 30000 cells.

Finally, Fig. 17 summarizes the options which enable the SSP to analyse separation under nearly arbitrary initial conditions, for any type of stores and taking into account any kind of additional items such as plume effects, active control modes and control surface deflections.

SSP CLEARANCE PROCESS

Following the above description the minimum data required to run a separation analysis data set consist of four main blocks:

- preprocessed freeflight aerodynamics in terms of sectional loads
- interference loads taken from wind tunnel measurements or preprocessed with Euler codes
- physical properties of the separation process such as rail dimensions, number of hook-off events, piston forces or rear hook release angles
- geometrical properties of the store and the aircraft.

With such a data base the separation behaviour of a store can be predicted involving all the options pre-installed to the SSP in a modular form, in order to define a pure theoretical clearance envelope. The qualification of this envelope is then achieved by flight test validation. Depending on the extension of the envelope on the number of carriage stations or the manoeuvring conditions to be cleared for separation, at least one or a minimum amount of test points are selected within the aircraft envelope.

If the store has been already qualified for safe separation with the same equipment on another aircraft, the validation can be achieved without further expensive flight test efforts by theoretical recomputations. If considerable differences are found between the flight tested and the computed trajectories the data base can be upgraded by sensitivity analysis and corrections of typical uncertainities such as:

- control surface misalignments
- store tolerances with respect to center of gravity position or moments of inertia
- aerodynamical damping derivatives
- interference-decay-factors if the flowfield option is not used or if the trajectory is processed iteratively in several steps
- ejection release unit asymmetries
- the accuracy of flight test data analysis if no telemetry is available.

The theoretically elaborated clearance is certified as soon as the agreement between experiments is stated to be acceptably good. Even in the case of divergencies in one or two dimensions, the validation statement will be accepted if the predictions are conservative, this means on the safe side or pessimistic as far as safety is concerned. Such a typical case is shown in Fig. 18, where the vertical displacement and the pitch angle of a drop launched missile are plotted versus time in comparison with flight test analysis results. In spite of the underpredicted pitch motion, the vertical displacement doesn't differ much. The computed pitch motion tends to indifferent values, whereas the pitch-down indicated by flight test is more favourable for safe separation.

A very good match is shown in Fig. 19 and 20, where the role rates and roll angles of a rail-launched missile are compared to flight test telemetry. During this firing case the roll-autopilot of the missile has been activated at about 0.4 s after motor ignition, in order to suppress the very strong roll disturbance during separation. With such a good validation of the theoretical result, as shown here at M=0.93 for the Tornado aircraft, the accuracy level is satisfying all safety aspects required to process the separation clearance even at corner points of the envelope.

CONCLUDING REMARKS

In general the quality of the predictions achievable with a store separation code is the key parameter which determines the total amount of required validation and qualification flight test points. In order to reduce these expensive experiments the main efforts performed in the last ten years on the SSP were dedicated to improve the evaluation of the aerodynamic effects during separation. Thereby, the change from potential theory to the Euler equations has realized a considerable gain in accuracy especially in the transonic and supersonic Mach number range. In addition to this a great part of nonlinearities, araising from reciprocal interference, from cross coupling terms and from unsteady effects, are now much better represented as in the past.

However, there are still some separation problems left which still cannot be perfectly matched within a flow angularity technique. Store separation out of a cavity as well as pivot hook releases as shown in Fig. 21, require more complex solutions as for instance provided by CHIMERA-type codes. A similar code is now under development at MBB.

REFERENCES

[1] A. Eberle et al.
Characteristic Flux Averaging Approach to the Solution of Euler's Equation.
VKI Lecture Series 1987-04 on Computational Fluid Dynamics, Belgium

[2] Th. Kühn et al.
Modelling and Analysis of the Separation of CEM Type B from Hermes
MBB-HERM-AN-001/1989

[3] M. Kraus et al.
Modelling and Analysis of the Separation of CEM Type A from Hermes
MBB-S-PUB-0396/1990

FIGURES

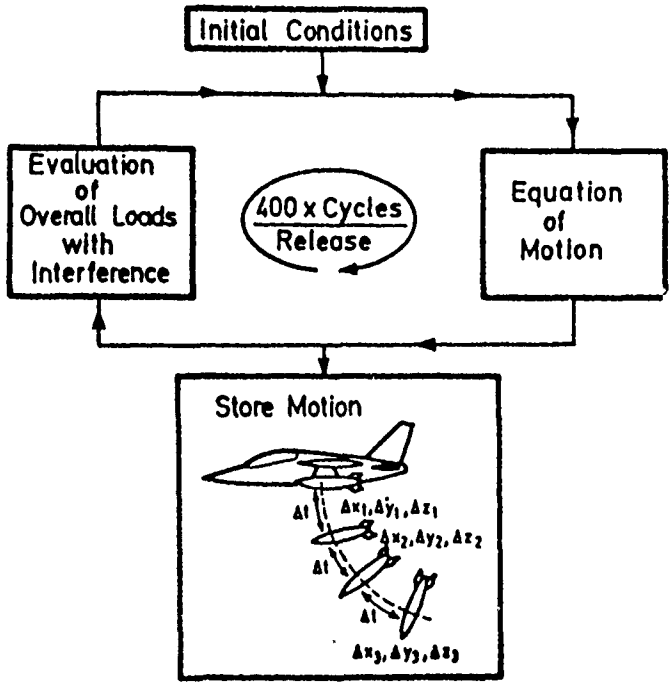

Fig. 1 Typical Program Design

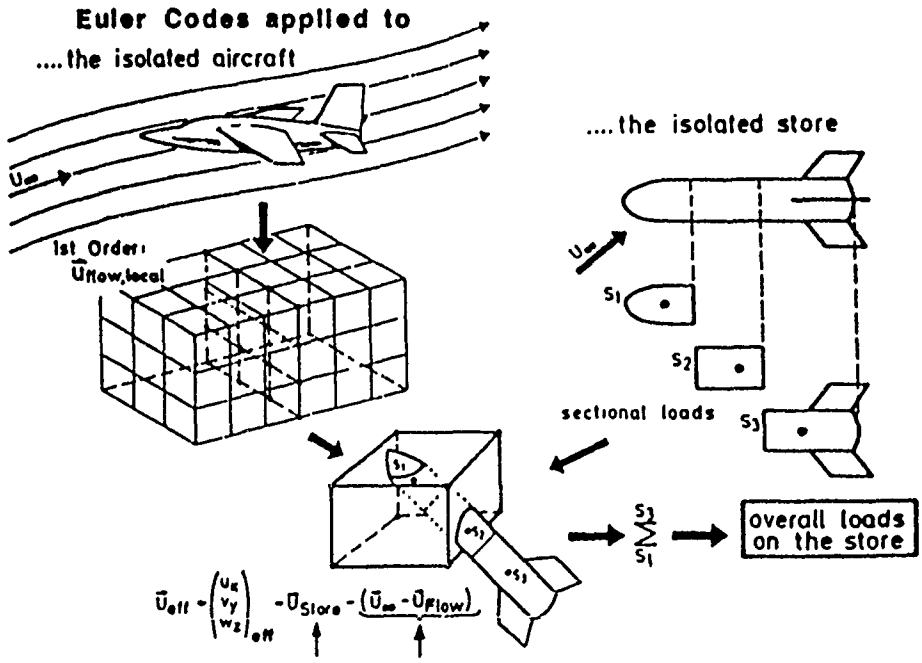

Fig. 2 Current Interference Concept (MBB-SSP)

$$\dot{\rho} + \rho(\dot{x}_x + \dot{y}_y + \dot{z}_z) + (l - \dot{x}\rho)_x + (m - \dot{y}\rho)_y + (n - \dot{z}\rho)_z = 0 ,$$

$$\dot{l} + l(\dot{x}_x + \dot{y}_y + \dot{z}_z) + [l(u-\dot{x})+p]_x + [l(v-\dot{y})]_y + [l(w-\dot{z})]_z = 0 ,$$

$$\dot{m} + m(\dot{x}_x + \dot{y}_y + \dot{z}_z) + [m(u-\dot{x})]_x + [m(v-\dot{y})+p]_y + [m(w-\dot{z})]_z = 0 ,$$

$$\dot{n} + n(\dot{x}_x + \dot{y}_y + \dot{z}_z) + [n(u-\dot{x})]_x + [n(v-\dot{y})]_y + [n(w-\dot{z})+p]_z = 0 ,$$

$$\dot{e} + e(\dot{x}_x + \dot{y}_y + \dot{z}_z) + [e(u-\dot{x})+pu]_x + [e(v-\dot{z})+pv]_y + [e(w-\dot{z})+pw]_z = 0$$

$$\frac{\dot{V}}{V} = \dot{x}_x + \dot{y}_y + \dot{z}_z \qquad V\dot{Q} + Q\cdot\dot{V} = (QV)^{\cdot}$$

$$(QV)^{\cdot} + V(E_{1x} + F_{1y} + G_{1z}) = 0 ,$$

Fig. 3 3D Flow Equations for Unsteady Moving Boundaries

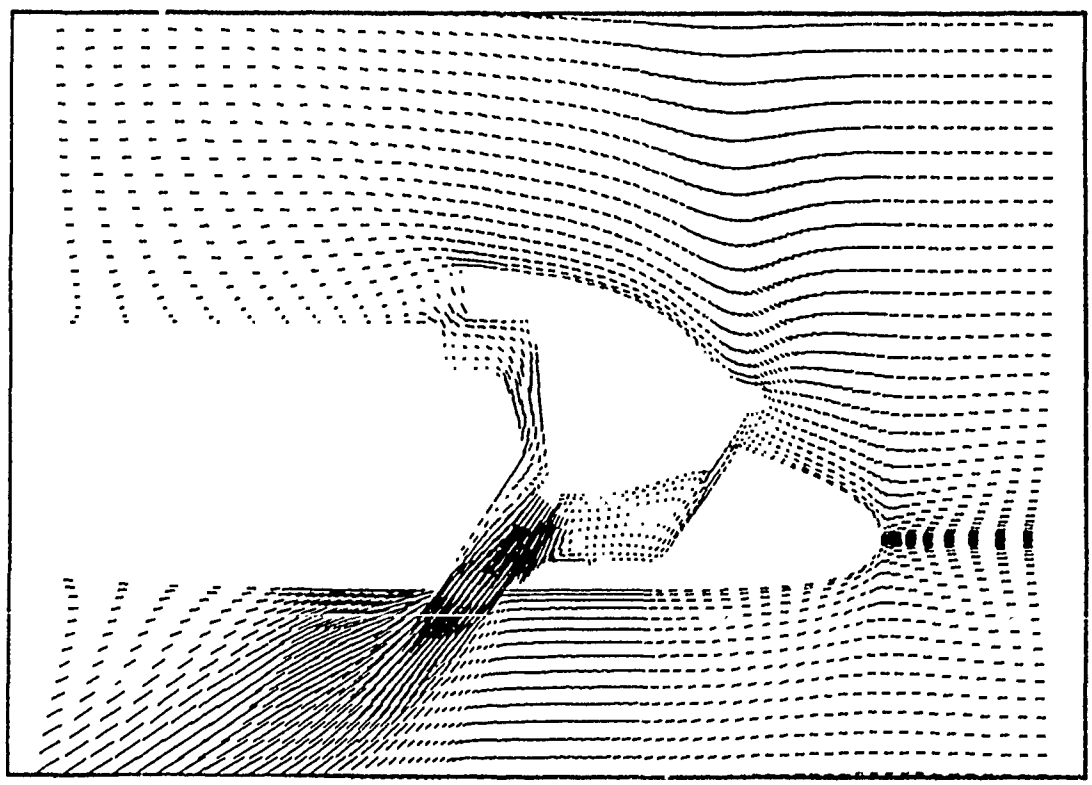

Fig.4 Velocityfield for Cem Separation at M=2.0

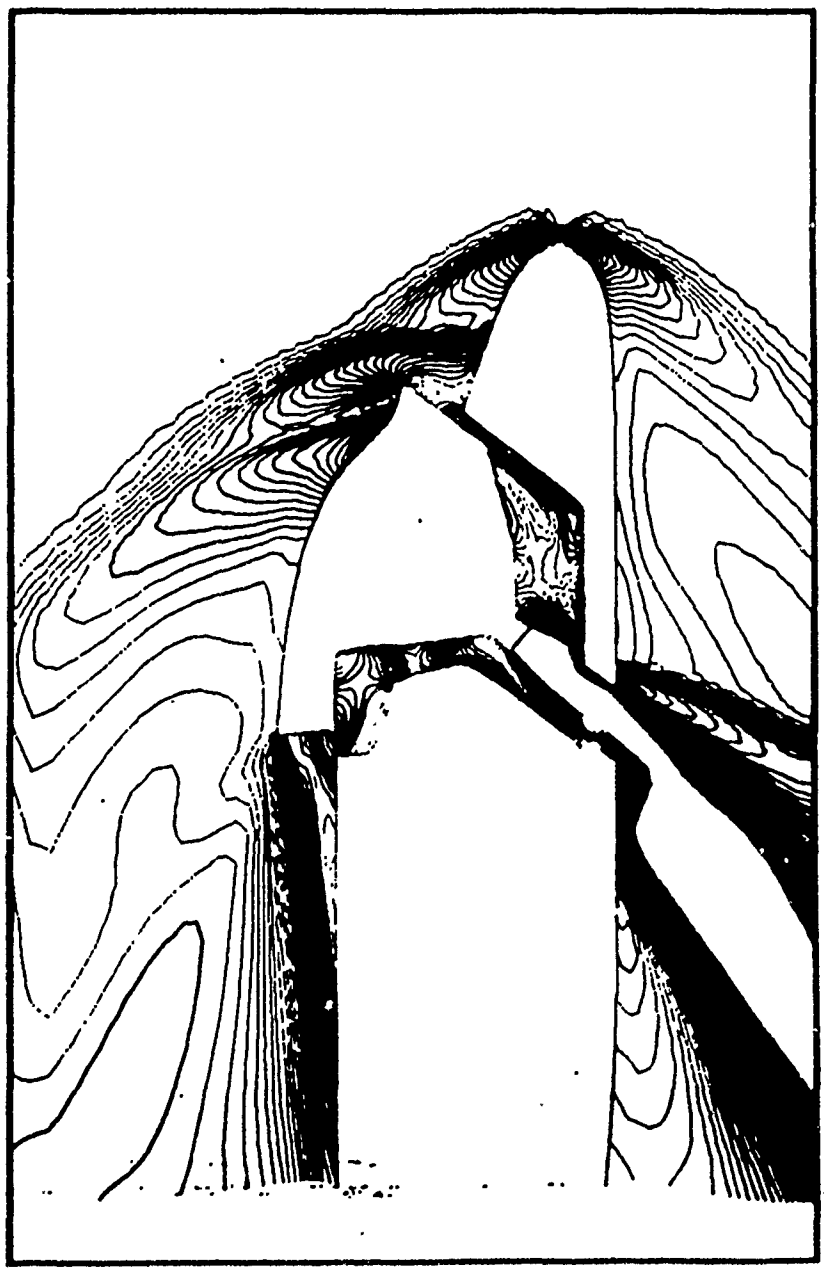

Fig.5 Isomachlines for Cem Separation at M=2.0

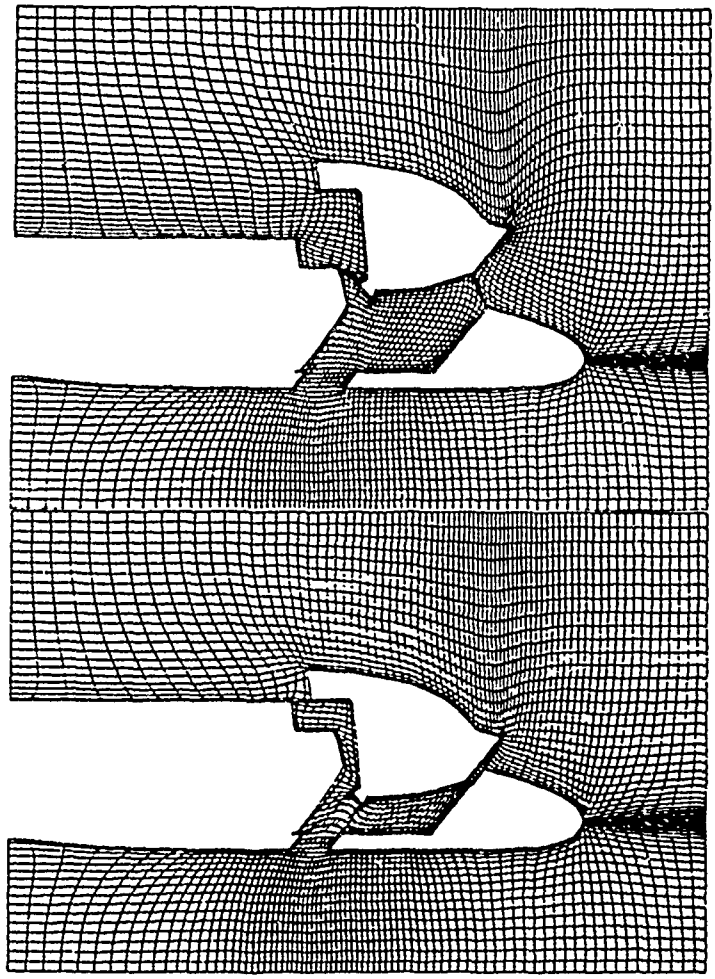

End of Cave Position

Interim Position

Fig.6

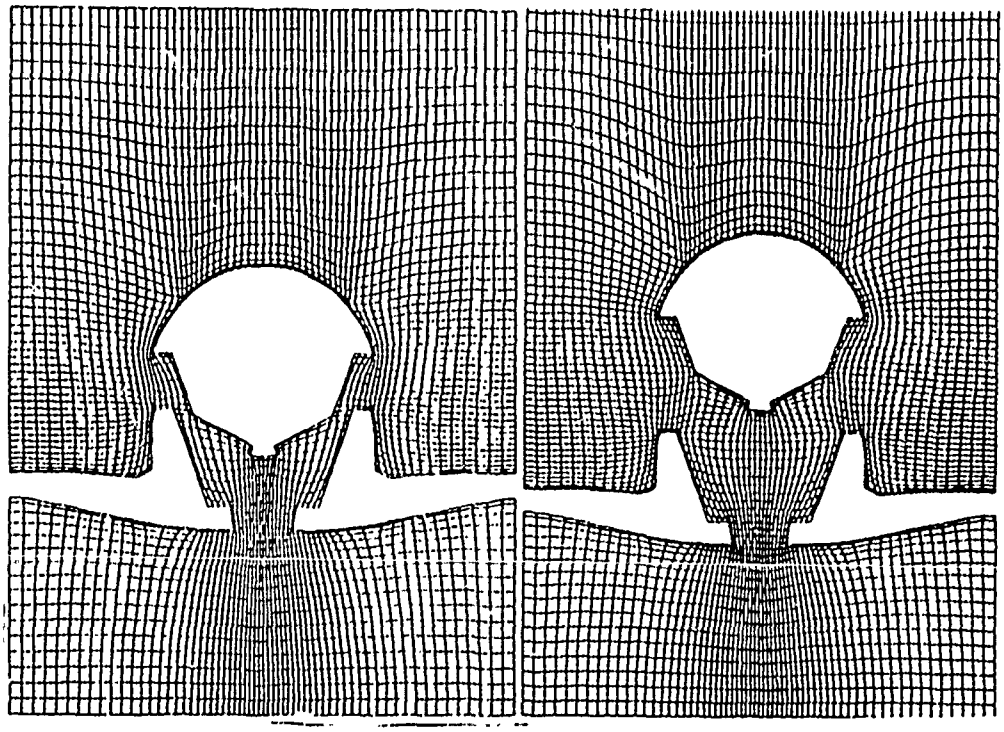

Fig.6 & 7 3D-Grids for Cem Separation Analysis

AXIAL FORCE AT M = 2.0

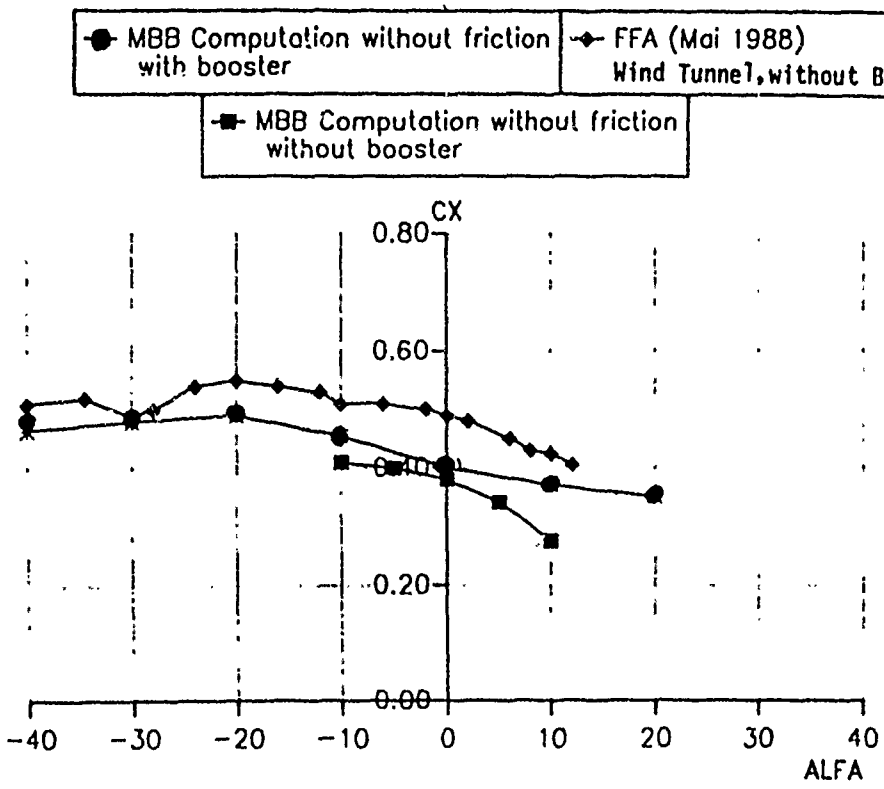

Fig.8

NORMAL FORCE AT M = 2.0

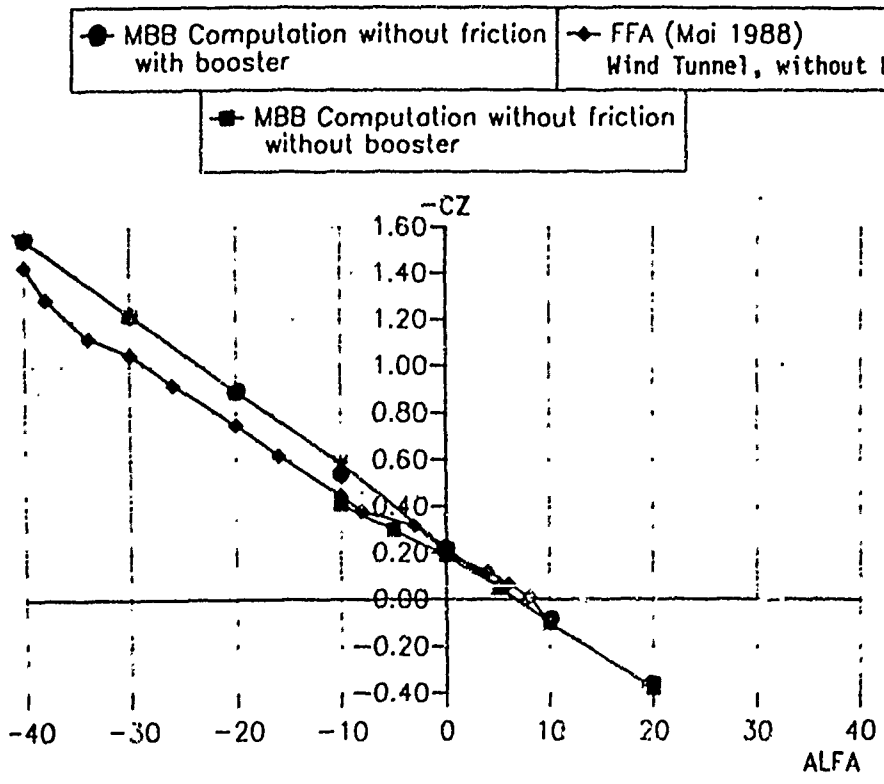

Fig.9

PITCHING MOMENT AT M = 2.0

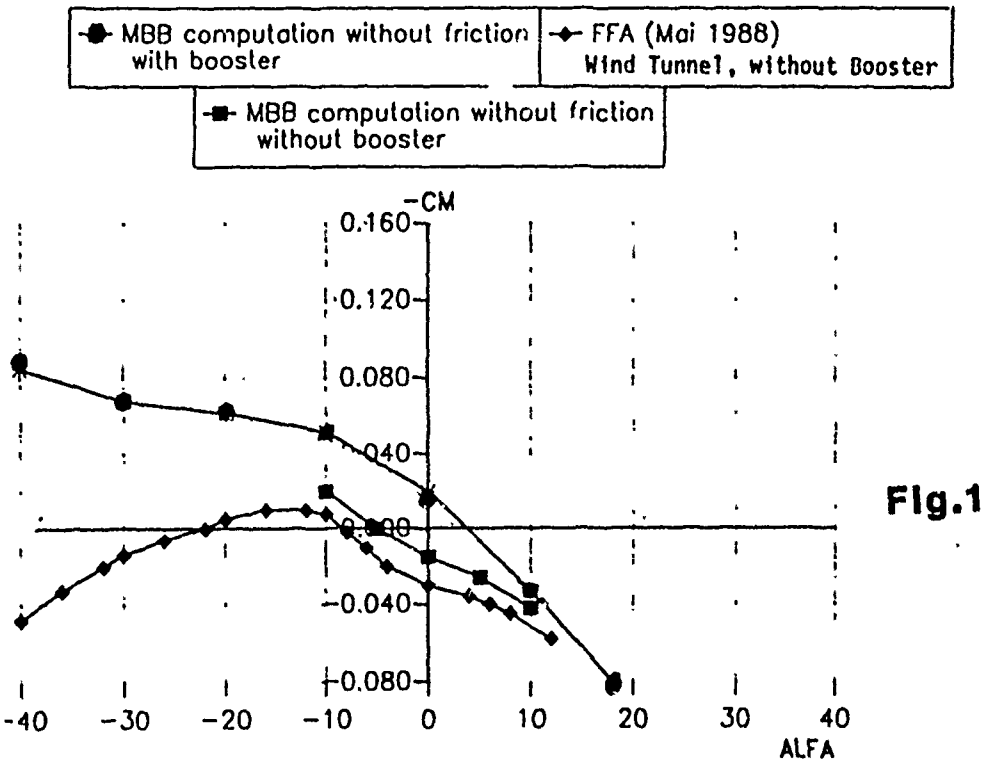

Fig.10

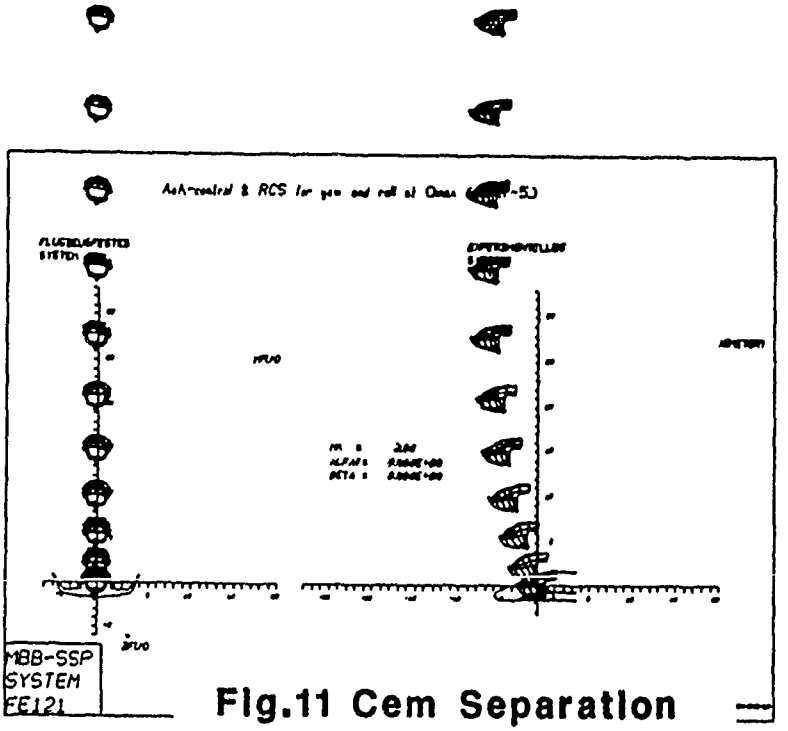

Fig.11 Cem Separation

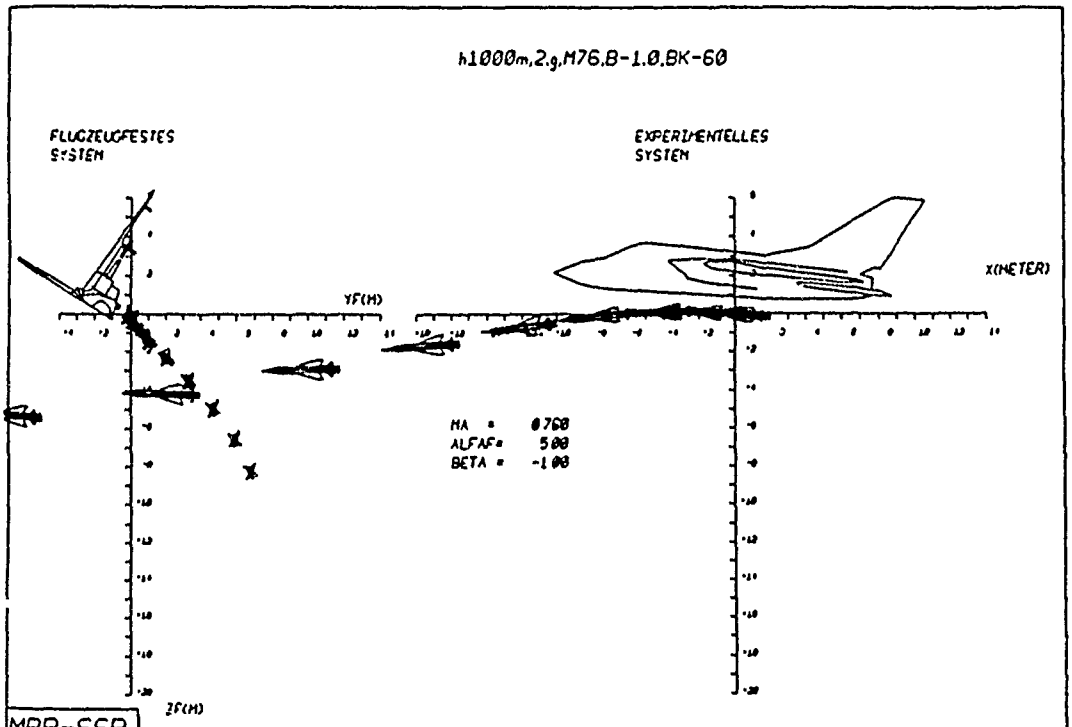

Fig.12 Rail-Launch assumed : safe

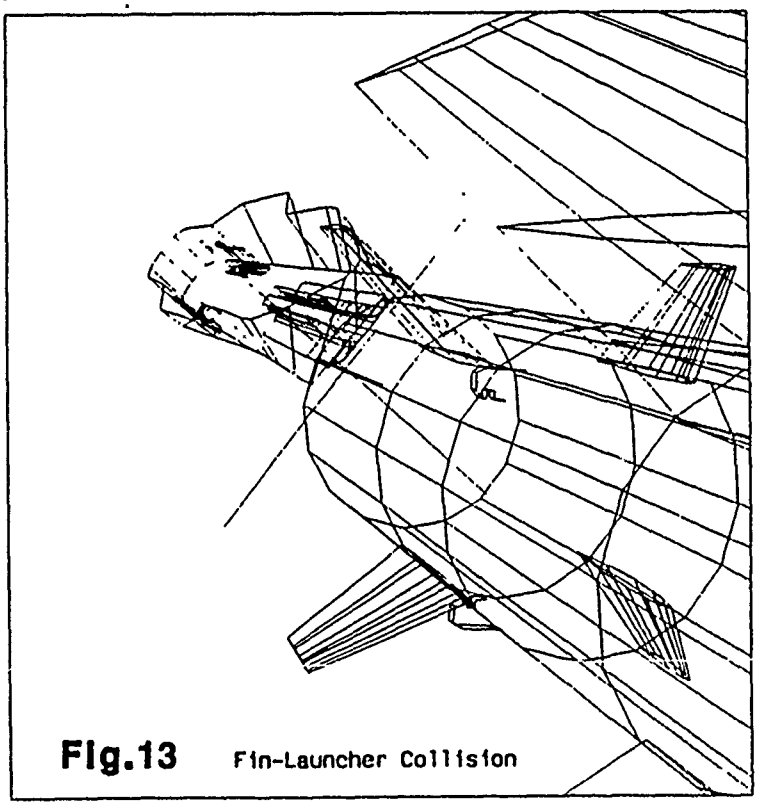

Fig.13 Fin-Launcher Collision

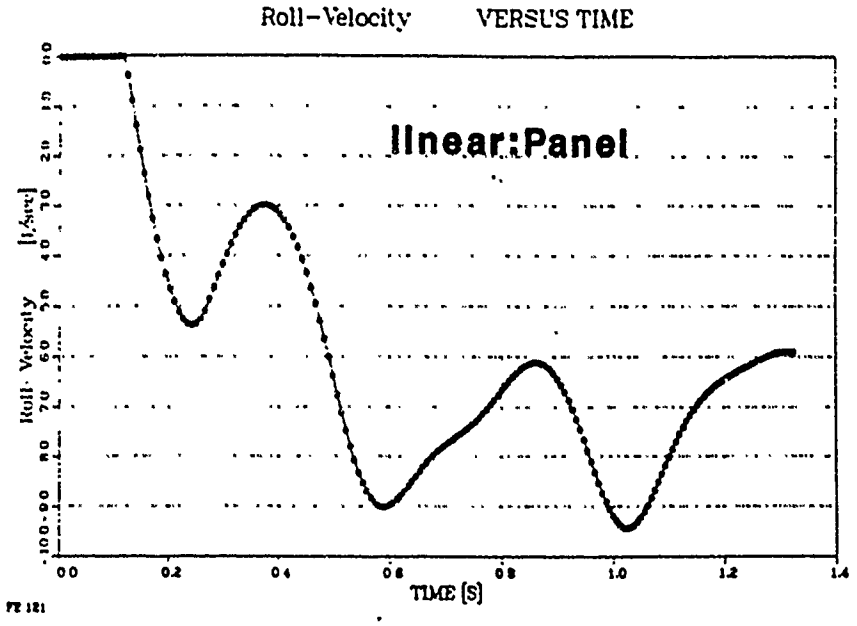

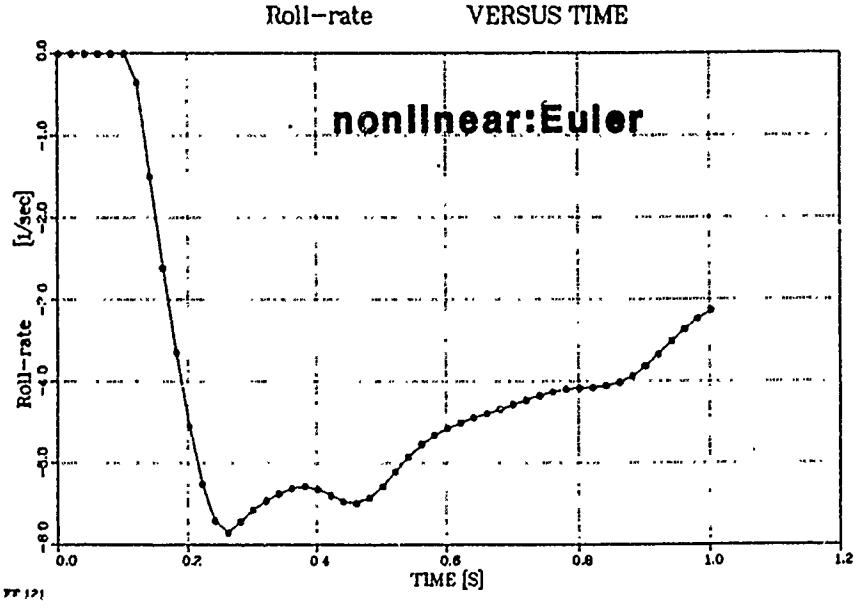

Influence of Cross-Coupling Terms Representation

Fig.14

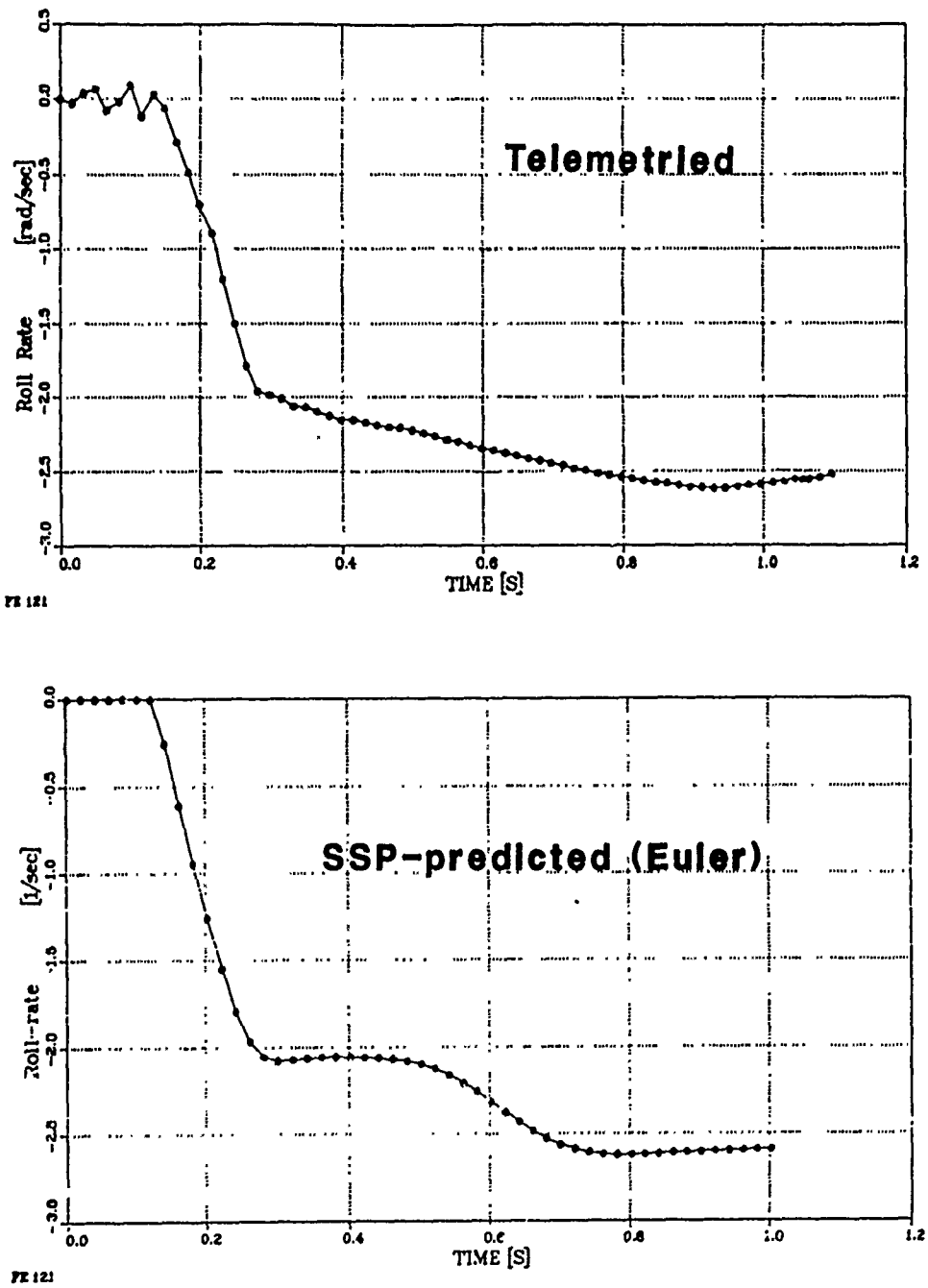

Comparison between Flight Test Telemetry and Theory

Fig.15

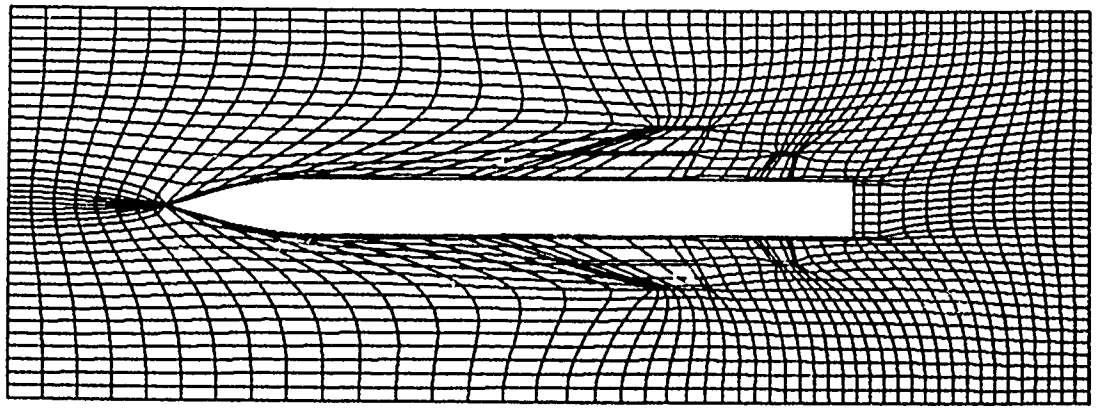

Fig.16 Freeflight 3D-Grid

① aircraft-parameters

orientation	load factor	rates	free stream conditions
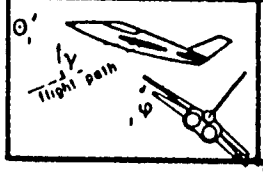	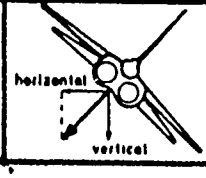	• pitch (q) • roll (p) • yaw (r)	• Mach number • angle of attack • sideslip angle • altitude • temperature • disturbances

② Ejection Release Unit - parameters

cartridges	throttles	[illegible]-position

③ store-parameters

type	physical characteristics	constraints
• missile • bomb • tank / pod • dispenser • ammunition • emergency device	• mass • inertias • c.g.-location • thrust • ignition-time • release sequence • arrangement • location	• rail • rear pivot • drag chute • floating fins • control deflection • wing extension • autopilot

Fig.17 SSP-Program Options

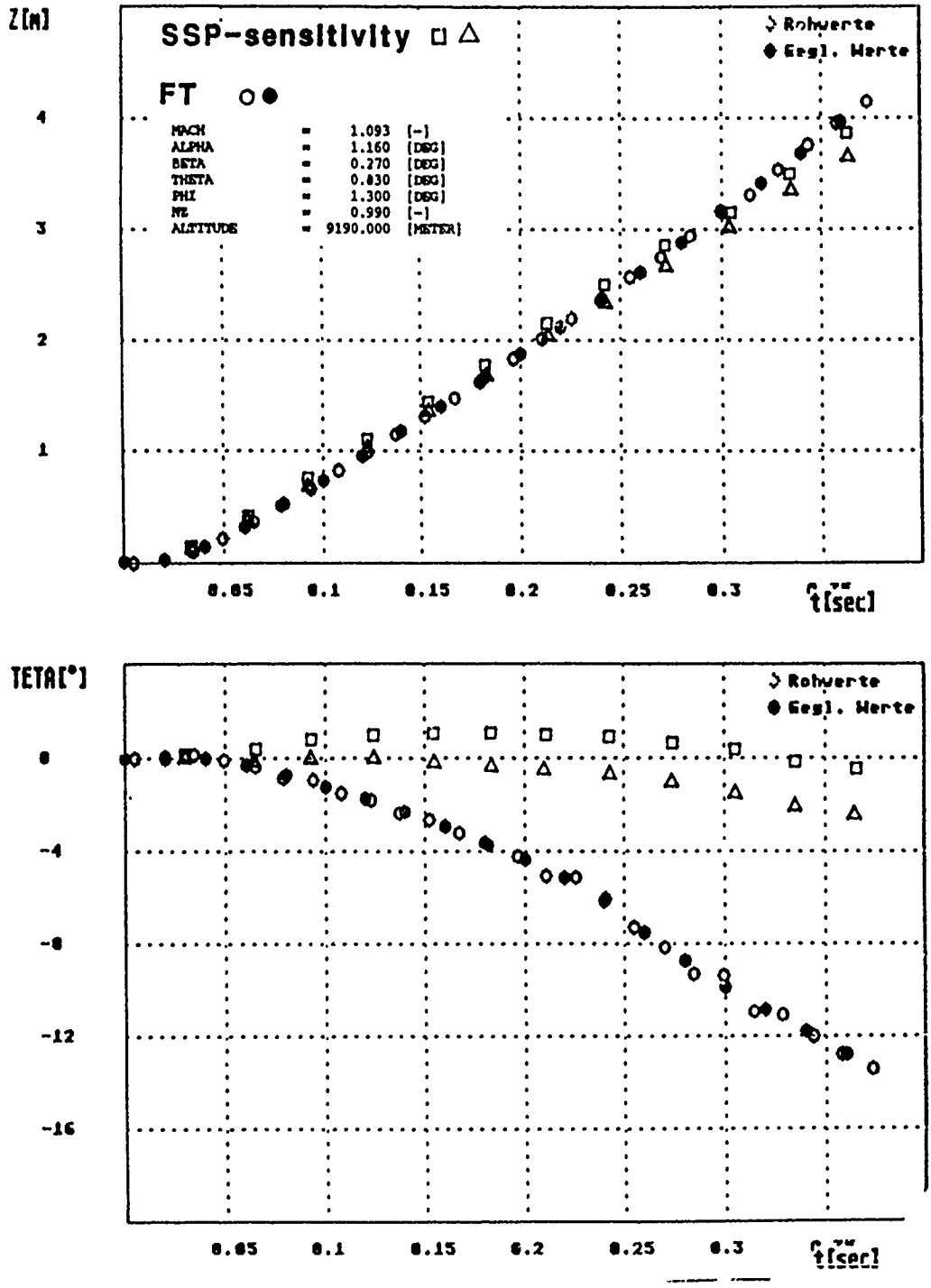

Comparison of FT-Movie-Analysis and SSP-Computation

Fig.18

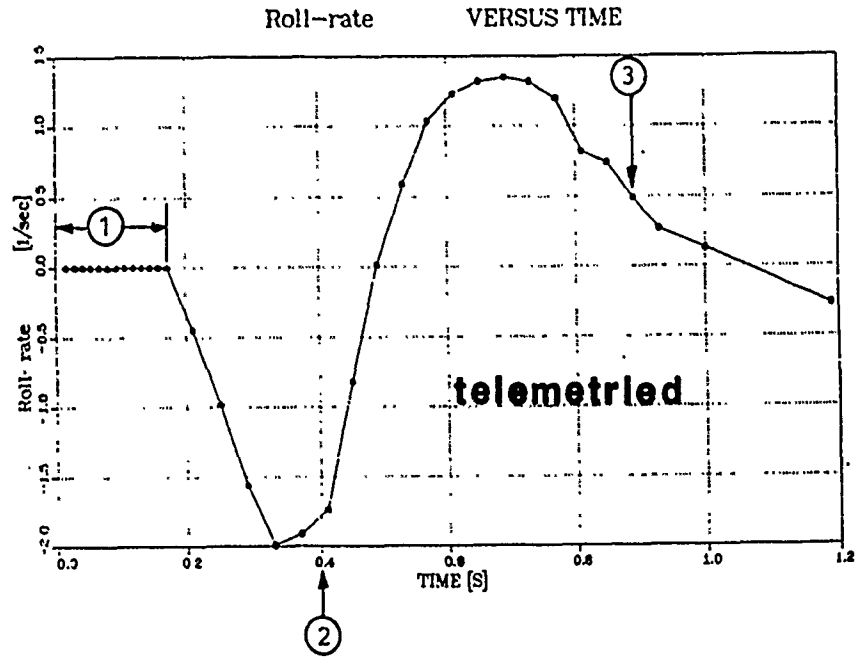

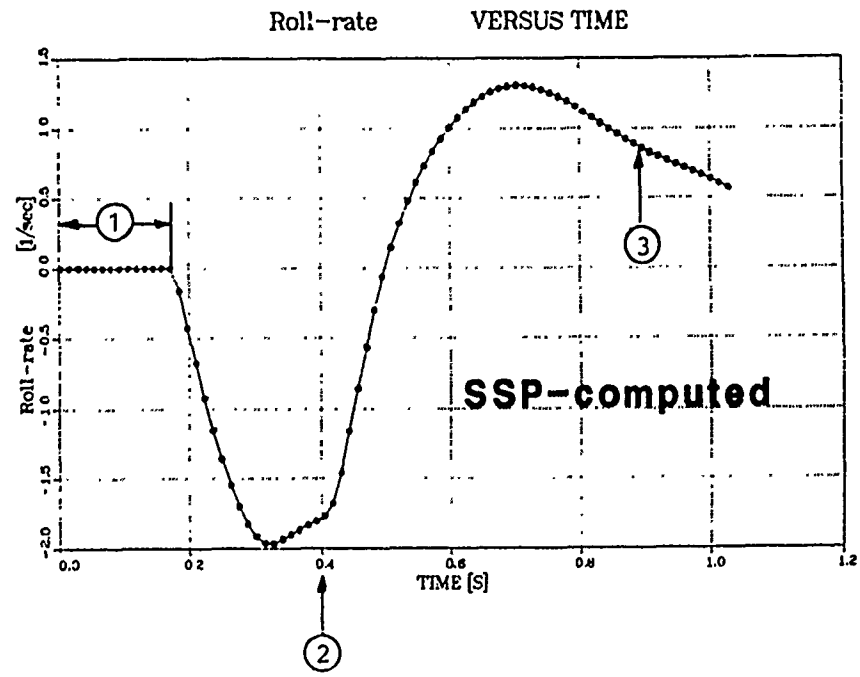

Fig.19 Validation of the SSP-Database

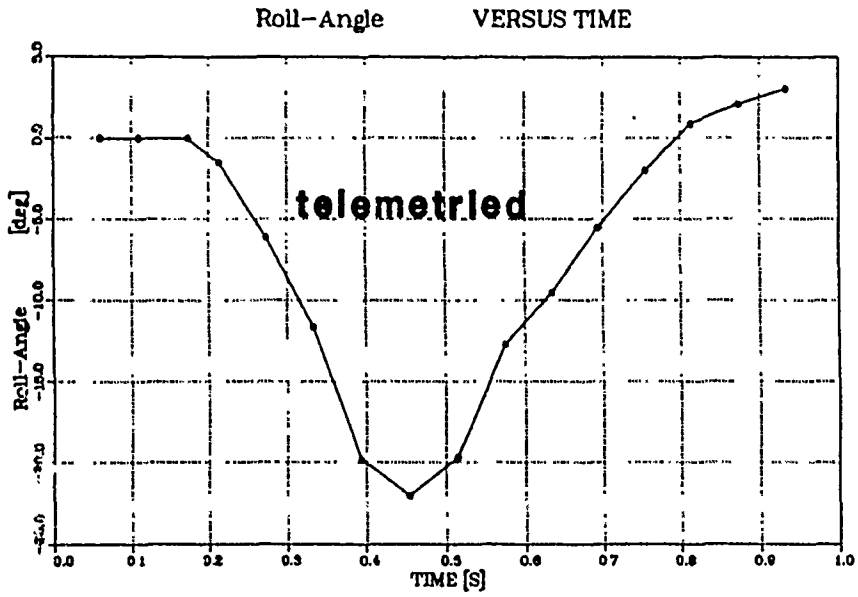

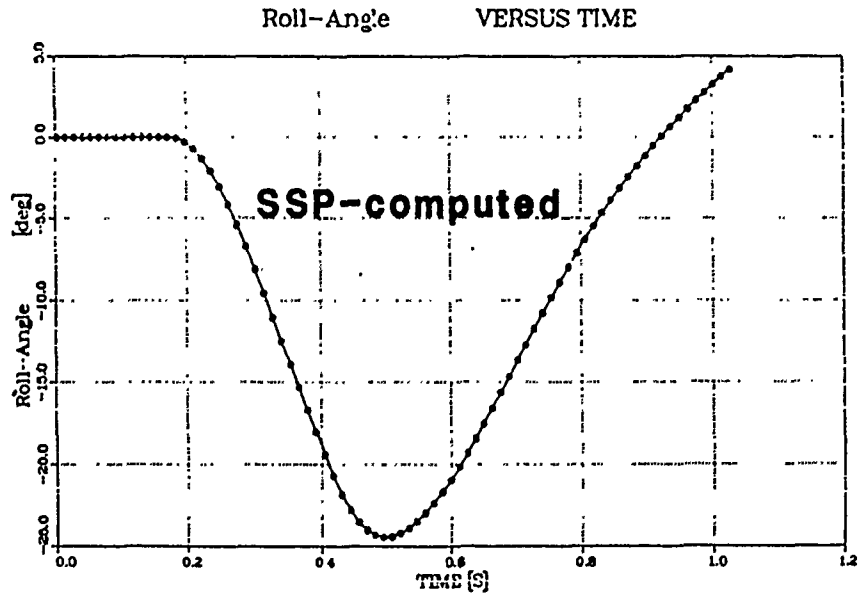

Fig.20 Validation of the SSP-Database

15-20

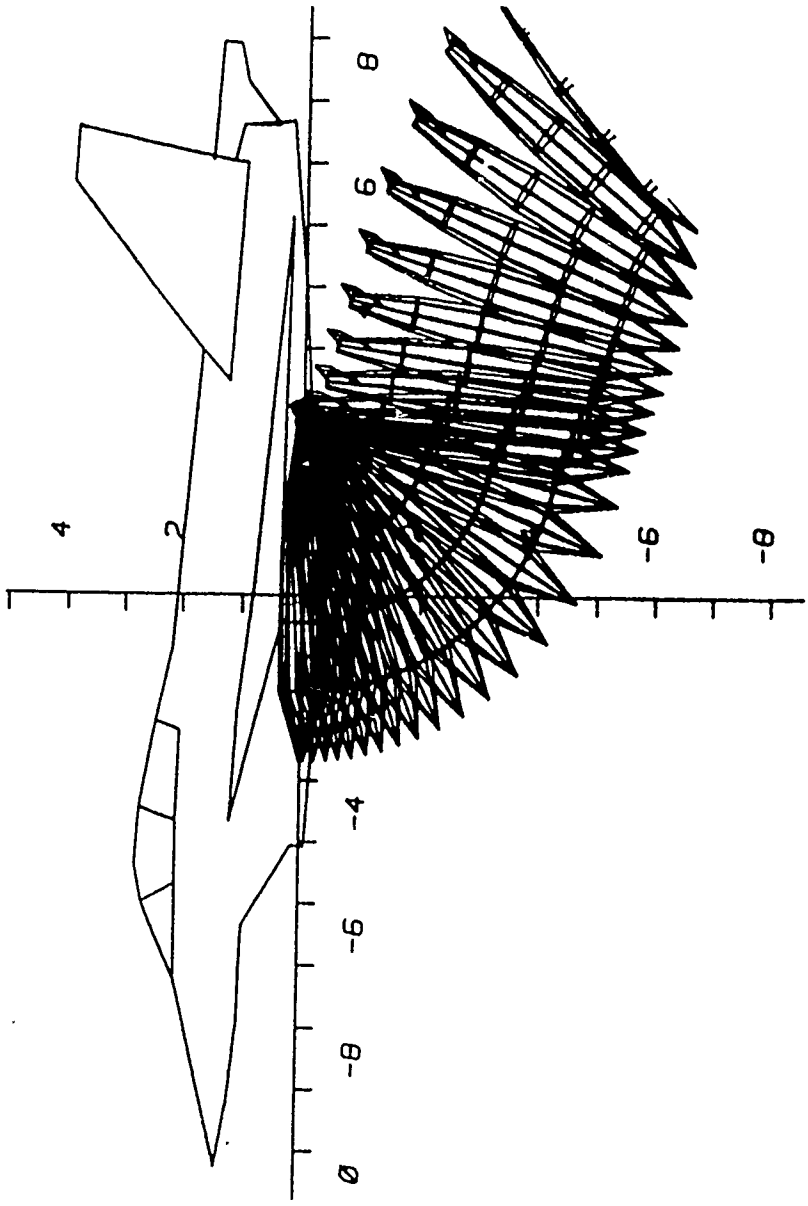

Fig.21 Limit of Reliability of Flow-Angularity-Technlques

BIOGRAPHY

Working since 1973 as a R/D-engineer in the field of computational fluid mechanics, Ronald M. Deslandes was tasked with the aerodynamic integration of stores on aircraft especially as far as store separation was concerned.

Since that time his main efforts concentrated in the development and improvement of mathematical models in order to achieve more confidence in the predictions of store separation. 1976 these efforts resulted in the first issue of the MBB-SSP (Store-Separation-Program) which has been successfully in operation for several common external store projects on the Tornado aircraft.

Always bearing in mind the considerable cost savings achieveable in wind tunnel experiments and flight tests by improving the accuracy of simulation, the linear theory formally taken into account, was replaced for the first time by advanced 3D-Euler terms in 1982-85.

1986 he achieved the degree of a Doctor Engineer at the University of Brunswick/FRG for a thesis about time accurate Euler-Solvers.

Recent successes are related to applications of the experience gathered since 1976 for advanced aircraft and space projects.

ENHANCEMENTS OF COMPUTER-GRAPHIC SYSTEMS FOR THE QUALITATIVE EVALUATION OF STORE-SEPARATION TRAJECTORIES

BY

K. Scott Keen, R. L. Clippard, W. G. Thomson
Calspan Corporation/AEDC Operations
Arnold Engineering Development Center
Arnold Air Force Base, Tennessee

For presentation at the Eighth Aircraft/Stores Compatibility Symposium, Ft. Walton Beach, Florida, October 23-25, 1990

The research reported herein was conducted at the Arnold Engineering Development Center (AEDC), Air Force Systems Command (AFSC), by Calspan Corporation/AEDC Operations, operating contractor for the aerospace flight dynamics effort at the AEDC, AFSC, Arnold Air Force Base, Tennessee. Further reproduction is authorized to satisfy the needs of the U. S. Government.

ENHANCEMENTS OF COMPUTER GRAPHIC SYSTEMS FOR THE QUALITATIVE EVALUATION OF STORE SEPARATION TRAJECTORIES

by

K. Scott Keen, R. L. Clippard, and W. G. Thomson
Calspan Corporation/AEDC Operations
Arnold Engineering Development Center
Arnold Air Force Base, Tennessee 37389

ABSTRACT

Qualitative understanding of store separation trajectory data can be greatly enhanced by visual displays of store and aircraft models on a computer graphics workstation. Methods for simplifying and streamlining the tasks required to generate and display store separation graphic 'scenes' have been developed. The preparation of numerical graphics models of the various items in a flight configuration is aided by the development of a series of conversion routines that can be used to generate graphic display models based on existing geometry models that may have been developed for use with a wide variety of readily available aerodynamic prediction programs. The actual specification of the relative positions of the various components to ensure the proper spatial relationship of the models on the graphics display screen has also been automated. As a result, the time and effort required to assemble graphics models representing flight configurations has been greatly reduced. In addition, improved scene display capabilities have been developed which include hidden-line and solid surfaces.

INTRODUCTION

The trajectory of an object separating from a carrier aircraft can be described by six motion quantities relating a coordinate axis system fixed in the separating body to another coordinate axis system fixed in the aircraft. The motion quantities are the longitudinal, lateral, and vertical linear translations and the yaw, pitch, and roll angular rotations of the separating store axis system relative to the aircraft-fixed axis system as functions of time after release. (The released object is generally referred to as a 'store' because it is stored on or in the aircraft prior to its release). The six motion quantities are often determined by a repetitive solution of the store equations of motion in a computational or wind tunnel trajectory simulation and are usually presented in plotted or tabulated form. The task of the analyst is to synthesize the six independent motion quantities obtained in the simulation into a single mental image of the spatial orientation of the store with respect to the aircraft as a function of time. Mental exercises of this sort, although difficult, are required to make value judgments concerning the safety and acceptability of the separation.

The research reported herein was conducted at the Arnold Engineering Development Center (AEDC), Air Force Systems Command (AFSC), by Calspan Corporation/AEDC Operations, operating contractor for the aerospace flight dynamics effort at the AEDC, AFSC, Arnold Air Force Base, Tennessee.

In recent years, capabilities for visualizing and evaluating the quality of store separation trajectories have been greatly improved through the implementation of a specialized computer graphics system at the AEDC. The system, designated the Store Separation Graphics Analysis Package (SGAP) (Ref. 1), allows manipulation and animation of three-dimensional (3-D) images of the aircraft and store geometries on a graphics screen. The computer graphic displays greatly enhance the ability of the aerodynamicist to make assessments of the quality of the separations as it allows the motion behavior of the store to be clearly 'seen.' Using a series of computer-generated images of representative store separation trajectories at a full range of aircraft flight conditions and store-loading configurations, the analyst is able to arrive at a quick global comprehension of the overall separation motion and thus make general assessments of the performance of the store/aircraft system throughout the release envelope. A black-and-white hard copy of a typical SGAP visualization is presented in Fig. 1.

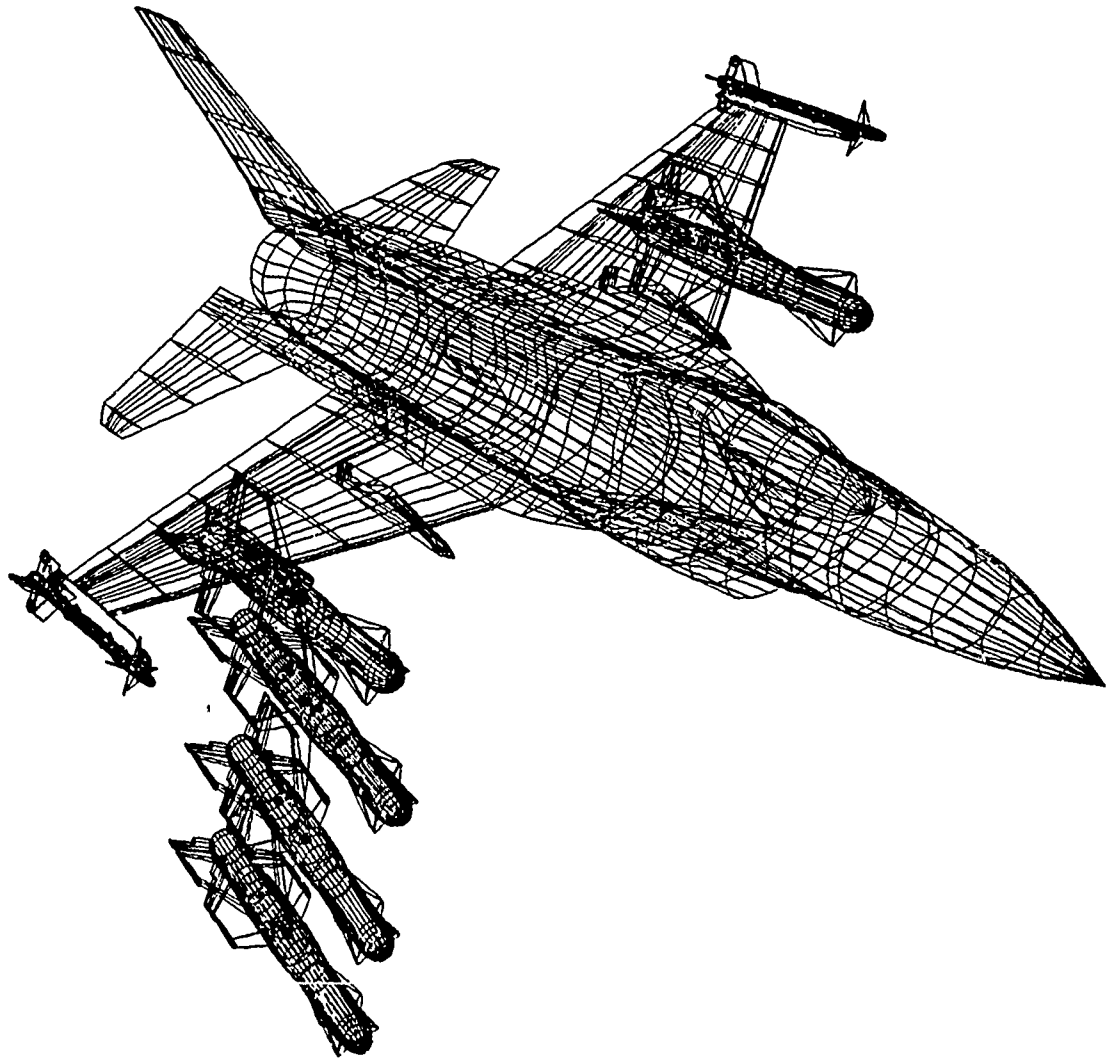

Fig. 1. Typical SGAP visualization.

Despite the increased data comprehension enabled by the graphic displays, improvements in the utility of the system were required to enable full realization of the benefits offered by graphic trajectory analysis. Actually, out of three major steps involved in the graphic process that is required for trajectory visualization, the SGAP system only performs the final (and arguably least difficult) step, the actual display of the images on the computer monitor. The other major steps of the graphics process include the preparation of numerical geometry models representing the various components in the configuration and the definition of the relative positions of the models in the graphics view. A major hindrance to production use of the SGAP system has been the rather extensive setup effort necessary to prepare the information required to satisfy the first two steps of the process. The present paper describes efforts to simplify and automate the tasks required to implement the modeling and configuration-assembly steps of the graphics process and represents the next logical step in the development of a user-friendly, production-oriented store separation graphic analysis capability. In addition, improvements in the graphics display capability itself, including hidden-line and shaded solid models are presented.

PREPARATION OF GEOMETRY MODELS

Arbitrary surface geometries are represented numerically by a set of points in 3-D space. The points are connected in some logical sequence by a series of straight-line segments to form a network of line vectors or panels that approximate the surfaces of the geometry. The creation of numerical models for complex geometries is a very difficult and often underestimated task. A large manhour expenditure may be required to define the x, y, and z coordinates of a sufficient number of points to adequately resolve the surface geometry of a body with the complex curvatures representative of a modern fighter aircraft. Often it is necessary to define thousands of points to provide the needed geometric resolution for a complex body. Once created, however, the numerical models may be permanently stored in the host computer for repeated future use.

Although the definition of the surface points used to describe a geometry can be an enormously tedious task, numerical models in some form may, fortunately, already exist for many aircraft and store geometries. Computer geometry models are often developed in the early stages of a vehicle design process to enable predictions of the aerodynamic properties of the vehicle or vehicle component. These models are used by a class of aerodynamic prediction codes known as panel methods. Panel-method aerodynamic prediction codes use points on the surface of the body organized into groups defining the corners of a series of four-sided surface panel elements which represent a faceted approximation to the geometry of the configuration. The aerodynamic properties of the vehicle in fluid flow are predicted by mathematically requiring the component of flow velocity, flow momentum, or mass flux normal to each panel to be zero. A wide variety of panel-method aerodynamic prediction codes are routinely used throughout the aerospace industry to support the development of new flight vehicles. Unfortunately, the many different panel codes also employ a wide variety of input formats to numerically define the vehicle geometries. It can be assumed, however, that panel models of some type have been developed for many, if not most, current flight vehicles. If existing panel models can be obtained, the creation of graphic geometry models for the SGAP system reduces to the relatively simple task of converting the existing panel code input files to the SGAP geometry format.

An effort to develop procedures for converting numerical panel code input models from one form to another was conducted several years ago at the AEDC in an attempt to reduce the large amount of duplicated effort that was formerly involved in preparing separate input models of the same configuration for each one of the different panel codes. A series of conversion programs were developed with the capability to convert the geometry as modeled for one panel code to the specific input items and formats used by another panel code. Based on the conversion procedures developed for the panel codes, a group of utility programs has been developed for creating graphics models in the SGAP format based on input models for many of the major panel codes in current use, including PAN AIR (Ref. 2), QUADPAN (Ref. 3), S/HAB (Ref. 4), USS AERO (Ref. 5), VSAERO (Ref. 6), and the NEAR Subsonic Trajectory Code (Ref. 7). Additional programs have been developed for converting geometry files created by CAD/CAM programs such as MOVIE.BYU (Ref. 8) and digital geometry tapes used by numerically controlled machining tools. A conversion program has also been developed (Ref. 9) for building store geometry models from the input descriptions used by the Interference Distributed Loads (IDL) Code (Ref. 10). The geometry conversion programs have been used in conjunction with techniques for building models from dimensioned drawings and a mechanical digitizing device which can physically measure the coordinates of the sub-scale AEDC wind tunnel models to enable the creation of an extensive computer library at the AEDC containing numerical models of many of the aircraft, bombs, missiles, pylons, launchers, and fuel tanks in the current U. S. Air Force and Navy inventories.

ASSEMBLY OF GRAPHICS CONFIGURATIONS

The spatial locations of each combination of aircraft, pylon, and store geometry components in the graphical geometry configuration are described by mathematically defining the translational positions and rotational orientations of each geometry component relative to the other components. Each physical flight or wind tunnel configuration has a corresponding digital configuration file consisting of a list of the names of the appropriate geometry files along with associated position and orientation information for each geometry component relative to the other components. The mathematical flexibility of being able to arbitrarily define the relative locations of each component relative to the other components is not characteristic, however, of the physical flight systems the numerical models are designed to represent. For the SGAP models to accurately represent an actual flight system, the numerical components of the graphics configuration must be assembled in a manner that is consistent with the actual physical interfaces between the flight hardware components. It is not productive, for example, for the graphics analyst to be responsible for mathematically specifying the spatial relationship between an aircraft wing geometry and an aircraft pylon geometry when the actual pylon hardware is physically designed to bolt onto the aircraft only at one specific wing location. A much better approach would be to numerically describe the positioning constraints associated with the hardware interfaces for each geometry component. The calculation of the geometry-referencing information and the creation of the SGAP configurations can then be automated using a specialized computer program. Such a program, designated the AUTOmatic CONFigurati. n (AUTOCONF) program, has been developed and is described in this section of the paper. Essentially the program builds up the graphics configurations by mating the appropriate hardware interface points on each geometry component. Assuming the numerical geometry models are available from an established graphics library, the setup effort required for a graphics session can be reduced simply to identifying which components are present in the configuration and specifying the coordinate axes in which the supplied trajectory data are defined.

The development of an automated graphic configuration-assembly capability is dependent on establishing a methodology for numerically describing the hardware interfaces connecting the various components of the configuration. Several different types of interface systems are commonly used to connect the various components of current military flight systems. Components such as electronic countermeasures pods, antennae, and pylons which are not designed to be released from the aircraft during flight are often bolted into place. Bombs, bomb racks, and fuel tanks are usually connected by a hook-and-eye type of mechanism whereby a pair of J-shaped hooks attached to one component are latched through a set of screw-eye suspension lugs attached to the other component. Lateral rigidity may be provided for hook installations by adjustable screw-in sway braces mounted on either side of the hooks. Air-launched missiles are often supported by T-shaped guides attached to the missile which slide inside a C-shaped rail attached to the aircraft or one of the aircraft pylons. Typical hook and rail installations are shown in Fig. 2.

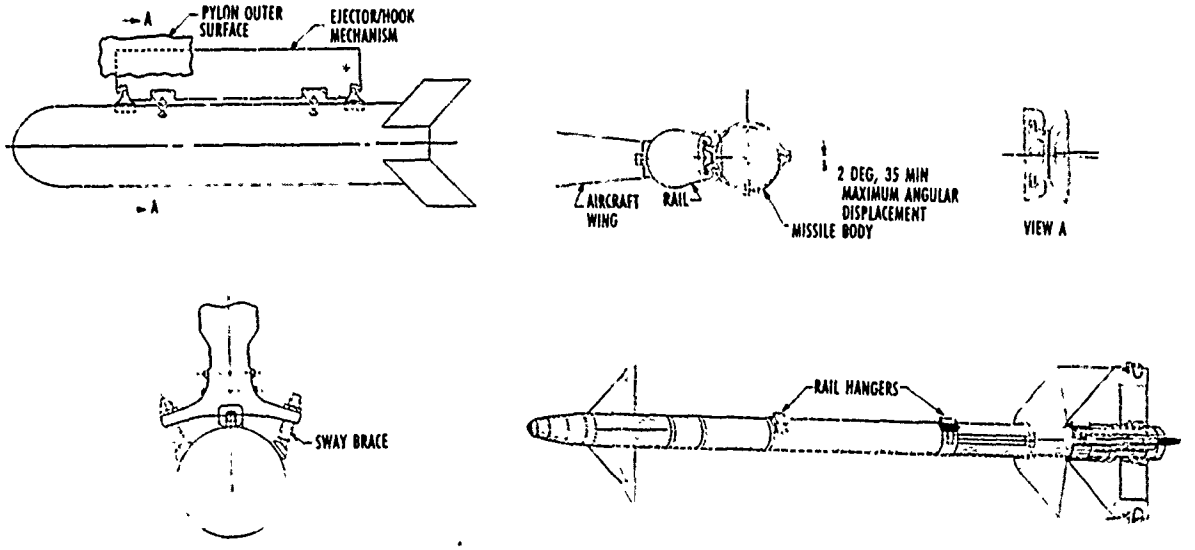

Fig. 2. Typical hook and rail installations.

Fortunately, over recent years much of the support hardware interface equipment has become standardized within the aircraft industry and the various military services. The standardization can be attributed in large part to the efforts of the Joint Ordnance Commanders Group (JOCG), Aircraft/Stores Compatibility Subgroup (formerly known as the Joint Technical Coordinating Group for Munitions Development, Working Party 6 for Aircraft/Stores Compatibility). The JOCG (like its forerunner, the JTCG) is made up of one or more high-level representatives from the Air Force Systems Command, the Air Force Logistics Command, the Naval Materiel Command, and the Army Materiel Command and was created to ensure the highest degree of cooperation and standardization between the various services. An important early product of the Aircraft/Stores Compatibility Group was a set of manuals describing interface hardware for many of the munitions in the U. S. inventory. The first of the manuals was released at a JTCG-sponsored symposium in 1973 (Ref. 11). The Aircraft Stores Interface Manuals (ASIM) (Ref. 12) contain detail drawings of current aircraft, pylons, racks, stores, and the associated interface mechanisms all presented in a standard format and drawn to a common scale. The ASIM was an important source for the interface information used by the graphics file-building procedures implemented in the AUTOCONF program. In a sense, the

AUTOCONF program and the SGAP display system can be considered to be a digital version of the ASIM manuals.

The method selected for describing hardware interfaces numerically in the AUTOCONF program is to specify the position and orientation of an interface-fixed axis system relative to the local geometry-axis system in which the surface coordinates of the model are defined. The origin of the interface system is fixed at the forward contact point of the interface, and the longitudinal interface axis is colinear with the line connecting the forward and aft contact points. The position and orientation of the interface systems for each geometry component are defined by specifying the longitudinal, lateral, and vertical coordinates of the interface-axis origin and the yaw, pitch, and roll incidences of the interface axis system relative to the local geometry axis system of the component. The interface position and orientation parameters for most geometry components are stored along with the surface geometry coordinates in each individual geometry file within the SGAP computer library.

The interface coordinates for a typical lug-mounted store are illustrated in Fig. 3. The figure is reproduced from the ASIM manual (Ref. 12) and is shown with notations indicating the local store geometry axes and the interface axes. Note that the interface-axis system origin is located at the point on the top inside rim of the forward suspension lug at which the lug and the corresponding hook on the matching support hardware make contact. Two primary types of suspension lugs are used by most of the stores in the current military inventory. Large stores are usually suspended from a pair of heavy-duty lugs screwed into the store body with a 30-in. axial spacing between them. Smaller stores are suspended from smaller lugs spaced 14 in. apart. An identifier indicating whether the store is equipped with 14-in. or 30-in. suspension lugs (or both) is included in the store geometry file, along with the definition of the interface systems. Also optionally included in the store geometry file are default nominal cg coordinates for the store which may be overridden with updated values at user discretion (most trajectory information is defined in terms of the translational motion of the store cg). In a similar manner, the geometry file for each store, missile, pylon, rack, or rail geometry in the SGAP geometry library also contains a numerical description of the associated hardware attachment points.

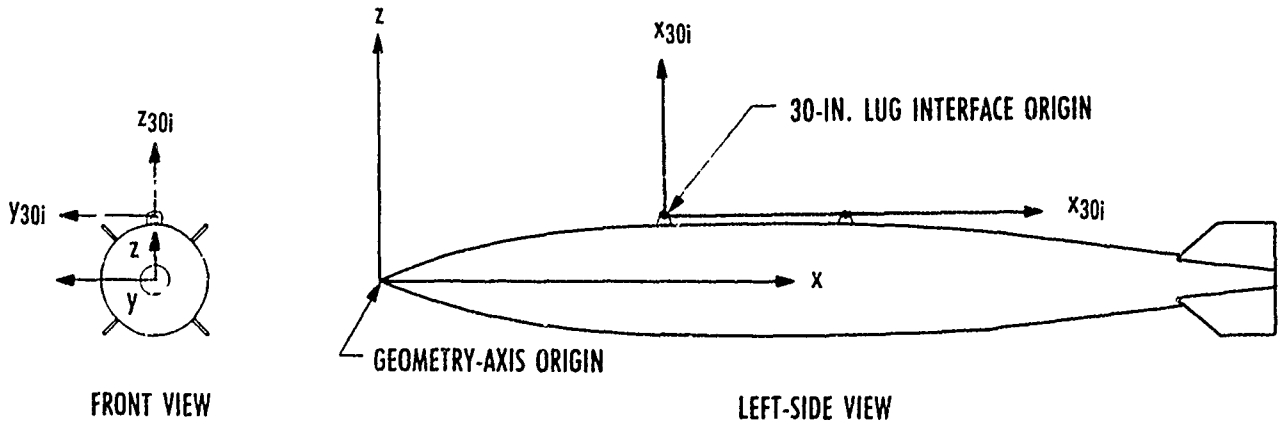

Modified Reproduction of Ref. 17 "Store Characteristics Manual" Figure 1-6A

Fig. 3. Interface axis systems for a typical store.

16--7

The interface axis systems for a typical multiple-station carriage rack geometry are illustrated in the annotated ASIM drawing shown in Fig. 4. The figure serves to illustrate how the configurations are assembled from the various components in the AUTOCONF program. Note that several different interface axis systems must be defined for multiple-carriage geometries. Both 14-in. and 30-in. lug interfaces (for attaching the rack to the aircraft pylon) and three sets of 14-in. hook interfaces (for attaching stores to the rack) are shown in the example of Fig. 4. For the rack/store/store case shown in Fig 4 the AUTOCONF is designed to determine the translational and rotational coordinates of each store relative to the rack which cause the store lug interface axes to be coincident with the corresponding hook interface axes on the rack. These translations and rotations are then specified in the graphics configuration. The AUTOCONF program is designed to select the proper size (14 in. or 30 in.) of hook interfaces to match the suspension lugs available on the attached component.

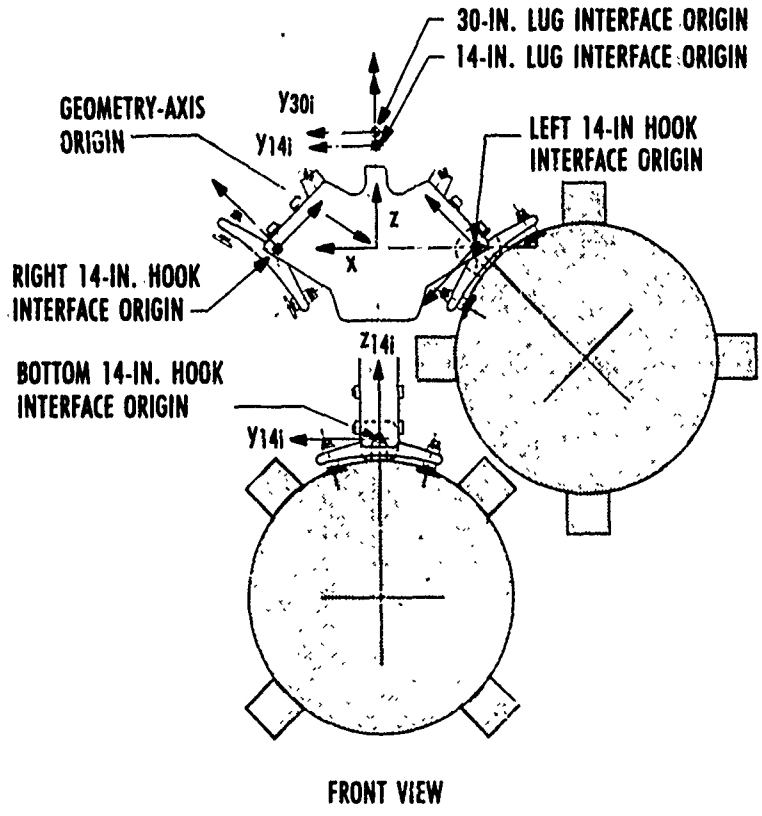

Fig. 4. Interface axis systems for a typical rack.

The AUTOCONF is menu driven and relatively easy to use. The first menu displays the aircraft models available in the graphics library. After the desired aircraft is selected, the program then displays structural points on the aircraft (often called hard points') at which items can be directly attached to the aircraft. Pylons, pods, antennae, rotary launcher shaft geometries, and open or closed weapons bay doors are usually added to the configuration at this level. If pylons have been specified in the configuration, the program then prompts for the pylon adaptor, rack, rail, or store to be attached at each pylon station in turn. Each of these items may be selected from a cataloged menu of items of that type (e.g., a menu of all missile

models available in the library is displayed if the user specifies that a missile is to be attached to a particular pylon). If a multiple carriage rack is selected, the user is prompted for stores to be attached at each rack station in turn. In addition to capabilities for assembling graphics configurations from scratch, the AUTOCONF also has significant capabilities for copying and editing pre-existing configurations, including adding additional components, deleting components, calculating the aircraft axis coordinates of the cg of the active store when it is at its carriage position, and combining several different components into a single combined geometry file. The AUTOCONF also has the capability to define the relationship between the coordinate axis system in which the store position and orientation trajectory information are defined and the coordinate systems in which the numerical geometry models are defined, a task which otherwise is often tedious for the analyst to define mathematically.

DISPLAY OF GRAPHICS CONFIGURATIONS

The store translation and rotation-versus-time trajectory data are used to position the images of the store on the screen in much the same manner that a physical store model would be positioned mechanically during a wind tunnel test. Trajectory visualization using 3-D computer graphics technology was proposed by Dix at the AEDC (Ref 1.) and was originally implemented on a then state-of-the-art graphics workstation by a contracted SGAP vendor, Amtek, Inc., of Atlanta, Ga. Since the introduction of the original SGAP system, major advances have been made in computer graphics technology allowing the development of improved display capabilities. The graphics workstation upon which the original SGAP display system was implemented employs a graphics process known as 'vector refresh' in which an electron beam traces each line across the face of the cathode ray tube, activating a low-persistence phosphor coating on the tube surface which causes the line to be displayed on the screen. Each line vector in the graphics model is traced on the screen in sequence and the beam must continuously cycle through all vectors in the model to reactivate (or 'refresh') the image. The short-life phosphor 'refresh' capability allows the vector images to be moved in real time on the graphics screen without leaving smeared or 'ghost' images on the screen. Unfortunately, because of the large number of vectors in a typical store-separation display, the vector-refresh workstation is not able to cycle through the vectors quickly enough to maintain a constant image. This produces an annoying 'flicker' phenomenon which results in visual fatigue for the user of the display system and poor-quality film or videotape records of the dynamic screen images. Other motivations for upgrading the system included slow turnaround time, hardware maintenance issues associated with the dated graphics workstation technology, scheduling difficulties in gaining access to one of the two available SGAP workstations because of a large AEDC test and analysis workload, and most importantly, inflexibility in adapting the display software for test-peculiar requirements (modifiable source code was not provided for many of the SGAP functions). The replacement SGAP capability has been implemented on modern mid-range raster workstations (some 40 of which are now available in the AEDC aerospace test facilities). Raster graphics technology is similar to conventional television and allows several improved display modes including an ability to display models using solid-filled panels under different lighting conditions rather than only as a network of line vectors. A typical solid-panel trajectory display is shown in Fig. 5. Efforts are currently underway to allow real-time animation of the solid panel models, although solid-model animation taxes the capabilities of most current top-of-the-line high-end graphics workstations.

Fig. 5. Typical solid-panel visualization.

The interactive graphics workstation represents, of course, the pinnacle of modern graphics technology, but there are instances where little or no interactive user intervention is necessary and the user is not interested in sitting at the graphics terminal for hours on end drawing trajectories. As a result, an alternate non-interactive display capability known as the Batch SGAP (BATGAP) has been developed. The BATGAP is designed to calculate fixed views (top, side,etc.) of all trajectories in a given test trajectory file at one time. Trajectories that are determined to be of interest upon examination of the fixed views can then be examined in more detail interactively using the SGAP capability. At the conclusion of a test, the analyst creates digital configuration files for all test configurations using the AUTOCONF, provides logic to the BATGAP code for the selection of which configurations are associated with particular test runs, submits the computer shot, and goes home. Pictures of all trajectories in the file should be generated by the next morning. The BATGAP is designed to run on a mainframe computer and create move/draw files for each trajectory which can be sent directly to a standard plotter or laser printer and requires no specialized graphics equipment.

Another alternate graphics display capability has been developed which combines portions of the SGAP geometry transformation capability with the hidden-line algorithm of Ref. 13. The hidden-line trajectory display program also runs in a batch mode and does not require high-end graphics equipment. The hidden-line trajectory representations are much less visually cluttered than the standard wire-frame drawings. A typical hidden-line trajectory display is presented in Fig. 6.

CONCLUSIONS AND FUTURE DEVELOPMENTS

Visualization of store trajectories using computer graphics technology has become a unique and valuable link in the analysis process that begins with test data and ends with an understanding of store/aircraft flight system performance. Recent improvements in configuration modeling, assembly, and graphics display capabilities are presented which greatly increase the utility and efficiency of the graphics analysis tools. Expanded graphics capabilities are currently under development to allow the addition of models of AEDC wind tunnel/model support system hardware

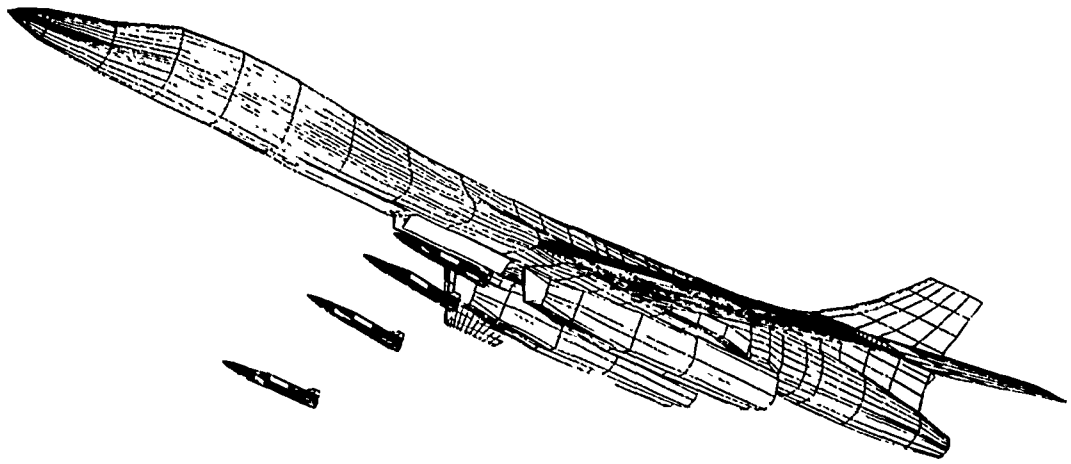

Fig. 6. Typical hidden-line visualization.

to the AUTOCONF/SGAP systems. Graphics modeling of wind tunnel hardware will facilitate the selection of model support sting components for wind tunnel testing. Much more importantly, however, a planned graphics-based support checkout capability could conceivably eliminate an average of a day in the tunnel from each future captive trajectory test. This amount of nonproductive wind tunnel occupancy time is presently dedicated to "grid checks" which involve the determination using the actual tunnel hardware of the limits of the available trajectory positioning motion and of potential physical interferences between the store and aircraft models and their corresponding sting or strut support systems. Use of graphics models rather than tunnel hardware for the grid check process will represent a major cost reduction for future wind tunnel trajectory testing efforts.

REFERENCES

1. Dix, R. E. "Advances in Store Separation Testing and Analysis Techniques."Paper presented at the AGARD 57th Symposium on Store-Airframe Aerodynamics,Athens, Greece, October 7-10,1985.

2. Sidewell, K. W., Baruah, P. K., and Bussoletti, J. E. "PAN AIR - A Computer Program for Predicting Subsonic or Supersonic Linear Potential Flows About Arbitrary Configurations Using a Higher Order Panel Method." NASA CR-3252, May 1980.

3. Youngsen, H. H. et al. "Comparison of Panel Method Formulations and Its Influence on the Development of QUADPAN, An Advanced Low Order Method." AIAA Paper No. 83-1827, July 1983.

4. Gentry, A. E., Smyth, D. N., and Oliver, W. R. "The Mark IV Supersonic-Hypersonic Arbitrary-Body Program." AFFDL-TR-73-159, November 1973.

5. Woodward, F. A. "USS AERO Computer Program Development, Versions B and C." NASA CR-3227, April 1980.

6. Maskew, B. "Prediction of Subsonic Aerodynamic Characteristics: A Case for Low-Order Panel Methods." Journal of Aircraft, Vol. 19, No. 2, February 1982, pp. 157-163.

7. Goodwin. F. K., Dillenius, M. F. E., and Nielsen, J. N. "Extension of the Method for Predicting Six-Degree-of-Freedom Store Separation Trajectories at Speeds up to the Critical Speed to Include a Fuselage with Noncircular Cross Section." AFFDL-TR-74-130, November 1974.

8. Christensen, H. N. "Movie.BYU" University Press, Brigham Young University, Provo, Utah 84602, 1983.

9. Keen, K. S. "New Approaches to Computational Aircraft/Store Weapons Integration." AIAA Paper No. 90-0274, January, 1990.

10. Morgret, C. H., Dix, R. E., and Lijewski, L. E. "Development of Analytical and Experimental Techniques for the Determination of Distributed Loads on Stores." AIAA Paper No. 81-1896R, August 1981.

11. Epstein, C. S. and Washmuth, H. L. "Working Party 12 Accomplishments." Aircraft/Stores Compatibility Symposium Proceedings, Vol. 1, Sacramento, California, September 18-20, 1973.

12. Joint Technical Coordinating Group for Munitions Development, Working Group for Aircraft/Stores Compatibility. "Aircraft Stores Interface Manual." "Aircraft Manual" JTCG/MD-WP-6-1, September 1973, Rev. 1, May 1974, Rev. 2, May 1976, Rev. 3, Oct. 1978, Rev. 4, Sept. 1980, Rev. 5, Oct. 1984, "Store Characteristics." JTCG/MD-WP-6-3, October 1978, Rev. 1, August 1980, Rev. 2, Oct. 1984.

13. Hedgley, D. R., Jr. "A General Solution to the Hidden-Line Program", NASA RP 1085, March 1982.

AUTOBIOGRAPHY

KENNETH SCOTT KEEN, Principal Research Engineer, Flight Dynamics Section, Technology and Analysis Branch, Calspan Corporation, AEDC Operations

Scott Keen has a Bachelor's Degree in Aerospace Engineering from the Georgia Institute of Technology, a Master of Science in AE from the University of Tennessee Space Institute, and is presently working toward a PhD in AE at UTSI. He is primarily responsible for the development and application of store-separation and free-flight motion simulations, aerodynamic predictions, and analysis of flight vehicle performance.

RICHARD LEE CLIPPARD, Computer Scientist IV, Technology Applications Section, Technology and Analysis Branch, Calspan Corporation, AEDC Operations.

Richard Clippard has a Bachelor's Degree in Mathematics and Computer Science from the University of Tennessee, Knoxville. He is primarily responsible for the development and application of test-support and post test analysis software on mainframe computers, workstations, and personal computers.

WILLIAM GEORGE THOMSON, Senior Research Engineer, Computational Fluid Dynamics Section, Technology and Analysis Branch, Calspan Corporation, AEDC Operations.

Bill Thomson has a Bachelor's Degree and a Master of Science Degree in Aeronautical and Astronautical Engineering from the University of Illinois and a PhD in Engineering from Wichita State University. He is primarily responsible for Graphics and Workstation systems and applications in the CFD Section.

THIS PAGE INTENTIONALLY LEFT BLANK

The Use of The C.T.S for Prediction of Trajectories to The Impact Point

(Article Unclassified)

By

Zilberman M.*, Shay M., Shlezinger A.,
Shruster I. and Cohen Ts.

Tashan-Engineering Center/Israel Aircraft Industries
and the Israeli Air Force

ABSTRACT

The Captive Trajectory System (C.T.S) at Israel Aircraft Industries (I.A.I) is mainly used for predicting separation of stores from parent vehicles. The system serves as a main tool in separation analysis, either by operating in a closed loop (C.T.S) or in an open loop (grid) scheme. Due to the high level of correlation between wind tunnel and flight test results, the use of the system has been extended to predict the effect of separation on the trajectory of a store to the impact point. Last year a long term effort, in which a full trajectory of several stores is predicted, has been initiated at IAI. This work presents the results which were obtained for the trajectories of low-drag Mk-84 and Mk-82 stores which were released from station 3 of a F-16 parent aircraft at several flight conditions in the transonic range.

It is shown that the aircraft/store interference has only little effect on the ground distance of the Mk-84. On the other hand, the ground distance which was obtained for the Mk-82 store was significantly affected by the interference and the ground distance was sensitive to the position on the TER (Triple Ejection Rack) from which it was released .

Aproved for Public Release; Distribution Unlimited

Presented at The JOCG 8th Aircraft/Stores Compatibility Symposium 23-25 October 1990/Ramada Beach Resort, Fort Walton Beach, Florida

List of Symbols

CEP- Circle of error probability

Cd - Drag coefficient

EJF- Ejection force

g - Load factor (=1 in level flight)

H - Altitude

Iyy- Moment of inertia, about the Y axis

Izz- Moment of inertia, about the Z axis

q - Rate in pitch

r - Rate in yaw

ΔR - Miss distance

S - Reference area of store

V - True air speed

W - Weight of the store

Xcg- Distance of center of gravity from nose

α - Angle of attack of aircraft

σ - Standard deviation of miss distance

ϑ - Angle of pitch

ψ - Angle of yaw

1. Introduction

The need for experimental and analytical investigation for certifying the release of a store from a new aircraft/store configuration is well accepted by the engineering community [1,2]. Although the contribution of computational methods to the certification process increases together with the computing power, it is clear to the authors that wind tunnel testing and the CTS will continue to contribute a major part in the certification process. The CTS suggests a compromise between the low cost computational methods and the "brute force" flight testing programs. On the one hand it will predict the trajectories when the configuration is complicated and analytical methods may fail, and on the other hand it will save risky and expensive flight test program.

A theoretical study (performed by the USAF, 1970 [4,1]) of the sensitivity of various parameters to ballistic accuracy for a Mk-82 store being released from a "generic" aircraft, has shown that those parameters related to the store separation, accounted for 30% of the total miss distance at 450 knots and to 21% at 860 knots.

The present study stresses the idea that the aerodynamic interference, during separation, may have a significant effect on the ground distance of a store. The positive experience which was gained by the authors while using the CTS as the main tool for predicting the separation of stores, has led to the present program.

It is shown that the ground distance of a store can be accurately predicted by inserting the separation results, which were obtained by the CTS, as the initial conditions for a 6DOF program which calculates the trajectory of a store to the impact point.

2. The CTS and the Test Procedure

The CTS is a 6DOF simulation system which is operated in the 4x4 ft. transonic test section of the blow down wind-tunnel at IAI. A 1:15 scale F-16 parent aircraft is attached to the ceiling of the test section on an angle of attack mechanism (see figure 1). The store model is mounted on a sting balance which is connected to the CTS by a roll sting. The real time calculations of the CTS are conducted by a DEC 11/73 minicomputer which can be programmed to simulate a complete trajectory or perform a predetermined grid test (Figure 2 is a schematic presentation of the CTS).

The simulated time duration of a typical trajectory is half a second. A typical simulated distance at which the aerodynamic coefficients converged to the free stream values is about four meters.

The results which are obtained during a CTS test are analysed by a 11/780 VAX computer. The final position, velocities and accelerations are fed to a 6DOF simulation program and a complete trajectory of the store is calculated to the impact point.

3. The Test Program

3.1 Test Configurations

Two stores were tested in the present study·

1) A Mk-84 store which was released from a single pylon, located at station 3.

2) A Mk-82 store which was released from all three positions of a triple ejection rack (TER) and was also located at station 3.

During the release of the Mk-84, the parent aircraft was loaded with a 300 gallon fuel tank at station 5, a/a missiles at stations 1 and 9 and Mk-84 at station 7.

During the release of the Mk-82 the parent aircraft was loaded with a 300 gallon fuel tank at station 5, 370 gallon fuel tanks at stations 4 and 6, a/a missiles at stations 1 and 9 and Mk-82 stores at station 7 (Table 1 summarizes the aircraft configurations for all the tests conducted in the present study).

Table 1

#	Store	Stat.1-9	Stst.2-8	Stat.3-7	Stat.4-6	Stat.5
1	Mk-84	A-9	empty	T o	empty	300g
2	Mk-82	A-9	empty	*┼*	370g	300g
3	Mk-82	A-9	empty	*┼o	370g	300g
4	Mk-82	A-9	empty	o┼	370g	300g

T - Single pylon, ┼ - TER, *- Dummy store, o- Metric store.

3.2 Test Conditions

The stores were tested in simulating the following flight conditions:

1) The MK-84 was tested at Mach numbers 0.7 and 0.95, at level flight and at an altitude of 10000 feet.

2) The Mk-82 was tested at Mach numbers 0.7 and 0.8 at -40^{o} dive and at Mach number 0.9 at -40^{o} dive and in level flight, all at 7000 feet altitude. Table 2 summarizes the simulated flight conditions for all the CTS tests.

Table 2

Store	Station	Mach	Tests #	γ	q	H
Mk-84	T	0.7	1	0°	1	10 kft.
Mk-84	T	0.95	2	0°	1	10 kft.
Mk-82	⊥	0.7	3-4	-40°	1	7 kft.
Mk-82	⊥	0.8	5-7	-40°	1	7 kft.
Mk-82	⊥	0.9	8-10	0°	1	7 kft.
Mk-82	⊥	0.9	11	-40°	1	7 kft.

⊥- release from positions on the TER; T- release from a single pylon.

4. Tests Results and Discussion

4.1 The Mk-84

In the first part of this work, two CTS tests were conducted with the MK-84 store which was released from station 3.(see table 1). The tests were simulating flight conditions at Mach 0.7 and at Mach 0.95 (see table 2, tests 1 and 2). Two trajectories were calculated for each CTS test. In one, the 6DOF program considered only the ejection forces exerted on the store and the calculations were performed in free stream conditions while in the second the program used the end point of the trajectory, obtained by the CTS as the starting point of its calculations. As a result at M=0.7, the ground distance of the trajectory with the separation effect was shorter in 7 m. than the trajectory which was obtained without it. At M=0.95 the difference in ground distance was 25 m. In both Mach numbers there was a good agreement between the reports from flight tests and the results which were obtained for the runs with the separation effects. It was clear from the above mentioned results and from the sensitivity study (which will be demonstrated in the next chapter) that the

contribution of separation effect is significant to the ground distance. However, in order to have more significant differences in the ground distances , we proceeded in our work with the Mk-82 store which has a ballistic factor (W/CdS) 30% smaller than that of the Mk-84.

4.2 The Mk-82

The Mk-82 was tested with the CTS by simulating its release from three positions on the TER and at three Mach numbers: 0.7, 0.8 and 0.9 (see tables 1 and 2).

At M=0.7 the store was released from the two side positions of the TER. The 6DOF simulation calculations exhibited differences of 12 m. and 18 m. in ground distances for the outboard and the inboard TER positions, respectively. Figure 3 present the time histories of the the angle of pitch (ϑ) and the angle of yaw (ψ) for a release from the inboard TER position (see left hand and right hand figures, respectively). Figure 4 present the time histories of the rates in pitch (q) and yaw (r) for the same run. The lines with the circles, in both pctures, present the run with the separation effect and the lines with squares present the run without it. It is observed that the absolute values of the initial perturbations in ϑ and q of both runs are similar. However, ϑ and q decay faster in free stream than in the proximity of the parent aircraft. In the lateral direction, the initial perturbation in ψ and r is greater at the run with the effect of separation, but the perturbations in both runs decay at the same time.

At M=0.8 the store was released from all the three positions on the TER. It was found that the difference in ground distance (between using the separation effect and without using it) was two times larger (82 m.) for the lower position of the TER than the

distance which was obtained for the inboard position (41 m.). The difference in ground distance which was obtained for the outboard TER position was the shortest (26 m.). Figure 5 is a time history of the angles θ (on the left) and ψ (on the right),which were obtained for the release from the inboard position on the TER. Figure 6 is the time history of q and r for the same run. It is observed that the absolute value of the initial perturbation in θ and q is much larger in the proximity of the aircraft than the one in the free stream. One can also observe that the run with separation effect is converged to a steeper angle.

At both Mach numbers,0.7 and 0.8, the agreement between wind tunnel and flight test was satisfactory. The results which were obtained for the runs with separation effect do not differ from flight test in more than 10 m.

At M=0.9 (test # 11, table 2) when the Mk-82 was released from the inboard position of the TER and in tests 10-12 when the store was released in level flight the differences between calculations with separation effect and without it were greater than those which were obtained at lower Mach numbers. Moreover, the results didn't agree well with the results which were obtained in flight tests.At Mach number 0.9, the extreme angular motions of the store (see figures 7 and 8 for the euler angles and the angular rates, respectively) exceded sometimes the boundaries of operation of the CTS. It may be argued that the main contribution to the difference in ground distance should be a consequence of the motion in pitch (see the left hand sides of figures 7 and 8). The operational difficulties which were mentioned above may be solved in two ways:

1) Modifying the CTS rig to enlarge the envelope of motion.
2) Extrapolating the CTS tests by grid tests.

5. Sensitivity Study

A sensitivity study was conducted on the Mk-82 store. The main objective of this study was to explore the separation effect on the Circle of Error Probability (CEP) and on the difference in distances on the ground. The store was given an initial perturbation in the rate of pitch (q_o) or yaw (r_o) and the 6DOF simulation program calculated the distance on the ground. The values for the perturbation were similar to the values which were obtained during the CTS tests. Eight parameters were chosen to take part in a "monte carlo" method. An uncertainty value σ was attributed to each parameter, where at each run a value between 0 to $3x\sigma$ was randomly chosen (Table 3 summarizes the errors attributed to each parameter).

Table 3

ΔH	ΔV	$\Delta\gamma z=\Delta\gamma y$	ΔEJF	ΔW	Iyy=Izz	ΔXcg
18m.	2.5m/s (5knts)	0.1°	100 lb	12kg (15%)	2.5 $kg\text{-}m^2$ (5%)	0.5in (5%)

The runs were repeatedly conducted at identical conditions until 90% of the events were sufficient to converge the hits to a finite CEP, at finite distance ΔR from the target and at a standard deviation of σ.

Table 4 summarizes the results which were obtained for the Mk-82 when it was tested at Mach numbers 0.7 and 0.9.

Table 4

	M	α^{o}	$q_{o}^{o/s}$	$r_{o}^{o/s}$	ΔR m.	CEP m.	σ m.
1)	0.7	0.0	0.0	0.0	1.3	9.5	15.0
2)	0.7	0.0	-100.0	0.0	-31.0	10.0	15.0
3)	0.7	0.0	0.0	50.0	-1.5	9.8	15.0
4)	0.7	0.0	-100.0	50.0	-33.0	10.5	15.0
5)	0.9	-1.0	0.0	0.0	2.0	12.0	16.0
6)	0.9	-1.0	-100.0	0.0	-19.7	12.0	16.0
7)	0.9	-1.0	-100.0	50.0	-20.0	12.0	16.0

The first line in the table presents a test which was conducted without any perturbation . The miss distance was 1.3 m. and the radius of CEP was 9.5 m.

The second line in table 4 presents a test in which a perturbation of -100 degrees per second in the rate of pitch was exerted on the store. As a result, a miss sdistance of 31. m. was obtained, but the radius of CEP was changed only slightly (10 m).

A perturbation of 50 degrees per second in yaw rate did not contribute any significant change in range (see line 3).

A superposition of perturbations in pitch and yaw have similar effect as to the perturbation in pitch alone (see line 4).

Lines 5 through 7 present similar results for M=0.9 as those which were obtained for M=0.7 in lines 1 through 4.

The conclusion one can draw from the present study is that aerodynamic interference during separation will affect the range of the store but it will not affect the CEP.

It can be observed that the miss distances which were obtained in table 4 are smaller than the values which are obtained for

separation effect. This is explained by the fact that the method was conducted in free stream . Moreover, performing the "monte-carlo" method in the vicinity of the parent aircraft had shown similar miss distances to those which were obtained from the CTS and the 6DOF simulation. The CEP, as expected, was not affected by the flow and remained the same as in the free stream.

6. Conclusions

The complete trajectories, from release to impact, of the Mk-84 and the Mk-82 were calculated by utilizing a 6DOF simulation program. The program used the end results of CTS tests as an input to the ballistic simulation. It was found that the aerodynamic interference affected the ground distances significantly.

The differences in ground distances which were obtained for the Mk-84 were smaller than those which were obtained for the Mk-82, due to the smaller ballistic factor and the weaker ejection force of the latter.

There is an increase in the difference of ground distance with Mach number between different positions on a TER.

The results which were obtained for the Mk-84 at M=0.7 and at M=0.95 and those which were obtained for the Mk-82 at M=0.7 and M=0.8 agreed well with flight test reports.

At M=0.9 the trajectory of the Mk-82 exceeded the boundaries of the CTS and the end point could not be considered as initial point for the 6DOF simulation.

Sensitivity study which was conducted on the Mk-82 store supported the hypothesis that the aerodynamic interference during separation contributes significantly to the ground distances. Therefore the CTS can be used as a main tool in predicting the complete trajectories of stores from release to impact.

References:

[1] Arnold R. J. and Epstein C.S., "AGARD Flight Test Techniques Series Volume 5 on Store Separation Flight Testing", AGARDograph No. 300.

[2] The "HORROR FILM" by Charles S. Epstein, Armcon INC.

[3] Maddox A.R., "Store Separation Trajectory Analysis", J. Aircraft Vol. 17, No. 11 November 1980.

[4] Gonzalez J.M. and Denney A.R., Lt. USAF, "Theoretical Sensitivity Analysis and System Delivery Accuracy Computations for High and Low Drag Weapons at Several Subsonic and Supersonic delivery Conditions". Technical Report AFATL-TR-70-110.

List of Figures

Figure 1. Mk-82 on the GIS at Israel Aircraft Industries

THIS PAGE INTENTIONALLY LEFT BLANK

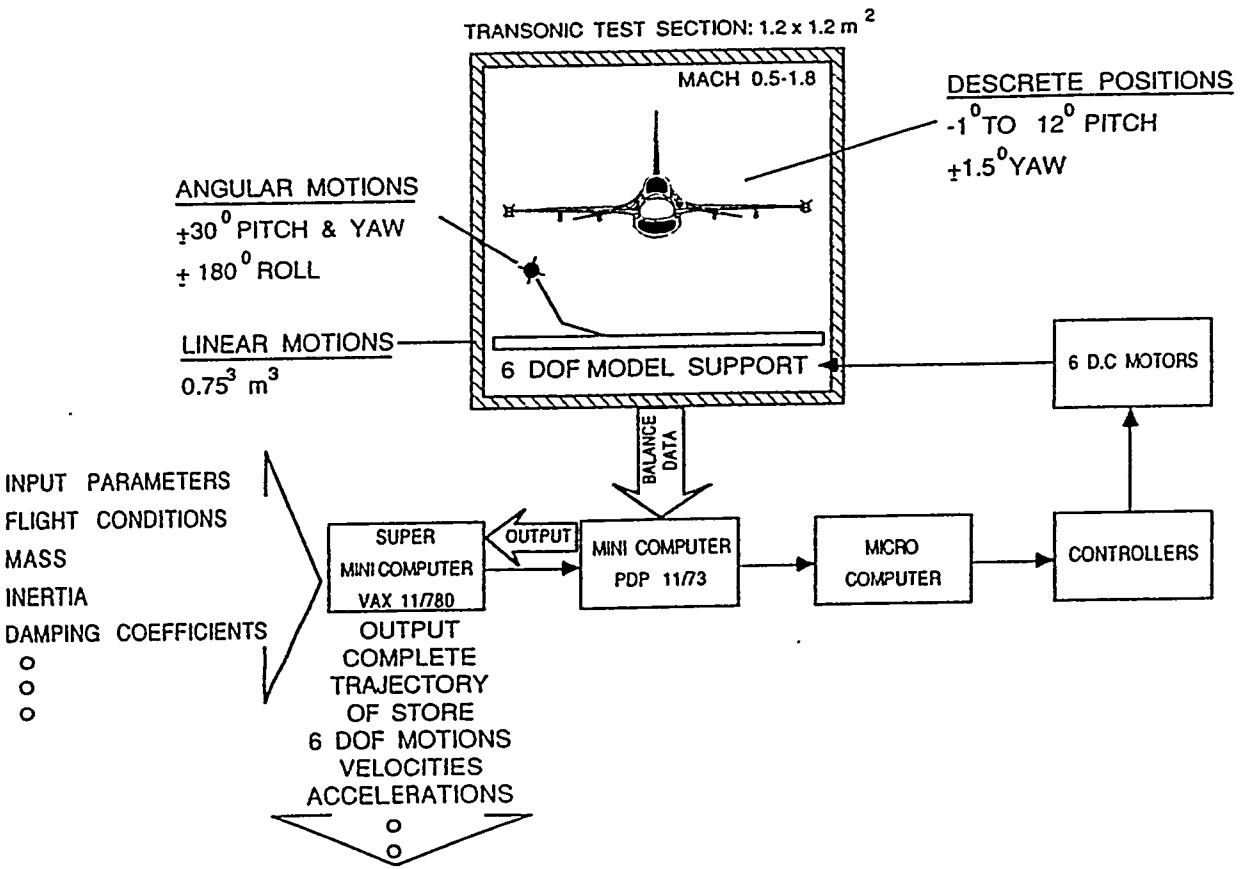

IAI TASHAN Engineering Center
AIRCRAFT DIVISION / ISRAEL AIRCRAFT INDUSTRIES LTD

Figure 2. A Schematic Chart of the CTS

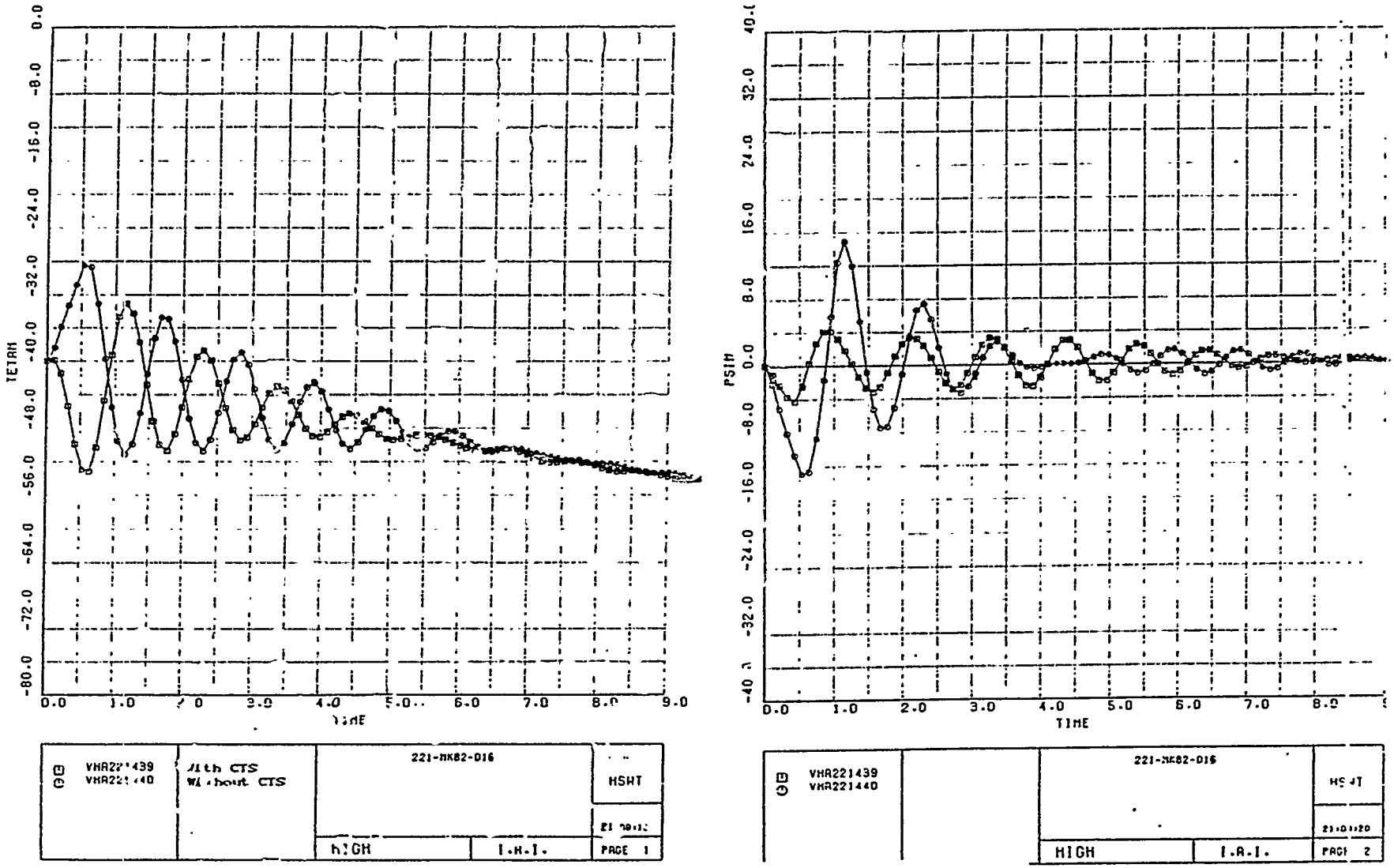

Figure 3. The Time History of Pitch (Left) and Yaw (Right) for A Release of Mk-82 From the Inboard TER Position at M=0.7

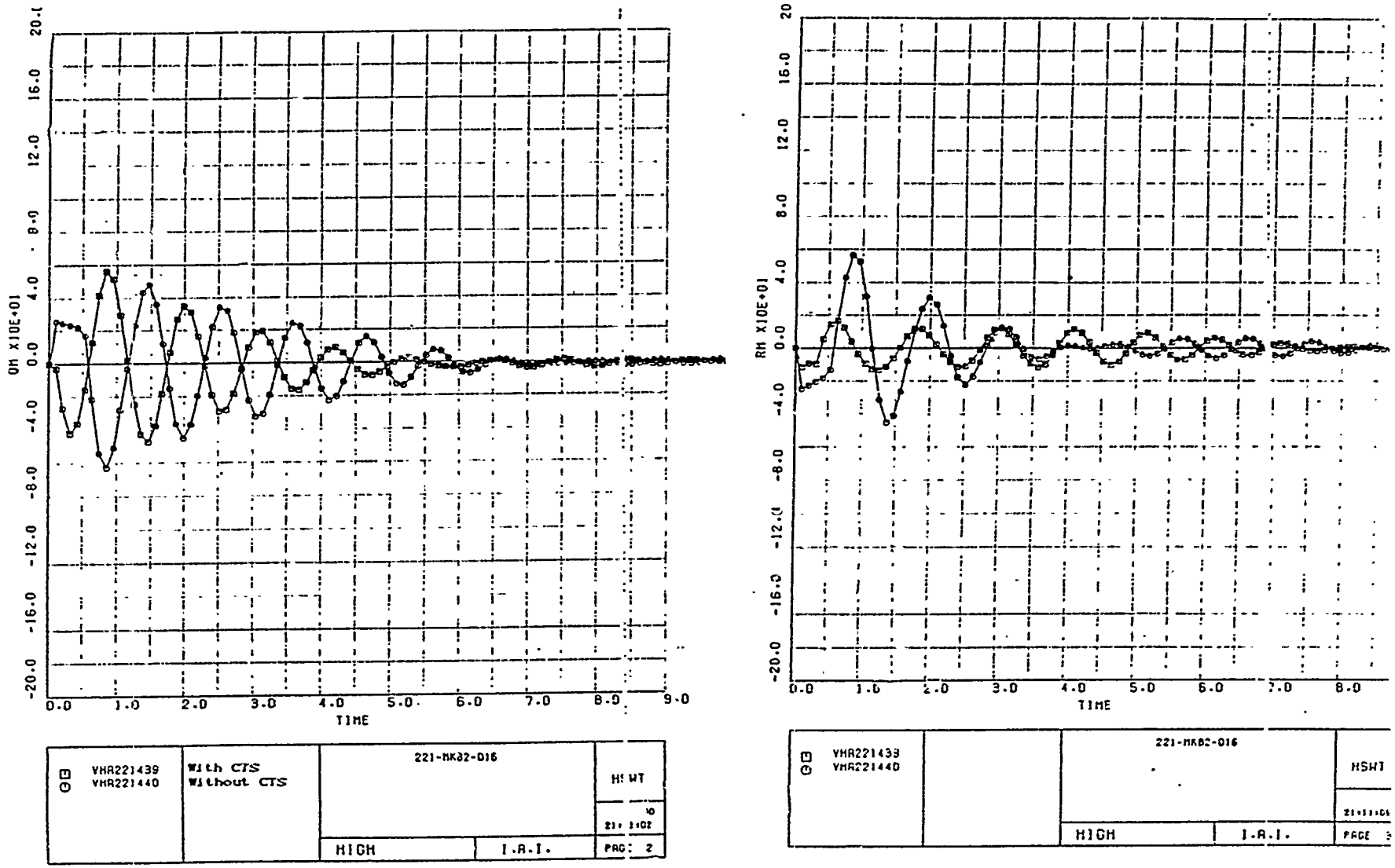

Figure 4. The Time History of the Rate of Pitch (left) and the Rate of Yaw (right) for A Release of Mk-82 From the Inboard TER Position at M=0.7

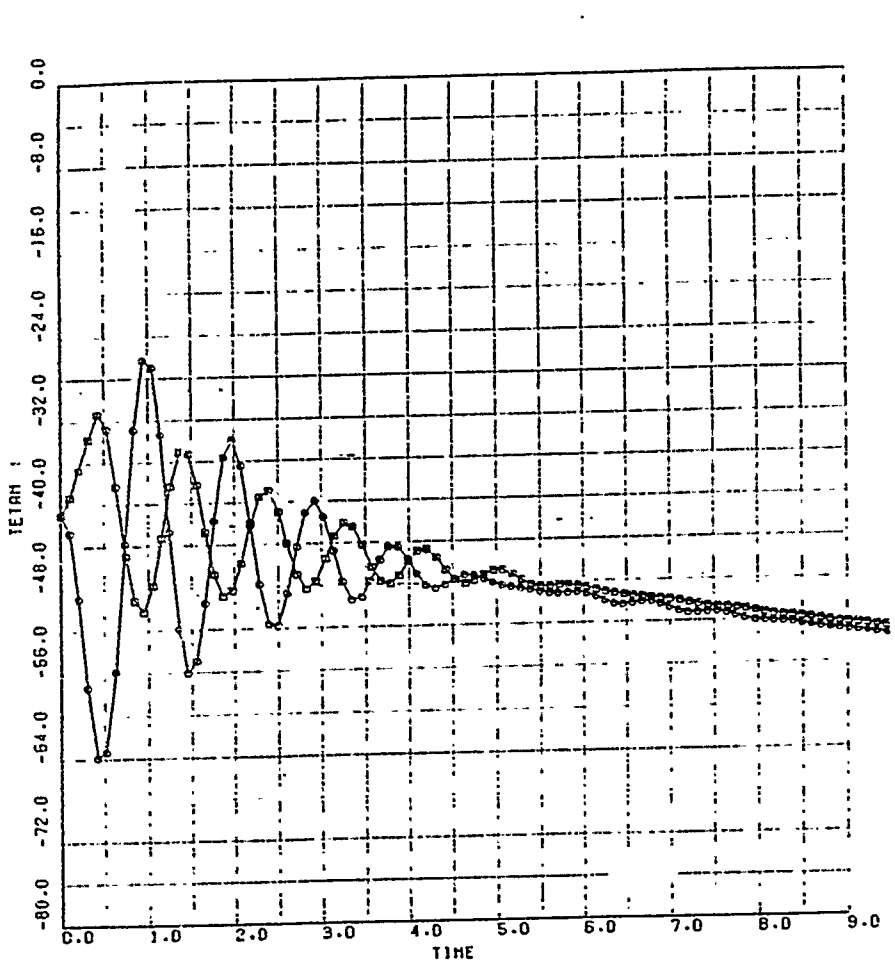

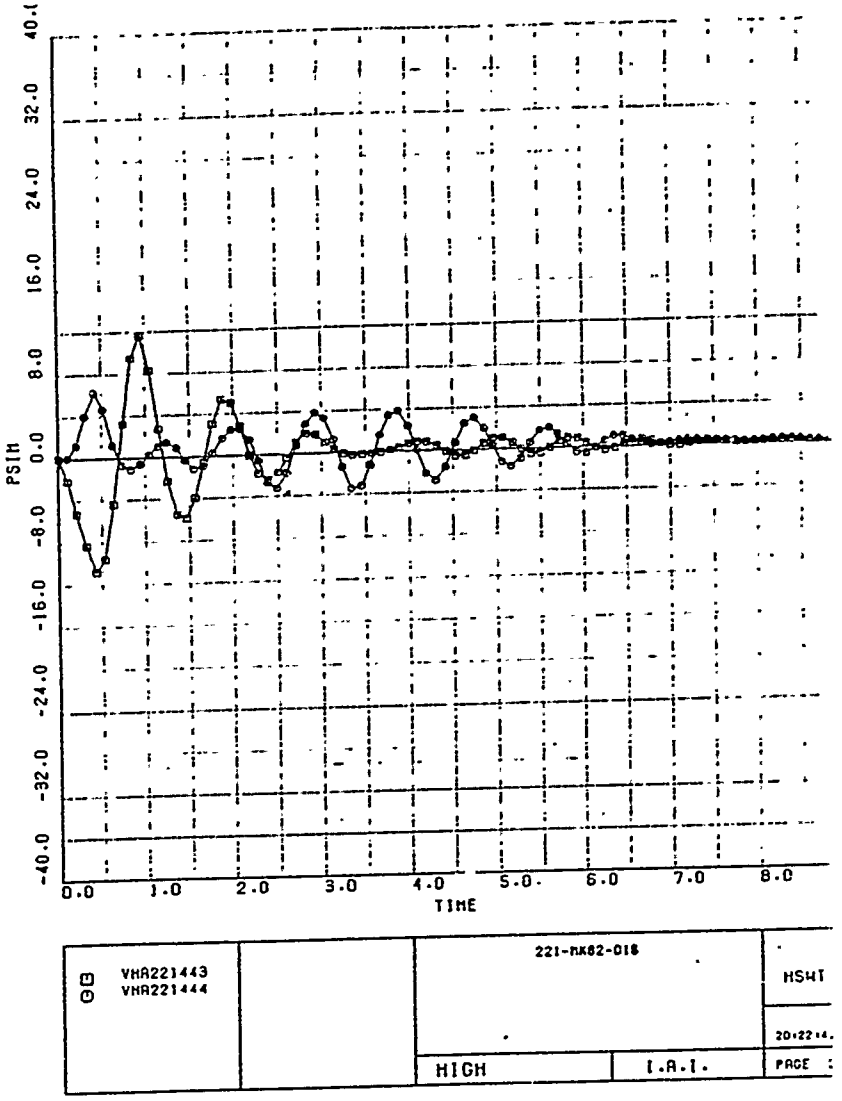

Figure 5. The Time History of Pitch (left) and Yaw (right) for A Release of Mk-82 From the Inboard TER Position at M=0.8

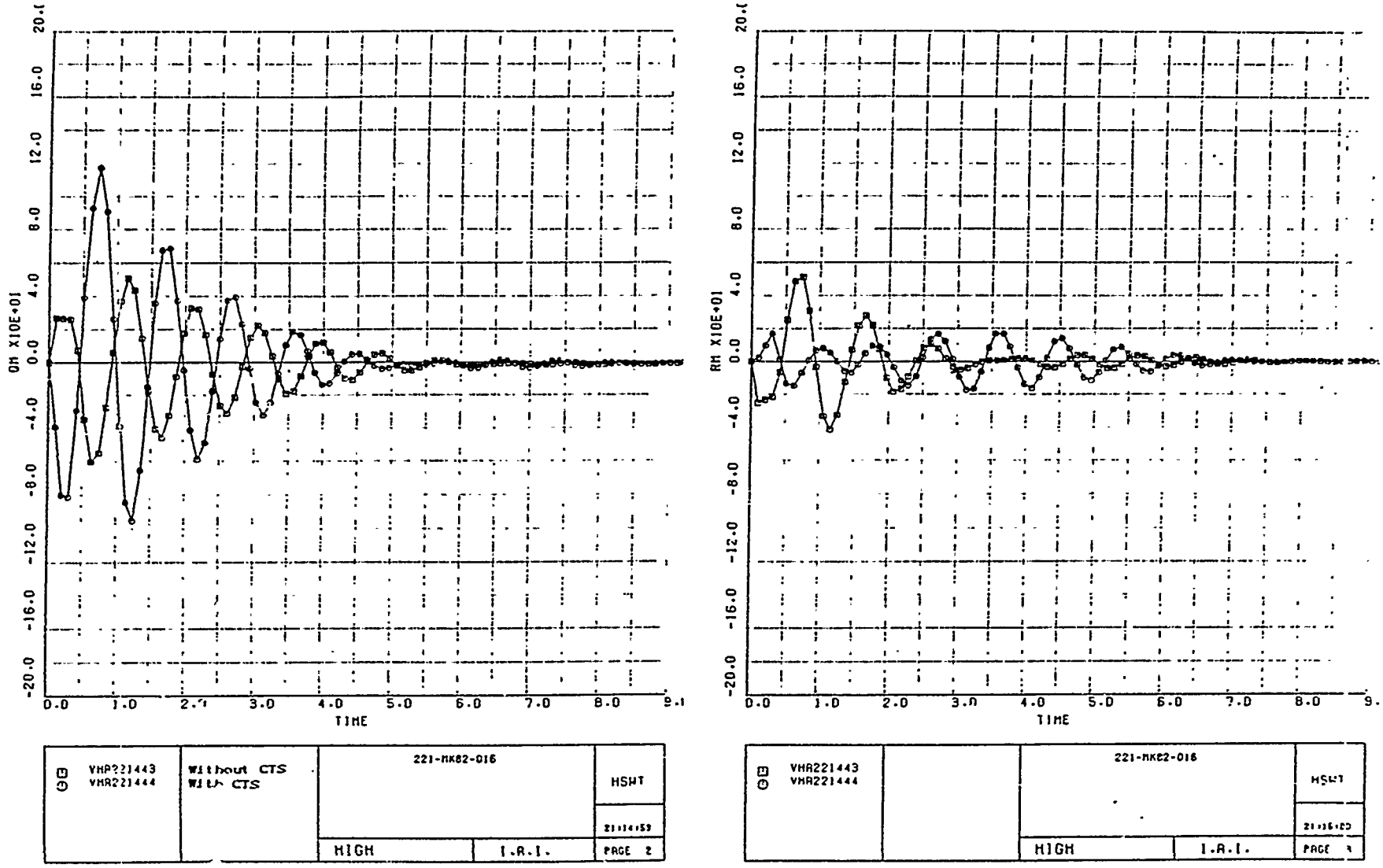

Figure 6. The Time History of the Rate of Pitch (left) and the Rate of Yaw (right) for A Release of Mk-82 From the Inboard TER Position at M=0.8

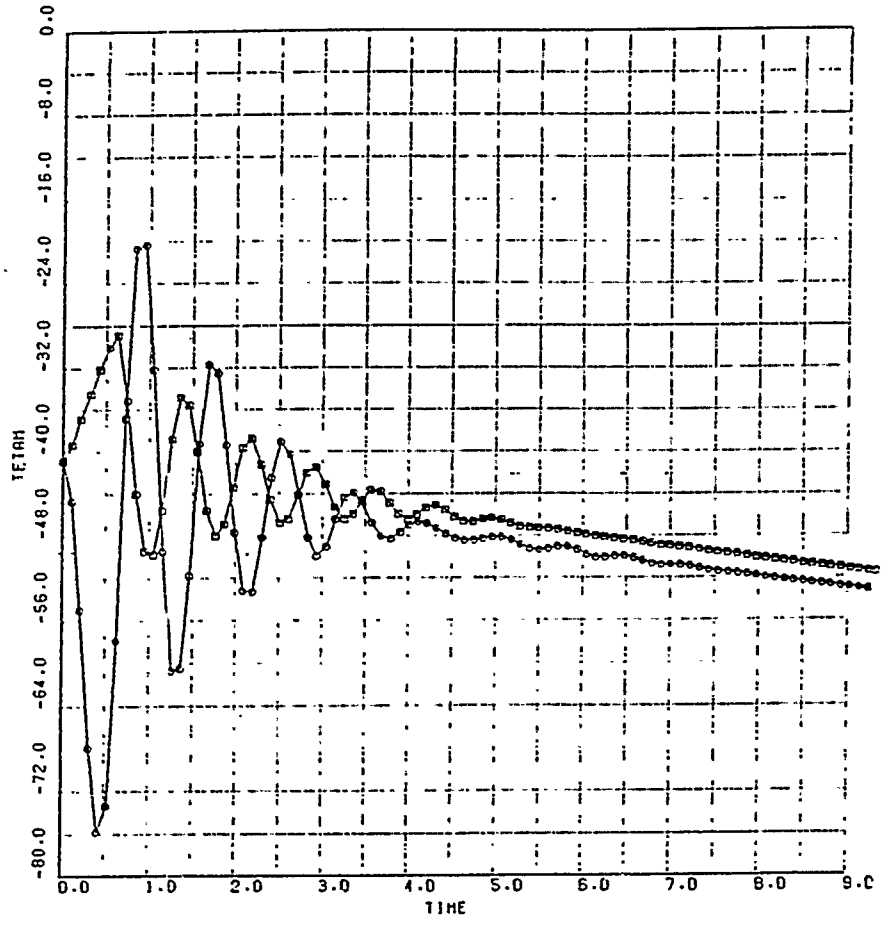

VHA221435 VHA221436	Without CTS With CTS	221-MK82-016	HSWT 20:40:23
		HIGH I.A.I.	PAGE 1

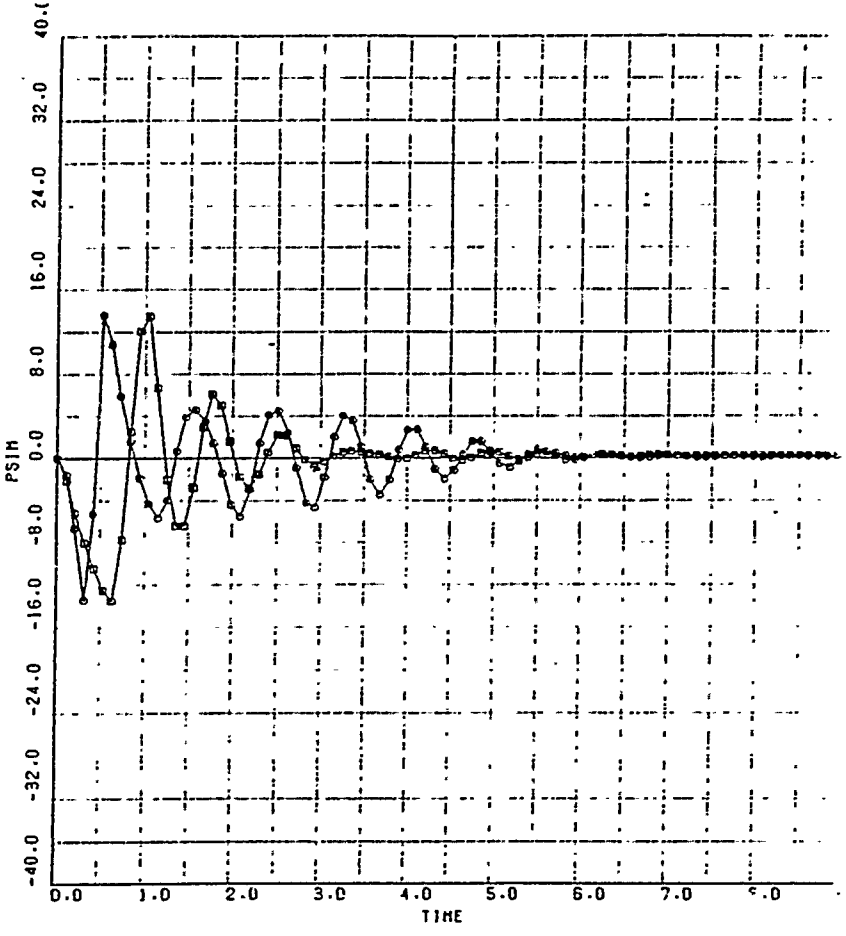

VHA221435 VHA221436		221-MK82-016	HSWT 20:40:29
		HIGH I.A.I.	PAGE 2

Figure 7. The Time History of Pitch (left) and Yaw (right) for A Release of Mk-82 From the Inboard TER Position at M=0.9

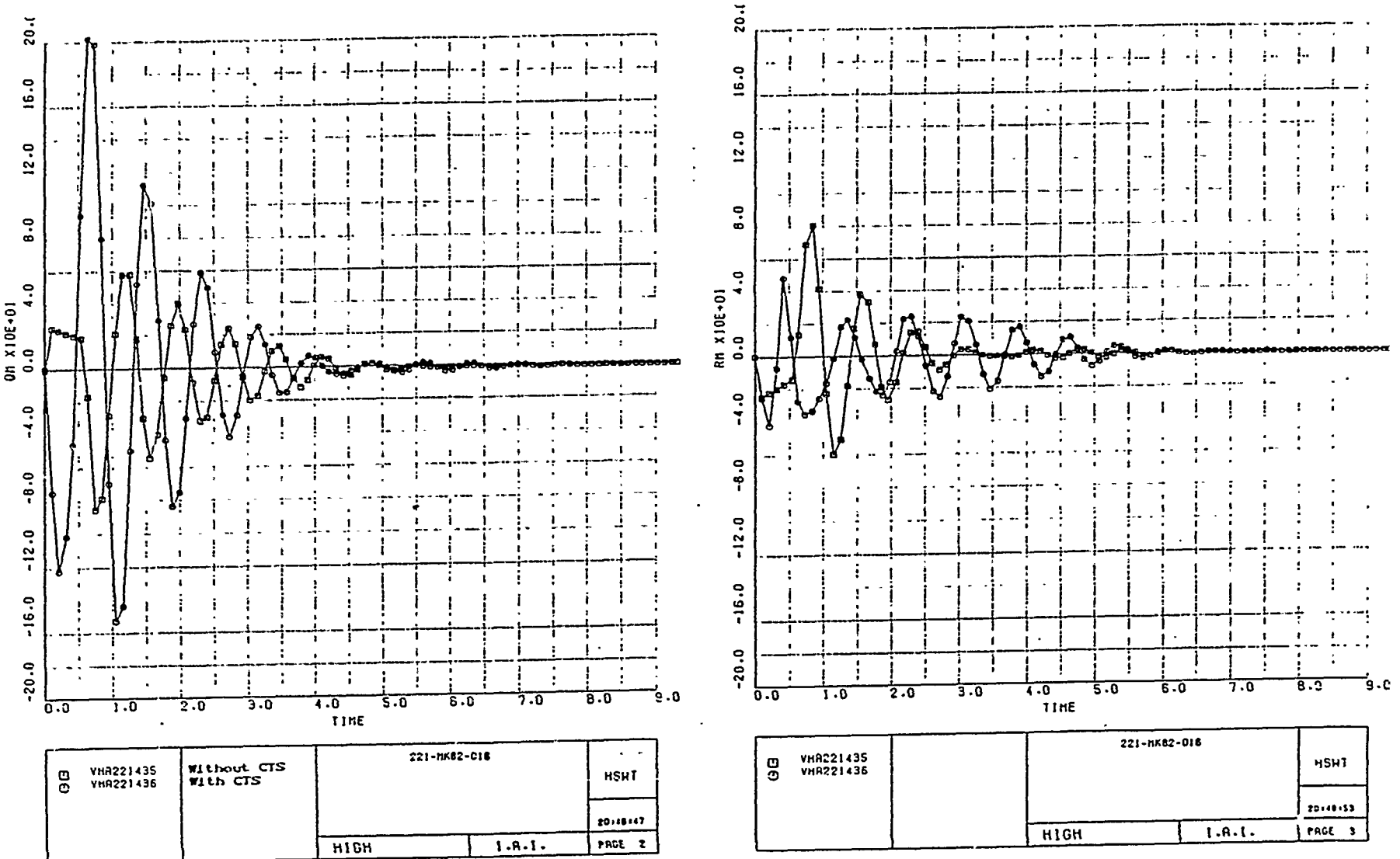

Figure 8. The Time History of the Rate of Pitch (left) and the Rate of Yaw (right) for A Release of Mk-82 From the Inboard TER Position at M=0.9

Biography of Authors

Dr. Moshe Zilberman received his B.Sc (1974), M.Sc (1976) and Ph.D (1981)from the Tel-Aviv University in ISRAEL. He has been working at IAI since 1979 on numerous R&D projects. Since 1988 he is the manager of R&D and Marketing in the Wind Tunnels Center at IAI. He is also a lecturer in the Faculty of Engineering in the Tel-Aviv University.

Maj. Alon Shlezinger received his B.Sc in Aeronautical Engineering from the Technion in 1981. Since then he has been part of the a/c store compatibility group of the IAF.

Lt. Tsahi Cohen (IAF) received his B.Sc in Aeronautical Engineering from the Technion-Israel Institute of Technology in 1988.Since then he has been assigned to the a/c store compatibility group in the IAF.

Israel Shruster received his B.Sc (1971) from the State University of Latvia, Riga and his M.Sc (1976) from the Technion in Israel. He is presently a senior engineer with Aerodynamic and Simulation department at MBT of IAI, ISRAEL.

Moti Shay received his B.Sc in Aerodynamic Engineering from the Technion of Haifa in 1977. He is a senior engineer with Aerodynamic and Simulation department at MBT of IAI, ISRAEL.

INSTRUMENTATION MEASUREMENT ACCURACY REQUIREMENTS (IMAR) FOR 6DOF BALLISTIC ANALYSES

by Gerald Solomon

Orlando Technology Incorporated
Shalimar, Florida

1.0 ABSTRACT

Instrumentation is available or in development which can provide measurements of weapon attitude (roll,pitch, and yaw rates and accelerations) during its flight. The measurements may be used to verify safe separation, to validate wind tunnel derived aerodynamics, and to determine aerodynamic coefficients required to match a simulated trajectory with the measured trajectory. The latter is used by ballisticians in developing ballistic models for delivery tables and for aircraft fire control ballistic computer applications. However, current ballistic analyses are limited to cinetheodolite tracking measurements from which weapon position, velocity, and acceleration are derived. In addition, these measurements produce intolerable position and velocity errors in the vicinity of the release aircraft. Since initial conditions are critical to accurate ballistic analyses, accurate measurements of the weapon attitude and position are needed from release to at least 3.0 seconds of flight. The emphasis on this time frame is because of the complex interaction of the weapon with the flowfield about the aircraft. The induced ballistic effects during separation are requiring large numbers of flight test drops to approximate. Weapon flight measurements in this area should lead to more accurate ballistic models with fewer flight tests. Flight variables to be measured and the level of the measurement accuracy needed are to be determined in the IMAR program.

The IMAR program will develop the analytical tools needed to determine the measurement accuracy requirements. The requirement is to develop accurate

ballistic models from the measurements. How accurate the ballistic models need to be depend on the aircraft accuracy (avionics/fire control) and the tactical application. IMAR will not assess ballistic model accuracy requirements but it will show the ballistic model accuracy in terms of the measurement accuracy. The analytical tools needed are methods to simulate measurement errors that may occur, methods to determine force and moment coefficients from the measurements, and methods to assess the ballistic accuracy as a result of using the coefficients to predict the weapon trajectory.

The first phase of the IMAR program will develop the method to determine the force and moment coefficients from flight test measurements. This development will be completed by October 1990. Similar methods have been applied to test where the vehicle is under control or the environment (mach number, air density, winds, etc.) is controlled. In this application the vehicle and the environment is uncontrolled so the aerodynamic force and moment models must be free to assume whatever form is needed to match the weapon's complex motion. In addition, the parameter estimation technique applied must be convergent with poor initial parameter estimates. The methodology (computer program) will provide a 6DOF ballistic analysis capability.

2.0 INTRODUCTION

In May 1988, the Air Force Armament Laboratory requested the 3246 Test Wing's assistance in defining instrumentation requirements for the SEEK EAGLE process relating to store separation and ballistic analysis. Orlando Technology, Inc. identified current instrumentation requirements for ballistic analyses using the ballistic analysis methods developed under the Ballistics Technology Improvement Plan (BTIP). These requirements directed improvements

in the 3DOF ballistic analysis area. In addition, an approach to advance the ballistics analysis capability to the 6DOF level was outlined. The approach outlined is:

1. Develop a method to determine 6DOF ballistics data from measurements of certain 6DOF state variables.
2. Develop a method to simulate the measurement of 6DOF state variables by embedding a simulation of the instrumentation measurement error in a 6DOF trajectory program.
3. Generate simulated 6DOF TSPI with various levels of instrumentation measurement error and determine the associated errors in the ballistics data determined from the 6 DOF ballistics analysis method.
4. Use the ballistics data (means and variances of the aerodynamic coefficients) in the BTIP program, BEAM, and determine the weapon MPI and CEP sensitivity to the errors in the ballistics data. Subsequently, establish the relationship between an instrument measurement error and its effect on the accuracy of the derived ballistics data.

The software development and studies in the approach were submitted to the SEEK EAGLE office as projects that could enhance the SEEK EAGLE process. The program was approved, funded, and given the acronym "IMAR". The IMAR program will provide data which show the effects of measurement errors on the derived ballistic coefficients and the subsequent accuracy of the derived ballistic models. These data will assist in selecting instruments with sufficient accuracy and reasonable cost. Figure 1 presents a flow diagram to illustrate how these data are to be determined. When the 6DOF instrumentation is operational, the 6DOF ballistic analysis capability developed under IMAR

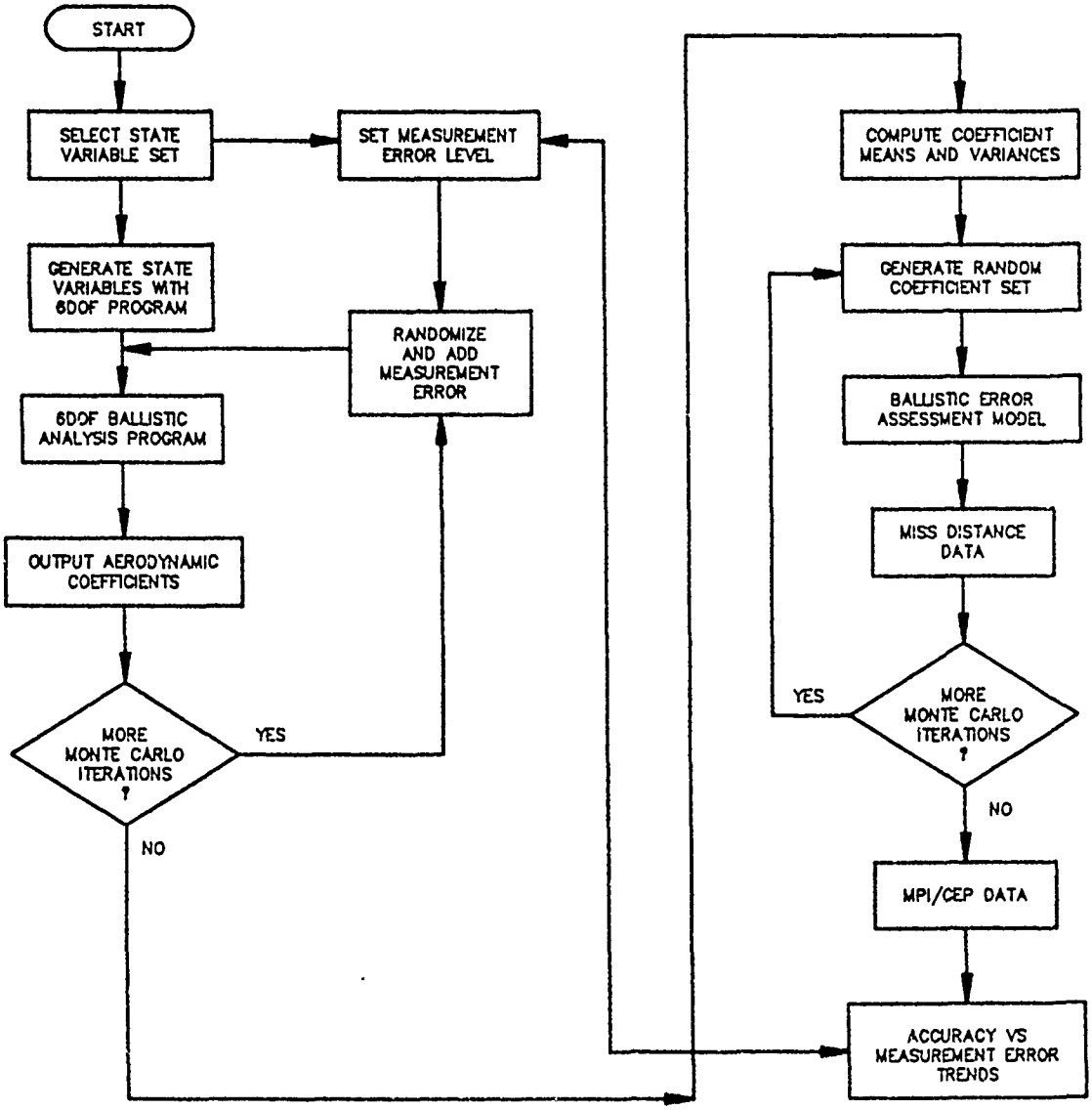

Figure 1. IMAR Program Functional Flow Diagram

will be available to determine the force and moment coefficients from the measured weapon motion. These data are to be used in developing accurate ballistic models and to compare with and possibly improve other approaches such as wind tunnel testing and computational fluid dynamics. Since more weapon state variables are measured in this process there are fewer unknowns in the ballistic equations. A reduction in the number of required weapon drops is anticipated with an additional improvement in ballistic model accuracy.

The IMAR program is dependent on the development of a 6DOF ballistic analysis method or computer program. Its development is the first task undertaken in the IMAR program. The theory applied and the results obtained as of August 15, 1990 are presented in this paper. The 6DOF ballistic analysis method is referred to as SDBAM.

3.0 6DOF BALLISTIC ANALYSIS METHOD (SDBAM)

SDBAM is a computer program which receives state variable measurements such as body axis angular acceleration and linear accelerations as input and derives the aerodynamic coefficients needed in the 6DOF equations of motion. The procedure employs non-linear least squares techniques referred to as the Newton, Gauss-Newton, or Newton-Raphson procedure [1]. The procedure is perhaps better known as the Chapman-Kirk method [2] because of their application of the Newton procedure to the problem of estimating aerodynamic coefficients from flight test data. In the IMAR application, an addition feature is added to the Newton method referred to as the Marquardt algorithm [3]. The Marquardt algorithm, as implemented, eliminates the need for an initial estimate of the aerodynamic coefficients to start the non-linear least squares procedure.

3.1 Least Squares Parameter Estimation

A review of parameter estimation theory is presented using both linear and non-linear scalar equations for illustrations. In SDBAM, the equations are the 6DOF differential equations of motion and the coefficients to be estimated are the aerodynamic force and moment coefficients.

The usual situation which requires a parameter estimator is a set of measurements (dependent variables) made at discrete intervals such as time or distance (the independent variable) of a process. The process is modeled mathematically and referred to as the state model. The state model usually contains proportionality constants, parameters or simply stated "fudge" factors which relate the model to reality (measured states). The values of these parameters are to be estimated in some "optimal" fashion to cause the model to "best" represent the set of measurements. If the mathematical model was absolutely correct then the measurements could be expressed as

$$Z = HX + V \tag{1}$$

where **Z** is an n x 1 vector of n measurements. **HX** represents the measurement as predicted by the mathematical model and **V** is an n x 1 vector of the errors in the measurements referred to as the instrumentation error. H is an n x m matrix which relates the measurements to the m x 1 vector of parameters **X**. If the measurement errors are unknown the "best" estimate of **X** is a least squares estimate.

3.2 Linear Least Squares Estimation

As an example, assume measurements of y are available as a function of time and that y is mathematically modeled as

$$y = C_1 + C_2 t + C_3 t^2 + C_4 t^3. \tag{2}$$

The measurement of each y is contaminated by an error in the instrumentation. The set of n measurements, Z, is expressed as

$$\begin{bmatrix} z_1 \\ z_2 \\ z_3 \\ . \\ . \\ . \\ z_n \end{bmatrix} = \begin{bmatrix} 1 & t_1 & t_1^2 & t_1^3 \\ 1 & t_2 & t_2^2 & t_2^3 \\ 1 & t_3 & t_3^2 & t_3^3 \\ . & . & . & . \\ . & . & . & . \\ . & . & . & . \\ 1 & t_n & t_n^2 & t_n^3 \end{bmatrix} \begin{bmatrix} C_1 \\ C_2 \\ C_3 \\ C_4 \end{bmatrix} + \begin{bmatrix} V_1 \\ V_2 \\ V_3 \\ . \\ . \\ V_n \end{bmatrix} \qquad (3)$$

In this example the system is linear in relation to the parameters C_1 through C_4. Linear estimation techniques may be applied.

The least squares method min'izes the sum of the squares of the residuals (SSR). A residual is defined as the difference between a measurement and the model prediction for that measurement. In matrix notation form SSR is

$$SSR = (Z - H\hat{X})^T(Z - H\hat{X}) = V^TV. \qquad (4)$$

T denotes a matrix transpose and the symbol $\hat{}$ specifies an estimate for X. SSR is differentiated with respect to $\hat{X}$, the derivative set to zero (to minimize), and the equation solved for $\hat{X}$. That is

$$\frac{\partial SSR}{\partial \hat{X}} = 0$$

$$-H^T(Z - H\hat{X}) + (Z - H\hat{X})(-H) = 0$$

$$- 2\, H^T(Z - H\hat{X}) = 0$$

$$H^T H\hat{X} = H^T Z$$

$$\hat{X} = (H^T H)^{-1} H^T Z \qquad (5)$$

The solution to (5) is obtained by performing the indicated matrix operations. In the form

$$(H^T H)\,\hat{X} = H^T Z$$

the linear example given in equation (3) becomes

$$nC_1 + \sum^n t_i C_2 + \sum^n t_i^2 C_3 + \sum^n t_i^3 C_4 = \sum^n z_i$$

$$\sum^n t_i C_1 + \sum^n t_i^2 C_2 + \sum^n t_i^3 C_3 + \sum^n t_i^4 C_4 = \sum^n z_i t_i$$

$$\sum^n t_i^2 C_1 + \sum^n t_i^3 C_2 + \sum^n t_i^4 C_3 + \sum^n t_i^5 C_4 = \sum^n z_i t_i^2 \qquad i=1 \text{ to } n$$

$$\sum^n t_i^3 C_1 + \sum^n t_i^4 C_2 + \sum^n t_i^5 C_3 + \sum^n t_i^6 C_4 = \sum^n z_i t_i^3.$$

The above system of linear equations in C_1 through C_4 may be solved using linear algebra (i.e. Cramer's method). The same results are obtained by the matrix operation in (5).

If the mathematical model is not linear in the coefficients or parameters, the least squares estimation process must be modified such that a solution may be found in a piece-wise linearization process. The following equation represents a mathematical model that is non-linear with respect to some of the parameters.

$$y = A\, e^{Bt}\cos(Ct) \qquad (6)$$

The model is non-linear with respect to B and C. If n measurements of a

process represented by (6) is made, the measurement model becomes

$$Z = h(x) + v \tag{7}$$

or

$$\begin{aligned} Z_1 &= A\, e^{Bt_1}\cos(Ct_1) + V_1 \\ Z_2 &= A\, e^{Bt_2}\cos(Ct_2) + V_2 \\ &\cdot \qquad\quad \cdot \qquad\quad \cdot \\ &\cdot \qquad\quad \cdot \qquad\quad \cdot \\ Z_n &= A\, e^{Bt_n}\cos(Ct_n) + V_n. \end{aligned}$$

Note that the parameters B and C are "embedded" in the mathematical model such that linear algebra or linear estimation cannot be applied to solve for the parameters. Equation (7) is similar to equation (1) with the mathematical model expressed as h (x) to denote a non-linear model in x.

The measurement model in (7) may be linearized about an estimate for x. Let the initial estimate for x be $\hat{x}_o$. Now expand h(x) about $\hat{x}_o$ in a Taylor series to obtain

$$h(x) = h(\hat{x}_o) + \frac{\partial h(\hat{x}_o)}{\partial x}(x - \hat{x}_o) + \frac{1}{2}\frac{\partial h(\hat{x}_o)}{\partial x^2}(x - \hat{x}_o)^2$$

$$+ \text{higher order terms.} \tag{8}$$

If $\hat{x}_o$ is sufficiently close to x, then the higher order terms are insignificant. Retaining linear terms only, equation (7) becomes

$$Z \simeq h(\hat{x}_o) + \frac{\partial h(\hat{x}_o)}{\partial x}(x - \hat{x}_o) + V. \tag{9}$$

or

$$Z - h(\hat{x}_o) = \frac{\partial h(\hat{x}_o)}{\partial x} (x - \hat{x}_o) + V \tag{10}$$

Now let

$$r = Z - h(\hat{x}_o),$$

$$G = \frac{\partial h(\hat{x}_o)}{\partial x},$$

and $\Delta\hat{x} = x - \hat{x}_o$

These substitutions into (10) gives

$$r = G\Delta\hat{x} + V. \tag{11}$$

Equation (11) is linear with respect to $\Delta\hat{x}$, that is, the error in the estimate. Using linear least squares $\Delta\hat{x}$ can be obtained. Note that (11) is of the same form as (1) and a solution is obtained similar to (5). That is

$$\Delta\hat{x} = (G^T G)^{-1} G^T r. \tag{12}$$

By adding $\Delta\hat{x}$ to the original estimate of $\hat{x}_o$ an improved or "better" estimate of x is obtained. This improved estimate suggests an iterative process which should converge in the limit to x. The iterative process is expressed as

$$\begin{aligned} \hat{x}_{i+1} &= \hat{x}_i + \Delta\hat{x}_i \\ &= \hat{x}_i + \left[\left(\frac{\partial h(\hat{x}_i)}{\partial x}\right)^T \frac{\partial h(\hat{x}_i)}{\partial x}\right]^{-1} \left(\frac{\partial h(\hat{x}_i)}{\partial x}\right)^T (Z - h(\hat{x}_i)). \end{aligned} \tag{13}$$

The method is now applied to the example model given by equation (6) where

$$h(x) = Ae^{Bt}\cos(Ct).$$

The first task is to determine the derivative of h(x) with respect to x. That is

$$\frac{\partial \hat{h}(x)}{\partial A} = e^{Bt}\cos(Ct)$$

$$\frac{\partial \hat{h}(x)}{\partial B} = Ate^{Bt}\cos(Ct)$$

and

$$\frac{\partial \hat{h}(x)}{\partial C} = -Ate^{Bt}\sin(Ct)$$

The expanded matrix $\frac{\partial h(\hat{x}_i)}{\partial x}$ is a matrix of the partial derivatives evaluated at each measurement point with the current estimate of x or A, B, and C. This matrix is often referred to as the sensitivity matrix. For n measurements the sensitivity matrix for the example becomes

$$\frac{\partial h(x_i)}{\partial x} = \begin{bmatrix} e^{Bt_1}\cos(Ct_1) & At_1e^{Bt_1}\cos(Ct_1) & -At_1e^{Bt_1}\sin(Ct_1) \\ e^{Bt_2}\cos(Ct_2) & At_2e^{Bt_2}\cos(Ct_2) & -At_2e^{Bt_2}\sin(Ct_2) \\ \cdot & \cdot & \cdot \\ \cdot & \cdot & \cdot \\ e^{Bt_n}\cos(Ct_n) & At_ne^{Bt_n}\cos(Ct_n) & -At_ne^{Bt_n}\sin(Ct_n) \end{bmatrix}$$

For an illustration of the application of the technique, values for y from equation (6) were generated with assumed values of A, B, and C. These y values were assumed to be measurements with zero measurement error. The iterative technique was applied with the results tabulated as a function of iteration cycle in Table 1. The parameter values at cycle "0" were the initial estimates.

TABLE 1. Convergence Example for Non-linear Least Squares

	ITERATION CYCLE							
PARAMETER	0	1	2	3	4	5	6	TRUE VALUES
A	20	22.19	25.95	24.92	25.01	25.99	25.00	25.00
B	0	-.712	-.783	-.496	-.503	-.499	-.500	-.500
C	2	2.544	3.352	3.075	3.141	3.14159	3.14159	3.14159

The Marquardt algorithm simply adds a factor, λ , to the G^TG matrix diagonal that causes the non-linear method to converge with relatively poor estimates of the parameters or coefficients. Thus,

$$\Delta X = (G^TG + \lambda I)^{-1}G^Tr. \qquad (14)$$

It can be shown that when λ approaches plus infinity, equation [14] approaches the same solution provided by the method of Steepest Descent. The Steepest Descent method is known to converge with poor initial parameter estimates but converges slowly. When the λ is zero (Gauss-Newton), poor initial estimates can cause divergence, but good estimates will converge and converge rapidly. Thus, the desired approach is to start the procedure with a large λ and then reduce it as the estimate improves to speed up convergence.

In the previous non-linear example, convergence was obtained within six iterations. At initial estimates values of 10, 0, and 1 for coefficients A, B, and C respectively, divergence occurred instantly. With λ set to 10,

convergence was achieved in approximately 15 iterations. With initial coefficient estimates of 0.1, 0.0, and 0.1, convergence occurred with 25 iterations.

3.3 Force and Moment Equations

The 6DOF equations used are the equations of motion used by the 3246 Test Wing in a number of applications, one of which includes trajectory simulation for safe separation assessments. In these equations there are ejection forces and moments acting in combination with aerodynamic forces and moments. The ejector forces and moments are assumed to be known in this presentation. However, they may be included as unknown forces in later developments. For the present, all forces and moments are of an aerodynamic origin. The equations and coordinate systems are further defined in Etkin[4]. The equations are listed in Figure 2 for reference.

The body axis equations for angular motion are integrated to provide body axis roll, pitch, and yaw rates. The Euler angle rate equations are integrated to provide Euler attitude angles of the weapon. The translational equations of motion are integrated in an earth fixed or test range coordinate system. The equations provide model estimates for measurements made directly by body mounted angular accelerometers and rate gyros. The Euler angles and rates could be provided by an inertial platform or other means.

The aerodynamic forces acting along the body axes are transformed to an earth fixed coordinate system using the transformation matrix as shown in Figure 2. These equations are best suited for ground based measurements of position, velocity, and acceleration. The body axis translational equations may also be integrated to provide body axis velocity components. The velocity components may be transformed to earth fixed velocity components from which

Body axis angular accelerations:

$$\begin{bmatrix} \dot{p} \\ \dot{q} \\ \dot{r} \end{bmatrix} = \bar{q}\,s\,d \begin{bmatrix} C_l / I_x \\ C_m / I_y \\ C_N / I_z \end{bmatrix} + \bar{q}\,s\,d^2 \begin{bmatrix} p\,C_{lp} / 2v\,I_x \\ q\,C_{mq} / 2v\,I_y \\ r\,C_{Nr} / 2v\,I_z \end{bmatrix} + \begin{bmatrix} 0 \\ (I_z - I_x)\,r\,p / I_y \\ (I_x - I_y)\,p\,q / I_z \end{bmatrix}$$

Euler angle rates:

$$\begin{bmatrix} \dot{\phi} \\ \dot{\theta} \\ \dot{\psi} \end{bmatrix} = \begin{bmatrix} 1 & \text{SIN}\,\phi\,\text{TAN}\,\theta & \text{COS}\,\phi\,\text{TAN}\theta \\ 0 & \text{COS}\,\phi & -\,\text{SIN}\,\phi \\ 0 & \text{SIN}\,\phi\,\text{SEC}\,\theta & \text{COS}\,\phi\,\text{SEC}\,\theta \end{bmatrix} \begin{bmatrix} p \\ q \\ r \end{bmatrix}$$

Earth axis linear accelerations:

$$\begin{bmatrix} \ddot{x} \\ \ddot{y} \\ \ddot{z} \end{bmatrix} = \bar{q}\,s/m \begin{bmatrix} a_{11} & a_{21} & a_{31} \\ a_{12} & a_{22} & a_{32} \\ a_{13} & a_{23} & a_{33} \end{bmatrix} \begin{bmatrix} C_x \\ C_y \\ C_z \end{bmatrix} + \begin{bmatrix} 0 \\ 0 \\ g \end{bmatrix}$$

a_{11} = COS θ COS ψ
a_{12} = COS θ SIN ψ
a_{13} = - SIN θ
a_{21} = SIN φ SIN θ COS ψ - COS φ SIN ψ
a_{22} = SIN φ SIN θ SIN ψ + COS φ COS ψ
a_{23} = SIN φ COS θ
a_{31} = COS φ SIN θ COS ψ + SIN φ SIN ψ
a_{32} = COS φ SIN θ SIN ψ - SIN φ COS ψ
a_{33} = COS φ COS θ

v = weapon velocity

$\bar{q} = 1/2\,\rho\,v^2$

$s = \pi\,d^2/4$

ρ = air density

d = reference diameter

m = weapon mass

g = gravity acceleration

I_x, I_y, I_z = Roll, pitch and yaw moments of inertia

Figure 2. SDBAM Equations of Motion

integration yields earth fixed position. This latter approach is best suited for body mounted linear accelerometers and may be used for ground based measurements of weapon position and velocity. When completed, SDBAM will be compatible with measured state variables in body coordinates, earth fixed coordinates, and combinations of both. At present, SDBAM is developed for body fixed angular measurements, Euler angle measurements, body axis linear accelerations, earth fixed axis linear accelerations, and positions.

3.4 Aerodynamic Coefficient Models

The aerodynamic force and moment coefficients for freestream flight are functions of angle of attack, angle of yaw, and mach number. In the flowfield of the aircraft, these parameters may vary significantly from point to point on the weapon body. In addition, since the weapon is in free unpowered flight, none of the parameters are constant. They are not accurately measured and do not serve well as independent variables to model the aerodynamic coefficients during separation from the aircraft. In this approach, the aerodynamic coefficients are modeled as simple polynomials with time as the independent variable. The order of the polynomial should be low to minimize the size of the matrices involved yet large enough to model the time variation of each coefficient. Successful results have been obtained with second order polynomials as well as fifth order polynomials.

For the second order model of the axial force coefficient, C_x

$$C_x = C_1 + C_2 t + C_3 t^2$$

there are three coefficients to be determined. Thus, second order models for three force coefficients and three moment coefficients requires a total of 18 coefficients to be determined. Likewise, a fifth order model of each coefficient requires 36 coefficients to be determined.

The damping moment coefficients are modeled in SDBAM as constants. They

are included as coefficients to be determined from the flight test data. However, poor results are obtained so they are currently not estimated and are assumed to be known. Similar problems with estimating damping moment coefficients using the Gauss-Newton procedure is reported in [5]. The dilemma is that moment coefficients are best estimated with short intervals of time (repeated intervals of less than a half yaw cycle) while damping coefficients need long measurement time intervals (several cycles) to estimate. Alternate methods are being considered to determine damping moment coefficients.

3.5 SDBAM Operation

A functional flow diagram of the computer program is shown in Figure (3). The inputs include weapon physical properties, the measurement data, and certain processing parameters. Physical properties such as weight, center of gravity location, and moments of inertia must be measured and provided for each test drop. A data file containing a measurement from each degree of freedom for each time interval must be provided. The time interval must be fixed and no data voids/drop-outs are permitted. The first set of measurements should include all state variable initial conditions. In general, the following state variables must be initialized.

p - body axis roll rate

q - body axis pitch rate

r - body axis yaw rate

ϕ - Euler roll angle

θ - Euler pitch angle

ψ - Euler yaw angle

$\dot{x}$ -)
$\dot{y}$ -) ground based velocity coordinates
$\dot{z}$ -)

x -)
y -) ground based position coordinates
z -)

Subsequent measurements need only to included a 6DOF measurement set such as p, q, r, x, y, and z as a function of time. Other sets are permitted by changing the measurement vector, Z, and by changing the G matrix. See equations 9 - 12. Five different measurement sets are currently programmed and more may be added for the user to select and enter as input.

The user specifies the segment length as the number of measurements per segment. The number of measurements per segment should be small because of the highly non-linear variation of the forces and moments. The number of segments may be as long as desired to process all the measurements. For example, 100 measurements may be made in 1.0 second at 0.01 intervals. To process the data, SDBAM inputs may be 10 for the number of measurements per segment and 10 for the number of segments.

Ordinarily, Gauss-Newton non-linear least squares require initial estimates for the parameters. The problem of inputting initial estimates for from 18 to 36 parameters is impractical because the user will have no basis for an estimate. In SDBAM all the parameters are initialized to be zero. If divergence occurs, the user increases the value of the initial Marquardt constant until convergence is achieved.

Convergence is achieved when the sum of squares of the residuals reaches a minimum. The residual is the difference between the measured value and the

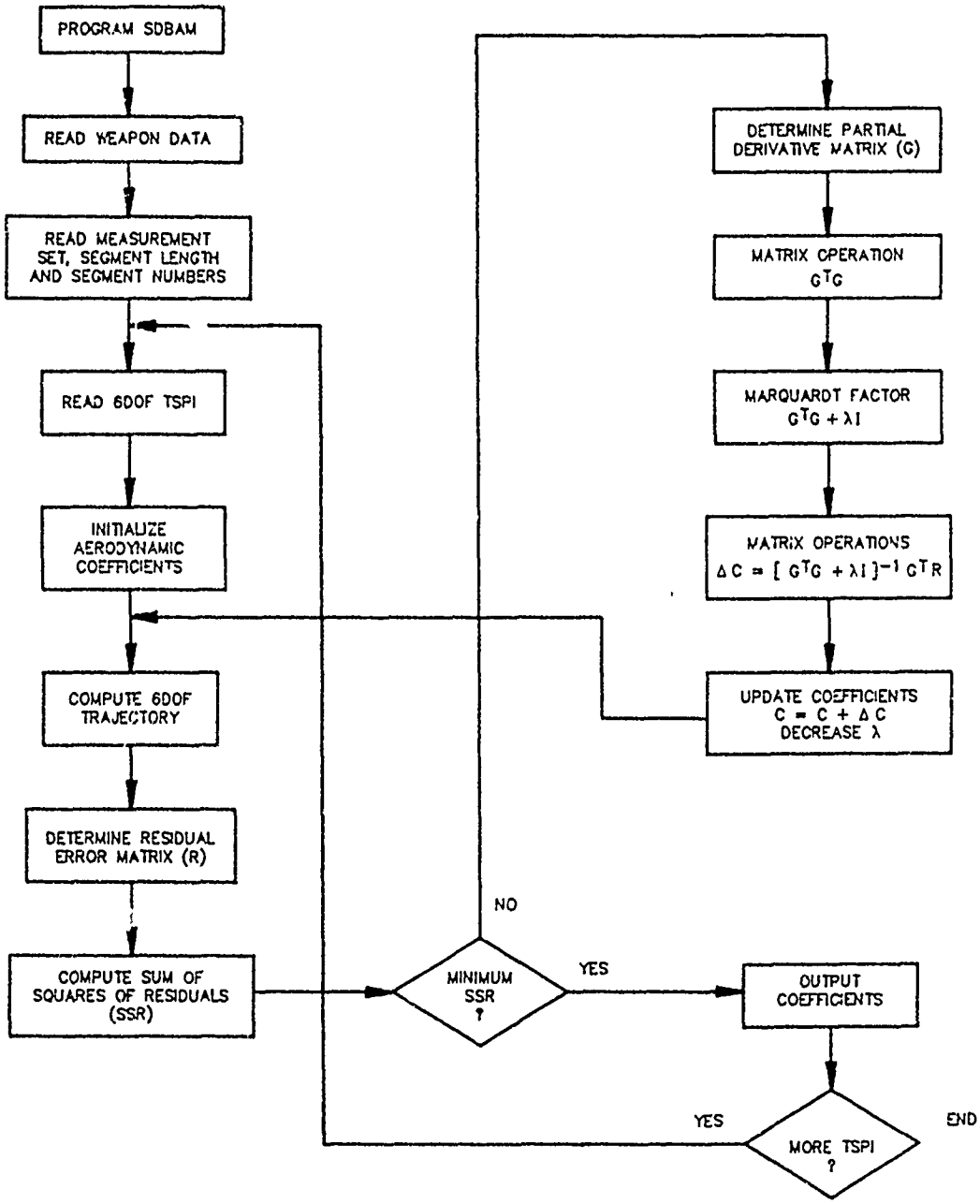

Figure 3. SDBAM Functional Flow Diagram

value computed in the 6DOF simulation which uses the parameter or aerodynamic coefficient estimates. When convergence occurs, the computed aerodynamic coefficients are written to a file. If there are additional segments, the program returns to read a new segment of the data. When completed, the output file will contain all the aerodynamic coefficients as a function of time. The coefficients in the polynomials are not retained.

3.6 Simulated Results

Inputs for the developmental SDBAM computer program from flight test data are not available. Throughout the development process, simulated flight test inputs have been generated with a 6DOF trajectory computer program. The simulated data include state variables such as roll, pitch, and yaw angular acceleration and weapon center of gravity accelerations as a function of time. Direct output simulates perfect measurements. A random measurement error or bias error may be added to each state variable to simulated possible measurement errors. In addition the simulated data also include the aerodynamic coefficients output as a function of time. The output of SDBAM may be compared with the perfect measurements and with the coefficients used to simulate the perfect measurements. These comparisons benefit the development process and are the simulated results presented here.

Trajectory data for the CBU-58 munition are generated using freestream wind tunnel aerodynamic coefficients. The initial conditions are selected to give the munition an angle of attack and an angle of sideslip. The total angle of attack is approximately 10^{o}. The release airspeed is 950 ft./sec. The trajectory data are body axis angular acceleration and rates, Euler angles, and translational position, velocity, and acceleration as a function of time. A trajectory data file is created and used as input to the SDBAM code.

In the following examples, measurement error is simulated and added to the state variables in the trajectory data file. The state variables selected are the angular and translational accelerations. The measurement error is simulated as a Gaussian distributed random variable with a zero mean (unbiased) and an input standard deviation. For each state variable and for each measurement a different random error is generated and added to the simulated error free (6DOF data) state variable.

With no measurement error, the SDBAM code should predict the coefficient time history as used in the 6DOF trajectory simulation. Figure 4 illustrates that SDBAM accomplishes this task. The plot essentially validates the code. The yaw moment and axial force coefficient are plotted. Similar results are obtained for the remaining coefficients.

An error budget representing the standard deviations of measurement error is selected. The simulated "measured" data are processed by SDBAM. The predictions determined are plotted in Figure 5 and Figure 6. The errors used are listed on the plots. The values listed are one standard deviation. Roll moment and axial force coefficient predictions are exhibiting more error than the yaw moment and side force predictions. However, the error exhibited may not induce a significant miss distance if the derived coefficients are used.

A significantly larger error budget is used to generate the prediction plotted in Figures 7 and 8. The measurement errors are so large that the predictions for roll moment and axial force coefficient are uncorrelated and meaningless. The side force coefficient predictions remain correlated and accurate although some error effects can be observed. The yaw moment coefficient predictions are extremely accurate and show little change with respect to the smaller error budget data.

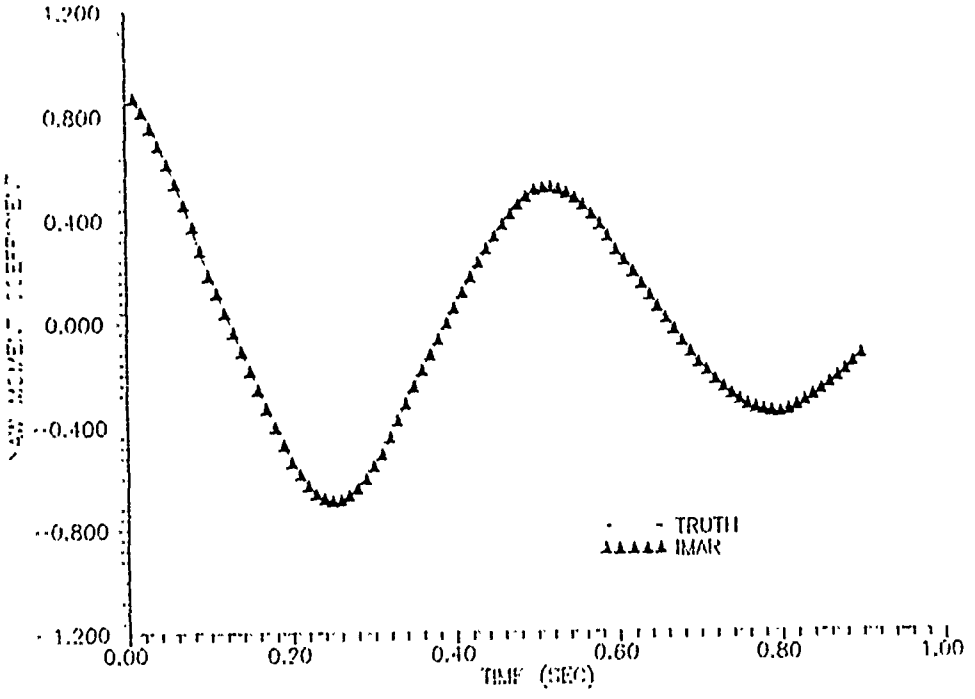

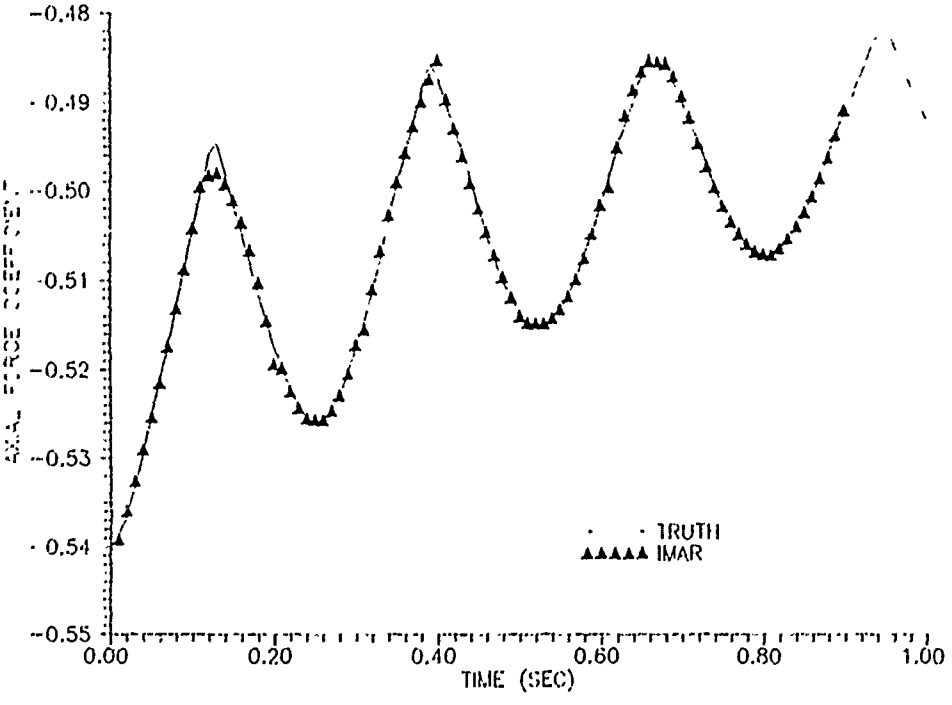

Figure 4. Yaw Moment and Axial Force Coefficient Predicted Time History with Zero Measurement Error.

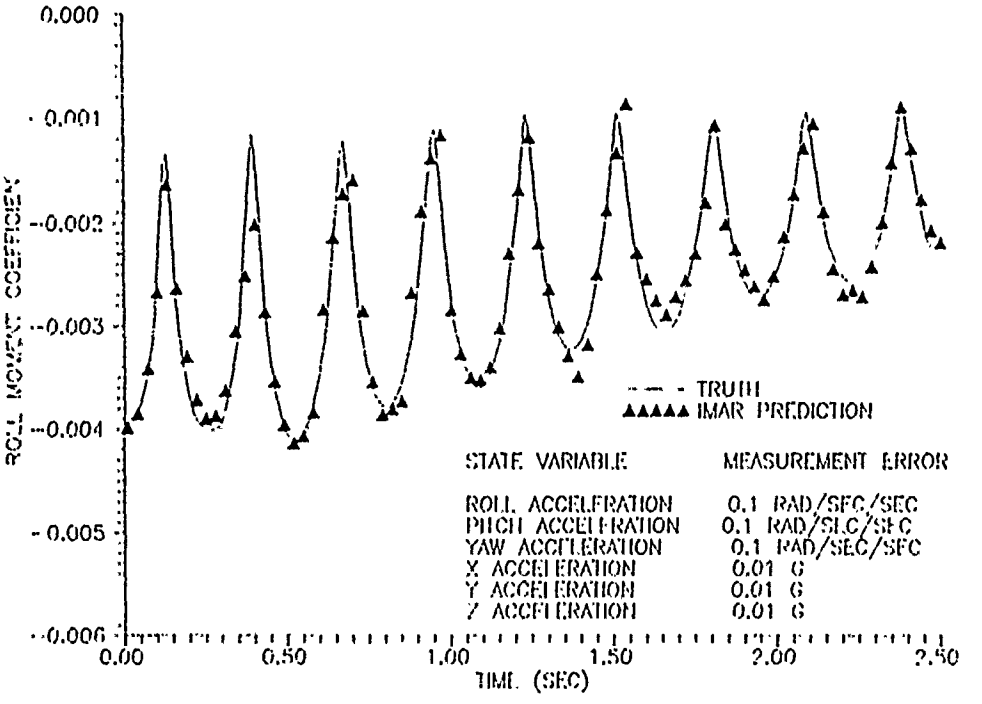

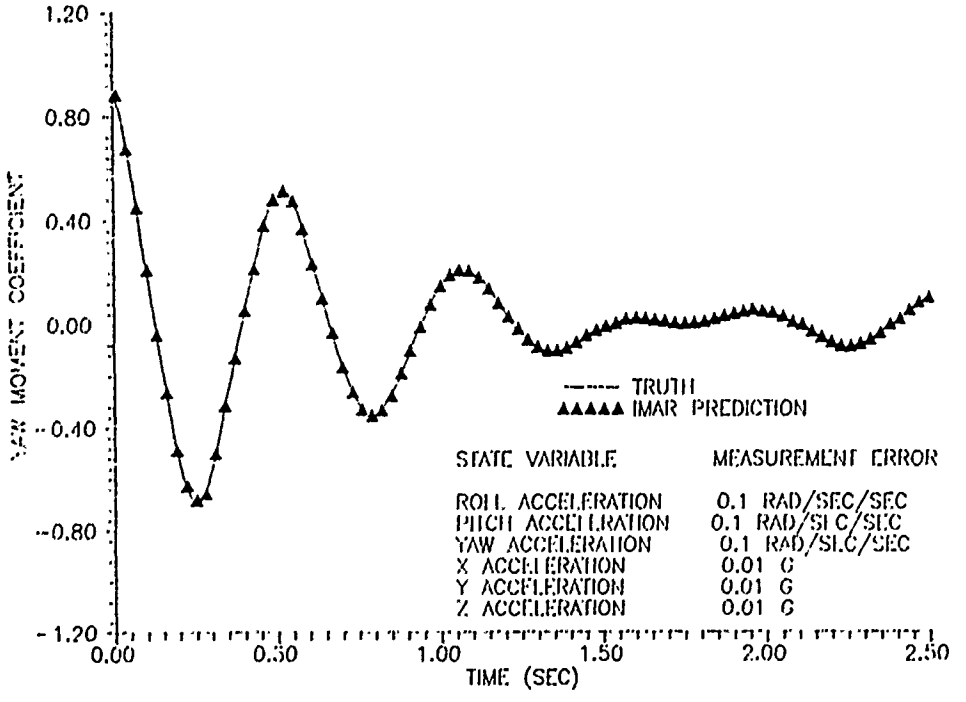

Figure 5. Roll and Yaw Moment Coefficient Predictions for 0.1 Rad/sec^2 Measurement Errors

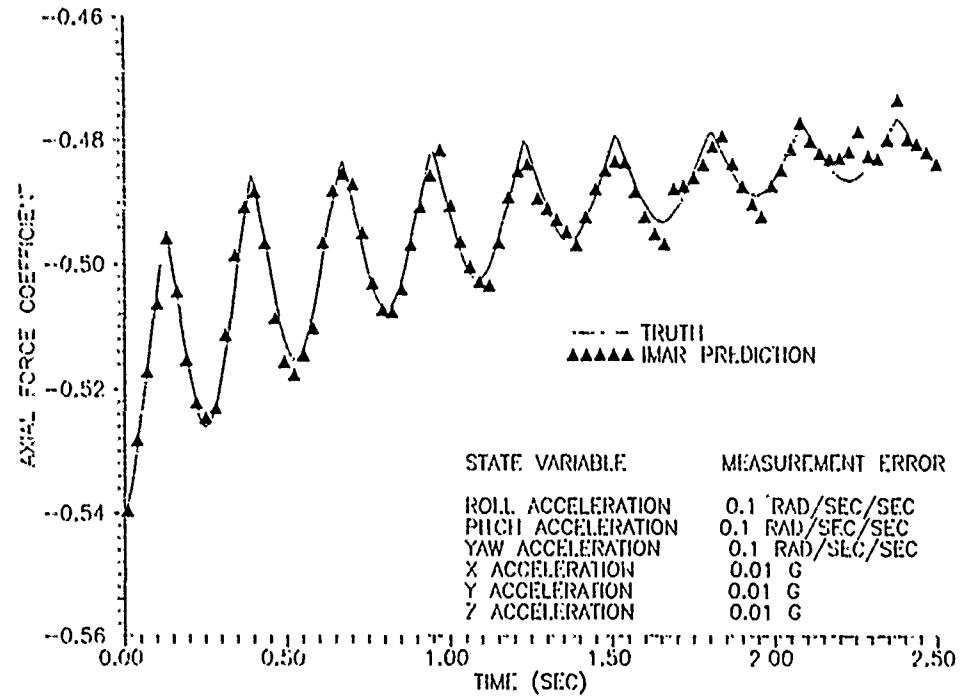

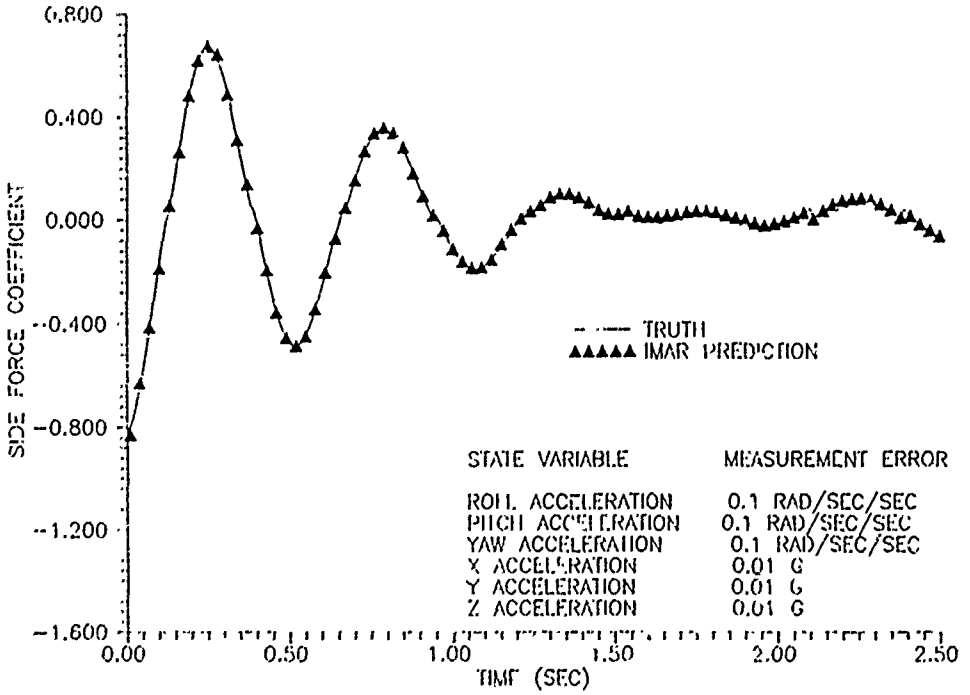

Figure 6. Axial and Side Force Coefficient Predictions for 0.01 G Measurement Errors

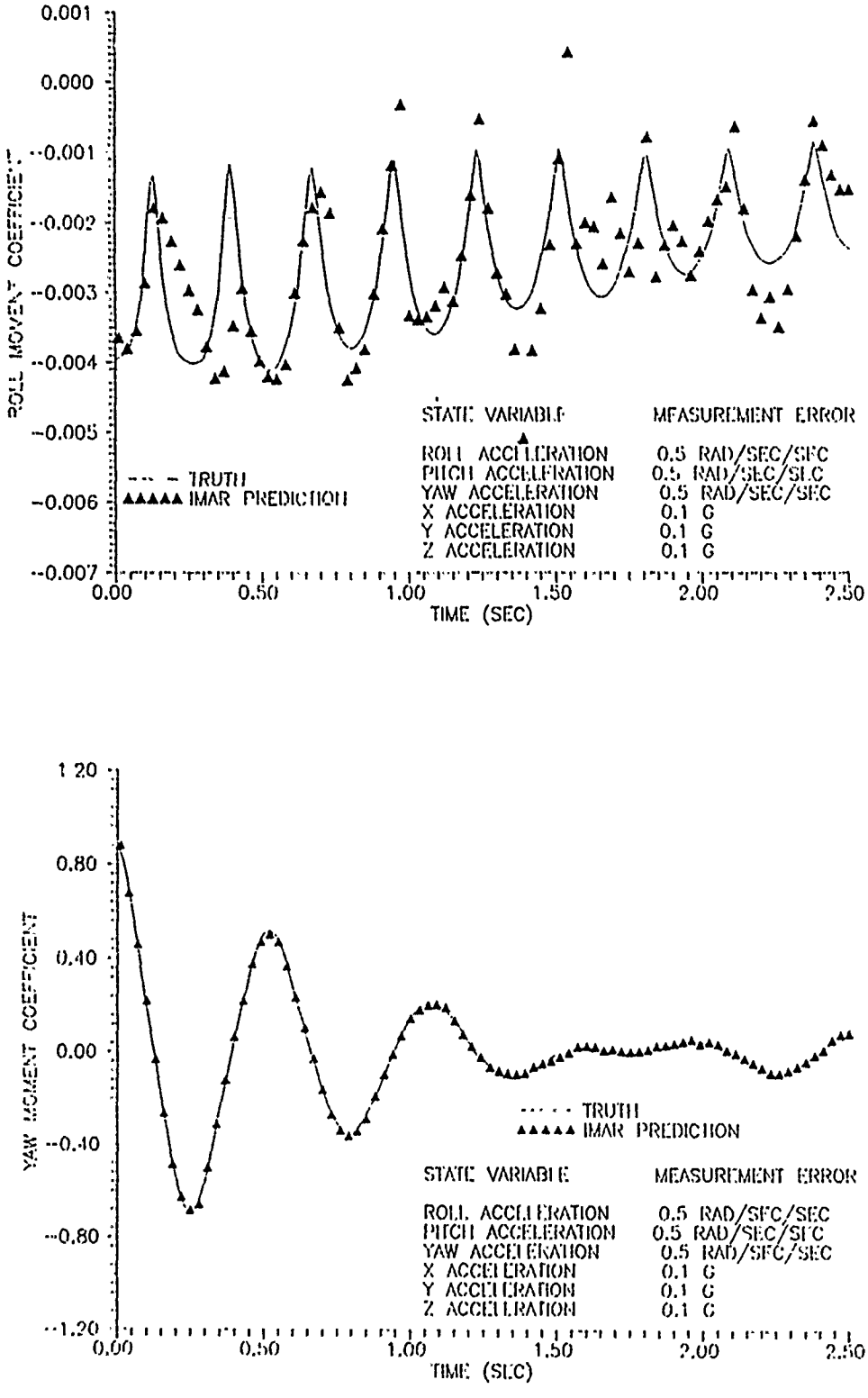

Figure 7. Roll and Yaw Moment Coefficient Predictions for 0.5 rad/sec^2 Measurement Error

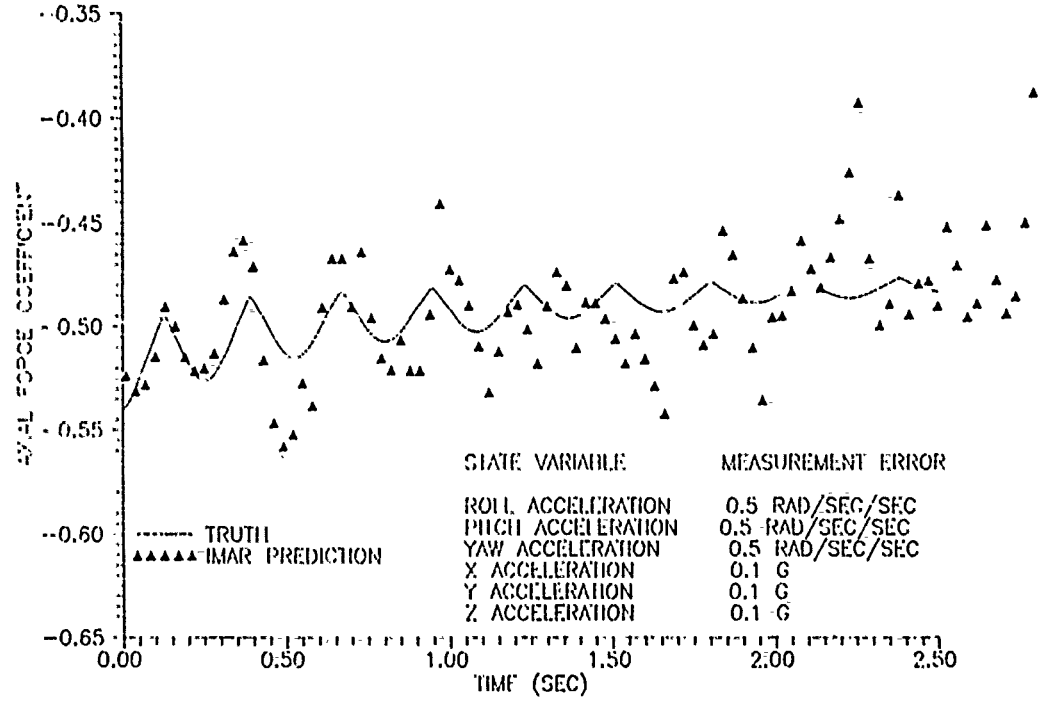

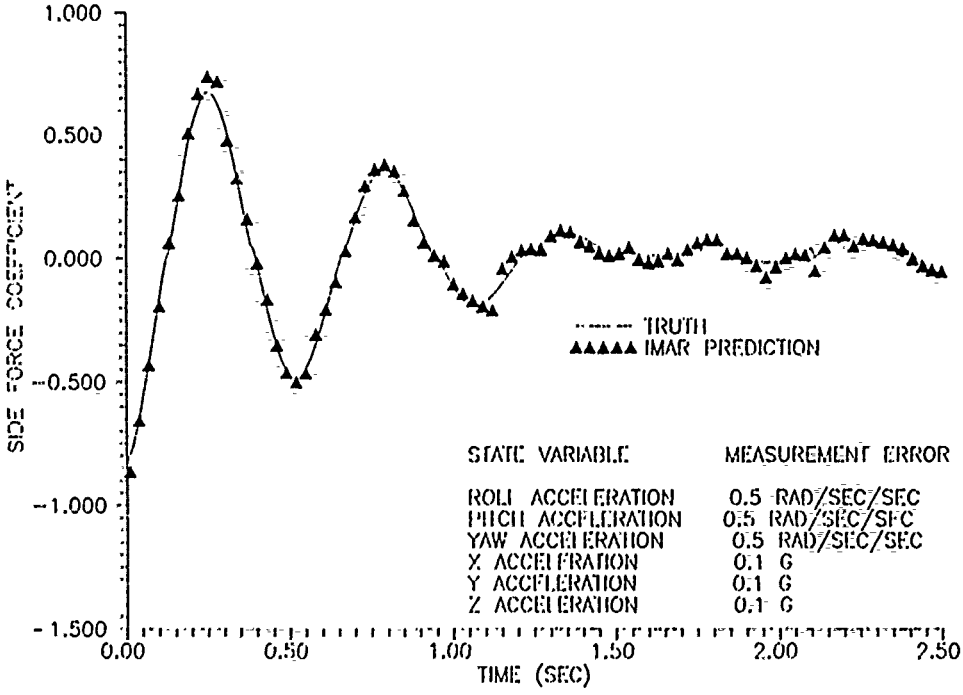

Figure 8. Axial and Side Force Coefficient Predictions for 0.1 G Measurement Errors

4.0 Conclusions

The SDBAM computer code is in development. Additional capabilities will be added before the IMAR program is completed. At the present time SDBAM could determine the aerodynamic force and moment coefficient time histories for a number of measured state variables. While any conclusions drawn are very preliminary, the data from the examples show

1. The SDBAM code is analytically validated.
2. Angular accelerometer used to measure roll acceleration need to be more accurate than pitch and yaw accelerometers.
3. Roll angular accelerometer error should be less than 0.5 radians/sec^2 from an analytical viewpoint.
4. Axial linear accelerometers need to be more accurate than the transverse accelerometers.
5. Axial linear accelerometer error should be less than 0.1 G from an analytical viewpoint.

The IMAR program will provide a 6DOF ballistic analysis capability (SDBAM) for the 3246 Test Wing. Although it will be operational in October 1990, some code revisions will be necessary to read operational flight test data. In the FY91 program, SDBAM will be used to determine state variable measurement error effects on the predicted coefficients.

BIOGRAPHY

Gerald Solomon has a Master of Science in Aerospace Engineering from the University of Florida with undergraduate degrees in physics and mathematics from Berry College. He has 25 years experience in weapon ballistic and effectiveness analyses. He was employed by the Air Force in 1965 and provided ballistic analysis support on a wide range of weapons from guns to air-launched nuclear missiles. In 1968 he was assigned to a team to determine gun system requirements to defeat a number of ground targets. The team's effort lead to the development of the 30 MM GAU - 8 gun. From 1969 to 1986 he participated in the effectiveness evaluation of the Air Force Armament Laboratory's (AFATL) technology programs related to air-to-air weapons. He served as technical director of the Weapons Effectiveness Branch in AFATL and as chairman of the Joint Technical Coordinating Group (JTCG) Gun Evaluation Group. He was employed by Orlando Technology in 1986 to devclop ballistic analysis methodology for both freestream and separation flight phases. He is the principal investigator for the IMAR program.

REFERENCES

1. Sorenson, Harold W., Parameter Estimation, Marcel Dekker, Inc, New York (1980)

2. Chapman, G.T., Kirk, D.B., "A Method for Extracting Aerodynamic Coefficients from Free-Flight Data," AIAAJ., Vol. 8, NO. 4, April 1970, pp. 753-758

3. Kuester, James L., Mize, Joe H., Optimization Techniques with FORTRAN, McGraw-Hill, New York (1973)

4. Etkin, Bernard, Dynamics of Atmospheric Flight, John Wiley & Sons, Inc, New York (1972)

5. Hozumi, Koichi, "Wind Tunnel Free-Flight Test by a Vertical Drop Technique at a Hypersonic Mach Number of 7", ICIASF 85 RECORD, pp. 241-250

AUTOMATED MISSION PLANNING

AND

BALLISTIC CALCULATIONS

by

Jacob G. Thorn, Jr.
3246 Test Wing/TYD
Eglin AFB, FL

INTRODUCTION

The following paper is a brief synopsis of where the Tactical Air Force has been, and is currently headed, in regard to computer-based mission planning and in specific, weapons delivery planning.

BACKGROUND

Tactical Air Command (TAC) first entered the field of small computer-based automation in 1981. TAC was one of the first groups in the Air Force to procure small personal computers for use at the squadron level. These computers were envisioned to help automate such operational functions as flight planning and weapons delivery planning. Up to this point in time, both functions were labor intensive tasks requiring aircrews to spend many hours planning both the route and delivery methods for a typical air-to-ground mission.

In the ensuing next few years, the Air Force and the technical community, as a whole, watched a technological explosion of capability become available on small table top computers. At the same time, the Tactical Air Force (TAF) was also experiencing a major upgrade in the capability of their fighter force. The F-15 and F-16 airframes were being updated to include a cartridge capability to load numerous amounts of data, to include route of flight, bomb load, weapons setting, etc., onto the airplane, relieving the aircrew from this time-consuming task of typing this data in after engine start. Mission planning automation began to broaden in its scope and also in its importance to the success of the mission.

The overall combat capability of a unit, including number of sorties generated per day and aircrew availability, became dependent upon a mission planning system being able to cut down on turn time.

As we moved into the 1990s, the computer technology explosion has caused a shift in all areas of how we perform in the combat arena. The scope of mission planning today has grown from the basics of flight planning to include such things as target area tactics, penetration and analysis of enemy threats, target area study, and support of advanced guided munitions.

It is clear as we move into the next decade, computer automation at the aircrew level is going to become a cornerstone of the success or failure of the TAF's capabilities to meet world-wide contingencies.

MISSION PLANNING TODAY

The Tactical Air Forces mission planning capabilities exist in two forms today -- a personal computer (PC) based system and a minicomputer system Mission Support System (MSS).

The PC based system consists of a group of software modules capable of doing basic mission planning to include flight planning, weapons delivery, and penetration analysis. These modules are designed to run on a basic Z-248 computer available in most squadrons.

The MSS, or minicomputer version, consists of a hardware set that was procured for the specific purpose of mission planning. The MSS offers all of the capabilities of the PC version, but also includes digital maps, imagery manipulation, and cartridge load capabilities.

There are many problems to be resolved in the area of mission support systems, such as logistic support, mobility capabilities, ease of operation, long-term support, and maintenance. Throughout the rest of this presentation, we will focus upon the one segment of the MSS that the Office for Aircraft Compatibility (TY) is involved with, i.e., automated weapons delivery calculations. We will attempt to present the lessons we have learned and where we think weapons delivery is headed in the future.

In a recent initiative sponsored by Headquarters Tactical Air Command (HQ TAC), TY has begun the development of a completely automated weapon delivery planning solution in the form of a highly interactive computer based program.

This computer program, which will be in the form of an automated Technical Order (T.O. 1-1M-34-2-D-A/B), is called the Non-Nuclear Weapons Delivery Planning Program (NNWDPP). This program will allow the aircrew of all fighter aircraft currently supported by T.O. 1-1M-34 to perform complete weapon delivery planning to include aircraft specification, geographic location entry (target, initial point, offset aim point, etc.), weapon specification (to include suspension and flying options), and delivery methods and parameters.

The scope of this program was to ensure that all missions meet the various criteria significant to the delivery of munitions, such as safe escape minimum release altitudes, dive recovery minimum altitude, and fuze arming altitudes and times.

The program will provide the pilot with error analysis capabilities to find useful trends significant to parameter variations at the time of the actual delivery; abort criteria calculations so that the pilot may determine the factors that drove the program to select particular minimum release altitudes, etc.; and the ability to generate -2 equivalent bombing tables as a form of paper-based "back-up" for the weapon delivery planning software.

At the beginning of this development, TY put together a team of programmers and engineers to take this project from its start to a full implementation in the field. The group established some basic goals from the beginning that we felt were lessons learned from past mission planning initiatives. These goals were as follows:

- the user interface had to be easy to use with little or no training.

- the system had to be fairly fast in its execution and be capable of running on today's Z-248 computer, already in place at the squadrons.

- early involvement of the user would ensure user acceptance in the end.

- the software would have to be written in a modular form allowing for ease of maintenance and quick response to user requested changes.

- the software would be designed in such a way as to be easily transported from one operating environment to another as the squadron's hardware grew with technology.

Keeping the above requirements in the forefront, the following sections show the approaches available to build a state-of-the-art user interface.

WEAPON DELIVERY USER INTERFACE DEVELOPMENT

Objective

Like any program's user interface, the purpose of a weapon delivery planning program's user interface is to obtain all necessary inputs from the user (and/or other sources), to correctly perform weapon computations, and to provide a method of producing high-quality output of the program's results. These computations involve several subject areas:

- ballistic calculations
- aircraft flight path calculations
- safe escape calculations
- dive recovery
- cluster munition pattern prediction

Additionally, the following capabilities have been identified for inclusion in future weapon delivery software:

- error analysis
- abort criteria determination
- and table generation.

Based upon these functional areas or capabilities, it is evident that the following types of information must be obtained from the user:

- aircraft and weapon specification
- target and other geographic point information
- delivery technique information (altitudes, airspeeds, angles, etc.)

There is obviously no "best" way to obtain this information, so the user interface for these programs must be developed in an iterative manner, with regular user feedback.

Pilot Requirements

In the development of weapon delivery planning program user interfaces, it is critical to obtain information, comments, and other requirements regarding the user interface from the community of

pilots that will be making use of the software. The following comments were gleaned from several requirements definition proceedings with Air Force combat pilots flying diverse aircraft in a variety of roles.

Easy to Learn and Use

Since the majority of pilots are not "computer gurus" or terribly good typists, it is necessary that any end-user software must be easy to learn and use in a minimum amount of time and with a minimum effort. The following section discusses several areas that have been identified to assist in making these characteristics possible.

Continuous On-Line Help

At any particular time, end-user software should provide applicable, context-sensitive on-line help so that the user can always infer from the screen what his range of options are and how they might be restricted. As an example, if the user were entering an airspeed value in a program, the software should display information explaining exactly what is significant about this airspeed ("it is release airspeed") and what is the range of accepted values for this airspeed ("250 to 600 KTAS").

In addition to continuous, context sensitive on-line help, it is also useful to provide complete and extensive on-line manual capabilities to the software so that the user can get additional, more specific information regarding any feature or capability of the program available.

Consistent, Forgiving Environment

The weapon delivery planning software must present a consistent face to the user, not allowing the user to enter incorrect information knowingly or unknowingly, and provide for the relatively easy reversal of commands or actions taken at any particular time.

Streamlining of Typical Data Entry "Path"

Like any other piece of software designed to perform a fairly well-defined task, there will be situations where a great deal of the normal information involved in weapon delivery planning is of a "boiler-plate" nature. Consequently, the program should take advantage of this fact so that pilots can "default" much of this information to nominal values for the missions and roles that they are involved in.

Target Hardware Platform

In spite of the fact that computer hardware has continued to advance to staggering heights, there is an existing installed base of moderately sophisticated hardware that makes up the greater portion of microcomputers that are immediately available to combat pilots. As a result, any weapon delivery planning software should be developed in such a manner as to be useable on these machines so that a maximum number of pilots can benefit from the program.

Custom Output

Another aspect of weapon delivery planning program user interfaces is their ability to produce high quality output in a format that is informative and useful to the pilot. Since there are so many types of combat aircraft, missions, and separate combat organizations, it is unreasonable to assume that all the needs of all of these organizations could be met with a single output format. As a result of this situation, a good user interface for weapon delivery planning programs will allow the user to control the format and information content of the output and customize it for his exact purposes.

Portable to the MSS

It is important in terms of training and developmental costs that any new planning software solutions be fairly transportable to other operational environments. In the case of weapon delivery planning software, it is important that the software be transportable to the MSS as this system is designed to be the fundamental planning system for all combat pilots in the future.

Easily Integrated with other Applications

Another equally important characteristic that must be supported by new planning software is to be easily integrated with other software packages. In the case of weapon delivery planning software, it is important that the software be be designed in such a way as to exchange flight planning information with other PC and MSS based software packages.

User Interfaces in General

What is a User Interface?

A User Interface (UI) is the computer software that mediates between a person and the program and allows the person to shape the computer into a tool to accomplish some goal. At one time, the UI was the last thing that was considered in the development of a software application, but now it is typically the first thing that is considered.

What are the Qualities of a Good UI?

UIs have come a long way in the past several years, primarily due to the increased capabilities of personal computers. In the process of improving and becoming more sophisticated, UIs have also begun to standardize to some extent.

Naturalness

What is natural to one person may not be natural to another, but there are several general characteristics that can be used in describing a "natural" UI:

- it does not force you to remember command names
- it does not allow unconfirmed, disastrous actions
- it allows a person to quickly perform useful work
- it allows you to make mistakes and change your mind
- it allows you to perform several actions at any given moment

Consistency

An UI is said to be consistent if its concepts, functions, and procedures apply across the application as a whole. This has the advantage of reducing the learning curve and users will develop an almost sub-conscious idea of what is the "right" command or action to use at any given moment.

Avoidance of Modes

A mode on an interactive computer system is a state of the UI that lasts for a period of time, is not associated with any particular object, and has no role other than to place an interpretation on operator input. Modes are generally frowned upon because of the fact that they place a special (maybe unknown or inconsistent) interpretation on the user's action.

Adapt to User's Level of Experience

A good UI will adapt to a user's level of experience in such a manner that both novice and expert users can operate the software in a efficient manner, making use of their knowledge (or lack thereof) of the system.

Why are Graphical User Interfaces (GUIs) Superior?

The objective of any UI is to create an illusion for the person that allows him to understand the system and know what to do next. One of the most powerful techniques used in strengthening this illusion is the adherence to a display technique known as WYSIWYG (What You See Is What You Get). High-resolution graphical displays provide much greater fidelity in creating the aforementioned illusion. When one combines this approach with a mouse for the direct manipulation of on-screen objects, the user's metaphor is reinforced to the point of being completely intuitive.

Some Popular GUIs and Industry Standards

In the last several years, the number of different GUIs has positively exploded. The user community now has the ability to run programs with a GUI on just about every popular personal computer, workstation, and many terminals.

GUIs are composed of several basic system components. The three most fundamental software/firmware components of GUIs are:

- the windowing system
- the imaging model
- the application program interface (API)

The following sections discuss four popular GUIs and the significant characteristics of each.

Macintosh™

While the initial techniques and concepts of GUIs were developed at Xerox™, Apple's Macintosh™ computer effectively made the GUI enormously successful. The Macintosh™ is currently the industry leader in terms of easy-to-learn and easy-to-use application software that, in spite of its diversity, is remarkably consistent and well-integrated.

In developing Macintosh™ applications, the programmer can choose from a variety of programming languages (e.g. Pascal, C, FORTRAN, Modula-2, Ada, etc.) and most applications will run on a baseline Macintosh™ since the all Macintosh™ computers have at least 1 megabyte (MB) of random access memory (RAM), a linear (Motorola) memory layout and an effective memory management capability built-in.

The Macintosh windowing and imaging models are "QuickDraw™", and its API is distributed for a variety of languages by Apple and third party sources.

Microsoft Windows

Microsoft™ Windows™ (version 3.0) is the IBM-compatible PC's answer to the Macintosh™ GUI. Windows™ is a very clean, attractive system that has the potential to challenge the Macintosh™ installed base and, perhaps, eventually in the number of application software packages available. Microsoft™ Windows™ conforms to IBM's (Software Application Architecture) SAA standards, and, consequently, holds considerable promise in terms of providing applications that operate in a familiar way on numerous platforms.

In developing Windows™ applications, the programmer is primarily restricted to the C and Pascal programming languages and, for the most part, larger applications will probably require at least 1 megabyte (MB) of random access memory (RAM) (as opposed to the standard 640K).

The Microsoft™ Windows™ API is distributed by Microsoft™.

OSF/MOTIF™

MOTIF™ is a GUI that has been developed by the Open System Foundation (OSF) in response to the large number of user-interfaces that have been unleashed upon the world with no concerted effort toward standardization.

MOTIF™ is built on top of the X-Windows windowing environment (developed at MIT), which is prevalent primarily on UNIX™ workstations, connected by Ethernet™ and equipped with a mouse, etc. In appearance, MOTIF™ is very similar to Windows™ 3.0 and Presentation Manager (a GUI for IBM's OS/2).

The primary advantage of MOTIF™ is that it attempts to conform to IBM's SAA standards concerning user interface characteristics, and is portable to most workstations that support UNIX™ and X-Windows.

NeXT

The NeXT™ computer's GUI is noteworthy for several reasons: it runs "on top of" UNIX™; it utilizes Postscript as both its imaging and display model; and (most importantly) it is supported by one of the most sophisticated GUI development systems in existence.

The NeXT™ computer provides development facilities that allow a typical programmer to generate virtually almost all of the source code associated with an applications user interface in a very short amount of time. This allows for rapid UI prototyping which has become critical in today's software development efforts.

The Approach Used in NNWDPP

In the previous sections, weapon delivery planning software and user interfaces were discussed in general. In this section, we will discuss the specific techniques and concepts that were used in the development of a user interface for a new weapon delivery planning program called NNWDPP (Non-Nuclear Weapon Delivery Planning Program).

Menus, Windows, and the Mouse

In keeping with well-researched information regarding the most useable user interfaces, the user interface for the NNWDPP was developed around the traditional metaphors of GUIs (being primarily influenced by Microsoft™ Windows™ and the Macintosh™). While the NNWDPP could not depend upon a graphic environment in which to operate, an attractive "character-based" GUI was developed utilizing a commercial toolkit.

The Metaphor: A Fill-in-the-Blank Form

Primarily due to the fact that graphics were not possible on the target hardware platform, the visual illusion or metaphor that is utilized by the NNWDPP was the next best thing: a form. The developers felt this was a logical choice as Air Force pilots are quite well-versed in filling out forms (much to their chagrin).

Ease-of-Use and Ease-of-Learning Features

The NNWDPP's user interface was developed in such as way that there is a minimum amount of knowledge required in the use of the program (note that this refers to the program's user interface, not the subject matter of weapon delivery). We have streamlined data entry as much as possible and provided extensive on-line help facilities.

Developmental Considerations

In the development of the NNWDPP's user interface (which as aforementioned utilized menus, windows and a mouse) we utilized a software toolkit call XVT™ (Extended Virtual Toolkit). This software package is designed to support numerous operating environments.

We combined the use of XVT™ with an adherence to object-oriented design techniques in order to support the easy maintenance and extendibility of the NNWDPP's user interface. XVT™ offers an additional advantage to the NNWDPP user interface: the XVT™ API is portable to a considerable number of operational environments (including graphical environments).

Having completed the user interface, the next step was to integrate this module with the calculation module.

WEAPON DELIVERY CALCULATIONS

The following is a brief description of the calculation model.

Weapon Trajectory

The basic problem that must be solved by the computer is that of determining the range of a non-thrusting body released from an aircraft in the earth's atmosphere. This problem, due primarily to the non-linear nature of the atmospheric properties, can not be solved in closed form. This logically leads to the use of numerical techniques to solve the underlying differential equations.

The differential equations of primary concern are a = F/M and are expressed as:

$$F = Ma = -C_D \rho S V^2/2$$

where

F = drag force

M = mass of bomb

a = acceleration

C_D = drag coefficient

ρ = air density

$S = \pi d^2/4$ = cross sectional area

d = weapon diameter

$\bar{V}$ = velocity relative to the air

thus

$$a = -C_D \pi \rho V^2 (d^2/4)/2M$$

or

$$a = -K_D \rho V^2 d^2/M = -K_D \rho \lambda V^2$$

where $K_D = \pi C_D/8$ is the drag coefficient as used in the program, and $\lambda = d^2/M$ is the weapon gamma.

Although the program is configured to solve the equations of motion in three dimensions and take into account the earth's rotational effects, the present version ignores rotational effects and computes the two-dimensional, downrange and vertical drop solution only.

The equations to be solved take the following form:

$$d^2x/dt^2 + H\ dx/dt = 0$$

$$d^2y/dt^2 + H\ dy/dt + G = 0$$

where x is the downrange travel of the bomb, y the vertical travel component, G the acceleration due to gravity and ($H = \lambda \rho K_D V$), the drag function.

The differential equations are solved using a modified Euler numerical integration process starting with the initial release conditions and terminating with the weapon impact.

Aircraft Flight Path

Aircraft flight path simulation is required to provide the weapon release parameters when a toss maneuver is run. Only level approaches with linear G and linear power applications are simulated. The equation is entered with approach altitude and airspeed, and the aircraft trajectory simulated until the specified release condition is obtained. Release may be on time, altitude, or flight path.

Pertinent aerodynamic data is stored in arrays and table lookup with linear interpolation is used to determine the angle-of-attack, available thrust, and drag coefficient as required during the simulation. The angle-of-attack and drag coefficient are stored as functions of lift coefficient and Mach number. Available thrust is a function of Mach number and density altitude.

To initialize the aircraft trajectory it is first necessary to determine the thrust to maintain steady state under the approach conditions. Since the approach is level, a force balance equation may be written as:

```
T = D/COS(ALPHA)
```

where

T = thrust required for steady state

D = drag

ALPHA = angle-of-attack

A second force balance equation may be also be written:

```
L = W-T*SIN(ALPHA)
```

where

L = lift

W = aircraft weight

Since the lift coefficient, C_L, ($C_L = L/QS$ where QS is the dynamic pressure) is required to look up C_D, the drag coefficient, and angle-of-attack in the aerodynamic data tables, the assumption that angle-of-attack equals zero is made initially and C_L becomes W/QS. The tables are then used to find a new value of ALPHA which in turn is used to compute a new C_L. The process is repeated until C_L changes by less than 0.001. Having a stable value for C_L, the thrust available is obtained by table lookup and P_0 , the ratio of required thrust to the available thrust, is computed. P_0 and ALPHA are then used to initialize the trajectory along with the approach altitude and airspeed. The program does not allow P_0 to be greater than 1.

Once the trajectory has been initialized at time zero, thrust is controlled using a linear multiplier that varies from P_0 to 1 over a time interval of one or two seconds depending on aircraft type. The G

force is controlled linearly with time from 1 to 3 or 4Gs over one or two seconds depending on aircraft type. The controlled G force, CG, is used in the computation of lift coefficient:

$$C_L = (W*CG-T*SIN(ALPHA))/QS$$

The force balance equations, which can no longer be simplified by assuming level flight, become:

$$F_x = T*COS(THETA+ALPHA)-D*COS(THETA)-l*SIN(THETA)$$

and

$$F_y = T*SIN(THETA+ALPHA)-D*SIN(THETA)+L*COS(THETA)-W$$

where

F_x = the force in the downrange direction

F_y = the force in the vertical direction

The acceleration components are obtained by dividing the associated force component by the aircraft mass. The resulting differential equations are then solved using a fourth order Runge-Kutta integration routine.

One limitation that was quickly identified was the burden imposed upon the significantly less powerful hardware platform (8-bit and 16-bit microprocessors) by the computation of store trajectories. This problem was satisfactorily solved by the development of a variable "step size" integration algorithm. Other limitations imposed by the target hardware platforms impacted the relative ease that databases could be modified and updated.

The automated weapons delivery program has been designed to be easily updated and incorporated into the weapons certification process. As new weapons are selected to be certified on a particular aircraft through the SEEK EAGLE process, these munitions are identified as needing support for mission planning. The required ballistics data is identified and any changes in delivery tactics are discussed with the user. As TY develops the new ballistic characteristics for the weapon, they are added to the weapons delivery program and provided to the responsible test organization (RTO) for verification, in conjunction with the testing of the weapon.

WHAT DOES THE FUTURE HOLD?

The future of mission planning, and in particular, the weapon delivery tasks are on the threshold of entering an entirely new domain of extremely sophisticated, integrated scenarios. The future will undoubtedly see these systems being interweaved with theater level battle management systems and high-volume, satellite information sources. It also seems likely that in an effort to provide unparalleled support for flexible weapon delivery planning in these systems, the systems of the future will be formed from complex software components that allow direct computation of ballistics and safe escape parameters on a "case-by-case" basis, in addition to providing large databases of pre-computed weapon delivery planning information for more traditional planning situations.

It is quite conceivable that, in the future, all operational aircraft data (stability and control, weight, and balance algorithms, etc.) and weapon information (guidance and control, thrust parameters, etc.), in the form of complex software packages, will be incorporated into an MSS. This system would allow complete and extremely high-quality simulation capability, conceivably to the point of simulating the combined trajectories of all aircraft, weapons and sub-munitions in a rigorous computational description of the entire air-to-surface environment.

While this sounds rather outlandish, it is possible, with today's hardware and software technology, to construct platforms capable, at least in terms of "raw" computing capability, of doing exactly this type of "simulation".

In addition to the outright capabilities of such systems, it is inevitable that we will see man/machine interfaces becoming equally sophisticated. Judging from the likely Initial Operating Capability (IOC) of such a system, it is probable that pilots will communicate with the system using voice, true 3D stereoscopic projection systems, and physical manipulation methods (like light pens, joy sticks, mice, etc.).

On an even broader horizon, it is likely that with the growing integration of weapon system and aircraft avionics, we will probably see weapon planning systems become mandatory components in all on-board combat aircraft computer systems (including support simulation platforms).

As we move to further automate the aircrews mission planning requirements, we must keep in mind the system must be highly portable, user friendly, and very reliable.

As we look to the future in areas such as target area tactics and mission simulation, we must answer the following questions before we even begin.

- how much accuracy is really needed?

- how close must ballistic calculations be when you include the overall performance of the weapons system?

As new technology becomes available we must make decisions on speed of computations versus costs. Is a speed-up from 5 minutes to 5 seconds worth about $100K per workstation?

As we look to the future, we must develop goals and standards for minimizing cost and maximizing flexibility of both the hardware and software platforms.

In conclusion, the TAF has come a long way in the last 10 years towards automating the aircrews' mission planning needs. We must learn from our past mistakes and seize the opportunity in the future to meet the demanding needs of future weapon systems.

SUMMARY

Throughout much of the history of automated mission planning systems, TY has provided its expertise in the form of technical assistance and software development in support of the weapon delivery aspects of this complex problem arena.

As aircraft and weapon systems become more complex and funding and schedule issues become more pronounced, the efficient management of these developmental issues will immediately impact operational readiness and effectiveness. With the inevitable move to a smarter, leaner inventory of guided weapon and sophisticated combat aircraft, the features, demands, and characteristics of these systems will, of course, be incorporated in the products that TY supplies to the project managers of future mission support systems.

TY is poised to support these efforts in the form of technological enhancements and expertise in weapon delivery issues.

REFERENCES

[1] Scientific American, September 1984, Volume 251, Number 3;
Computer Software, Alan Kay.

[2] User Interfaces in C: Programmer's Guide to State-of-the-Art
Interfaces, Mark Goodwin, 1989,
Management Information Source, Inc., Portland Oregon.

[3] User-Oriented Computer Languages: Analysis and Design, Melvin Klerrer,
Macmillian Publishing
Company 1987, New York.

[4] The NeXT Book, Bruce F. Webster, Addison-Wesley Publishing Company,
1989, Reading
Massachusetts.

[5] Byte, July 1988, MacGraw-Hill Publications, A Guide to GUIs, Frank
Hayes and Nick Barnas.

[6] Object-Oriented Programming for the Macintosh, Kurt J. Schmucker,
Hayden Book Company,
Hasbourough Heights, New Jersey 1986.

[7] NNWDPP Software Requirements Analysis, 1990, 3246 Test Wing/ TYD

[8] NNWDPP Software Requirements Specification, 1990, 3246 Test Wing/TYD

BIOGRAPHY

Mr Jake Thorn is an Electronic Engineer with the 3246 Test Wing in charge of Weapon Delivery Mission Support System Software.

Born in Pascagoula Mississippi, Mr Thorn graduated from Mississippi State University as a President's Scholar, receiving a degree in Electronic Engineering and a commission as a Distinguished Graduate of the U.S. Air Force Reserve Officers Training Corps program. Mr Thorn worked as a graduate fellow at MSU while awaiting pilot training. Following pilot training at Columbus AFB MS, he was assigned to the first operational A-10 Aircraft Wing, Myrtle Beach AFB SC, as an instructor pilot and wing weapons officer; then as an operational test and evaluation pilot at Eglin AFB FL. Following a tour as the A-10 standardization and evaluation pilot at Tactical Air Command headquarters, Langley AFB VA, Major Thorn served with the Air Force Thunderbirds as the number eight pilot and advance man.

Just prior to leaving the Air Force in December of 1989, Major Thorn was the Chief of the Tactical Air Forces Mission Support System projects office at the Tactical Air Warfare Center at Eglin AFB FL. Major Thorn currently is a member of the 919 Special Operations Group flying AC-130s at Duke Field FL.

Mr Thorn and his wife Elizabeth, have two children: Katie and Chip.

THIS PAGE INTENTIONALLY LEFT BLANK

An Approach for Correlating External Store Wind Tunnel Measured Aerodynamic Loads to Flight Test Derived Loads

John T. Rodgers, Jr.
Engineer

Structural Loads and Criteria
GENERAL DYNAMICS/Fort Worth Division

ABSTRACT

Loads flight testing is performed to validate analytical methods and data used to compute loads. To achieve the validation, analytical loads are predicted for the flight test maneuvers so a comparison with flight test derived loads can be made. During recent flight loads testing of an F-16, these predicted and derived loads for an underwing carried external store differed significantly. A study was conducted to determine the cause of this unusual discrepancy.

Investigation into the causes lead to examining the accuracy of the following load sources: 1) Flight test instrumentation - both aircraft/store and ground station, 2) Loads prediction methods, 3) Load prediction basic data. The investigation concluded that inaccuracies in the loads prediction data were the apparent cause for the discrepancy. Sources of this data included digital computer maneuver simulation, dynamic load environment, and wind tunnel tests.

A detailed comparison of the predicted data to measured flight data showed significant differences. These differences were due to the dynamic load environment and the aerodynamic data. The unexpected presence of high magnitude low cycle oscillations caused the differences in the dynamic load environment. Causes of the differences in the aerodynamic data were unknown. The predicted data was in the form of non-dimensional aerodynamic coefficients obtained from wind tunnel tests of a 1/9th scale model. The experimental error of the test was insignificant, therefore, some aerodynamic flow phenomenon must have occurred to cause the load discrepancies. The study task became the development of a procedure to correlate the existing wind tunnel data to the flight test derived loads.

The procedure development involved deriving flight measured aerodynamic coefficients and comparing these to coefficients from the wind tunnel test. This process was complicated by the lack of flight test data needed to transfer the moments to a common reference axis. Store only forces and moments (i.e., loads acting on the store in the presence of the pylon and F-16) and store plus pylon forces (i.e., forces acting on the store/pylon combination in the presence of the F-16) were not measured during flight; only store plus pylon moments were obtained. Several assumptions, about the relationship of the forces and moments not measured during flight to both the flight measured moments and the wind tunnel test forces and moments, were made to overcome this lack of flight test data. A "realistic" aero data base was then developed for the purpose of setting aircraft operational limits when carrying this underwing external store.

As evidenced by the investigation of this unique situation, scaled wind turnel tests may not always reflect full scale aerodynamic loads. Variances in flexibility, Reynolds number, wall effects and probably other unknowns can be significant between the modeled external store and the actual external store and might cause differences in external store carriage loads.

1. INTRODUCTION

Loads flight testing is performed to validate analytical methods and data used in computing loads. Maneuvers are selected to be flown based on maximizing loads on aircraft components such as external store hardpoints. Analytical methods are employed to predict the loads acting on each component during the selected maneuvers. Flight loads are derived from the test instrumentation and compared to predicted values. During recent flight testing of an F-16, these predicted and derived loads for an underwing carried external store differed significantly. A study was conducted to ascertain the cause of this unusual discrepancy and to determine the necessary action for adjusting the unrepresentative loads since the differences were severe enough to possibly impact final flight operational limits.

2. INVESTIGATION OF DISCREPANCY

Investigation into the causes of the discrepancy lead to examining the accuracy of the following load sources: 1) Flight test instrumentation - both aircraft/store and ground station, 2) Analytical methods, 3) Load prediction basic data.

The flight test instrumentation consists of two subsystems: measuring and recording. The measuring subsystem includes the strain gage bridges and electrical bridge combination networks (modules). The pylon has strain gage bridges installed on load-carrying members. For each measurement, selected bridges feed voltages to a module which simulates regression equations using attenuating resistors. The equations are developed using calibration data.

The recording subsystem entails a gain multiplier, a data tape, a telemetry transmitter, a telemetry receiver and a strip chart recorder. Measured strains are translated into three components of load (pitch, roll and yaw moments) by the gain multiplier. The derived moments along with aircraft response parameters are recorded at a rate of 200 samples per second on the onboard data tape and also is transmitted via telemetry to the ground station. The strip chart recorder provides traces of the store plus pylon moments. A schematic diagram of the entire system is shown in Figure 3. Both subsystems were checked for accuracy.

The system check was accomplished by positioning a loading ram between two dummy stores mounted on the instrumented pylon and an adjacent pylon (see Figure 4). Known forces were applied to the store by the ram. The measuring subsystem was checked by obtaining the values from the module and manually multiplying the values by the module slopes to determine the measured moments. The applied moments, obtained at the forward attach point of the wing/pylon interface (Flight Test Reference) based on the applied ram forces, and the measured moments were compared and found to correspond. Since the recorded and applied moments agreed, the flight test instrumentation loads equations were validated.

The recording subsystem was checked separately by reapplying the ram forces and comparing the recorded strip chart moment traces to the applied moments. The second application of loads reaffirmed the loads equation as well as verified the recording subsystem. The predicted loads were determined to be the unrepresentative loads as a result of this verification of the flight test instrumentation.

The predicted loads were calculated using an external store loads analysis computer program written at General Dynamics for the F-16. The program computes the store only and store plus pylon air, inertia, and net loads. However, the analytical methodology does not account for dynamic loads.

The flight test data showed that unexpected Limit Cycle Oscillations (LCO) were experienced by the store. The dynamic load increments must be accounted for in the loads predictions due to the low frequency and high magnitude of the oscillations. Load versus time plots were used to ascertain the increments. An example of these plots is shown in Figure 6. The increments were used to determine the static flight derived loads which were compared with the predicted loads.

The method of computing the air and inertia loads was examined. A flight test maneuver's loads were predicted by hand calculations. The hand calculated loads corresponded to the computer predicted loads. Therefore, the discrepancy was determined to have been caused by the basic data used in predicting the external store loads.

The aircraft response parameters used in computing the external store loads are listed in Figure 8. A comparison between the computer simulation and the actual flight recorded values showed no significant differences with the exception of the axial load factor. Instead of being predicted by the simulation, the axial load factor is assumed to be zero g's. Flight measured values ranged from zero to 1.25 g's in the forward direction with a mean value of 0.5g's. This difference in axial load factor did contribute to the discrepancy, but accounts for only a small percentage of the pitch moment differences.

Net loads are the sum of the air and inertia loads. Since the predicted inertia loads are similar to the derived inertia loads but the predicted net loads to the derived net loads are not, the cause of the majority of the discrepancy must be the difference in air loads. An example of the discrepancies in the aerodynamic loads is shown in Figure 9. Hence, the non-dimensional aerodynamic coefficients from the wind tunnel tests do not reflect the actual aerodynamic loads. The experimental error of the wind tunnel tests is insignificant (+/-0.1%), therefore, some aerodynamic flow phenomenon must have occurred to cause the differences.

The value for the axial load factor was updated to the mean value by a simple change in the computer program inputs. The inclusion of the dynamic load environment was an easy task since the incremental loads could be derived from the net load vs time plots. The only remaining data still requiring adjustment was the aerodynamic coefficients.

The adjustment of the aerodynamic coefficients can be accomplished in one of two manners. The first is to perform a new wind tunnel test while the second is to correlate the existing coefficients to the flight test derived loads. Since the first method involves the cost of a second wind tunnel test which still might not reflect the actual aerodynamics, the second technique is considered more practical and was chosen.

3. BACKGROUND ON WIND TUNNEL DATA BASE

A description of the existing wind tunnel data is provided as background information.

The existing wind tunnel data consists of non-dimensional aerodynamic coefficients for drag, side, and normal forces plus

pitch, roll, and yaw moments. The side force, normal force, pitch moment, roll moment and yaw moment are measured in loads wind tunnel tests for store only (i.e., the store in the presence of the pylon and F-16) on the left wing and for store plus pylon (i.e., the store/pylon combination in the presence of the F-16) on the right wing at various Mach numbers. The coefficients are obtained for three combinations of angle of attack (alpha), angle of sideslip (beta), and trailing edge flap deflection (delta flap). The first of these is the alpha sweep, which has varying alpha with zero beta and zero flap deflection. The second, the beta sweep, has varying beta, alpha equal to five degrees and no flap deflection. This data is converted to incremental coefficients at zero angle of attack. The final combination is the flap influence sweep and is another sweep of varying alpha with zero beta. This data, however, is obtained with either $+20^{o}$ or -20^{o} degrees deflection of the trailing edge flap and is also converted to incremental coefficients to represent the influences of the flap deflection. For all of these sweeps, the angles range in two degree increments from -5 to +27 degrees for alpha and from -10 to +10 degrees for beta. The total aerodynamic coefficient is the sum of the three sweeps with the flap influence sweep being linearly interpolated from the wind tunnel value ($+/-20^{o}$) to the actual value. The drag force coefficient is measured in a separate test (force balance test) for various Mach numbers. This coefficient is independent of alpha, beta and delta flap.

These sets of coefficients are obtained for several different external store loadings to determine the proximity effects of adjacent stores. A sample listing of a wind tunnel test run log is contained in Figure 10. All coefficients are referenced to the store center of gravity (Aerodynamic Reference).

4. CORRELATION PROCEDURE

The basis of the correlation is the comparison of the flight test derived aerodynamic coefficients to the existing wind tunnel coefficients. To accomplish this comparison, the coefficients must be at the same conditions (i.e., the values of alpha, beta, and delta flap must be the same plus the moment coefficients must be at the same reference point). The flight measured values and reference point are chosen as the

conditions. As noted previously, the wind tunnel data, which is referenced to the Aerodynamic Reference, is at two degree increments for alpha and beta and is at -20, 0, and +20 degrees of flap deflection. It is, therefore, interpolated and transferred to obtain the coefficients at the flight test conditions. The delta store plus pylon moment coefficients are the results of this first series of comparisons.

Achieving the rest of the comparisons was not as easy, several complications due to the lack of flight test data had to be resolved. These complications included the following:

1. Store plus pylon forces (i.e., forces acting on the store/pylon combination in the presence of the F-16) were not measured during flight.

2. Store only forces and moments (i.e., loads acting on the store in the presence of the pylon and F-16) were not measured during flight.

3. Flight test data was not available for all wind tunnel Mach numbers and store loadings. The load discrepancies were not localized problems. Various speeds and loadings showed discrepancies. Therefore, all store loadings and Mach numbers not flown also must be correlated.

4. The wind tunnel test coefficients are referenced to the Aerodynamic Reference while the flight test loads were referenced to the Flight Test Reference. The new correlated moment coefficients have to be referenced to the Aerodynamic reference for incorporation into the database. This was hampered by the lack of flight test measured force data (see #1).

Several assumptions, about the relationship of the forces and moments not measured during flight to both the flight measured moments and the wind tunnel test force and moment coefficients, were made to overcome this lack of flight test data.

5. ASSUMPTIONS INVOLVED IN THE APPROACH

The store plus pylon force coefficients must be correlated for two reasons. First the force coefficients are needed to

determine the actual load environment of the store plus pylon. Store carriage loads influence wing aerodynamics/loads and thus aircraft operation. Second, correct force coefficients are necessary for transferring the moment coefficients from one reference point to another. To achieve the correlation of the store plus pylon coefficients, the forces were derived from the flight test data.

The drag coefficients were accepted as correct as measured in the force balance test. This can be done since the force balance test is completely separate from the loads test with regards to procedure and model. Drag force coefficients computed from theoretical equations verified this supposition. The normal force coefficients were also accepted as correct as measured in the wind tunnel test. Since the fuselage station moment arms are relatively small between the Flight Test Reference and the Aerodynamic Reference, unrealistic delta normal forces would be necessary to cause significant changes in pitch moment. Therefore, the change in normal force can be ignored.

These two approximations simplify the procedure of determining the store plus pylon pitch moment coefficients at the Aerodynamic Reference by eliminating any affects of the change in normal force or drag force on the pitching moment. It is simpler to add a couple than to determine the change in each force. No increase in accuracy would be gained by determining arbitrary delta forces.

The side force coefficients were assumed to account for the entire difference in roll moment between flight and wind tunnel. This was based upon a survey of wind tunnel side force center of pressures (CP's) that showed reasonably consistent CP locations about the store plus pylon center of area. This meant there is a roll moment couple coefficient to be added to the existing wind tunnel coefficients at the Aerodynamic Reference that is caused by the change in side force at the center of area.

The yaw moment differences at the Aerodynamic Reference are, thus, made up by the incremental moment due to the delta side force and by a couple. The store plus pylon coefficients are now defined based on these equations and the flight measured moment coefficients can be transferred from the Flight Test Reference to the Aerodynamic Reference.

The store only load coefficients were defined at the Flight Test Reference based on assumptions about the relationship between store only and store plus pylon loads.

The store only drag and normal force coefficients were taken as correct in the existing data for the same reasons as stated for the store plus pylon coefficients. The store only side force coefficients, however, could not be derived in the same manner since there was no flight test derived store only roll moments. The store plus pylon delta side force was assumed to be distributed to both store and pylon based upon their relative side areas because the large side area of pylons carry approximately this percentage of the total load. Therefore, the store only side force coefficients are equal to the flight derived store plus pylon force coefficients multiplied by the ratio of store only to store plus pylon side areas.

The delta pitch moment was believed to act only on the store. Justification of this is that the pylon, a thin rigid body, has a smaller wetted area compared to the store. Thus, it was accepted that the discrepancies were not caused by differences in pylon loads. This allowed the store plus pylon delta pitch moment coefficients to be added directly to the wind tunnel store only coefficients. The delta store only roll moment coefficients were considered to be due entirely to the delta store only side force coefficients. The reasoning is that as for the store plus pylon, the store only side force causes the entire change in rolling moment. The yaw moment coefficients were defined by accounting for the change in the side force's influence on yaw moment and by dividing the store plus pylon moment couple into the store only and pylon only components based on the side areas. This is an extension of the side force distribution assumption. The store only moment coefficients are then transferred to the Aerodynamic Reference for incorporation into the database.

The flight test program did not include maneuvers at each Mach number tested in the wind tunnel. To correlate the coefficients when flight test data was unavailable, the Mach effects between consecutive Mach numbers tested in the tunnel were taken as correct. This is based on the fact that differences between flight and wind tunnel are independent of Mach number. Therefore, the delta between existing and correlated coefficients at one Mach number (i.e., 0.6M) can be added to the existing coefficients for the next Mach number (i.e., 0.9M).

This premise can also be used for correlating store loadings that are not flown in flight tests. Only certain store loadings, including the configuration carrying only the store, were able to be flown during the program. The influences of an adjacent store on the aerodynamic coefficients in the wind tunnel test were believed to be correct. Since the discrepancies were found for several flight test store loadings, the reasoning of the adjacent store influences not being dependent on the flow phenomenon is verified. The existing delta, between the coefficients without adjacent stores, can be added to the correlated coefficients for the store without influence to obtain the correlated coefficients with influences.

The flight test derived coefficients were separated into three categories corresponding to the sweeps described for the wind tunnel data. The categories are the three maneuver types performed during the flight test program symmetric, sideslip and roll. Symmetric maneuvers with varying alpha, negligible beta, and small trailing edge flap deflections were paired with the alpha sweep. The beta sweep corresponded to sideslip maneuvers which have varying beta, small alpha, and insignificant flap deflection. Finally, roll maneuvers were associated with the flap influence sweep because of the varying alpha, minor beta, and significant deflections involved. By these associations, the correlation method involves three types of existing flight measured coefficients and three types of unknown "to be adjusted" wind tunnel coefficients based on flight test maneuvers. Due to the flight test plan, sideslip maneuvers were flown at only one Mach/altitude point during the program. This lack of maneuver data again caused complications with the correlation since the equations became indeterminate (four unknowns and three equations). Another assumption was made to alleviate this situation. The correlation was restricted by this complication to using only symmetric and roll maneuvers. The beta values measured during flight testing for these maneuvers were small. Therefore, the beta sweep coefficients were accepted as correct as measured in the tunnel. The correlation of alpha cured the discrepancies in the sideslip maneuver loads that were measured, therefore, this supposition was proven valid. This reduced the correlation to two unknowns to two equations. For symmetric maneuvers, the trailing edge flap deflections are insignificant. Therefore the equation for total coefficient is solved for the alpha sweep. The flap influence sweep is then correlated knowing the correlated alpha and beta coefficients.

6. THE APPROACH

Flight test data was obtained from the onboard tape at 40 samples per second. The data was chosen for analysis based on the following criteria: 1) symmetric maneuver data with a wide range of alpha was selected at one degree intervals of alpha and; 2) roll maneuver data with a smaller range was selected at one-half degree intervals of alpha. Data was selected as a function of alpha since both sweeps to be correlated cover a range of alpha.

The investigation procedures and the assumptions were combined to develop the approach. The flight test derived air moments were determined by subtracting the inertia loads and dynamic incremental loads from the recorded moments. The inertia loads were calculated using the flight measured aircraft parameters listed in Figure 8. The LCO for each time hack selected defined the values of the dynamic increments. The aerodynamic moments were then converted to non-dimensional coefficients based on the surface area and mean aerodynamic chord of the F-16 wing.

Once the three sweeps of coefficients for both store only and store plus pylon were defined at the Aerodynamic Reference, trends of coefficient with alpha were determined and compared to trends of the wind tunnel coefficients.

The trends of flight measured and wind tunnel coefficients versus alpha were compared because of the amount of flight test data available. The range of alpha during flight test maneuvers was not as large as tested in the wind tunnel. While wind tunnel tests ranged from -5^{o} to $+27^{o}$, the range for symmetric maneuvers was only -3^{o} to $+19^{o}$ (see Figure 15). This deficiency was worse for roll maneuvers where the range typically totaled a maximum of 4 degrees (see Figure 16). The comparison was performed to expand the trend of flight test data.

The extrapolation of the alpha sweep data consisted of taking the percentage change between the end points of the flight measured curve to wind tunnel and maintaining it over the rest of the alpha range. The flap influence sweep could not be extrapolated in the same manner due to the small range of flight measured data and the fact that trends for the flap influence sweep could not be determined. The mean flight measured coefficient was determined and the delta between it and its corresponding wind tunnel value was applied to the whole range of wind tunnel coefficients. By applying this

delta across the board, the flap influence adjustment became a shift in intercept rather than including any change in slope.

The curves of correlated wind tunnel data were generated from the extrapolations and incorporated into the aero data base. This realistic data base was then used to set aircraft operational limits when carrying this underwing external store.

7. CONCLUSIONS

This approach associated the unknown flow phenomenon with differences in certain aerodynamic loads. The phenomenon was attributed with causing a pitch moment couple, a roll moment couple, a yaw moment couple, and a change in side force on the store plus pylon at the Aerodynamic Reference. By including these changes along with the adjustments for axial load factor and LCO dynamic load increments, the flight test derived loads are now accurately represented by the analytical loads as shown by the plots in Figure 17.

As evidenced by the investigation of this unique situation, scaled wind tunnel tests may not always reflect full scale aerodynamic loads. Variances in flexibility, Reynolds number, wall effects and probably other unknowns can be significant between the modeled external store and the actual external store and might cause differences in external store carriage loads. This technique developed at General Dynamics is generic in nature and could be utilized (depending on the circumstances) if this occurrence would ever happen again with another external store.

ORAL PRESENTATION CHARTS FOLLOW

AN APPROACH FOR CORRELATING EXTERNAL STORE WIND TUNNEL MEASURED AERODYNAMIC LOADS TO FLIGHT TEST DERIVED LOADS

JOHN T. RODGERS, JR.
ENGINEER

STRUCTURAL LOADS AND CRITERIA
GENERAL DYNAMICS/FORT WORTH DIVISION

FIGURE 1

INTRODUCTION

- LOADS FLIGHT TESTING
  - * VALIDATES ANALYTICAL METHODS AND DATA
  - * TEST PROGRAMS DEVELOPED TO DEMONSTRATE MAXIMUM LOADS
  - * LOADS FOR ALL PROGRAM MANEUVERS PREDICTED ANALYTICALLY
  - * FLIGHT LOADS DERIVED FROM STRAIN GAGE INSTRUMENTATION
- DISCREPANCY BETWEEN FLIGHT DERIVED AND ANALYTICALLY PREDICTED LOADS
- POSSIBLE CAUSES OF DISCREPANCY
  - * FLIGHT TEST INSTRUMENTATION ~ AIRCRAFT/STORE AND GROUND STATION
  - * ANALYTICAL METHODS FOR PREDICTING LOADS
  - * LOAD BASIC DATA

FIGURE 2

FLIGHT TEST INSTRUMENTATION SCHEMATIC DIAGRAM

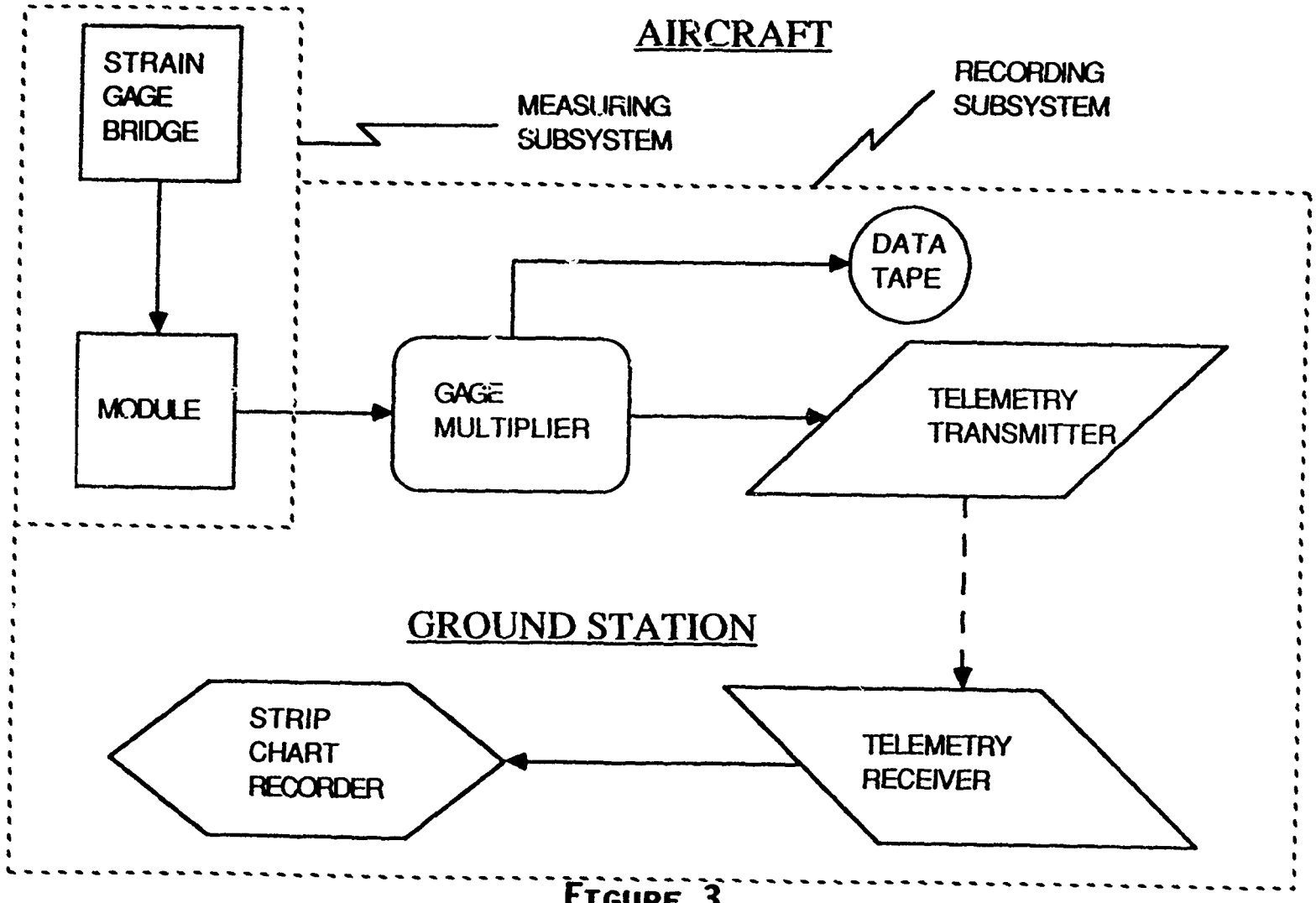

FIGURE 3

INSTRUMENTATION VALIDATION SYSTEM

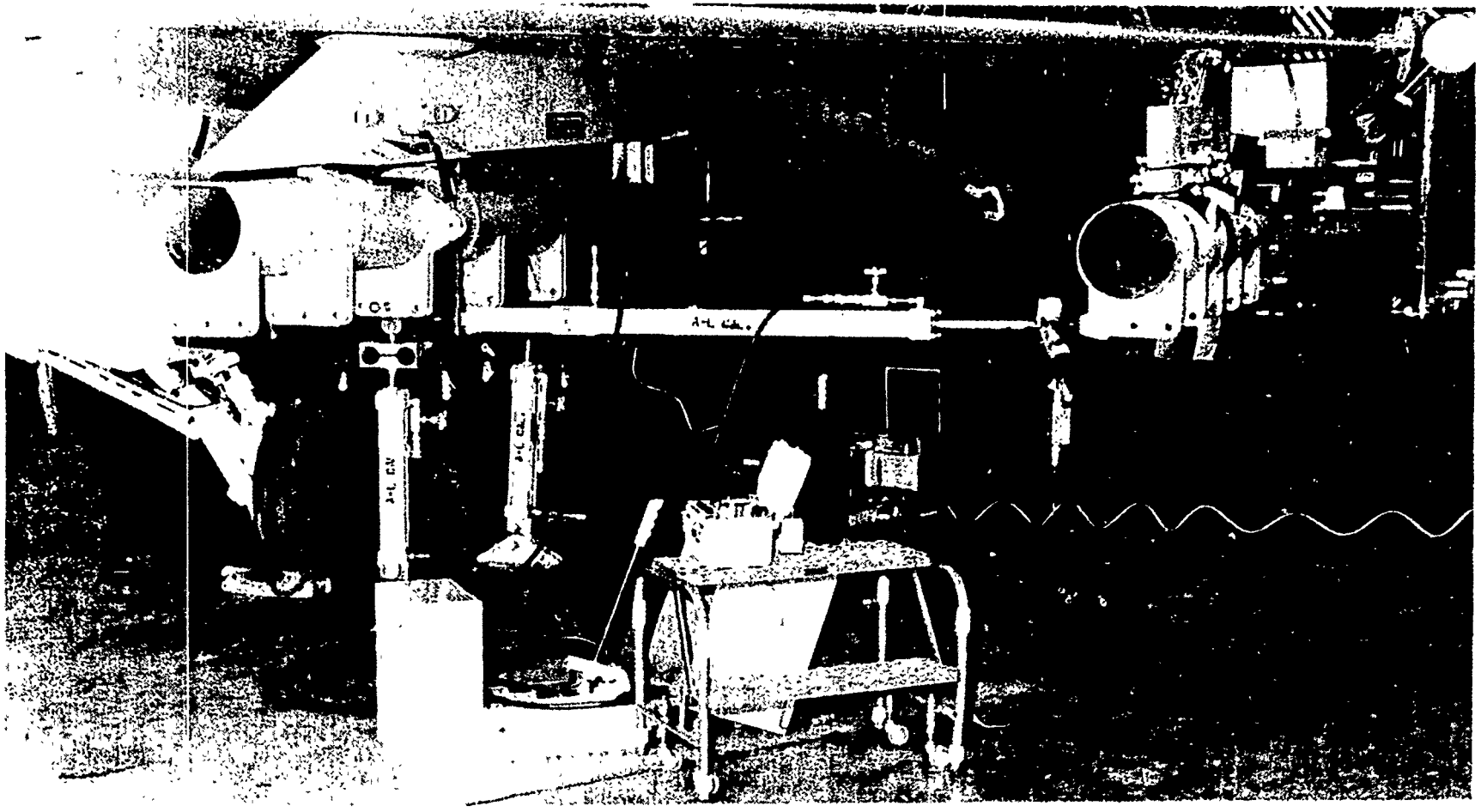

FIGURE 4

POSSIBLE CAUSES OF DISCREPANCY

- o ANALYTICAL METHODS
  - * GENERAL DYNAMICS EXTERNAL STORE LOADS COMPUTER PROGRAM
  - * PROGRAM CALCULATES AIR, INERTIA AND NET LOADS
  - * DOES NOT ACCOUNT FOR DYNAMIC LOADS

FIGURE 5

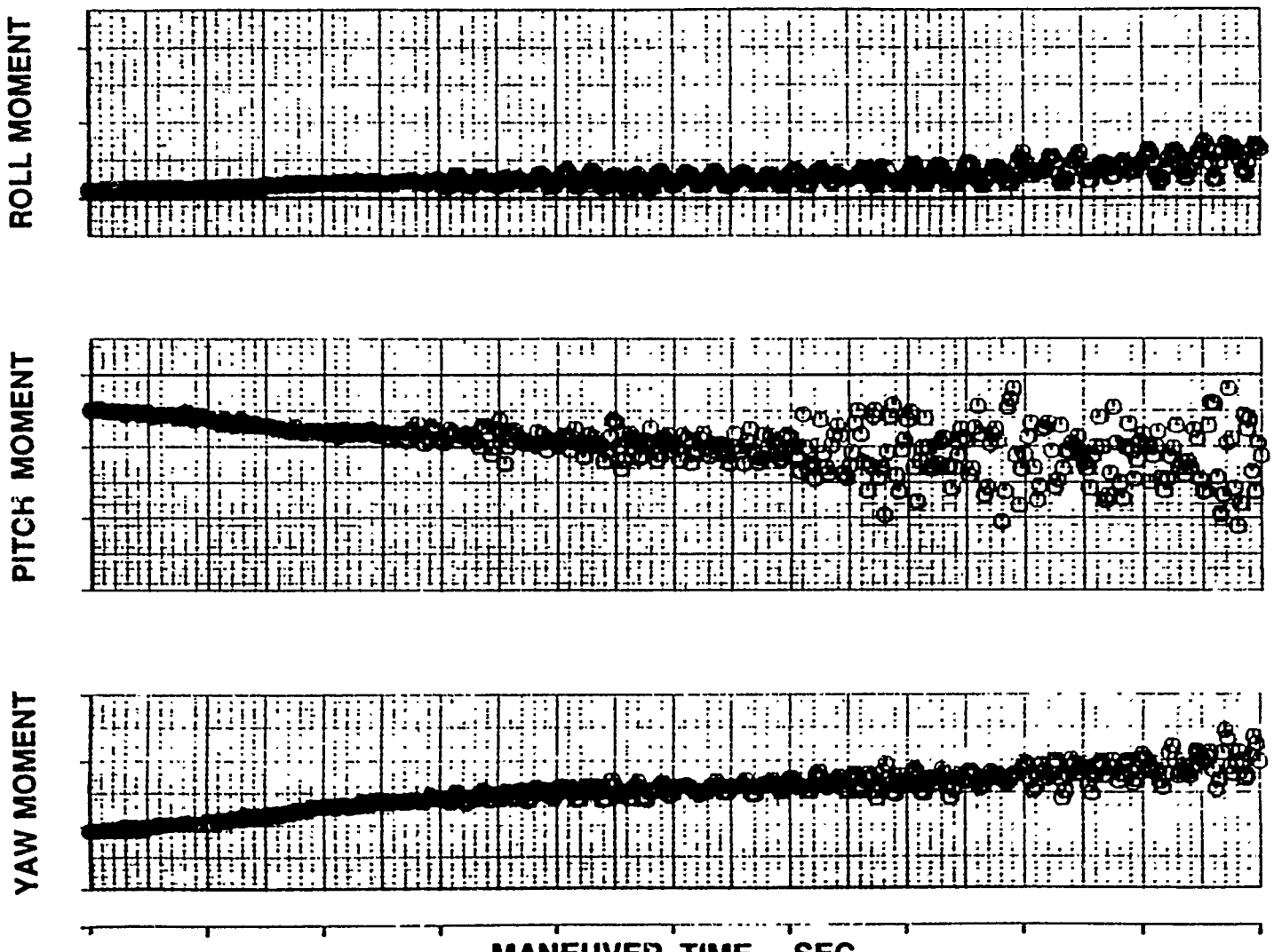
FLIGHT DERIVED LOADS VS TIME
ROLL MOMENT
PITCH MOMENT
YAW MOMENT
MANEUVER TIME - SEC

FIGURE 6

POSSIBLE CAUSES OF DISCREPANCY (CONT'D)

- o STATIC LOAD COMPARISON
  - * DISCREPANCY BETWEEN STATIC FLIGHT DERIVED LOADS AND STATIC ANALYTICALLY PREDICTED LOADS
  - * FLIGHT DERIVED LOADS VALIDATED
  - * PREDICTED LOADS CHECKED BY HAND COMPUTATIONS
  - * DISCREPANCY RESULTS FROM BASIC DATA

17

- o BASIC DATA
  - * ACTUAL MASS PROPERTIES OF STORE MEASURED (DATA NOT IN QUESTION)
  - * AIRCRAFT MANEUVER RESPONSE DATA FROM DIGITAL COMPUTER SIMULATION
  - * STORE AERODYNAMIC COEFFICIENT DATA MEASURED IN 1/9TH SCALE MODEL WIND TUNNEL TESTS

FIGURE 7

AIRCRAFT MANEUVER RESPONSE PARAMETERS

PARAMETER	UNITS
MACH NUMBER	-
ALTITUDE	f t
AIRCRAFT CENTER OF GRAVITY	% M.A.C.
ANGLE OF ATTACK	degrees
ANGLE OF SIDESLIP	degrees
LEFT HAND TRAILING EDGE FLAP DEFLECTION	degrees
RIGHT HAND TRAILING EDGE FLAP DEFLECTION	degrees
ROLL RATE	deg/sec
PITCH RATE	deg/sec
YAW RATE	deg/sec
ROLL ACCELERATION	rad/sec**2
PITCH ACCELERATION	rad/sec**2
YAW ACCELERATION	rad/sec**2
AXIAL LOAD FACTOR	g's
LATERAL LOAD FACTOR	g's
VERTICAL LOAD FACTOR	g's
DYNAMIC PRESSURE	lbs/ft**2

FIGURE 8

COMPARISON OF PREDICTED AND MEASURED AERODYNAMIC LOADS

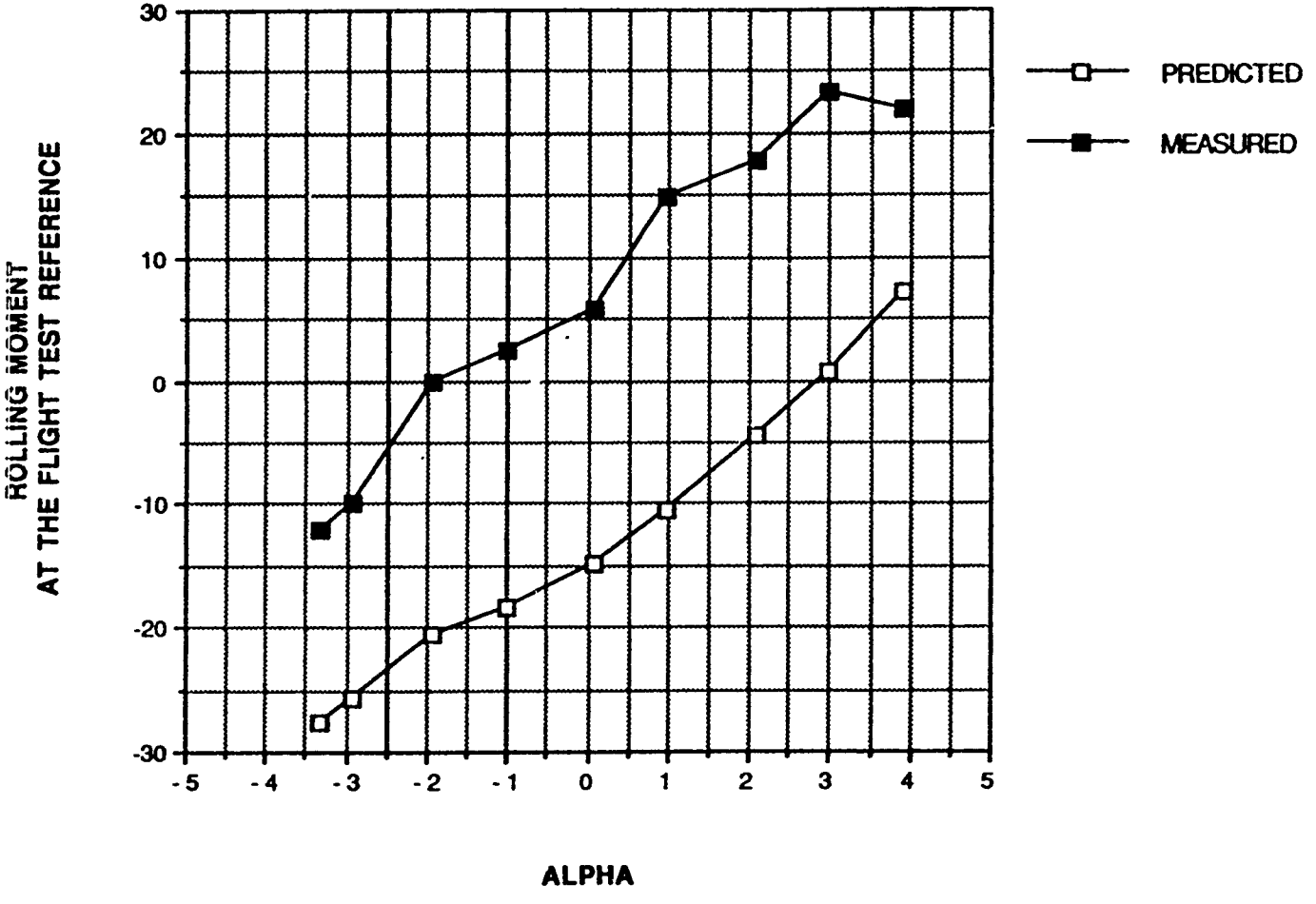

FIGURE 9

SAMPLE WIND TUNNEL TEST SUMMARY SHEET

TEST TF-397

EXTERNAL STORES					CONTROLS			MACH NUMBER						
BL 0	BL. 71	BL 120	BL 157	TIP	alpha	beta	Δ te	0.6	0.85	0.9	0.95	1.1	1.2	1.55
ALQ-119-12	370 TK	MK-84		AIM-9J	V	0	0	269	271	272				
ALQ-119-12	370 TK.	MK-84		AIM-9J	5	V	0	275	276	277				
	370 TK			AIM-9J	V	0	0	282		285	286	289	290	293
	370 TK			AIM 9J	5	V	0	283		284	287	288	291	292
	370 TK			AIM-9J	V	0	20	296	430	297	298	299	300	301
	370 TK			AIM-9J	V	0	-20	429	431	432	433	434	435	436
ALQ-119-12		MK-84		AIM-9J	V	0	0	328	330	332				
ALQ-119-12		MK-84		AIM-9J	5	V	0	329	331	333				
ALQ-119-12		MK-84		AIM-9J	V	0	20	321	332	323				
ALQ-119-12			AIM-9J	AIM-9J	V	0	0	350		348	346	344	340	342
ALQ-119-12			AIM-9J	AIM-9J	5	V	0	351		349	347	345	341	343

FOR ALL RUNS : Δr=0 Δh=0 Δle=0

$$\text{TOTAL AERODYNAMIC COEFFICIENT} = \text{COEFFICIENT DUE TO ALPHA SWEEP} + \text{DELTA COEFFICIENT DUE TO BETA SWEEP} + \text{DELTA COEFFICIENT DUE TO FLAP DEFLECTION} * \left(\frac{\text{ACTUAL DEFLECTION}}{\text{TEST DEFLECTION}} \right)$$

FIGURE 10

THE APPROACH

- CORRELATION IS A COMPARISON OF WIND TUNNEL COEFFICIENTS TO FLIGHT TEST COEFFICIENTS AT THE FLIGHT CONDITIONS OF ANGLE OF ATTACK, ANGLE OF SIDESLIP, FLAP DEFLECTION ANGLE, AND MACH NUMBER

- COMPLICATIONS OF THE COMPARISON
  - * STORE PLUS PYLON FLIGHT DERIVED FORCES NOT AVAILABLE
  - * STORE ONLY FLIGHT DERIVED LOADS NOT AVAILABLE
  - * DIRECT CORRELATION OF ENTIRE WIND TUNNEL NOT POSSIBLE DUE TO LACK OF FLIGHT TEST DATA (COST PROHIBITED)
  - * DIFFERENT MOMENT REFERENCE POINTS (AERODYNAMIC REFERENCE VS. FLIGHT TEST REFERENCE)

- STORE PLUS PYLON FORCES
  - * WIND TUNNEL DRAG FORCE AND NORMAL FORCE ARE ACCEPTED AS CORRECT
  - * SIDE FORCE ACCOUNTS FOR THE DISCREPANCY IN ROLL MOMENT AT THE FLIGHT TEST REFERENCE LOCATION

FIGURE 11

THE APPROACH (CONT'D)

- RESULTS OF FORCE ASSUMPTIONS ON THE MOMENTS AT THE AERODYNAMIC REFERENCE
  - * DELTA PITCH MOMENT WHICH EQUALS THE PITCH MOMENT DISCREPANCY AT FLIGHT TEST REFERENCE
  - * DELTA ROLL MOMENT WHICH IS DUE TO THE CHANGE IN SIDE FORCE AT THE CENTER OF AREA (TYPICAL CP LOCATION OF THE WIND TUNNEL DATA)
  - * DELTA YAW MOMENT WHICH EQUALS THE YAW MOMENT DISCREPANCY MINUS THE CHANGE IN MOMENT DUE TO THE SIDE FORCE DELTA

- DETERMINATION OF STORE ONLY DATA ~ BASED ON RELATIONSHIP OF STORE AND PYLON AERODYNAMICS
  - * DRAG FORCE AND NORMAL FORCE ARE ACCEPTED AS CORRECT
  - * STORE PLUS PYLON SIDE FORCE CHANGE IS DISTRIBUTED BETWEEN STORE AND PYLON BASED ON RESPECTIVE SIDE AREAS

FIGURE 12

THE APPROACH (CONT'D)

- DETERMINATION OF STORE ONLY DATA ~ BASED ON RELATIONSHIP OF STORE AND PYLON AERODYNAMICS (CONT'D)
  - * STORE PLUS PYLON PITCH MOMENT COUPLE IS CAUSED ENTIRELY BY A SHIFT IN STORE ONLY CP
  - * NO STORE ONLY ROLL MOMENT COUPLE SINCE CP LOCATION IS CONSISTENT
  - * YAW MOMENT COUPLE DUE TO THE DISTRIBUTION OF STORE PLUS PYLON COUPLE BASED ON SIDE AREAS MINUS THE INCREMENT CAUSED BY THE SIDE FORCE CHANGE
- CORRELATION OF WIND TUNNEL DATA WITHOUT CORRESPONDING FLIGHT TEST DATA
  - * MACH EFFECT TRENDS VALIDATED BY FLIGHT TEST DATA
  - * STORE PROXIMITY INFLUENCES FROM WIND TUNNEL TAKEN AS STILL VALID

FIGURE 13

THE APPROACH (CONT'D)

- o CORRELATION PROCEDURE
  - * FLIGHT TEST MANEUVERS ASSOCIATED WITH WIND TUNNEL TEST RUNS
  - * SYMMETRIC DATA USED FIRST TO CORRELATE ALPHA SWEEP (NO SIGNIFICANT BETA OR FLAP DEFLECTIONS TO ACCOUNT FOR)
  - * BETA SWEEP NOT CHANGED, SIDESLIP MANEUVER LOADS CAN NOW BE PREDICTED USING A CORRELATED ALPHA SWEEP
  - * ROLL DATA AND CORRELATED ALPHA/BETA SWEEPS ALLOW CORRELATION OF FLAP DEFLECTION SWEEP

FIGURE 14

PITCH MOMENT COEFFICIENT VS ALPHA
SYMMETRIC MANEUVER SAMPLE

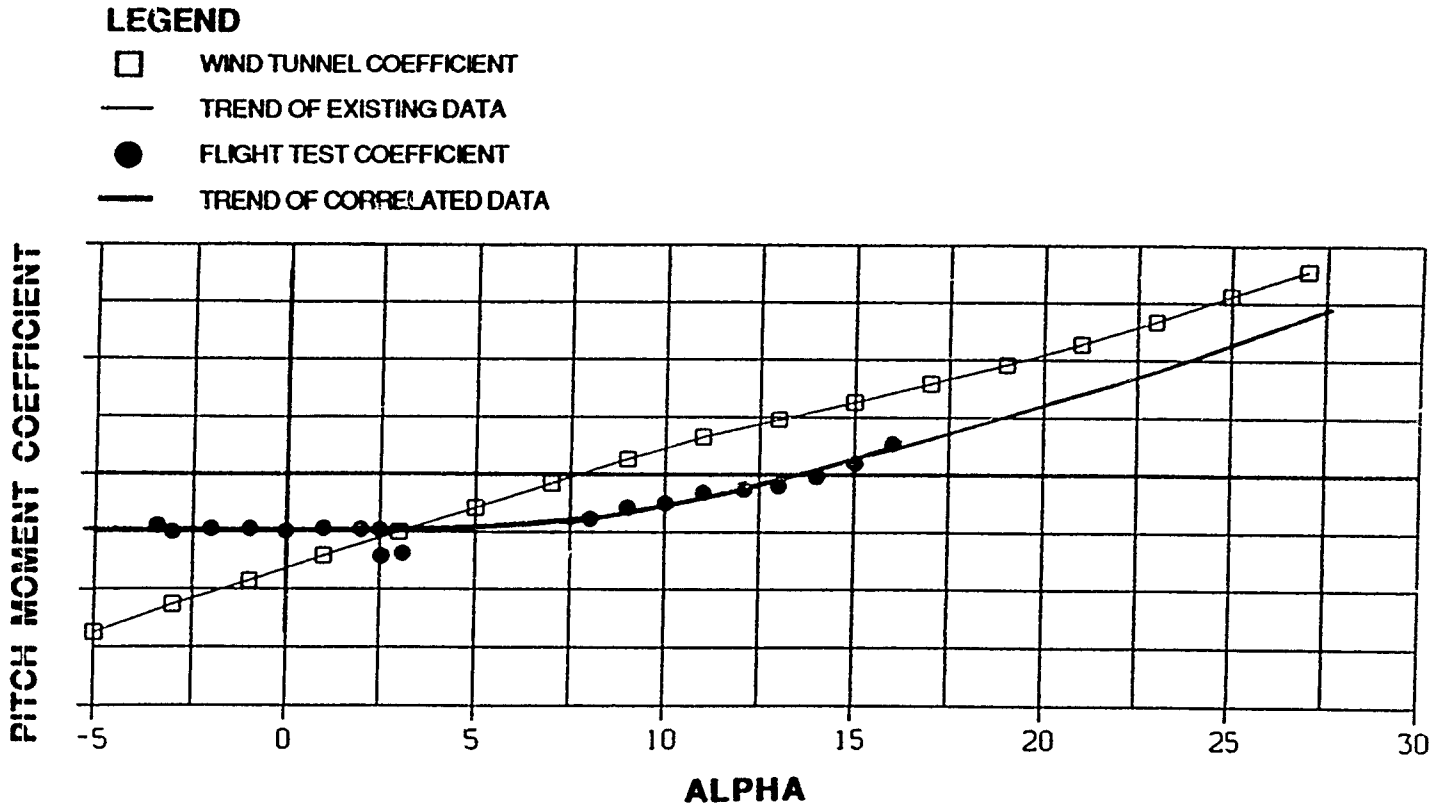

COEFFICIENTS ARE AT THE AERODYNAMIC REFERENCE

FIGURE 15

PITCH MOMENT COEFFICIENT VS ALPHA
ROLL MANEUVER SAMPLE

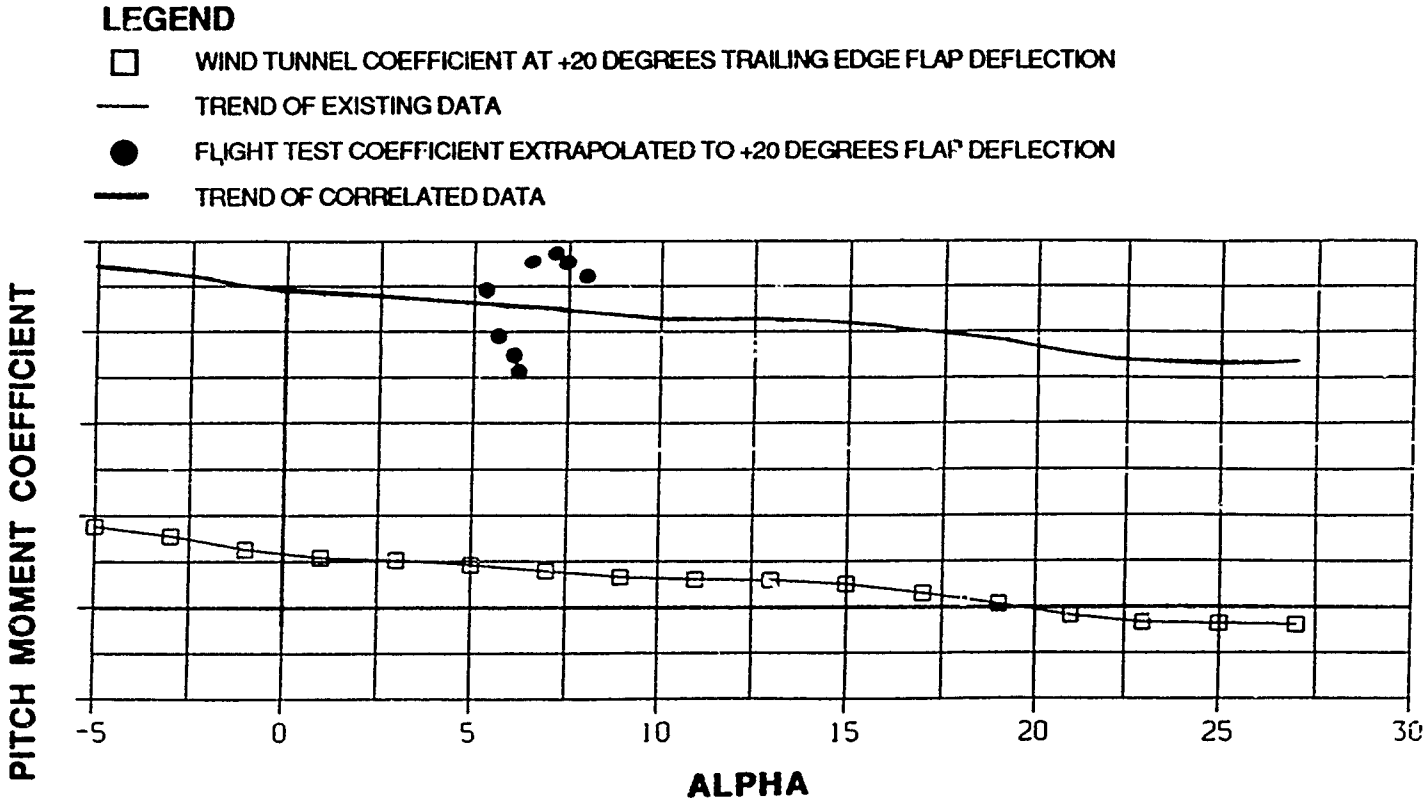

COEFFICIENTS ARE AT THE AERODYNAMIC REFERENCE

FIGURE 16

COMPARISON OF AERODYNAMIC LOADS AFTER CORRELATION

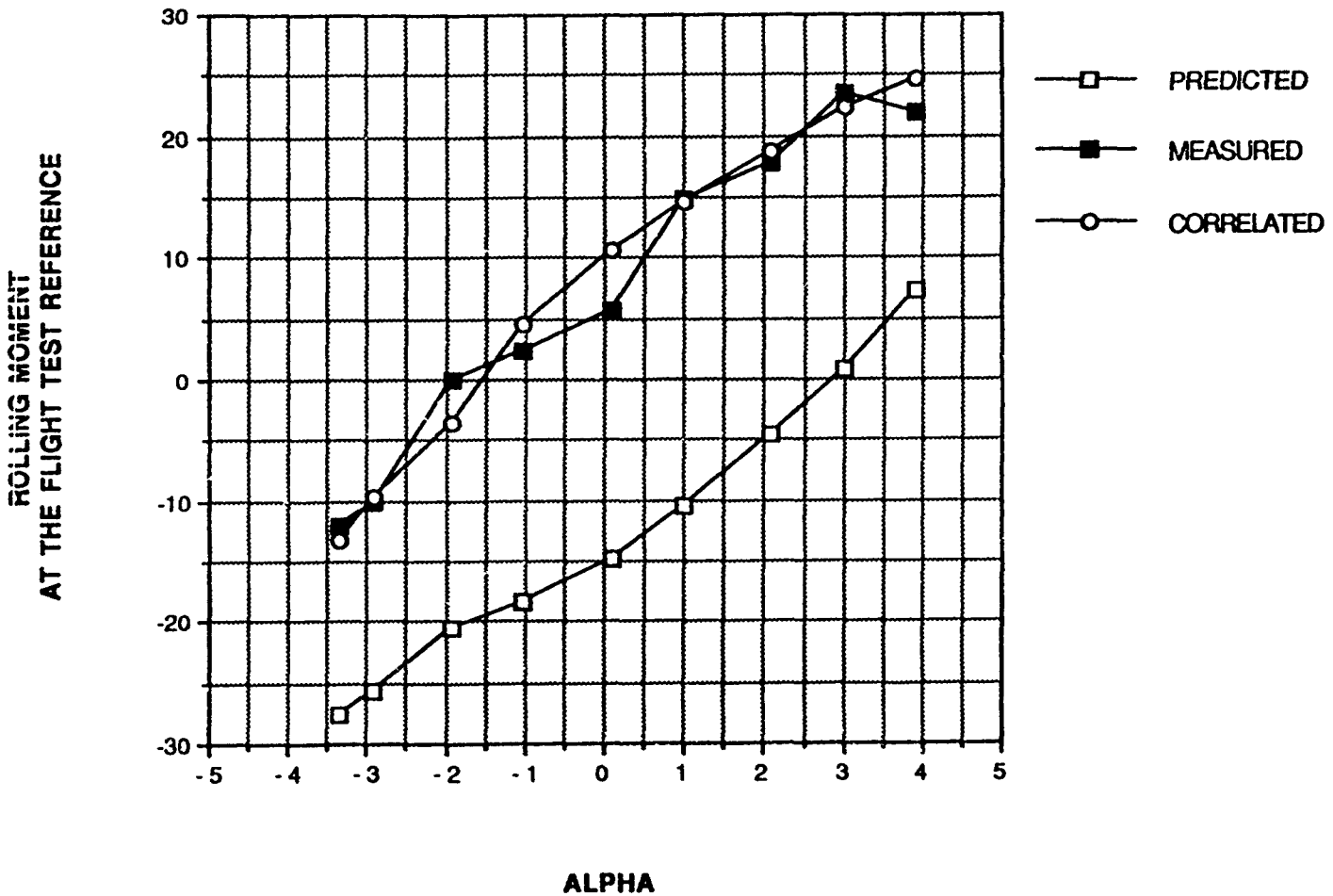

FIGURE 17

BIOGRAPHY

JOHN T. RODGERS, JR.

Mr. Rodgers received his B.S. degree in Aerospace Engineering from the University of Notre Dame in 1987. In January 1988, he assumed his current position as an engineer in the Static Loads and Criteria Group at General Dynamics/Fort Worth Division. His primary responsibilities have included computing external store carriage loads for pylon design and F-16 structural certification. His efforts have included supporting loads flight testing by accomplishing pre-flight and post-flight load predictions, correlating external store aerodynamics data acquired from wind tunnel tests to flight test data, and performing external store carriage loads analysis based on flight test derived loads results.

THIS PAGE INTENTIONALLY LEFT BLANK

CAVITY AEROACOUSTICS*

Richard E. Dix
Calspan Corporation, AEDC Operations
Arnold Air Force Base, Tennessee
and
Carroll Butler
AFATL/FXA, Eglin AFB, Florida

INTRODUCTION

Aircraft design decisions often depend on the two factors, weight and drag. Since the first powered flight, aircraft designers have smoothed, faired, retracted, and hidden as many external excrescences as possible in the quest for additional vehicle performance and efficiency. However, the jocular observation that "there is no free lunch" becomes a real conclusion as the designer dutifully pursues the aerodynamic grail. As an example, consider the retraction or hiding of items in a cavity that is closed and smooth to the flow over the body. At an appropriate time, doors or panels open as part of a desired operational sequence, and the storage volume, or cavity, together with the contents, are exposed to the external flow. Regardless of the purpose or contents of the cavity, two of the important flow phenomena that occur with exposure of the cavity are: 1) the development of a shear layer within which the transition occurs from the stagnant cavity environment to the active external flow; and 2) the creation of a concomitant fluctuating pressure environment in the cavity. The fluctuations often resonate at characteristic frequencies, and are generally detectable as audible tones, leading to the term "aeroacoustic" to describe the fluid dynamic environment. Over the years, various investigators have focused on the action of the shear layer passing over the cavity (a vortex-acoustic coupling) as a cause of the aeroacoustic phenomena (Refs. 1-3). In 1970, Covert (Ref. 4) offered a good historical perspective, citing Strouhal, Rayleigh, and Kohlrausch in works dating back to the 1870s, 1880s, and 1890s. More recently, Stallings and Wilcox (Ref. 5) at NASA/Langley summarized current models of supersonic flow over shallow (closed flow), medium (transitional flow), and deep (open flow) cavities, illustrated in Fig. 1.

Many sets of experiments have been completed in studies of the cavity aeroacoustic environment, among these Rossiter's predictions of the modal frequencies (Ref. 6) and Clark's studies of techniques of controlling the modal amplitudes (Ref. 7). The effect of cavity shape on the static pressure distribution over the surfaces of the cavity was reported by Plentovich (Ref. 8), and Stallings and Wilcox (Ref. 5), and computational fluid dynamic (CFD) efforts to predict cavity flow fields have been described by Suhs (Ref. 9), Rizzetta (Ref. 10), and Baysal (Ref. 11). These documents represent only a fraction of the active authors and programs setting about to better define, predict, and interact with cavity aeroacoustic phenomena. The present paper, for example, documents a program of experiments that has been underway for three years at the Arnold Engineering Development Center (AEDC), and has resulted in a rather large data base describing the aeroacoustic environment associated with cavities of three different length-to-height ratios (L/H), equipped with a variety of acoustic suppression devices and doors, and exposed to external flows of subsonic to supersonic speeds.

---

* The research reported herein was performed by the Arnold Engineering Development Center (AEDC), Air Force Systems Command. Work and analysis for this research were done by personnel of Calspan Corporation/AEDC Operations, operating contract for the AEDC aerospace flight dynamics facilities. Further reproduction is authorized to satisfy needs of the U. S. Government.

SHEAR LAYER

Aerodynamic Loads

Both the presence of the shear layer between the open cavity volume and the external flow field and the existence of tones in the cavity represent challenges to aircraft and systems designers. If, for instance, it is desired to move a body out of a cavity, the variation of aerodynamic forces acting on the body as it passes through the shear layer must be known. In 1983, Stallings at NASA/Langley reported large changes in loads acting on a store passing through a cavity shear layer (Ref. 12). The loads were noted to depend on the length-to-height ratio (L/H) of the cavity, Fig. 2. Using a device designed to translate the body in small increments along one axis only (the "Z-Rig," Ref. 13, Fig. 3), Dix at the Arnold Engineering Development Center (AEDC) confirmed the existence of substantial gradients in body loads when passing through the shear layer, Fig. 4 (Ref. 13). The importance of the gradients must be assessed case by case, but one must clearly proceed with caution if tempted to construct a simple curve through three data points measured at coarse intervals as indicated in Fig. 4.

Strong variations in aerodynamic loads could affect somewhat the structural integrity of any body passing through a shear layer, but perhaps the most critical question is the influence on the trajectory of a body released inside the cavity and passing outward through the shear layer. At the AEDC, Dix has measured and calculated trajectories of a store jettisoned out of a cavity. Trajectories were measured using the Captive Trajectory Support (CTS) system in the 4-ft transonic wind tunnel AEDC Aerodynamic Wind Tunnel (4T), Fig. 5 and Ref. 14. Several sets of cavity dimensions (L/H), cavity door configurations, and flow suppression devices were used to vary the configuration of the cavity, but the ejection conditions were constant. Store motion was predicted from a point at the end of a Z-axis ejector stroke. The end-of-stroke translational velocity (V_{Zeos}) was 30 ft/sec in the Z-axis direction (down and away from the cavity), and the angular pitching velocity of the store was -1 rad/sec (nose down). During the same test, aerodynamic loads acting on the store at a spatial grid of locations in and near the cavity were recorded to provide a basis for predictions of store separation trajectories using post-test computational techniques. The post-test computer code, developed by Morgret (Ref. 15) called the Multiple Degree-of-freedom Interpolation and Trajectory Generation Program, or MDITGP, is in fact a code similar to the code used to predict trajectories in the wind tunnel using the CTS system. During a test, forces and moments acting on the store in the wind tunnel are used as inputs to the code, while for the post-test trajectory predictions, the store loads inputs are interpolated from the grid data. A clear advantage of the post-test computational technique is the ease with which initial conditions, such as the end-of-stroke store velocities, can be changed to predict many different trajectories from the same set of wind tunnel data. A description of the MDITGP is contained in Ref. 15.

Using different end-of-stroke store velocities, it was possible to gain an appreciation of the effect of a cavity shear layer on the trajectory of a jettisoned store. As illustrated in Fig. 6, with the end-of-stroke Z-axis translational velocity above approximately 1.5 percent of the free-stream velocity, store motion was negligibly affected by passing through the shear layer, so long as the end-of-stroke pitch velocity, θ, was -1 rad/sec (nose-down). When the initial pitch rate of the store was $-1 < \theta \leq 0$ (or even worse, nose-up, $\theta > 0$), passage through the shear layer was not smooth, and jettison under these conditions would not be considered safe. Clearly, to assure reliable traverse through the shear layer at all jettison conditions, the store would have to be constrained in some way, such as with the use of a trapeze, a device dating back at least as far as the JU 87 Stuka of 1935. Constraint has been used much more recently, as for example, on the F-106 and the Tornado.

Acoustics

The cause-and-effect relationship between the shear layer and the acoustic-frequency fluctuations in the cavity has been studied extensively, but is not completely understood. Under contract to the U. S. Air Force, Heller and Bliss, of the firm of Bolt, Beranek, and Newman conducted a series of water table studies in 1972 (Ref. 16) during which it was demonstrated that the expansion of an approaching

supersonic flow into the cavity (for cavities of appropriate L/H values) would generate a pressure disturbance or wave that would travel to the downstream bulkhead, where it would be reflected. As fluid was forced from the cavity by the brief increase in pressure, the shock at the downstream edge of the cavity opening detached. When the pressure was reduced by the reflection and mass ejection, the shock again attached to the downstream edge. Meanwhile, the forward traveling reflection forced the shear layer away from the cavity until expansion at the upstream edge again took place, and the cycle began anew. A sketch illustrating the above model is shown in Fig. 7.

Further experimentation by Heller and Bliss showed that the fluctuating shear layer could be stabilized through the use of various baffles in the cavity and bulkhead edge shaping. Unfortunately, the entire effort was experimental, not at all proceeding from fundamental fluid-dynamic relationships. Consequently, no attempt was made to predict frequencies or amplitudes of the acoustic-frequency pressure oscillations in the cavity.

The flow expansion-compression-ejection model appeals to intuition, and has been proffered by many investigators. Indeed, fluctuating pressures acting on the surfaces of flat plate and cavity models have been observed by both Dix at the AEDC (Ref. 13) and Plentovich at NASA/Langley (Ref. 8). In both studies, conventional measurements of static pressures acting on surfaces in steady flow were made, with the disappointing result that repeatability was poor. A sketch of the AEDC model is shown in Fig. 8, and a typical profile of surface pressure coefficient along the centerline of the plate-cavity model with L/H = 4.5 is shown in Fig. 9, for a transonic condition. There are actually 12 profiles shown in Fig. 9, recorded at random intervals of 20 to 60 sec. Repeatability on the plate upstream of the cavity is excellent - well within the quoted statistical 95-percent confidence interval for one standard deviation of the pressure coefficient, i.e., a C_p of ± 0.01. In the cavity, the data points indicate decreasing repeatability with increasing X/L. On the plate downstream of the cavity, a convergence toward acceptable repeatability occurs. Sample profiles of both statistical mean and standard deviations are shown in Figs. 10a and 10b, respectively.

When dynamic pressure transducers are used to sense the fluctuating components of surface pressures, there is convincing correlation between the power spectra in the frequency domain at various locations and the standard deviation profile determined from the 12 repeat points. Sample spectra are shown in Fig. 11 for several locations on the plate/cavity model. Near the downstream wall in the cavity, where the one-standard-deviation profile is maximum in value, the modal and broadband amplitudes are greatest, as are the overall root-mean-square (RMS) levels. Consistently, near the upstream wall in the cavity, both low standard deviation in the static measurements and lower modal and RMS levels of fluctuating pressures are observed.

ACOUSTIC PREDICTIONS

In his 1962 RAS paper, Rossiter offers an empirical method of predicting modal frequencies,

$$f = \frac{V(m - \gamma)}{L\left(1 + \frac{\gamma - 1}{2} M^2\right)^{\frac{1}{2}} \left(\frac{V_v}{V_\infty}\right)} \quad \text{(Ref. 6).}$$

The influence of the shear layer is addressed via the vortex velocity ratio, and cavity shape in the flow direction is acknowledged through the γ term, which Rossiter presents as a function of cavity L/H. When Rossiter's values of γ are displayed graphically as a function of L/H, a mathematical relationship is difficult to propose for the purpose of interpolation and/or extrapolation, Fig. 12. For example, the cavities used by the authors in a recent set of experiments require both interpolation and extrapolation. Both first and second-order relationships were attempted, with mixed results. Interpolation via either

linear or parabolic relationships yielded similar values of γ, but extrapolation beyond the range of Rossiter's results could be undertaken only subjectively (Fig. 12).
Comparison of frequency predictions with data from the recent AEDC wind tunnel experiments illustrates the limitation (Fig. 13). Tonal frequencies in a deep cavity (L/H = 4.5) are predicted quite well for modes 1 and 2 through M = 1.20, but less well for the third and higher modes. Furthermore, the predicted frequencies are underestimated for all modes at Mach numbers greater than 1.20, which happens to be the limit of Rossiter's data base. The trend of prediction quality is downward as the height of the cavity decreases (Fig. 13b, L/H = 9.0), but the issue of γ choice becomes moot for a most shallow cavity of L/H = 14.4, illustrated in Fig. 13c, for which no sharp tones are detected. Of course Rossiter's data base is also limited to L/H = 10.

Amplitude predictions represent a much more complicated situation. It may be inferred from data in the literature that the amplitude of a tone, expressed as a static pressure coefficient, is dependent on many parameters, e.g.,

$$c_p = c_p\left(\frac{tc_\infty}{L}, \bar{x}/L, L/H, W/H, M_\infty, \theta/H, \gamma\right),$$

where L, W, and H are cavity dimensions, θ is the displacement thickness of the approaching boundary layer, c_∞ is the free-stream speed of sound, t is time, x is the axial length from the leading edge of the cavity to a location in the cavity, and γ is the ratio of specific heats.

Recent AEDC data confirm no strong effect of unit Reynolds number (Fig. 14) and of Mach number (Fig. 15). However, tonal amplitude can be affected by model size, as observed by Shaw (Ref. 17). Using the authors' generic plate/cavity model (Fig. 8), filler blocks were installed which decreased the dimensions of the cavity in small steps, while maintaining the shape of the cavity, i.e. the L/H and L/W ratios were constant (W = cavity width). The same pressure transducer was used in all measurements by mounting it in the same relative location in each cavity. With the size ratio, or scale factor, represented by λ, Shaw's data can be shown in graphical form as in Fig. 16. It must be noted that the boundary layer at the leading edge of the cavity opening was constant, since the inserts were installed beginning at the downstream end of the cavity. With so many parameters interacting, development of an amplitude-prediction algorithm will be difficult, indeed. A research effort is underway at the AEDC to attempt such a correlation.

MODULATION OF THE CAVITY ACOUSTICS

A large part of the authors' series of wind tunnel experiments at the AEDC has been a study of the effectiveness of various techniques in modulating the cavity aeroacoustic environment. Two passive devices were evaluated: 1) spoiler devices mounted at or near the leading edge of the cavity, and 2) 45-deg ramp surfaces installed in the cavity at the downstream wall, illustrated in Fig. 17. Of course, cavities are usually equipped with doors, and several types were also included in the experiments (Fig. 18). Clearly, a very large data base was compiled as the many combinations of these devices were evaluated, and it will be possible to present only a small amount of the data.

Spoiler and Door Effects on Cavity Aeroacoustics

The effectiveness of a spoiler erected perpendicular to the flow at the leading edge of the cavity opening in modulating or suppressing pressure fluctuations in the cavity of an F-111 aircraft was described by Clark (Refs. 7 and 18). Although Clark identified the superior effectiveness of a combined leading-edge sawtooth spoiler and rear bulkhead ramp (Fig. 19), the internal ramp requires a cavity length that is longer than otherwise required, and is therefore not regarded with favor by the structural

designer. Consequently, only spoiler-door combinations are described here. Three types of data support conclusions about the effectiveness of spoiler-door combinations, and will be discussed here.

Static Pressure Distribution

First, static pressure measurements taken along the longitudinal centerline of the cavity walls and ceiling can be used to identify the regions of high and low aerodynamic pressure acting on a body in the cavity that strongly influence the subsequent behavior of the body. In the case of a store jettisoned from a cavity, the influence of a properly designed spoiler can be extremely beneficial. For example, in Fig. 20, the influence of a sawtooth spoiler mounted at the leading edge of a cavity of L/H = 4.5, and in the presence of square-leading-edge bifold doors open to 90 deg (SBF 90) is illustrated for a transonic Mach number. Two heights of the sawtooth spoiler were used during the test, one about three times the boundary-layer height (3δ) and one approximately equal to the boundary layer (1δ). For comparison, the centerline pressure distribution of the clean cavity (no spoilers, no doors) is also shown. In this case, the store model is suspended 4.5 store diameters below the cavity opening, as if just jettisoned. Note that in the clean cavity, the pressure distribution is benign over 60 percent of the length of the cavity, but that near the rear bulkhead, the stagnation of flow causes a high pressure to build in the region of the cavity nearest the tail fins of a typical store. With the 1δ spoiler installed, there is a reduction in surface pressure to below free-stream static throughout the cavity, and a significant reduction in the stagnation region. This influence is made stronger when the 3δ spoiler is installed.

Store Loads

Spoiler influence is also illustrated in Fig. 21 using the second type of data, store aerodynamic loads. Store loads were measured using a strain-gage balance inside the sting-mounted store model. The important pitching moment is almost neutral as the store leaves the clean cavity. When the 1δ spoiler is installed, the desirable nose-down pitch is improved, and with the 3δ spoiler, dramatically improved. Unfortunately, the benefit does not remain as Mach number increases, and at low supersonic conditions, the influences of a spoiler are indistinguishable from the clean cavity (Fig. 22).

That the spoiler influence is not so much dependent on the type of doors but rather on the leading edge shape can be seen in Figure 23. The 3δ sawtooth spoiler was mounted on the L/H = 90 cavity with three different doors: square leading-edge single fold, or "cafe", doors open to 90 deg (SC 90); the SBF 90 doors mentioned above; and tapered-leading-edge cafe doors open to 90 deg (TC 90). The spoiler effect is the same for the square leading-edge doors, but significantly less effective for the tapered leading-edge doors until the low supersonic regime, where the shock structures emanating from the doors dominate the store loads. These loads are summarized as a function of Mach Number in Fig. 23b.

While the qualitative effects of spoilers and doors on surface pressures and store loads are quite understandable from the aerodynamist's intuition, what is not available is an easy-to-use method of predicting the magnitude of the effects. CFD techniques can be brought to bear on the problem, but the complex mesh that must be defined, with separate grids for each component, drive computing costs to exorbitant levels.

Acoustic Environment

The third measure of spoiler/door influence is the acoustic environment of the cavity. Advances in transducer technology have reduced the differences between "static" and "unsteady" pressure-measuring techniques to largely a matter of where the transducer is located. In most wind tunnel models, internal volume is severely limited, so transducers are usually located outside the model and connected to the orifice on the model via small tubes. The output voltage of the transducer is sampled tens of thousands of times each second for a period of time considered adequate to determine a valid mean value of the pressure at the orifice. Unsteady, or fluctuating pressures are sensed in much the

same way, except that contemporary transducers are self-contained in a relatively small package that is mounted directly in the surface of the model.

During the AEDC cavity tests, a total of 45 transducers were mounted in the plate/cavity model, most serving as alternates in case of loss of signal from an adjacent transducer. Along the longitudinal centerline of the cavity, the transducers were mounted with a spacing of approximately 0.9-in. center-to-center (Fig. 24). The output of each transducer was recorded 10,000 times each second for 5 secs. Data were reduced via FFT techniques using 1,024-point ensembles, so that the bandwidth of the analysis was 9.77 Hz.

As a sample of the data, the effectiveness of a spoiler in modulating the tonal amplitudes sensed by transducer number 16 at the rear bulkhead of a deep cavity (L/H = 4.5) is illustrated in Fig. 25 for a transonic condition. (Spoiler effectiveness in a shallow cavity, say L/H = 9.0, at the same condition is not as noticeable as for the deep cavity since the tones diminish as L/H is decreased.) The noise-reduction effectiveness of the coarse sawtooth and the fine sawtooth 3δ spoilers is compared in Fig. 25b. The ordinate, $\Delta P_{RMS}/q_\infty$ represents the difference in the overall SPL (coverted to an rms pressure and normalized by free-stream dynamic pressure) at tranducer K16 between a cavity with the coarse sawtooth 3δ spoiler and a cavity with the fine sawtooth 3δ spoiler. Although the noise reduction using the coarse sawtooth is beneficial at subsonic conditions, their is no clear advantage of coarse over tine sawtooth in the supersonic regime, where the presence of shock structures overwhelm turbulence.

The authors' AFATL/AEDC data base contains over a thousand spectra representing many combinations of spoilers, doors, and ramps. Clearly it would be impossible in a survey paper to discuss more than a few cases. The data discussed herein tend to substantiate results reported by others. What is new is the compilation into one data base of experimental data defining the many interactions in the flow field caused by the presence of multiple physical features.

CFD CALCULATIONS

Using a CRAY XMP computer, Suhs at the AEDC has predicted flow fields in empty cavities (Ref. 9). His technique has been to use a time-accurate full Navier-Stokes solver with viscosity effects confined to a thin layer adjacent to the surfaces. A stretched Cartesian grid was also used, increasing the density of grid cells close to the model surfaces, and increasing cell size in regions well away from the walls (Fig. 26). Good agreement with measurements has been obtained (Fig. 27), but solutions for an empty cavity have required 10 to 20 hours of computation to complete. Sketches of the mass flux through the plane of a cavity opening are shown in Fig. 28. The sketches were recorded at 0.4 of a time characteristic (0.00085 sec) intervals (see Ref. 9 for more details). At present, grids for a store model and a sting are being added, with the concomitant increase in calculation time - upwards of 40 hours of CPU time. Current flow models include a modified Baldwin-Lomax turbulence model. Further discussion of CFD results will be left to other authors.

SCHLIEREN EVIDENCE - SUPERSONIC REGIME

During a series of tests at supersonic conditions, some schlieren movies were recorded at a rate of 4,000 frames/sec. Visual evidence of laminar-to-turbulent-to-laminar behavior was observed as the boundary-layer flow moved downstream from over the plate to over the cavity (Fig. 29). Although this behavior was not expected, the effect on cavity pressure distributions and acoustic tonal amplitudes was not detected. In fact, at a constant unit Reynolds number of approximately 3 x 10^6 per foot, the overall (rms) level at transducer 16 tended to peak in the transonic regime and decrease as Mach number increased. Furthermore, tonal amplitudes abate as Mach number increases, so that in the supersonic regime only broadband noise is evident (Fig. 30).

CONCLUDING REMARKS

Cavity aeroacoustics - a challenge of recurring practical interest for the past 60 years - has yielded stubbornly to researchers to date. The engineering method of Rossiter for predicting modal frequencies to be expected in certain simple rectangular cavities exposed to grazing transonic flow provides adequate, if not perfect, guidance to the designer. Beyond the limits of Rossiter's data base in cavity geometry and flow velocity, however, the method falters. Although there is at least a possibility of predicting modal frequencies, there is unfortunately no easily applied method of predicting modal amplitudes. Not only are wind tunnel tests conducted at incorrect Reynolds numbers, but scale effects on acoustic levels have also been observed. CFD solutions are being reported, but the complex grids and turbulence models required represent computation-intensive demands on expensive Class VI computing machines. Efforts underway at the AEDC to organize and correlate existing data could produce at least a first-order amplitude-prediction technique within a year.

In the meantime, a large data base of cavity pressure measurements - both static and unsteady - and store loads has been assembled at the AEDC under the sponsorship of AFATL. From these data, some helpful general trends have been observed, to wit: 1) spoilers mounted at the leading edge of a cavity opening are effective in suppressing aeroacoustic phenomena only in the subsonic-transonic regime, losing effectiveness at supersonic conditions, 2) the effectiveness of a spoiler is independent of square leading-edge door type (single-fold or bifold), but the effectiveness is weakened by the strong flow field around a tapered leading-edge door, especially as velocity increases, and 3) the overall (rms) acoustic amplitude in a cavity is not a function of Reynolds' number.

Fortunately, safe separation of stores jettisoned from a cavity can be assured if sufficient outward velocity and pitch rate are imparted to the store. In other words, the shear layer can be defeated if the residence time of the store passing through it is minimized, so that inertia dominates. Whether the structural and functional integrity of the bodies in the cavity can be assured after the imposition of the necessary forces and acceleration is quite another question, as is the question of survival of exposure to acoustic tones on the order of 170 db. These questions are beyond the scope of this paper.

BIBLIOGRAPHY

1. Krishnamurty, K., "Acoustic Radiation from Two-Dimensional Rectangular Cutouts in Aerodynamic Surfaces," NACA TN 3487, August 1955.

2. Tam, C.K.W. and Block, P. J. W., "On the Tones and Pressure Oscillations Induced by Flow Over Rectangular Cavities," Journal of Fluid Mechanics, Vol. 89, 1978, pp. 373-399.

3. Bilani, A. J. and Covert, E. E., "Estimates of Possible Excitation Frequencies for Shallow Cavities," AIAA Journal, Vol. 11, 1953, pp. 347-351.

4. Covert, Eugene E., "An Approximate Calculation of the Onset Velocity of Cavity Oscillations," AIAA Journal, Vol. 8, No. 12, December 1970, pp. 2189-2194.

5. Stallings, Robert L., Jr. and Wilcox, Floyd J., Jr., "Experimental Cavity Pressure Distributions at Supersonic Speeds," NASA Technical Paper 2683, June 1987.

6. Rossiter, J. E., "Wind Tunnel Experiments on the Flow Over Rectangular Cavities at Subsonic and Transonic Speeds," Ministry of Aviation, Aeronautical Research Council Reports and Memoranda, R&M No. 3438, October 1964.

7. Clark, Rodney L., "Weapons Bay Turbulence Reduction Techniques," AFFDL-TM-75-147-FXM, December 1975.

8. Plentovich, E. B., "Study of Three-Dimensional Cavity Flow at Transonic Speeds," AIAA Paper No. AIAA-88-2032, presented at the AIAA 15th Aerodynamic Testing Conference, San Diego, California, May 18-20, 1988.

9. Suhs, N. E., "Computations of Three-Dimensional Cavity Flow at Subsonic and Supersonic Mach Numbers," AIAA Paper No. AIAA-87-1208, presented at the AIAA 19th Fluid Dynamics, Plasma Dynamics, and Lasers Conference, June 8-10, 1987, Honolulu, Hawaii.

10. Rizzetta, Donald P., "Numerical Simulation of Supersonic Flow Over a Three-Dimensional Cavity," AIAA Paper No. AIAA-87-1288, presented at the AIAA 19th Fluid Dynamics, Plasma Dynamics, and Lasers Conference, June 8-10, 1987, Honolulu, Hawaii.

11. Baysal, O., Srinivasan, S., and Stallings, R. L., Jr., "Unsteady Viscous Calculations of Supersonic Flows Past Deep and Shallow Three-Dimensional Cavities," AIAA Paper No. AIAA-88-0101, presented at the AIAA 26th Aerospace Sciences Meeting, January 11-14, 1988, Reno, Nevada.

12. Stallings, R. L., Jr., "Store Separation from Cavities at Supersonic Flight Speeds," Journal of Spacecraft, Vol. 20, No. 2, March-April 1983, pp. 129-132.

13. Dix, R. E., "On Simulation Techniques for the Separation of Stores from Internal Installations," SAE Technical Paper No. 871799, presented at the SAE Aerospace Technology Conference and Exposition, Long Beach, California, October 5-8, 1987.

14. Carman, J. B., Jr., Hill, D. W., Jr., and Christopher, J. P., "Store Separation Testing Techniques of the Arnold Engineering Development Center, Volume II, Description of Captive Trajectory Store Separation Testing in the Aerodynamic Wind Tunnel (4T)," AEDC-TR-79-1 (AD-A087561), June 1980.

15. Keen, K. Scott, "New Approaches to Computational Aircraft/Store Weapons Integration," AIAA Paper No. AIAA-90-0274, presented at the 28th Aerospace Sciences Meeting, January 8-11, 1990, Reno, Nevada.

16. Heller, H. H. and Bliss, D. B., "Aerodynamically-Induced Pressure Oscillations in Cavities - Physical Mechanisms and Suppression Techniques," AFFDL-TR-74-133 (AD-B002701), February 1975.

17. Shaw, L. L., "Scale Effect on the Flow-Induced Acoustic Environment in Cavities - Wind Tunnel Test Results," WRDC-TM-89-159-FIBG, February 1989.

18. Clark, Rodney L, "Evaluation of F-111 Weapon Bay Aero-acoustic and Weapon Separation Improvement Techniques," AFFDL-TR-79-3003, February 1979.

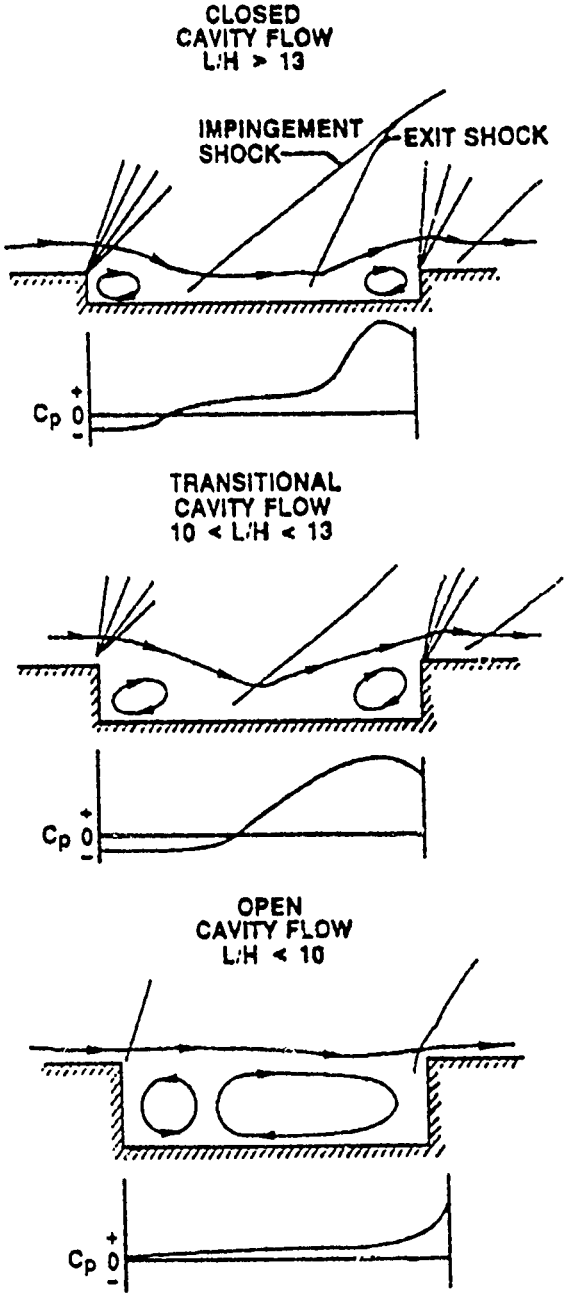

Fig. 1. Cavity flow field models (Ref. 5.)

Fig. 2. Gradients in store loads through a shear layer (Ref. 12).

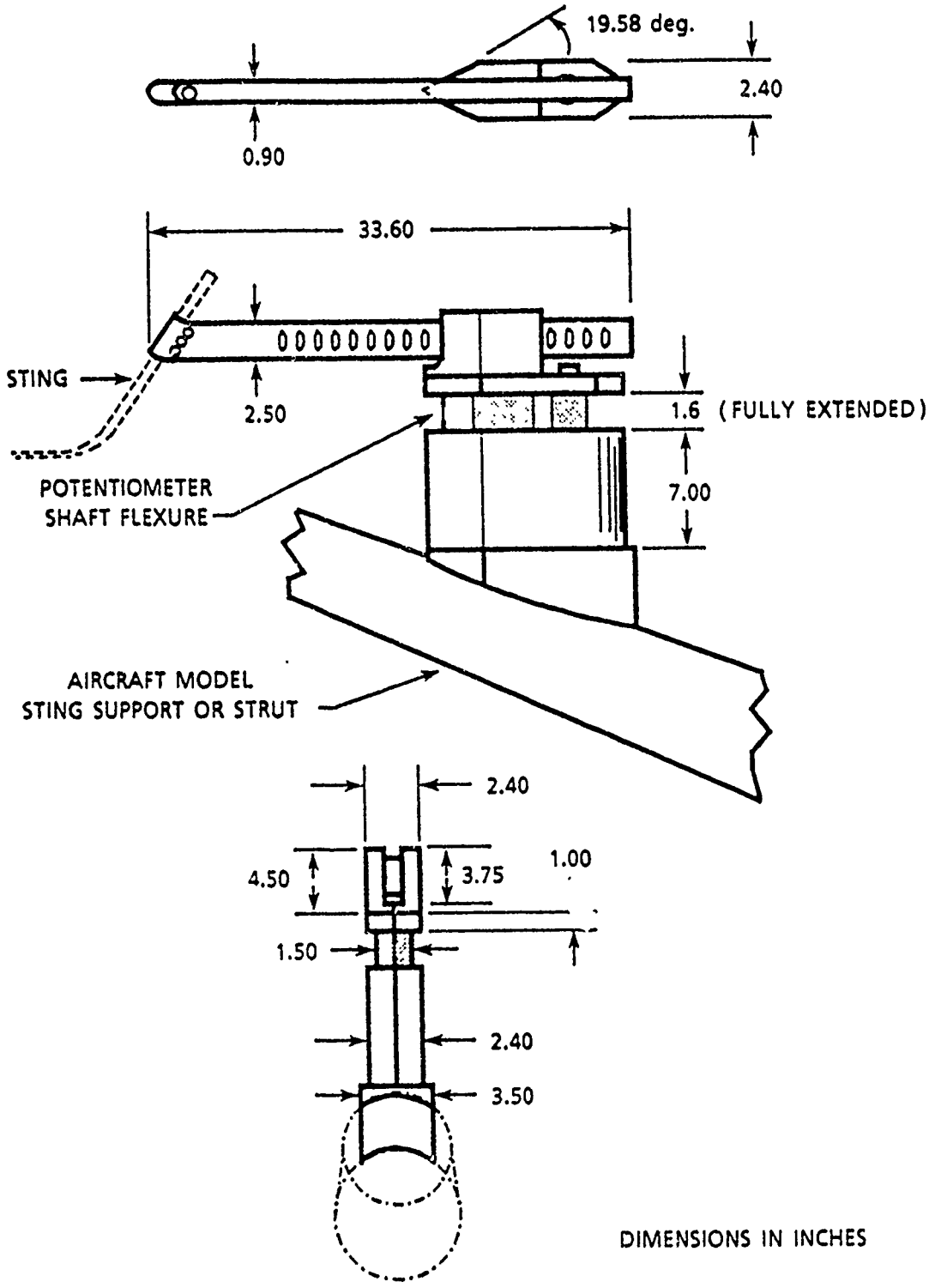

Fig. 3. Sketch of the single-axis translating sting support (Z-Rig).

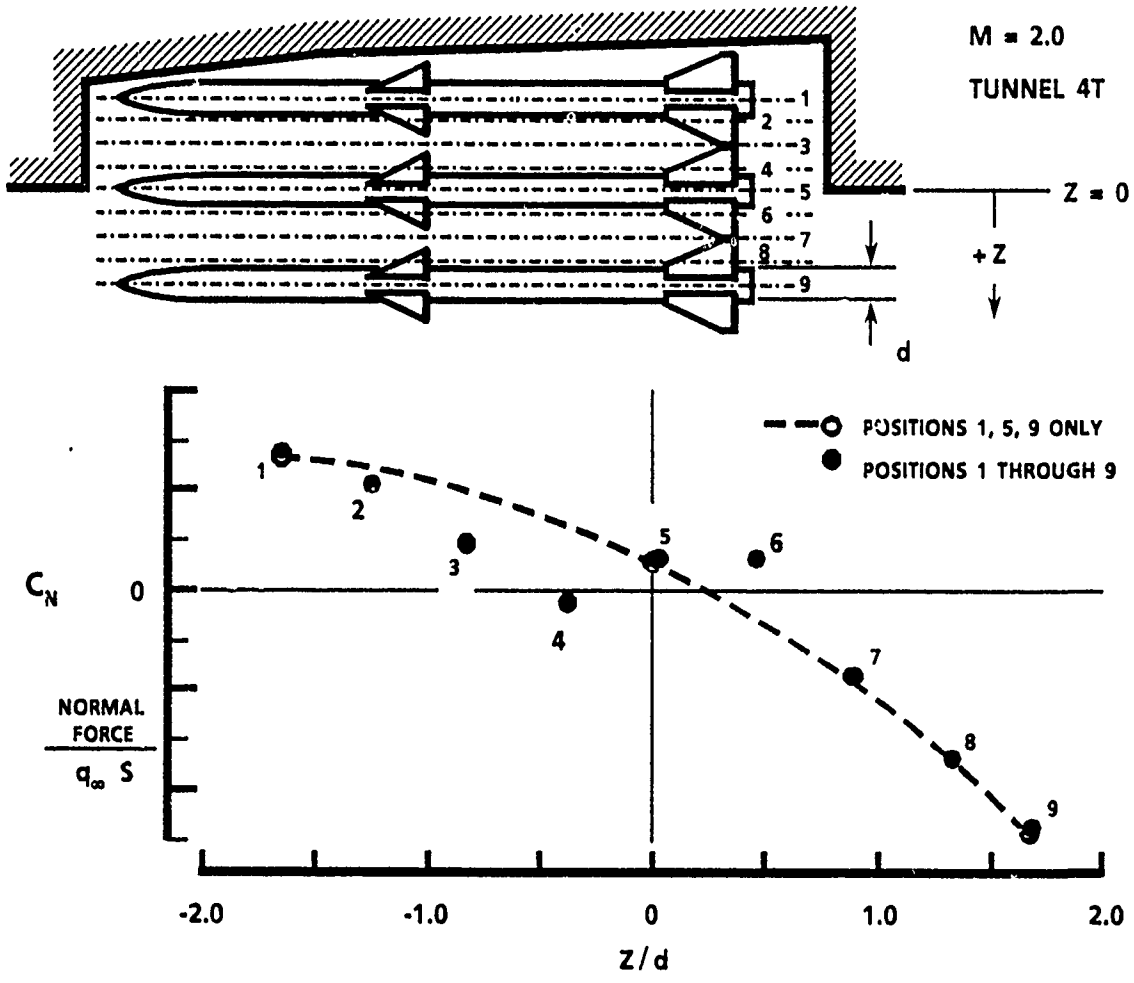

Fig. 4. Incomplete loads from limited data in a shear layer.

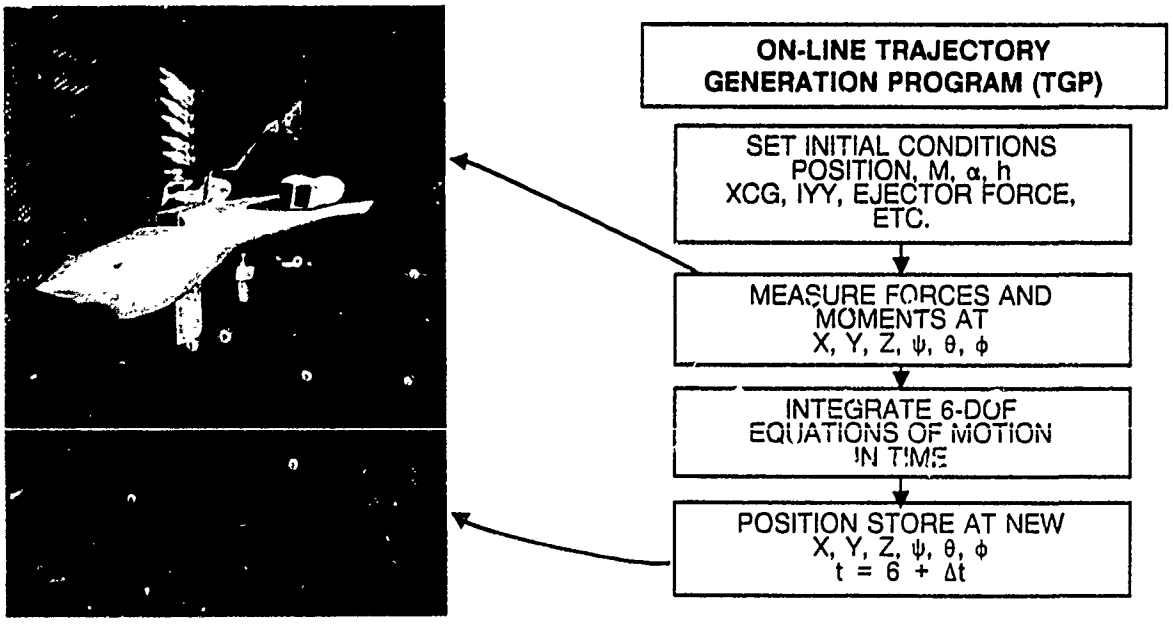

Fig. 5. The two-sting Captive Trajectory System (CTS) system at the AEDC.

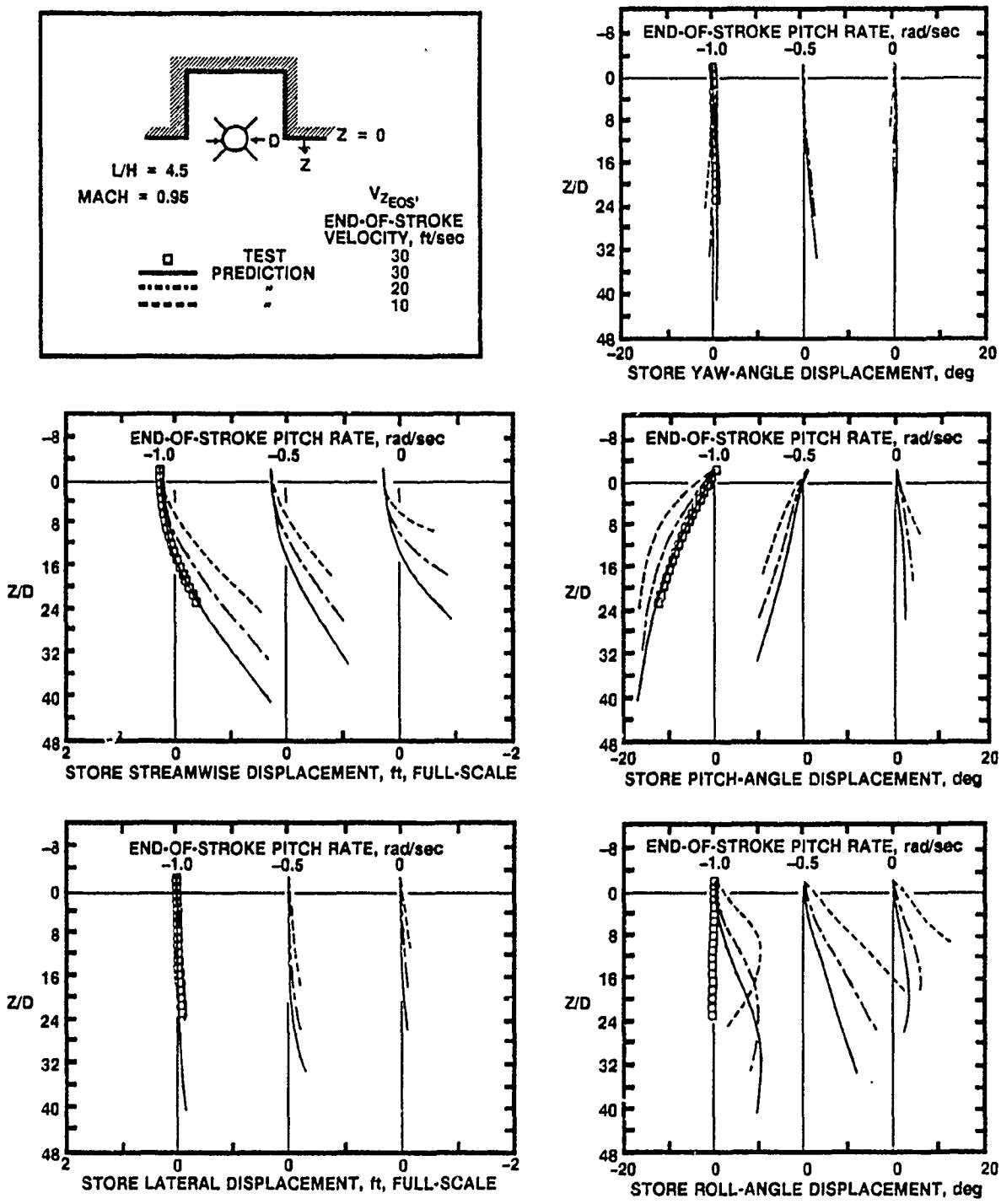

Fig. 6. Examples of calculated separation trajectories for a store ejected from a generic cavity.

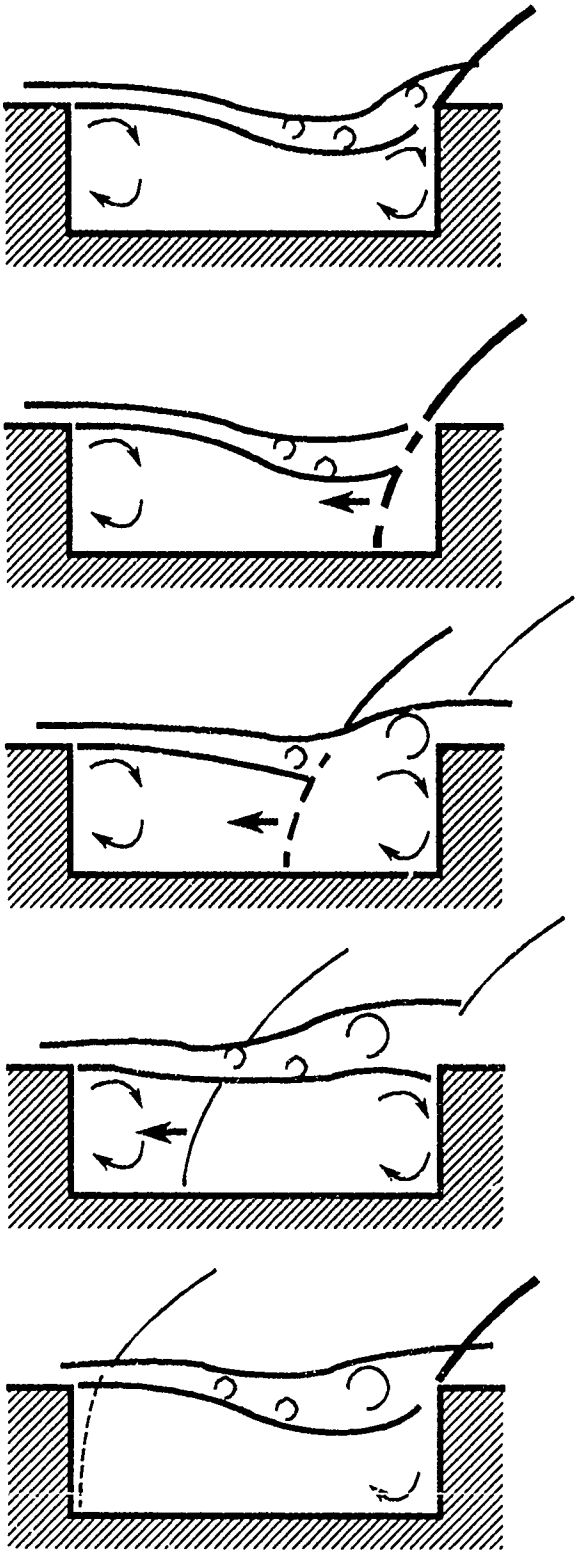

Fig. 7. Qualitative sketch of the flow-development over a cavity (from water-table experiments).

DIMENSIONS IN INCHES

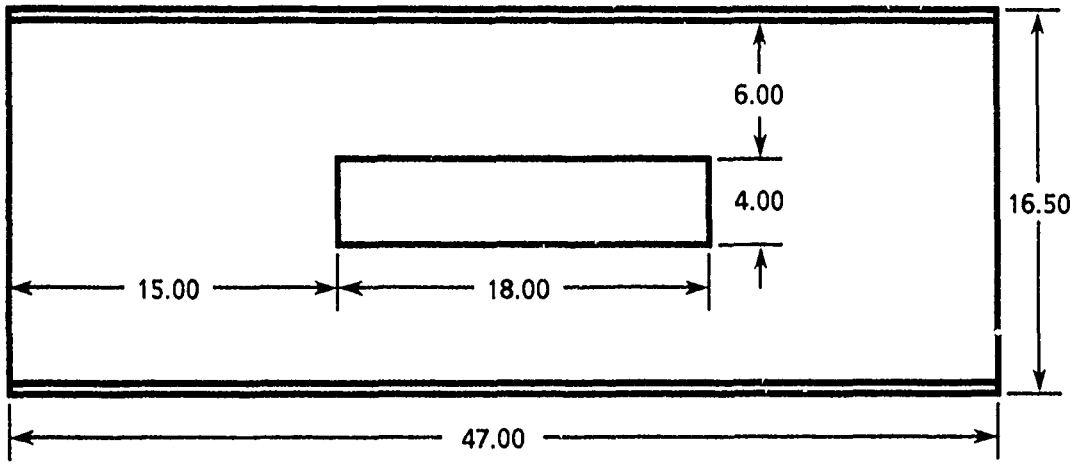

TOP VIEW (AS MOUNTED IN WIND TUNNEL) OF PLATE/CAVITY MODEL

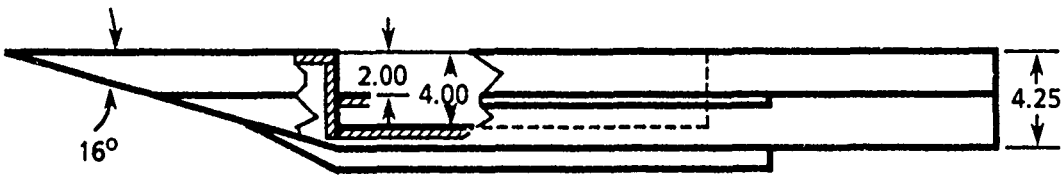

SIDE VIEW OF PLATE/CAVITY MODEL

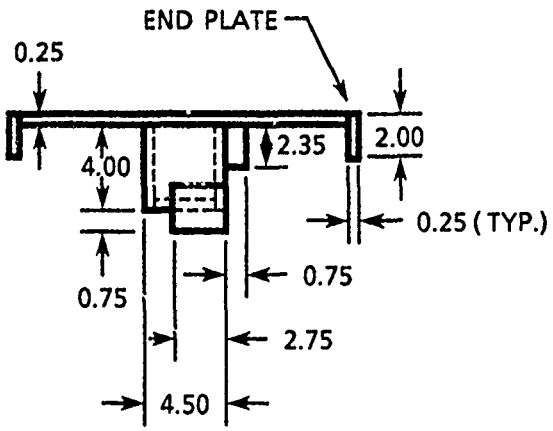

FRONT VIEW OF PLATE/CAVITY MODEL
LOOKING DOWNSTREAM

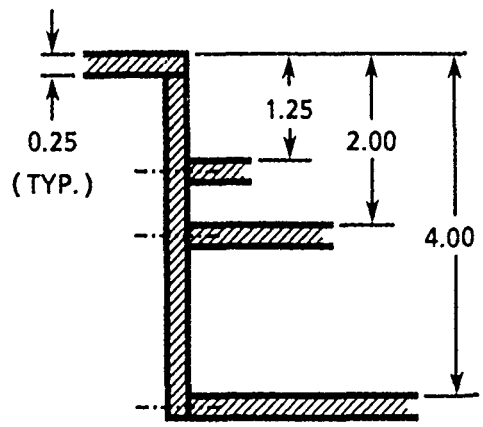

SECTION THROUGH CAVITY
SHOWING ADJUSTABLE CEILING

Fig. 8. Generic flat-plate/cavity model, mounted inverted in the wind tunnel.

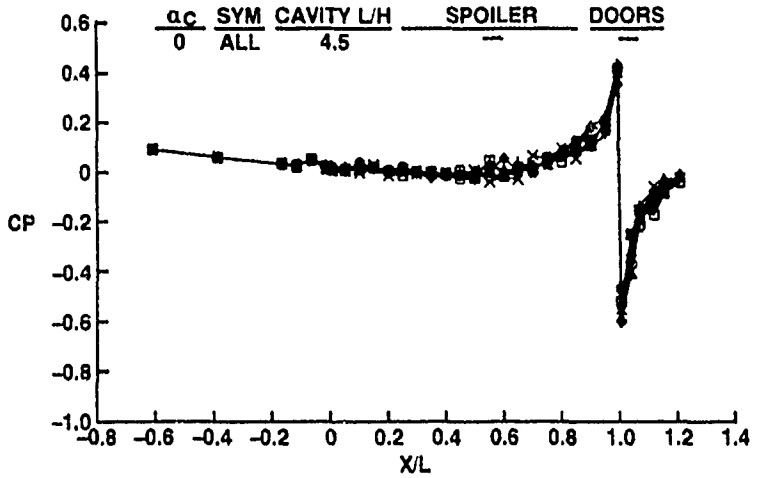

Fig. 9. Variation in centerline surface pressures acting on a generic flat-plate cavity.

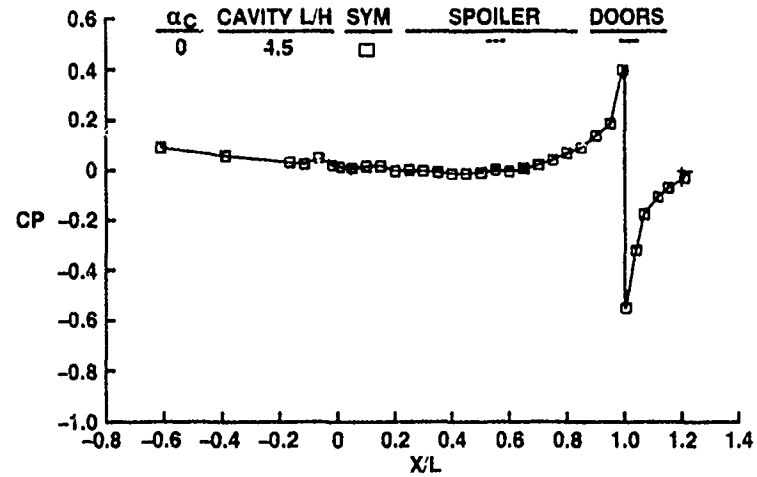

a. Mean pressure profile

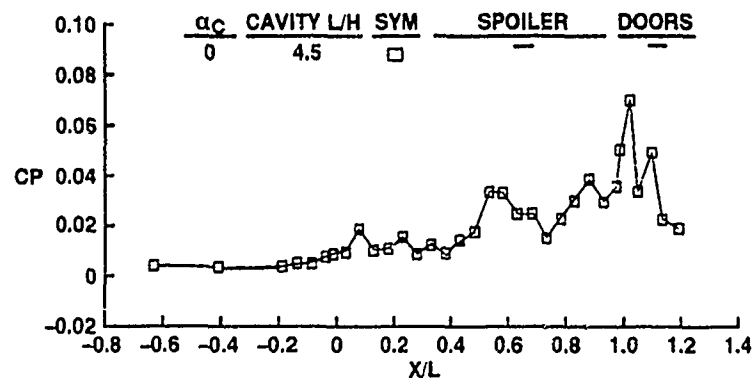

b. Profile of one standard deviation

Fig. 10. Statistical profiles for twelve repeated measurements of plate/cavity surface pressure.

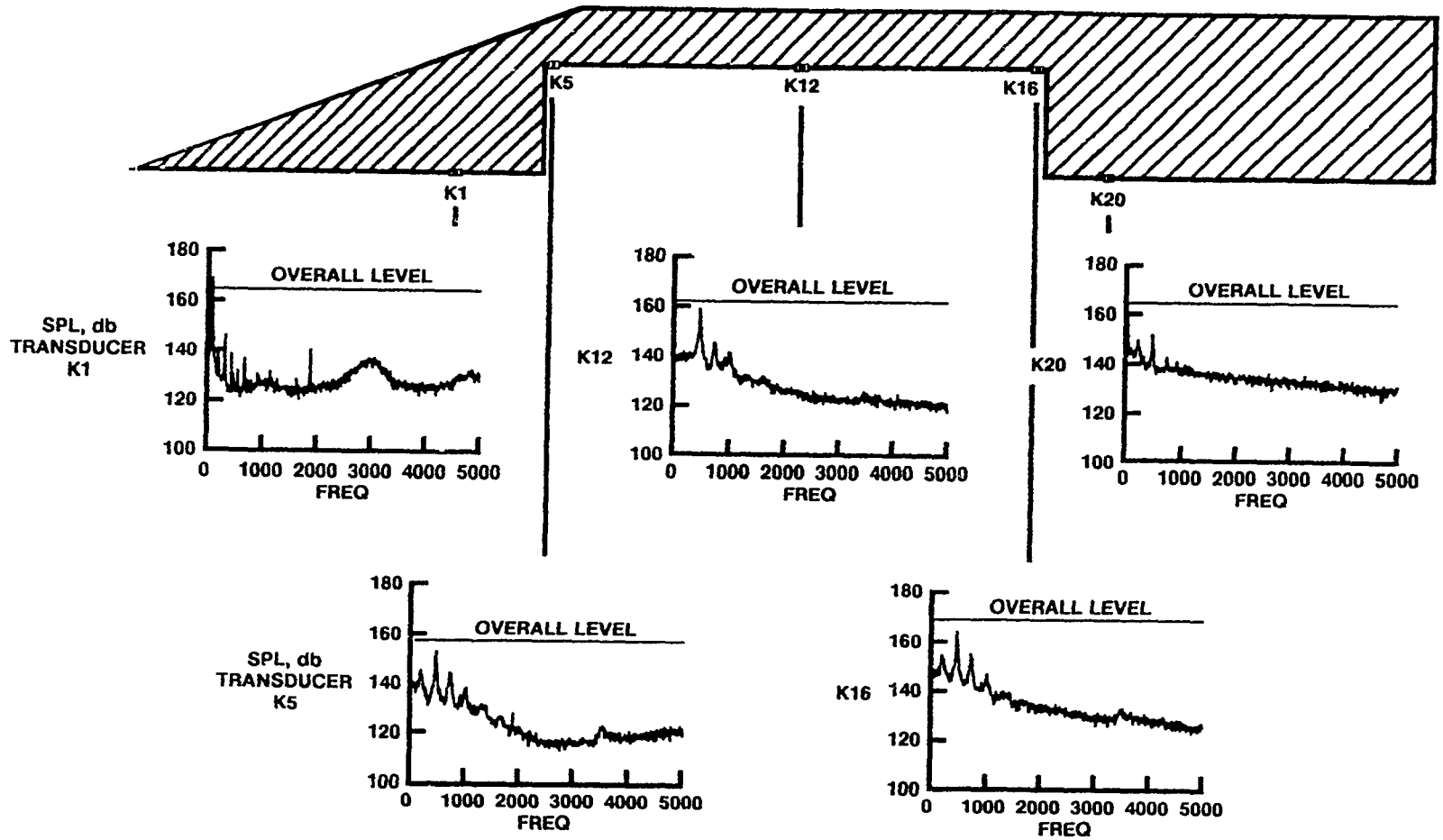

Fig. 11. Characteristic centerline acoustic spectra.

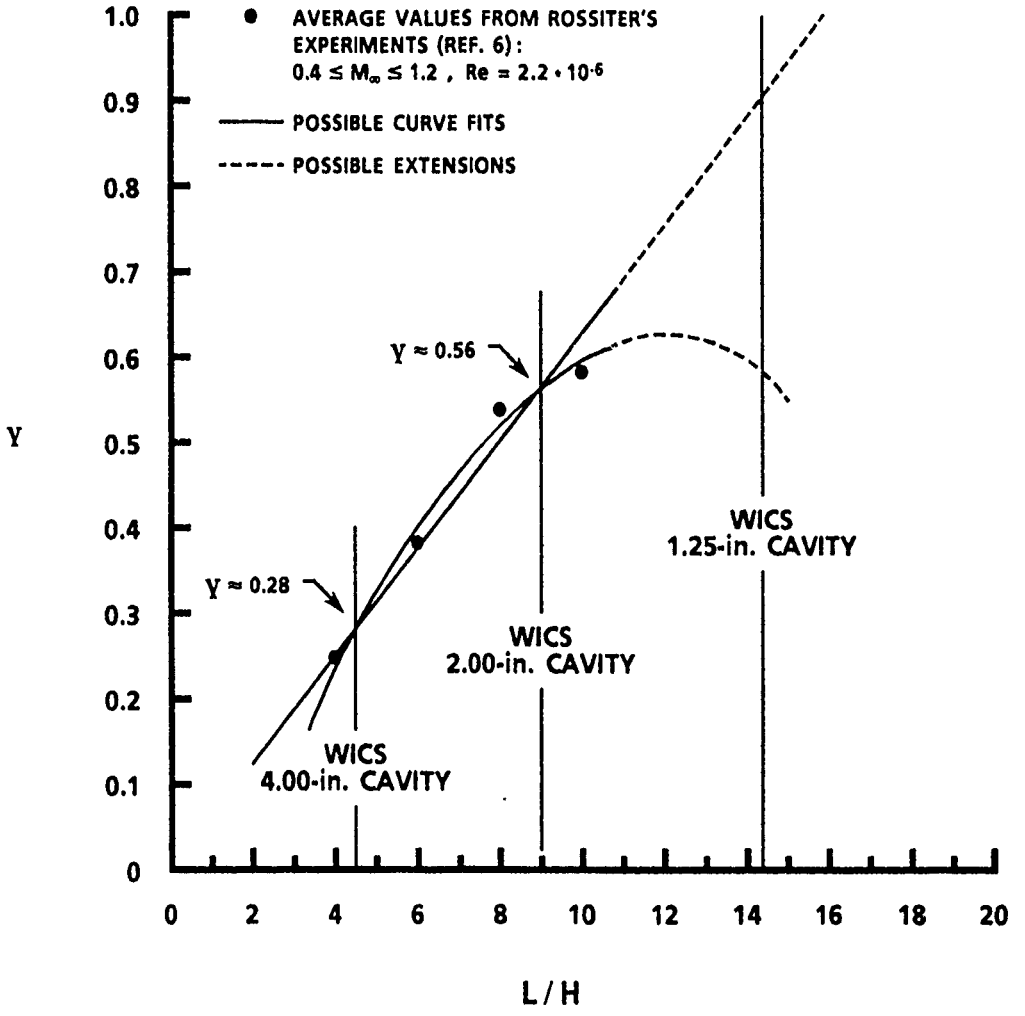

Fig. 12. Rossiter's γ term (Ref. 6).

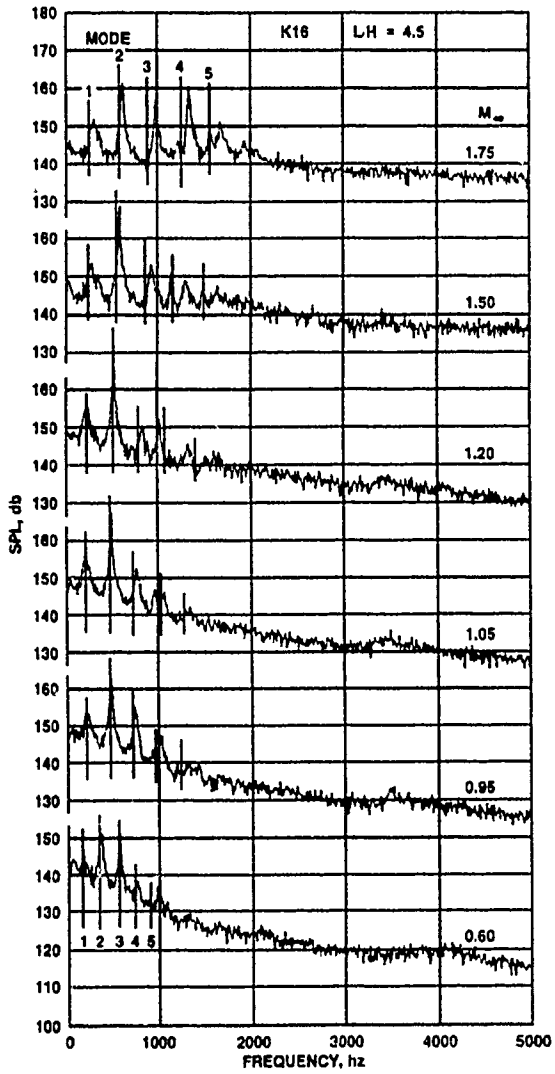

a. Cavity L/H = 4.5, transducer K16

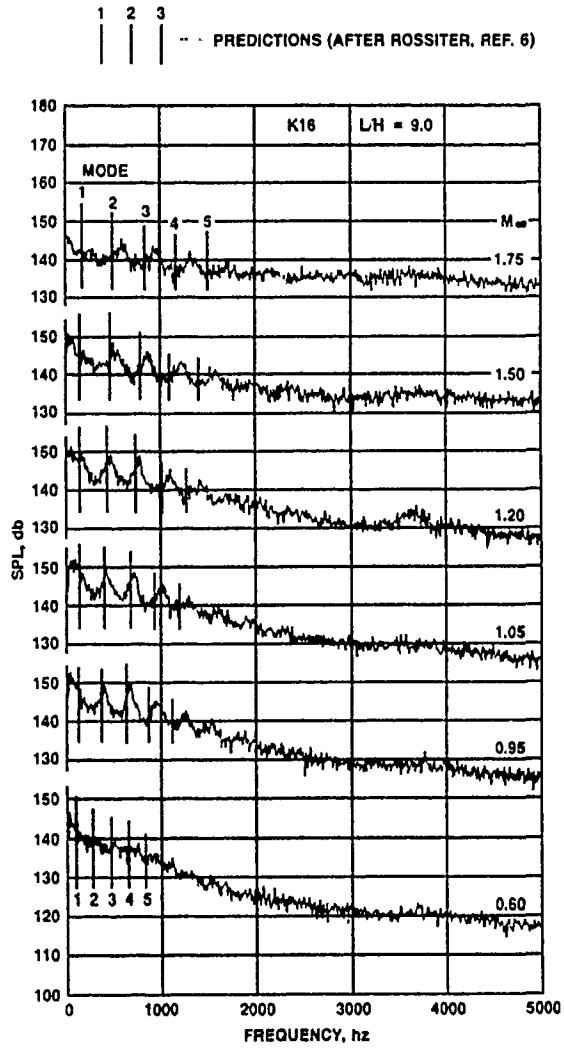

b. Cavity L/H = 9.0, transducer K16

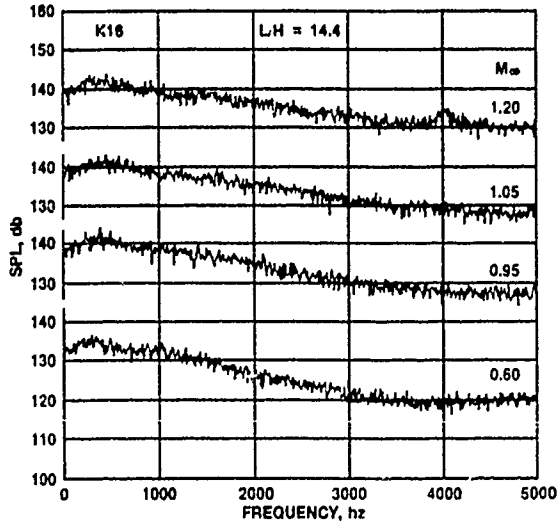

c. Cavity L/H = 14.4, transducer K16

Fig. 13. Comparison of measured and predicted modal frequencies.

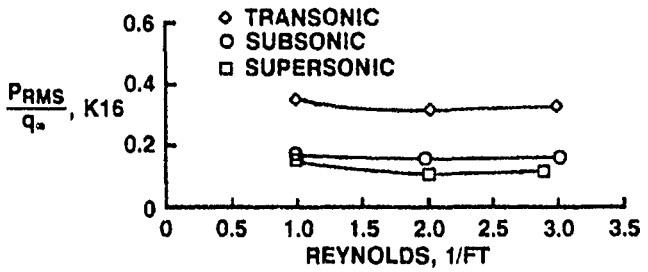

Fig. 14. Reynolds number effect on overall sound pressure level.

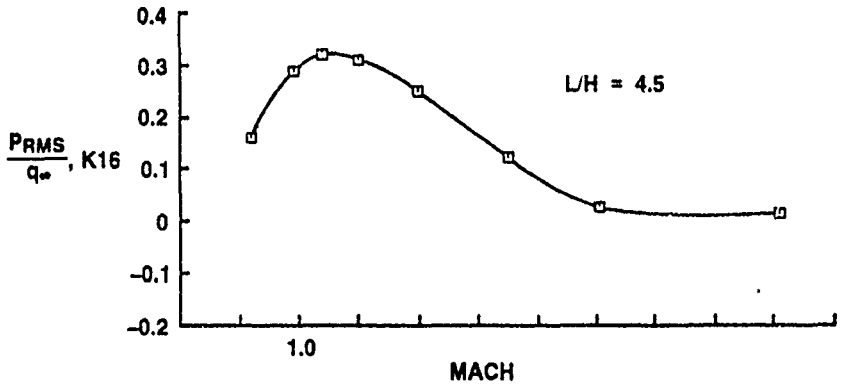

Fig. 15. Mach number effect on overall sound pressure level.

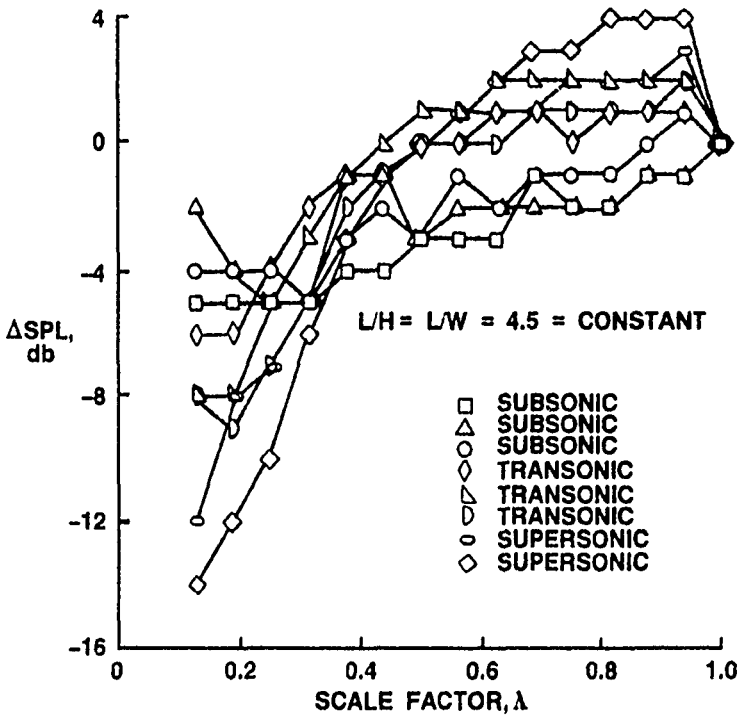

Fig. 16. Scale effect on overall sound pressure level.

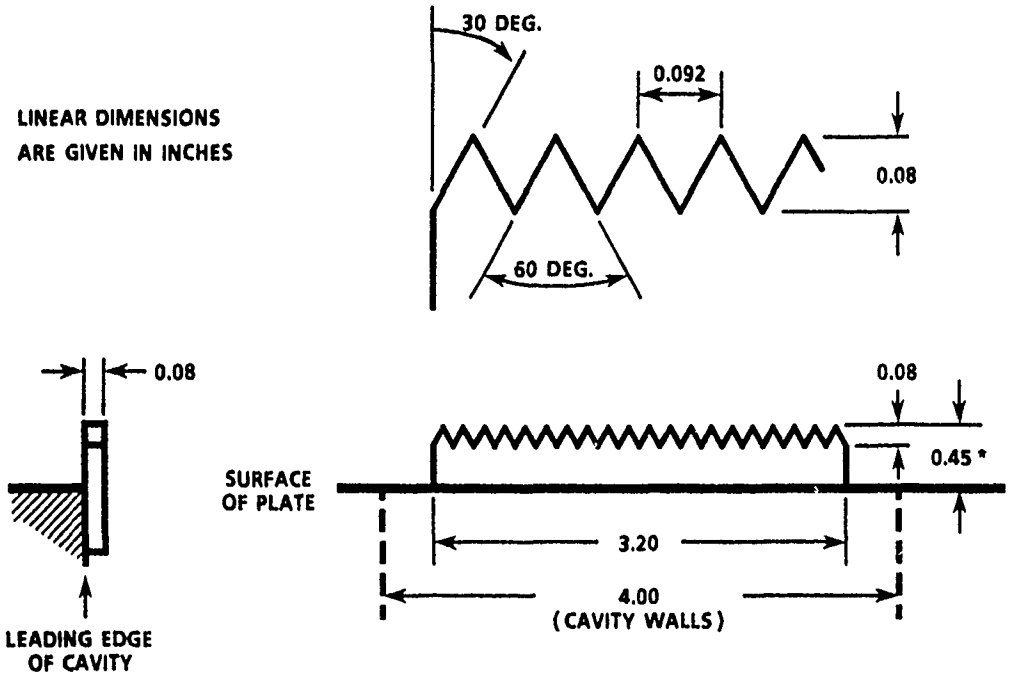

0.45-IN.* SAWTOOTH SPOILER, FINE PITCH

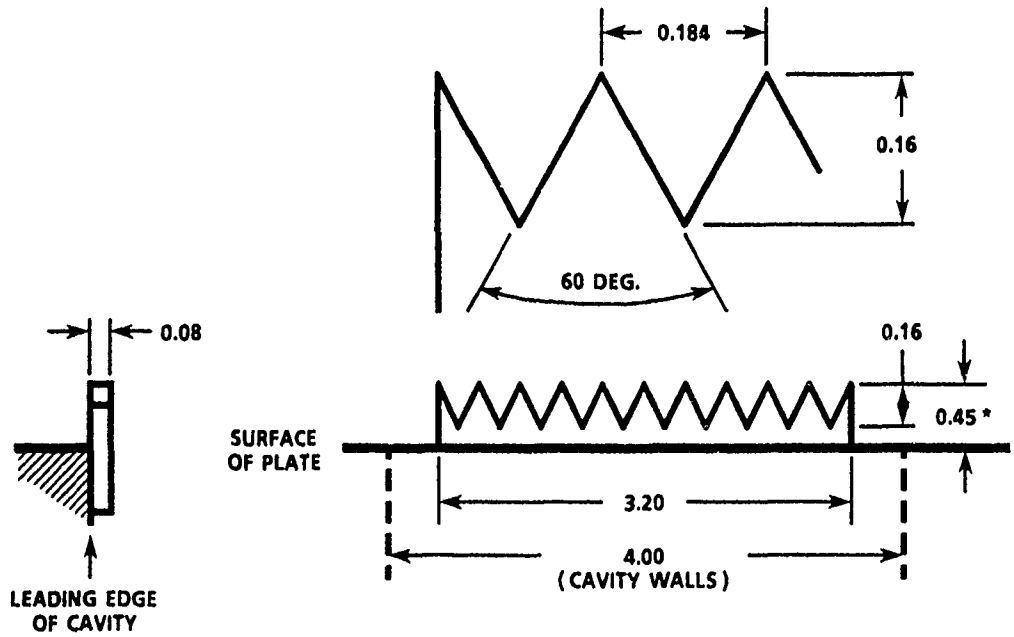

0.45-IN.* SAWTOOTH SPOILER, COURSE PITCH

* 0.45-in. Spoiler shown; 0.15-in. and 0.30-in. differ in total height, not in sawtooth design

a. Sawtooth spoilers

Fig. 17. Spoiler and ramp model sketches.

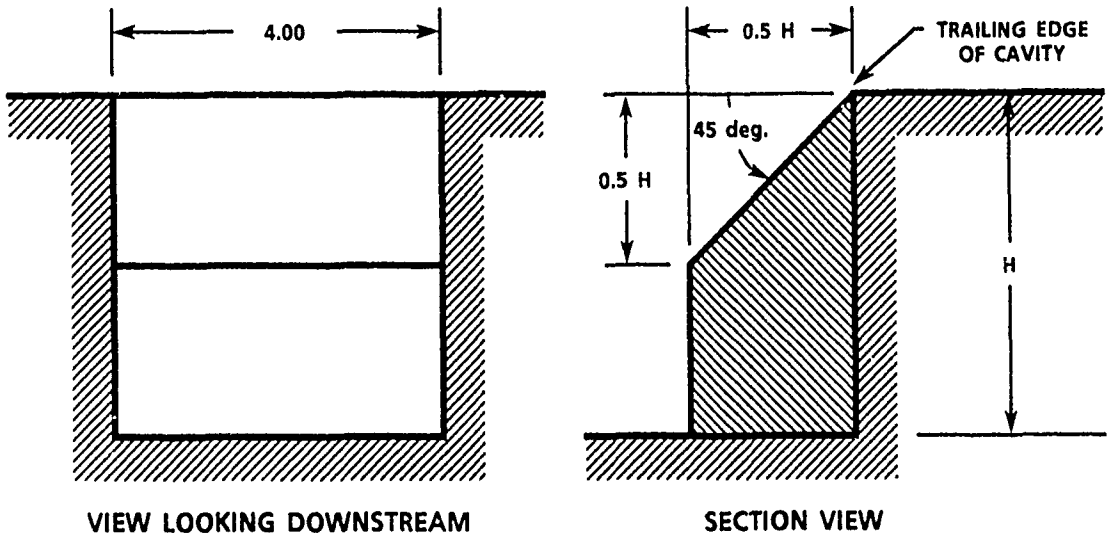

45-DEGREE SOLID RAMP

LINEAR DIMENSIONS ARE GIVEN IN INCHES

NOTE: H = 4.00, 2.00, OR 1.25 in.

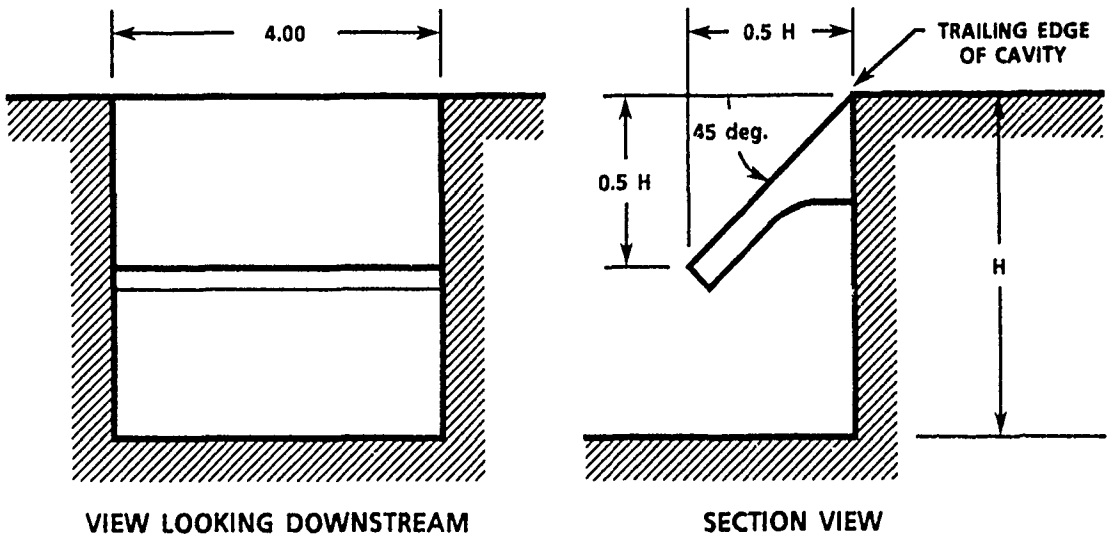

45-DEGREE SIMULATED HINGED RAMP

b. Ramp models
Fig. 17. Concluded.

LINEAR DIMENSIONS ARE GIVEN IN INCHES

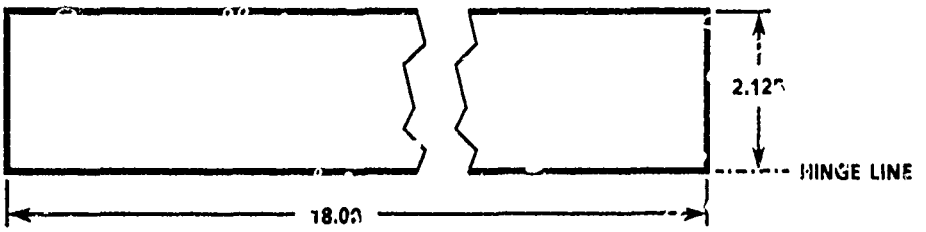

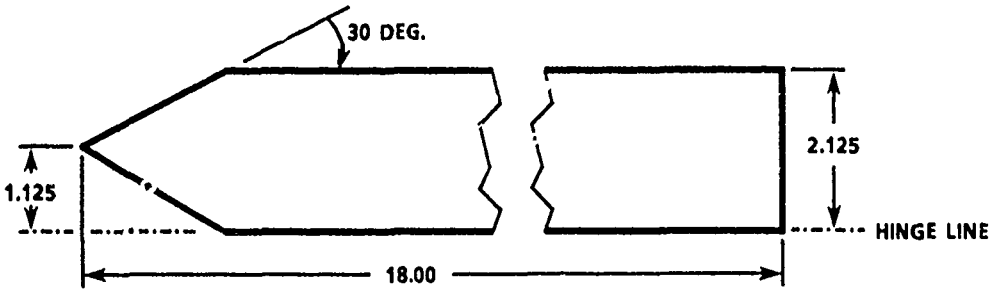

TAPERED LEADING EDGE (TC)

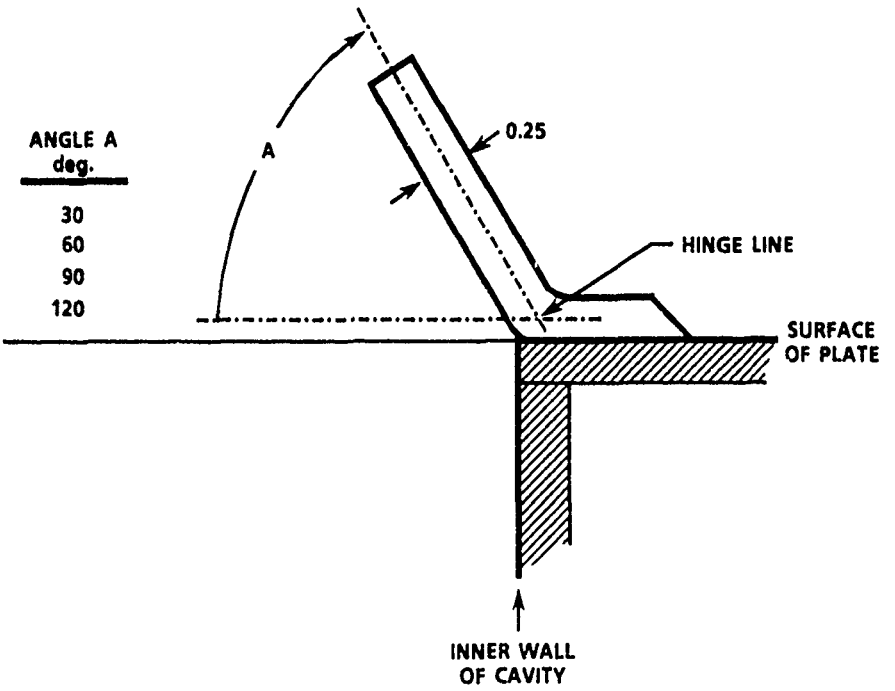

a. Cafe doors

Fig. 18. Cavity door model sketches.

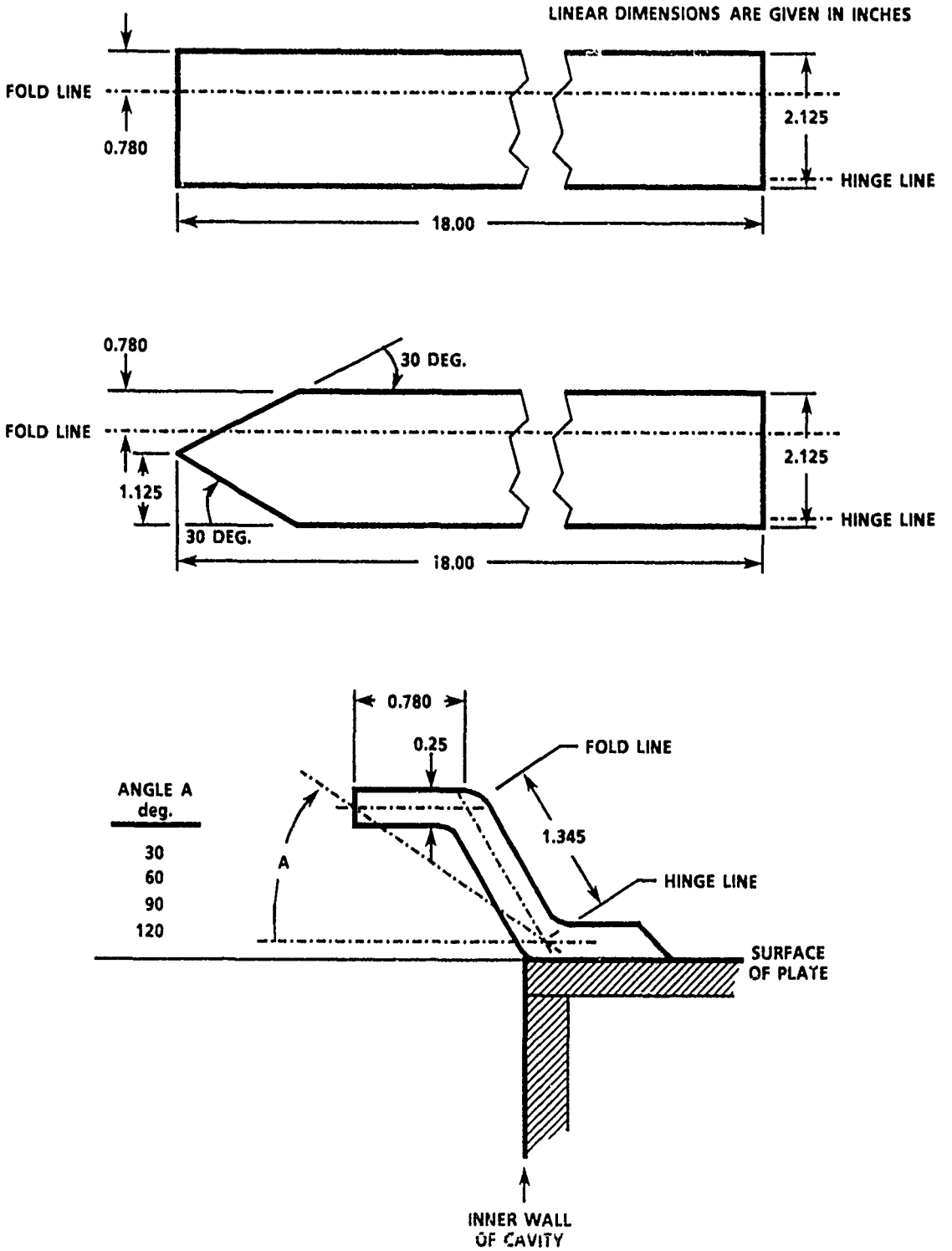

b. Bi-fold doors
Fig. 18. Concluded.

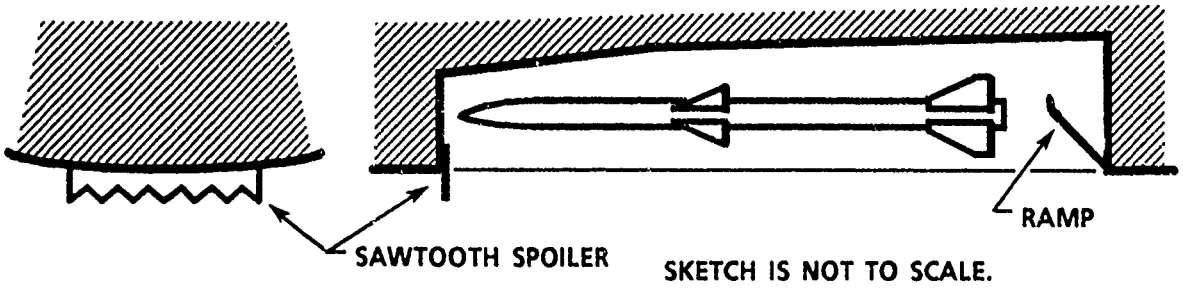

Fig. 19. Sketch of combined sawtooth spoiler and rear bulkhead ramp (Ref. 18).

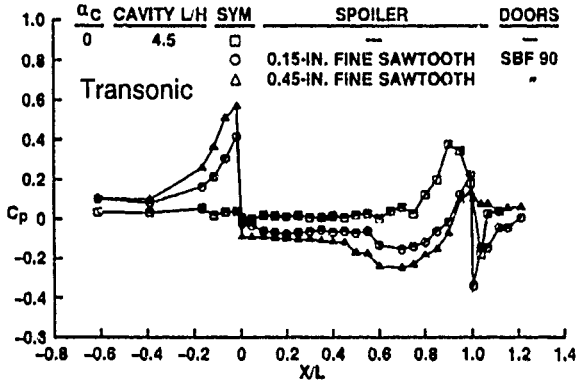

Fig. 20. Centerline surface pressure profile with a store model suspended 4.5 diameters outside the cavity opening.

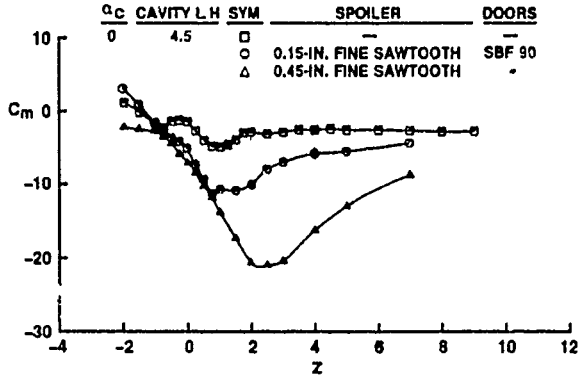

Fig. 21. Pitching moment acting on a store model along a constant-attitude Z-axis translation, transonic condition.

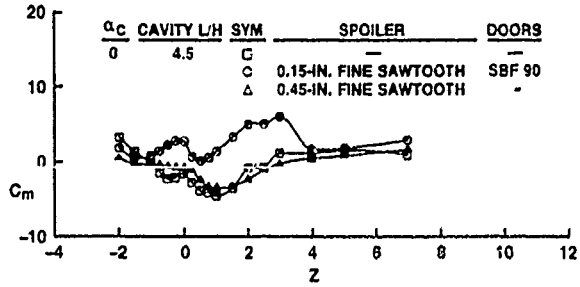

Fig. 22. Pitching moment acting on a store model along a constant-attitude Z-axis translation, supersonic condition.

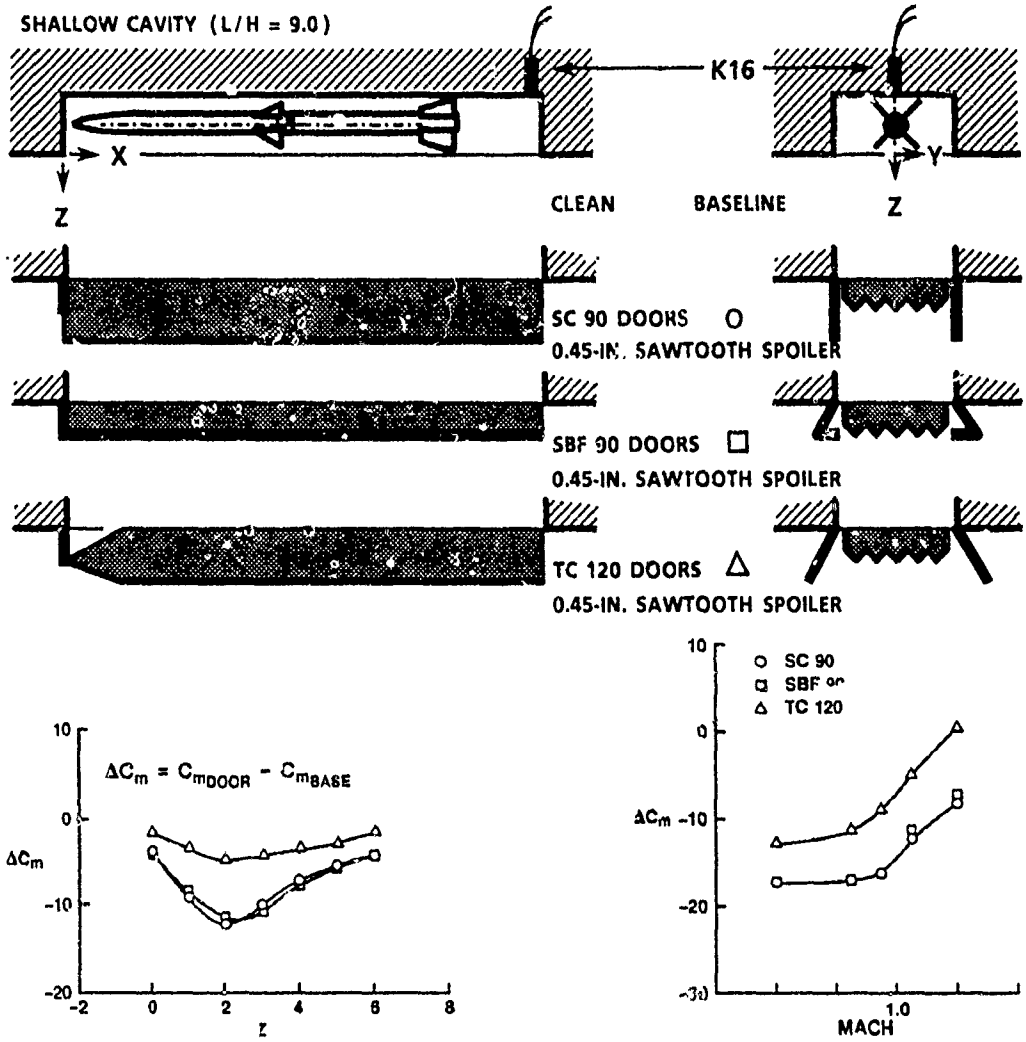

a. Transonic condition

b. Variation with Mach number at Z = 2 ft (full scale)

Fig. 23. Difference in pitching moment acting on a store model along a Z-axis translation out of a cavity with a 3δ sawtooth spoiler and various styles of doors.

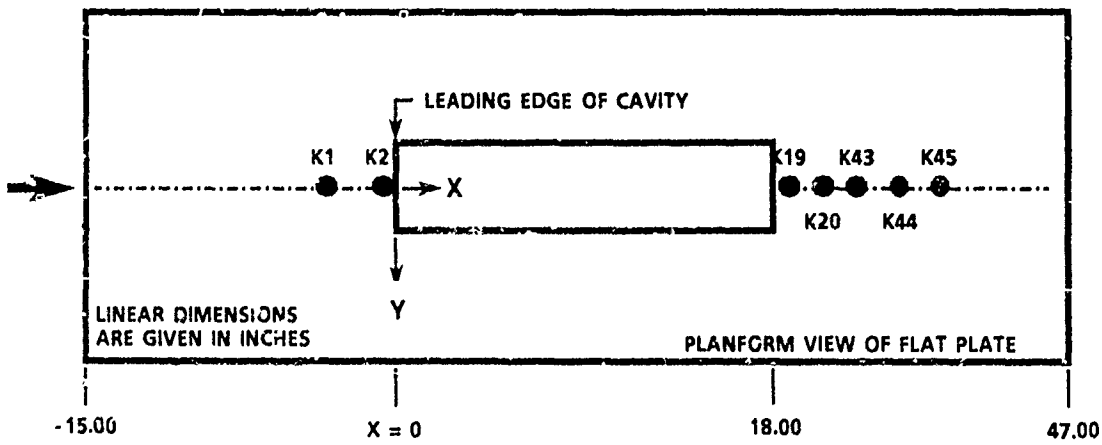

a. Locati n of pressure transducers on the flate plate

Fig. 24. Pressure transducer locations.

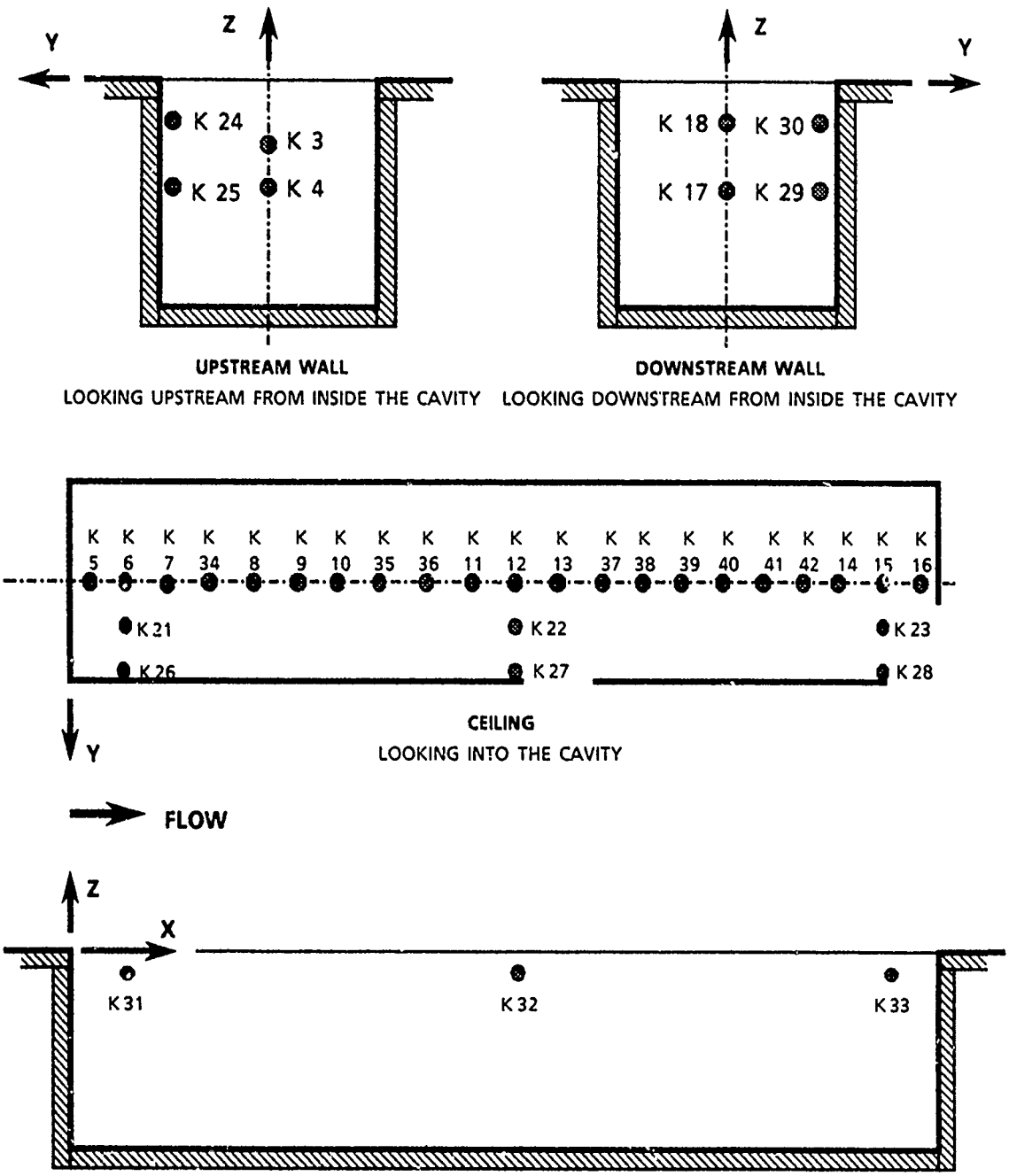

b. Location of pressure transducers in the cavity
Fig. 24. Continued.

TRANSDUCER NUMBER	X MODEL INCHES	X/L	Y MODEL INCHES	Y/W/2	Z MODEL INCHES	TRANSDUCER NUMBER	X MODEL INCHES	X/L	Y MODEL INCHES	Y/W/2	Z MODEL INCHES
K 1	−3.175	−0.176	0	0	0	K26	1.075	0.060	1.8	0.90	−H
K 2	−0.475	−0.026	0	0	0	K27	9.175	0.510	1.8	0.90	−H
K 3	0	0	0	0	−1.125	K28	16.925	0.940	1.8	0.90	−H
K 4	0	0	0	0	−1.975	K29	18.000	1.000	1.9	0.95	−1.975
K 5	0.275	0.015	0	0	−H	K30	18.000	1.000	1.9	0.95	−0.725
K 6	1.075	0.060	0	0	−H	K31	1.075	0.060	2.0	1.00	−0.35
K 7	1.975	0.110	0	0	−H	K32	9.175	0.510	2.0	1.00	−0.35
K 8	3.775	0.210	0	0	−H	K33	16.925	0.940	2.0	1.00	−0.35
K 9	4.675	0.260	0	0	−H	K34	2.875	0.160	0	0	−H
K10	5.575	0.310	0	0	−H	K35	6.475	0.360	0	0	−H
K11	8.275	0.460	0	0	−H	K36	7.375	0.410	0	0	−H
K12	9.175	0.510	0	0	−H	K37	10.975	0.610	0	0	−H
K13	10.075	0.560	0	0	−H	K38	11.875	0.660	0	0	−H
K14	16.025	0.893	0	0	−H	K39	12.775	0.710	0	0	−H
K15	16.925	0.940	0	0	−H	K40	13.675	0.760	0	0	−H
K16	17.725	0.985	0	0	−H	K41	14.575	0.810	0	0	−H
K17	18.000	1.000	0	0	−1.975	K42	15.475	0.860	0	0	−H
K18	18.000	1.000	0	0	−0.725	K43	21.950	1.219	0	0	0
K19	18.875	1.049	0	0	0	K44	23.950	1.331	0	0	0
K20	20.275	1.126	0	0	0	K45	25.950	1.442	0	0	0
K21	1.075	0.060	0.9	0.45	−H						
K22	9.175	0.510	0.9	0.45	−H	K46	TUNNEL WALL				
K23	16.925	0.940	0.9	0.45	−H						
K24	0	0	1.9	0.95	−0.725	K101	GMPM STORE MODEL (See Fig. 11)				
K25	0	0	1.9	0.95	−1.975	106					

c. Pressure transducer locations

Fig. 24. Concluded.

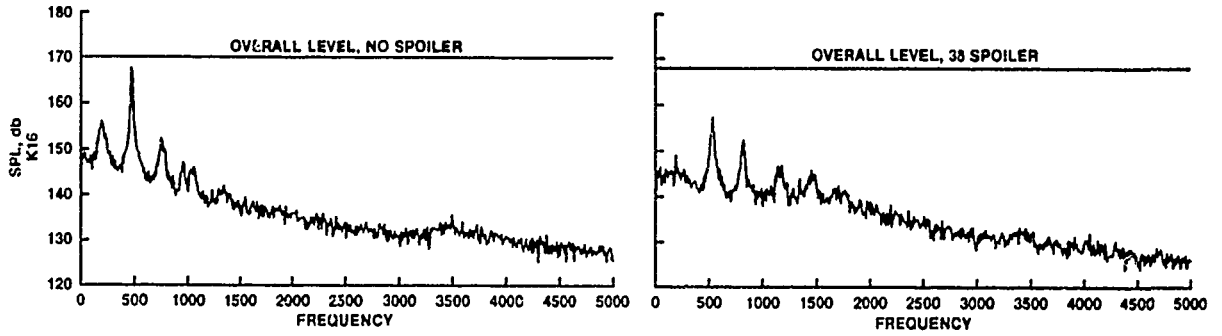

a. Fine sawtooth spoiler

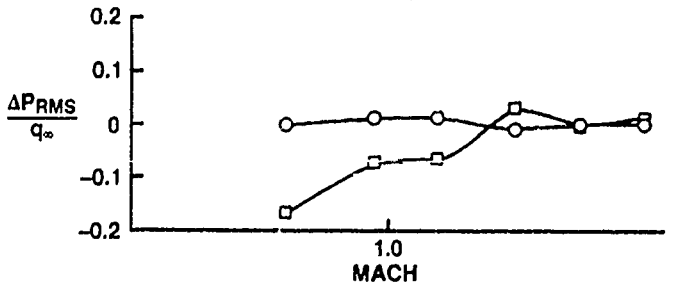

b. Comparison of the fine and coarse sawtooth spoilers

Fig. 25. Effectiveness of 3δ sawtooth spoilers, deep cavity (L/H = 4.5), transonic condition.

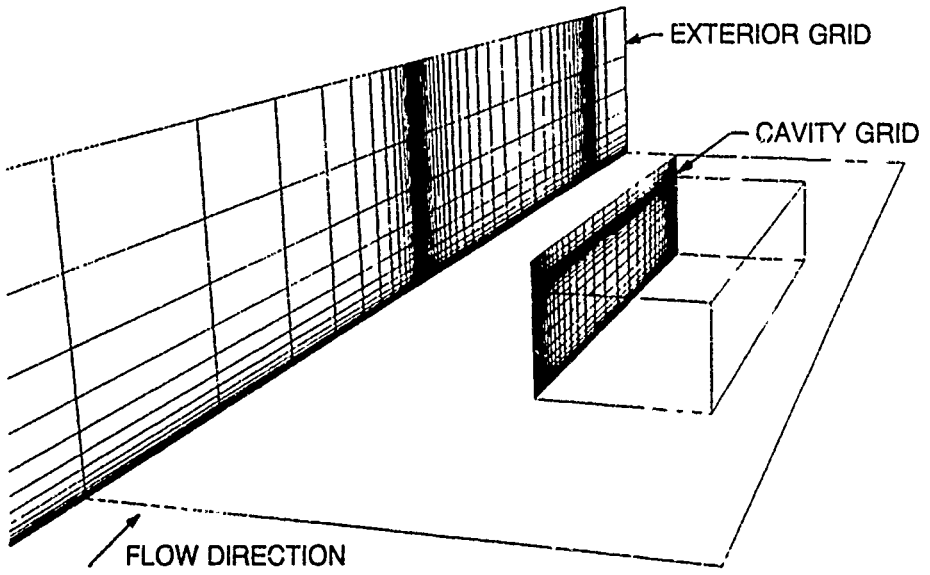

Fig. 26. Computational grids for a generic cavity (Ref. 9).

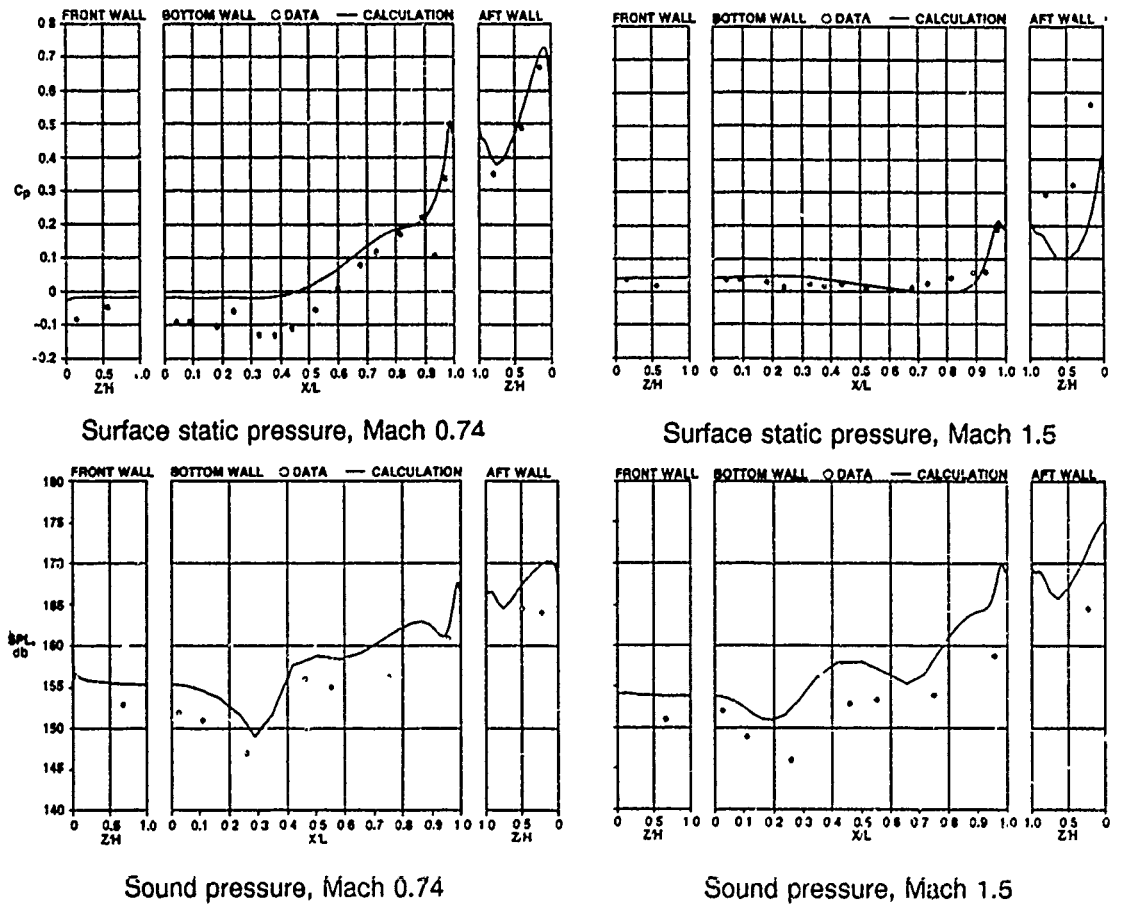

Surface static pressure, Mach 0.74

Surface static pressure, Mach 1.5

Sound pressure, Mach 0.74

Sound pressure, Mach 1.5

Fig. 27. Comparison of calculated and measured static pressure and sound pressure levels for a deep cavity (L/H = 5.6) (Ref. 9).

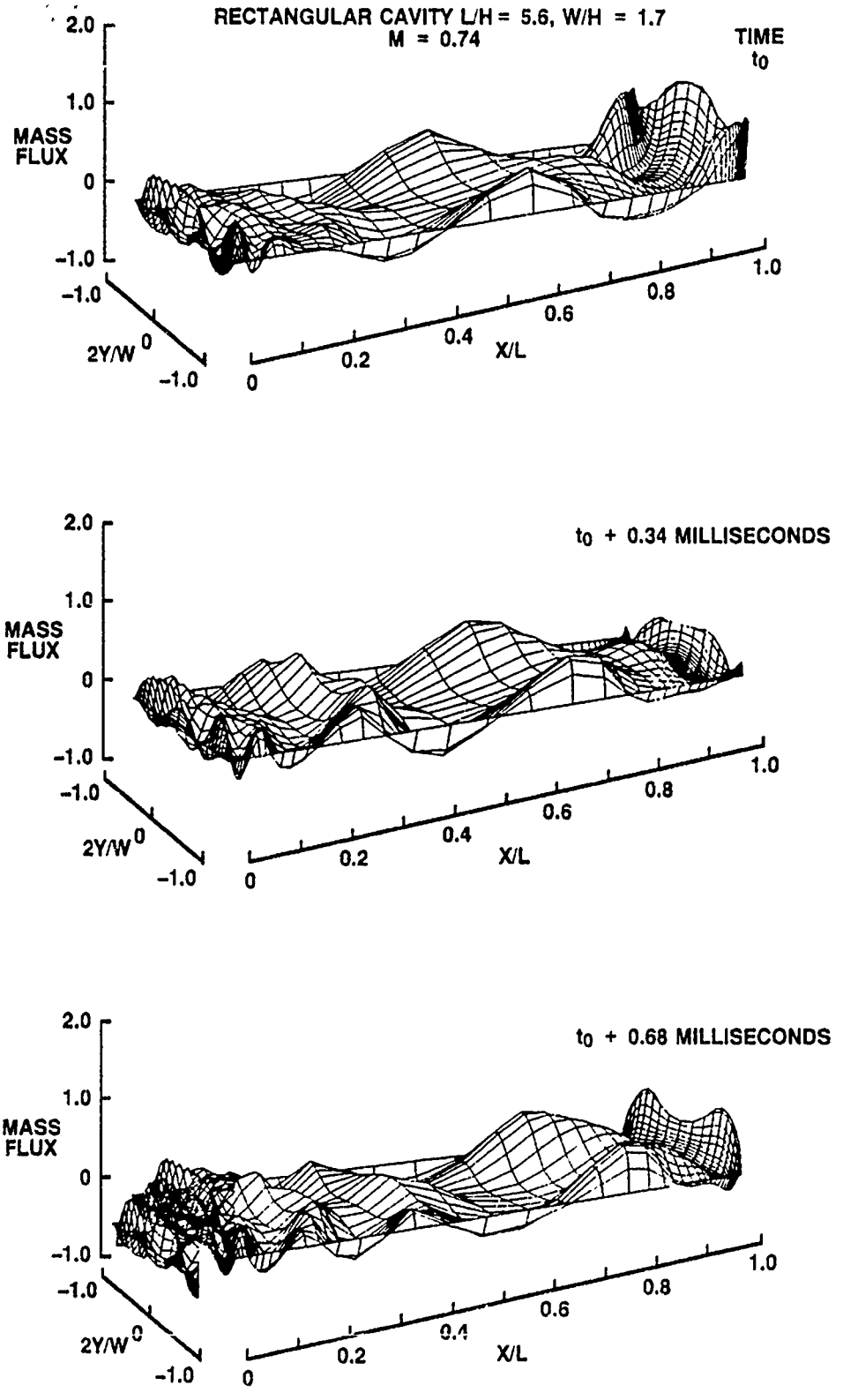

Fig. 28. Predictions of mass flux in the plane of a rectangular cavity opening (L/H = 5.6) at M = 0.74 (Ref.9).

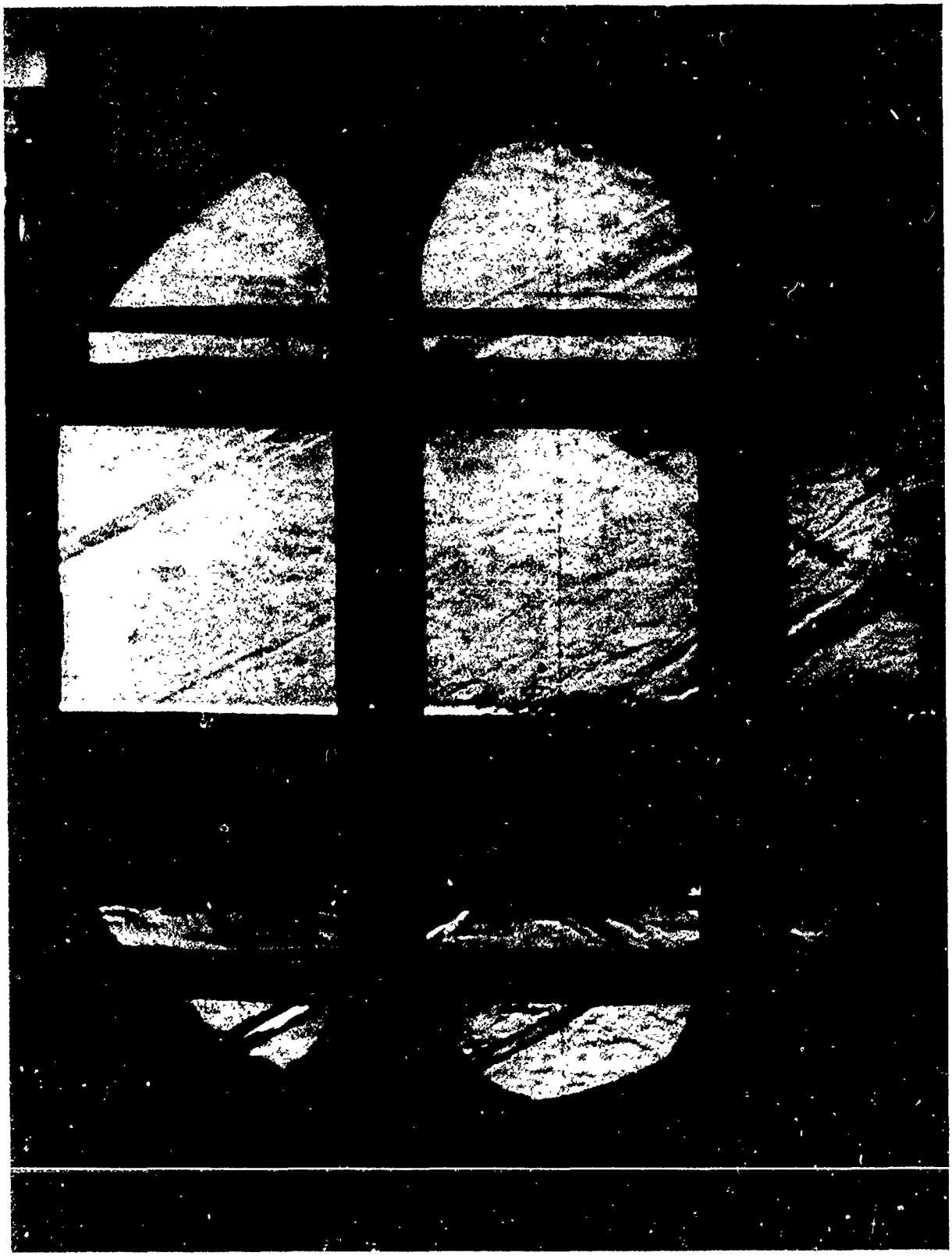

a. Clean cavity

Fig. 29. Schlieren photographs of flow over a transitional cavity (L/H = 9.0) equipped with various spoiler and door configurations.

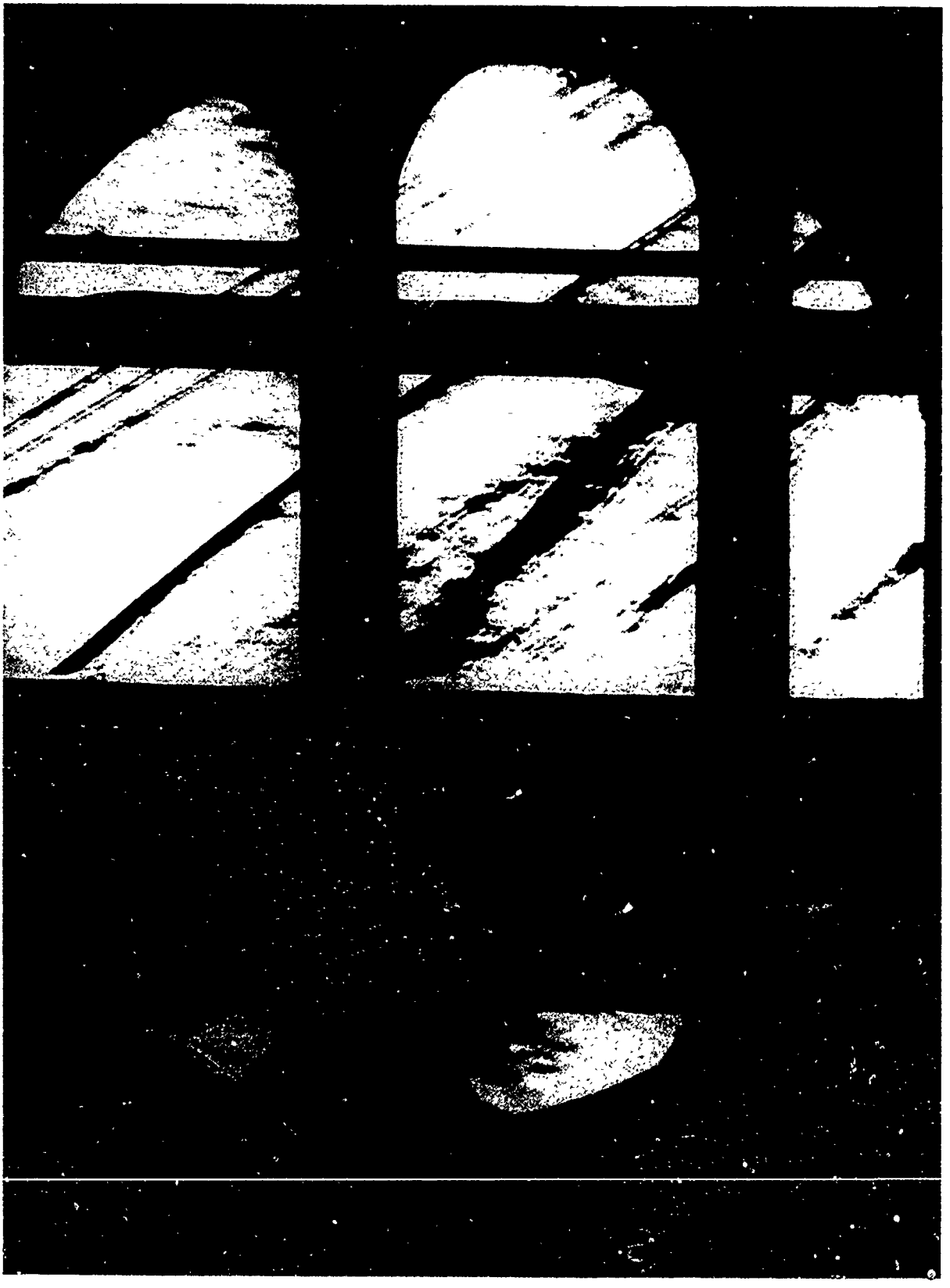

b. Cavity with 3δ sawtooth spoiler at leading edge of cavity
Fig. 29. Continued.

c. Cavity with SC 90 doors and 3δ sawtooth spoiler
Fig. 29. Continued.

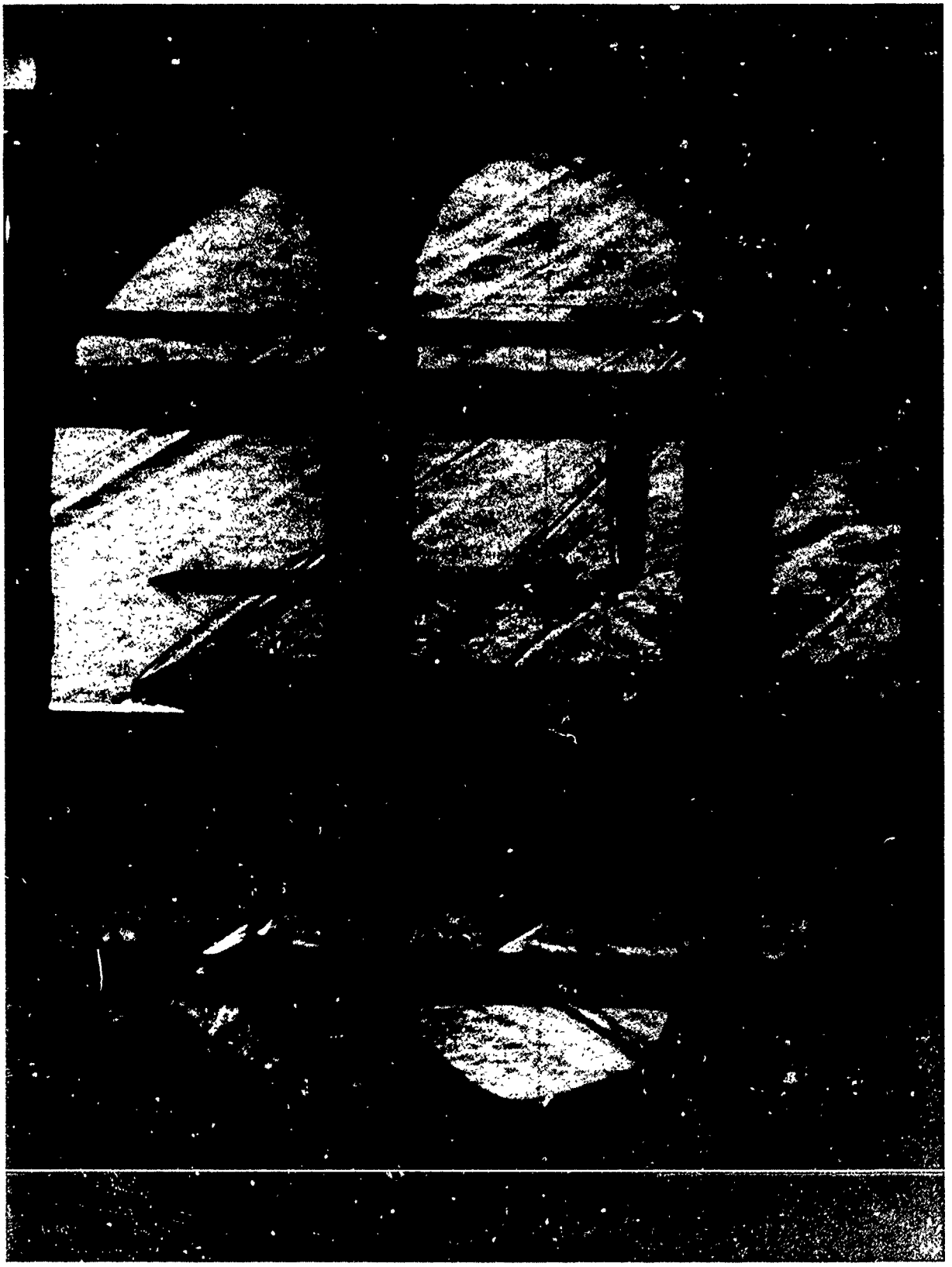

d. Cavity with TC 120 doors and 1δ sawtooth spoiler
Fig. 29. Concluded.

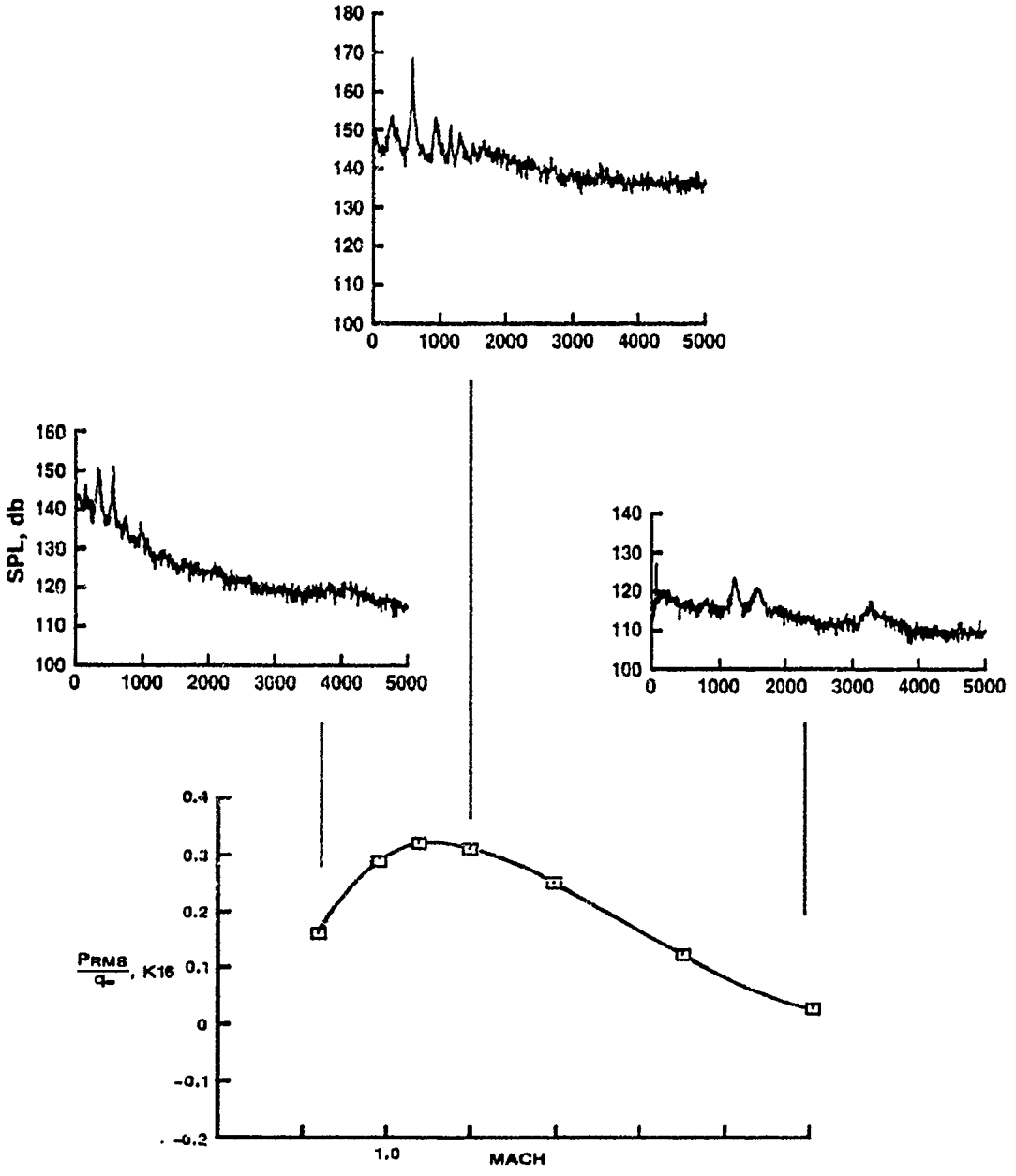

Fig. 30. Variation with Mach number of tonal amplitudes and overall sound pressure levels in a deep cavity (L/H = 4.5) with no spoilers or doors.

Vita - Richard E. Dix

A graduate of Georgia Tech with BS and MS degrees in Aeronautical Engineering, Mr. Dix has been involved in applied research at the AEDC for many years, concentrating on improvements in wind tunnel testing and data analysis. Shortly after the AEDC four-foot transonic wind tunnel, Tunnel (4T), came on-line in 1968, Mr. Dix became involved in developing store separation test techniques, looking for new or improved applications of the captive-trajectory support (CTS) system. He has just completed a four-year test program sponsored by AFATL/FXA that produced a large data base dealing with the carriage and separation of internal stores.

THIS PAGE INTENTIONALLY LEFT BLANK

A SEMI-EMPIRICAL APPROACH TO PREDICT TRANSONIC LIMIT CYCLE OSCILLATION CHARACTERISTICS OF FIGHTER AIRCRAFT

J.J. MEIJER†
A.M. CUNNINGHAM, Jr.‡
R.J. ZWAAN§

October 19, 1990

(Article UNCLASSIFIED)

†Senior research engineer
National Aerospace Laboratory (NLR)
Amsterdam, The Netherlands

‡Engineering Staff Specialist
General Dynamics Fort Worth Division
Fort Worth, Texas, U.S.A.

§Head Aeroelastic Department
National Aerospace Laboratory (NLR)
Amsterdam, The Netherlands

"Approved for public release; distribution unlimited"

This investigation is a cooperative General Dynamics/NLR program, funded by:
United States Air Force
The Netherlands Ministry of Defense
General Dynamics, Fort Worth Division, Texas, United States
National Aerospace Laboratory, Amsterdam, The Netherlands

Abstract

Flutter analysis for fighter aircraft in the transonic speed regime (M = 0.9 to 1.1) is difficult to treat analytically since the governing aerodynamic equations are inherently nonlinear due to the presence of shocks embedded in the flow fields. When flow separation occurs, the analytical simulation becomes even more complicated. Nevertheless, flutter predictions are needed in this speed regime because flutter stability is often critical and is very sensitive to store configurations and downloadings.

In addition, fighter aircraft must perform "high g" maneuvers at transonic speeds which may lead to conditions that are strongly dominated by separated flows. These types of flows usually produce either aircraft buffet or, in some cases, a more severe transonic nonlinear structural oscillation of limited amplitude commonly known as limit cycle oscillations (LCO). LCO is a limited amplitude self-sustaining oscillation produced by a structural/aerodynamic interaction. It is related to flutter but affects aircraft performance in a manner similar to buffet.

An analysis of steady wind tunnel data, obtained for a fighter type aircraft, has indicated that shock-induced and trailing edge separation plays a dominant role in the development of LCO at transonic speeds. On this basis, a semi-empirical LCO prediction method is being developed which makes use of such steady wind tunnel data. The preliminary method has been applied to several configurations and has correctly identified those which have encountered LCO. The advantage of the method, at least for qualitative predictions, is the potential for application early in the design process of new aircraft to determine and understand the aeroelastic characteristics. The method is still being evaluated and upgrading and refinements are expected from unsteady wind tunnel pressure measurements to be obtained from oscillating models as part of an extensive investigation into the aerodynamic nature of LCO. The method will be described in its present form and results of preliminary predictions will be compared with flight test trends and those from classical flutter predictions.

Contents

LIST OF FIGURES

1 Introduction

Requirements of fighter aircraft to operate with high maneuverability in the transonic speed regime increase the potential to encounter a transonic nonlinear flutter, known as limit cycle oscillations (LCO). LCO is a limited amplitude self-sustaining oscillation produced by a structural/aerodynamic interaction. The phenomenon is related to buffet but has characteristics similar to classical flutter in that it usually occurs at a single frequency. From an operational point of view, LCO results in an undesirable airframe vibration that limits the pilot's functional abilities and produces extreme discomfort and anxiety. More importantly, targeting accuracy is degraded, e.g. wing mounted missiles cannot be fired because of high levels of wing motion that prevent target lock-on.

Examples of recordings of LCO for two type of fighter aircraft are shown in figures 1 and 2. The LCO in figure 1 was encountered during flight flutter tests of fighter-type aircraft I with a new type of external fuel pylon/tank (Ref. 1). Figure 2 shows the results during flight flutter tests of fighter-type aircraft II equipped with a chaff dispenser pod. In both cases the maximum amplitudes occur during aircraft deceleration, thus pointing to some hysteresis effect. LCO is experienced by highly swept wings as well as high aspect ratio wings, although different flow mechanisms may be involved. In references 2 to 6 such cases were analyzed in relation to wing bending oscillations.

For fighter aircraft, LCO is characterized by an almost harmonic oscillation which appears at Mach numbers ranging from 0.8 to 1.1, and at moderate angles of attack depending on the Mach number, but usually less then 10 deg. The flow conditions during LCO are characterized by mixed attached/separated flow and correspond to flight conditions as indicated by the shaded area in figure 3, which represents a typical performance map of lift coefficient versus Mach number for fighter aircraft (Ref. 7). Lowly damped vibration modes tend to respond provided they have the proper characteristics to couple with this type of flow. This coupling frequently occurs near flutter boundaries, which implies that classical flutter predictions with linear theory may be applied as a guidance to establish LCO sensitivity. An example of flutter predictions for fighter-type aircraft I is shown in figure 4. Similar calculations were carried out for other configurations, which gave rise to unstable or lowly damped modes in the transonic speed range (Refs. 1, 8 and 9). The almost harmonic characteristic of the oscillation essentially eliminates classical buffet as a forcing mechanism. Because of the wide range of frequencies observed on various configurations, however, it is also unlikely that the forcing mechanism is due to an aerodynamic resonance at some specific frequency, which is known from wind tunnel tests with two-dimensional wings (Ref. 10). In the next chapter the basis of a prediction method for LCO is discussed, and the arguments are given which support its validity.

2 Basis of prediction method

In reference 11 a prediction method for LCO was proposed based on a timediscretized solution of equations of motion which can be written in matrix form as:

$$[M]\{\ddot{q}\} + [C]\{\dot{q}\} + [K]\{q\} = \{A(q)\} + \{B(\dot{q})\}\,, \qquad (2.0.1)$$

The left hand side represent inertia, damping and stiffness terms. $[A]$ and $[B]$ are the aerodynamic stiffness and damping terms which are nonlinear functions of the generalized coordinate vector $\{q\}$. This equation was considered in reference 11 as the multi-DOF generalization of the

1-DOF Van der Pol's equation. The latter equation is characterized by a nonlinear damping term which is negative for small amplitudes (unstable system) and becomes positive for large amplitudes (stable system). The result is that an initially small amplitude increases until an LCO is formed. Preliminary applications of this method in reference 11 to fighter-type aircraft I showed that LCO could indeed be predicted, although the amplitudes were unrealistically high. The following two conclusions were drawn:

1. The nonlinear aerodynamic forces as derived from steady wind tunnel tests were sufficient to produce qualitatively correct predictions.
2. At least two DOFs proved necessary to arrive at LCO, just as in "classical" flutter cases.

Since reference 11 was released the aeroelastic mechanisms of the above flutter cases were studied extensively, because the last conclusion contrasted with the solution of the 1-DOF Van der Pol's equation which for proper aerodynamic damping characteristics could produce an LCO. The results of this more recent study are:

1. For all cases considered at least two DOFs were necessary to produce LCO. Elimination of all but one DOF always led to a stable system.
2. Elimination of the coupling terms in $[A]$ of (2.0.1) always led to a stable system; elimination of the coupling terms in $[B]$ only changed the amplitude of the LCO.

These results confirmed indeed that LCO was the result of usual flutter mechanisms with two or more DOFs but with nonlinear aerodynamic terms, rather than a generalized formulation of Van der Pol's equation. Solving (2.0.1) using steady aerodynamic data forms the basis of the present prediction method. This development follows the suggestion to use steady data as given previously in references 2, 4 and 12. In the following discussions this method will be evaluated to determine if it may be applicable to the early stages of the aircraft design process.

3 Aerodynamics for LCO

A crucial question of course is whether aerodynamic data of fighter-type wings exist which hold the prospect of success in applying the preceding principle. In this connection steady pressure data for a full-span wind tunnel model representing aircraft I were analyzed at NLR which were made available by the aircraft manufacturer (Ref. 13). The objective of that test was to obtain pressure data for investigating the role of shock-induced trailing-edge separation in LCO as suggested in reference 12. Pressure data were acquired on the wings, the horizontal tails and the fuselage for the following test conditions: Mach number ranging from 0.90 to 0.96, with increments of 0.01, and angle of attack ranging from 0 to 10 deg, with increments of 0.5 deg. During these tests different tip launchers and leading-edge-flap settings were also included in the configuration matrix.

The wing pressures were integrated by NLR to both sectional and overall forces. The wing planform of the wind tunnel model provided with pressure orifices is shown in figure 5. Also shown is the panel distribution used in the chordwise and spanwise integration.

Results of the analysis are presented for one type of tip launcher and leading-edge-flap setting. In figures 6 and 7 the steady normal force and moment coefficients are shown for stations 1 and 6 (most inboard and outboard, respectively) as function of angle of attack (0 to 10 deg) and Mach number (0.90 to 0.96). The coefficients for the intermediate stations show a gradual transition. It is immediately clear that the coefficients in station 1 do not show any irregular behavior, whereas in station 6 both lift and moment coefficients show rapid changes in short intervals of the angles of attack (centered on about 5 to 7 deg) in the greater part of the Mach number interval. These rapid changes might give rise to LCO as discussed in chapter 2 and are typical of those described in reference 12 that were shown to drive LCO.

To analyze the kind of pressure distributions which lead to the rapid changes in the aerodynamic coefficients, the pressure distributions on the upper and lower wing surface in stations 1 and 6 at Mach number 0.92 are presented in figures 8 and 9. The pressure distribution at the upper surface in station 1 shows a very gradual development with angle of attack, with a small upstream shift of the shock along with a slight trailing edge flow separation at the highest angle of attack. In station 6 a strong upstream shift of the shock starts at about 5 to 7 deg coupled with a rapidly developing flow separation at the trailing edge. This occurs after a merging of the weaker nose and aft shocks into a much stronger single shock that induces the extensive separation as is discussed in detail in reference 14. The shock motion also reverses at this point which coincides with breaks in the sectional lift and pitching moment coefficients. The pressure distributions on the lower side show only very gradual developments. For the other type of tip launcher and leading edge flap settings the same kind of trends were observed. Having established the cause of the rapid changes in the sectional coefficients, the question remains whether they are capable of producing LCO. The answer should come from solving the equations of motion for the elastic aircraft structures, i.e. carrying out time integration of equation 2.1 with these typical nonlinear aerodynamics as was done in reference 12.

4 Discussion of prediction method

In this chapter the aeroelastic equations of motion and the time-marching solution procedure are described.

4.1 Aeroelastic equations of motion

The aeroelastic equations of motion are be written in a usual matrix form as:

$$[M]\{\ddot{q}\} + [C]\{\dot{q}\} + [K]\{q\} = \{L\}\,, \tag{4.1.1}$$

where q is the vector of generalized coordinates, M is the generalized mass matrix, C is the structural damping matrix, and K is the stiffness matrix. L is the vector of generalized aerodynamic forces. An adequate description of the displacements of the unrestrained aircraft structure is obtained by taking the symmetric and antisymmetric natural vibration modes as generalized coordinates, completed by adding the rigid body modes. The modes with the lowest natural frequencies are fully utilized, whereas the remaining higher modes may be treated with the concept of residualization. In the present study, however, the presence of these remaining modes is neglected altogether. The equations of motion are expressed then in matrix form as:

$$\begin{bmatrix} M_R & 0 \\ 0 & M_E \end{bmatrix} \begin{Bmatrix} \ddot{q}_R \\ \ddot{q}_E \end{Bmatrix} + \begin{bmatrix} 0 & 0 \\ 0 & 2\zeta_E M_E \omega_E \end{bmatrix} \begin{Bmatrix} \dot{q}_R \\ \dot{q}_E \end{Bmatrix} + \begin{bmatrix} 0 & 0 \\ 0 & M_E \omega_E^2 \end{bmatrix} \begin{Bmatrix} q_R \\ q_E \end{Bmatrix} = \begin{Bmatrix} L_R \\ L_E \end{Bmatrix}, \tag{4.1.2}$$

in which the indices R and E refer to the rigid body and elastic modes. Their number is N_R and N_E , respectively. ζ and ω are the damping factor and natural frequency of each elastic mode. The generalized aerodynamic force for the i-th coordinate is formulated as:

$$L_i = \frac{1}{2}\rho V^2 \int_S \phi_i\langle x,y\rangle \Delta C_p\langle x,y,\alpha\langle t\rangle\rangle dS\,, \tag{4.1.3}$$

in which $\frac{1}{2}\rho V^2$ is the dynamic pressure, $\phi_i\langle x,y\rangle$ is the natural mode shape and $\Delta C_p\langle x,y,\alpha\langle t\rangle\rangle$ is the pressure difference distribution over the wing depending on the dynamic angle of attack distribution α . This distribution is expressed by:

$$\alpha = \alpha_m + \Delta\alpha, \quad \Delta\alpha = \Delta\alpha\langle x,y,t\rangle\,, \tag{4.1.4}$$

$$\Delta\alpha = \sum_{N_R+N_E} \left(\frac{\partial}{\partial x} + \frac{1}{V}\frac{\partial}{\partial t}\right) \phi_j(x,y) q_j(t) \,. \tag{4.1.5}$$

α_m is the mean angle of attack and $\Delta\alpha$ the time-dependent variation at point x, y. In the present approach, the pressure distribution ΔC_p in (4.2.1) is a time-independent nonlinear function of α . It is this relation by which the aerodynamic peculiarities discussed in chapter 3 enter the equations of motion (4.1.3), weighted by an appropriate mode shape ϕ_i . After substituting (4.2.2) and (4.2.3) in (4.2.1), L_i can be interpreted as:

$$[L_i] = Aq + B\dot{q}, \tag{4.1.6}$$

where A and B are time-independent coefficients. This expression shows that L_i involves an aerodynamic stiffness term, Aq, and an aerodynamic damping term, $B\dot{q}$. In the numerical solution of the equations of motion the aerodynamic forces L_i are discretized as follows:

$$L_i = \frac{1}{2}\rho V^2 \sum_k (\phi_i(x,y)\Delta C_p(x,y,\alpha(t)))_k \, \Delta S_k \,, \tag{4.1.7}$$

in which ΔS_k is the k-th panel area, and the product $\langle \phi_i \Delta C_p \rangle$ is taken constant over the whole k-th panel, being evaluated at the $\langle x, y \rangle$ position of the k-th pressure orifice. Because of the nonlinear aerodynamics, (4.1.3) has to be evaluated for both right and left wing and added at each time step of the time simulation. It should be noted that in the present study only aerodynamic forces on the wing have been taken into account and those on the wing stores, fuselage and empennage surfaces ignored.

Before solving, the equations of motion are brought into state space form. Writing (4.1.2) as:

$$[M]\{\ddot{q}\} + [C]\{\dot{q}\} + [K]\{q\} = \{L(q,\dot{q})\} \,, \tag{4.1.8}$$

their state space form is:

$$\begin{aligned} \{\dot{s}\} &= [M]^{-1}(\{L(q,\dot{q})\} - [C]\{s\} - [K]\{q\}), \\ \{\dot{q}\} &= \{s\}, \end{aligned} \tag{4.1.9}$$

or the usual form:

$$\{\dot{x}\} = [A]\{x\} + [B]\{u\} \quad , \tag{4.1.10}$$

where A and B are constant matrices that result from the change of the variables $x = [s, q]^T$ and u is the generalized force $L(q, \dot{q})$.

4.2 Time-marching aeroelastic solution

The aeroelastic solution procedure implemented for integrating (4.1.10) is similar to that described by Edwards et al (Ref. 15). Since (4.1.10) is a finite-dimensional differential equation, its solution (Ref.16) is given by:

$$x_i(t) = \Phi(t)x_i(0) + \int_0^t \exp[A(t-\tau)]\, Bu(\tau)d\tau \,. \tag{4.2.1}$$

The state transition matrix ,$\phi(t) = exp[At]$ in general, can be calculated to any assigned accuracy by using a sufficient number of terms of the series expansion of the matrix exponential function. As explained in reference 16, the first term in (4.2.1) is the homogeneous response portion of (4.1.10), while the second term is a convolution integral giving the forced response. Numerically, the solution is advanced from any time step n to step n+1, by:

$$x_i[(n+1)\Delta t] = \Phi(\Delta t)x_i(n\Delta t) + \int_{n\Delta t}^{(n+1)\Delta t} \exp[A((n+1)\Delta t - \tau)]Bu(\tau)d\tau, \qquad (4.2.2)$$

where Δt is the time step. Since $u(\tau)$ is not known over the interval $n\Delta t < t < (n+1)\Delta t$, the integral in (refeq:vttwee) must be approximated. The simplest approximation for the integral is to assume that $u(\tau)$ is constant, i.e. $u(\tau) = u(n\Delta t)$ over the interval. A better approximation may be obtained by assuming u to vary linearly from $u(n\Delta t)$ and $u((n+1)\Delta t)$:

$$u^{n+1} = u^n + \left(u^{\cdot} - u^{n-1}\right). \qquad (4.2.3)$$

The resulting algorithm is:

$$x_i^{n+1} = \Phi x_i^n + \Theta B\left(3u^n - u^{n-1}\right)/2, \qquad (4.2.4)$$

where Θ is the integral of the state transition matrix Φ. The integration matrices Φ and Θ were calculated using the program described in reference 17. The final result of the time integration process is the variation of the generalized coordinates q and their time derivatives as functions of time. They can easily be reduced to quantities of practical interest, like wing tip acceleration, pilot seat acceleration, etc.

4.3 Number of applied vibration modes

The choice of which and how many modes to use in the solution of (4.1.10) is a critical decision. A trade-off must be made between

1. the time required for the analyst to reduce the number of modes to a minimum and
2. the computer cost required to run a full "unedited" set of modes within the frequency range of interest.

In the investigation described in reference 12, it was possible to reduce the number of modes to a single DOF as a result of knowledge gained from flight test measured LCO characteristics. Also, since LCO did not occur near a flutter boundary, the natural modes were essentially unchanged and represented those of the full-scale aircraft at flight LCO conditions. This is not the general case, however, particularly where LCO occurs near the flutter boundary. In this case, the modified modes resulting from the flutter eigenvectors may be quite different from the natural modes. The concept of a single DOF response in LCO still applies, however, but it applies to a complex mode as prescribed by the eigenvectors.

Some guidance for mode selection may be derived from the results of routine linear flutter calculations for a complete multi-DOF system in attached flow. Modes that exhibit low aerodynamic damping values within the flight conditions of interest, are good candidates for producing LCO. Along with the damping values, the eigenvectors are also available for constructing the appropriate complex modes if they are significantly different from the natural modes. However, the LCO potential of each mode, real or complex, is governed by its shape and how this shape interacts with the nonlinear flow fields. Such evaluation by visual inspection is a qualitative judgement process which requires a high level of aerodynamic expertise, and its outcome may not always be the right answer. Finally, if the LCO conditions are near a flutter boundary, it is also quite possible that the eigenvectors are significantly modified by nonlinear aerodynamic

forces. Thus, even with all of this information, the analyst would have to spend a significant amount of time making the mode selections but would have no guarantee that he made the right decisions and the results could be entirely misleading.

In spite of the additional computer costs, a better alternative is to use the full set of vibration modes within the frequency range of interest. This has the advantages that (1) the system can filter out the mode(s) that will respond in LCO, (2) the time requirement and uncertainty of the decision process for mode selection is eliminated, and (3) more modes are available to describe a possible shift in mean angle of attack due to static wing deflections. The mean angle of attack due to aircraft maneuvering and/or static aeroelastic effects has a major influence on the aerodynamic loads during LCO. Modes that contribute dynamically to LCO may differ from the modes that contribute to static deflections. The representation of the latter modes in the equations of motion may be simplified by the concept of modal residualization.

5 Applications

A number of configurations is considered to which the wind tunnel data presented in chapter 3 are applicable. Configurations A, B and C include the same type of underwing missiles. Their differences are that configurations A and B have different empty tip launchers, whereas configuration C is configuration A with tip missiles and external fuel tanks installed. Finally, configuration D and a number of its downloadings are considered. This configuration includes external fuel t 500 lbs stores and tip missiles. For all configurations modal characteristics were calculated and "classical" flutter calculations were performed based on the subsonic doublet lattice method. For some configurations the transonic FTRAN3 method was also applied. tex paper Conditions for the LCO calculations are given below, unless otherwise mentioned.

1. Natural vibration modes were considered, antisymmetric and unrestrained, with frequencies up to a maximum of 15 Hz. Structural damping was varia- ble.
2. Only aerodynamic forces on the wings were considered. Mach number and altitude were variable. No deflections of wing flaps and control surfaces were assumed.
3. The calculated responses are (1) the normal acceleration at the front end of the tip launcher, (2) the same at the rear end and (3) the lateral ac- celeration at the pilot seat. All accelerations in g. Initial disturbances were given to the vibration modes which develop in limit cycle oscillations.

Flight test data are available for all configurations.

5.1 Generic model

The structural properties of the generic model are slightly different from the original configuration A, because after the first calculations one of the mass points of the outboard underwing launcher/missile combination was found to be located too far aft. Classical flutter calculations for M = 0.9 showed a serious instability of an antisymmetrical mode at a frequency of 7.6 Hz inside the flight envelope, neglecting structural damping. Because of this pronounced flutter sensitivity this generic model was maintained to investigate typical features of transonic LCO. Steady wind tunnel data for configuration A were used. The two vibration modes (of the generic model) which will turn out to be dominant in the development of LCO are shown in figure 10. The frequency difference is small. Both modes show a torsional deflection of the outer wing parts. The bending deflections are opposite.

1. 2-DOF system

   The system consists of the two vibration modes presented in figure 10. Calculations were started at a mean angle of attack of 6 deg, where in view of the sectional coefficients presented in figure 7 the occurrence of LCO was expected. The other conditions were sea level, M = 0.92 and g = 0.02. An initial disturbance was given of the second vibration mode. Calculations were made of the three response accelerations during 20 s. The results are presented in figure 11. All three accelerations, 1) tip launcher front end, 2) tip launcher rear end and 3) pilot seat, lateral, pass clearly into LCO with a frequency of 7.7 Hz and amplitudes of 27.5 g, 10.5 g and 3.1 g, respectively. Obviously the second vibration mode seems dominating in the LCO. At the right bottom of figure 11 the dynamic angle of attack of the wing tip station is presented. Its amplitude increases to 1.8 deg. Such large responses are attributed to the flutter sensitivity mentioned above.

2. Two 1-DOF systems

   Response calculations were made for the two vibration modes separately over a period of 20 s. The other conditions were the same as for the 2-DOF system. Neither of the isolated modes showed any LCO. The conclusion is that the interaction of at least two vibration modes is necessary for LCO to develop in this case, just as in most "classical" flutter cases, but now with nonlinear aerodynamics.

3. 12-DOF system

   Calculations were also made for the generic model at the same structural damping, Mach number and altitude to demonstrate that LCO can be detected without previous knowledge of sensitive natural modes and angle of attack range. This was done by using all natural modes up to a frequency of 15 Hz and allowing the mean angle of attack to vary linearly from 1 to 10 deg as it would during a maneuver. The results are shown in figure 12 where it is apparent that, in addition to LCO at higher angles, large amplitude oscillations at 7.7 Hz occur at angles much less than 6 deg. This is again attributed to the flutter sensitivity mentioned earlier. The LCO disappears at about 7.4 deg. Thus it has been demonstrated that the model predicts LCO without any assumption on critical modes or angles of attack. In view of the 2-DOF results it is advisable not to rely only on an interpretation of the aerodynamic loads to establish possible LCO conditions, but to include sufficient variations of the flight conditions in the response calculations.

   The large amplitude responses shown in figure 12 raise the concern that values of α developed during the solution process may exceed the limits of the aerodynamic data base. Results for the tip launcher angle of attack are shown in figure 13. For a structural damping of 0.02, the maximum amplitudes are very close to the data base limits of 0 and 10 deg. Response predictions for which the angle exceeds the data base limits, such as those for a structural damping of 0.01, would no longer be valid and would have to be rejected.

   Another feature apparent in figure 13 is the occurrence of several break points in the amplitude envelope. These angles are noted in the figure and are also noted along the normal force and pitching moment curve for station 6. There are many complicated relationships implied in these results concerning the effect of previously encountered oscillations that have not been damped before a significant mean angle of attack change has occurred during the α-sweep. As an example, LCO at a lower mean angle may be amplified when encountering a more severe instability at a higher angle. This is illustrated at point 2 where the maximum angle of attack has reached about 5.5 to 6.0 deg after which the amplitude grows more rapidly with increasing angle. A major change as shown in the pitching moment curve, develops between 5 and 7 deg (strong negative slope) and is believed to be the source of accelerated amplitude growth with angle of attack at point 2.

The disappearance of LCO at about 7.4 deg (point 5) is not clearly understood, however, the bump in mean angle between 8.5 and 9.5 deg (point 6) is possibly attributed to static aeroelastic response of the wing to an abrupt change in normal force slope.

Since the response levels in this example are unrealistically high, study of this problem is academic; however, it does serve as a means of understanding the nonlinear dynamics associated with LCO during aircraft maneuvering. The problem shown in figure 12 and 13 was re-run with the linearly increasing mean angle which was then held constant upon reaching 6 deg at 15 s. These results are shown in figure 14 where it is seen that a damping occurs after reaching 6 deg. This damping is acting on the residual oscillations remaining from LCO encountered at lower angles. The remaining oscillations are thus representative of LCO at a mean angle of 6 deg.

5.2 Flow characteristics during LCO

To demonstrate the potential role of shock-induced trailing edge separation during LCO (Ref. 12) the wing motion and the pressure distributions on the upper surface were plotted during one cycle of oscillation for the example shown in figure 14. The cycle starts at 25.1 s and the time intervals are 0.005 s. The results are presented for four time steps, viz. 25.115 s, 25.155 s, 25.175 s and 25.215 s. These time steps were chosen to correspond to the extremes of angle of attack variation at wing tip station 6 about $\alpha = 6$ deg. These deflections are highlighted as a heavy line in figure 15 and represent the incremental angle of attack for (I) maximum nose down, (II) zero with positive pitch rate (III) maximum nose up, and (IV) zero with negative pitch rate.

The results in figure 15 along with the C_N and C_m trends for station 6 in figure 13, may be used to clearly demonstrate the relationship between shock induced trailing edge separation and LCO. At point I in figure 15, the wing tip is at a minimum total angle of attack (i.e.$\alpha = \alpha_m + \Delta\alpha$) of about $\alpha = 4.7$ deg and a large positive (up) deflection as indicated by the deflections (heavy line) at station 6. Two shocks (nose and aft shocks) are distinctly seen in the chordwise pressure distributions (heavy line) also at station 6. The flow is attached at the trailing edge as indicated by the nearly zero value of the pressure coefficient. In figure 13 at $\alpha = 4.7$ deg, C_N is at its lowest value during the cycle and C_m is at its highest value. Thus, attached flow with two shocks is providing a nose up pitching moment increment at the minimum angle and a downward acting normal force incremental at a large upward deflection.

Continuing on to point II in figure 15, the wing tip is at $\alpha = 6$ deg and a maximum downward deflection. The two shocks have merged into a single strong shock and the trailing edge pressures are indicating that separation has begun. In figure 13, C_N is higher but at a plateau that continues up to $\alpha = 8.5$ deg . C_m is lower (less nose up). At point III in figure 15, the wing tip is at a maximum angle of attack of about $\alpha = 7.3$ deg . The single strong shock formed at point II has fully separated the flow to the trailing edge which in turn has driven the shock forward as shown in the pressures at station 6. In figure 13, the C_N is still about the same as it was at point II, however, C_m is now lower and more nose down. Finally, at point IV in figure 15, the wing tip is at about $\alpha = 6$ deg but maximum upward deflection. The trailing edge pressures are indicating that re-attachment is going on and a strong single aft shock is now present. In figure 13, C_N is the same as it was at $\alpha = 7.3$ deg at point III but C_m is higher giving less nose down pitching moment. From point IV, the cycle continues to point I where the two-shock system is re-formed.

The relationship just illustrated between shock induced trailing edge separation, pitching moment and torsion response at station 6, is identical to that described in reference 12 where it was concluded that a nonlinear aerodynamic spring was the principal driving mechanism for LCO. For the current example, however, significant vertical translation in the LCO (or eigen)

mode was opposed by C_N variations at point III. For angles of attack above α = 6 deg , C_m was was constant and did not affect the wing motion which would make it a neutral spring for half of the cycle. Thus, the existence of an additional nonlinear spring for opposing translation for half of the cycle further substantiates the above conclusion of reference 12.

5.3 LCO sensitive parameters

Since the response levels of LCO became quite large for the example shown in figure 14, the knowledge of LCO sensitive parameters becomes important in order to investigate under which conditions the LCO becomes more realistic. Therefore the calculations of the example presented in figure 14 were repeated for varying altitude, angle of attack, Mach number and structural damping. The initial disturbance applied to the LCO sensitive natural mode was kept still the same. The responses were calculated over a period of 30 s to 60 s, until stabilized LCO condition were achieved. In figure 16 maximum LCO amplitudes of the normal acceleration at the front end of the tip launcher are presented as function of altitude (Fig. 16a), structural damping (Fig. 16b), mean angle of attack (Fig. 16c) and Mach number (Fig. 16d). Responses for which the angle of attack exceeds the data base limits were left out. Although a limited search was performed, the presented results demonstrate very well the sensitivity of the considered parameters to LCO.

The interesting features to note are that the amplitude decreases rapidly when the altitude is increased from 0 ft to 5K ft (Fig. 16a) and/or the structural damping of each natural mode from g = 0.0 to 0.02 (Fig. 16b). Variations of altitude from 5K ft to 15K ft and/or structural damping from 0.02 to 0.04 leads to small amplitude changes. A rapidly growing amplitude for increasing mean angle of attack and structural damping values smaller than 0.02 is shown in figure 16c. When the angle of attack becomes greater than 6 deg it appears that the amplitude decreases rapidly and disappears at about 7 deg, which was already observed in figure 12 and 13. Finally, figure 16d shows that the responses are highly influenced by changing Mach number. The increase of amplitude at M = 0.90 is not clearly understood and need further investigation. The trends for higher Mach numbers than 0.96 could not be determined due to limitations of the data base.

Due to the nonlinear aerodynamics it should be evident that more parameter combinations have to be worked through to illuminate the sensitivity of LCO.

5.4 Configuration A

Response calculations were carried out for configuration A with the correct structural representation. Classical flutter calculations show an unstable antisymmetrical mode at a frequency of 7.6 Hz just above the desired maximum speed of 600 KEAS, neglecting structural damping. The LCO calculations were made for a system with natural modes up to 15 Hz (12 DOF) and varying structural damping values. The flight conditions were: Mach number 0.92 and altitude 5K ft. Just as for the generic model, mean angles of attack were chosen at which maximum responses were expected. The results are presented in figures 17 and 18 for acceleration 1 and structural damping values of 0.01, 0.02 and 0.03. The frequency is about 7.6 Hz. It appears that for a mean angle of attack of 6 deg and structural damping values of 0.01 and 0.02 rapidly developing LCO was obtained (Fig. 17), whereas for a structural damping of 0.03 the calculations had to be continued to 60 s to obtain sustained oscillations. The LCO response levels for acc.1 (Fig. 17) are 14.2 g, 13.5 g and 10.0 g, and those for acc.3 are 2.0 g, 1.8 g and 1.4 g, respectively. The results presented in figure 18, show a near-LCO for a mean angle of attack of 2 deg and structural damping values of 0.01 and 0.02. Continuation of the calculations up to 40 s led to constant amplitude LCO. The LCO response levels are for acc.1: 20.3 g and 4.1 g (Fig. 18), and for acc.3: 2.8 g and 0.55 g. For a structural damping value of 0.03 g no LCO was found. The response levels are high and follow the trends found with the generic model

(Fig. 16c). A reason for the still high response levels could be the missing correct aerodynamic damping due to unsteady flow effects.

Flight test results for configuration A yielded LCO at M = 0.9 (during a wind-up turn) at an altitude of 5K ft. The frequency of acceleration 1 was about 7.5 Hz and the amplitude 2 g. The conclusion is that, at least the calculated LCO and the flight test data seem to agree qualitatively.

5.5 Configuration B

Configuration B has the same loading conditions as configuration A, but different type of tip launchers, implying changes in the structural representation. Classical flutter calculations show again an unstable antisymmetrical mode at a frequency of 7.6 Hz speed of 600 KEAS. Steady wind tunnel data for configuration B are also present, which differ only slightly from the data of configuration A. It would be expected therefore that differences in LCO of configurations A and B are caused mainly by the difference in structural representation.

Response calculations were carried out for the same conditions as for configuration A, including a system with natural modes up to 15 Hz (12 DOF) and varying structural damping values. Results of acceleration 1 for mean angles of attack of 6 and 2 deg, and varying structural damping are presented in figures 19 and 20. The frequency is about 7.7 Hz. For both cases, after the calculations were continued to 40 s, sustained oscillations were found. At a mean angle of attack of 6 deg the LCO amplitude levels are for acc.1: 17.1 g (Fig. 19), acc.2: 5.9 g and acc.3: 2.2 g, and for a mean angle of attack of 2 deg these levels become for acc.1: 2.3 g (Fig. 20), acc.2: 0.5 g and acc.3: 0.3 g. For both cases LCO was suppressed by increasing the structural damping. Obviously the calculated responses of configuration B show a weaker sensitivity to LCO then was calculated for configuration A, because at lower structural damping values LCO disappears. This observation is also confirmed by the results of flight tests.

The flight test results for configuration B yielded LCO at M = 0.95 (during a wind-up turn) at an altitude of 5K ft, while at M = 0.90 and same altitude no LCO was observed. The frequency of acceleration 1 was about 7.5 Hz and the amplitude 2.4 g. Again, the conclusion is that the calculated LCO and the flight test data seem to agree qualitatively.

5.6 Configuration C

The loading conditions of configuration C are the same as configuration A, but now tip missiles are installed. No appropriate wind tunnel data are available for configuration C, but it is certainly justified to apply the data of configuration A, because the typical transonic flow phenomena occur on the upper surface of the wing. Response calculations were made for a system with natural modes up to 15 Hz (17 DOF) over a period of 20 s, while the angle of attack changed linearly from 1 to 6 deg in 15 s, after which the angle of attack was kept constant at 6 deg. The other conditions were kept the same as for configuration A. The results are shown in figure 21 for the responses at the tip launchers. It appears that LCO is completely absent. The responses are very irregular and well damped. Classical flutter calculations do neither show any instability.

In flight tests of configuration C no LCO was observed, so that again the conclusion is that calculated LCO and flight test data correlate well in this respect.

5.7 Configurations D

Finally, predictions were carried out for configurations D and a number of its downloadings, D.1 to D.3 (Fig. 22). These configurations equipped with multi-store racks and 500 to 600 lbs stores in combination with external fuel tanks and missiles are comparable with those in which heavy stores are installed instead of multi-store racks. Classical flutter calculations show

for downloading D.2 a severe unstable mode at about 5 Hz and for downloading D.4 a mild instability at about 7.5 Hz for full to half full external fuel tanks. Configuration D, the alternate downloading D.3 instead of D.2 and the downloadings D.1 and D.4 with empty tanks do not show any problem.

No appropriate wind tunnel data are available for those configurations. Therefore, the aerodynamic data of configuration B were used instead because the same type of tip launchers are installed. The reason applying these data was already argumented in chapter 5.6 for configuration C in the same situa tion.

Responses were calculated for the same flight conditions as above and struc- tural damping of 0.01. For each configuration shown in figure 22 natural modes up to 15 Hz were applied which lead to DOF numbers mentioned in the figure for the separate configurations. The calculations were carried out over 30 s, while the angle of attack changed linearly from 1 to 10 deg. No LCO is observed for all configurations with empty external fuel tanks, but with full external fuel tanks downloading D.1 shows a serious LCO at about 5 Hz and downloading D.2 shows a latent LCO sensitivity at about 7.5 Hz. Maxi mum response levels were predicted at about mean angles of attack of 6 and 2 deg. Repeating the calculations for downloading D.3 and constant mean angle of attack of 6 deg yielded the following acceleration levels: acc.1: 16.0 g (Fig. 22), acc.2: 6.3 g and acc.3: 1.6 g. The conclusion can be drawn that downloading D.3 is a good substitute for D.2, but might pose problems after releasing stores and downloading D.4 is generated.

Configurations D.1 and D.2 show again that the flutter stability of fighter aircraft, which are expected to carry a wide range of external stores, is highly affected by the variations in vibrational characteristics of the aircraft structure. These characteristics depend to a large extent on the inertial parameters of the individual stores and the way in which they are combined into specific configurations. Moreover, during a mission the struc- tural modes may change considerably due to fuel consumption from external tanks and to release of stores.

Available flight test data for these configurations correlate qualitatively quite well with the calculated responses. This might lead to the additional conclusion that the aerodynamic characteristics of the underwing stores play a minor role in predicting LCO. That store inertial characteristics are dominant has become clear from the above examples.

The results of all applications in this chapter justify the conclusion that the proposed prediction method is promising. The method has been formulated in a manner to allow for further refinements discussed in the next chapter.

6 Improvements of the prediction method

The development of the present prediction method is still in progress. The following extensions are being realized or foreseen:

1. Refinements of the aeroelastic model
   In chapter 4 the concept of modal residualization was proposed as a means to account for the elastic modes with natural frequencies higher than those in the basic set of modes used in the LCO calculations. This extended structural model is expected to provide an improved determination of the aeroelastic deflections and slopes. Another improvement to be considered is to include the aerodynamic forces on fuselage and tail surfaces.

2. Use of unsteady wind tunnel data
   The use of unsteady wind tunnel data obtained by pressure measurements with oscillating models will improve the accuracy of the method for predicting LCO. The inherent phase difference between the aerodynamic loading and generating oscillations is expected to influence the predicted sensitivity of aircraft to LCO. Therefore, as a major part of this

extensive investigation into the aerodynamic nature of LCO, unsteady transonic wind tunnel tests are to be conducted during 1991 at NLR (Ref. 18). In these tests pressure distributions and overall aerodynamic loads will be measured on an oscillating semi-span wing model (Fig. 23) with the same planform as the model for which steady data (Ref. 13) were shown in chapter 3.

Unsteady nonlinear aerodynamic loads due to harmonic model oscillations, however, are less appropriate for straight-forward application in the present prediction method. Useful empirical techniques to transform unsteady nonlinear aerodynamic loads during dynamic stall in a suitable form for use in time simulation methods are described in references 19 to 21. The technique described in references 19 and 20 was developed by ONERA, in France, for two- dimensional wings. This technique is based on splitting the aerodynamic force into a "linear" part F_1 and a "nonlinear" part F_2 (Fig. 24) each of which are modeled by differential equations. The various parameters in these equations are deduced from matching with unsteady wind tunnel data. A similar type of approach is presented in reference 21. Such techniques may be applicable to fighter type wings as well and will be utilized to transform the unsteady wind tunnel data from the current investigation.

3. Use of theoretical unsteady data
   Although this study is limited to utilizing steady and unsteady wind tunnel data, the prediction method may also use of theoretical data in a similar manner as described in reference 22. However, current predictions of 3-D unsteady transonic separated flows with Navier-Stokes solvers or vortex and zonal methods are not yet reliable due to uncertainties in turbulence modeling, etc., and are much more expensive than wind tunnel testing. Thus, the use of theoretical data is premature at this time but could be implemented in the future.

7 Conclusions

In this paper a semi-empirical method has been proposed and evaluated to predict LCO characteristics of fighter aircraft. The evaluation has been performed based on steady wind tunnel data. Some conclusions are drawn concerning the prediction method:

1. Data from steady wind tunnel tests were sufficient for predicting the es- sential features of LCO.
2. A minimum of two natural modes must be included, although the LCO appears as a single eigenmode system.
3. Running the method using many modes through an angle of attack sweep (to simulate a maneuver) provides a means for calculating LCO trends without prior knowledge of natural modes or angle of attack that are sensitive to LCO. There is, however, a significant effect of pitch rate.
4. It has been clearly demonstrated that shock-induced trailing edge separa tion plays a dominant role in the development of LCO at transonic speeds.
5. Altitude, mean angle of attack, Mach number and structural damping turned out to be sensitive parameters in LCO.
6. The effects of store configurations on LCO trends were qualitatively pre dicted in all cases.
7. In agreement with linear flutter analyses, aerodynamic effects of under- wing stores were found to be negligible with this modeling technique. Store mass effects on the modes were dominant.
8. Unsteady effects are needed to properly quantify the driving force and damping characteristics which are important for developing a consistent LCO model.

8 References

1. Meijer, J.J., "NLR Contributions to the Flutter Certification of Aircraft with External Stores", 7th Aircraft/Stores Compatibility Symposium, Wright-Patterson AFB, Ohio, 8-10 April 1986 and at the 17th Annual Symposium of the Society of Flight Test Engineers, Washington, D.C., USA, 10-14 August 1986.
2. Ericsson, L.E., "Vortex-induced Bending Oscillation of a Swept Wing", J. Aircraft, Vol. 24, No. 3, March 1987, pp. 195-202.
3. Dobbs, S.K., Miller, G.D., Stevenson, J.R., "Self Induced Oscillation Wind Tunnel Test of a Variable Sweep Wing", AIAA-85-0739, August 1985.
4. Moss, G.F., Pierce, D. "The Dynamic Response of Wings in Torsion at High Subsonic Speeds", AGARD-CP-226, 1977.
5. Seidel. D.A., Eckstrom. C.V., Sandford, M.C., "Investigation of Transonic Region of High Dynamic Response Encountered on an Elastic Supercritical Wing", AIAA-87-0735-CP, April 1987. Also J. Aircraft, Vol. 26, No. 9, September 1989, pp. 870-875.
6. Eckstrom. C.V., Seidel. D.A., Sandford, M.C., "Unsteady pressure and structural Response Measurements on an Elastic Supercritical Wing", AIAA-88-2277.
7. Bradley, R.G., "Practical Aerodynamic Problems - Military Aircraft", Transonic Aerodynamics, Edited by David Nixon, Vol. 81 Progress in Astronautics and Aeronautics, AIAA, 1982.
8. Hounjet, M.L.H., Kolk, J.T. van der, Meijer, J.J., "Application of NLR's Numerical Simulation Methods to the Transonic Potential Flow about Oscillating Wings", AIAA-84-1564, June 1984.
9. Hounjet, M.L.H., Meijer, J.J., "Application of Time-Linearized Methods to Oscillating Wings in Transonic Flow and Flutter", AGARD CP 374, September 1984.
10. Boer, R.G. den, Houwink, R. "Analysis of Transonic Aerodynamic Characteristics for a Supercritical Airfoil Oscillating in Heave, Pitch and with Oscillating Flap", AGARD-CP-374, 1985.
11. Meijer, J.J., Zwaan, R.J., "Investigation of a Semi-empirical Method to Predict Limit Cycle Oscillations of Modern Fighter Aircraft", Paper presented at the AGARD Specialists Meeting on Aircraft Dynamics Loads due to Flow Separation, Sorrento, Italy, 1-6 April 1990.
12. Cunningham, Jr., A.M., "The Role of Shock-Induced Trailing-Edge Separation in Limit Cycle Oscillations", NASA-CP-3022, 1987.
13. Elbers, W.K., "Wind Tunnel Data Report 1/9-Scale F-16A Pressure Model Investigation of Shock-Induced Separation for Limit Cycle Oscillation Studies (AEDC PWT-16T Test TF-695)", General Dynamics, Fort Worth Division Report 16PR4694, September 1985, (Contract No. F33657-84-C-2034).
14. Cunningham, Jr., A.M., Spragle, G.S., "A Study of the Effects of Reynolds Number and Mach Number on Constant Pressure Coefficient Jump for Shock-Induced Trailing-Edge Separation", NASA-CR-4090, August 1987.
15. Edwards, J.W., Bennett, R.M., Whitlow, Jr., W., Seidel, D.A., "Time-marching Transonic Flutter Solutions including Angle-of-attack Effects", J. Aircraft, Vol. 20, No. 11, Nov. 1983, pp. 899-906.
16. Brockett. R.W., "Finite Dimensional Linear Systems", John-Wiley and Sons, Inc. 1970.
17. Armstrong, E.S., "ORACLS: A Design System for Linear Multivariable Control", Control and Systems Theory, Vol. 10, 1980.

18. Boer, R.G. den, Cunningham, Jr., A.M. "Unsteady Transonic Wind Tunnel Testing of Fighter Type Wings", 31st AIAA/ASME/ASCE/AHS/ASC Structures, Structural Dynamics, and Materials Conference, Long Beach, California, April 2-4, 1990.

19. Dat, R. "Development of the Basic Methods Needed to Predict the Aeroelastic Behavior of Helicopters", Rech. Aerosp. 1983-1.

20. Petot, D., "Differential Equation Modeling for Dynamic Stall", Rech. Aerosp. 1989-5.

21. Leishman, J.G., Crouse, Jr., G.L., "State-space Model for Unsteady Airfoil Behavior and Dynamic Stall", AIAA-89-1319.

22. Reddy, T.S.R., Kaza, K.R.V., "A Comparitive Study of Some Dynamic Stall Models", NASA TM 88917, 1987.

9 Autobiographies

9.1 J.J. Meijer

J.J. Meijer
Senior Research Engineer
Nationaal Lucht- en Ruimtevaartlaboratorium
National Aerospace Laboratory, NLR
Amsterdam, The Netherlands

Mr. Meijer received an "Ingenieur" degree in Aeronautical Engineering from Delft Technological University in 1968. Upon graduation he performed two years of postgraduate studies on structural and aeroelastic subjects. In 1970 he joined the Department of Aeroelasticity at the National Aerospace Laboratory. Since that time he is responsible for the development of computer codes for dynamic response and flutter calculations. He was involved in the flutter clearance and dynamic responses during store releases of the Northrop NF-5 aircraft. In 1976/1977 he participated in a F-16 ride quality study (carried out under contract for General Dynamics) where he was responsible for the aeroelastic modeling and calculations. In the period 1980 up to 1984 he was involved in a flutter study of a wind tunnel model of a supercritical transport type wing. From 1984 up to 1989 he was also involved in the aeroelastic modeling of a rotary-wing system, applied to wind energy converters. Since 1984, he is responsible as a project leader for the flutter clearance of new F-16 configurations and the development of new techniques to investigate aeroelastic matters of fighter aircraft. Recently, he participates in an aeroelastic study of limit cycle oscillations of fighter aircraft (partly under contract for General Dynamics).
Professional society: Member AIAA.

9.2 A.M. Cunningham, Jr.

A.M. Cunningham, Jr.
Engineering Staff Specialist
General Dynamics Fort Worth Division
Fort Worth, Texas

Ph.D. - Mechanical Engineering, University of Texas at Austin, 1966
M.S. - Mechanical Engineering, University of Texas at Austin, 1963
B.S. - Mechanical Engineering, University of Texas at Austin, 1961

Dr. Cunningham has worked at General Dynamics Fort Worth Division since 1965 and is currently a member of the Aerospace Technology Staff. He worked in the Computational Fluid Dynamics Group of Aerospace Technology from 1983 to 1989 and in the Aeroanalysis Group of Aerospace Technology from 1979 to 1983. Prior to that he worked in the Structural Dynamics Group of Airframe and Structures Technology.

In the Aeroanalysis Group, Dr. Cunningham has conducted many studies leading to developments in the area of analytically predicting aerodynamic characteristics of various configurations in subsonic, transonic, and supersonic flows as well as in high-angle-of-attack vortex flows. He was program manager for a contract in which he developed aerodynamic load prediction methods for bomber and logistic-type airplane wing tail loads.

Since 1983, Dr Cunningham has conducted basic investigation on the nature of unsteady separated flows associated with rapid aircraft maneuvers at very high angles of attack.

9.3 R.J. Zwaan

Head Department of Unsteady
Aerodynamics and Aeroelasticity
Nationaal Lucht- en Ruimtevaartlaboratorium
National Aerospace Laboratory, NLR
Amsterdam, The Netherlands

"Ingenieur" (M.S. equivalent) - Aeronautical Engineering, Delft University of Technology, 1962.

Mr. Zwaan has worked at NLR in the field of unsteady aerodynamics and aeroelasticity since 1960. He has conducted analytical studies in unsteady lifting surface methods and in aeroelastic characteristics of civil and fighter aircraft. He has contributed to several wind tunnnel tests concerning unsteady aerodynamic loads and flutter, and to flight tests with fighter aircraft. In 1979 he became head of the Department of Unsteady Aerodynamics and Aeroelasticity.

Since 1984, Mr Zwaan is part-time professor at the Delft University of Tech nology, where he gives courses on aircraft vibrations and aeroelasticity.

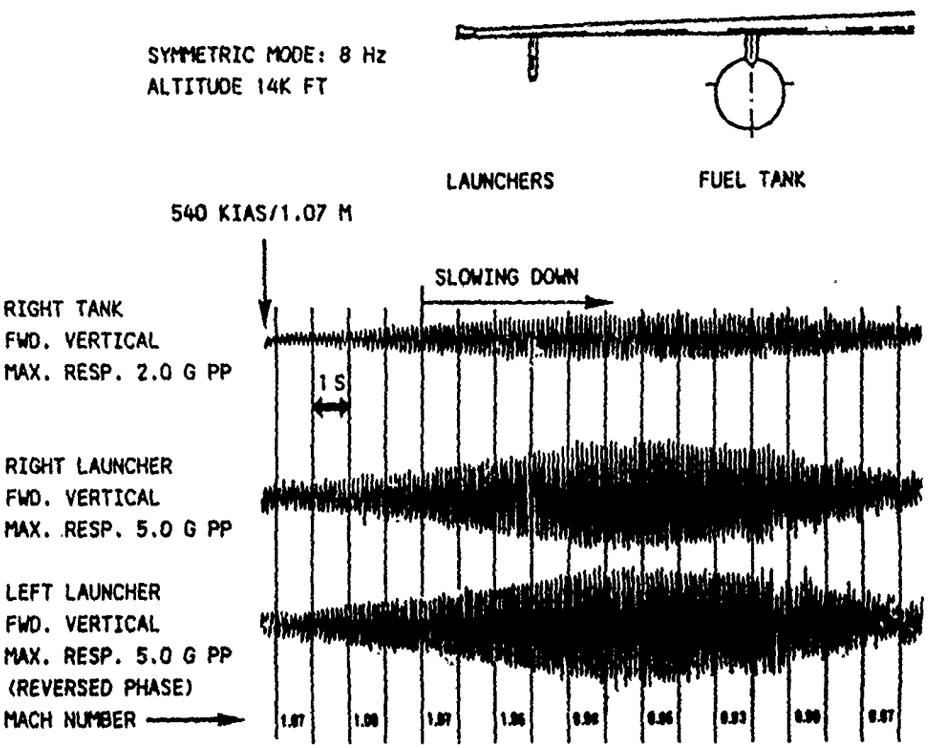

1. Recordings of accelerometers during flight flutter testing of fighter-type aircraft I.

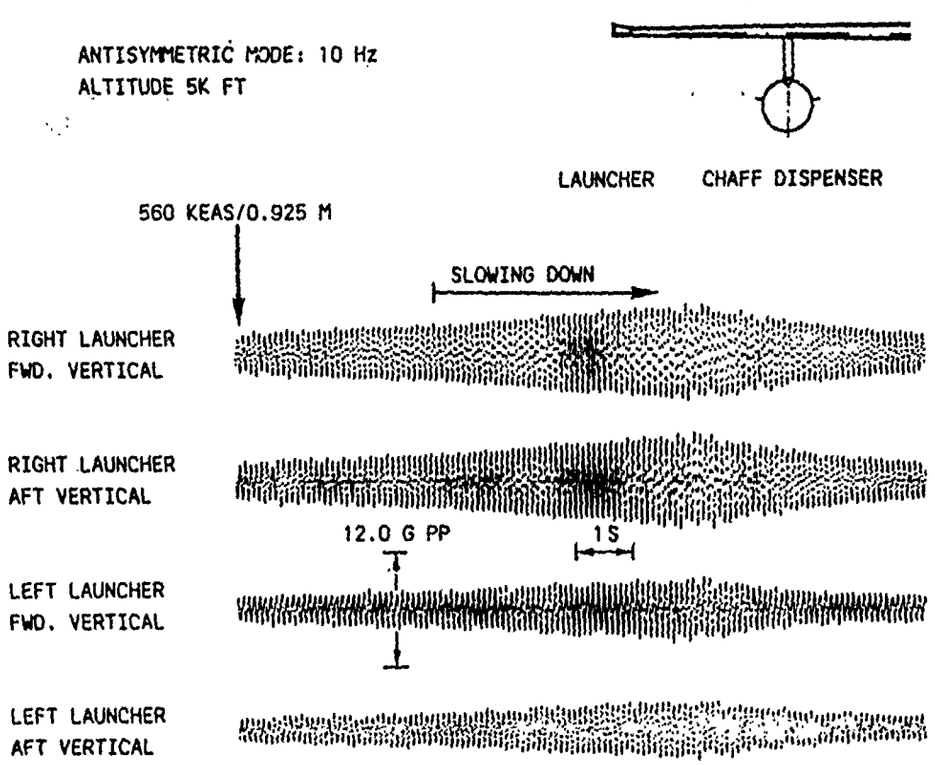

2. Recordings of accelerometers during flight flutter testing of fighter-type aircraft II.

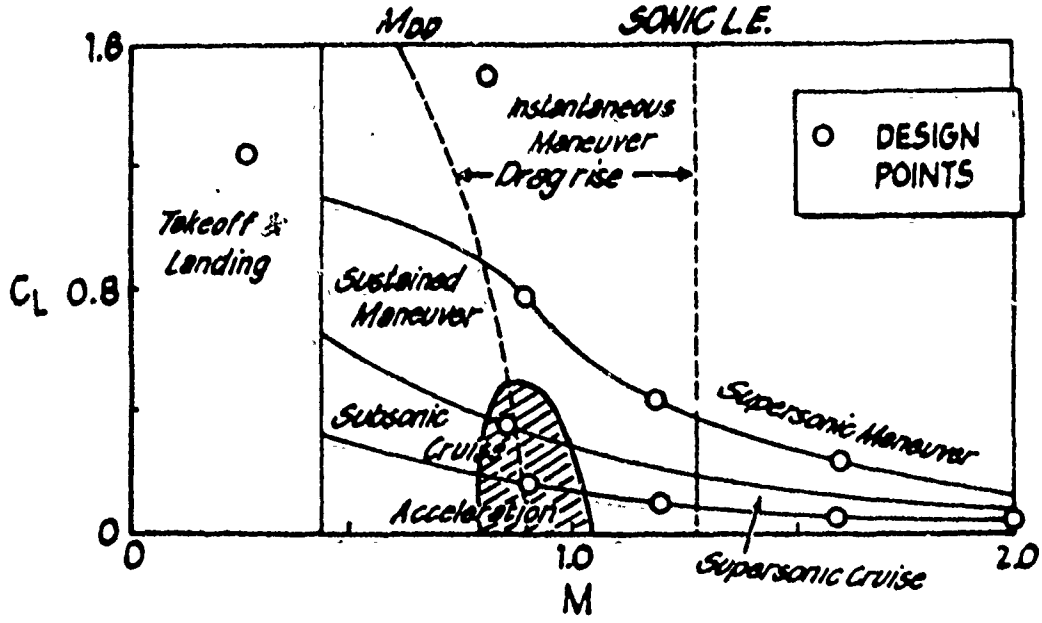

3. Typical performance map for fighter aircraft.

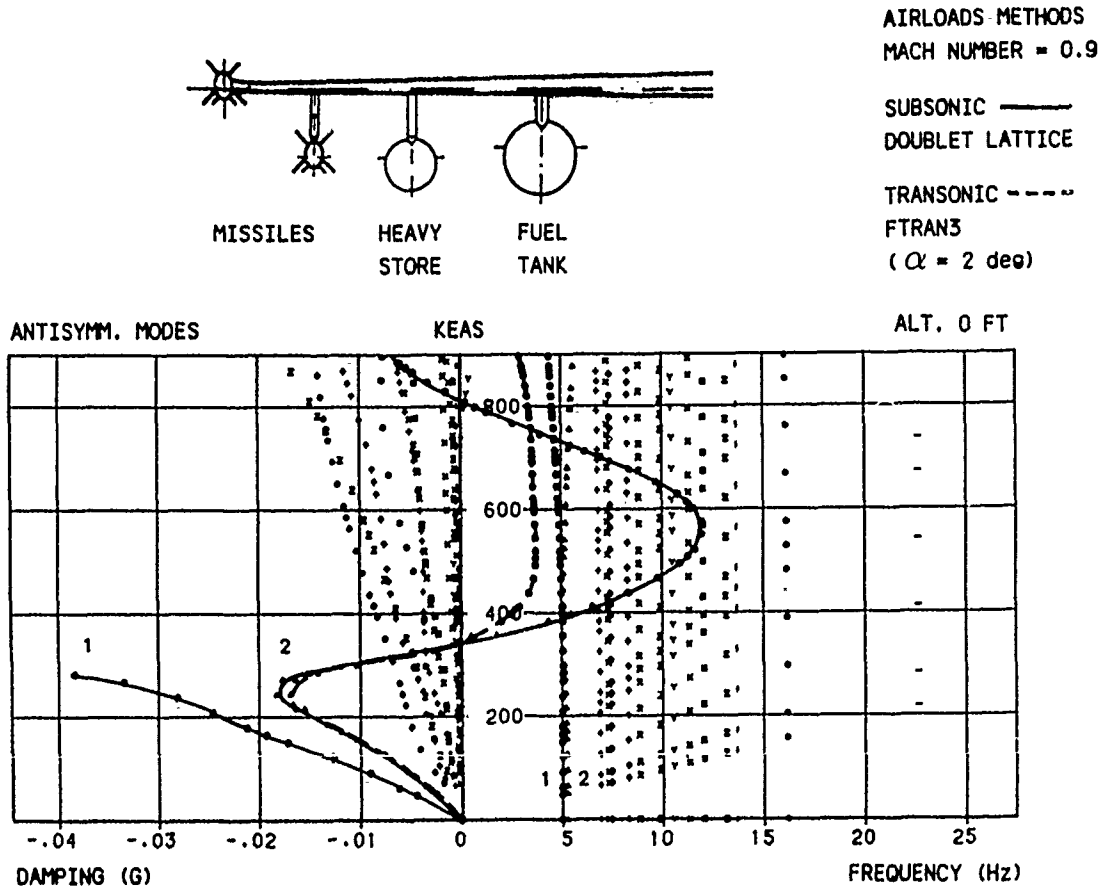

4. Example of calculated flutter characteristics with linear theory for fighter-type aircraft I.

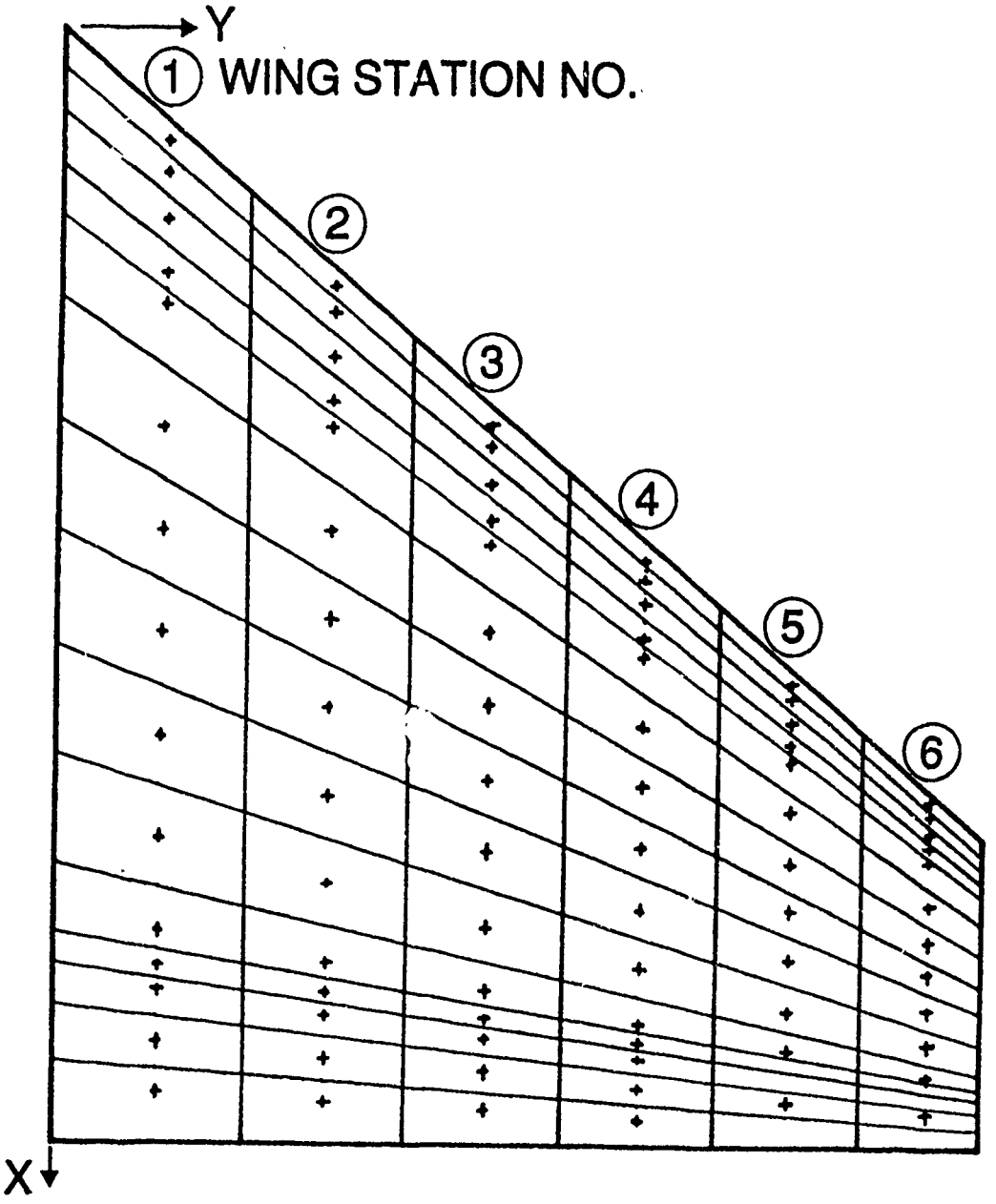

5. Location of pressure orifices and corresponding panels on the model wing planform.

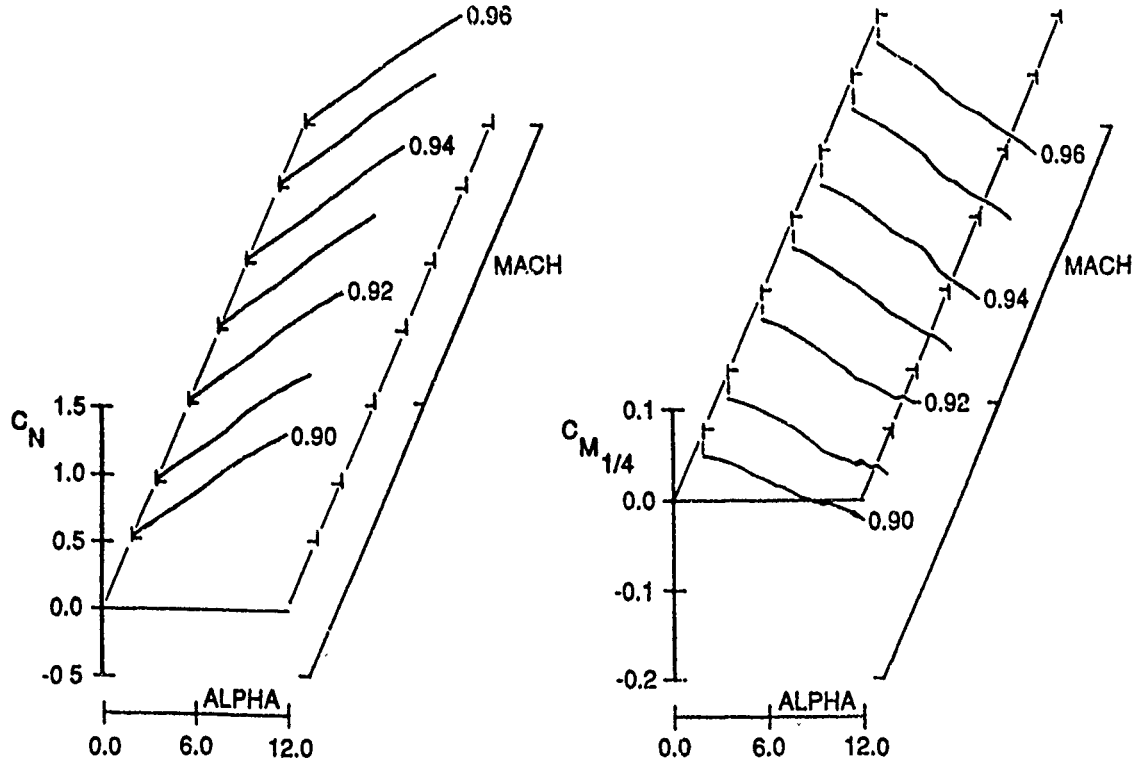

6. Steady lift and moment coefficients in station 1 as function of Mach number and angle of attack.

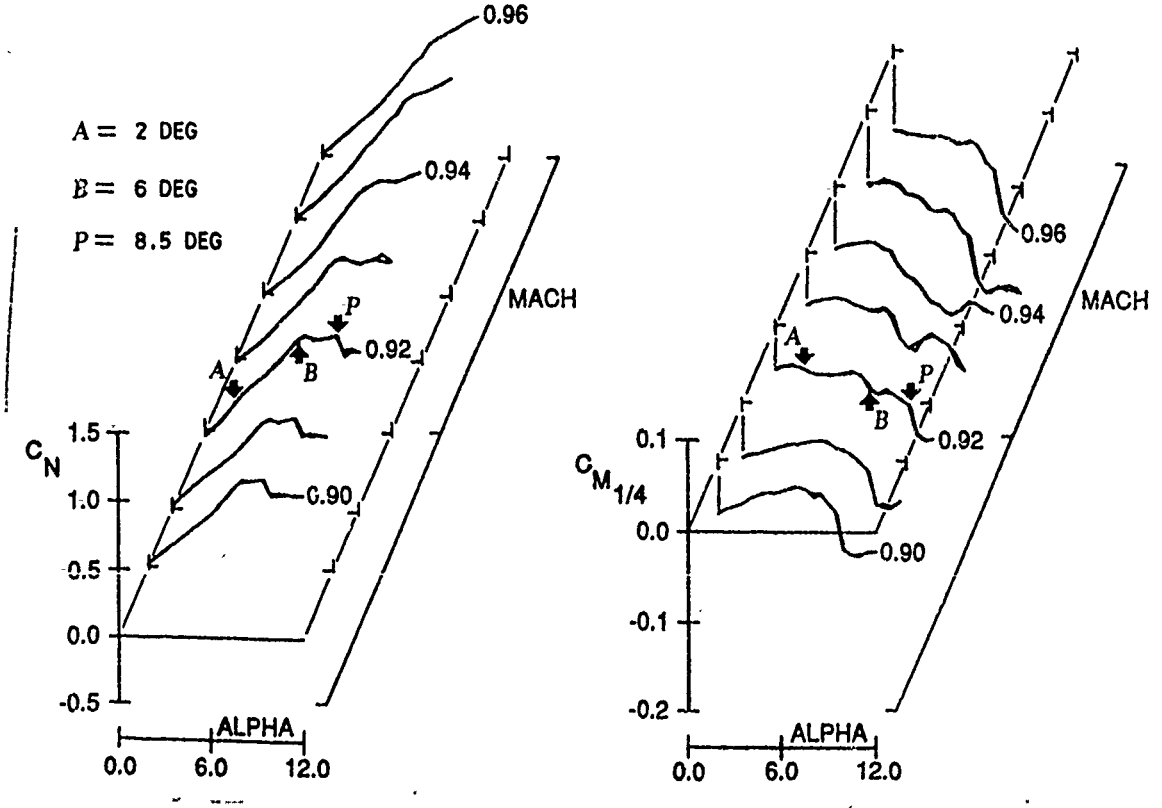

7. Steady lift and moment coefficients in station 6 as function of Mach number and angle of attack.

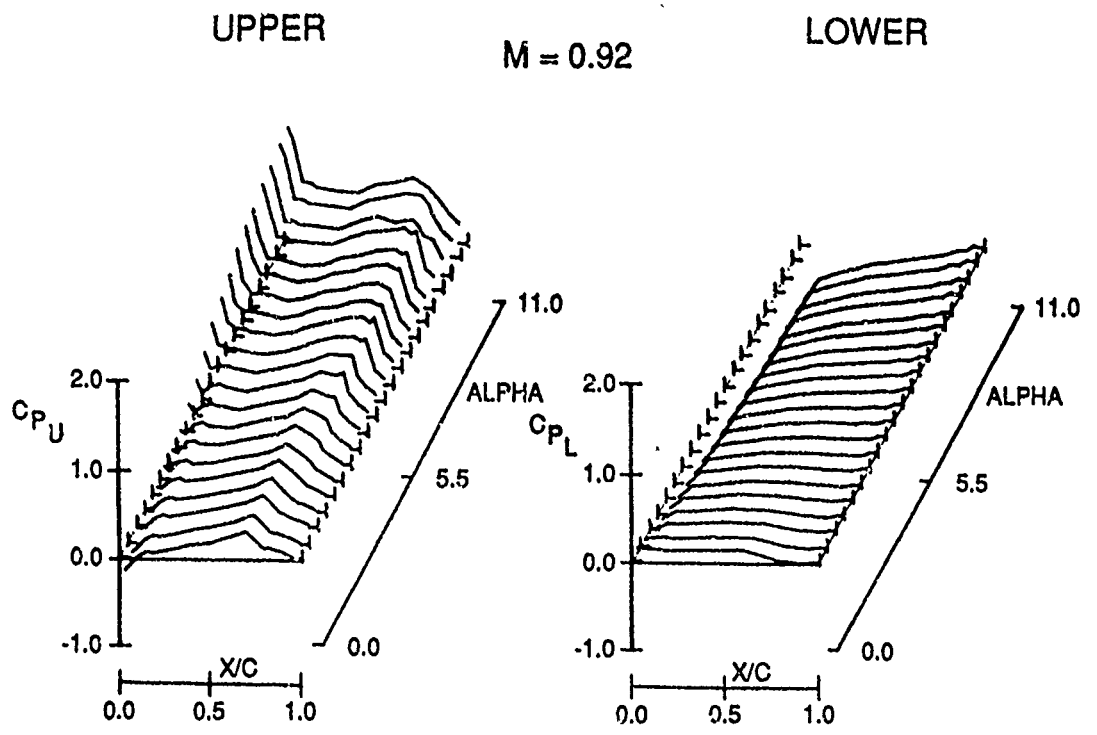

8. Steady pressure distributions in station 1 as function of angle of attack and constant Mach number (M = 0.92).

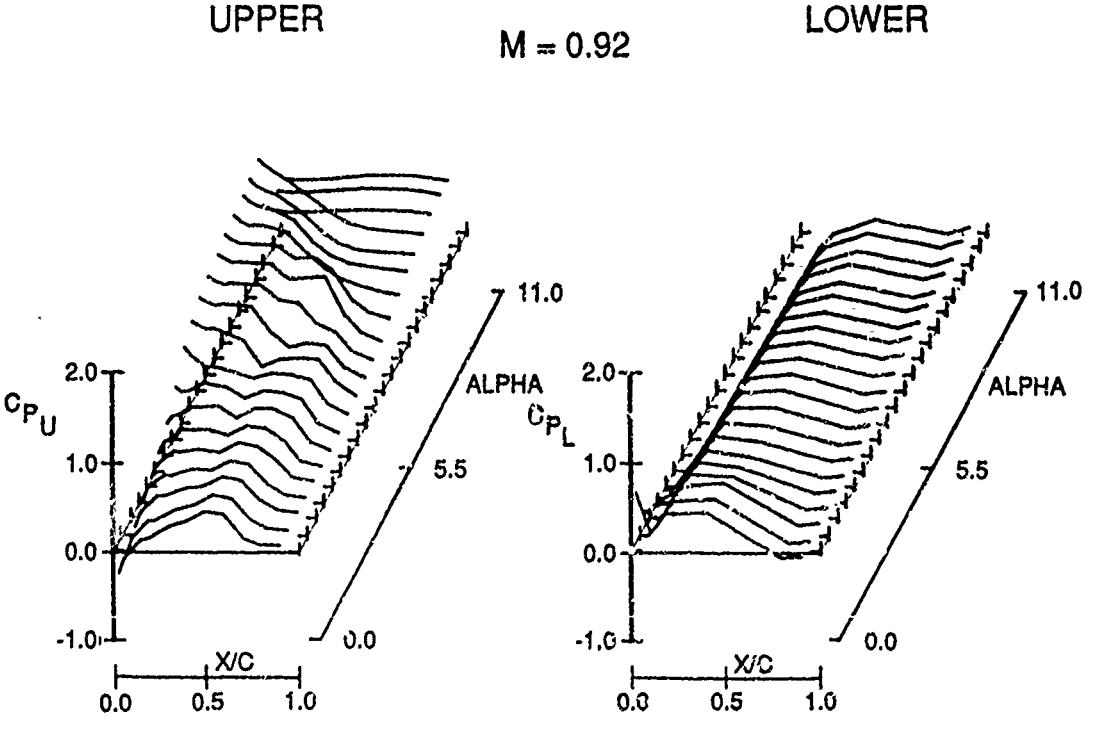

9. Steady pressure distributions in station 6 as function of angle of attack and constant Mach number (M = 0.92).

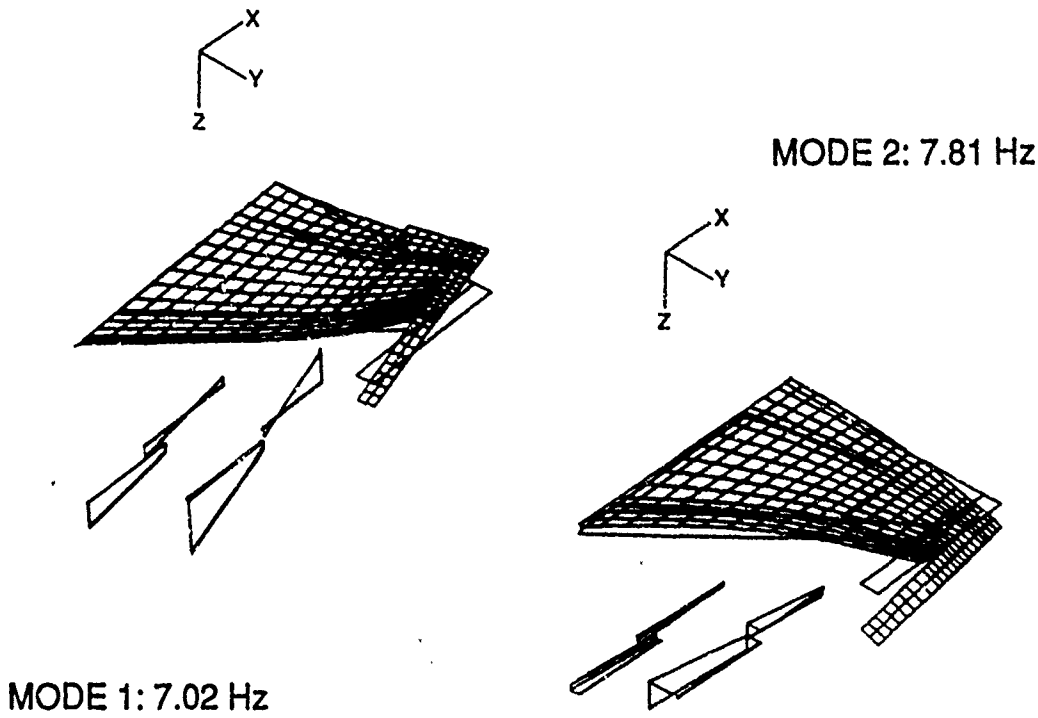

10. First two unrestrained vibration modes of generic model.

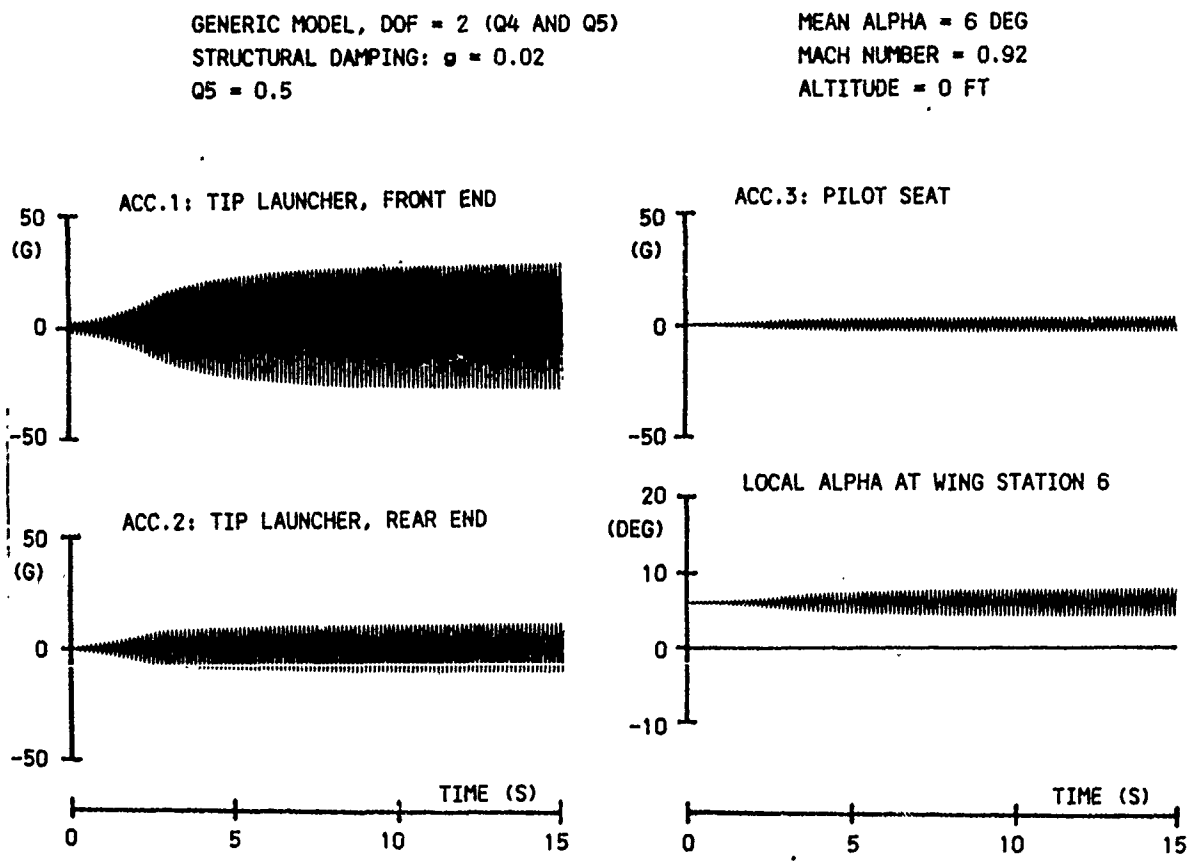

11. Response calculations for generic model; 2 DOF, M = 0.92, α= 6 deg, altitude = 0 ft, structural damping: g = 0.02

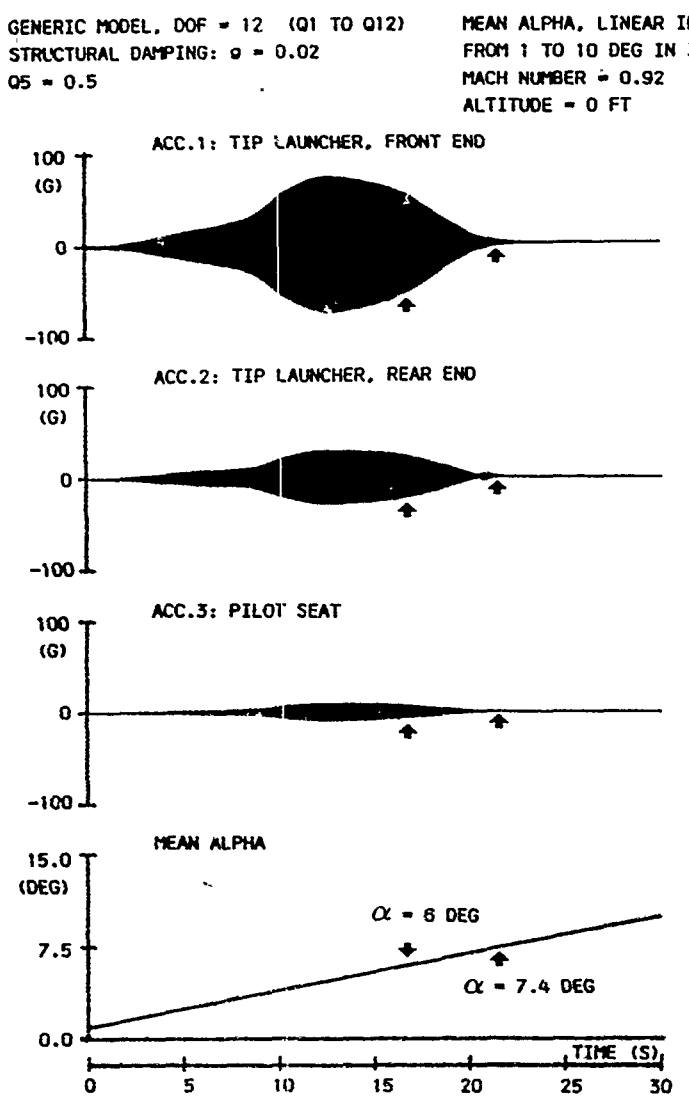

12. Response calculations for generic model; 12 DOF, M = 0.92, α variable, altitude = 0 ft, structural damping: g = 0.02.

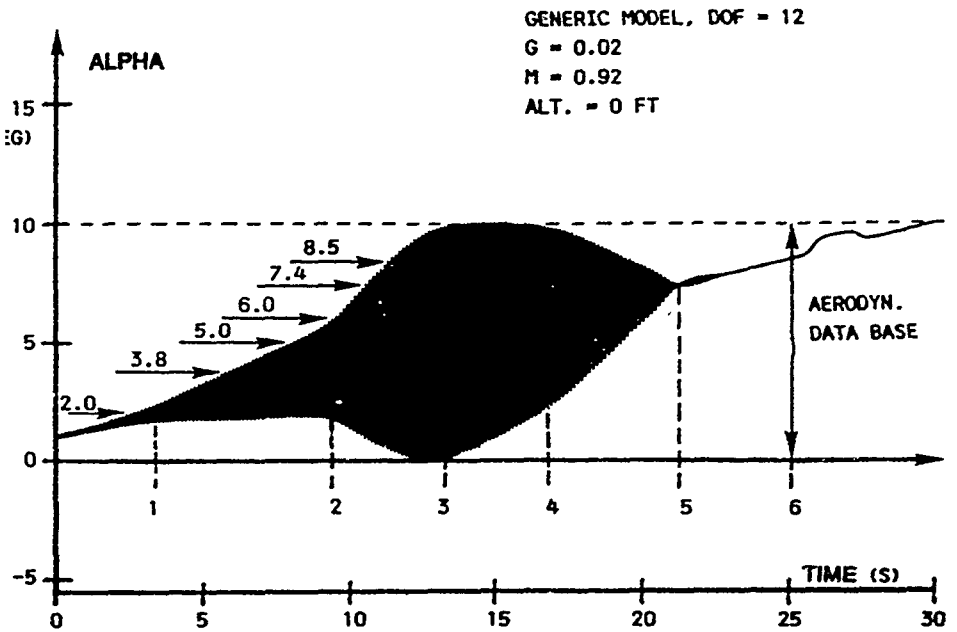

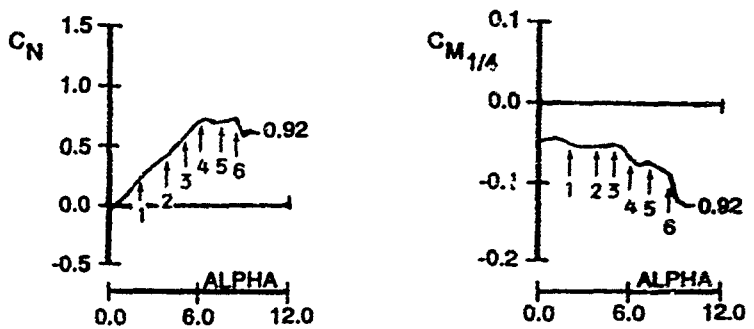

13. Local alpha and sectional aerodynamic coefficients at wing station 6

GENERIC MODEL, DOF = 12 (Q1 TO Q12)
STRUCTURAL DAMPING: g = 0.02
Q5 = 0.5

MEAN ALPHA, LINEAR INCREASE
FROM 1 TO 6 DEG IN 15 S
MACH NUMBER = 0.92
ALTITUDE = 0 FT

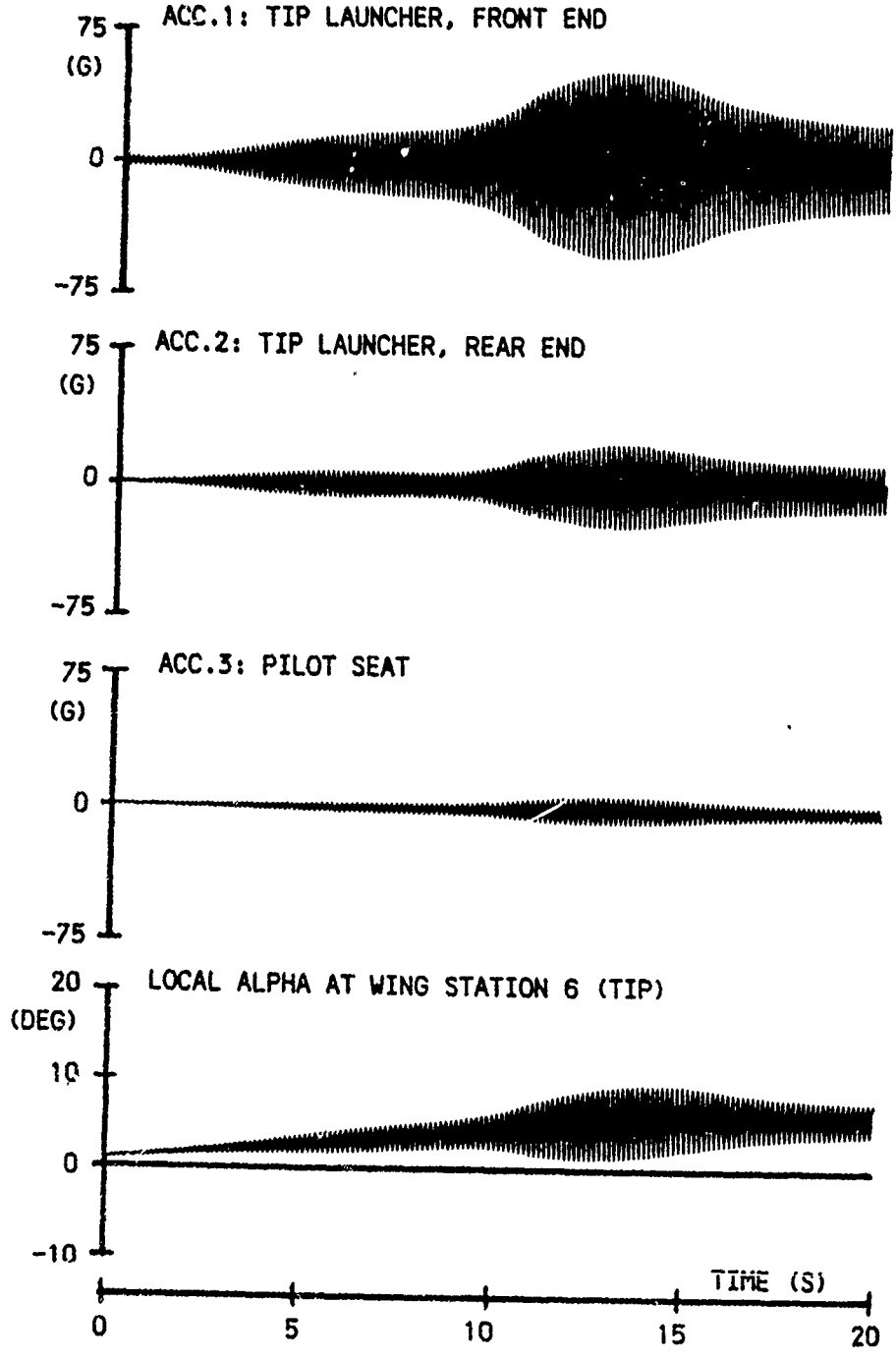

14. Response calculations for generic model; 12 DOF, M = 0.92, α variable, altitude = 0 ft, structural damping: g = 0.02.

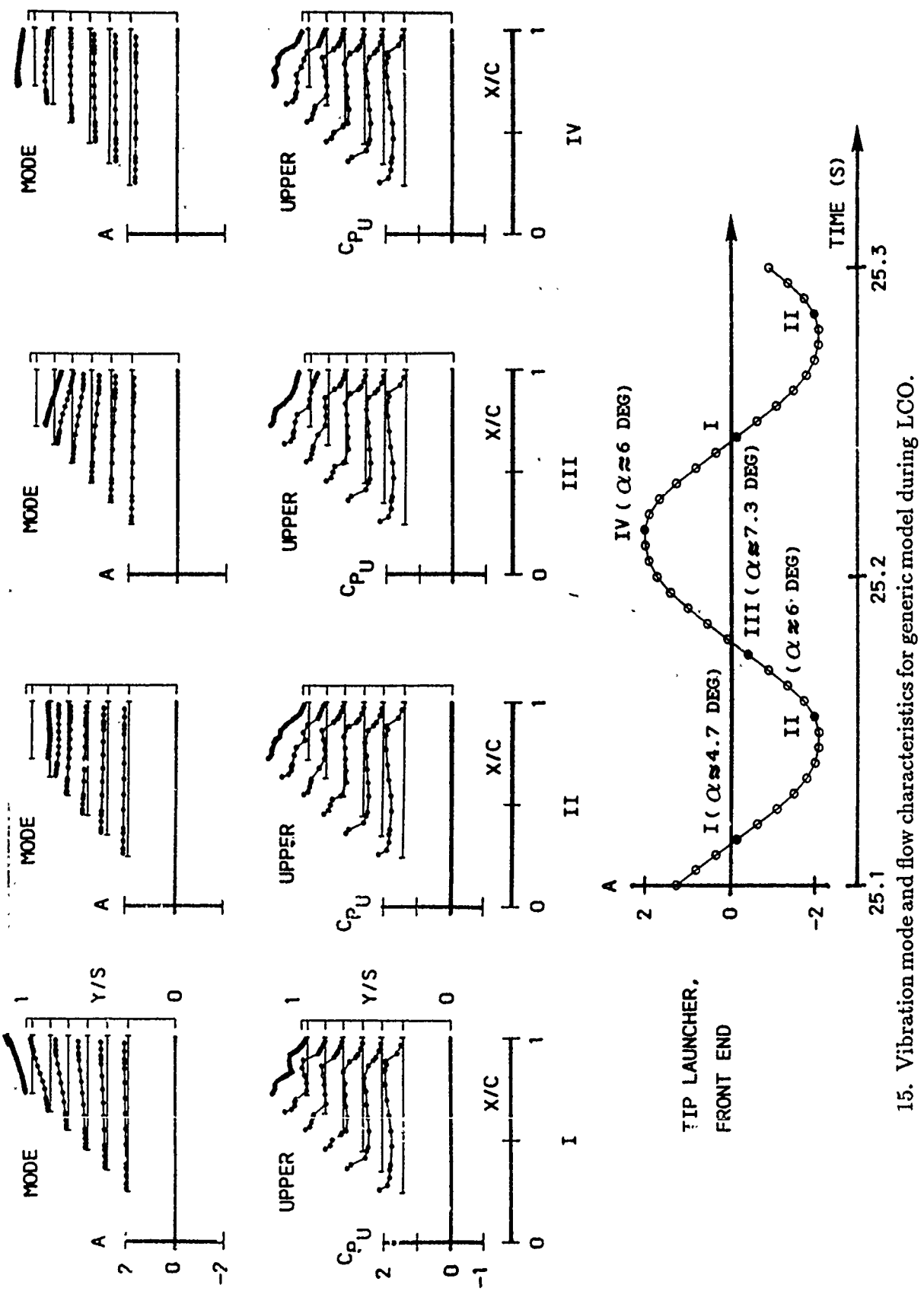

15. Vibration mode and flow characteristics for generic model during LCO.

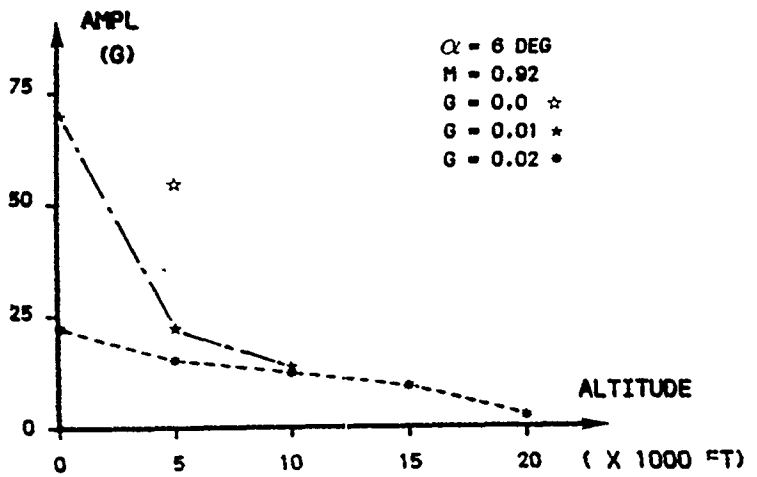

16a. Maximum LCO amplitude as function of altitude.

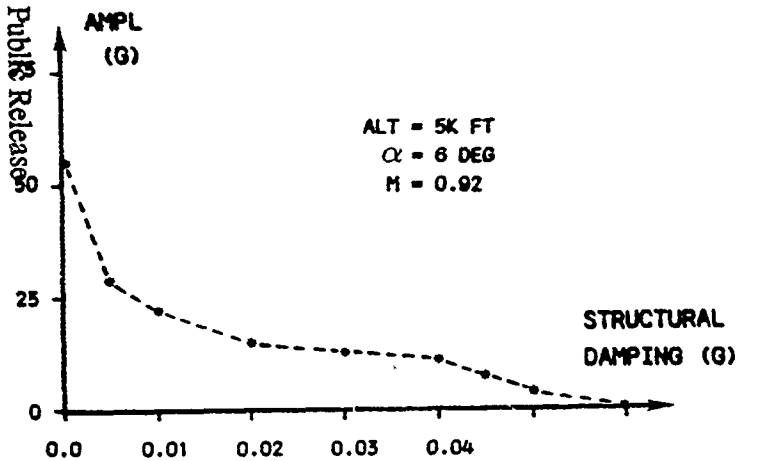

16b. Maximum LCO amplitude as function of structural damping.

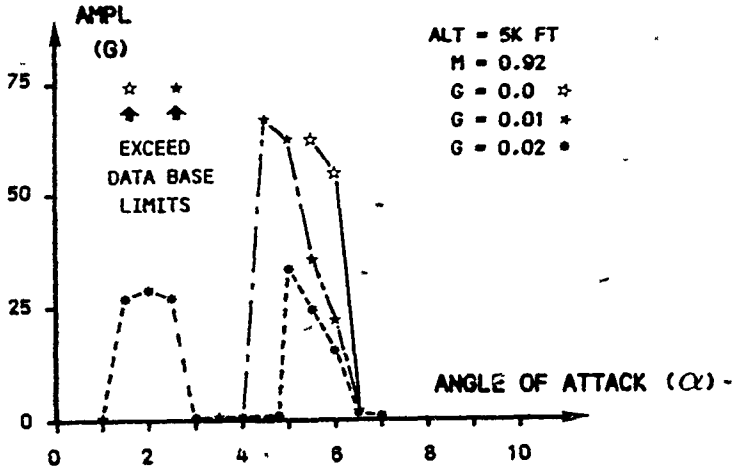

16c. Maximum LCO amplitude as function of angle of attack.

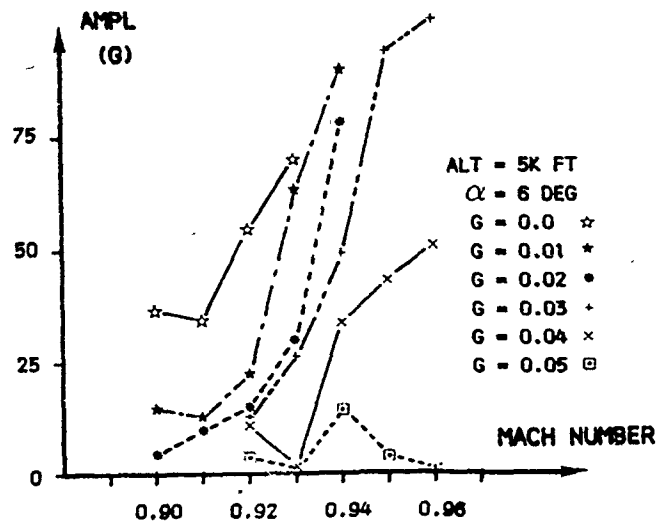

16d. Maximum LCO amplitude as function of Mach number.

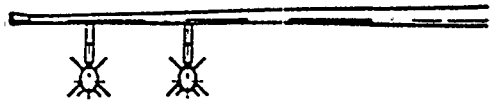

CONF.: A, DOF = 12
MEAN ALPHA = 6 DEG
M = 0.92, ALT. = 5K FT

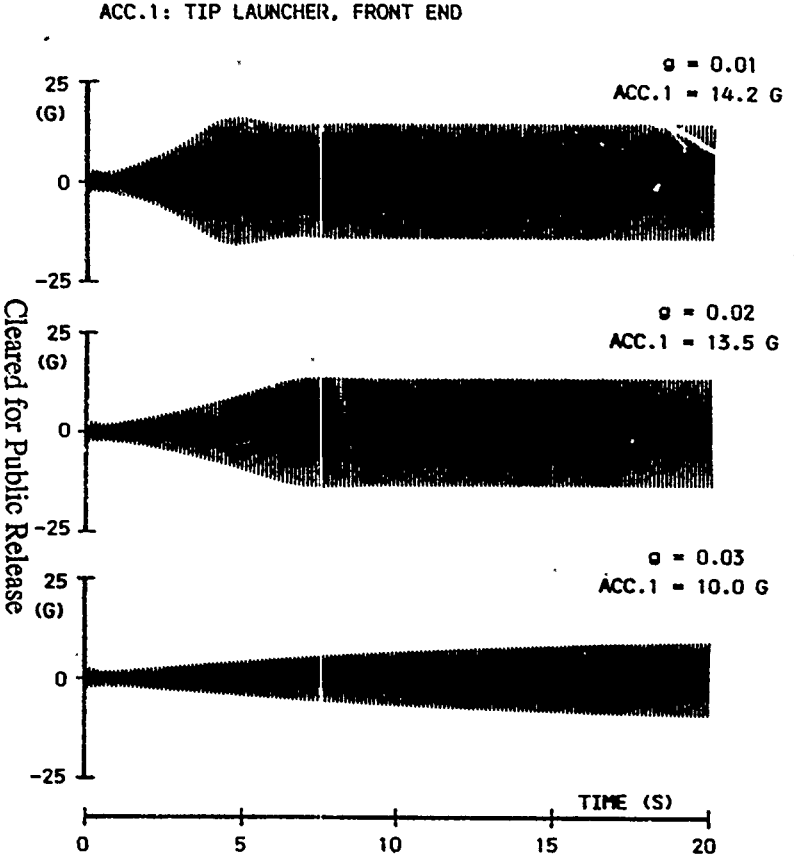

17. Response calculations for configuration A; 12 DOF, M = 0.92, $\alpha = 6$ deg, altitude = 5K ft, structural damping variable.

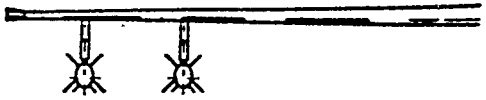

CONF.: A, DOF = 12
MEAN ALPHA = 2 DEG
M = 0.92, ALT. = 5K FT

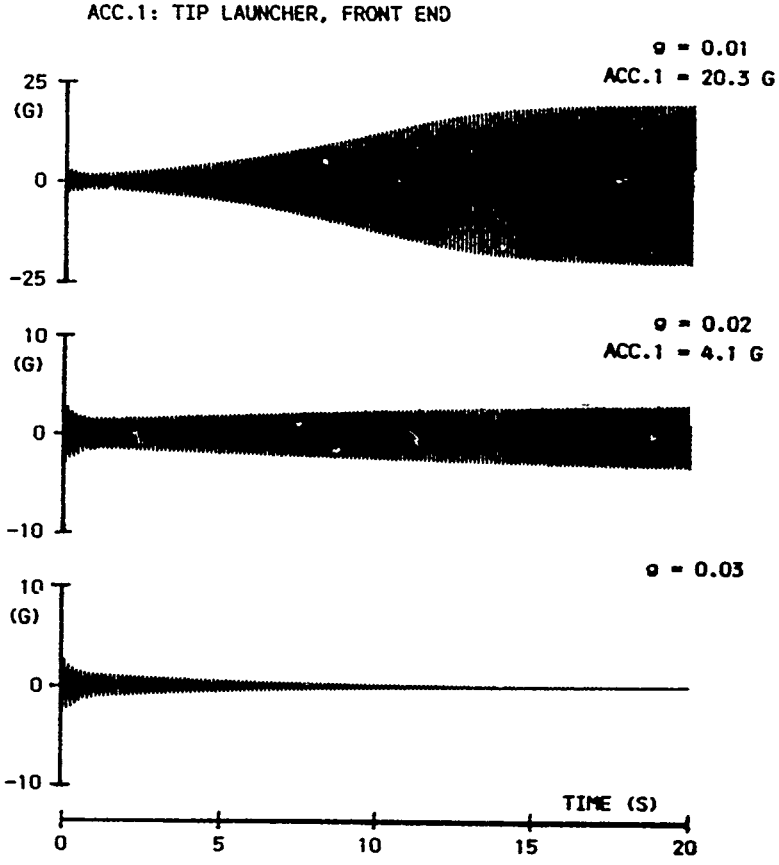

18. Response calculations for configuration A; 12 DOF, M = 0.92, $\alpha = 2$ deg, altitude = 5K ft, structural damping variable.

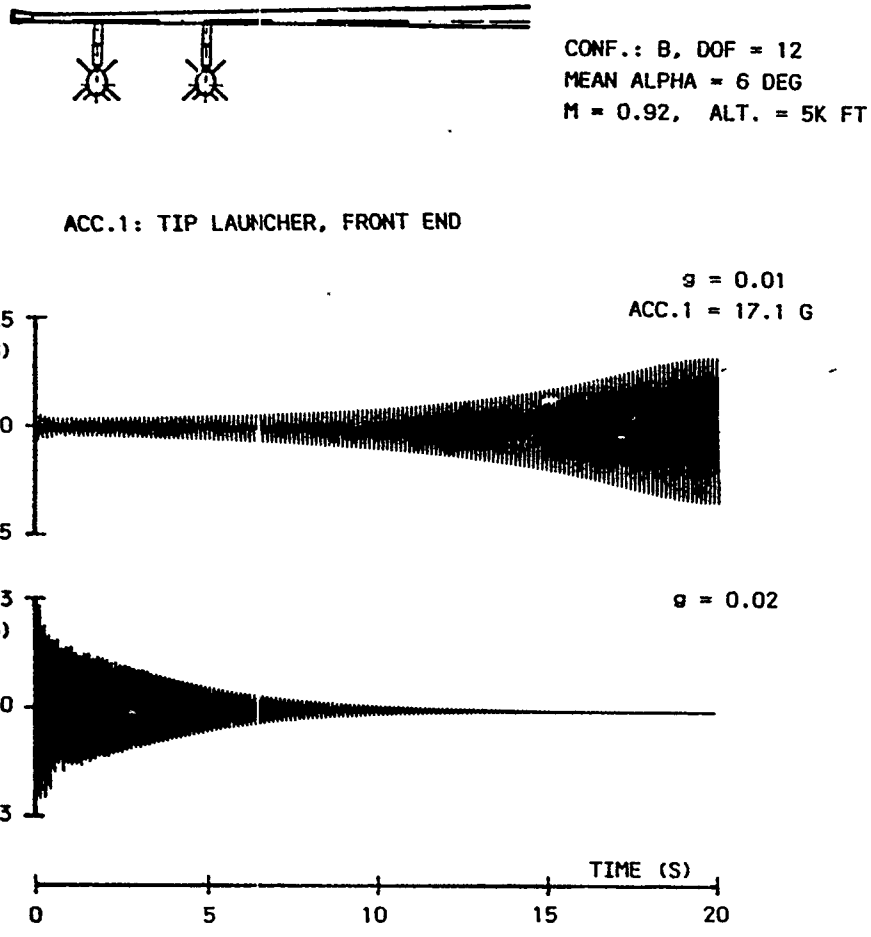

19. Response calculations for configuration B; 12 DOF, M = 0.92, $\alpha = 6$ deg, altitude = 5K ft, structural damping variable.

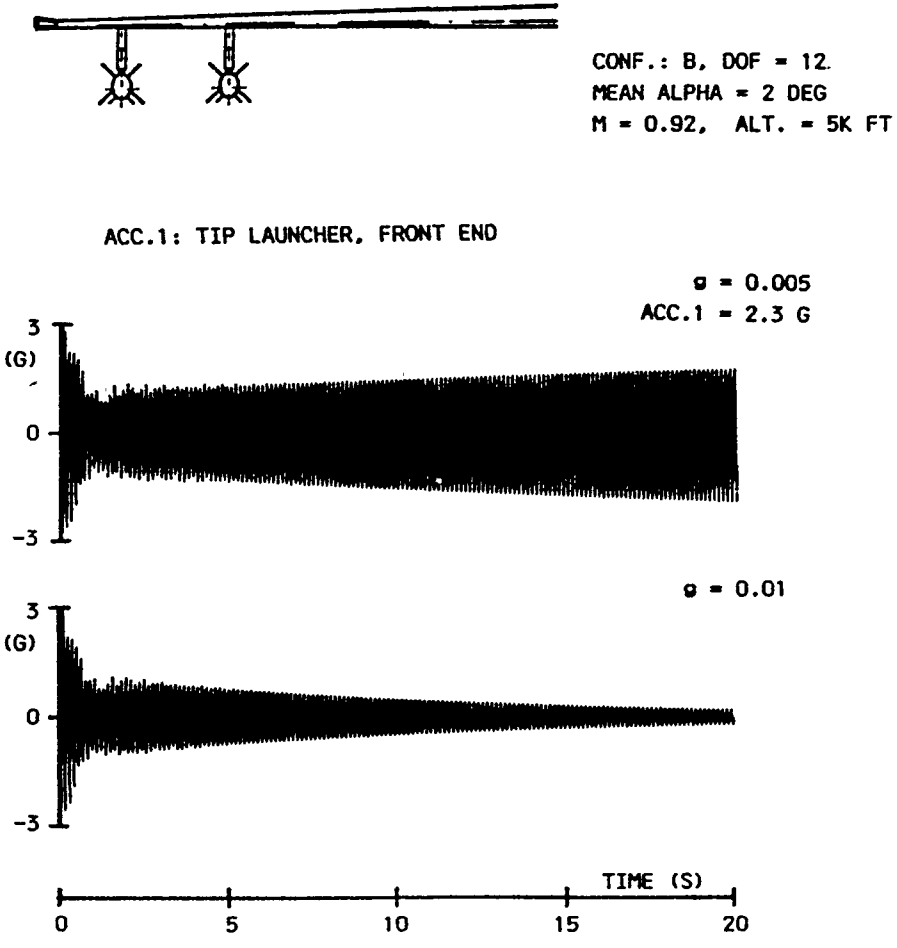

20. Response calculations for configuration B; 12 DOF, M = 0.92, $\alpha = 2$ deg, altitude = 5K ft, structural damping variable.

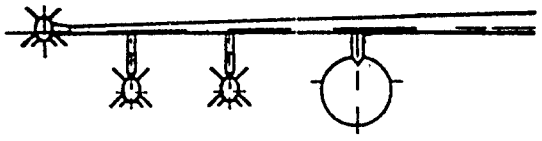

CONF.: C, DOF = 17
MEAN ALPHA, LINEAR INCREASE
FROM 1 TO 6 DEG IN 15 S,
THEN CONSTANT
M = 0.92, ALTITUDE = 5K FT
g = 0.01

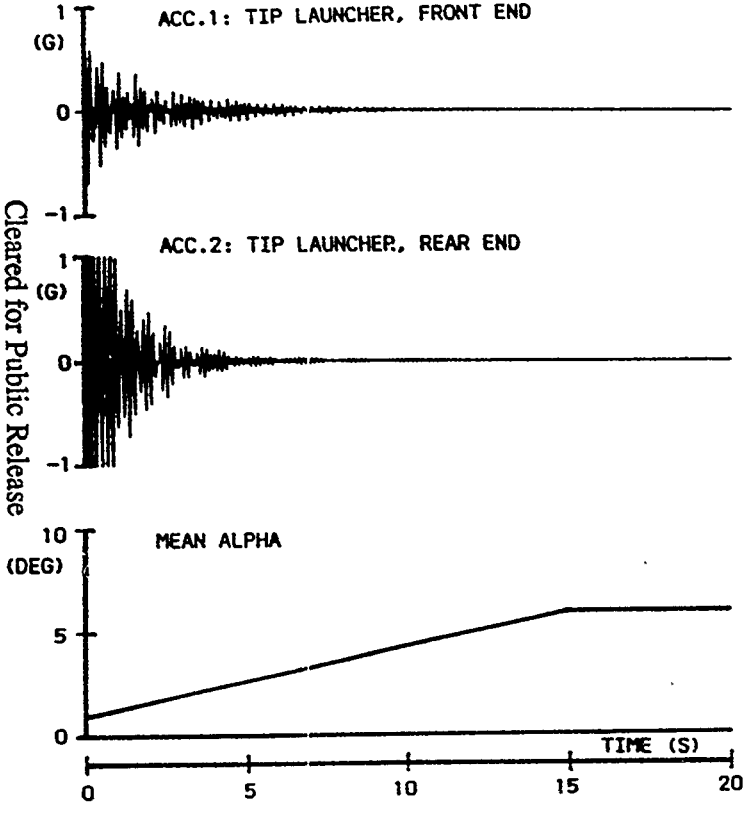

21. Response calculations for configuration C; 17 DOF, M = 0.92, α-variable, altitude = 5K ft, structural damping: g = 0.01.

CONF.: J, DOF = 20
MEAN ALPHA = 6 DEG
M = 0.92, ALT. = 5K FT
g = 0.01

TK FULL : NO LCO
TK EMPTY: NO LCO

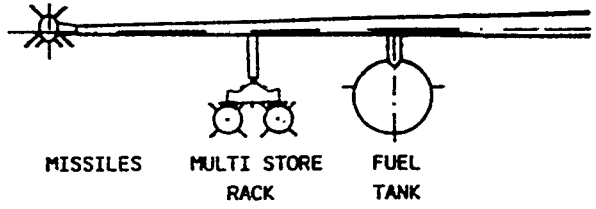

CONF.: D.1, DOF = 16
TK FULL : LCO (ACC.1 = 16 G)
TK EMPTY: NO LCO

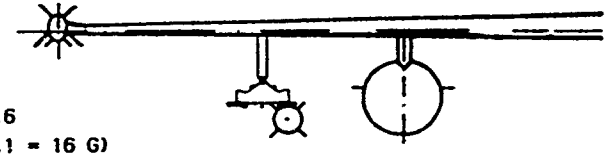

CONF.: D.2, DOF = 18
TK FULL : NO LCO
TK EMPTY: NO LCO

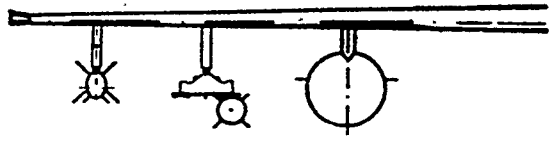

CONF.: D.3, DOF = 14
TK FULL : LCO SENSITIVE
TK EMPTY: NO LCO

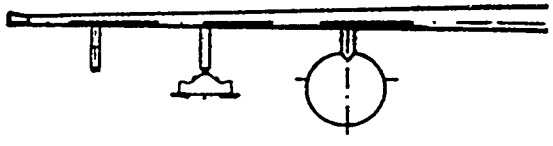

22. Results of responses for configuration D and downloadings; M = 0.92, altitude = 5K ft, structural damping: g = 0.01.

LCO configuration (oscillating outboard wing)

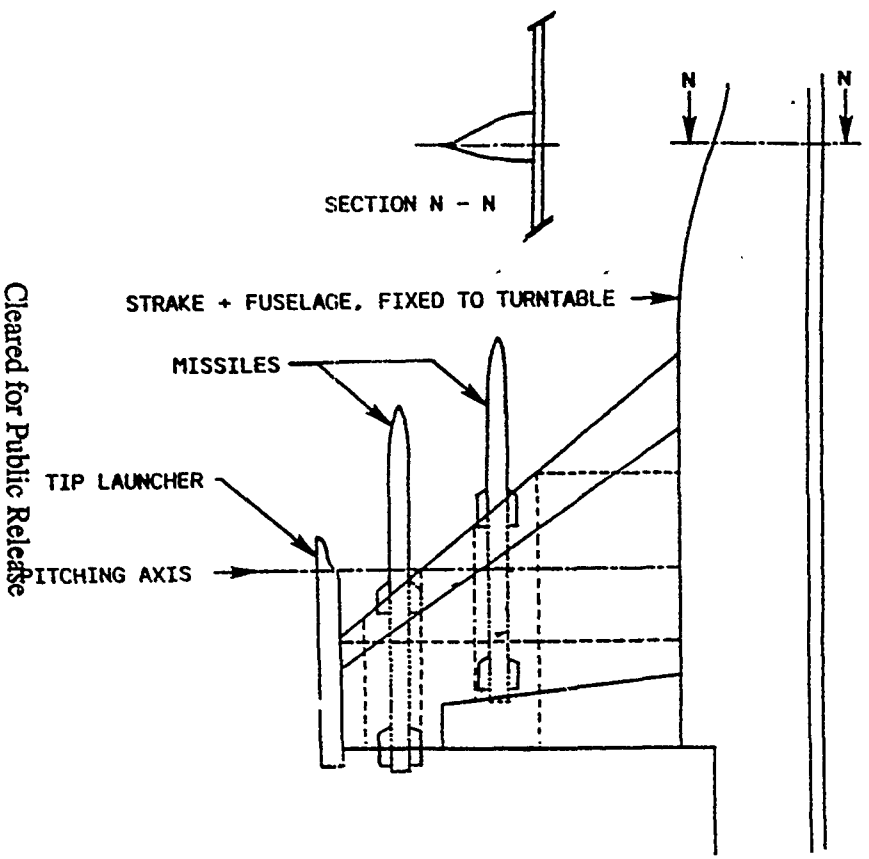

23. Wind tunnel model of fighter type wing for LCO investigation.

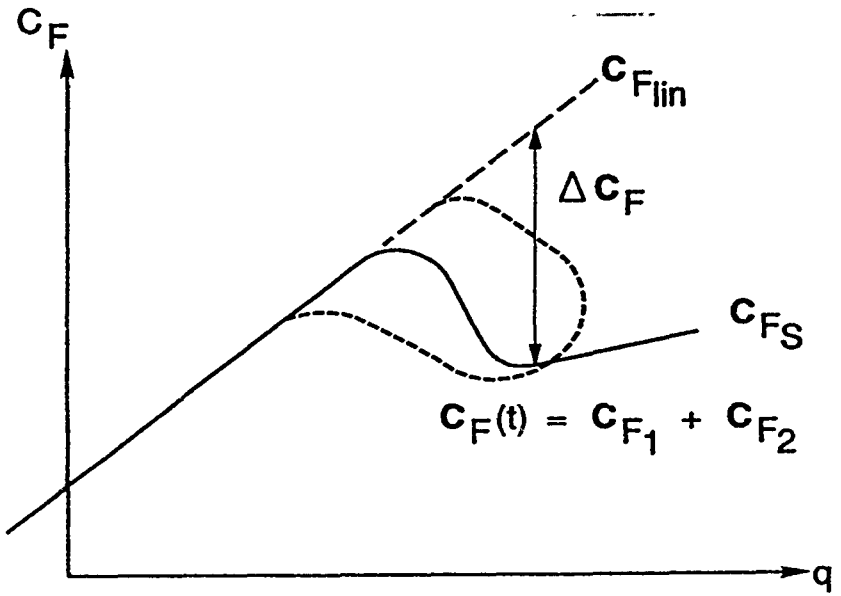

$$C_F = C_{F_1} + C_{F_2}$$

$$\dot{C}_{F_1} + a_1 C_{F_1} = f_1 (q, \dot{q}, \ddot{q})$$

$$\ddot{C}_{F_2} + a_2 \dot{C}_{F_2} + a_3 C_{F_2} = f_2 (q, \dot{q}, \ddot{q}, \Delta C_F)$$

24. Generalized "ONERA" dynamic stall model.

AMRAAM VIBRATION SPECTRUM DEFINITION USING FLIGHT TEST DATA

BY

William O. Dreadin

Orlando Technology, Incorporated

CLEARED FOR PUBLIC RELEASE

ABSTRACT

Since the AMRAAM missile was fielded there have been requirements for missile improvements. These requirements have dictated the need for a better definition of the qualification vibration spectrum and test durations to be employed in ground tests. Most recently, spectrum tailoring was accomplished using flight test data representing real world conditions of the AMRAAM on the F-15 during air combat maneuvering (ACM).

INTRODUCTION

This paper documents the findings of an effort which was undertaken to employ test data to improve the specification of vibration test levels and durations for AMRAAM qualification testing. The intent was to assure more realistic test levels and durations for lot acceptance and missile improvement programs. Hundreds of missions of flight test data were used to develop a basis on which vibration spectrum level and test duration could be defined.

Power spectral density profiles from instrumented measurement vehicle (IMV) flights on a variety of aircraft were employed to determine that the F-15 introduces the most severe vibration environment during the mission segment labeled air combat maneuvering (ACM).

Structural data recorders in the F-15 fleet are monitored by the logistics command and the aircraft prime manufacturer for fatigue history studies. This recorded data was one primary source used to define the "typical" mission profile by investigating parameters such as total length of a mission, altitude, mach, angle of attack, accelerations, and the number and type of maneuvers in each mission. For our purposes the "average or typical" intercept mission was defined in 3 segments. The three segments being: 1) taxi/takeoff/and cruise to target area 2) ACM 3) return to base and land.

Another primary source of data used to enhance the definition of the ACM portion of an intercept mission was flight test data from Red Flag (simulated air combat) exercises.

IMV response stripouts were used to help establish parameter interactions and define maneuvers based on test data so that computer codes could be written for data sorting. The number and duration of exposures to wind-up-turns, accels-delcel's, loaded turns, etc. were established from these data. Using the definition of a "typical" mission and the spectral content of mission segments allowed qualification test levels and durations to be defined in concert with the desired missile life cycle.

THE DATA ANALYSES

When it was first decided that refinement of the vibration test spectrum was needed to meet the objective of the missile improvement program, a major search for technical information was begun. Reviews of data from sidewinder and sparrow test programs were undertaken. The prime aircraft manufacturers for the AMRAAM carriage platforms were contacted for data. Navy and Air Force tests agencies were contacted to gain the benefit of unique experiences and input they could contribute.

After reviewing flight test data from instrumented AMRAAM captive carriage vehicles on the F-14, F-15, F-16, and F-18 it was determined that the most severe and potentially damaging environment existed on the F-15. The literature search yielded a mission profile (Figure 1) which had been presented in the Naval Weapons Center report NWCTP6833. For the mission profile segments defined it was determined that test requirements could be satisfactorily defined for all segments except the ACM portion. During the ACM segment, particularly damaging phenomenon were being experienced on the F-15.

F-15 MISSION SEGMENTS

	Role	
	ACM Training	Alert Scramble
Percent of Missions	95	5
Mission Duration (min)		
Total Mission	≤80	≤80
Mission Segments		
1. Taxi	1-5	1
2. Takeoff	0.1	0.1
3. Climb	5	2
4. Cruise	10-20	5-20
5. Loiter/Vector	10-30	5-10
6. ACM*	5-10	5-20
7. Return to Base	10-20	5-20
8. Descend	7-8	7-8
9. Land	0.1	0.1
10. Park	1-5	1-5

* ACM is usually similar to TACTS/ACMI training missions. However, in about 10% of missions, ACMI will be conducted at altitudes well below the TACTS range floor (i.e., 300-5000 ft AGL).

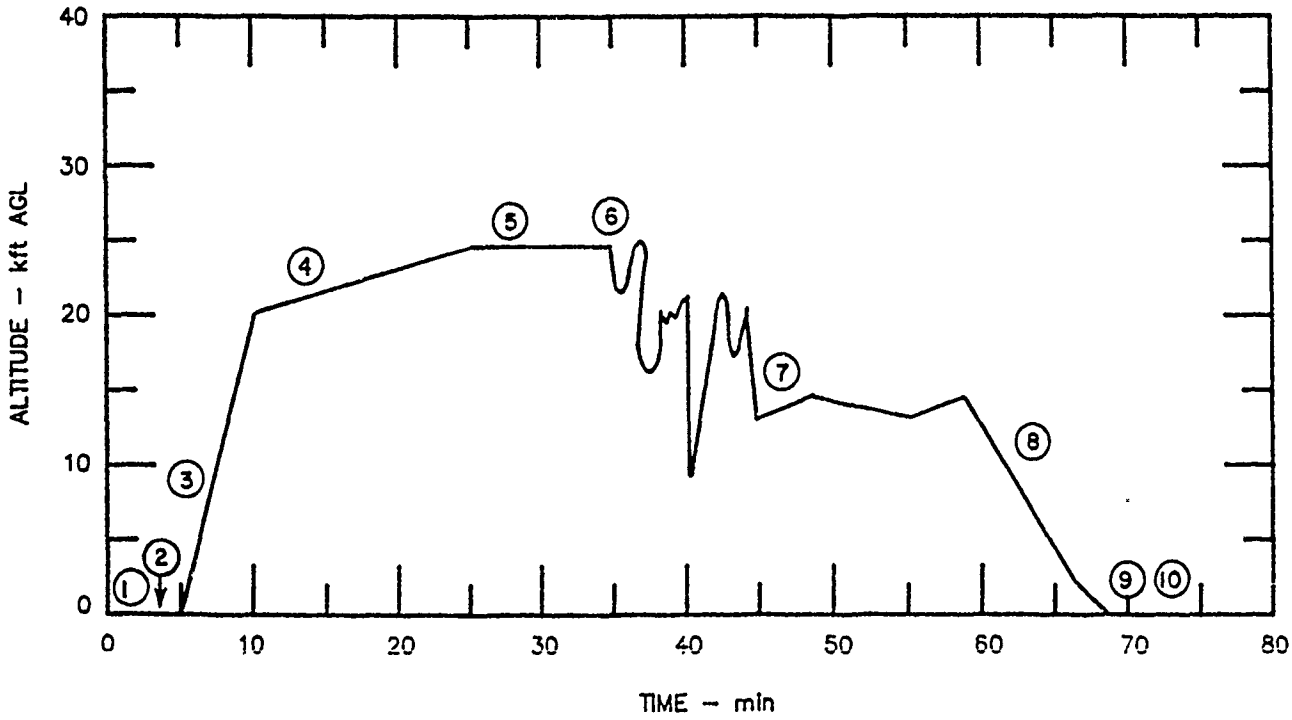

(N) Refer to the mission segments listed in the table above.

Figure 1

Aircraft buffet, extensive high g maneuvering, and throttle chops were cited as drivers in the vibration environment being experienced. A throttle chop is defined as a reduction in engine power which results in a severe oscillatory flow field near the engine inlet. This phenomenon particularly affects the fuselage mounted missiles.

Now our goal was to achieve a better definition of the ACM segment by gaining a better understanding of these three phenomonena.

Eglin AFB test data provided two primary pieces of information. First, vibration intensities under various flight conditions were defined as power spectral density records from instrumented AMRAAM flights. Dozens of flights had been analyzed with the AMRAAM/IMV on various stations on the aircraft and power spectral densities had become fairly well defined. Additionally, the test points were correlated with real time strip plots of aircraft and missile data to aid in the recognition of maneuvers. What we now wanted to accomplish was to define the number of events, the duration of exposure, and intensities experienced during ACM. An example of flight test points or a flight card is shown in Figure 2 with a portion of the corresponding strip chart data shown in Figure 3. A detailed study of similar data helped in the design of computer codes which had filters that could identify combinations of parameters which would indicate wind-up-turns, or throttle chops, or other maneuvers of interest.

Pilot interviews were conducted early in the process and provided the following content for the ACM segment:

1. Maneuvering from 5,000 feet to 25,000 feet at military power
2. Continuous hard break turns of 6-7 g's with occasional spikes to 9 g's

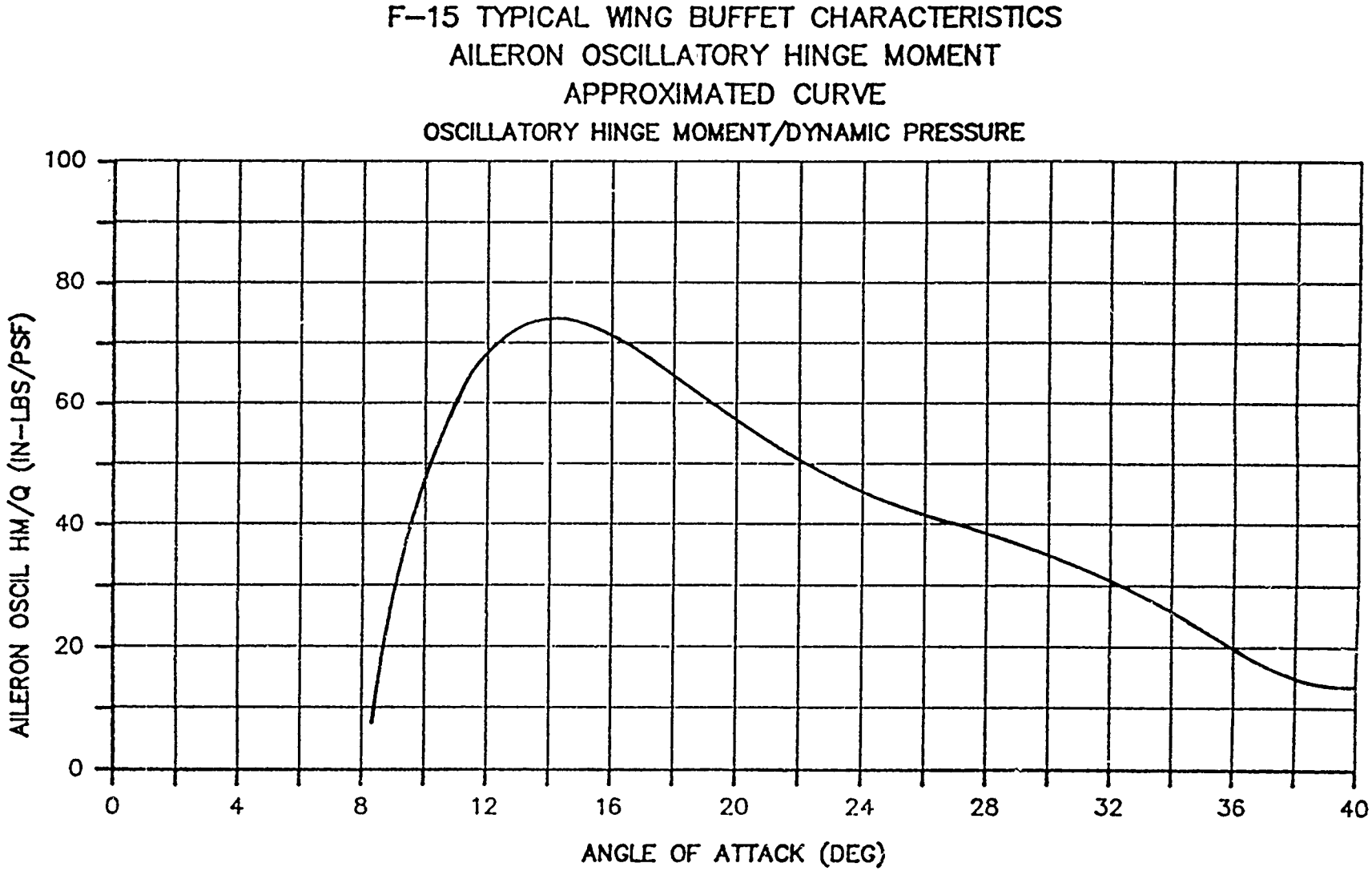
F–15 TYPICAL WING BUFFET CHARACTERISTICS
AILERON OSCILLATORY HINGE MOMENT
APPROXIMATED CURVE
OSCILLATORY HINGE MOMENT/DYNAMIC PRESSURE
AILERON OSCIL HM/Q (IN-LBS/PSF)
100
80
60
40
20
0
0
4
8
12
16
20
24
28
32
36
40
ANGLE OF ATTACK (DEG)

Figure 2

F-15E BUFFET INTENSITY

Nz = 6

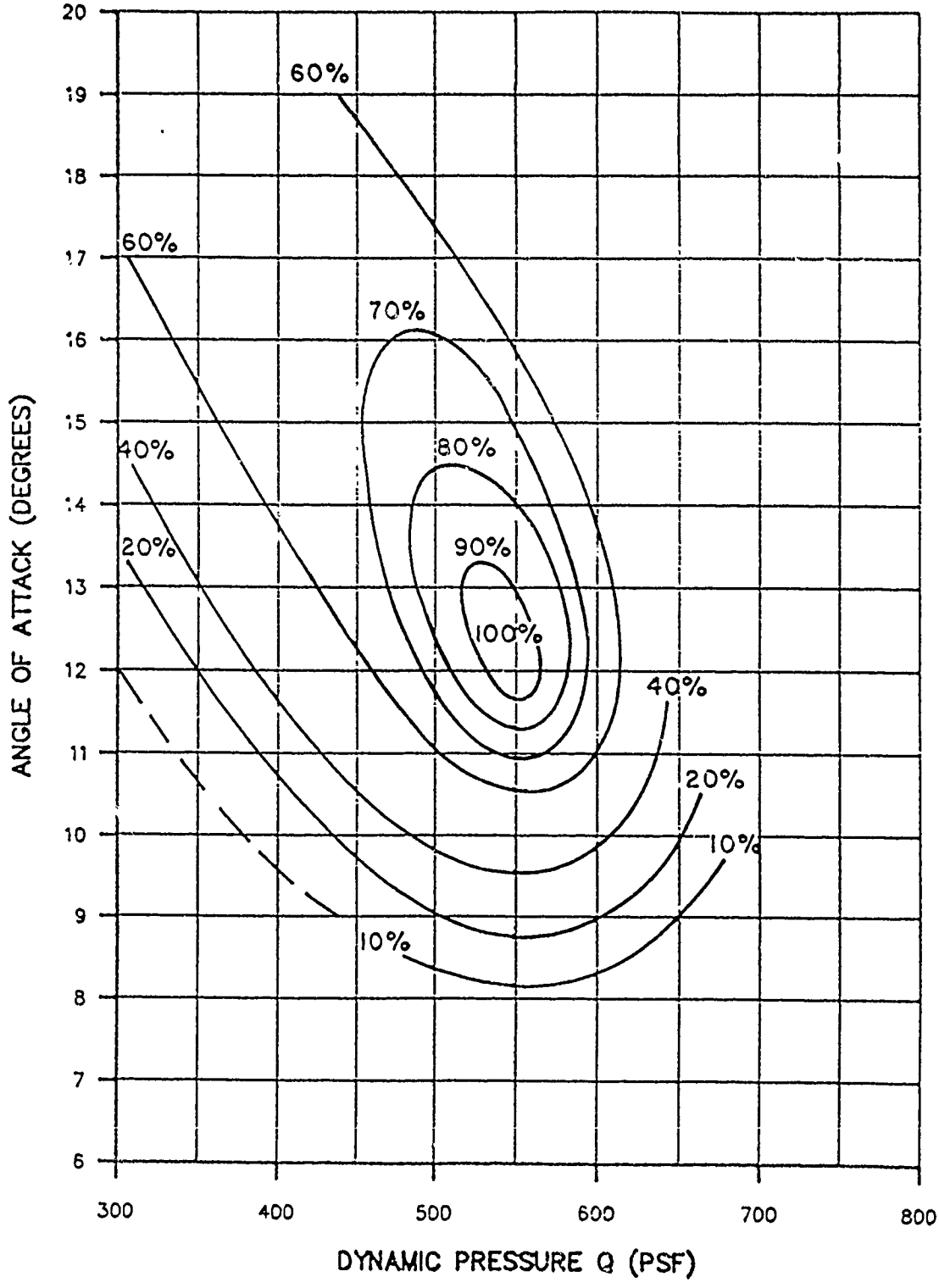

Figure 3

3. Not uncommon to feel aircraft buffet for up to 2 minutes continuously.

4. The duration of ACM per mission is about 20 minutes

It was not immediately obvious, but subsequent analysis of data showed that what the pilot perceives and definitions that engineers typically apply are not totally coincident. In particular in no case in the data did we see where the aircraft was exposed to buffet for durations approaching 2 minutes. The engineering definition of wing buffet is a resonant oscillatory condition which, unlike flutter, is not immediately catastrophic. For the F-15 buffet is well defined on the basis of aircraft angle of attack and dynamic pressure (Figures 4 and 5). The pilot feels aircraft shuttering due to separated flow but that is not necessarily buffet and low level buffet may be present before the pilot can feel it. Additionally, data indicates that the pilots observation of the g meter in the cockpit and data recorded by the structural data recorder are not in agreement (i.e. no 9g maneuvers were recorded under any conditions). This can be seen in Tables 1A - 1E. Once we realized these differences, we were better able to correlate pilot reports with test data.

The structural data recorder (SDR) data acquired from the Logistics Command and McDonnell Douglas provide a large data base of flights from take-off to landing. Some 173 flights of data were included in the generation of the average or typical mission duration of 69 minutes. Using the values of angle of attack and dynamic pressure (Figures 4 and 5) present during buffet as filters, an average of 3.6 seconds of buffet per mission would have been possible in the missions analyzed. Similarly, each mission would result in an average of 82.7 seconds of high g maneuvering. We were now faced with a discrepancy of the reported exposures from pilot interviews and this set of data.

— B4 A —

F-15 FLOW DOWN TEST POINTS

POINT	SPEED	ALTITUDE	MANEUVER
1	0.96M	0K	5.5G windup turn left, idle throttles in 3s hold Gs until 0.8M, deploy speed brake and hold, terminate at 0.7M.
2	0.96M	20K	5.5G windup turn left, idle throttles in 3s hold Gs and terminate at 0.7M
3	0.96M	20K	5.5G windup turn right, idle throttles in 3s hold Gs and terminate at 0.7M
4	0.96M	20K	1.0G decel w/ throttle chop, terminate at 0.8M
5	0.96M	20K	1.0G decel w/ throttle chop, deploy speed brake and hold, terminate at 0.8M
6	0.80M	20K	1.0G steady state (no maneuver)
7	0.90M	20K	1.0G steady state (no maneuver)
8	0.90M	20K	1.0G steady state (no maneuver)
9	1.1M	20K	1.0G steady state (no maneuver)
10	1.3M	20K	1.0G steady state (no maneuver)
11	0.96M	20K	7.3G windup turn right w/ throttle chop, hold Gs and terminate at 0.7M

MISSION NUMBER	JON NUMBER	SHORT TITLE	DATE
1656	24370449	AIM-120A	22 JUNE 8
RANGE A4, AL W151 C2, C4	PROFILE STD WATER	ALTITUDE 0-25 K FT	TIME 0830-1030
CONTROL CALL SIGN: MISSION	FREQUENCIES 314.8 314.1/	STEP / START	CHECK IN / T/O 0830
CALL SIGN	AIRCRAFT TYPE/NO. F-15/045	CREW	JOKER/BINGO
	F-4/800		

STATION	STORES	WEIGHT (EACH/TOTAL)	CATEGORY
5	CLT	4400	
BB	IMV S/N 002	335	

LIMITS	AIRSPEED MIN	AIRSPEED MAX	AIRSPEED MACH	ACCEL G SYM +/-	ACCEL G UNSY +/-	ROLL RATE
CARRIAGE		-1 limits				
EMPLOYMENT		N/A				
JETTISON		-1 limits				

MISSION SUMMARY

GATHER ACCELERATION DATA WITH THE IMV AND AN INSTRUMENTED PRODUCTION LAU-128.

FLIGHT CLEARANCE: 8C-101 (AMEND 4L)

FLY 20K pts @ 21K

VPS WX

T WX

J65F DATE		GR/WT		CG LOC		FCIF / PUBS
TAKE OFF	TEMP	PA	MAX ABORT	N/WLO	T/O SPEED	T/O DISTANCE
LAND	IMMEDIATE /		PILOT			CWSOF

Figure 4

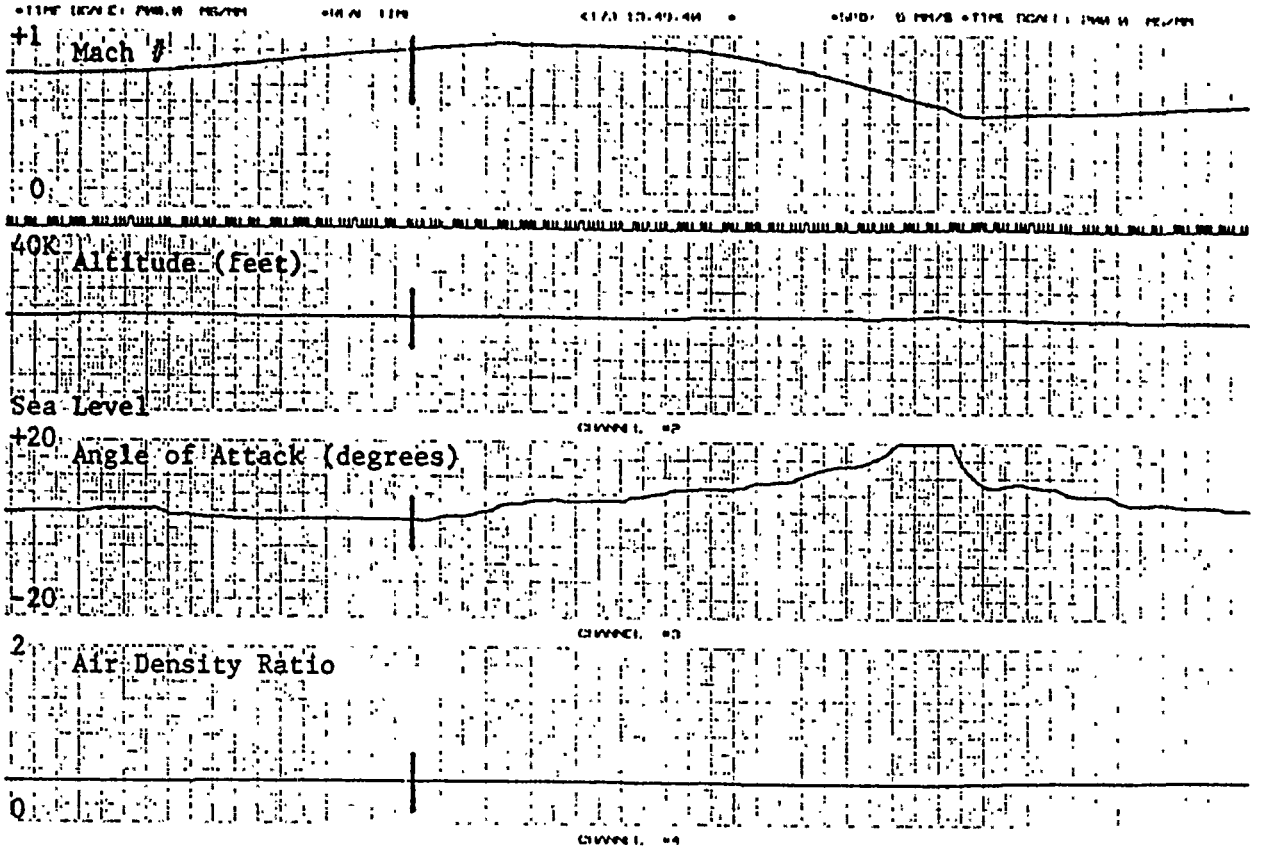

TEST POINT #1 461

Astro-Med, Inc. MT-9500 MULTI-TASK RECORDER

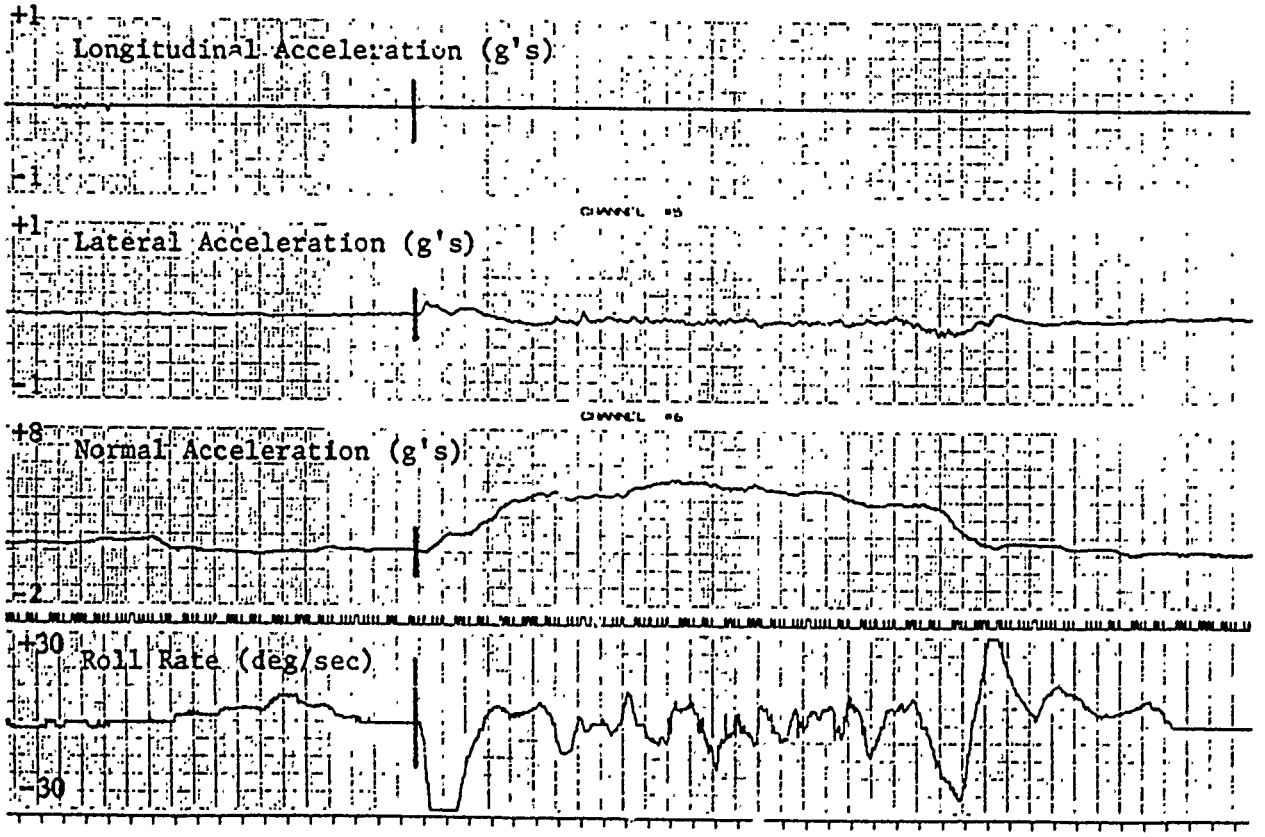

Figure 5

Table 1A. Normal Acceleration Distribution From 835 Minutes of SDR Data

NORMAL ACCELERATION (g's)	TIME SPENT (SECONDS)
< - 1	0
-1 - -.5	0
-.5 - 0	1.6
0 - .5	146.6
.5 - 1.0	19,170.2
1.0 - 1.5	21,794.4
1.5 - 2.0	3,804.1
2.0 - 2.5	1,505.3
2.5 - 3.0	1,081.9
3.0 - 3.5	843.6
3.5 - 4.0	641.9
4.0 - 4.5	476.3
4.5 - 5.0	300.9
5.0 - 5.5	171.1
5.5 - 6.0	73.7
6.0 - 6.5	44.4
6.5 - 7.0	24.0
7.0 - 7.5	13.2
>7.5	5.3

Table 1B. Angle Of Attack Distribution From 835 Minutes of SDR Data

ANGLE OF ATTACK (DEGREES)	TIME SPENT (SECONDS)
< - 10	0
-10 - 0	7.0
0 - 5	38,803.0
5 - 10	7,592.6
10 - 15	2,744.2
15 - 20	602.0
20 - 25	233.5
25 - 30	104.3
30 - 35	22.8
>35	0

Table 1C. Mach Distribution From 835 Minutes of SDR Data

MACH NUMBER	TIME SPENT (SECONDS)
0 - .1	.2
.1 - .2	14.2
.2 - .3	1,414.0
.3 - .4	17,121.8
.4 - .5	3,539.2
.5 - .6	4,910.2
.6 - .7	8,222.3
.7 - .8	9,101.7
.8 - .9	4,074.4
.9 - 1.0	1,635.6
1.0 - 1.1	57.5
1.1 - 1.2	8.3
>1.2	0

Table 1D. Altitude Distribution From 835 Minutes of SDR Data

ALTITUDE FEET	TIME SPENT (SECONDS)
0 - 5K	9,915.6
5 - 10K	4,453.1
10 - 15K	5,286.1
15 - 20K	10,986.8
20 - 25K	10,698.2
25 - 30K	6,881.6
30 - 35K	1,930.6
35 - 40K	122.5
>40K	0

Table 1E. Dynamic Pressure Distribution From 835 Minutes of SDR Data

DYNAMIC PRESSURE (PSF)	TIME SPENT (SECONDS)
0 - 100	1,972.4
100 - 200	3,536.8
200 - 300	9,160.6
300 - 400	16,282.4
400 - 500	10,934.2
500 - 600	5,633.3
600 - 700	1,609.8
700 - 800	832.3
>800	138.3

We recognized that the SDR data base had missions of four basic types included:

1. ACM with guns and ammo, or practice gun fire pass
2. ACM with missile installed on practice missile fire pass
3. Intercept practice
4. ACM camera only

Even breaking the data base down and looking at the four types individually did not offer any significant alteration of the above averages.

In order to achieve a better definition of the ACM segment we turned to the data bases existing at Nellis AFB where simulated dog fight scenarios are flown during Red Flag exercises. The entire mission from take-off to landing is not recorded, only the engagement portion of the mission. These engagements are expected to be the most realistic of any data source we could find. The reduction of data from these missions resulted in better correlation with the pilot reports of such engagements. Some parameters of interest were not included in the Red Flag data set, but sufficient data was available to accommodate the generation of tables 2A - 2D. There were 76 aircraft engagements containing from 4.4 minutes to 20.7 minutes of recorded

data each. The average recorded engagement was 11.8 minutes with two engagements per mission. The potential exposure to buffet in an intercept mission is an average 646 seconds. The typical mission would contain an average of 36 throttle chops, 6 wind-up-turns, and expose the missile to 130 seconds of normal accelerations in excess of 3 g's. Additional data analyses were conducted but at this point we were able to meld data from our 3 primary sources into table 3.

The AMRAAM Joint Systems Project Office (JSPO) established the next generation of test requirements for the AMRAAM using these data. Having applied the specification required margins of safety for the test limits, Table 4 was established.

Table 2A. Normal Acceleration Distribution From 880 Minutes of Nellis Data

NORMAL ACCELERATION (g's)	TIME SPENT (SECONDS)
< - 1	188.0
-1 - -.5	75.0
-.5 - 0	5,606.0
0 - .5	3,453.0
.5 - 1.0	14,416.0
1.0 - 1.5	14,646.0
1.5 - 2.0	4,460.0
2.0 - 2.5	2,426.0
2.5 - 3.0	2,052.0
3.0 - 3.5	1,625.0
3.5 - 4.0	1,027.0
4.0 - 4.5	900.0
4.5 - 5.0	640.0
5.0 - 5.5	526.0
5.5 - 6.0	189.0
6.0 - 6.5	52.0
6.5 - 7.0	1
7.0 - 7.5	0
>7.5	0

Table 2B. Angle Of Attack Distribution From 880 Minutes of Red Flag Data

ANGLE OF ATTACK (DEGREES)	TIME SPENT (SECONDS)
< - 10	0
-10 - 0	0
0 - 5	115.0
5 - 10	25,693.0
10 - 15	24,015.0
15 - 20	3,138.0
20 - 25	233.0
25 - 30	50.0
30 - 35	0
>35	0

Table 2C. Mach Distribution From 880 Minutes of Red Flag Data

MACH NUMBER	TIME SPENT (SECONDS)
0 - .1	0
.1 - .2	0
.2 - .3	415.0
.3 - .4	848.8
.4 - .5	2,219.0
.5 - .6	5,101.0
.6 - .7	7,625.0
.7 - .8	11,974.0
.8 - .9	12,254.0
.9 - 1.0	7,248.0
1.0 - 1.1	604.0
1.1 - 1.2	50.0
>1.2	290.0

Table 2D. Altitude Distribution From 880 Minutes of Red Flag Data

ALTITUDE (FEET)	TIME SPENT (SECONDS)
0 - 5K	246.0
5 - 10K	22,138.0
10 - 15K	3,692.0
15 - 20K	3,059.0
20 - 25K	5,025.0
25 - 30K	7,817.0
30 - 35K	2,775.0
35 - 40K	1,015.0
>40K	7,458.0

Table 3.

Dynamic Pressure (PSF)	Missile Station 32 (Overall GRMS)		Missile Station 137 (Overall GRMS)	
	VERT	LAT	VERT	LAT
0 - 300	2.6	1.3	3.4	4.0
300 - 500	2.9	2.0	6.6	6.5
500 - 800	4.1	3.0	1.0	7.8
>800	7.4	6.1	14.8	14.3

(From 20 - 2000 HZ)

TABLE 4.

JSPO Recommended Tests
(450 Hour Missile Life)

Non-Buffet (20 - 2000 HZ) Duration (MIN)	Missile Station 32 VERT GRMS	Missile Station 32 LAT GRMS	Missile Station 137 VERT GRMS	Missile Station 137 LAT GRMS
30	9.6	6.7	16.1	16.1
30	7.2	5.1	12.1	12.1
1200	6.2	4.4	10.5	10.5
Buffet* (20 - 300 HZ) Duration (MIN)	GRMS	GRMS	GRMS	GRMS
106	2.7 - 5.1	3.4 - 6.8	5.5 - 12.4	5.5 - 10.5

* The buffet test is to be accomplished in segments within the GRMS range since it is realized that the entire buffet exposure is not at maximum intensity.

We had now accomplished vibration spectrum tailoring using the most thoroughly tested external store in rememberable history.

CONCLUSIONS

The Red Flag and SDR programs were conducted without environmental qualification testing in mind; hence, the data available was less than 100% of what a test engineer would request if he were allowed to design the test. Regardless, we were able to acquire adequate data to complete our stated objective. With a better definition of the air combat maneuvering portion of a mission and data that showed that we already had a reasonable definition of the vibration character for other mission segments, we were able to complete the spectrum tailoring tasks.

One question that had surfaced during these investigations was whether adequate military standards and specifications existed since we were continually attempting to refine environmental test requirements. It is this author's opinion that as long as new generations of weapons and aircraft are developed that standards and specifications will always require modernization to reflect new performance criteria found through testing. This suggests that standards and specifications will always follow fast moving high technology programs. Our salvation is that the concept of spectrum tailoring allows us to actively acquire data to improve our ground tests.

RESUME

MR. WILLIAM O. DREADIN

Mr. Dreadin is a Senior Engineer with Orlando Technology, Incorporated of Shalimar, Florida. He has a degree in Physics with a minor in Aerospace Engineering from Auburn University. He has over seventeen years in the aerospace industry specializing in aircraft/store compatibility engineering with emphasis on flutter analysis, modal testing, and environmental qualification test and analysis.

Mr. Dreadin leads a compatibility engineering team which supports the Office for Aircraft Compatibility at Eglin AFB, Fl in the technical disciplines of flutter analyses and instrumented flight tests, store loads analyses and tests, aircraft loads analyses and tests, store safe separation and six-degree-of-freedom simulations and tests, stability and control analyses, and a variety of computer code development and maintenance tasks.

ACKNOWLEDGEMENTS

The author wishes to express his appreciation to Messers Cliff Gornto and Henry Bester of OTI and Lt Col Tom Johnson and Capt Keith Topham of the AMRAAM JSPO for their input and assistance in the preparation of this paper.

THIS PAGE INTENTIONALLY LEFT BLANK

Evaluation of the Spoiler Excitation System in F-111/CBU-87/89 Flutter Flight Tests

Ms Mary A. Marshall

Air Force Development Test Center

ABSTRACT

Tactical Air Command (TAC) requested carriage of BRU loaded CBU-87/89 dispenser weapons on the F-111. Analysis of these loadings indicated that at certain aerodynamic conditions the potential for flutter existed. In order to determine the maximum safe airspeed, it was necessary to flight test. This program was given to the Air Force Development Test Center at Eglin AFB.

Since the F-111 has a relatively stiff wing, it was not easily excited by stick raps or turbulence. Engineers and pilots from the 3246th Test Wing worked with General Dynamics Fort Worth Division to develop the Spoiler Excitation System (SES). The SES provided forcing functions tailored to excite the modes of interest. Testing was accomplished by stabilizing at a benign condition and executing random, sine sweep, and sine burst excitations. Wingtip and store data were telemetered to the control room for real time power spectral density (PSD) analysis. If the results were satisfactory, airspeed was increased and the test procedure repeated until a limit was established. The SES proved to be an efficient and effective means of flutter flight testing the F-111.

BACKGROUND

The F-111 is a United States Air Force all-weather tactical strike aircraft. As part of the F-111 SEEK EAGLE program, TAC asked for the operational capability to carry multiple CBU-87/89 stores on BRU-3A/As. Since

past flight tests demonstrated this aircraft had the potential to flutter, General Dynamics performed a flutter analysis of the CBU-87/89 configurations and their downloads. Several were predicted to have aeroelastic instabilities. According to their analyses, it was possible that the aerodynamics at certain conditions could cause the first wing bending symmetric mode to coalesce (merge) with the store pitch mode and drive the wing into divergent oscillations. The flutter model was considered accurate in predicting flutter sensitive configurations, but it was believed to be conservative in predicting flutter speed. In order to give TAC the maximum carriage airspeed possible, it was necessary to flutter flight test all configurations predicted to have instabilities within the requested envelope.

PAST METHODS

Hydraulic Wing Vane Exciter System. Flutter flight testing the F-111 has always been difficult. General Dynamics conducted the first flutter flight tests under the Full-Scale Engineering Development and HARVEST REAPER programs. They used a hydraulic wing vane exciter system. This system successfully stimulated modes of interest, making it possible to determine damping and frequency trends and clear configurations. However, the hydraulics frequently leaked. This was an undesirable test method from a reliability standpoint.

Gust Probe Tests. It was believed that the F-111 SEEK EAGLE program could be flutter tested quickly and inexpensively using random air turbulence as the source of excitation. The forcing function would be measured by an instrumented gust boom. Response accelerometers were mounted on the wingtips and stores. Damping and frequency were determined from PSD plots and frequency response plots. The data obtained using this technique was obviously questionable. Significant coherence, (at best it was approximately

0.70), was only achieved by flying low level among the mountains at Edwards AFB, but then data could not be transmitted to a control room for real time analysis. Under all other conditions, the turbulence did not put enough energy into wing and store modes to give them sufficient amplitude for frequency analysis. The response plots obtained were basically noise, and any frequency or damping results drawn form them were likely to be incorrect.

Stick Rap Tests. At the conclusion of gust probe testing, an attempt was made to flutter flight test using stick rap and logarithmic decrement analysis of the stripchart data:

$$\xi = \ln (A_0/A_n)/(\pi n)$$

where ξ = the damping
A_0 = amplitude of first cycle (in gs)
A_n = amplitude of nth cycle (in gs)

This technique was also ineffective because the response did not have enough decay for an accurate damping solution. The damping appeared to be non-linear; the signal would be of uniform frequency, but it would decay quickly then slowly trail out for several cycles. In addition, maintenance crews felt that the stick rap tests were detrimental to the test aircraft as it experienced excessive fuel leaks at that time.

SPOILER EXCITATION SYSTEM

Air Force and General Dynamics test personnel agreed that some sort of exciter system was needed to flutter flight test the F-111. Maj Dan Isabel, a 3247th Test Squadron pilot, theorized that an exciter similar to the F-16s Flutter Excitation System (FES) could be developed for the F-111. The FES used flapperon movement to provide excitation to the aircraft and stores. After some research, it was decided that the outboard spoilers could be used in the same way. Since the outboard spoilers are not part of a flight control

feedback loop, a voltage signal could drive them to provide and any type of forcing function desired. The SES was designed such that when it was actived, normal aircraft stick commands to the outboard spoiler were replaced by the excitation signal. The designers were General Dynamic engineers John Perez, Santi Bulnez, Hal Morrison, and J. C. Cooper.

The SES control panel is shown in Figure 1. It was located in the cockpit next to the TFR scope (Fig. 2), where it was easily operated by the Weapons Systems Officer (WSO). It provided three types of excitation: sine sweep (up or down), sine burst, and random (Fig. 3). The duration, frequency or frequency range, sweep rate, and spoiler amplitude of the excitation could be varied as needed. Both symmetric and antisymmetric forcing functions could be generated.

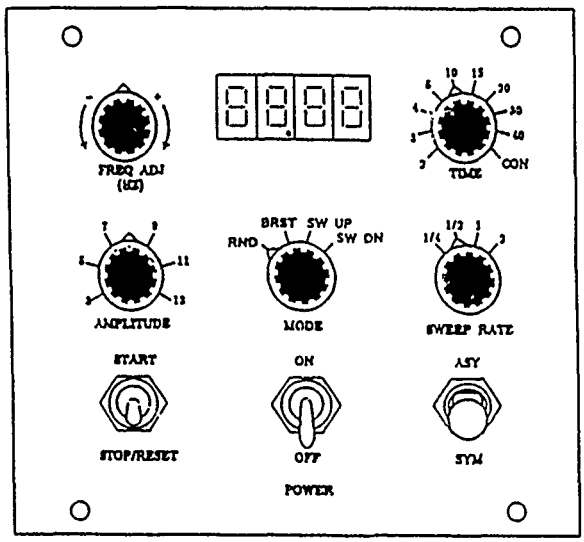

Figure 1. The variety of settings allowed a forcing function to be generated that was tailored to excite the modes of interest.

Several safety features were built into the design of the SES. A failure monitor was incorporated. If a failure was detected at any time it would have caused a display of 88.88 on the control panel. The display would have been reset by cycling the START-STOP/RESET switch. If the failure persisted, the

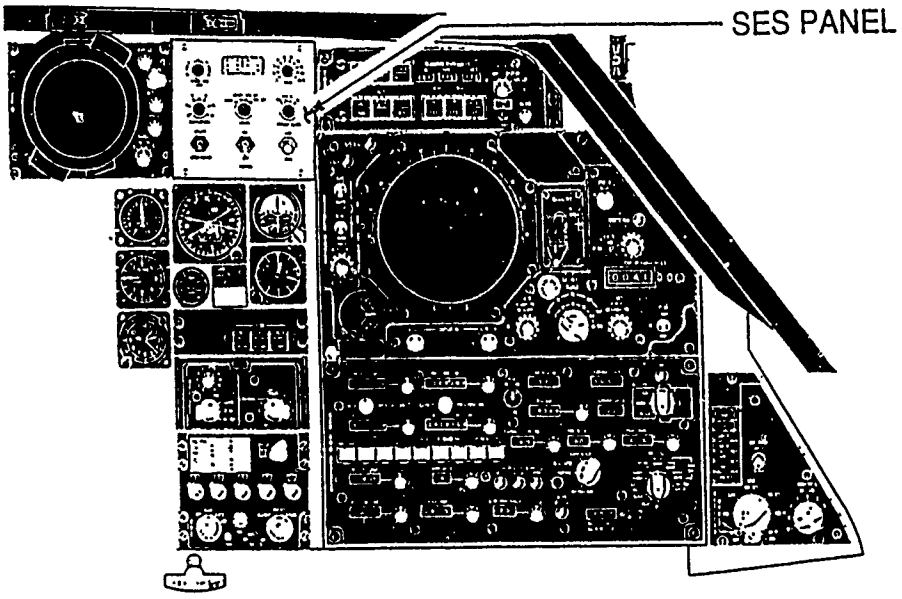

Figure 2. The SES control panel was located in front of the WSO in the righthand forward instrument panel.

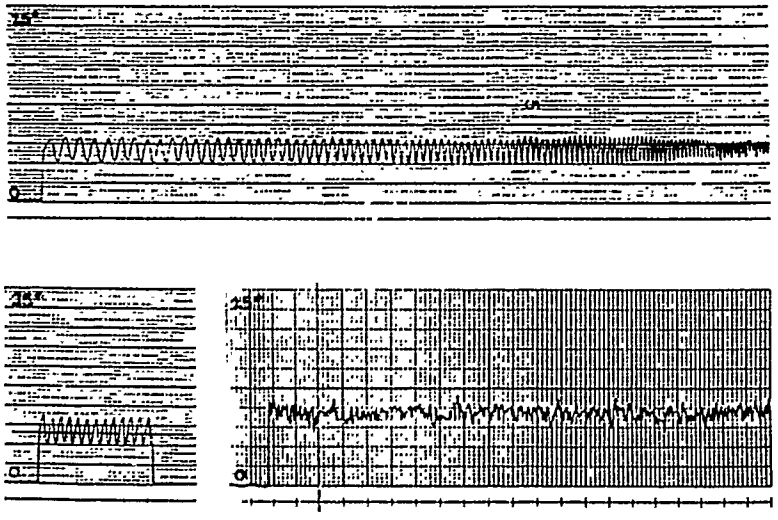

Figure 3. Spoiler traces are pictured for the (a) sine sweep, (b) sine burst and (c) random excitations. For symmetric excitations, the lefthand and righthand spoiler traces were identical. For antisymmetric excitations the lefthand and righthand spoilers were 180 degrees out of phase about the spoiler amplitude line, (pictured in (b) as —— – ——).

power to the SES would have been removed at the control panel, at the paddle switch or at the master modification instrumentation switch. SES failures would have resulted in the outboard spoilers being locked down but the inboard spoilers still would have been active.

INSTRUMENTATION

Instrumention was placed to record the two input forces and the response modes of interest (Fig. 4). The first and second input forces were measured by position sensors at the lefthand and righthand outboard spoilers, respectively. The response, or output, was measured by accelerometers placed on each wingtip and weapon station at the forward and aft ends. In addition, maneuver quality parameters, such as stick and rudder position, were instrumented. The bulkhead was instrumented to detect fuselage bending or torsion; however these modes were not predicted to cause an instability, so this data was not monitored realtime. The horizontal stabilizer was instrumented to record flight control anomalies encountered during tests. All data was sampled and transmitted to the control room real time at a rate of 200 samples per second.

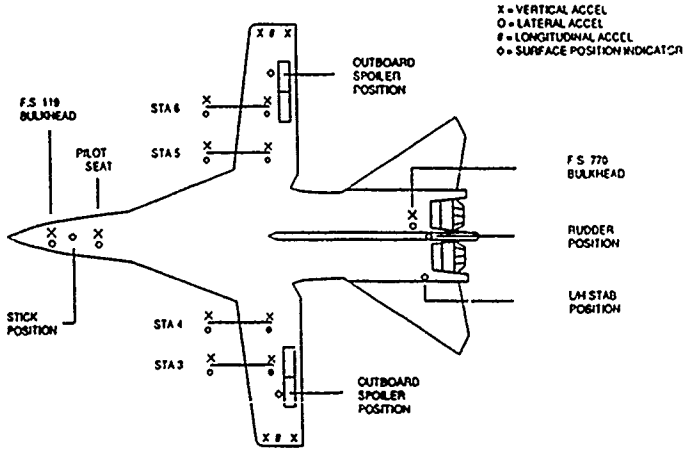

Figure 4. The test aircraft was instrumented for modal information, maneuver quality parameters, forcing function data and limited flight control surveys.

SOFTWARE

Eglin AFB and General Dynamics Data Systems Division personnel developed the software used in the F-111 CBU-87/89 flutter tests. The program was called "The Enhanced Flutter Program." It ran on a VAX 8600 with a Computer Signal Processing, Inc. array processor which performed the Fast Fourier Transforms (FFT) algorithms using a blocksize of 1024. It could process twenty channels of data including the summation and difference of parameters. The software was capable of performing several damping solutions; however, the PSD and frequency response solutions were used exclusively.

PSD Solution. The PSD plots described the response acceleration at a given frequency. In order to obtain the response PSD, the accelerometer data was collected in blocks, denoted as y(k). A Kaiser-Bessel window (Fig. 5) was applied to the block which forced the window to be periodic and reduced leakage. The discrete Fourier Transform was given by the following equation:

$$Y(j) = 2 \sum_{k=0}^{N-1} y(k)w(k)\exp\left(\frac{-2\pi i j k}{N}\right), \quad j = 0,1,2,\ldots,(N/2)-1$$

where $w(k)$ = the Kaiser-Bessel window

$i = \sqrt{-1}$

N = blocksize (1024)

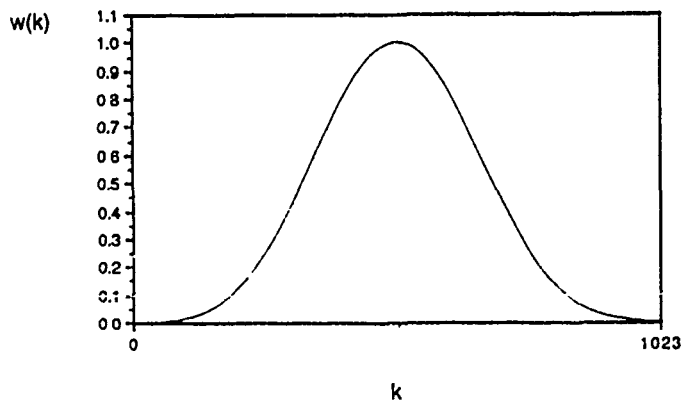

Figure 5. The Kaiser-Bessel window shown was used to prevent leakage.

The PSD for that block was given by

$$G_{yy}(j) = \frac{T|Y(j)|^2}{4NW} \quad j = 0,1,2,\ldots,(N/2)-1$$

where T = the time between samples in seconds
W = the mean square of the Kaiser-Bessel Window

This PSD was the raw PSD computed after the first 1024 samples. After another 256 samples were taken, another PSD would be computed from the most recent block of data; again the block was 1024 samples. The two PSD were then averaged. By applying this averaging technique to several blocks of data an accurate represenation of the true PSD was obtained. For a random excitation, twenty averages were taken. For a sine sweep excitation approximately twelve averages were taken.

Peaks on the PSD represented the natural frequency (f_n) of active modes. The damping was related to the bandwidth of the spike at half the peak power. This was known as the half power technique:

ζ = bandwidth/($2f_n$)

and was illustrated in Figure 6.

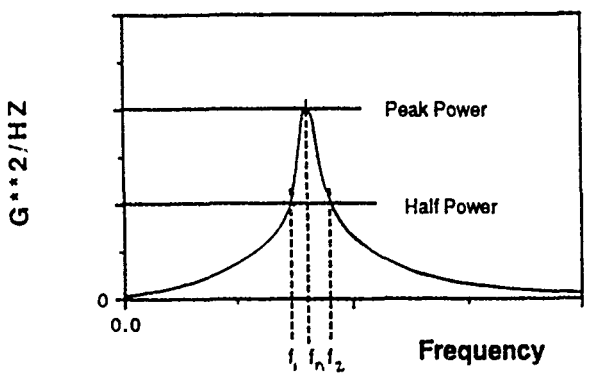

Figure 6. The half power technique determines damping based on the bandwidth at half the peak power and the natural frequency.

Frequency Response Plots. Frequency response plots represented the phase shift and transmissibility at various input frequencies. The frequency

response functions were computed from the input PSD and Cross-PSD. The input data x(k) was computed from the input forces using the following equations:

$$q = ((1+.2M^2)^{3.5} - 1) * p_o * (1 - 6.87535(10^{-6}) * H_p)^{5.2561}$$

where q = dynamic pressure in pounds per square foot
M = Mach No.
p_o = static pressure in pounds per square foot
H_p = Pressure Altitude in feet

and

$$x(k) = (F_1 - F_2) * q/2$$

where F_1 = first force, (lefthand spoiler position)
F_2 = second force, (righthand spoiler position)

The dynamic pressure at a given test point was essentially a constant. In theory it "weighted" the input data so that the magnitude of the frequency response plots were comparable for different test conditions.

The input PSD was calculated exactly the same as the output PSD but used the input data. The Cross-PSD is calculated in a similar manner but used both the input and output data. The discrete Fourier transform of the input data block is found from

$$X(j) = 2 \sum_{k=0}^{N-1} x(k)w(k)\exp(\frac{-2\pi ijk}{N}),\ j=0,1,2,\ldots,(N/2)-1$$

The raw estimate of the Cross-PSD is computed from

$$G_{xy}(j) = \frac{TX(j)^* Y(j)}{4NW},\ j = 0,1,2,\ldots,(N/2)-1$$

where $X(j)^*$ = the complex conjugate of X(j)

The Cross-PSD was averaged in the same way as the PSD.

The frequency response function was found by dividing the averaged Cross-PSD by the averaged forcing function PSD.

$$H(j) = \frac{G_{xy}(j)}{G_{xx}(j)},\ j = 1,2,\ldots(N/2)-1$$

note: j = 0 was the DC component of the PSD and Cross PSD

Since H(j) was a complex vector, the magnitude frequency response was found by taking the absolute value, and the phase frequency response was determined by taking the inverse tangent of the imaginary component divided by the real component.

On the phase plots, a singular mode was represented by a +/- 90 degree crossing, (Fig. 7). For a perfect single degree of freedom system the damping and phase were related by

$$\tan \phi = \frac{-2\xi f f_n}{f_n^2 - f^2}$$

where f = a frequency in the vicinity of f_n
ϕ = phase angle

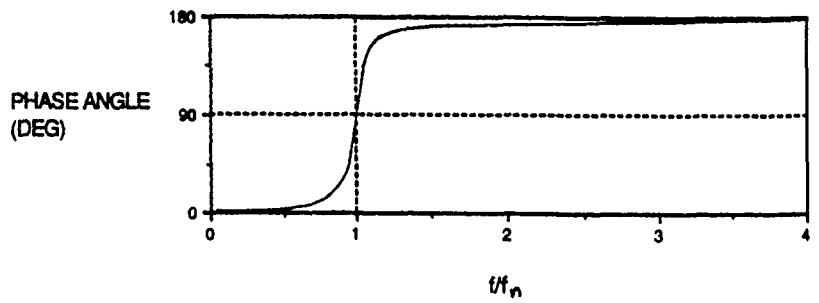

Figure 7. The phase angle for a single degree of freedom mode is $\pm$90 degrees at the natural frequency.

Since test data was not perfect, errors are introduced to both sides of the equation

$$\tan (\phi + c) = \frac{-2\xi f f_n + g(f_n, \xi, c)}{f_n^2 - f^2}$$

where c = an error constant to account for other modes
g = noise in the data and other errors

A solution for ξ, f_n, and c is determined by selecting a range of data in the vicinity of a mode and performing a least squares fit.

The peaks on the magnitude plot represented modes much like the PSD plots. Damping was determined using the half power equation, except that the bandwidth was taken at 70.7 percent the peak magnitude.

Coherence Function. The coherence (γ) was a function of the averaged input PSD $G_{xx}(j)$, the averaged output PSD $G_{yy}(j)$ and the averaged Cross-PSD $G_{xy}(j)$. It was computed as follows

$$\gamma(j) = \frac{|G_{xy}(j)|^2}{G_{xx}(j)G_{yy}(j)} \qquad j=1,2,\ldots,(N/2)-1$$

The coherence value ranged from zero to one. One meant perfect coherence; the output was a direct result of the input.

TEST TECHNIQUES

Test Points. The object of the flutter test was to safely determine the maximum carriage airspeed TAC could be given. As in most flutter flight testing, the F-111 SEEK EAGLE test was accomplished using a build-up procedure. By nature, the potential for flutter increased with the dynamic pressure. Therefore testing began at high altitude, low airspeed, and proceeded to low altitude, high airspeed.

The variable wingsweep (16 - 72.5 deg) of the F-111 complicated flutter flight testing even further. The modal characteristics were quite different for the wings fully swept forward and fully swept aft. In the interest of time and money, only a small number of wingsweeps could be analyzed and tested. Earlier General Dynamics tests had established standard wingsweeps in flutter testing the F-111. They believed it was possible to clear from 16 to 49 degrees by flight testing at 26 degrees, and it was possible to clear from 50 to 72.5 degrees by flight testing at 50 degrees. Since the outboard spoilers locked out at 45 degrees, an intermediate set of test points were accomplished at 44 degrees. The 26 degree wingsweep was not always most flutter critical. The wingsweep predicted to be the most flutter critical was tested last.

Maneuvers. The test condition was evaluated by stabilizing on condition and performing the following maneuvers:

1. Stick fixed pitch and roll raps -- a sharp pulse input and return to neutral
2. Rudder free kicks -- a pulse to a rudder pedal with the stick held fixed
3. Modal excitations
   a. Random Symmetric for 20 FFTs at a fixed spoiler amplitude, typically 11 degrees
   b. Sweep up Symmetric generally from 1 to 10 Hz at a fixed spoiler amplitude, typically 7 degrees; the frequency was increased every cycle by .05 Hz
   c. Sweep up Antisymmetric also from 1 to 10 Hz at a fixed spoiler amplitude, typically 7 degrees
   d. Bursts at a fixed spoiler amplitude, typically 7 degrees
4. Wind-up turn and reversal

Abort/Test Termination Criteria. The test engineers were to call an abort or terminate testing if one of the four following events occured:

1. Damping reached 3 percent or less
2. Damping was predicted to reach 3 percent or less at the next test point and the damping trend suggested a rapid decrease in damping
3. Two modes appeared to be coalescing
4. Response to a flutter maneuver reached +/-4 gs at the wingtip

The test aircrew was given the right to execute an abort at any time they felt it necessary.

DATA ANALYSIS

Real Time. During the flutter missions, only key parameters were analyzed and monitored for coalesence and decreased damping. The forward vertical wingtip summation and difference, and the aft vertical stores summation and difference were analyzed using the Enhanced Flutter Program. Because the testing needed to proceed as quickly as possible, only the PSD frequency and damping solutions were taken. These values were plotted against dynamic pressure. It was only necessary to analyze the sine sweep and random excitation data using the flutter program.

On the strip charts, the forward and aft wingtip and store accelerometers were monitored. The exponential decay response of the stick rap and bursts were analyzed real time using logarithmic decrement technique. Specifically, a "quick" damping solution, the Half Amplitude method, was used; the damping was determined by dividing 0.22 by the number of cycles to half amplitude (Fig. 8). In general, these damping solutions were higher than the frequency analysis results. During the wind-up turns, the accelerometer time-history data were qualitatively analyzed for any sort of sustained oscillation.

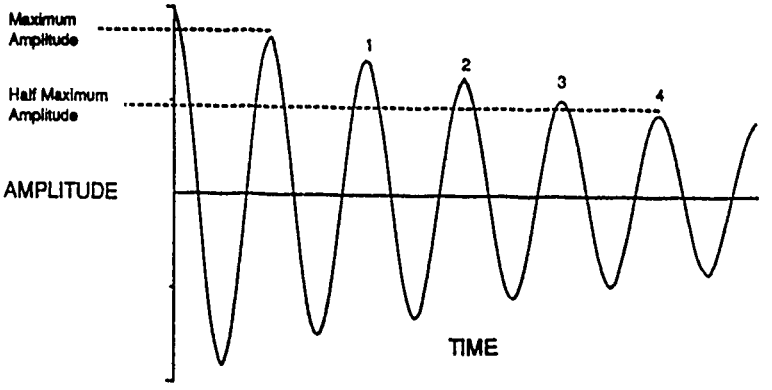

Figure 8. For the Half Amplitude damping solution, the maximum amplitude was generally taken at the first cycle of steady state response. The damping was determined by dividing 0.22 by the number of cycles to half that amplitude. For this particular response, the damping is approximately 5.5%.

Post Flight. After each mission a more thorough analysis took place. All vertical wingtip and store accelerometers were analyzed using the Enhanced Flutter Program for both indivdual and combined solutions.

TEST RESULTS

F-111 CBU-87/89 flutter flight testing took place from September 1989 to March 1990. Eleven flutter sensitive configurations were tested. At this time, most of the post flight data reduction has been accomplished. Preliminary data surveys suggest that all modes were well damped and

sufficiently separated from each other. Coherence values for primary modes range from 0.70 to 0.95. However, 3246 TESTW/TYE is still tabulating the post flight results to form frequency and damping trends.

TEST EVALUATION

Overall, 3246 TESTW/TY felt the SES was an excellent tool in flutter flight testing the F-111. The power level and coherence indicated sufficient excitation which resulted in data believed to be representative of the aircraft and stores. Also, the flutter flights were accomplished relatively quickly since it only took four minutes per test condition to collect the data and perform preliminary analysis. In addition, the test technique was not detrimental to the aircraft which led to as many as eight flutter missions flown in one month. A few anomalies were noted with the SES and are discussed here.

The symmetric sine sweep and symmetric random excitation successfully activated wing and store modes. However, when the two excitations were analyzed, they did not give identical solutions. In general, the random data yielded higher frequency and lower damping than the sine sweep. The output power level of the sine sweep was much higher than the random although the spoiler amplitude was less.

The individual accelerometers had good coherence for the symmetric sine sweep and symmetric random excitation. The antisymmetric sine sweep PSDs exhibited wing and store excitation and reasonable power levels. Despite this, the individual accelerometers had poor coherence, but the difference of the left and right side had good coherence.

The sine burst was successful in activating the first wing bending symmetric, inboard store pitch, and outboard store pitch modes. The responses were classic exponential decays. Frequency analysis indicated

that the first wing bending antisymmetric mode was more lowly damped than the symmetric mode. Also, the antisymmetric mode appeared to be easily excited since it responded to both the random symmetric and symmetric sine sweep excitations. Contrary to logic, the first wing bending antisymmetric mode did not respond to antisymmetric bursts.

Throughout these tests, it was difficult to isolate the store modes. For the forward store accelerometers, the wing mode often bled over and masked the store mode, especially for the symmetric sine sweep response. This hindered PSD and magnitude frequency response analysis. The random symmetric excitation was more successful in determining the store mode frequency, but it was still difficult to determine damping since the bandwidth was affected by the wing mode. The aft store accelerometers isolated the store mode better. In general, the wing mode was of a much lower power level while the store mode was much higher. Frequently, the store mode was completely isolated from the wing mode making it possible to obtain PSD and magnitude frequency response solutions.

FUTURE ENDEAVORS

At this time, the CBU-87/89 test aircraft (F-111E 67-0118) is in periodic depot maintenance at SM/ALC and another F-111 (F-111 67-0115) is being instrumented for both flutter and separations flight testing. In October 1990, validation flight testing should begin for the new aircraft. Soon after that, the Mixed Loads program will be flutter flight tested. Eleven configurations involving various combinations of Mk-82s, Mk-84s and GBU-15s will be tested. The test technique for this program will be identical to that successfully utilized for the CBU-87/89 flight test program. Upon its return, F-111 67-0118 will be reinstrumented for both flutter and separations flight

testing giving the 3246th Test Wing two F-111 aircraft capable of supporting future SEEK EAGLE testing.

CONCLUSIONS

The objective of the F-111 SEEK EAGLE flutter tests was successfully accomplished using the SES. Since the forcing function could be specifically designated to excite the modes of interest, it was possible to determine the frequency and damping of critical modes at several points throughout the flight envelope. Except for the transonic test points, all data had acceptable coherence.

The SES was a cost effective tool in flutter flight testing the F-111. Its development was relatively inexpensive when compared to the gust probe technique. The SES was easily installed into the F-111 and has required little maintenance. The excitation response levels were high enough that confidence could be established in the damping solutions making it possible to gather flutter data in less time and leading to greater mission productivity. The SES proved to be an excellent tool in flutter flight testing the F-111.

BIBLIOGRAPHY

1. Charleston, J. R. Class II Modification Documentation to Install a Flutter Excitation System on Aircraft F-111E No.4 (AF S/N 67-118) FZM-12-11067. Ft. Worth: General Dynamics, 1988.

2. Craig, Roy R. Structural Dynamics An Introduction to Computer Methods. New York: John Wiley and Sons, 1981.

3. Eubanks, A. L. Real-time Flutter Monitoring System Software Documentation. Ft. Worth: General Dynamics Corporation Data Systems Division Central Center, 1989.

4. Marshall, Mary A., and Shirley, Benjamin M. "F-111 Flutter Flight Testing," Technical Memorandum. Feb. 1990.

5. Stanley, William D., Dougherty, Gary R., and Doughtery, Ray. Digital Signal Processing, 2nd ed. Reston: Reston Publishing Company, Inc, 1984.

6. Structural Dynamics Research Laboratory, "Modal Analysis Basic Theory and Practice." Intensive short course by the University of Cincinnati, 1990.

7. Tustin, Wayne, and Mercado, Robert. Random Vibration In Perspective. Santa Barbara: Tustin Institute of Technology, 1984.

ACKNOWLEDGEMENTS

The following people were consulted in writing this paper:

Capt Larry Coleman
Mr Al Eubanks
Maj Mark Fish
Ms Vicki Fowler
Capt Paul Freeman
Maj Jim Jimenez
Mr John Perez
Mr Andy Rheinhart
Mr Ben Shirley
Flt Lt Mal Tutty

Their help was greatly appreciated.

BIOGRAPHY

Mary Marshall graduated from California Polytechnic State University San Luis Obispo in March 1986 with a Bachelor's of Science Degree in Mechanical Engineering. Her work experience began as a Co-Operative Education student engineer working for Solar Turbines, Inc. analyzing gas turbine engines. After graduation, she was hired by the Federal Government and worked at Edwards AFB. During this time she was involved with B-52 and F-16 flutter flight testing and X-29 loads tests. Ms Marshall transfered to Eglin AFB in 1988. Since that time she has performed F-111 flutter flight tests.

CAVITY ACOUSTICS IN HIGH REYNOLDS NUMBER TRANSONIC FLOWS

M. B. Tracy, E. B. Plentovich, J. Chu, and J. G. Shearin

NASA Langley Research Center

Hampton, Virginia

Paper Submitted to the

Eighth Aircraft/Stores Compatibility Symposium

Eglin Air Force Base, Florida

October 23-25, 1990

Abstract

An experiment was performed in the NASA Langley 0.3-Meter Transonic Cryogenic Tunnel to study the internal acoustic field generated by rectangular cavities in transonic flow and to determine the effect of Reynolds number and yaw angle. The cavity studied was 11.25 inches in length and 2.5 inches wide. The cavity depth was varied to obtain length-to-height (l/h) ratios of 4.4, 6.7, 12.67, and 20.0. Data were obtained for the Mach number range 0.20 through 0.90, the Reynolds number range 2 through 100 million per foot, and for two yaw angles, 0° and 15°. Results show that Reynolds number has little effect on the acoustic field in rectangular cavities at 0° yaw. Cavities with l/h equal to 4.4 and 6.7 generated tones at high transonic speeds while those with l/h equal to 20.0 did not. This agrees with data obtained previously at supersonic speeds. As Mach number decreased, the amplitude and band width of the tones changed. No tones appeared for Mach equal 0.20. For a cavity with l/h equal 12.67, tones appeared at Mach = 0.6, indicating a change in flowfield type. Changes in acoustic spectra with yaw angle were inconsistent, varying with Reynolds number, Mach number, l/h, and acoustic mode number.

Symbols

f	frequency, Hz.
f_m	frequency of acoustic mode, Hz.
FPL	fluctuating pressure level, db re q_∞.
h	cavity height, ft.
$k(M_\infty)$	empirical ratio of shear layer and free-stream velocities.
l	cavity length, ft.
M_∞	free-stream Mach Number.
m	acoustic mode number
p	measured fluctuating pressure, psf.
q_∞	free-stream dynamic pressure, psf.
Re_∞	free-stream unit Reynolds number, per foot.

$T_{t\infty}$	free-stream total temperature, ° K.
U_∞	free-stream velocity, fps.
w	cavity width, ft.
$\alpha(l/h)$	empirical phase between instabilities in shear layer and pressure waves.
γ	ratio of specific heat of air at constant pressure to that at constant volume.

Introduction

While internal carriage of weapons provides aerodynamic advantages in flight, difficulties such as large nose up pitching moments or store structural vibration can arise when a store is required to separate from a cavity exposed to an external flow. In order to insure safe separation (a store exiting from a cavity), it is necessary to study the flow disturbances generated when a rectangular cavity is introduced into uniform flow. In addition to changes in the mean pressure distribution in the cavity, an acoustic pressure field with high intensity tones can be generated as reported in references 1-10. This paper addresses the acoustic tone generation under transonic conditions.

Four types of flow have been observed for cavities under supersonic conditions: closed, transitional-closed, transitional-open, and open, as described in reference 11. (Reference 12 describes open and closed cavity flows.) Closed cavity flow, in which the shear layer attaches to the floor of the cavity, is observed for cavities with length-to-height ratios greater than 13 at supersonic speeds. Such flow produces an adverse static pressure gradient in the cavity which causes a separating store to experience large nose up pitching moments. Open cavity flow, in which the shear layer bridges the cavity, is seen at supersonic speeds for cavities with l/h ratios less than 10. Although this type flow produces a more uniform static pressure distribution, it is this flow regime that can produce high intensity acoustic tones. These tones can induce structural vibrations in a separating store as shown in reference 13. Transitional-open and transitional-closed flow are two distinct transitional flows for which the corresponding acoustic fields have not been determined.

The mechanism that produces the acoustic tones is understood to be a reinforcement between instabilities in the shear layer that bridges the cavity and pressure waves generated

in the cavity when the shear layer impinges on the aft wall. Acoustic tones occur at discrete frequencies which correspond to characteristic pressure patterns, or modes, in the cavity. Although there is no satisfactory method to predict tone amplitude (or whether or not they occur at all), the frequencies at which they occur can be predicted by a semi-empirical equation determined by Rossiter in reference 1 and modified by Heller, Holmes and Covert in reference 2,

$$f_m = \frac{U_\infty}{l} \frac{m - \alpha(\frac{l}{h})}{\frac{M_\infty}{\sqrt{1+(\frac{\gamma-1}{2})M_\infty^2}} + \frac{1}{\kappa(M)}}$$

The purpose of this study was to determine if tones are generated at transonic speeds for the same geometries (l/h ratios) as at supersonic speeds and to determine the effect of Reynolds number and cavity yaw angle.

Experimental Description

Test Facility

The experimental study was performed in the 13-inch by 13-inch test section of the NASA Langley Research Center 0.3-Meter Transonic Cryogenic Tunnel (0.3-m TCT) shown in figure 1. (References 14 and 15 describe the facility and operation in more detail.) The 0.3-m TCT is a continuous, fan-driven, cryogenic pressure tunnel which uses nitrogen as a test gas. The test section has adaptive upper and lower walls (reference 16) which were steamlined during the test.

The Mach number can be varied continuously from 0.20 through 0.95 and the stagnation pressure and temperature are variable over the range of 1.2 to 6.0 atmospheres and 80 to 320 K, respectively, which permits unit Reynolds numbers up to 100 million per foot.

Model

A rectangular cavity model was mounted on a turntable which was installed in the sidewall of the 0.3-m TCT. Figure 2 shows the cavity with dynamic pressure intrumentation prior to installation in the tunnel. The cavity was 11.25 in. long by 2.50 in. wide and the depth was variable to obtain l/h ratios of 4.4 (h = 2.56 in.), 6.7 (h = 1.68 in.), 12.67

(h = 0.89 in.), and 20.0 (h = 0.56 in.). The turntable could be rotated with respect to the flow, to position the cavity with a yaw angle of 0° and 15°.

Instrumentation

The model was instrumented with 18 dynamic pressure transducers (16 of which were along the centerline) as shown schematically in figure 3. The origin of the coordinates used is the center top of the forward cavity wall. The transducers were miniature, high-sensitivity, piezoresistive, differential dynamic pressure transducers with a full scale range of ± 10 psid. The reference pressure was local static (Transducers 1 - 3, and 15 - 17 were manifolded to a static pressure port identified as SR1 in figure 3: Transducers 4 - 11 were manifolded to SR2: and transducers 12 - 14, 18 and 19 were manifolded to SR3.) and a calibration at 1000 Hz verified that the temperature compensation maintained a sensitivity that was within 10 percent of a reference sensitivity at 100 K. Analog data were recorded on two 14-channel FM tape recorders using Medium Band Format at 30 inches per second. A sine wave calibration was applied to each transducers several times throughout the test.

Test Matrix

Data were obtained for Mach numbers of 0.20, 0.60, 0.80, and 0.90. The Reynolds number was varied from 4 through 100 million per foot, at yaw angles of 0° and 15°.

Boundary Layer Thickness

The thickness of the boundary layer at the leading edge of the cavity was measured with a total pressure rake. For Mach 0.6, the boundary layer thickness was found to range from 0.58 in. at a Reynolds number of 5 x 10^6 / ft. to 0.47 in. at a Reynolds number of 85 x 10^6 / ft. For Mach 0.9, it ranged from 0.51 in. at a Reynolds number of 13 x 10^6 / ft. to 0.49 in. at a Reynolds number of 100 x 10^6 /ft. Measurements were made with the cavity floor positioned flush with the turntable (h = 0.00 in.)

Data Analysis

An antialiasing filter was applied at 5 kIIz and the analog data was sampled at 12.5 kHz. The digitized data were divided into 50 blocks (assumed independent) of 4096 points each. Each block was fourier analyzed using a Hanning window and the resulting spectra

points each. Each block was fourier analyzed using a Hanning window and the resulting spectra were averaged. This produces spectra with a frequency resolution of 3 Hz and 95% confidence that the spectral estimate is within ± 1 dB of the true spectra based on a Chi-square distribution.

Results and Discussion

Since the data were obtained for a wide range of temperature and dynamic pressure, the data were nondimensionalized using free-stream parameters. The pressure is presented in decibels (db) as is customary for acoustic data and is nondimensionalized with free-stream dynamic pressure as is customary for aerodynamic data,

$$FPL = 20 \log \frac{p}{q_\infty}$$

The frequency is nondimensionalized using the cavity length, l, and the free-stream flow speed, U_∞.

An illustration of an acoustic mode shape in the cavity can be obtained by plotting the amplitude of a tone, at a given frequency, as a function of position along the length of the cavity. Figure 4 presents three different mode shapes (corresponding to fl/U_∞ approximately equal to 0.7, 1.1, and 1.5) in a cavity with l/h = 6.7, Mach = 0.80, yaw = 0°, and Re = 99 x 10^6/ft. Subsequent data will be presented as acoustic spectra. Data from transducer 1 (see figure 3) will be used in this report because the least amount of broadband noise was measured at that location. Except where indicated, all data are presented for yaw of 0°. For reference, the nondimensional frequencies predicted by the modified Rossiter equation are given in Table 1.

Effect of l/h

One of the main objectives of this study was to determine if the tones that correspond to the predicted Rossiter frequencies are generated by cavities with the same l/h ratios at transonic speeds as they are at supersonic speeds. Figure 5 presents plots comparing FPL spectra for the four l/h configurations at each Mach 0.6, 0.8 and 0.9. Data are presented for the highest Reynolds number obtained (85, 100, and 100 x 10^6/ft, respectively). The

modal frequencies predicted by the modified Rossiter equation are also indicated by labels below the abscissa. As discussed in reference 17, the modified Rossiter equation is a semi-empirical equation which was determined for a limited parameter range. This may account for the disagreement between the predicted values and those observed in this test.

A first observation is that the deeper the cavity (or greater the volume), the greater the acoustic pressures. Tones are observed for cavities with l/h equal to 4.4 and 6.7 and not 20.0 which agrees with data obtained previously under supersonic conditions. (The tones that appear in the data for l/h = 20.0 coincide with the tunnel fan blade passing frequency; fl/U_∞ of 1.21 for M = 0.60, 1.13 for M = 0.80, and 1.07 for M = 0.90.) An unanticipated result is the presence of tones for l/h of 12.67 at Mach 0.60 but not at 0.80 or 0.90.

Data for M = 0.20 was only available for l/h equal to 4.4 and 6.7. There were no tones apparent and no notable differences between the spectra.

Effect of Reynolds Number

Figures 6, 7 and 8 illustrate the effect of Reynolds number on the cavity FPL for each l/h configuration at Mach = 0.6, 0.8 and 0.9, respectively. It is apparent that there is little change above Reynolds number of 30 x 10^6/ft. The differences in FPL below 30 x 10^6/ft. may be due to a thermal shift in the transducer sensitivity over the test range of 104 to 320 K. Data for M = 0.20 was only available for low Reynolds numbers (less than 30 x 10^6/ft.) and are not presented.

Effect of Mach number

Mode amplitude and band width changed with Mach number. Different tones dominated the spectra for different Mach numbers. Figure 9 gives spectra comparing cavity FPL for the Mach number range for each l/h configuration at yaw = 0° and Re = 30 x 10^6/ft.

For cavities with l/h equal to 4.4 and 6.7, figures 9 a) and b), Mach 0.20 spectra contained no identifiable features. Mach 0.60 spectra contained broad peaks. As the Mach number increased to 0.80, the second mode (fl/U_∞ approximatly equal to 0.7) sharpened

and became dominant while higher order modes (fl/U_∞ equal to 1.2 and greater) decreased in amplitude. Spectra for Mach 0.90 was similar to the Mach 0.80 spectra with the exception that the second mode that was prominent at Mach 0.80 decreased in amplitude and the first mode (fl/U_∞ approximately equal to 0.3) becomes more prominent. The broadening of the tones, i.e. high pressure levels over a range of frequencies about the modal frequency, may indicate a destabilization of the feedback mechanism as the Mach number decreases.

Data from l/h = 12.67, given in figure 9 c), show the most dramatic change, indicating a possible change in flowfield type. The tones are eliminated as the Mach number increases from 0.6 to 0.8. Static pressure distributions (see reference 18) are expected to aid in identifying the flowfield types at each Mach number.

Spectra for l/h = 20.0, given in figure 9 d) contain no tones and show only a slight increase in broadband noise with increasing Mach number.

Effect of Yaw

Changes in the cavity fluctuating pressures with yaw angle were inconsistent, varying with Mach number, Reynolds number, l/h and mode order. There was no case in which the tones were eliminated altogether indicating a change from open to closed cavity type flow. Except where noted later, the frequencies at which tones were observed coincided for both yaw angles. Figures 10 through 12 give spectra comparing data for yaw of 0° with 15°, for cavities with l/h equal to 4.4, 6.7, and 12.67 respectively. Each figure presents data for high and low Reynolds numbers at Mach numbers of 0.60, 0.80, and 0.90.

The effect of yaw coupled with Reynolds number is most clearly seen in comparing figure 10 c) with d) where there a is significantly different decrease in amplitude of the second mode (fl/U_∞ approximately equal to 0.8) with yaw angle. Comparing figure 10 a) with c), and 10 b) with d) shows how Mach number can couple with yaw to either increase or decrease tone amplitude. There are cases in which tones appear or disappear with yaw. An example of the former is the third mode (fl/U_∞ approximately equal to 1.1) in figure 10 d). The opposite effect is seen for the first mode (fl/U_∞ approximately equal to 0.3)

in figure 11 f).

An interesting phenonema is observed at Mach equal 0.90, as seen in figures 10 e), 10 f), 11 e), and 11 f). Beginning with the third mode (fl/U_∞ approximately equal to 1.1), there is a shift down (to the left) in the higher modal frequencies with increased yaw. This may result from the cavity appearing longer to the shorter wavelength modes when it is in the yawed position. (The apparent shift up in tone frequencies with yaw in figure 10 c) is due to a difference in flow velocity used to normalize the frequency.)

As the cavity becomes more shallow, the effects described above become less dramatic as seen in figures 11 and 12. There was no effect of yaw in the l/h = 20.0 configuration. The effect of yaw at M = 0.20 was minimal. At Mach = 0.20, spectra for cavities with l/h equal to 4.4 and 6.7 showed only a slight increase in broadband noise with increased yaw.

Conclusions

Reynolds number appears to have little effect on the acoustic spectra generated by rectangular cavities at yaw = 0° for Mach numbers 0.20 though 0.90.

Tone generation in rectangular cavities occurs for the same l/h ratios at high transonic speeds as at supersonic speeds. As Mach number decreases to M = 0.6, a cavity of l/h of 12.67 (transitional at supersonic speeds) begins to generate tones indicating a change in flowfield type.

Mode amplitude and band width depended on Mach number. Prominent tones at Mach 0.80 and 0.90, broaden and change in amplitude as Mach becomes 0.60. There we' no tones apparent at M = 0.20.

The effect of yaw on cavity acoustics was inconsistent. Changes in acoustic spectra with yaw varied with Reynolds number, Mach number , l/h, and mode number. Higher order modes shifted down in frequency with yaw at Mach equals 0.90.

References

1. Rossiter, J.E.: Wind-Tunnel Experiments on the Flow over Rectangular Cavities at Subsonic and Transonic Speeds. RAE Report No. 3438, October 1964.

2. Heller, H.H.; Holmes, D.; and Covert, E.E.: Flow-Induced Pressure Oscillations in Shallow Cavities. AFFDL-TR-70-104, December 1970.

3. Heller, Hanno H. and Bliss, Donald B.: Aerodynamically Induced Pressure Oscillations in Cavities - Physical Mechanisms and Suppression Concepts. AFFDL-TR-74-133, February 1975.

4. Bartel, H.W. and McAvoy, J.M.: Cavity Oscillation in Cruise Missile Carrier Aircraft. AFWAL-TR-81-3033, June 1981.

5. Clark, Rodney L.: Evaluation of F-111 Weapons Bay Aero-Acoustic and Weapon Separation Improvement Techniques. AFFDL-TR-79-3003, February 1979.

6. Kaufman, Louis G.; Maciulaitis, Algirdas; and Clark, Rodney L.: Mach 0.6 to 3.0 Flows Over Rectangular Cavities. AFWAL-TR-82-3112, May 1983.

7. Shaw, L.; Clark, R.; and Talmadge, D.: F-111 Generic Weapons Bay Acoustic Enviroment. AIAA-87-0168, January 1987.

8. Gates, Roger S.; Butler, Carroll B.; Shaw, Leonard L ; and Dix, Richard E.: Aeroacoustic Effects of Body Blockage in Cavity Flow. AIAA-87-2667.

9. Shaw, Leonard and Banaszak, Dave.: Weapons Internal Carriage/Separation-'WICS' Aeroacoustic Research. AFWAL-TM-86-243-FIBG, March 1987.

10. Dix, R.E.: Weapons Internal Carriage and Separation at Transonic Conditions. AEDC-TMR-89-P4, October 1989.

11. Wilcox, Floyd J., Jr.: Experimental Measurement of Internal Store Separation Characteristics at Supersonic Speeds. Presented at the Store Carriage, Integration, and Release Conferencem April 4-6,1990.

12. Stallings, Robert L., Jr. and Wilcox, Floyd J., Jr.: Experimental Cavity Pressure Distributions at Supersonic Speeds. NASA TP-2683, June 1987.

13. Tracy, Maureen B. and Stallings, Robert L., Jr.: Coupling of Acoustic Enviroment in Rectangular Cavity with Store Vibration Characteristics During Simulated Separation in Supersonic Flow(U). NASA TP-2986, June 1990. CONFIDENTIAL.

14. Ladson, Charles L. and Ray, Edward J.: Evolution, Calibration, and Operational

Characteristics of the Two-Dimensional Test Section of the Langley 0.3-Meter Transonic Cryogenic Tunnel. NASA TP-2749, September 1987.

15. Rallo, Rosemary A.; Dress, David A.; and Siegel, Henry J.A.: Operating Envelope Charts for the Langley 0.3-Meter Transonic Cryogenic Wind Tunnel. NASA TM-89008, August 1986.

16. Mineck, Raymond E.: Hardware and Operating Features of the Adaptive Wall Test Section for the Langley 0.3-Meter Transonic Cryogenic Tunnel. NASA TM-4114, June 1989.

17. Dix, Richard E., and Butler, Carroll: Cavity Aeroacoustics.: Presented at the Store Carriage, Integration, and Release Conference, April 4-6,1990.

18. Plentovich, E. B., Chu, Julio, and Tracy, M. B.: Experimental Study of a Rectangular Box Cavity at High Reynolds Numbers. NASA TM-4209, 1990.

TABLE 1

Predicted Nondimensional Modal Frequencies

$$f_m \frac{l}{U_\infty} = \frac{m - \alpha\left(\frac{l}{h}\right)}{\frac{M_\infty}{\sqrt{1+\left(\frac{\gamma-1}{2}\right)M_\infty^2}} + \frac{1}{k(M)}}, \alpha = 0.25(\text{Ref.1}), k = 0.57(\text{Ref.1})$$

Mode	Mach Number			
	0.20	0.60	0.80	0.90
1	0.38	0.32	0.30	0.29
2	0.90	0.75	0.70	0.68
3	1.41	1.18	1.10	1.06
4	1.92	1.61	1.50	1.45
5	2.44	2.04	1.90	1.84
6	2.95	2.47	2.30	2.22
7	3.46	2.90	2.70	2.61

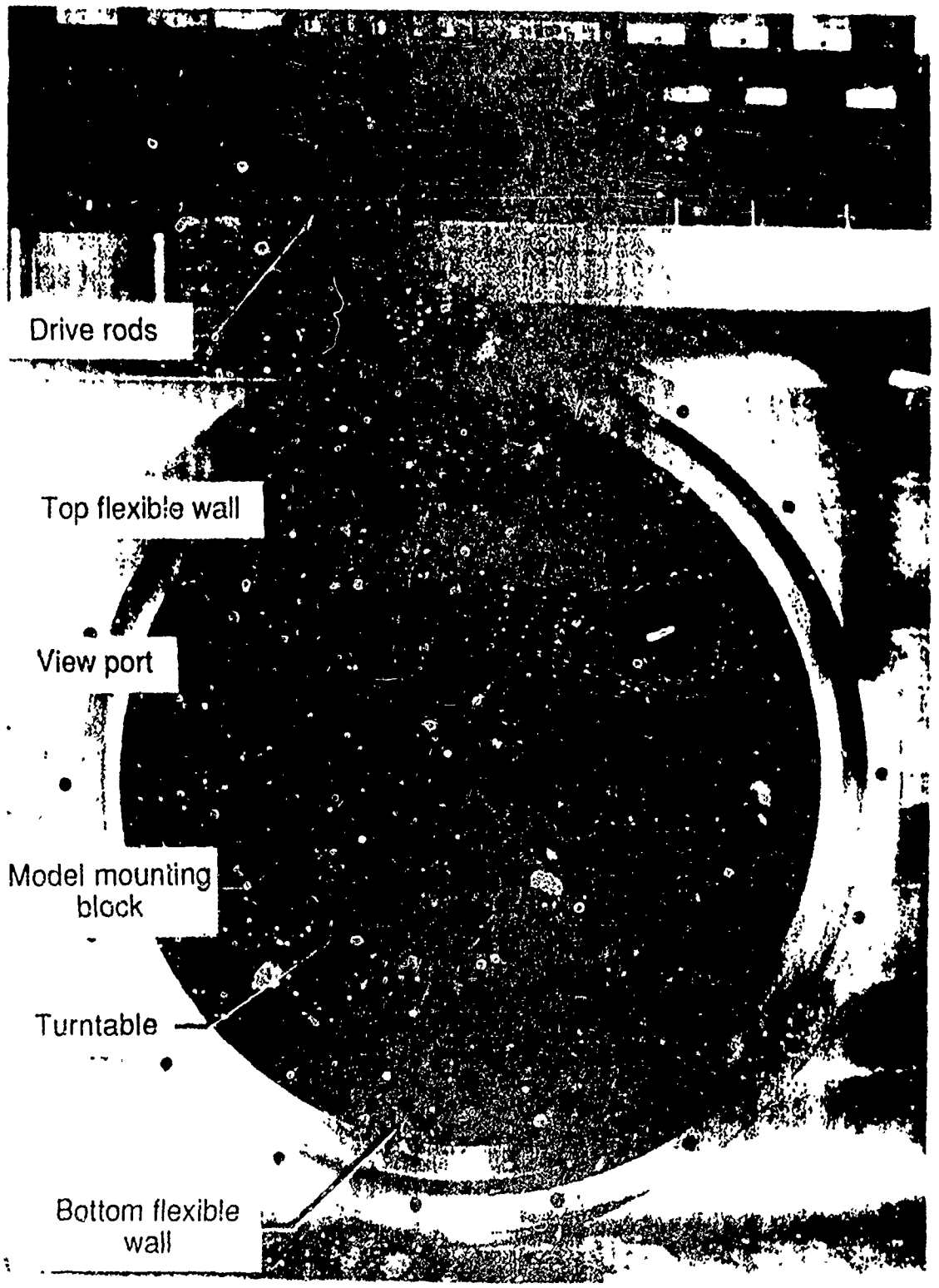

Figure 1. Interior of 0.3-m TCT 13-in. by 13-in. test section.

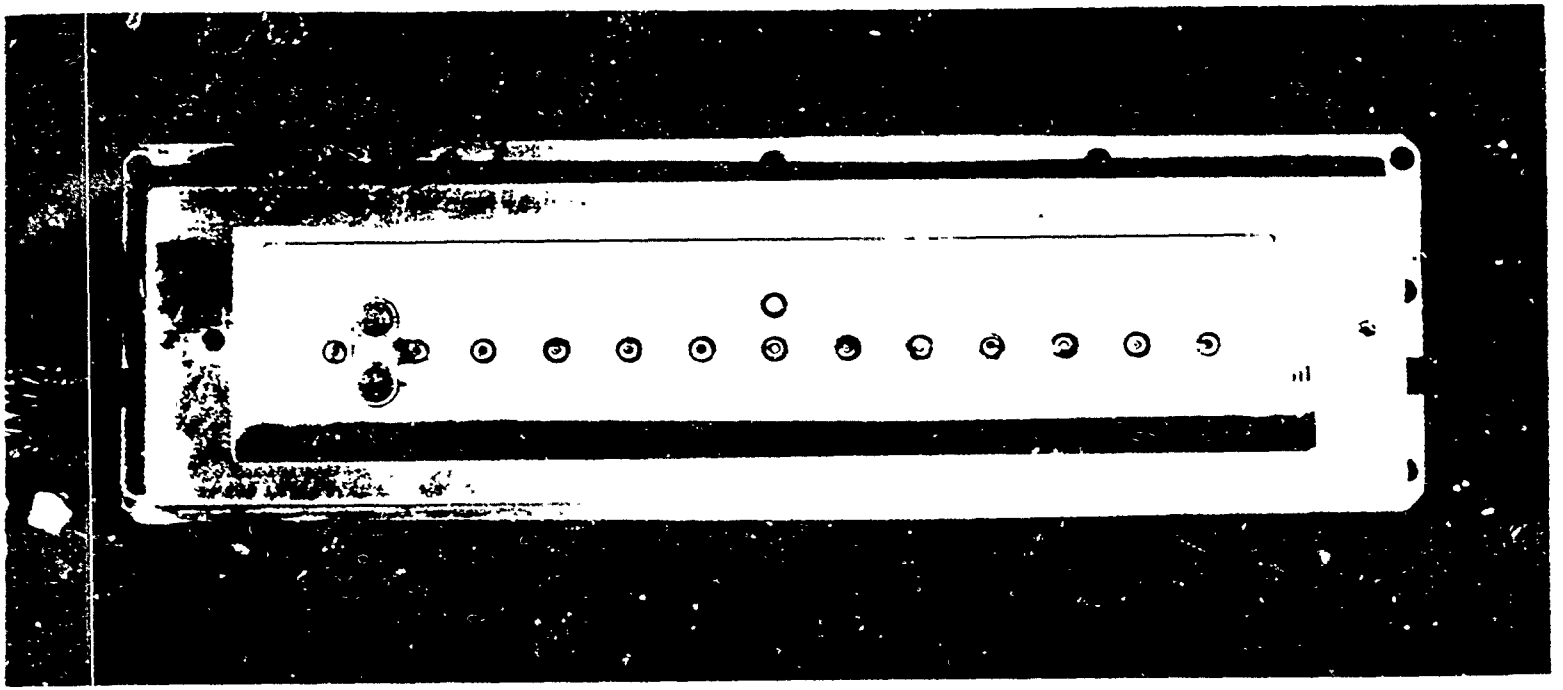

Figure 2. High Reynolds number cavity model.
(Dynamic pressure transducers are shown.)

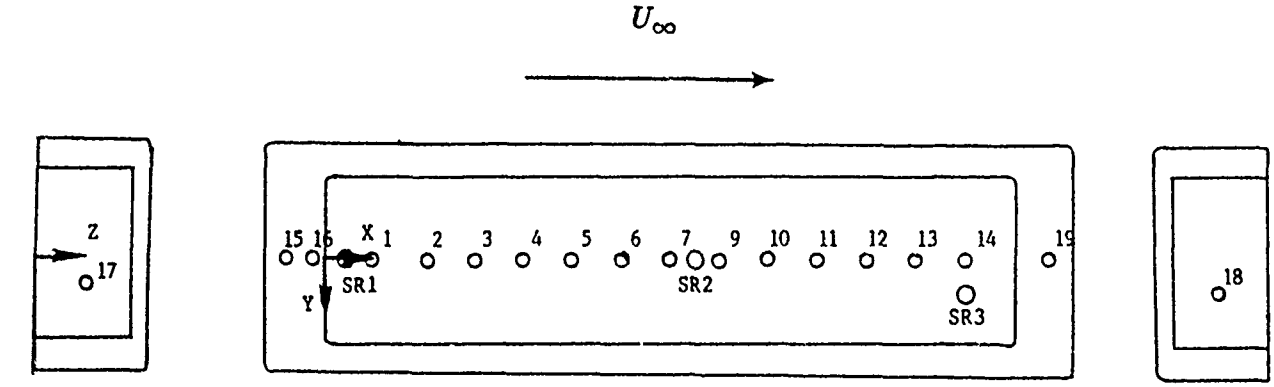

Transducer No.	x(in)	y(in)	z(in)	Model Location
1	0.800	0.0	h	cavity floor
2	1.700	0.0	h	cavity floor
3	2.460	0.0	h	cavity floor
4	3.254	0.0	h	cavity floor
5	4.058	0.0	h	cavity floor
6	4.862	0.0	h	cavity floor
7	5.666	0.0	h	cavity floor
9	6.470	0.0	h	cavity floor
10	7.274	0.0	h	cavity floor
11	8.078	0.0	h	cavity floor
12	8.882	0.0	h	cavity floor
13	9.686	0.0	h	cavity floor
14	10.490	0.0	h	cavity floor
15	-0.690	0.0	0.0	tunnel sidewall, fwd
16	-0.230	0.0	0.0	tunnel sidewall, fwd
17	0.000	0.47	h/2	forward cavity wall
18	11.260	0.47	h/2	aft cavity wall
19	11.800	0.0	0.0	tunnel sidewall, aft
Reference Orifice				
SR1	0.401	0.0	h	cavity floor
SR2	6.071	0.0	h	cavity floor
SR3	10.486	0.5	h	cavity floor

Figure 3. Dynamic instrumentation layout.

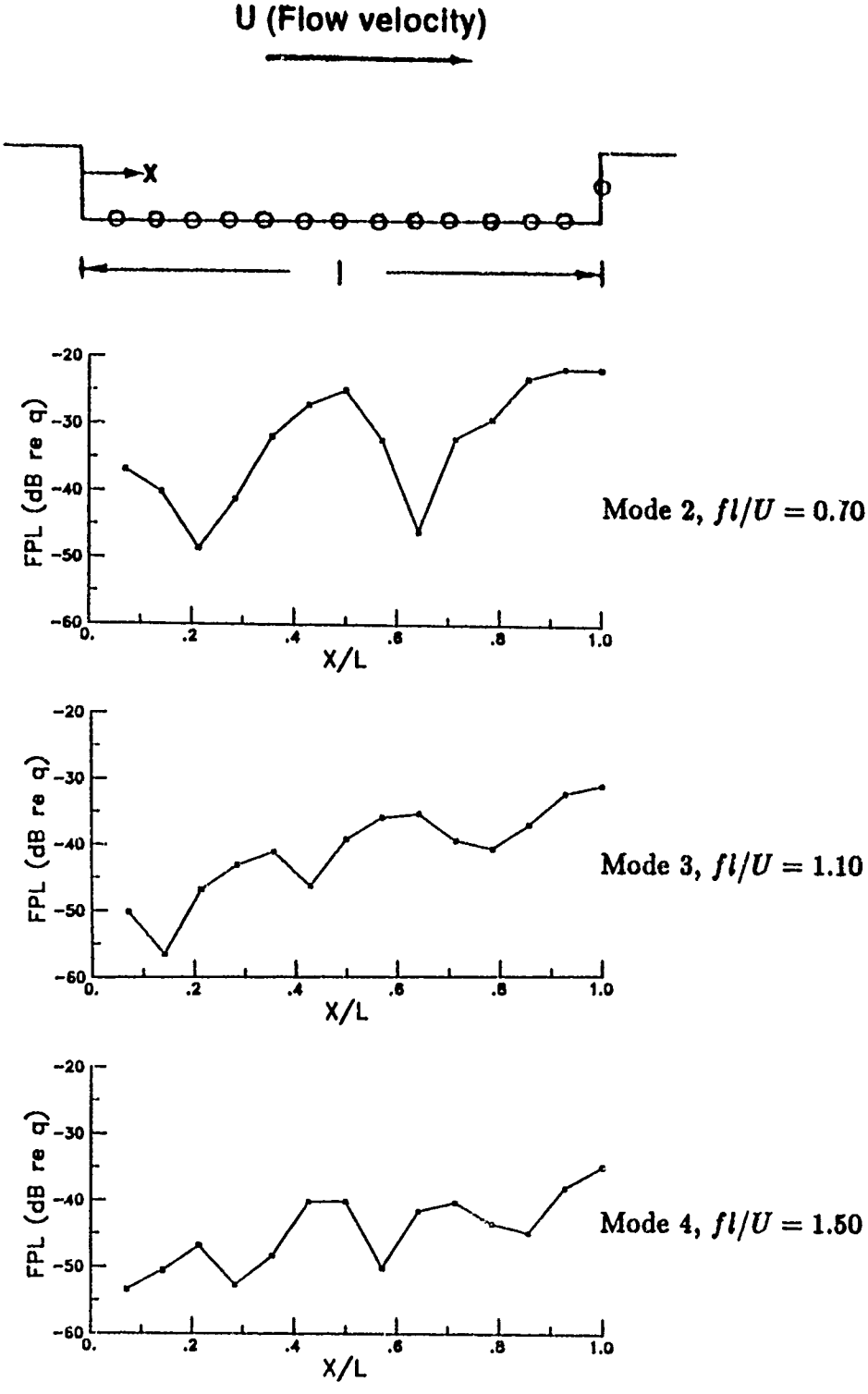

Figure 4. Mode shapes in cavity. M = 0.8, Yaw = 0°, l/h =6.70, R = 99 x 10^6 / ft.

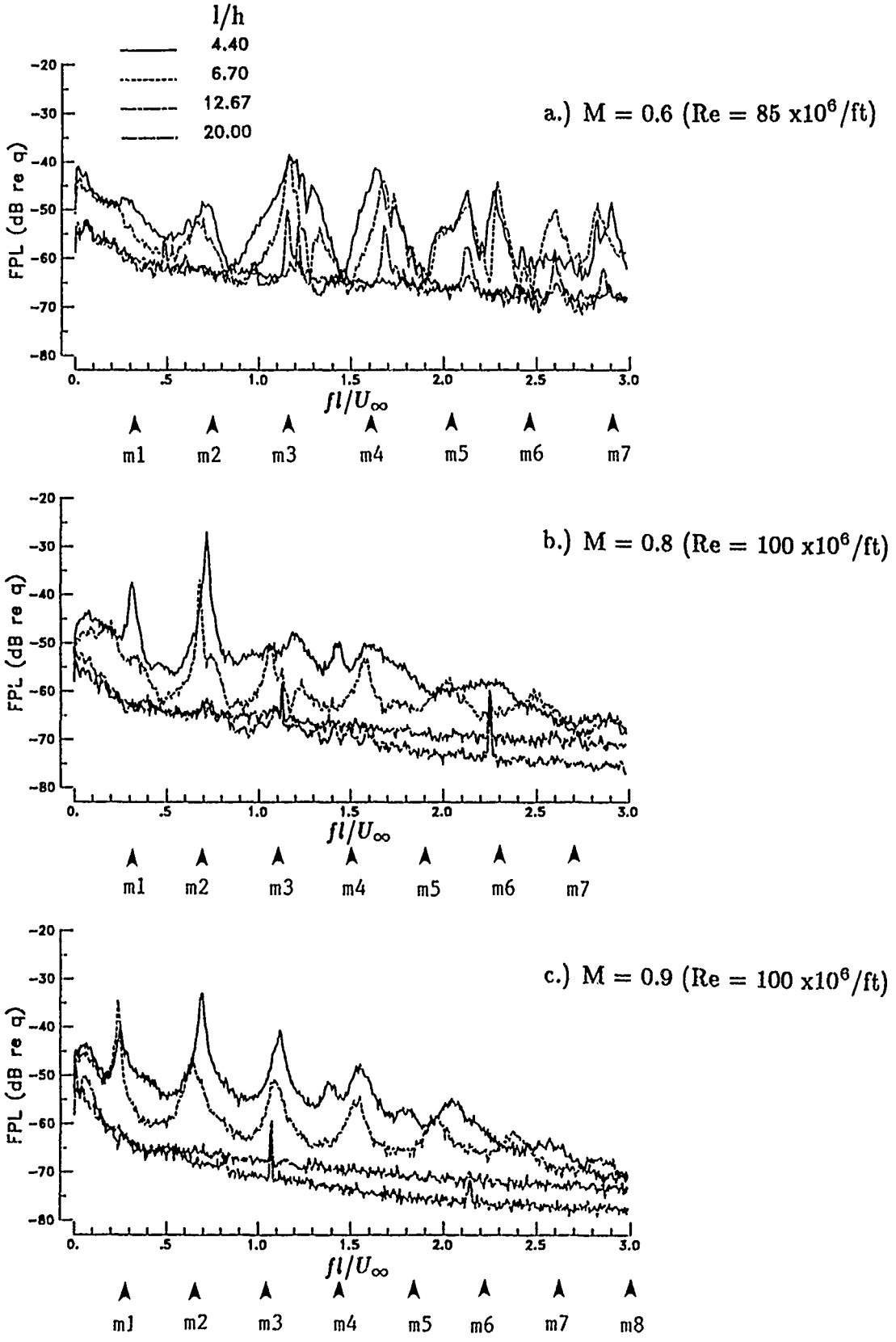

Figure 5. Effect of l/h of cavity fluctuating pressures. Yaw = 0°
Predicted modes indicated by m number.

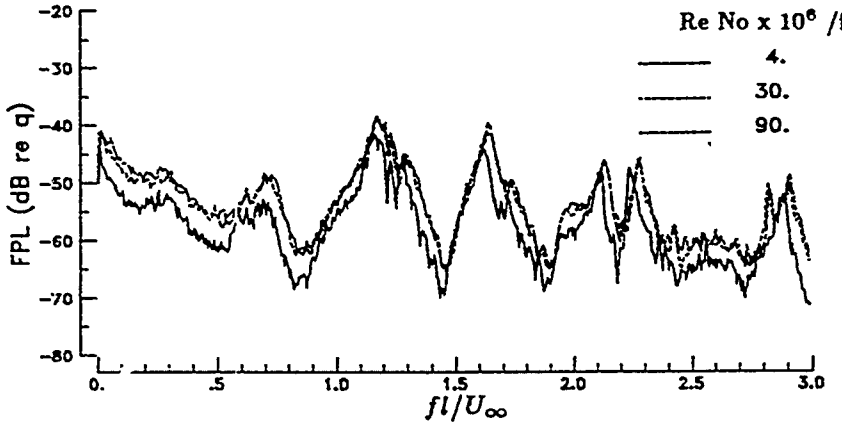

a.) l/h = 4.40

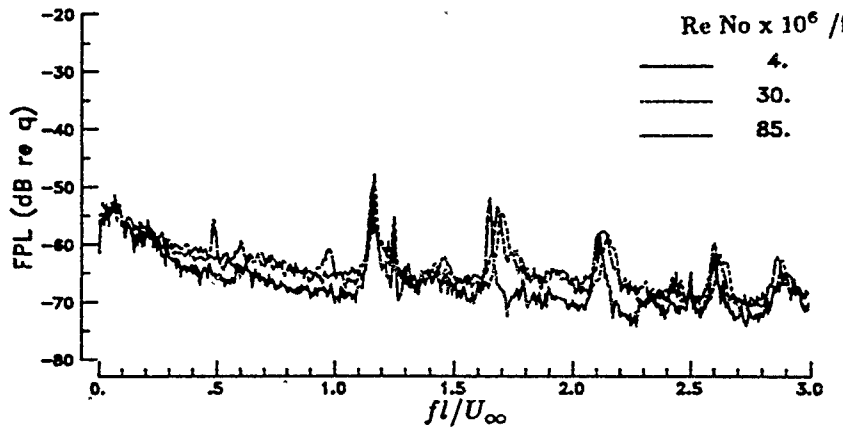

c.) l/h = 12.67

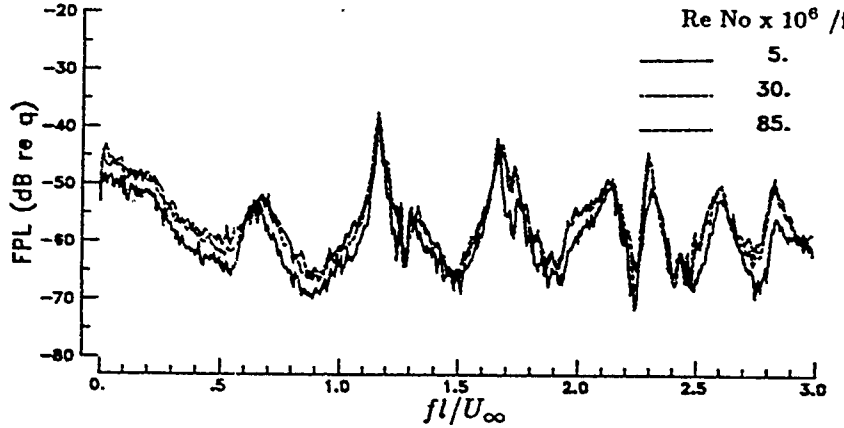

b.) l/h = 6.70

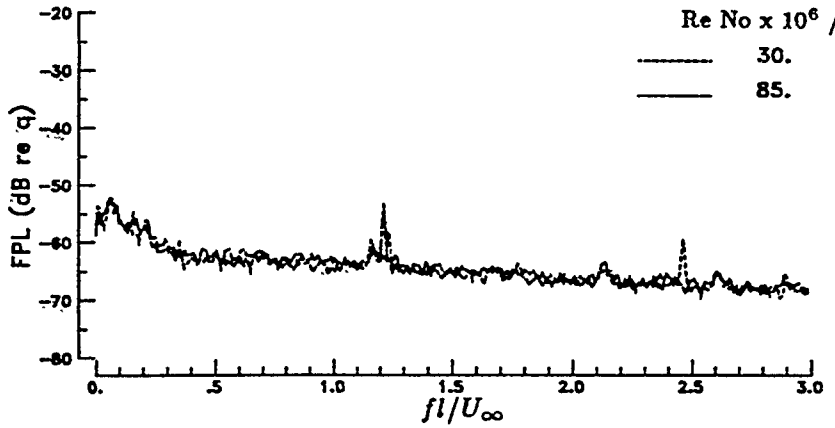

d.) l/h = 20.00

Figure 6. Effect of Reynolds number on cavity fluctuating pressures. Yaw = 0°, M = 0.6.

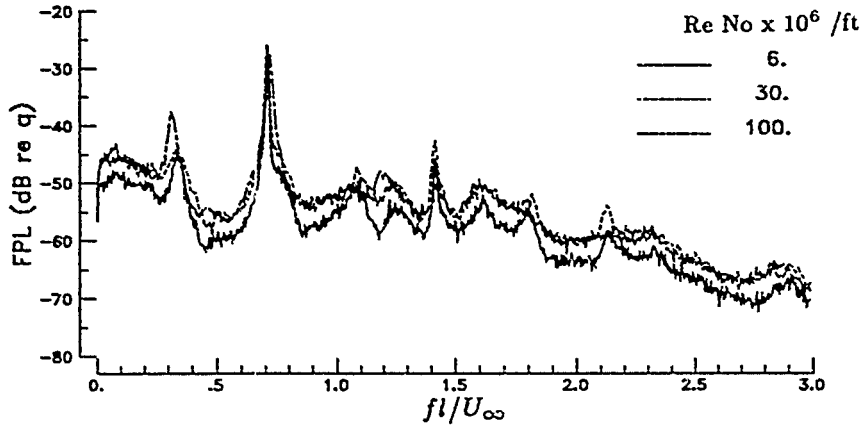

a.) l/h = 4.40

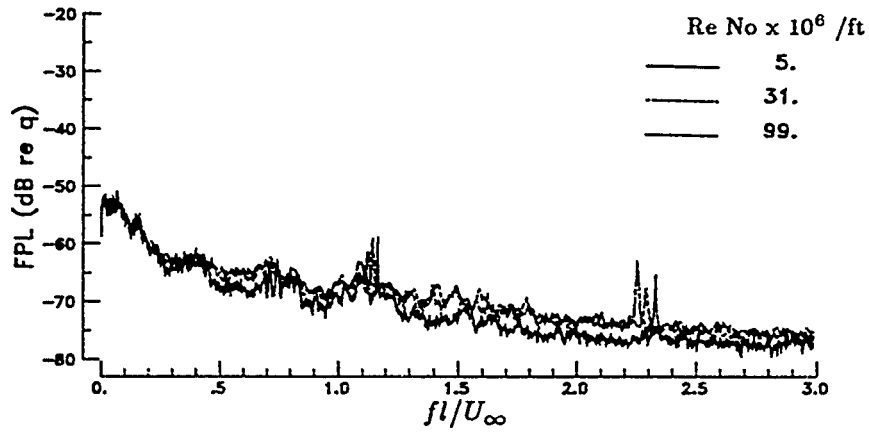

c.) l/h = 12.67

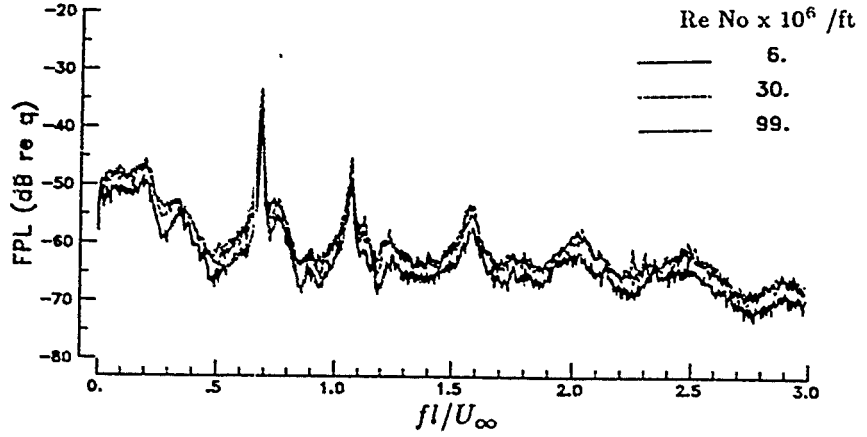

b.) l/h = 6.70

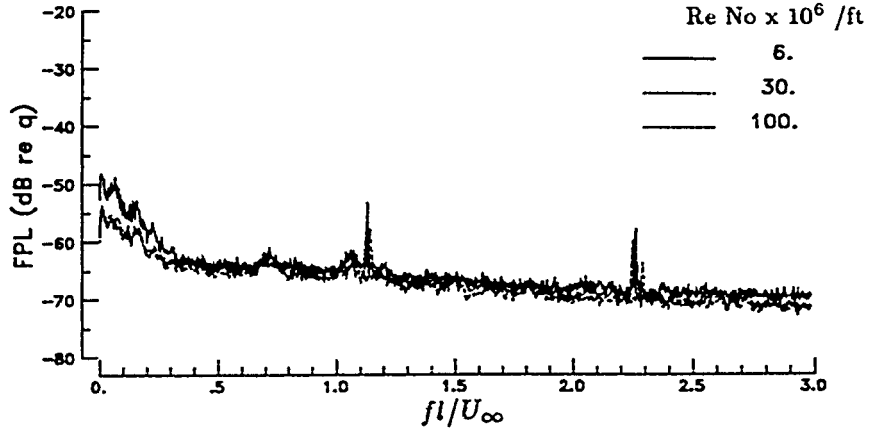

d.) l/h = 20.00

Figure 7. Effect of Reynolds number on cavity fluctuating pressures. Yaw = 0°, M = 0.8.

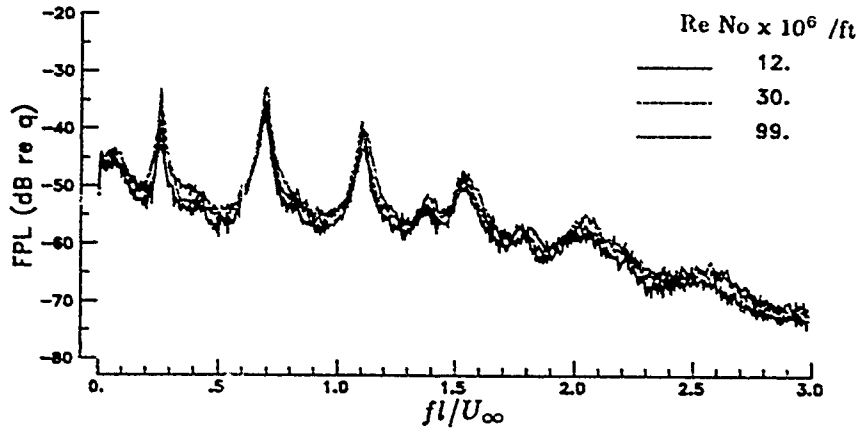

a.) l/h = 4.40

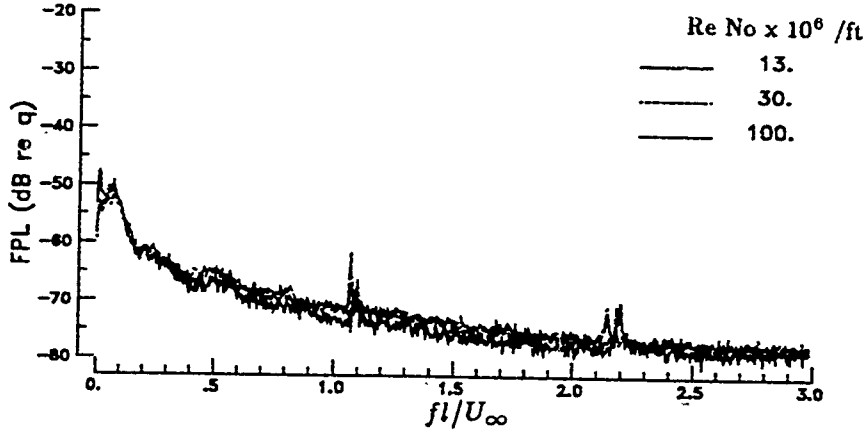

c.) l/h = 12.67

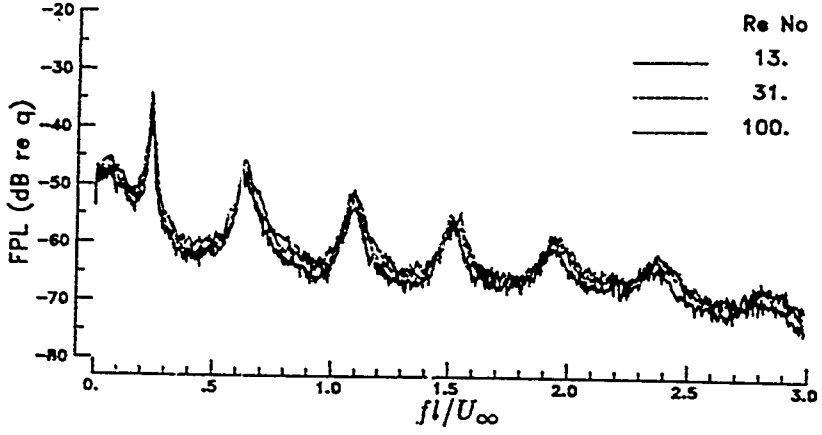

b.) l/h = 6.70

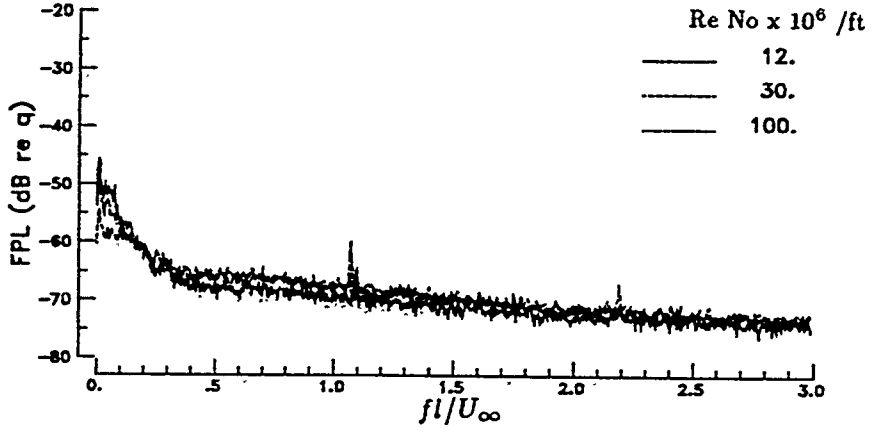

d.) l/h = 20.00

Figure 8. Effect of Reynolds number on cavity fluctuating pressures. Yaw = 0°, M = 0.9.

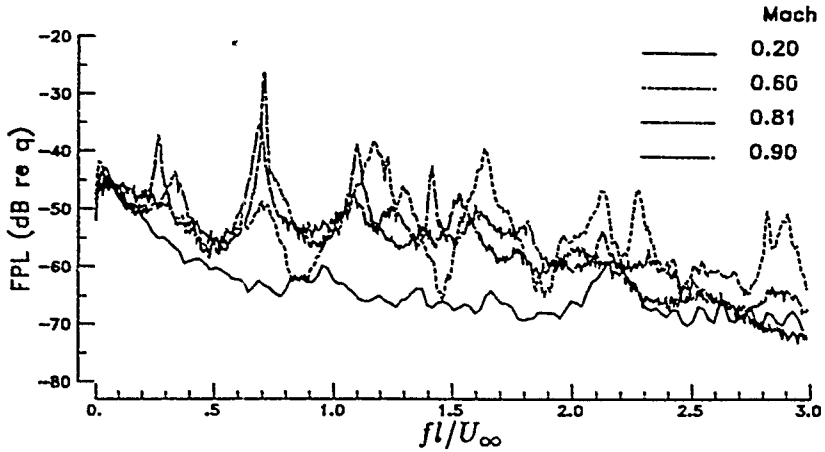

a.) l/h =4.40

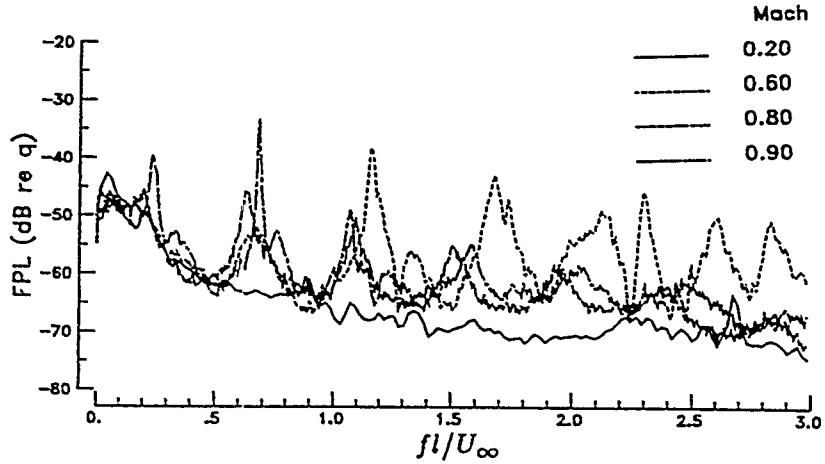

b.) l/h = 6.70

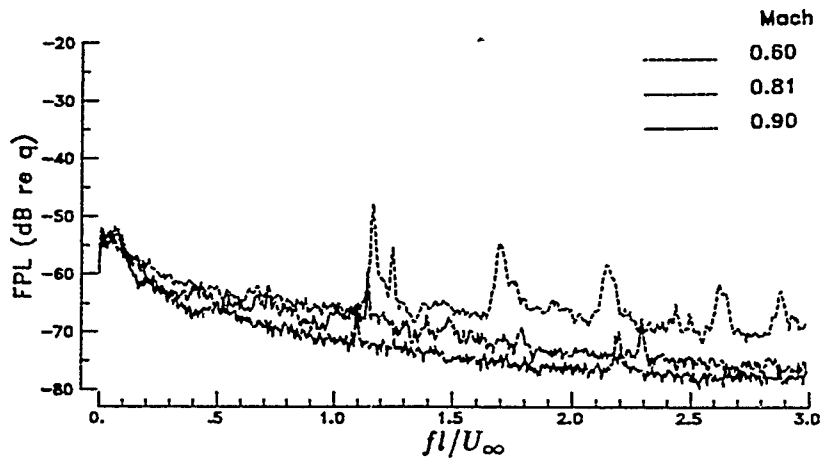

c.) l/h = 12.67

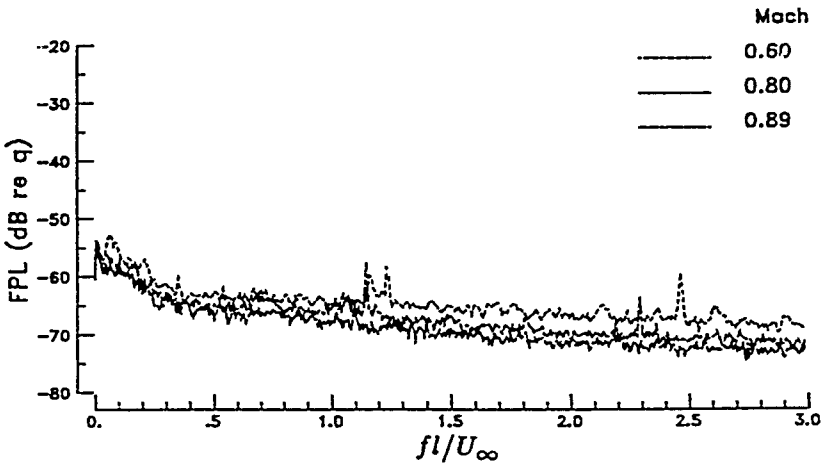

d.) l/h = 20.00

Figure 9. Effect of Mach number on cavity fluctuating pressures. Yaw = 0°, Re = 30 x 10^6 /ft.

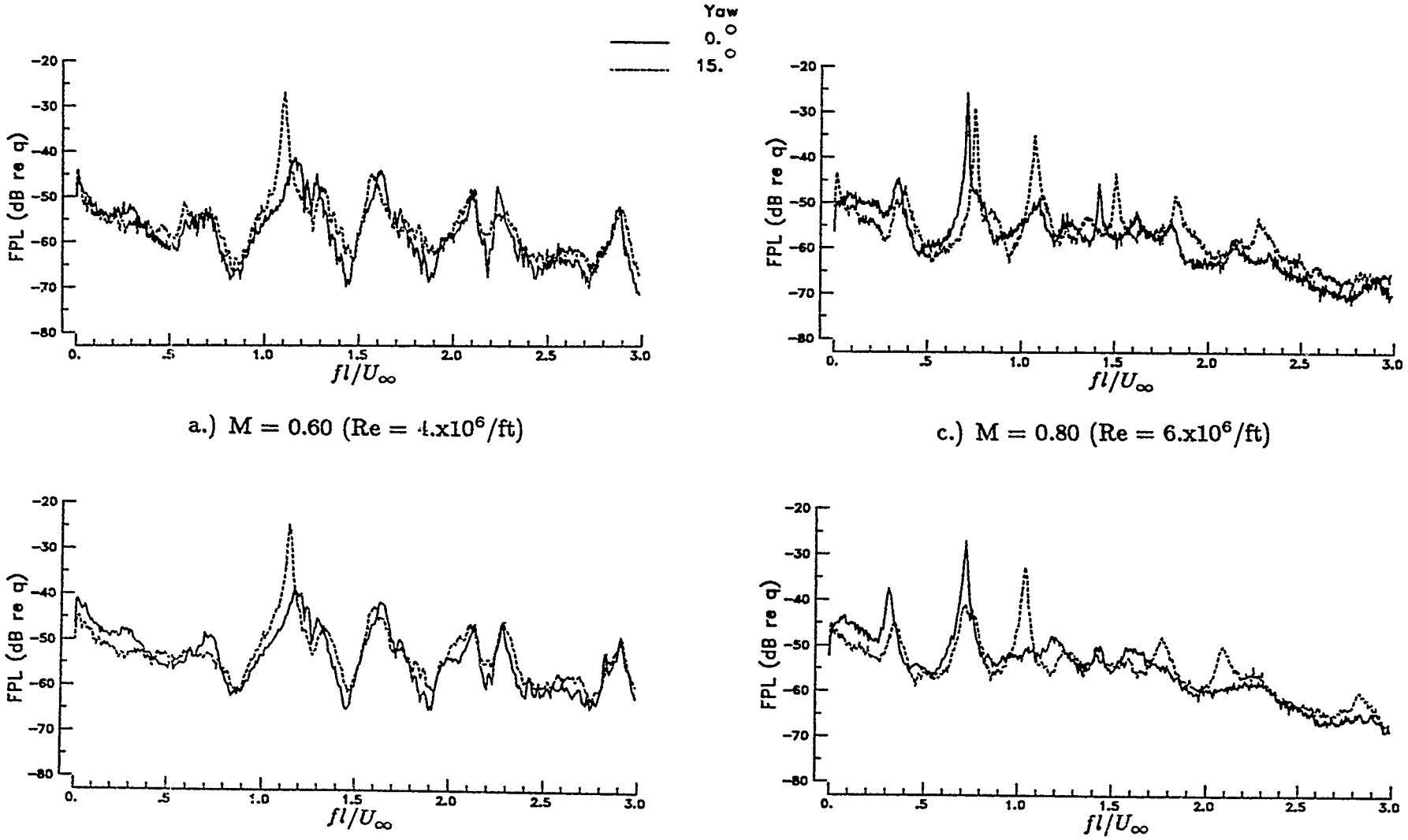

Figure 10. Effect of yaw on cavity fluctuating pressures. l/h = 4.4.

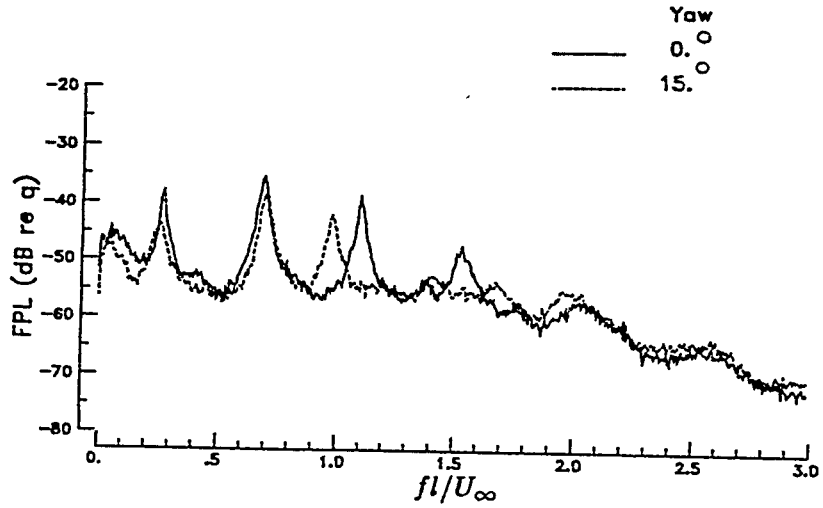

e.) M = 0.90 (Re = 30.x10^6/ft)

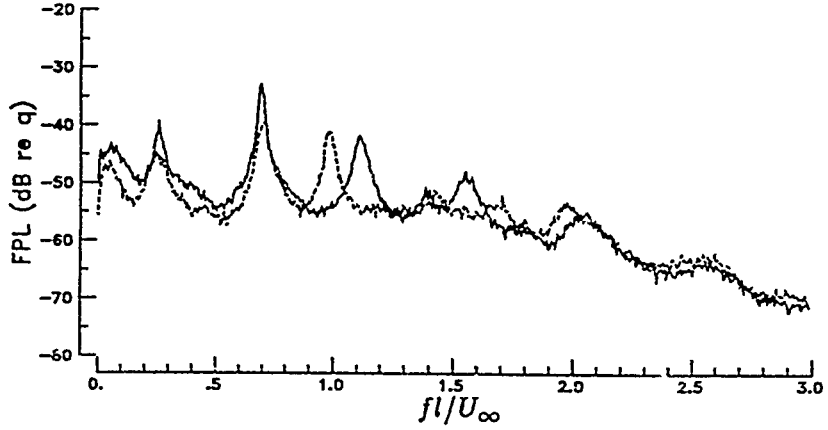

f.) M = 0.90 (Re = 90.x10^6/ft)

Figure 10. Continued.

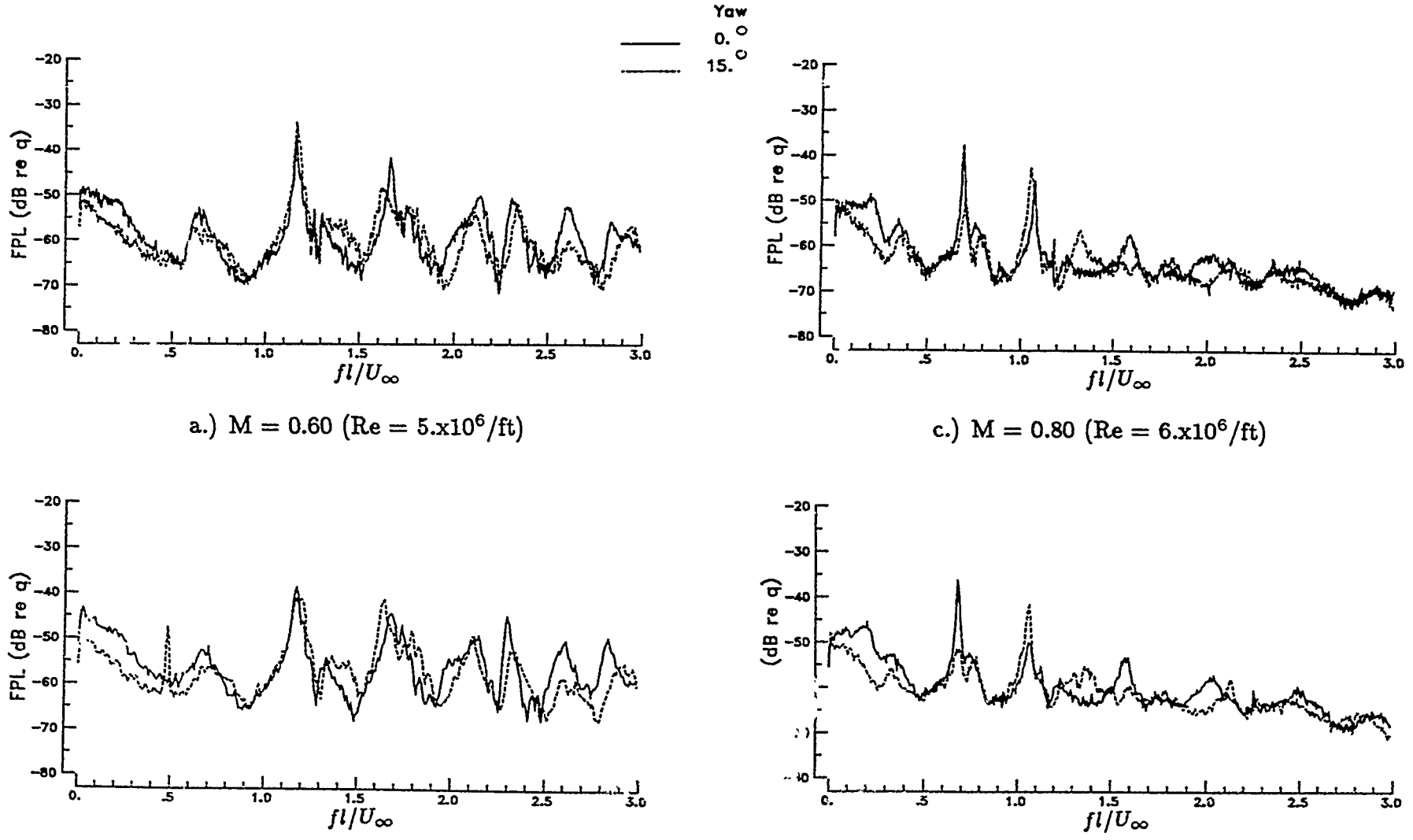

Figure 11. Effect of ... tion pressures. l/h = 6.7.

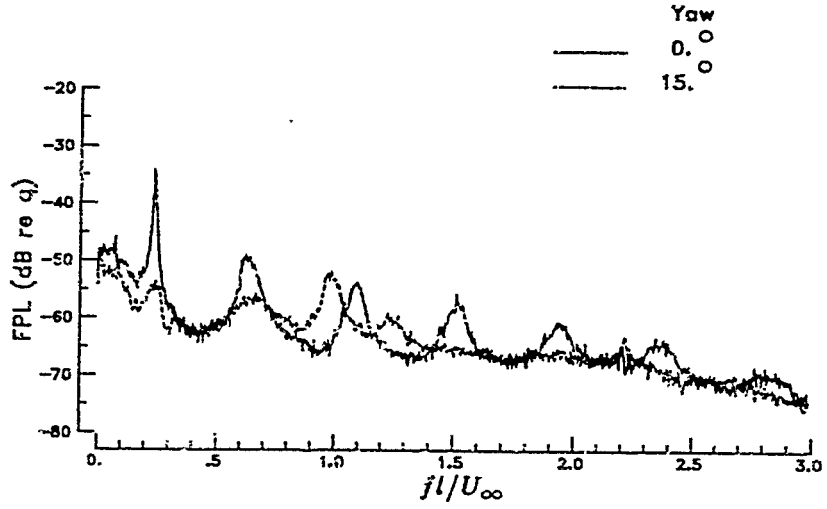

e.) M = 0.90 (Re = 12.x10^6/ft)

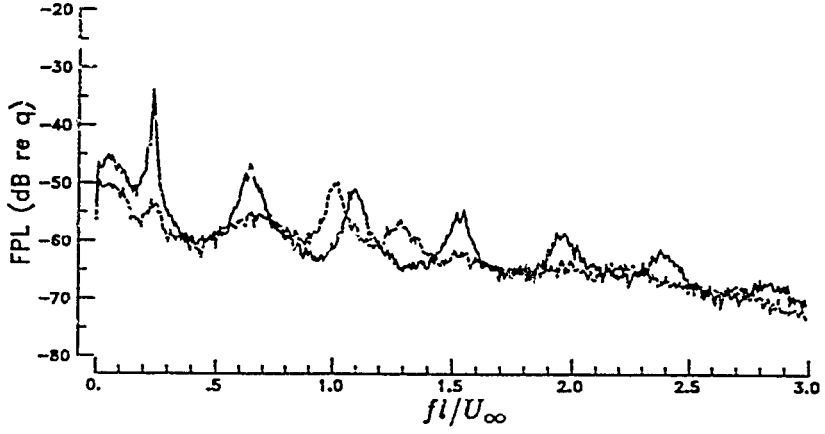

f.) M = 0.90 (Re = 100.x10^6/ft)

Figure 11. Continued.

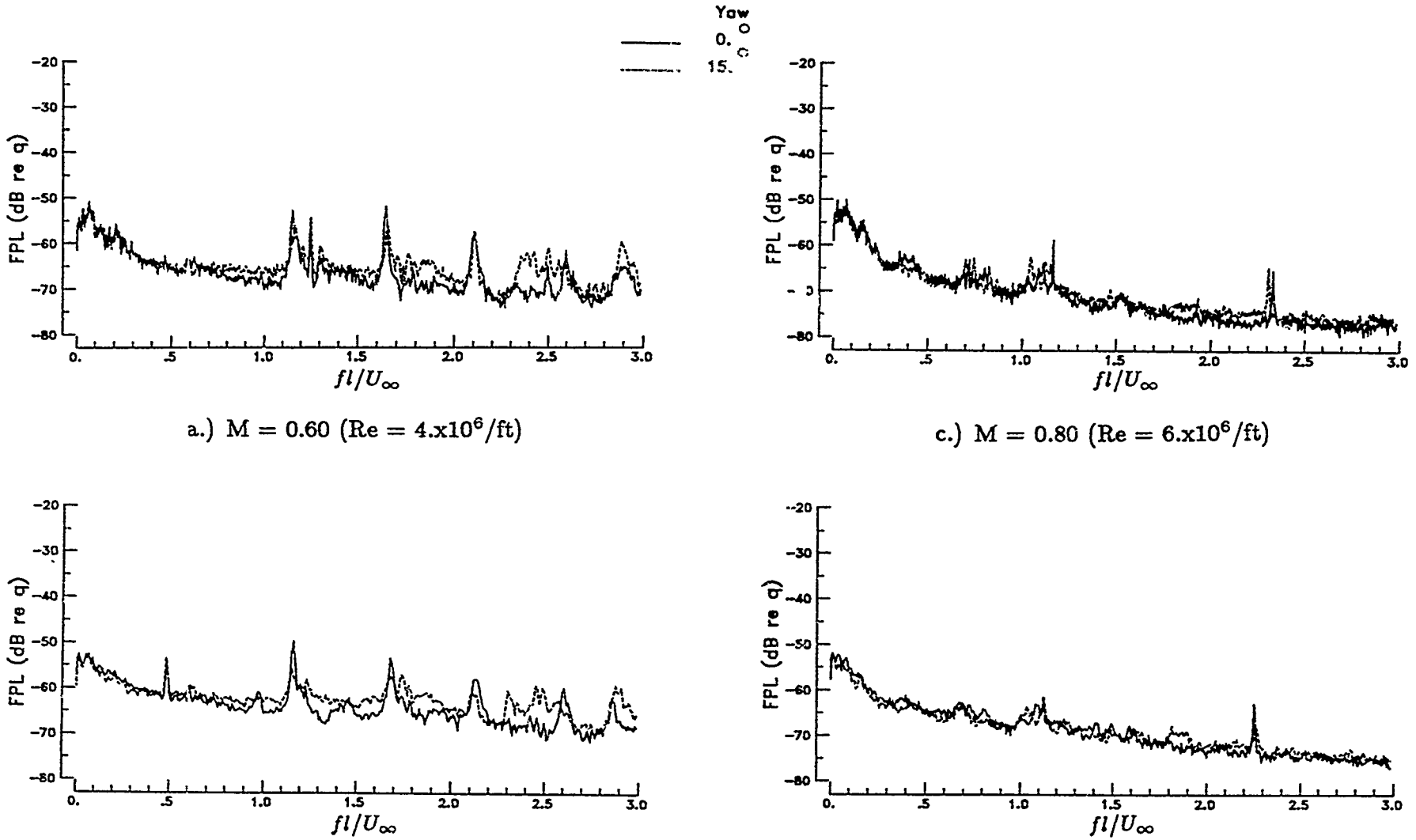

a.) M = 0.60 (Re = 4.x10^6/ft)

c.) M = 0.80 (Re = 6.x10^6/ft)

b.) M = 0.60 (Re = 85.x10^6/ft)

d.) M = 0.80 (Re = 99.x10^6/ft)

Figure 12. Effect of yaw on cavity fluctuating pressures. l/h = 12.67.

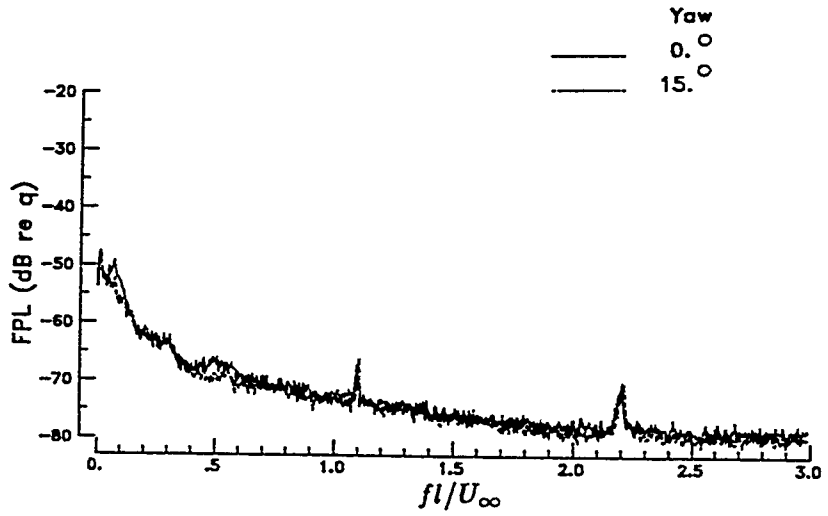

e.) M = 0.90 (Re = 13.x10^6/ft)

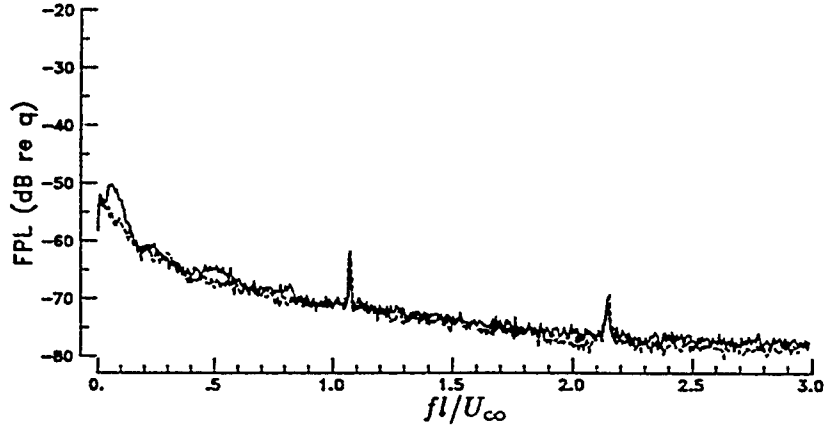

f.) M = 0.90 (Re = 100.x10^6/ft)

Figure 12. Continued.

Author's Autobiographies

Ms. M. B. Tracy has just been hired by NASA LaRC and will be working in the area of unsteady flow phenomena at transonic speeds. For the past 5 years, she has been employeed at LaRC as a contractor and was involved in the prediction of rotor-tone noise and experimental cavity acoustics. Ms. Tracy has been involved in studies of the coupling between cavity generated acoustic tones and structural vibrations of a store undergoing separation at supersonic speeds. She has also studied acoustic wave propagation in absorbing materials while employeed by the David Taylor Research Center. Ms. Tracy has a B.S. in physics from Loyola College and an M.S. in mechanics from The Johns Hopkins University.

Ms. E. B. Plentovich has been employed by the NASA Langley Research Center (LaRC) since 1980. She is currently working in the area of transonic store carriage and separation and is developing a program that would produce design strategies for store/aircraft integration that has recently received funding. Ms. Plentovich has been involved in many experimental studies, including store internal carriage, orifice induced pressure error, transport tests, and 2-D airfoil tests. She has a B.S. in aerospace engineering from Virginia Polytechnic Institute and State University (VPI&SU) and an M.S. in mechanical engineering from George Washington University.

Mr. J. Chu has been employed by NASA LaRC since 1981. He is currently working in the area of transonic, cryogenic, high-Reynolds-number aerodynamic research. This research includes commercial- and supersonic-transport tests and static- and fluctuating-pressure measurements on 2-D airfoil investigations. In the past, Mr. Chu has conducted experiments in a variety of facilities ranging from the low-speed regime of water tunnels and spin tunnels to the higher regime of transonic tunnels. He holds a B.S. in aerospace engineering from the Polytechnic Institute of New York.

Overview of Transonic Research on Internal Carriage at NASA Langley Research Center

E. B. Plentovich, M. B. Tracy, J. Chu
NASA Langley Research Center
Hampton, VA

R. L. Stallings, Jr.
Lockheed Engineering and Sciences Company
Hampton, VA

Introduction

NASA Langley Research Center (LaRC) has been involved in store carriage and separation research for many years with emphasis on the supersonic speed regime. Recently however, NASA LaRC has begun research into internal carriage at transonic speeds. This paper will present an overview of the two transonic experimental studies that have been conducted to provide information on the flow in cavities at transonic speeds, high Reynolds numbers, and at yaw. These tests are identified as the Transonic Cavity Flow Test and the High Reynolds Number Cavity Test. A new program being initiated to develop design strategies to provide soft optimization of store carriage and separation at transonic speeds will also be discussed. This program is referred to as the Transonic Store Carriage and Separation Program.

Transonic Cavity Flow Test

The first experimental investigation was conducted to expand the data base and the knowledge of flow in cavities over the subsonic and transonic speed regimes. A rectangular, three-dimensional cavity was tested in the David Taylor Research Center (DTRC) 7- by 10-Foot Transonic Wind Tunnel (TWT) over a Mach number range from 0.30 to 0.95 and at unit Reynolds numbers from 1×10^6 to 4.2×10^6 per foot. Two cavities were tested with length-to-height ratios (l/h) of 4.4 and 11.7 and with rectangular and nonrectangular cross-sections. Extensive static pressure data on the model walls were obtained. A more complete analysis and tabulation of these data can be found in ref. 1.

Wind Tunnel Description

The DTRC 7x10 TWT is a continuous flow, transonic facility which is capable of operating over a Mach number range from 0.2 to 1.17. The tunnel can obtain Reynolds numbers per foot from approximately 1.0×10^6 to 5.5×10^6. More information on this facility is documented in reference 2.

Model Description

A rectangular, three-dimensional cavity was mounted in a flat plate; a photograph of the model mounted in the tunnel is shown in figure 1. A flat plate was chosen as the parent body to allow a well defined two-dimensional flowfield to develop ahead of the cavity. The model was supported in the center of the tunnel by six legs. The forward two legs on each side were swept to longitudinally distribute the model cross-sectional area for blockage considerations. Two guy wires were attached to either side of the plate to increase lateral stiffness and stability. A fairing was placed around the cavity on the underside of the plate for aerodynamic purposes.

The cavity had a length of 3.5 ft., a width of 0.8 ft., and a maximum depth of 0.8 ft. The model dimensions are shown in figure 2. The floor of the cavity could be moved from the maximum depth of 0.8 ft. to a depth of 0.3 ft. or to the plate surface. The configuration with no cavity, the floor at the plate surface, was employed when the boundary layer thickness was

measured. The cavity l/h values tested were 4.4 for the deeper configuration (h = 0.8 ft.) and 11.7 for the more shallow configuration (h = 0.3 ft.).

The model was instrumented with 262 static pressures orifices. The majority of the orifices were concentrated on the cavity walls. Figure 3 shows the regions on the model where the orifices were located.

Test Conditions

The model was tested at Mach numbers from 0.3 to 0.95 and at unit Reynolds numbers ranging from 1.0 x 10^6 to 4.2 x 10^6 / foot. The Reynolds number was varied for fixed Mach numbers between 0.60 and 0.90.

Discussion of Results

In the data presentation, both instantaneous and time averaged pressures will be shown. The instantaneous measurements demonstrate the variation in pressures over a 1.25 second sampling period. (These measurements are noted on the figure title as 'individual data samples plotted.') To compare results between cavity configurations, Mach numbers, and Reynolds numbers, the data will be presented as the time average of all measurements taken at the specified test condition. (These measurements are noted on the figure title as 'average of 100 data samples plotted'.)

Static Pressure Unsteadiness.

Figure 4 shows the variation in pressure coefficient (C_p) along the cavity floor centerline for several individual samples taken during a 1.25 second period. (Note that x is the longitudinal distance on the model, see fig. 2.) Each sample is an instantaneous, unaveraged record of the data. Samples were chosen to show the wide variation in instantaneous static pressure measurements. As can be seen in the plots, there is a sizable change in the magnitude and shape of the pressure distribution on the cavity floor over time (t). Figure 4 is representative of the deep cavity data obtained at all Mach numbers tested and for Reynolds numbers of 3.3 x 10^6 / foot or greater. As the Reynolds number decreased, the unsteadiness also decreased, as illustrated by comparing the data in figures 4 and 5. Figures 4 and 5 also show that the pressure distribution is relatively smooth with no discontinuities. Notice that at $x/l \approx 0.275$ on fig. 4 and at $x/l \approx 0.45$ on fig. 5, there appears to be a node, all curves passing through approximately the same point. This is indicative of the presence of a standing wave which may be resulting from the interaction of the compression waves inside the cavity. Compression waves are formed as the shear layer dips into the cavity and the external flow contacts the rear cavity wall. Reference 3 gives specific details for the method by which the compression waves are formed and interact.

For the shallow cavity, the flow unsteadiness was much less than was seen for the deep cavity (see fig. 6). The increased steadiness of the flow in the shallow cavity would be expected because there is not a fluctuating shear layer as there is in a deep cavity.

Effect of Boundary Layer Thickness.

The shallow cavity was tested utilizing two methods for developing the boundary layer. In the first method, the boundary layer was artificially thickened using a 2 ft. band of no. 60 grit downstream of the leading edge, see fig. 2. The boundary layer in the second method developed naturally after being tripped near the leading edge of the flat plate. The boundary layer over the cavity, for both methods, was turbulent; however, these methods should generate different boundary layer thicknesses and the boundary layer that developed after being tripped at the leading edge should be the thinner. Because of time constraints, the boundary layer thickness was not measured when the leading edge trip was used; however, with the relatively simple model configuration of a flat plate with a turbulent boundary layer, the 1/7th power law of Stratford and Beavers, ref. 4, was used to provide an estimate of the boundary layer

thickness. The boundary layer thickness was computed to be approximately 0.60 in. (δ/l = 0.014) for M = 0.95, and R = 1.8 x 10^6, as compared to a 0.88 in. measured value for the artificially thickened configuration. The calculation of the thickness of the boundary layer that was generated with the leading edge strip does not need to be exact. What is important for this comparison is that there is a difference in the boundary layer thickness. Figure 7 shows the sensitivity of the shallow cavity pressure distribution to the boundary layer thickness (δ) entering the cavity. As can be seen, the effect is for the pressure distributions in the aft region of the cavity to become slightly more positive, and downstream of the cavity to become slightly more negative, when the boundary layer entering the cavity is thinner.

Summary

To aid in the understanding of the flow in cavities at transonic speeds, an experimental study was conducted in the DTRC 7x10 TWT. For this investigation, cavities with length to height ratios of 11.7 and 4.4 were tested at Mach numbers from 0.3 to 0.95 and at unit Reynolds numbers from 1.0 x 10^6 to 4.2 x 10^6 / foot. Static pressures were measured on the model and the boundary layer thickness was measured 2 in. upstream of the leading edge of the cavity. For the shallow cavity (l/h = 11.7), runs were made with and without artificially thickening the boundary layer. The comparison between artificially thickened and not-thickened boundary layers showed the pressure distribution in the aft portion of the cavity to be sensitive to boundary layer thickness entering the cavity. The measured pressures in the aft portion of the cavity were greater for the thinner boundary layer runs. For the deep cavity (l/h = 4.4) configuration at Reynolds numbers greater than 3.0 x 10^6 / foot, the instantaneous 'static' pressure samples on the cavity floor were seen to fluctuate significantly over the 1.25 second sampling period. For the deep cavity at lower Reynolds numbers and for all conditions tested with the shallow cavity, the data showed much less unsteadiness. Though mean static pressure distributions have been used in past deep cavity analysis with transonic free-stream conditions, the data presented here indicate that averaged data may not be adequate when determining cavity dynamic loads or instantaneous cavity flowfields.

High Reynolds Number Cavity Test

The second experimental investigation was conducted to more fully evaluate the effect of Reynolds number on the flowfield in a rectangular, box cavity. This investigation was conducted in the NASA LaRC 0.3-Meter Transonic Cryogenic Tunnel (TCT) at Mach numbers from 0.2 to 0.9 and at unit Reynolds numbers from 2 x 10^6 to 100 x 10^6 per foot. Cavity variables were length-to-height ratio, 4.4, 6.7, 12.67, and 20.0, (cavity length = 11.25 in.) and yaw angle, 0° and 15°. Mean static and fluctuating pressure data were obtained. Instantaneous static pressure data were not available; therefore, only the mean static pressure data are discussed herein. The analysis of the fluctuating pressure data are contained in a separate paper in this Symposium, ref. 5.

Wind Tunnel Description

The tests were conducted in the 13-inch by 13-inch two-dimensional adaptive wall test section of the NASA LaRC 0.3-m TCT. The 0.3-m TCT is a fan-driven, cryogenic pressure tunnel which uses gaseous nitrogen as a test medium. It is capable of operating at stagnation temperatures from approximately 80K to 327K, and at stagnation pressures from 1.2 atmospheres to 6.0 atmospheres. The fan speed is variable so that the empty test section Mach number can be varied continuously from about 0.20 to 0.95. This combination of test conditions provides a test envelope of chord Reynolds numbers up to about 100 million based on a model chord of 12 inches. Additional details of the tunnel may be found in references 6 and 7.

Model Description

The model tested was a rectangular, three-dimensional box cavity mounted on the sidewall of the 0.3-m TCT test section. The cavity model was centered in a sidewall turntable, about sta. 0. The position of the turntable in the test section is shown in fig. 8. The model was fabricated to allow the use of the angle-of-attack drive for positioning of the model to 0 and 15° yaw angles.

The cavity had a length of 11.25 in., a width of 2.50 in. and a maximum depth of 2.56 in. The floor of the cavity could be positioned at various depths to produce the cavity configurations while length and width were fixed. The cavity l/h values tested were 4.4 (h = 2.56 in.), 6.7 (h = 1.68 in.), 12.67 (h = 0.89 in.), and 20.0 (h = 0.56 in.). A configuration with no cavity, the floor at the plate surface, was used to provide a solid sidewall for determining boundary layer thickness. Photographs of the model are provided in figures 9 and 10. Figure 9 shows the model prior to tunnel installation with the floor of the cavity positioned at a depth of 2.56 in. (l/h = 4.4). Figure 10 shows the model mounted in the tunnel in the configuration for measuring the boundary layer (no cavity and the boundary layer rake installed).

The model was instrumented with 21 static pressure orifices and 18 flush-mounted fluctuating pressure transducers, figure 11 is a sketch of the instrumentation layout. The forward and aft walls of the cavity are instrumented with only a single fluctuating pressure transducer located at the center of the wall in each configuration.

Test Conditions

The model was tested at Mach numbers from 0.2 to 0.90, unit Reynolds numbers ranging from 2.0 x 10^6 to 100 x 10^6 / foot, and yaw angles of 0° and 15°. The model was tested at a reduced set of conditions and configurations for yaw = 15°. The flexible test section walls were set to a 'streamlined' shape for each test condition. The term 'streamlined' walls refers to the setting of the test section walls such that they have been contoured to reduce the interference on the model from the walls.

Discussion of Results

Reynolds Number Effects.

The effect of Reynolds number on cavity flowfield was a principle focus of the test. For this study the model was mounted on the sidewall of the tunnel. This method of mounting resulted in the sidewall boundary layer thickness being the boundary layer thickness entering the cavity. The use of the sidewall boundary layer created a very thick boundary layer entering the cavity and one that was relatively insensitive to Reynolds number. Because of the use of the sidewall boundary layer, the value of δ/l changes little as compared to the factor of 50 change in free-stream Reynolds number, so the effects shown are due to the Reynolds number itself.

Figure 12 shows a comparison of Reynolds numbers at M = 0.80 for the various cavity configurations at yaw = 0°. As can be seen in the plots, there is very little change in the mean C_p distribution over the range of Reynolds numbers tested.

The pressure distributions at yaw = 15° are provided in figure 13. Again Reynolds number is seen to have no significant impact on the pressure distributions. There are some slight differences in the measured pressures; however, these differences have minimal effect on flowfield characteristics. (Data were not taken for the l/h = 20.0 cavity configuration at yaw = 15°.)

Effect of l/h Change.

Figures 14 and 15 provide a comparison of cavity pressure measurements for the different cavity configurations. The cavity length remained fixed at 11.25 in., but depth was varied to generate cavities with l/h ratios of 4.4, 6.7, 12.67, and 20.0. Because of the minimal variation in pressure distribution with Reynolds number this comparison is shown for R = 90 x 10^6 / foot. Figure 14 compares the data at yaw = 0°. The cavity flowfield type for l/h = 4.4 is an open

cavity flowfield and for l/h = 20.0 is a closed cavity flowfield, as anticipated from supersonic results. Also based on supersonic results, the cavity configuration of l/h = 6.7 was expected to be an open flowfield, but the pressure distribution of the present test shows that the flowfield is transitional-open at M = 0.60 and has a tendency toward the open type at higher Mach numbers. Also, a cavity with a length-to-depth ratio of 12.67 would be expected to be transitional in nature; however, at M = 0.60 the flowfield is closed and becomes transitional-closed at higher Mach numbers.

Figure 15 compares the data for yaw = 15° and at R = 90 x 10^6. Here it is seen that the flow is transitional-closed for l/h ratios of 4.4 and 6.7 and of the closed type for l/h = 12.67. (The l/h = 20.0 cavity configuration was not tested at yaw = 15°.)

Effect of Yaw Angle.

Figure 16 compares mean pressure distributions for the two yaw angles tested at various Mach numbers for each cavity configuration. (The l/h = 20.0 cavity configuration was not tested at yaw = 15°.) The effect of yaw angle on a closed or a transitional cavity flow was seen to be minimal, see figs. 16(b) and (c). However, if the flowfield was open at yaw = 0°, when the cavity was yawed to 15° the flowfield became transitional in type and a much larger change in the mean pressures was seen, fig. 16(a).

Summary

To provide information on the effect of Reynolds number on cavity flowfields at subsonic and transonic speeds, an experimental study was conducted in the NASA LaRC 0.3-m TCT. For this investigation cavities with length to height ratios of 4.4, 6.7, 12.67, and 20.0 were tested at Mach numbers from 0.2 to 0.90 and at unit Reynolds numbers from 2 x 10^6 to 100 x 10^6 / foot. Static and fluctuating pressures were measured on the model and the boundary layer thickness was measured at the cavity leading edge position. For the range of Reynolds number tested, Reynolds numbers had no significant effect on the mean pressure distribution. The effect of yaw on the cavity mean pressure distribution was most pronounced if the flowfield was of the open type at yaw = 0°; the flowfield became transitional at yaw = 15°. However, if the flowfield at yaw = 0° was transitional or closed, the effect of yaw on the cavity pressure distribution was very minimal. This test also showed that the types of flowfield at subsonic conditions will occur for a different range of l/h ratios than is seen at supersonic conditions.

Transonic Store Carriage and Separation Program

Research in the area of store carriage and separation at supersonic speeds has been ongoing at NASA LaRC for many years. At transonic speeds; however, there is insufficient information on store and parent aircraft flowfields and the interaction between them for providing information to the designers of the integrated system. To support this effort, LaRC has begun a long-term program to study store carriage and separation at transonic speeds. It is the goal of the program to investigate, understand, and model the transonic flow physics associated with store carriage and separation. In achieving this goal we will develop design strategies related to generic stores and parent aircraft that will simultaneously optimize low observability; low, acceptable drag; and safe, accurate separation over the desired speed regime.

NASA LaRC has several unique capabilities that will enable it to accomplish this program. Among them are the talents and tools for conducting basic and applied research. The program will require that experimental and computational people work as a team to fulfill the goal. At NASA LaRC there is a strong base of experimental, theoretical and applied computational capability from which the necessary expertise can be drawn. A third capability at NASA LaRC is that the program will be conducted with consideration of the flow physics independent of a specific configuration. The program was developed to enable concepts that can be applied to any configuration to be developed.

DOD/ Industry Approach

The usual approach used by DOD and industry to study store carriage and separation is the captive trajectory system (CTS). Other methods which are also used are:

1. drop the store and use a camera to observe the trajectory or
2. measure the flow angularity around an aircraft and estimate the trajectory of the store from the data.

These approaches are oriented toward qualifying a specific configuration, so tests are conducted for each new store/aircraft combination. The CTS method is very complex and only allows for the testing of small-scale models. The small size limits the amount of instrumentation that can be placed within the model and therefore limits the amount of information that can be obtained relative to store carriage and separation. Information on the CTS method and computational approaches to predict store separation trajectories can be found in ref. 8.

NASA LaRC Approach

The approach to be used by NASA LaRC will be oriented to generic configurations. The steps are sketched in fig. 17.

The first step in the approach will be to generate the flowfield around a parent aircraft. Two methods were considered for accomplishment of this step. The first was experimentally oriented. A 3-component laser doppler velocimeter was considered for use to survey the flowfield under the parent aircraft. This method was not currently available for transonic testing and is very time extensive, so it was not chosen, but it is still considered as a means to verify the method that was chosen. The second method, the one planned for use, is to computationally generate the flowfield. Computational methods can provide accurate information on the flowfield around an aircraft in a reasonable length of time. Additionally, because the flowfield in the region where the store will be carried is the critical area to be modeled, the aircraft grid will not be as complex because the lower surface of an aircraft is fairly flat. The reduction in grid complexity will also decrease the computation time required. Another beneficial aspect that arises from the consideration of generic configurations is that only the gross properties of the flow in the region of the store will need to be modeled. From this standpoint, an Euler solution may be all that is necessary to determine the large-scale flow properties.

The next step will be to configure the flow over a flat plate to simulate the calculated flow properties around the parent aircraft. The flat plate used in the previously described cavity test at the DTRC 7x10 TWT has been modified for installation in the NASA LaRC 8-Foot Transonic Pressure Tunnel (TPT). This model will become the generic parent aircraft surface from which store carriage and separation testing will be conducted. To simulate the desired flowfield, inserts will be placed on the tunnel walls and the flat plate. The design of the tunnel and model insert configurations will be done computationally.

The use of a flat plate and inserts to simulate the flow around the parent aircraft will enable many flowfields to be modeled with minimal expense for model costs. The size of the flat plate/cavity model will also enable larger scale store models to be tested than could be done with the CTS. A five-hole probe will be used to verify the flowfield around the cavity.

The last step will be to conduct the store carriage and release studies in a flowfield that simulates the flow under an aircraft. For this step, a store positioning system would need to be developed. The system envisioned would use a twin-screw arrangement to provide vertical movement and angle-of-attack and a separate roll mechanism. This system would be mounted downstream of the flat plate and would be used not only for positioning the store, but also for the five-hole probe survey of the flowfield. An important benefit from this method of testing is its flexibility. The current program is based on store carriage and separation characteristics in an internal cavity so that low observability aspects are optimized; however, the configuration

could be easily adapted to look at external and conformal carriage if the need arose. This set-up could also be arranged to test a specific configuration.

Another aspect of this approach is the development and verification of computational programs and the critique of design and problem-solving methods. In most programs, this aspect is generally treated as a separate problem. In this program it is planned to have the theoretical, analytical and experimental people work as a single team so resources, knowledge and ideas can be readily exchanged.

FY91 Plans

The majority of the effort in FY91 will be concentrated in two areas. The first being the design and construction of the store positioning hardware that was described in the above section. The second area consists of two tests currently scheduled for testing in the 8-ft. TPT.

The first test will determine the length-to-height ratios where the flowfield transitions from closed to open flow. The cavity model described previously for the DTRC test has been modified to allow the aft wall of the cavity to be remotely positioned to various lengths. The cavity width and depth will be manually positioned. Cavity length-to-height ratios from 2 to 20 will be able to be obtained. Two other aspects of this investigation are under consideration. The first aspect is the study of the effect of cavity scale on cavity flowfields. For scaling it is necessary to hold the ratios of length-to-height, width-to-depth, and boundary layer thickness-to-depth constant. To scale the boundary layer thickness, methods are being considered which would double the thickness of the boundary layer. A second aspect being studied is the use of a large eddy breakup device (LEBU) as proposed in ref. 9. The pressure fluctuations downstream of the LEBU are expected to be reduced which would possibly have an affect on the cavity acoustics. Consideration is being given to the design of a simple LEBU to determine if there is an improvement in the cavity acoustic level.

The second experimental investigation planned will use the same flat plate/cavity model. Inserts will be placed within the cavity to study passive venting concepts. The concepts being considered are designed to passively alter the cavity flowfield to generate an environment more conducive to store separation and to attenuate acoustic intensity. Three methods of passively venting the cavity will be studied and are sketched in fig. 18. The arrows in fig. 18 describe the expected pattern for pressure venting. In all methods static and fluctuating pressure measurements will be obtained. The first method will consist of a porous floor plate, see fig. 18(a). This method has been tried at supersonic speeds, ref. 10, and was found to successfully modify a closed cavity flowfield pressure distribution to one of an open cavity type. With the porous plate the high pressures at the rear of the cavity will be allowed to vent to the low pressures at the forward region of the cavity through a vent chamber under the porous floor. The second method for consideration with shallow cavities is the pipe vent, see fig. 18(b). This method is similar to the porous floor in that the high pressure region in the rear of a shallow cavity is allowed to vent to the low pressure region in the forward portion of the cavity; however, the method through which the venting is accomplished is different. In the pipe vent concept, circular pipes are placed on the floor of the shallow cavity. Both ends of the pipes are open to allow the venting of the pressure from the rear of the cavity to the front. This concept is being considered as a possible means of altering the cavity flowfields in existing aircraft. The third method has been proposed for deep cavities and is termed a lip vent, fig. 18(c). This method results from the idea that altering the vortex formation at the cavity leading edge could cause the acoustic intensity within the cavity to be decreased. The lip vent operates by venting the high pressure on the outer edge of the cavity rear face to the lower pressure region on the outer edge of the cavity front face. Again, the venting is accomplished through a vent chamber outside of the cavity.

Concluding Remarks

NASA LaRC has been involved in the area of store carriage and separation for several years.

In the past, supersonic speeds have been the primary focus; however, currently the transonic speed regime is of primary interest. A long-term program has been undertaken to look at the characteristics of store carriage and separation at transonic speeds. This effort will team theoretical, analytical and experimental capabilities to develop design strategies for the soft optimization of low observability; low, acceptable drag; and safe, accurate separation. The approach to be used will develop strategies for application to any configuration. Until the store positioning hardware is built, several tests with a clean cavity configuration are planned. These tests will look at defining the length-to-height (l/h) ratios at which the flowfield transitions from close to open. (Recall that in the previously described test in the 0.3-m TCT, it was found that the l/h ratios where the flowfield transitioned were different than occurred for supersonic speeds.) The second test will investigate the effects of three passive venting concepts on the static and fluctuating pressure distributions inside deep and shallow cavities.

References

1. Plentovich, E. B.: Three-Dimensional Cavity Flowfields at Subsonic and Transonic Speeds. NASA TM-4209, 1990.
2. ASED staff: Transonic Wind-Tunnel Facility at the Naval Ship Research and Development Center. Report ASED 332, June 1975.
3. Heller, Hanno H. and Bliss, Donald B.: Aerodynamically Induced Pressure Oscillations in Cavities - Physical Mechanisms and Suppression Concepts. AFFDL-TR-74-133, February 1975.
4. Stratford, B.S. and Beavers, G.S.: The Calculation of the Compressible Turbulent Boundary Layer in an Arbitrary Pressure Gradient - A Correlation of certain previous Methods. R. & M. No. 3207, September 1957.
5. Tracy, M. B.; Plentovich, E. B.; Chu, J.; and Shearin, J. G.: Cavity Acoustics in High Reynolds Number Transonic Flows. Presented at the Eighth Aircraft/Stores Compatibility Symposium, Oct. 23-25, 1990.
6. Mineck, Raymond E.: Hardware and Operating Features of the Adaptive Wall Test Section for the Langley 0.3-Meter Transonic Cryogenic Tunnel. NASA TM-4114, June 1989.
7. Ladson, Charles L. and Ray, Edward J.: Evolution, Calibration, and Operational Characteristics of the Two-Dimensional Test Section of the Langley 0.3-Meter Transonic Cryogenic Tunnel. NASA TP-2749, September 1987.
8. Keen, K. Scott: New Approaches to Computational Aircraft/Store Weapons Integration. AIAA-90-0274, January 8-11, 1990.
9. Komerath, N. M.; Ahuja, K. K.; and Chambers, F. W.: Prediction and Measurement of Flows Over Cavities - A Survey. AIAA-87-0166, January 12-15, 1987.
10. Wilcox, F. J., Jr.: Passive Venting System for Modifying Cavity Flowfields at Supersonic Speeds. AIAA Journal, vol. 26, no. 3, March 1988, pp. 374-376.

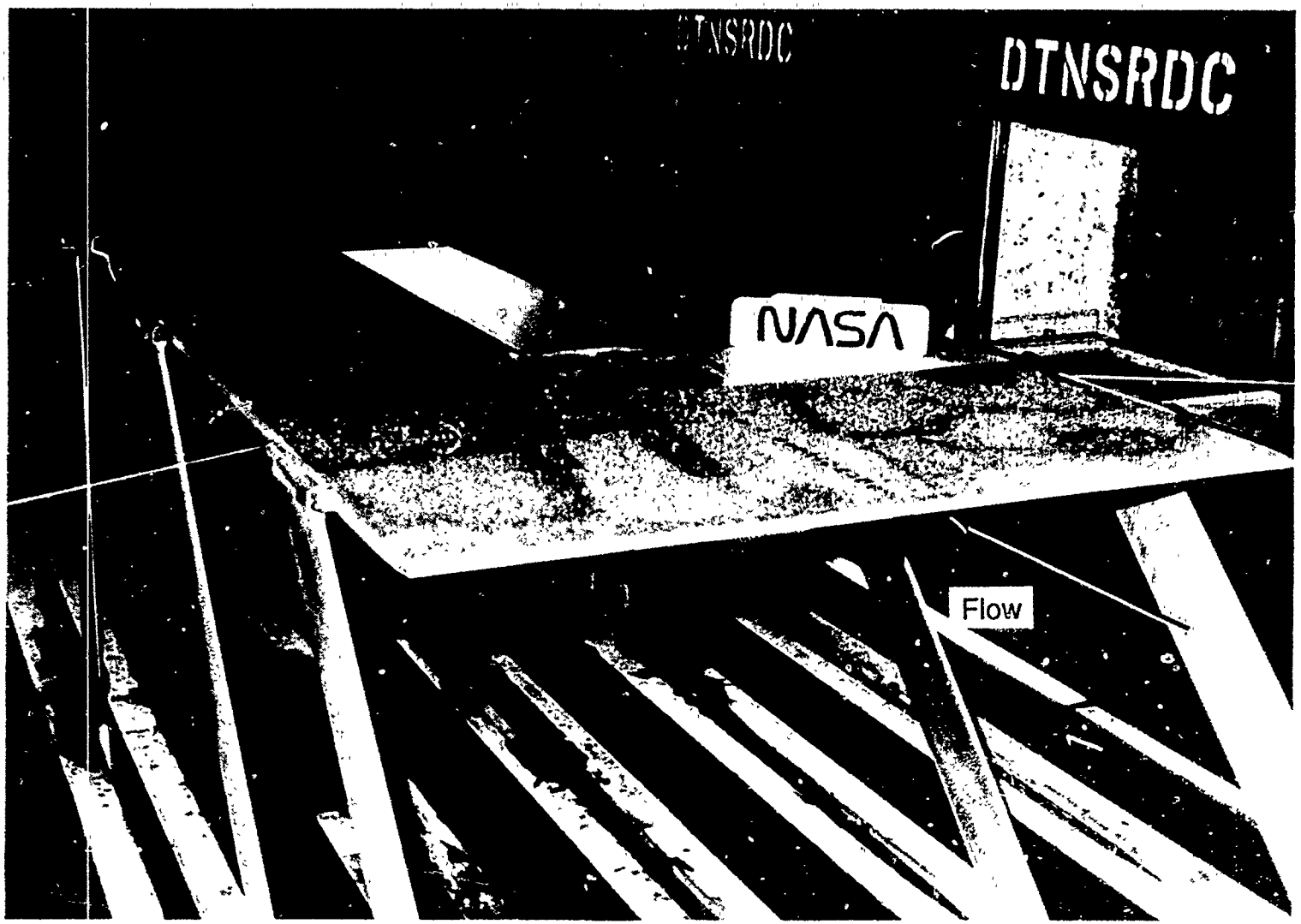

Figure 1.- Transonic cavity flow model installed in DTRC 7x10 TWT.

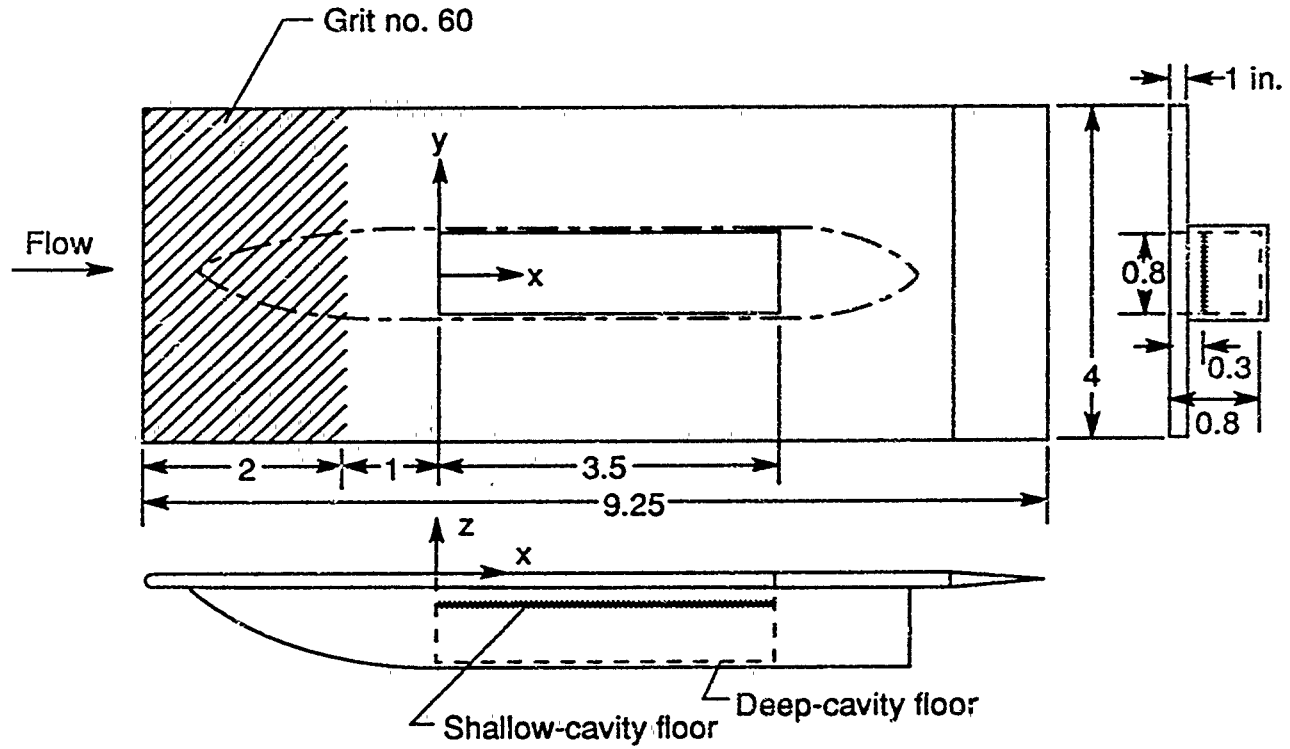

Figure 2.- Schematic drawing of transonic cavity flow model. (All dimensions are in feet unless otherwise noted.)

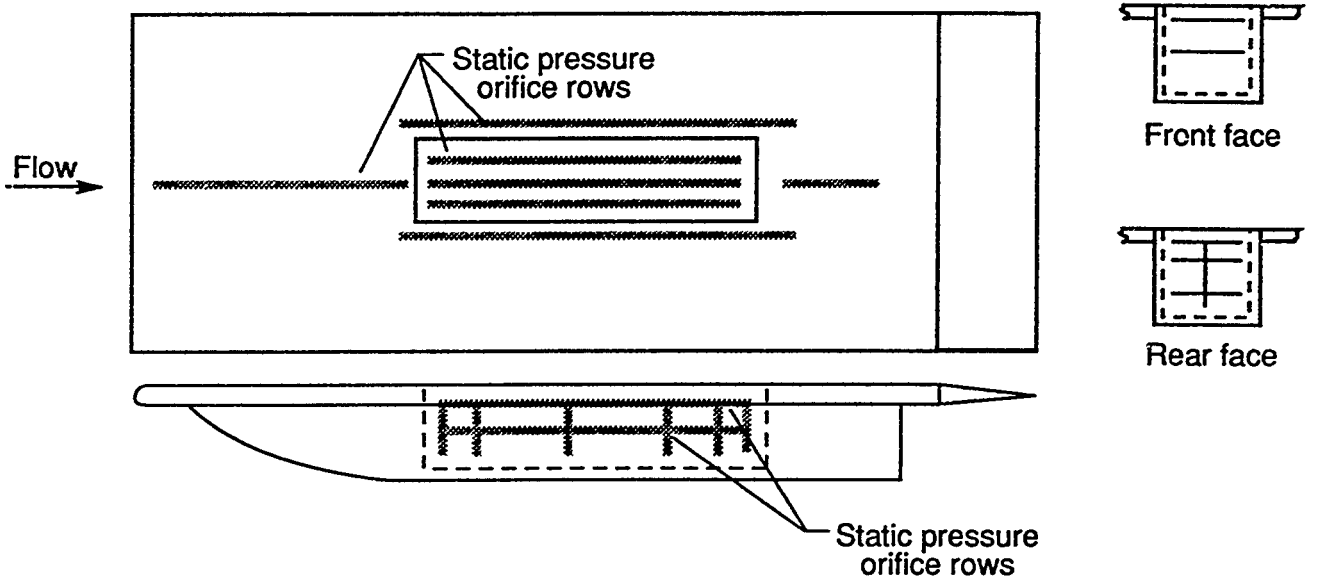

Figure 3.- Static pressure orifice locations.

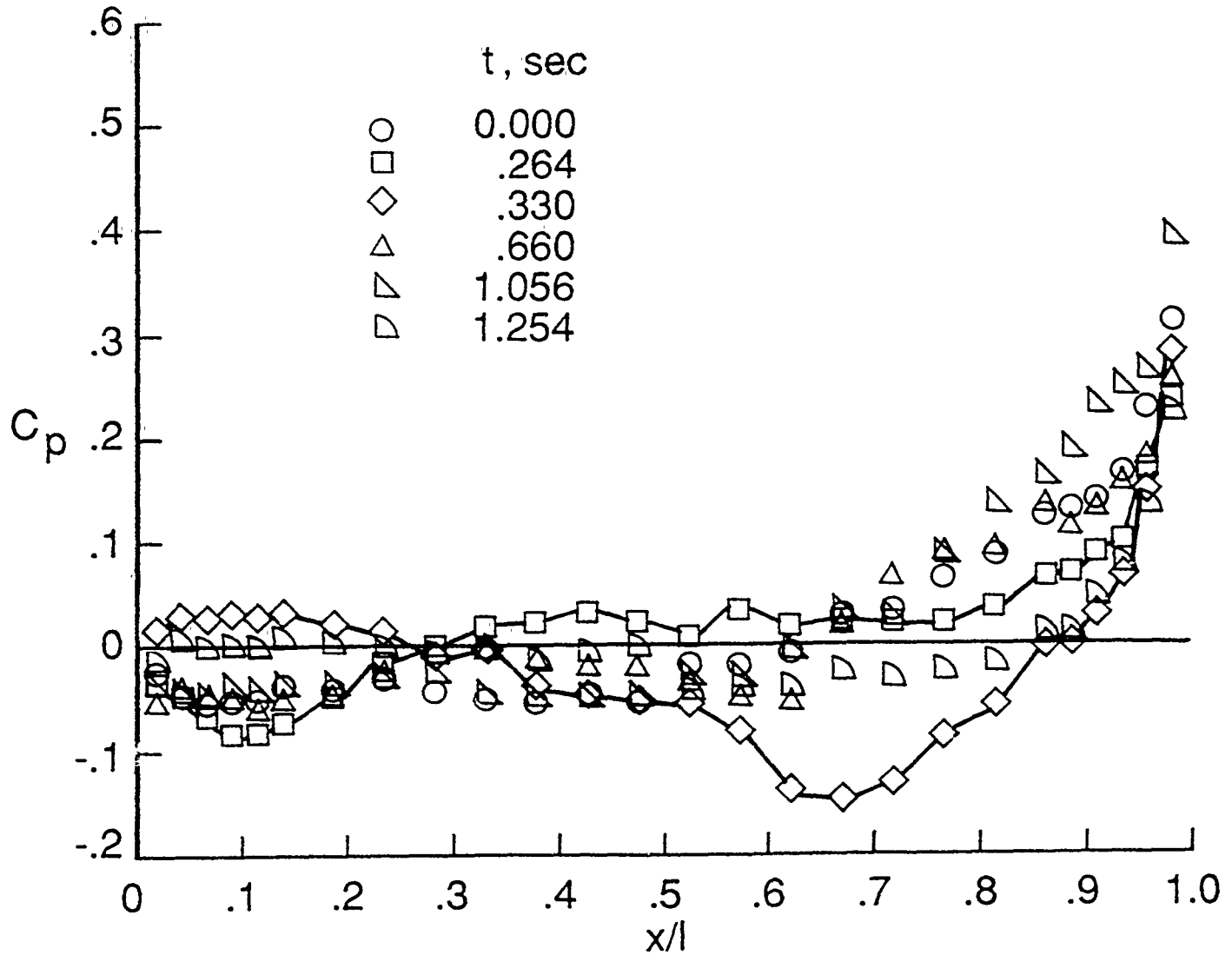

Figure 4.- Variation of cavity floor centerline pressure distributions with time, l/h = 4.4, M = 0.60, R = 3.5 x 10^6. (Individual data samples plotted.)

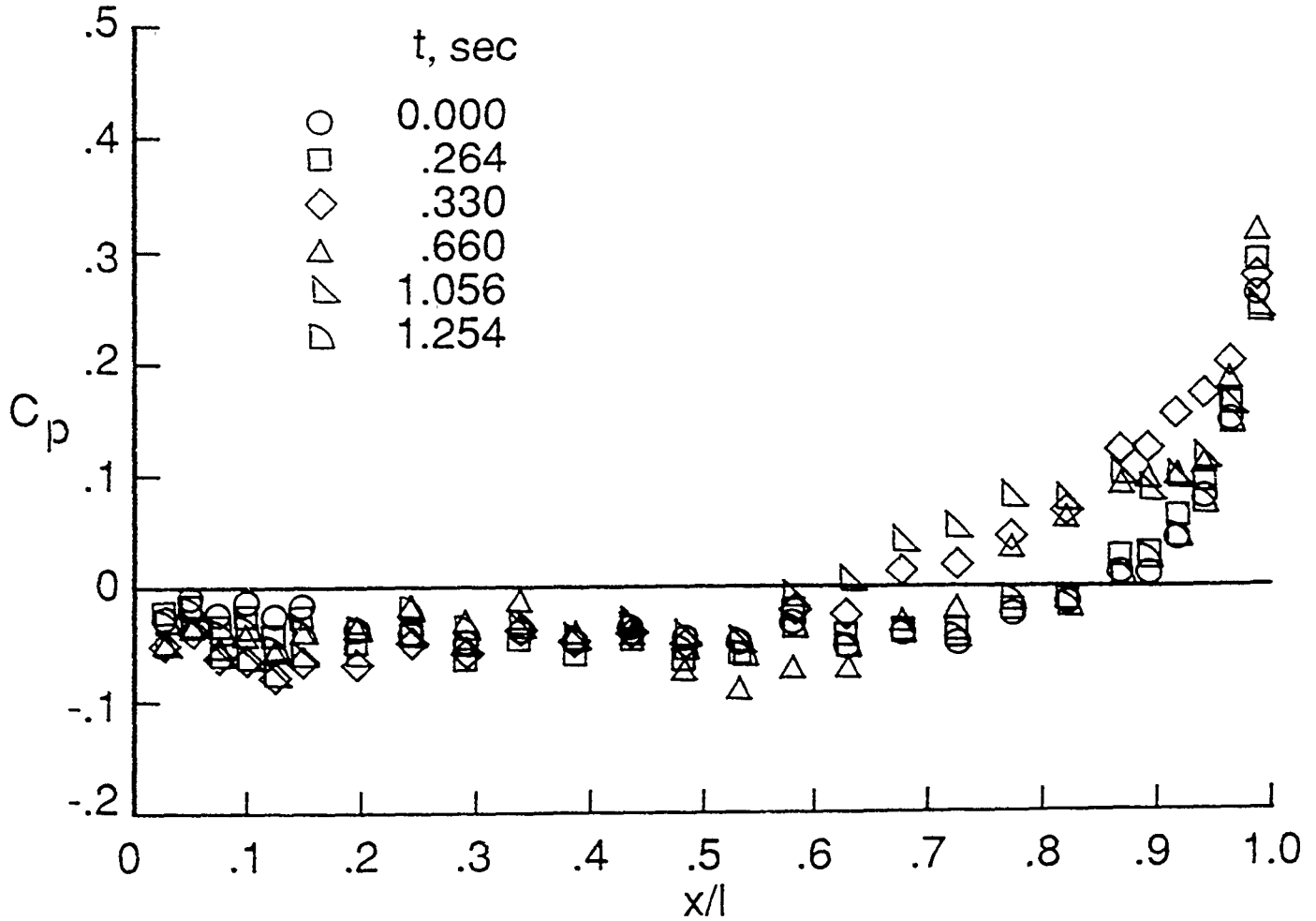

Figure 5.- Variation of cavity floor centerline pressure distributions with time, l/h = 4.4, M = 0.60, R = 1.6 x 10^6. (Individual data samples plotted.)

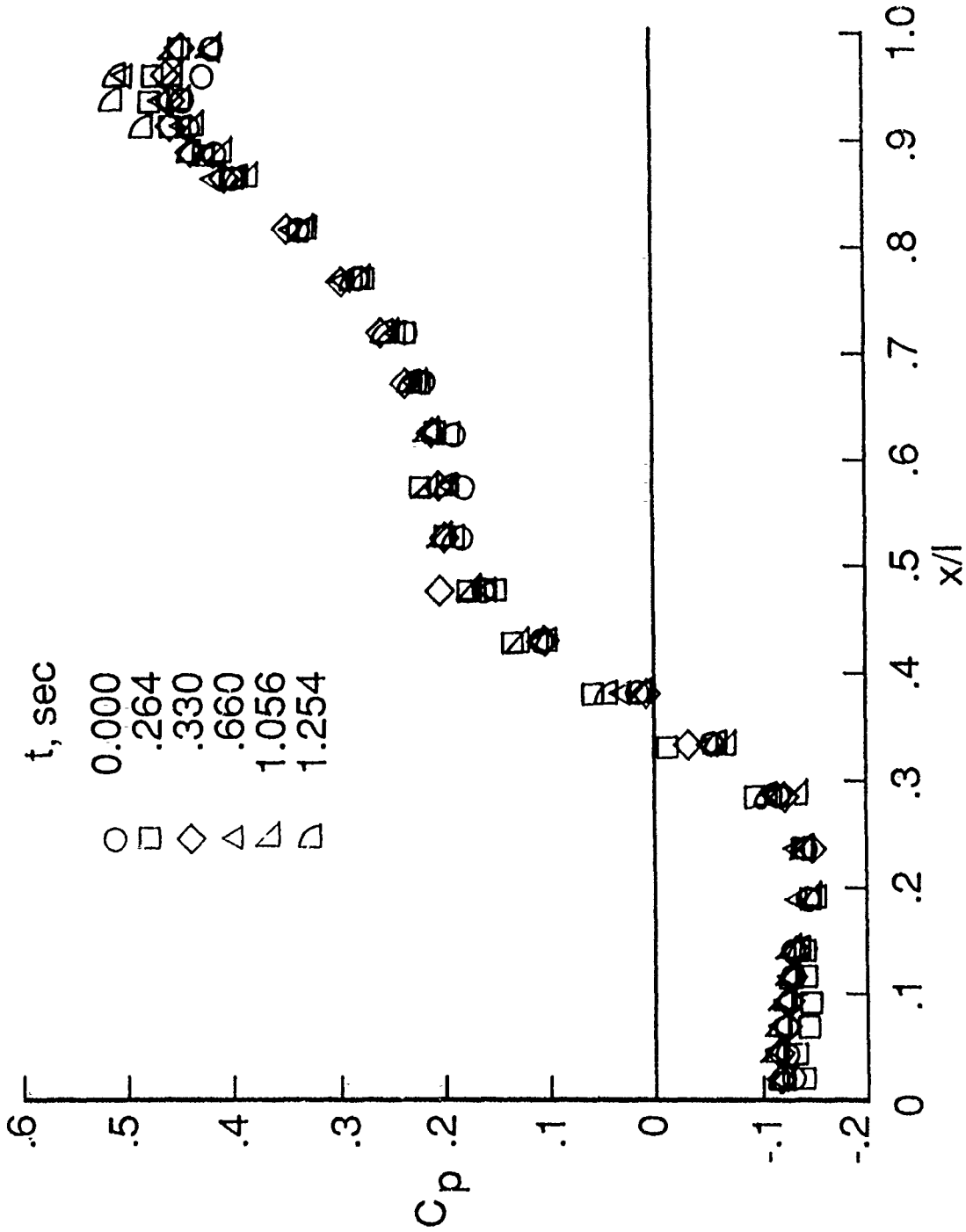

Figure 6.- Variation of cavity floor centerline pressure distributions with time, l/h = 11.7, M = 0.60, R = 3.5 x 10^6. (Individual data samples plotted.)

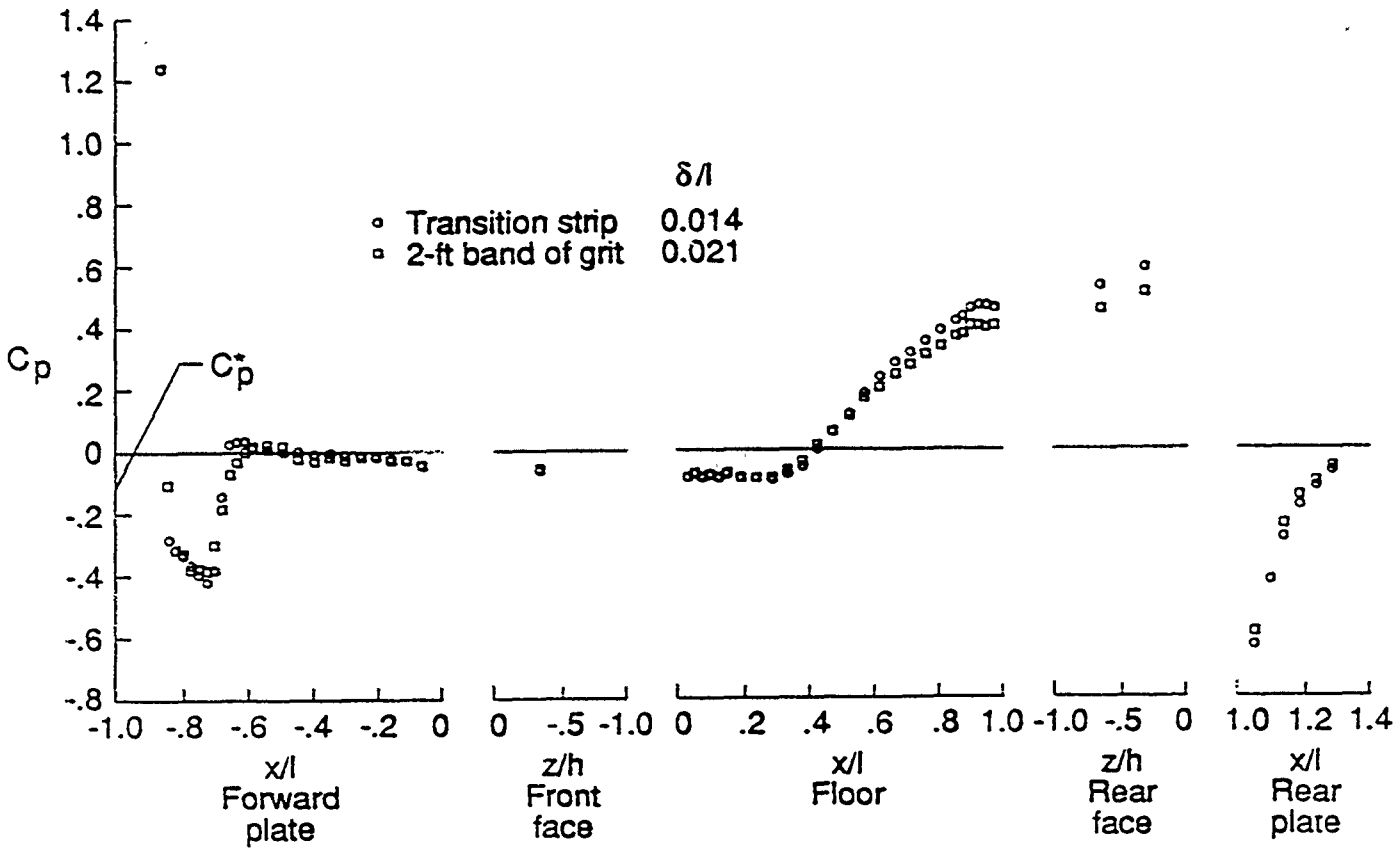

Figure 7.- Effect of boundary-layer thickness on centerline pressure distributions, l/h = 11.7, M = 0.95, R = 1.7 x 10^6. (Average of 100 data samples plotted.)

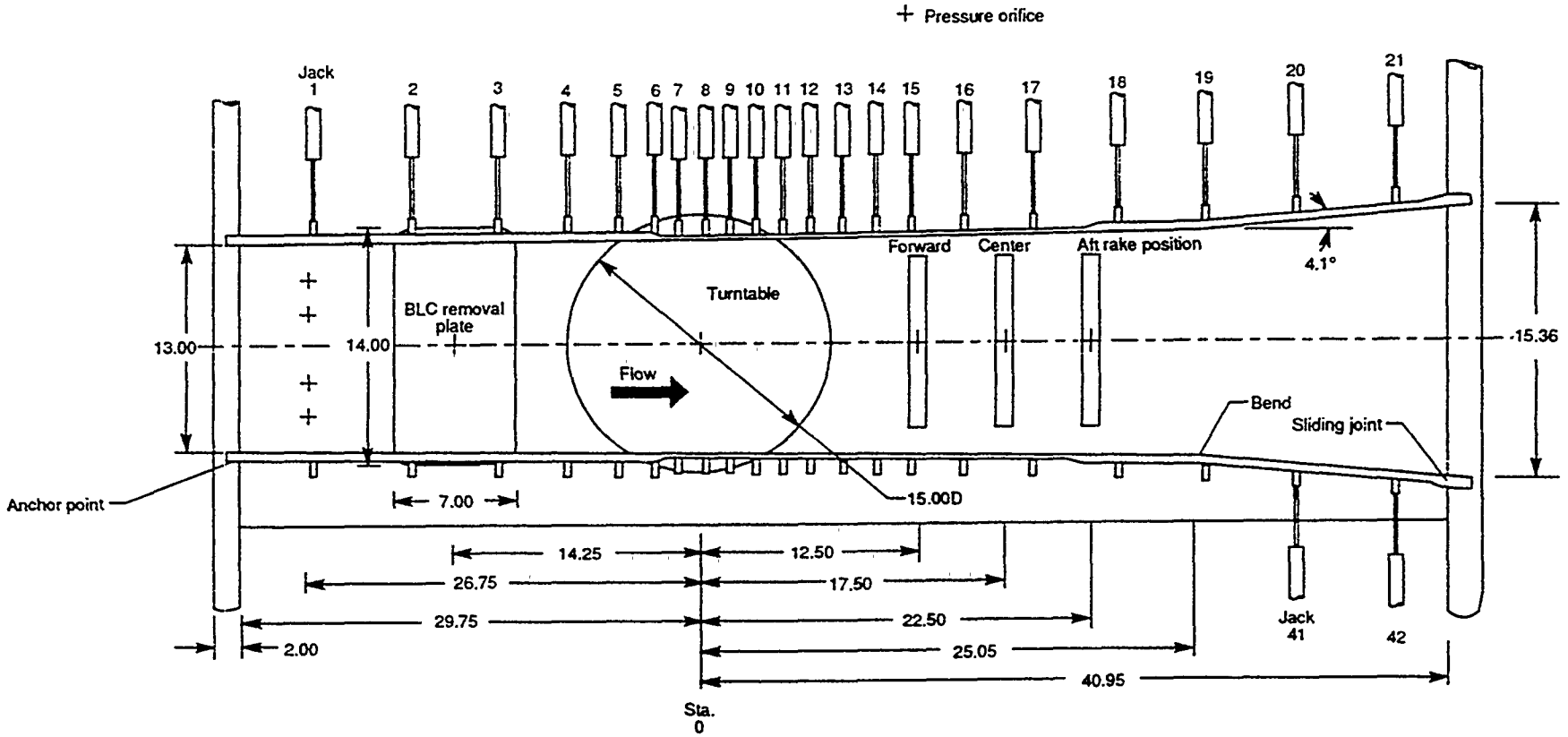

Figure 8.- Details of flow region of 13- by 13- inch adaptive wall test section; some lower wall jacks omitted for clarity, ref. 6. (All dimensions are in inches.)

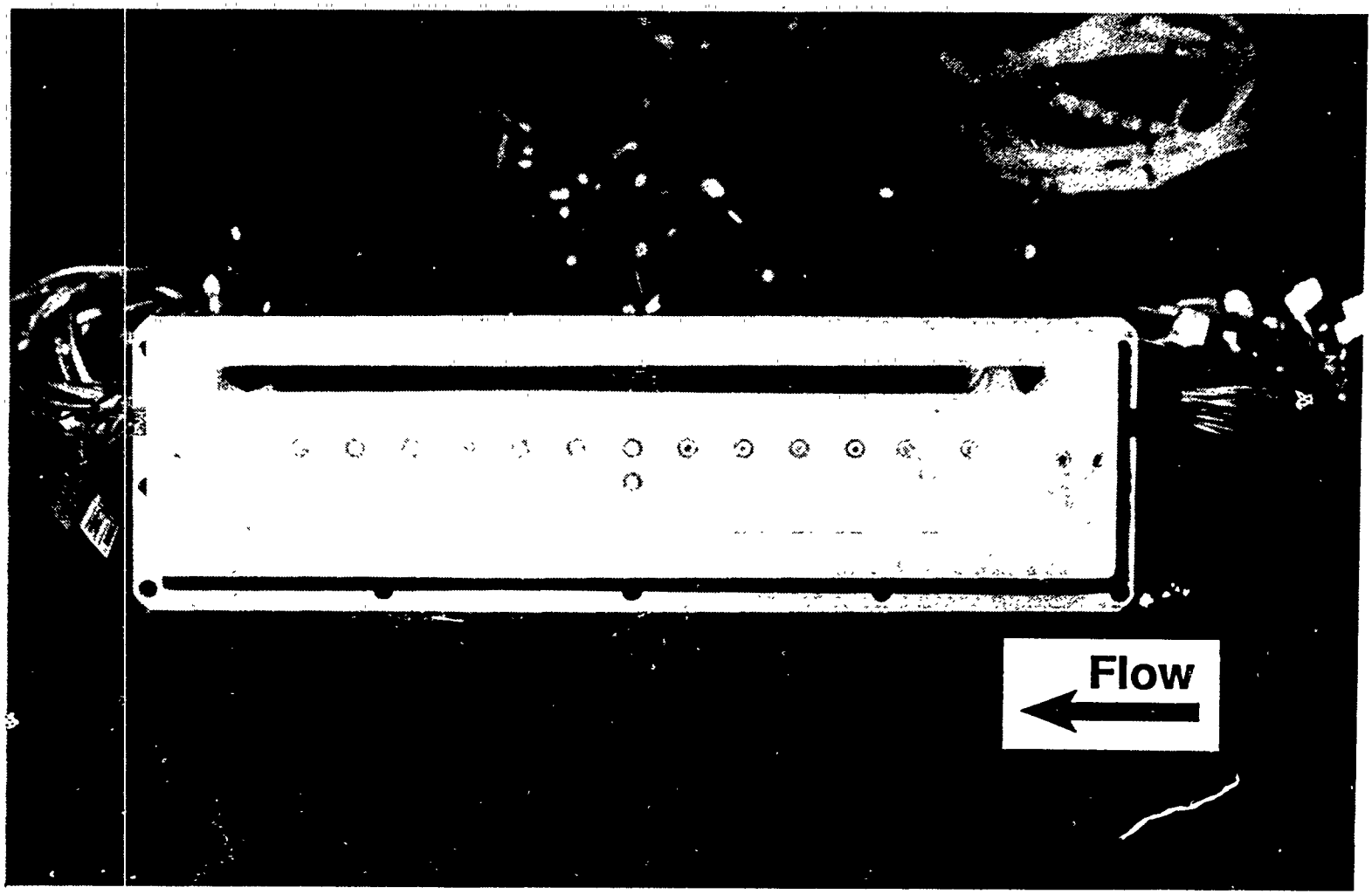

Figure 9.- Photograph of high Reynolds number cavity model prior to tunnel installation.

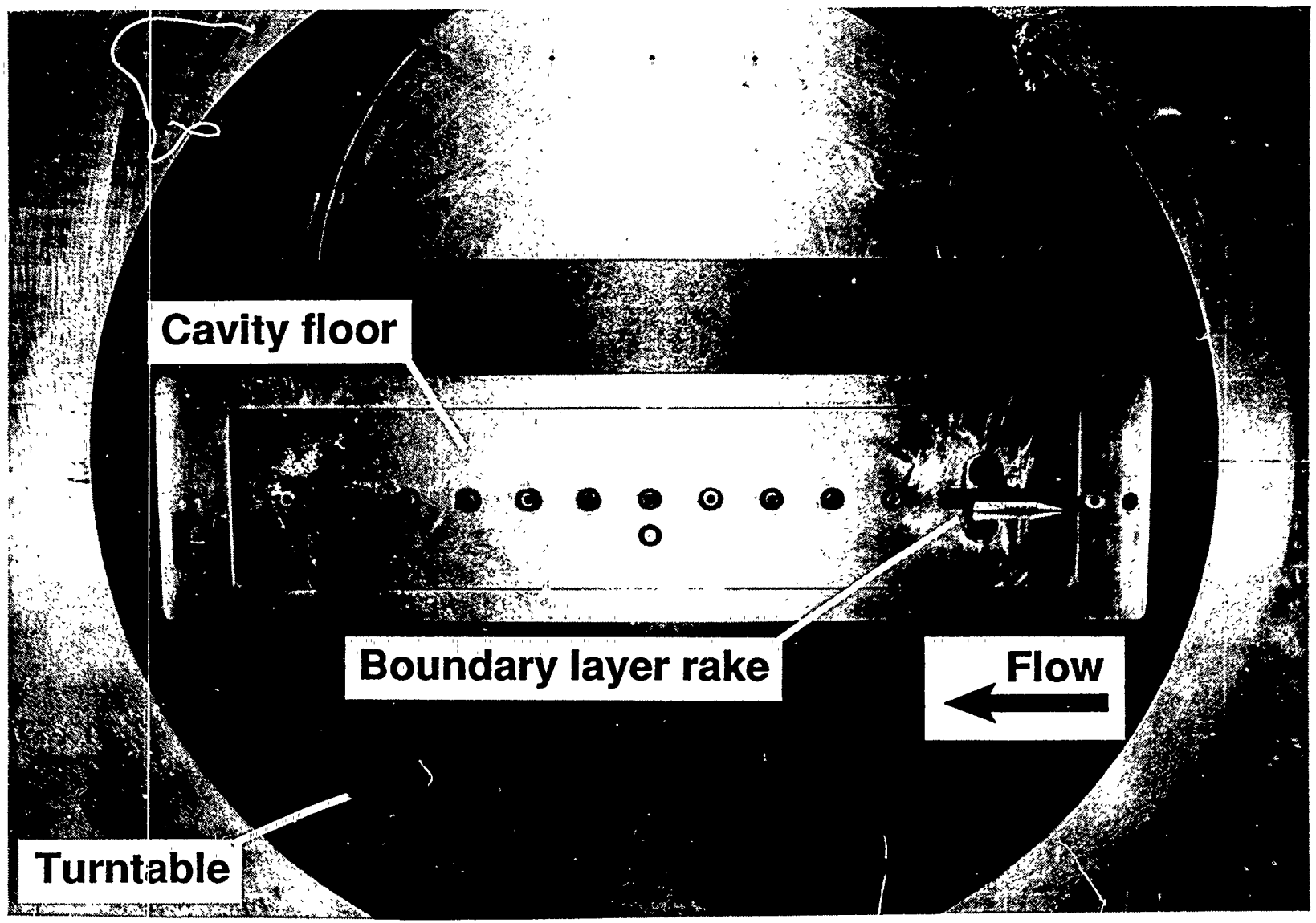

Figure 10.- Photograph of model installed in tunnel.

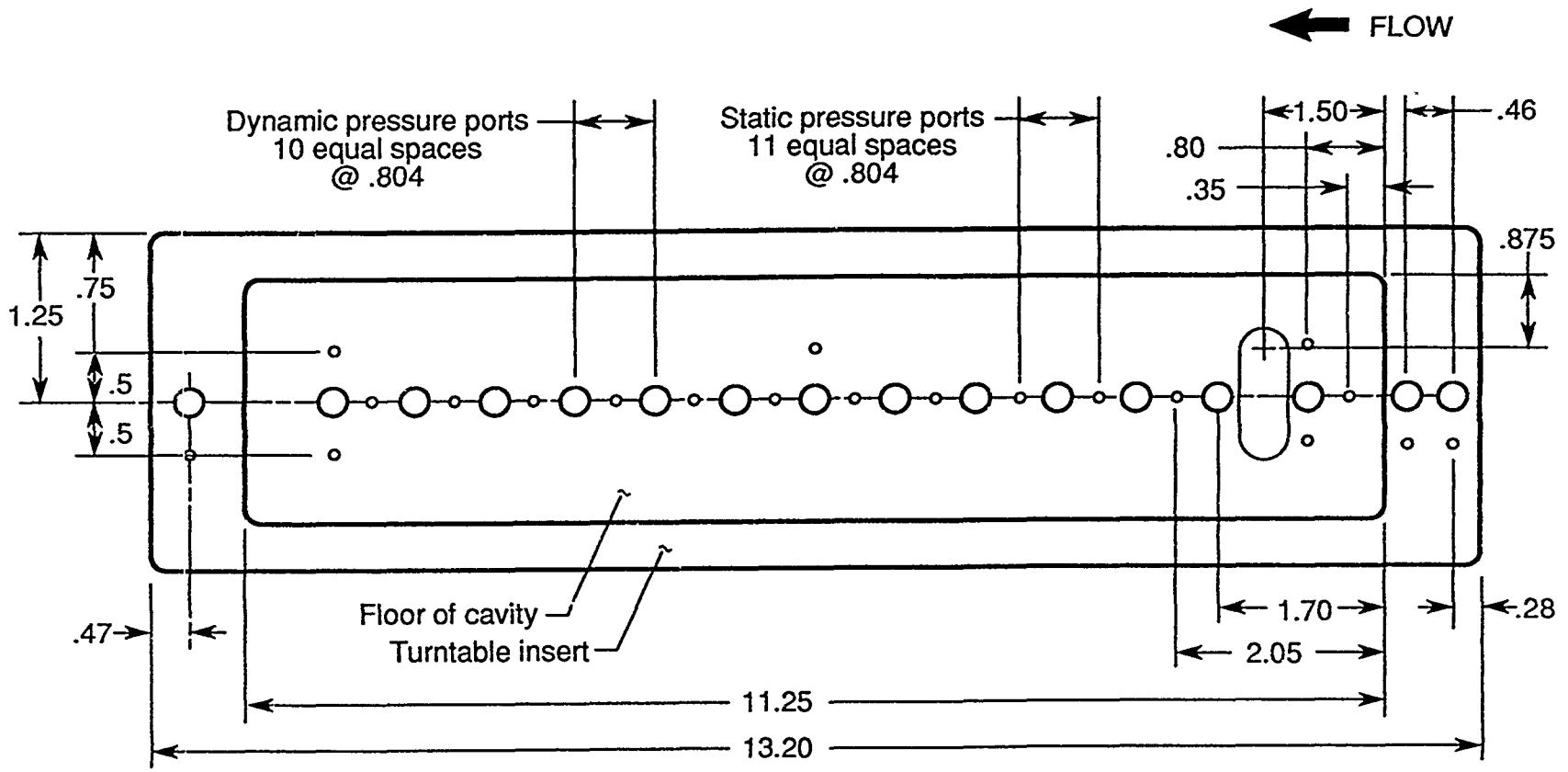

Figure 11.- Sketch of instrumentation layout.

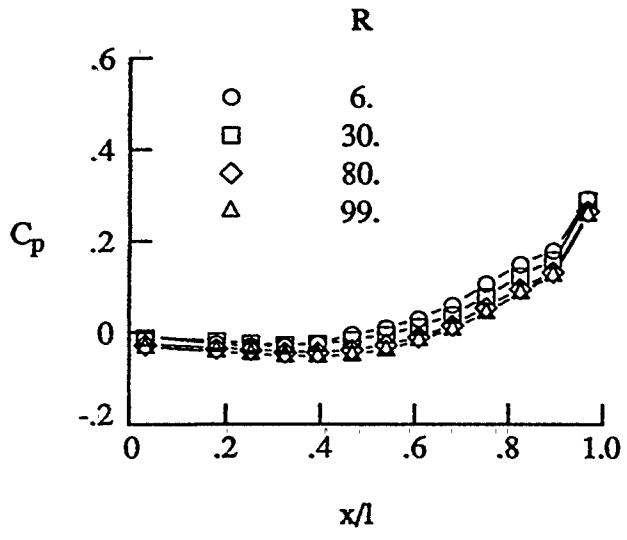

(a) l/h = 4.4

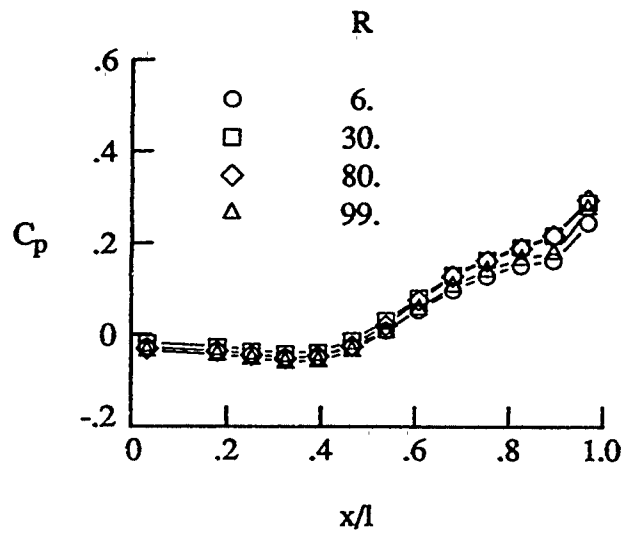

(b) l/h = 6.7

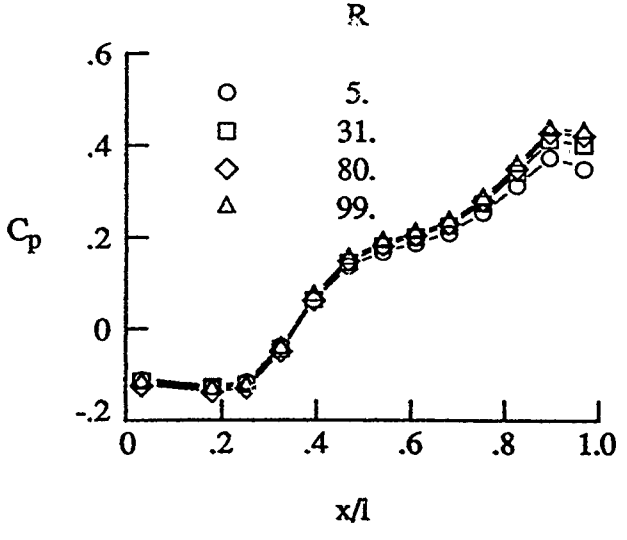

(c) l/h = 12.67

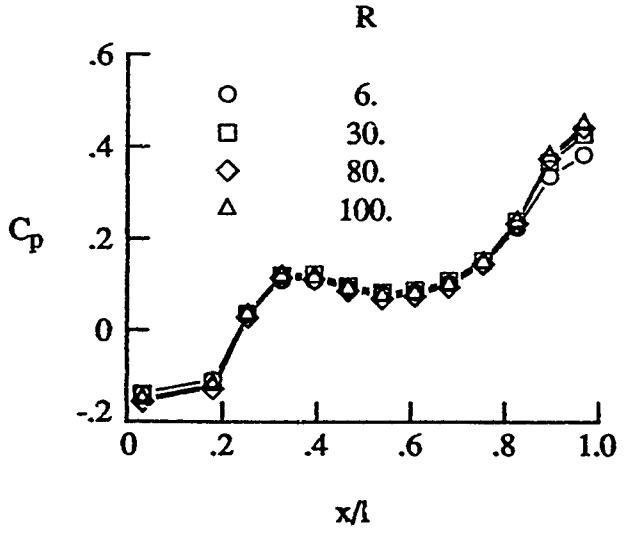

(d) l/h = 20.0

Figure 12.- Effect of Reynolds number on cavity pressure distributions at M = 0.80 and yaw = 0°.

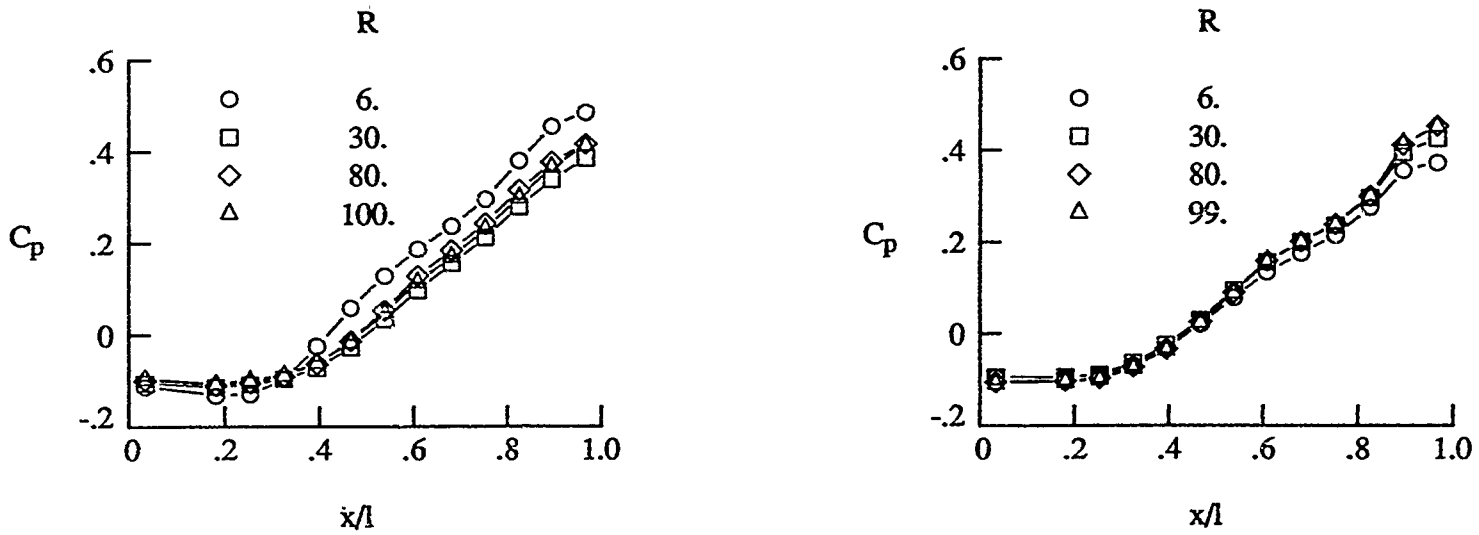

(a) l/h = 4.4

(b) l/h = 6.7

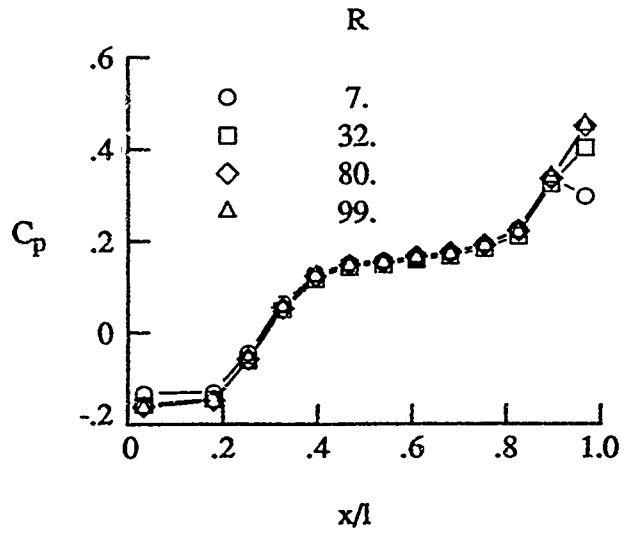

(c) l/h = 12.67

Figure 13.- Effect of Reynolds number on cavity pressure distributions at M = 0.80 and yaw = 15°.

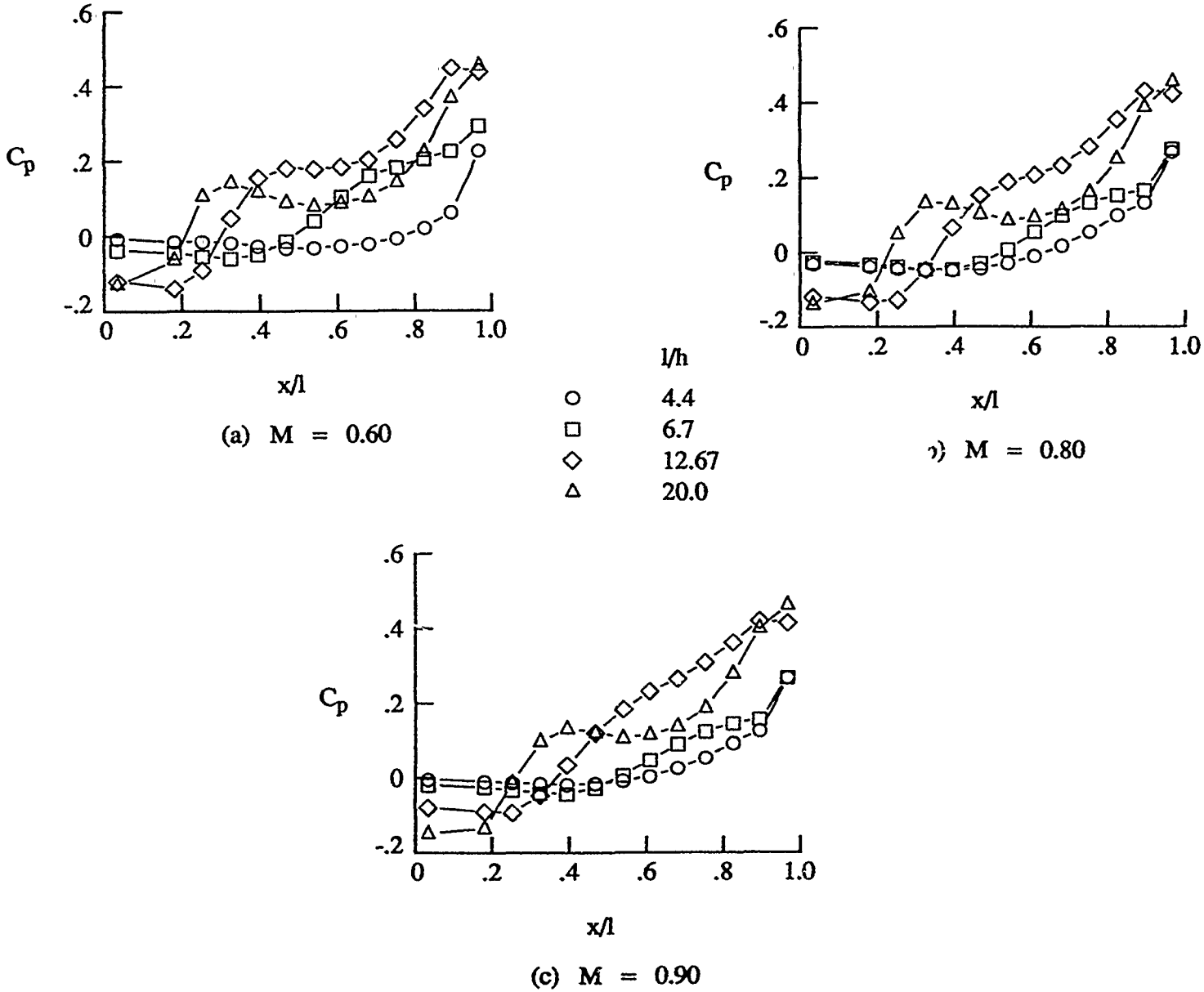

(a) M = 0.60

(b) M = 0.80

(c) M = 0.90

Figure 14.- Effect of cavity depth on pressure distributions, R = 90 x 10^6 and yaw = 0°.

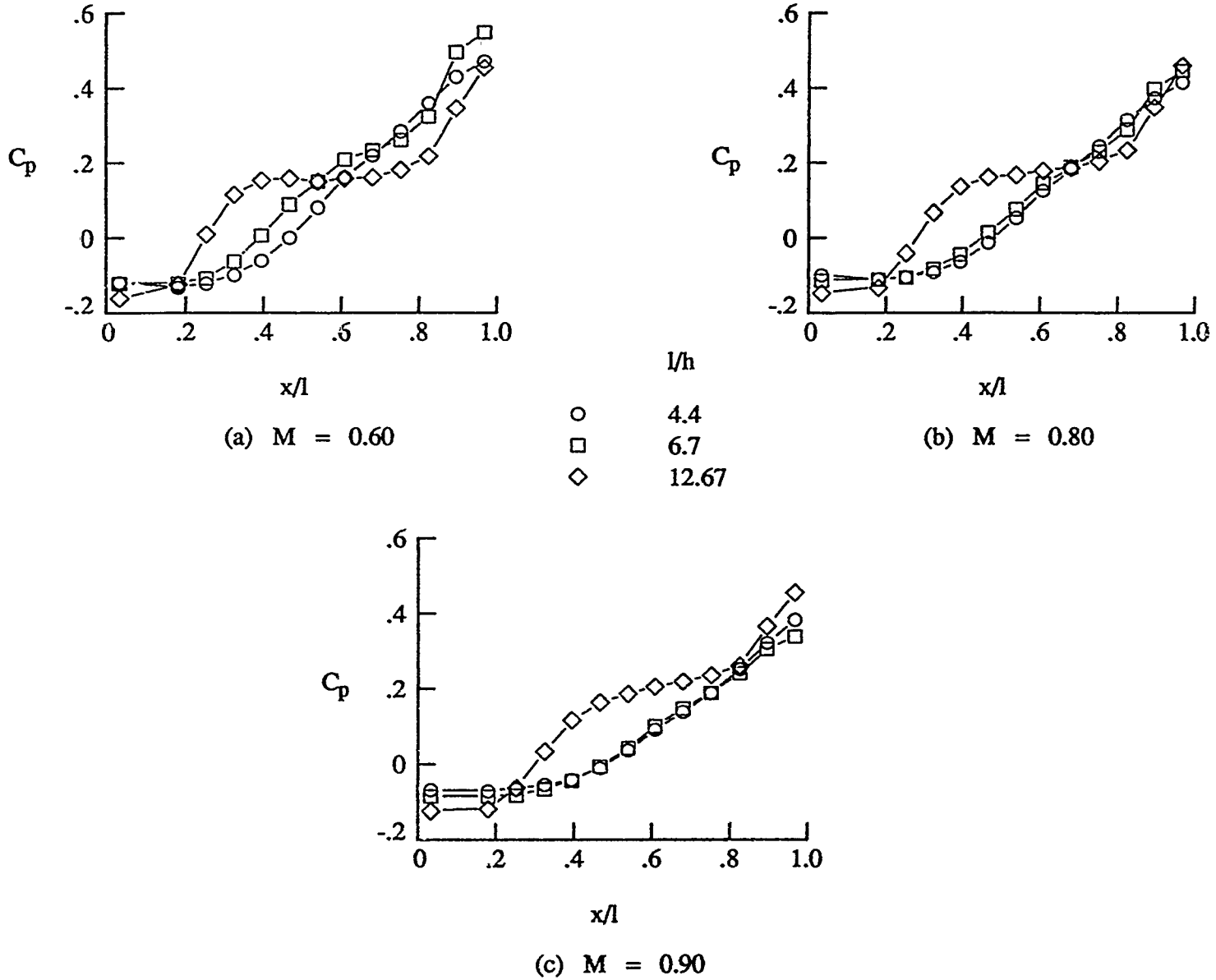

Figure 15.- Effect of cavity depth on pressure distributions, R = 90 x 10^6 and yaw = 15°.

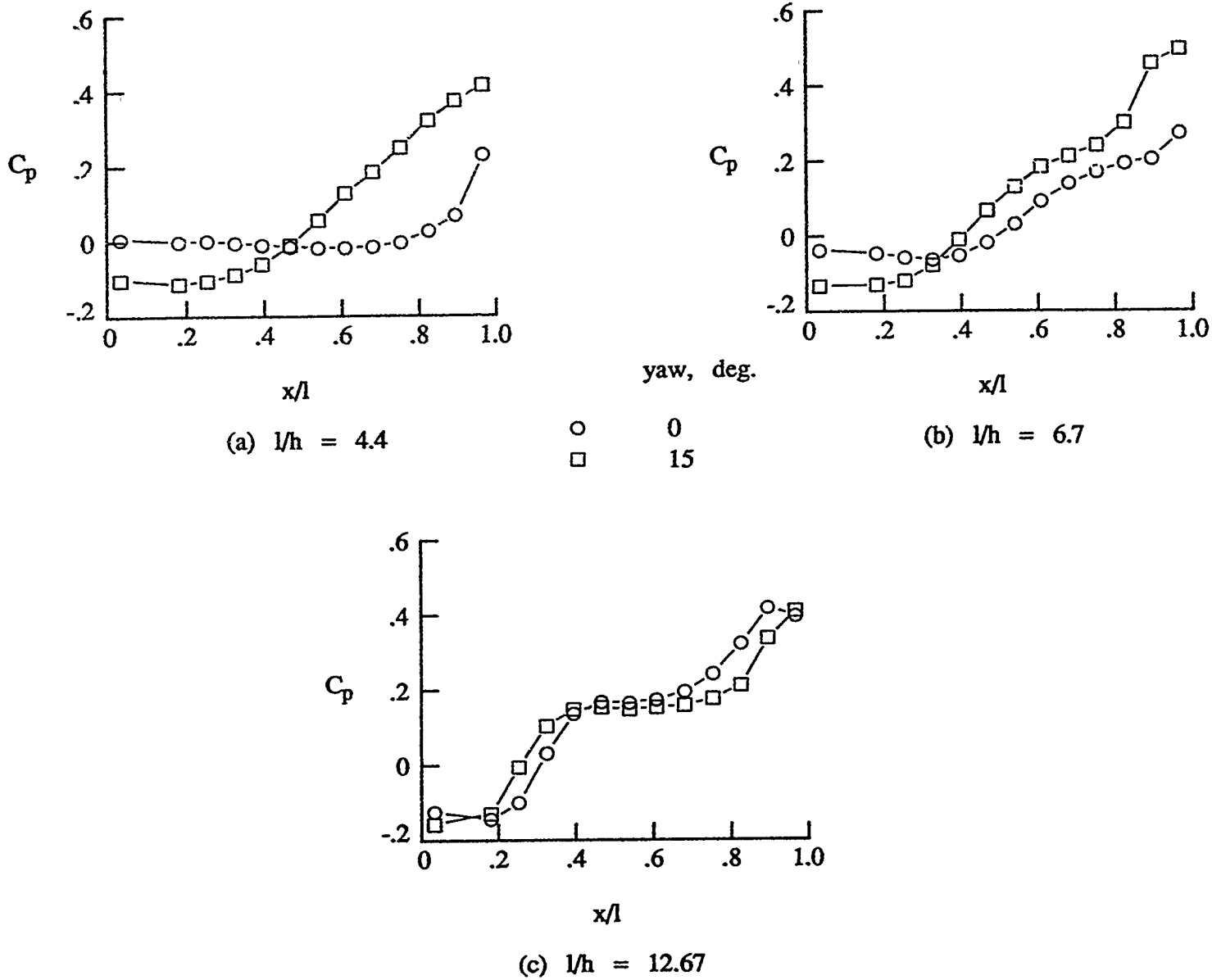

Figure 16.- Effect of yaw angle on cavity pressure distributions at M = 0.60 and R = 30 x 10^6.

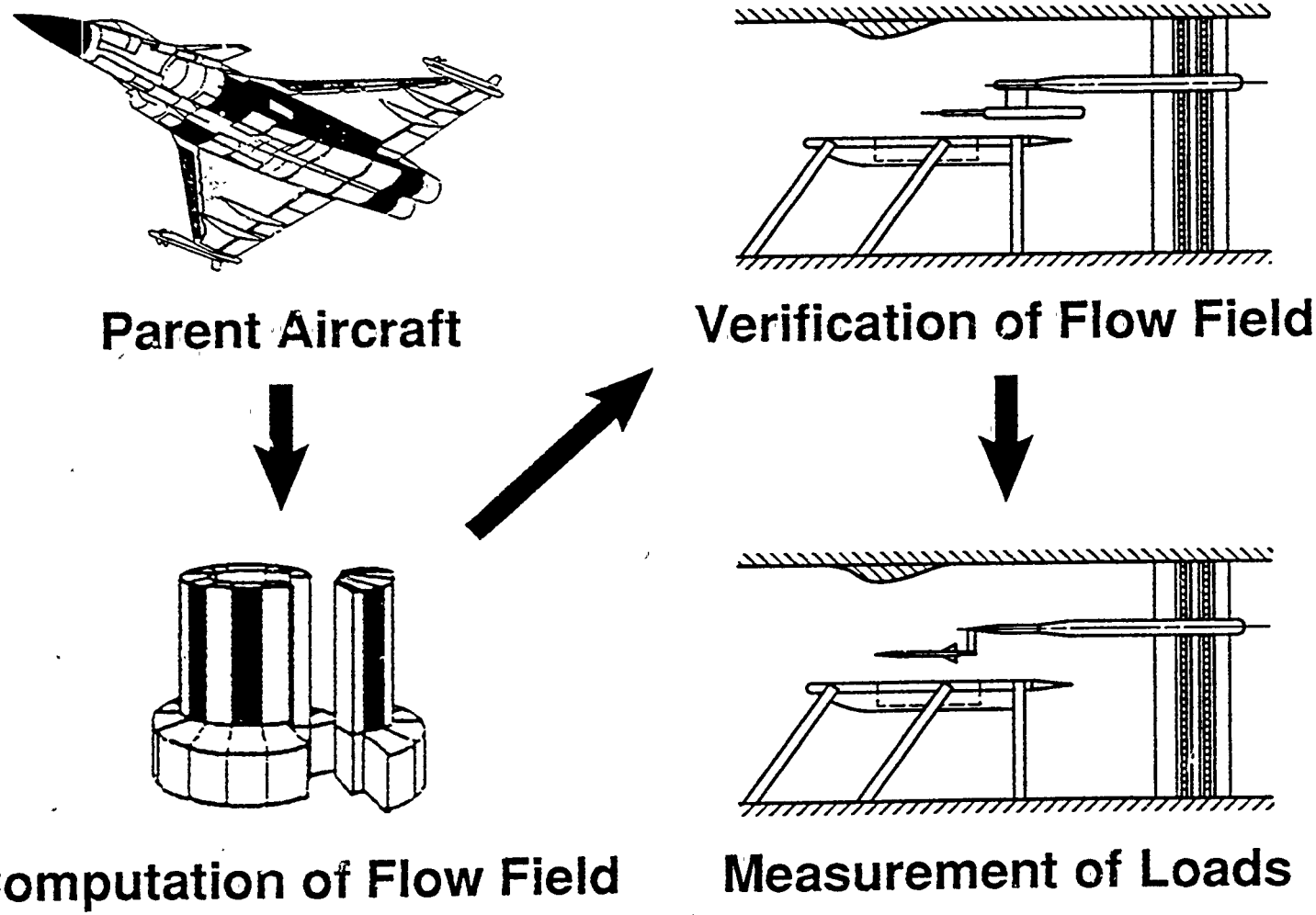

Figure 17.- NASA LaRC approach.

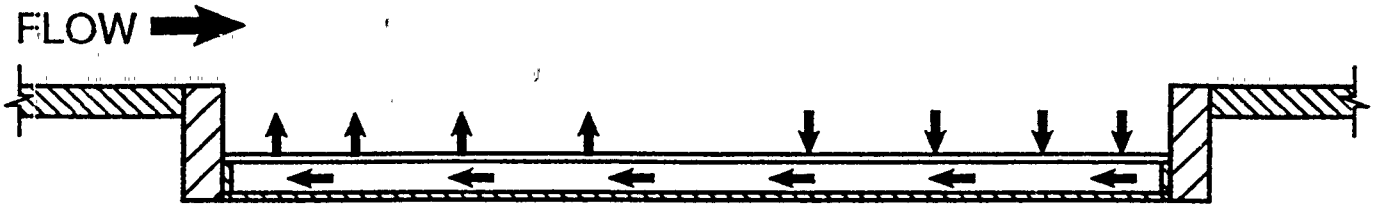

(a) Porous plate. l/h = 13.40, 17.50

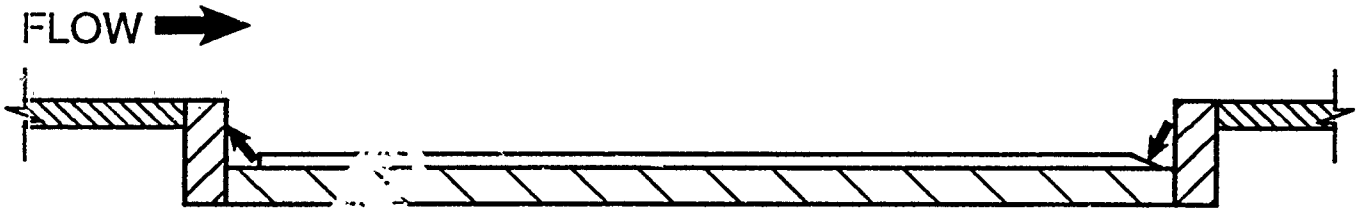

(b) Pipe vents. l/h = 13.40, 17.50

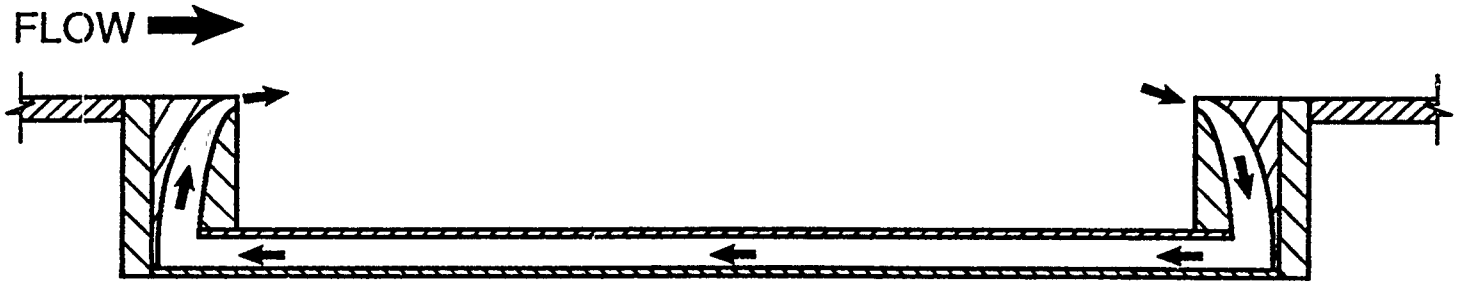

(c) Lip vent. l/h = 6.70

Figure 18.- Passive venting concepts.

Author's Autobiographies

Ms. E. B. Plentovich has been employed by the NASA Langley Research Center (LaRC) since 1980. She is currently working in the area of transonic store carriage and separation and is developing a program that would produce design strategies for store/aircraft integration that has recently received funding. Ms. Plentovich has been involved in many experimental studies, including store internal carriage, orifice induced pressure error, transport tests, and 2-D airfoil tests. She has a B.S. in aerospace engineering from Virginia Polytechnic Institute and State University (VPI&SU) and an M.S. in mechanical engineering from George Washington University.

Ms. M. B. Tracy has just been hired by NASA LaRC and will be working in the area of unsteady flow phenomena at transonic speeds. For the past 5 years, she has been employeed at LaRC as a contractor and was involved in the prediction of rotor-tone noise and experimental cavity acoustics. Ms. Tracy has been involved in studies of the coupling between cavity generated acoustic tones and structural vibrations of a store undergoing separation at supersonic speeds. She has also studied acoustic wave propagation in absorbing materials while employeed by the David Taylor Research Center. Ms. Tracy has a B.S. in physics from Loyola College and an M.S. in mechanics from The Johns Hopkins University.

Mr. J. Chu has been employed by NASA LaRC since 1981. He is currently working in the area of transonic, cryogenic, high-Reynolds-number aerodynamic research. This research includes commercial- and supersonic-transport tests and static- and fluctuating-pressure measurements on 2-D airfoil investigations. In the past, Mr. Chu has conducted experiments in a variety of facilities ranging from the low-speed regime of water tunnels and spin tunnels to the higher regime of transonic tunnels. He holds a B.S. in aerospace engineering from the Polytechnic Institute of New York.

Mr. R. L. Stallings has been employed by Lockheed Engineering and Sciences Co., since 1989, and is currently working under contract to the Transonic Aerodynamics Branch at the NASA LaRC in the field of transonic store separation. He retired from NASA LaRC in 1989 after 34 years of service. While at NASA, he has been principal investigator of numerous supersonic experimental investigations in the areas of store carriage and separation, aerodynamic heating of missiles and launch vehicles, and high-angle-of-attack aerodynamics. Before joining NASA, he was a maintenance officer in the United States Air Force. He has a B.S. in mechanical engineering, aeronautical option from North Carolina State University and an M.S. in aeronautical engineering from VPI&SU.

THIS PAGE INTENTIONALLY LEFT BLANK

NADC APPROACH TO PREDICTING STORE CARRIAGE LOADS

A. Cenko
NADC, Warminster, Pa.
K. Phillips
DTRC, Carderock, Md.

ABSTRACT:

Recent advances in Computational Fluid Dynamics (CFD) methods have enabled the analytic calculation of the carriage loads for stores mounted on complex aircraft. The latest results have demonstrated excellent agreement with test data for the F-15 at M = 0.98. However, in a preliminary design environment, the necessity of generating and validating an Euler grid to fit the aircraft and store arrangement may not be feasible. For that reason alternative approaches which require less time to arrive at an answer deserve consideration. The paper presents an engineering .pproach which can give acceptable estimates of store carriage loads in a timely manner.

NOMENCLATURE:

A_i Normal Force Influence Coefficient.

B_i Pitching Moment Influence Coefficient.

ALFXY: Indicated angle in yaw (δ_i) between the projection of the local flow velocity vector onto the probe X_B-Y_B plane and the probe X_B axis, positive in the positive Y_B direction, deg.

ALFXZ: Indicated angle in pitch (α_i) between the projection of the local flow velocity vector onto the probe X_B-Z_B plane and the probe X_B axis, positive in the negative Z_B direction, deg.

BL: Aircraft Butline, positive outboard, in.

C_N Normal Force Coefficient.

C_{N0} Normal Force Coefficient at $\alpha = 0$.

C_m Pitching Moment Coefficient.

C_{m0} Pitching Moment Coefficient at $\alpha = 0$.

C_Y Side Force Coefficient.

C_n Yawing Moment Coefficient.

FS: Aircraft Fuselage Station, positive aft, in.

M: Mach number

WL: Aircraft Waterline, positive up, in.

X_B: Parallel to the probe longitudinal axis, positive forward as seen by the pilot.

Y_B: Perpendicular to the X_B and Z_B directions, positive to the right as seen by the pilot.

Z_B: Perpendicular to the X_B direction, positive downward as seen by the pilot.

α: Angle of attack, deg.

INTRODUCTION:

The most accurate analytic tool for determining store carriage loads for all conditions would be a solution to the Navier Stokes equations. However, for most configurations of interest, such a solution is beyond the state of the art for predicting store carriage loads. The Euler equations, which have been solved for various complex shapes[1], require the development of a grid that accurately fits the configuration and extends out into the flowfield. The generation of such a grid is a time consuming process that needs to be repeated anytime slight configuration changes are made.

Computational tools that need only a surface description of the aircraft geometry are far easier to use. Although these are at present capable of only solving the full potential equations[2] or their linearized[3] equivalents, that may be all that is required since the wing lower surface pylon location may not be subject to the non-linear supercritical effects usually associated with the wing upper surfaces. One major advantage of using the PAN AIR program is that the aircraft panel models can be run with minor changes[4] on the TranAir program, and PAN AIR models for most NAVY aircraft already exist.

Another method for predicting store carriage loads is the Influence Function Method[5] (IFM) which uses the angularity distribution along the store to predict store loads along a horizontal traverse. The principal advantage of the IFM technique is that estimates of store carriage loads can be made in minutes once the aircraft flowfield near carriage is known.

BACKGROUND:

The IFM technique is a three step process that alternatively employs the following equations:

$$C_N - C_{N0} = \sum_{i=1}^{N} A_i \alpha_i \qquad 1)$$

$$C_m - C_{m0} = \sum_{i=1}^{N} B_i \alpha_i \qquad 2)$$

These equations represent the relationship between the forces and moments acting on a store, and the interaction of the local flow angle on each store element with the store normal force and pitching moment influence coefficients (hence the terminology Influence Function Method) A_i and B_i, respectively. Note that although these equations are linear in form, they do not represent linearized aerodynamic effects. The equations are actually analogous to regression equations where the non-linear terms are included in the influence coefficient term as well as a general nonlinear angularity represented by α_i. The formulation for the sidewash as a function of side force and yawing moment is identical, and the following comments concerning angularity apply to both the pitch and yaw plane.

The first step in the IFM process is calibration, i.e., determining the store's influence coefficients so that it's response to a nonuniform flowfield can be estimated. This requires at least N values of C_N and C_m and angularity α_i along an axial traverse. Originally, these values were obtained in a wind tunnel test. It has since been demonstrated that[6] these influence coefficients can also be determined by reproducing the experimental calibration process using an analytic CFD approach. However, the IDL/IFM[7] code has demonstrated an excellent ability to determine a symmetric store's influence coefficients at all Mach numbers. The technique also appears to work, within the inherent limitations of the IFM approach, for nonsymmetric configurations[8]. Since the IDL/IFM code can provide a set of influence coefficients in minutes of both set-up and computing time, it is the only method used for influence coefficient determination in this paper.

Once the influence coefficients have been determined, Eqs. 1) and 2) may be solved for the unknown angularity distributions along an axial traverse. The procedure adopted has been to solve the two sets of equations simultaneously for the unknown angularities α_i. Since the simultaneous solution has more equations than unknowns, the unknown

angularity can be determined for regions of the traverse forward and aft of the actual test data.

The final step in the IFM procedure is to combine the deduced α_i flowfield with influence coefficients for another store to determine that store's normal force and pitching moment in an axial traverse at the same conditions. Another approach is to use aircraft angularity data, derived either from a probe flowfield test or a CFD calculation, to predict the store loads in an axial traverse.

An inherent assumption of the IFM technique is that the mutual interference between the aircraft and store can be neglected in considering the effect of the aircraft flowfield on the store. Previous comparisons with probe flowfield test data indicated that the mutual interference effects are negligible up to one store diameter of pylon carriage, as may be seen in Fig. 1 and 2, where the IFM predicted F-15 upwash and sidewash are in very good agreement with yaw probe test data at M = 0.95 and 1.2. The assumption that mutual interference effects may be ignored may not be valid for the store in the carriage position.

Recent test data have suggested[9] that the IFM could provide useful information at the carriage position. Three tow targets, designated TDU-34A, TDU-34G and TDU-34H that differed only in their tail configuration, were tested at the A-6E launch position, Fig. 3. Axial traverses at this location provided an IFM predicted flowfield that was in close agreement for all three configurations. This flowfield differed considerably with PAN AIR predictions at this traverse location, Fig. 4. The IFM predicted flowfield, however, when used with IDL/IFM predicted influence coefficients, provided an excellent prediction of the targets C_N and C_m behavior in an axial traverse along the carriage position, Fig. 5. It appears that the reason the IFM predicted flowfield differed from the PAN AIR predictions may be attributed to mutual interference between the aircraft and store at carriage. This implies that IFM predictions can be used at carriage for stores of similar geometry to actually predict the mutual interference effect between the aircraft and store.

NAVY APPROACH TO ESTIMATING STORE CARRIAGE LOADS:

The first step in the NADC approach to calculating store carriage loads is estimating the aircraft flowfield. The primary analytic tool for this purpose is the PAN AIR program. Although this code is only applicable in the linear speed regime, it is relatively easy to model complex aircraft configurations which can be subsequently used in the TranAir program, which has shown[4] good correlation with transonic test data. Furthermore, changes in configuration shape such as fuel tanks, pylons and other

stores can be easily incorporated. PAN AIR models for most NAVY aircraft have been generated and are readily available when aircraft or store configuration modifications are envisioned.

Although the PAN AIR program has demonstrated the ability to predict complex aircraft flowfields in the linear speed regime, yaw head probe flowfield test data, when available, are always used to validate the PAN AIR aircraft models. At present, extensive yaw head probe test data are available at various Mach numbers and aircraft attitudes for the A-6 and F-18 aircraft, and a limited set of data exist for the F-14 configuration. An example of the ability of the PAN AIR code to predict aircraft flowfields can be seen in Fig. 6-9, which compare PAN AIR predictions with DTRC yaw head probe test data for the outboard pylon with a fuel tank present (Fig. 6-7) and absent (Fig. 8-9) on the inboard pylon. Although at this Mach number linear theory is not expected to work, the predictions are in reasonable agreement with the flowfield test data, with the exception of the region of the wing trailing edge. PAN AIR seems to be able to predict the fuel tank effect on the aircraft flowfield. One reason for the good agreement with the test data might be that although the wing upper surface at this condition is highly supercritical, the transonic effects on the wing lower surface might be confined to the region of the trailing edge shock.

Once the aircraft flowfield has been validated an IDL/IFM model of the store has to be developed. For symmetric configurations this is a relatively simple matter, and excellent predictions of the freestream aerodynamic coefficients is generally achieved as may be seen in Fig. 10-11 for the MK-82 bomb.

If the store is asymmetric the IDL/IFM code theoretically should not be used. Although a method of calibrating non-symmetric stores has been developed[10], it is inherently more difficult and costly to apply. Furthermore, since the IFM technique is applied along an axial traverse representing the store's C.G. locations, calibrations that take into account complex geometric effects (i.e. wing and tail surfaces out of the plane of symmetry) are beyond the inherent limitations of the technique. For asymmetric stores the recommended[8] approach is to model the configuration approximately as two symmetric shapes in the pitch and yaw planes, and perform the IDL/IFM calibrations separately for the two planes. The calibration is considered to be successful if the IDL/IFM predicted freestream values are in reasonable agreement with the test data. An example of this approach can be seen in fig. 12-13 for the BQM-126 configuration shown in Fig. 14 in the launch position for the F-18 aircraft.

The last step in the IFM procedure is to combine the aircraft flowfield with the store's influence coefficients to predict the store loads along an axial traverse. Good agreement with carriage loads test data was achieved for the BQM-126 when it's pitch plane influence coefficients were combined with F-18 probe flowfield test data, as may be seen in Fig. 15. However, since the carriage loads occur in a region of rapidly changing normal force and pitching moment, and only one experimental location was available for comparison purposes, the agreement might have been fortuitous. Grid loads data at an axial traverse near the carriage position would be needed to substantiate that the trends predicted by IFM are reasonable.

AIWS F-18 CARRIAGE LOADS:

A good example of the NAVY approach to predicting store carriage loads is available from the Advanced Interdiction Weapons System program. For this program three separate weapon configurations were developed by three separate teams of contractors. These weapons were all asymmetric, with different folding wing and tail arrangements. Since the air launch certification effort for the three weapons from the F-18 aircraft had to be completed in less than one year, generating an Euler grid for the F-18 aircraft which would accommodate the three different weapon arrangements prior to the three separate wind tunnel tests was not a feasible alternative.

The approach adopted was to develop an IDL/IFM model of the three weapon configurations. As may be seen in Fig. 16 the IDL predicted normal force for one of the configurations is in good agreement with the test data. The pitching moment prediction does not match the non-linear behavior exhibited by the test data. However, $C_{m\alpha}$ (which represents the sum of the B_i influence coefficients) is reasonably well predicted for positive angles of attack.

Both experimental and analytic F-18 flowfield test data were available at Mach numbers M = 0.6, 0.8 and 0.95. Using these flowfields and the IDL/IFM influence coefficients, IFM predictions for the three different weapon configurations were made for a grid ranging from the two pylon carriage position to a position 30 inches below the pylon. On the basis of these preliminary calculations it appeared that the critical launch conditions, as evidenced by large variations in pitching and yawing moments, would occur for M = 0.95 at the outboard pylon carriage location, for a fuel tank mounted on the inboard pylon. Accordingly, axial traverse test data were taken at this location during the grid portion of the AIWS wind tunnel test.

Fig. 17 and 18 compare these IFM predictions with the test data. Two sets of predictions are shown, one based on

the DTRC yaw head probe data and the other on the PAN AIR predicted flowfield at the same traverse location, as previously shown in Fig. 6 and 7.

As may be seen in Fig. 17 and 18 the IFM predicted moment variation using the PAN AIR predicted flowfield is in better agreement with the test data than that using the DTRC yaw head probe flowfield test data. This is surprising since previous experience has suggested that yaw head probe test data would provide the best IFM predictions. It must be realized, however, that this example represents an attempt to use the IFM technique at the limit (or beyond) it's range of applicability. When the AIWS configuration is near the pylon carriage position there is no doubt a great deal of mutual interference between the store and the aircraft induced flowfield. As may be seen in Fig. 6 and 7 the major difference between the PAN AIR predicted α_i and δ_i and the test data occurs in the region where the shock from the wing trailing edge should intersect the traverse. PAN AIR does not predict this shock effect; it is entirely possible that the mutual interference effect between the aircraft and store would tend to dissipate and smooth out this transonic flowfield behavior. It is expected that at subsonic speeds, and locations somewhat further away from the carriage position, probe flowfield test data would provide the best IFM predictions. It should also be mentioned that at subsonic speeds the PAN AIR predicted flowfield is usually in better agreement with probe flowfield data[11].

Both sets of IFM predictions are in reasonable agreement with the test data and both predicted, prior to the wind tunnel test, that the peak pitching and yawing moment would occur near the carriage position, fuselage station 450. Considering the fact that IFM predictions for three Mach numbers for both pylon carriage locations for three different AIWS configurations were generated in less than one days time, the cost effectiveness of the IFM approach should be apparent.

CONCLUSIONS:

Although advances in CFD techniques have enabled the calculation of store carriage loads for complex configurations at transonic speeds, these methods require a considerable expenditure of time and manpower. Furthermore, the impact of configuration changes can not be easily examined. The Influence Function Method, on the other hand, permits an estimate of store carriage loads to be made in a timely fashion, prior to the wind tunnel test, and the effects of configuration modifications can be evaluated in a matter of hours. The method cannot be expected in all cases to give quantatively correct answers since it ignores the effect of mutual interference; for stores of similar shape, it might be also able to account[9] for this effect.

REFERENCES:

1. Keen, K. S., "New Approaches to Computational Aircraft/Store Weapons Integration," AIAA paper 90-0274, Jan. 1990.

2. Erickson, L. L., et al., "Applications of the TranAir Full-Potential Code to Complete Configurations," ICAS Paper ICAS-86-1.3.5, 1986.

3. Magnus, A. E. and Epton, M. A. "PAN AIR - A Computer Program for Predicting Subsonic or Supersonic Linear Potential Flows About Arbitrary Configurations Using a Higher Order Panel Method," NASA CR-3251, 1980.

4. Tseng, W., et al., "TranAir Applications to Fighter Configurations," AIAA paper 89-2220, 1989.

5. Cenko, A., "IFM Applications to Trajectory Predictions - Past, Present and Future," SAE paper 871792, 1987.

6. Cenko, A., et al., "Further Development of the Influence Function Method for Store Aerodynamic Analysis, "J. Aircraft, Aug. 1986, pp 656-661.

7. Keen, K. S., "Inexpensive Calibrations for the Influence Function Method Using the Interference Distributed Loads Code," J. Aircraft, Jan. 1985, pp 85-87.

8. Cenko, A., et al. "IFM Applications to Complex Store Configurations," AIAA Paper 90-0275, Jan. 1990.

9. Cenko, A., et al., "Ground Testing Techniques for Tethered Systems," AIAA Paper 90-1428, June 1990.

10. Cenko, A., et al., "IFM Applications to Theoretical Trajectory Predictions," AIAA Paper 87-0210, Jan. 1987.

11. Cenko, A., "Evaluation of Methods for Predicting Transonic Aircraft Flowfields," NADC Report, in press.

BIOGRAPHY

Alexis Cenko

Dr. Cenko received his B.S. from Penn State, his Masters from Cornell and his terminal degree from West Virginia University, all in Aerospace Engineering. In 1969, he joined the Grumman Aerospace Corporation, where he developed methods for transonic airfoil analysis and supersonic aircraft design. He also served as the program manager of the transonic wing design program and the principal investigator on the Influence Function Method contract for the Air Force. In 1984 he accepted a position as Associate Professor of Engineering at Hofstra University. Finding himself temperamentally unsuited to an academic environment, he joined the Aerodynamics Division at the Naval Air Development Center in August of 1987. Presently, he is involved with air launch certification efforts on the AIWS, A-6/TDU-34, F-18/UAVMR and P-7 programs.

Kenneth A. Phillips

A 1964 graduate of West Virginia University with a degree in Aerospace Engineering, Mr. Phillips joined the staff at David Taylor Research Center in 1965. He spent several years working in the area of dynamic stability, missile stability and control and weapon design. He was a member of the team that developed the Conformal Carriage System for the F-4 aircraft and was responsible for conceptual weapon design for that program. A transfer to another area at the Center provided experience in the Aircraft/Ship interface and shipboard operations of aircraft with additional work in air-cushion vehicles for the Navy. For the past 10 years, Mr. Phillips has been involved in Aircraft/weapon compatibility and has been in charge of the experimental efforts in captive trajectory techniques, grid testing, and carriage loads testing. Presently, he is head of the Applied Aerodynamics Group and has served on the Aircraft/Store Compatibility Panel of JOCG.

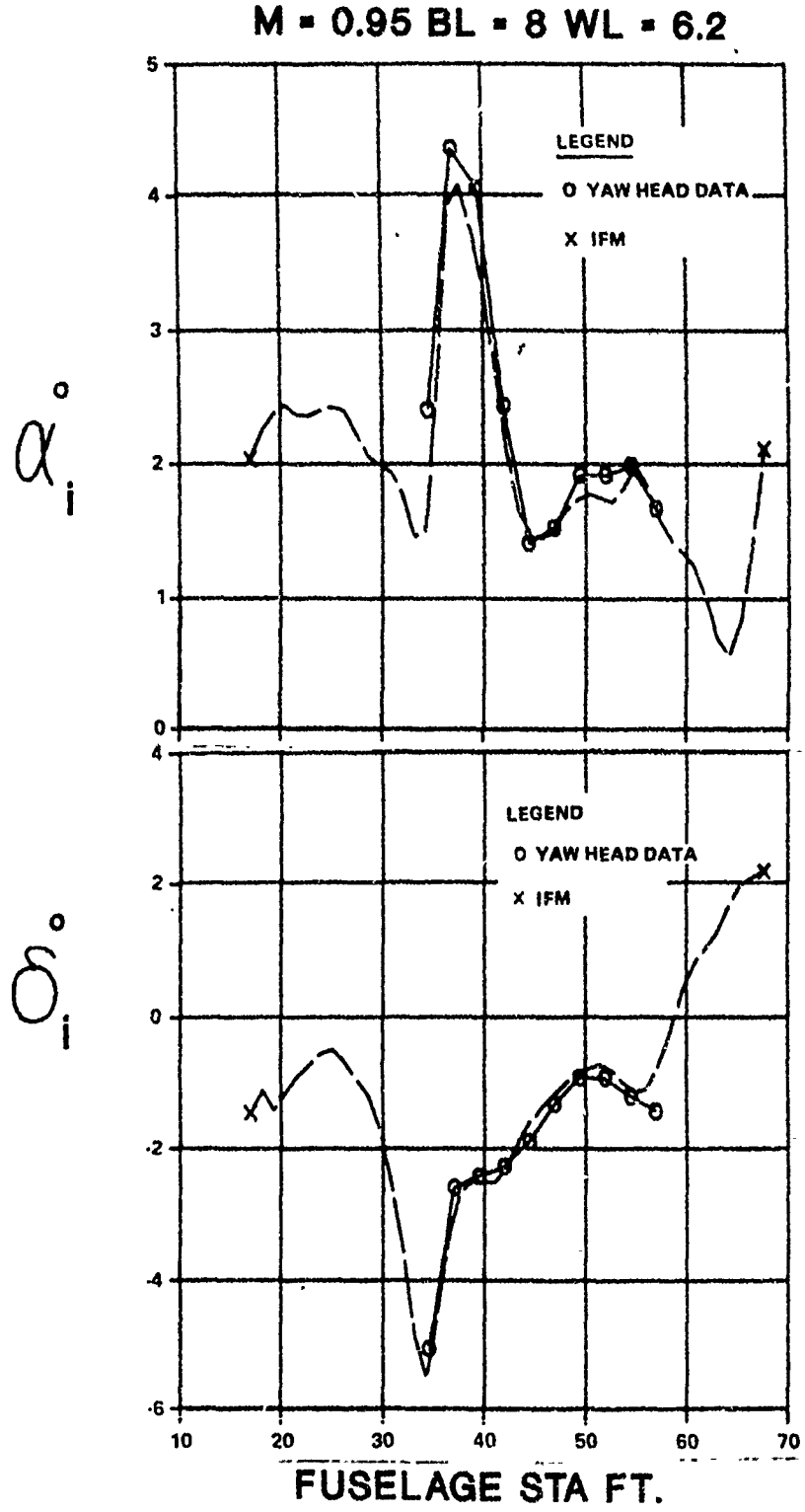

FIG 1 IFM PREDICTED F-15 FLOWFIELD

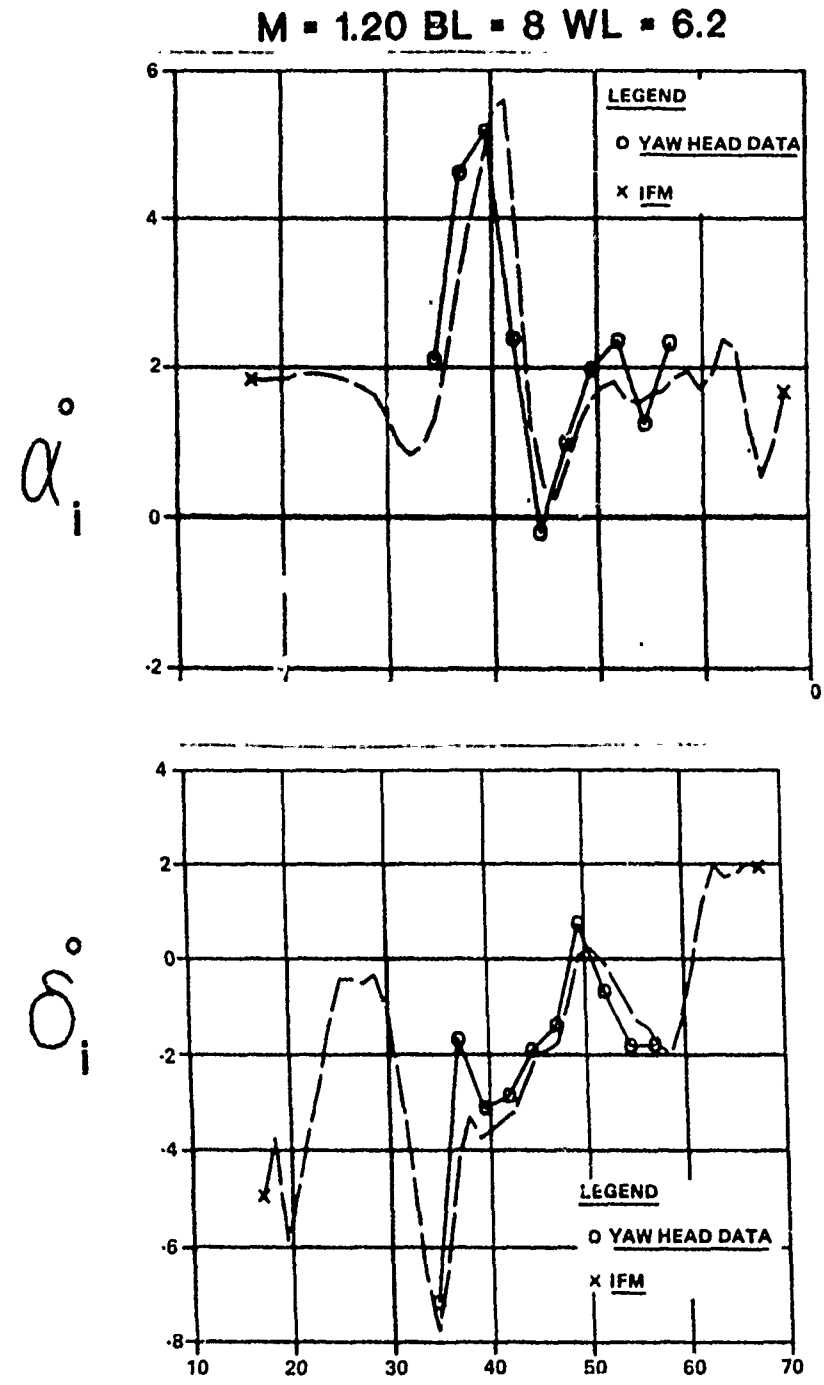

FIG 2 IFM PREDICTED F-15 FLOWFIELD

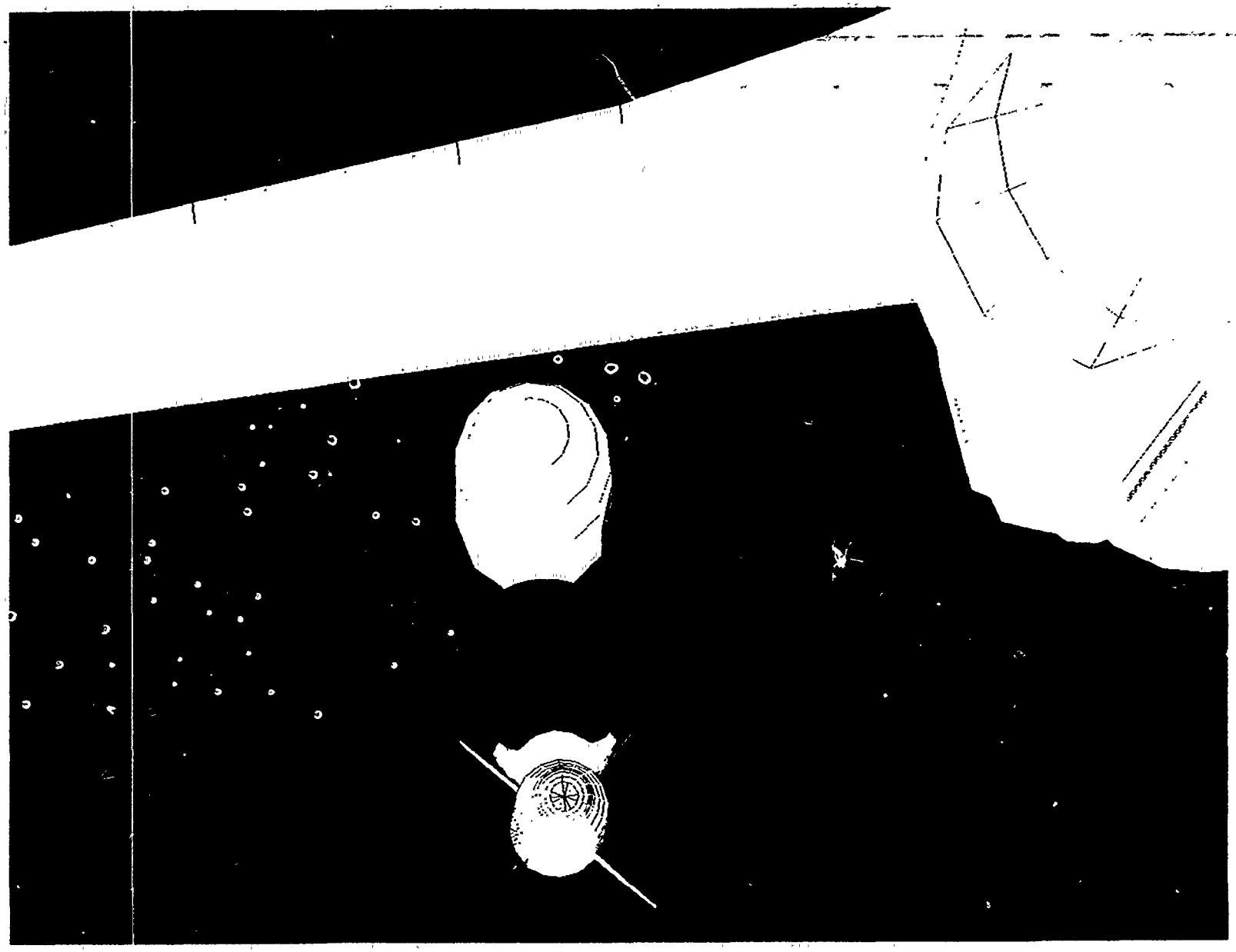

FIG. 3 TDU-34A TARGET IN A-6E LAUNCH POSITION

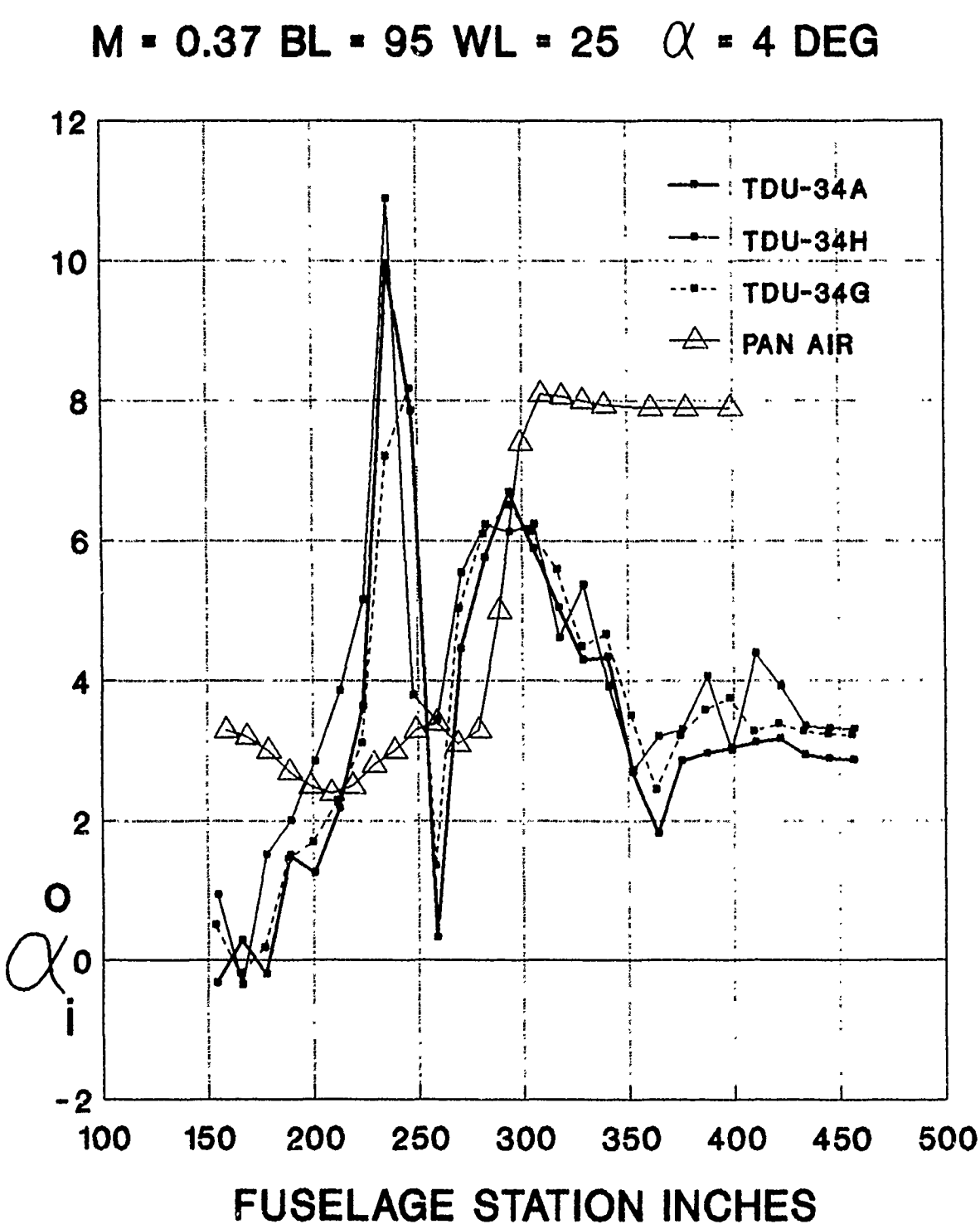

FIG. 4 IFM PREDICTED A-6 ALFXZ

M = 0.37 BL = 95 WL = 25 α = 4 DEG

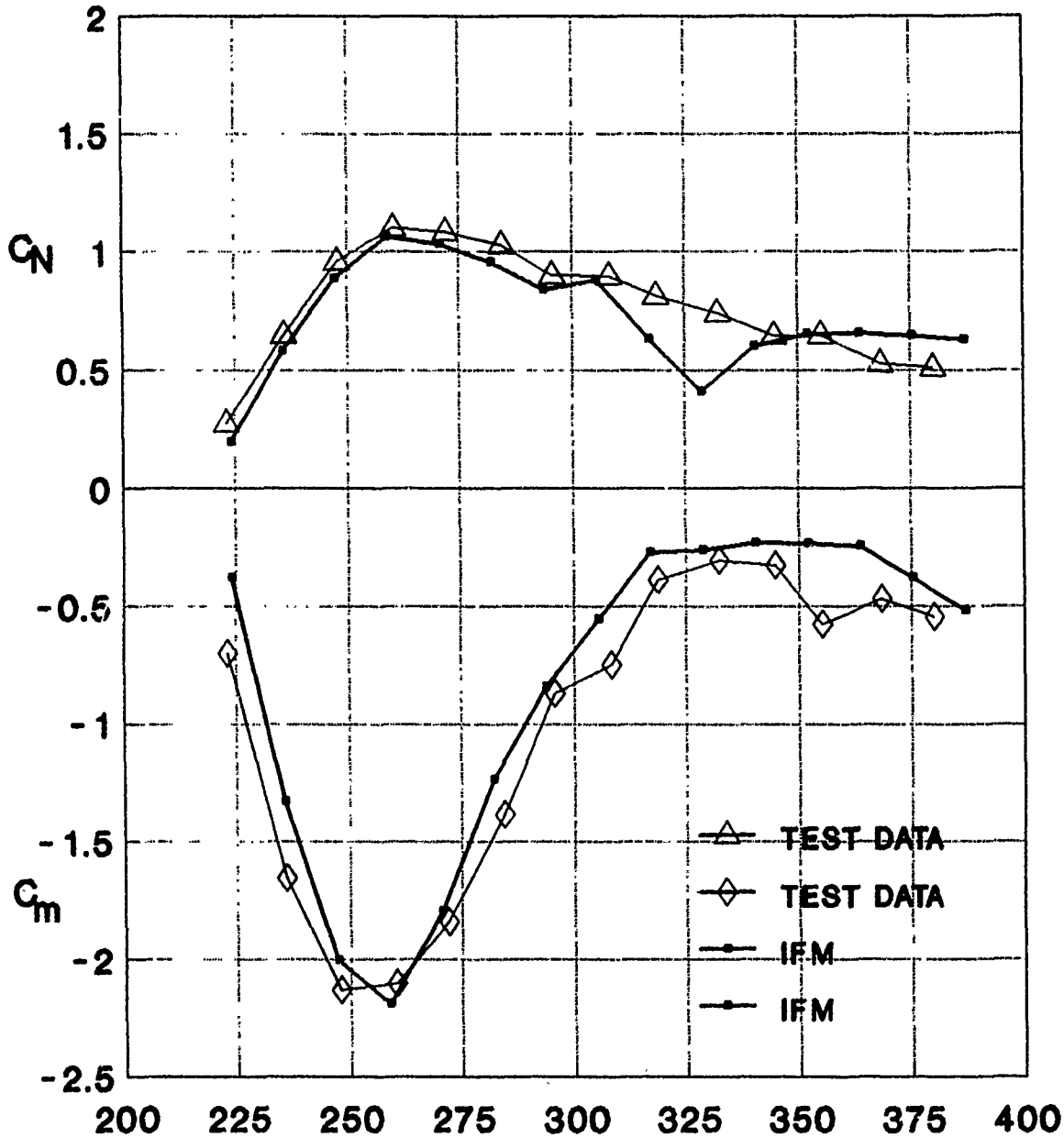

FIG 5 TDU-34G PREDICTIONS FROM TDU-34A

M = 0.95 WL = 62 BL = 134

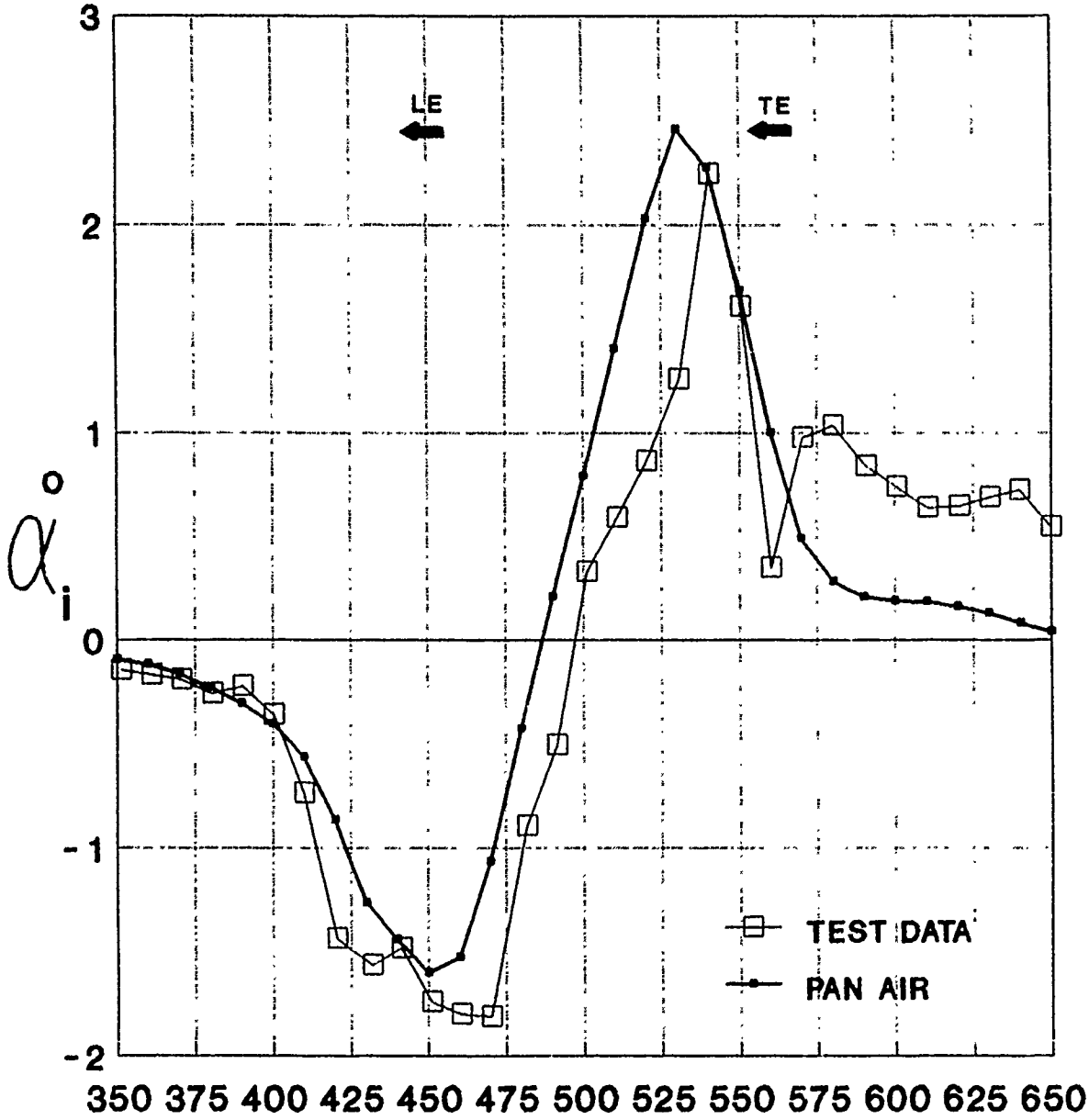

FIG 6 PAN AIR PREDICTED ALFXZ

M = 0.95 WL = 62 BL 134

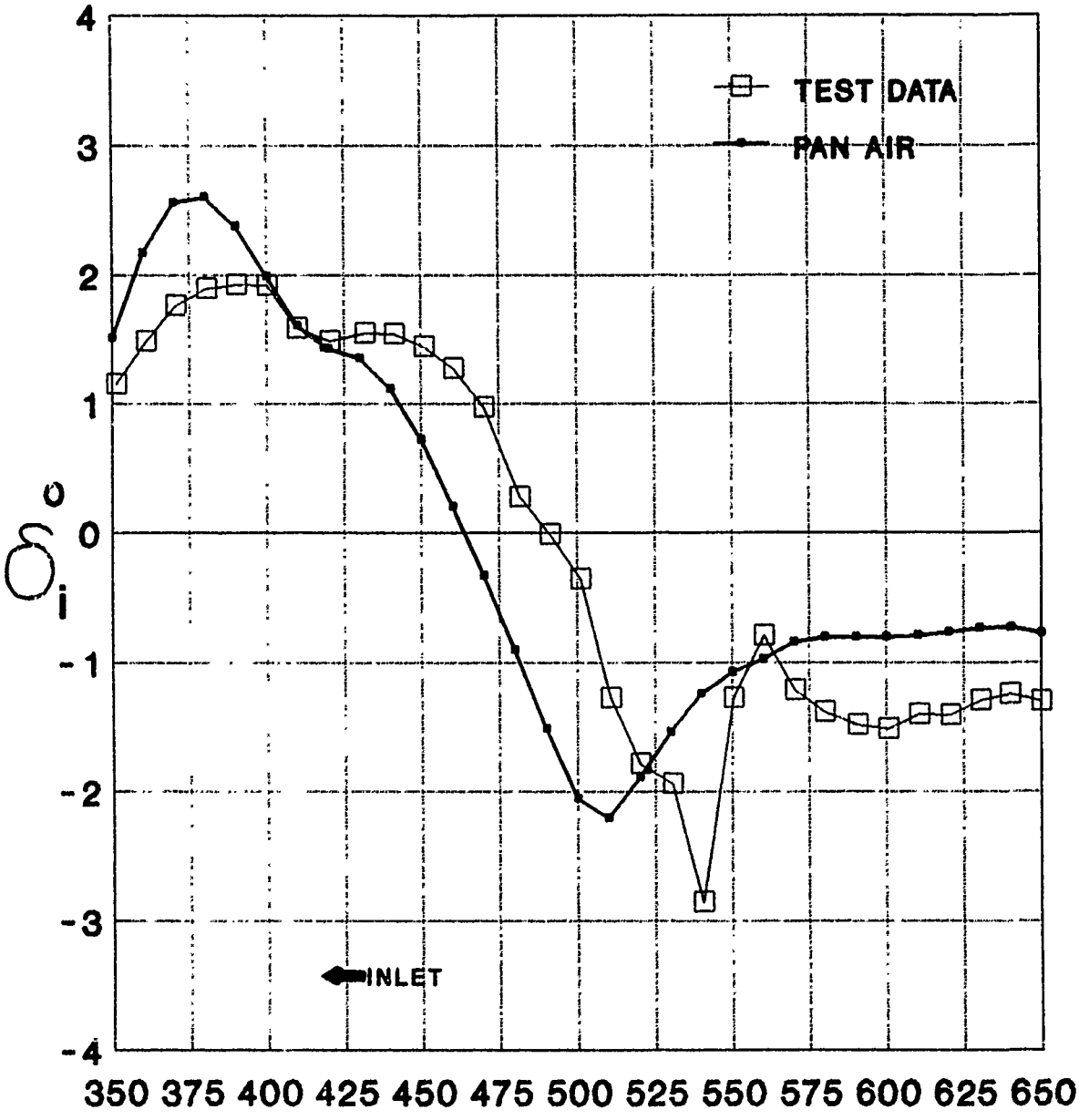

FIG. 7 PAN AIR PREDICTED ALFXY

M = 0.95 ALPHA = 0.0 BL 134

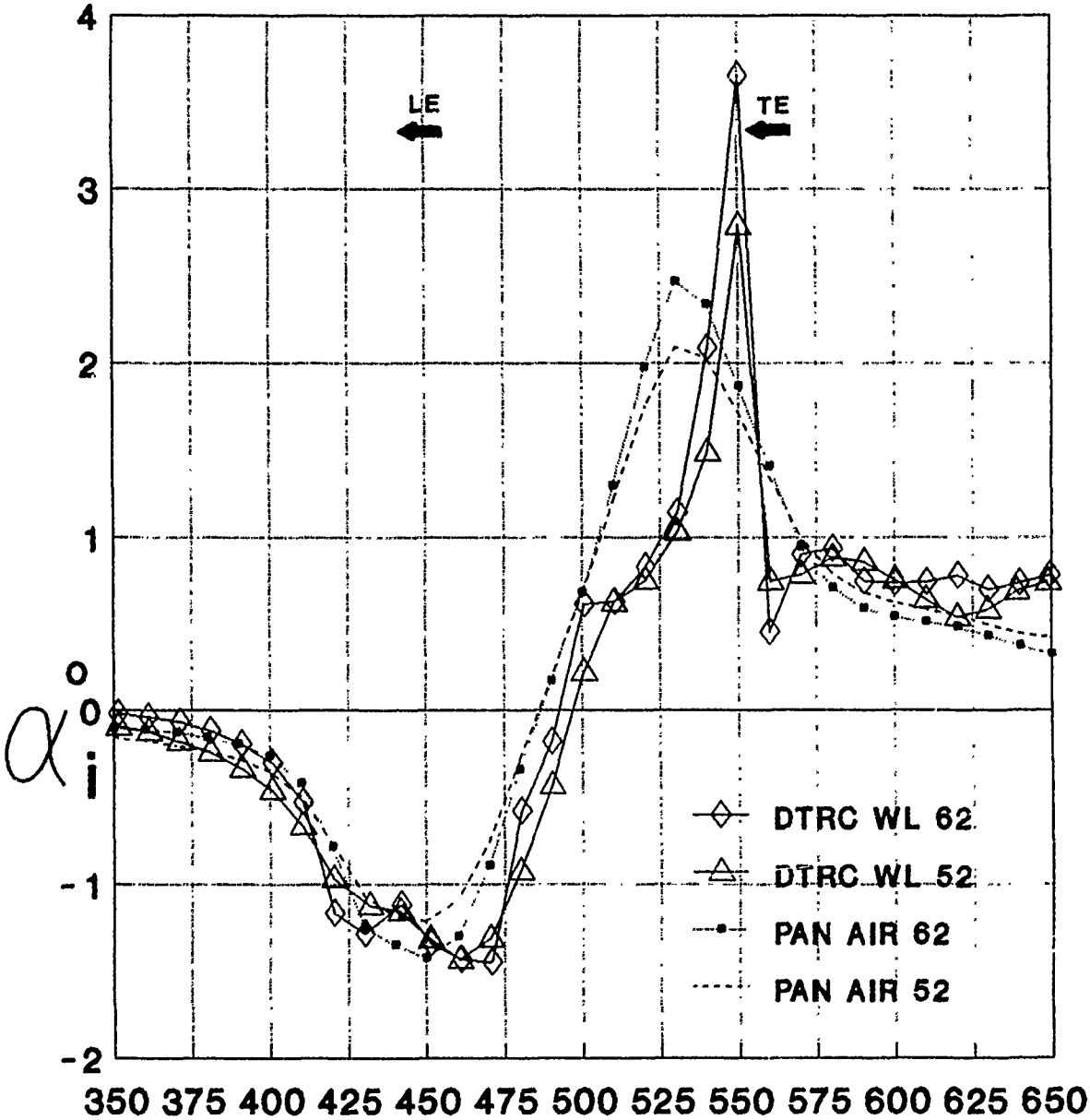

FIGURE 8 PAN AIR PREDICTED F-18 ALFXZ

M = 0.95 ALPHA = 0.0 BL 134

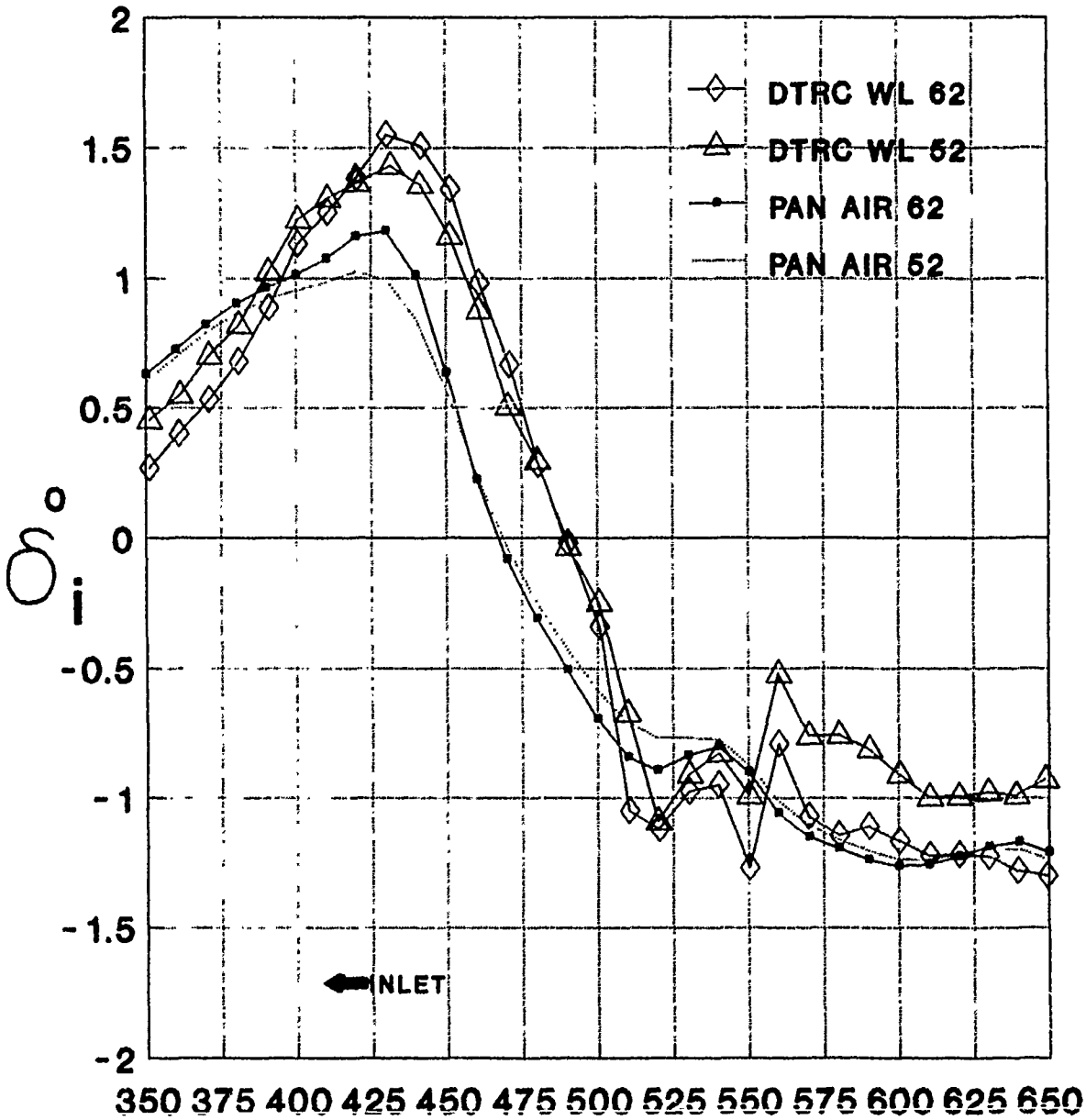

FIG. 9 PAN AIR PREDICTED F-18 ALFXY

MK-82 CONFIGURATION M = 0.85

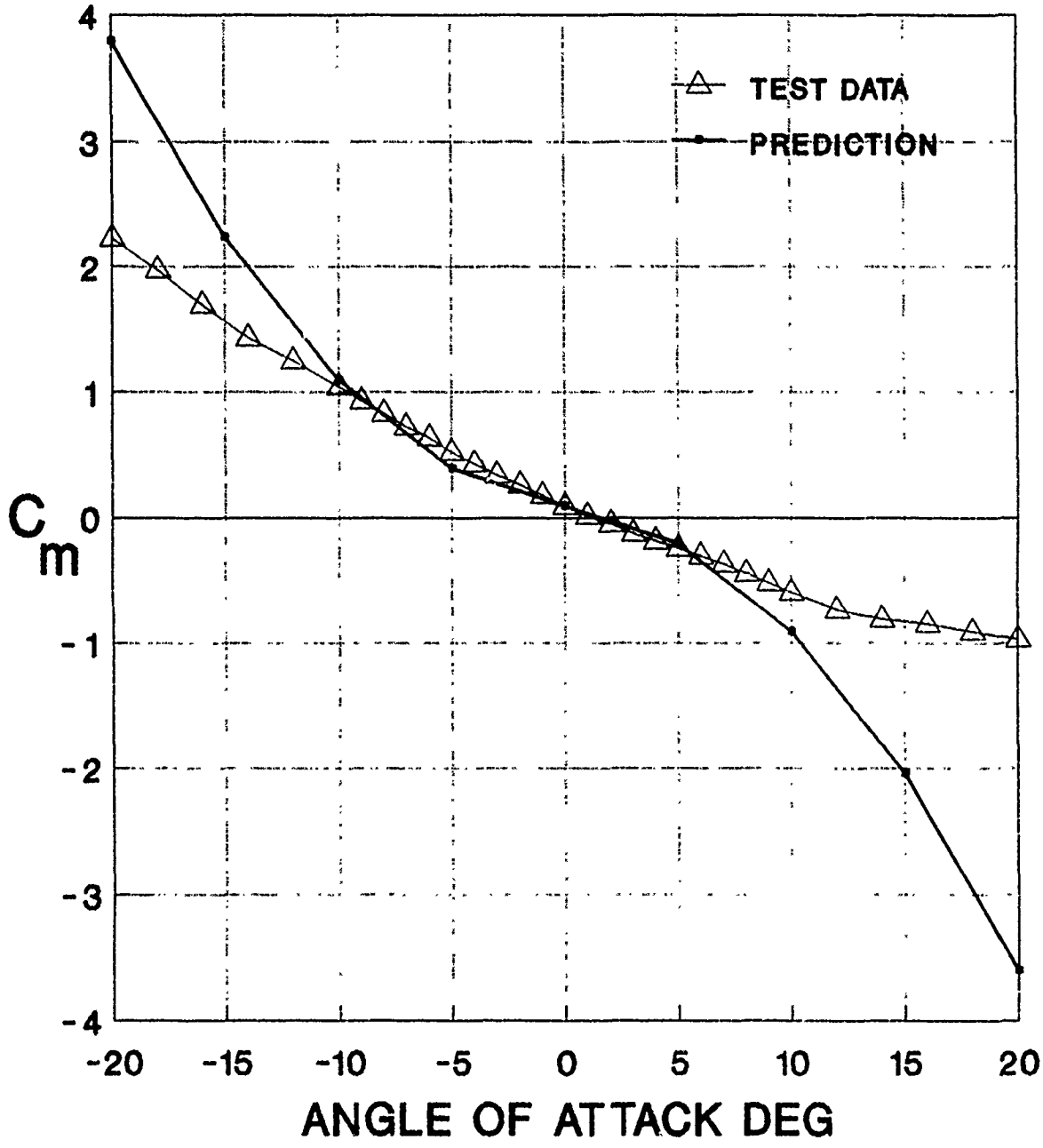

FIG 10 IDL/IFM PREDICTED MOMENT

MK-82 CONFIGURATION M = 0.85

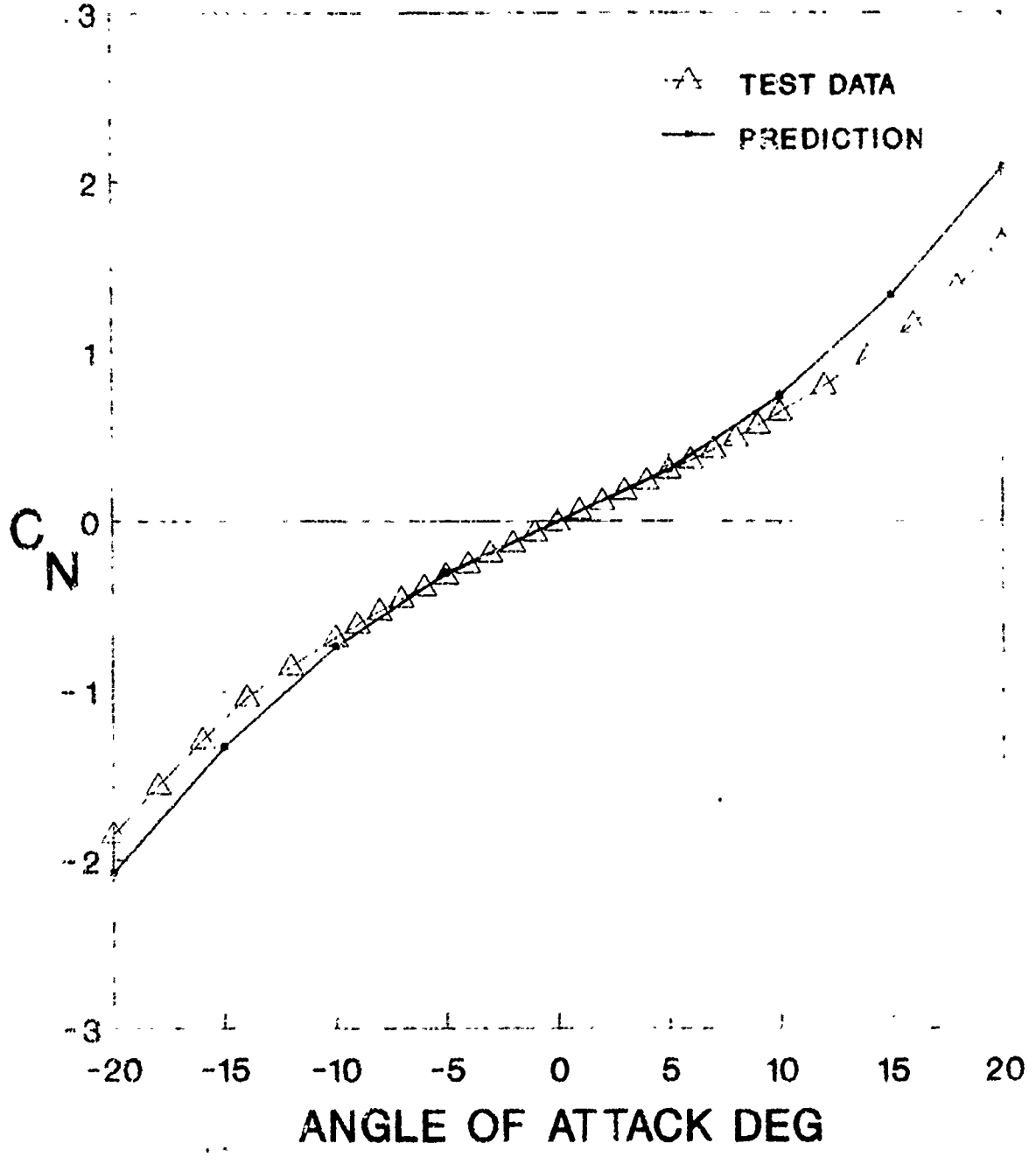

FIG 11 IDL/IFM PREDICTED NORMAL FORCE

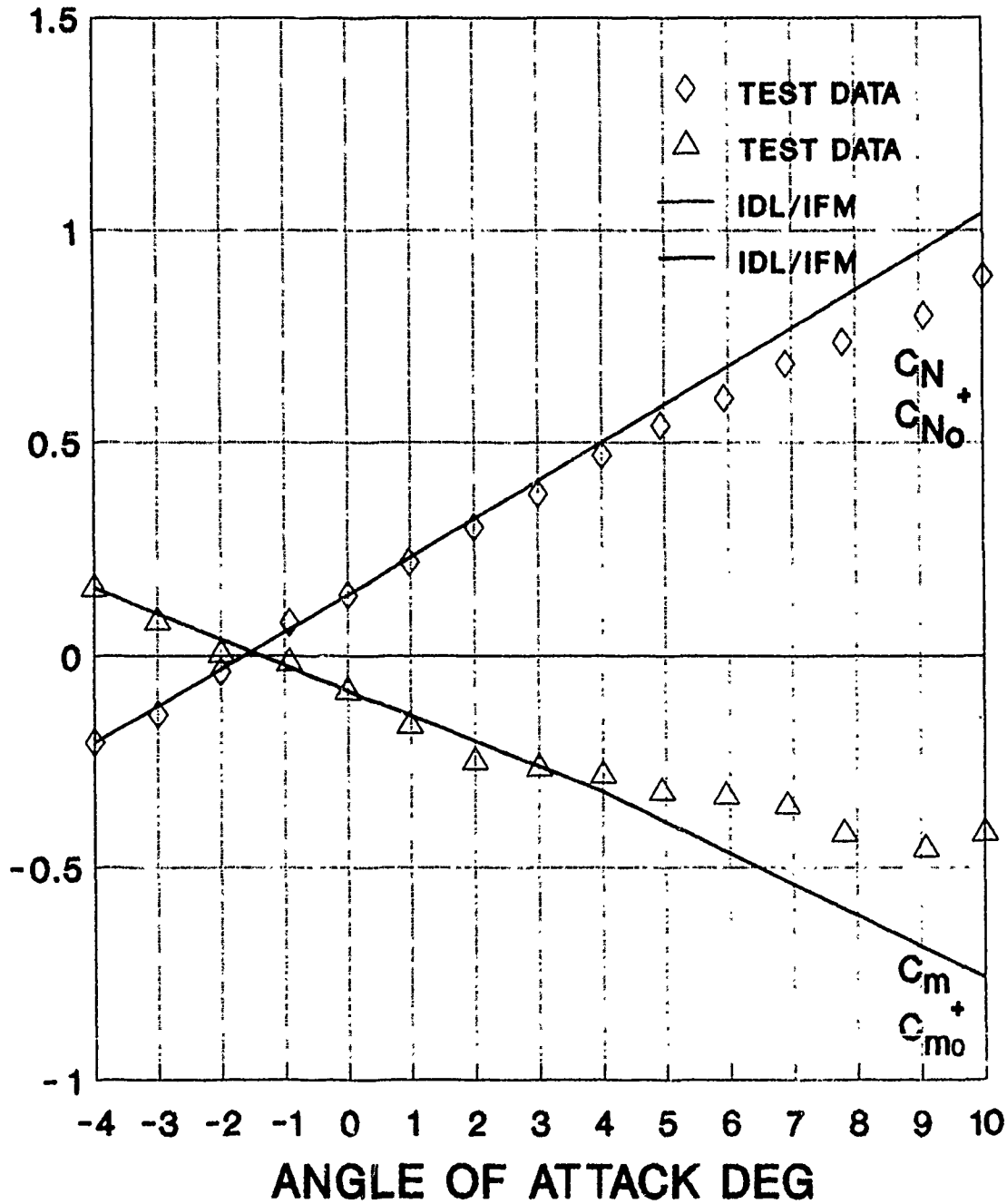

FIG 12 BQM-126A FREESTREAM DATA M = 0.5

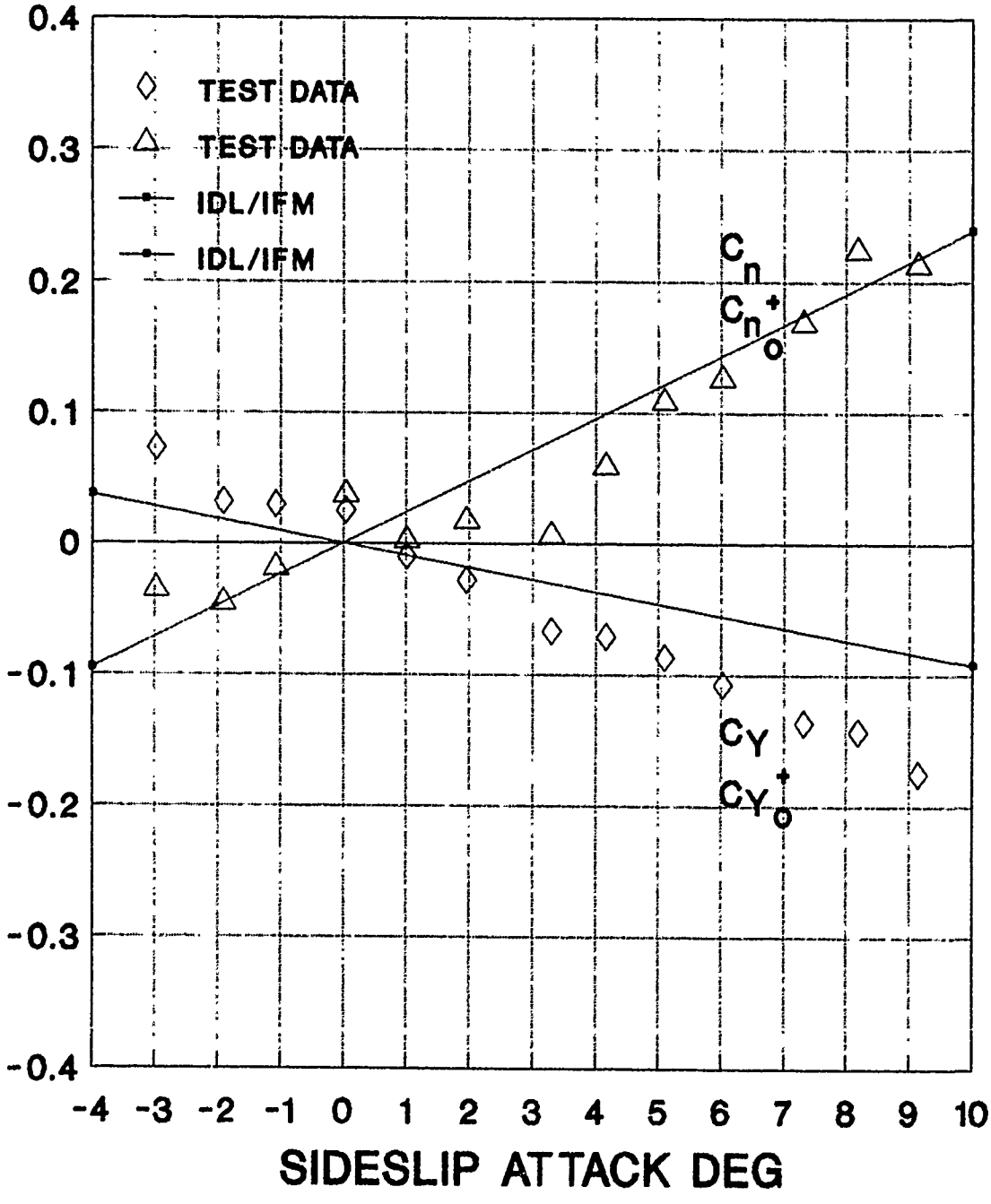

FIG 13 BQM-126A FREESTREAM DATA M = 0.5

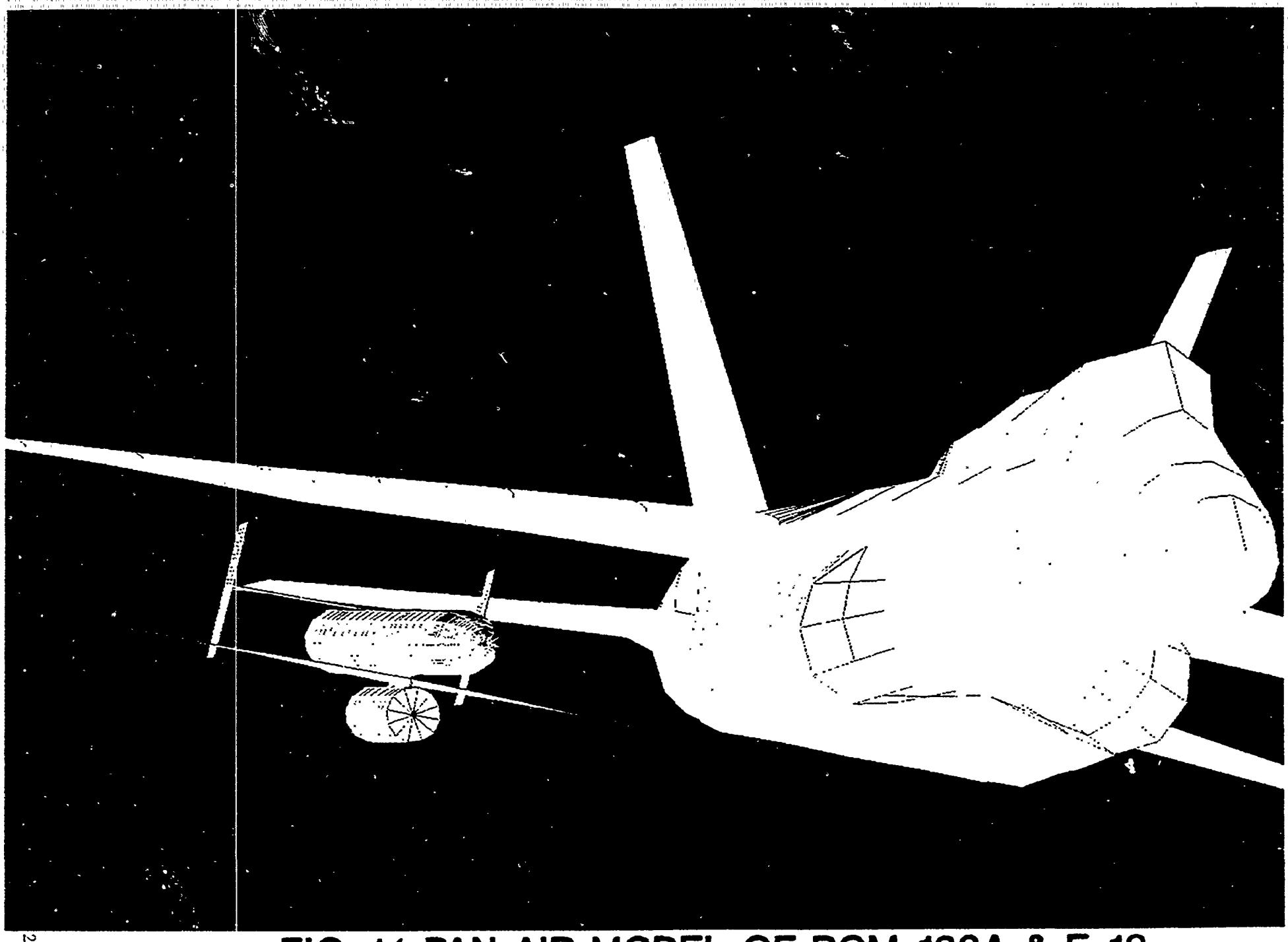

FIG. 14 PAN AIR MODEL OF BQM-126A & F-18

M = 0.45 WL = 70 BL = 134

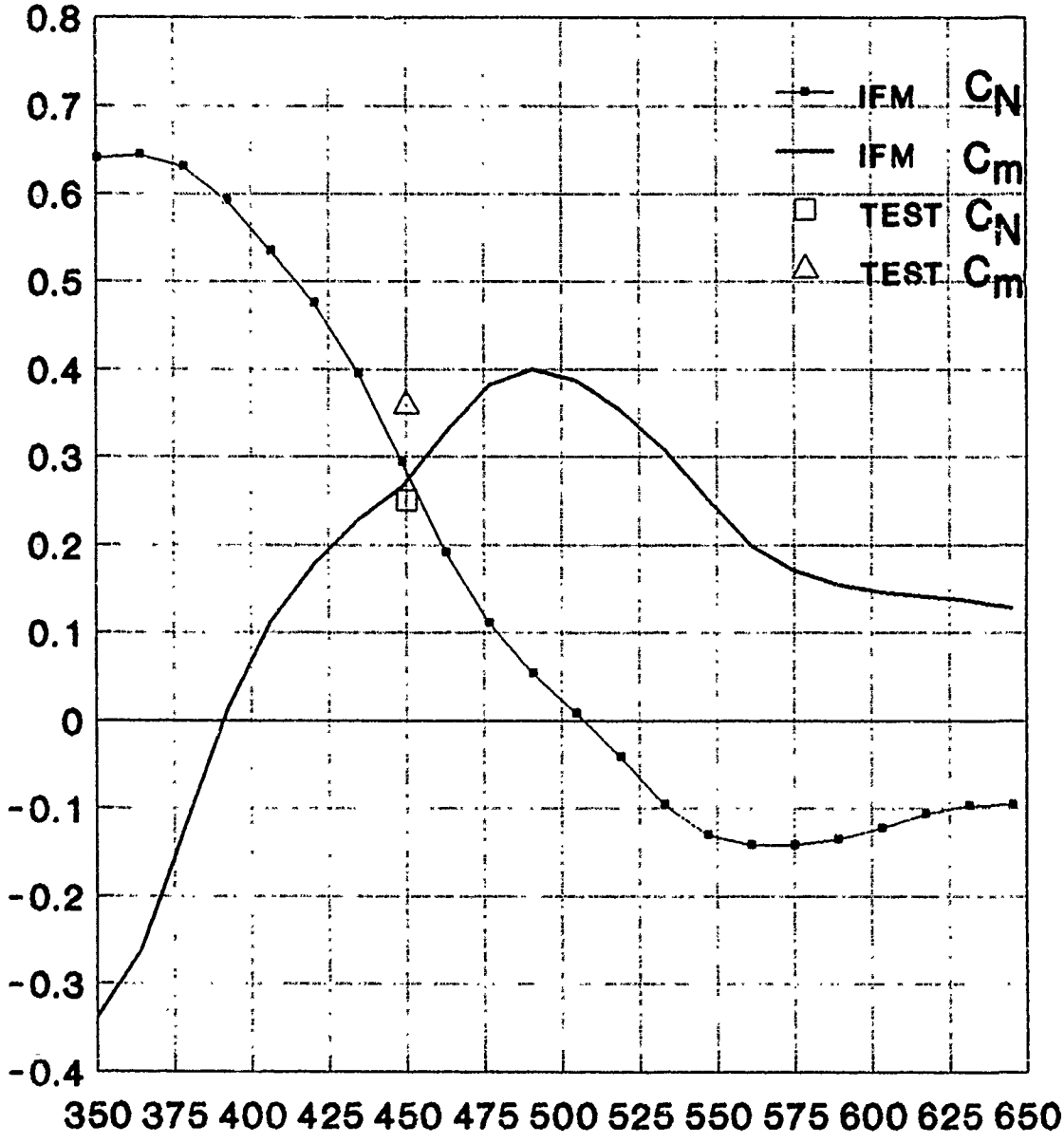

FIG 15 BQM-126 F-18 CARRIAGE LOADS

AIWS CONFIGURATION M = 0.95

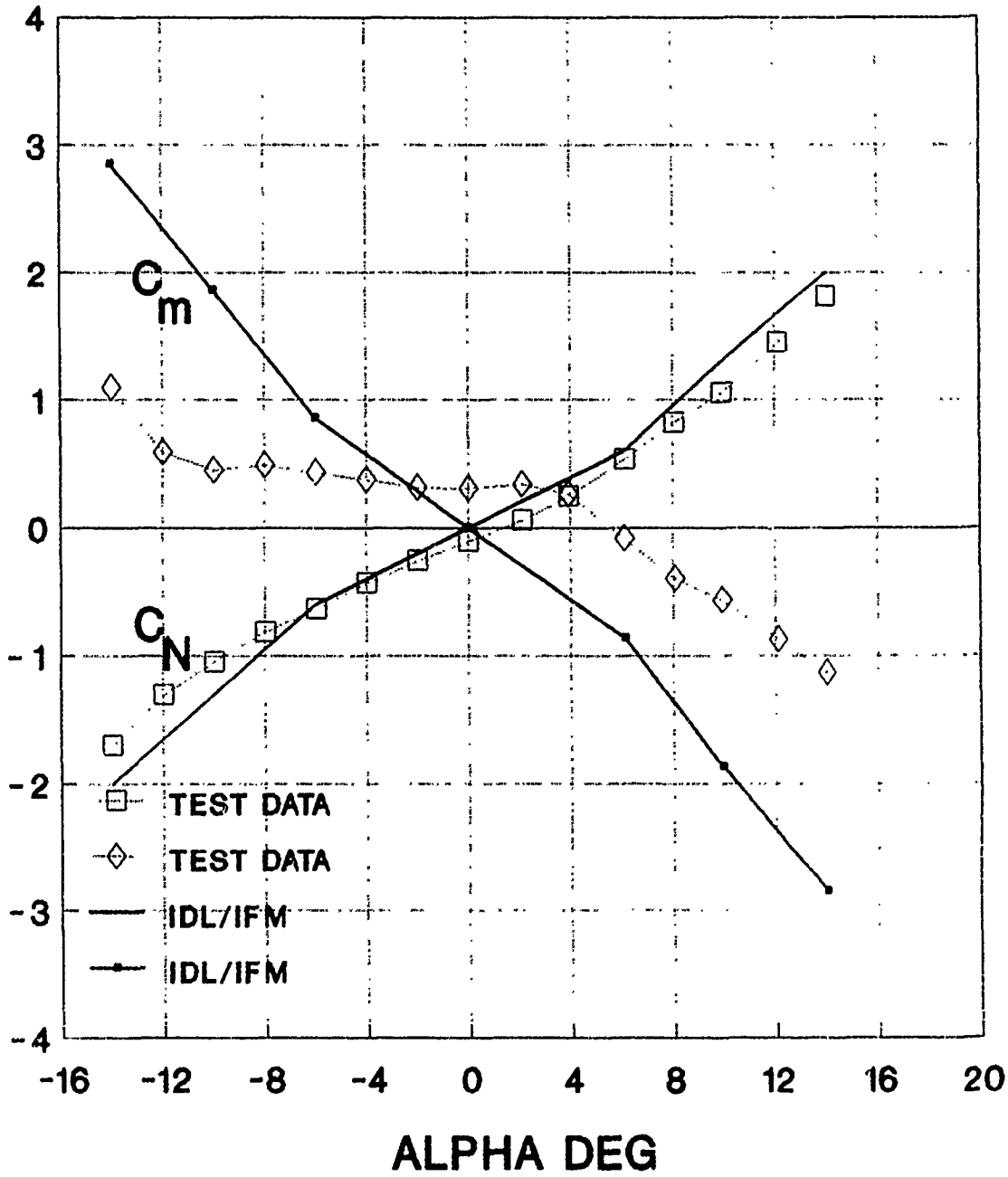

FIG. 16 IDL FORCE AND MOMENT CORRELATION

AIWS CONFIGURATION M=.95 WL=62 BL=134

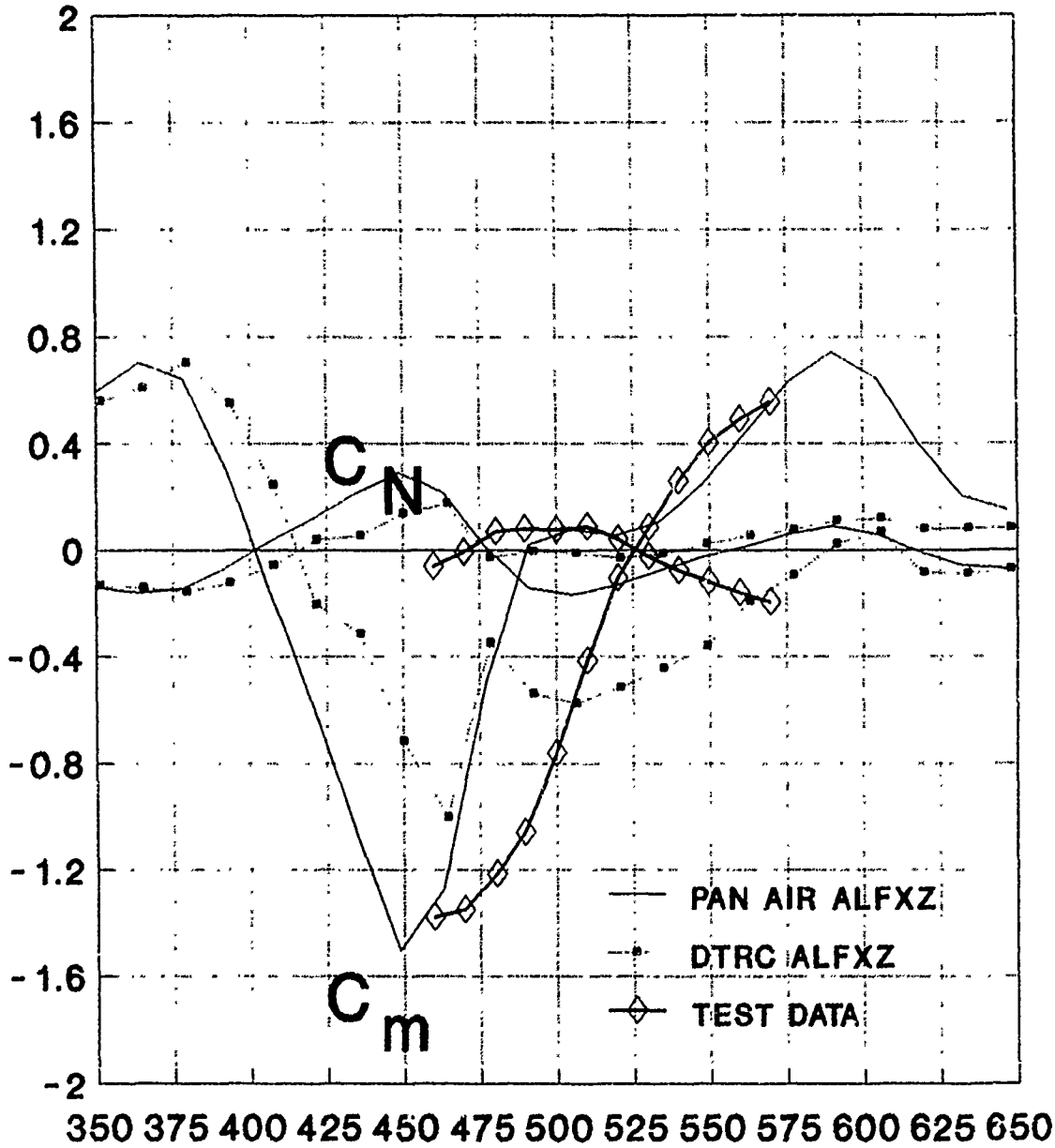

FIG. 17 IFM FORCE AND MOMENT COMPARISON

AIWS CONFIGURATION M=.95 WL=62 BL=134

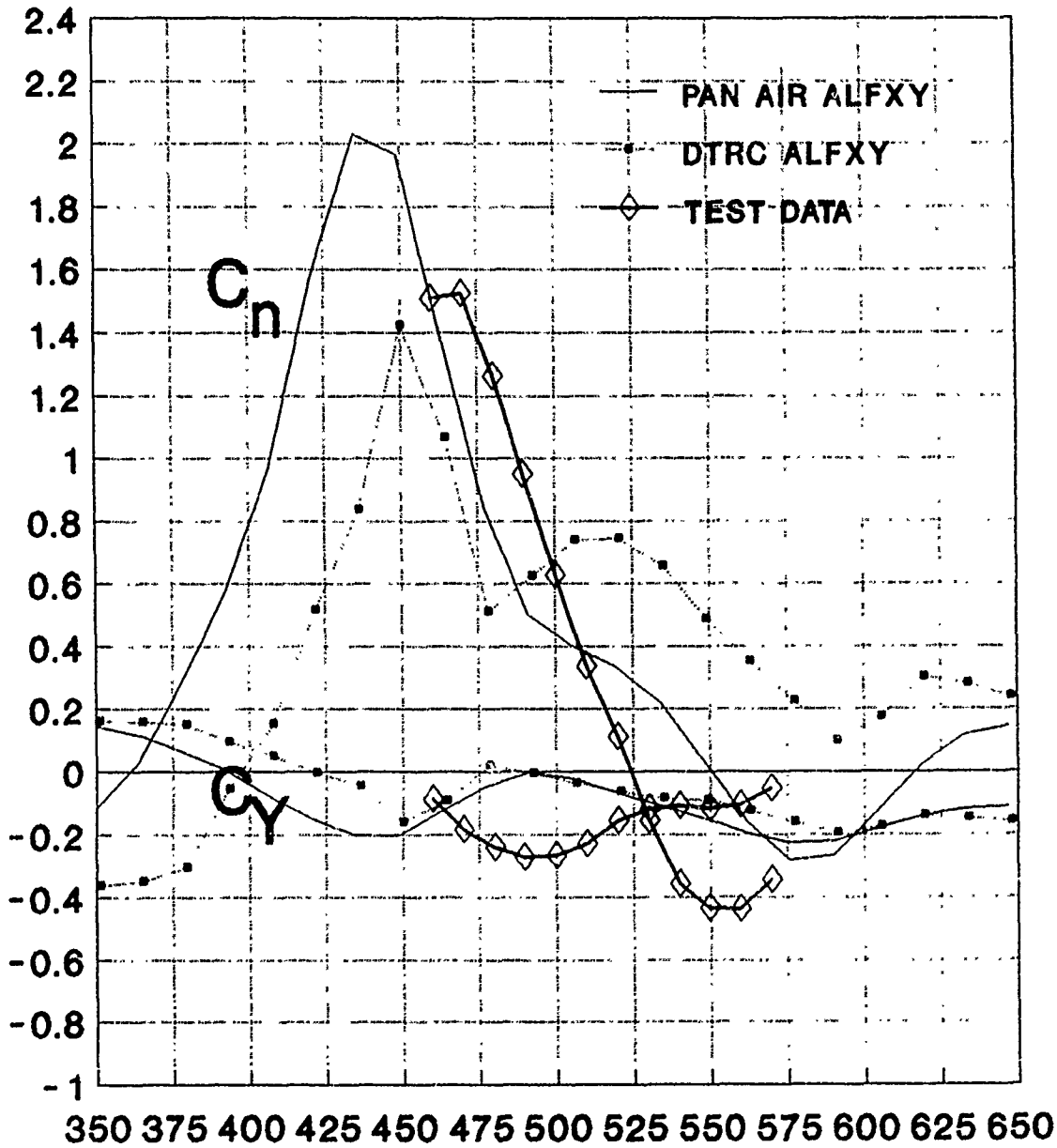

FIG. 18 IFM FORCE AND MOMENT COMPARISON

BIOGRAPHY
A. CENKO

EDUCATION:

B.S. PENN STATE UNIVERSITY 1965
M.E. CORNELL UNIVERSITY 1967
Ph.D. W. VIRGINIA UNIVERSITY 1970

PROFESSIONAL EXPERIENCE:

ASSO. ENGINEER, BOEING VERTOL, 12/65-9/66
Analysed helicopter rotor performance.

ENGINEER, GRUMMAN AEROSPACE, 7/69-9/72
Developed transonic wing design methods.

ASST. PROFESSOR, DOWLING COLLEGE, 9/72-5/77
Taught courses in Aeronatics and Mathematics.

SENIOR ENGINEER, GRUMMAN AEROSPACE, 5/77-1/85
Developed methods for A/C design and store separation.

ASSO. PROFESSOR, HOFSTRA UNIVERSITY, 1/85-8/87
Taught courses in Aerospace and Mechanical engineering.

AEROSPACE ENGINEER, NAVAL AIR DEV. CTR, 8/87-PRESENT.
Developed methods to predict tow target trajectories and the behavior of stores separating from a cavity. Responsible for recommending to NAVAIR the Air Launch Certification of stores from Navy aircraft.

ANALYTICAL INVESTIGATION OF AIRCRAFT/STORE FLIGHT LOAD ENVELOPES: VALIDATION OF MIL-A-8591G*

By: R. L. York, V. M. Gallagher, and R. H. Monahan
SRI International
Menlo Park, California

Military specification MIL-A-8591G (Reference 1)† identifies and quantifies the aircraft flight parameters required to analyze the structural interface between an aircraft and its stores. These flight parameters are sufficient to completely define the inertial and aerodynamic loads applied to a store when subjected to high dynamic flight. The specific flight parameters include load factors, angular rates, angular accelerations, and angles of attack/sideslip. The specified flight envelope is a function of the flight characteristics of the aircraft, the geometry of the aircraft store combination, and the store weight. The purpose of this investigation is to analytically examine the flight envelope defined in MIL-A-8591G and to quantify the changes in the envelope as aircraft type changes and store location varies.

1 INTRODUCTION

Figure 1 presents four load factor envelopes taken from previous stores identification reports. The envelopes are for the following applications:

Figure 1(a): F-111 Outboard Pylon (Reference 2)

Figure 1(b): F-18/AIM-9L (Reference 3)

Figure 1(c): F-15 Wing Station (2 and 8) (Reference 4)

Figure 1(d): F-14/AIM-7 Pylon (Reference 5).

The maximum/minimum vertical and lateral load factors are presented in Table 1. Point load factors vary between 50% and 900%, a significantly large variation. To investigate these differences, SRI has developed a model of the store/aircraft combination that is capable of predicting store load factors. The approach is to identify and define the flight performance characteristics of modern combat aircraft. The performance characteristics (mainly angular rates and accelerations) are then used to generate a theoretical flight envelope using the basic laws of mechanics. Outputs of the model are summarized and quantitatively discussed. The results are used to explore the sensitivity of MIL-A-8591G loads. These loads were developed to cover the broad spectrum of aircraft flown today and are satisfactory for most stores carried on a variety of aircraft. In some cases MIL-A-8591G loads may be inappropriate for specific applications. That is, for specific aircraft/store combinations these loads may be over-restrictive in some cases or not stringent enough in others, depending on the application.

*This effort was supported partially by ASD Det 24/YIC, Eglin AFB, FL.

†References are listed at the end of this paper.

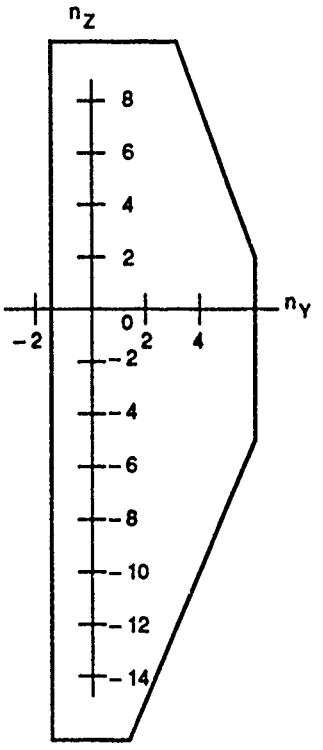

(a) F-111 OUTBOARD PYLON (Reference 2)

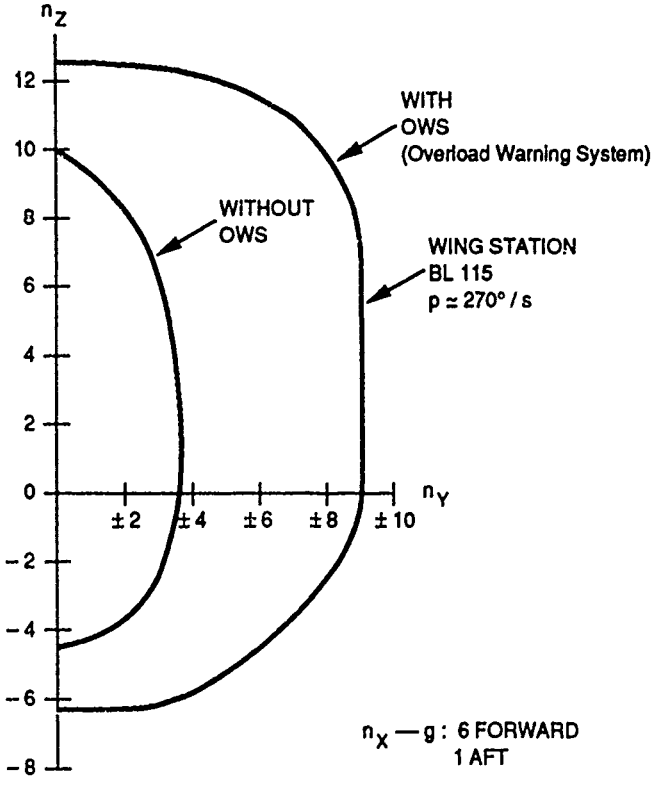

(b) F-15 WING STATION (Reference 4)

TMS-3503

FIGURE 1 AIRCRAFT / STORE FLIGHT ENVELOPES

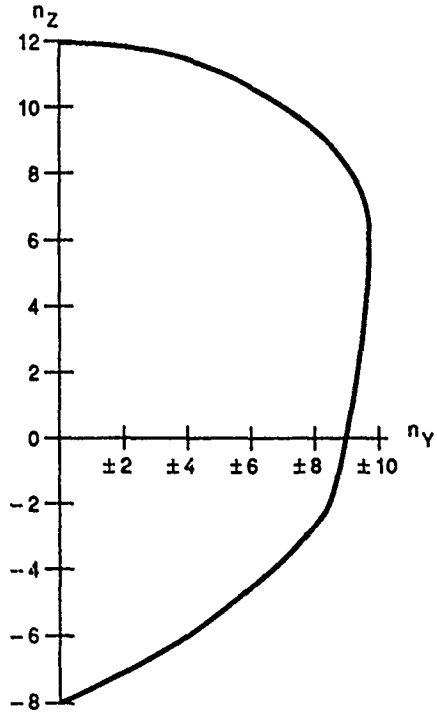

(c) F-18 / AIM-9 (Reference 3)

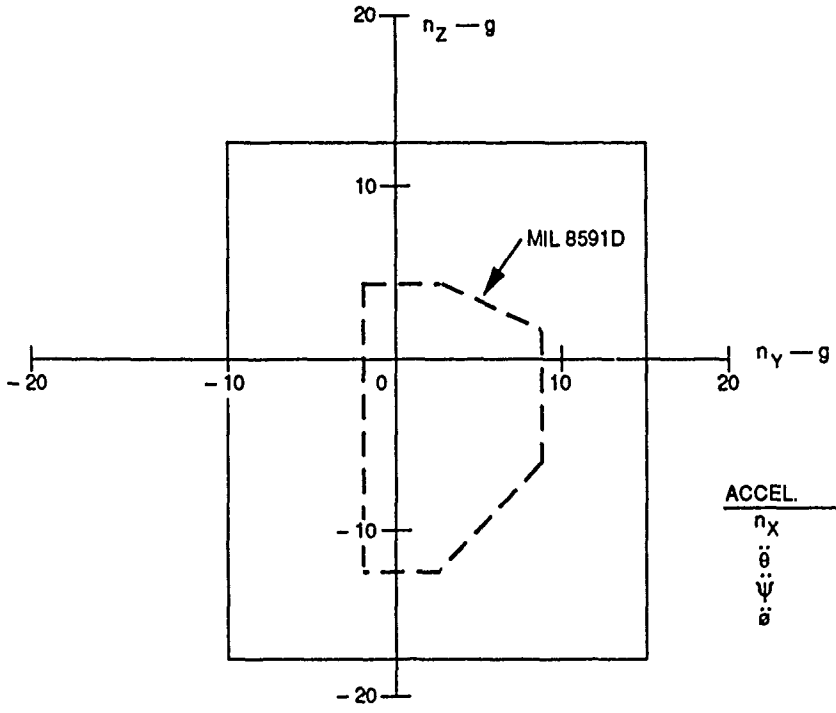

ACCEL.	MIL 8591D	F-14 / SPA.
n_X	±5	—
$\ddot{\theta}$	±25	±100
$\ddot{\psi}$	—6	+76 / –60
$\ddot{\varnothing}$	—	+1860 / –1120

(d) F-14 / AIM-7 PYLON (Reference 5)

TMS-3503

FIGURE 1 (continued)

Table 1: STORE LOAD FACTOR COMPARISONS

Source	Reference 2	Reference 3	Reference 4	Reference 5	Maximum % Difference
$n_{z_{max}}$	15.0	12.0	12.5	17.5	45.8
$n_{z_{min}}$	-10.0	-8.0	-6.0	-12.5	108.3
$n_{y_{max}}$	6.0	10.0	9.0	15.0	150.0
$n_{y_{min}}$	2.0	1.5	3.0	15.0	900.0

II STORE/AIRCRAFT MANEUVER ENVELOPE

Appendix B of MIL-A-8591G defines analysis methods for determining design loads to which a store can be subjected during flight. SRI used these methods to validate and substantiate the inertial load factor envelope for AIS pods mounted on an F-16 aircraft (References 6 and 7).

A. F-16 AIS Pod Mounting Locations

The AIS pod can be mounted at six locations on the F-16C, three on each side of the aircraft (References 8 and 10). Figure 2 shows these locations and specifies the distance of each location from the centerline of the fuselage. SRI developed load factor envelopes for midwing stations 3 and 7 and wingtip stations 1 and 9.

B. Store Load Factor Model

To determine the critical points on the inertial load factor envelope, SRI developed a computer model of the aircraft/store combination. The program modeled the F-16 as a rigid body and used the distances, rates, and accelerations given in reference documentation to calculate the load factors on the pod at each location. The equations of motion used (which follow) were taken from Appendix B of MIL-A-8591G.

Store load factors:

$$n_{x_S} = -a_x + \frac{1}{g}\left[\omega_z \Delta Y - \omega_y \Delta Z + (\omega_y^2 + \omega_z^2)\,\Delta X - \omega_x \omega_y \Delta Y - \omega_x \omega_z \Delta Z\right]$$

$$n_{y_S} = -a_y + \frac{1}{g}\left[\omega_x \Delta Z - \omega_z \Delta X + (\omega_x^2 + \omega_z^2)\,\Delta Y - \omega_x \omega_y \Delta X - \omega_y \omega_z \Delta Z\right]$$

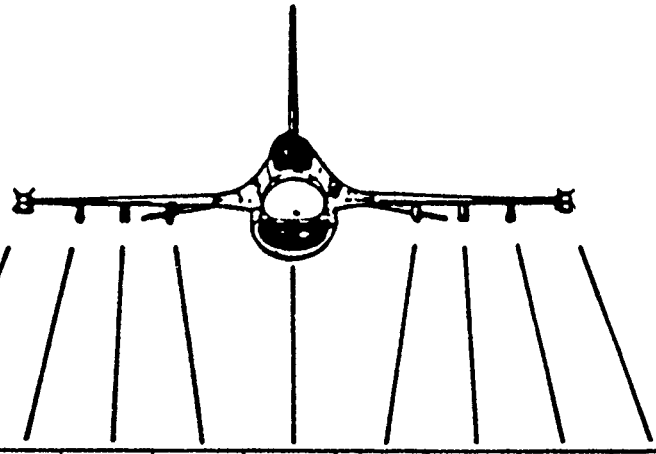

	STA 9	STA 8	STA 7	STA 6	STA 5	STA 4	STA 3	STA 2	STA 1
AIM-9 SIDEWINDER	YES	YES	YES	NO	NO	NO	YES	YES	YES
AIS PODS	YES	YES	YES	NO	NO	NO	YES	YES	YES
DISTANCE FROM CG (ft)	15.8	13.1	10.0				-10.0	-13.1	-15.8
ROLL (deg)	-90	0	0				0	0	90

TMS-3503

FIGURE 2 F-16 AIS POD MOUNTING LOCATIONS

$$n_{z_S} = -a_z + \frac{1}{g}\left[\dot{\omega}_y \Delta X - \dot{\omega}_x \Delta Y + (\omega_y^2 + \omega_x^2)\,\Delta Z - \omega_x \omega_z \Delta X - \omega_y \omega_z \Delta Y\right].$$

Adaptation parameters:

$\Delta X = X_{\text{store cg}} - X_{\text{aircraft cg}}$

$\Delta Y = Y_{\text{store cg}} - Y_{\text{aircraft cg}}$

$\Delta Z = Z_{\text{store cg}} - Z_{\text{aircraft cg}}$.

C. Aircraft Flight Data Sources

To calculate the load factors at the four aircraft/store attachment locations, SRI identified that values of a number of flight parameters (i.e., linear accelerations; roll, pitch, and yaw rates/accelerations) and displacements were required to determine the store flight envelope. Four sources of data were utilized to define the required data. Each source is described below.

1. F-16 Flight Manual Data

Linear normal acceleration and roll rate were found in the F-16C Flight Manual (Reference 8). Table 2 lists the specific values used.

Table 2: F-16 FLIGHT DATA CARRYING THE AIS POD

Parameter		Value
Name	Symbol	
Maximum Roll Rate	$\dot{\omega}_x$	270°/s (4.7 rad/s)
Maximum Positive Z Load Factor	a_z	9.0 g
Minimum Negative Z Load Factor	a_z	-3.0 g

2. MIL-A-8591G Data

Roll, pitch, and yaw accelerations were not available in the F-16 Flight Manual. Therefore, the peak values for these parameters were taken from Table B-2 of Appendix B of MIL-A-8591G. This information is duplicated in Table 3.

Table 3: AIRCRAFT FLIGHT CONDITIONS FOR DESIGN OF STORES ON HIGH-PERFORMANCE AIRCRAFT (Limit Loads)

Condition	Dynamic Pressure (psf)	Aircraft Angles (deg)		Linear Accelerations (g)			Peak Angular Rates* (rad/s)			Peak Angular Accelerations* (rad/s^2)		
		Attack α	Sideslip β	a_x	a_y	a_z	$\dot{\omega}_x$	$\dot{\omega}_y$	$\dot{\omega}_z$	$\ddot{\omega}_x$	$\ddot{\omega}_y$	$\ddot{\omega}_z$
1. Pullout	2500	5	0	±1.5	±1.0	+7.0	...	...	...	±0.25	±0.5	0
2. Pullout	1000	13	0	±1.5	±1.0	+8.5	...	...	...	±0.5	±0.5	0
3. Pullout	500	25	0	±1.5	±1.0	+10.0	...	...	...	±0.5	±0.5	0
4. Rolling-pullout	650	6	±2	±1.5	±0.5	+7.0	±5.0	...	...	±11.0	±3.0	±2.0
5. Rolling-pullout	2500	3	±1	±1.5	±0.25	+6.5	±4.5	...	...	±13.0	±1.0	±1.0
6. Rolling-pullout	2500	2	±1	±1.5	±0.25	+6.0	±4.5	...	...	±17.0	±1.0	±1.0
7. Barrier *engagement*	150	0	0	-4.0	±1.0	+2.0	...	...	...	0	±6.0	±4.0
8. Max. sink rate landing	150	0	0	-1.0	±1.0	+4.0	...	...	...	0	±4.0	±2.0
9. Bank-to-bank roll	2500	3	±1	±1.5	±1.0	+6.0	...	...	...	±13.0	±0.5	±1.0
10. Rudder-kick release (1 g)	400	2	±10	±1.5	±1.5	+1.0	...	...	...	±1.0	0	±1.5
11. Pushover	2500	-2	0	±1.5	±1.0	-1.0	...	...	...	0	0	0
12. Pushover	1800	-4	0	±1.5	±1.0	-3.0	...	...	...	0	0	0
13. Pushover	1000	-6	0	±1.5	±1.0	-6.0	...	...	...	±0.5	0	0

*These are peak values and do not occur simultaneously.

3. TACTS/ACMI Data

Pitch and yaw rates were more difficult to establish. Neither the F-16 Flight Manual nor MIL-A-8591G contain adequate information to define these parameters. In a previous study (Reference 9), SRI collected and analyzed flight data from high-dynamic segments of TACTS/ACMI training missions. Five different aircraft types were involved in the study: F-18 (wingtip), F-14, F-5 (wingtip), F-4, and A-4. This study indicated the AIS pitch rate is ±0.4 rad/s and the yaw rate ±0.5 rad/s. These data are summarized in Table 4.

Table 4: ADDITIONAL AIRCRAFT/STORE FLIGHT PARAMETERS

Parameter		Value
Name	Symbol	
Pitch rate	$\dot{\omega}_Y$	±0.4 rad/s
Yaw rate	$\dot{\omega}_Z$	±0.5 rad/s
Roll acceleration	$\ddot{\omega}_X$	±10.0 rad/s^2

4. TACTS/ACMI Aircraft/Pod Interface Manual Data

This document (Reference 10) describes the capability of the AIS pod, which is designed to be carried on any aircraft/store location capable of carrying a Sidewinder. The TACTS/ACMI system assesses aircrew training and, therefore, must translate pod-measured performance data from pod coordinates to aircraft coordinates. This translation requires the displacement vector (referred to as adaptation parameters) from the pod center of gravity (cg) to the aircraft cg. The Interface Manual defines, along with other data, the adaptation parameters for each aircraft/pod combination.

D. Aircraft Flight Data Selection

Review of the data sources identified in Section II-C establishes that there is insufficient flight data available to describe specific flight maneuvers for the F-16. Therefore, a rationale was developed to generate the required information from available sources.

1. Approach

The nine-step approach illustrated in Figure 3 describes the methodology SRI followed to determine the parameters required to generate a store load factor envelope. Each step is explained further in the following paragraphs.

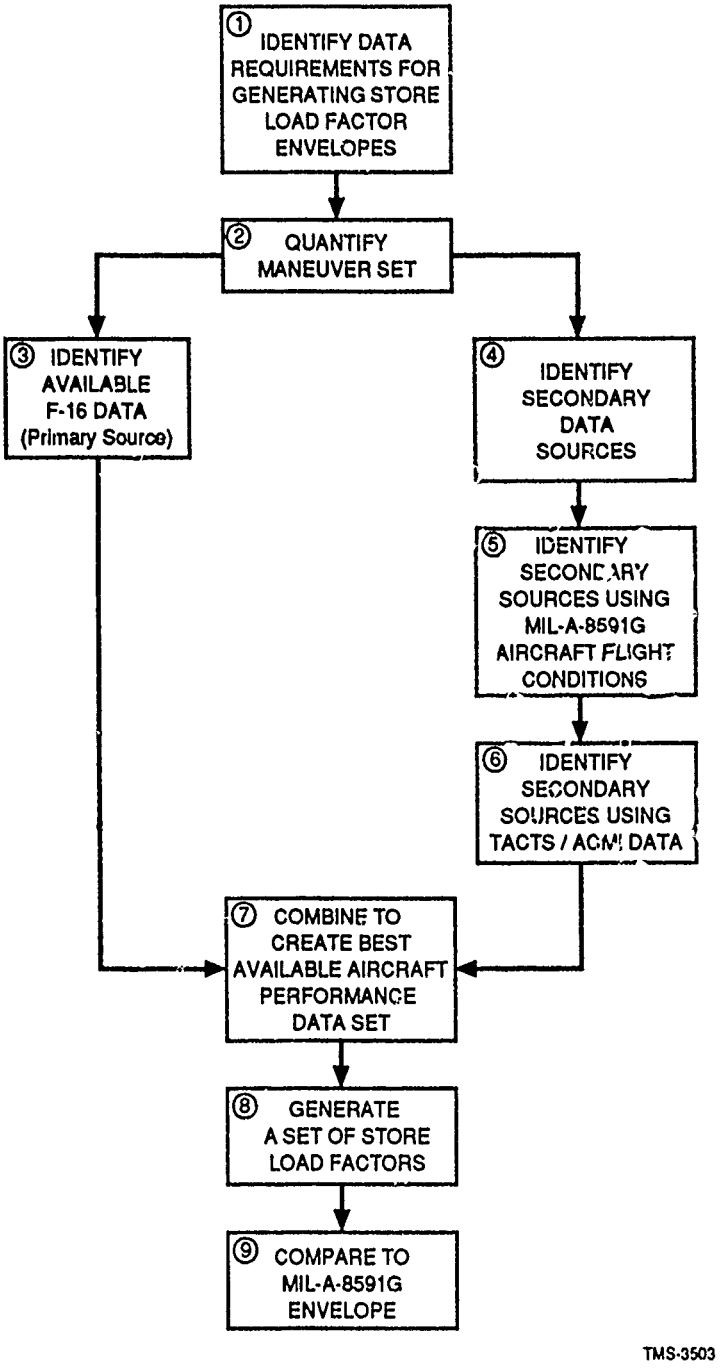

FIGURE 3 STEPS REQUIRED TO SYSTEMATICALLY DERIVE A STORE LOAD FACTOR ENVELOPE

Step 1: The procedure begins by identifying the data required to generate a store load factor envelope. The equations of motion indicate the aircraft load factors, angular rates/accelerations, and adaptation parameters are required for the calculation.

Step 2: SRI selected four general types of maneuvers (as identified in MIL-A-8591G) that stress stores during captive flight: (1) Pushover, (2) Rolling Pushover, (3) Rolling Pullout, and (4) Pullout.

Step 3: Identification of aircraft performance data begins by review of existing and available F-16 data, including the F-16 Flight Manual.

Step 4: Twelve parameters are potentially required to address every factor that contributes to generating loads on a store: three linear load factors, three angular velocities, three angular accelerations, and three displacements. The F-16 Flight Manual addresses only a limited number of these parameters. Other sources are required to define an adequate set of parameters.

Step 5: If F-16-specific data are not available, the default parameters allowed by and defined in MIL-A-8591G are then used.

Step 6: If default values are not identified in MIL-A-8591G, worst-case values that have been recorded during TACTS/ACMI training exercises are then selected.

Step 7: The "best" set of parameters is selected by selectively using all available data. Data is first taken from the F-16 Flight Manual, then from MIL-A-8591G, and finally from TACTS/ACMI exercises to fill any remaining voids.

Step 8: This "best" set of parameters is used with the model presented in Section II-B to generate a store load factor envelope.

Step 9: The theoretical envelopes generated in Step 8 will then be compared with the envelopes provided in MIL-A-8591G.

2. Maneuver Selection

Table 3 (Table B-2 of MIL-A-8591G) was used as a guide to identify specific stressing maneuvers. The peak values of the flight performance parameters associated with an aircraft do not occur simultaneously (i.e., maximum acceleration does not occur at the same time as maximum velocity). To address this problem, the parameters in Table 3 have been modified (using the procedures identified in the previous section) as follows for each maneuver considered.

- Pushover (Table 3, condition 12) with
  - Minimum angular velocity
  - Maximum angular acceleration.
- Rolling Pushover #1 (Table 3, condition 12) with
  - Moderate angular velocity
  - Moderate angular acceleration.

- Rolling Pushover #2 (Table 3, condition 11) with
  - Maximum angular velocity
  - Minimum angular acceleration.
- Rolling Pullout #1 (Table 3, condition 4) with
  - Maximum angular velocity
  - Minimum angular acceleration.
- Rolling Pullout #2 (Table 3, condition 4) with
  - Moderate angular velocity
  - Moderate angular acceleration.
- Pullout (Table 3, condition 2) with
  - Minimum angular velocity
  - Maximum angular acceleration.

3. Load Factors

Minimum and maximum values of aircraft normal load factor (a_Z) were taken from the F-16 Flight Manual: a_Z (minimum) = -3.0 g and a_Z (maximum) = 9.0 g. Nominal values of a_X (±1.5 g) and a_Y (±1.0 g) were taken from MIL-A-8591G.

4. Angular Velocity/Acceleration

The contribution of angular velocity and acceleration must be determined for each maneuver. To assess the overall potential contribution of each parameter, SRI considered each extreme (all angular velocity/no acceleration and no angular velocity/all acceleration) and explored one point between these two limits.

Paragraph 3.11.3.2 and Figure 12 of MIL-A-8591G state that load factors and angular accelerations shall be represented by a half sine wave amplitude profile (Figure 4). Figure 5 extends this acceleration profile to generate an angular velocity profile and identifies the three specific points (A, B, and C) that are used to create the parameter set for each maneuver.

5. Adaptation Parameters

Table 5 gives the specific displacement vector associated with the AIS pod when it is carried on each of the six potential Sidewinder stations on the F-16.

6. Summary of Model Input Parameters

Table 6 summarizes the optional parameter set generated from review and assessment of the available aircraft performance data.

FOR FLIGHT:	t = 0.20 s to 1.0 s
FOR ARRESTED LANDING: (with longitudinal load factors up to 2.0)	t = 0.03 s to 0.10 s
FOR ARRESTED LANDING: (with longitudinal load factors above 2.0)	t = 0.15 s to 0.50 s
FOR CATAPULTING:	t = 0.02 s to 0.40 s
FOR NON-ARRESTED LANDING:	t = 0.03 s to 1.0 s

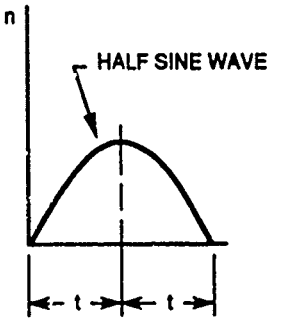

FOR ALL CASES ABOVE, n = LOAD FACTOR

TMS-3503

FIGURE 4 TIME-LOAD FACTOR CURVE

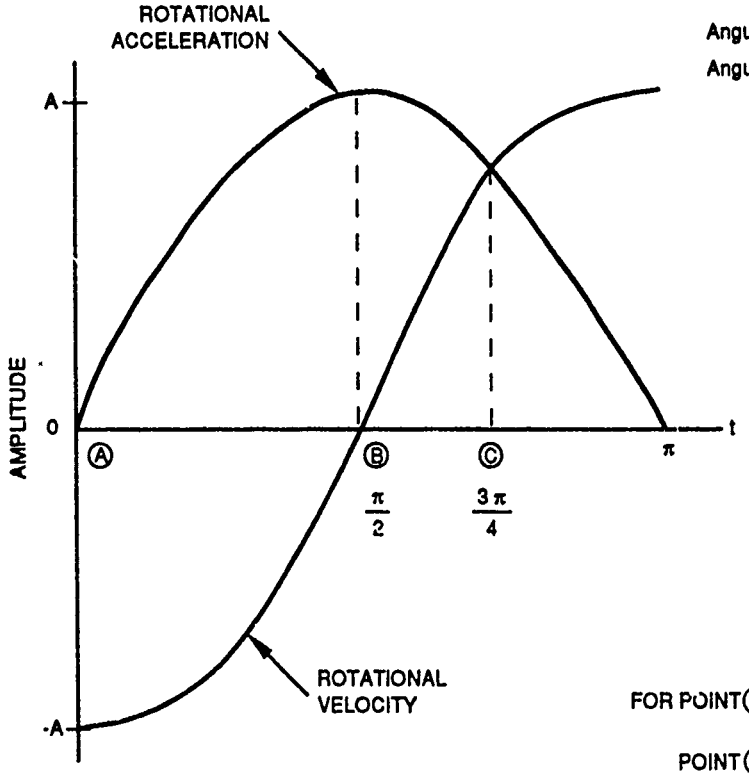

Angular Acceleration: $\ddot{\omega} = A \sin t$

Angular Velocity: $\dot{\omega} = A \int \sin t \, dt = A \cos t + c$
(assume c = 0)

FOR POINT Ⓐ : Rotational Acceleration @ Minimum
Rotational Velocity @ Maximum

POINT Ⓑ : Rotational Acceleration @ Minimum
Rotational Velocity @ Maximum

POINT Ⓒ : Simultaneous Contribution
of Rotational Velocity and Acceleration
(0.707 of maximum amplitude of each)

TMS-3503

FIGURE 5 ANGULAR VELOCITY / ACCELERATION RELATIONSHIP

Table 5: ADAPTATION PARAMETERS (Reference 10)

Station	Store Displacement from A/C cg (ft)		
	ΔX	ΔY	ΔZ
1	9.7	-15.7	0.7
3	6.4	-10.0	-0.8
7	6.4	+10.0	-0.8
9	9.7	+15.7	0.7

Table 6: SUMMARY OF MODEL INPUT PARAMETERS

Maneuver Description			Aircraft Parameters				
Maneuver	Angular Velocity	Angular Rate	a_x (g)	a_y (g)	a_z (g)	$\dot{\omega}_x$ (rad/s)	$\ddot{\omega}_x$ (rad/s^2)
Pushover (Condition 12)	Minimum	Maximum	-1.5	-1.0	-3.0	0.0	-10.0
Rolling Pushover #1 (Condition 12)	Moderate	Moderate	-1.5	-1.0	-3.0	-3.3	-7.1
Rolling Pushover #2 (Condition 11)	Maximum	Minimum	-1.5	0.0	-1.0	-4.7	0.0
Rolling Pullout #1 (Condition 4)	Maximum	Minimum	-1.5	0.0	9.0	-4.7	0.0
Rolling Pullout #2 (Condition 4)	Moderate	Moderate	-1.5	-1.0	9.0	-3.3	7.1
Rolling Pullout (Condition 2)	Minimum	Maximum	-1.5	-1.0	9.0	0.0	10.0

E. Store Load Factors

SRI has generated two store load factor sets corresponding to the maneuvers identified in Section II-D-2 and using the parameter values indicated in Table 6. The first set of load factors was calculated for a store mounted on a midwing pylon ($\Delta Y = 10.1$ ft) and the second set for a store mounted on the wingtip ($\Delta Y = 15.8$ ft).

1. Calculated Midwing Pylon Store Load Factors (Stations 3 and 7)

Table 7 presents the calculated store factors for midwing pylon carriage. Figure 6 shows these data and also the MIL-A-8591G pylon envelope. The average deviations of the calculated load factors from the comparable boundaries are given in Table 8.

Table 7: CALCULATED PYLON STORE LOAD FACTORS

Maneuver*	Store Load Factor (g)		
	n_x	n_y	n_z
Pushover	1.50	0.75	6.11
Rolling Pushover #1	1.50	4.21	5.48
Rolling Pushover #2	1.50	6.87	1.55
Rolling Pullout #1	1.50	6.87	-8.45
Rolling Pullout #2	1.50	4.56	-10.94
Pullout	1.50	1.25	-12.11

*Section II-D-2 describes the parameters for each maneuver.

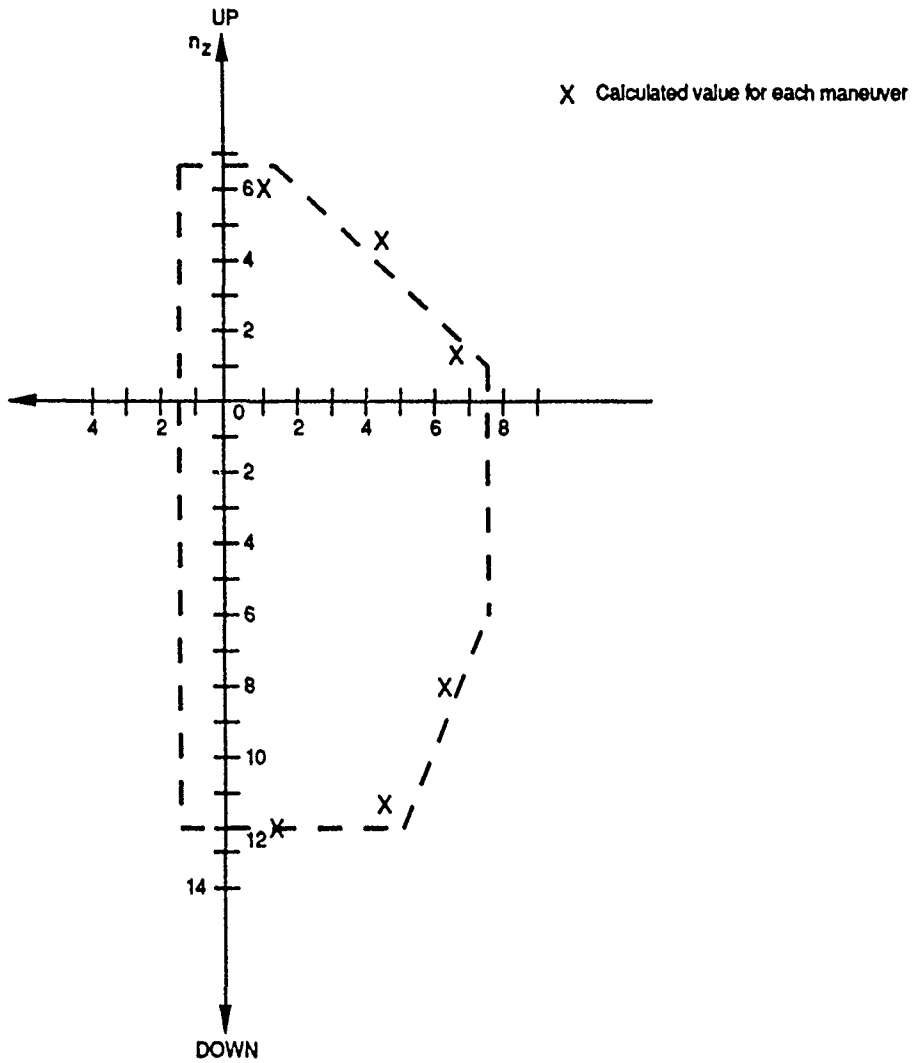

FIGURE 6 CAPTIVE FLIGHT LOAD FACTOR ENVELOPES – PYLON CASE

Table 8: MIDWING PYLON LOAD FACTOR COMPARISONS

Load Factor	Average Deviation (%)
n_y (max)	1.6
n_z (max)	-6.0
n_z (min)	-1.0

2. Calculated Wingtip Store Load Factors (Stations 1 and 9)

Table 9 presents the calculated store load factors for wingtip carriage. Figure 7 shows these data and also the MIL-A-8591G wingtip envelope. The two calculated points at the top of Figure 7 were chosen as comparable to the top boundary (max n_Z) of the envelope; the two calculated points at the bottom were chosen as comparable to the bottom boundary (min n_Z); and the two points to the right of the envelope were chosen as comparable to the right vertical boundary (max n_Y). Table 10 indicates the average of the deviations of the calculated load factors from the comparable boundaries.

Table 9: CALCULATED WINGTIP STORE LOAD FACTORS

Maneuver*	Store Load Factor (g)		
	n_x	n_y	n_z
Pushover	1.50	1.22	7.88
Rolling Pushover #1	1.50	6.47	6.23
Rolling Pushover #2	1.50	10.78	0.52
Rolling Pullout #1	1.50	10.78	-9.48
Rolling Pullout #2	1.50	6.16	-12.70
Pullout	1.50	0.78	-13.88

*Section II-D-2 describes the parameters for each maneuver.

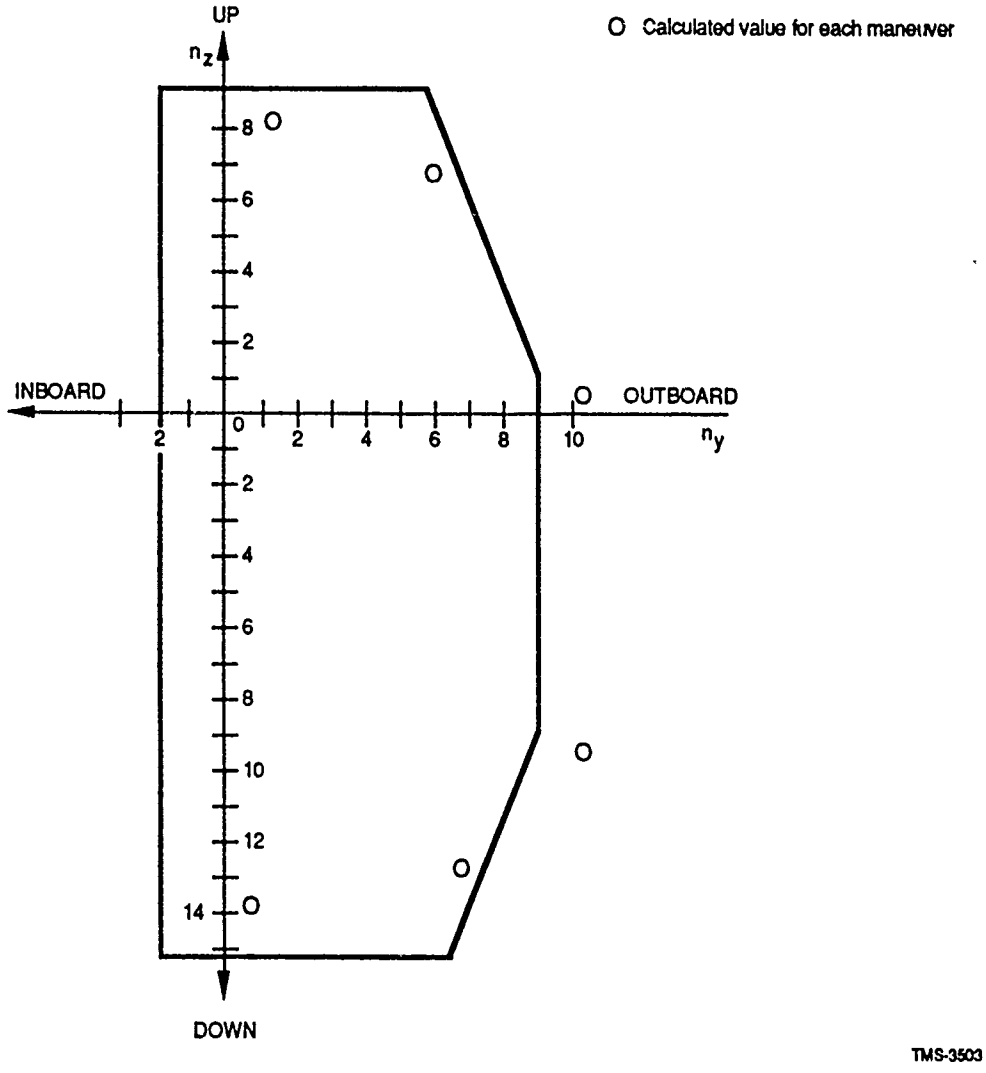

FIGURE 7 CAPTIVE FLIGHT LOAD FACTOR ENVELOPE – WINGTIP CASE

Table 10: F-16 WINGTIP LOAD FACTOR COMPARISONS

Load Factor	Average Deviation (%)
n_y (max)	19.8
n_z (max)	-12.4
n_z (min)	-10.5

III DISCUSSION

When the calculated store load factor and the MIL-A-8591G load factor envelopes are compared, the following range of percentage deviations are indicated: -12.4% to 19.8% for wingtip-mounted stores and, significantly smaller, -6.0% to 1.6% for midwing-mounted stores. The load factor trend for both cases (wingtip and midwing pylon) are similar. The MIL-A-8591G wingtip envelope may be too restrictive for normal loads and potentially not restrictive enough for lateral loads. Supplemental data would be required before this issue can be resolved. The overall procedures identified in MIL-A-8591G again have been shown to be comprehensive and flexible. In a large majority of cases, the procedures are totally appropriate. However, some judgement should be applied when an extremely heavy or lightweight store is to be considered for carriage. In these cases, a modified envelope, as allowed by MIL-A-8591G, may be more appropriate.

REFERENCES

1. "General Design Criteria for Airborne Stores, Associated Suspension Lugs, and Aircraft-Store Interface," MIL-A-8591G, Department of the Navy (1 December 1983).
2. "The Proper Use of Military Specification MIL-A-8591E for Design of Stores to be Used by the United States Air Force," Dyess, W. W., Air Force Armament Laboratory (DLJC), Eglin AFB, Florida, presented at JTCG Symposium (7 October 1977).
3. "Interface Control Document F-18 Aircraft/AIM-9L Missile," Kohl, R. L., Report No. ICD-F-18-003, McDonnell Aircraft Company, St. Louis, Missouri (24 February 1978).
4. "Minutes of the 53rd Quarterly Meeting of the JTCG/MD Working Party 6, Aero-Structures Study Group," Smith, R. E., Naval Weapons Center, China Lake, California (19 June 1984).
5. "F-14/AWG-9/AIM-7E and 7F System Interface Program Final Report," Part 1, Sections 1 through 5, Report No. BR-8596, Raytheon Co., Lowell, Massachusetts (July 1975).
6. "AIS Pod Static Stress Analysis: Procedure and Applications," R. L. York, J. W. Prausa, SRI International Report 8350-80-RM-33 (November 1980).
7. "AIS Pod Flight Compatibility/Certification Analysis (P4, P4A, P4AX, P4AM)," Gallagher, V. M., R. H. Monahan, R. L. York, and M. W. Eliot, SRI International Report 6301-89-FR-128 (September 1989).
8. "Flight Manual, F-16C/D, Blocks 25, 30, and 32," T.O. 1F-16G-1, General Dynamics (Fort Worth Division), Change 3 (27 June 1988).
9. "Experimental Investigation of Aircraft Flight Load Envelopes: Validation of MIL-A-8591F," York, R. L., R. E. Ford, and I. M. Wadsworth, Presented at 6th Biennial Aircraft/Stores Compatibility Symposium, Naval Surface Weapons Center, White Oak, Maryland (26-28 October 1982).
10. "TACTS/ACMI Aircraft/AIS Interface Manual," prepared by SRI International for AD/YIC, Eglin AFB, Florida (January 1989).

BIOGRAPHY OF PRESENTER

As a Senior Research Engineer in the Systems Development Division at SRI International, Mr. York has been involved with many systems analysis and development projects for military test ranges, instrumentation, and weapons systems. Since 1978, Mr. York's work at SRI has included responsibility for evaluating the structural interface between externally carried instrumentation packages developed as a part of a range instrumentation system. This work has expanded to include evaluating this interface for a number of military weapon systems. Clients have included the Naval Air Systems Command, Armament Division U.S. Air Force, Naval Air Development Center, and the Naval Weapons Center. Mr. York has a B.S.A.E. (1970) from California Polytechnic University and an M.S.M.E. (1975) from the University of California.

BIOGRAPHY OF AUTHOR

As a Senior Systems Analyst in the Systems Development Division at SRI International, Mrs. Gallagher has been involved in technical analysis and software development for a variety of Navy and Air Force training and weapons systems. She has conducted studies in which data from the TACTS/ACMI ranges were used to support fatigue analyses and to help determine future hardware requirements for the ranges. Mrs. Gallagher has a B.A. in Statistics from the University of California and an M.S. in Statistics from Stanford University.

BIOGRAPHY OF AUTHOR

As a Senior Operations Analyst in the Systems Development Division at SRI International, Dr. Monahan has been involved in numerous studies and analyses related to the effectiveness and operational use of various military weapons systems and associated equipment. He has developed and applied several computer models required for analyses directed toward the structural certification of weapons/stores. Dr. Monahan has a B.S. (1960) and M.S. (1963) in Mathematics from Syracuse University and a Ph.D. (1973) in Statistics from Stanford University.

ACER

ITS SELF-RECHARGEABLE ENERGY SOURCE AND THE LESSONS LEARNED

(ARTICLE UNCLASSIFIED)

By

Lynn D. Seal
EDO Corporation, College Pt., NY 11356

INTRODUCTION

Advanced tactical fighter studies project very high threat scenarios for future air combat zones. In order to accomplish the air-to-ground mission, aircraft performance and survivability must be improved significantly. Current fighter aircraft use pylon or multiple rack carriage for air-to-ground weapons. Study results to date show that conformal, blended, semi-submerged or submerged types of carriage can increase aircraft performance and survivability to acceptable levels. These carriage concepts greatly reduce the weapons contribution to the overall system drag and radar cross section. The benefits of conformal carriage have already been flight demonstrated with existing weapons on the F-4 in 1973 and on the F-15 in 1983. One significant deficiency was repeatedly highlighted during these tests: a suitable ejector mechanism does not exist for conformal applications. Present inventory ejector mechanisms require access to the breech to install impulse cartridges and to the swaybraces to secure the weapon. Both functions must be performed after the weapon has been loaded which prevents the ejector from being embedded in the airframe. In the past several years technology advances have been made which eliminate the need for access to the ejector mechanism after weapon loading. Energy sources are available to both eject the weapons and operate the swaybracing system. The use of these technologies will allow the ejector mechanisms and associated energy sources to become aircraft subsystems embedded directly in the airframe.

The conformal carriage and ejection of stores implies a need for ejector mechanisms integrated into an aircraft's fuselage and hands-off operation of these mechanisms once stores are loaded. The resulting requirement is for completely remote operation of the suspension equipment in all regards, and the need for an energy source that:

- does not have to be replaced after each store ejection and;
- does not contaminate the suspension equipment thereby eliminating the need for periodic cleaning.

The Air Force recognizing the growing need for conformal carriage suspension equipment - further enhanced by its stated intent to develop conformal carriage energy sources - began in late 1984 to develop the concepts that would lead to design of the Alternate Conformal Ejector Rack.

The objective of the Alternate Conformal Ejector Rack (ACER) program was to demonstrate an innovative rechargeable energy source in a carriage and release (C&R) mechanism designed specifically for conformal carriage and release of weapons. Further, not only should the energy source be remotely rechargeable, but the carriage and release mechanism should also be remotely controlled. This results in a ejection system that can be totally integrated into the aircraft so that the only "hands-on" operation by ground crews is loading the weapon onto the ACER. EDO Corporation, under contract FO8635-85-C-0170 and the direction of Mr. Don Larson of the Air Force Armament Laboratory, designed, fabricated, tested, and delivered the ACER System to the Air Force. Not only will this paper present the ACER design and performance, it will more importantly discuss some important "lessons learned" during the course of the program.

DESCRIPTION OF DESIGN

It was realized during the course of the ACER design that the key to the entire system was the energy source and that this source would out of necessity have to be self-rechargeable. A self-recharging energy source is needed because of the inaccessibility of the ejection mechanisms in conformal carriage installations and the stated Air Force policy of limiting maintenance on next generation aircraft. Figure 1 shows the ACER before integration into an aircraft. The approach taken for the ACER design was to use existing, proven mechanisms and methods uniquely

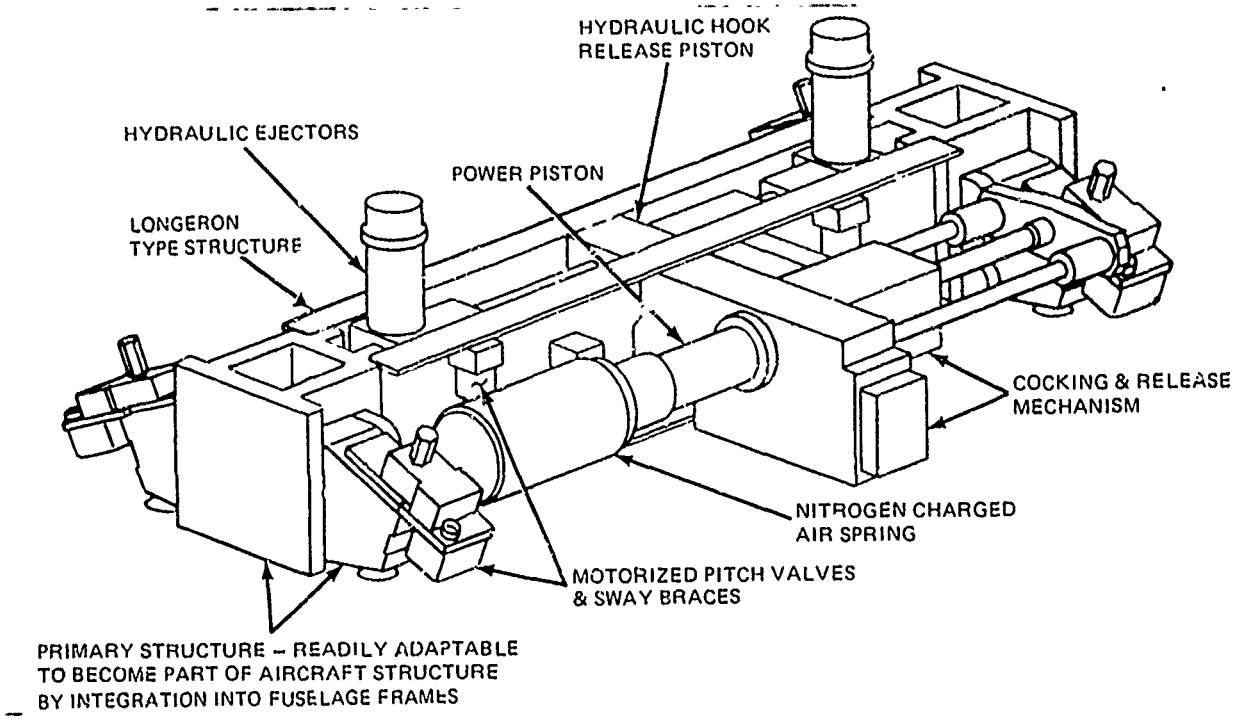

Figure 1. ACER System

packaged to meet the Air Force requirements. This would, for the overall system, increase reliability while greatly reducing risk.

The theory of operation for the ACER system is shown schematically in Figure 2. As can be seen from the schematic, the operation is straight forward. Most importantly, the system contains no hydraulic valves and the oil is only pressurized during the ejection cycle. The gas is charged at 3000 psi when the power module is fully released. The volume of the nitrogen chamber is sized such that when the cocking mechanism drives the power piston to the locked position the gas is compressed to a level of 4000 psi. This feature enables existing Air Force flight line equipment to be used to charge the ACER power module. The real key to the ACER system, as previously stated, is the power module. The mechanism, as shown in Figure 3, combines a series of commonly used aircraft components so that only aircraft electrical power is required to ready the ACER for ejection.

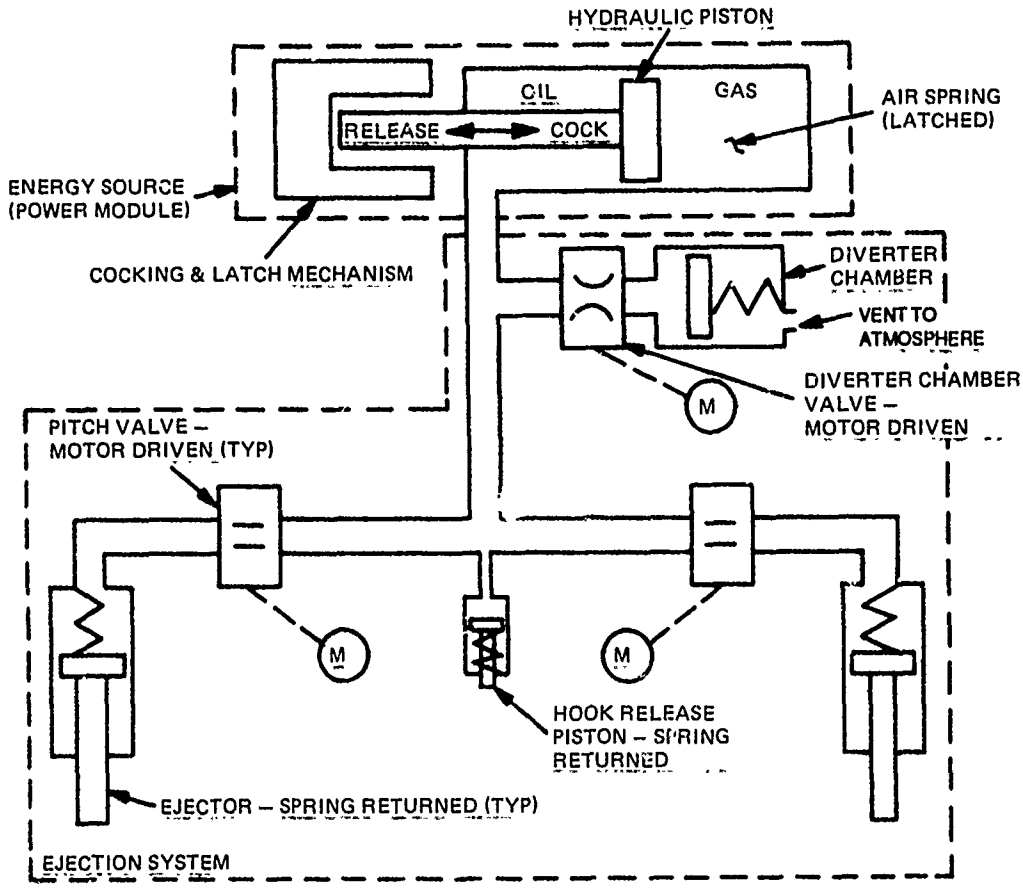

OPERATION

- The motor driven cocking mechanism drives the hydraulic piston off its stop to the cocked position which further compresses the nitrogen gas of the air spring.
- The hydraulic piston is held in the cocked position by a mechanical latch. There is no pressure in the oil at this time and the cocking mechanism returns to its starting position.
- A solenoid releases the latch and the air spring drives the hydraulic piston to the released position. This action forces the oil out of the power module into the ejection system to release the hooks and eject the carried store.
- The diverter chamber provides for expansion/contraction of the oil due to temperature changes and provides storage for oil from the retracting ejectors until the power module is cocked.

Figure 2. Energy Source/Ejection System Schematic

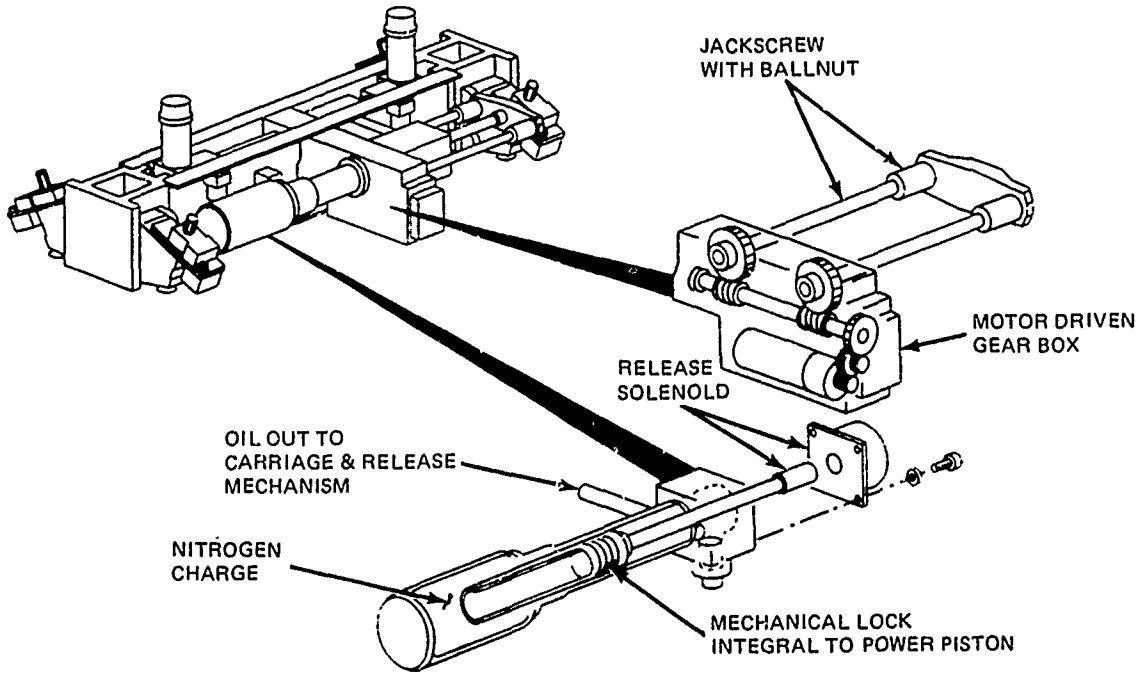

Figure 3. Key Power Module Components

The power module consists of a piston powered by high pressure nitrogen gas. The piston is prevented from moving by a mechanical lock. When the lock is released by a solenoid, the piston is free to move and force high pressure hydraulic oil to power the ejectors. When the piston has forced all oil into the ejectors, it comes to rest against a mechanical stop. The nitrogen gas is retained but at lower pressure due to the increased volume of the nitrogen gas chamber. An electric motor driving a series of jackscrews forces the power piston back into the locked position. This recompresses the nitrogen gas and draws the hydraulic fluid from the diverter chambers back into the power module. The ACER is now fully energized and ready for another ejection. About five minutes is needed for the motor driven jackscrews to cock the piston and return to the stowed position. Figures 4 and 5 schematically show operation of the power module. Note that several interesting points are evident:

- The nitrogen and hydraulic oil are each sealed independently and separated by an annulus vented to atmosphere to prevent mixing if leakage of either should occur.

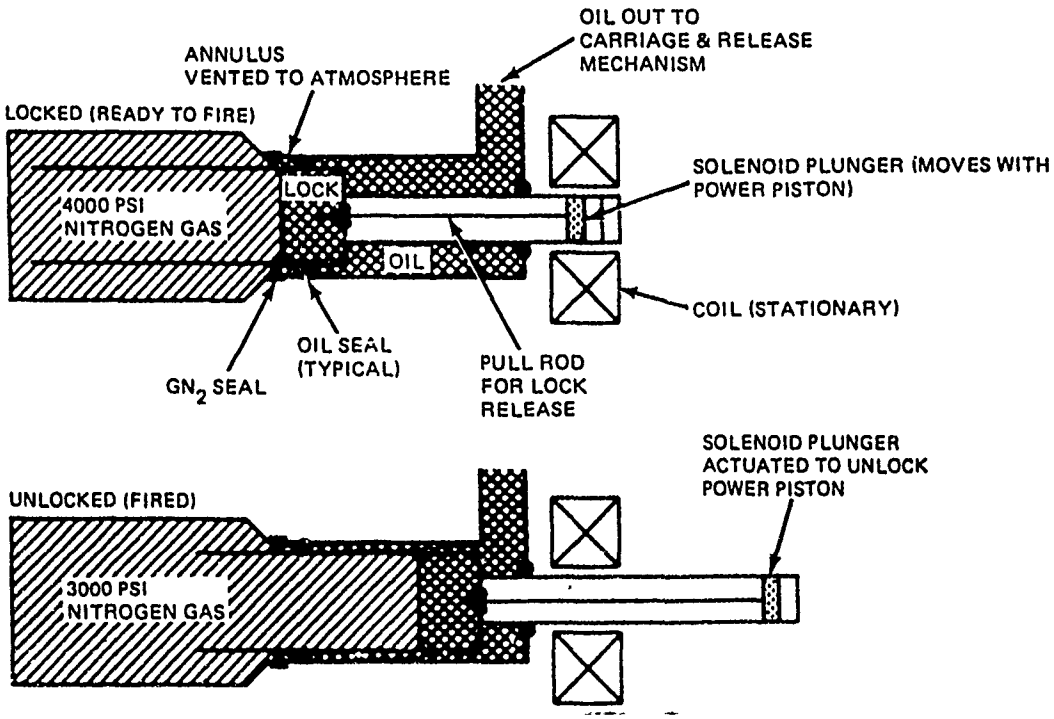

Figure 4. Power Module Operation

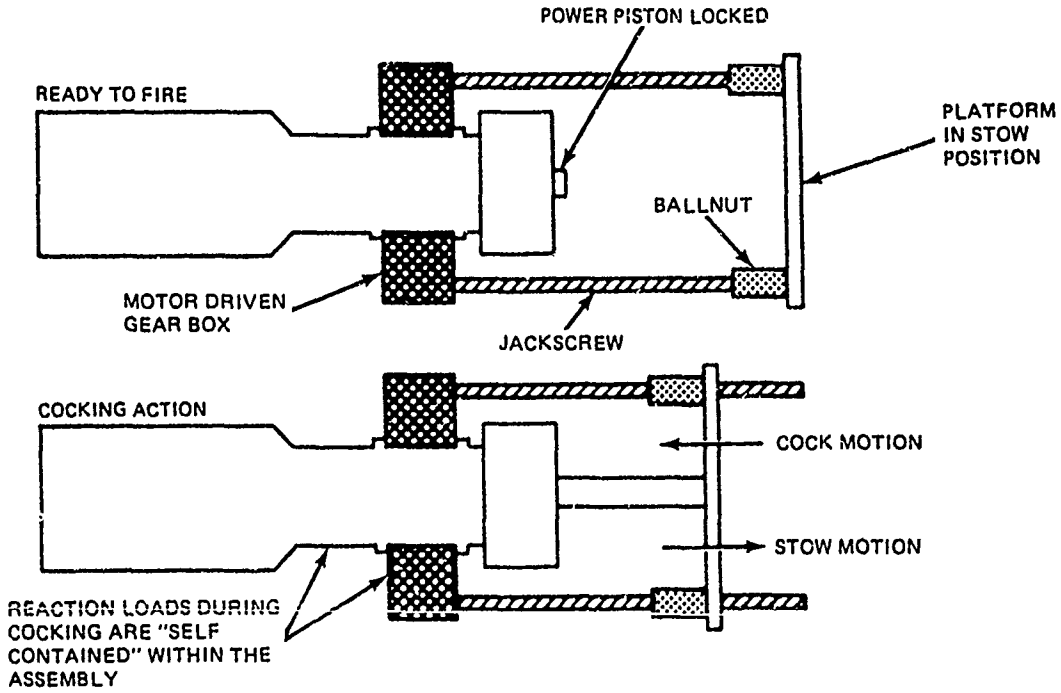

Figure 5. Cocking Mechanism Operation for Power Module

- The lock mechanism is lubricated by the hydraulic fluid to prevent wear.

- The release solenoid is unique in that its coil is stationary to the ACER structure while its plunger and stop move with the power piston (once the lock is released) so that the coil supply wiring does not have to "shoot" back and forth with the piston.

- Except during flight with a store, the ACER nitrogen charge can be kept at 3000 psi to minimize possible leakage.

As the power module design progressed, it was evident that the most critical component was the lock itself. EDO therefore looked for an existing, proven lock that could meet this criteria and teamed with Dowty Decoto, Inc. (Yakima, WA). Dowty provided a scaled down version of their hold-back-bar lock for carrier launches of F-14/-18 aircraft. This lock is incorporated into the power module and provides a proven mechanism capable of retaining the piston which releasing with a solenoid force of only 50 to 60 lbs.

A second important component of the power module is the release solenoid. Here, a concept initiated by EDO was refined and developed by Sterer Engineering and Manufacturing Co. (Los Angeles, CA). The design eliminated the problem of supplying power to a solenoid whose coil would travel at the same end-of-stroke velocity as the ejected store if it were attached to the power piston. The design provides a standard solenoid plunger and stop which are directly attached to the power piston. The plunger is attached to a pull rod that releases the lock (see Figure 4).

When the power module is cocked (locked), the coil (mounted to the power module housing) surrounds its plunger/stop. The coil is powered by an electrical pulse. This action causes the plunger to move and release the lock via the pull rod it is attached to. The lock cannot reset once the power piston has moved only a few hundredths of an inch. Thus, the lock can not relock when the plunger moves out of the coil's magnetic field and loses force.

The final difficult design problem (volume and weight limitations were at a premium) for the power module was the cocking mechanism which is required to operate against high loads as the power module piston is locked. Again, looking for existing, proven mechanisms that could be repackaged to meet the ACER requirements, Aircraft Control Division of Eaton Corp. (Denville, NJ) was selected because of their expertise in electromechanical actuators for military and commercial aircraft.

Aircraft Control's design also provided positive secondary benefits. First, the power module piston housing passes through a hole in the gear box so that the two can be clamped together during assembly. This permits all loads to be reacted within the two structures so that only light fasteners are needed to hold the assembly in the aircraft. Second, by disconnecting only one hydraulic connection (fluid tube from power module to ejector rack), the power module is isolated and removed from the carriage and release mechanism.

Figure 6 shows the completed ACER as delivered to the Air Force. Its associated control console for remote operation is also shown.

As illustrated by Figure 2, the ACER is a closed hydraulic system in that as hydraulic fluid is added all air is evacuated. Thus, once the ACER is charged with hydraulic oil, the extension of any one piston must be compensated for by the retraction of another piston. For example, consider the following scenario (which describes a routine ejection and recocking):

- The power module is cocked, both ejectors are fully retracted, and the diverter chamber holds a small amount of fluid for temperature compensation. Note that the diverter chamber valve is in an orificed position. This provides sufficient flow for slowly expanding/contracting fluid due to temperature changes.

- The ACER is fired and a solenoid releases the mechanical latch that holds the power module piston against the nitrogen gas charge.

- The power module pumps hydraulic fluid into the ejection system. Since the diverter chamber valve is in an orificed position (.040 inch flow diameter), it chokes fluid flow and all fluid flows into the ejection system to release the suspension hooks and eject the store.

- When both ejectors reach the end of their stroke, there is still a small amount of fluid in the power module. This fluid acts as a "shock absorber" to slowly bring the power module piston against its stop. This is because the remaining fluid in the power module must be forced through the small orifice diverter valve into the diverter chamber.

- Immediately after store ejection, the power module has pumped all fluid into the ACER ejection system and its piston, the hook release piston and both ejector pistons are fully extended and against their respective stops.

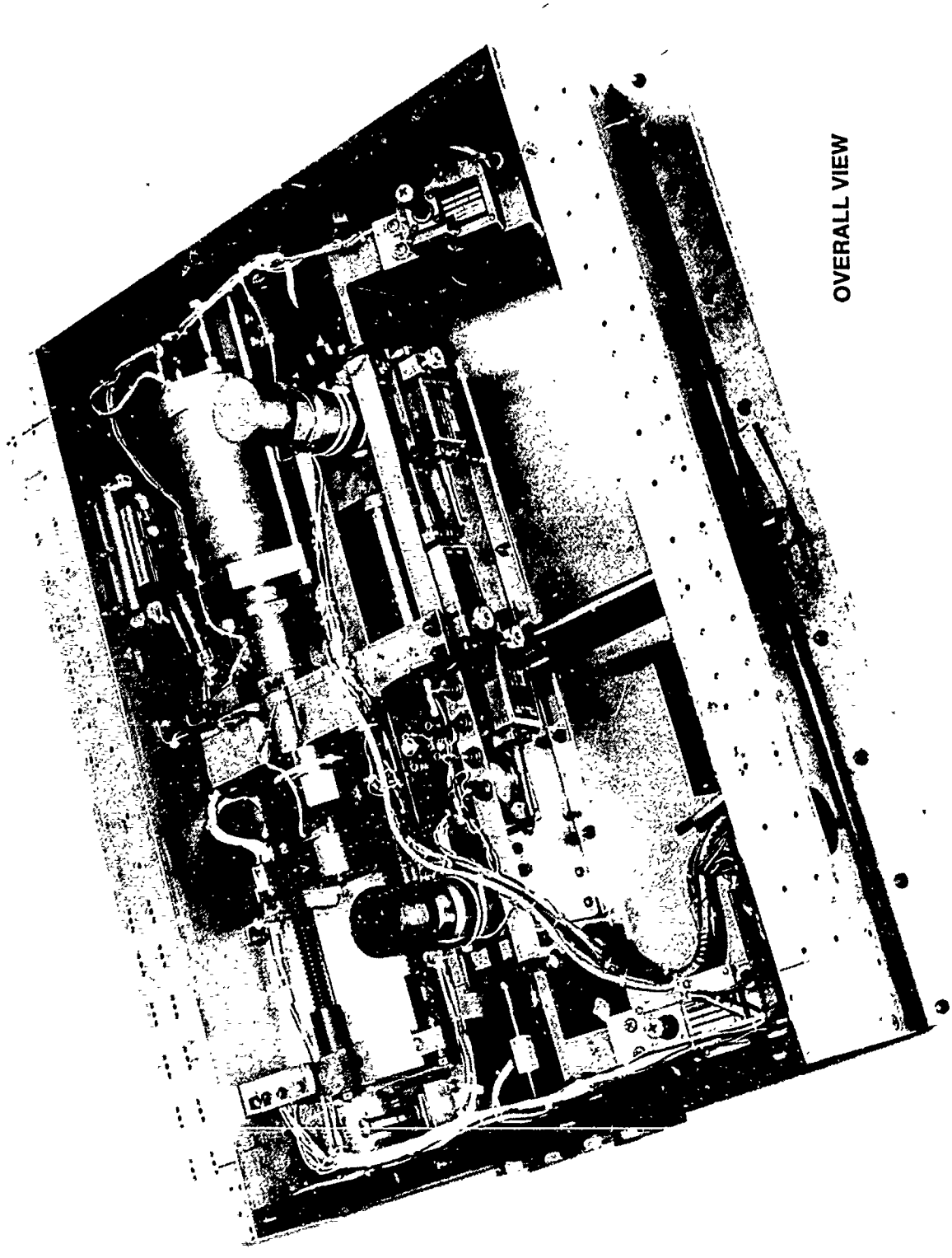

OVERALL VIEW

Figure 6. ACER and Remote Control Panel (Sheet 1 of 2)

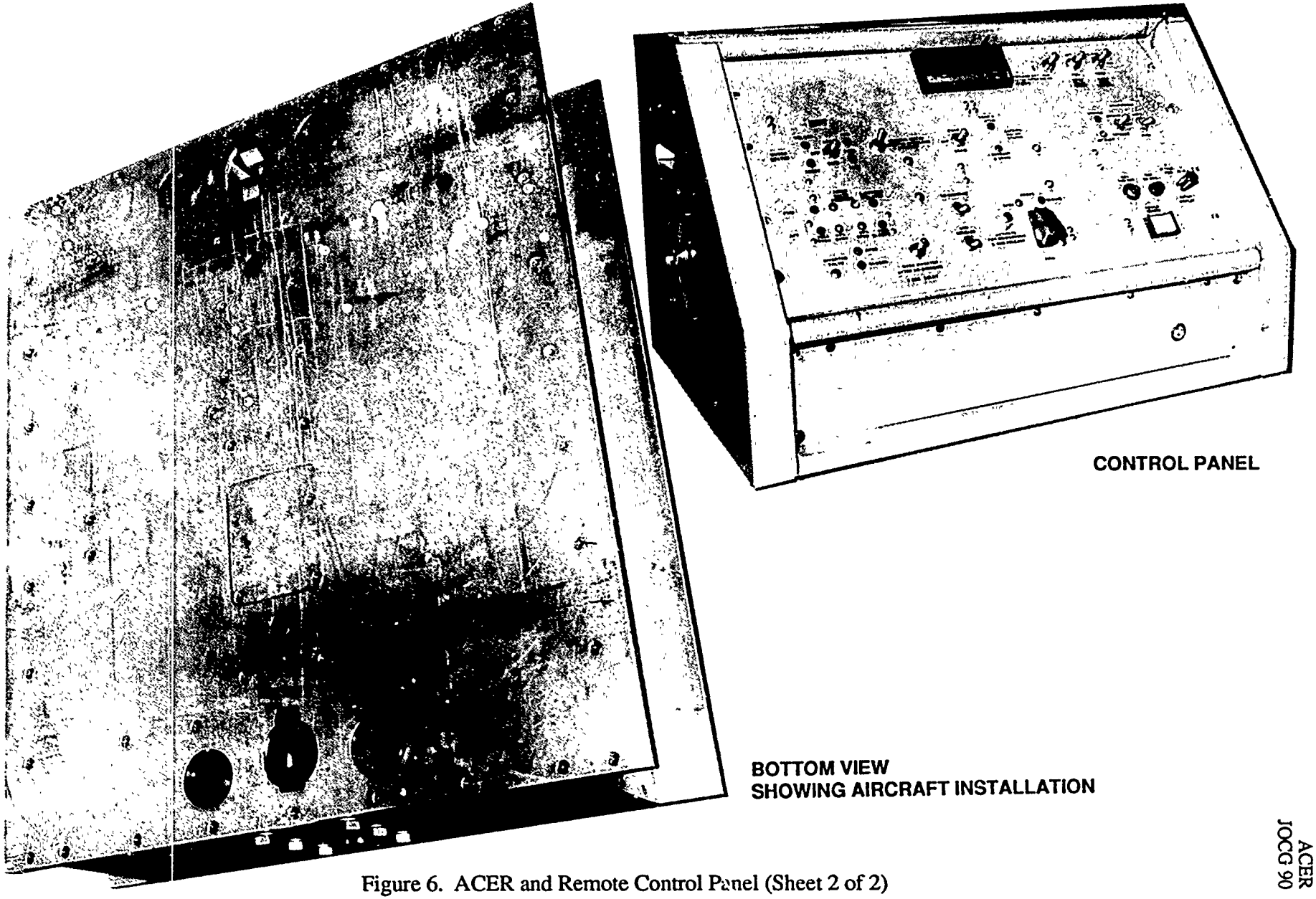

Figure 6. ACER and Remote Control Panel (Sheet 2 of 2)

- At this point, the motor controlling the diverter valve automatically opens the diverter valve to permit free fluid flow. This enables springs to retract the hook release and ejector pistons by "pumping" fluid into the diverter chamber. All fluid that was in the power module before store ejection is now in the diverter chamber.

- The ACER is recocked for the next ejection by turning on the cocking motor. This pushes the power module piston off its stop to compress the 3000 psi nitrogen gas to 4000 psi when the piston is again captured by its mechanical lock. As the piston is being recocked, atmospheric pressure drives fluid from the diverter chambers into the power module (a vacuum cannot be created). When the power module piston is cocked (recaptured by its mechanical lock), the diverter valve is automatically positioned in the orificed position by its motor. The ACER is now ready for the next ejection when the cocking motor returns to the stowed position.

TEST RESULTS

The ACER, as delivered to the Air Force, provided the performance shown in Table 1. A typical ejection trace for a 1000 lb store is shown in Figure 7.

Table 1. ACER Performance

Store Wt (lbs)	Firing Temperature (°F)	EOS Velocity (ft/sec)
500	Room	18.5
1000	Room	14.5
1000	–5	12.9
1000	+120	15.2
2000	Room	11.5
NOTE: Total peak reaction load for a room temperature ejection was 17,000 lbs.		

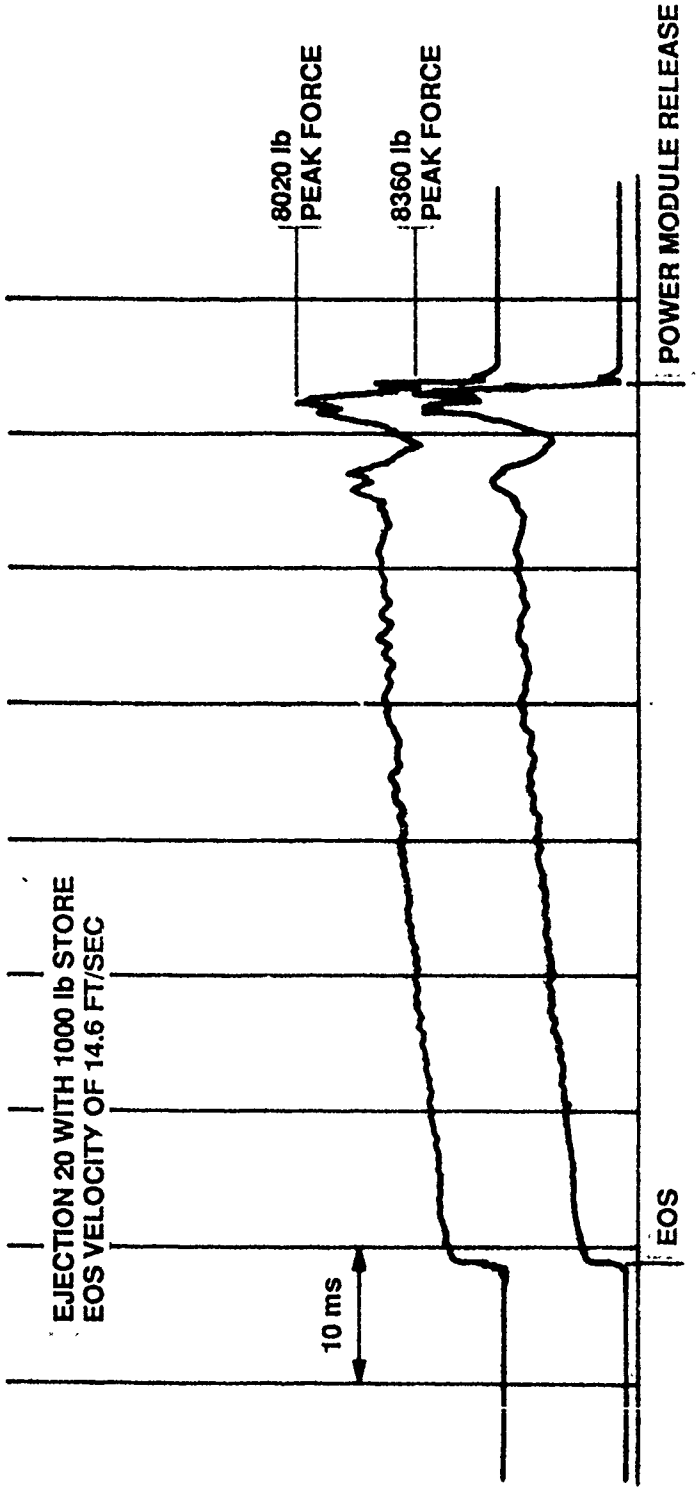

Figure 7. Typical ACER Ejection Trace

The overall test program for the ACER consisted of performance/operational tests (at room, high, and low temperature), structural load tests and vibration tests. The ACER completed each of these tests with the following results:

- A 129 room temperature ejections were performed over a 38 day period. There was no difference in performance between the first and last ejection. This met the Air Force requirements of 100 ejections over a 30 day period with no degradation in performance nor any scheduled maintenance. Note that the ACER was originally required to eject a 1000 lb store at 20 ft/sec. However, due to the surge damper described under "lessons learned," the performance was decreased to the Table 1 values.

- The ACER successfully demonstrated all specified remote operational requirements.

- The ACER was required to eject stores from –65°F to +200°F. Testing showed the actual range to be from about –5°F to +120°F. This is further discussed under "lessons learned."

- The ACER successfully completed all specified structural load tests.

- The ACER successfully completed the specified MIL-T-7743E random vibration test.

The ACER, after completion of testing, was overhauled and delivered to the Air Force. It is certified for Safety-of-Flight testing and has been fitted to a specially designed F-111 bomb bay pallet. This will permit simulated conformal carriage flights to be conducted with the ACER.

LESSONS LEARNED

Many interesting problems were discovered and overcome before the ACER was tested and delivered to the Air Force. Additionally, some important observations were also made that may be of assistance to future designers of similar mechanisms. Discussion of the various conditions follows:

- Linkage Snubbers – The hydraulic pressure in the ACER system rises very quickly once the power module is released, as shown in Figure 7. The rate of rise is even faster than that of impulse cartridges. As a result, the mechanical linkage stops normally used in hot

gas ejector racks would not arrest the ACER hook release linkages without damage. A 180 ft-lb capacity hydraulic shock absorber had to be used to safely snub each hook linkage set. Because the shock absorbers were reset with an integral spring, they performed double duty by also resetting the hook sears and release linkages when a store was loaded.

- Surge Damper – Initial store release tests with the ACER revealed a disturbing fact. When the power module released, its locked piston "smacked" into the static hydraulic fluid causing a significant hammer shock effect, as shown in Figure 8.

  It was clear that the hammer shock effect (which always caused about 2 1/2 times the theoretical force output) had to be reduced or eliminated to meet stated ejection peak force requirements. Hydraulic accumulators were added to the power module to reduce the hammer shock pressure peak. Both bladder and piston type accumulators were tested. Both types reduced the hammer shock peak to between 1 1/2 to 2 times the theoretical. However, the bladder type would not always return all fluid back to the system, and finally ruptured dumping its nitrogen charge into the closed ACER hydraulic system. The piston type accumulator did not fail, but because of the bladder type's failure it was recognized that any nitrogen leakage from an accumulator into the ACER would cause a safety problem. The safety problem being that enough pressure may be inadvertently built up to release the store suspension hooks. Thus, accumulators were abandoned as a method of damping the pressure spike.

  One possibility remaining was to place some type of "orifice" or mechanical surge damper between the power module and the ACER ejection system. The only place to package this mechanism was in the hydraulic supply tube between the power module and ejection system. Sterer Engineering was contacted and proposed a mechanism based on a design they had previously manufactured. The method of operation is as follows:

  (a) The initial pressure spike from the power module must force open a sliding valve controlled by a flow limiting orifice. The orifice is sized to open the valve after the pressure spike has naturally damped in the power module.

  (b) Flow from the ejection system (diverter chambers) is not controlled in that free flow is permitted for proper cocking of the power module.

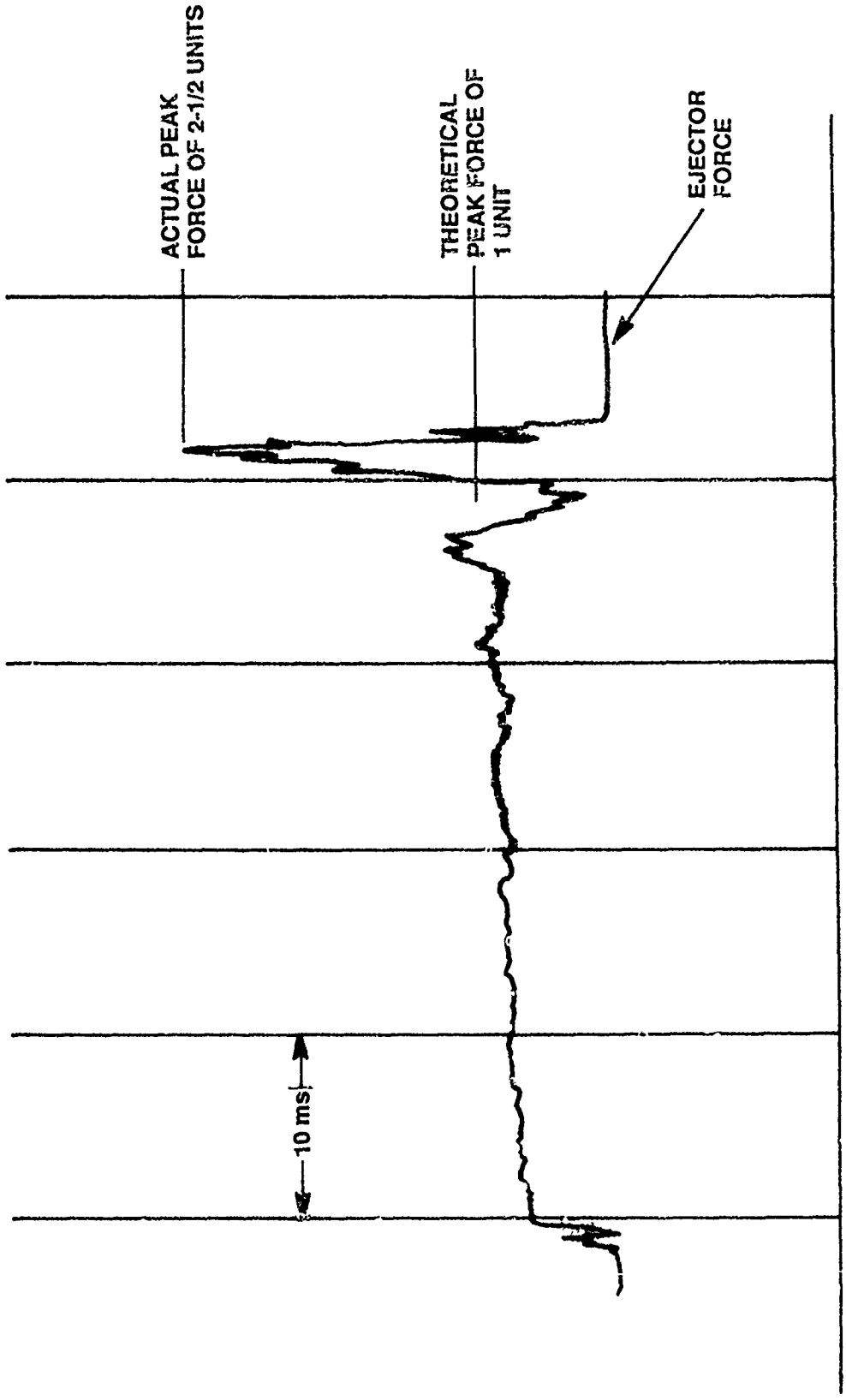

Figure 8. Hammer Shock Effect

The surge damper had to be packaged in the limited volume of the supply tube. As such, the flow rate the supply tube was originally designed for was compromised. As shown in Figure 9, the damper worked as advertised, but did not permit full flow into the ACER's ejection system. Rework (orifice sizing and sliding valve body diameter changes) to the damper improved the performance, but it was still not considered sufficient. The damper was then modified and the ACER performance was considerably improved as shown in Figure 10. The modified damper provided acceptable ACER performance (at a 4000 psi cocked power module nitrogen charge) while limiting the hammer shock spike to 1-1/2 times the theoretical force. The modified surge damper is incorporated into the ACER. Note that if the surge damper had been designed into the ACER from the beginning of the program, sufficient space for a higher flow mechanism could have been provided that would have completely damped the hammer shock effect.

- Power Module Piston – The most serious problem discovered during testing of the ACER dealt with "air" entering the power module hydraulic fluid. This happened twice and caused severe damage to the ACER each time because the released power module piston would do no work (it would simply compress very low pressure air) and would strike its stop at a very high velocity. Many reasons were hypothesized for this a problem such as:

  (a) Air leaking through hydraulic seals during ejection or cocking.

  (b) Accidentally cocking the ACER with the diverter valve "closed" (this caused an electrical interlock that prevents cocking motor operation with a closed diverter valve to be added to the ACER).

  (c) A faulty power module nitrogen gas seal and a plugged vent to atmosphere between it and the power module hydraulic seal (see Figure 4).

  (d) Minute cracks in the power module piston between the nitrogen gas/hydraulic fluid interface.

  (e) The diverter pistons jamming as the ACER is cocked so that air is drawn past their unenergized hydraulic seals.

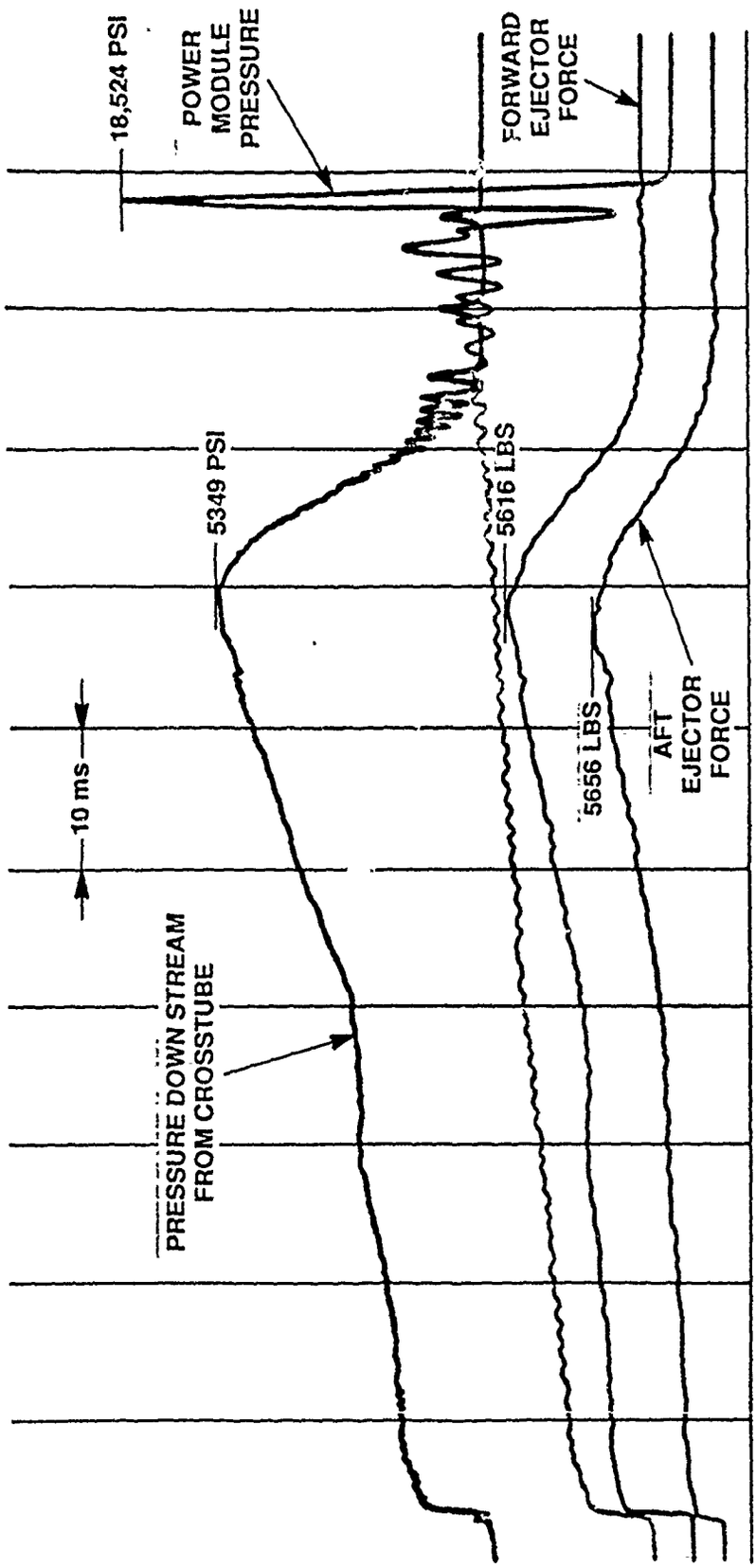

Figure 9. Surge Damper Performance

29-17

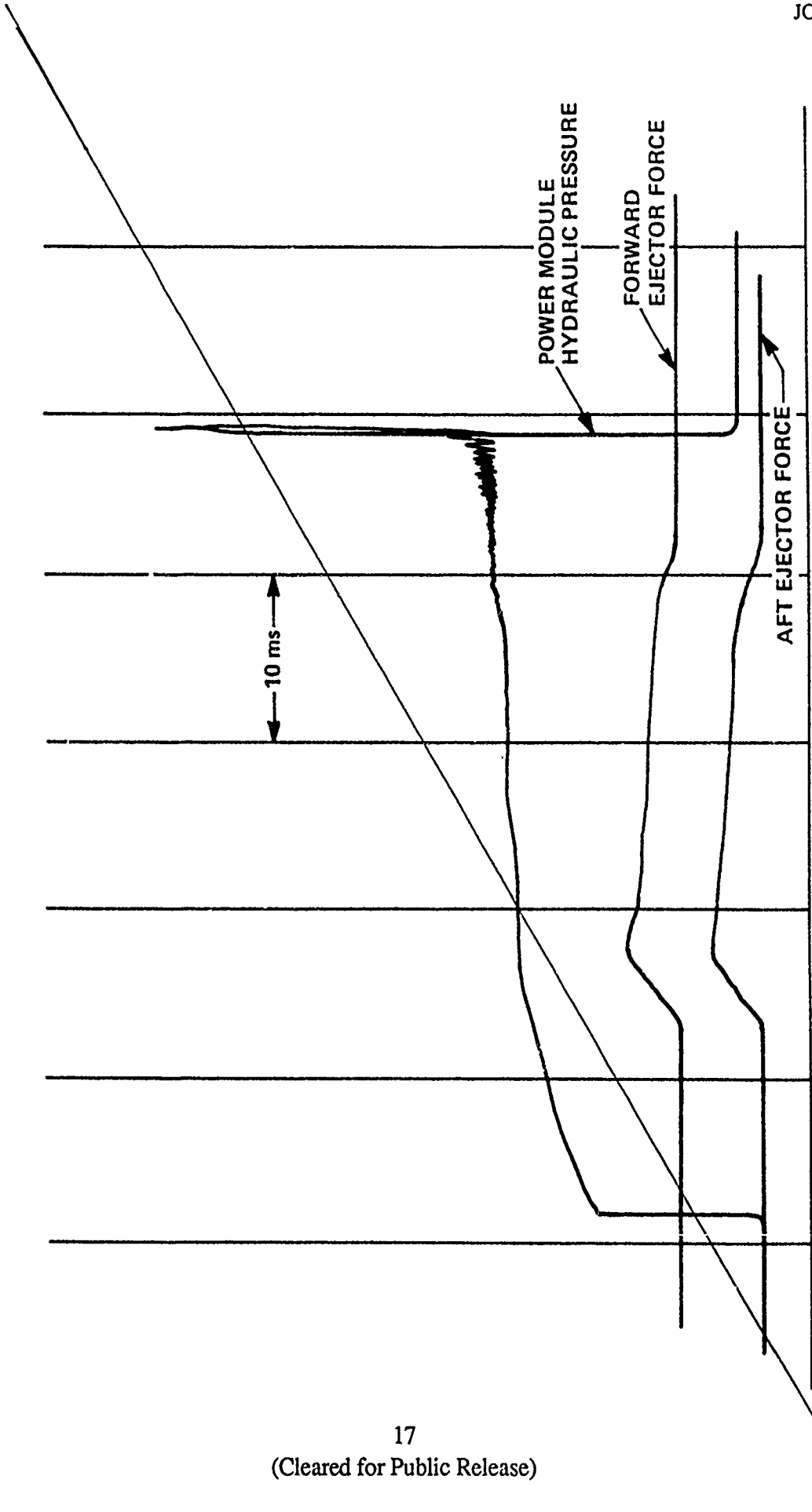

Figure 9. Surge Damper Performance

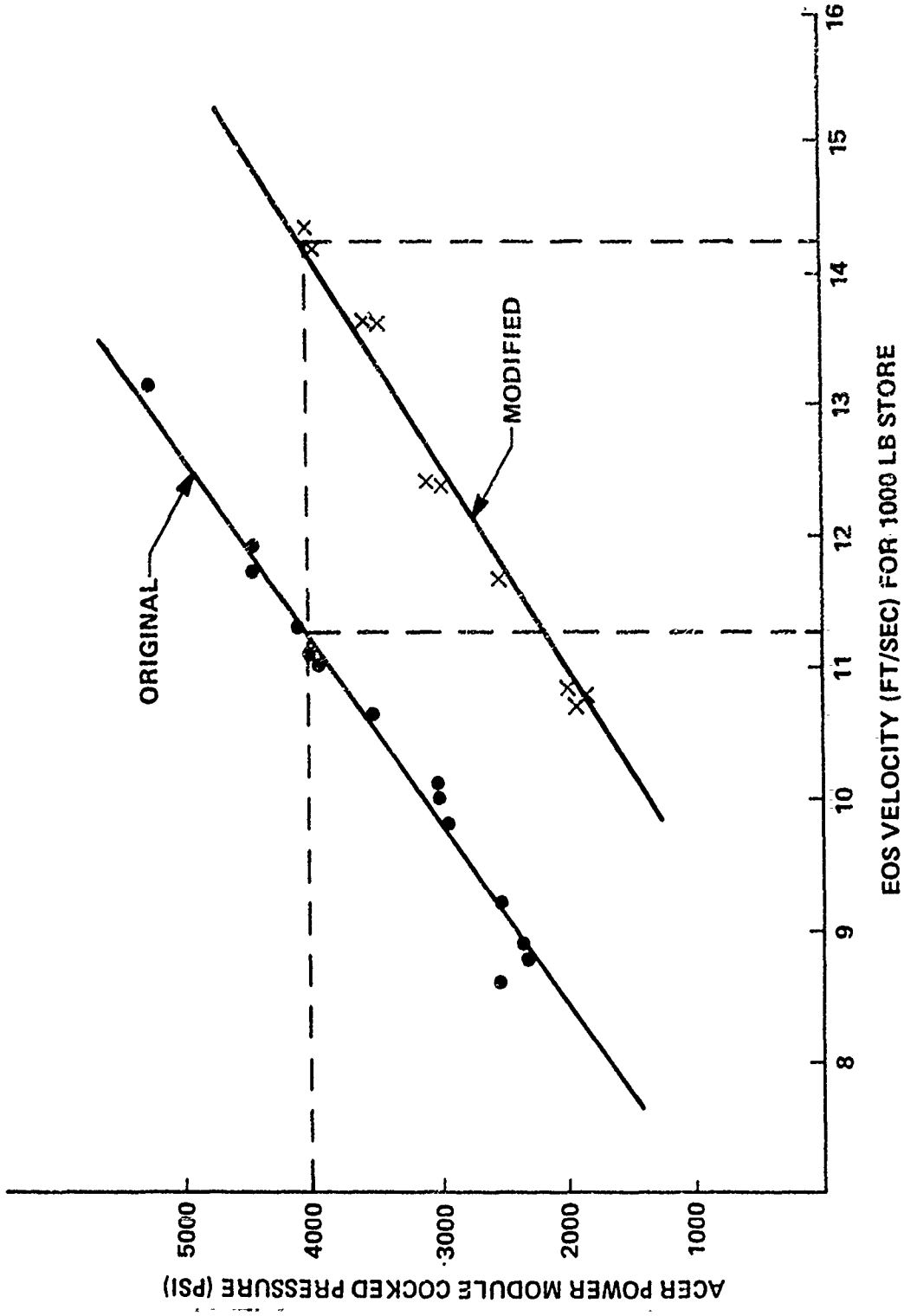

Figure 10. Modified Surge Damper Performance

All of these possible reasons were investigated, with a new power module piston even being manufactured and tested in the ACER. Eventually, all were eliminated as the source of the problem.

The original power module piston was sent to a metallurgical laboratory for radiography and destructive testing in an attempt to determine an unusual leakage path. It was examined for hydrogen embrittlement, fatigue and/or quench cracks. No definite anomalies could be determined.

However, during the course of the investigation, one of the metallurgical tests required sectioning and etching of the piston to look for cracks in the base material. The photographs of the sectioned piston clearly showed the chrome the piston had been plated with to reduce wear. Although the chrome was of uniform thickness and properly bonded to the piston, it was somewhat porous in nature (not at all unusual for hard chrome plating). It was at this time that the possibility of very small amounts of nitrogen gas traveling under the chrome plating (by passing the seals and vented annulus) into the hydraulic fluid was proposed, as shown in Figure 11.

An exhaustive study was conducted which showed this to be the case. Note, that even though very small amounts of gas were leaking, once a bubble of very low pressure nitrogen entered the ACER's hydraulic charge the hydraulic fluid would not properly be "sucked back" into the power module during cocking. This caused the released power module piston to rapidly accelerate into the nitrogen bubble and damage the mechanism. Once the chrome plating was established as the reason for "air entering the ACER fluid charge", a new power module piston was manufactured with its surface hardened by nitriding, and the "air" problem was completely eliminated.

- Power Module Lock – The power module piston lock is a key to the entire concept. During the course of testing, it became evident that small amounts of wear and/or galling to the lock segments and lock retainers increased the force needed to release the power module. While the absolute value of the increase was small (an increase from 50 lbs to about 75 lbs of lock release force was needed to release the 11,200 lb power module load), problems were caused because the release solenoid was already designed and fixed at a maximum of 60 lbs of release force.

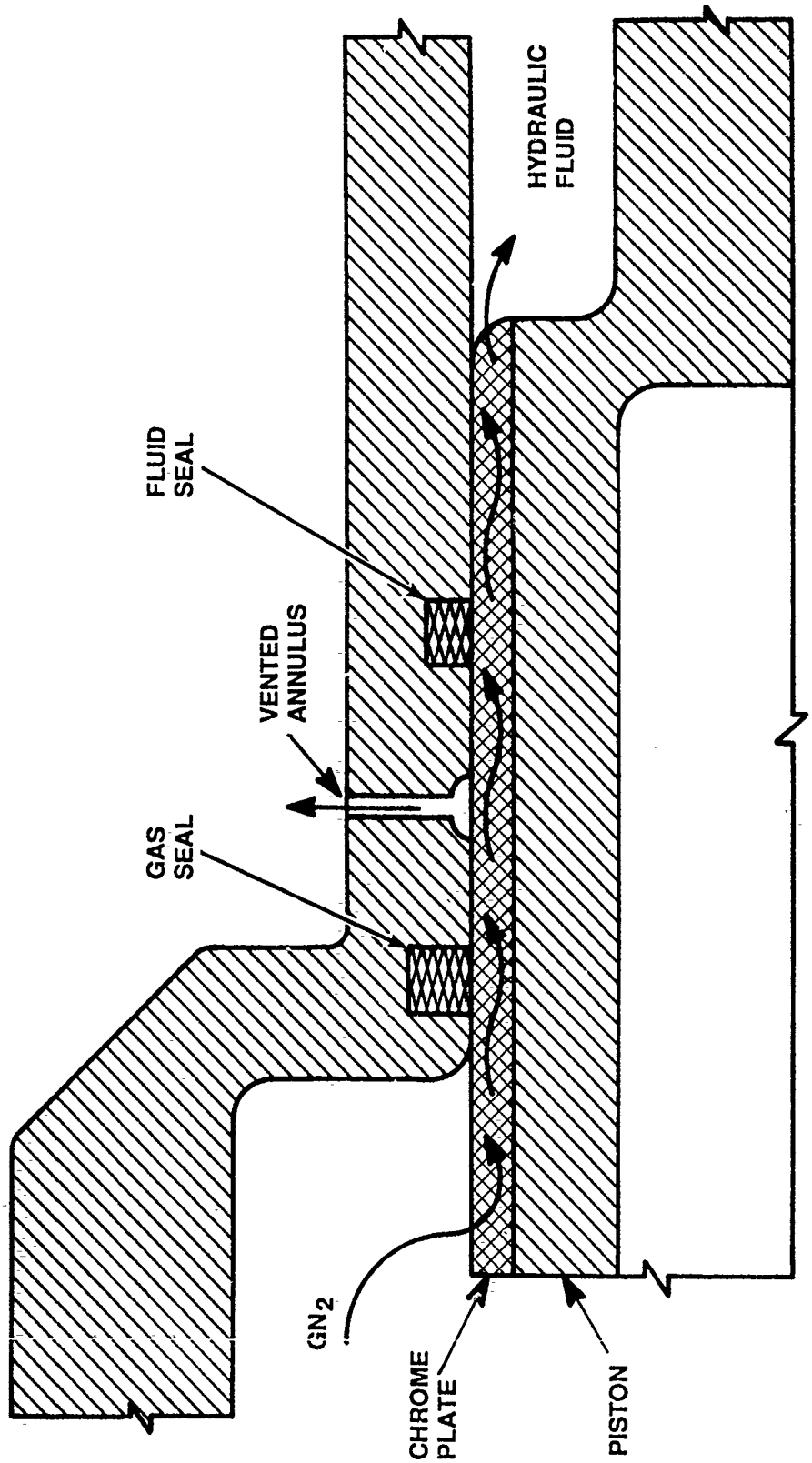

Figure 11. Nitrogen Gas Path through Chrome Plate

Several changes to the two-stage lock mechanism were made, such as changing lock segment release angles and reducing the reset spring forces. These changes helped, however, the minor and expected wear to the lock segments continued to cause minor difficulties.

Finally, the lock segments were changed to beryllium-copper alloy so that less wear and galling would occur between them and the hard steel surfaces they operated against. This change eliminated the lock problems.

- Hydraulic Seals – No problems were encountered with the ACER's hydraulic seals. Impulse pressures up to 18,000 psi were satisfactorily sealed during the course of the program. Shamban "Plus Seal II" and Green-Tweed "T-Seal" were used. Both types had teflon back-up rings on each side.

- Swaybraces – The ACER swaybraces are motor driven and automatically swaybrace the store. Each motor turns off at a specified preload value. During vibration testing, the motors were left in the "on" or "engage" position. This caused the swaybraces to continually tighten as the store vibrated, making manual release almost impossible due to the high store preload. Although it should have been initially recognized, it is apparent that motorized swaybracing systems should be "shut-down" once they properly engage and swaybrace. This will prevent vibrational and/or inertial store movements from causing additional and unwanted swaybrace preload.

- Temperature – As previously stated, the ACER would not function over the required –65°F to +200°F temperature range. These problems occurred because either the power module would not unlock once cocked or the power module lock would not reset once released (this happened only at high temperatures).

  Investigation of the problem indicated that the release solenoid was simply not providing sufficient force to unlock the power module. This was most likely due to expansion/contraction of the various lock parts which caused minor binding and a corresponding slight increase in release force. Further, in the case of low temperature testing, considerable condensation in the temperature box may have exacerbated the problem by forming ice around the solenoid pull-rod to the lock release mechanism.

The solenoid used to release the ACER is already large and heavy. To continue to increase its size to provide more lock release force would not be productive. The only solution for positive release of the power module is to use the aircraft hydraulic pressure. While this would violate the ACER program requirement that only aircraft electrical power was available for ACER operation, at least the high (100 to 200 lbs) force needed to insure lock release would be readily available.

- Weight – The completed ACER weighed 168 lbs against a goal of 120 lbs. Some of the excess weight resulted because funding and time constraints did not allow for an optimium weight design. However, even if the 120 lbs weight goal had been met, the ACER would still be heavy and would penalize any host aircraft.

  An important reason for the ACER's high weight was that a key program requirement was that only aircraft electrical power could be used for ACER operation. This necessitated the use of solenoids and electrical motors for all functions. For example, the ACER power module weighs 50 lbs, with almost half of the weight consisting of the cocking motor and release solenoid. This weight could be reduced to less than 30 lbs if aircraft hydraulic pressure could be used to cock and then release the ACER.

  Further by truly integrating the ACER ejector mechanisms into an aircraft's structure, the weight could be further reduced. For example, the two ACER structural fittings weighed 19 lbs each. If they could be replaced by aircraft frames to support the ACERs hooks, swaybraces and ejectors, significant weight reduction is again possible.

CONCLUSIONS AND RECOMMENDATIONS

The ACER program proved there are viable concepts that can replace impulse cartridges as C&R mechanism energy sources. While none of these concepts can compete with the weight to power ratio of impulse cartridges, careful design to integrate ACER type components into existing aircraft structure could provide a self-recharging, remotely controlled C&R mechanism that weighs less than 100 lbs.

The key to reducing weight is to permit the suspension equipment designer to use both electrical and hydraulic power from the aircraft. This would allow the best weight to power trade-offs to be made for all design aspects. Recall that the ACER program specified only the use of aircraft electrical power. While this seemed appropriate at the time, efforts to date suggest the changes shown in Table 2 for the next generation ACER.

Table 2. Suggested ACER Design Changes

ACER Component	Present Design	Future Design
Power Module	Nitrogen Charged, Electrically Cocked (motor), Electrically Released (solenoid)	Nitrogen Charged, Hydraulically Cocked, Hydraulically Released
Reversible Inflight Lock	Electrically Driven by Linear Actuator	No Change
Pitch/Diverter Valves	Electrically Driven by Linear Actuator	No Change
Ejector Piston Preload	Electrically Released (solenoid) Compression Spring	Hydraulic Pressure
Ejector Piston Retraction	Spring Retur .ed	Hydraulic Pressure
Structure	Self Contained	Make Maximum Use of Aircraft Frames and Structure

ABOUT THE AUTHOR

Mr. Lynn D. Seal is the Manager for Advanced Aircraft Systems at EDO Corporation. He received his B.S. in Metallurgy from Case Institute of Technology in 1965.

As a Captain in the USAF, he gained intimate familiarity with aircraft maintenance and flight line operation as a C-130E maintenance officer during the Vietnam era. He joined EDO in 1979 with 10 years of previous armament experience. Some of his key programs were introducing PH13-8Mo to the U.S. Navy as a low maintenance ERU hook material, and various design efforts on the Tornado/F-15 ejector racks and the YF-22 AMRAAM eject launcher.

MBB
Deutsche Aerospace

Rail Launched Missile/Launcher Interface for Aircraft

by

Stephan Lösch
Military Aircraft Division
Messerschmitt-Bölkow-Blohm GmbH
Munich, West-Germany

Foreword

Data and facts given in the presentation hereafter were evaluated with the aim to extract requirements for an equipment specification which is dedicated to a modern fighter aircraft. However the intention is to avoid a special to type equipment and to ensure adaptability to further aircraft with minimized modifications. This was considered as a principal task of an aircraft developer and producer in view of the equipment to be specified and lateron delivered by a supplier and purchased as performant system to the customer.

Background

The requirement for standardization in aircraft armament is getting more and more important under the conditions of decreasing budgets but steady increasing requirements to the aircraft weapons systems. It is now to find a concept which allows a broad use of newly developed equipment. In the special case of air to air missile launcher the provision must

be for cross use with various missiles and carriers within the NATO countries. Fulfilment of this aspect is the dominating requirement to get international customers acceptance for new development of air to air role equipment.

The interface of a rail launched missile to its carrier is the most important feature to achieve mechanical integration into the aircraft. It comprises first the load carrying mechanical components like hangers, their location and geometry and secondly the electromechanical requirements: location, dimension and operation of the connectors. Further it is recommended to look upon the interface aircraft/launcher in terms of form, fit and function. The last step is the full integration of the aircraft weapon system. This is expressed in NATO requirements for an Advanced Rail Launcher:

- Level 1 Launcher/Missile
- Level 2 Aircraft/Launcher
- Level 2 Aircraft weapon system integration

The way forward to a feasible concept does not end with defining requirement but subsequently has to analyze the available status in respect to missiles and aircraft and the related planning for future weapons. The presentation will therefore analyze the most important current and future air to air missiles used within NATO. Due to the complexity this presentation is limited to aspects related to level 1 and 2 of NATO-ADVANCED RAIL LAUNCHER requirements.

Analysis of air to air missile mechanical interface

Missiles interfere with the launcher by hangers, buttons, fin retainers, snubbers and not at least by the electrical connectors. The connectors may be of shear wafer type or operated by an umbilical retract mechanism. Missiles with a digital interface generally require umbilical retract actuating. Fig.1 gives key data of the weapons which are candidates for the later proposed rail concept.

These weapons represent medium range and short range missiles; currently developed or in service use. Missiles are now analyzed concerning the mechanical interface which a launcher rail concept has to accomplish.

This first analysis (Fig. 2) indicates fundamental differences in missile attachment philosophy. Aspide, Sky Flash and Sparrow are attached via two hangers, a button and a C-shaped hanger. Short range missiles and the AMRAAM are fixed via three hangers. Sidewinder and ASRAAM use three T-shaped hangers, whilst the AMRAAM centre attachment is a C-shaped hanger.

The differences in respect to electrical connectors are obvious. There are digital and analogue interfaces to be applied with; connections which require umbilical retract or which simply shear the connector off. AMRAAM, ASRAAM and MICA require an umbilical retract mechanism due to their digital interface. The bus wiring is too resistant to be sheared off. All the other missiles dispose over an electrical interface which has to be cut off during launch. Thereby induced shear off forces are not negligible. As a next step (Fig. 3) it is now to evaluate the position and the cross section of the hangers on the missile to assess the geometrical compatibility with the rail defined by STANAG 3842 and the proposed rail geometry.

Longitudinal position of hangers and connectors show the possibility of a common rail concept because buttons and hangers have in first order the same distance. This fact offers the possibility to operate the missiles via identical detent mechanisms.

ARLA launcher requires the missile to be kept on the launcher in case of an inadvertent firing. In the light of this requirement for the ARLA-Launcher the medium range missiles with only a forward button should be restrained via the C-hanger, due to expected strength limits of the button if the missile thrust is applied. This lead to the conclusion to

go for two detent mechanisms: Medium weight missiles shall be restrained longitudinally via their centre C-hanger the short range missiles via their forward T-hanger or button.

Electrical connector locations present a complex integration task due to the different locations of Aspide, Sky Flash and Sparrow motor fire connectors. However this task is considered feasible for a launcher supplier because the motor fire connectors are small and of shear wafer type; no electrical umbilical actuation mechanism is required. The connectors for AMRAAM, ASRAAM or AIM-9 are already covered by STANAG 3842. Provision for cooling air supply is via the AIM-9 umbilical at missile nose section.

Examination of cross sectional condition displays a foul to harmonize the geometrical requirements of STANAG 3842 and the body of Aspide, Sky Flash and Sparrow. These missiles interfere with the rail defined in the standard. It is not possible to operate Aspide, Sky Flash or Sparrow from a rail shaped according to STANAG 3842 definition for class A. The rail beam would penetrate into Aspide, Sparrow and Sky Flash missile body (Fig. 4).

Advanced rail concept

A rail concept must now be established to combine the requirements of most of previously mentioned missile types. Launcher bottom structure must be designed to react the loads during carriage and release, provide sufficient guidance for the moving missile and serve other facilities like connectors, attachments, detents, snubbers,... .

A way ahead is to modify the cross sectional shape of the rail. Fig. 5 indicates necessary reshaping to cope for the missiles subject of this analysis.

After detailed evaluation of the requirements of a high performance fighter aircraft currently developed a rail concept had been devised. The current status of which is shown in figure 6. In the carriage position all hangers are engaged and thus no limitation of flight envelope due to the rail geometry occurs. The moving missile is sequentially disengaged. AIM-9 suspension is as on current Sidewinder launchers: FWD - CTR - AFT hangers leave the rail serially. AMRAAM first disengages the FWD hanger. Second the AFT attachment leaves the rail. AFT hanger is further guided

upwards and sidewards. CTR hanger detaches as last contact point to the launcher. Aspide, Sky Flash and Sparrow which dispose of two hangers only disengage successively, first button and then C-hanger which is the maximum achievable guidance for this type of missile.

This new concept now caters for all missiles subject of the analysis in terms of mechanical and kinematic compatibility. It is now to cover the aspect of safe separation and to introduce it into the relevant standards.

STANAG 3842

Purpose of STANAG 3842 is to standardize the mechanical interface between rail launched missiles and launchers. The agreement covers four missile mass classes of which primarily class A and B are of interest (Fig. 7).

The French MICA missile should be allocated to missile mass class A but is intentionally not mentioned in the table because the hanger geometry cannot be fully harmonized with the requirements laid down in the standardization agreement.

Rail geometry of mass class B missiles is not defined. This may be due to the fact that most of these missiles were already in service when the standard was established. It is however of great importance to consider these missiles in conjunction with class A missiles just because of similar operational dedication. AMRAAM as well as Aspide, Sky Flash and Sparrow are medium range missiles. The latter three are likely to be upgraded and to remain in service for the next decade. Current procurement plans call for the US Air Forces and the US Navy to be equipped with more than 17000 AIM-7 missiles. Further the latest version of (AIM-7P) is still under development. Sky Flash is in operational use in the UK and the intention is emphasized to develop an advanced version within an international collaboration. Aspide is in final development stage and one of the candidates for the inventory of air to air missiles for the Italian Air Force.

It is thus not appropriate to only concentrate on the class A missiles and to dedicate rail launchers and associated concept only to AIM-9, AIM-120 and ASRAAM. These are obviously performant representatives of air to

air missiles. However with the exception of AIM-9 type missiles they are not yet fully developed and international procurement intention is still pending.

Above explained technical solution to combine both missile classes must now been seen in combination with the available status of the standard. The basic contradiction appears quite evidently that the requirements in the STANAG 3842 if so remaining, prevent the solution due to very strict limitation on rail geometry for class A missiles. Class B missiles cannot be carried or fired from launcher which only comply to STANAG 3842 rail requirements. It is therefore proposed to the relevant NATO-Military Agency for Standardization (MAS) to envisage an enhanced edition of the STANAG 3842 which should respect the combined requirements of class A + B missiles

We attempt to approach this working group with a proposal in terms of new standardized rail geometry which caters for the above mentioned missile types and which kinematically will resemble to the approach above.

Safe separation requirements

The proposed rail concept does not change the mechanical guidance restrictions for the short range missiles during carriage and release. The carriage interaction points are not affected by the new rail concept; all hangers are engaged in carriage position and thus no limitation of flight envelope due to the new rail concept must be expected. The only difference occurs in the mechanical release guidance for the AMRAAM. Its third aft T-hanger which will not be guided until the leading edge of the launcher. It appears that the aft T-hanger is only present due to the need of carriage load reaction to the launcher. The other medium range missiles, Aspide, Sparrow and Sky Flash do not dispose of a rear hanger, which implies the conclusion that it is not required for safe separation from rail launchers; the mechanical release guidance is thus not affected by the new rail concept.

Safe separation analysis is a task to be carried out separately for each aircraft type. It cannot be concluded therefore that safe separation is guarantied by a standardized rail concept. Even a rail compliant with STANAG 3842 as it currently stands, does not guarantee safe separation over all aircraft types. It is however

of great interest to get indication of the safe separation behaviour of particular type of aircraft to support the new rail concept. MBB carried out investigations on a high performance delta wing fighter aircraft type for AMRAAM release under different extremes of the flight envelope. The result can only be shown by its tendency due to security restrictions. Two critical cases out of the various examples are shown below:

AMRAAM	high 'g'	no adjacent stores
AMRAAM	low 'g'	adjacent stores

Both cases established safe separation behaviour within the missile limits when the new rail concept is used. The station is considered critical concerning safe separation behaviour at the outer wing with adjacent stores in the next proximity. It is intentionally used for the analysis because a positive result at this wing station provides good indication for safe separation from other wing stations. Fig's. 8 and 9 show the separation trajectory for above mentioned cases. Analysis took care of all kinematic parameters, and missile safe separation was demonstrated.

Concluding we cannot detect any disadvantage in terms of safe separation for this type of aircraft when the new rail concept is used. Similar positive results were evaluated on the wing station of a wing sweep fighter aircraft.

Interoperability and cross servicing

The current rail definition of STANAG 3842 will prevent suppliers for a rail launcher for modern fighter aircraft to offer a rail concept common for class A+B missiles. The consequence would be the need to exchange mechanical rail components if role changes are required from class A to class B missiles.

NATO countries currently use fighter aircraft such as F-14, F-15, F-16, F-18, TOR-ADV, MIRAGE 2000, Harrier, F-4F which all dispose over wing stations for air to air missile carriage. Between two and six missiles can be rail launched from these aircraft. Currently available armament comprises AIM-9 type,

AIM-7, Sky Flash and eventually Aspide. Within the next future as well AMRAAM is expected to be entered into service in the principal NATO air forces.

Western Europe, for example, offers immense possible combinations between aircraft and armament due to the dense agglomeration of different national equipment. Cross servicing, which is certainly not limited to armament, is and will be a challenging task. Here the requirement of NATO-ADVANCED RAIL LAUNCHER group reappears, that 'for interoperability reasons, it is desired that module changes to accommodate different missile types be avoided'. This expresses the fact, that after operational engagement, it is likely for a fighter aircraft not to land on its home base.

Intentionally NATO Allied Tactical Air Force carry out periodical exercises to establish the capability of cross servicing amongst the NATO Air Forces with different type of aircraft, role equipment and weapons. One of the tasks is to rearm an aircraft on different air bases with different weapons. This requirement is difficult to cope with under the condition of role equipment dedicated to a particular weapon. Effectivity of an air force is very much depending on the cross servicing capability, which in terms of air to air missiles is much related to the available carriers. Here the rail launched missile/launcher interface is of great importance. A first step was already done by the STANAG 3842 as it currently stands, but an enhancement in the light of the proposed rail concept could further improve the situation. US fighters would be in the position to use Sparrow, AIM-9 and AMRAAM whichever is available on the particular air base. These missiles can be operated from the same rail launcher without the need to have role change items available.

Prime attempt of cross servicing is to enable the air forces to carry out 'Stage A' activities which is to refuel the aircraft. 'Stage B' is then refuel and rearm the aircraft which requires that relevant weapons can be fitted and operated. Universal rail launcher with appropriate rail for most of the relevant air to air missiles is thus an appropriate means to get closer to the requirement of 'Stage B' across the NATO air forces. Apart from the aircraft inherent capabilities as attack and identification performance it is not at least the rail with adapted launcher components to ensure fit and function of the weapons. Todays modern technology with the capability for intelligent launcher electronics in combination with standard MilStd 1760 interface will most probably reduce the integration effort. The rail launcher has to

transform the software controlled data transfer from and to the aircraft to the individual missile needs (Fig. 10).

Synthesis

Abstracts of a study were presented which was carried out at MBB Military Aircraft Division to evaluate the rail geometry of a future rail launcher and to influence the relevant specifications for current development programmes in the light of the results.

Analysis of technical as well as procurement and operational requirements lead to a proposal for a rail launched missile/launcher interface which caters for the majority of air to air missiles used in the NATO countries. Feasibility study is supported by safe separation exercise using the possible new rail concept on modern high performance aircraft. This ended with positive results. Relation of missile interface to STANAG 3842 and cross servicing aspects were offered with the result that a new rail concept will improve cross servicing capabilities. It appears mandatory to respect cross servicing requirements when specifying future role equipment. It is further realized that such an idea can only expect broad acceptance and thus important influence on future equipment if it is reflected in the relevant standards and agreements. The ambition to approach NATO-Standardization Agency was expressed intentionally at this symposium

Further aspects - future activities

In excess of the presented main topic, other aspects of a rail launcher have to be considered to end up with equipment requirements leading to real cross integration capability. The launcher has to incorporate integrated electronics with the capability to switch to individual missile application. One important condition here is the provision of a MilStd 1760 interface or similar subsets to simplify electrical function with the carrier aircraft. Envisaged integration of digitally operated missiles such as AMRAAM provide

for the necessary upgrade of aircraft sensors and computers as well as software provision and handling up to the aircraft launcher interface.

The launcher has to incorporate cooling facility for IR missiles. Cooling most probably has to be accomplished by use of a gas bottle with the provision for future replacement by a pure air generator, mainly depending on its development status.

Most of the requirements will be reflected in the specification for European Fighter Aircraft Rail Launcher which will be issued for tendering within the next future.

	User Countries	Weight [kg]	Guidance	Status
AMRAAM (AIM-120)	USA GE UK + NATO	150	Command, inertial & active radar	Development
ASRAAM (AIM-132)	International	65	IR	Development
Sidewinder (AIM-9L/M)	All NATO	87	IR	Operational
Aspide	Italy	220	Semi active radar	Development
Sky Flash	UK Sweden	195	Semi active radar	Operational
Sparrow (AIM-7M)	USA + NATO	227	Semi active radar	Operational
MICA	France	110	Active radar & IR versions	Development

Fig. 1 Air to air missile key data

	FWD	CTR	AFT	Umbilical	Motor Fire	Remarks
	Hangers			Electromechanical		
AMRAAM	T+B	C	T	×	-	Umbilical retract
ASRAAM	T	T	T	×	-	Umbilical retract or AIM-9L umbilical
AIM-9L/M	T	T	T	×	-	external cooling air supply
Aspide	B	C	-	×	×	shear connectors
Sky Flash	B	C	-	×	×	shear connectors
Sparrow	B	C	-	×	×	shear connectors
MICA	T	T	C	×	-	Umbilical retract

Explanation

T T-Hanger
B Button
C C-Hanger

Fig. 2 Air to air missile mechanical and electromechanical interface

Pictures will be presented only

Fig. 3 Position of hangers and electrical connectors

Fig. 4 Hanger to rail interface conflict

Fig. 5 Modified rail cross section

Fig. 6 Sequencial release

Class	Weights [kg]	Rail	Missiles
A	68 - 159	defined	AMRAAM ASRAAM AIM-9L/M
B	159 - 363	not defined	Aspide Sky Flash Sparrow

Fig. 7 Definition of mass classes in STANAG 3842
(Edition 1 + Amendment 1)

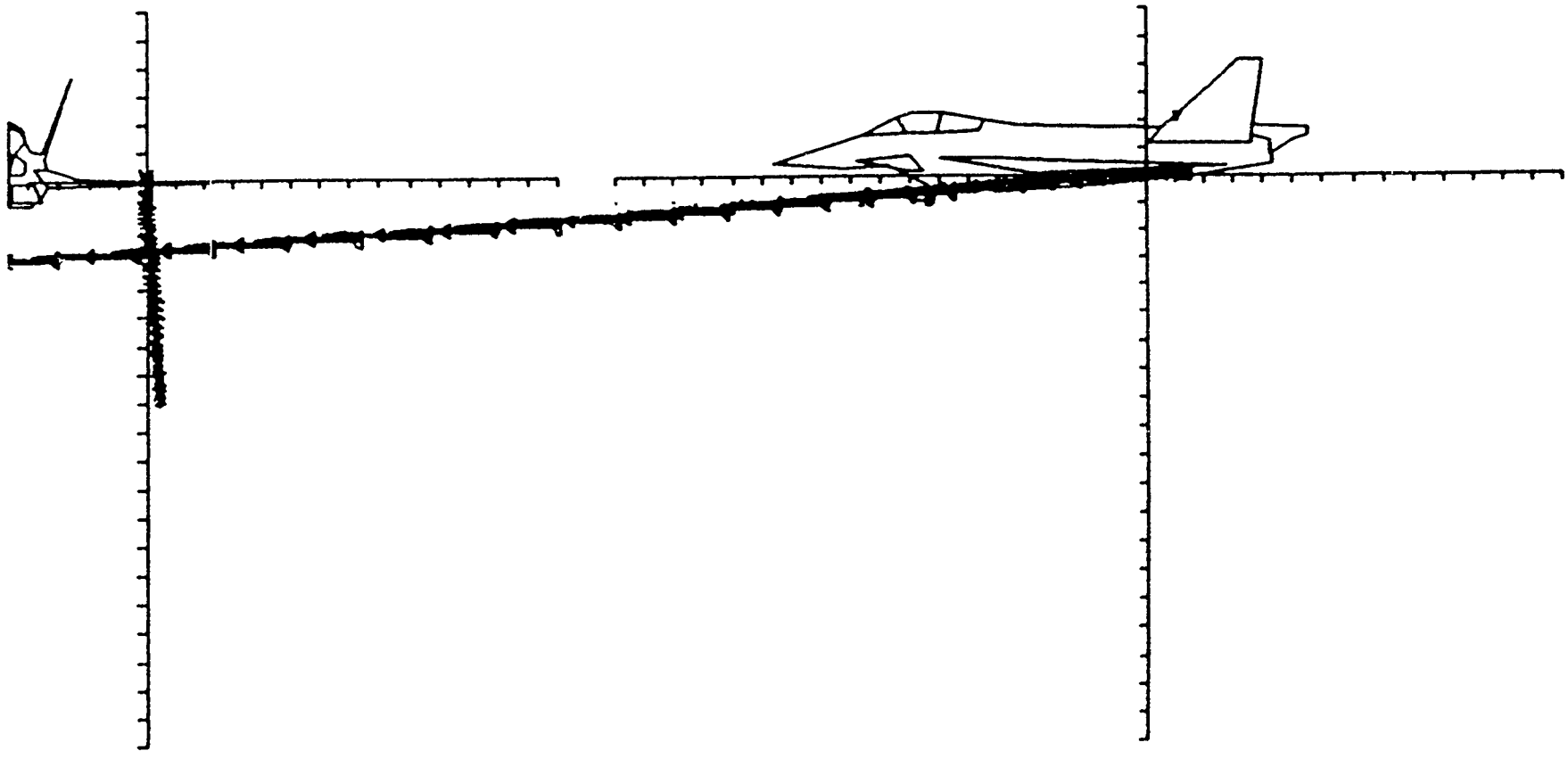

Fig. 8 Separation trajectory - low 'g' - adjacent tank

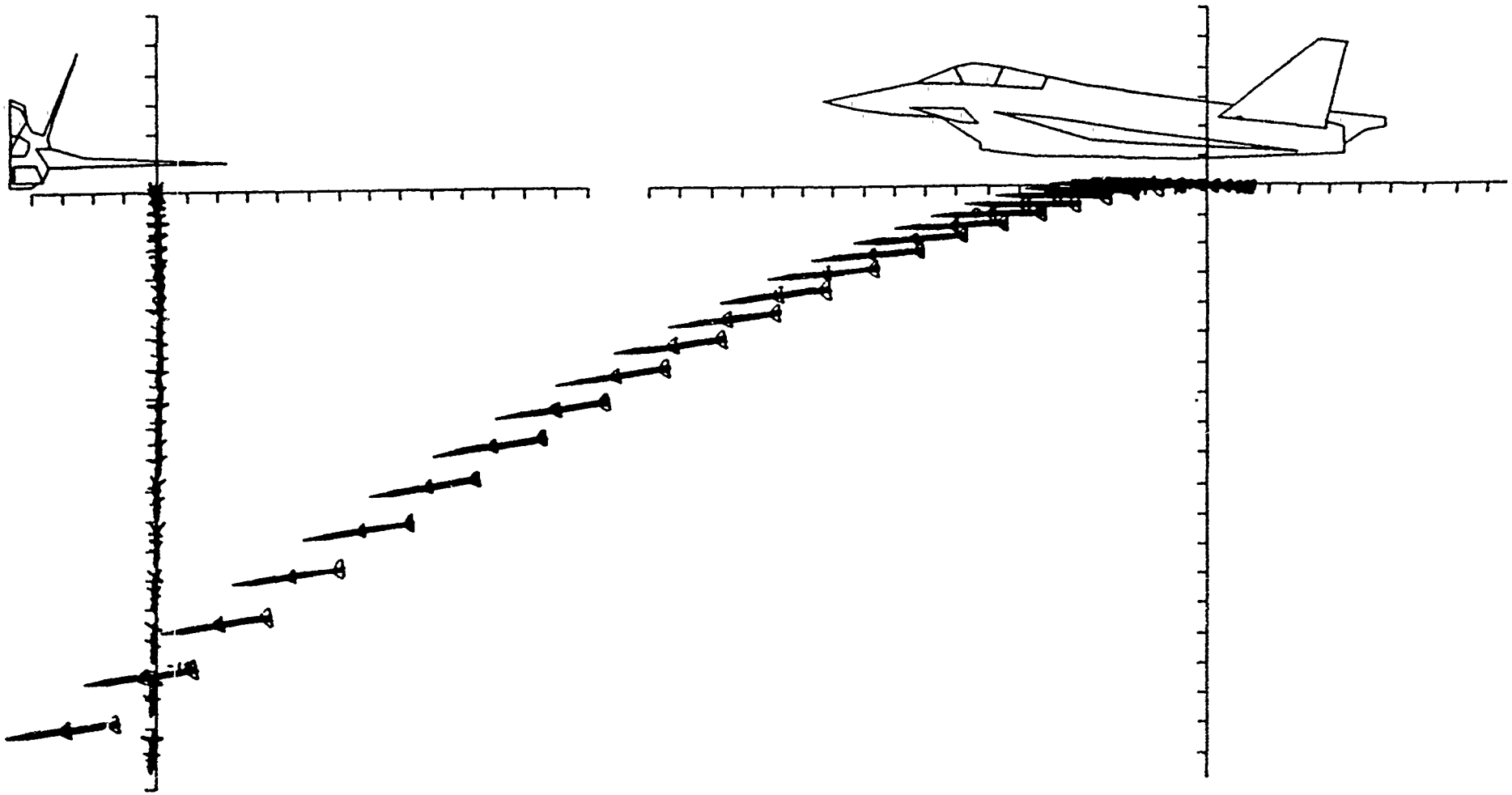

Fig. 9 Separation trajectory - high 'g'

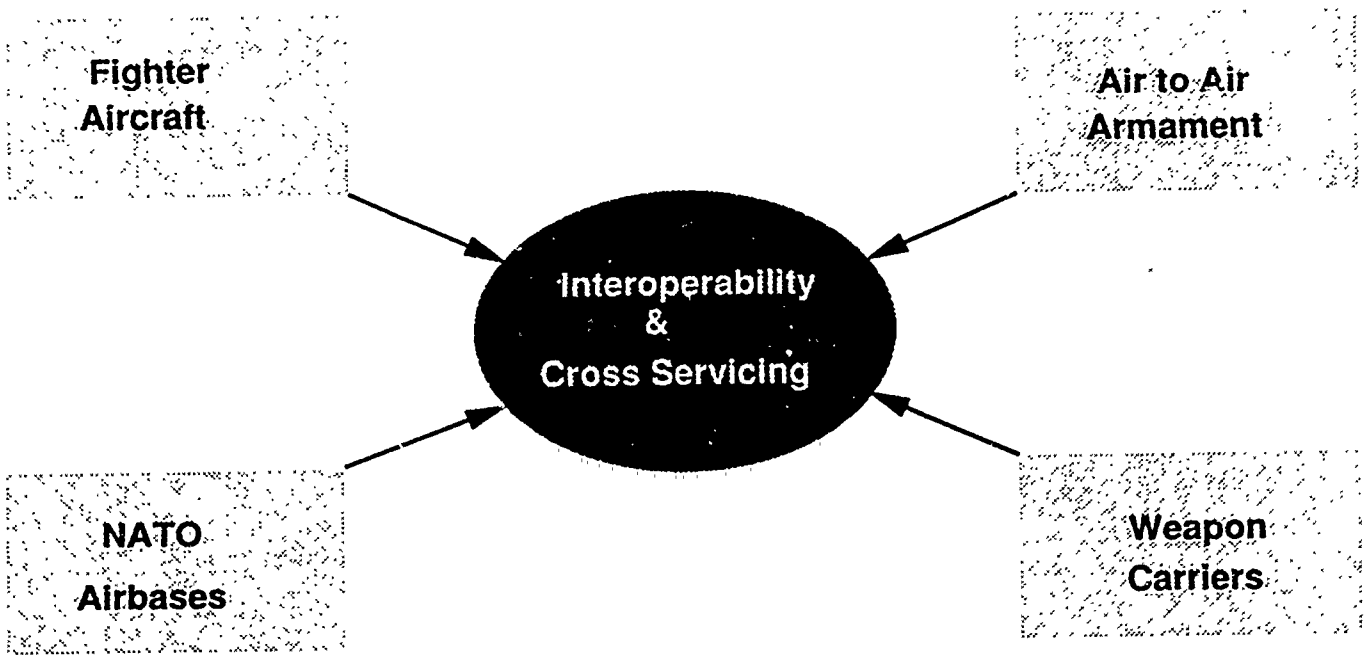

Cross Servicing:

Stage 'A' : Gas & Go
Stage 'B' : Gas & Go & Weapons

Fig. 10 Interoperability & cross servicing

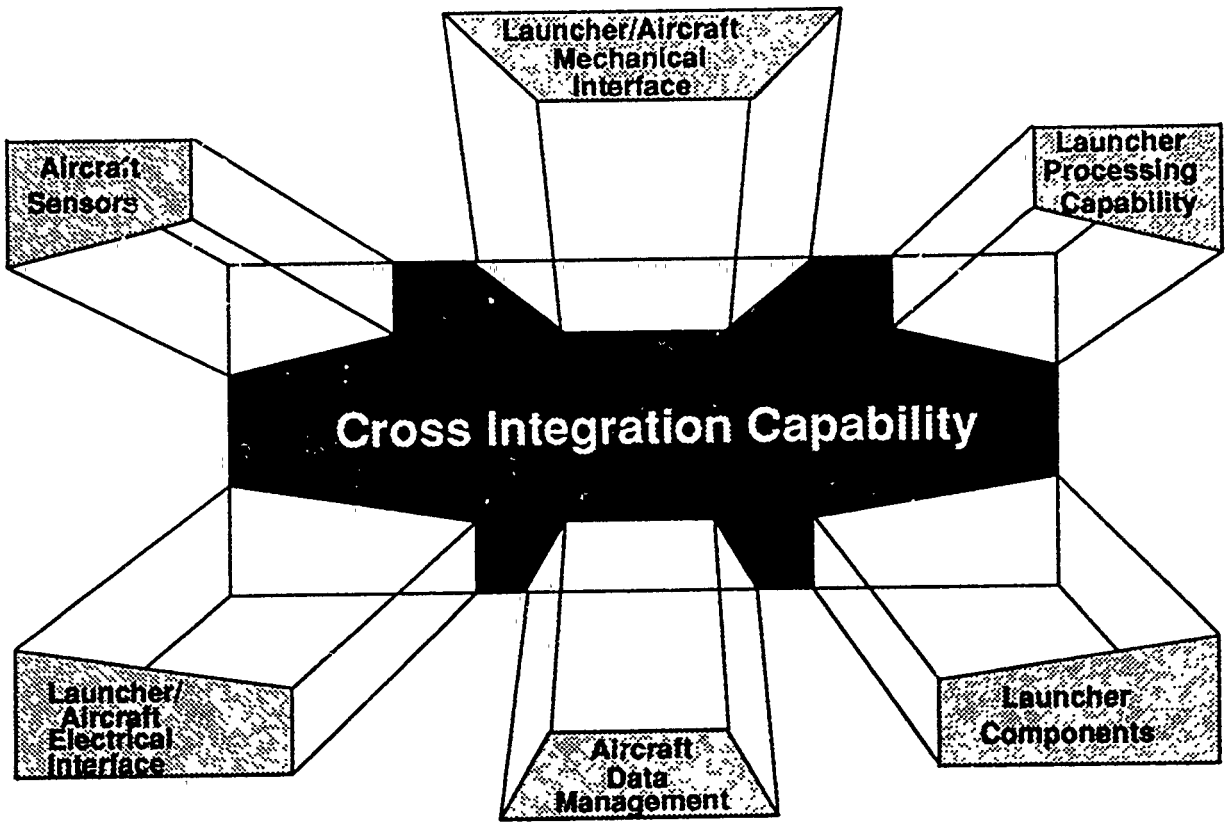

Fig. 11 Cross integration capability

Autobiography

Stephan Lösch

Stephan Lösch studied mechanical engineering at the technical university of munich and achieved the diploma in June 1988. He carried out his final thesis at the facility of Airbus Industry in Toulouse, France in 1987/88, supported by two scholarships.

During his studies Stephan Lösch gathered experience in various companies as trainee: Diehl - Nürnberg, MAN - Nürnberg, Bosch - Munich, BMW - Munich, MBB - Munich, Rodenstock - Munich.

1988 he joined the Military Aircraft Division of Messerschmitt Bölkow Blohm GmbH at Munich as system engineer for role equipment and launching systems. Stephan Lösch was responsibly involved in the EFA project representing his branch internationally and in relation to the customer and inside the company.

In summer 1989 Stephan Lösch was promoted as 'group leader for role equipment and launching systems' within the system department. He is involved in aircraft programs such as EFA, Tornado and Phantom Combat Efficiency Improvement.

Technical system aspects -electrical and mechanical-, equipment specifications, supplier assessment and selection as well as commercial involvement are his tasks in the new position.

THIS PAGE INTENTIONALLY LEFT BLANK

AIR CARRIED MISSILE INTERFACE DESIGN FOR RAIL AND EJECTION LAUNCH - SOME OBSERVATIONS AND IDEAS

By D.GRIFFIN, Frazer-Nash Defence Systems Limited, Leatherhead, U.K.

ABSTRACT

The purpose of this paper is to catalyse both discussion and review of air carried missile/launcher interfaces, so that future weapons will be more launcher-friendly as well as being potentially more aerodynamic. It is evident that in terms of missile suspension features, we in NATO have got where we are today by a series of independent procurement decisions combined with minimum-short-term-cost motivations and a "too little, too late" attitude to standardisation. The time is now ripe for seriously reviewing where we should go from here.

A missile's suspension lugs/hangers serve no useful purpose when the missile is in free flight, so they should be optimised for carriage and launch and must be either of a low drag design, or else retractable after launch. The paper explores some potential concepts in this area of design.

Key to the acceptability of future missile design is the increasing emphasis on eject launch capability, so this will be given close examination without necessarily compromising the rail launch option. Moreover, when required for rail launch, the ability to tolerate more severe carriage environments than at present will be an essential feature of future air launched weapon systems. In an ideal world, a common hanger arrangement for all sizes of missile, is favourite. It has to acknowledged, however, that this may be an ephemeral hope, when all practical considerations are reviewed.

It may be that the evolutionary process of missile refinement and family development has come to an end, and that a quantum change is now called for. This will involve some difficult decisions by those who shape the policies of our air forces, but it is inescapable that these decisions will get even more difficult (and expensive) with the passage of time. The writer, therefore, recommends early action, in the interests of operational effectiveness and longer term economics.

INTRODUCTION

Unlike ballistic stores, air launched guided missiles are not yet the subject of ratified STANAGS controlling their carriage interfaces. The main reason for this, is may be argued, is that their electronic interfaces have tended to be unique, (for various reasons) and that there is therefore no point in providing "semi-interoperability"! However, matters are changing. With the adoption of MIL STD 1760 and 1553, the opportunity for total interoperability will become more dependant upon mechanical interfaces, and hence the subject of this paper.

Stanags 3726, 3842 and MIL 8591 adequately define and control aircraft interfaces for free-fall stores, and where possible, they have been used for some "missiles", such as air-to-surface or standoff weapons. However, missiles with energetic booster rockets, such as air-to-air types, have been designed primarily (or perhaps even solely) for rail launch; and ejection launch has been adopted on some such weapons, almost as a bonus feature! The attraction of rail launching is understandable; it confers an ability to conveniently attach the missile in a state of launch readiness, to many points on the aircraft, indeed, almost at each and every weapon station. The opportunistic nature of such self-defence weaponry makes it attractive to users who can dedicate "spare" weapon stations to such a useful facility, and with comparative ease.

The AIM7 and AIM9 series of missiles are archetypal examples of this philosophy and their deserved popularity is testimony to the soundness of the original concept. However, when these weapons were conceived in the 1950s it would have been nothing short of miraculous if it could have been envisaged that their mechanical interfaces would be good for all time. Regrettably, there are some people who would have us believe that this can be so. Good as the Sparrow and Sidewinder interfaces are, they are rapidly being overtaken by events, and it is nothing short of fanciful to imagine that future ultra high performance air-to-air missiles (AAM) can live up to expectations and performance requirements when burdened with the "hand-me-down" suspension features of the 40 year old designs. Despite this, the existence of numerous old missiles is used to justify their compatibility with new launch systems, and the existence of numerous old launchers is used to justify their compatibility with new missiles. Even now, events are unfolding, which could, by means of STANAGS 3844 and 3842, effectively perpetuate the old AAM interfaces. Can this be allowed to happen without a critical review of its implications? The writer is an advocate of STANAGS but believes that in this instance, the wrong decision could be regretted for a long time to come.

RAIL VERSUS EJECTION LAUNCH

With recent advances in ejection launch technology and increasing future emphasis on stealth and low drag carriage, it may be argued that all future AAMs should have an eject launch capability, whereas current ones all do not. But it would be foolishly parochial to dismiss rail launching completely, for reasons discussed above, i.e., it confers flexibility of weapon fitment to meet the air defence role.

In the past, however, rail launching has been the dominant influence on interface design; but in the future, at least equal importance should be attached to ejection launching.

CURRENT INTERFACES

To those people familiar with AIM9 and AIM7 interfaces (and of course AIM120 - which is a mix of both), their principal drawback is fairly obvious, and it relates to the aerodynamic drag caused by the suspension features when the missiles are in free flight. Less obvious to the uninitiated is the inability of the suspension features to accurately align and constrain the missile during carriage and launch, together with the problems of load redundancy and difficulties of reliably predicting carriage forces at the interface. If these were not problem enough, they also have little strength in hand for further performance enhancements in the host aircraft. Such factors provide ample justification for future improvements, so let us consider them in turn:

Aerodynamics

Crudely, in order to minimise drag, suspension hanger lugs should be few in number, have minimal frontal area and should be carefully shaped, avoiding blunt leading edges and certain other geometrical features. Better still, there should be no exposed lugs at all! Figure 1 shows some possible approaches to the lug design problem, wherein it will be appreciated that the optimum for rail launch is not necessarily best for ejection launch (and vice versa). This begs the question of whether missiles should be differently configured for the two methods of launching. (more on this later). The best aerodynamic solution; namely, recessed lugs, is not favoured by the missile designer as it complicates the rocket motor or warhead design or introduces other internal packaging problems. It should be a future aim to cut toal lug drag to 5% or less of the total weapon figure, whereas it often contributes 15% or more with current interfaces.

Load Reaction

The load component that causes the worst reaction difficulties is Rolling Moment (M_x). For some installations, this issue represents the critical design case from a strength viewpoint, and requires some complex roll reaction mechanisms during carriage and eject launch. The principal problems arise due to the small moment arm usually available for generating a resisting couple (see fig 2). Also, M_x is often the most indeterminately reacted load -there usually being several available force couples capable of contributing to M_x reaction. The difficulty lies in defining how much load is reacted by which mechanism - each varying with dimensional tolerances, local stiffnesses, and initial contact conditions. Fig 3 shows a hypothetical interface with a possible load reaction system which aids accurate force prediction. What is not shown, however, is how these pure forces may be reconciled with rail or ejection launcher functional requirements. It appears that some form of compromise interface is virtually inevitable when practical considerations are included.

Location During Launch

During carriage the missile must have six "degrees of captivity". During launch, it still needs five! In other words, during launch, the missile must move only axially (rail launch) or vertically (ejection launch), despite aerodynamic and inertial influences to the contrary. Let us consider the ramifications of this truism.

Rail Launching

In the case of rail launch there are two schools of thought concerning the best way to let go. One says the lugs should disengage in sequence, with rolling moment and a degree of pitch control being effected by one hanger at the rearmost part of the missile, (fig 4). The other says that five degrees of captivity should give way to zero at the instant when the last two lugs disengage simultaneously. Neither system is a clear winner, as the former suffers from tip-off effects caused by pitching moments generated by the last lug to leave the rail launcher during high 'g' launches. The latter system does not suffer this problem, but the missile is totally unconstrained while in the vicinity of the forward section of the launcher. This can lead to collisions with the launcher and possible launcher or missile damage. Interestingly, both systems seem to work well, and the second solution does at least enable a more practical two-hanger suspension system to be employed, with other attendant advantages (e.g. drag and load determinism).

Eject Launching

The biggest problem faced during eject launching is that of preventing yaw, sideslip and roll of the missile as it is being accelerated downwards. Features which enable the ejector feet to locate on the missile lugs (see fig 5) would be a great help in resolving this present difficulty. The orientation of the missile fins and/or wings during carriage also has a significant bearing on this issue, and presents one powerful reason for having different interfaces on the ejectable versions of AAMs. This will now be explained: Fig 6 shows frontal views of a missile carried in the + (plus) and x (*x*) configurations. To keep the aerodynamic surfaces clear of the launcher, rail suspension lugs are located circumferentually between the surfaces. If the aerodynamic surfaces are of small span, the lugs may be used for ejection carriage in a semi-conformal manner as shown in figure 5 . This orientation is also favourite for internal carriage and eject launch. If full conformal or semi-buried carriage is required, however, the wings and fins must be vertical and horizontal ("plus" carriage). This complicates the eject launch interface if rail launch is also to be possible with the same missile. Alternatively, if rail launch compatibility is not required, the suspension features may be located in the plane of the fins. (Fig 7)

Carriage Alignment

Precise alignment is important for two reasons; firstly, it enables a close fit of missile and airframe during conformal carriage - without undesirable contacts arising from in-flight carriage forces, and secondly, if the missile has a guidance system requiring an accurate orientation datum reference, minimal positioned variability improves operational success envelopes.

Rail launchers, require reasonable running clearances between lugs and rail tracks and this degrades alignment, but the longitudinal distance between lugs is favourable, so alignment is rarely a critical problem.

Eject launchers, however, especially when carrying current missiles in the 'plus' orientation, suffer from the inherent limitations of the interface geometry, and because the suspension is effectively rotated through 45°, there is coupling between pitch, yaw and roll misalignments. Here is another powerful argument for carriage in the 'x' configuratioin, or for the addition of precise yaw locations to the existing interfaces.

OPTIMAL SOLUTIONS - ARE THERE ANY?

The following is a list of questions which will influence the choice of suspension geometry :-

a) Is the missile dedicated to rail launch?

b) Is the missile dedicated to ejection launch?

c) Is the missile to be ejection and rail launchable?

d) Does the missile have aerodynamic surfaces?

e) What is the span of these surfaces?

f) Is the missile body capable of reacting point loads?

g) Can retractable lugs be accommodated?

h) What is the mass of the missile?

j) What is the diameter of the missile?

k) What range of lug fore-aft locations are possible?

l) Can wings/fins be used to react suspension forces?

m) Is the missile to be carried in the "plus" or "*x*" position?

n) What is the maximum allowable drag increment due to lugs?

o) What is the carriage manoeuvre/speed envelope?

It is a design aim, of course, to find a suspension layout that eliminates the relevance of most, if not all, of the above questions, but this is an unlikely outcome. However, for every different combination of answers there is a possible discrete interface standard, so that minimising the impact of differences is certainly a worthwhile objective!

Other Interfaces

The foregoing has assumed that the other connections between aircraft and missile are of a lower order of importance (or difficulty to incorporate). This assumption may be overly simplistic; umbilical connections have already been sources of considerable discussion and numberous attempts at standardisation - and are known to complicate launcher interfaces if their positioning or mechanical requirements for engagement and disengagement become too specific. There is a powerful argument for attempting to standardise such connections, if only in position; and eject launchers are much less able to tolerate arbitrary positioning of this facility, as they tend to be more compact in size and mechanically complex. The ideal position would appear to be midway between eject launch suspension, features - to allow space for linkages or holdback detents - for ejection and rail respectively. Whatever the final decision it is imperative that this feature is commonised, if future standardisation is to be meaningfully implemented.

CONCLUSIONS

The writer believes that any future air-to-air missile's aerodynamic surfaces should be severely restricted in span to allow semi-conformal carriage on ejection launchers in the 'x' position. Rail launching will also then be possible with compromise lugs, which should be designed such that two are used for rail launch and another combination of two are used for eject launch (see fig 5). The aerodynamic 'strakes' should be configured to permit wrap around ejector yokes in the region of the 'T' lugs used for ejection launcher carriage. The load reaction systems of this proposal are not perfectly deterministic, but offer a vast improvement over present 'standards'.

And what about all of the existing launch hardware? We can use it for the existing missiles, but let us invest in new launchers if we're really serious about staying ahead of the competition. Compared with missiles, launchers are very inexpensive, and at least one rail launcher already developed (by Frazer-Nash) will offer scope for compatibility with old and new missiles!

DES/DG/REP-0120/ljd

BIOGRAPHY

Dennis Griffin - obtained an honours degree in Mechanical Engineering at Brunel University, London in 1968. Since then he has been employed by Hawker Siddeley Aviation, Kingston, UK, and Frazer-Nash. Throughout his career, he has had an interest in stores carriage systems. His current role is that of Chief Engineer at Frazer-Nash Defence Systems, Leatherhead, England.

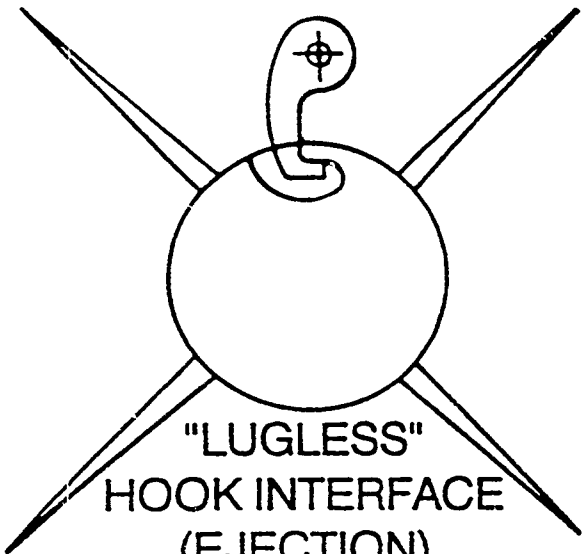

"LUGLESS"
HOOK INTERFACE
(EJECTION)

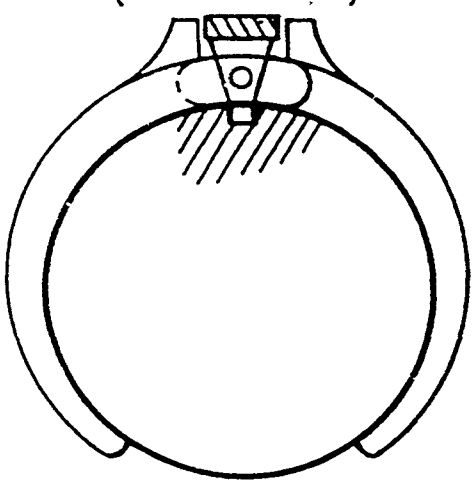

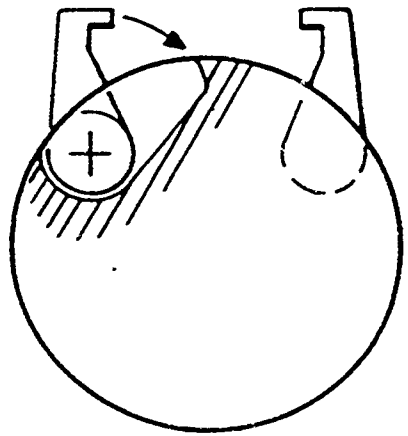

FOLDING RAIL LUGS

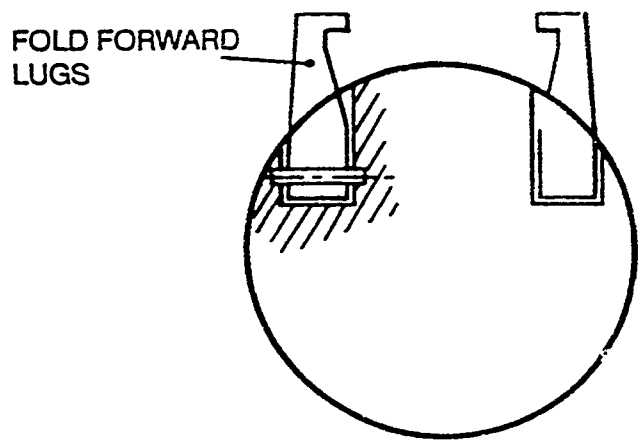

Fig 1

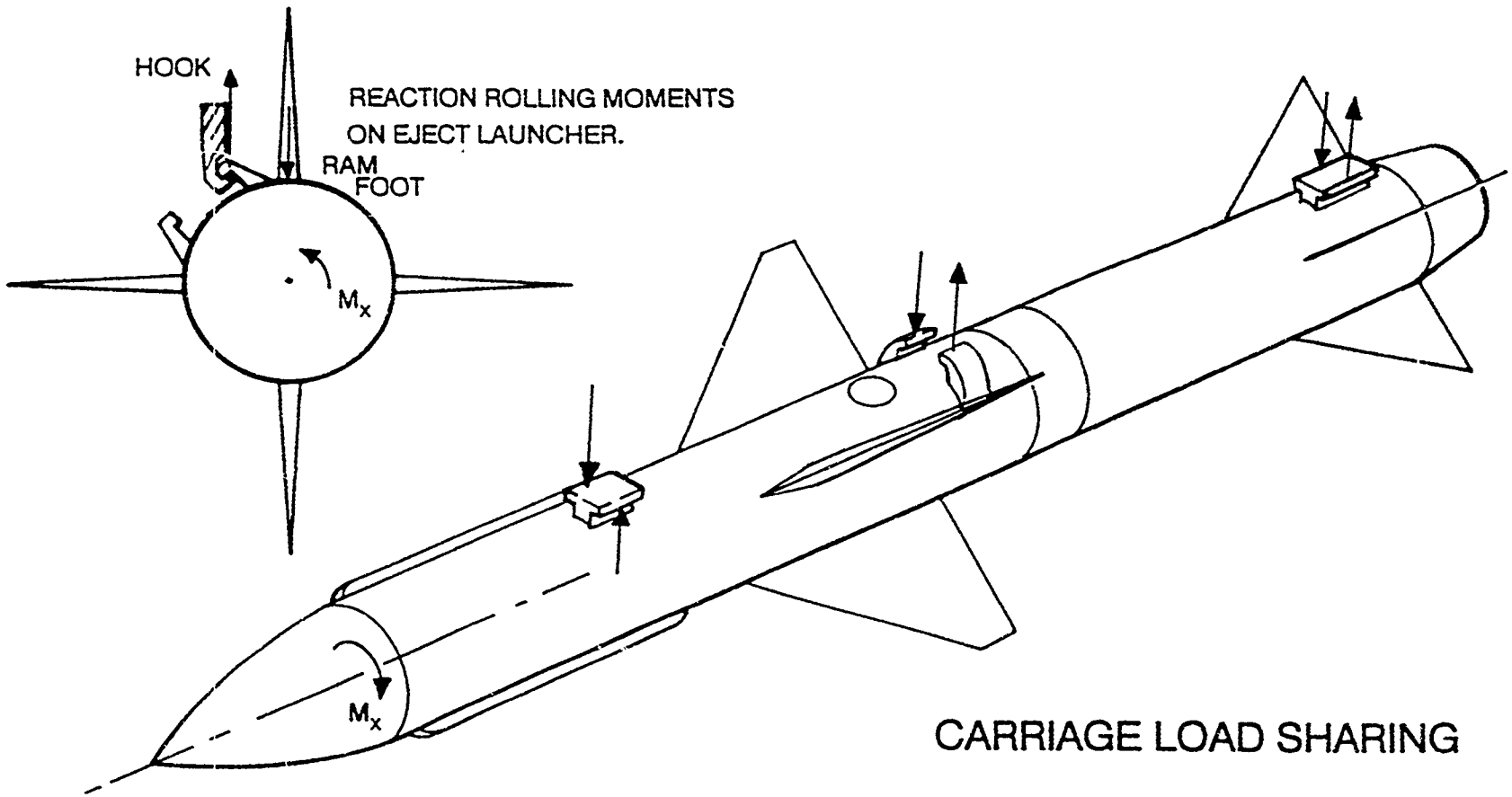

CARRIAGE LOAD SHARING

Example of M_x, F_z, M_y redundancy in rail carriage

Fig 2

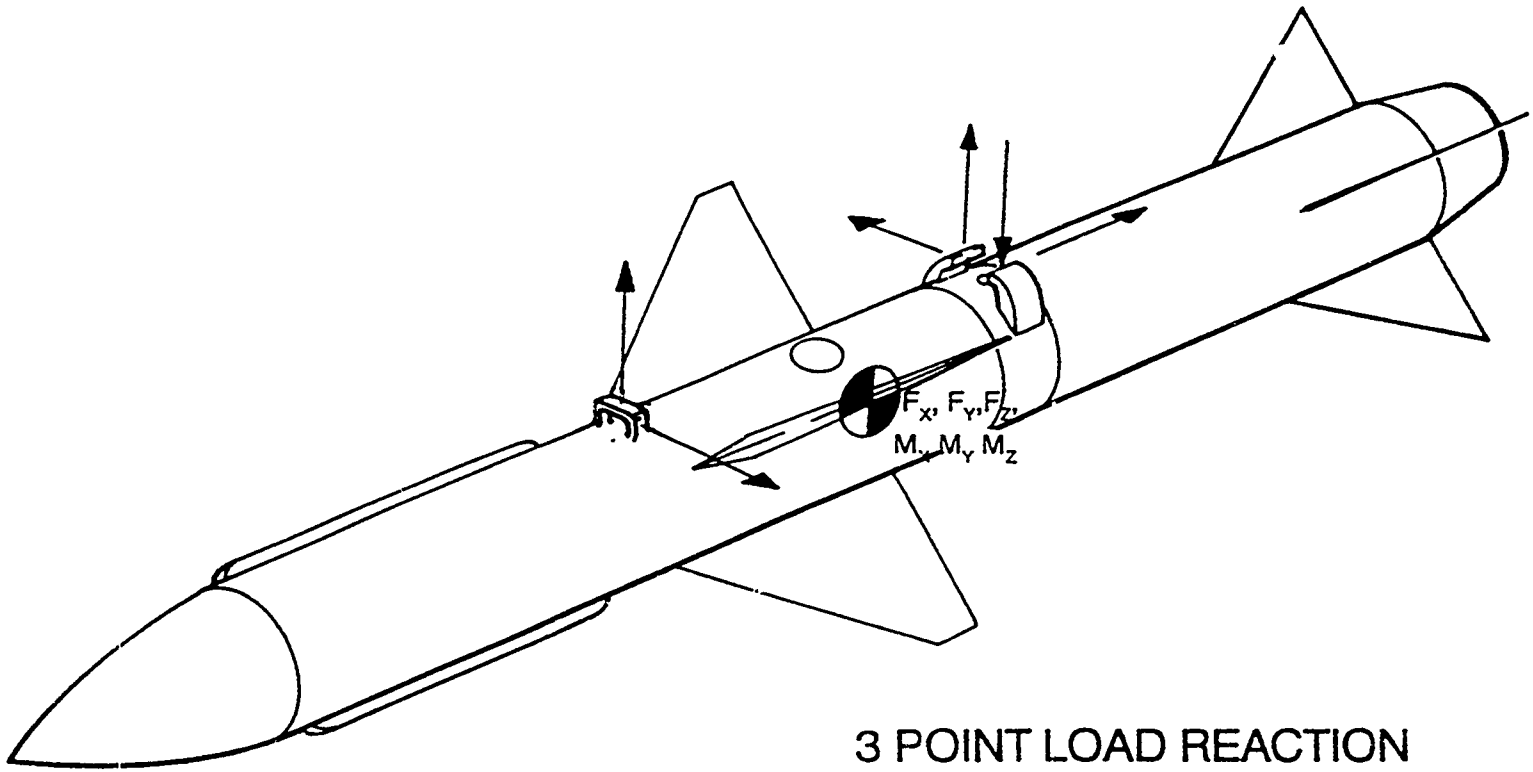

3 POINT LOAD REACTION

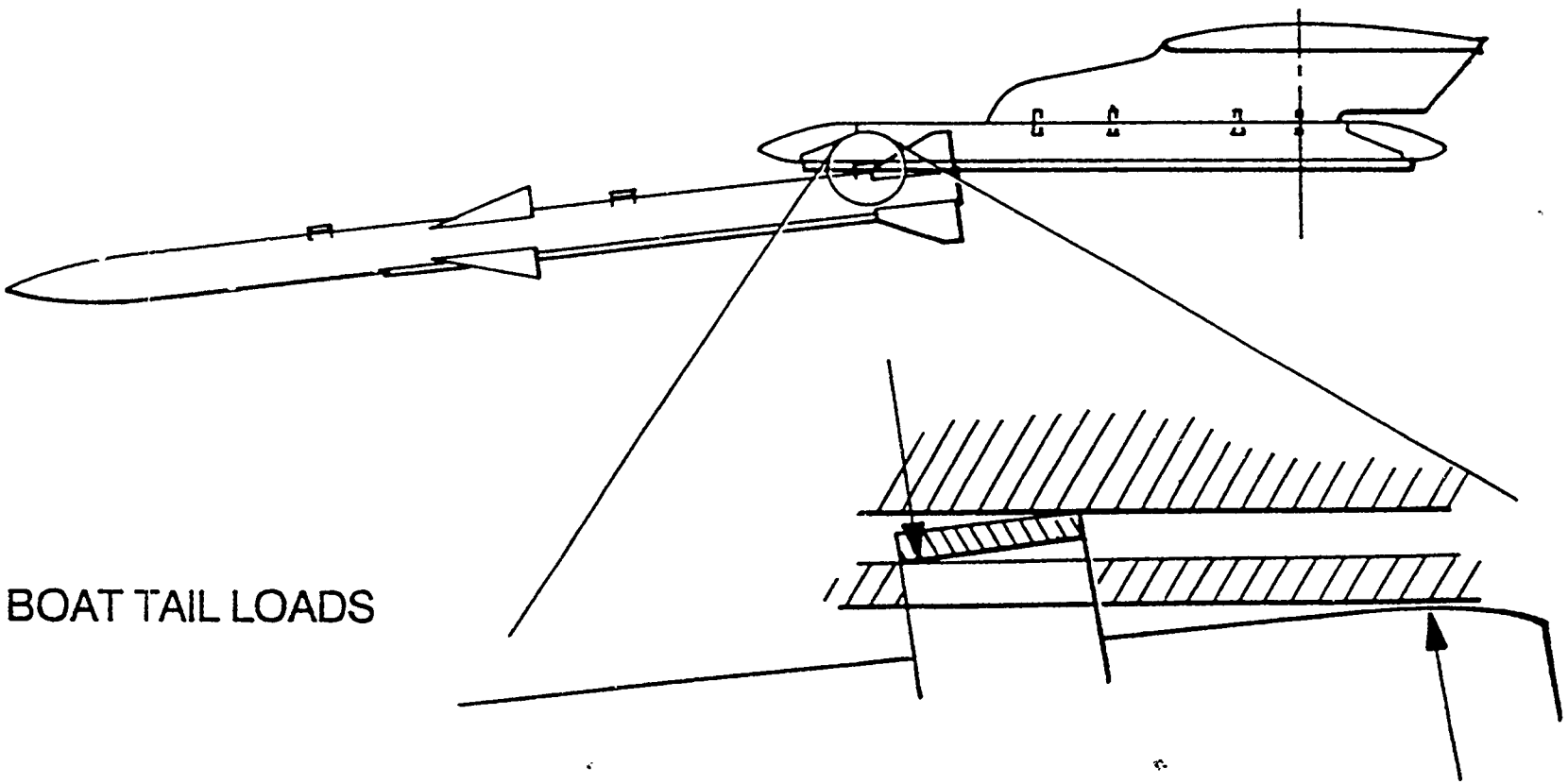

BOAT TAIL LOADS

Fig 4

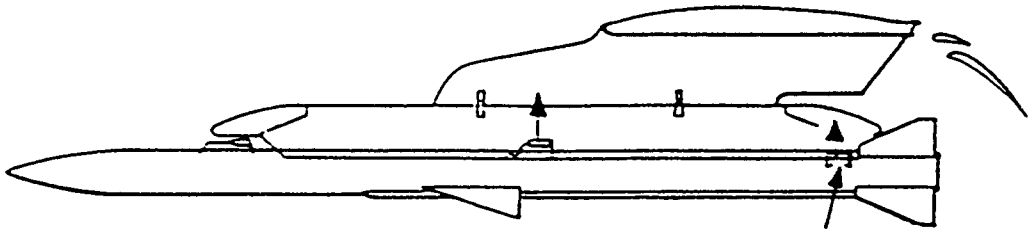

RAIL LAUNCH

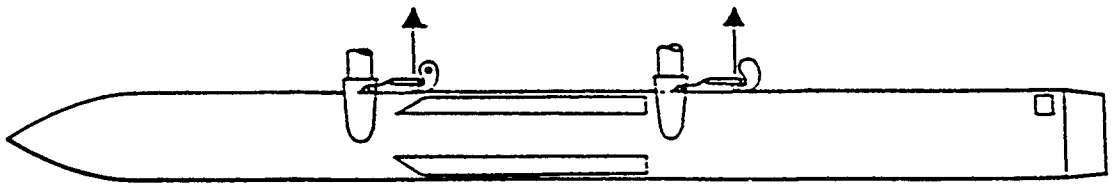

EJECT LAUNCH

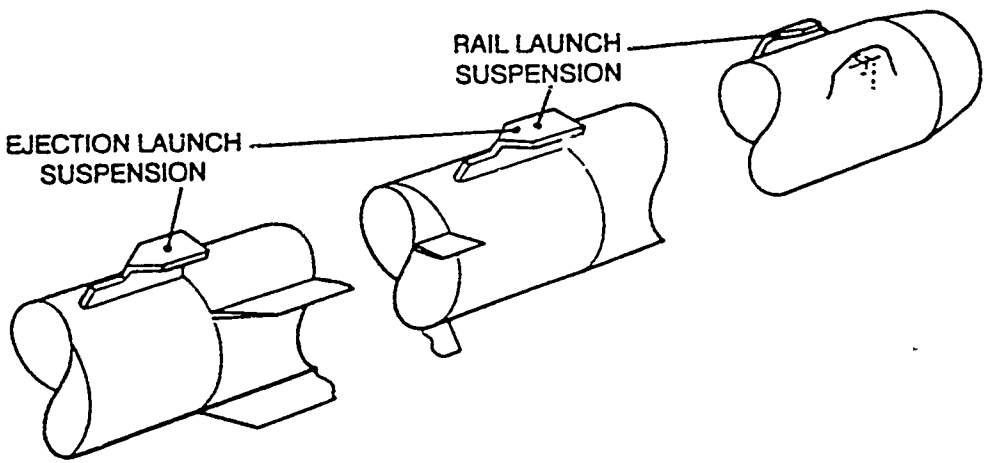

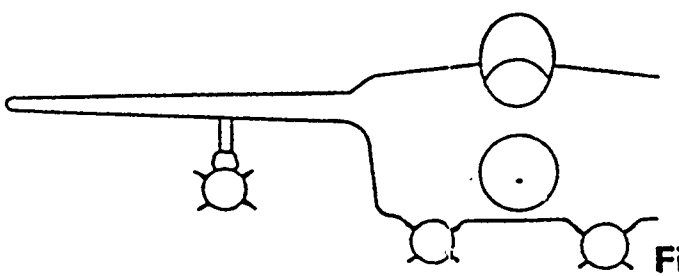

Fig 5

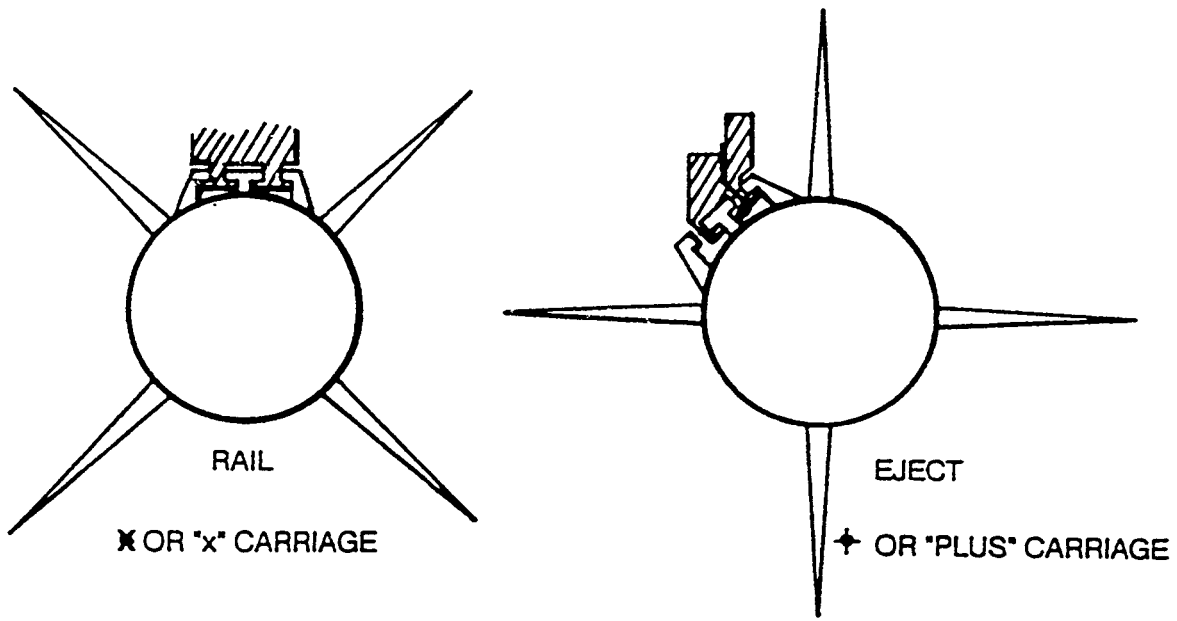

Fig 6

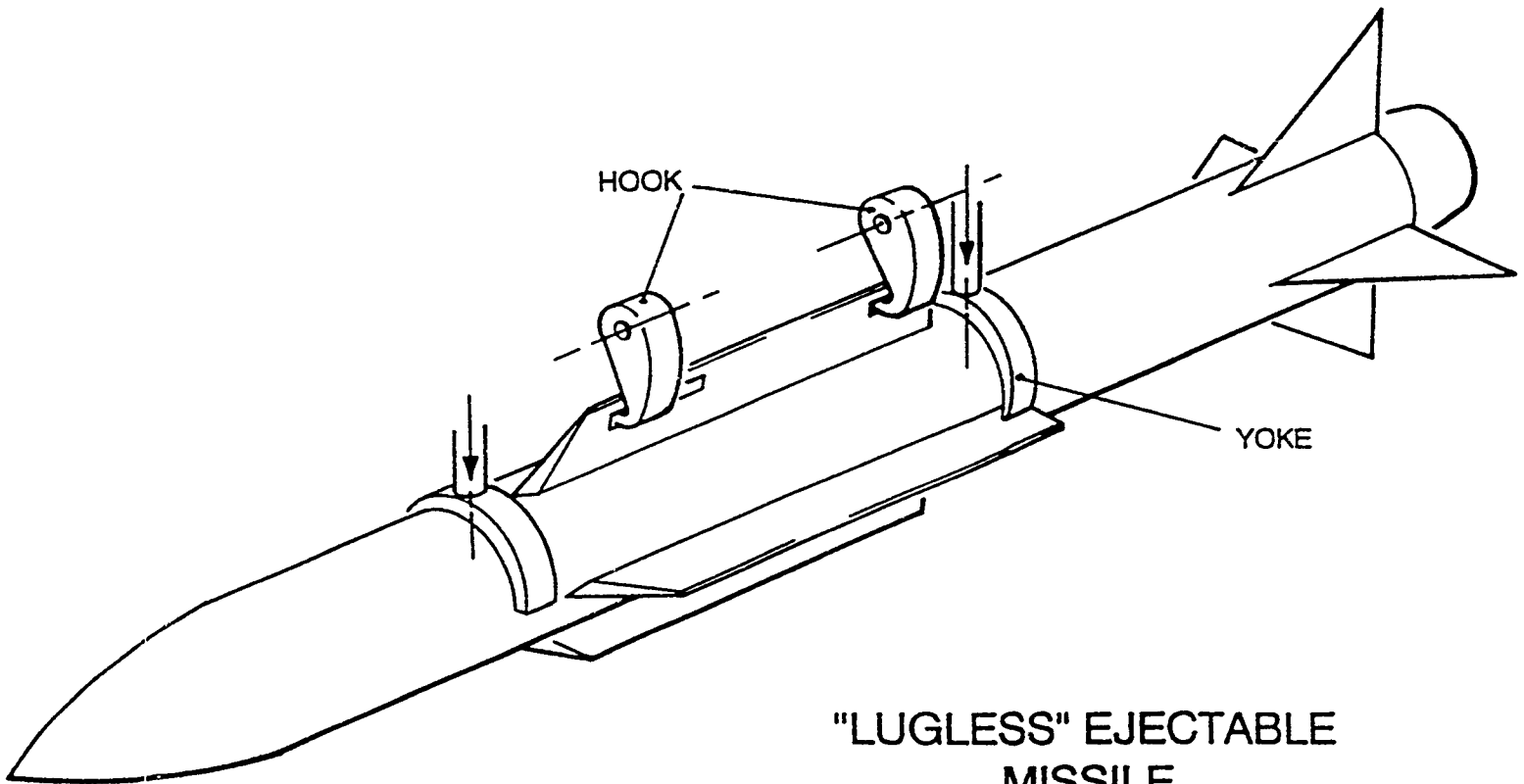

"LUGLESS" EJECTABLE
MISSILE

Fig 7

BIOGRAPHY

D E N N I S G R I F F I N

Dennis Griffin has been employed by Frazer-Nash since 1970, having obtained a Technology Degree at Brunel University, England, in 1968. He started his aeronautical training at Hawker Siddeley Aviation (now British Aerospace) in 1964, and has been associated with stores carriage and release since 1969, with specific specialisation in missile rail and eject launcher design in the last decade.

A member of both the Institute of Mechanical Engineers and Royal Aeronautical Society, he enjoys problem solving and is named as inventor in 10 Patents - mostly in the area of stores carriage equipment design.

Mr Griffin is now Technical Director of Frazer-Nash Defence Systems, Leatherhead, England and has given papers at two previous ASC symposia.

DES/DG/REP-0095/1jd

THIS PAGE INTENTIONALLY LEFT BLANK

NEWS TRENDS FOR COMBAT AIRCRAFT PYLONS

by

Philippe GUITAUT
and
Jean-Pierre MATTEI

R. ALKAN & Cie
Rue du 8 mai 1945
94460 VALENTON

- France -

A. PYLON STRUCTURES MADE OF COMPOSITE MATERIALS FOR COMBAT AIRCRAFT

1. GENERAL

ALKAN has specialized, for the last 50 years, in the development of supporting pylons for the combat aircraft of the French and Foreign Air Forces. The structure of these pylons is made of aluminium, generally manufactured from a solid block of metal. Despite the lightening weight saving method the inboard pylons of a MIRAGE 2000 of the French Airforce weigh 220 lbs (100 kg) in flying order.

Considering the increase of the loading conditions of the future aircraft and the weight specifications laid down by the aircraft manufacturers, ALKAN has, since 1980, envisaged the use of new materials for the manufacture of aircraft pylons of the next century.

Therefore an important development has been made by using composite materials.

The aim of this development was to :

- Validate the use of composite materials for the manufacture of pylon composite structures of combat aircraft,
- Determine the acceptable gains in weight,
- Determine the good resistance of these structures under vibration conditions (rigidity),
- Identify the utilization risks of these pylons in usual conditions.

In order to improve the mechanical behaviour of the structures, ALKAN was led to develop several manufacturing processes, i.e. :

1. The manufacture of totally monolithic structures with singular points, without any gluing or assembly (SIMS process).

   This method guarantees to the composite structures :

   . a 30 to 40 % weight reduction,
   . good resistance to vibration,
   . unlimited life,
   . insensitiveness to corrosion.

ALKAN

MIRAGE 2000 INBOARD CARBON FIBER PYLON

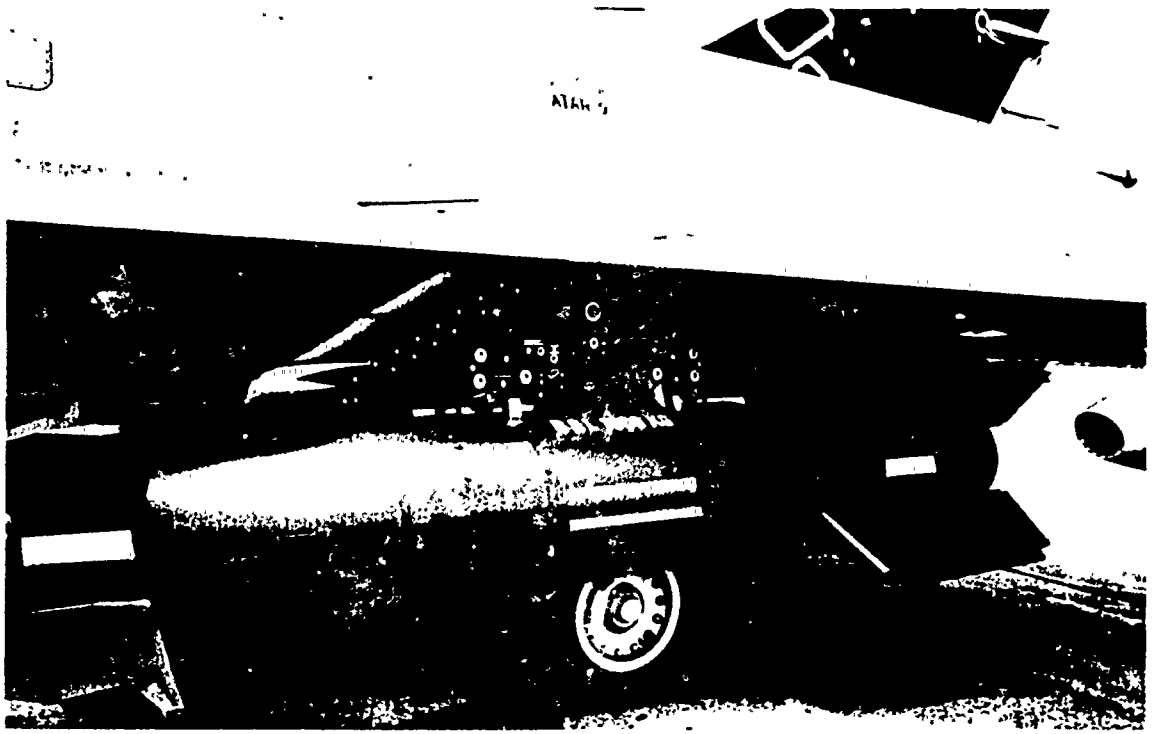

2. Protection of these structures by a deposit (metal or ceramic) transferred during polymerization (RAC process).

These deposits confer a good resistance to the following aggressions to composite structures :

. Rain and sand erosion,
. Impact,
. Lightning,
. Thermal shock.

In addition, they guarantee an improved electrical conductivity, a good protection against EMI and a radar stealthiness.

CARBON FIBER PYLON

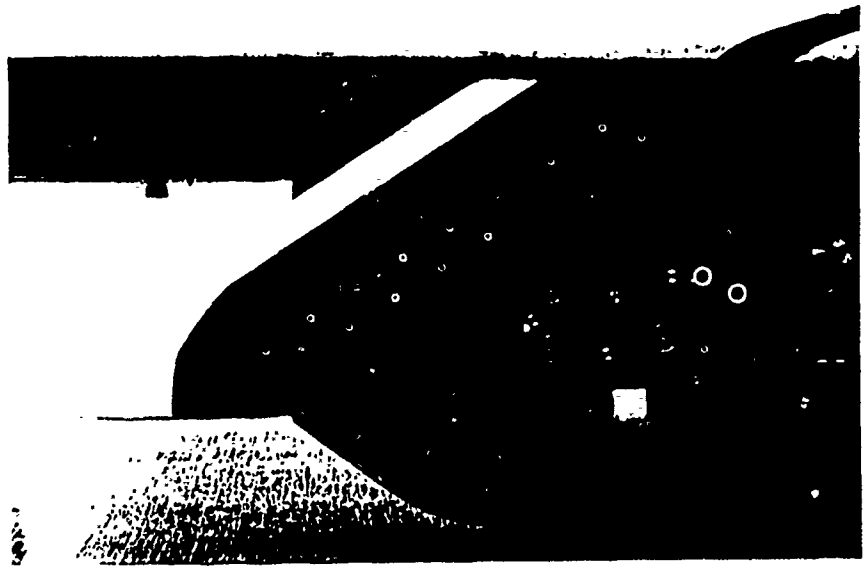

Front fairing with protective coating against

- **Erosion**
- **Rock fire**

2. TECHNICAL CLAUSES OF THE DEVELOPMENT

ALKAN manufactured the first armament pylons made of composite materials in 1985 with the above mentioned processes. The structures of these 9020 type pylons are made of preimprenated carbon fiber and epoxy resin. The chosen fiber is TORAY's T300 and the resin is CIBA's VICOTEX 10B.

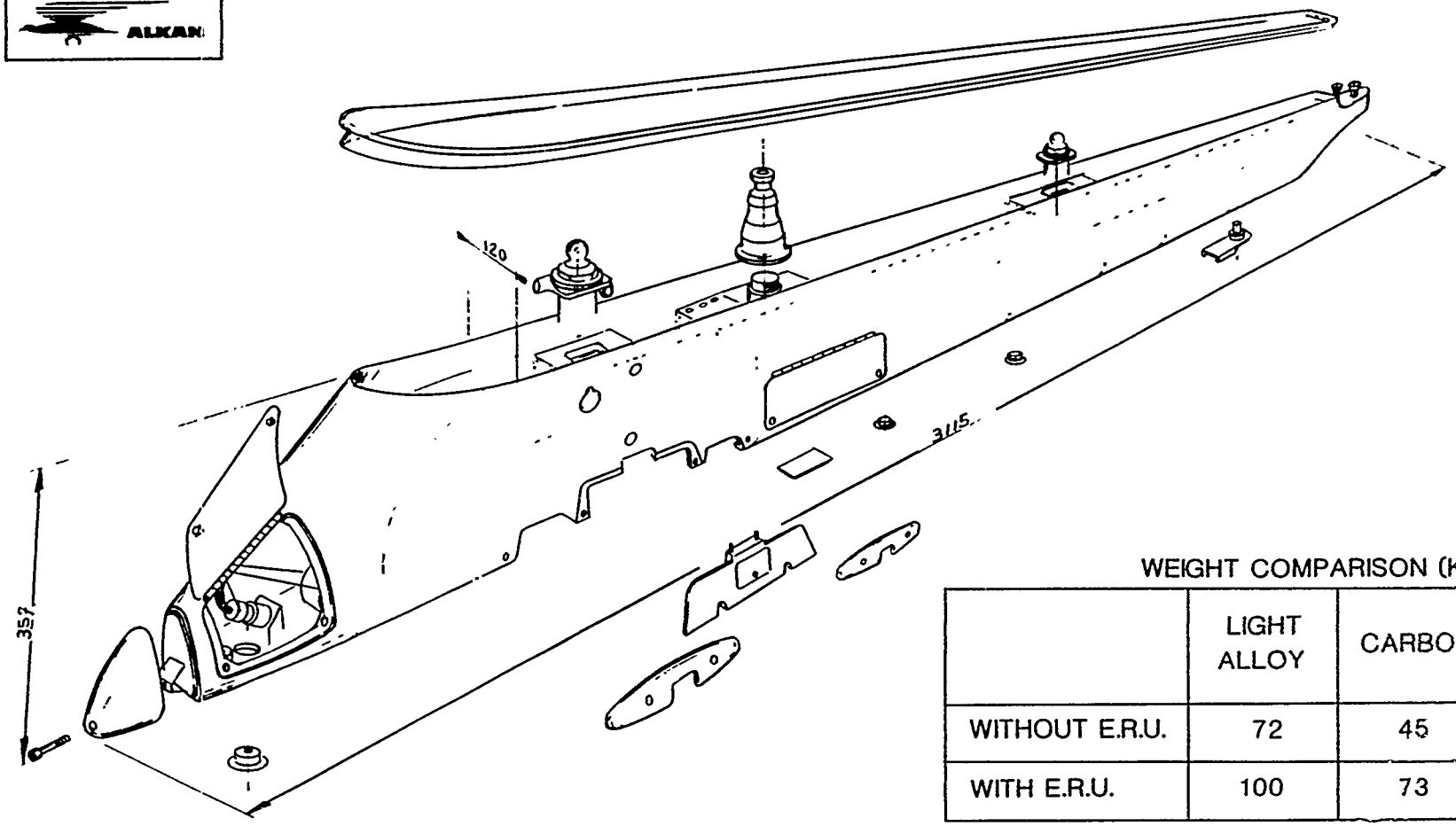

WEIGHT COMPARISON (Kg)

	LIGHT ALLOY	CARBON
WITHOUT E.R.U.	72	45
WITH E.R.U.	100	73

MIRAGE 2000 INBOARD CARBON FIBER PYLON

These pylons were defined in compliance with the specifications of the MIRAGE 2000 by DASSAULT AVIATION. They can withstand 1500 kg loads with a 6 g acceleration factor. They are fitted with composite front fairing which are resistant to rockets and to rain and sand erosion.

A total of 9 pylons were manufactured.

Five of these were used for ground tests and four for airborne tests. All these structures were instrumented and checked by ultra-sounds.

3. DESCRIPTION OF THE STRUCTURE

It is a monolithic structure which is polymerized in a single passage ; it is not assembled or glued. The manufacturing method alloved us to :

- Reduce the weight (- 35 %),
- Increase the rigidity of the structure. Relatively to an aluminium structure :
  . equivalent rigidity along OY,
  . greater rigidity along OX and OZ (+ 30 %),
- Considerably increase its lastingness,
- Reduce manufacturing costs.

The structure is composed of :

- 1 central body,
- 1 screwed-on front fairing,
- 1 screwed-on rear fairing.

3.1. The body

The body is composed of one hollow main longitudinal beam made of carbon fiber and epoxy, tape-laid on a mandrel.

The function of this beam is to absorb :

. The torsional stresses of the structure,

. The fixation stresses of the pylon to the wings,

. The fixation stresses induced by the store through the ejector.

The following elements are placed on this beam during the tape-laying procedure :

. The inserts for the fixation to the wings,

. The structural body of the ejector,

. The lower structures to absorb the bending stresses.

And the end of the tape-laying process a netting is place on the structure for the conduction of electrical charge (lightning).

3.1.1. Wing fixation inserts

Three titanium inserts are fixed to the main beam :

. The front insert includes the ball joint housing for the front bearing of the pylon into the wing. This bearing was specially designed. It guarantees a vertical freedom to the wing and to the pylon although it maintains their contact. This system was necessary because of the difference in rigidity between the wing and the pylon ;

. The central insert allows the mounting of an attachment device for the fastening to the wing. Stresses (approximatively 20,000 daN) are diffused into the composite structure through the insert. The design of this insert is of vital importance : the insert must be both sufficiently rigid to transmit stresses and sufficiently flexible to diffuse them into the structure.

3.1.2. The structural body of the E.R.U.

It is a hollow tank for the mounting of the E.R.U. This carbon/epoxide tank is taped onto the main beam.

It is machined and drilled after polymerization, in order to receive the E.R.U.

3.1.3. The bending tanks

These tanks are situated behind the structural body of the E.R.U. and suspended to the main beam. They are used to lodge the electronic equipment.

3.2. The front fairing

The front fairing is made of carbon/epoxide. It is covered, before polymerization, with an anti rain and sand erosion ceramic protection.

The fairing is mounted onto the structure with mechanical fixing devices.

3.3. The rear fairing

The rear fairing is made of carbon/epoxide. It is mounted onto the structure with mechanical fixing devices.

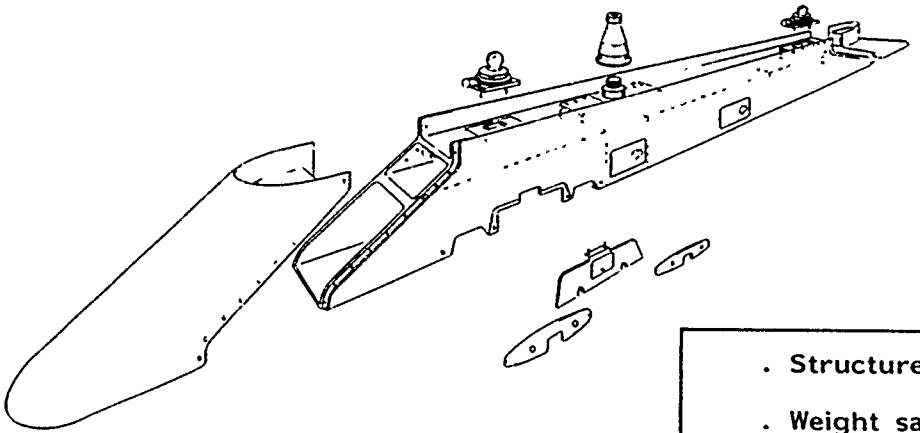

ALKAN

- Structure weight = 34 kg
- Weight saving compared with light alloy structure = 35 %

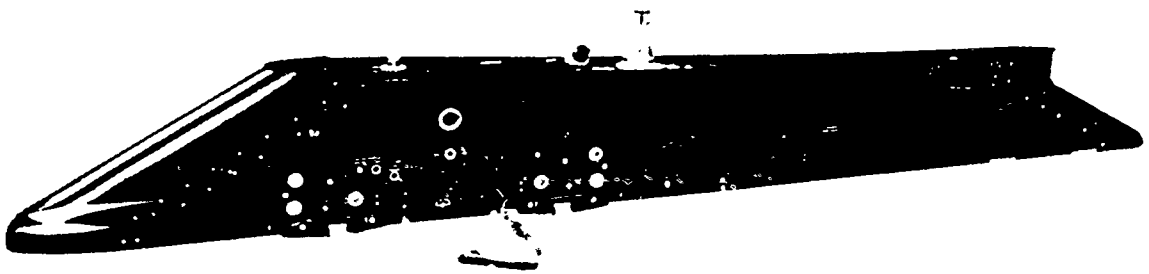

CARBON FIBER PYLON

COMPLETE CARBON FIBER STRUCTURE WITH SEPARATE FRONT AND REAR FAIRINGS

4. GROUND TESTS

4.1. Static tests

Several types of fixing devices to the aircraft were tested using the five pylons which were manufactured for the static tests.

The chosen load case was that of the MIRAGE 2000, as it is the most demanding for the attachment to the aircraft.

All the tests were made with acoustic emission (EPA system).

The influence of the wing flexibility on the pylon was specially designed. Underwing tests were made up to n = 0.8 of the chosen load case. The pylons underwent, in addition, n = 1.5 of the chosen load case on rigid frame.

The internal supports of the pylon have been modified to obtain a greater rigidity (30 %) along My as compared to that of the metal pylon, whereas the rigidity along Mx was fairly close.

4.2. Fatigue Tests

One of the pylons (N° 004) was used to validate the resistance of the structure to fatigue. This structure was placed in a climatic chamber and a hydraulic system for the application of loads (Z and Y) was associated to it. The temperature ranged from - 40 °C to + 70 °C with a succession of humid (95 % RH) and dry periods (0 % RH). The test lasted six months. The structure underwent 40,000 load cycles, each one representing 1 hour of flight of the MIRAGE 2000.

This test was carried out under monitoring by acoustic emission.

After this test the structure was checked on a static test bench. No loss of performance was measurable.

On the other hand, and separately, the mechanical fixing devices used to fix the pylon to the aircraft have been validated. They underwent 17,000 load cycles along Z and 22,000 combined load cycles along Z and Y.

4.3. Flutter tests under the wings

Two pylons were mounted under the wings of a MIRAGE III and 400 and 700 kg bombs were loaded. The aircraft underwent vibration tests in order to determine the first flutter modes. The results have shown that the aircraft equipped with composite pylons and loads had no unfavourable behaviour which could lead to the flutter of the aircraft.

4.4. Firing tests

Ground check firing tests were carried out. The firing results show that the ignition time is slightly longer with composite pylons thant with metal pylons. But, as this difference is very slight (5 milliseconds), it was considered as acceptable. The pylon's mechanical behaviour was perfect.

5. FLIGHT TESTS

5.1. Rain tests

The pylons were submitted to rain tests, in flight, at the Centre d'Essais en Vol at Cazaux (France). The longest flight took place on 9th March 1986. It lasted 17 minutes in the rain, 12 of which at 500 Kt. The front fairings were not damaged during this flight, nor during the following ones.

5.2. Structural tests

The structural tests, in flight, took place at the Centre d'Essais en Vol at Istres (France).

Two programmes were carried out :

- The first one, with pylons n° 005 and 006, between 6th January 1986 and 22nd September 1987,
- The second one, with pylons n° 007 and 009, between 26th October 1989 and 15 July 1990.

All the pylons underwent ultra-sound identification tests as well as a static validation test. Modifications had been made to pylons 007 and 009. They essentially concerned, on the front, an elastic fixing device to the aircraft and a main attachment device which improved the rigidity of the structure. All these pylons were equipped with automatic control instruments, such as strain gauges, vibration and displacement sensors.

The flight tests aimed at opening the range of store of the ALKAN 9020 composite pylons, on the MIRAGE III auxiliary aircraft, by loading them progressively with :

- 125 kg bombs,
- 250 kg bombs,
- 400 kg bombs,
- 700 kg bombs.

The 700 kg bomb was equipped with automatic control instruments. The stresses developed between the bomb and the pylon, as well as those between the pylon and the aircraft were measured.

Over 20 flights were made. The maximum loading conditions made with success were :

- M..... 0.95
- V..... 600 Kt
- Z..... 13,000 feet
- Rolling..... 180 °/sec
- N..... 5.5 g

6. CONCLUSIONS

Type 9020 composite pylons were flight qualified in the above defined range. Complementary flights will be undertaken with an extension of the range for 400 kg stores :

- V < 650 kt
- Z < 40,000 feet
- N < 7 g
- Mach < 1.4

The pylons are already ground and flight qualified. ALKAN has also got organized to guarantee the quality of manufacture and the acceptance test of this type of structure. It is therefore possible to envisage the use of this type of structure on combat aircraft. This is why ALKAN suggests, for the RAFALE, composite material structures.

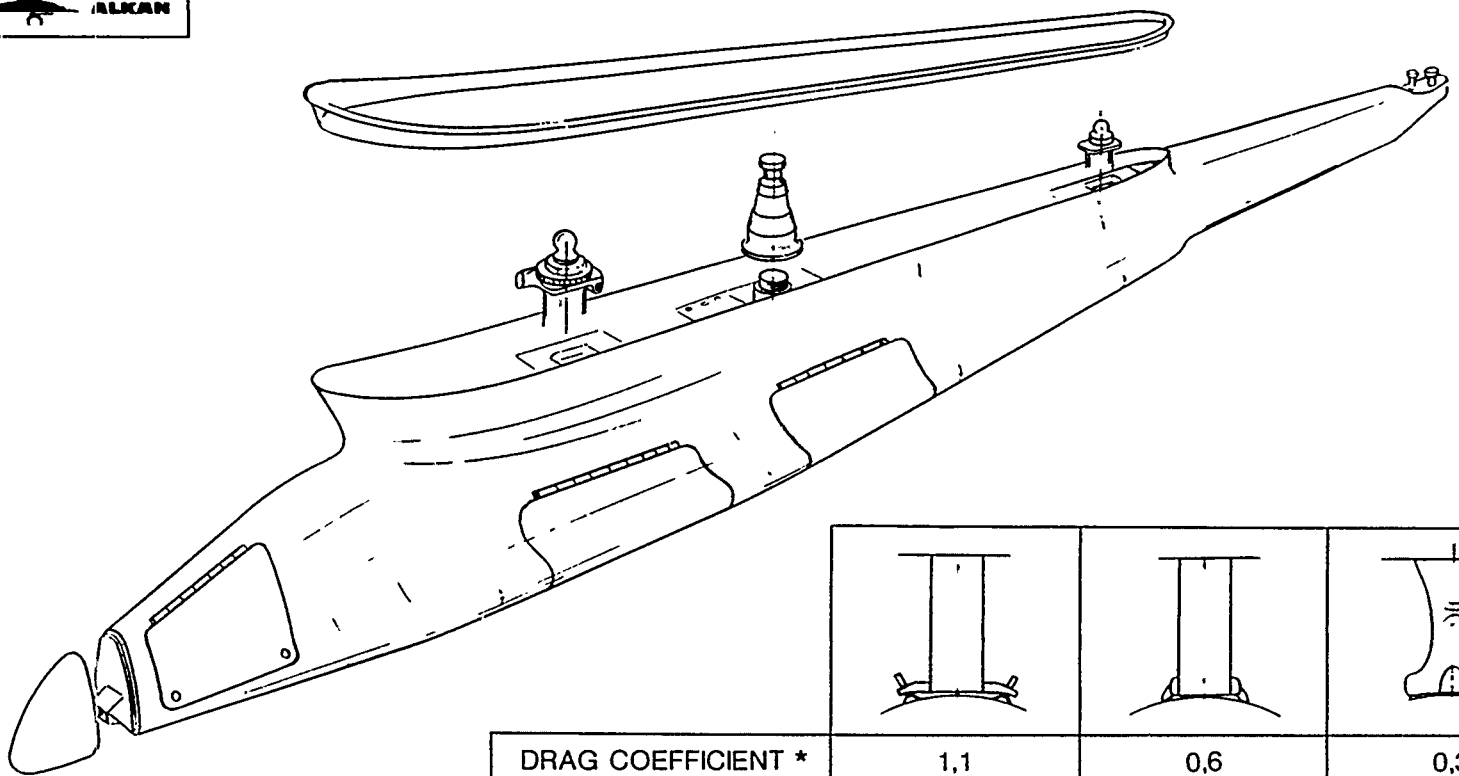

DRAG COEFFICIENT *	1,1	0,6	0,3
AIRCRAFT	MIRAGE F1	MIRAGE 2000	RAFALE

* From HOERNER

NEXT GENERATION PYLON

The gain in weight is foreseen to be 30 kg per pylon (i.e., approximately 200 kg per aircraft). Furthermore, new manufacturing methods let us envisage more and more aerodynamic and stealthy shapes. Finally a cost analysis of the structure has shown that such structures would not cost more than metal structures.

B. PNEUMATIC EJECTOR RELEASE UNIT

For many years, the usual technique for store separation and ejection has been to call for pyrotechnical energy ensured by electrically energized cartridges. This technique has been widely described and experimented and although improvements have been implemented, well known disadvantages have never been overcome.

These drawbacks are specially restricting in :

- Operational use :

Cartridge combustion is a fast chemical reaction which involves a steep pressure rise.

Forces applied on the store, when ejected, are linked to the gas pressure curve and therefore have the same variations. The result is that high reaction forces are encountered at the beginning of the ejection phase and, consequently, high accelerations are applied to the store.

- Servicing and maintenance :

Corrosion of gas-exposed parts involved in the pyrotechnic sub-assembly calls for either costly corrosion-resistant materials or frequent cleaning of these parts.

In order to fulfil the modern operational requirements, a study of alternative energy sources has been conducted ; its main characteristics would lead to :

. almost maintenance-free unit,
. improved and reliable ejection characteristics,
. ground operation safety,
. high performance reliability.

Following this study, ALKAN has developed an Ejector Release Unit operated by pneumatic energy provided by a gas storage container.

When energized, the electrovalve releases the pneumatic energy and gas is routed to the ejection pistons through two adjustable regulators ensuring :

- an output pressure almost independent from the input pressure ; constant ejection characteristics are achieved regardless the temperature (see figure 3) ;

- an adjustment of the ejection parameters allowing stepless thrust settings for both pistons for pitch control or variable flat ejection characteristics (see figure 2) ;

- a drastic improvement of ejection velocities and the use of a clean gas allow an active control of the gas flow. Therefore, when compared to pyrotechnic E.R.Us characteristics :

  ---> for a given reaction force, pneumatic E.R.U. ejection velocities are higher,
  ---> for a given ejection velocity, pneumatic E.R.U. reaction forces are lower (see figures 4 and 5).

PNEUMATIC E.R.U.

BLOCK DIAGRAM

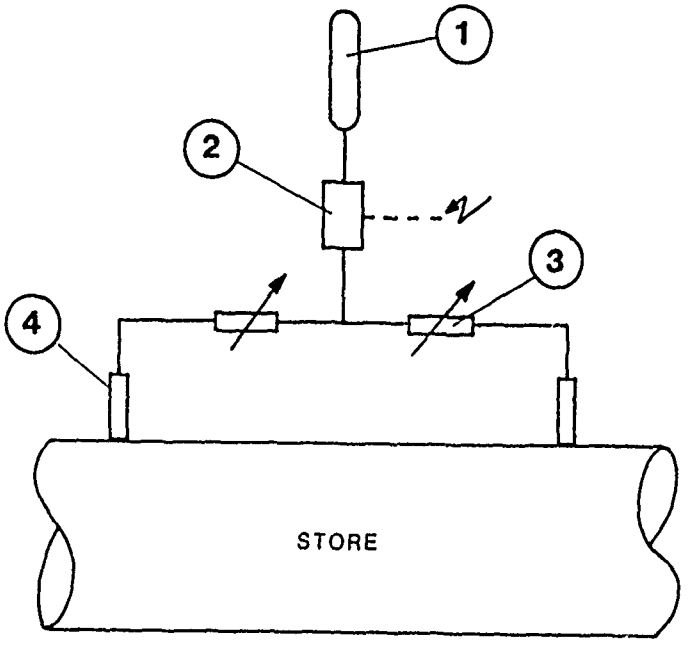

Fig. 1

1 - GAS STORAGE CONTAINER
2 - ELECTRO VALVE
3 - REGULATORS
4 - EJECTION RAMS

At both ends of the E.R.U., three-stage pistons connected to the egulator outputs impart the pneumatic energy to the store.

These parameters can be controlled either manually on the ground or remotely in flight.

This possibility to have the ejection parameters vary in flight is a new advantage offered to aircraft manufacturers. They can totally master the ejection conditions and put them under the control of the aircraft operations.

The pneumatic energy source is a bottle of 1/3 litre under a pressure of 350 bars (5000 psi). These volume and pressure conditions allow the ejection of a 250 kg store (500 lbs) at the same speed as that which is obtained with a pyrotechnic ejector.

The value of the pressure is due to the existence, on most NATO bases, of pressure boosters which can supply 300 to 350 bars. In terms of interoperability, the use of pneumatic energy is therefore perfectly compatible with the Air Force requirements.

Reloading conditions

The design of the pneumatic E.R.U. integrated in a pylon made of composite materials must be such that is allows :

- either an easy removal of a gas storage container to be exchanged with a full container,
- or the "in situ" filling of this container.

It was imagined, however, that the reloading of this container could be done during the flight without the need of any manual operation. The idea of an embarked miniature air booster was developed and will soon be experimented.

The advantage of this component is double :

- allow the refilling of the compressed gas bottle as soon as a store has been ejected and, hence, be available for another ejection.
- obtain a constant pressure in the bottle at any temperature by combining a pressure sensor and a valve to the pressure booster so that the pressure can be increased when the temperature decreases, or reduced when the pressure increases.

One should noticed that, under these conditions, the presence of regulators is no longer an absolute necessity.

PNEUMATIC E.R.U. (1405)

EJECTION CHARACTERISTICS

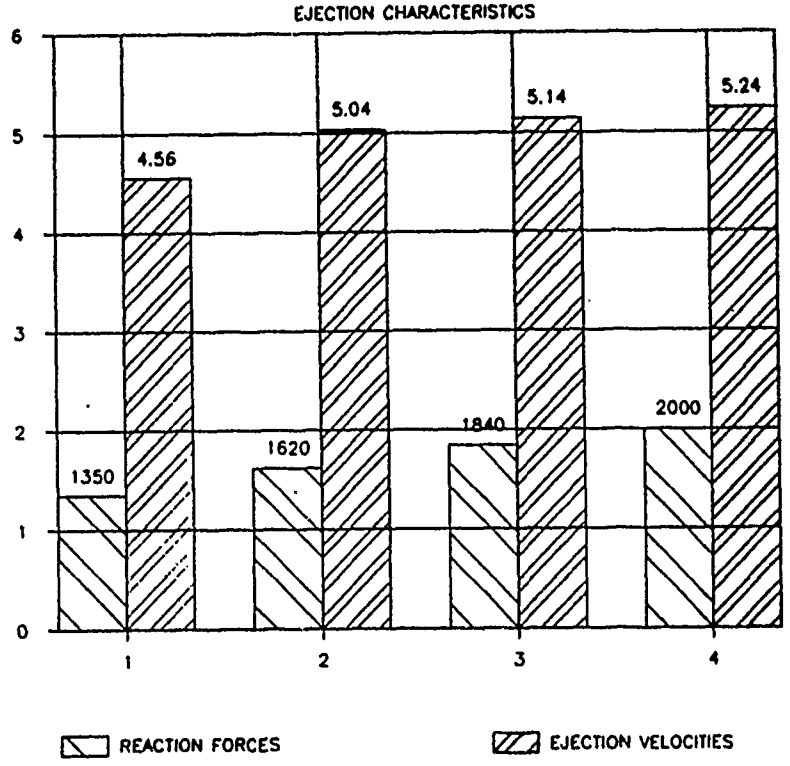

Fig. 2

PNEUMATIC E.R.U. (1405)

EJECTION CHARACTERISTICS

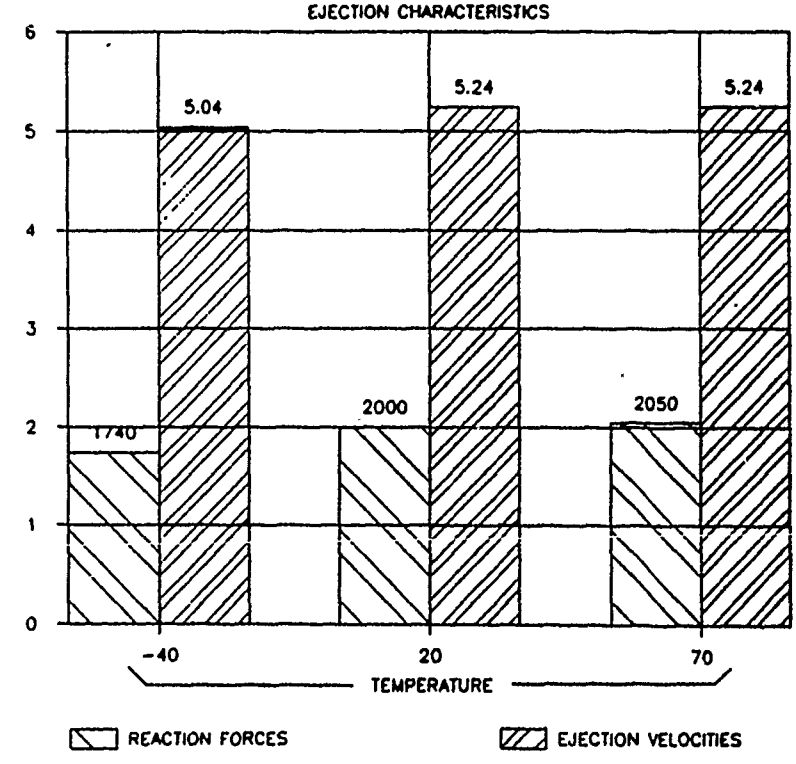

Fig. 3

PNEUMATIC E.R.U. (165B)

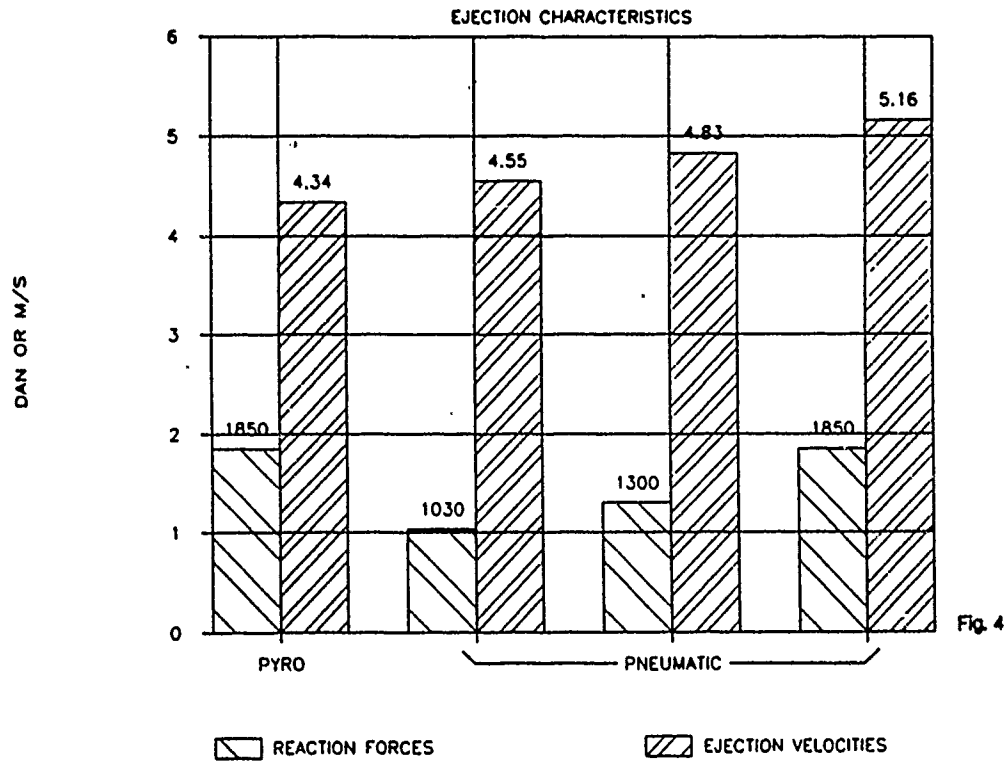

Fig. 4

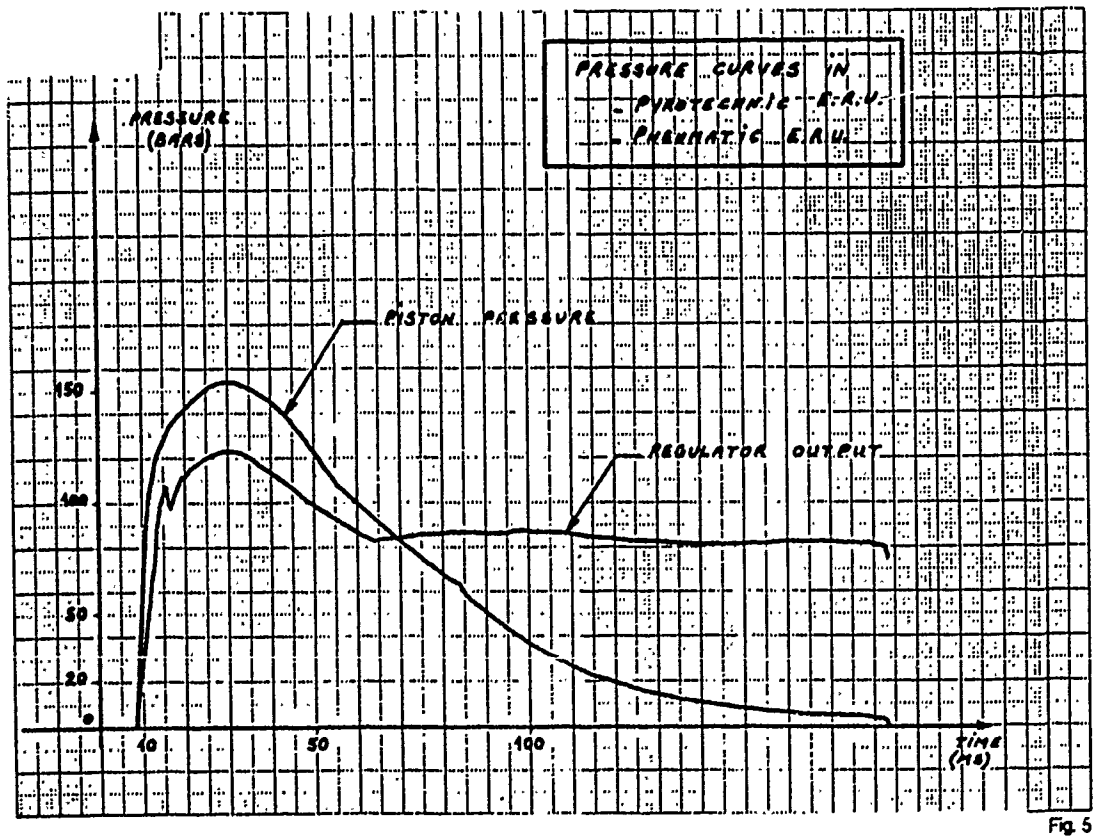

Fig. 5

Application to multiple adaptors

The use of pneumatic energy is also favourable when several ejectors are associated either in a multiple store adaptor or in a "conformal".

A bottle of sufficient capacity can supply several ejectors in sequence. A single source of energy is sufficient.

Conclusion

Pneumatic energy which is characterized by :

- a clean gas which suppresses the cleaning and maintenance operations,
- an adiabatic release for a notable performance increase on the ejection characteristics,
- easiness of storage and filling of the used bottles,
- an operational cost which is almost nil,

will probably be the energy which will be used to power the ejectors of the 21st century.

This century has already begun for the "RAFALE" for which this energy has been chosen.

About the authors :

Philippe GUITAUT graduated from the **"ECOLE NATIONALE D'INGENIEURS DE BREST"** (FRANCE) in 1973.

He started work with THOMSON-CSF as a design engineer in the Airborne radar Division.

He joined ALKAN in 1978 as a project engineer in charge of the design and development of ejector release units and wing pylons.

He is now the Carriage Equipment Division Manager of ALKAN.

Jean-Pierre MATTEI

Mr Matteï joined R. ALKAN Company in 1973 to participate in the widely diverse engineering projects undertaken by the Company most of which were French Ministry contracts for military and associated equipment.

In 1979 he was assigned the responsibility of the design, the manufacturing processes and the testing of composites structures, mainly made of Carbon-Epoxy.

At present he is the Chief of Composite Material Division.

Launcher Technology for Internal Carriage

Lt. James P. Solti
and
Diane M. Wright

Air Force Armament Laboratory
Flight Vehicles Branch
Eglin Air Force Base, Florida

Abstract

To prepare for the high density threat projected in the future, the USAF must improve aircraft performance and survivability. Internal carriage of weapons can provide significant improvements in these areas. However, internal carriage poses unique launching difficulties. The near cavity airflow associated with a weapons bay is severe and control of the missile is necessary until the missile is outside of the bay. The technology used to launch from weapons bays in the past is unacceptable for the high Mach and high g environment of advanced aircraft. To further complicate the problem, some air-to-air missiles can be eject launched while others must be rail launched. To allow for weapon loadouts with any mix of air-to-air missiles, a dual mode, eject/rail launcher is required. Currently, no existing single launcher is capable of both eject and rail launch.

Under the Advanced Missile Eject Launcher Technology (AMELT) program, the Air Force Armament Laboratory has developed technologies to safely eject launch air-to-air missiles from internal weapons bays. A launcher concept was designed, fabricated, and laboratory-tested to demonstrate the required technologies. The AMELT launcher consists of scissor-like linkages powered by an 8000 psi hydraulic servoactuator. The AMELT hardware provides tri-axial missile restraint for 19 inches of a 22-inch stroke, variable eject velocities to 40 feet per second, and variable nose-down pitch rates to 1.5 radians per second. The AMELT program addressed some of the supportability problems encountered with loading and maintaining launchers in weapons bays. The AMELT hardware has automatic hook latching and swaybracing as well as remotely-operated umbilical connect/disconnect, launcher safe/arm, and missile download.

To expand on the AMELT design and provide some of the basic technologies for the dual mode, eject/rail capability, the Dual Mode Launcher (DML) program has been established. The DML concept will be capable of eject launching an AIM-120 missile and rail launching an AIM-9 missile with no reconfiguration to the launcher. The launcher will be required to interface with the suspension hangers and electrical connectors of both missiles. To minimize size and weight, short rail technology will be developed under the DML program. The existing AMELT hardware will be modified to incorporate this advanced "short rail". The AMELT control system will be modified to ensure slow extension and retraction as separate events and will provide for prolonged extension to enable the missile's seeker to lock onto the target in the rail mode. Along with these new technologies, the DML concept will retain the AMELT capabilities in the eject mode. Similar to AMELT, the DML will be designed, fabricated, and laboratory-tested to demonstrate the technologies and performance.

Introduction

Studies have projected extremely high threat densities for future air combat. In order for the USAF to successfully accomplish its mission, aircraft performance and survivability must be improved. One approach is to carry air-to-air missiles internally to reduce the performance and survivability degradation associated with external carriage. This concept, however, is very different from the way we currently carry and launch missiles from inventory aircraft. Historical data bases were queried and the technology voids were identified. It was concluded that several areas of launcher technology must be developed to support this internal carriage configuration. This paper documents the technology base research and the resulting technology challenges yet to be accomplished.

Background

The F-102 and F-106 aircraft were designed with internal weapons bays. The United States Air Force Museum, in Dayton Ohio, was a valuable source of historical data on these century series aircraft. The museum archives contained a collection of technical documents, performance data, and news clippings of the subject aircraft. Both aircraft were capable of carriage and launch of AIM-4 Falcon air-to-air missiles. During launch, the AIM-4 hangers were designed to slide off a rail when the motor was ignited. The F-106 could carry four in a two-by-two, tandem arrangement. The forward two missiles and their respective rails were lowered into the airstream on a single pallet. The aft two could be lowered individually on trapeze-type launchers (Figure 1). Both the pallet and the trapeze mechanisms were powered by 3000 psi pneumatics and both swung through an arc, moving the missile forward during extension. This trapeze motion results in a long bay to accommodate the forward displacement. The F-102 aircraft carried and launched six AIM-4 missiles. The F-102 had a center fuselage bay and two shoulder bays. Each of which could carry two AIM-4s in tandem. A bi-fold mechanism, operated by 3000 psi pneumatics, lowered the missile in a purely vertical motion (Figure 2). This vertical stroke allowed the aircraft designers to make the bay shorter. The launcher systems for both aircraft were large and cumbersome.

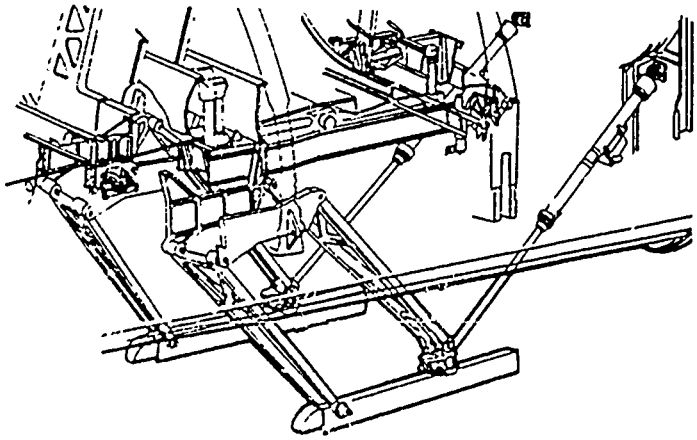

Figure 1. F-106 Aft Launchers (Extended)

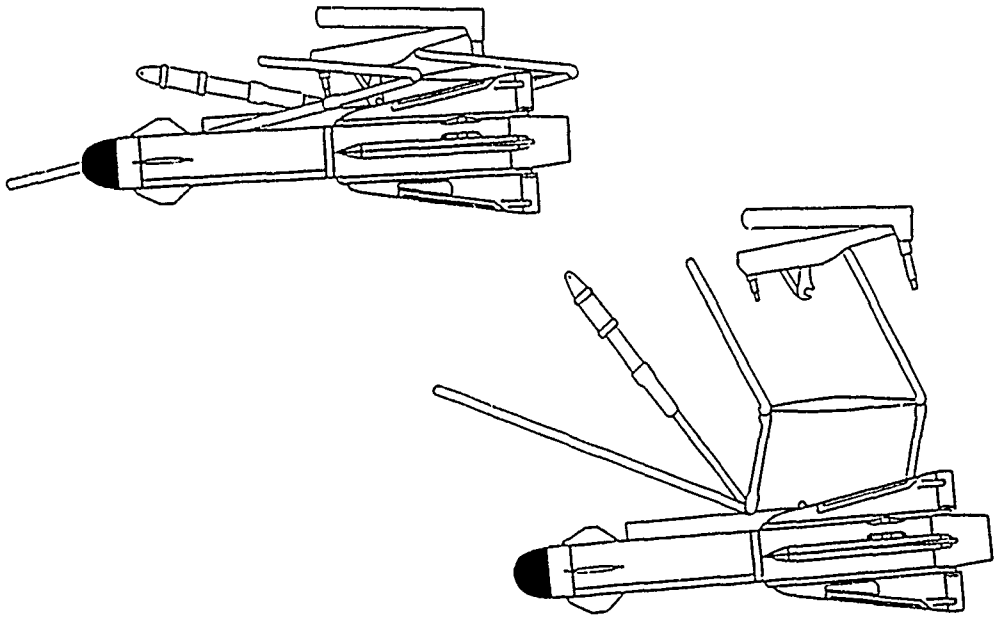

Figure 2. F-102 Launcher (Retracted and Extended)

Some of the attractive features of these historical launching systems should be considered for future launchers. The non-pyrotechnic power source for reduced maintenance and the vertical stroke which reduces the length of the bay are both desirable characteristics. However, in general, it was determined that these historical concepts are unacceptable for the high Mach and high g environments of future fighter aircraft. The F-102 and F-106 launchers, already large and heavy, would require resizing to structurally support the current AIM-120, Advanced Medium Range Air-to-Air Missile (AMRAAM), which is nearly twice the weight of the AIM-4 missile. Additionally, these launchers were limited to rail launch operation. Some of today's missiles are compatible with eject launch concepts, which push the weapon away from the aircraft. The eject mode of operation can be advantageous for internally-carried weapons since it limits the time that the bay doors are opened. The opened doors significantly reduce the aircraft performance and survivability. Ultimately, a single launcher with dual mode, eject/rail, capability would be the most desirable for future aircraft to allow for maximum flexibility in weapon loadout. This provides for the carriage of both eject and rail launched missiles on a single launcher and minimizes the time between missions since replacing the launcher is not necessary.

For advanced aircraft to effectively release internally-carried weapons in the projected flight envelopes, launcher technology must be substantially improved. One of the current AMRAAM eject launchers, the LAU-106, utilizes explosive cartridges which supply hot gas pressure to the two ejector pistons. The pistons stroke 7.5 inches to push the missile away with typical end-of-stroke velocities of 21 feet per second and nose-down pitch rates of .42 radians per second. The LAU-106 also is equipped with a

forward yoke which enables some limited yaw control of the weapon. The performance characteristics of the LAU-106 are acceptable for external carriage, but, as discussed below, will be unacceptable for separation of internally-carried weapons.

A significant amount of resources have been expended to define the airflow around aircraft. The Weapons Internal Carriage and Separation (WICS) program has focused its efforts on the airflow specifically generated in the vicinity of a weapons bay to identify the unique problems associated with launching internally carried weapons. The program objective was to investigate and determine the bay environment for a wide range of bay sizes and configurations. Extensive wind tunnel testing was performed using a generic bay. Metal blocks and missile models were used to provide variations in bay dimensions and configuration changes. Conclusions from the WICS program have indicated that the inner cavity airflow associated with weapon bays is severe in terms of aerodynamic and acoustic levels. Typically, the airflow enters at the forward wall of the weapons bay, travels along the ceiling, and exits at the aft wall of the bay. The airflow pattern forces the missile's nose up and tail down. This missile attitude can be disastrous if it is not restrained or corrected. Therefore, the launcher must control the missile and maintain the proper attitude until it is outside of the weapons bay's turbulent environment. The LAU-106 launcher cannot provide this control. Additionally, while the bay doors are open, a standing acoustic wave can travel between the forward and aft walls causing destructive sound pressure levels. Consequently, the launcher mechanism must extend and retract quickly to minimize the time that the doors must be open.

Discussion

Based on the WICS data and advice from knowledgeable aircraft designers and weapons separation experts, performance requirements were defined. To ensure a safe and successful separation from a bay, the launcher must provide end-of-stroke velocities of 30 to 40 feet per second and nose-down pitch rates to 2.0 radians per second. The launcher must also maintain tri-axial control of the missile throughout the stroke. The missile must be extended approximately one missile diameter below the mold line of the aircraft to avoid the interference flow field. The launcher must operate quickly. A maximum of 500 milliseconds from first launcher motion to stowed position after launch was established. The Air Force Armament Laboratory initiated the Advanced Missile Eject Launcher Technology (AMELT) program in an attempt to satisfy these requirements. For proof-of-concept, the AMELT program centered around an AMRAAM-type missile and eject launch was the selected launch concept.

The AMELT program objective was to develop technologies to safely eject launch air-to-air missiles from internal weapons bays. A launcher concept was designed, fabricated, and laboratory-tested. The AMELT launcher consists of a pair of scissor-like linkages powered by an 8000 psi hydraulic system. Figure 3 shows the AMELT launcher in the retracted position and Figure 4 the extended position. Two nitrogen-filled, piston-type accumulators supply pressurized hydraulic fluid to a servoactuator upon the launch command. The servoactuator, located between the accumulators, forces the drive body down the support rail. The two large support arms, suspended

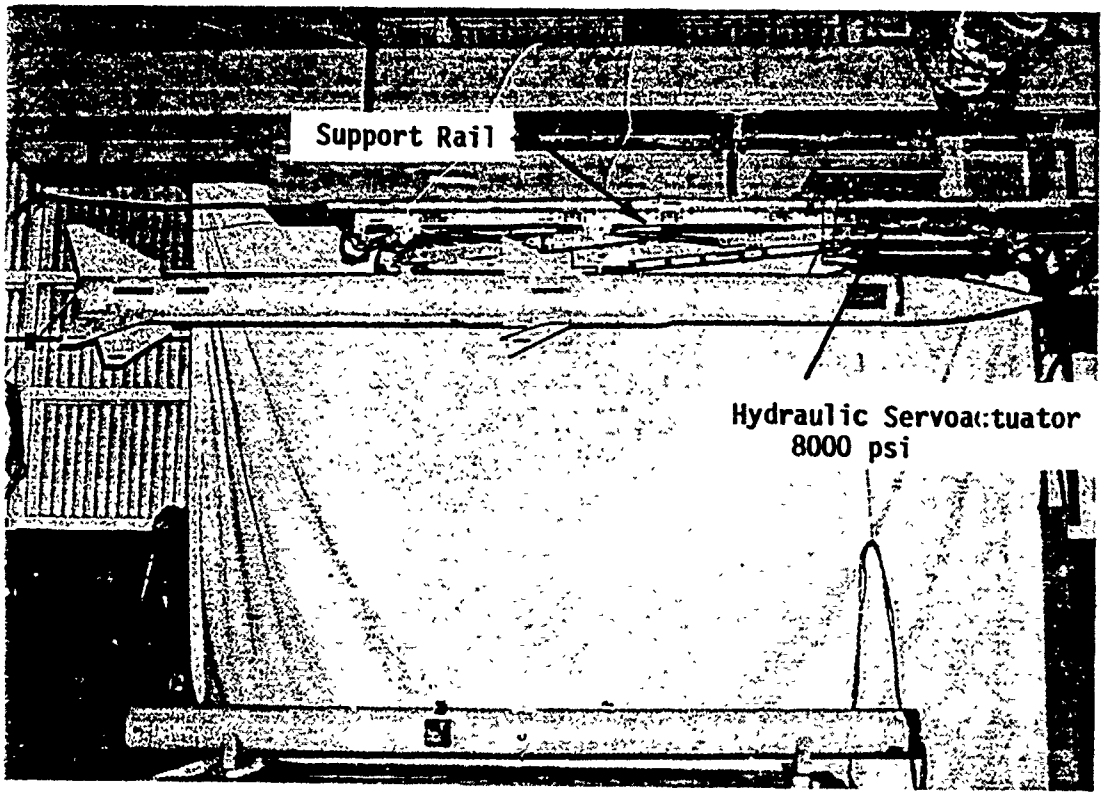

Figure 3. AMELT Launcher/AMRAAM Missile - Retracted

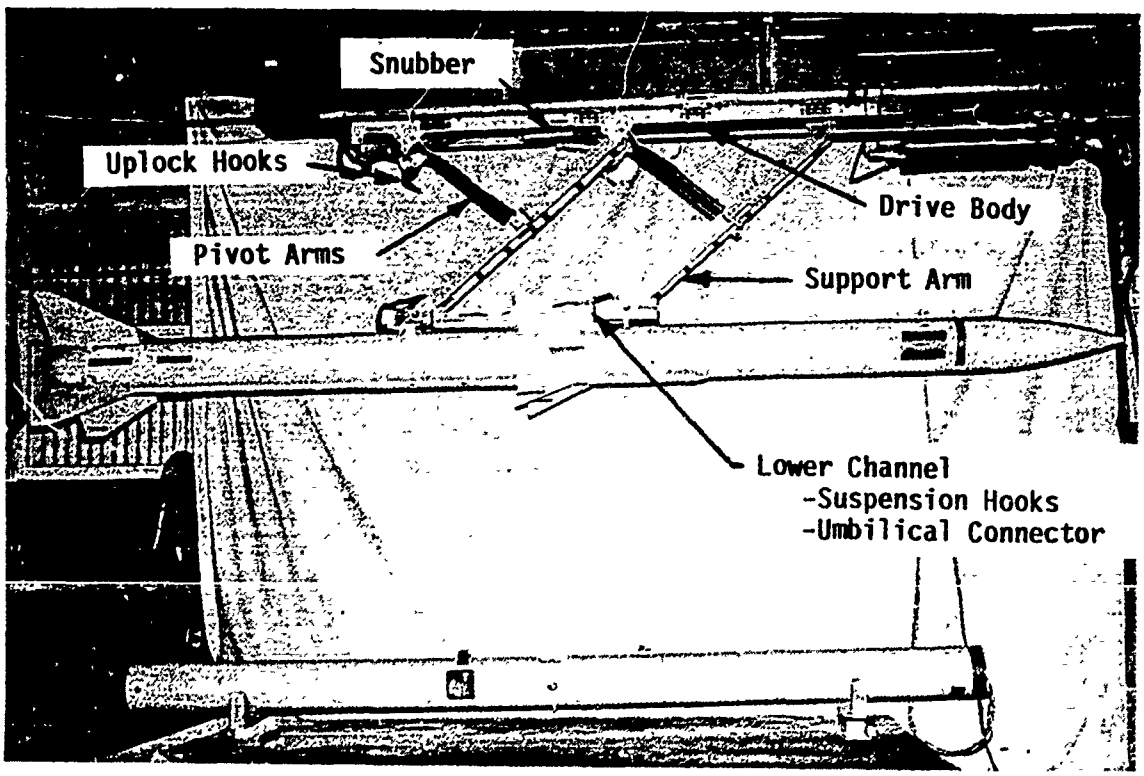

Figure 4. AMELT Launcher/AMRAAM Missile - Extended

from the drive body, rotate about four short pivot arms. The geometry is such that the missile extends in a purely vertical motion. Shown in Figure 5, the lower channel, which is supported by the two large arms, contains the hooks, linkages, umbilical and a small drive motor. When extended through 19 inches, the hook linkages are mechanically and dependently forced open. At 22 inches, the launcher mechanism is decelerated by an external snubber and the missile is ejected from the aircraft. The AMELT hardware has a series of wedges which bear on the missile hangers to provide tri-axial missile restraint. This tri-axial restraint, variable eject velocities to 40 feet per second, and variable nose-down pitch rates to 1.5 radians per second were demonstrated in a ground test program.

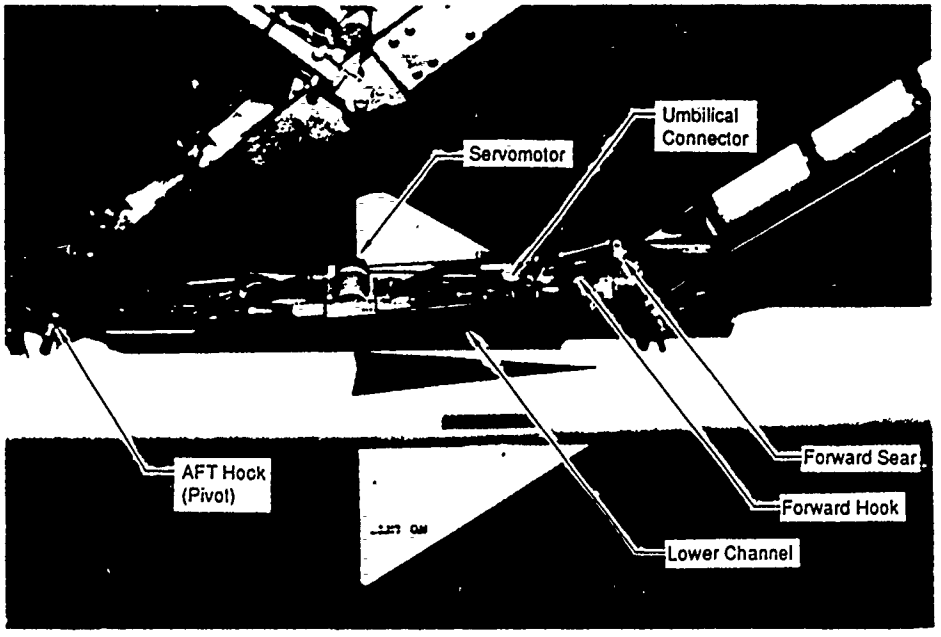

Figure 5. AMELT Lower Channel

During the AMELT program, some of the current launcher supportability, loading, and maintenance problems were also addressed. Standard eject launchers, including the LAU-106, use pyrotechnic impulse cartridges to separate the weapon from the aircraft. The carbon and debris released from these cartridges clog the venting tubes and require the equipment to be cleaned as often as once every five ejections. To alleviate this problem, the AMELT hardware is operated by an all hydraulic power supply. Additionally, standard missile launchers require access for installation and inspection of the impulse cartridges. A hydraulic system has no such requirement, making it more desirable for a bay environment where access is limited. Hydraulics also eliminate the logistic problems associated with storage, inventory, and accountability of pyrotechnic devices.

With respect to performance, cartridges impart a high impulse load onto the missile often causing undesirably high g loads. Hydraulic systems offer the designer the ability to control the input force signal. A hydraulic system can be tailored to produce a near constant input force signal. Properly designed, the launcher can provide higher end-of-stroke velocities, lower g loading, and offer greater control. During the AMELT test program, it was shown that the input force curve should have an initial ramp to reduce the impact loading on the linkages and eliminate the box-car effect. This provided the most stable separations. A feedback control system can be incorporated into the hydraulics, creating a "smart launcher." The AMELT launcher has a feedback control loop which enables the launcher to increase the velocity throughout the stroke if less than the desired end-of-stroke velocity is sensed. AMELT, however, cannot slow the launcher linkages if the mechanism is moving too quickly.

Reliability and supportability were also considered very important in the AMELT program. Due to the space and visual limitations of a bay, "blind loading" technologies were developed. The AMELT hardware has automatic hook latching and swaybracing for ease in loading the missile. The missile is loaded onto the retracted launcher and the missile hangers trip the hooks which can be independently latched. Additionally, umbilical connect/disconnect, launcher safe/arm, and missile download operations are controlled from a panel which is remote from the launcher mechanism. A small drive motor in the lower channel performs the umbilical and download functions. The AMELT launcher has proven that these technologies are viable for improved loading and downloading in a weapons bay.

The AMELT program was successful in demonstrating the basic technologies required for the eject launch of internally-carried air-to-air missiles. However, some missiles cannot be eject launched because of the impact loads experienced during ejection or because they need to be in the airstream to track the target prior to launch. These missiles must be rail launched. Ideally, to allow for loadouts with any mix of air-to-air missiles without swapping launchers or reconfiguration, a dual mode, eject/rail launcher is desired. No existing single launcher is capable of both eject and rail launch. With this in mind, the Air Force is establishing the Dual Mode Launcher (DML) Technology program to fill this void. The DML hardware will be designed to retain the AMELT eject performance. Similar to the AMELT hardware, the DML launcher must physically restrain the missile in three axes during extension. In the eject mode, the launcher must be capable of fast extension and retraction as one continuous motion (less than 500 milliseconds). In the rail mode, the launcher must extend more slowly (approximately one second) and hold the missile below the aircraft to allow the missile's seeker to lock onto the target (at least ten seconds) before launching. The launcher must be capable of slow retraction (approximately one second) if the missile is not launched by the pilot or fast retraction without the missile. To further simplify loading, the DML should be loaded in the extended position and retract the weapon into the bay under its own power.

For proof-of-concept, the DML will be designed for eject launching an AIM-120 missile and rail launching an AIM-9 missile with no reconfiguration to the launcher. The launcher will be required to interface with the missile hangers and electrical connectors of both missiles. This will be an

engineering challenge. Each missile has three suspension hangers and an electrical connector. The forward hanger on each missile is essentially the same. However, the remaining hangers are physically different and are spaced differently. The electrical connectors are also different in configuration and location (Figure 6).

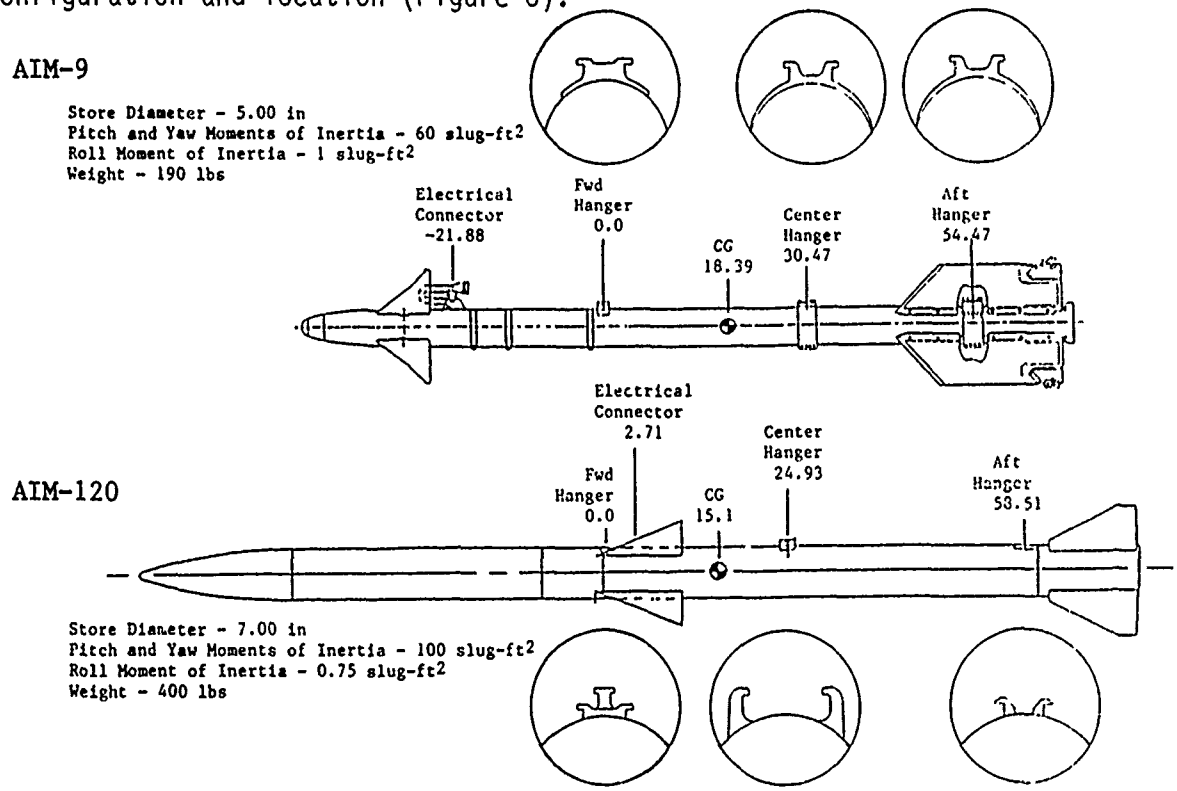

Figure 6. AIM-9 and AIM-120 Missile Physical Characteristics

To minimize size and weight, revolutionary rail technology will be explored. This technology will include a short rail concept which is less than the existing rail length of 93.3 inches. This concept will allow for the carriage of the AIM-9 missile using only two of the three available hangers. The shorter rail length will minimize the weight of the lower channel and reduce the loading on the launcher when extended. The existing AMELT hardware will be modified to incorporate this advanced "short rail." A major emphasis of the DML program will be investigation of the AIM-9 performance during launch from the shorter rail. The program will analyze the structural integrity of the missile when supported by only the forward and center hangers. Analysis of the aerodynamic stability and performance capabilities of the missile are also critical. Soft eject launch technology for the AIM-9 will also be examined. Presently, the missile is held on the rail until the rocket motor reaches a specified thrust to override a mechanical detent, allowing the missile to be propelled down the rail. It is hypothesized that the missile could be extended down into the airstream; locked onto the target, and held by the launcher until the missile motor reaches the detent thrust. Then, the missile could be slowly ejected (1 to 2 feet per second) from the aircraft. This vertical eject force would allow the missile to fly safely away from the aircraft. Investigation of the maximum eject velocity for maintaining seeker lock-on will be critical.

Conclusion

The vast advancements of aircraft and missile systems, combined with ever changing mission requirements and threats require tomorrow's missile launchers to have improved performance, reliability, and maintainability. Failure to successfully launch a missile could easily result in the loss of life and catastrophic loss of a multimillion dollar aircraft. Though a difficult task, development of a DML concept is critical for advanced aircraft weapons systems. The AMELT and DML programs have taken the initial steps toward filling existing technological voids. These programs have established a good technology base and provided risk reduction for future development of these technologies.

ABOUT THE AUTHORS

James P. Solti, 1Lt, USAF

B.S. Engineering Sciences, U.S. Air Force Academy, CO. Lt Solti is a project engineer responsible for the development and testing of carriage and release technology. He is assigned to the Weapons Integration Technology Section, Flight Vehicles Branch, Air Force Armament Laboratory, Eglin Air Force Base, FL.

Diane M. Wright

B.S. Mechanical Engineering, University of Dayton, OH. Ms Wright is a program manager responsible for the development of carriage and release technology for advanced weapon systems. She is assigned to the Weapons Integration Technology Section, Flight Vehicles Branch, Air Force Armament Laboratory, Eglin Air Force Base, FL.

UNCLASSIFIED

Cleared for Public Release

THE USE OF MISSILE LAUNCHERS WITH DETACHABLE RAILS TO PROVIDE A NOVEL MEANS OF MISSILE JETTISON

by

JOHN R PEARCE

(FRAZER-NASH DEFENCE SYSTEMS LTD)

AND

HOWARD A TORODE

(ROYAL AEROSPACE ESTABLISHMENT, FARNBOROUGH)

PART I - CONCEPTION AND DESIGN DESCRIPTION

PART II - CFD MODELLING AND ASSESSMENT TESTING

PART I COPYRIGHT

RANDALLS WAY, LEATHERHEAD, SURREY KT22 7TX
Tel: LEATHERHEAD (0372) 379717 Fax: 0372 377879 Telex: 929947G

PART II COPYRIGHT

PART I - CONCEPTION AND DESIGN DESCRIPTION

I.1 This paper describes the implementation of what we believe is a new and novel means of missile jettison from rail launchers. This capability arises from a number of unique features inherent in the design for the Common Rail Launcher and it is appropriate to first outline the design of the Common Rail Launcher and to consider how its unique features both contribute to the problem of store jettison as well as providing a unique solution.

I.2 The Common Rail Launcher (CRL) has been privately developed by Frazer-Nash Defence Systems Ltd resulting in a rail launcher meeting the requirements of RAE Specification WE2188. In its most basic, this specification requires a rail launcher that can interface a wide variety of missiles onto a wide variety of aircraft. The novel concept of rail jettison emerged during the PV phase, its further development and testing being carried out under a contract from Attack Weapons Department, RAE Farnborough.

A truly modular design approach has been adopted as can be seen (fig 1) with various gas system options, ECM unit options and appropriate modules to suit various missiles. Fundamental to the design is a quickly detachable rail which enables different missile suspension lug geometries to be accommodated.

Another cornerstone of the design is the use of a monolithic body extrusion (fig 2) which on its upper surface can be machined to accept aircraft suspension fittings at appropriate positions and which on its lower surface has machined a series of interlocking 'Tee' features which engage with appropriate features on the rail. The use of a hollow extrusion provides maximum available volume for power supplies, detent units etc whilst providing a simple structural element.

In addition, the use of a hollow structural extrusion for the body of CRL, together with suitable lug fittings that locate into the roof of the extrusion, offers almost infinite potential for the positioning of the mechanical and electrical interfaces between the launcher and the aircraft (fig 3). In practice the physical size of each of the interface fittings, and the need to retain sufficient material between adjacent apertures to provide structural integrity, limits the total number of apertures to a maximum of 7 or 8. Since each interface typically requires 3 apertures, it is obvious that overlaying 2, 3 or more set of interface apertures is likely to result in mutual interference or lack of structural integrity. However, practical results show that whilst it is almost impossible to meet quadruple interface requirements certain triple and many double combination can be catered for.

I.3 There is a tendency nowadays to equip fairly small aircraft with a large array of powerful weapons - to give big teeth to small aircraft (fig 4). The versatility of longitudinal mounting on the CRL greatly aids this trend enabling large MRAAM's to be positioned under small wings. However, one major problem arises when fitting large missiles on small wings (fig 5). Generally, if the missile is positioned to give adequate clearance to control surface envelopes and ground clearance lines it has to be positioned further forward than would ideally be the case. In these cases it can be difficult, if not impossible to arrange for the launcher plus missile centre of gravity to match the thrust line of the jettisoning ERU: the thrust line usually ends up well aft of the launcher-plus-missile centre of gravity resulting in unacceptable pitch-up moments preventing safe jettison. This effect is especially true with ERU's of 14 inch spacing where, even with extreme throttling, a thrust line variation of ± 5.0" is rarely available. Since the ability to jettison unserviceable explosive stores is a highly desirable if not mandatory requirement it was obvious that some way to facilitate jettison without using the ERU would greatly enhance the CRL's capability.

I.4 Two factors came together in the generation of an idea to overcome the difficulties of missile jettison from such forward mounted locations. The first was the realisation that if the jettison forces could be generated between the rail launcher and the missile they could always be made to act in the correct relative position to the missiles centre of gravity. The second was the realisation that if it was possible to reverse the rail locking motion, the result would be to decouple the missile and rail from the launcher with a fairly small amount of relative motion (see fig 6).

This was developed into a concept whereby the rail and the missile were moved rearwards to disengage the rail 'tee' features and thus "disconnect" the missile and rail from the launcher (fig 7). The mechanism that provided the rearwards motion was designed also to produce a downwards force, once the rail was disconnected, such that forward mounting of such a device would result in the imparting of a nose down pitching moment on the missile.

I.5 Unfortunately, to move both the missile and the rail back, a large number of missile to launcher interfaces need to be released or removed. Figure 8 shows a list of such interfaces. It includes all of the interfaces seen on most (if not all) of current in-service missiles - a given missile then, will have perhaps 5 of 6 out of the list. Many of these features would need to be actively disengaged to permit rearward missile motion eg the umbilical connector and both the forward and aft snubbers. To disengage or actuate all of these features, especially on a launcher which may not possess full power supplies or may be damaged in some way, the concept of rail jettison rapidly becomes impracticable.

I.6 It was then realized that the rail could be disengaged by a rearwards movement of the rail alone, without a corresponding movement of the missile. Under these circumstances the missile could be retained by the horizontal constraints and the rail would be slid backwards until the vertical coupling provided by the 'Tee' lugs, was lost. At this point the rail and missile are free to fall away downwards since none of the restraints act in the vertical direction, only the horizontal.

Figure 9 shows this point more clearly with each of the features highlighted imparting only longitudinal constraint to the missile.

I.7 With the motion of the rail now defined (ie the rail engagement stroke applied rearwards) and the need to provide a small nose down bias to widen the jettison envelope, some means of actuation is required to implement the idea. The first action is thus to select a suitable power source since this will determine the detail of the actuator. The tabulation shown in figure 10 is a list of possible power sources that were considered and scored. As may be expected for such a mechanism, which needs to be stored in the stand-by condition for many years and then needs to operate reliably and powerfully on a one-shot basis, the most suitable power source turned out to be some form of pyrotechnic cartridge.

I.8 Such a power source, acting as a hot gas generator is classically used to operate a piston in a cylinder to generate mechanical output. With all the accumulated knowledge of such actuators it is the obvious choice here, and a scheme integrating the cartridge breeches and the cylinder into one block was generated. Mounted on this block was the necessary linkage to generate the 'L' shaped motion needed.

Figure 11 shows the likely implementation of such a device which, in its non activated state, engages with the launcher rail and prevents it moving longitudinally. The linkage on the side of the unit generates an 'L' shaped motion where the first movement disengages the rail whilst the second movement, at right angles to the first, imparts a nosedown pitching moment onto the rail and missile.

I.9 Other configurations of the scheme which relied on reversing the store loading motion on conventional, integral rail launchers were also investigated. Although the actuation of such schemes was shown to be feasible, it was deemed not to be practical for two major reasons. Firstly the device required two, long stroke pannier mounted actuators and secondly, in these schemes it was necessary to release all the interfaces between the rail launcher and the missile.

I.10 Once the design of a jettisonable rail from a rail launcher was shown to be both feasible and practicable, a series of practical tests were planned by, and carried out in conjunction with the Royal Aerospace Establishment.

These tests, which explored the likely jettison envelope of the Sea Harrier will be described in Part II of this paper.

PART II - CFD MODELLING AND ASSESSMENT TESTING

II.1 GENERAL APPROACH

Aerodynamic studies formed an important part of the development cycle of the Rail Jettison system to aid the MoD funded study. Specifically, prediction work was necessary to establish design data in the following areas for the installation and flight clearance of the AMRAAM on the Sea Harrier outboard wing pylon station:

a) Installed Carriage Loads
b) Quasi Steady-State Down Rail Aero Loads during Launch
c) Jettison Trajectory (free fall and eject assisted).

The limited resources and timescale of the Frazer-Nash programme precluded any physical testing for design loads. Therefore for all of these aspects a Computational Fluid dynamics approach was sought. These modelling calculations were carried out by RAE Farnborough using the British Aerospace (MAD), SPARV Panel Code (Ref 1). The panelling techniques used took full cognicence of the needs to represent correctly the details of wing/fuselage carry over of the base flow effects (see Ref 2 and Fig 12). SPARV (Source Patch and Rig Vorticity) is a Panel method applicable to subcritical flows, which has demonstrated a considerable flexibility in this arena, and has been utilised on a very wide range of UK stores integration programmes. The ability to address all of these issues using the same computational modelling utility greatly assisted in expediting the early stages of the programme in an economic fashion.

II.2 INITIAL RESULTS COMMENTARY

II.2.1 Weapon Loads

This phase was required to demonstrate that the FN installation did not create any loading cases that were outside the missile airframe capability. Early work for the simple installed loads data showed encouraging agreement with similar carriage cases. This phase became virtually a model validation exercise since it was clearly anticipated that the conventional external design of the CRL launcher unit would have only a minor effect on weapon carriage loads compared to the aircraft overall flowfield.

Encouraged by the success of the validation process, further missile loads were calculated at 'down rail' positions in quasi steady flow. The data gathered during this phase was necessary to define fully the launch environment for more comprehensive simulations of the full dynamics of the aircraft/launcher/weapon system during launch (fig 13).

Results which have subsequently become available in UK for this case have shown good agreement with these prediction.

II.2.2 Jettison Trajectory Prediction

One of the strengths of the SPARV utility is its ability to be coupled to a 6 degree of freedom simulation for modelling of release trajectories (known as TSPARV). This utility has been used to predict 'rail jettisons' over a wide flight envelope (figs 14 and 15). While sufficient runs were carried out within the conventional envelope to test the model and establish a working database, the emphasis of this exercise was placed on lower speed regimes where it was expected that a jettison would offer improved operational safety.

These configurations naturally led to significant flight incidences up to the point where a Harrier configuration would normally become semi jet borne. Gravity releases showed acceptable trajectories at most conditions tested. However, at higher incidences, and particularly lower speeds, there developed a tendency to hesitate at the released pitch attitude before finally pitching down in a stable fashion.

II.3 THE NEED FOR PRACTICAL TRIALS

At this early stage of the programme it was considered that these provisional trends required more serious consideration. The aim of this rail design was to establish the ability to jettison the weapon at all flight conditions including the Harrier's unique capabilities in jet borne and semi jetborne flight where loading becomes critical in an emergency situation.

The effects of the aircraft's jet efflux on the flowfield in the region of the weapon have not been evaluated and were not capable of representation within the available CFD codes. Early studies by RAE have shown that jet induced loads on a statically suspended weapon could be substantial (ref 3), but the implication for release trajectory have not been studied. It was therefore decided to mount a wind tunnel trial to evaluate this particularly novel aspect of the capability and to establish greater confidence in prediction data.

The number of configuration parameter options in the trial was large: including stores configuration, flap setting, nozzle angle, and jet velocity. Added to these was the option to use the FN ejection pitch thruster. All these combined with the basic parameter set of tunnel speed, model incidence and sideslip required a highly critical selection process of the cases to be investigated. This option set was further complicated by the need to establish repeatability of results, known historically as a limitation of this sort of trial. Our compromise was to trial each data point at least 3 times to evaluate consistency.

The programme, as completed, investigated 30 combinations of configuration and flight condition (see figure 17). Note that most cases were trialed above the appropriate level flight incidences for given airspeeds to anticipate a failure condition when the aircraft would find itself in a dynamic manoeuvre at high transient incidence. A typical release is shown in figure 18.

Detailed analysis of the trial is in hand at this time but early evaluation of the film records has shown encouraging trends. In consideration of the wing borne case, the CFD predictions have been confirmed, showing pitch trajectory hesitation at elevated incidence, both with and without aft blowing jets (no visible interaction). The lateral disturbance has also been shown to be small in all cases including some sideslip conditions.

In semi jet borne flight with nozzles deflected and jet efflux flow activated the jettison trajectory remains relatively benign, and flight incidence remains the most sensitive parameter. There appeared to be no cases where the weapon model became entrained directly in the jet efflux flow, although this was not expected for a tip pylon shielded by the large inboard store. There were perceptible differences in lateral behaviour in semi-jet borne flight, with an exaggerated tendency for the store to yaw outboard with the tail approaching the inboard tank. On no occasion did this appear limiting.

The fully jet borne cases focused on the limiting incidence value and maximum nozzle flow throughout. In these cases there emerged a combined stabilizing effect of onset and jet efflux flow on the weapon trajectory. With no tunnel flow the weapon tended to remain pitched up throughout the near trajectory, but with only modest onset flows this tendency was suppressed and indeed reversed into pitch down. This would suggest that any limitation in the jettison envelope would probably be an airspeed/incidence boundary given that jet efflux flow tends to stabilise the weapon trajectory.

The Frazer-Nash pitch down assist system was also trialed at 7 flight conditions during the programme. This performed well at limit incidence completely eradicating any pitch hesitancy. However, in more benign cases it could be considered over effective in pitching the weapon tail into the rear of the launcher as has been seen on some CFD runs. The power of the pitch assist clearly needs further fine tuning.

II.3 REVIEW OF AERODYNAMIC ISSUES

This programme has again demonstrated the utility of the computational method in establishing concept feasibility early in a weapons integration programme. Development risk areas have been identified, and in the case study of rail jettison further wind tunnel trials have expanded on the initial database to a point where the novel features of the system have passed initial feasibility.

REFERENCES

1. J A Petrie, Development of an Efficient and Versatile Panel Programme for Aerodynamic Problems. Leeds University Doctoral Thesis, March 1979.

2. C D S Clarkson, Prediction of Stores Carriage/Release Behaviour Using Computational Fluid Mechanics. Paper Presented at RAes Symposium on Stores Integration & Release, Bath, UK, April 1990.

3. J W Peto and J A Ross, Low Speed Wing tunnel Tests on the Effect of Jet Blowing on Adjacent Stores. RAE Tech Memo, to be Published.

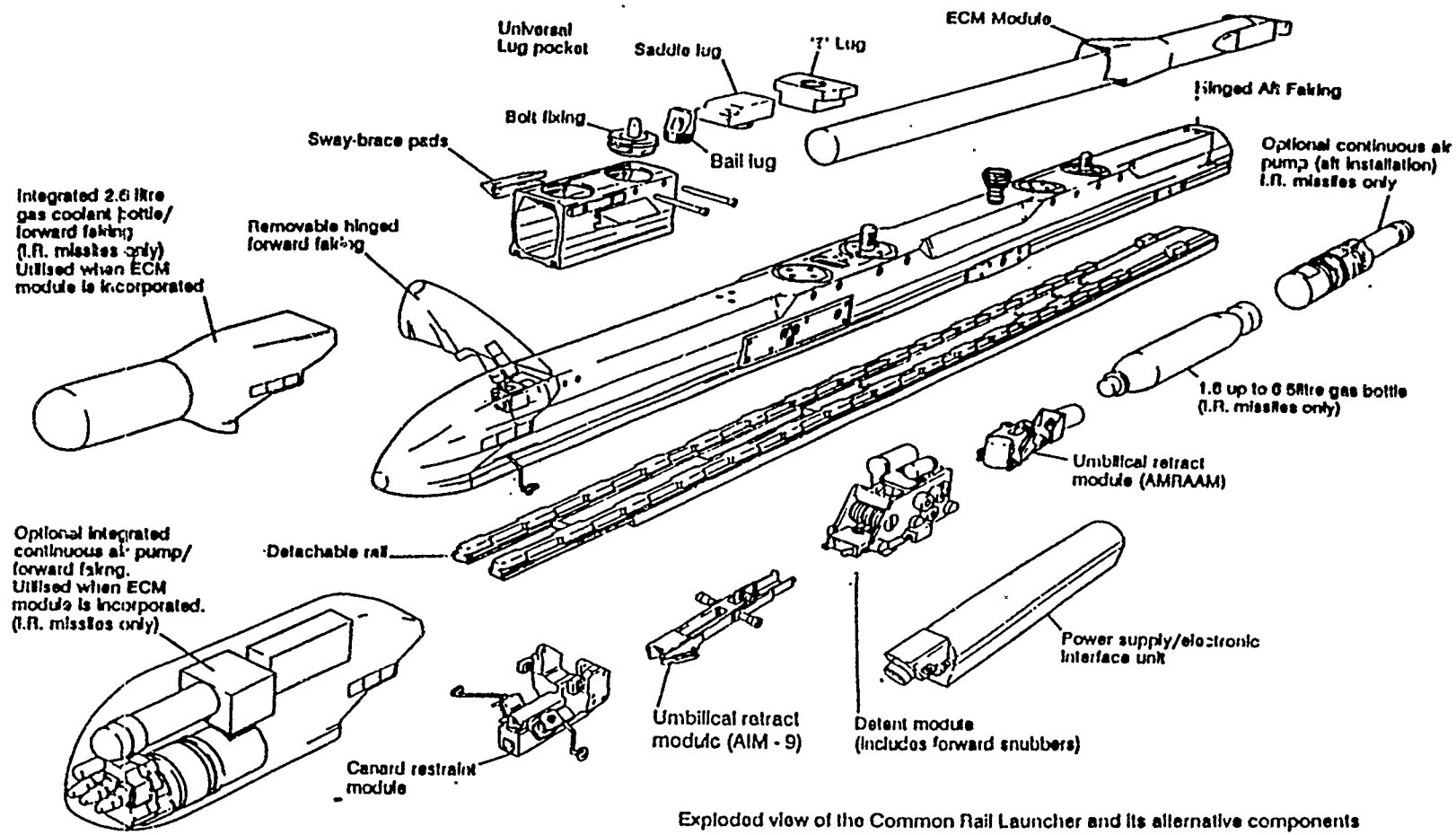

Exploded view of the Common Rail Launcher and its alternative components

FIGURE 1.

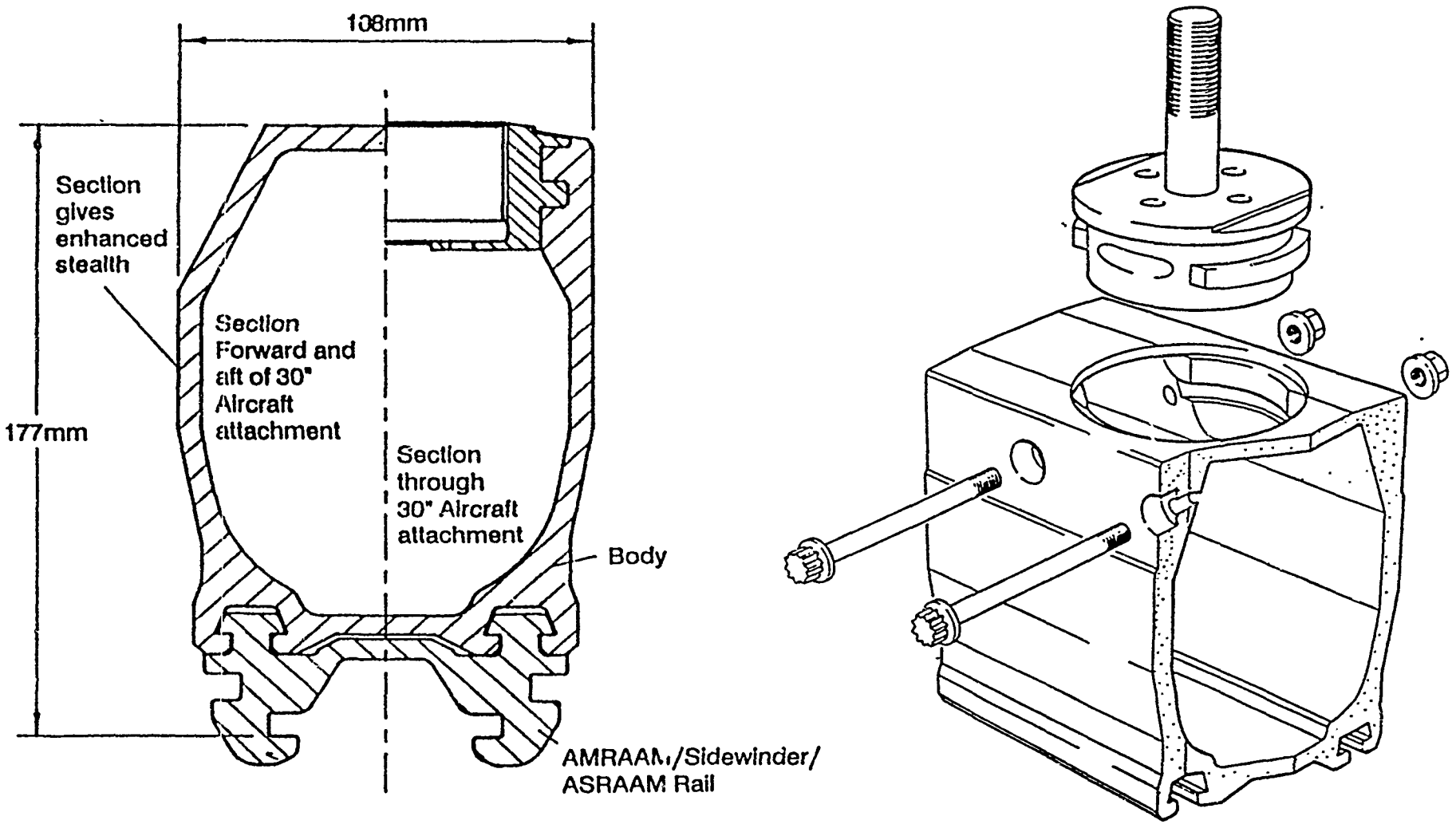
108mm
177mm
Section gives enhanced stealth
Section Forward and aft of 30° Aircraft attachment
Section through 30° Aircraft attachment
Body
AMRAAM/Sidewinder/ ASRAAM Rail

FIGURE 2.

Adaptability of longitudinal mounting.

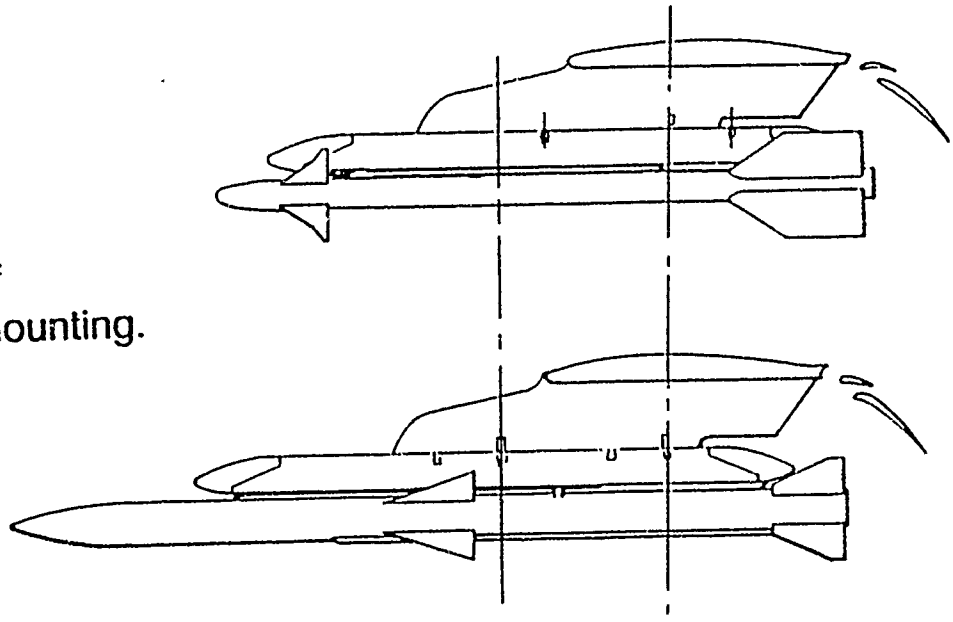

FIGURE 3.

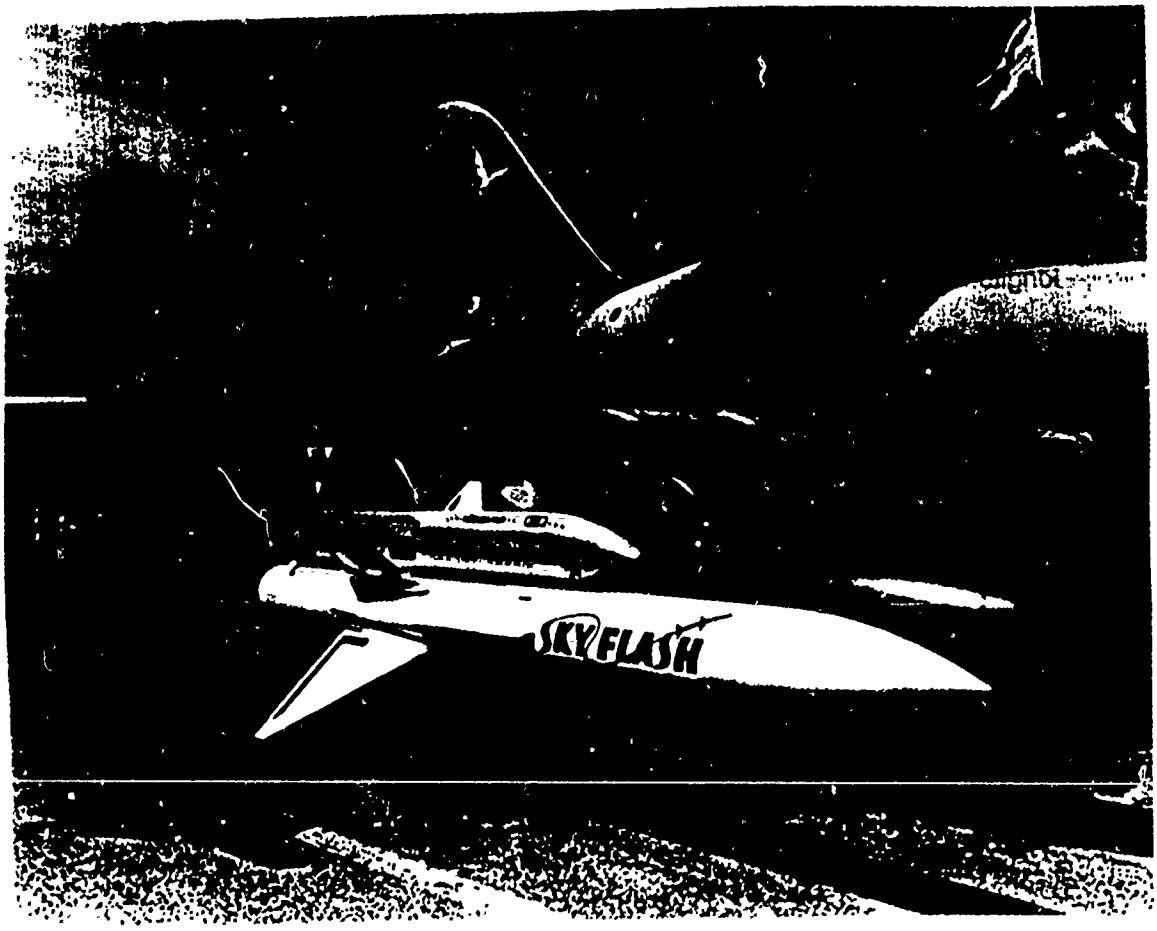

FIGURE 4.

Problems with ERU thrust lines on small aircraft.

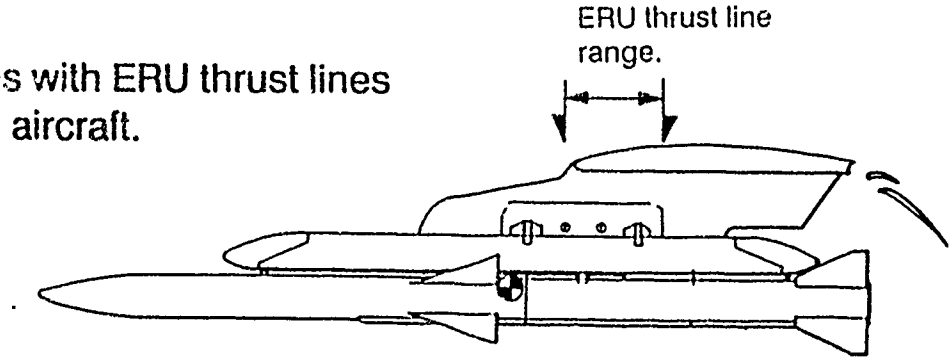

FIGURE 5.

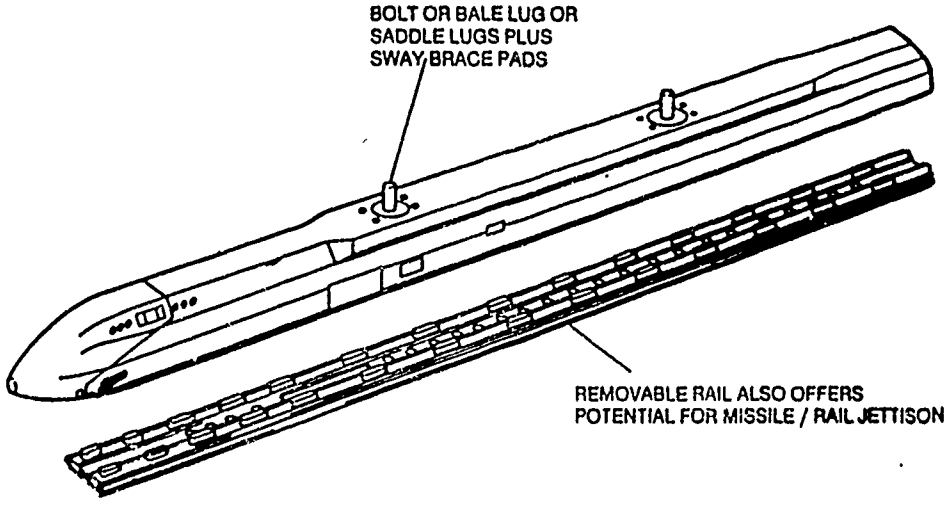

FIGURE 6.

Jettison using the detachable rail.

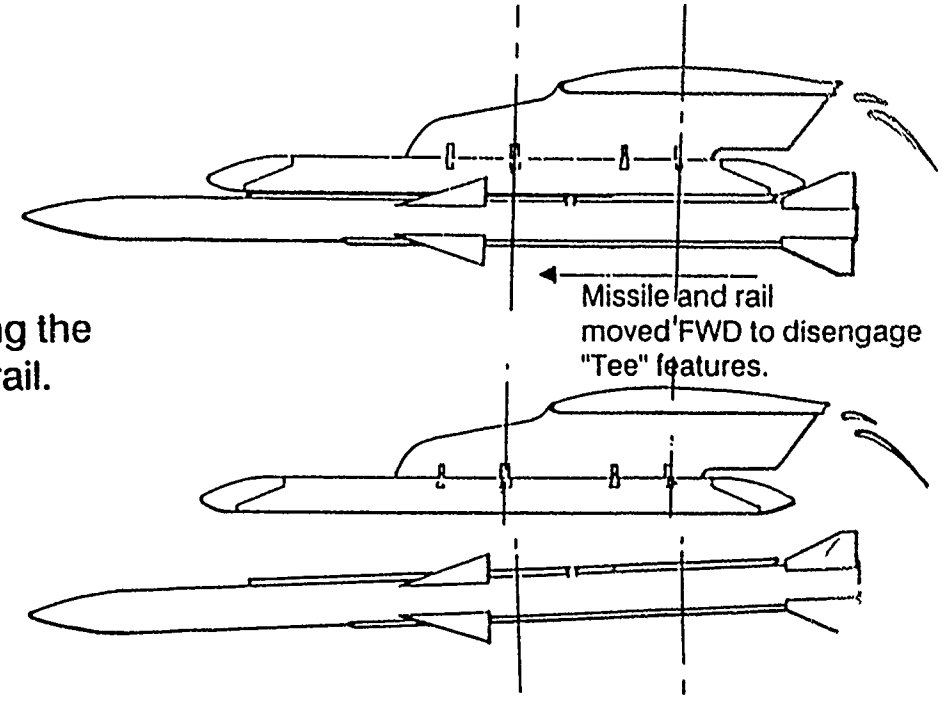

FIGURE 7.

Forward detent.

Forward lock.

Aft restraint.

Forward snubber.

Aft snubber.

Umbilical connecter.

Motor fire connector.

Control surface restraints.

Missile to launcher interface features.

FIGURE 8.

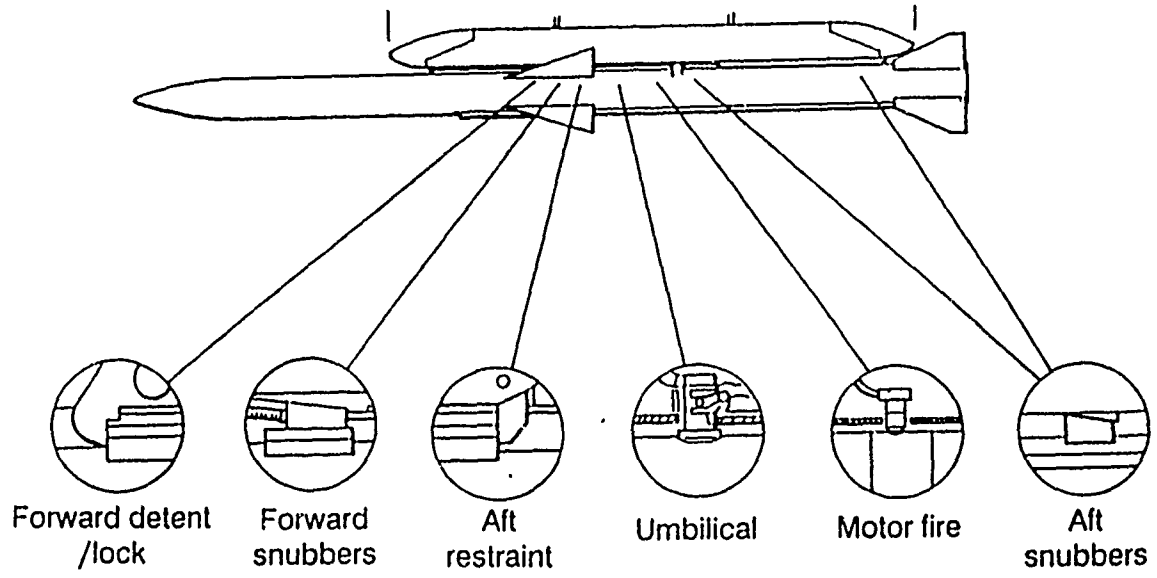

Considerations leading to "rail only" movement.

FIGURE 9.

Aerodynamic.

Electric.

Hydraulic.

Hot gas.

Cold gas.

Spring.

Elastomer.

Explosive.

Possible power sources.

FIGURE 10.

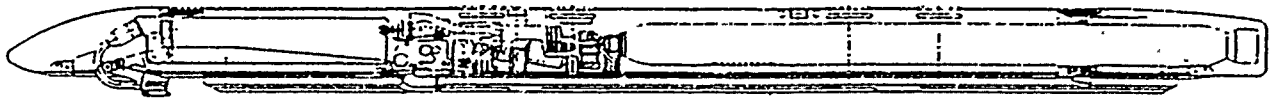

Launcher after fitment of rail eject mechanism

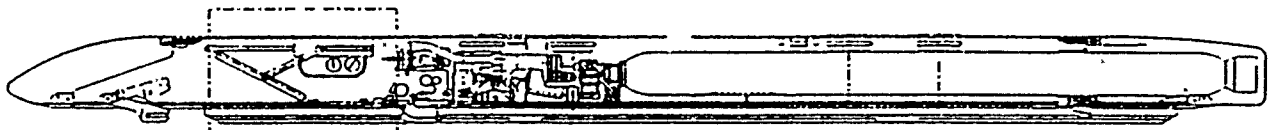

Launcher before fitment of rail eject mechanism

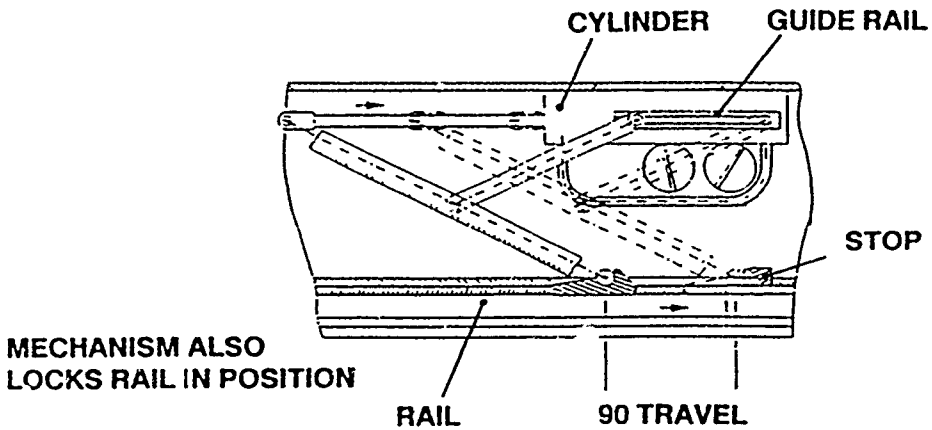

Detail "A" showing eject mechanism

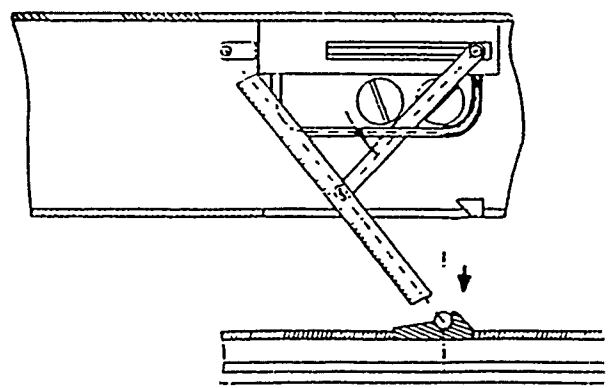

Detail of rail fully ejected

FIGURE 11.

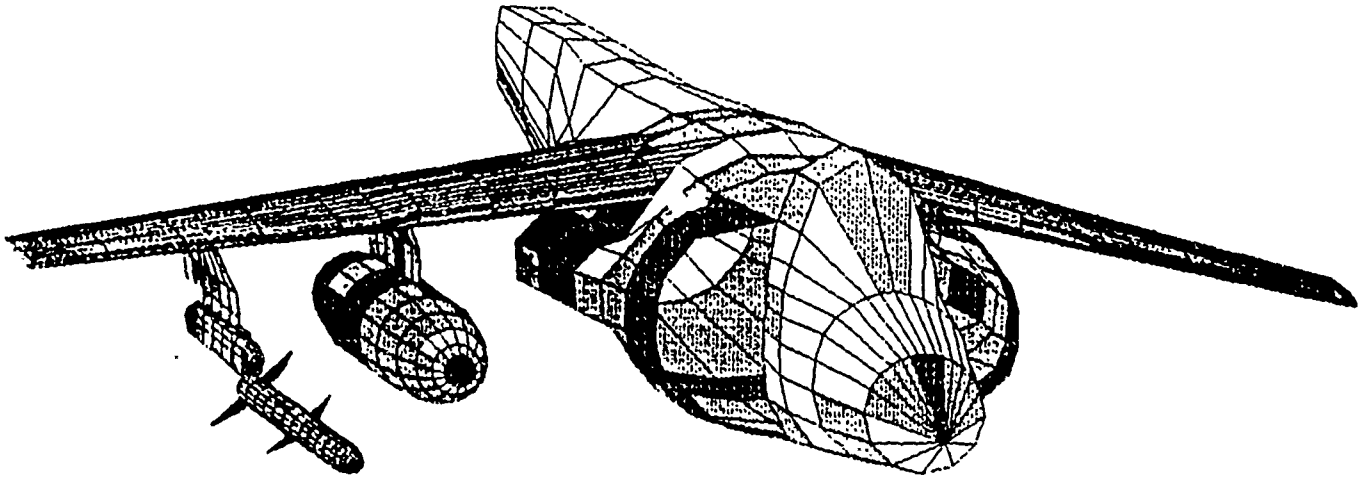

FIGURE 12.
SEA HARRIER/AMRAAM/CRL SPARV CFD MODEL CONFIGURATION

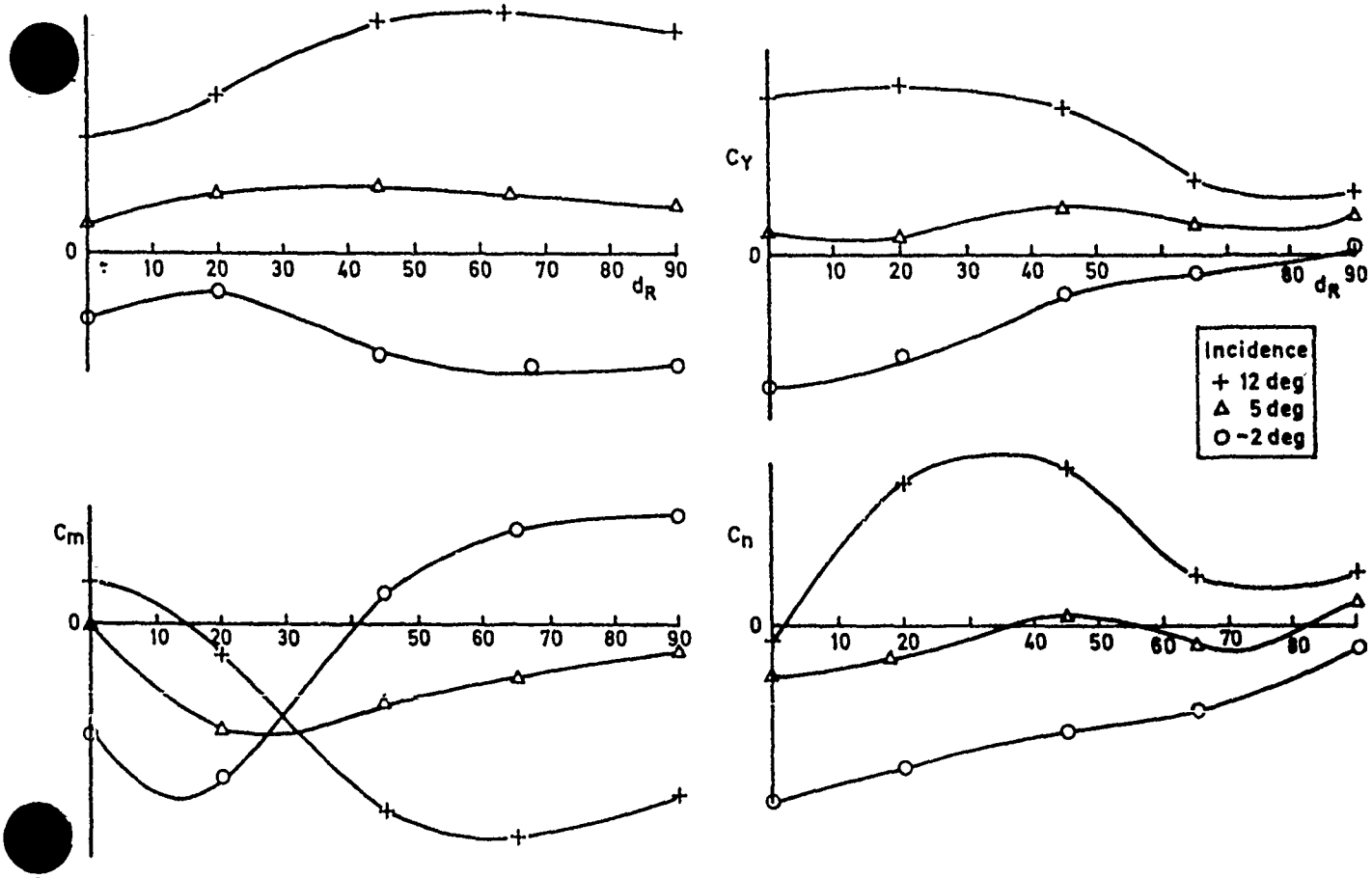

FIGURE 13. AMRAAM on CRL Down rail loads prediction

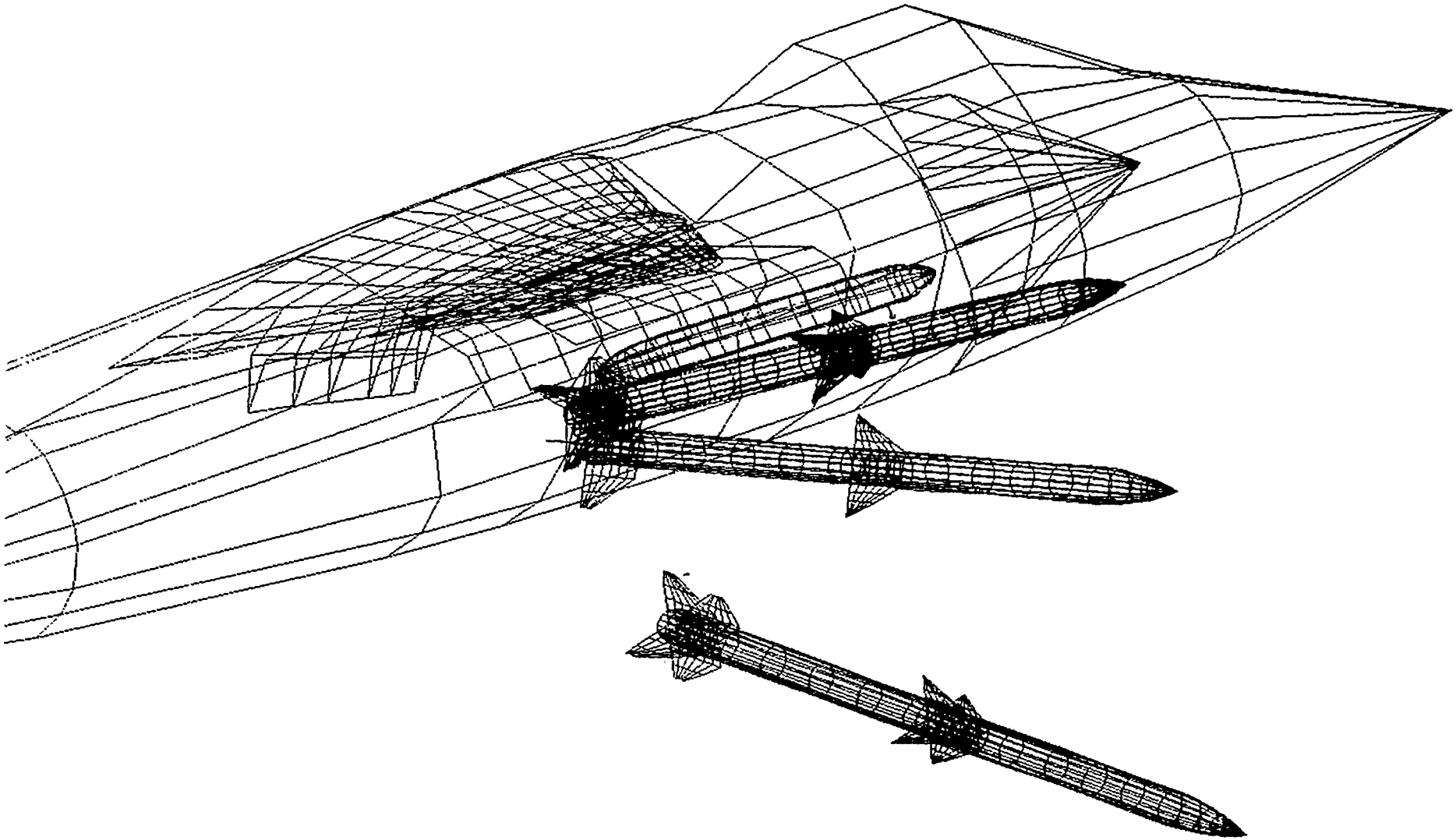

FIGURE 14.

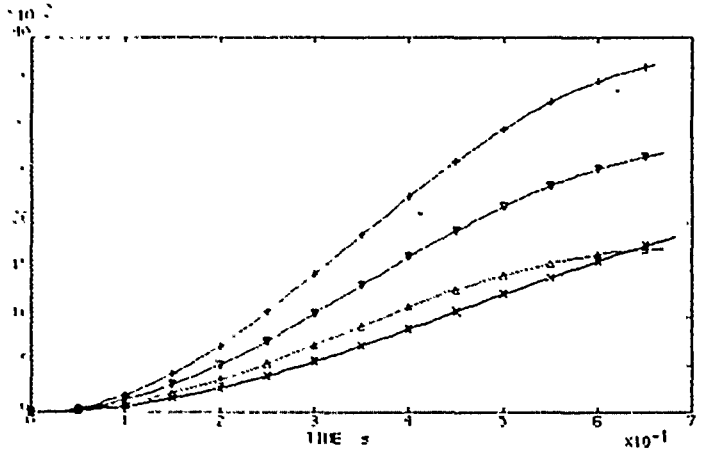

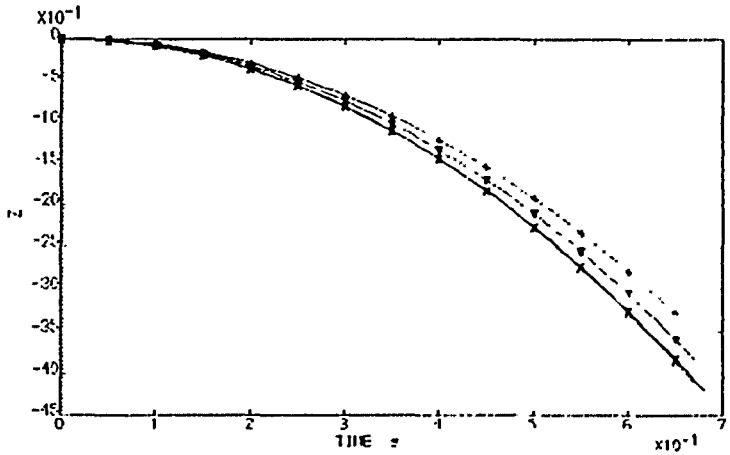

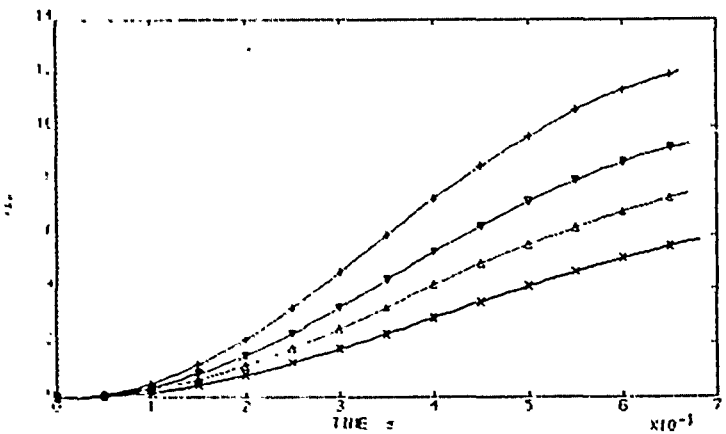

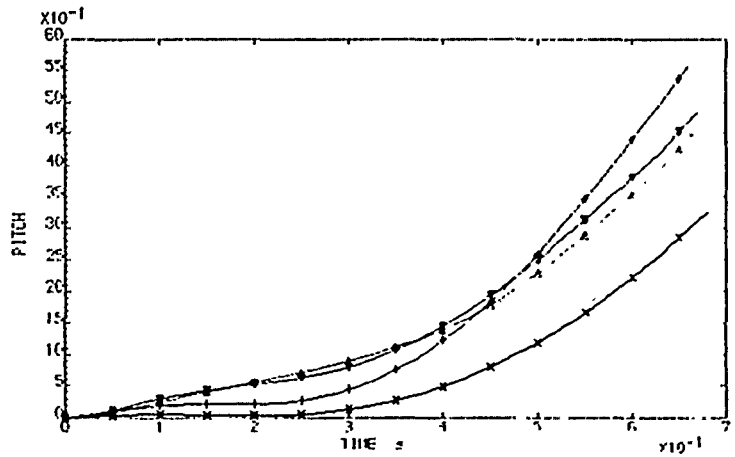

SYMBOL	MACHNO	AIRSPEED	INCIDENCE	V.EJECTION
Δ	0.25	240	5.0	0.0
∇	0.25	240	10.0	0.0
+	0.25	240	15.0	0.0
×	0.15	120	15.0	0.0

FIGURE 15.

SPARV TRAJECTORY SIMULATION
SEA HARRIER/AMRAAM/CRL

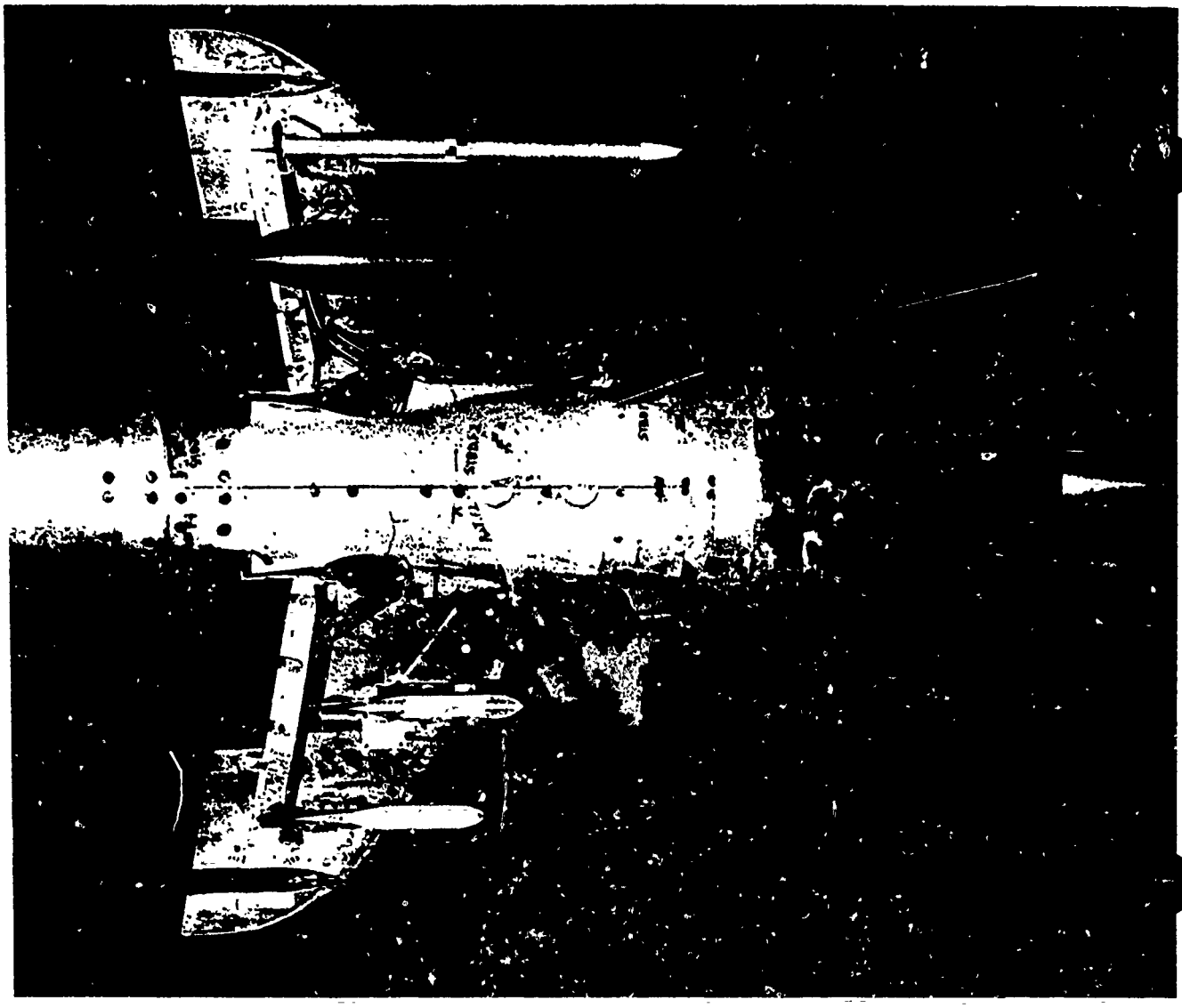

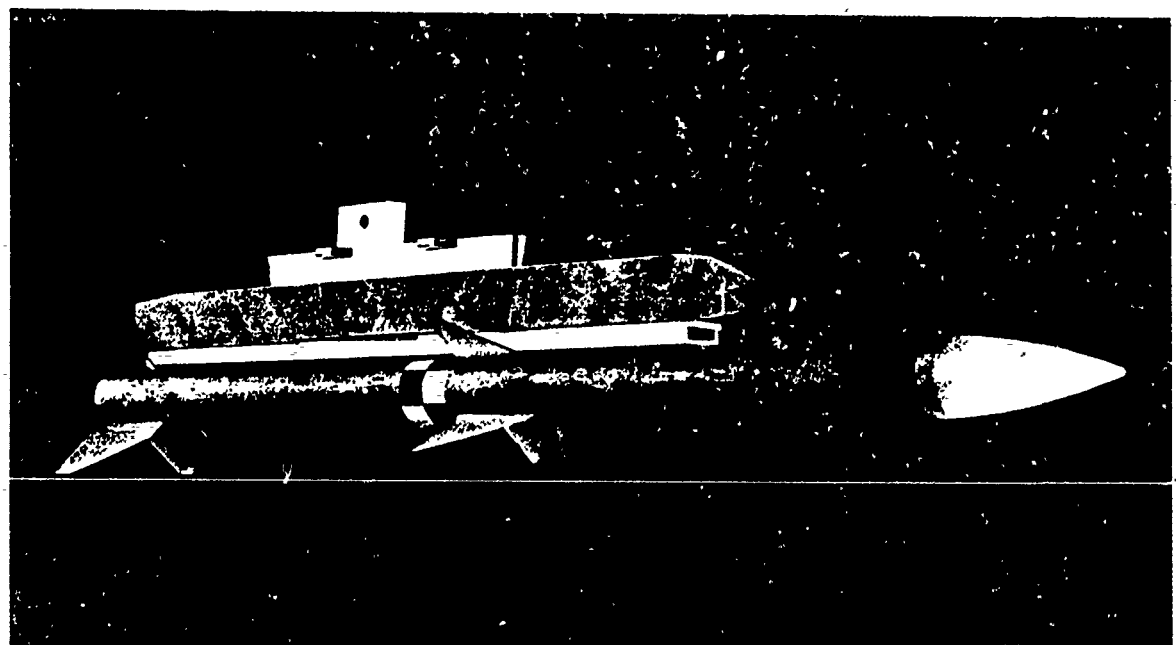

FIGURE 16.

SEA HARRIER and AMRAAM/CRL MODELS for WIND TUNNEL DROP TRIAL

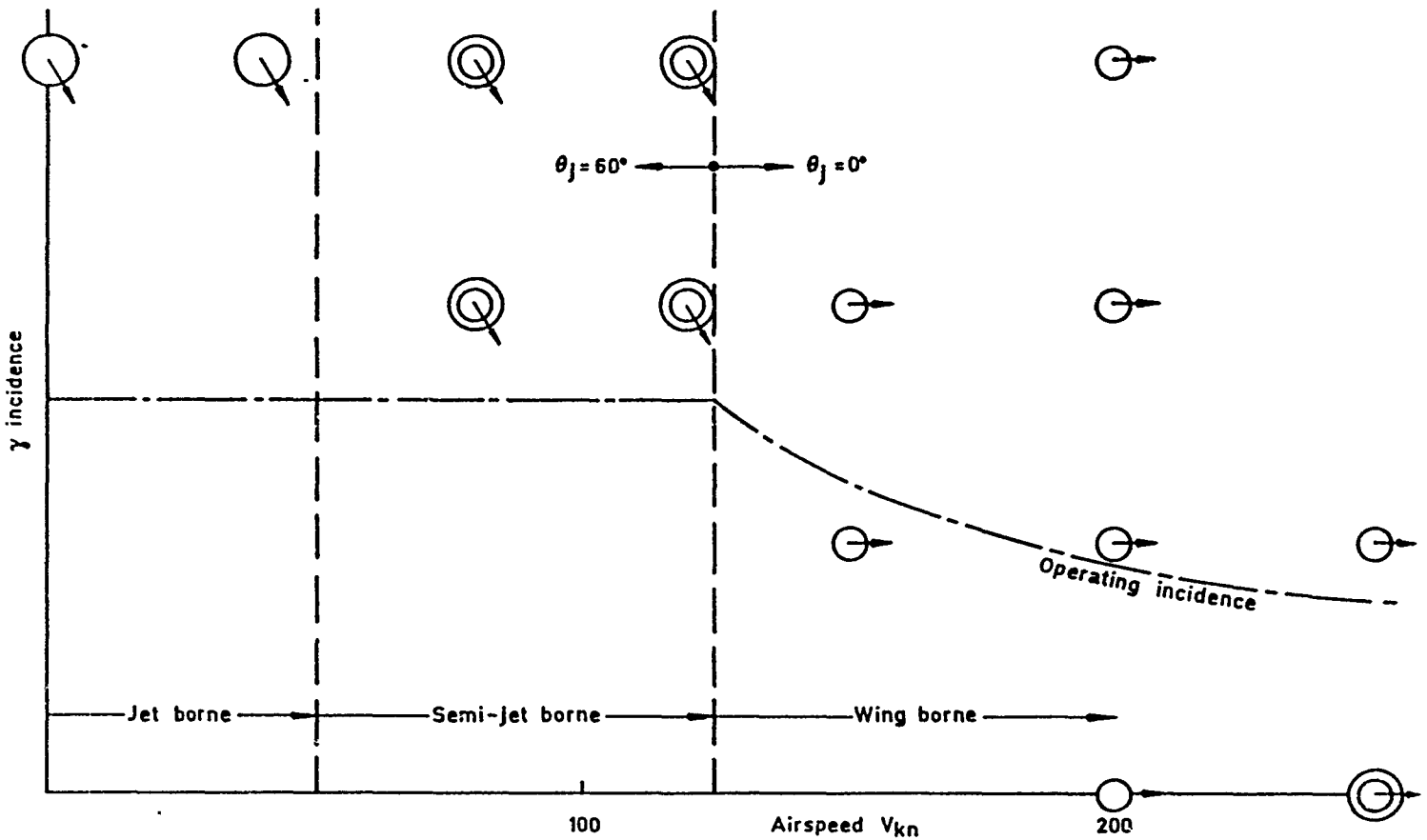

FIGURE 17. Harrier – AMRAAM – CRL separation trial conditions

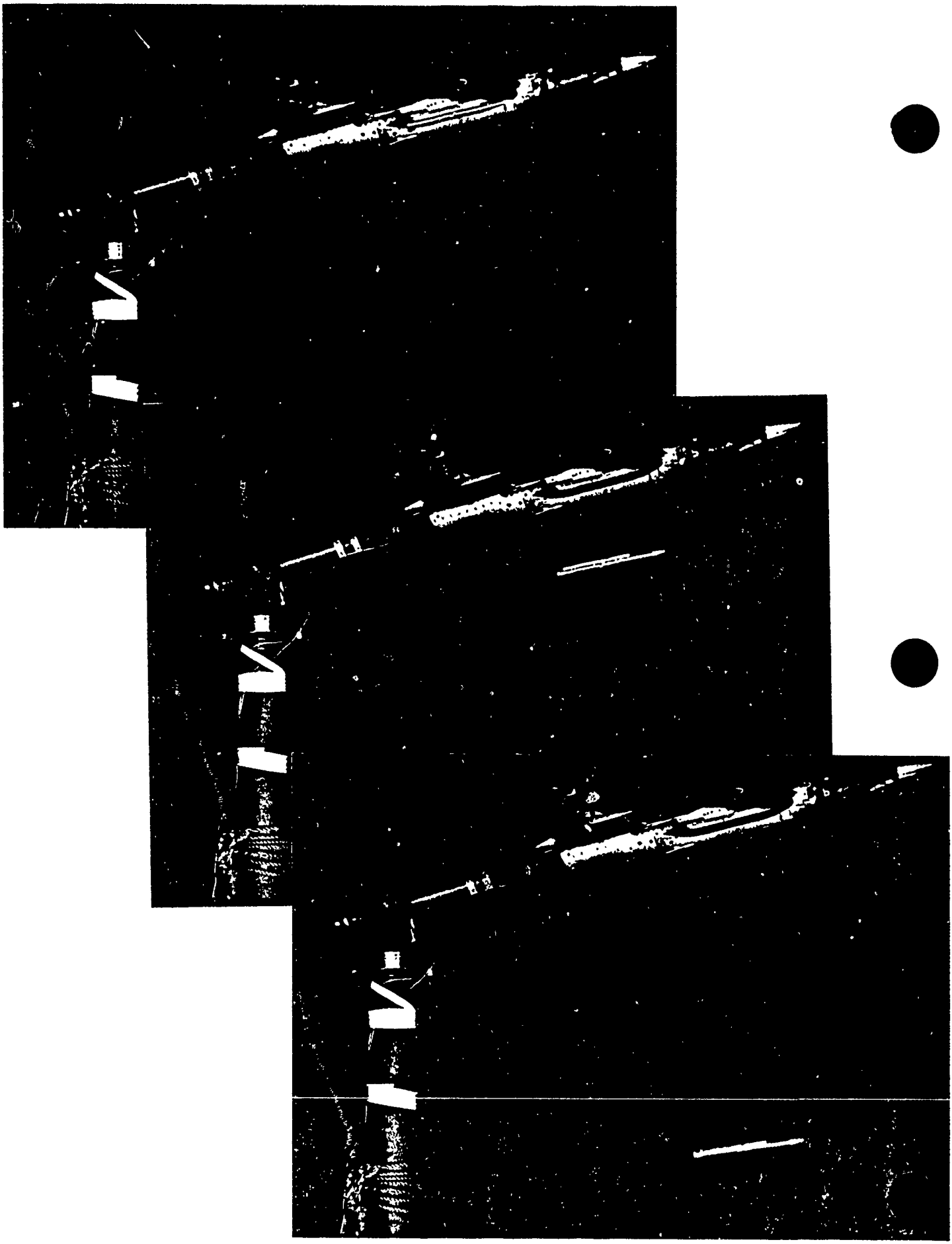

FIGURE 18.
AMRAAM MODEL JETTISON IN RAE 24 ft TUNNEL

AUTHORS BACKGROUNDS

JOHN R PEARCE, Technical Manager, Frazer-Nash Defence Systems Ltd., has been responsible for the technical design and development of the Common Rail Launcher and its derivatives. He has also led studies into the development of pneumatic and liquid propellant powered, advanced technology eject launchers. Before specialising in missile ejection and release technology, his previous experience covered the design and development of weapon system fuses and safety and arming systems. He spend some time on the design and development of some major TGSM programmes. He is a Chartered Engineer and holds a Polytechnic Diploma in Advanced Mechanical Engineering. He started his engineering career with an Indentured Apprenticeship at Hawker Aircraft.

HOWARD A TORODE is a Principal Scientist at RAE(F) leading a section concerned with Weapon Carriage, Release and Ballistics in Attack Weapons Department. He graduated in Aeronautical Engineering at Imperial College London in 1968 and also as a licensed Flight Test Engineer from the French Test Centre (1978). He joined UK MOD in 1974 and has worked diversely at MOD HQ and also at RAE Bedford where he was involved with VSTOL flight control and piloted simulation. In 1984 he was seconded to NATO/AGARD in Paris, France, where he was Executive Officer for the Flight Mechanic Panel. Current weapons interests range from practical applications of CFD, wind tunnel and flight validation trials.

THIS PAGE INTENTIONALLY LEFT BLANK

Title: KEY FEATURES IN THE DESIGN OF CARRIAGE-AND-RELEASE EQUIPMENTS FOR AGILE COMBAT AIRCRAFT

Author: R R Evans

SUMMARY

This paper examines the demands that modern combat aircraft make on the design of new weapon carriage-and-release equipments, and briefly outlines some key features which can be included in such designs to meet those demands. The weapon carriage requirements of a modern combat aircraft such as F-16, F-18 or European Fighter Aircraft (EFA) typically include under-wing pylon mounted ejector release units (both light duty and heavy duty) for carriage of external stores, eject launchers for short and medium range air-to-air missiles carried conformally or internally in the fuselage, and rail launchers for short and medium range air-to-air missiles carried on under-wing pylons or on wing-tips.

Modern combat aircraft present significant challenges to the designer of carriage-and-release equipments because they combine the capacity for ever-increasing agility with the need for the controlled and safe separation of weapons at all points of their flight envelopes. Additionally, as equipments become more sophisticated, the end-user demands that the cost of ownership, and complexity of operation and support for those equipments are more and more reduced. The critical features of the equipments are thus:-

*HIGH PERFORMANCE

*LOW MASS

*ADAPTABILITY TO A WIDE RANGE OF WEAPONS

*EASE OF OPERATION AND SUPPORT

*EASE OF MAINTENANCE

This paper will describe the typical design details which address these requirements using, as illustrative

examples, features from a family of weapon carriage-and-release equipment technology demonstrators, developed as a collaborative European venture over the past four years. In particular, the discussion concentrates on the application of a novel design of force-control valve and the use of titanium alloys for expulsion systems, and design improvements for multi-functionality and simplified ground support activities.

Design solutions here described, result from the work of the ACMA Consortium (AEREA of Italy, CASA of Spain, MBB-UW of Germany and ML Aviation of the United Kingdom). The Consortium was formed initially to respond to the specific requirements of the European Fighter Aircraft, but its extensive self-funded experimental and development programmes have since been tailored to meet the perceived needs of post-1992 Europe and the wider world markets.

Throughout the paper, the emphasis is placed on design solutions which present comparatively low technical risk, and which can be manufactured without significant increase in costs or development of new production processes when compared to conventional equipments.

1. INTRODUCTION

1.1 Fighter aircraft with high agility impose significant challenges to the designer of weapon carriage-and-release equipments. He must ensure a performance which offers controlled and safe weapon separation regardless of aircraft manoeuvre. This normally results in a requirement for the highest possible ejection velocity within the particular force and acceleration constraints imposed by the limitations of aircraft and missile structural strengths. As aircraft combat performances improve, there is a demand for increasing weapon separation velocities but generally no relaxation of the other constraints. In addition, the higher inertia and aerodynamic loading conditions associated with weapon release from lighter, more agile aircraft produce a demand for stronger equipments without undue penalties of increased mass or aerodynamic drag.

1.2 The current condition of military budgets throughout the world is resulting in purchasers giving equal weight to the affordability of weapon carriage-and-

release equipments. Thus the designer, now as never before, must combine optimum performance with low procurement cost and low life-cycle costs. Technical excellence is no longer desirable at any price; it must be achieved without compromising ease of operability, high reliability, low maintenance, or the capability of different weapon carriage with little or no role-change activity. Hence the end user is provided with fast turn-around capability and low costs of ownership.

1.3 ML Aviation, together with its partners in the ACMA Consortium (AEREA of Italy, CASA of Spain and MBB-UW of Germany) and in collaboration with other European Defence Contractors (eg. MATRA of France), has made a considerable investment in design and prototype programmes over the past four years in order to investigate innovations in equipment design required to meet the technical and commercial requirements of the users of agile combat aircraft. The aim of the programme has been to create an integrated family of carriage-and-release equipments, including light and heavy-duty bomb racks, Medium Range Air-to Air Missile (MRAAM) Eject Launchers, and Short and Medium Range Missile (SRAAM and MRAAM) Rail Launchers, with a high commonality of features, and which offers high performance and low operating costs for aircraft such as F-16, F-18 and EFA.

1.4 This paper presents elements from the design studies, performed as part of the collaborative programmes, as examples of practical approaches to providing carriage and release equipments with optimum separation performance, high strength with low mass, adaptability to a wide range of weapons, ease of maintenance, and ease of operation and support.

1.5 All of the design elements here discussed have been proven in programmes of ground and flight-testing with technology demonstrators and several of the elements are incorporated in equipments which have now been selected for the European Fighter Aircraft (EFA).

2. OPTIMISED SEPARATION PERFORMANCE

2.1 For equipments such as bomb racks and missile eject launchers, safe separation of weapons from agile aircraft normally requires the maximum possible

ejection velocity. However, the ejection velocity is often limited by other design constraints such as the forces which the local aircraft or missile structures can withstand, or the acceleration levels which can be imposed on particular missile components. Thus the essential criterion of an optimised ejection system is that it should apply an acceleration to the weapon which is as close as possible to constant acceleration.

2.2 The majority of weapon ejection devices employ standard pyrotechnic cartridges as the power source. Use of cartridges for this purpose is well-proven, and they currently offer unrivalled advantages of mass and volume over alternative power sources such as high-pressure cold gas or hydraulics. Unfortunately, they also have two distinct disadvantages in terms of system contamination, and the high transient reactions they induce during the ejection sequence. The contamination problem will be discussed later so, for the moment, this paper will concentrate on one possible approach to smoothing out the impulsive effects of pyrotechnic cartridges.

2.3 All pyrotechnic cartridges generate a pressure-time characteristic which is essentially triangular in shape with a sharp rise to peak pressure and a more gradual decay. It is the apex of this triangle which produces the maximum pressure over the ejection system rams and hence the maximum, albeit transient, forces and reactions on the weapon and aircraft structures. When structural limitations dictate a lower allowable maximum, the peak gas pressure on the ejector rams must somehow be reduced. Conventional approaches to reducing the maximum reaction (ie. simple orifice throttling) inevitably result in a loss of potential ejection energy and hence a reduction of weapon separation velocity One alternative is to use a variable orifice system to "flatten" the pressure-time curve for the rams and hence maximise the available energy within the reaction "ceiling". A comparison of conventional orifice and variable orifice throttling pressure-time curves is shown in Figure 1.

2.4 The variable orifice is created by feeding gas to the ram through a tube which houses a tapered valve. The tapered valve is par of the ram assembly and is hence withdrawn from the feed tube as the ejection

stroke progresses, creating an anular orifice of varying area. The taper itself need not be constant and can be tailored to the particular gas system to produce a faster rise to peak pressure and a more gradual decay so as to maximise the useful energy derived from the cartridges. This system, installed in a long-stroke two-stage telescopic ram, is shown in Figure 2.

2.5 A secondary method of alleviating the impulsive characteristics of standard cartridges is to control the problem at source, ie. to modify the pressure-time curve within the breech itself. This can be done by installing a valve which is opened at a defined "trigger-pressure" to increase the breech volume and smooth out the peak pressure. The system avoids overboard venting and permits most of the generated gas to be used during the ejection cycle. This variable-volume supplementary breech cavity is shown in simplified illustration in Figure 3. It has the advantage of limiting pressure variations due to changes in cartridge type or ambient temperature and thus allows more controlled conditions for the optimisation of the downstream variable throttles.

2.6 These ram-installed variable orifices, combined with breech pressure-regulation and conventional pitch-control orifices create a system which offers optimised ejection performance, with a wide variety of cartridge types and under a wide range of environmental conditions. The system is applicable to many different types of ejectors such as the light-duty bomb rack, heavy-duty bomb rack, and MRAAM eject launcher design proposals shown in Figures 4, 5 and 6 respectively.

2.7 A large number of ground firings have now been performed with long-stroke variable-throttled technology demonstrators and the initial results with these unrefined, experimental units show that, within a given reaction constraint, variable throttling offers an increase in end-of-stroke ejection velocity of in excess of 30% when compared with conventional orifice throttling. ACMA consider that the technology demonstration programmes have not only confirmed the technical aspects of this approach to optimisation of weapon separation performance, but has shown also that these design elements impose no significant increase in manufacturing complexity, in

either choice of materials, or tolerances, or surface treatments.

3. LOW MASS AND HIGH STRENGTH

3.1 For bomb racks such as those shown in Figures 4 and 5, and particularly for a long-stroke eject launcher such as that shown in Figure 6, a significant proportion of the total mass is found in the gas system. The majority of ejection equipments have hitherto relied on the use of high strength maraging or corrosion-resistant steels for gas system components. These materials have a high strength/weight ratio, but the complex shapes of gas system components often present manufacturing difficulties in the realisation of minimum wall thicknesses etc. and hence minimum mass.

3.2 An obvious approach to mass reduction is therefore to investigate the possible application of alternative high strength, lightweight materials which have hitherto not been widely used in conventional ejector design. For this reason, one of the ACMA experimental programmes involved the manufacture and testing of an ejection system which used titanium alloy as the primary material. Firing trials with Ti-6Al-4V components have demonstrated that this alloy combines the benefits of low mass with excellent resistance to contamination from the by-products of cartridge ignition.

3.3 The use of titanium does have certain drawbacks, including the problem of its propensity for galling or high friction on rubbing surfaces, and treatments have to be applied to prevent this. The experimental titanium ejector programme successfully identified a method of surface nitriding which not only reduces the surface friction and increases its resistance to wear and erosion, but can also be applied as a relatively cheap variation of an existing standard low-risk industrial process.

4. ADAPTABILITY TO A WIDE RANGE OF WEAPONS

4.1 It is accepted practice for bomb racks, such as those shown in Figures 4 and 5, to be designed to meet the arming, fuzing, carriage, swaybracing and release requirements of any weapon or store which can be carried on standard portal lugs at 14-inch or 30-inch

centres. Often such bomb racks will be capable of interfacing with stores that vary from flat-topped down to 9 inches diameter. Until quite recently however, the approach to missile launcher design, whether rail or eject launched, tended to be towards single-weapon dedicated equipments.

4.2 It is now recognised that the end user of missile launchers has a growing interest in procuring equipments which can support more than one weapon. It is the contention of the ACMA Consortium that this type of adaptability is both feasible and affordable, providing that the range of candidate missiles for a particular launcher is limited to some kind of sensible grouping, in particular by mass range and mechanical interface. In this way, adaptability may be achieved with minimum or non role-change requirement and without the extreme penalties of structural mass associated with the capability of supporting too wide a mass range of missiles, eg. 90 kg to over 300 kg.

4.3 It is equally important for the designer to recognise that the introduction of design modularity, whenever possible, in multi-role launchers greatly increases their potential application. If variants of a widely-adaptable launcher can be configured and sold in a one, two, three or more weapons role, then it offers benefits both to industry and the end user. The high commonality of parts among such variants allows larger production lot sizes and greater markets to the producer, and better logistic support and choice of application for the customer. The ACMA programmes have concentrated closely on achieving this synthesis of adaptability of weapon support and flexibility of final configuration by modular design.

4.4 The first example of this approach is given by the proposed design for an Advanced MRAAM Eject Launcher as shown in Figure 6. The launcher is shown in its dual mode configuration whereby it is capable of carriage-and-ejection of AMRAAM or Sparrow-class missiles (eg. Skyflash or Aspide) by the use of role-change items which allow simple and rapid on-aircraft conversion. Due to the "building block" approach used in this design, the launcher can be delivered as a simpler and lighter single missile-dedicated configuration, or converted from dual to single mode at base workshop level. All

launcher variants derive from a common structure, gas system and basic carriage mechanism, with missile-dedicated mechanical and electrical functions provided as extra built-in modules or role-change items. This design approach offers maximum choice and flexibility to the end user and minimises the production costs due to the very high degree of common parts among the various configurations.

4.5 The second example of this approach is the ACMA proposal for the design of an Advanced Multi-Purpose Rail Launcher (MPRL) shown as Figure 7. The MPRL is designed to be capable of supporting Sidewinder, Sparrow variants, AMRAAM, and anticipated developments such as ASRAAM and digital Sidewinder on a wide variety of aircraft. The missiles, like the aircraft themselves, divide into digital and analogue types, and for this reason a multi-purpose rail launcher capable of supporting all these candidate missiles on a wide variety of aircraft can offer considerable benefits of simplified logistics and increased serviceability, availability and cross-operability.

4.6 As with the Eject Launcher, adaptability and flexibility is assured by modularity of design. The significant design elements of an advanced MPRL include an integrated electronics unit, front and rear detent assemblies, umbilical connectors with their engage and release mechanisms, rear snubbers, a central operating handle for all launcher function selection modes, and the cooling system for the IR Seeker. A 4.1 litre nitrogen bottle is shown in the figure but the launcher will accept a pure-air generator as an alternative.

4.7 All these elements are housed in a stiff lightweight structure formed from an attachment frame and the rail sections. The integrated rail concept permits the carriage and launch of all the candidate missiles without the need for adapters or interchangeable components. The attachment frame is capable of being fitted with 30-inch suspension bolts, 14-inch bail lugs, detachable swaybraces, a front launcher-aircraft connector at the standard LAU-7 position, a rear launcher-aircraft connector to MIL-STD 1760 Class 2, or a connector in an intermediate position. The launcher is completed by detachable nose and tail fairings which give access to the forward AIM-9

umbilical position, electronics box and cooling system.

4.8 As previously stated, the detail design of the launcher is specifically targeted at ensuring maximum flexibility of application. The MPRL offers a choice of mechanical and electrical interfaces which allow it to carry and launch all of its candidate missiles on all modern fighter aircraft. At the same time, the launcher is capable of lighter and simpler configuration. It can, for instance, be built as a dedicated missile launcher fitted with the appropriate off-the-shelf power supply unit and cooling system (if necessary). An example of this single-missile configuration is the Sidewinder Dedicated Launcher (SDL-21) shown as Figure 8.

In other configurations, the redundant multi-purpose modules would be omitted and could be replaced by other equipments, eg. chaff or flare dispensers as shown in Figure 9, and this flexibility of alternative configurations is demonstrated by the family tree of variants derived from the MPRL shown in Figure 10.

4.9 Again this philosophy of flexible design within practical limits ensures that production costs and logistic support costs are reduced, and cross-operability is enhanced by the fact that all variants of the launcher share approximately 70% commonality of parts.

4.10 Joint studies with MATRA are currently under way to extend further the application of the MPRL to other candidate missiles such as MICA and MAGIC

5. EASE OF OPERATION AND SUPPORT

5.1 Ease of operation and logistic support is important in any equipment, and becomes even more so for multi-role equipments of complex functionality. The designer must carefully address these requirements in order to minimise operating costs, reduce on-ground turn-around times, maintain reliability and avoid the possibilities of ground-crew errors.

5.2 The family of weapon carriage-and-release equipments previously discussed has been carefully structured as a package which offers the end user the benefits of simplified operation and support. As will also be seen from the following examples, considerable emphasi has been placed on maximising the commonality of components between the equipment types and variants so that procurement costs can be reduced and spares planning can be simplified.

5.3 The proposed designs for the light and heavy-duty bomb racks share a large number of identical components to reduce costs and simplify spares support. The two units use the same electrical subsystem, the same breech assembly and the same central kinematics box with identical mechanism components between the 14-inch carriage hooks. Of equal importance is the fact that both bomb racks are powered by the same NATO standard cartridge as is proposed for the MRAAM eject launcher. Only one cartridge type would be required for an aircraft fitted with these pyrotechnic release equipments, thus simplifying the operational logistics and avoiding the possibility for errors which arise with mixed cartridge installations. Rapid and easy weapon loading is ensured for both bomb racks by self-latching carriage hooks and a single point square drive system for swaybracing. All ground operations are performed using integral handles or standard square drives, without the need for special tools.

5.4 The MRAAM eject launcher design follows a similar pattern to that of the bomb racks. All ground functions can be performed using integral handles or standard tools. Rapid reconfiguration for the dual mode version of the launcher (see Figure 4) is achieved by ensuring that all missile-specific components (pitch-control throttles, force-control throttles, carriage-hook inserts, and ram yokes) are role-change items, capable of removal and replacement from the underside of the unit without disruption of the installation.

5.5 The MRAAM Eject Launcher is intended primarily for buried installations with restricted access and therefore ease of ground operation during weapon loading must be given the highest design priority. For this reason, all the ground-functioned points are concentrated in a single area, as illustrated in Figure 11. In this way ease of access can be

achieved without the need for multiple doors in the local structure. An added advantage of this design is that all ground operations (cartridge insertion and removal, pitch throttle adjustment or replacement, umbilical insertion and removal, ground lock insertion and removal, and opening and closing of carriage hooks) are possible with the missile attached to the launcher.

5.6 The details of the ACMA Multi-Purpose Rail Launcher proposal provide the most comprehensive example of what can be achieved when ease of operation is given equal design priority to the technical requirements. The integrated electronics unit is semi-modular in that it automatically supports all the candidate missiles and can be converted to different aircraft applications by simple board replacement. This, combined with the on-board installation of all candidate missile umbilical mechanisms and the common rail design, means that the electrical and mechanical interfaces of Sidewinder, ASRAAM, AMRAAM, and Sparrow variants are available without the need for role-change activities.

5.7 Loading and unloading of missiles with this design is further simplified by a centrally located three-position operating handle. There is a single load/unload position which disengages backstops, snubbers and firing circuits for all candidate missiles. The remaining two positions of the handle create flight-ready conditions for the candidate missile with the appropriate backstop, snubbers and firing circuitry engaged. All other ground functions - insertion and removal of umbilicals, and fitment or removal of fairings - can be performed using a standard square drive tool, and all operations can be performed from either side of the launcher.

6. EASE OF MAINTENANCE

6.1 A key factor in the costs of ownership for all types of carriage-and-release equipment is the time and cost of scheduled and unscheduled maintenance activities. A high maintenance requirement has the added drawback of reducing reliability. "If it ain't broke, don't fix it" is a truism born from the bitter service experience that, regardless of training and procedural controls, many equipment defects arise from damage or errors occurring during maintenance.

6.2 Low maintainability is not a characteristic which can simply be added as a design improvement at some point downstream in the programme when all other requirements have been met. It must be integrated at the beginning of any development and given weight with other design factors. The experience of the ACMA programmes is that, once a design team is committed to the principle of minimising the need for maintenance, this approach does not result in having to compromise other important design factors.

6.3 Necessary maintenance of bomb racks and missile eject launchers arises primarily from the need to combat the erosive and corrosive effects of cartridge combustion, and the need to prevent the reduction in performance that can arise from the accumulation of spent cartridge debris. The ACMA proposals for these equipments attack these problems in three ways - by restricting the dispersal of contaminants in the gas systems, by selection of contaminant resistant materials and processes, and by designing for easy cleaning.

6.4 The design details which have been introduced to improve maintainability include coarse filters in the cartridge holders which retain most of the cartridge debris in the breech volume, and the use of stainless steel and titanium alloys with surface treatments such as chromium plating, polymer-impregnated electroless nickel coatings and nitriding which all contribute to wear-resistance, low friction, corrosion resistance and resistance to contaminant adhesion. Attention to detail design of the gas system avoids the creation of contaminant traps and maximises the gas flow conditions and the ejection performance.

This disciplined approach results in equipments fitted with gas systems that can be subjected to more than 50 firings without cleaning (and which can be subsequently cleaned using standard detergents rather than specialised cleaning fluids), and fitted with mechanisms which require no regular lubrication. A final feature that is common to the ACMA proposals for bomb racks and missile eject launcher designs is that when scheduled cleaning of the ejection systems

is required, it can be performed with relative ease and with no special tools. All critical gas-affected parts (eg. cartridge holders, throttles, valves and pistons) are designed to be removable without disrupting the installation of the parent equipments in the aircraft.

6.5 In the design of the proposed missile rail launchers, any significant maintenance activity is virtually eradicated. Experience shows that the area of a rail launcher most likely to require maintenance or repair

is the rail itself. Traditional treatments such as plain hard anodising, simple molybdenum-disulphide greases or dry-film lubricants require considerable maintenance and refurbishment when subjected to the mechanical and efflux damage associated with missile launch. The rails of the ACMA launcher variants are comprised of sections manufactured from high strength aluminium and steel alloys. The aluminium alloy is treated to create a polymer-impregnated hard-anodised surface and the steel alloy is coated with polymer-impregnated electroless nickel. Both treatments are established commercially-available low-risk processes which offer durable surfaces with low and consistent friction characteristics. Our testing shows that the infusion of the polymers in a porous metallic matrix ensures their survivability under conditions of temperature and bearing pressure well beyond the ranges normally associated with such materials. The entrapment of the plastic lubricant ensures that the low friction characteristics continue to be maintained even under conditions of slow surface wear.

7. CONCLUSIONS

7.1 The concepts presented in this paper represent practical responses to the needs of current agile combat aircraft. The approach taken by the ACMA teams depends upon the innovative use of materials and processes and refinement of detail design rather than some high-risk radical departure from current technology. The concepts have now been proven in ground trials of prototype ejection equipments and ground and flight trials of prototype rail launchers. Our belief is that the programmes have resulted in a family of carriage-and-release equipments which matches the cost, performance and support requirements of users of current aircraft.

7.2 The long term future for missile rail launchers will undoubtedly see the continuation of the drive for multi-role equipments capable of supporting a range of weapons. The extent of that range is currently subject to the practical limitations of commonality of weight class and mechanical interface. Any future attempt to extend the carriage capability of launchers beyond that of 4 or 5 missiles would be totally dependent on new weapon design interfaces being more closely restricted to a common interface.

7.3 For weapon ejection devices powered by pyrotechnic cartridges, such as those described in this paper, the designer is now at the limits of what can be achieved in terms of performance and maintainability etc. A new generation of higher performance, no-maintenance equipments would certainly require alternative energy sources which were cleaner and more controllable than cartridges. Such options already exist in the form of high pressure cold gas, hydraulic fluids or combinations of both. The ACMA design studies would indicate however that these alternatives have yet to overcome the disadvantages of increased weight, increased volume and a requirement for a radical change in user support equipments. A deciding factor in the development of new power sources will be whether future aircraft trends are towards internal or external weapon carriage. The former would certainly have a greater need for equipments with low access requirements and high controllable performance and would place less emphasis on the need for low weight, low volume and minimum drag profile.

7.4 Regardless of the future technical requirements which may appear for carriage-and-release equipments, two customer requirements can be confidently predicted - low procurement costs and low life-cycle costs. These requirements are not met simply by production efficiencies and product improvement - they must evolve from day one of the programme as the very foundation of the design.

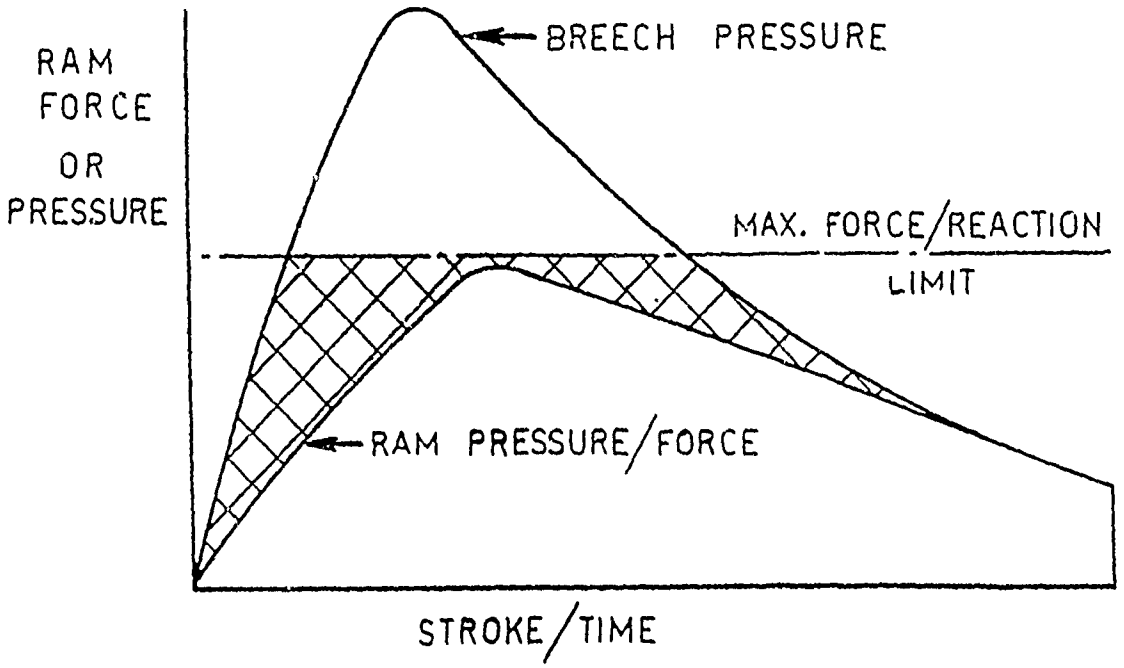

Fig.1a Pressure-time Curve for Conventional Orifice Throttle

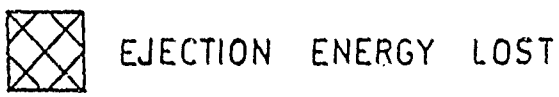

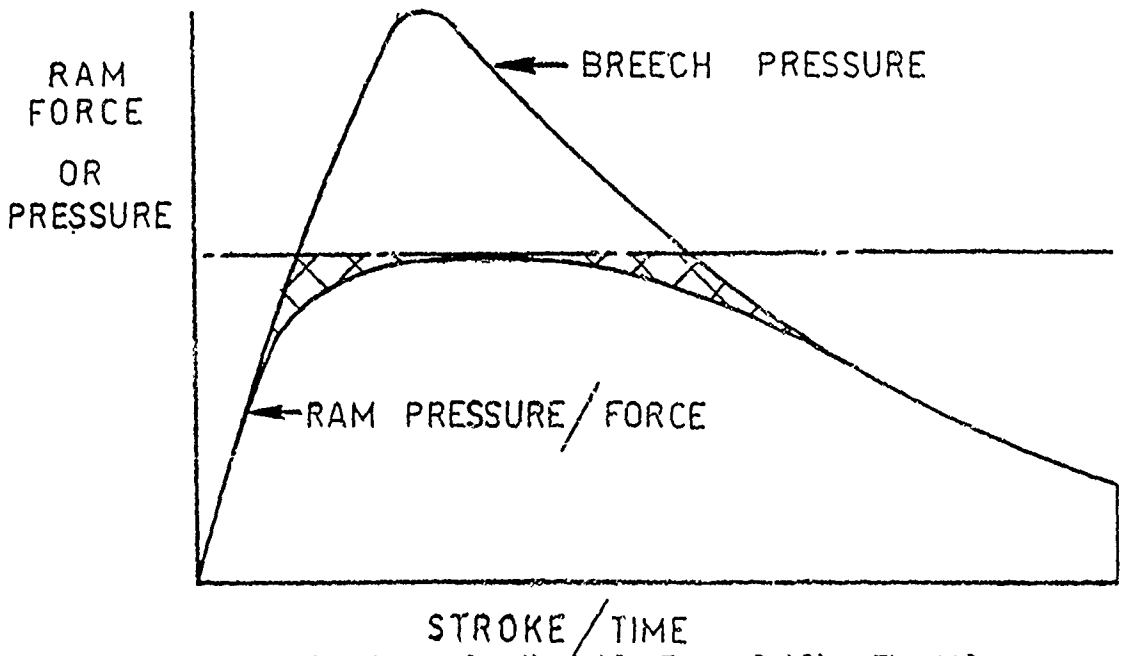

Fig. 1b Pressure-time Curve for Variable Taper-Orifice Throttle

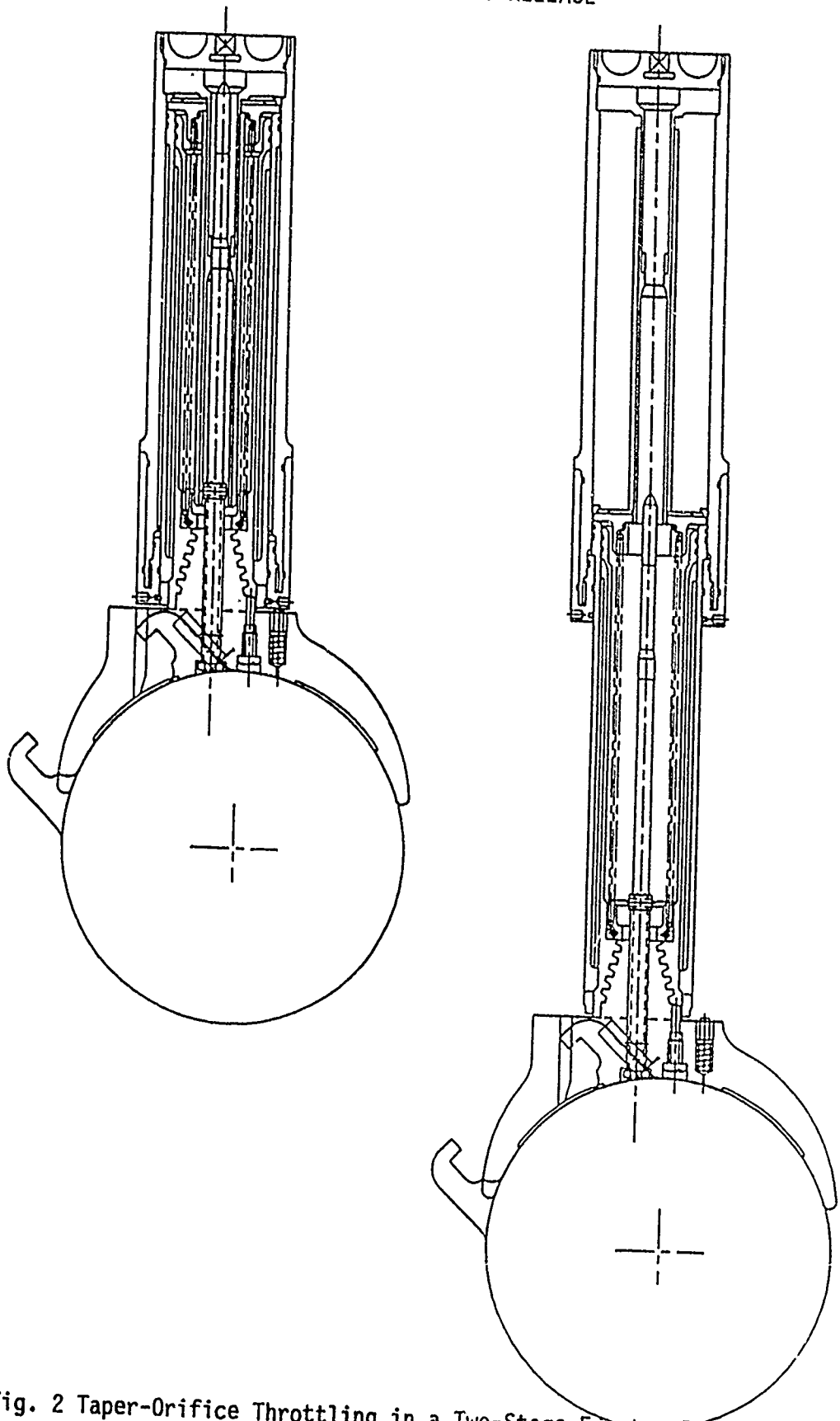

Fig. 2 Taper-Orifice Throttling in a Two-Stage Ejector Ram

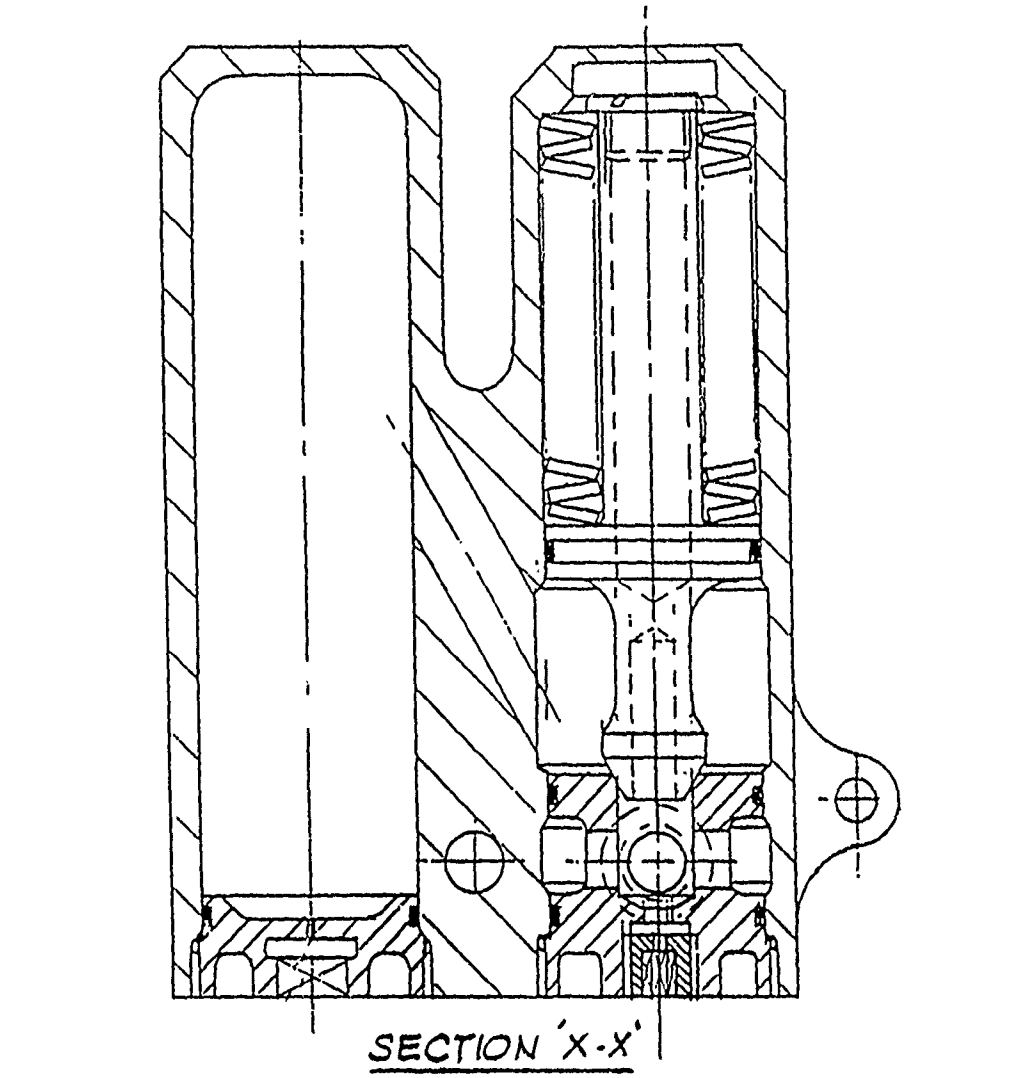

Fig. 3 Breech Volume Control System

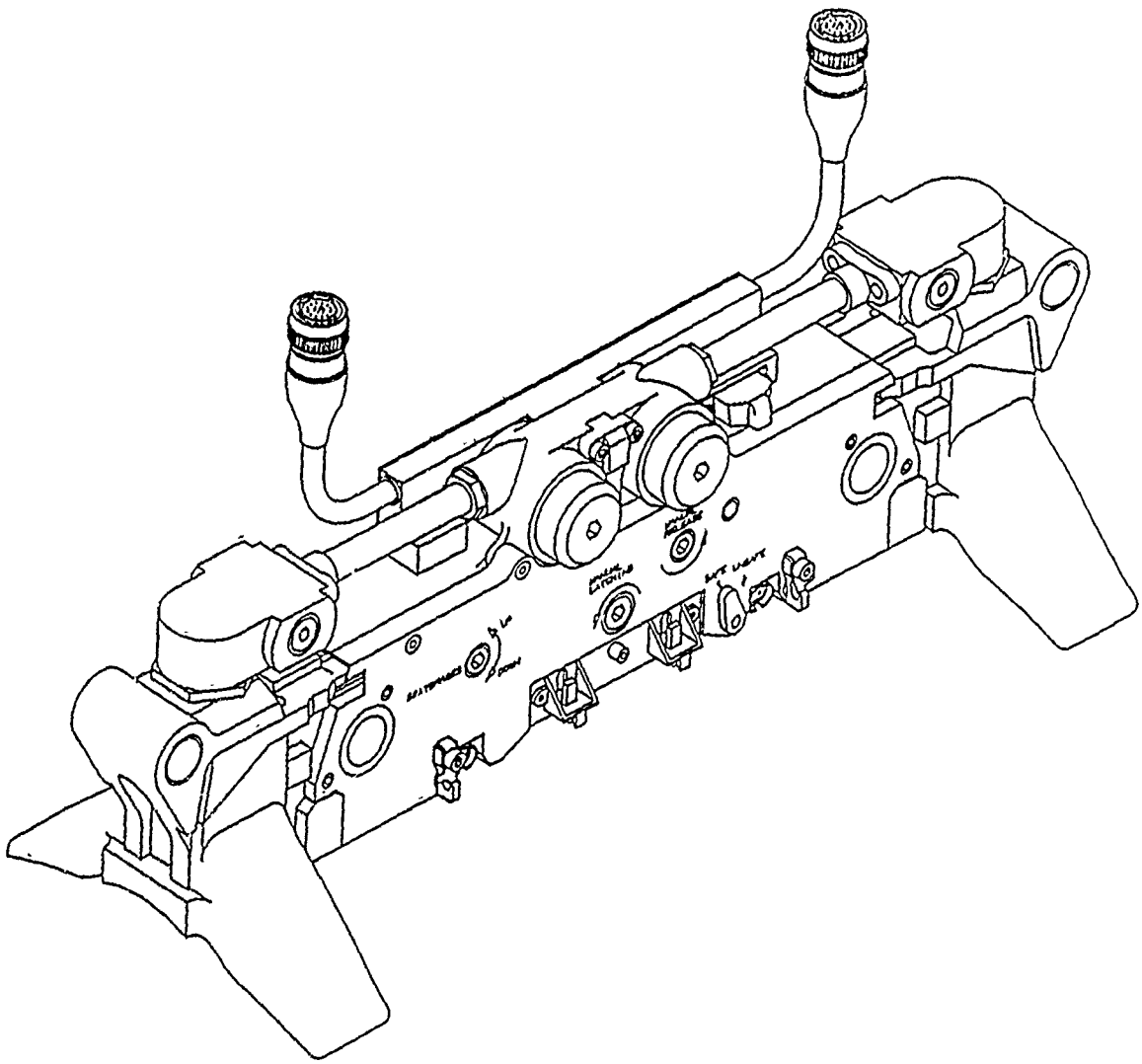

Fig. 4 Proposal for Advanced Light-Duty Bomb Rack

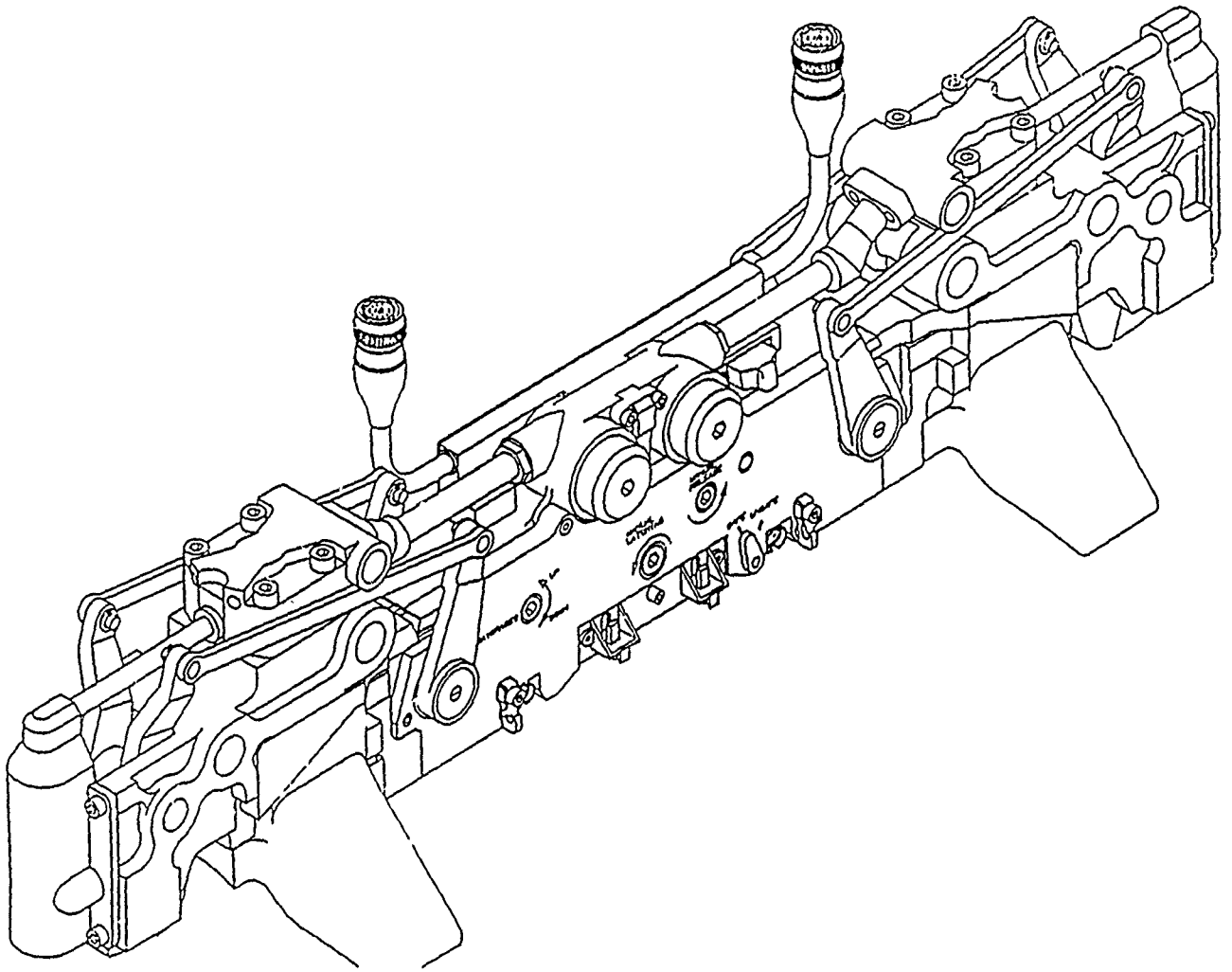

Fig. 5 Proposal for Advanced Heavy-Duty Bomb Rack

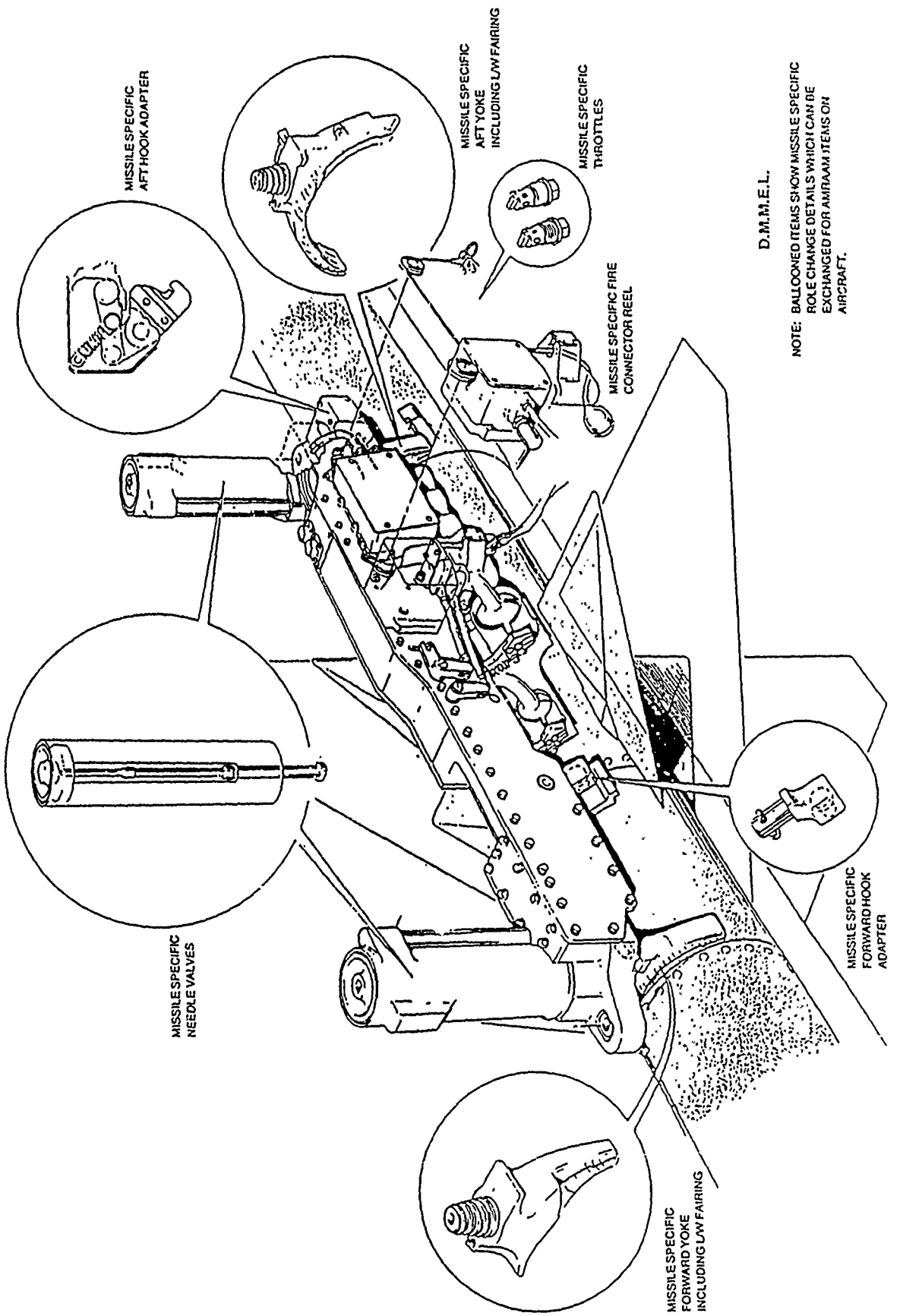

Fig. 6 Proposal for Advanced MRAAM Eject Launcher

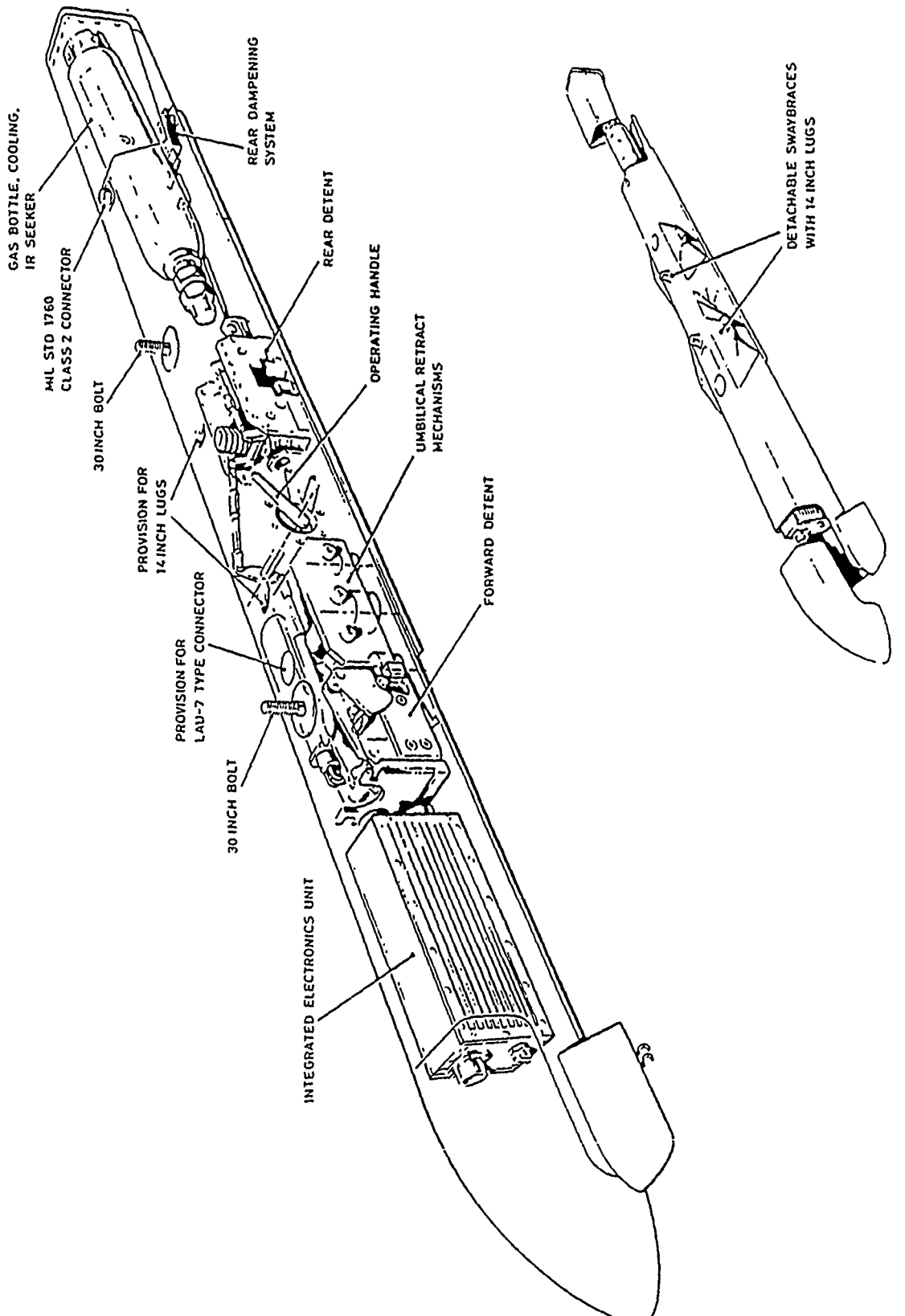

Fig. 7 Proposal for an Advanced Multi-Purpose Rail Launcher

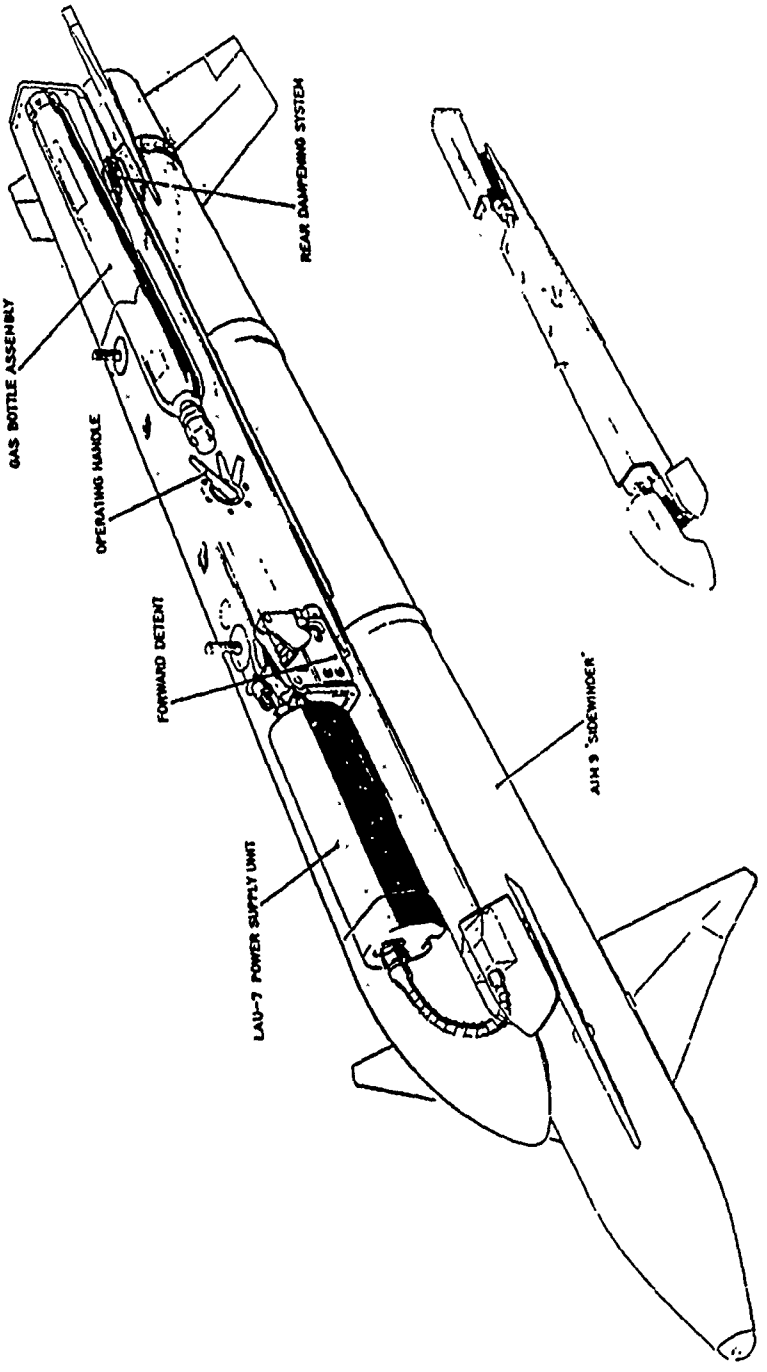

Fig.8 Proposal for Sidewinder-Dedicated Rail Launcher, SDL-21 Page 22

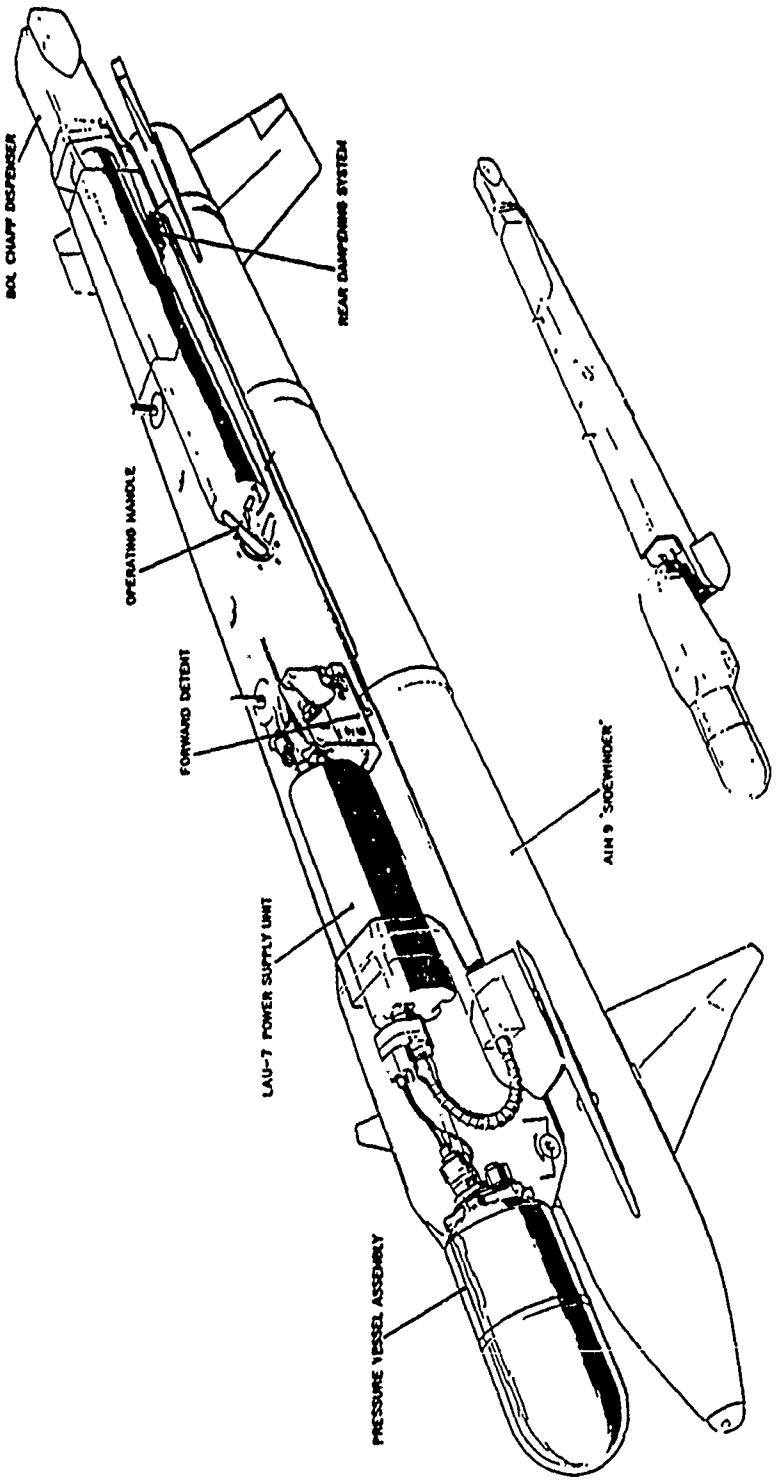

Fig. 9 Proposal for a Sidewinder-Dedicated Rail Launcher with chaff dispenser, SDL-21 CF

CLEARED FOR PUBLIC RELEASE

MPRL FOR AIM-9, ASRAAM, AMRAAM, SPARROW VARIANTS

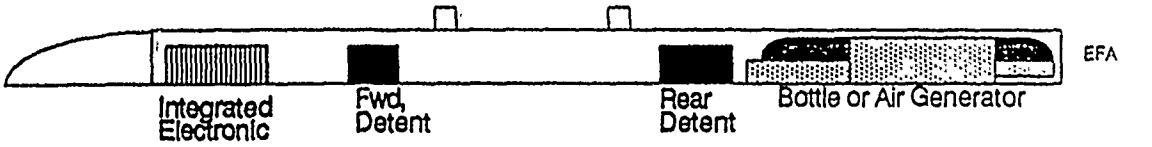

SDL 21 For AIM - 9

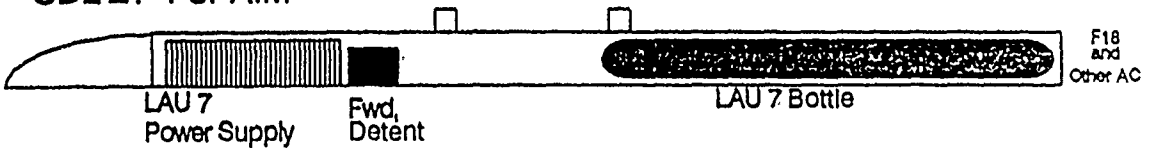

SDL 21 C/F For AIM-9

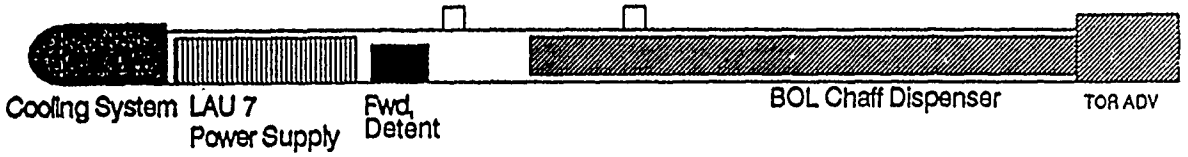

COMBI LAU For AIM -9

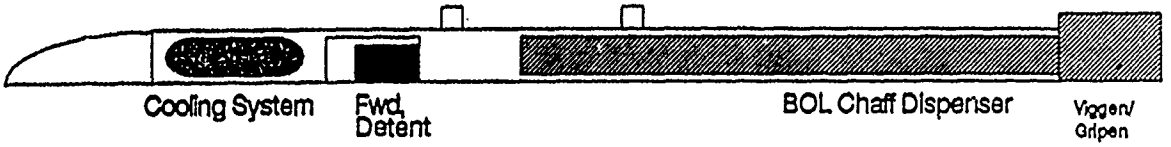

COMBI LAU For AIM -9

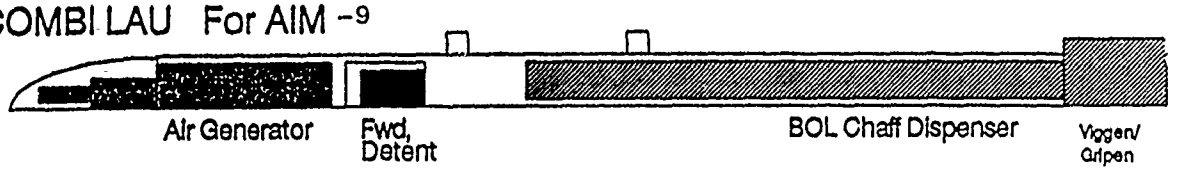

SDL 21 For AIM-9

FIG.10 MPRL FAMILY TREE PAGE 24

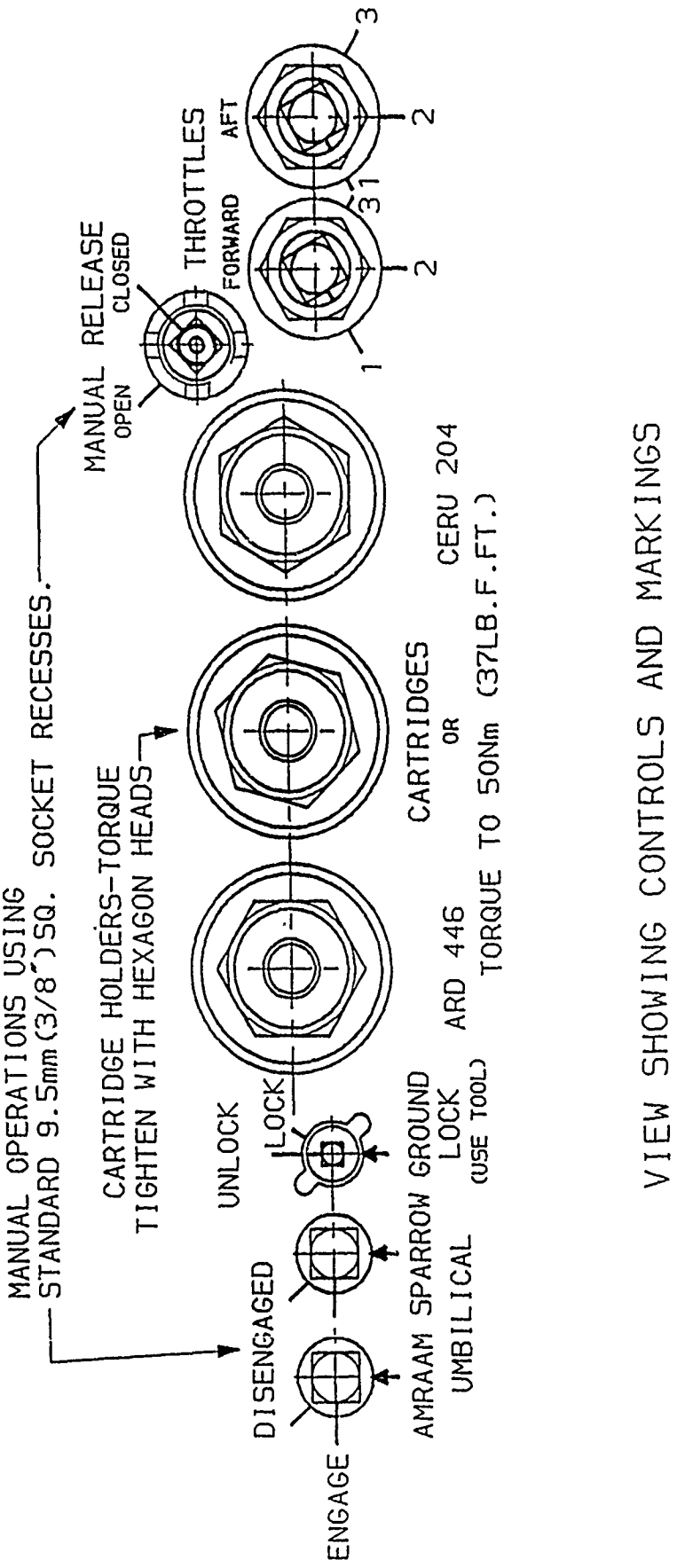

Fig. 11 View of Ground Functioning Points, MRAAM Eject Launcher

CATEGORY: Store Suspension and Release

TITLE: Key Features in the Design of Carriage-and Release Equipments for Agile Combat Aircraft.

AUTHOR: R R Evans, Head of Projects, ML Aviation Ltd, UK.

BIOGRAPHY OF AUTHOR

After completion of a student apprenticeship in 1969, the author joined the Structures Office of British Aerospace at Filton, Bristol where he worked on structural analysis and detail stressing for the Concorde and Tornado programmes.

In 1977 the author transferred to the Guided Weapons Division (later to become BAe Dynamics) at Filton where he became a design group leader for missile system installations (Swingfire, Rapier and Seawolf) on a variety of vehicles.

In 1979 he joined ML Aviation, initially as a Principal Design Engineer and then as Technical Services Manager and Chief Engineer, before reaching his current post as Head of Projects Department. During the course of his career with ML Aviation, the author has been closely involved with a number of weapon-carriage-and-release equipments developments including the BRU36A/A for the AV-8B aircraft, the Sea Eagle Missile Eject Launcher, the Alarm Rail Launcher and a number of proposals in collaboration with European partners for the Eurofighter programme.

Thus on close analysis of the author's career, both in the commercial and military fields, it will be seen that his involvement has always been with things that go bang - either sonically or pyrotechnically. Furthermore, his special and abiding interest has always been that - after the bang - the aircraft should at least remain intact.

So far, so good.

COMPUTERIZED PHYSICAL FIT OF STORES ON AIRCRAFT

(AIR FORCE FEASIBILITY STUDY: APPLICABILITY AND BENEFIT STUDY)

DANIEL SPEYER

3246 TEST WING/TY
OFFICE FOR AIRCRAFT COMPATIBILITY
EGLIN AIR FORCE BASE, FLORIDA

OCTOBER 1990

ABSTRACT

Most fit check methods which the Air Force compatibility engineer presently uses are not very accurate and are time consuming. An engineer does not have an accurate analytical tool to perform fit checks. The Aircraft Stores Interface Manual (ASIM) is available to the compatibility engineer; however, engineers use this manual only as a rough estimate. The engineer has to depend on flight line fit checks with tangible stores on tangible aircraft before he can feel confident that the stores fit on the aircraft. During development of new stores, computer based fit checks are usually conducted on a limited number of candidate aircraft by the aircraft prime contractors. As the store enters the inventory, certification requirements often change or are broadened versus the original requirement. In order to be responsive and provide the Air Force with the capability to perform broader compatibility studies on more aircraft and additional store configurations, the Air Force needs an in-house analytical tool. Furthermore, the current dependence within the Air Force for hardware oriented fit checks often results in unanticipated discoveries of fit interference that negatively impact certification schedules and cost. An early analytical based approach using computers would avoid many of these "show-stopping" problems which often appear late in the certification effort. Since there have been great advances in computer graphics software, hardware speed, and memory, it is feasible to develop an analytical computerized tool to perform fit checks. However, during the survey reported herein, the lack of a system which can easily and accurately perform a fit check in accordance with MIL-STD-1289A became apparent. Many systems are out-dated and cumbersome to work with. A compatibility engineer would have to train for many months before he could model aircraft and stores to perform a fit check on these systems. Software will have to be modified to make it more user-friendly, less cumbersome, and meet the requirements of MIL-STD-1289A. Recommend the following: (1) survey software packages (preferably three-dimensional, solid modeling, computer aided design software packages) which can be modified to perform fit checks of armament on aircraft in accordance with MIL-STD-1289, and purchase (or lease) the software package; (2) modify the software to perform fit checks easily and accurately; (3) survey and purchase graphics work stations; (4) develop lines of communications with government offices and aircraft/ armament contractors for exchanging external dimension model data; (5) develop methods for verifying data and evaluate whether a measurement lab is required to collect accurate data.

TABLE OF CONTENTS

LIST OF FIGURES

SECTION I

INTRODUCTION

A. Purpose of Report: This report was written to:

1. Explore the need for developing better methods to determine geometrical physical fit of stores on aircraft

2. Investigate the feasibility of using a computer to perform this task

3. Survey current capabilities to perform fit checks with a computer

4. Recommend an approach to develop the system which could be used most effectively and easily by a compatibility engineer

Most fit check methods which the Air Force compatibility engineer presently uses are not accurate and are time consuming. Because fit checks are so important to the certification process, the use of a computer as an engineering tool to complete fit checks needs to be investigated. Advances in computer graphics software, hardware speed, and memory make computers a viable solution.

B. Description of Fit Check: A fit check is a process where an engineer using drawings, computerized models, or physical items assesses whether a store will contact the aircraft, ground, or any other store during the full operation of an aircraft flight mission. Stores are objects (e.g., launchers, pylons, bombs, and missiles) which bolt onto or hang from aircraft. Using specifications in MIL-STD-1289A, the compatibility engineer ensures stores are separated (some distance) from the aircraft, other stores, and from the ground. MIL-STD-1289A specifies distances which stores must be separated to clear other objects to ensure the following circumstances do not occur:

1. Stores do not contact or vibrate against the aircraft/stores during flight or contact each other during separation.

2. Stores do not interfere with the aircraft control surfaces and/or landing gear.

3. Stores clear the ground during take-off and landing.

4. Stores can be loaded/unloaded using ground loading equipment.

(See Addendum I for overview of MIL-STD-1289A)

C. The Importance of a Fit Check: When HQ TAC/SAC/MAC requests a store to be certified on an aircraft, there are many engineering disciplines which need to be addressed. The store's mass properties and added aerodynamic drag require engineers to analyze aircraft stability and control, aircraft loads

(attachment strength and wing strength), aircraft flutter, and store separation. The first engineering discipline which should be addressed is geometrical fit. A fit check will determine whether a store can be loaded and captive carried on the aircraft (at a particular station, on a particular pylon).

If the compatibility engineer determines the store will fit on the requested aircraft, other engineering disciplines can begin their analysis. For example, separation engineers can begin their wind tunnel test, systems engineering can begin their integration/electrical modification analysis, aircraft flutter engineers can begin their computer analysis, etc. If wind tunnel testing or electrical modifications are completed before a fit check is completed, wind tunnel testing/integration analysis may have to be re-accomplished if the fit check uncovers a requirement for a modification to the aircraft/store. For example, if the store interferes with the aircraft control surface, an adaptor may need to be fabricated to separate the store from the control surface. If the store scrapes the ground during landing or interferes with the operation of the landing gear, the store may never be certified on the pylon or aircraft for which the separation/integration engineer has already invested time and money in the analysis, testing, and procurement of software and hardware.

In conclusion, fit check analysis must be one of the first engineering disciplines to be completed in the certification process. This analysis will support or cancel further analysis.

SECTION II

CURRENT ENGINEERING TOOLS

The current methods used by the compatibility engineer to obtain the geometrical information are not accurate and are time consuming. An Air Force compatibility engineer has three methods of obtaining the geometrical data necessary to perform a fit check analysis.

A. Paper Fit Check: The first method is to perform a paper fit check using paper drawings. The drawings can be obtained from System Program Offices (SPO), System Program Managers (SPM), Contractors, or the Aircraft Stores Interference Manuals (ASIM: ASIM contains two-dimensional (2-D) paper drawings of aircraft and stores). The engineer combines the relevant drawings and manually places the stores on the aircraft. This process is susceptible to mistakes. If the many drawings which the engineer combines are not in the same scale, he has to redraw them. Rotation and pitch angles are hard to manipulate manually on paper. Paper drawings are in two dimensions (2-D) only, while a fit check requires analysis and observation in all three dimensions (3-D).

B. Contracted Computer Fit Check: The second method which the Air Force engineer uses to perform a fit check is to contact the Aircraft Systems Program Office/Manager who will, in turn, contract the aircraft contractor to model the stores and perform the fit check using computerized physical fit programs. This method is time consuming and costly. All present-day aircraft (F-15, F-16, F-111, F-4, etc.) are modeled in computers in 2-D or 3-D wire frame models. The aircraft contractors can perform a fit check using these models. This places the Air Force dependent solely on aircraft contractor capability, which makes it difficult to perform quick studies.

C. Flight Line Fit Check: The third method is to actually obtain all the relevant stores/aircraft and perform the fit check on the flight line. This method is costly, very time consuming, and sometimes impossible (when dealing with a developmental store or aircraft). This method does not take into account the problems associated with large manufacture tolerances and attachment tolerances. When a fit check is conducted on one aircraft with one store, the distances measured could differ when the store is loaded on another aircraft because of changes of external dimensions of stores and shifting of stores on their attachments. When using a computer, these tolerances can be taken into account (the computer could examine the worst case fit check situation).

When investigating whether a store will contact the ground during takeoff and landing, there is not a method of actually raising the aircraft's nose on the flight line to simulate pitch attitude during take-off and landing. A fit check engineer uses the ASIM for an estimate and verifies the distance between the store and the ground using video cameras during an actual flight mission.

This method does not verify landing with a flat tire and/or compressed strut. When investigating whether a store will contact the ground with a flat tire and fully compressed strut, the ground support crew must deflate the tires and drain the struts. This can damage the tires and struts so that they have to be replaced.

SECTION III

THE NEED FOR A BETTER ENGINEERING TOOL

As can be seen in the previous section, a compatibility engineer can complete a fit check either by contracting aircraft contractors or by conducting a preliminary paper fit check (using paper drawings, ASIMs) and validating it after tangible assets are delivered to the flight line. A compatibility engineer cannot draw a complete conclusion regarding a fit check without an actual flight line fit check. Many times the ASIM drawings are not detailed enough to use for certification of a weapon on an aircraft. Two-dimensional drawings are used only as an estimate or prelude to an actual fit check on the flight line. Many drawings can not be found in the manuals. A compatibility engineer needs a better tool then just ASIMs to determine whether a store will fit.

When conducting a flight line fit check, an engineer must keep in mind that he is conducting a fit check with one store on one pylon on one aircraft. There are many statistical tolerances (manufacture or interface variables) which one fit check will not address. Only during a flight test program will a compatibility engineer be able to address statistical tolerances. During a flight test program, the store will be carried on many different aircraft on many different pylons. Frequently a fit check problem appears during a flight test program which was not identified during the initial fit check. A compatibility engineer needs a better tool for determining whether a store will fit early in the program rather than waiting for a problem to appear during flight testing.

If a store is in design and not available for a flight line fit check, the compatibility engineer can recommend that the aircraft contractor perform the fit check. Most stores are carried on more than one aircraft, so the compatibility engineer will have to contract more than one aircraft contractor. Because of the differences in contractor systems and methodologies, the fit checks by the different contractors will result in different degrees of accuracy. Also, the time and expense of utilizing multiple contractors through multiple contractors through multiple contracts becomes a responsiveness issue. If one methodology or system is used to perform the fit checks, the analysis will be more consistent and the accuracy will be more constant.

Many benefits would result from an Air Force computerized fit check capability. This tool would give the engineer an analysis capability which is not available today. When modeling the stores, the engineer could place any desired dimensions in the computer. He would not have to depend so much on a flight test program to determine fit in accordance with MIL-STD-1289A. This tool would allow the Air Force to be more efficient.

SECTION IV

FEASIBILITY AND BENEFITS OF USING A COMPUTER

This section discusses the following benefits of computerized fit checks: (a) how a computer can be used more efficiently and effectively than paper drawings by a compatibility engineer, (b) different model formats (mathematical description of a store or aircraft in a computer) and why certain formats could be used more accurately, (c) tolerance issues which a engineer needs to address with any fit check analysis and how a computer can help solve these issues, and (d) the desired engineering features which need to be incorporated in the system for a proper fit check to be conducted.

A. Paper Versus Computer:

1. Paper: Paper has inherent problems. Paper is subject to tearing, misplacement, and even expansion and shrinking due to atmospheric humidity. The drawings are drawn to a predetermined scale (e.g., 1:16, 1:10, etc.). Not all drawings are in identical scale. When different drawings are combined, those which are out of scale will have to be redrawn or modified. Paper drawings are hard to manipulate accurately, especially in regard to such details as angles and attachment placement. The drawings of stores are loaded on aircraft drawings with adhesive tape. Fit checks are documented by placing the taped drawings on a copier machine. Most important, paper can not function in three dimensions.

2. Computers: Computers store the drawings magnetically, so tearing and loss (if backed-up correctly) do not occur. Adding stores to aircraft is completed using exact attachment coordinates. Pitch, roll, and yaw angles of stores can be easily computed/verified. Print out of drawings and fit check analysis is easier to complete. Interference and separation distances can be computed automatically with certain software algorithms. Computers are very accurate. Computers can work in three dimensions. The only problem with computers is the large amount of time spent developing and maintaining the database.

B. Different Model Formats (Two Dimensions Versus Three Dimensions):

1. Two Dimensions: Two-dimensional models have many drawbacks. They do not fully represent a real-life flight line fit check. Fit checking a store on an aircraft is a three-dimensional problem. When a fit check engineer tries to determine the separation clearances between a store and a pylon, he positions his head by bending down, looking up, and possibly rotating in such a position to obtain a perpendicular view of the clearance distance. This movement cannot be modeled using two-dimensional software. When a three-dimensional problem, such as fitting a store on an aircraft, is modeled in two dimensions, the designer of the 2-D model decides which perspectives are more usable for latter fit check use. The 2-D model designer usually decides on a front, top, and side view. When the compatibility engineer tries to determine

whether a store will contact the aircraft, he will most likely find that the views he has at his disposal will not give him the right perspective to determine the interference or separation distance. This is especially true for curved surfaces (fairings on pylons or conformal fuel tanks). To obtain all aspects of all possible interferences between a store and an aircraft, the length of the store and aircraft interface area would have to be broken up into a multitude of cross sections with three views of each cross section. Using the cross section approach, the model designer again makes the decision, beforehand, which cross sections are best for the compatibility engineer.

2. Three Dimensions: When the model designer constructs the aircraft and store models in a computer, he does not have to decide which views are best for the compatibility engineer because he models the entire surface of the store in length, width and depth. The engineer can use the computer viewing options to rotate, pitch, and yaw the aircraft store combination because the models are built in three dimensions. Two-dimensional files are modeled only in length and width. For example, if you rotate a 2-D side view of a store model 90 degrees to view the nose of the store, it becomes a one-dimension line instead of another 2-D image. The drawback of 3-D models is that the data files take more time to input because of the added dimension. This section explains the attributes and drawbacks of defining 3-D models in wire frame, surfaces, and solids.

a. Wire Frame: Wire frame models are the simplest models to create. They can offer precise data about surface edges of an object. However, they do not contain information about surfaces between the edges and do not differentiate between the inside and outside of an object. As a result, wire frame models representing complex geometries often are ambiguous (Figure 1). They do not provide enough information to represent a solid object with complex surfaces. The wire frame model is created by the relationship that exists between the 3-D points, which are connected with lines.

Interference is sometimes roughly approximated when wire frame models are used, and in some instances, is impossible to determine. For example, a compatibility engineer may want to determine the interference between a store fin and an aircraft conformal fuel tank. In reality, the fin interferes with the fuel tank; however, if the aircraft surface is defined with wire frame squares, the fin interference may not be identified because the fin model penetrates the aircraft surface model between the defined wire frame lines.

Complex wire frame models are very difficult to interpret. They are visually ambiguous not only to the model designer but also to the compatibility engineer. For example, in Figure 2, is the missile's fin (on the top of missile) in front of or behind the launcher? It is not possible to shade a wire frame model because there is no concept of faces to reflect light. Because of this ambiguity, hidden line images cannot be generated. A compatibility engineer can see through the store, pylon, and aircraft; therefore, it is difficult to determine which lines represent which object.

b. Surface: A surface model holds a description of a model by storing the points, edges, and faces between the edges. It conveys no concept of the space occupied by the material or of the connectivity between the

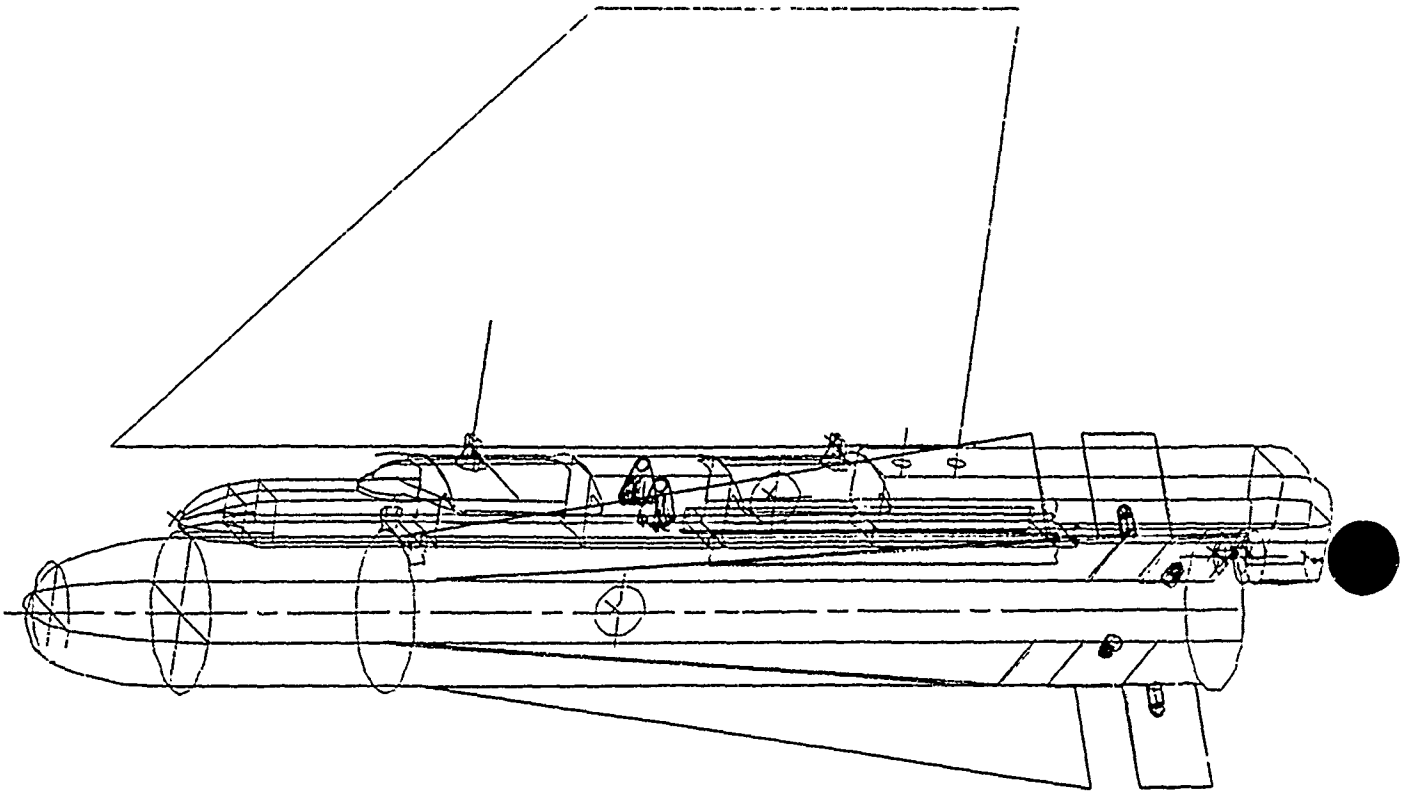

Figure 1: AGM-65 on a LAU-117, Showing the ambiguity of viewing wire frame drawings. Model was printed using McDonnell Douglas's CAD D software.

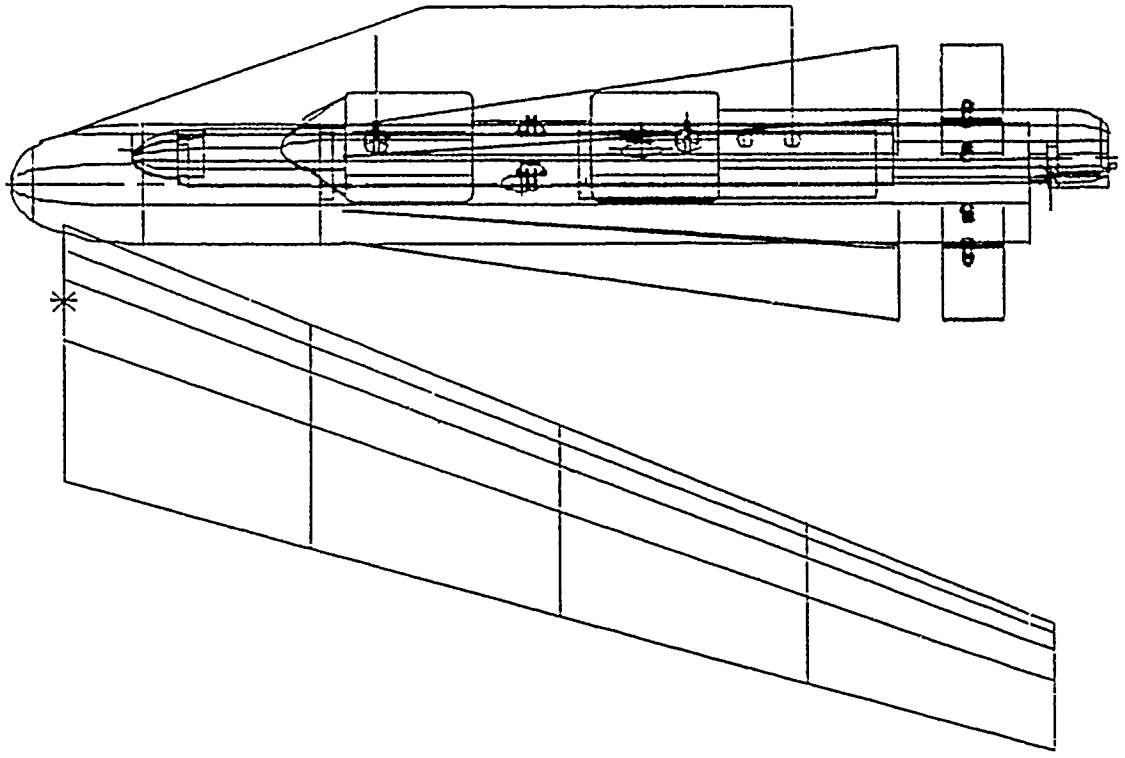

Figure 2: AGM-65 on a LAU-117, Showing the ambiguity of determining interference between two wire frame drawings (missile and a mock aircraft surface). Model was printed out using McDonnell Douglas's CAD D software.

faces. Surface models, the next higher level of modeling, avoid many of the wire frame ambiguities by connecting various user-selected surfaces to represent a part's geometry. However, they contain no information on the interior of a part. Interference can be calculated using surface models when the surface normals are pointing in the correct direction. If surface normals are not defined, a surface model cannot determine the amount of interference an object has within another object. When viewing an object, the fit check engineer cannot view automatically sectioned and hidden line images, because the models contain insufficient information for the software to produce these images.

c. Solid: Solid models, the highest level of sophistication in modeling, overcome the drawbacks of wire frame and surface models by defining parts mathematically as solid objects (volume). While conventional wire frame and surface models represent only edges and envelopes of a part, solid models define the material inside and eliminate any ambiguity in interpreting the model (Figure 3). This representation also creates a more nearly complete database for performing a range of other functions. Unlike wire frame and surface models, solid models can be used to determine if a specified point lies inside, outside, or on the surface of a part. Solid models demand more computer processing time and memory than do wire frame or surface models, but they can readily be used to compute mass properties. They also lend themselves to 3-D kinematic studies (e.g., operation of landing gear) and interference checking.

Interference between solid models can be defined and measured by extracting the interference volume or separation distance (if the two objects do not interfere). Solid models can also be used to determine whether a solid object moving through space interferes with another object by extruding a surface on the solid object in a specified direction. For example, to determine whether a missile being launched down a rail will contact an adjacent store, the aft surface of the missile wing is extruded in the direction in which it would be translating down the rail. The extruded surface becomes a new solid. The new solid represents all positions the missile wing would have occupied during the entire launch cycle. An interference check is now completed between the new solid and the adjacent store.

D. Tolerance Issues: There are many problems associated with tolerances. Below are tolerance problems which should be addressed by a compatibility engineer in performing a fit check on the flight line.

1. Manufacture Problems: To cut costs, weapons are mass produced. Therefore, the manufacture tolerances can sometimes be very large (especially for older 1950/1960 bombs). The newer missiles' and guided weapons' tolerances are smaller; however, most guided bombs use the old (large tolerance) bomb bodies.

Computers can help solve this problem. At the present time, when a compatibility engineer goes to the flight line to check the fit of a store on an aircraft, he is checking one combination of one store on one pylon on one

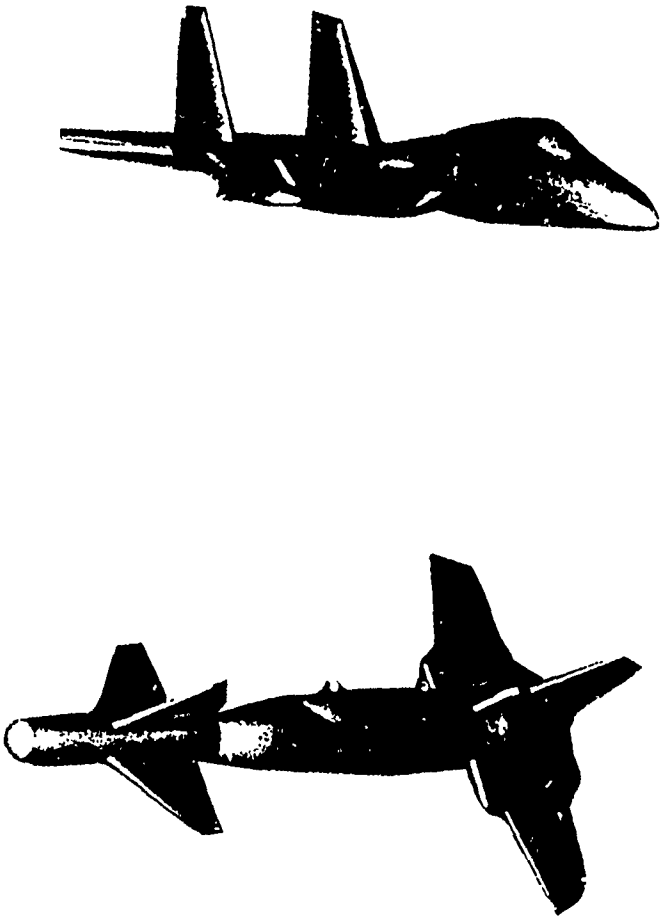

Figure 3: F-15 and GBU-24A/B, Solid models eliminate ambiguity while viewing. Model was photographed from the ASD/XRC (M) computer monitor.

aircraft. An engineer does not perform a hundred fit checks to determine whether all inventory stores fit on all aircraft. A model in a computer can be defined with any dimensions. To represent different stores, a few models could be designed: largest, smallest, and nominal. Tolerance data could be obtained from the contractor; however, build-up tolerances (guided systems on old bombs) would have to be measured. A database could be developed using a statistical sample methodology. For example, a survey would be taken at different weapon depots, and a crew could travel to the depots to measure a sample of different weapons. The measured data could be compared to the solid model dimensions to determine needed tolerances for particular objects. Aircraft could be measured approximately in the equivalent manner.

2. Attachment Shifting/Loading: The pylons/stores being carried on Air Force aircraft are built by many different contractors. When a pylon, suspension equipment, and store are mated, there is a possibility of having different overall distances for every pylon, store, and aircraft combination. In fact, if you mate the same pylon and store on an aircraft and measure the distance between the store and the flap and then load the exact pylon and store combination on a similar aircraft, the distances will be noticeably different.

Again, computers can help. Attachment distances and angles can be manipulated in a computer, while on the flight line they can not. The collection of data would be the difficult part to solve in this method. Statistical measurements would have to be obtained from actual store/aircraft combinations so as to educate the model designer about the amount of shifting which can occur.

3. Wear: The most difficult of the four tolerance issues is wear tolerance problems. As pylons/stores and especially suspension equipment are used on the flight line, they receive changes to the external dimensions (dents, bends, etc.). Aircraft skin and structure stretch during their life cycle. Maintenance technical orders give guidelines of allowable deformities of stores being loaded on aircraft. A multi-weapon ejector rack can be worn/deformed in a manner that allows stores to be closer to each other than they would normally be.

Wear can be modeled in a computer; however, wear data would be nearly impossible to obtain from the contractors. Wear would have to be measured from actual items, and then the nominal model could be duplicated and modified to represent a stretched or bent model.

4. Dynamic Effects: The distances between the stores and the aircraft when the aircraft is at rest will be different when the aircraft is in flight. When the aircraft is in flight, the aircraft and stores experience forces, accelerations, and aerodynamic loads (pressures/vibrations). These forces result in movement of stores and adjacent aircraft structure.

To model the dynamics of a static model, deflection/displacement information would have to obtained from the structures and vibrations groups. The nominal models could be duplicated and modified to represent worse case deflections and displacements.

When an engineer performs a fit check on the flight line, he needs to keep in mind that he is performing a fit check with one store on one pylon. The store is most likely new and is being loaded on an aircraft which is static (no vibration or acceleration/inertia effects). MIL-STD-1289A attempts to solve the above problems by specifying required clearances by which a store must be separated from another store/aircraft/ground. If the compatibility engineer abides by the clearances specified by MIL-STD-1289A, the above tolerance problems should not cause a store to rub or contact another store/aircraft/ ground.

E. Desired Software Engineering Tool Features: It is important to emphasize what is being modeled and to manipulate these models to perform the fit check analysis. A computerized fit check entails modeling aircraft, suspension equipment, and stores into a database; combining specific databases into one database, and conducting interference checks during the following processes: static fit of stores on aircraft, simulated separation of stores down rail launchers or ejected from suspension equipment, simulated landings with and without simulated gear failures (flat tire and/or strut failures), and movement of all aircraft control surfaces, parts, and access panels. The following paragraphs describe the above process and define system functions required for the performance of the above tasks.

1. Modeling Aircraft, Suspension Equipment, and Stores Into a Database: To build models, the computer software must have a computer aided design (CAD) package built into it, or the software must interface with a CAD system. The software must be able to model in 3-D solid models.

2. Combining Specific Databases Into One Database: When a compatibility engineer is performing a fit check, he will first read an aircraft model and then read pylon models and store models in combination with the aircraft model. The software must be able to combine databases into one database on command and place an object tangent to another object on command (placing missile hangers level with rail launcher or store lugs tangent with pylon suspension hooks).

3. Interference Checks: Static Fit of Stores on Aircraft: The software must be able to perform interference calculations and identify the closest distance between two objects if they do not interfere. It is desirable for the software to identify the interference volume.

4. Interference Checks: Separation of Stores: The software must be able to translate a surface or a solid in a defined trajectory, and at the same time, perform interference calculations between identified objects. It is desirable that the software be able to sweep out a volume to represent a new solid. This new solid can be checked in this manner for interference instead of using an iteration routine which checks interference after every slight movement of the model being translated.

5. Interference Checks: Simulated Landings With and Without Simulated Gear Failures (Flat Tire and/or Compressed Strut): The software must be able to rotate a solid (aircraft/store combination) about another solid (ground)

and at the same time perform interference calculations between identified objects.

6. Interference Checks: Movement of All Aircraft Control Surfaces, Parts, and Access Panels: The software must be able to perform kinematic functions. To represent proper movement of landing gear, or rotation of aircraft slats or flaps, software must be able to model the movement of the objects as closely as possible. The software must define how solids are connected (fixed, degrees of freedom of movement, etc.) to each other. During the simulation of the movement of objects, the software performs interference calculations between objects in perspective.

SECTION V

SURVEY CURRENT COMPUTER CAPABILITIES FOR PERFORMING FIT CHECKS

This section discusses the different computer systems which the government has or could use to perform computerized fit check of stores on aircraft. This section also discusses the systems the aircraft contractors are using and will be using in the future to perform this task.

A. Government Computer Systems:

1. ASD/XRC (M): XRC has a 3-D solids model based computerized fit check program which is the most usable system found during this survey. The program's solid model generator was designed by Brigham Young University's (BYU) Civil Engineering Department. The Navy contracted BYU to design a solid model program (NAVGRAPH) and deliver the model's Fortran Source Code. The program is free to any government organization. XRC contracted APTEK to develop a program (CALIPER) which uses the NAVGRAPH CAD models to determine interference distances. The program also calculates minimum separation distance between two objects. Figure 3 was modeled using this software. F-15A and many stores have already been modeled by APTEK. The program can sweep, rotate, and extrude surfaces to make new solid models. This capability can be used to represent aircraft flaps and landing gear doors to sweep an area.

2. Arnold Engineering Development Center (AEDC): AEDC has developed a program, Store-Separation Graphical Analysis Package (SGAP) which uses 3-D wire frame models to represent the output of wind tunnel test trajectories. This program helps the store separation engineer visualize/analyze store trajectories. AEDC-TR-88-39 Technical Report describes the SGAP geometry in the following manner: "Arbitrary surface geometries are represented numerically by a set of points in 3-D space. The points are connected in some logical sequence by a series of straight-line segments to approximate the surfaces of the geometry. Three-dimensional representations of this type are commonly referred to as wire-framed models." The SGAP program has a capability (using AUTOCONF) to place stores on aircraft in a specified orientation, build surfaces (or facets) using the wire frame points, and calculate collision of an object with another object. However, when a curved surface is being defined by points and lines, SGAP connects the points with straight lines instead of arcs or curved lines. With this method, a multitude of points and lines would have to be used to define a curved surface accurately enough for our purposes. AEDC has an extensive aircraft and stores model library. However, most models are not detailed enough to be used for fit check purposes. If the model database is transferred to a solids software database, many hours will have to be spent extracting the points from the database and curve-fitting the points to approximate the solid's surfaces.

3. Hill AFB, Wright Patterson AFB, Robins AFB, Edwards AFB: All of the engineering groups and aircraft program managers who were contacted at the above Air Force bases stated they do not have a computer fit check

capability and that they depend completely on aircraft contractors to perform the computer fit check tasks.

4. Pacific Missile Test Center (PMTC): Associated with the ASIM system, the Navy has tasked a contractor to model all the drawings in ASIM in 2-D wire frame. The contractor is performing this task with a scanner type system. The data are put into the model database by placing a set of drawings on a device similar to a copier machine. This machine defines the 2-D drawing lines mathematically with 2-D coordinates (X,Y). There can be many inaccuracies involved with modeling objects in this manner. The scanner has software which decides where the objects surface coordinates start and end. So, if the paper drawing is slightly faded or creased, the software may be incorrect on the placement of the object's coordinates. PMTC does not have an in-house system to perform fit checks in a computer.

5. Marines: To support the AV-8B (Harrier), the marines purchased McAir's 3-D wire frame CAD-D computerized fit check system. See paragraph B.2. for further description about CAD-D.

B. Contractor Computer Systems:

1. General Dynamics (GD): GD purchased a Lockheed developed 2-D wire frame computer program (CAD M). GD modeled the F-16 and portions of the F-111 in this system and also many stores and pylons. To determine whether a store interferes with the aircraft, the fit check engineer tasks the Lines Group (group in GD who controls the aircraft LOFT [surface data base]) to send 2-D cross-sections of the area of concern. This system is cumbersome, especially when working with moving parts or rounded surfaces. LOFT data are available for the F-16 and some F-111 parts. GD models advanced aircraft designs using a 3-D solid modeler called Catia. Catia is designed by a French company called Daasault, and IBM distributes the software in the United States. Catia which can accept LOFT data, model movement of landing gear, and calculate separation/interference distances, is a very powerful software that should be seriously reviewed.

2. McDonnell Douglas Aircraft (McAir): McAir developed a 3-D wire frame computer program (CAD D) in the early 1970's. This program interfaces with the aircraft surface description data (LOFT). To determine whether a store interferes with the aircraft, the engineer brings in a small specified amount of surface data from the large aircraft database using a program called Parametric Evaluator. This system works accurately; however, stores/pylons are not described with surfaces. Only the aircraft is described in surface data. Also, to determine whether a store interferes with an aircraft, the fit check engineer has to visually search the wire frame drawings for the interference (Figure 2). This task is time consuming and can produce errors.

Loft or surface data are available for the F-15A/B/C/D/E, F-18, AV-8, and some F-4 parts. McAir has decided to begin designing new aircraft with solid models (using Unigraphics). For example, the new transport aircraft (MD-12) will be designed using solids models.

3. Northrop: Northrop developed a 3-D wire frame computer program called N CAD. N CAD has a hidden line capability but does not have a surface shading capability. This program interfaces with the aircraft surface description data (LOFT) approximately the same way McAir's program does. Loft data are described in a software called N COW. LOFT or surface data are available for some aircraft. The armament group has no plans to upgrade to a solid modeler at the present time.

4. Boeing: Since Boeing is Northrop's subcontractor for the B-2 program, they purchased Northrop's 3-D wire frame program N CAD and surface database N COW. Boeing is designing the weapon suspension equipment for advanced aircraft. For future programs, Boeing plans to design aircraft using the solid model program Catia.

5. Grumman: Grumman uses the 2-D wire frame program that GD uses for the F-14. They are modeling their new program, EA-6B, using the solid model program Catia.

In Figure 4, a matrix of systems versus desired features can be found.

Features / Systems	2-D/ 3-D	Solids	Interfer. Calculator	Interfer. Accuracy	Modeling Accuracy	User-Friendly	Kinematic Tools	Macro. Tools
ASD/XRC	3-D	yes	yes	accurate	accurate	yes, but needs mod	none	none
AEDC	3-D	no	yes	Inaccur.	Inaccur.	unfriendly	none	none
GD								
CAD M	2-D	N/A	no	N/A	Inaccur.	unfriendly	none	none
Catia	3-D	yes	yes	accurate	accurate	yes, but needs mod	alot	some
Mc Air								
CAD D	3-D	no	no	N/A	Inaccur.	unfriendly	none	none
Unigraph	3-D	yes	yes	accurate	accurate	yes, but needs mod	unknown	some
Northrop								
N CAD	3-D	no	no	N/A	Inaccur.	unfriendly	none	none

Figure 4: Matrix of Current Computer Capabilities Versus the Desired System Attributes

SECTION VI

RECOMMENDED APPROACH

All aircraft contractors have been conducting fit checks using 2-D or 3-D wire frame drawings for the past two decades with much success. Aircraft contractors are designing future aircraft with 3-D solid models and will be conducting fit check of stores on aircraft with solid models. Without building a mock-up of the aircraft, aircraft contractors are building new production aircraft from the models in the computer. For example, the advanced bomber was built by Northrop using only computer models. This shows how much confidence aircraft contractors have in the accuracy of their model generators.

Discussions with the aircraft contractor engineers indicate that computer software and hardware have matured greatly in the past two decades. Contractors recommend solid model generating software to be used to perform this engineering task. Solid models are more accurate and are easier to use than the models used in the past. Since most stores/pylons will have to be modeled from 2-D paper drawings, it is prudent to spend a little more time now modeling in solids (instead of wire frame or surfaces), because the models could be later used for other purposes. Solid models have volume, so mass properties can be easily determined with algorithms. With the models being geometrically/externally defined as well as internally defined, these models could be used in future compatibility analytical tools (store separation, computational fluid dynamics, structural analysis, flutter analysis, etc.).

Much work is being accomplished in human factors engineering. Engineers are modeling the human body in computers. Torsos, arms, legs, and movement of joints are being modeled, so loading crews will be able to be modeled in the future. Lanyard routing could later be modeled, as well as store loading equipment (jammers). There are endless possibilities for which solid models could be used in the future.

If computer models of aircraft and stores have to be developed, performing production fit checks may take some time. It may also take some time before databases and the model generator can be trusted to a point where flight lire fit checks do not occur. However, as the system matures, fitting a store on an aircraft on the flight line will be performed less often. Engineers will no longer have to wait until actual hardware is built and delivered to the flight line before determining actual physical fit, nor will they have to videotape actual landings to determine whether stores will scrape the ground when landing. Engineers will no longer have to deflate tires, drain struts, or put aircraft on jacks to operate landing gear to determine clearances. Programs will not have as many surprises and delays due to problems with physical fit. As soon as TAC documents requirements, an engineer can model the store and perform fit checks before any time and money is spent on the program.

The following is a discussion of a recommended approach for deciding on the software and hardware which will best perform this engineering task, modifying software, and acquiring and verifying the database.

RECOMMENDATION #1: SURVEY SOFTWARE PACKAGES (PREFERABLY THREE-DIMENSIONAL, SOLID MODELING, COMPUTER-AIDED DESIGN SOFTWARE PACKAGES) WHICH CAN BE MODIFIED TO PERFORM FIT CHECKS IN ACCORDANCE WITH MIL-STD-1289 AND PURCHASE (OR LEASE) THE SOFTWARE PACKAGE

A. Software Survey: During the above survey, many different CAD software companies were contacted to determine whether a software has already been developed which can perform this task. The system which best matched requirements was the ASD/XRC (M) system, although it still would have to be modified. Many off-the-shelf software packages can be modified to perform this task. A group of compatibility engineers would have to decide which software has the basic tools which could be modified. Purchasing software and modifying it is recommended rather than designing new software. (See Figure 5 for a recommended system description.)

A group of software evaluators will need to work with many software packages and choose the one which requires least modification. Important criteria for evaluating the software must be established. The software evaluators will need to attend training classes, model stores with the software, and coordinate with the intended users. The evaluators must decide on a fit check problem which represents as many different problems as are described in Section IV.E and model the same fit check problems on the different software being considered. Other then section IV.E, there are some additional criteria which the software must meet:

1. Accuracy: The most important aspect of any engineering tool is how accurately the tool measures a process. The software must model stores accurately and perform interference checks and kinematic operations accurately. When modeling an aircraft or a store, the model generator must be able to represent the complex curves very closely. When an engineer builds a model of a store, he inputs points, connects the points to make lines, and connects lines to make surfaces. At this point, the computer is approximating the surfaces by connecting the points with a straight line or a curved line with a radius. How accurately does the computer determine a point on a surface when not all points are defined directly by the user? Most models have different types of mathematical methods for defining where every point is inside or on the surface of a solid.

2. Interference Calculation: For any software being reviewed, the emphasis must be placed on how the modeler performs the interference checks. How accurately does the system calculate interference? Does the software highlight closest proximity of object to object specified? Can software view and print out any view during static fit or simulated activities?

3. User-Friendliness: Since most of the time and money spent on this system will be in manhour cost to model stores and aircraft, some important questions to ask are: Is the software capable of generating solid models easily? How easy is the software to use? Does the software have easy-to-use manuals with examples? Are macros easy to write? Are kinematic models easy to define? Can solid models be transferred and manipulated easily? Is the software working in a "pull-down menu/window environment" with mouse-controlled cursor? How much time does it take to manipulate and build models?

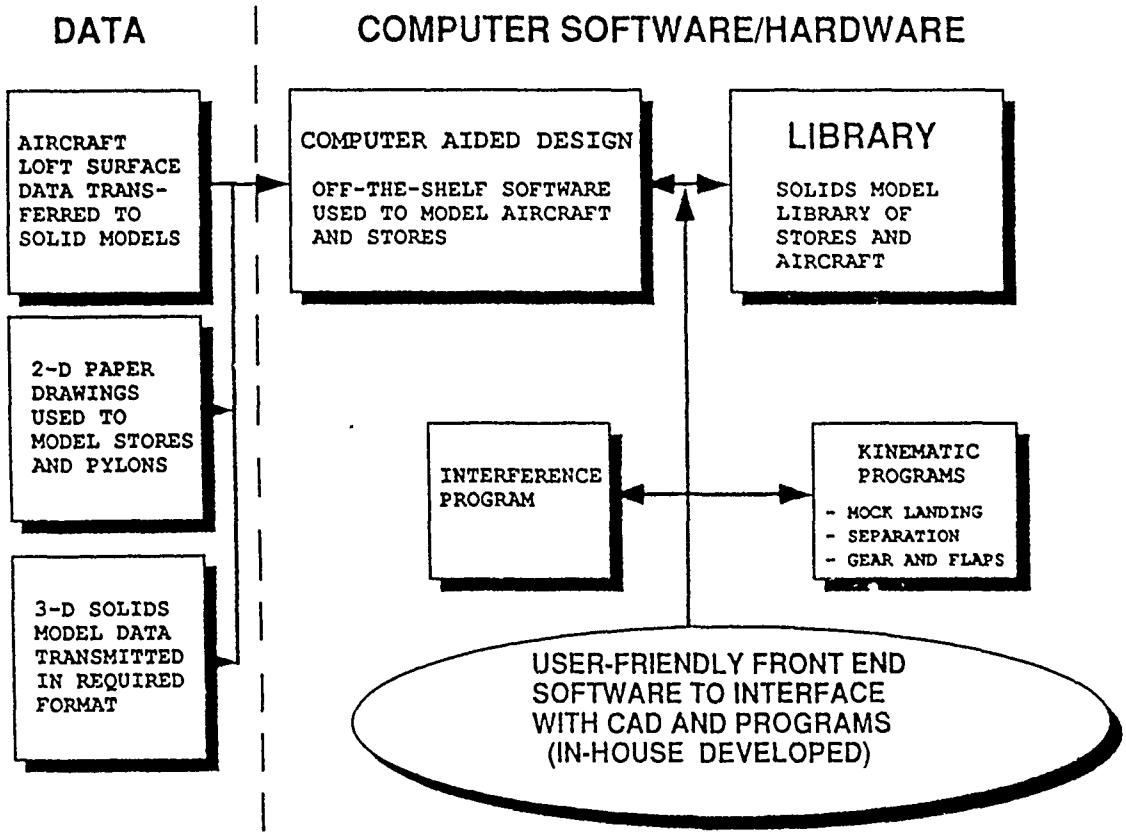

Figure 5: Description of Recommended Fit Check System

An engineering tool is just that, a tool. If the tool is too complicated to learn and use, then the engineers will find easier methods to answer their questions. So user friendliness is an extremely important criteria.

4. Add/Modify Software: If the software comes with a source code, is the computer language in Fortran, C, Basic, Pascal, etc.? If software is not supplied with the source code, can external programs be interfaced with software?

5. Read Data from Different Sources: Since the fastest method of obtaining a model is to directly receive the aircraft or stores model electronically (using magnetic tapes or telephone lines) from the contractors who designed and manufactured the item, it is very prudent to purchase a software which is involved in the standardization of database formatting. Most contractors do have their products defined mathematically in their computer systems. However, because of formatting differences between software companies and lack of standardized formatting regulations, a model built on one system cannot be brought into another modeling system without a large transformation effort. An effort headed by the United States Department of Commerce is being conducted to standardize CAD model format. Models built in solids can not be transferred using the old standard, Initial Graphics Exchange Specification (IGES). A new standard is being developed, Product Data Exchange Specification (PDES), to give solid model users the capability to transfer models.

6. Software Cost: Cost of a software is an important criterion, as long as the above criteria are judged first. Because the cost of software will be very small in comparison with the cost of the manhours to build the amount of models to put this system in operation, the cost of software is not as important as other criteria. Some software can be bought, and some software can only be leased. Some software can be used by a large amount of users at one time, and some software can be used by only one user at one time for each copy bought. Since CAD software is very fluid and can be out-dated in a short amount of time, the people judging which software to purchase need to decide which of the above purchasing methods would best fit their requirements.

7. Maintenance Cost of Software: Since most solid generators are fairly new software in the market, many software "bugs" can be found when using the software. Having a maintenance contract will allow the compatibility engineer to interface with the software engineers and ask questions about how to manipulate the software or "bug" work around. How expensive is the maintenance?

RECOMMENDATION #2: MODIFY SOFTWARE TO PERFORM FIT CHECKS EASILY AND ACCURATELY

B. Software Modification: During the survey (Section V) of currently used fit check computer systems, it became apparent that not all systems can perform a fit check in accordance with MIL-STD-1289A easily and accurately. Some software packages have many of the desired functions built into the software, yet an engineer would have to interface with the software many

months before he can model stores and much longer to manipulate models and perform fit checks. In other words, some software packages have the capability, yet are not user-friendly. Software engineers will have to modify off-the-shelf software for it to become more user friendly (See figure 6 for example of user-friendly, front-end software interface directorate.)

RECOMMENDATION #3: SURVEY AND PURCHASE GRAPHICS WORK STATION

C. Hardware Survey: This section details a recommended approach to decide which hardware would perform this engineering task most effectively. Software should be picked before hardware. Some software can be interfaced with only a particular hardware. For example, Dassault's software "Catia" can be interfaced with only IBM hardware. However, most commercial software can be interfaced with many different hardware.

1. Type of Hardware: There are basically three different types of hardware which were being used by compatibility engineers during the survey. The first type was a main frame. The large aircraft contractors use this type of hardware. They have hundreds of terminals interfacing with the mainframe at the same time, and the individuals have to share time using this type of hardware. Because of the type of interaction which is needed to use CAD software, mainframes are too slow. When an engineer wants to manipulate a model on the screen, he has to wait for the command to be sent to the mainframe, then wait its turn to be worked on. Then the monitor is updated. This can take from 30 seconds to 10 minutes, depending on the amount of users on-line with the mainframe.

The second type is a mini-mainframe (for example: mini-VAX). This is exactly what it sounds like, a smaller office mainframe (three-foot-high hardware which does not allow as many users to interface with the system). This can be faster than a mainframe; yet the computations are still being sent to the mini-mainframe which means that the system is slow, especially if the user has to wait his turn for his model to be updated. ASD/XRC (M) uses this type of hardware.

The third and most preferable type of hardware is the work station. This is a desk top computer which can operate independently from other systems. All computations are done for one user, and the system can be very fast.

2. Hardware Decision Criteria: After purchasing the software, decide upon a fit check problem which can be modeled and manipulated. The following criteria should be kept in mind when deciding on the type of hardware:

a. Speed: Modeling stores in a computer is very time consuming. The longer an engineer has to wait for the model he is generating to be updated, the longer (hundred-fold) it will take to model complex stores. It would be inefficient for an engineer to wait 30 minutes to finish each calculation when performing many interference calculations or kinematic operations. Speed is an important criterion.

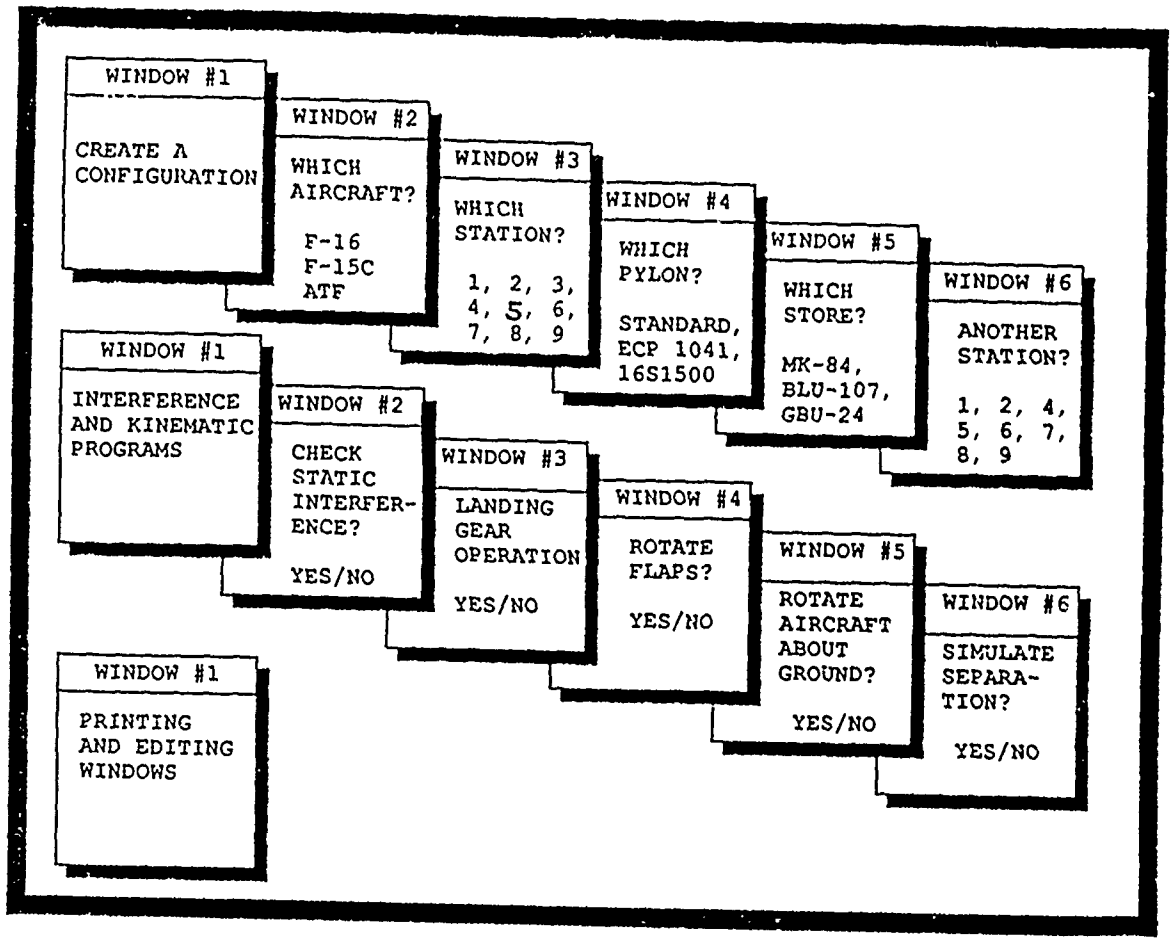

Figure 6: Example of User-Friendly, Front-End Software, Interface Directorate

b. Tools to Manipulate Software: Many user-friendly tools can be purchased with the hardware. These tools can be used to manipulate the software commands. For example, a mouse can be used instead of the keyboard. To manipulate the view of the model, a dial board can be used instead of function keys on the keyboard. These are only a few examples of the different tools which can be purchased with the hardware. However, it should be kept in mind that not all hardware uses all type of user-friendly tools. Some hardware interfaces with only certain types of manipulating tools.

c. Memory: To perform this engineering task successfully, a large library of models will be developed. In what format should the models be stored? Should a group of models be stored in such a manner that the data could be accessible at all times to all users? Or should the data be stored on some type of disk on a shelf? When the user wants to input a model which is stored on the shelf, he can read the data into the computer when he wants to use the data. If the shelf storage method is used, the cost of the hardware could be lowered.

d. Cost of Hardware and Maintenance: The cost of the hardware is a very important criterion. There are many tradeoffs of speed and cost. The judges should also keep in mind the cost of hardware maintenance. Is there an on-going base support contract for a particular brand of hardware?

RECOMMENDATION #4: DEVELOP LINES OF COMMUNICATION WITH GOVERNMENT OFFICES AND AIRCRAFT/ARMAMENT CONTRACTORS FOR EXCHANGING EXTERNAL DIMENSION MODEL DATA

D. Collecting Data: Much of the manhours spent trying to put this engineering tool in production will be in modeling the multitude of different stores, pylons, and aircraft. Before an engineer can model a store, he must obtain accurate external dimensions of the store and aircraft. The accuracy of the computerized fit system is extremely dependent on the accuracy of the data in generating the models. Most of the data will be obtained from two different sources (Figure 7):

1. 2-D Paper Drawings: Since most stores, pylons, and aircraft are more than 10 years old, obtaining data in the exact computerized format (3-D Solids using a specific software) will be extremely rare. The most abundant form of usable data will be in 2-D paper drawings. The drawings will have dimensions and a few cross sectional views down the length of the store/pylon. Transferring 2-D data accurately into 3-D models will not be easy. Most drawings do not have enough dimensions and enough cross sectional views to be transferred accurately. If a definition of a curved surface is not available on the drawing, the engineer will have to approximate the placement of the points on the curved surfaces. To make this method as nearly accurate as possible, blueprint drawings obtained directly from the store designer will be required. Obtaining 2-D paper drawings will not be an easy task either. Much time will be spent making phone calls and writing messages to item managers and contractors to obtain the quality drawings needed to make accurate models.

2. 2-D or 3-D Computer Data: Most aircraft contractors have their products defined mathematically in their computer system in some format. For

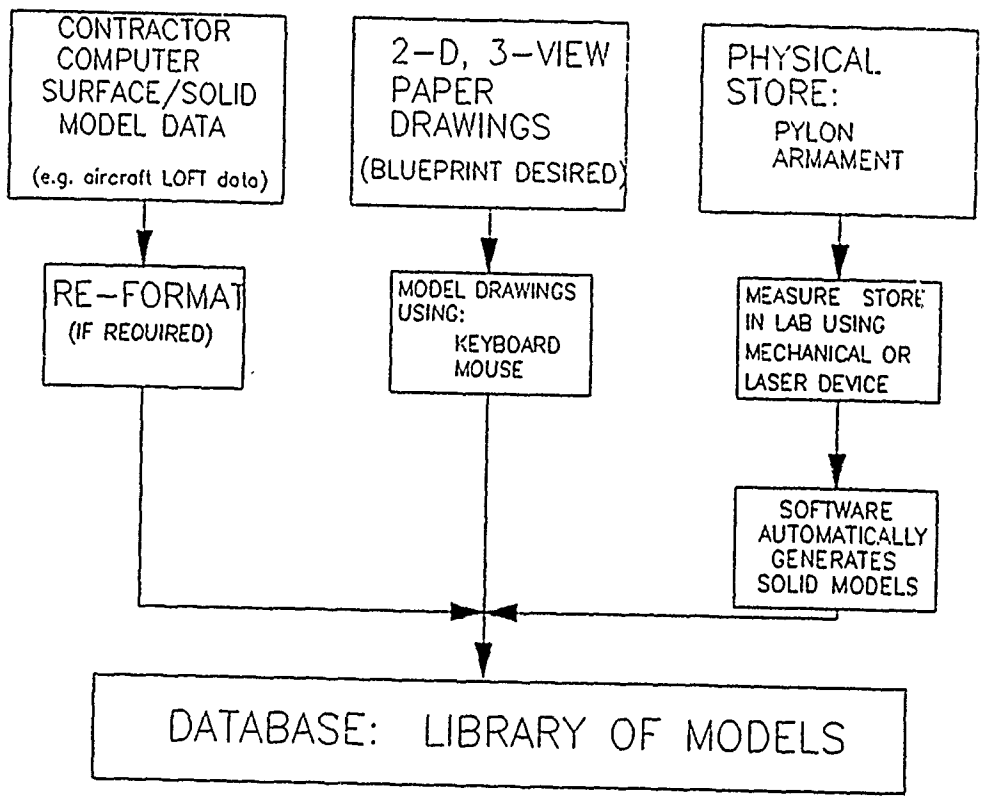

Figure 7: Description of Data Input Resources

example, McDonnell Douglas has the entire F-15E aircraft's surface defined in their LOFT system. It may be cost-effective for the Air Force to pay aircraft contractors to translate their aircraft surface data (LOFT) into the desired software format. In fact, this method may be the only method to obtain the accurate data required. In the future, when all contractors can translate data easily among themselves, transfer/exchange of solid models will be an everyday occurrence; however, at the present time, transfer of data will be a very complex task.

RECOMMENDATION #5: DEVELOP METHODS FOR VERIFYING DATA AND EVALUATE WHETHER A MEASUREMENT LAB IS REQUIRED TO COLLECT ACCURATE DATA

E. Verifying Data: After models have been generated and the process of fit checking stores on aircraft can be accomplished, how does the engineer know that the interference distances he is obtaining from the software algorithms are accurate? Even a more simple problem: after a store model has been generated, how accurately does the model in the computer represent the stores being delivered to the flight line? The only method for verifying the accuracy of the data is to actually measure the external dimensions of aircraft, pylons, and stores and compare those measured dimensions to the models in the computer. How does an engineer go about performing this task? What type of measuring instrumentation or tools does an engineer use to perform this task accurately? Even if an engineer measures one store, that one store does not represent every store which will be delivered to the flight line. The store measured may be the smallest store ever delivered to the flight line, it may be the largest store. To solve this statistical problem, an engineer would have to measure many stores from different production lots.

Measurement instrumentation systems are being developed and used by the government and contractors. Contractors have been using measurement systems during the quality control aspects of their production cycle. Some systems use a mechanical robot probe to measure accurate distances. Other systems use light and radar as well as light and video.

If fit check results have been found to be not accurate enough, the Air Force may want to build a lab or purchase some mobile equipment to measure stores and aircraft. This equipment will be expensive, and computer software will probably have to be developed to transfer measured data into solid computer models. This measurement system would solve many of the data acquisition problems. If it is impossible to obtain accurate drawings of a store or pylon, the stores could be measured and modeled. A statistical database of manufacture tolerances can also be obtained with this system.

SECTION VII

SUMMARY

Most fit check methods which the Air Force compatibility engineer presently uses are not very accurate and are time consuming. An engineer does not have an accurate analytical tool to perform fit checks. The Aircraft Stores Interface Manual (ASIM) is available to the compatibility engineer; however, engineers use this manual only as a rough estimate. The engineer has to depend on flight line fit checks with tangible stores on tangible aircraft before he can feel confident that the store fits on the aircraft. During development of new stores, computer based fit checks are usually conducted on a limited number of candidate aircraft by the aircraft prime contractors. As the store enters the inventory, certification requirements often change or are broadened versus the original requirement. In order to be responsive and provide the Air Force with the capability to perform broader compatibility studies on more aircraft and additional store configurations, the Air Force needs an in-house analytical tool. Furthermore, the current dependence within the Air Force for hardware oriented fit checks often results in unanticipated discoveries of fit interference that negatively impact certification schedules and cost. An early analytical based approach using computers would avoid many of these "show-stopping" problems which often appear late in the certification effort.

Since there have been great advances in computer graphics software, hardware speed, and memory, it is feasible to develop an analytical computerized tool to perform fit checks. However, during the survey reported herein, the lack of a system which can easily and accurately perform a fit check in accordance with MIL-STD-1289A became apparent. Many systems are out-dated and cumbersome to work with. A compatibility engineer would have to train for many months before he could model aircraft and stores to perform a fit check on these systems. A software will have to be modified to make it more user-friendly, less cumbersome, and meet the requirements of MIL-STD-1289A.

Major Recommendations:

1. Survey software packages (preferably three-dimensional, solid modeling, computer-aided design software packages) which can be modified to perform fit checks of armament on aircraft in accordance with MIL-STD-1289, and purchase (or lease) the software package.

2. Modify the software to perform fit checks easily and accurately.

3. Survey and purchase graphics work stations.

4. Develop lines of communications with government offices and aircraft/armament contractors for exchanging external dimension model data.

5. Develop methods for verifying data and evaluate whether a measurement lab is required to collect accurate data.

It is recommended that the Air Force survey and purchase a three-dimensional solid modeling computer aided design software (off-the-shelf), survey and purchase graphics work stations, and modify the software to develop this analytical tool. Most of the funding spent in developing this capability will be in manhours cost. To modify the software and to develop a large library of stores and aircraft will take time and funding. To collect the source data to develop the aircraft and store models will also be time consuming. To make accurate models, it is recommended that aircraft contractor LOFT surface data be used to develop the aircraft models and that contractor blueprint drawings be used to develop store/pylon models.

SECTION VIII

ADDENDUM I: MIL-STD-1289A OVERVIEW

A. External Carriage:

1. Store-to-Aircraft Clearance: Minimum clearance between all required stores and the aircraft including flight control surfaces, landing gear, access doors, etc., shall be one inch with the surface deflected to the point of closest proximity to the store.

2. Store-to-Store Clearance: Minimum of one inch clearance between adjacent stores. Additional clearance may be required for fuse clearance for the stores mounted on the aircraft suspension equipment. For stores configured in tandem, this distance shall be measured from a plane tangent to the rearmost surface of the forward store to the closest surface of the aft store or fuse to ensure clearance during separation. For stores that ordinarily are made safe by removal of fuses, adequate clearance shall be provided to remove or install fuses on the loaded store without removing the stores from their loaded positions.

3. Store-to-Pylon (Ejector Rack) Clearance: A minimum of 0.5 inch shall be provided between any component along the length of the store and the pylon it is suspended on, except for suspension lugs, store sensing switches, and after careful consideration, bomb charging well electrical power generator components. A minimum of 0.625 inch shall be provided between ejector rack and the store.

4. Store-to-Ground Clearances: The minimum ground clearance shall be no less than 3 inches (6 inches for aircraft designed to operate on rough terrain) in the worst condition of any tire flat and a completely depressed strut with the aircraft in either a static, takeoff, or landing attitude.

B. Internal Carriage: Except for the closed bomb bay doors and side rails, no part of the aircraft nor any other obstruction, except such as required sway braces, displacing gear, etc., which are automatically removed from their obstructive positions as each store is released, shall lie within the clearance space envelope bounded by the imaginary plane surfaces defined as follows:

1. The plane tangent to the uppermost extremity of the store parallel to the armament datum line and parallel to the pitch axis of the aircraft.

2. Four planes tangent to the foremost, rearmost, right, and left extremities of the store and at an angle 10 degrees away from the vertical and out from the bomb bay. Minimum clearance between stores shall be 2.5 inches to prevent contact between stores.

SECTION IX

BIBLIOGRAPHY AND ACKNOWLEDGEMENT

Bibliography:

1. "Review of Current Geometric Modeling Technology," 1990 Shape Data Ltd, Cambridge England.

2. "Why Solid Modeling?" Thomas Boulter, Aerospace America, Jan 85.

3. "An Overview of Analytic Solid Modeling," Malcolm S. Casale and Edward L. Stanton, PDA Engineering, IEEE PG&A, Feb 85.

4. "An Introduction to Solid Modeling," George Allen, Computers and Graphics, 1984.

5. AEDC-TR-88-39, Procedures for the Preparation of Computer-Graphic Models for Separation Trajectory Analyses, Feb 89.

Acknowledgements:

During the collection of background data to develop this report, I met with many people to discuss their recommended approaches or capabilities. They all provided a great deal of information and advice which aided immensely in the development of this study.

1. Government:

   a. Wright Patterson AFB: Bill Allen (ASD/EN)

   b. Hill AFB: Lt Steve Hardy (OO-ALC/MMETM)

   c. Warner Robins AFB: Bob Wade (WR-ALC/MMETMF)

   d. Edwards AFB: Capt Bill Norton (6[illegible] TW/DOES)

   e. Fort Meade: Col Bruce Altchuler

   f. Eglin AFB: Al Smith (Math Lab), Allen Baker (ASD/XRC [M]), Bob Cross

   g. PMTC: Jerry Harnes, Harold Washmuth, Terry Elliot, Lynn Agalier

2. Contractors:

   a. General Dynamics: Lewis Tovar, Jon Judd, Fred Newman, Sam Majors

   b. Boeing: Frank King, Dwight Numamaker, Art Hartwig, Joe Fox

   c. Northrop: Ken Hyssong, Scott Collins, Mike Laurent

d. Florida International University: Dr Gautam Ray, Assistant Dean of Computer Sciences

e. Daasault: Fran Aldridge (Catia)

f. McDonnell Douglas Aircraft Company: Thomas Melson and Tom Johnson

g. APTEK: Mark Landon and Jerry Udy

h. Unigraphics: Allen Messer

i. Grumman: Phil Jacknis

j. IBM: Jim Wrench

k. Hewlett Packard: Brian Hill

l. TASC: Michael W. Nowotny, Alfred E. Bills, Joel W. Cartwright

m. SDRC: John Watson (Ideas)

BIOGRAPHY

Mr Daniel Speyer is a Compatibility Program Manager with the 3246 Test Wing in charge of Geometrical Physical Fit Check Software development.

Born in Summit New Jersey, Daniel Speyer graduated from Auburn University receiving a bachelors of science degree in Aerospace Engineering. After graduation, Mr Speyer was offered a program management job with the Office for Aircraft Compatibility. He worked with many aircraft and armament compatibility test programs including F-16, F-15, and AMRAAM.

Mr Speyer is single.

IMPROVEMENT OF SEPARATIONS OF PRACTICE BOMBS FROM A MULTIPLE BOMB ADAPTER

K.R. Rijzebol
National Aerospace Laboratory NLR
Amsterdam, The Netherlands

Paper to be published in the Proceedings of the Eighth "Aircraft/Stores Compatibility Symposium" at Fort Walton Beach, Florida, USA, 23-25 October 1990.

The investigation has been carried out under a contract awarded by the Royal Netherlands Air Force (RNLAF), Directorate of Materiel Air, Scientific Support Division.

SUMMARY

In search for a small and easy to handle practice bomb rack to replace the aging SUU-20B/A, the Royal Netherlands Air Force (RNLAF) investigated the Multiple Practice Bomb Adapter. This MPBA is required to be used on the F-16 for training with the BDU-33D/B and Mk-106 practice bombs.

The RNLAF executed an initial exploratory flight test program with this tandem two-place MPBA. The results did not show adverse characteristics. A report on flight tests of this rack with the A-7 Corsair II was also positive. In a subsequent delivery flight test program to collect scoring data, high-speed 16 mm movie cameras were used to monitor separation behaviour. The recordings on film revealed bomb-to-pylon or bomb-to-adapter contact of both the Mk-106 (at moderate airspeed) and the BDU-33D/B (at higher speed) within the required release envelope.

In a first effort to improve the separation characteristics of the practice bombs, the aerodynamic shape of the bomb adapter was modified. Also an extension of the ejector pistons was applied to bridge a small gap between the ejector piston and the bomb in captive position. Flight tests with the modified rack showed still unacceptable separation behaviour.
Additional mechanical modifications, consisting of spring type "tail-up restrictors", were applied to both the original and the aerodynamically modified bomb rack. The modified bomb racks produced satisfactory separation characteristics for the BDU-33D/B practice bomb throughout the required release envelope. The Mk-106 produced considerable deflection of the tail-up restrictors.

A more rigid, production prototype design of the tail-up restrictor was then constructed for the original MPBA (with the 7 mm longer ejection piston maintained), and was flight tested in May 1990. The test results showed that the tail-up restrictors do prevent collisions of bomb tails with the MPBA, the parent pylon or the aircraft. The practice bombs, the BDU-33D/B as well as the MK-106 show a gentle pitch down after release and separate positively and clear from the aircraft for all flight conditions.

Although some carriage tests, already performed with the original MPBA, have to be repeated for the final model of the MPBA, it can be concluded, that the F-16 with the loaded, modified MPBA will be cleared for employment up to M = 0.85 / 550 KIAS for normal accelerations of 0.5 to 5.0 g and for carriage up to M = 0.95 / 550 KIAS for all configurations. With empty, modified MPBA the supersonic carriage envelope will be the same as for the comparable aircraft configurations with empty TER-9/A.

The paper presents a comparison of the bomb adapter before and after the modifications and gives the results of the flight test programs.

CONTENTS

LIST OF SYMBOLS AND ABBREVIATIONS

AFRES	USAF Reserves
AIAA	American Institute of Aeronautics and Astronautics
DGLR	Deutsche Gesellschaft fuer Luft- und Raumfahrt
DPBA	Dual Practice Bomb Adapter (Aerodynamically modified MPBA, 1989)
FCC	Fire Control Computer
fps	frames per second
KIAS	knots indicated airspeed
KLu	Koninklijke Luchtmacht (RNLAF)
KTAS	knots true airspeed
M	Mach number
MPBA	Multiple Practice Bomb Adapter
MPBR	earlier name of MPBA
NLR	Nationaal Lucht- en Ruimtevaartlaboratorium
	National Aerospace Laboratory NLR
RNLAF	Royal Netherlands Air Force
SETP	Society of Experimental Test Pilots
SFTE	Society of Flight Test Engineers
SOF	safety of flight
TAC	Tactical Air Command
TER	Triple Ejector Rack
USAF	United States Air Force
USG	United States Gallon

1 INTRODUCTION

From 1985 the Royal Netherlands Air Force (RNLAF) has considered the Multiple Practice Bomb Adapter (MPBA) as a candidate practice bomb rack for use on the General Dynamics F-16 aircraft of the RNLAF. The original MPBA is a small, easy to handle bomb rack, that can be carried at the standard weapon pylons of the aircraft. It is illustrated in the figures 1 and 2. The light rack (31 lb) is intended to be used for practice bombs listed in table 1. The practice bombs have to be equipped with a bomb lug. The MPBA consists of a simple, light alloy extrusion beam, machined to provide accommodation for two ejector units for one bomb each, a pylon / MPBA interface unit and a nose cap. The ejector units have electro-mechanically operated bomb hooks and spring-loaded ejector pistons. The rack can be used in gravity drop mode (no initial ejection velocity) or the ejector can be spring loaded with resulting ejection velocities shown in table 1. The bomb release is initiated by an electrical release signal which electro-mechanically opens the bomb hook. The two bombs can be released in "single mode" or "ripple mode" with a minimum interval of 20 milliseconds.

The MPBA was successfully tested on the A-7 Corsair II of the US Air National Guard. The RNLAF acquired two test articles of the MPBA for flight testing on the F-16. The required operational flight envelope for use with the F-16 is more extended than for the A-7 Corsair II. A preliminary RNLAF test program was executed in 1985. No adverse flight characteristics were noted, but no separation characteristics were recorded at that time. A preliminary assessment of the suitability of the Fire Control Computer (FCC) software of the SUU-20B/A or of the TER-9/A was carried out. In both cases all BDU-33D/B and Mk-106 bombs fell over, and consequently a software adaption for the MPBA was recommended.

In November and December 1988 the RNLAF executed a more extensive flight test program, using experimental FCC software for both the BDU-33D/B and the Mk-106. The separation characteristics were recorded with 16 mm high-speed cameras. Releases utilizing the spring-loaded ejectors showed better separations than gravity releases, and consequently most releases were done with ejector preload. The recordings showed that the Mk-106 did hit either the MPBA rack or aircraft pylon at aircraft speeds of 450 KTAS. Even at 380 KTAS a hit was observed (Fig. 3). The BDU-33D/B did hit either the MPBA or pylon at 500 and 550 KTAS. Figure 4 shows these results. The required release limits were identical to the limits which apply to releases of practice bombs from the SUU-20B/A and the TER-9/A, i.e. 0.5 g and 550 KTAS for the BDU-33D/B or 0.7 g and 550 KTAS for the Mk-106.

A modification of the MPBA was recommended to improve the release characteristics. Two different modifications were applied before a final solution yielded favourable separation characteristics for both types of practice bombs. The results of the test programs are reported in the following chapters.

In table 2 the mass properties of the original MPBA, the aerodynamically modified DPBA and the final version of the modified MPBA are compared with the mass properties of the empty TER-9/A and the empty SUU-20B/A. Figure 5 compares the original MPBA with the TER-9/A.

2 INITIAL, AERODYNAMIC MODIFICATION: DPBA

Indications were obtained that the flow field about the original MPBA was probably the major contributor to the observed unsatisfactory separation behaviour. An aerodynamic modification of the MPBA was designed and constructed. Figure 6 illustrates this aerodynamically cleaned-up MPBA (renamed DPBA for Dual Practice Bomb Adapter).

The flight test program with the DPBA was executed in October and November 1989. All releases were executed with spring-preloaded ejectors. Released from the aft bomb position, the BDU-33D/B showed slightly increased pitch-down (compare figure 7a to figure 4a). The releases from the forward position were severely degraded (compare figure 7b to figure 4b. The results of the flight tests demonstrated that the aerodynamically cleaned-up MPBA (resulting in the DPBA) with supposedly a better aerodynamic flow around the ejector units, did not provide the expected better separation behaviour of the BDU-33D/B. Because of the unfavourable results the planned separation tests of the Mk-106 were cancelled.

In order to obtain an insight in the aerodynamic flow pattern, an investigation was executed using tufts fixed to the BDU-33D/B body and fins, as well as to the DPBA. The 16 mm film recordings showed a favourable airflow for the larger part of the bombs for most flight conditions. For some flight conditions a turbulent airflow existed around the upper fins of the bomb in the wake behind the forward ejector unit.
The observed flow phenomena could not likely be the (only) cause of the degraded separation behaviour of the bombs. Thus, an explanation was searched for. The most likely interpretation of the results is that the flow around the practice bombs did improve, which means a higher air velocity around the rack, hence an increased drag of the bombs, especially of the one on the forward station. With a bomb lug, initially only free to move downward out of its stored position (Fig. 8), the increased bomb drag yielded an increased nose-down, tail-up moment, rotating the bomb around the aft "sway braces" of the ejector unit, which acted thus as a pivot point. The tail fins in this way entered the wake of the ejector unit before developing a sufficient tail-down force.

The conclusions from the analysis of the separation results and the flow investigation were that an aerodynamic solution of the pitch-down problem causing bomb-to-rack or bomb-to-pylon contact would be highly unlikely, and that a mechanical solution might be more successful. It was therefore proposed to restrict the tail-up rotation of the practice bombs by applying a mechanical modification.

3 MPBA WITH FLEXIBLE TAIL-UP RESTRICTORS

To prevent the observed excessive nose-down / tail-up rotation and consequently tail-to-rack collision, a common design of a "tail-up restrictor" was accepted to be fitted to both the DPBA and to the original MPBA. In this way different results of the two models would indicate which model would be the best final choice. The construction consisted of two flexible steel rods, interconnected by an adjustable tail support bar (to accommodate BDU-33D/B as well as Mk-106 bombs), which provided a small preload to the fins of the practice bomb. Figure 9 shows the MPBA with the flexible tail-up restrictors on both ejector units while figure 10 shows the DPBA with an identical set.

The simple design and construction of the tail-up restrictors was considered as a "demonstration-of-the-concept" model; in case of success a more durable, less fragile and probably more rigid design was envisaged.

An additional modification was applied to the ejector pistons, which were provided with a 7 mm extension to bridge an idle gap of about 7 mm of ineffective ejection stroke of the original pistons.

The flight tests with these tail-up restrictors took place from December 1989 to February 1990. Testing mainly concentrated on releases at 1 g and 0.5 g, from 450 to 550 KTAS. The results showed excellent separation characteristics for the DPBA as well as for the MPBA, for both the aft position and the forward position. The separation results for the DPBA are presented in figure 11. The results for the MPBA are shown in figure 12. Both sets of results should be compared to the results in figure 7.

The successful testing of the BDU-33D/B suggested a reconsideration of testing the Mk-106 high drag practice bomb. In a separation test at 450 KTAS and 1 g, the Mk-106 showed an almost identical pitch-down for all bombs, from the DPBA as well as from the MPBA. The results are also plotted in the figures 10 and 12 to be compared to the BDU-33D/B results. The drag, combined with the pitch-down moment (tail-up moment) of the Mk-106 was that large, that the tail-up restrictors of the forward position showed a deflection of about one bomb diameter (100 mm). Neither the tail fins of the Mk-106, nor the tail-up restrictors did touch the DPBA or MPBA, or the parent pylon. Due to the considerable deflection and pitch-down, no additional tests with the Mk-106 were executed. However, the conclusion was, that a successful certification of the DPBA or MPBA in combination with the Mk-106, should be possible with a more rigid tail-up restrictor.

Following the success obtained with the flexible tail-up restrictors, a production prototype tail-up restrictor was designed and constructed. Because the results with the MPBA were slightly better than with the DPBA and because the aerodynamically improved model would increase the cost of the rack significantly, the original MPBA was chosen as the basis for the final model of the practice bomb rack.

4 IMPROVED MPBA WITH FINAL MODEL TAIL-UP RESTRICTORS

As explained in the previous chapter the original MPBA was selected as the basis for the final MPBA to be modified with the final version of the tail-up restrictor. This final version features increased stiffness when compared to the "proof of concept" model and consequently deflects at higher loads. Figures 13 and 14 illustrate the added construction, which is intended to counteract the bomb tails upward rotation sufficiently to prevent a collision with the MPBA or parent pylon. The construction is designed to support or touch the tail fins of the practice bombs. The tail-up restrictor can hinge at the forward attachment points and is connected to an off-the-shelf shockmount in the MPBA backbone above the bomb tail. This shockmount is the actual spring element in the system and allows for differences in the bomb tail dimensions and bomb mounting inaccuracies, or heights relative to the MPBA body and / or provide a light preload to give the tail a minimal initial downward velocity. The modified MPBA retains the internal mechanical properties of the original MPBA.

The modification applied to the ejector pistons was retained. Originally in the loaded situation, the piston showed a gap of about 7 mm to the top of the BDU-33D/B. So 7 mm of the ejector stroke was unused, while the ejection spring load is the highest in the first part of the ejection stroke. A 7 mm lengthening of the ejector pistons was therefore realized to bridge this 7 mm gap.

In May 1990 a series of separation flight tests was executed in which, in general, in one pass all four practice bombs were released while recorded with high speed 16 mm film cameras operating at 200 frames per second. Both Mk-106's from the left hand MPBA and both BDU-33D/B's from the right hand MPBA were released in the "rippled pair" mode in which a long release interval between 0.3 and 0.5 seconds provided sufficient time spacing to guarantee independent release characteristics of the aft and the forward bombs. This technique, combined with the carefully timed manually run activation and de-activation of the high-speed cameras, resulted in short film lengths, which provided short processing times. In this way short turn around times were possible during the separation flight test program.

The intended release conditions for the BDU-33D/B as well as for the Mk-106 were

- airspeeds of : 380, 450, 500 and 550 KTAS
- normal loads of: 1.0 and 0.5 g

Releases at higher normal loads than 1.0 g were envisaged for the scoring program, although the earlier programs demonstrated clearly that the separations showed increasingly better characteristics with higher load factors due to the larger difference in normal acceleration of the aircraft and the released practice bombs.

With the new production prototype of the tail-up restrictors, the BDU-33 and the Mk-106 practice bombs showed excellent separation characteristics. The initial situation, with the bomb tails resting against the tail-up restrictors with a light or with no preload, prevented a collision of the bomb tails with the MPBA or aircraft pylon, as did occur in the tests with the original MPBA and with the aerodynamically modified MPBA.

a. BDU-33D/B separations

The BDU-33 pitched down gently in all separations. The tail moved away from the tail-up restrictor smoothly with hardly a noticeable initial contact. The maximum pitch down angles increased with airspeed. This is illustrated in figure 15, showing the maximum pitch down attitude separately for the aft ejector and the forward ejector. Bombs from the forward ejector unit pitched down about five degrees more than from the aft ejector unit. There is little difference between the maximum pitch down angles of the releases at 1.0 g and of releases at 0.5 g. This is an improvement in relation to the situation with both the original and the aerodynamically modified MPBA. Relative to the MPBA with the flexible tail-up restrictors, the maximum pitch down angles increased again about 5 to 10 degrees, which might be caused by a smaller preload of the new tail-up restrictors.

Nevertheless, the separations of the BDU-33D/B are positive, gentle and smooth, with a favourable pitch down, creating a negative angle-of-attack, resulting in a downward aerodynamic force on the BDU-33D/B. In all separations the BDU-33D/B showed a damped oscillation, while falling clear and away from the aircraft.

b. Mk-106 separations

The Mk-106 pitched down as gently as the BDU-33, although the Mk-106 first made a firm contact with the tail-up restrictor, with an increasing deflection of the shockmounts as a function of the increasing airspeed. Following initial release the Mk-106 moved away gently.

The maximum pitch down angles of the Mk-106 are shown in figure 16, for both the aft ejector unit and the forward unit. The results show a maximum pitch down angle almost independent of airspeed; e.g. the higher airspeeds pitch down was about five degrees more for the 0.5 g releases than for the releases at 1.0 g. The releases of the Mk-106 at 450 KTAS from the earlier flexible tail-up restrictor model of the MPBA showed a slightly larger pitch down of about 35 to 40 degrees, but with an unacceptably large deflection of the restrictors.

Compared to the results of the early separation tests with the original MPBA, the separation characteristics improved significantly, resulting in a positive, gentle and smooth clearing of the Mk-106 from the MPBA as well as from the parent pylon. The pitch down angle results in a negative angle-of-attack for the Mk-106, providing a favourable downward aerodynamic force. In all separations the high-drag Mk-106 practice bomb showed a damping oscillation, while falling downwards and aft.

c. Minimum release intervals

The MPBA can provide ripple release signals with a minimum interval of 20 milliseconds. A couple of closely spaced ripple releases were executed during the last separation test program.

The high drag Mk-106, when released from the aft ejector unit, moves down and aft rapidly and is separated well from the MPBA when the forward Mk-106 is released after 60 milliseconds. The recommended minimum interval of 60 milliseconds can be maintained.

The low drag BDU-33D/B, when released from the aft ejector unit, moves down and shows hardly any rearward movement. The forward BDU-33D/B (which is carried lower than the aft bomb), when released 60 milliseconds later than the aft bomb, is only a few inches higher than, and almost just in front of the aft bomb. With only small ejection velocities (nominally of about 3 ft/s) the aft bomb will have a chance to enter the wake of the forward bomb and catch-up with that bomb. Due to the narrow angle lens of the 16 mm high-speed camera, the two BDU-33D/B's, while closely together, were out of view at an early stage and the development of the separat' trajectories could not be analyzed completely. Because of the initial separation characteristics it is recommended to use a minimum release interval of 120 milliseconds for ripple releases of BDU-33D/B's from one MPBA.

d. Employment limits

The conclusions of the analyses of the separation results are that the MPBA, modified with the production prototype tail-up restrictors, provide positive, clean separations of the BDU-33D/B and the Mk-106 practice bombs for release conditions up to 550 KTAS and for normal accelerations of 0.5 g and more. The BDU-33D/B can thus be released at the same conditions as from the SUU-20B/A and from the TER-9/A with adapter. The release envelope for the Mk-106 is an improvement, because the lower acceleration limit for the Mk-106 is 0.7 g, when released from the SUU-20B/A, while the Mk-106 is not certified in combination with the TER-9/A.

Actually the separations of the Mk-106 at 380 KTAS and at 550 KTAS and of the BDU-33D/B at 550 KTAS, were not at the intended 0.5 g but at a still lower value of 0.3 g, as is marked in figures 15 and 16. The separation characteristics proved to be quite satisfactory even with those release conditions. This guarantees a welcome safety margin for the intended and cleared employment envelope which will be as shown below.

BDU-33D/B and Mk-106, both with a bomb lug, can safely, positively and clearly be released from the modified MPBA with final model tail-up restrictors as tested at

airspeeds up to M=0.85 / 550 KTAS whichever comes first, and at normal accelerations between 0.5 g and 5.0 g.

5 SCORING PERFORMANCE

In the last two flight test programs two different software systems were used to release the practice bombs and to judge the scoring performance of the MPBA. The Mk-106 was only tested in the last program, using a preliminary version of the FCC software program. The results of the software tests are discussed below.

a. TER-9/A / BDU-33D/B software

In the tests of January and February 1990, a number of probing tests were executed to compare the scoring performance of the BDU-33D/B's when released from the MPBA and from the TER-9/A. The existing software of the Fire Control Computer (FCC) for the BDU-33D/B + TER-9/A (with adapter) combination was used. (The Mk-106 is not to be released from the TER-9/A.) In this software the ejection velocity of the BDU-33D/B is set to 0 ft/s. However the spring ejectors of the DPBA / MPBA were armed, providing an ejection velocity of about 3 ft/s (Tab. 1).

To monitor the separate bomb trajectories and impacts during the scoring tests, a 16 mm high speed (100 fps) "trail" camera was mounted, aimed aft and about 50 degree down. Using the release signal event marking, the time synchronization signal, both at the film edges and the frame with the impact, also the time of fall of the bombs could be derived and used for analyses. The impacts were also reported by the crew of the bomb ranges. In general the BDU-33D/B's were delivered from low altitude and in nominally level flights (1.0 and 0.5 g). The impacts of the bombs, released in "pairs" from the MPBA and the TER-9/A, showed comparable bomb ranges. In several deliveries the impacts were only some tens of feet separated, with extremes of about one hundred feet difference. The only one LOFT release resulted in a difference in impacts of about 500 ft.

The initial assessment is, that the bombs from the MPBA have a longer range. The differences in ballistic performance can be caused by differences in:

- ejection velocities
- interference effects

The ejection velocity of the BDU-33D/B from the MPBA is about 3 ft/s. Nominally the ejection velocity of the BDU-33D/B when released from the TER-9/A is 0 ft/s, according to the data in the FCC of the F-16. During the flight tests the MPBA separations were controlled using this FCC software for the TER-9/A / BDU-33D/B combination. In a ground test, however, the spring force of the BDU-33D/B-adapter of a TER-9/A, proved to be higher than that of the MPBA spring ejector. Differences in bomb-to-rack interference, for example large pitch oscillations, might contribute to differences in bomb ranges. One separation (at 550 KTAS and 1 g) from the TER-9/A was recorded on 16 mm high speed film. The oscillation characteristics, however, were almost identical with those of the BDU-33D/B released at the same moment from the MPBA. Therefore the shorter range for the BDU-33D/B from the TER-9/A most probably is due to the higher ejection velocity of the BDU-33D/B from the TER-9/A. A more extensive scoring program should provide the proper FCC software data.

b. MPBA / BDU-33D/B / Mk-106 software

In June 1990 the RNLAF executed a flight test program to examine a preliminary version of the software of the FCC. With this program available, containing also software to operate the MPBA, a limited number of dedicated BDU-33D/B and Mk-106 release flight tests were executed for scoring purposes.

The BDU-33D/B generally fell short of the target. The next conclusion is only valid if the TER-9/A / BDU-33D/B software (as tested in January and February 1990) is correct, i.e. causing the BDU-33D/B to hit the target well. (Records did not include absolute input positions.) If the TER-9 / BDU-33 software is correct the BDU-33D/B from the MPBA is falling over when using that software. Using the preliminary MPBA software the BDU-33D/B did clearly fall short of the target. This indicates in which direction the software for the BDU-33D/B has to be corrected.

The Mk-106 was also reported to fall short of the target, but the errors were not large, The tested software model of the MPBA / Mk-106 combination is acceptable, but can still be improved.

With the limited data available from a small, "probing" scoring program, no final conclusions can be drawn. A dedicated, more extensive scoring test program, to provide the required release and trajectory data for the BDU-33D/B as well as the Mk-106, is planned to be executed in the USA in the fall of 1990.

6 OTHER CERTIFICATION SUBJECTS

For a complete flight clearance of the desired F-16 / MPBA configurations, the subjects of flutter, loads, stability and control characteristics and performance are required to be investigated.

Most subjects are analyzed well and the results are reported separately. A few demonstration flights to the edges of the intended supersonic flight envelope, for the empty improved MPBA, are still to be executed.

7 CONCLUSIONS

A successful analysis and flight test program was executed by the National Aerospace Laboratory NLR and the RNLAF to demonstrate adequate flight and employment characteristics of the F-16 in combination with a modified MPBA. After a less successful aerodynamic modification, a mechanical modification, using simple, but flexible "tail-up restrictors", provided highly satisfactory separation characteristics. The final modifications relative to the original MPBA, are the addition of more rigid and ruggedized tail-up restrictors with limited-stroke shockmounts and a 7 mm extension to the spring-loaded ejector pistons.

The conclusions of the analysis and flight test program are listed below.

a. Store separation

The separations of the BDU-33D/B improved well and the separations of the Mk-106 improved significantly after addition of "tail-up restrictors" to the original MPBA. The tail-up restrictors prevent collisions of the bomb tails with the MPBA, the parent pylon or the aircraft. The practice bombs show a gentle pitch down after release and separate positively and clear from the aircraft.
The release envelope for the BDU-33D/B as well as for the Mk-106 is established as

M = 0.85 / 550 KIAS and 0.5 to 5.0 g.

Minimum release intervals for ripple releases from one MPBA are recommended as:
120 milliseconds for the BDU-33D/B and
60 milliseconds for the Mk-106.

b. Scoring performance

In a limited scoring program, two software programs were used for the BDU-33D/B releases. When using the TER-9/A / BDU-33D/B software, the bombs from the MPBA seem to fall over. Using a preliminary MPBA software program for the BDU-33 and Mk-106 the bombs fall short of the target.
A dedicated ballistic test program is planned to take place in the fall of 1990.

The final conclusion of the analysis and flight test program is that the MPBA, modified with more rigid, final model tail-up restrictors and longer ejection pistons, with or without BDU-33D/B or Mk-106 practice bombs, can be carried and employed with the F-16 aircraft to the same limits as the TER-9/A with BDU-33D/B practice bombs. After successful execution of a few remaining demonstration flights the F-16 / MPBA configurations will be cleared for the complete intended flight envelope.

Table 1 Practice bomb compatibility and performance chart

Store type	Mass lb	Ejection force lb	Ejection stroke in	End-of-stroke velocity ft/s
MK-106 Mod 1	5	43	0.78	4.2
MK-106 Mod 5	5	43	0.78	4.2
MK-48	10	45	0.8	3.4
BDU-48	10	45	0.8	3.4
BDU-33	25	55	1.0	3.3
MK-76 Mod	25	54	1.0	3.2

Table 2 Comparison of MPBA, TER-9/A and SUU-20B/A configurations

	Length in	Mass lb	C.G. position in	Moment of Inertia lb.in2
Weapon pylon (MAU-12)	98	260		110000
Original MPBA, empty	49.7	31		4000
loaded 2 * 25 lb		81	8.1 *)	18000
Weapon pylon + loaded MPBA		341		
Weapon pylon (MAU-12)	98	260		110000
Aerod. mod. MPBA= DPBA, empty		49		5200
loaded 2 * 25 lb		99		19200
Weapon pylon + loaded DPBA		359		
Weapon pylon (MAU-12)	98	260		110000
Final version of MPBA, empty (rigid tail-up restrictor)	52	37	8.2 *)	5200
loaded 2 * 25 lb		87		19200
Weapon pylon + loaded MPBA		347		
Weapon pylon (MAU-12)	98	260		110000
TER-9/A, empty	68	93	16.4 $)	15300
Weapon pylon + empty TER-9/A		353		
Weapon pylon (MAU-12)	98	260		110000
SUU-20B/A, empty	122	276	14.7 $)	227000
Weapon pylon + empty SUU-20B/A		536		

*) Center of gravity position aft of center of forward MPBA carriage lug (14 inch hooks)

$) Center of gravity position aft of center of forward 30 inch carriage lug which is 8 inch in front of the forward 14 inch pylon hook

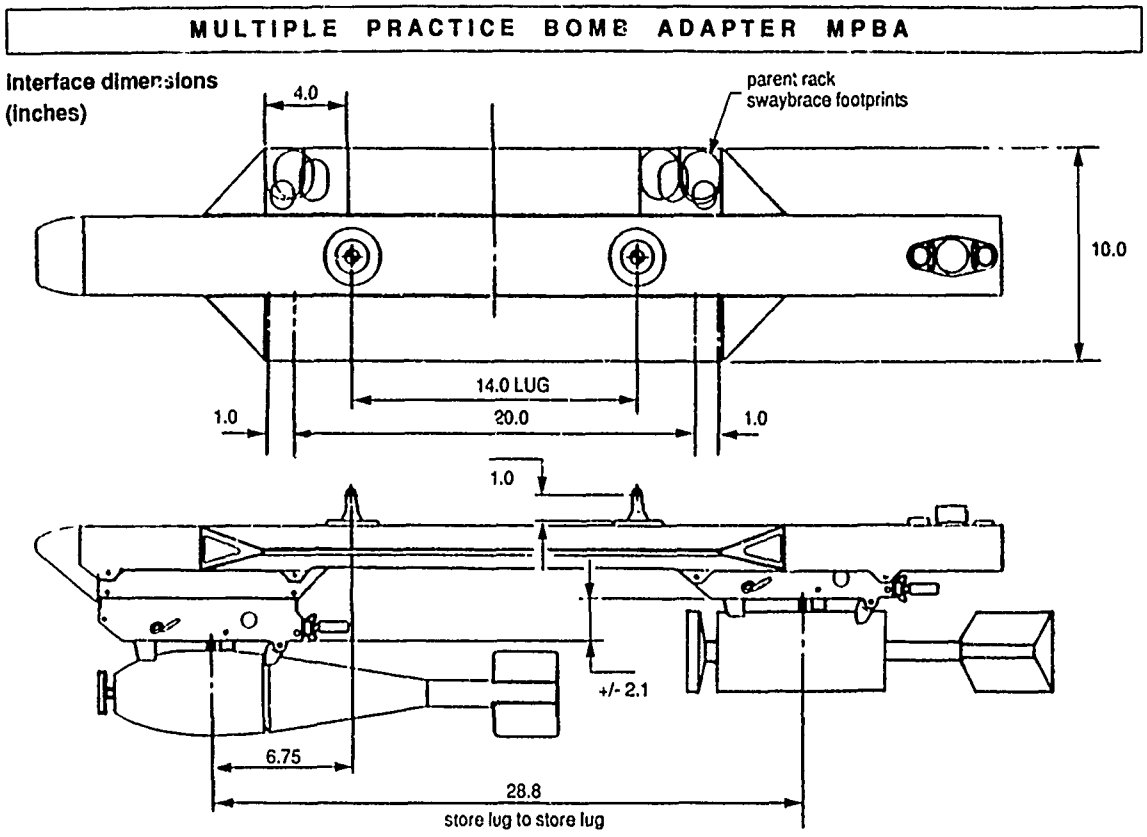

Fig. 1 Original MPBA with BDU-33D/B (fwd) and Mk-106 (aft)

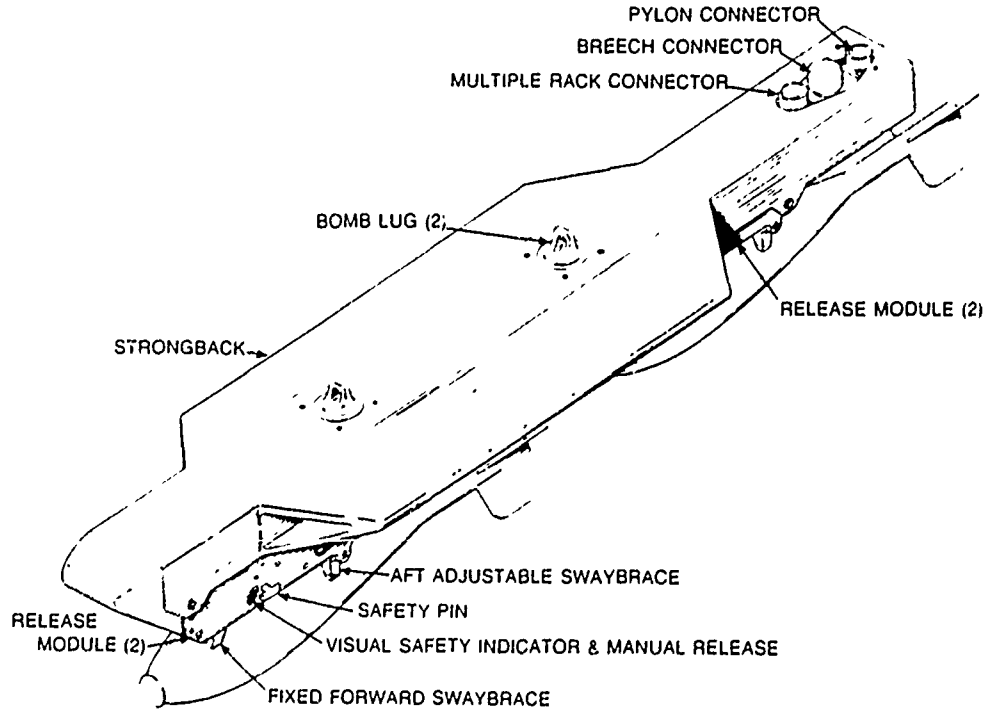

Fig. 2 Original MPBRack (front ejector not lowered)

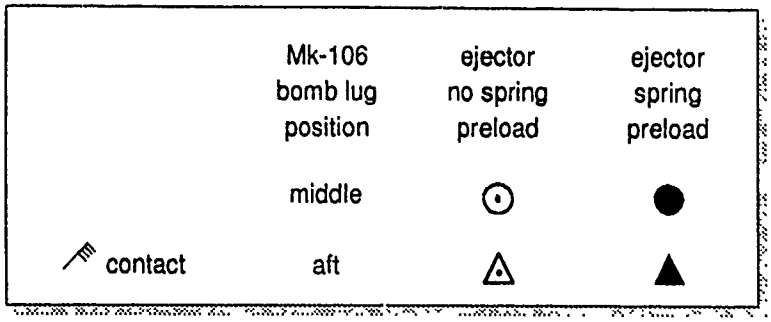

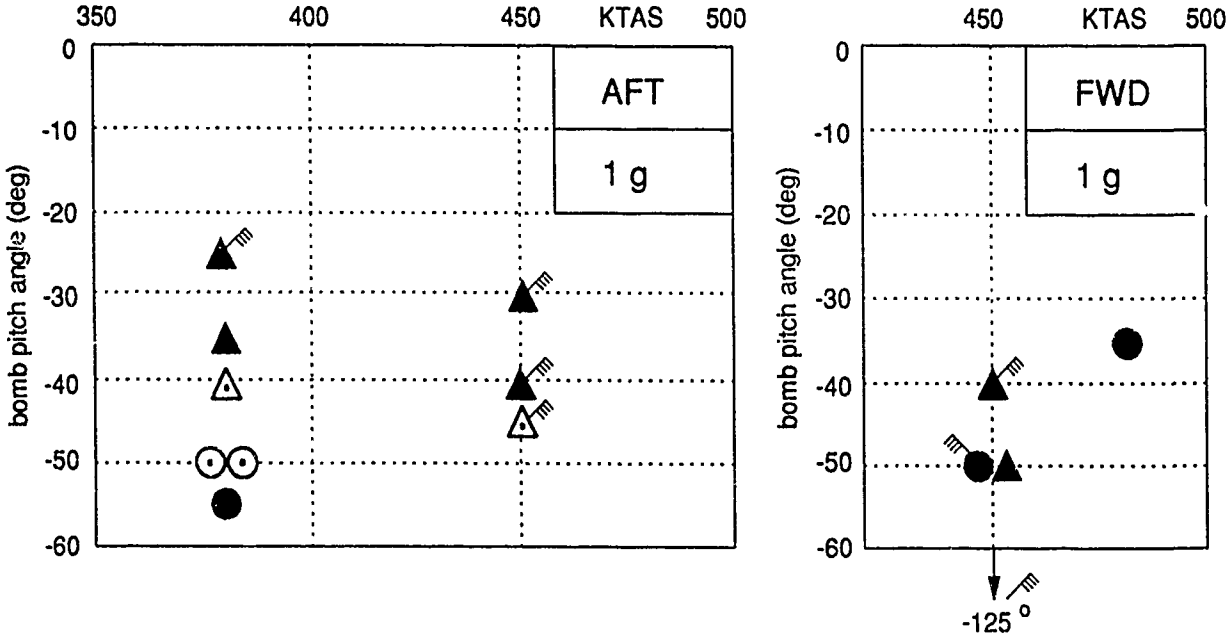

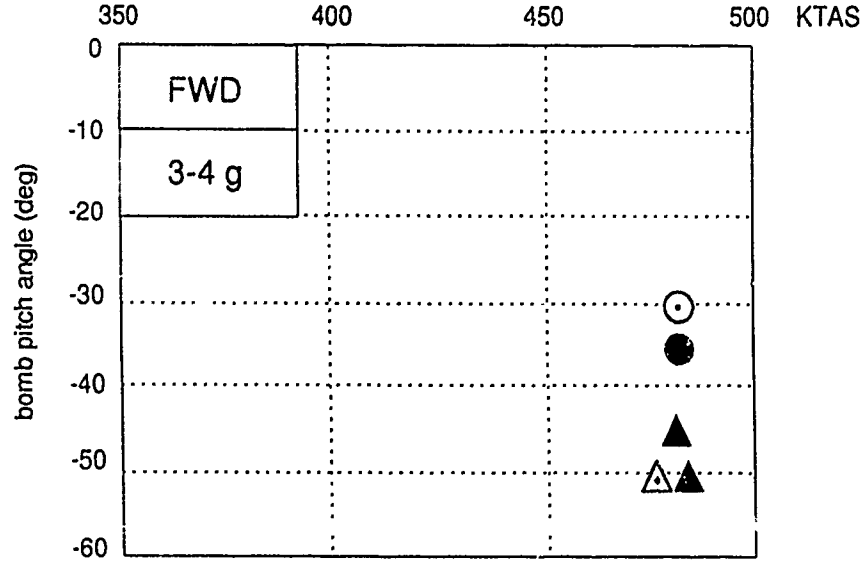

Fig. 3 Results of separations of Mk-106 from original MPBA (tests in 1988)

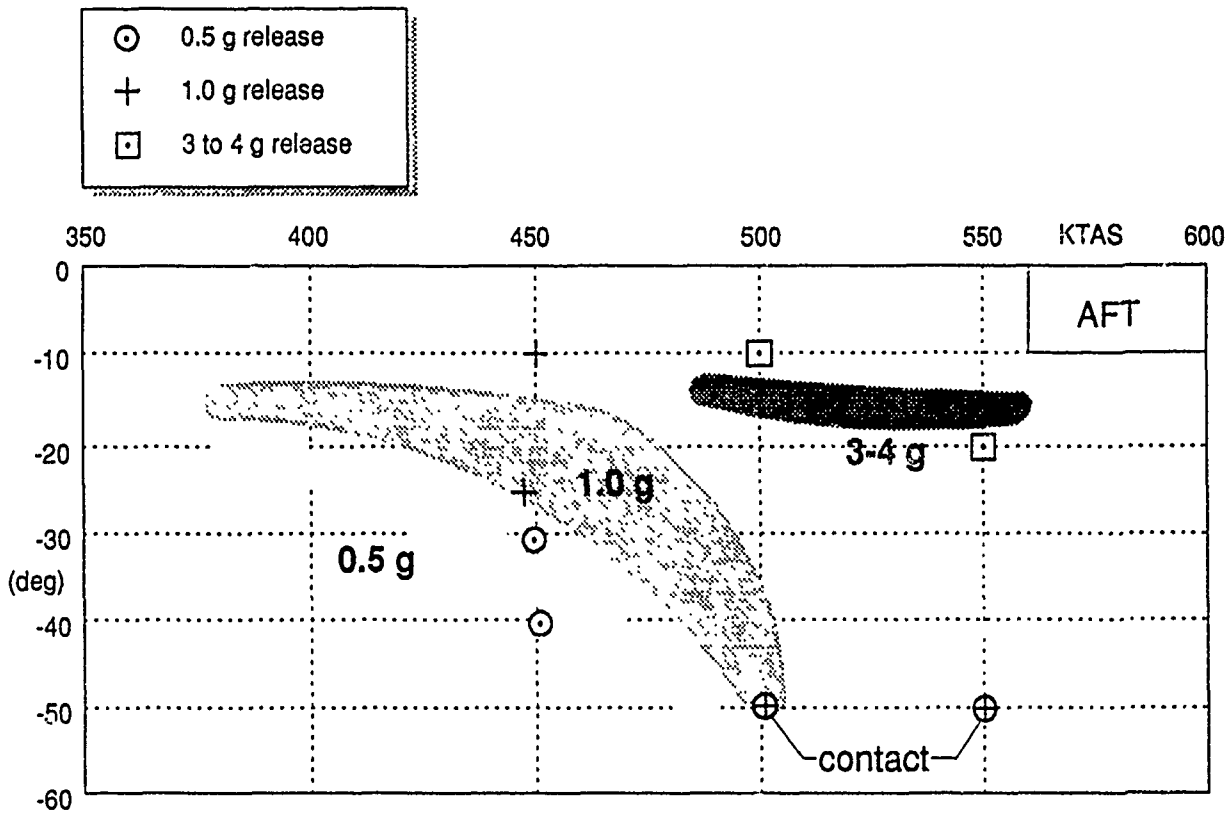

a) Maximum pitch down angle of BDU-33D/B from AFT position

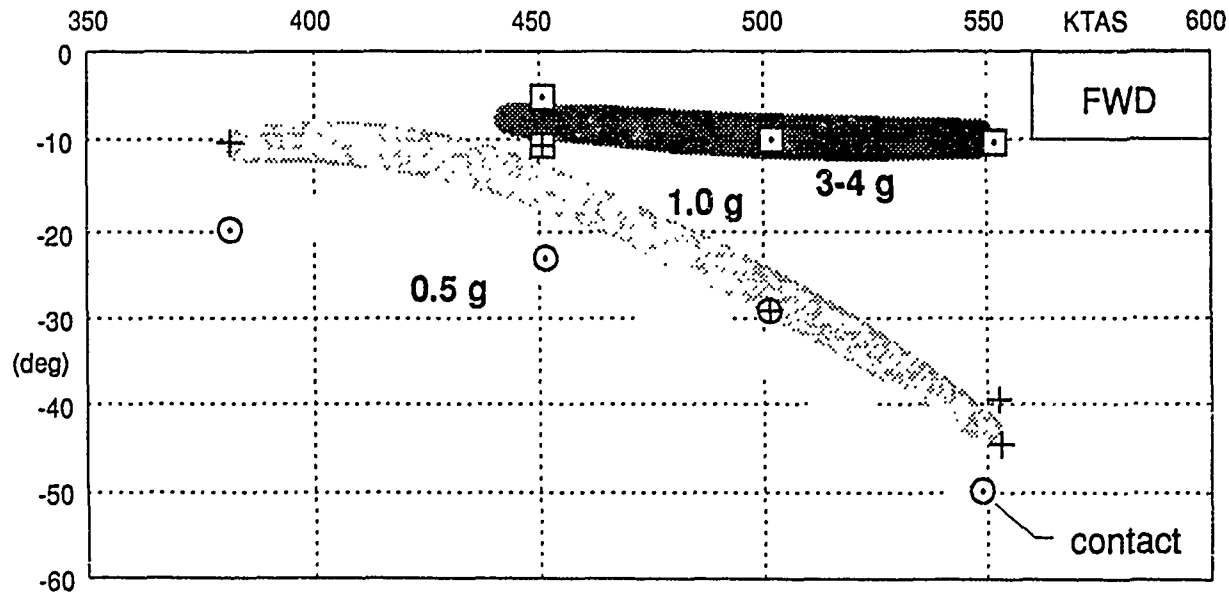

b) Maximum pitch down angle of BDU-33D/B from FWD position

Fig. 4 Results of separations of BDU-33D/B from original MPBA (tests in 1988)

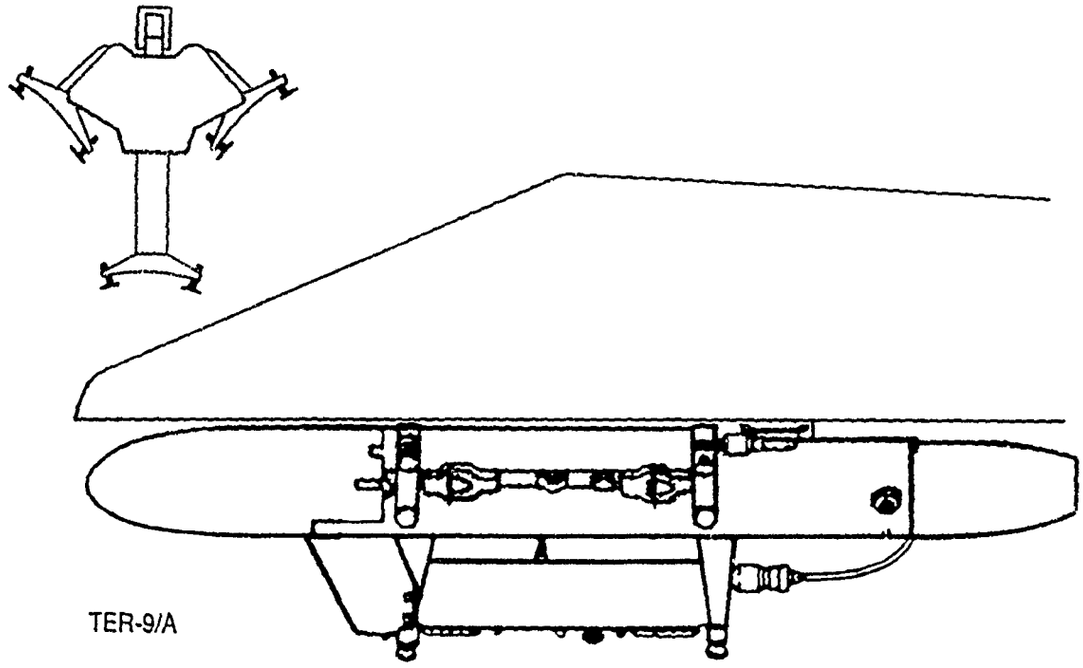

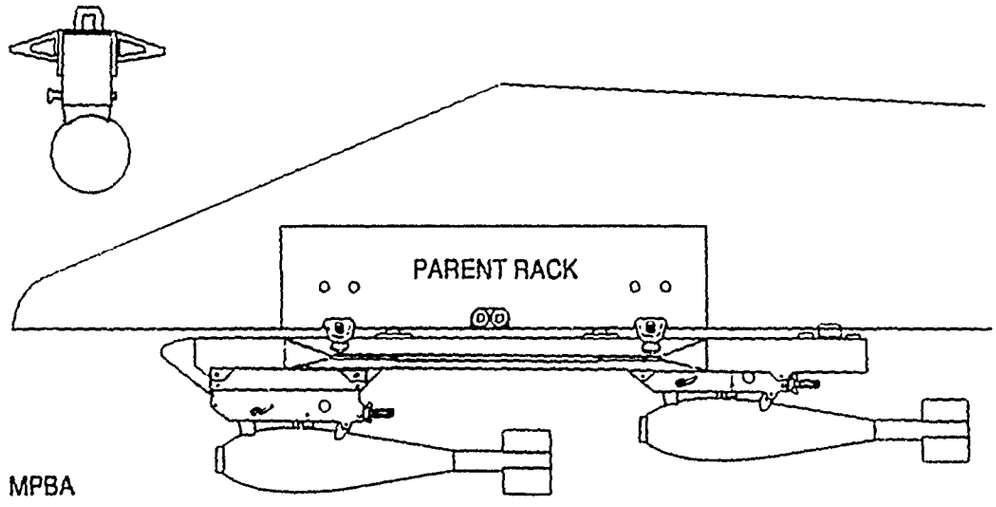

Fig. 5 Original MPBA, compared to the TER-9/A

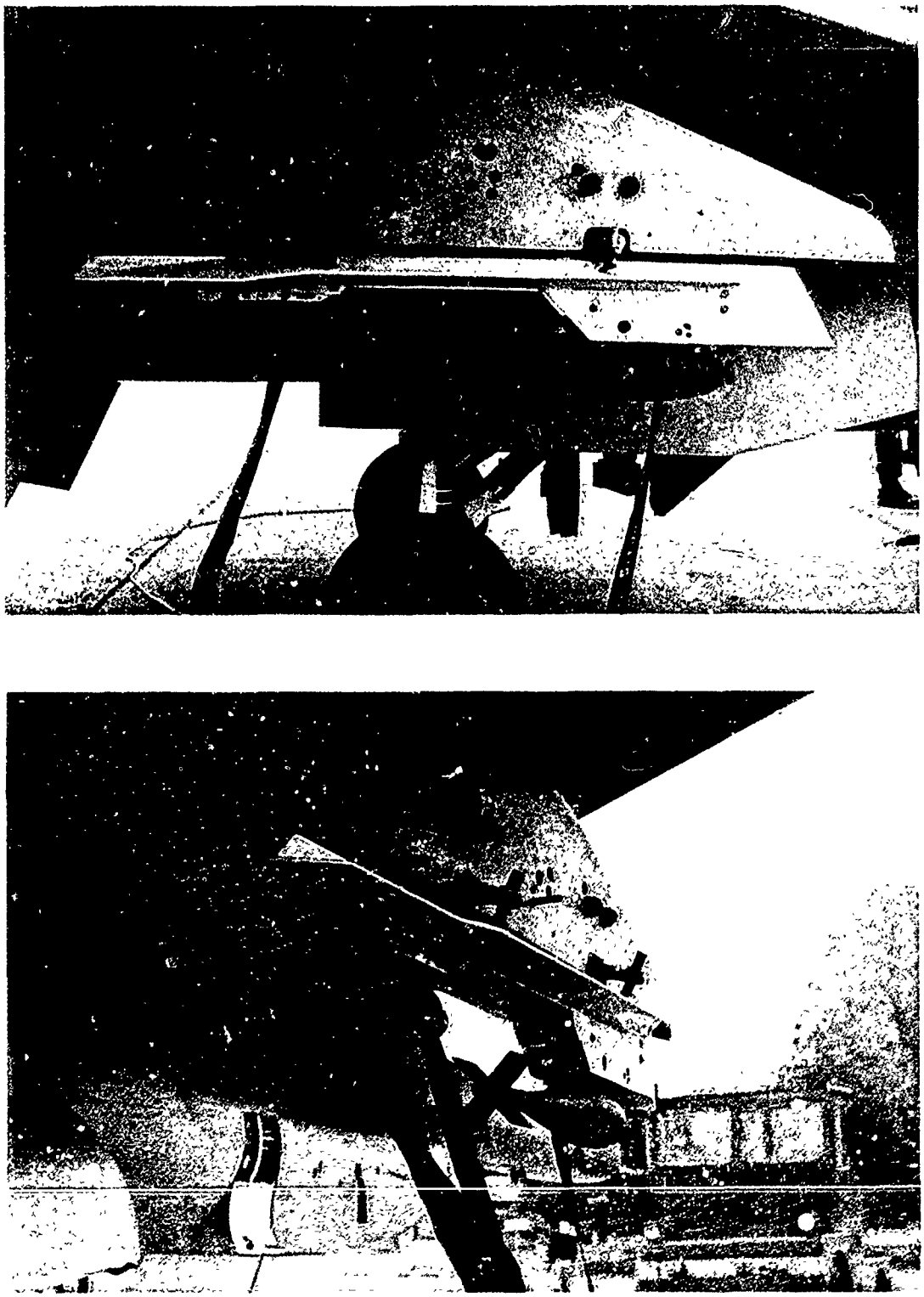

Fig. 6 DPBA, aerodynamically modified MPBA

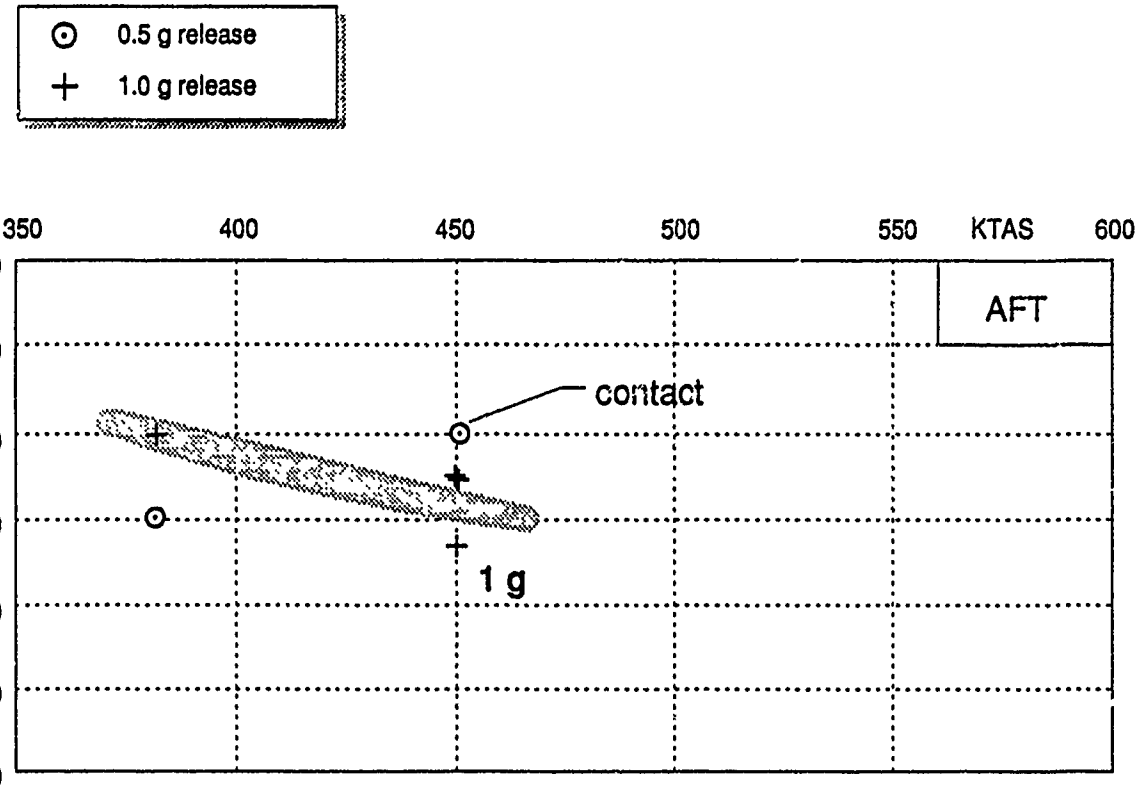

a) Maximum pitch down angle of BDU-33D/B from AFT position

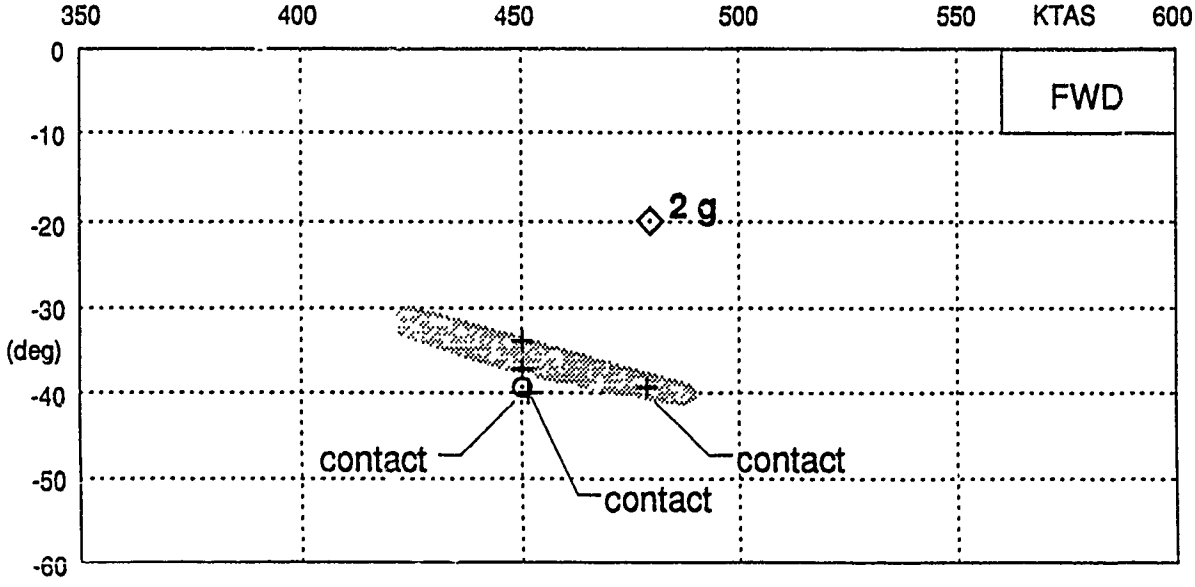

b) Maximum pitch down angle of BDU-33D/B from FWD position

Fig. 7 Separation results for the DPBA (aerodynamically modified MPBA) no tail-up restrictor (tests in October 1989)

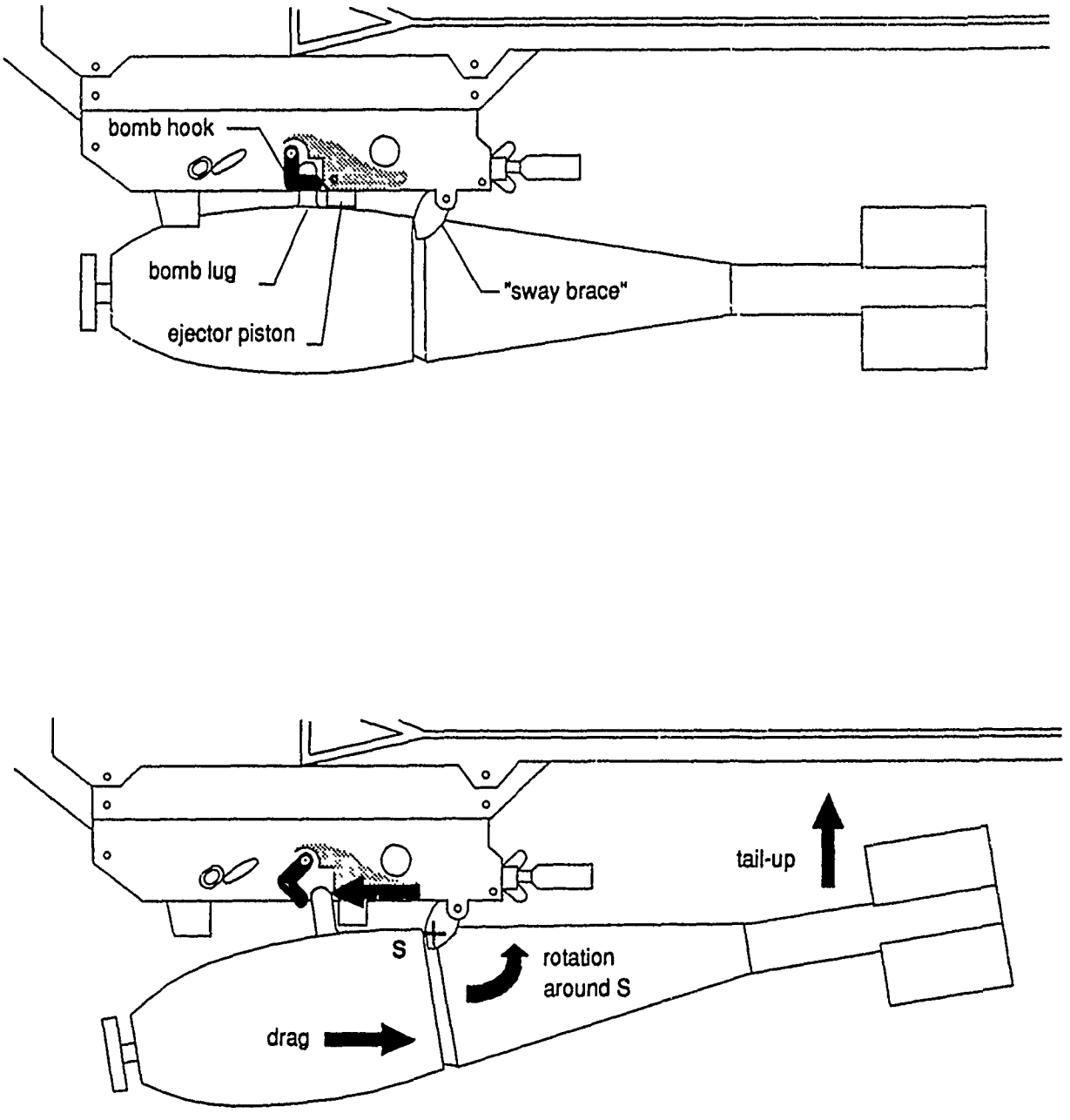

Fig. 8 Explanation of mechanical pitch-down moment, due to drag force and reaction force in bomb lug cavity, creating a rotation around support S, hence a tail-up movement.

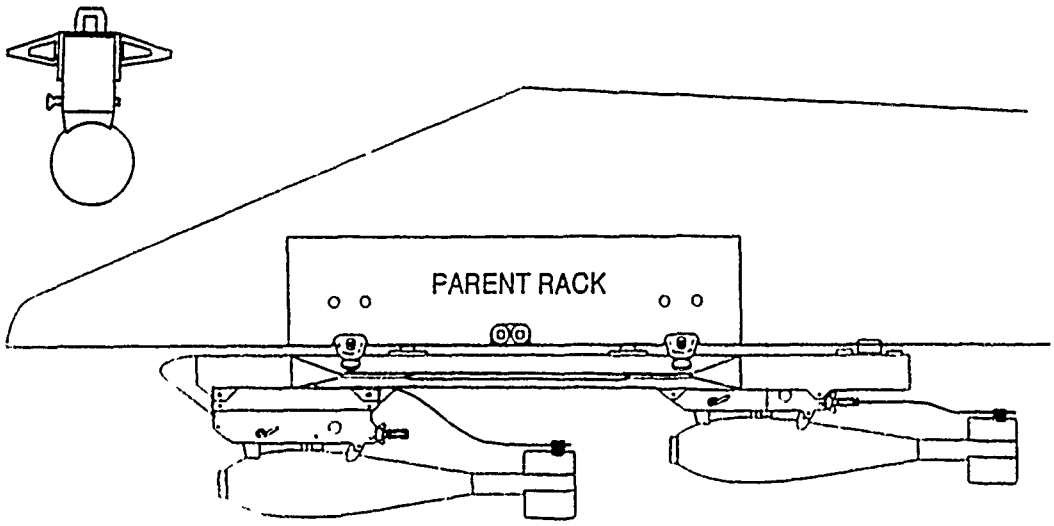

Fig. 9 MPBA with flexible tail-up restrictor (compare with Fig. 5)

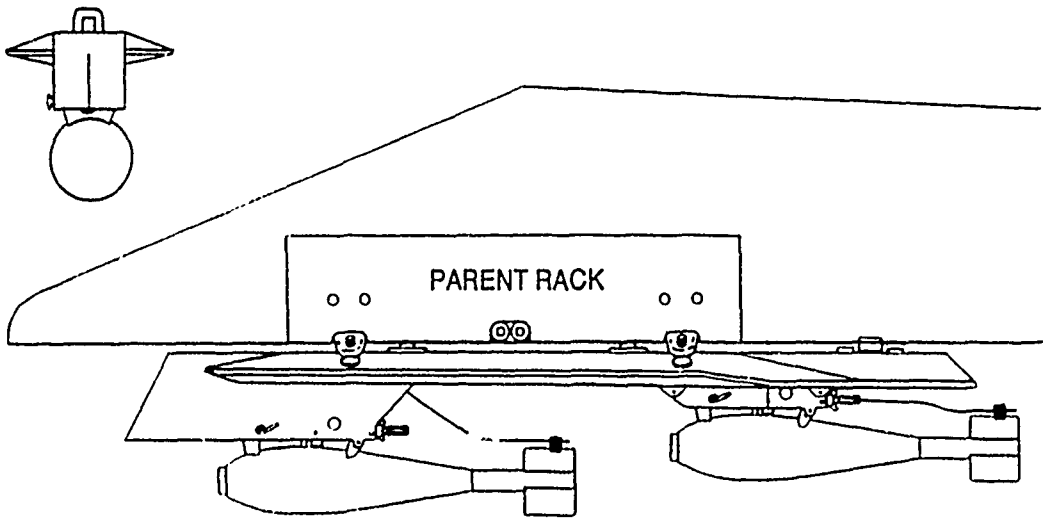

Fig. 10 DPBA with flexible tail-up restrictor

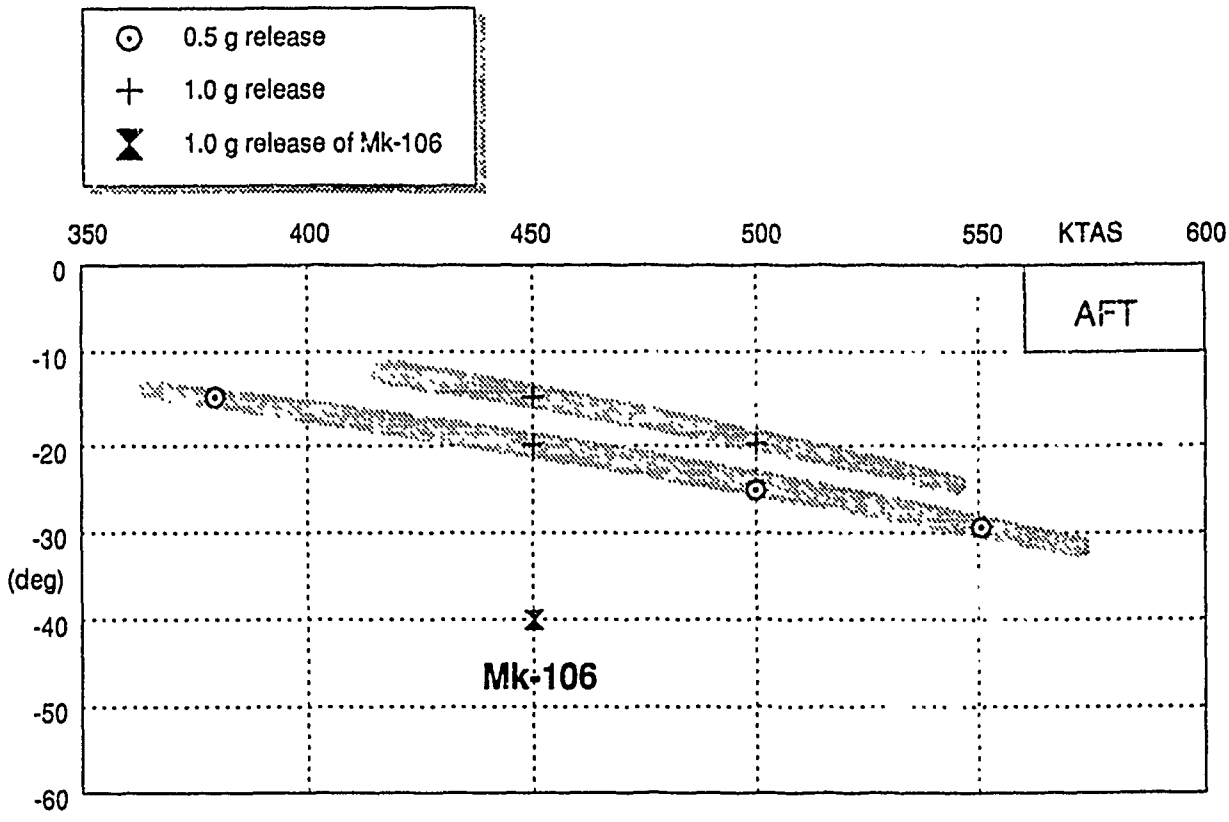

a) Maximum pitch down angle of BDU-33D/B and one Mk-106 from AFT position

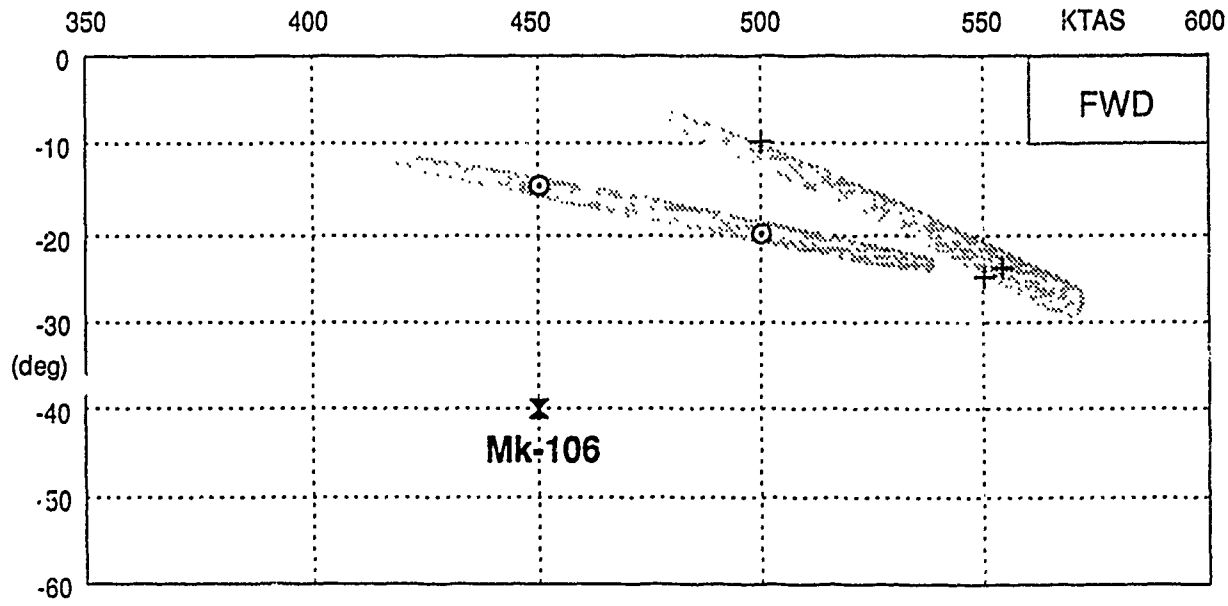

b) Maximum pitch down angle of BDU-33D/B and one Mk-106 from FWD position

Fig. 11 Separation results for the DPBA with flexible tail-up restrictor

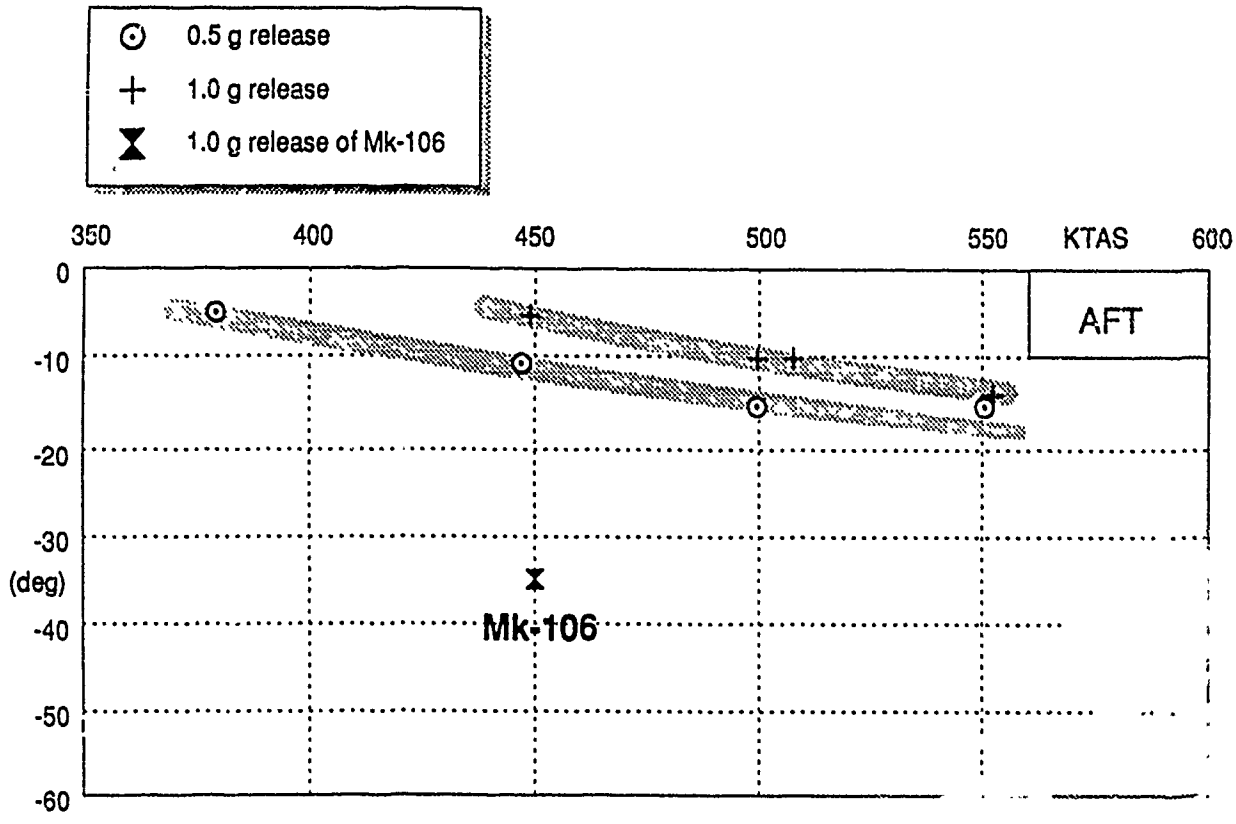

a) Maximum pitch down angle of DBU-33D/B and one Mk-106 from AFT position

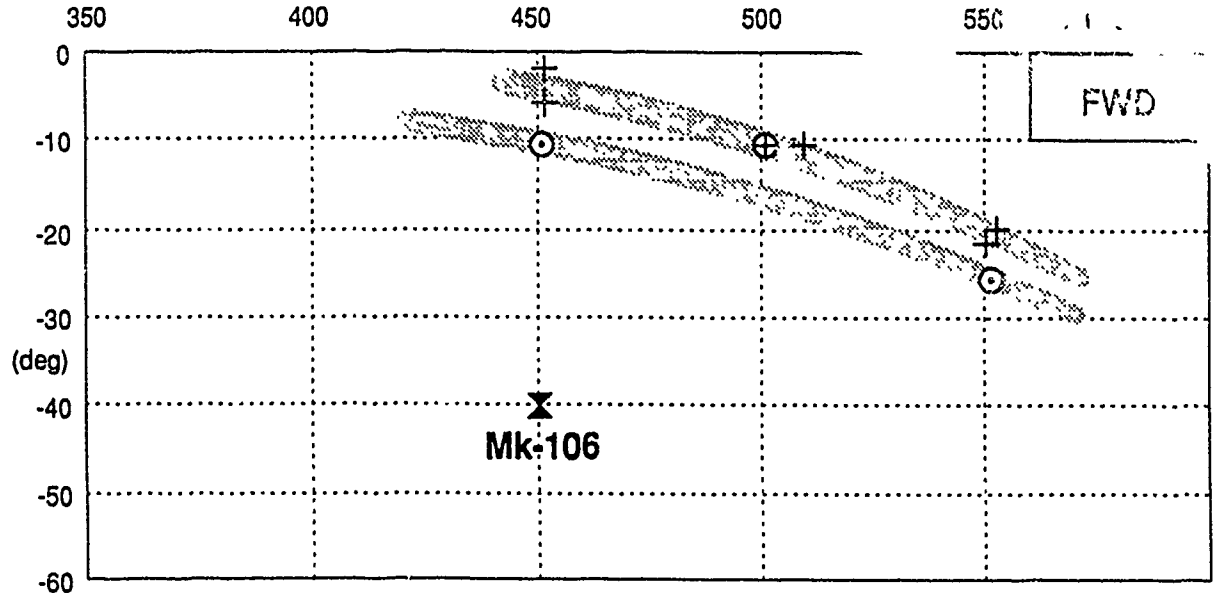

b) Maximum pitch down angle of BDU-33D/B and one Mk-106 from FWD position

Fig. 12 Separation results for the MPBA with flexible tail-up restrictor

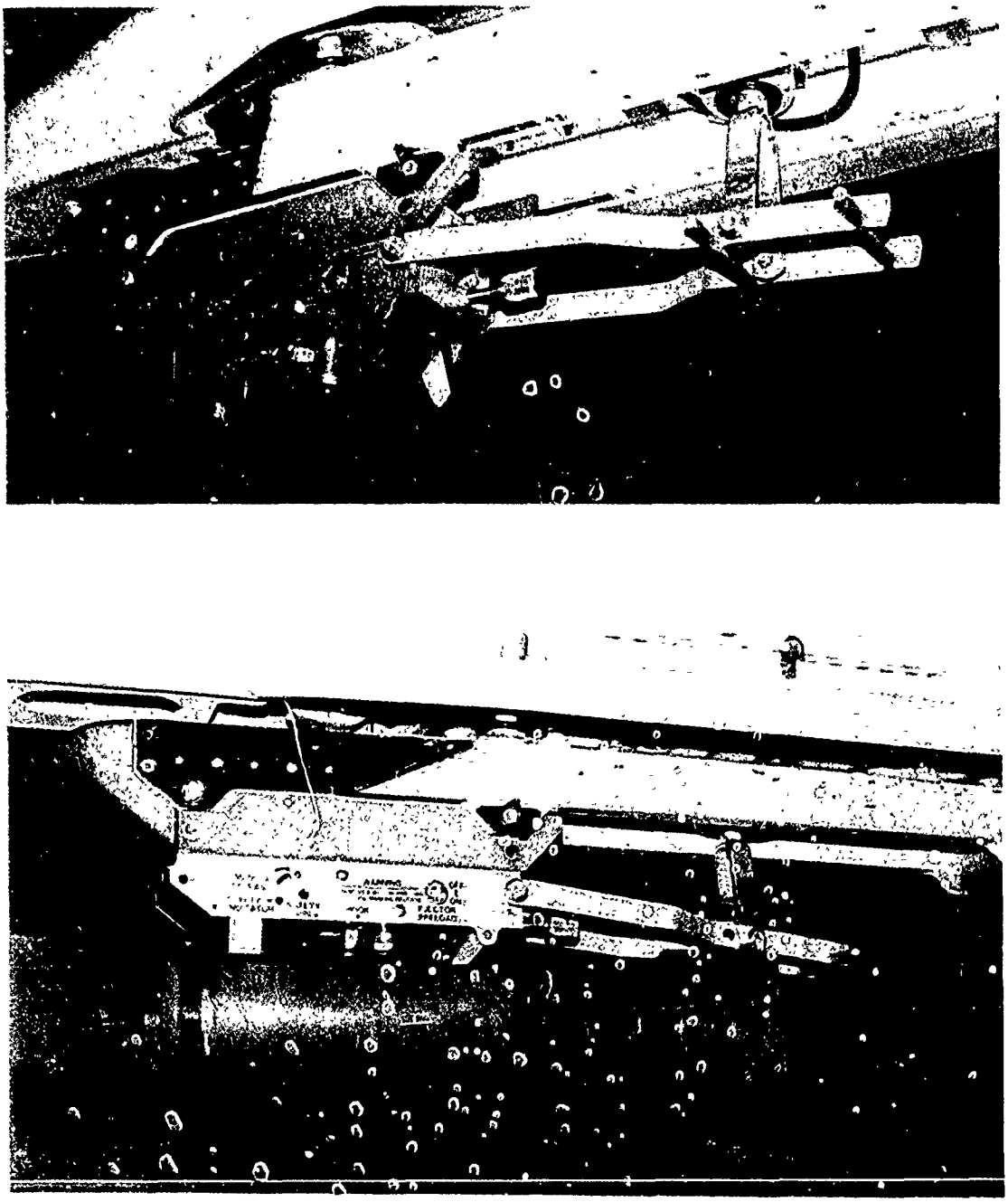

Fig. 13 The front ejector unit of the MPBA with the tail-up restrictor and the 7 mm longer ejector piston (upper picture) and a Mk-106 high drag practice bomb mounted (lower picture)

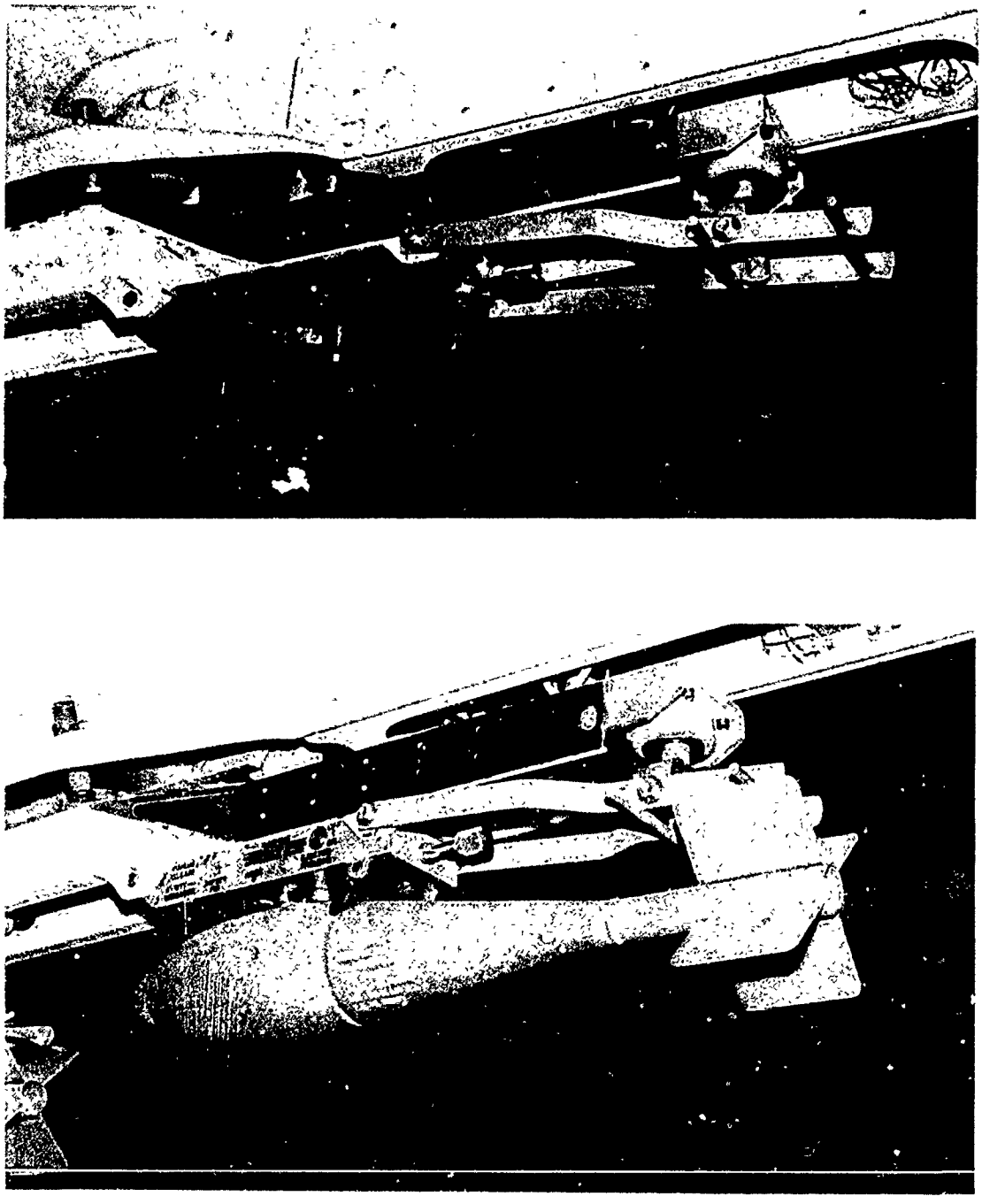

Fig. 14 The aft ejector unit of the MPBA with the tail-up restrictor and the 7 mm longer ejector piston (upper picture) and a BDU-33D/B low drag practice bomb mounted (lower picture)

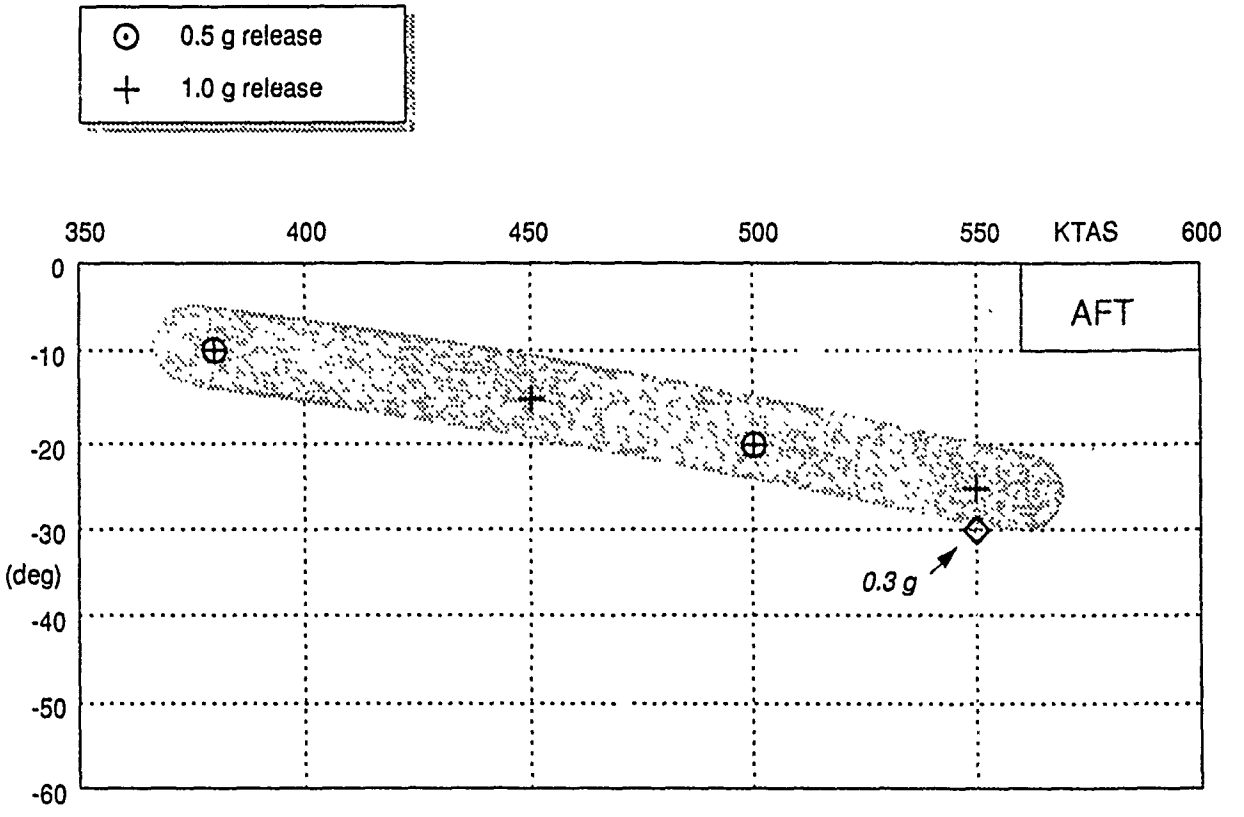

a) Maximum pitch down of angle of BDU-33D/B from AFT position of modified MPBA

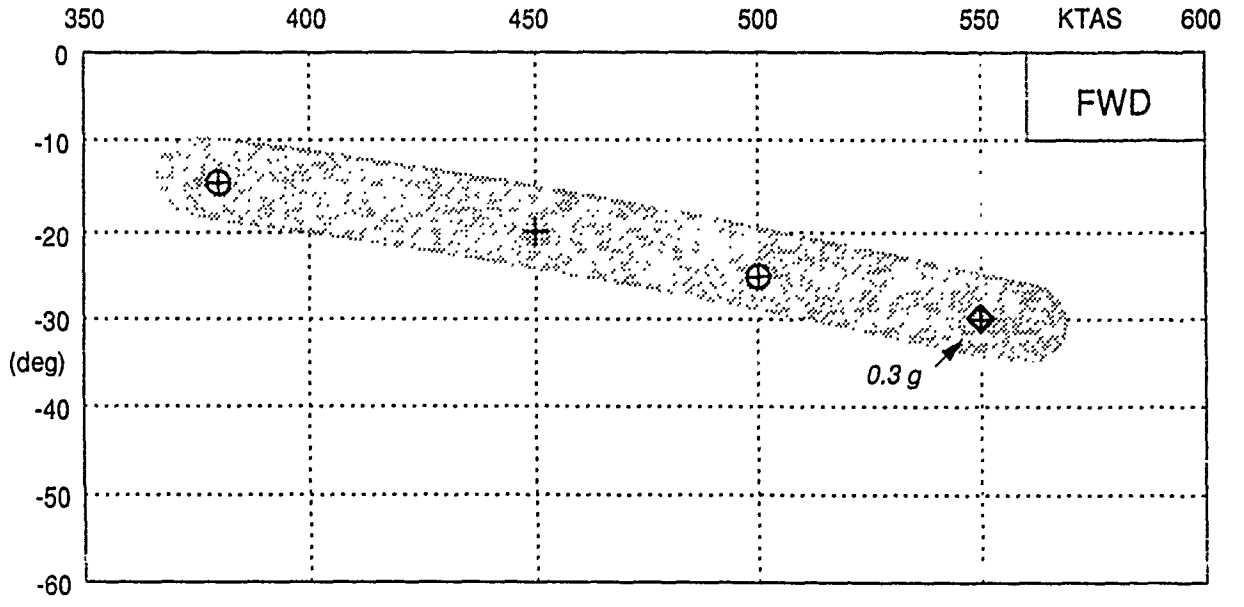

b) Maximum pitch down angle of BDU-33D/B from FWD position of modified MPBA

Fig. 15 Results of BDU-33D/B separations from modified MPBA

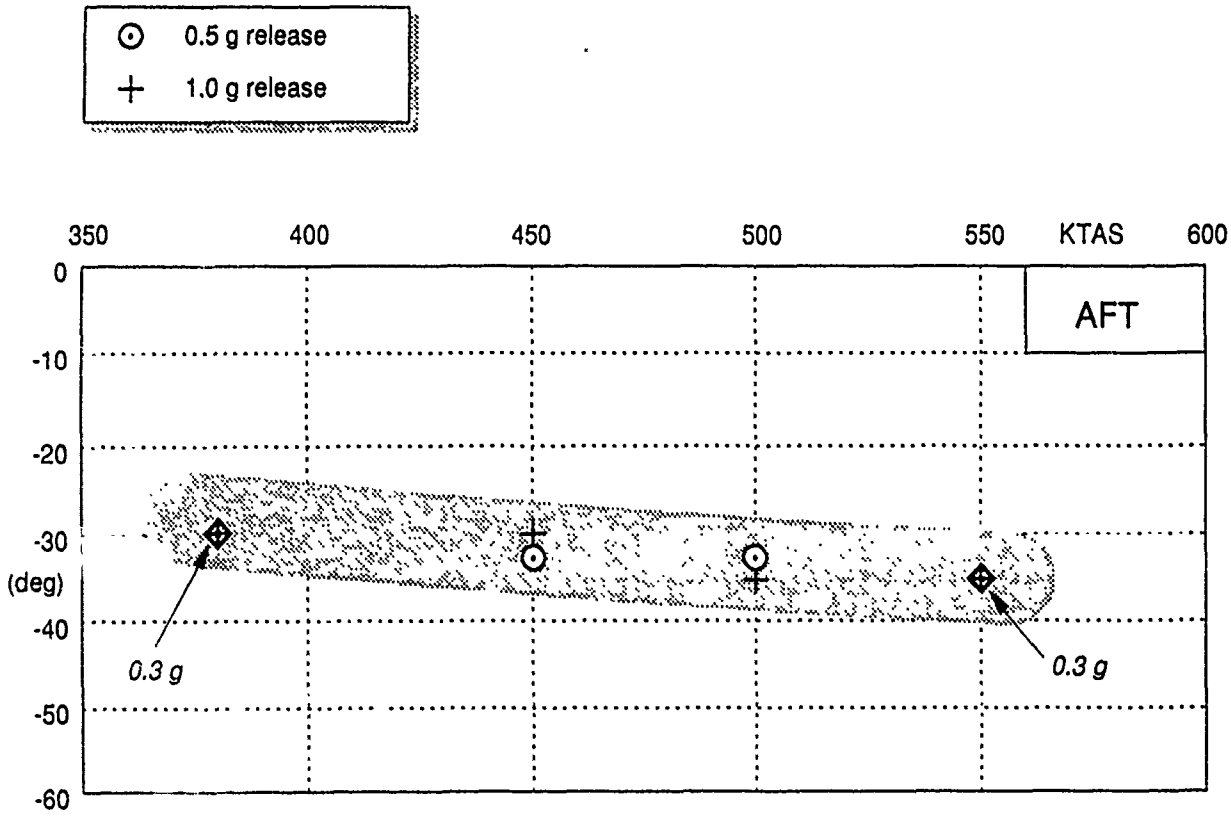

a) Maximum pitch down angle of Mk-106 from AFT position of modified MPBA

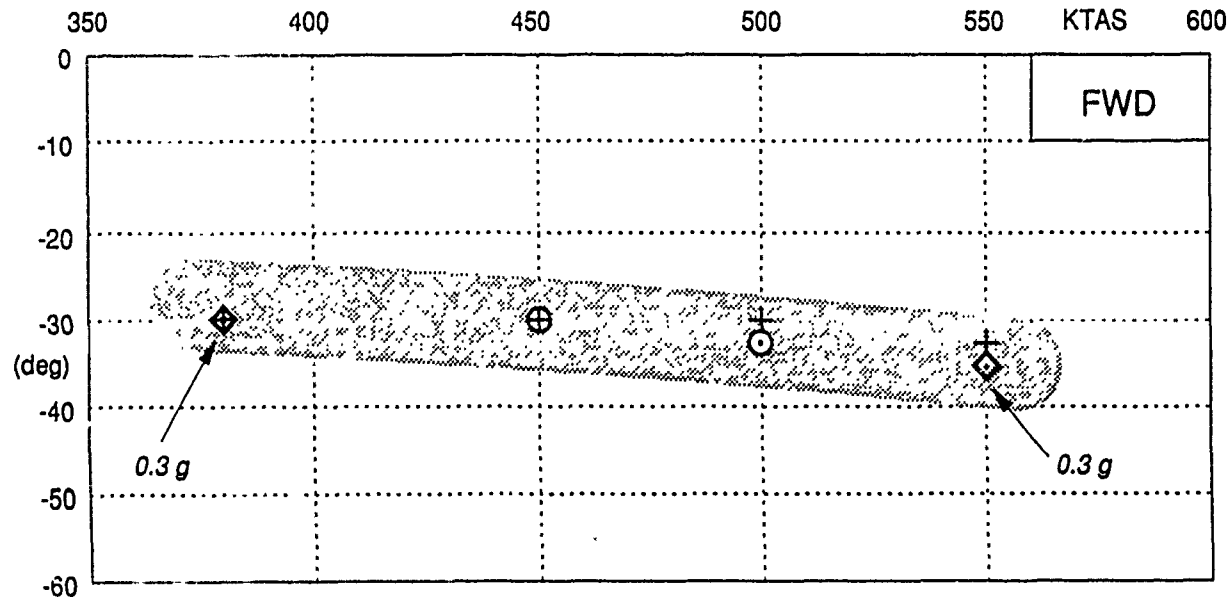

b)Maximum pitch down angle of Mk-106 from FWD position of modified MPBA

Fig. 16 Results of Mk-106 separations from modified MPBA

Biography of author

Kornelis R. Rijzebol (in English: "Case" Ryzebol) was born in 1941 in Warffum, in the Netherlands. Before going to University, he completed his military service in the Royal Netherlands Air Force. In 1970 he finished his study at the Technical University of Delft as a M.Sc. in Aerospace Engineering.

Since 1970 he is an employee of the National Aerospace Laboratory NLR at Amsterdam. From the beginning he was and still is involved in studies and flight test programs for the F-104G, (N)F-5 and F-16 of the Royal Netherlands Air Force, patrol aircraft of the Royal Netherlands Navy and the armed Fokker F-27 Maritime/Enforcer, mainly concerning aircraft-store compatibility, and most of all store separation prediction, flight testing, analyzing and NLR project management. As a flight test engineer / observer he was actively involved in separation tests of stores or air-to-air tow targets (F-104G and F-16).

In 1989 and 1990 he was involved in NAVSTAR/GPS test program planning and in-flight test management, testing NAVSTAR/GPS based research systems on board of the NLR Fairchild / Swearingen Metro II laboratory aircraft,

THIS PAGE INTENTIONALLY LEFT BLANK

THE DESKTOP ENGINEER

by

John C. Marshall

General Research Corporation

For Presentation To The

Eighth JOCG Aircraft/Stores Compatibility Symposium

Fort Walton Beach, Florida

23 - 25 October 1990

CLEARED FOR PUBLIC RELEASE

THE DESKTOP ENGINEER

by
John C. Marshall
General Research Corporation

INTRODUCTION

Every engineering task has a requirement for some type of analysis. It may be preliminary in nature to sort through the solutions available; it may be somewhat more involved to evaluate the relative merits and performance parameters of the candidate solutions; or it may be very extensive to resolve details of the system or activity being investigated. Most probably, several types of analysis will, or should, be brought to bear at various stages of the task.

Over the past several decades, tremendous strides have been made in the development of new "tools of the trade" to assist the engineer in his efforts - primarily as the result of the advent and subsequent explosive growth of high-speed digital computers. Word processing software makes it quick and easy to prepare text (this paper is an obvious example), from the first rough draft to the final product with no illegible handwriting to decipher, simple editing, and output that is letter quality - truly "camera ready." Computer-aided design tools have revolutionized the drafting room. And the presence of large-capacity, number-crunching computers has permitted solutions to be obtained never dreamed possible by those who first stated the problems.

In this environment, there is a tendency to always throw the maximum computer power available into the analysis process. It is often assumed that a large machine running a complex program, which creates great mounds of data with many significant digits, is the engineer's "dream machine." In many instances, however, there will be no direct correlation between the quantity of data produced and the amount of useful information obtained. It is an axiom of the engineering profession that a job has been properly engineered if,

and only if, the analysis and development have been carried out in an economical manner and if the end product represents the most economical solution that satisfies the operational criteria. The emphasis on the word "economical" is intentional, and is the purpose of this presentation. By this axiom, simpler methods are frequently the proper choice to carry out the analysis required, and the simpler tools are typically well suited to produce the desired information.

This premise is demonstrated herein by describing the tools and methods which were devised to carry out an aircraft/stores separation analysis without the benefit of a mainframe computer or extensive CFD analytic codes. Certainly, the benefits of computer assistance were not ignored, but it was determined early in the analysis process that a modest desktop system would do the job very nicely. An investment on the order of $2,000 to $3,000 is all it takes to provide both the hardware and the software to do the job described herein.

THE PROBLEM AND THE APPROACH

The basic problem to be resolved by this analysis was an age-old one in the annals of aircraft/store compatibility; how much clearance is required between a weapon at carriage and an adjacent fuel tank in order to assure safe separation of the weapon over a wide range of flight conditions. The weapon was somewhat typical of the general class of small, subsonic glide vehicles, with a modest lift-to-drag ratio to permit it to be launched from a comfortable standoff distance. The need for enough aerodynamic lift to provide the glide capability added two undesirable effects; 1) the aerodynamic responsiveness made the vehicle sensitive to flow-field variations near carriage, even over the short time interval of the separation event, and 2) the required size of the lifting surfaces encroached significantly on the normally-desired physical clearances. The aerodynamicists who designed the weapon were thus battling tooth and nail with the compatibility engineers

over what constituted an acceptable weapon configuration. Does this sound familiar?

Three items were needed in order to perform the separation analysis for this problem; 1) a definition of the flow field that the weapon would traverse during the initial separation event, 2) a determination of the aerodynamic forces and moments acting on the weapon in this flow field, and 3) a multi-degree-of-freedom flight simulation to integrate the equations of motion to produce the resultant flight path. Details of the methods of addressing these three requirements are given in the following paragraphs.

THE FLOW FIELD

The carrier vehicle which was to deliver the weapon was a low-wing, high-speed, fighter aircraft which could operate in either an interceptor or attack mode. In the attack mode, it was equipped with a large fuel tank carried under the fuselage on the centerline of the aircraft. The fuel-tank shape consisted of an ogive nose (slightly blunted), a cylindrical center section, and a short ogive tail fairing, all with a circular cross section. The tank was mounted from a very stubby pylon so that it was quite close to the underside of the fuselage, and thus to the plane of the wing lower surface. The weapon was pylon-mounted alongside the tank so that its centerline was slightly closer to the wing than was that of the tank. The nose of the weapon was somewhat forward of the tank nose, and the weapon tail fins were opposite the center section of the tank. Thus, the weapon was in the most non-uniform region of the tank flow field.

A composite flow field was developed to account for the effects of the fuel-tank size and shape, the proximity of the weapon to the aircraft wing, and the aircraft angle of attack. It was assumed that the three effects could be combined by the method of superposition. Since the fuel tank was a body of revolution, it lent itself very nicely to representation, in a mathematical

sense, by a line source distribution along the tank centerline. Although the method is based on incompressible flow analysis, Mach number effects can be included by use of the Prandtl-Glauert rule, which is suitable as long as the local flow field is subsonic throughout.

In the general case, where the body shape can be defined in terms of an analytic function, the line source distribution is found by an integral solution which requires the flow to be tangent to the body along its entire length. When the body shape is known only in terms of specific coordinates, an approximate solution can be found by substituting a finite series of "n" equal-length segments for the line distribution. The larger the value of "n," the better the approximation, but very good results are found with relatively small numbers of segments. For the present case, a source distribution made up of ten segments was used. The strength of each segment was determined by the condition of flow tangency at ten points along the tank surface, located at stations corresponding to the center of each segment. This produced a set of ten equations to determine the ten segment strengths. An iterative procedure was used to resolve this set, which converged to a solution with an acceptably low number of iterations. An additional condition which states that the sum of the strengths of the individual segments must be zero if the body is a closed body was used as a check on the validity of the solutions obtained. The velocity components at any point in the flow are then determined by adding the effects from all source segments to the uniform rectilinear flow of the free stream. An example of the type of flow field produced by this solution is shown in Figure 1. Even the streamline closest to the body is a surprisingly rational solution, given the coarseness of the segment distribution chosen.

With the low-wing configuration of the aircraft, the wing and fuselage lower surfaces were nearly planar. Although the wing was a far cry from being infinite in dimensions, the short range of the tank flow field as seen in Figure 1 suggested that an image-field

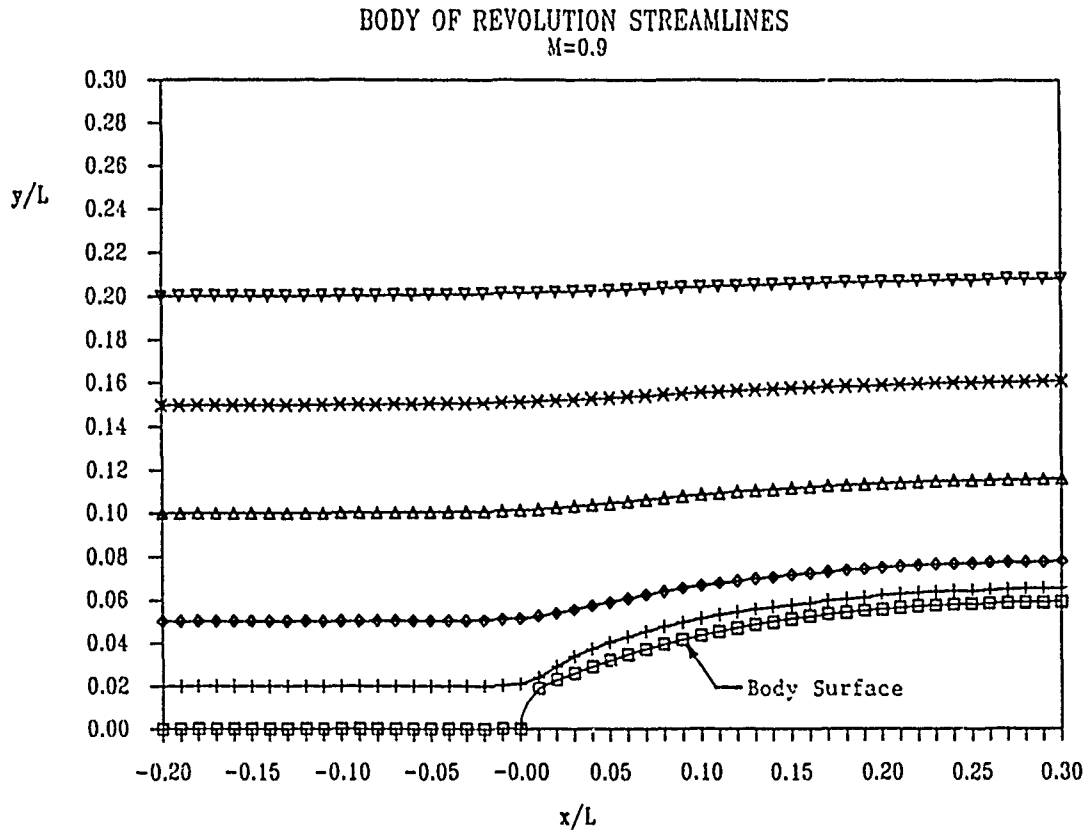

Figure 1. Fuel-tank Flow Field Representation

approach might be a reasonable way to produce the desired composite effect of the wing and the fuel tank. In this approach, a second line source distribution, equal in strength to that used to represent the tank, was located (mathematically) above the tank. The vertical spacing was twice the distance from the centerline of the tank to the wing lower surface. At the planar surface midway between the two line sources, the vertical components of velocity just cancel out - the desired condition of a solid interface. At the surface of the tank, the effect of the image field is equivalent to a distortion of the shape of the tank. A few calculations showed that this effect was very small. If desired, an adjustment could have been made to the strength of the source segments to account for the image field effect at some selected points on the tank, but the complexity of the added computations was not deemed necessary for the present analysis.

Aircraft angle of attack, for small angles only, was accounted for by adding a constant incremental flow angle which was modified by a one-dimensional exponential decay factor. The decay factor was selected to just cancel out the flow angle at the vertical location of the wing lower surface while becoming negligible at a distance of a few meters below the wing. As with the image-tank flow field, this adjustment effectively distorts the tank shape without some correction to the source strengths. However, since it was used only for angles of attack of a few degrees, and only to investigate relative effects of angle of attack on weapon flight behavior, no changes were made in the basic fuel-tank flow field when non-zero values of angle of attack were used.

THE WEAPON AND ITS AERODYNAMICS

The weapon configuration was quite simple. The body was a circular cylinder with an elliptically-blunted nose. The major lifting surfaces were four rectangular fins (wings) mounted at the rear of the body in an "X" configuration. Two small fins (canards) were mounted near the nose in the horizontal plane to produce a near-neutral static margin in pitch while retaining sufficient static stability in the yaw plane. Moveable trailing-edge surfaces were incorporated in all four of the rear-mounted fins to provide combined pitch, yaw, and roll control.

The configuration had been thoroughly evaluated in a wind tunnel, so a comprehensive set of body-buildup aerodynamic data was available. This permitted the effects of each component of the weapon to be defined separately. Since it was not expected that the weapon would undergo large pitch or yaw excursions in the short period of time during which it traversed the fuel-tank flow field, the critical period for this analysis, all component aerodynamic data were assumed to be linear. The six static force and moment aerodynamic coefficients of the full configuration were determined on the basis of composite flow-field velocities calculated at the weapon center of gravity (c.g.). The flow field was also evaluated

at the body-axis stations of the canards and the rear-mounted fins. For each fin set, an incremental force coefficient was determined by multiplying the incremental flow angle (difference between the local value and that at the c.g.) by the slope of the corresponding force-coefficient. These incremental force coefficients were multiplied by the appropriate distance terms to obtain the incremental moment coefficients. The incremental coefficients were then added to the values obtained for the full configuration to determine the total forces and moments acting on the weapon at any instant in time.

The aerodynamic contributions of the control surfaces were handled in a similar fashion. The aerodynamic coefficient slopes due to control surface deflection were determined for each fin, at each flight Mach number, from the wind tunnel data. Multiplying these slopes by the desired deflection angles produced control-induced increments in each of the aerodynamic coefficients. These increments were then introduced into the calculation as constants in the input-data string, and were added to the basic coefficients for the configuration.

For completeness, the aerodynamic damping derivatives were included in the calculations. However, for the type of motion being evaluated in this analysis, only the roll-damping term was of any significance.

Samples of typical aerodynamic data are shown in Figures 2 through 4. Although the numerical values are not shown in these figures, the data for each coefficient are plotted to the same scale for comparison. These curves show that the assumption of linearity is reasonable at least up to 6 degrees angle of attack, and possibly a bit higher. Calculations of the analysis verified that the angles experienced were within this range. Also, over this same range, the contr. effects were essentially constant.

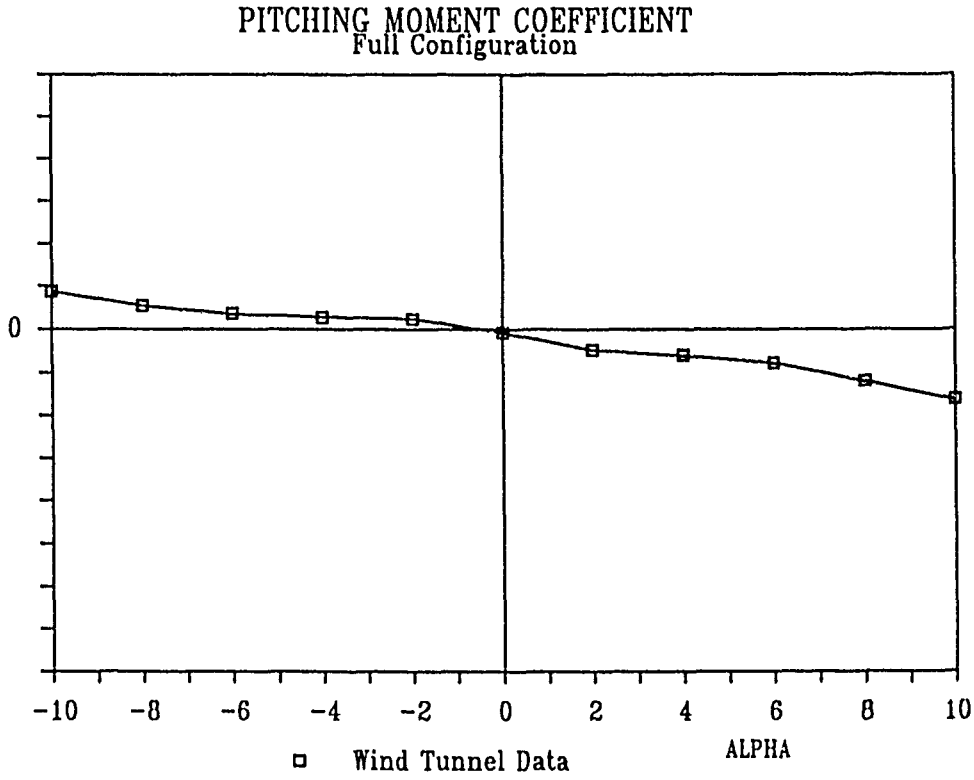

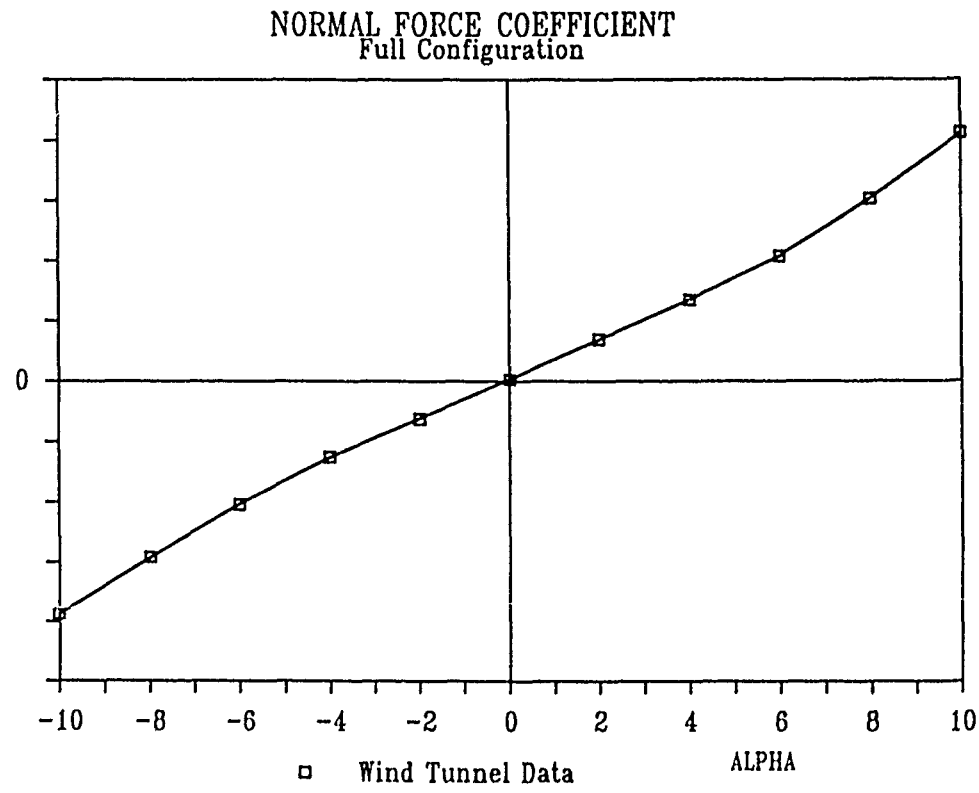

Figure 2. Aerodynamic Coefficients for the Complete Configuration

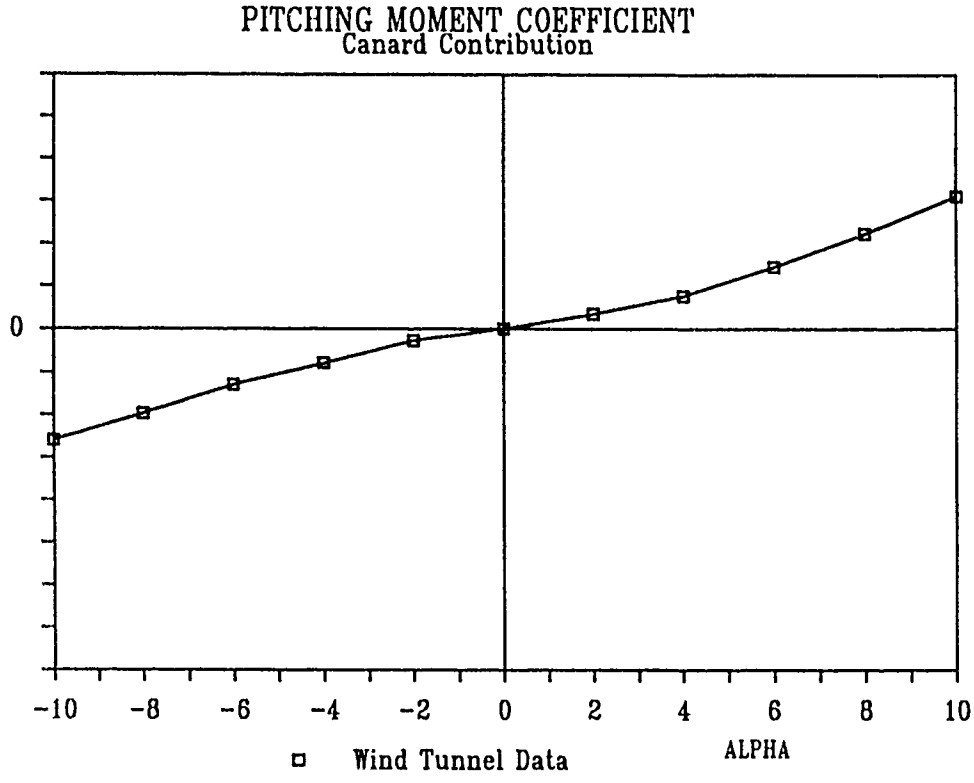

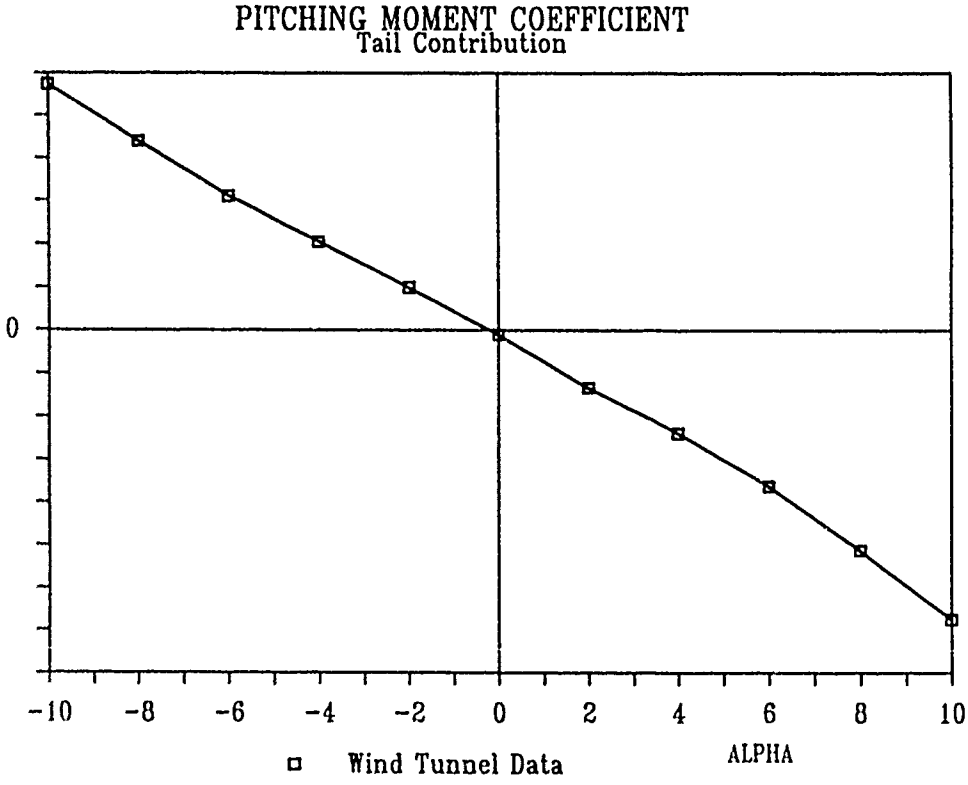

Figure 3. Pitching-Moment Coefficients for the Canard and Tail

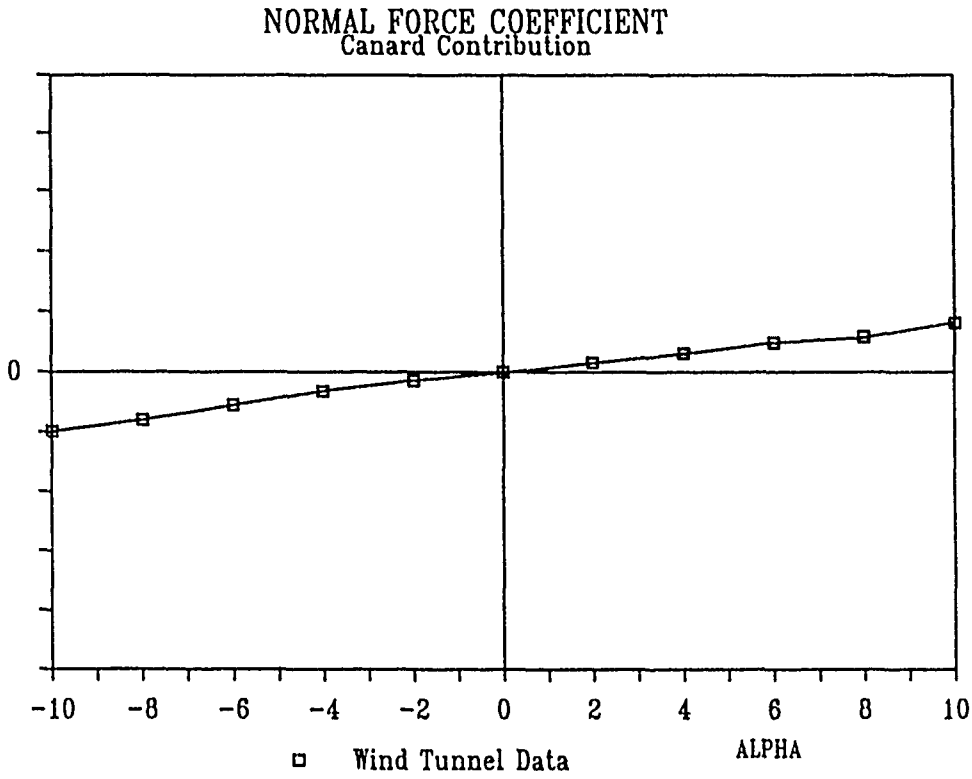

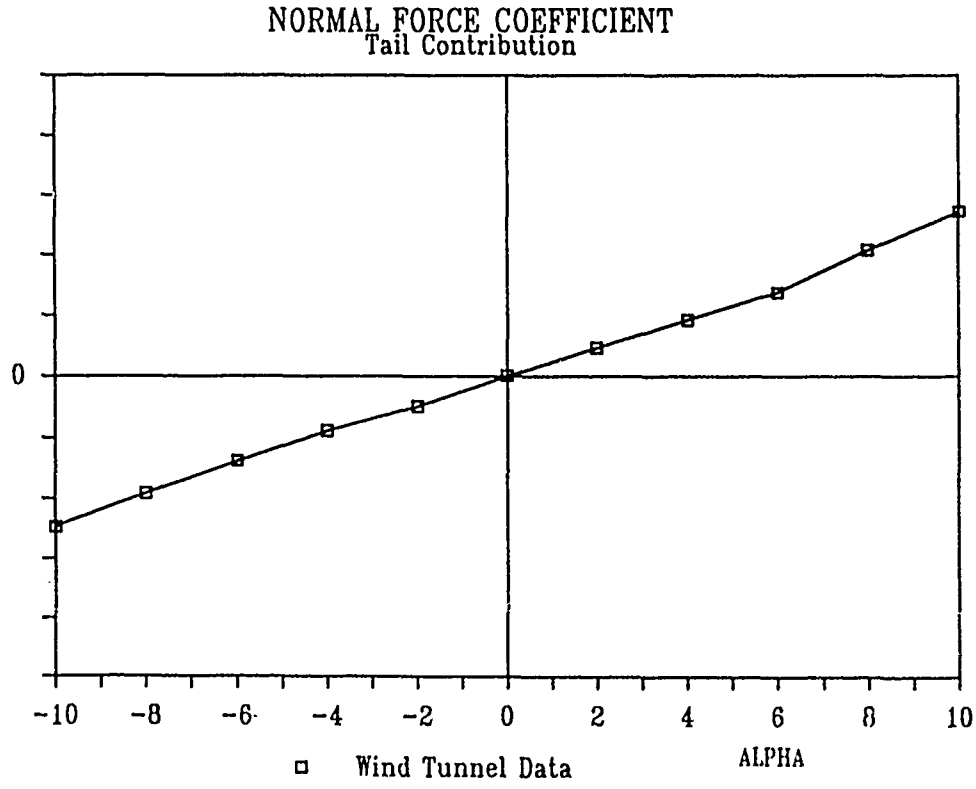

Figure 4. Normal-Force Coefficients for the Canard and Tail

THE FLIGHT SIMULATION

There were several criteria established which guided the development of the flight simulation. These were:

1. The weapon would experience a three-dimensional flow field so that a full six-degree-of-freedom (6-DOF) simulation would be required.

2. A simple structure was desired both to facilitate modifications and to keep the computational time low.

3. The integration process should maintain reasonable accuracy while not requiring excessive computational time. An adjustable integration step size was desired in order to establish the proper compromise between these two goals.

4. Data handling among the component modules of the simulation should be such that addition or modification of variables in one module do not require a change to other modules.

5. It should be easy to change the input values and to change the quantities being written to the output file.

The result of applying these criteria was a full 6-DOF simulation with a simple modular structure. The main program, or executive, routine was quite short. It directed the program flow through the input and initialization processes, a repetitive loop of evaluating flow-field parameters and integrating the equations of motion, a periodic storing of selected data in a temporary internal file, and a program-ending dump of these data into a conveniently structured output file. In the initial program structure, since the configuration to be studied was fixed, the fuel-tank flow-field structure was evaluated prior to running the simulation and the

strength parameters for the segments of the line source distribution were included in the input-file data string. In a later modification, developed to improve the flexibility of the program, a separate module was included in the initialization process to calculate these segment strength parameters. In this case, the input string contained fuel-tank geometric parameters (local radius versus station).

The cycle through the integration loop began with an evaluation of the flow-field velocity components at the three locations corresponding to the positions of the weapon canards, c.g., and tail fins. Local angles of attack and sideslip angles were determined from these velocity components and the body attitude. With these data, the aerodynamic coefficients could be calculated and summed to provide total aerodynamic forces and moments. External forces and moments (ejectors, thrust, and others as desired) were added to these and the resultant body linear and angular accelerations were calculated. Integration of the accelerations, calculation of positions in several reference coordinate systems, and storage of data in the temporary file completed the cycle. Time was then incremented and the process repeated until the desired end point was attained.

A trapezoidal integration scheme was selected which uses a linear extrapolation of second derivatives to start the process. Because the pitch and yaw angular motions were not expected to be large, the body angular positions were obtained by a direct integration of the angular velocities. The use of quaternions to track the angular motion and more elaborate extrapolation and/or integration schemes was considered, but the additional complexity of using these was not deemed justified within the constraints of the present problem definition.

Data handling within the program structure was accomplished with a dimensioned common array. Variables to be transferred to or from another module were equivalenced to locations in this

common array at the beginning of the modules in which they were used. The array dimension was set at a large enough value that many additions could be made without a major resizing. The array size was changed only once - when the program was being adapted to another problem at a later date. In the case of the flow-field subroutine, a.. argument string was also used in the call statement to facilitate use of the same code to determine the flow angles at several geometric locations at each time step.

An input scheme was developed with the intent of being both "user friendly" and flexible. A series of messages appear on the terminal screen which guide the user to the proper input. At program start up, the user enters an identifying Run No., the flight Mach number, and the flight altitude. The corresponding stored input file is selected based on this Mach number input, and the file is read. The user is then given an opportunity to change any, or all, of the input data manually from the terminal keyboard. A standard structure was established for the input file in which any combination of values can be input to stated locations in the common array. Each line of input data in this file contains the variable name (for user reference only), its common-array location number, and the numerical value to be assigned in either fixed or floating point notation. Since all locations in the common array are zeroed out when the input file is called for, only those quantities which have a non-zero value must be included in the input string. However, for completeness, the full set of 62 standard input values were included in all of the input files.

The input file also includes instructions for establishing the quantities to be sent to the output file. Each line of output data in this part of the file contains the variable name to be used to identify the quantity in the output listing (column heading) and the common-array location number of the quantity. The output file is structured to print four quantities on each page - the first column is always the simulation time. The other quantities are printed in the order in which they appear in the input file. Input

data and output data are identified in the input file by an integer code at the beginning of each line. If the input data are manually entered from the keyboard, then no output file instructions will be given and no data are stored. In this case, the only output is the standard terminal screen display during the course of the computations.

The simulation was coded in standard Fortran 77 language. It was coded, compiled, and run on a run-of-the-mill desktop personal computer (PC) of the type found in most engineering offices and many homes. The combined source-code files require approximately 30 kilobytes of disk storage space while the executable code occupies about 51 kilobytes. Trajectory runs simulating the first 0.4 second following release, with an integration step size of one millisecond, were generally used in this analysis. Using a microprocessor with a clock speed of 4.77 megaHertz, such a run would require 3.5 minutes of computer time, of which 0.9 minute was for setup and input processing, 1.8 minutes was computational time, and 0.8 minute was used in writing the output file. Typical input and output files, with 60 output variables at time steps of 0.02 sec., for a run of this length required 3.6 and 35 kilobytes, respectively, of disk space. These are indeed modest numbers.

The editor and compiler software are readily available for a few hundred dollars at any computer store or through the many catalog operations extant. The total time required to develop the flow-field models, evaluate and interpret the wind tunnel aerodynamic data, structure and code the simulation, and carry out validation runs and the separation analysis was on the order of four months. This was essentially a one-man effort of the author, with outside assistance coming only in the structuring of the input and output files and the code needed to manage them. So this was indeed a very low-cost effort to deal with a problem of such considerable importance.

BUT DOES IT WORK?

Having made the original premise of promoting the use of only the most "economical" methods, and having presented the details of a low-cost analysis to demonstrate this premise, it is only fair to ask the question "does it work?" The desired result of economizing is to achieve a specific goal at the lowest unit cost and, after all, even a small number (low-cost effort) divided by zero (no useful results) still yields infinity (high unit cost of output). It would take a most naive reader, I would presume, to expect to find anything but a positive answer here.

To justify the "yes" answer, let us consider the outcome of the analysis and other supporting information. Although specific weapon details and performance results cannot be presented here, some general comments can be made with regard to the trajectory runs produced with the simulation described above.

1. The flow field around the nose of the fuel tank produced a cross-flow velocity which tended to push the nose of the weapon away from the tank. At the tail-fin location, there was little compensating cross flow so that the tail tended to move towards the tank.

2. The aerodynamic characteristics of the weapon were such that the flow-field distortions produced a rolling moment that rotated the top, inboard fin towards the horizontal position. This further aggravated the tank clearance problem.

3. Since the magnitude of the aerodynamic forces increases as the square of the flight velocity, the reduction in clearance between weapon and fuel tank became more serious as the aircraft speed increased. At a flight Mach number of approximately 0.9, the clearance became zero; i.e., there was a collision.

4. Because the offending motion was generated primarily from aerodynamic forces, the only effective way found to compensate for them was by aerodynamic means; e.g., by a bias offset in the control surface positions.

These results were used to aid in structuring a wind tunnel test program to study the separation characteristics. Data from this test series corroborated the above results for flight speeds up to, and including, Mach number 0.8. At somewhat higher speeds, local supersonic flow (and its attendant shock waves) was encountered between the tank and the weapon which reversed the direction of the weapon motion. This type of flow, of course, is beyond the scope of the flow-field representation used in the analysis. Thus, the wind tunnel data both verified the usefulness of the preliminary analysis and defined one of the limitations of its applicability.

Another verification of the quality of the present results came from a later analysis of the same weapon system. This later analysis utilized a r cher extensive program which required the use of one of the larger, faster computing systems. In this program, the aircraft flow field was modeled in considerable detail using both source-sink and panel methods to define the shape of the aircraft, but it was subject to the same subsonic flow limitation as for the present analysis. With such a code, the setup time is quite large and the computational time is costly. This analysis produced results which also corroborated the desktop simulation. There was a small difference in the flight Mach number at which contact between tank and weapon was first encountered, but it was a difference of no practical significance.

POSTLOGUE

Based on the success of the above-described analysis effort, the desktop trajectory simulation was pressed into service on another program. The configurations of both the aircraft and the vehicle to be released were quite different from those modeled in

the original simulation, as were the source and nature of the flow-field data. Thanks to the simple modular structure of the simulation, it was a relatively easy task to modify it for the new usage. There were three major modifications required.

1. The only available source of information on the flow-field characteristics was a set of wind tunnel data from an unrelated program, in which aerodynamic loads were measured on a different vehicle in proximity to the fuselage of the same aircraft. These data were evaluated in comparison to the basic freestream characteristics of the missile to determine the local flow angles in the region just below the fuselage. The matrix of missile positions was such that flow angles could be determined at eight axial stations for each of several vertical distances from the bottom of the fuselage. Analytic curve-fit functions were developed to represent the local flow angle in the vertical plane in terms of both the axial and vertical positions. Since the vehicle was to be carried on, and released from, the fuselage centerline with no other external stores mounted on the aircraft, no lateral flow angles were included. The flow-field subroutine used in the original simulation was replaced by a new one in which local flow angles were calculated from these analytic functions.

2. It was desired to evaluate the flight motion of the vehicle not only during the separation event, but also through transition to a sustained-flight attitude after it had cleared the aircraft. Therefore, it would be expected to reach higher angles of attack than previously considered. To accommodate this difference, a new subroutine for the aerodynamic coefficients was created which used a more elaborate curve-fit process, and which accounted for significant changes in the vehicle flight Mach number over the course of a trajectory run. The

aerodynamic coefficient functions which were derived were based on wind tunnel data for the complete vehicle and its components, including the effects of control surface deflection.

3. Also because of this more elaborate flight profile, a rather sophisticated autopilot routine was required. A first-order lead-lag filter representation was used, based on the onboard-software design, with variable gains and both angle-error and angular-rate inputs. The actuator response was modeled as a second-order lag system with torque limits imposed. When its use was specified, this routine was called at the beginning of the aerodynamics subroutine and its output was a set of control-surface deflection angles. These angles were then multiplied by the appropriate control derivatives to obtain the control increments to the aerodynamic coefficients.

The major part of the effort in making these modifications was in developing the curve-fit functions to the flow-field and vehicle aerodynamic data. For the vehicle aerodynamic data, polynomials of up to the third order in both angle of attack and Mach number were found to be sufficient. For the flow-field data, a linear combination of both polynomial and exponential functions was required to get a satisfactory representation. Shock waves at supersonic speeds were noted in the data by sudden shifts in the level of the flow angle, and these were accounted for, to a large degree, in the selection of the curve-fit functions.

Once the aerodynamic data representations were selected, the task of modifying the simulation was quite simple. Because of the added complexity of the modifications, the executable code file size was increased to about 67 kilobytes and the computational time was increased by about 20 percent. The nature of the flight to be simulated also required that the calculations be extended over a

longer flight time. If only the separation was being analyzed, a flight time of one second was usually sufficient. To examine the transition to the sustained-flight condition, a flight of six seconds duration was typically calculated. The computational time required for these runs was about 5.5 minutes and 30.5 minutes for simulated flight times of one second and six seconds, respectively.

The primary requirement of the analysis was to aid in planning for a separation-trajectory wind tunnel test. The results showed that the vehicle would separate properly at subsonic speeds. However, at transonic and supersonic speeds, the nature and strength of the aircraft flow field were such that the vehicle would tumble in a nose-down direction. This motion was confirmed by the results of the test program. The analysis also indicated that the only effective means of controlling the tumbling motion was to initiate autopilot control immediately after release, and to increase the gain on the pitch-rate input by a significant amount over that initially planned. Because of the magnitude of the aerodynamic forces, making rational changes in such variables as ejector forces and vehicle incidence at carriage were shown to be of no benefit.

The analysis of transition to a sustained-flight condition was carried out to study the aerodynamic responsiveness of the vehicle and, secondarily, the stability of the autopilot system. Some areas of possible concern were identified in this latter area. Again, later more extensive and elaborate calculations showed that the desktop analysis produced results which correctly identified trends and basic characteristics. No conclusions based on the desktop results were refuted by the later analyses.

AND IN CONCLUSION

In spite of the often ready availability of complex and extensive engineering tools by which to carry out elaborate analyses, the engineer should keep in mind the need for cost

effectiveness in choosing the approach to be used in analyzing a new system, or a new use for an old system. A simplified approach may often be the better choice when the simplifying assumptions can be made on the basis of sound engineering evaluation and judgement. This is almost always the case when basic characteristics and trends, rather than precise numbers, are the desired result, or when it is necessary to narrow the range of choices among several alternative approaches to resolving a problem.

With the capability, ease of use, ready availability, and low cost of today's engineering tools, even the individual and small-office engineer has the capacity to make significant contributions to the solution of important problems. It may require more careful thought in the beginning and even a touch of cleverness, both hallmarks of the successful entrepreneur, but the results are usually both satisfying and cost effective.

BIOGRAPHY

MR. JOHN C. MARSHALL

Mr. Marshall received his engineering education at the California Institute of Technology, being granted a Bachelor of Science degree in Mechanical Engineering in 1949 and a Master of Science degree in Aeronautics in 1951. He was associated with the Arnold Engineering Development Center (AEDC) from 1951 through 1984, where he developed transonic wind tunnel test procedures and was responsible for conducting wind tunnel test programs, with special emphasis in the later years on store separation testing in the 4T wind tunnel using grid survey, captive trajectory, and freedrop test techniques. He retired from his AEDC associations in 1984 and joined General Research Corporation in Fort Walton Beach, Florida, where he is currently involved with systems analysis and simulation development. Mr. Marshall is an Associate Fellow of the AIAA, a registered Professional Engineer in Tennessee, and a consultant to the SAB Division Advisory Group of the Aeronautical Systems Division (AFSC/ASD), Wright-Patterson Air Force Base.